RONALD L. EISENBERG NANCY M. JOHNSON

Comprehensive Radiographic PATHOLOGY

SIXTH EDITION

EVOLVE STUDY RESOURCES FREE WITH TEXTBOOK PURCHASE
EVOLVE.ELSEVIER.COM

ELSEVIER

ELSEVIER evolve

YOU'VE JUST PURCHASED MORE THAN A TEXTBOOK!

Evolve Student Resources for *Eisenberg: Comprehensive Radiographic Pathology, Sixth Edition,* include the following:

- Image collection
- Review questions for each chapter

Activate the complete learning experience that comes with each textbook purchase by registering at

http://evolve.elsevier.com/Eisenberg/pathology/

REGISTER TODAY!

You can now purchase Elsevier products on Evolve!
Go to evolve.elsevier.com/html/shop-promo.html to search and browse for products.

Comprehensive Radiographic PATHOLOGY

SIXTH EDITION

Ronald L. Eisenberg, MD, JD, FACR
Associate Professor of Radiology
Harvard Medical School
Staff Radiologist
Beth Israel Deaconess Medical Center
Boston, Massachusetts

Nancy M. Johnson, MEd, RT(R)(CV)(CT)(QM), FASRT
Faculty, Diagnostic Medical Imaging
GateWay Community College
Phoenix, Arizona

ELSEVIER

ELSEVIER

3251 Riverport Lane
St. Louis, Missouri 63043

COMPREHENSIVE RADIOGRAPHIC PATHOLOGY, SIXTH EDITION
Copyright © 2016 by Mosby, Inc., an affiliate of Elsevier Inc.

All rights reserved. No part of this publication may be reproduced or transmitted in any form or by any means, electronic or mechanical, including photocopying, recording, or any information storage and retrieval system, without permission in writing from the publisher, except that, until further notice, instructors requiring their students to purchase Comprehensive Radiographic Pathology by Eisenberg, may reproduce the contents or parts thereof for instructional purposes, provided each copy contains a proper copyright notice as follows: Copyright © 2016 by Elsevier Inc.

Details on how to seek permission, further information about the Publisher's permissions policies and our arrangements with organizations such as the Copyright Clearance Center and the Copyright Licensing Agency, can be found at our website: www.elsevier.com/permissions.

This book and the individual contributions contained in it are protected under copyright by the Publisher (other than as may be noted herein).

Permission is hereby granted to reproduce the test questions in this publication in complete pages, with the copyright notice, for instructional use and not for resale.

Although for mechanical reasons some/all pages of this publication are perforated, only those pages imprinted with an Elsevier Inc. copyright notice are intended for removal.

Notices

Knowledge and best practice in this field are constantly changing. As new research and experience broaden our understanding, changes in research methods, professional practices, or medical treatment may become necessary.

Practitioners and researchers must always rely on their own experience and knowledge in evaluating and using any information, methods, compounds, or experiments described herein. In using such information or methods they should be mindful of their own safety and the safety of others, including parties for whom they have a professional responsibility.

With respect to any drug or pharmaceutical products identified, readers are advised to check the most current information provided (i) on procedures featured or (ii) by the manufacturer of each product to be administered, to verify the recommended dose or formula, the method and duration of administration, and contraindications. It is the responsibility of practitioners, relying on their own experience and knowledge of their patients, to make diagnoses, to determine dosages and the best treatment for each individual patient, and to take all appropriate safety precautions.

To the fullest extent of the law, neither the Publisher nor the authors, contributors, or editors, assume any liability for any injury and/or damage to persons or property as a matter of products liability, negligence or otherwise, or from any use or operation of any methods, products, instructions, or ideas contained in the material herein.

Previous editions copyrighted 2012, 2007, 2003, 1995, 1990.

Library of Congress Cataloging-in-Publication Data

Eisenberg, Ronald L., author.
Comprehensive radiographic pathology / Ronald L. Eisenberg, Nancy M. Johnson. -- Sixth edition.
p. ; cm.
Includes index.
ISBN 978-0-323-35324-3 (pbk. : alk. paper)
I. Johnson, Nancy M., author. II. Title.
[DNLM: 1. Radiography--methods. 2. Pathology. WN 200]
RC78
616.07'572--dc23

2015016178

Content Strategist: Sonya Seigafuse
Content Development Manager: Laurie Gower
Content Development Specialist: Laura Goodrich
Publishing Services Manager: Jeff Patterson
Project Managers: Jeanne Genz and Lisa A. P. Bushey
Design Direction: Julia Dummitt

Printed in China

Last digit is the print number: 9 8 7 6 5 4 3 2 1

This text is dedicated to all the students and medical imaging professionals
who wish to better understand the value
of pathology to improve their diagnostic images.

Thank all of you who helped in making this endeavor successful.
Special credit to the contributors of this edition who
assisted in updating the content and images.

–

Raymond Johnson, BS, NMTCB, PET
and
Bartram Pierce, BS, RT(R)(MR), FASRT

Nancy M. Johnson

This page intentionally left blank

REVIEWERS

Elaine Beaudoin, MS, RT(R)
Clinical Coordinator
Niagara County Community College
Sanborn, New York

Chris Beaudry, MEd, ARRT(R)(M)(CT)
Program Coordinator
Yakima Valley Community College
Yakima, Washington

Dena L. Blevins, BSRT(R)
Clinical Coordinator
Collins Career Technical College
Chesapeake, Ohio

Robin T. Cornett, MAEd, RT(R)(CV)
Program Director, Radiography
Catawba Valley Community College
Hickory, North Carolina

Kristi Klein, MSEd, RT(R)(M)(CT)
Program Director
Madison Area Technical College
Madison, Wisconsin

Nancy I. Lamouroux, BS, RT(R)
Clinical Coordinator/Instructor
Kilgore College
Kilgore, Texas

Joy Menser, EdD, RT(R)(T)
Program Director of Radiography
Owensboro Community and Technical College
Owensboro, Kentucky

Cynthia A. Meyers, MSRT(R)
Program Director, Professor
Niagara County Community College
Sanborn, New York

Sandra E. Moore, MA, RT(R)(M)
Radiography Program Director
The Johns Hopkins Hospital
Baltimore, Maryland

April H. Pait, BS, RT(R)(M)
Clinical Coordinator
Guilford Technical Community College
Jamestown, North Carolina

Paula Pate-Schloder, MS, RT(R)(CV)(CT)(VI)
Associate Professor
Misericordia University
Dallas, Pennsylvania

Lorrie Scott Teeter, MS, RT(R)(CT)
Assistant Professor
Adventist University of Health Sciences
Orlando, Florida

This page intentionally left blank

PREFACE

Understanding the basic principles of pathology is an essential part of the radiologic technologist's education. Knowing how disease processes work and recognizing the radiographic appearance of specific diseases aids the technologist in selecting proper modalities and determining the need for repeat radiographs in different situations. This kind of knowledge enables the radiologic technologist to become a more competent professional and a contributing member of the diagnostic team.

ORGANIZATION

Fully illustrated and well organized, *Comprehensive Radiographic Pathology* meets the needs of today's student and practicing image personnel. The book opens with a chapter on disease processes that introduces the pathologic terms used throughout the text. Chapter 2 describes the advantages and limitations of eight widely used modalities: mammography, ultrasound, computed tomography (CT), magnetic resonance imaging (MRI), nuclear medicine, single-photon emission computed tomography (SPECT), positron emission tomography (PET), and fusion imaging. Summary tables describe imaging terminology used in each of the seven modalities.

Each of the remaining chapters is a systematic approach to the diseases involving a specific organ system. These chapters begin with an overview of physiology. For each of the most common pathologic conditions associated with the system, there is a brief description of the disease and its clinical manifestations, followed by imaging findings and treatment. Summary tables follow each major discussion, reiterating the location, imaging appearance, and treatment of the diseases just presented.

DISTINCTIVE FEATURES

- Comprehensive coverage provides the most thorough explanations of any radiographic pathology text of those pathologies that can be diagnosed with medical imaging.
- Navigating the chapters is easy with the standardized heading scheme and chapter outlines for the systems chapters.
- *Radiographer Notes* in every chapter instruct students on how to deal effectively with varying patient needs and provide perspective on why learning pathology is important for radiography practice.
- A systems approach makes it easy to locate information and to study one area at a time, assimilating details in a logical sequence. It provides the best framework for building understanding of pathology.
- Summary tables list the imaging appearance and treatment of each disease and have been updated to include pathologic conditions included in the text.
- Coverage of the alternative imaging modalities that supplement radiographic imaging for diagnosis of some pathology conditions orients readers to other modalities that may be needed to ensure proper diagnosis of certain pathologies.
- Treatment sections provide useful background treatment and prognosis.
- The student workbook provides extra opportunities for review and self-assessment.

NEW TO THIS EDITION

- Expanded terms related to disease process and imaging features
- Updates and additions of the following: fusion imaging, SPECT, PET/CT, MR pulse sequences, and their correlation with general radiography
- Color images, where appropriate, of MR, nuclear medicine, and PET/CT
- Updated *Radiographer Notes* to incorporate analog and digital information

PEDAGOGICAL FEATURES

- Each chapter opens with an outline and a key terms list to aid the student in navigating the content.
- *Radiographer Notes* offer helpful suggestions for producing optimal radiographs of the organ system featured in each chapter. Information especially relevant to radiologic technologists is included, such as positioning and exposure factor adjustments for patients with specific conditions and special patient handling requirements. If multiple imaging modalities can be used, the most appropriate initial procedure is indicated, as well as the sequence in which various imaging studies should be performed.
- The body system chapters are organized as follows: physiology, identification of anatomic structures on anatomy figures and radiographs, pathologic conditions, radiographic appearance, and treatment.
- Each section of related pathologies is summarized in a table at the end of the section. The table names the disorder and then lists the location, radiographic appearance, and treatment for easy review and enhanced retention.
- Finally, each chapter ends with a series of review questions to help readers assess their comprehension of the material. An answer key is found at the back of the book, along with several appendices, an extensive glossary, and a list of major prefixes, roots, and suffixes to help readers determine the meaning of unfamiliar words.

ANCILLARIES

For the Instructor

- Instructor Resources on Evolve include a test bank with approximately 500 questions, PowerPoint slides, and an image collection with approximately 900 images.

For the Student

- The Evolve site offers 10 student review questions per chapter and access to the image collection for further review.
- The workbook contains a variety of exercises for each of the 12 chapters in the book. Examples include matching terms with their definitions; labeling diagrams; fill-in-the-blank, short-answer, and multiple-choice questions; pathology case studies; and a post-test. Completing the workbook activities will ensure understanding of disease processes, their radiographic appearance, and their likely treatment. The answers for the exercises are located in the back of the workbook.
- By understanding the disease processes, their image appearance, and their treatment, the technologist will be prepared to contribute to the diagnostic team.

CONTENTS

Preface, vii

1 Introduction to Pathology, 1
Disease, 2
Inflammation, 3
Edema, 4
Ischemia and Infarction, 5
Hemorrhage, 5
Alterations of Cell Growth, 6
Neoplasia, 7
Hereditary Diseases, 9
Disorders of Immunity, 11
Infectious Disease Exposure, 11
Acquired Immunodeficiency Syndrome, 12

2 Specialized Imaging Techniques, 15
Diagnostic Imaging Modalities, 15
Imaging Features, 16
Mammography, 16
Ultrasound, 17
Computed Tomography, 20
Magnetic Resonance Imaging, 24
Nuclear Medicine, 28
Single-Photon Emission Computed Tomography, 28
Positron Emission Tomography, 29
Fusion Imaging, 31

3 Respiratory System, 36
Physiology of the Respiratory System, 38
Internal Devices, 40
Endotracheal Tube, 40
Central Venous Catheters, 40
Swan–Ganz Catheters, 41
Transvenous Cardiac Pacemakers, 42
Congenital/Hereditary Diseases, 43
Cystic Fibrosis, 43
Hyaline Membrane Disease, 44
Inflammatory Disorders of the Upper Respiratory System, 44
Croup, 44
Epiglottitis, 44
Inflammatory Disorders of the Lower Respiratory System, 45
Pneumonia, 45
Anthrax, 47
Lung Abscess, 48
Tuberculosis, 49
Pulmonary Mycosis, 52
Respiratory Syncytial Virus, 53
Severe Acute Respiratory Syndrome, 53
Diffuse Lung Disease, 54
Chronic Obstructive Pulmonary Disease, 54
Sarcoidosis, 57
Pneumoconiosis, 59
Neoplasms, 61
Solitary Pulmonary Nodule, 61
Bronchial Adenoma, 63
Bronchogenic Carcinoma, 63
Treatment of Pulmonary Neoplastic Diseases, 65
Pulmonary Metastases, 65
Vascular Diseases, 68
Pulmonary Embolism, 68
Septic Embolism, 71
Pulmonary Arteriovenous Fistula, 72
Miscellaneous Lung Disorders, 72
Atelectasis, 72
Adult Respiratory Distress Syndrome, 73
Intrabronchial Foreign Bodies, 74
Mediastinal Emphysema (Pneumomediastinum), 75
Subcutaneous Emphysema, 75
Treatment of Mediastinal and Subcutaneous Emphysema, 75
Disorders of the Pleura, 76
Pneumothorax, 76
Pleural Effusion, 77
Empyema, 79
Mediastinal Masses, 80
Disorders of the Diaphragm, 82
Diaphragmatic Paralysis, 82
Eventration of the Diaphragm, 83
Other Causes of Elevation of the Diaphragm, 83

4 Skeletal System, 85
Physiology of the Skeletal System, 87
Congenital/Hereditary Diseases of Bone, 89
Vertebral Anomalies, 89
Spina Bifida, 89
Osteopetrosis, 90
Osteogenesis Imperfecta, 91
Achondroplasia, 92
Congenital Hip Dysplasia (Dislocation), 92
Inflammatory and Infectious Disorders, 95
Rheumatoid Arthritis, 95
Rheumatoid Variants: Ankylosing Spondylitis, Reiter's Syndrome, and Psoriatic Arthritis, 96
Osteoarthritis (Degenerative Joint Disease), 98
Infectious Arthritis, 98
Treatment of Arthritis, 100
Bursitis, 101
Rotator Cuff Tears, 102
Tears of the Menisci of the Knee, 103

Bacterial Osteomyelitis, 103
Tuberculous Osteomyelitis, 106
Metabolic Bone Disease, 108
Osteoporosis, 108
Osteomalacia, 109
Rickets, 110
Gout, 111
Paget's Disease, 112
Lead Poisoning, 114
Fibrous Dysplasia, 116
Ischemic Necrosis of Bone, 116
Benign Bone Tumors, 119
Treatment of Benign Bone Tumors, 123
Malignant Bone Tumors, 124
Treatment of Malignant Bone Tumors, 127
Bone Metastases, 127
Fractures, 131
Types of Fractures, 131
Fracture Healing, 134
Pathologic Fractures, 135
Stress Fractures, 136
Battered-Child Syndrome, 137
Common Fractures and Dislocations, 137
Fractures and Dislocations of the Spine, 141
Herniation of Intervertebral Disks, 144
Scoliosis, 147
Spondylolysis and Spondylolisthesis, 148

5 Gastrointestinal System, 152
Physiology of the Digestive System, 153
Esophagus, 156
Tracheoesophageal Fistula, 156
Esophagitis, 158
Ingestion of Corrosive Agents, 160
Esophageal Cancer, 161
Esophageal Diverticula, 163
Esophageal Varices, 163
Hiatal Hernia, 165
Achalasia, 166
Foreign Bodies, 166
Perforation of the Esophagus, 168
Stomach, 170
Gastritis, 170
Pyloric Stenosis, 170
Peptic Ulcer Disease, 171
Cancer of the Stomach, 174
Small Bowel, 176
Crohn's Disease (Regional Enteritis), 176
Small Bowel Obstruction, 177
Adynamic Ileus, 180
Intussusception, 181
Malabsorption Disorders, 182
Colon, 183
Appendicitis, 183
Diverticulosis, 185
Diverticulitis, 186
Ulcerative Colitis, 187
Crohn's Colitis, 189
Ischemic Colitis, 191
Irritable Bowel Syndrome, 191
Cancer of the Colon, 191
Large Bowel Obstruction, 193
Volvulus of the Colon, 193
Hemorrhoids, 195
Gallbladder, 197
Gallstones (Cholelithiasis), 197
Acute Cholecystitis, 198
Emphysematous Cholecystitis, 199
Porcelain Gallbladder, 199
Liver, 201
Hepatitis, 201
Cirrhosis of the Liver, 202
Hepatocellular Carcinoma, 203
Hepatic Metastases, 205
Pancreas, 206
Acute Pancreatitis, 206
Chronic Pancreatitis, 206
Pancreatic Pseudocyst, 208
Cancer of the Pancreas, 209
Pneumoperitoneum, 210
Spleen, 212
Enlargement, 212
Rupture, 213

6 Urinary System, 216
Physiology of the Urinary System, 216
Congenital/Hereditary Diseases, 218
Anomalies of Number and Size, 218
Anomalies of Rotation, Position, and Fusion, 219
Anomalies of Renal Pelvis and Ureter, 220
Treatment of Congenital/Hereditary Anomalies, 221
Ureterocele, 221
Posterior Urethral Valves, 222
Inflammatory Disorders, 224
Glomerulonephritis, 224
Pyelonephritis, 224
Tuberculosis, 225
Papillary Necrosis, 226
Cystitis, 227
Urinary Calculi, 228
Urinary Tract Obstruction, 231
Cysts and Tumors, 234
Renal Cyst, 234
Polycystic Kidney Disease, 236
Renal Carcinoma, 237
Wilms' Tumor (Nephroblastoma), 240
Carcinoma of the Bladder, 240
Renal Vein Thrombosis, 242
Acute Renal Failure, 243
Chronic Renal Failure, 245

7 Cardiovascular System, 248
Physiology of the Cardiovascular System, 248
Congenital Heart Disease, 252
Left-to-Right Shunts, 252
Tetralogy of Fallot, 254
Coarctation of the Aorta, 254
Acquired Vascular Disease, 256
Coronary Artery Disease, 256
Congestive Heart Failure, 260
Pulmonary Edema, 261
Hypertension, 263
Hypertensive Heart Disease, 265
Aneurysm, 266
Traumatic Rupture of the Aorta, 267
Dissection of the Aorta, 268
Atherosclerosis, 270
Thrombosis and Embolism, 271
Valvular Disease, 275
Rheumatic Heart Disease, 275
Mitral Stenosis, 275
Mitral Insufficiency, 276
Aortic Stenosis, 277
Aortic Insufficiency, 278
Infective Endocarditis, 278
Pericardial Effusion, 280
Venous Disease, 281
Deep Venous Thrombosis, 281
Varicose Veins, 281

8 Nervous System, 286
Physiology of the Nervous System, 287
Infections of the Central Nervous System, 290
Meningitis, 290
Encephalitis, 291
Brain Abscess, 292
Subdural Empyema, 293
Epidural Empyema, 293
Treatment of Subdural and Epidural Empyemas, 294
Osteomyelitis of the Skull, 294
Tumors of the Central Nervous System, 295
Glioma, 295
Meningioma, 299
Acoustic Neuroma, 299
Pituitary Adenoma, 300
Craniopharyngioma, 303
Pineal Tumors, 305
Chordoma, 306
Metastatic Carcinoma, 307
Traumatic Processes of the Brain and Skull, 309
Skull Fracture, 309
Epidural Hematoma, 311
Subdural Hematoma, 311
Cerebral Contusion, 312
Intracerebral Hematoma, 313
Subarachnoid Hemorrhage, 313
Carotid Artery Injury, 313
Facial Fractures, 313
Vascular Disease of the Central Nervous System, 317
Cerebrovascular Disease, 317
Stroke Syndrome, 317
Transient Ischemic Attacks, 319
Intraparenchymal Hemorrhage, 320
Subarachnoid Hemorrhage, 321
Multiple Sclerosis, 324
Epilepsy and Convulsive Disorders, 326
Degenerative Diseases, 327
Normal Aging, 327
Alzheimer's Disease, 327
Huntington's Disease, 328
Parkinson's Disease, 329
Cerebellar Atrophy, 329
Amyotrophic Lateral Sclerosis (Lou Gehrig's Disease), 330
Hydrocephalus, 330
Sinusitis, 332

9 Hematopoietic System, 336
Physiology of the Blood, 336
Diseases of Red Blood Cells, 337
Anemia, 337
Polycythemia, 342
Treatment of Polycythemias, 342
Diseases of White Blood Cells, 342
Leukemia, 342
Lymphoma, 344
Infectious Mononucleosis, 349
Diseases of Platelets (Bleeding Disorders), 349
Hemophilia, 350
Purpura (Thrombocytopenia), 350

10 Endocrine System, 354
Physiology of the Endocrine System, 354
Adrenal Glands, 355
Physiology of the Adrenal Glands, 355
Diseases of the Adrenal Cortex, 355
Diseases of the Adrenal Medulla, 360
Pituitary Gland, 364
Physiology of the Pituitary Gland, 364
Diseases of the Pituitary Gland, 364
Thyroid Gland, 367
Physiology of the Thyroid Gland, 367
Diseases of the Thyroid Gland, 367
Parathyroid Glands, 374
Physiology of the Parathyroid Glands, 374
Diseases of the Parathyroid Glands, 374
Diabetes Mellitus, 378

11 Reproductive System, 383
Infectious Diseases of Both Genders, 383
Syphilis, 383
Gonorrhea, 385

Male Reproductive System, 386
Physiology of the Male Reproductive System, 386
Benign Prostatic Hyperplasia, 387
Carcinoma of the Prostate Gland, 388
Staging, 389
Undescended Testis (Cryptorchidism), 390
Testicular Torsion and Epididymitis, 391
Testicular Tumors, 393
Female Reproductive System, 394
Physiology of the Female Reproductive System, 394
Pelvic Inflammatory Disease, 396
Cysts and Tumors, 397
Ovarian Cysts and Tumors, 397
Dermoid Cyst (Teratoma), 400
Uterine Fibroids, 400
Endometrial Carcinoma, 402
Endometriosis, 403
Carcinoma of the Cervix, 404
Breast Lesions, 407
Breast Cancer, 407
Benign Breast Disease, 409
Imaging in Pregnancy, 414
Ectopic Pregnancy, 416
Trophoblastic Disease, 416
Female Infertility, 417

12 Miscellaneous Diseases, 419
Nutritional Diseases, 419
Vitamin Deficiencies, 419
Hypervitaminosis, 421
Protein–Calorie Malnutrition (Kwashiorkor), 422
Obesity, 422
Systemic Lupus Erythematosus, 423
Melanoma, 424
Muscular Dystrophy, 425
Hereditary Diseases, 426
Chromosomal Aberrations, 426
Genetic Amino Acid Disorders, 428

Answers to Review Questions, 432
Illustration Credits, 435
Appendix A: Prefixes/Suffixes/Roots, 439
Appendix B: Laboratory Values and Their Significance, 441
Glossary, 442
Index, 449

1

Introduction to Pathology

OUTLINE

Disease
- Inflammation
- Edema
- Ischemia and Infarction
- Hemorrhage
- Alterations of Cell Growth
- Neoplasia

Hereditary Diseases

Disorders of Immunity

Infectious Disease Exposure

Acquired Immunodeficiency Syndrome

KEY TERMS

abscess
acquired immunodeficiency syndrome (AIDS)
active immunity
anaphylactic
anaplastic
antibodies
antigens
asymptomatic
atrophy
autosomes
bacteremia
benign
cancers
carcinomas
community acquired
diagnosis
dominant
dysplasia
edema
epidemiology
etiology
grading
granulation tissue
hematogenous spread
hematoma
hemorrhage
hereditary diseases
hyperplasia
iatrogenic
idiopathic
immune
infarct
inflammation
ischemia
lymphatic spread
malignant
metastasize
morbidity
mortality
mutations
neoplasia
nosocomial
oncology
permeable
personal protective equipment
prognosis
pyogenic
recessive
sarcomas
signs
staging
Standard Precautions
symptoms
syndrome
toxoid
Transmission-Based Precautions
undifferentiated
vaccine

OBJECTIVES

After reading this chapter, the reader will be able to:

- Classify the more common diseases in terms of their attenuation of x-rays
- Explain the changes in technical factors required for obtaining optimal quality radiographic images in patients with various underlying pathologic conditions
- Define and describe all boldface terms in this chapter
- Differentiate inflammation, edema, infarction, hemorrhage, and neoplasia
- Characterize the various alterations of cell growth
- Describe the various immune reactions of the body
- Describe AIDS and the precautions necessary when taking a radiograph of patients with AIDS or any patient with whom contact with any body fluid is possible (Standard Precautions)

DISEASE

Pathology is the study of diseases that can cause abnormalities in the structure or function of various organ systems. In essence, a *disease* is the pattern of the body's response to some form of injury that causes a deviation from or variation of normal conditions. Diseases may be hereditary or may result from a broad spectrum of traumatic, infectious, vascular, or metabolic processes manifesting as a set of characteristics known as **signs** and **symptoms**. Signs represent the measurable or objective manifestations of the disease process. The experiences the patient feels and describes are the symptoms, those (subjective) manifestations that are not measurable or observable. A patient showing no evidence of diseases is considered **asymptomatic**. Symptoms may reflect alterations of cell growth, as in neoplasia (tumors), or may even be caused by physicians and their treatment (**iatrogenic**). Imaging modalities are used to assist in making a **diagnosis**, the precise disease process affecting the patient. To best treat a disease process, it is important to discover its underlying cause, known as the **etiology**. If the underlying cause is unknown, the disease is termed **idiopathic**. Once the specific diagnosis and etiology are confirmed, the physician offers a **prognosis**, which describes the expected patient outcome. A condition characterized by a group of signs, symptoms, and disease processes may be categorized as a **syndrome**.

Incidences of the development of infections at the acute care facility are called **nosocomial**, whereas infections that develop outside the healthcare facility are known as **community acquired**.

This chapter discusses several basic reactions of the body that characterize the underlying mechanisms for the radiographic manifestations of most pathologic conditions. These processes are inflammation, edema, ischemia and infarction, hemorrhage, and alterations of cell growth leading to the development of neoplasms (tumors). In addition, this chapter deals with hereditary diseases and immune reactions, such as acquired immunodeficiency syndrome (AIDS).

Summary of Terms for Disease

Term	Definition
Signs	Measurable or objective manifestations
Symptoms	Feelings that the patient describes—subjective manifestations
Asymptomatic	Without subjective or objective manifestations
Diagnosis	Identification of disease process
Etiology	Study of the cause of the disease process
Idiopathic	Underlying cause is unknown
Prognosis	Probable patient outcome
Syndrome	Linked combination of signs and symptoms
Iatrogenic	Disease caused by physician or treatment
Nosocomial infections	Infections contracted in the acute care facility
Community-acquired infections	Infections contracted in a public setting outside of the acute care facility

RADIOGRAPHER NOTES

Radiography of patients with underlying pathologic conditions can present problems for even the most experienced radiographers. Adjustments in patient position may be necessary to prevent excessive pain caused by the body's response to trauma or certain disease processes. A change in routine projections may be indicated to visualize subtle alterations in the normal imaging appearance. Many disease processes also alter the density of the structures being radiographed and therefore require changes in technique. For example, extensive edema may require an increased technique, whereas severe atrophy may require a decreased technique. Unless the radiographer has access to previous images with recorded exposure factors, a standard technique chart should be used to determine the initial exposures. Any necessary adjustments can then be made on subsequent images.

Box 1-1 lists the relative attenuation of x-rays that can be expected in advanced stages of various disease processes. In chest radiography, 110 to 125 kilovolts peak (kVp) is optimal; therefore, milliampere-second (mAs) factors should be adjusted to control density. In skeletal radiography, when bone *quality* changes are expected, the best exposure factor to change is the kilovolt peak (beam quality change for structural change). When bone *quantity* changes, the milliampere-second (mAs) value is the exposure factor to change to control density (beam quantity increases to ensure that enough radiation reaches the image receptor without changing the contrast). For example, in osteoporosis there is a decrease in bone quantity and quality; however, a decrease in kilovolts produces a higher-quality image. The normal kilovolt peak easily penetrates the diseased bone, producing a low-contrast image with loss of visibility of detail. As imaging progresses into the digital imaging arena, the same theories apply; however, the processing algorithm will control brightness (density) and contrast. The exposure index (number) will represent the over- or underexposure of the image.

Certain diseases suppress the normal immune response. Immunocompromised patients (e.g., those with advanced leukemia) may require special care to prevent their acquiring a disease from the radiographer. Personal protective equipment (PPE) aids in preventing the spread of microorganisms to the patient and to the healthcare worker. The patient may have to be placed in protective isolation (or "reverse" isolation), and the radiographer may be required to put on a mask, gown, and gloves before approaching the patient. Diseases such as AIDS and hepatitis require that the radiographer wear rubber or latex gloves to be protected against exposure to blood and body fluids, which could contaminate any area near the patient. When examining a patient with AIDS who has a productive cough, the radiographer must wear a mask and possibly protective eye goggles if there is a need to be very close to the patient's face. It is important to remember that many patients undergoing radiographic procedures have not been diagnosed, and thus all patients should be treated as though they may have a communicable disease. Therefore, whenever exposure to any type of body secretion or blood may occur, the healthcare worker should wear appropriate PPE.

BOX 1-1 Relative Attenuation of X-Rays in Advanced Stages of Diseases

Skeletal System

Additive (Increased Attenuation)

Acromegaly
Acute kyphosis
Callus
Charcot's joint
Chronic osteomyelitis (healed)
Exostosis
Hydrocephalus
Marble bone
Metastasis (osteosclerotic)
Osteochondroma
Osteoma
Paget's disease
Proliferative arthritis
Sclerosis

Destructive (Decreased Attenuation)

Active osteomyelitis
Active tuberculosis
Aseptic necrosis
Atrophy (disease or disuse)
Blastomycosis
Carcinoma
Coccidioidomycosis
Degenerative arthritis
Ewing's tumor (in children)
Fibrosarcoma
Giant cell tumor
Gout
Hemangioma
Hodgkin's disease
Hyperparathyroidism
Leprosy
Metastasis (osteolytic)
Multiple myeloma
Neuroblastoma
New bone (fibrosis)
Osteitis fibrosa cystica
Osteoporosis/osteomalacia
Radiation necrosis
Solitary myeloma

Respiratory System

Additive (Increased Attenuation)

Actinomycosis
Arrested tuberculosis (calcification)
Atelectasis
Bronchiectasis
Edema
Empyema
Encapsulated abscess
Hydropneumothorax
Malignancy
Miliary tuberculosis
Pleural effusion
Pneumoconiosis
  Anthracosis
  Asbestosis
  Calcinosis
  Siderosis
  Silicosis
Pneumonia
Syphilis
Thoracoplasty

Destructive (Decreased Attenuation)

Early lung abscess
Emphysema
Pneumothorax

Circulatory System

Additive (Increased Attenuation)

Aortic aneurysm
Ascites
Cirrhosis of the liver
Enlarged heart

Soft Tissue

Additive (Increased Attenuation)

Edema

Destructive (Decreased Attenuation)

Emaciation

Even though disease processes increase or decrease the attenuation of the x-rays, it is important to produce a quality image to demonstrate the change in attenuation. Excessive variation of the technical exposure factors may obscure the pathophysiologic changes due to the disease process.
From Thompson TT: *Cahoon's formulating x-ray techniques*, ed 9, Durham, NC, 1979, Duke University Press.

Inflammation

Acute **inflammation** is the initial response of body tissues to local injury. The various types of injury include those caused by blunt or penetrating trauma, infectious organisms, and irritating chemical substances. Regardless of the underlying cause, the inflammatory response consists of four overlapping events that occur sequentially (Box 1-2).

The earliest bodily response to local injury is dilation of arterioles, capillaries, and venules, leading to a dramatic increase in blood flow in and around the injury site. This hyperemia produces the heat and redness associated with inflammation. As hyperemia develops, the venules and capillaries become abnormally **permeable**, allowing passage of protein-rich plasma across vessel walls into the interstitium. This inflammatory exudate in the tissues results in the swelling associated with inflammation, which produces pressure on sensitive nerve endings and causes pain. The protein-rich exudate of inflammation must be differentiated from a transudate, a low-protein fluid such as that seen in the pulmonary edema that develops in congestive heart failure.

Very early in the inflammatory response, leukocytes (white blood cells, especially neutrophils and macrophages) of the

BOX 1-2 Events That Occur in Inflammatory Response

1. Alterations in blood flow and vascular permeability
2. Migration of circulating white blood cells to the interstitium of the injured tissue
3. Phagocytosis and enzymatic digestion of dead cells and tissue elements
4. Repair of injury by regeneration of normal parenchymal cells or proliferation of granulation tissue and eventual scar formation

circulating blood migrate to the area of injury. These white blood cells cross the capillary walls into the injured tissues, where they engulf and enzymatically digest infecting organisms and cellular debris, a process called *phagocytosis*.

The removal of necrotic debris and any injurious agents, such as bacteria, makes possible the repair of the injury that triggered the inflammatory response. In many tissues, such as the lung after pneumococcal pneumonia, regeneration of parenchymal cells permits reconstitution of normal anatomic structure and function. However, some tissues, such as the heart after myocardial infarction, cannot heal by regeneration. A fibrous scar replaces the area of destroyed tissue with **granulation tissue**. Granulation tissue refers to a combination of young developing capillaries and actively proliferating fibroblasts, which produce connective tissue fibers (collagen) that replace the dead tissue. Eventually, the strong connective tissue contracts to produce a fibrous scar. In the abdomen, such fibrous adhesions can narrow loops of intestine and result in an obstruction. The accumulation of excessive amounts of collagen (more common in African Americans) may produce a protruding, tumor-like scar known as a keloid. Unfortunately, surgery to remove a keloid is usually ineffective because the subsequent incision tends to heal in the same way.

Many injuries heal by a combination of regeneration and scar tissue formation. An example is the response of the liver to repeated and persistent alcoholic injury; the result is cirrhosis, in which irregular lobules of regenerated liver cells are crisscrossed and surrounded by bands of scar tissue. Scar tissue formation consists of fibrous connective tissue, which can be divided into primary union (surgical incision) and secondary union (nonsurgical; gunshot wound).

The five clinical signs of acute inflammation are rubor (redness), calor (heat), tumor (swelling), dolor (pain), and loss of function. The localized heat and redness result from increased blood flow in the microcirculation at the site of injury. The swelling occurs because the exudate increases the amount of interstitial fluid, resulting in pressure on nerve endings and thus pain, which results in a loss of function.

Acute inflammation can also lead to systemic manifestations. Fever is especially common in inflammatory conditions associated with the spread of organisms into the bloodstream. The number of circulating white blood cells also increases (leukocytosis).

Some bacterial organisms (e.g., staphylococci and streptococci) produce toxins that damage the tissues and incite an inflammatory response. The presence of **pyogenic** bacteria leads to the production of a thick, yellow fluid called *pus*, which contains dead white blood cells, inflammatory exudate, and bacteria. A suppurative inflammation is one that is associated with pus formation. When a pyogenic infection occurs beneath the skin or in a solid organ, it produces an abscess, a localized, usually encapsulated, collection of pus. All pyogens, wherever they become implanted, have the ability to invade blood vessels to produce **bacteremia**, with the potential involvement of other organs and tissues in the body.

A granulomatous inflammation manifests as a distinct pattern seen in relatively few diseases, including tuberculosis, syphilis, and sarcoidosis. A granuloma is a localized area of chronic inflammation, often with central necrosis. It is characterized by the accumulation of macrophages, some of which fuse to form multinucleated giant cells.

Summary of Terms for Inflammatory Process

Term	Definition
Inflammation	Initial response of the tissue to local injury
Permeable membrane	Allows fluids/cells to pass from one tissue to another tissue or location
Granulation tissue	Fibrous scar replaces destroyed tissue
Pyogenic bacteria	Thick, yellow fluid called pus (dead white cells)
Abscess	Localized, usually encapsulated, collection of fluid
Bacteremia	Potential involvement of other organs and tissues in the body by organisms invading the blood vessels

Edema

Edema is the accumulation of abnormal amounts of fluid in the intercellular tissue spaces or body cavities. Localized edema results from an inflammatory reaction, whereas generalized edema occurs with pronounced swelling of subcutaneous tissues throughout the body (anasarca). Localized edema may result from inflammation, with the escape of protein-rich intravascular fluid into the extravascular tissue. It may also result from a local obstruction to lymphatic drainage; for example, in filariasis, a parasitic worm causes lymphatic obstruction, and the resulting localized edema is termed elephantiasis. Generalized edema occurs most frequently in patients with congestive heart failure, cirrhosis of the liver, and certain forms of renal disease. Because of the effect of gravity, generalized edema is usually most prominent in dependent portions of the body. Thus, ambulatory patients tend to accumulate fluid in tissues around the ankles and lower legs, whereas in hospitalized patients who are nonambulatory or sedentary, the edema fluid collects most prominently in the lower back, sacral areas, and lungs.

Extravascular fluid can also accumulate in serous cavities to produce pleural and pericardial effusions and peritoneal ascites. Edema may produce minimal clinical symptoms or be potentially fatal. If localized to the subcutaneous tissues, large amounts of edema may cause minimal functional impairment. In contrast, pulmonary edema, pericardial effusion, or edematous swelling of the brain may have dire consequences.

Summary of Terms for Edema

Term	Definition
Edema	Accumulation of abnormal amounts of fluid in the intercellular tissue spaces or body cavities
Anasarca	Generalized edema that occurs with pronounced swelling of subcutaneous tissues throughout the body
Elephantiasis	Localized lymphatic obstruction resulting in localized edema

Ischemia and Infarction

Ischemia refers to an interference with the blood supply to an organ or part of an organ, depriving the organ's cells and tissues of oxygen and nutrients. Ischemia may be caused by a narrowing of arterial structures, as in atherosclerosis, or by thrombotic or embolic occlusion (Figure 1-1). Depending on several factors, occlusion of an artery or vein may have little or no effect on the involved tissue, or it may cause death of the tissue and even of the individual. A major determinant is the availability of an alternative or newly acquired route of blood supply (collateral vessels). Other factors include the rate of development of the occlusion, the vulnerability of the tissue to hypoxia, and the oxygen-carrying capacity of the blood. Slowly developing occlusions are less likely to cause tissue death (necrosis) because they provide an opportunity for the development of alternative pathways of flow. Ganglion cells of the nervous system and myocardial muscle cells undergo irreversible damage if deprived of their blood supply for 3 to 5 minutes. Anemic or cyanotic patients tolerate arterial insufficiency less well than normal individuals do, and thus occlusion of even a small vessel in such a patient may lead to death of tissue.

An **infarct** is a localized area of ischemic necrosis within a tissue or organ produced by occlusion of either its arterial supply or its venous drainage. The two most common clinical forms of infarction are myocardial and pulmonary. Almost all infarcts result from thrombotic or embolic occlusion. Infrequent causes include twisting of an organ (volvulus), compression of the blood supply of a loop of bowel in a hernia sac, or trapping of a viscus under a peritoneal adhesion.

In cases in which ischemia continues to progress, resulting in an infarction, necrosis may occur as a result of lack of blood flow. This progressive situation can lead to a condition called *gangrene*. Severe arterial disease of the lower extremities may result in necrosis of several toes or a large segment of the foot, causing gangrene. A frequent presenting symptom in diabetic patients is ischemia of the foot, which may progress to infarction and result in gangrene.

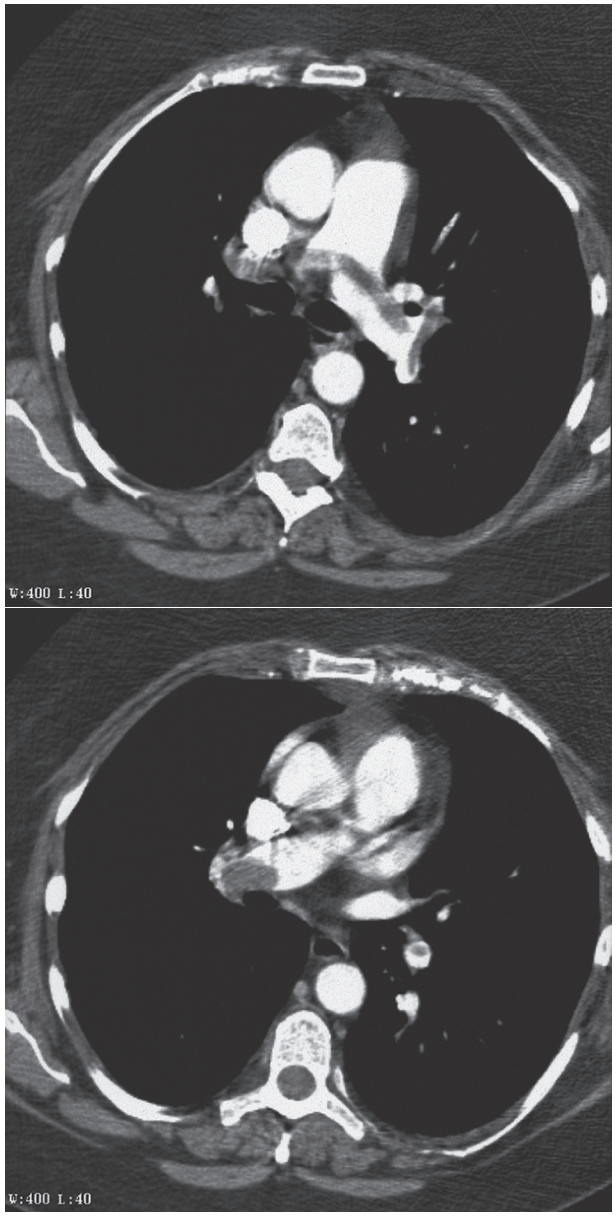

FIGURE 1-1 Computed tomography (CT) scan of pulmonary embolism. **(A)** Filling defect in both the right and the left pulmonary arteries (saddle type), and **(B)** a blockage (filling defect) nearly complete on the right.

Infarctions tend to be especially severe because they occur more often in the patients least able to withstand them. Thus, infarcts tend to occur in elderly individuals with advanced atherosclerosis or impaired cardiac function and are more likely to occur after surgery or delivery.

Hemorrhage

The term **hemorrhage** implies rupture of a blood vessel. Rupture of a large artery or vein is almost always caused by some form of injury, such as trauma, atherosclerosis, or inflammatory or neoplastic erosion of the vessel wall. Hemorrhage may be external, or the blood may be trapped within body tissues, resulting in an accumulation termed a **hematoma** (Figure 1-2). The accumulation of blood in a body cavity results in hemothorax, hemopericardium, hemoperitoneum, or hemarthrosis (blood in a joint).

FIGURE 1-2 Subdural hematoma. Concave appearance of increased attenuation on the left causing midline shift of the ventricles.

Minimal hemorrhages into the skin, mucous membranes, or serosal surfaces are called *petechiae*; slightly larger hemorrhages are termed *purpura*. A large (>1 to 2 cm) subcutaneous hematoma, or bruise, is called an *ecchymosis*.

The significance of hemorrhage depends on the volume of blood loss, the rate of loss, and the site of the hemorrhage. Sudden losses of up to 20% of the blood volume or slow losses of even larger amounts may have little clinical significance. The site of the hemorrhage is critical. For example, an amount of bleeding that would have little clinical significance in the subcutaneous tissues may cause death when located in a vital portion of the brain. Large amounts of external bleeding lead to the chronic loss of iron from the body and anemia. In contrast, internal hemorrhages into body cavities, joints, or tissues permit the iron to be recaptured for the synthesis of hemoglobin and the development of normal red blood cells.

Summary of Terms for Blood Vessels

Term	Definition
Ischemia	Interference of blood supply to an organ; deprives cells and tissues of oxygen and nutrients
Infarct	Localized area of ischemic necrosis; produced by occlusion of either arterial supply or venous drainage
Hemorrhage	Implies rupture of a blood vessel
Hematoma	Accumulation of blood trapped within body tissues

Alterations of Cell Growth

Changes in the number and size of cells, their differentiation, and their arrangement may develop in response to physiologic stimuli. **Atrophy** refers to a reduction in the size or number of cells in an organ or tissue, with a corresponding decrease in function. It must be distinguished from hypoplasia and aplasia, in which failure of normal development accounts for small size.

An example is the disuse atrophy that occurs with immobilization of a limb by a plaster cast. The muscle mass of the encased limb reduces dramatically. Because the cast also removes the stress and strain from the enclosed bone

Summary of Terms for Alterations of Cell Growth

Term	Definition
Atrophy	Reduction in the size or number of cells in an organ or tissue, with a corresponding decrease in function
Hypertrophy	Increase in the size of the cells of a tissue or organ in response to a demand for increased function
Hyperplasia	Increase in the number of cells in a tissue or organ
Dysplasia	Loss of uniformity of individual cells and their architectural orientation
Neoplasia	Ungoverned abnormal proliferation of cells
Oncology	Study of neoplasms (tumors)
Benign	Growth that closely resembles the cells of origin in structure and function
Malignant	Neoplastic growth that invades and destroys adjacent structures
Metastasize	Malignant neoplasms that travel to distant sites
Carcinoma	Malignant neoplasm of epithelial cell origin
Anaplastic	Undifferentiated cell growth—without form (bizarre)
Sarcoma	Highly malignant tumor originating from connective tissue
Lymphatic spread	Major route by which carcinoma metastasizes
Hematogenous spread	Malignant tumors that have invaded the circulatory system and travel as neoplastic emboli
Grading	Assessment of aggressiveness or degree of malignancy
Staging	(1) Extensiveness of tumor at the primary site (2) Presence or absence of metastases to lymph nodes and distant organs
Epidemiology	Study of determinants of disease events in given populations
Morbidity	Rate that an illness or abnormality occurs
Mortality	Reflects the number of deaths by disease per population

that normally stimulates new bone formation, normal bone resorption continues unchecked and the loss of calcified bone can be detected on radiographs. In this situation, there is rapid recovery from the atrophic appearance when the cast is removed and normal function is resumed.

Pathologic, irreversible atrophy may be caused by loss of innervation, by hormonal stimulation, or by decreased blood supply. For example, stenosis of a renal artery may cause atrophy of the kidney with shrinkage of individual nephrons and loss of interstitial tissue.

Hypertrophy refers to an increase in the size of the cells of a tissue or organ in response to a demand for increased function. This must be distinguished from **hyperplasia**, an increase in the number of cells in a tissue or organ (Figure 1-3). Hypertrophy occurs most often in cells that cannot multiply, especially those in myocardial and peripheral striated muscle. Myocardial hypertrophy is necessary to maintain cardiac output despite increased peripheral resistance in patients with arterial hypertension or aortic valve disease. After the loss of a normal kidney, hypertrophy of the other kidney occurs in an attempt to continue adequate renal function.

Examples of hyperplasia include: (1) proliferation of granulation tissue in the repair of injury and (2) the increased cellularity of bone marrow in patients with hemolytic anemia or after hemorrhage. Hyperplasia of the adrenal cortex is a response to increased adrenocorticotropic hormone (ACTH) secretion; hyperplasia of the thyroid gland occurs with increased thyrotropic hormone secretion by the pituitary gland.

Dysplasia is a loss in the uniformity of individual cells and their architectural orientation; it is typically associated with prolonged chronic irritation or inflammation. Removal of the irritant may result in a return to normal, but often the tissue change persists, and it may evolve into a totally abnormal growth pattern. Thus, dysplasia is generally considered at least potentially premalignant—a borderline lesion that may heal or progress to cancer.

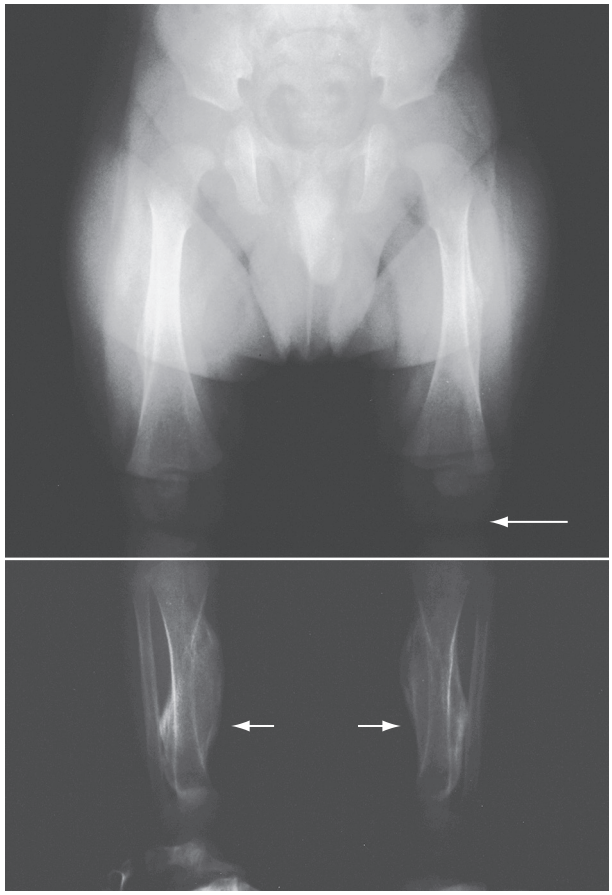

FIGURE 1-3 Infantile cortical hyperostosis (Caffey's disease). Affected bones demonstrate cortical thickening with new periosteal bone formation bilaterally on the femurs **(A)** and tibias **(B)** (*arrows*).

Neoplasia

Neoplasia, from the Latin word for "new growth," refers to an abnormal proliferation of cells that are no longer controlled by the factors that govern the growth of normal cells. Neoplastic cells act as parasites, competing with normal cells and tissues for their metabolic needs. Thus, tumor cells may flourish and the patient becomes weak and emaciated, a condition termed *cachexia*.

Neoplasms are commonly referred to as tumors; indeed, the study of neoplasms is called **oncology**, derived from the Greek word *oncos*, meaning "tumor." Although the word *tumor* originally referred to any swelling, which could also be produced by edema or hemorrhage in tissue, the word now refers almost exclusively to a neoplasm.

Neoplasms are divided into benign and malignant categories on the basis of their potential clinical behavior. **Benign** tumors closely resemble their cells of origin in structure and function. They remain localized, without spreading to other sites, and thus can usually be surgically removed with resultant survival of the patient.

Nevertheless, some benign tumors can have severe consequences because of their position or hormonal secretion. For example, a benign pituitary tumor can cause pressure atrophy and destruction of the surrounding gland, and a benign tumor of the islets of Langerhans in the pancreas can produce excessive amounts of insulin, resulting in possibly fatal low levels of blood glucose. Other potentially dangerous benign tumors include those arising in the brain or spinal cord, which may influence central nervous system function. Tumors of the trachea or esophagus may occlude the air supply or make it impossible to swallow.

Malignant neoplasms invade and destroy adjacent structures and spread to distant sites (**metastasize**), causing death. Malignancies tend to be poorly differentiated so that it may be impossible to determine the organ from which they originate. Malignant tumors are collectively referred to as **cancers**. This term is derived from the Latin word for "crab," possibly because the finger-like projections that extend into underlying tissue resemble crablike claws.

All tumors, both benign and malignant, have two basic components: (1) the parenchyma (organ tissue), made up of proliferating neoplastic cells, and (2) the supporting stroma (supporting tissue), made up of connective tissue,

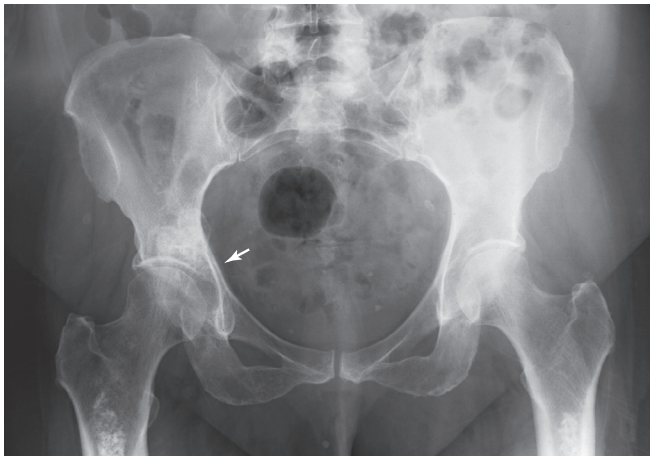

FIGURE 1-4 Enchondroma. A lobulated area with increased bone density in the supra-acetabular region on the right side (*arrow*).

blood vessels, and possibly lymphatic vessels. The parenchyma of the neoplasm largely determines its biologic behavior and is the component that determines how the tumor is named.

Most benign tumors consist of parenchymal cells that closely resemble the tissue of origin. Their names come from adding the suffix *-oma* to the cell type from which the tumor arose. For example, benign tumors of fibrous tissue are termed *fibromas*, whereas benign cartilaginous tumors are *chondromas* (Figure 1-4). The term *adenoma* is applied to benign epithelial neoplasms that grow in glandlike patterns. Benign tumors that form large cystic masses are called *cystadenomas*. *Lipomas* consist of soft fatty tissue, *myomas* are tumors of muscle, and *angiomas* are tumors composed of blood vessels. An epithelial tumor that grows as a projecting mass on the skin or from an inner mucous membrane (e.g., the gastrointestinal tract) is termed a *papilloma* or a *polyp*.

Malignant neoplasms of epithelial cell origin are called **carcinomas**, from the Greek word *karkinos*, meaning "crab." Carcinomas affect epithelial tissues, skin, and mucous membranes lining body cavities. *Adenocarcinoma* refers to malignancies of glandular tissues, such as the breast, liver, and pancreas, and of the cells lining the gastrointestinal tract. *Squamous cell carcinoma* denotes a cancer in which the tumor cells resemble stratified squamous epithelium, as in the lung and head and neck regions. At times, the tumor grows in such a bizarre pattern that it is termed **undifferentiated** or **anaplastic** (without form).

Sarcomas are highly malignant tumors arising from connective tissues, such as bone, muscle, and cartilage. Although they are less common than carcinomas, sarcomas tend to spread more rapidly.

Substantial evidence exists indicating that most tumors arise from a single cell (monoclonal origin). The rate of growth generally correlates inversely with the level of parenchymal differentiation. Thus, well-differentiated tumors tend to grow slowly, whereas bizarre, undifferentiated neoplasms have a rapid growth rate.

Although the cause of cancer is still unknown, many possible causative factors (*carcinogens*) have been implicated. Chemical carcinogens may cause structural alteration of the deoxyribonucleic acid (DNA) molecule (mutation), which may lead to the development of a neoplasm. Examples of chemical carcinogens include air and water pollution, cigarette smoke, asbestos, and a variety of other substances used in industry, food, cosmetics, and plastics. The development of specific types of cancer in certain families suggests a possible genetic predisposition. Excessive exposure to ultraviolet radiation (sunshine) may lead to the development of skin cancer. Survivors of the atom bomb who received huge doses of radiation have demonstrated a high incidence of leukemia. A greater-than-expected rate of leukemia was also seen in persons working with x-radiation before the need for proper protection was appreciated.

The study of experimental animal tumors has offered convincing evidence that DNA and ribonucleic acid (RNA) viruses can induce neoplastic transformation. Viruses that invade normal cells may alter their genetic material, leading to the abnormal cell divisions and rapid growth observed in malignant tumors.

The clinical symptoms of cancer vary with the site of malignancy. A blood-tinged stool, a change in bowel activity (e.g., intermittent constipation and diarrhea), or intestinal obstruction is suggestive of gastrointestinal malignancy. Difficulty in swallowing (dysphagia) or loss of appetite (anorexia), especially if accompanied by rapid weight loss, suggests a neoplasm in the esophagus or stomach. Hematuria may indicate kidney or bladder cancer, whereas difficulties in urination (e.g., urgency, a burning sensation, or an inability to start the stream of urine) in an elderly man may be a sign of prostate tumor. Hemoptysis (coughing up blood), a persistent cough, or hoarseness may suggest a neoplasm in the respiratory tract. Severe anemia may develop from internal bleeding or from malfunction of the bone marrow caused by growth of a malignant lesion in the skeleton.

It should be stressed that these clinical symptoms may also be caused by benign disease. Nevertheless, because they may signal an underlying malignancy, they should be carefully investigated to exclude the presence of cancer.

Pain is frequently not an early sign of cancer. Unfortunately, pain may be appreciated only when the malignancy has spread too extensively to be curable. Secondary infections are common and an increasing cause of death. Most cancer patients are immunologically compromised, either because of their original disease or as a result of irradiation or chemotherapy. In addition to having typical bacterial and viral infections, immunocompromised patients with malignancy are especially susceptible to unusual opportunistic infections, such as *Pneumocystis jirovecii* (formerly *Pneumocystis carinii*) pneumonia and cytomegalovirus.

Some cancers that are still at a curable stage can be detected by screening procedures. Routine mammography

may identify nonpalpable breast cancer; a Papanicolaou (Pap) smear may show otherwise unsuspected cancer of the cervix. Surgical removal of these small tumors without metastatic spread offers an excellent prognosis.

Malignant neoplasms disseminate to distant sites by one of three pathways: (1) seeding within body cavities, (2) lymphatic spread, and (3) hematogenous spread.

Seeding (diffuse spread) of cancers occurs when neoplasms invade a natural body cavity. For example, a tumor of the gastrointestinal tract may penetrate the wall of the gut (visceral peritoneum), permitting metastases to enter the peritoneal cavity and implant at distant sites. A similar sequence may occur with lung cancers in the pleural cavity. Neoplasms of the central nervous system (medulloblastoma and ependymoma) may spread from the cerebral ventricles by means of the cerebrospinal fluid to reimplant on the meningeal surfaces within the brain or in the spinal cord.

Lymphatic spread is the major metastatic route of carcinomas, especially those of the lung and breast. The pattern of lymph node involvement depends on the site of the primary neoplasm and the natural lymphatic pathways of drainage of that region. Carcinomas of the lung metastasize first to the regional bronchial lymph nodes and then to the tracheobronchial and hilar nodes. Carcinoma of the breast usually arises in the upper outer quadrant and first spreads to the axillary nodes. Medial breast lesions may drain through the chest wall to nodes along the internal mammary artery.

The **hematogenous spread** of cancer is a complex process involving several steps. Tumor cells invade and penetrate blood vessels, traveling as neoplastic emboli in the circulation. These emboli of tumor cells are trapped in small vascular channels of distant organs, where they invade the wall of the arresting vessel and infiltrate and multiply in the adjacent tissue. The localization of hematogenous metastases tends to be determined by the vascular connections and anatomic relationships between the primary neoplasm and the metastatic sites. For example, carcinomas arising in abdominal organs, such as the gastrointestinal tract, tend to metastasize to the liver because of the flow of portal vein blood to that organ. Cancers arising in midline organs close to the vertebral column (e.g., prostate and thyroid) tend to embolize through the paravertebral venous plexus to seed the vertebral column. Neoplasms in organs drained by the inferior and superior vena cava, such as the kidney, tend to metastasize to the lung. However, several well-defined patterns of metastatic spread cannot be easily explained by vascular–anatomic relationships. Some examples are the tendency for carcinoma of the lung to involve the adrenal glands, simultaneous metastatic deposits in the brain and adrenal glands, and pituitary metastases occurring from breast carcinomas.

The **grading** of a malignant tumor assesses aggressiveness, or degree of malignancy. The grade of a tumor usually indicates its biologic behavior and may allow prediction of its responsiveness to certain therapeutic agents. **Staging** refers to the extensiveness of a tumor at its primary site and the presence or absence of metastases to lymph nodes and distant organs, such as the liver, lungs, and skeleton. The staging of a tumor aids in determining the most appropriate therapy. Well-localized tumors without evidence of metastases may be surgically removed. Fast-growing, undifferentiated tumors, such as those found in patients with Hodgkin's disease, may respond best to radiation therapy. Cancer of the prostate responds to hormonal therapy, which consists of either the removal of the sources of male gonadal hormones that stimulate tumor growth or the administration of the female gonadal hormone (estrogen) that inhibits it. Chemotherapy uses one or a combination of cytotoxic substances that kill neoplastic cells, but these drugs may injure many normal cells and result in significant complications.

Upon determination of the type of neoplastic involvement, a study of determinants is compiled for the specific disease in a given population, which is called **epidemiology**. Using epidemiology and the grading of the neoplasms then becomes part of establishing morbidity. **Morbidity** is the rate that an illness or abnormality occurs. Depending on the stage of the tumor, **mortality** is calculated by reviewing the population involved to statistically calculate the expected death rate. These factors will be taken into consideration when the best course of treatment for the patient is being determined.

HEREDITARY DISEASES

Hereditary diseases pass from one generation to the next through the genetic information contained in the nucleus of each cell. They reflect an abnormality in the DNA, which provides the blueprint for protein synthesis in the cell. In many hereditary diseases, an error in a single protein molecule leads to enzyme defects; membrane receptor and transport system defects; alterations in the structure, function, or quantity of nonenzyme proteins; and unusual drug reactions.

The most common hereditary abnormality is an enzyme deficiency. This leads to a metabolic block that results either in a decreased amount of a substance needed for normal function or in an accumulation of a metabolic intermediate that may cause injury. An example of the first mechanism is albinism, the absence of pigmentation resulting from an enzymatic deficiency that prevents the synthesis of the pigment melanin. An example of the second mechanism is phenylketonuria, in which the absence of an enzyme leads to the accumulation of toxic levels of the amino acid phenylalanine.

A defect in the structure of the globin molecule leads to the development of the hemoglobinopathies, such as sickle cell disease and thalassemia. An example of a genetically determined adverse reaction to drugs is glucose 6-phosphate dehydrogenase deficiency, in which an insufficient amount of the enzyme results in a severe hemolytic anemia in patients receiving a common antimalarial drug.

Despite our extensive knowledge of the biochemical basis of many genetic disorders, there are a large number of conditions for which the underlying mechanism is still

unknown. This list includes neurofibromatosis, retinoblastoma, and familial colonic polyposis (see Chapter 5). Each human cell contains 46 chromosomes divided into 23 pairs. The chromosomes in turn contain thousands of genes, each of which is responsible for the synthesis of a single protein. Forty-four of the chromosomes are called **autosomes**; the other two are the X and Y chromosomes, which determine the sex of the person. A combination of XY chromosomes results in a male, whereas an XX configuration results in a female.

Each person inherits half of his or her chromosomes from each parent. If the genes inherited from each parent are the same for a particular trait, the person is *homozygous* for that trait. If the genes differ (e.g., one for brown eyes and one for blue eyes), the person is *heterozygous* for that trait. **Dominant** genes always produce an effect regardless of whether the person is homozygous or heterozygous; **recessive** genes manifest themselves only when the person is homozygous for the trait. In determining eye color, brown is dominant, whereas blue is recessive. It must be remembered that although a recessive trait must have been contributed by both parents, the possibility exists that neither parent demonstrates that trait. For example, two parents, each with one gene for brown eyes and one gene for blue eyes, would show the dominant brown coloration, although they could each contribute a blue-eye gene to their offspring, who would manifest the recessive blue-eye trait.

For some traits, the genes are codominant so that both are expressed. An example is the AB blood type, in which the gene for factor A is inherited from one parent and that for factor B is inherited from the other.

Mutations are alterations in the DNA structure that may become permanent hereditary changes if they affect the gonadal cells. Mutations may result from radiation, chemicals, or viruses. They may have minimal effect and be virtually undetectable or may be so serious that they are incompatible with life, causing the death of a fetus and spontaneous abortion.

Autosomal dominant disorders are transmitted from one generation to the next. These disorders affect females and males, and both can transmit the condition. When an affected person marries an unaffected person, half the children (on average) will have the disease. The clinical manifestations of autosomal dominant disorders can be modified by reduced penetrance and variable expressivity. *Reduced penetrance* means that not everyone who has the gene will demonstrate the trait; *variable expressivity* refers to the fact that a dominant gene may manifest somewhat differently in different individuals (Figure 1-5) (e.g., polydactyly may be expressed in the toes or in the fingers as one or more extra digits). Examples of autosomal dominant disorders include achondroplasia (see Chapter 4), neurofibromatosis, Marfan's syndrome (see Chapter 12), and familial hypercholesterolemia.

Autosomal recessive disorders result only when a person is homozygous for the defective gene. The trait does not usually affect the parents, although siblings may show the disease. On average, siblings have a one-in-four chance of being affected; two out of four will be carriers of the gene, and one will be normal. Recessive genes appear more frequently in a family, and close intermarriage (as between first cousins) increases the risk of the particular disease. Unlike in autosomal dominant diseases, the expression of the defect tends to be uniform in autosomal recessive diseases and the age of onset is frequently early in life. Examples of autosomal recessive disorders are phenylketonuria (see Chapter 12), cystic fibrosis (see Chapter 3), galactosemia, glycogen and lipid storage diseases (see Chapter 12), Tay–Sachs disease, and sickle cell anemia (see Chapter 9).

FIGURE 1-5 **Polydactyly.** Right foot image with seven metatarsals and eight digits.

Sex-linked disorders generally result from defective genes on the X chromosome because the Y chromosome is small and carries very few genes. Most of these conditions are transmitted by heterozygous female carriers virtually only to sons, who have only the single, affected X chromosome. Sons of a heterozygous woman have a one-in-two chance of receiving the mutant gene. An affected man does not transmit the disorder to his sons, but all his daughters carry the genetic trait. In rare cases, a female may have the sex-linked disease if she is homozygous for the recessive gene. Virtually all sex-linked disorders are recessive. The most common example of a sex-linked disorder is color blindness. Other conditions are glucose 6-phosphate dehydrogenase deficiency and some types of hemophilia (see Chapter 9) and muscular dystrophy (see Chapter 12).

Summary of Terms for Hereditary Diseases

Term	Definition
Hereditary process	Genetic information contained in the nucleus of each cell passed to the next generation
Autosomes	44 chromosomes other than X and Y
Dominant gene	Always produces an effect
Recessive gene	Manifests when a person is homozygous for the trait
Mutation	Alteration in the DNA structures that may become permanent hereditary change

DISORDERS OF IMMUNITY

The immune reaction of the body provides a powerful defense against invading organisms by allowing it to recognize foreign substances (**antigens**), such as bacteria, viruses, fungi, and toxins, and to produce **antibodies** to counteract them. The antibody binds together with the antigen to make the antigen harmless. Once antibodies have been produced, a person becomes **immune** to the antigen.

Antibodies, or immunoglobulins, form in lymphoid tissue, primarily in the lymph nodes, thymus gland, and spleen. Although an infant has some immunity at birth, most immunity is acquired either naturally by exposure to a disease or artificially by immunization. There are two types of artificial immunity: active and passive. In **active immunity**, a person forms antibodies to counteract an antigen in the form of a vaccine or a toxoid. A **vaccine** consists of a low dose of dead or deactivated bacteria or viruses. Although these organisms cannot cause disease, they are foreign proteins containing antigens that stimulate the body to produce antibodies against them. A **toxoid** is a chemically altered toxin, the poisonous material produced by a pathogenic organism. As with a vaccine, the toxin cannot cause disease but does trigger the development of antibodies. Examples of active immunity are the vaccines given to prevent smallpox, polio, measles, tetanus, and diphtheria. Active immunity persists for a long time, although a relatively long time is required to build up immunity, and a booster shot frequently gives a stronger effect.

Passive immunity refers to the administration of a dose of preformed antibodies from the immune serum of an animal, usually a horse. This type of immunity acts immediately but lasts for a relatively short time. It is used in situations in which a person is exposed to a serious disease (hepatitis, rabies, and tetanus) but has no immunity against it and thus requires an immediate supply of antibodies to prevent a possibly fatal infection.

Several fundamental mechanisms of immunologic responses to antigens exist. The first type is a rapidly occurring reaction in which antigens are attacked by antibodies previously bound to the surface of mast cells. The mast cells release histamine, which causes a local increase in vascular permeability and smooth muscle contraction. Disorders resulting from localized reactions of this type (which probably have a genetically determined predisposition) include hay fever, asthma, and gastrointestinal allergies. Generalized, or systemic, **anaphylactic** reactions are characterized by hypotension and vascular collapse (shock) with urticaria (hives), bronchiolar spasm, and laryngeal edema. This reaction causes sudden death in patients who are hypersensitive ("allergic") to the sting of bees, wasps, and other insects and to medications, such as penicillin and the iodinated contrast materials used in radiology.

In the second type of immune reaction, called a *cytotoxic reaction*, either the antigen is a component of a cell or it attaches to the wall of red blood cells, white blood cells, platelets, or vascular endothelial cells. The reaction with an antibody leads to cell destruction by lysis or phagocytosis. Examples of a cytotoxic immune reaction include the transfusion reaction occurring after the administration of ABO-incompatible blood, and erythroblastosis fetalis, the hemolytic anemia of the Rh-positive newborn whose Rh-negative mother has produced anti-Rh antibodies.

The third type of immune reaction, a *delayed reaction*, occurs in an individual previously sensitized to an antigen. As an example, the first time a person touches poison ivy, no reaction occurs. However, on the next exposure to poison ivy, antibodies are present to attack the antigen, and the patient develops the typical rash and irritation. A similar process produces a reaction to tuberculosis, leprosy, many fungal diseases, and other infections. This process also represents the principal component of rejection in organ transplants.

INFECTIOUS DISEASE EXPOSURE

Working in the healthcare environment means that exposure to infectious microorganisms will occur. To minimize exposure, all healthcare workers should follow the Centers for Disease Control and Prevention's (CDC) **Standard Precautions**. Exposure to blood-borne pathogens such as human immunodeficiency virus (HIV) and hepatitis B virus (HBV) can be minimized for all persons involved with the use of the appropriate **personal protective equipment** (PPE). The CDC recommends that all such persons be considered potentially infected and that Standard Precautions be applied when they are delivering health services to every patient. In cases of highly transmissible pathogens, additional precautions are necessary; **Transmission-Based Precautions** should be used for persons with pathogens transmissible by contact, droplet, or through air (airborne). Each healthcare facility is responsible for administering the precautions; educating, training, and monitoring its employees; and providing a protective environment. Every healthcare worker must take personal responsibility to help contain the infectious process in the work environment by following CDC standards.

Summary of Terms for Immunity Disorders

Term	Definition
Antigens	Foreign substance that evokes an immune response
Antibodies	Immunoglobulins responding to the antigens to make them harmless
Immune	Protected against antigens; antibodies binding with antigens to make them harmless
Active immunity	Forming antibodies to counteract an antigen by way of vaccine or toxoid
Vaccine	Contact with dead or deactivated microorganisms to form antibodies
Toxoid	Treated toxin with antigenic power to produce immunity by creating antibodies
Anaphylactic reaction	Hypersensitive reaction resulting in a histamine release
Standard Precautions	Protection used when delivering healthcare services to any person
Personal protective equipment	PPE—gowns, gloves, masks, shoe covers, and eye protection used to prevent transmission of potential infectious agents
Transmission-Based Precautions	Additional protective equipment to prevent the spread of highly infectious pathogens through contact, droplet, or airborne transmission

ACQUIRED IMMUNODEFICIENCY SYNDROME

Acquired immunodeficiency syndrome (AIDS), which most commonly affects young homosexual men and intravenous drug abusers, is characterized by a profound and sustained impairment of cellular immunity that results in recurrent or sequential opportunistic infections and a particularly aggressive form of Kaposi's sarcoma. AIDS has also been reported in a substantial number of hemophiliac patients, in recipients of transfusions, and increasingly in heterosexual partners of affected individuals. AIDS is attributable to infection with retroviruses (RNA viruses) known as human immunodeficiency viruses (HIV). This immune deficiency predominantly involves the lungs, gastrointestinal tract, and central nervous system. Pulmonary infections are extremely common in patients with AIDS and are frequently caused by organisms that only rarely produce disease in individuals with normal immune systems. Approximately 60% of AIDS victims experience one or more attacks of *P. jirovecii* pneumonia, which is characterized by a sudden onset, a rapid progression to diffuse lung involvement, and a considerable delay in resolution. The fungus cannot be cultured, and the disease is usually fatal if untreated. An open-lung biopsy is often necessary to make the diagnosis if a sputum examination reveals no organisms in a patient in whom this disease is suspected.

FIGURE 1-6 Kaposi's sarcoma. Small bowel study shows multiple intramural nodules (predominantly involving the jejunum) that distort the mucosal pattern and produce contour defects and intraluminal lucencies.

Gastrointestinal manifestations of AIDS include a variety of sexually transmitted diseases involving the rectum and colon, infectious processes (e.g., shigellosis, amebiasis, candidiasis, and giardiasis), and alimentary tract dissemination (spread) of Kaposi's sarcoma. Kaposi's sarcoma, a systemic disease, characteristically affects the skin and causes an ulcerated hemorrhagic dermatitis. Metastases to the small bowel, which are relatively common, consist of multiple reddish or bluish red nodules that intrude into the lumen of the bowel (Figure 1-6). Similar lesions can develop throughout the gastrointestinal tract. Central ulceration of the metastases causes gastrointestinal bleeding and a characteristic radiographic appearance of multiple "bull's-eye" lesions simulating metastatic melanoma.

Approximately 40% of all AIDS victims have neurologic symptoms, most commonly progressive dementia. Patients with mass lesions of the brain commonly have focal neurologic symptoms and signs.

Imaging appearance. The typical early radiographic finding of *P. jirovecii* pneumonia is a hazy, perihilar, granular infiltrate that spreads to the periphery and appears predominantly interstitial. In later stages, the pattern progresses to patchy areas of air-space consolidation with air bronchograms, indicating the alveolar nature of the process (Figure 1-7). The radiographic appearance may closely resemble that of pulmonary edema or bacterial pneumonia.

Magnetic resonance imaging (MRI) best demonstrates the multiple manifestations of AIDS in the central nervous system, where areas of increased signal intensity can be seen on T2-weighted images. Atypical brain abscesses and meningeal infection often occur, most commonly related to toxoplasmosis, cryptococcosis, cytomegalovirus, and herpesvirus

FIGURE 1-7 *Pneumocystis jirovecii* pneumonia. Diffuse bilateral air-space consolidation is suggestive of severe bacterial pneumonia or pulmonary edema.

(Figure 1-8). Increasing evidence indicates that cerebral infections may manifest from the HIV itself. Patients with AIDS also have a high incidence of lymphoma involving the central nervous system.

Treatment. Although much research has been initiated, no cure for AIDS has been found. Currently, treatment assists in maintaining quality of life and managing symptoms as they manifest. Antiviral drugs help suppress the HIV infection. A healthy lifestyle free of stress, alcohol, and illegal drugs is recommended. An HIV carrier should avoid infections if possible because they may accelerate the HIV process.

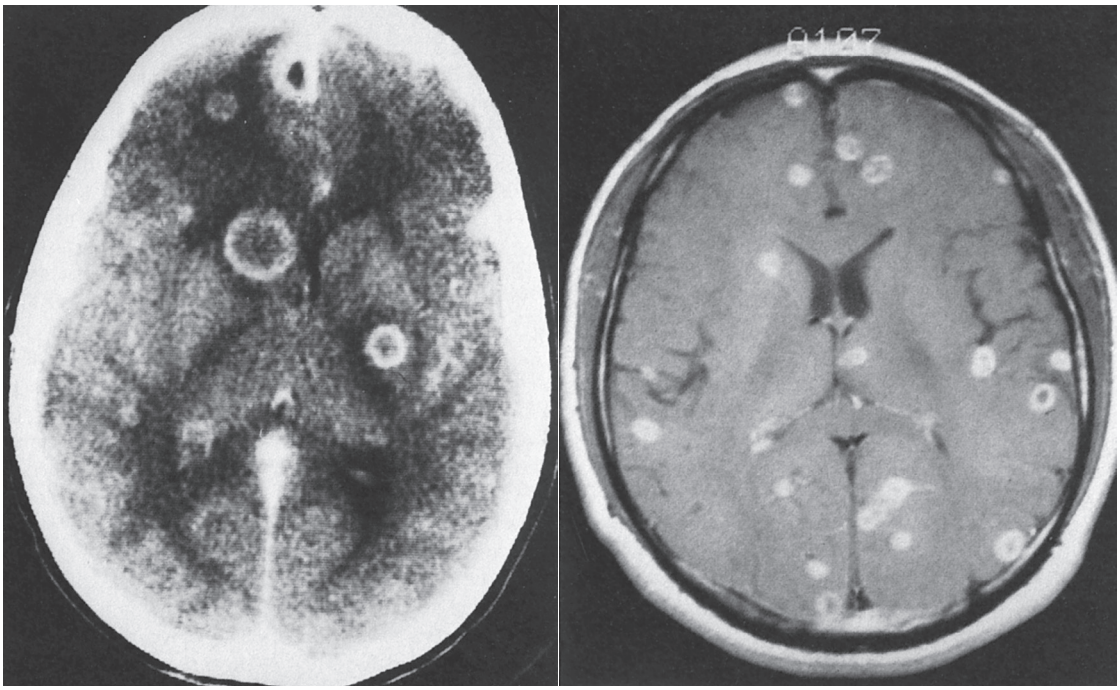

FIGURE 1-8 Neurologic manifestations of AIDS. **(A)** Computed tomography (CT) scan shows multiple ring-enhancing lesions caused by cryptococcal brain abscesses. **(B)** MRI, after intravenous administration of contrast medium, demonstrates multiple enhancing abscesses caused by toxoplasmosis.

REVIEW QUESTIONS

1. The accumulation of abnormal amounts of fluid in the spaces between cells or in body cavities is termed _____.
2. _____ is the process by which white blood cells surround and digest infectious organisms.
3. A tumor-like scar is referred to as a(n) _____.
4. Inflammation with pus formation is termed _____.
5. An interruption in the blood supply to an organ or body part is referred to as _____.
6. A localized area of ischemic necrosis in an organ or tissue is termed a(n) _____.
7. A swelling caused by bleeding into an enclosed area is termed _____.
8. A decrease in function of an organ or tissue because of a reduction in the size or number of cells is termed _____.
9. The term _____ means new growth.
10. The term for benign epithelial neoplasms that have a glandlike pattern is _____.
11. The study of determinants of disease events in given populations is _____.
12. Statistically, _____ reflects the number of deaths by disease per population.
13. The rate that an illness or abnormality occurs is called _____.
14. Gowns, gloves, masks, shoe covers, and eye protection used to prevent transmission of potential infectious agents are _____.
15. _____ determines the additional protective equipment needed to prevent the spread of highly infectious pathogens through contact, droplet, or airborne transmission.
16. The cause of the disease process is called _____.
17. A(n) _____ is the combination of signs and symptoms used to determine the disease process.
18. When a combination of signs, symptoms, and disease processes are linked, it is known as a(n)_____.
19. _____ is when a patient does not show any evidence of disease.
20. The expected outcome of a disease process is _____.

2

Specialized Imaging Techniques

OUTLINE

Diagnostic Imaging Modalities
- Imaging Features
- Mammography
- Ultrasound
- Computed Tomography
- Magnetic Resonance Imaging
- Nuclear Medicine
- Single-Photon Emission Computed Tomography
- Positron Emission Tomography
- Fusion Imaging

KEY TERMS

anechoic
annihilation
collimator
computed tomography (CT)
CT number
diffusion imaging
direct fusion
fat suppression
functional MRI (fMRI)
gamma camera
helical
hyperechoic
hypoechoic
imaging features
integrated imaging
isoechoic
magnetic resonance imaging (MRI)
mammography
nuclear medicine
perfusion imaging
positron emission tomography (PET)
radiofrequency (RF) pulse
radiopharmaceutical
single-photon emission computed tomography (SPECT)
T1-weighted images
T2-weighted images
ultrasound
virtual reality
volume-rendered imaging

OBJECTIVES

After reading this chapter, the reader will be able to:

- Define the imaging features most commonly used by radiologists to indicate pathophysiology changes
- Differentiate screening and diagnostic mammography imaging protocols and how the protocols are used to demonstrate pathology
- Describe the theory of image production with ultrasound and why this modality becomes the optimal choice to demonstrate pathologic conditions
- Describe the theory of image production with computed tomography (CT) and the body structures best demonstrated
- Briefly describe the theory of image production with magnetic resonance imaging (MRI) and the different sequences used to demonstrate specific tissue
- Describe the theory of image production with nuclear medicine, single-photon emission computed tomography (SPECT), and positron emission tomography (PET)
- Identify the fusion imaging techniques required to produce optimal quality images in patients with various underlying pathologic conditions
- Define and describe all boldface terms in this chapter

DIAGNOSTIC IMAGING MODALITIES

As the world of technology advances, medical imaging modalities have become more technical. This change requires the radiographer to have a broader and more specific skill set to produce quality images. An example of this trend in diagnostic imaging is the expansion of the department with the development of specific x-ray tubes to produce high-quality mammographic images of the breast.

The first of these new modalities was ultrasound, which was capable of producing images without the use of ionizing radiation, providing a diagnostic tool to view soft tissues, especially in the fetus. In the early to mid-1970s, computed axial tomography (now known as CT) provided revolutionary new images of the brain that demonstrated the bone structure, white and gray matter, and the fluid-filled ventricles. Eventually, CT eliminated the need for pneumoencephalography and replaced many cerebral angiograms. Scientists integrated

the use of strong magnets and radiofrequencies to provide another mode of producing images without the use of ionizing radiation—nuclear magnetic resonance (now known as magnetic resonance imaging). MRI offers clinicians images with high soft tissue resolution and the ability to visualize structural and functional tissue. CT and MRI now provide diagnosticians with three-dimensional (3D) (axial, sagittal, and coronal) images and offer a way to separate overlapping anatomic structures. With continuing research, nuclear medicine expanded its role by adding movement and a computer that allowed more than anterior and posterior projections, resulting in the development of single-photon emission computed tomography. Additional research developments in radiopharmaceuticals led to the creation of a positron-emitting radionuclide, which resulted in the newest modality—positron emission tomography. Now the concept of multiplanar imaging and gamma camera movement (tomography) has provided healthcare with two new perspectives in molecular imaging.

Computerized technology has become prevalent in imaging today. Imaging modalities with special software can now be integrated to create a fused image (superimposition of images from two different modalities). PET/CT is the most prominent hybrid equipment available today. As computed technology continues to become more complex, the modalities of today's imaging department will also become more complicated. However, these positive changes result in images that are more precise and have greater sensitivity. This offers the radiologist opportunity to make a quicker, more accurate diagnosis for the patient.

RADIOGRAPHER NOTES

A medical radiographer is one of the patient's healthcare team, providing care, diagnosis, and treatment, especially in the diagnostic imaging department. The role of the radiographer as a team member is to produce the best quality images for diagnosis. Not only radiologists and physicians view the images; technologists using other imaging modalities—such as mammography, ultrasound, CT, MRI, nuclear medicine, SPECT, and PET—view these images as a basis for producing studies in their respective modalities.

For the healthcare team, communication is especially important. To communicate effectively, the radiographer may need to gather information from the patient (patient history). Once the added information is recorded, the technologist may confer with the radiologist to ensure that the correct examination has been ordered. In some cases, even though the examination is correct, it also would be beneficial if further history were gathered or additional image projections were taken to provide supplementary information. The better radiographers understand their role in imaging, the more adept they will be at producing the correct images for the specific pathophysiologic condition of the patient.

To best demonstrate the pathology, all imaging technologists must do their part to provide added information. The imaging team is responsible for providing the best images to complement one another. The collection of images from all modalities aids the diagnostician in making the most accurate diagnosis.

Imaging Features

When radiologists interpret images, they use a common terminology called **imaging features**, imaging descriptors that the technologist should become familiar with to better understand the pathophysiologic changes reflected in the diagnostic image. Common features or descriptors include *location, size, density, structure, shape, demarcation, perfusion,* and *integration*. The *location* descriptor indicates the site where the changes in the anatomic features are evident, whereas the *size* descriptor refers to the measurements of those changes on the image. The tissue *density* and *structure* describe the abnormal appearance in comparison with what is expected as normal. *Shape* and *border (demarcation)* describe anatomic structure changes and involvement. *Perfusion* of abnormal tissue relates to its degree of vascularity, which may be of value in distinguishing between cystic and solid-tissue lesions. Depending on the type of pathologic process, the tissue changes may be described as being space-occupying or *integrated* in the anatomic structure. Imaging features and descriptors are essentially a common language used by radiologists in interpreting images and conveying this information to referring physicians reviewing them. Each specific diagnostic modality utilizes a series of imaging descriptors that may have to be modified for it.

Summary of Imaging Descriptors

Term	Definition
Where	Location, lateralization, relative position to organs and vessels
Size	Diameter or width and length (millimeters or centimeters)
Density	Relative to surrounding tissue (isodense, hyperdense, or hypodense; radiolucent or radiopaque)
Structure	Heterogeneous (septate) or homogeneous (fluids)
Shape	Tubular (vessels or muscles) Nodular (tumor or lymph nodes) Reticular (resembling a net) Striate or diffuse (streaked or widely spread)
Demarcation	Sharply marginated (more likely benign) Indistinctly marginated (infiltration into surrounding tissue—inflammation or malignancy)
Perfusion	Peripheral, homogeneous, or heterogeneous enhancement
Integration	Space-occupying effect

Mammography

Most modern imaging departments have a separate area where breast imaging procedures are performed. The most common imaging technique for diagnosing breast cancer is full-field digital mammography (FFDM). Some centers still use the conventional screen-film imaging, which employs a specially designed x-ray screen that permits the proper exposure of film by many

fewer x-rays than would otherwise be necessary. This procedure produces a conventional black-and-white image at a very low radiation dose. Full-field digital **mammography** relies on radiation captured by multiple cells that convert the radiation energy to electrical energy to produce a numerical value (i.e., a digitized image). The advantages of digital mammography are faster image acquisition with lower dose (shorter exposure), increased contrast resolution with the ability to manipulate images to visualize specific areas of interest, decreased need to repeat studies, and the ease of sharing images with other professionals. *Screening* mammography consists of two images of each breast, the craniocaudal and mediolateral oblique projections. For a woman with a palpable nodule, the first choice may be a *diagnostic* mammogram, which includes an additional 90-degree mediolateral projection. When screening mammography demonstrates a suspicious area or a definite abnormality, additional images, such as coned-down or magnification projections, can be completed to compliment the study. In some cases, ultrasound supplements mammography images by demonstrating the lesion to be fluid filled (cystic) or solid.

Summary of Imaging for Mammography—Anatomic Imaging	
Image creation	Ionizing radiation—x-ray attenuation of breast tissue
Image receptor	Digital plate or analog system
Imaging descriptors	Same as used for general x-ray

Ultrasound

Ultrasound (also called ultrasonography) is a widely accepted cross-sectional imaging technique because of its low cost, availability, and ability to differentiate cystic (gallbladder), solid (liver), and complex (liver tumor) tissue. A noninvasive imaging modality, ultrasound uses high-frequency sound waves produced by electrical stimulation of a specialized crystal (Figure 2-1). When the high-frequency sound waves pass through the body, their intensity is reduced by different amounts depending on the acoustic properties of the tissues through which they travel. The crystal mounted in a transducer sends the signal and also acts as a receiver to record echoes reflected back from the body whenever the sound wave strikes an interface between two tissues that have different acoustic properties. The transducer records the tiny changes of the signal's pitch and direction. A water-tissue interface can produce strong reflections (echoes), whereas a solid tissue mass that contains small differences in composition can cause weak reflections. The display of the ultrasound image on an imaging monitor shows both the intensity level of the echoes and the position in the body from which they were scanned. Ultrasound images may be displayed as static grayscale images or as multiple (video) images that permit movement to be viewed in real time. Color display on a sonogram is used to detect motion (specifically, blood flow). Depending on the equipment used, the interactions of the tissue with the sound wave determine how the tissue or organ is visualized and described.

In general, fluid-filled structures have intense echoes at their borders, no internal echoes, and good transmission of the sound waves. **Anechoic** tissue or structures (which are *echo free,* or lacking a signal) transmit sound waves easily and appear as the dark region on the image; examples are the gallbladder and a distended urinary bladder. Solid structures (e.g., liver and spleen) produce internal echoes of variable intensity. The terms **hyperechoic** and **hypoechoic** are used to make comparisons of echo intensities between adjacent structures. For example, the normal liver can be described as being hyperechoic to the normal renal cortex because the hepatic parenchymal tissue appears as a lighter shade of gray. Conversely, because the normal renal cortex appears as a darker shade of gray than the normal liver parenchyma, it can be described as being hypoechoic to the liver. The term **isoechoic** is used to describe two structures that have the same echogenicity even though the tissue may not be the same; for example, liver tissue is often isoechoic to the spleen. Complex tissue types have both anechoic and echogenic areas (Figure 2-2).

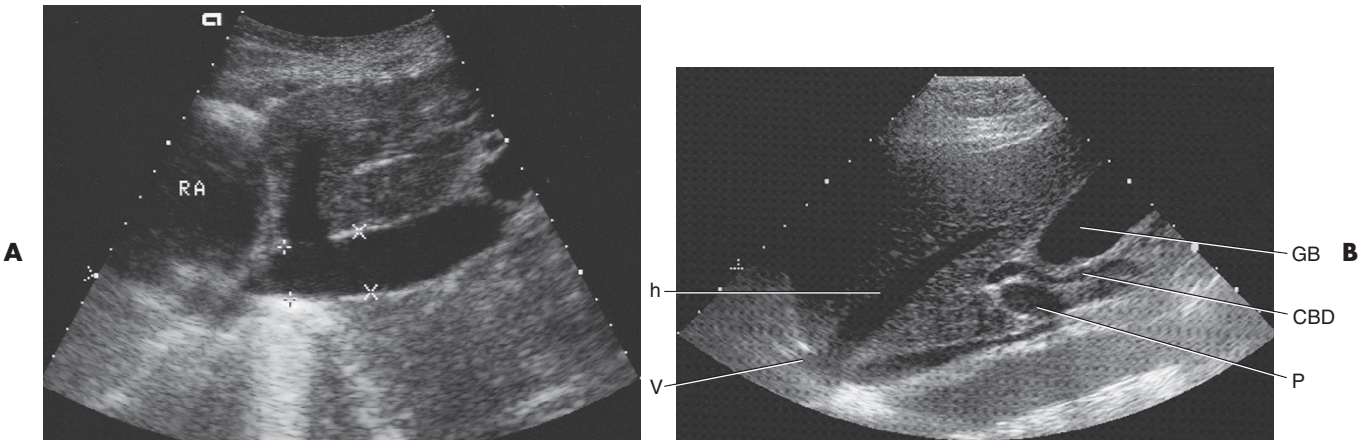

FIGURE 2-1 Ultrasound images of normal abdomens. **(A)** Right atrium of the heart (RA), the inferior vena cava (marked for measurement), and the hepatic vein joining the inferior vena cava. **(B)** Gallbladder (GB), common bile duct (CBD), portal vein (P), hepatic vein (h), and inferior vena cava (V).

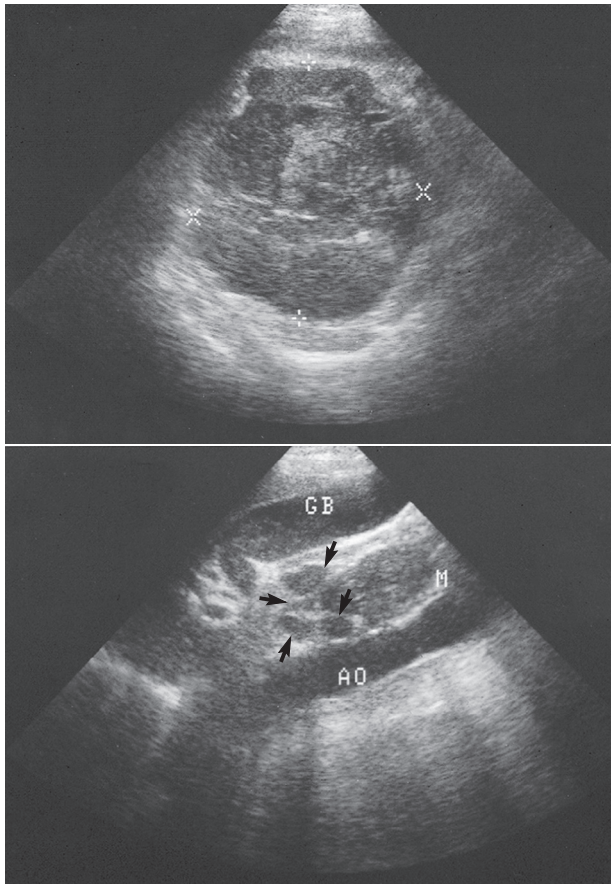

FIGURE 2-2 Ultrasound images of the abdomen. (A) Transverse right kidney demonstrates a hyperechoic area (*white*) within the mass caused by renal cell carcinoma. (B) Gallbladder (GB) and aorta (AO) are hypoechoic compared with the pancreas. Focal masses (*arrows*) are isoechoic (i.e., similar in density) to the adjacent pancreatic tissue.

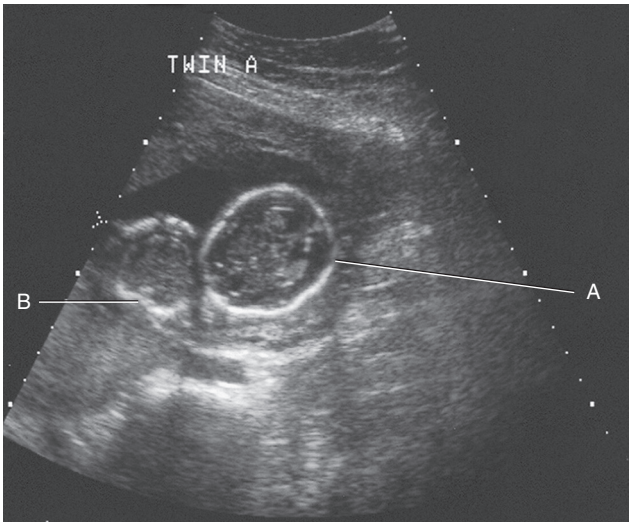

FIGURE 2-3 Sonogram of the abdomen of a woman with a multiple pregnancy. Cranial architecture is normal in fetus A and abnormal in fetus B, a finding that documented demise of fetus B (and also fetus C, which is not imaged).

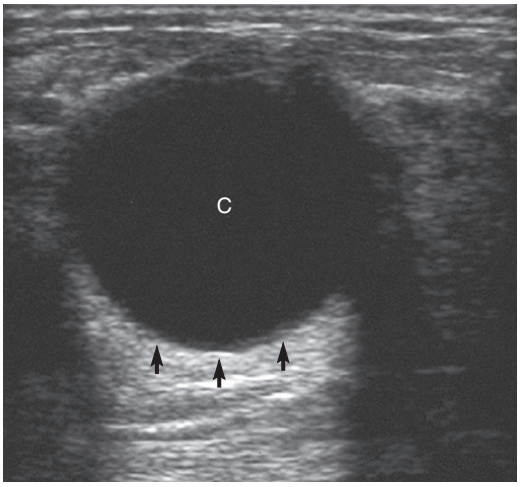

FIGURE 2-4 Ultrasound image of a focal area of breast tissue. The sonogram shows an anechoic mass (C) with a well-defined back wall and distal enhancement (*arrows*).

The major advantage of ultrasound is its safety. There has been no evidence of any adverse effect on human tissues at the intensity level currently used for diagnostic procedures. Therefore, ultrasound is the modality of choice for examinations of children and pregnant women in whom a potential danger exists from the radiation exposure involved with other imaging studies. Ultrasound is by far the best technique for evaluating fetal age and placenta placement, congenital anomalies, and complications of pregnancy (Figure 2-3). Abdominal ultrasound is used extensively to evaluate the intraperitoneal and retroperitoneal structures, to detect abdominal and pelvic abscesses, and to diagnose obstruction of the biliary and urinary tracts. Pelvic ultrasound images of the prostate gland aid in the detection and accurate staging of neoplasms. Pelvic imaging is performed via a transabdominal (through the abdominal wall), transvaginal (through the vagina), or transrectal (through the rectum) approach.

Vascular or color-flow Doppler studies assess the patency of major blood vessels, demonstrating obstructions (stenoses), blood clots, plaques, and emboli. The color-flow duplex system, in which conventional real-time imaging is integrated with Doppler imaging (to produce quantitative data) and with color, depicts motion and the direction and velocity of blood flow. The color and intensity represent the direction of flow and the velocity, respectively (e.g., in the carotid artery).

Other uses of ultrasound include breast imaging (to differentiate solid from cystic masses) (Figure 2-4), musculoskeletal imaging (to detect problems with tendons, muscles, and joints and also soft tissue fluid collections or masses) (Figure 2-5), and as an imaging guide for invasive procedures (biopsies, aspirations, and drain placement) (Figure 2-6).

Ultrasound is a quick, inexpensive procedure for evaluating postoperative complications, although it may be difficult to perform in some patients because of overlying dressings, retention sutures, drains, and open wounds,

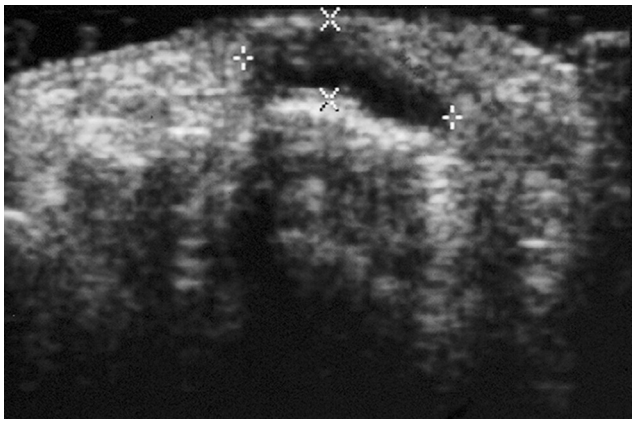

FIGURE 2-5 Ultrasound image of a wrist demonstrating the musculoskeletal architecture. A cystic structure (15 × 5 mm) can be seen near the dorsal aspect of base of the fourth and fifth metacarpals.

which may prevent the transducer from being in direct contact with the skin. In children with open fontanelles, ultrasound can image the intracranial structures. High-resolution, real-time ultrasound systems can assist surgeons during operative procedures. This technique has been applied to the neurosurgical localization of brain and spine neoplasms, to the evaluation of intraventricular shunt tube placement, to the localization of renal calculi, and to surgical procedures involving the hepatobiliary system and pancreas.

The role of ultrasound imaging has expanded as a result of the availability of multifrequency transducers (2–15 MHz) and advances in software (signal-processing) technology. The resultant higher-resolution images are used in musculoskeletal, breast, and small-parts imaging. The latest technologies include harmonic imaging (which involves a broad band of low frequencies and can suppress reflection from surrounding tissue) to reduce image noise and artifact, real-time compound imaging (a combination of multiple lines of sight that increases image clarity and provides more diagnostic information), and contrast agents (microbubble echo-enhancing agents) that increase vasculature definition. Harmonic imaging produces diminished noise images, increasing the resolution in a hypersthenic patient so that patient size does not prevent obtaining diagnostic images. Contrast agents, injectable low-solubility gas bubbles (<5 μm) such as perfluorochemicals (inert dense fluids), increase the differentiation of tissues and enhance visibility of detail in tumors, small and stenotic vessels, heart studies, and ultrasound hysterosonograms.

Ultrasound imaging requires an expanded knowledge of anatomy, physiology, and pathology to locate and demonstrate the specific region of interest. The quality of the scans is operator dependent, and extensive instruction and guidance are required to produce optimal images.

The major limitation of ultrasound is the presence of acoustic barriers, such as air, bone, and barium. For example, air reflects essentially the entire ultrasound beam so that structures

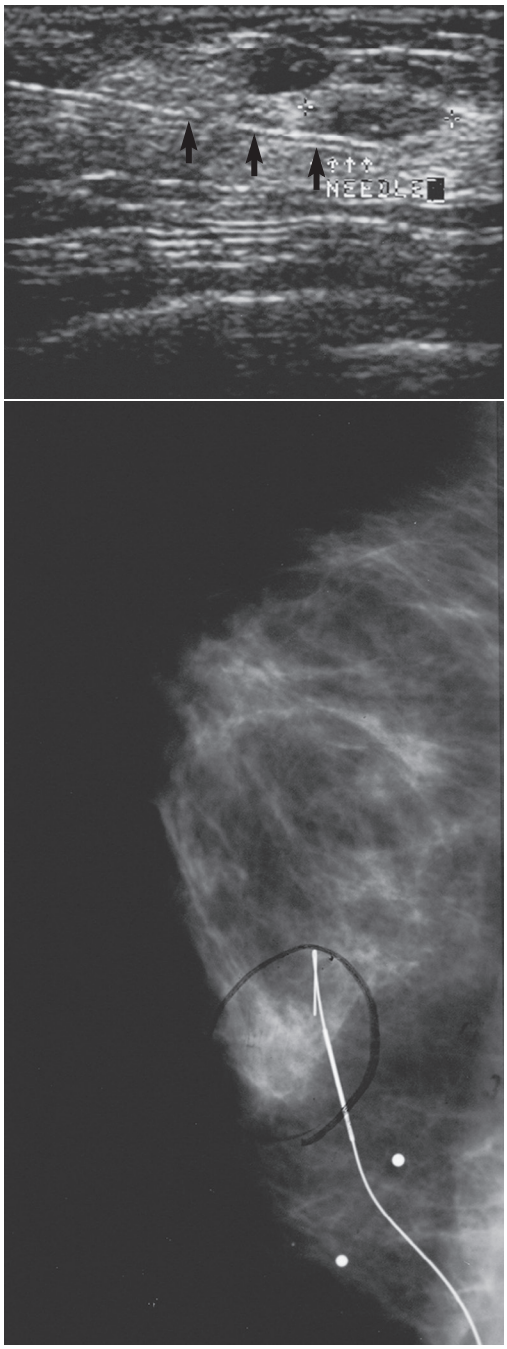

FIGURE 2-6 Ultrasound-guided localization. (A) Ultrasound needle localization for surgical biopsy of the breast. (B) Mammography image verifying needle localization.

beneath cannot be imaged well. This special problem interferes with imaging of the solid abdominal organs (e.g., the pancreas) in a patient with adynamic ileus, and it is the major factor precluding ultrasound examination of the thorax. For an ultrasound examination of the pelvis, the patient usually drinks a large amount of fluid to fill the bladder, thus displacing the air-filled bowel from the region of interest. More information on ultrasound imaging can be found on the following websites: http://www.aium.org, http://www.sdms.org, and http://www.ardms.org.

Summary of Imaging for Ultrasound—Anatomic Imaging	
Image creation	Transducer production of multifrequency sound waves
Image receptor	Transducer receiving echoed signal
Imaging descriptors	Anechoic (dark region)—echo-free tissue or structure
	Hyperechoic (lighter shade) and hypoechoic (darker shade)—comparison of echo intensities for adjacent tissue
	Isoechoic (same shade)—two structures that have the same echogenicity

Computed Tomography

Computed tomography (CT) produces cross-sectional tomographic images by first scanning a slice of tissue from multiple angles with a collimated x-ray beam, then calculating a relative linear attenuation coefficient (representing the amount of radiation absorbed in tissue for the various tissue elements in the section), and finally displaying the computed reconstruction as a grayscale image on a imaging monitor. Unlike other imaging modalities (except for the more recent MRI), CT permits the radiographic differentiation of a variety of soft tissues from each other (Figure 2-7). CT is extremely sensitive to slight (1%) differences in tissue densities; for comparison, detection by conventional screen-film radiography requires differences in tissue density of at least 5%. Thus, in the head, CT can differentiate between blood clots, white matter and gray matter, cerebrospinal fluid, cerebral edema, and neoplastic processes.

The **CT number** (Hounsfield number) reflects the attenuation of a specific tissue relative to that of water, which is arbitrarily assigned a CT number of 0 and appears gray on the image. The highest CT number (1000) represents bone, which appears white, and the lowest CT number (–1000) denotes air, which appears black. Fat has a CT number less than 0, whereas soft tissues have CT numbers greater than 0. The use of the computer allows the image to be manipulated by adjustment of the window width (grayscale—contrast scale) and window level (density or brightness). From the radiographer's perspective, the window width determines the number of densities that can be visualized on the monitor. The window level is the midpoint or center of the total number of densities being viewed in a selected window width. Predetermined window widths and window levels are used to demonstrate specific parts of the anatomy (lung, liver, and bone). Technical improvements in CT instrumentation and tube heat unit capacity have greatly reduced the time required to produce multiple slices (1 or 2 seconds), permitting the CT evaluation of virtually any portion of the body. In most instances, some type of preliminary image is obtained (either a radiograph or a CT-generated image—topogram or scout) for localization, the detection of potentially interfering high-density material (metallic clips, barium, and electrodes), and correlation with the CT images. An overlying grid with numeric markers permits close correlation between the subsequent CT scans and the initial scout image (Figure 2-8).

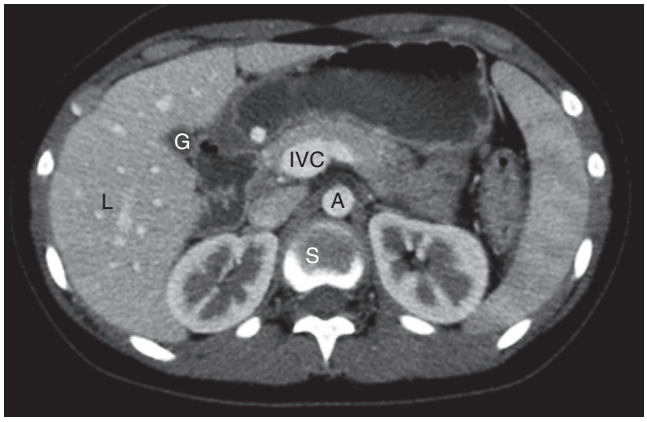

FIGURE 2-7 Normal contrast-enhanced CT scan of lower abdomen. A, aorta; L, liver; G, gallbladder; S, spine; IVC, inferior vena cava.

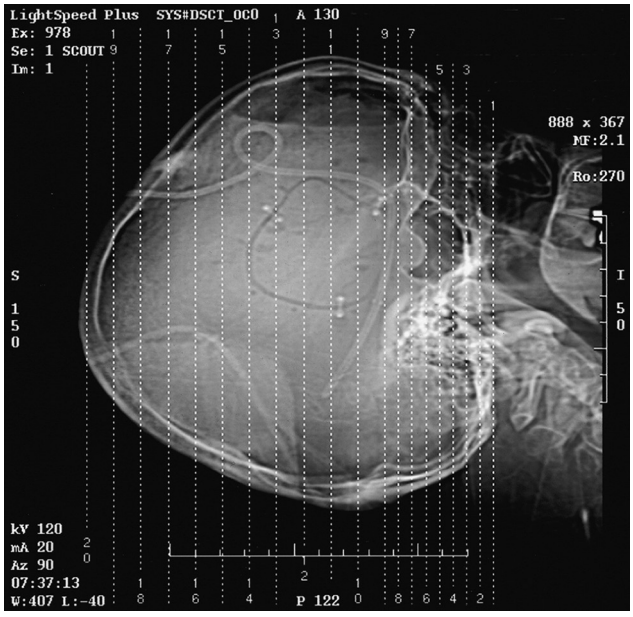

FIGURE 2-8 CT scout image. Overlying grid represents scan slices.

The intravenous injection of iodinated contrast material has become an integral part of many CT examinations. Scanning during or immediately after the administration of contrast material permits the differentiation of vascular from nonvascular solid structures. Differences in the degree and the time course of contrast enhancement may permit the detection of neoplastic or infectious processes within normal parenchymal structures. Because of its relatively low CT number, fat can serve as a natural contrast material and can outline parenchymal organs. In patients with malignant lesions, the loss of adjacent fat planes strongly suggests tumor extension. For abdominal studies, especially those of the pancreas and retroperitoneum, dilute oral contrast material (1% to 3% weight per volume barium sulfate or a water-soluble material) is frequently given to demonstrate the lumen of the gastrointestinal tract, and it permits the distinction between loops of bowel and solid abdominal structures.

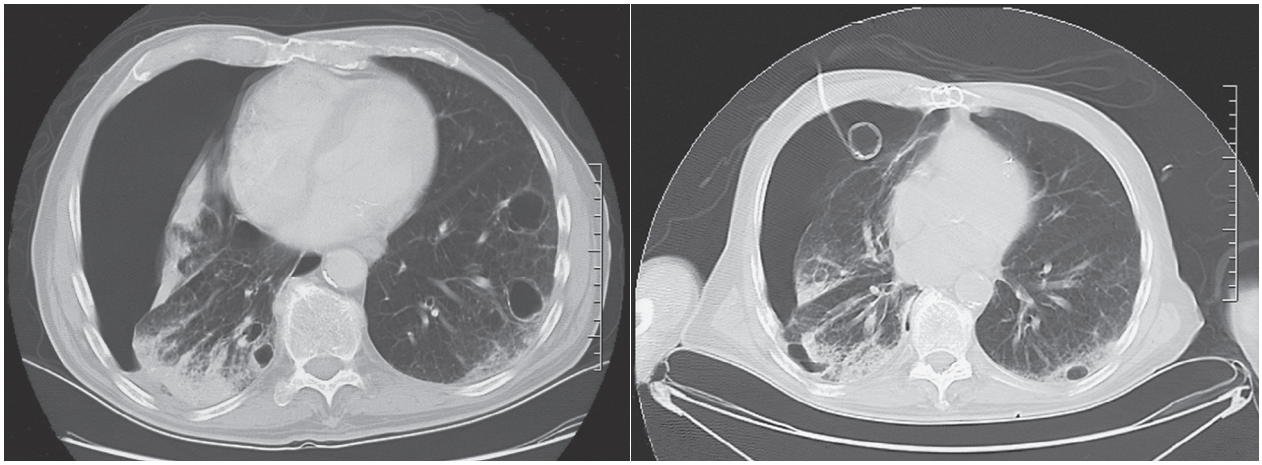

FIGURE 2-9 High-resolution CT scan of the lung. **(A)** A pneumothorax can be seen in the right side of the lung of an emphysematous patient, and blebs (high-density areas) can be seen in the left lung. **(B)** Visualization of catheter placement in the treatment for the pneumothorax.

Conventional CT produces images using a section thickness of 1 to 10 mm. In high-resolution CT, thin sections (1.5- to 2.0-mm slices) are used to produce a very detailed display of lung anatomy. High-resolution CT is far more sensitive and specific than plain chest radiographs (or conventional CT) for the diagnosis of parenchymal lung disease (Figure 2-9).

CT technology has moved to spiral (**helical**) scanning. In this technique, continual CT scanning is performed as the patient moves through the gantry (unlike the multiple single scans in conventional CT) (Figure 2-10). This approach permits much faster scanning without respiratory motion and provides volumetric data that can be easily reformatted in coronal and sagittal planes, and in the standard axial plane. Helical scanners with subsecond scanning abilities produce images of the chest (taking less than 20 seconds to complete the scan protocol) that demonstrate the pulmonary arteries without motion and can detect pulmonary emboli. CT imaging protocols for some procedures (e.g., obtaining images of the kidneys and liver) may require three-phase scanning (arterial, capillary, and venous phases and an excretory phase) to demonstrate all anatomic (tissue) structures (Figure 2-11). The single-scan protocol changed with subsecond scanning because the intravenous bolus injection appears very dense on the image and may obscure the pathologic features. Subsecond scanning requires delayed scanning and second and third phases to demonstrate a higher sensitivity than single-slice scanning. Subsecond scanning also produces abdominal studies with much less peristaltic motion, resulting in a higher-quality examination. Spiral CT allows reconstruction of images in three dimensions, because the data collected is a volume, and can demonstrate vascular lesions without the need for arteriography (Figure 2-12). With the thin slices of spiral scanning, the ability to reconstruct at thinner slice than in conventional CT scanning, and the addition of 3D software, the reconstruction can produce virtual colonoscopy and bronchoscopy images.

The sixth-generation scanners perform multiple slices consisting of multidetectors producing 8 to 64 slices per rotation, offering pitch variability (table movement) and variable rotation speed of the tube. It also contains software programming for instantaneous 3D images (Figure 2-13). Using a coned x-ray beam, the seventh-generation scanners can collect 16 to 320 sections of data in one rotation, and therefore they are known as multisection multidetector (MSMD) scanners or multiple array scanners. With the development of multidetector scanners, CT angiography (CTA) has become more precise and prevalent. The faster scanning times and thinner slices have made cardiac scanning possible well beyond what the electron-beam CT scanner could image. Clinicians and radiologists are quickly accepting the use of CT for vascular imaging; however, the complexity of the imaging protocol creates the need for extensive specialized education for the radiographer to produce the highest-quality images while keeping the patient dose to a minimum. An understanding of vascular anatomy, blood flow rates related to blood pressure, and ejection fraction rates and possible pathophysiologic conditions that can influence protocol is necessary.

Some postprocessing techniques used in CT include maximum intensity projections (MIPs), minimum intensity projections (MinIPs), shaded surface rendering, volume rendering, and virtual reality images. For CT angiography, MIPs are used to highlight the brightest pixels and thus enhance the image. The MinIPs, which enhance the lowest intensities (darker structures), are used for virtual colonoscopy. Shaded surface rendering reconstructions take the two-dimensional image and then add depth and shape to make a 3D image. With the use of **volume-rendered imaging** and 3D volume rendering, the vascular system can be viewed from all perspectives (360 degrees) as well as from the surface or internally. **Virtual reality** (VR) reconstructions are used in virtual colonoscopy to demonstrate the area inside of the bowel lumen.

As scanning technology becomes more complex, the technologist must utilize appropriate exposure settings to minimize patient radiation dose. The newest CT scanners provide dosage calculations that can be recorded as evidence of following ALARA (as low as reasonably achievable) practices.

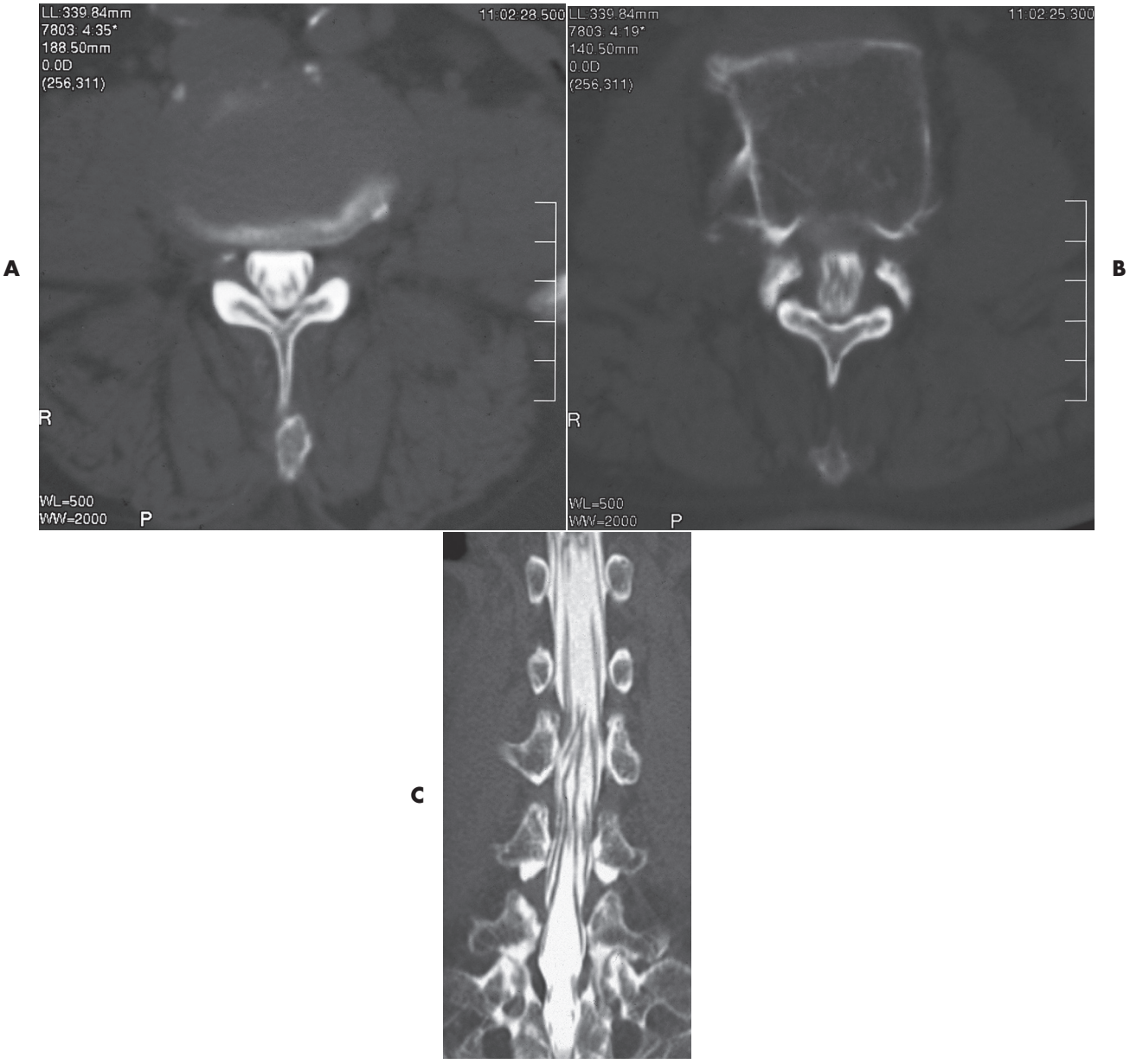

FIGURE 2-10 CT myelogram. Nonionic contrast agent (10 mL) was injected into the subarachnoid space. Following the myelogram, CT images using 3-mm slices were taken on a 16-slice scanner. On axial projections, image **A** demonstrates subarachnoid (SA) space enhancement with the vertebral disk anteriorly, and image **B** illustrates the SA shifted to the left. The coronal reconstruction **(C)** better demonstrates an impingement on the right at the level of L2–L3.

Summary of Imaging for Computed Tomography—Anatomic Imaging

Image creation	Collimated x-ray beam attenuation detection
Image receptor	Detectors receiving the attenuated signal
Imaging descriptors	CT number (Hounsfield number)—reflects the attenuation of a specific tissue relative to water, which equals "0"
	Highest CT number is 1000—represents bone (appears white)
	Lowest CT number is –1000—represents air (appears black)
	Window width—grayscale—contrast scale
	Window level—midpoint or center of total number of densities
Postprocessing	Maximum intensity projections (MIPs)—enhancing brightest intensities
	Minimum intensity projections (MinIPs)—enhancing lowest intensities (colonoscopy)
	Shaded surface rendering and volume rendering—3D rendering demonstrating the surface or selected structures
	Virtual reality (VR)—demonstrates internal structures for virtual bronchoscopy or colonoscopy

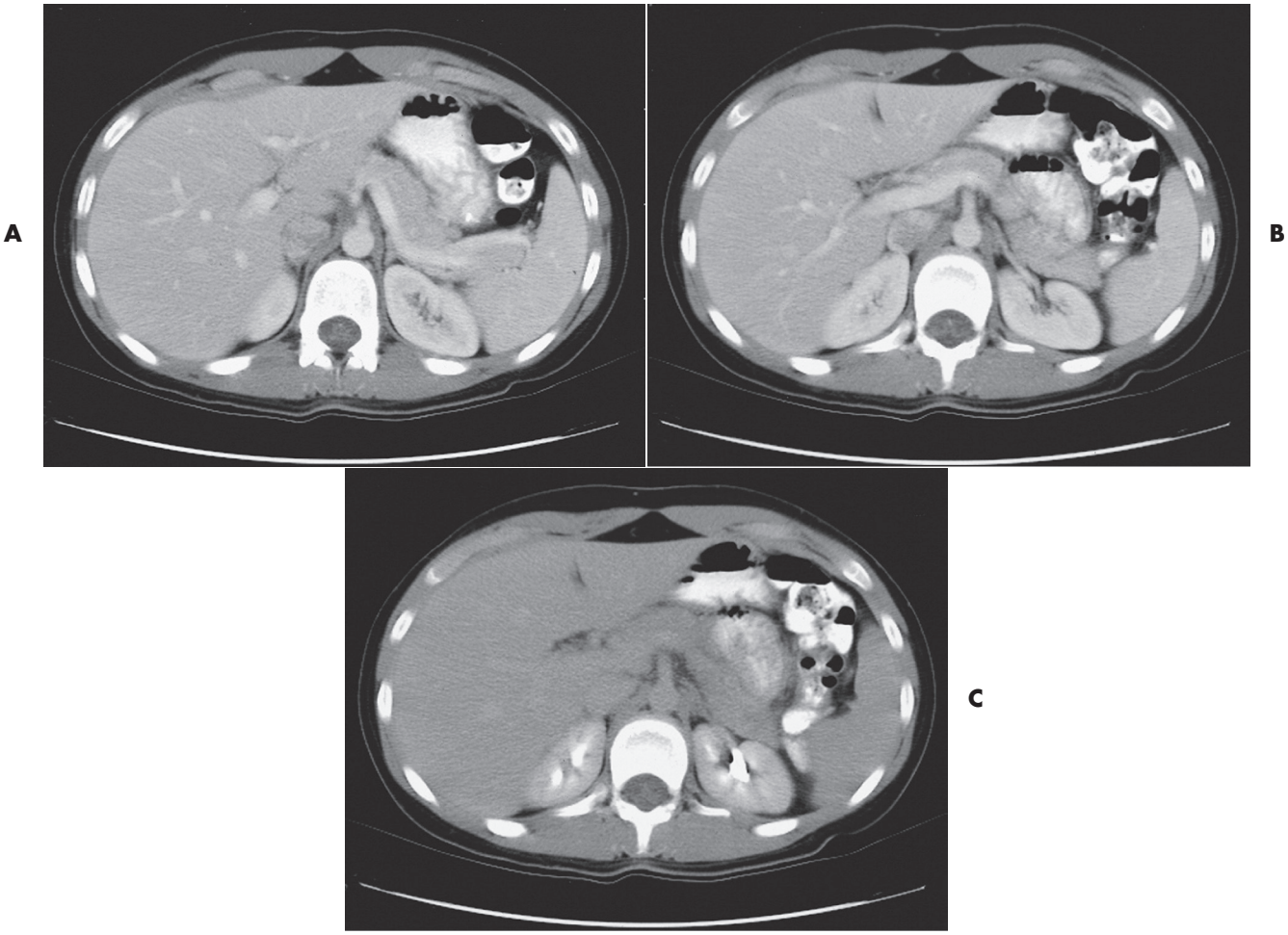

FIGURE 2-11 Three-phase CT scanning protocol for an abdomen. **(A)** Arterial phase demonstrating the abdominal aorta and kidney nephrogram. **(B)** Portal venous phase seen in the liver. **(C)** Excretory phase of the kidneys is visualized.

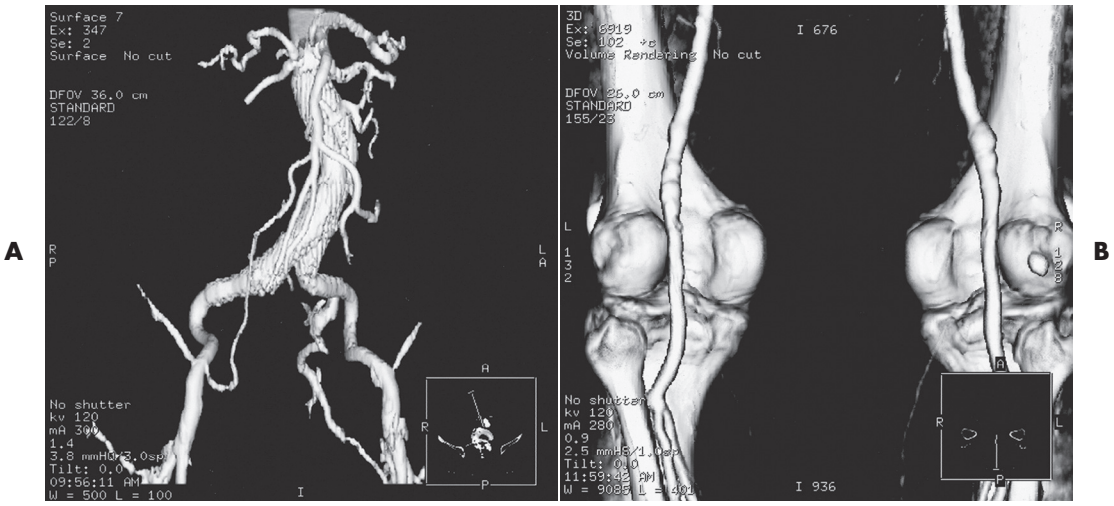

FIGURE 2-12 CT angiography. **(A)** Special software is used to demonstrate the abdominal aorta, the renal arteries, the superior mesenteric artery, and the iliac arteries. **(B)** Three-dimensional software in a femoral arterial runoff is used to demonstrate the popliteal arteries.

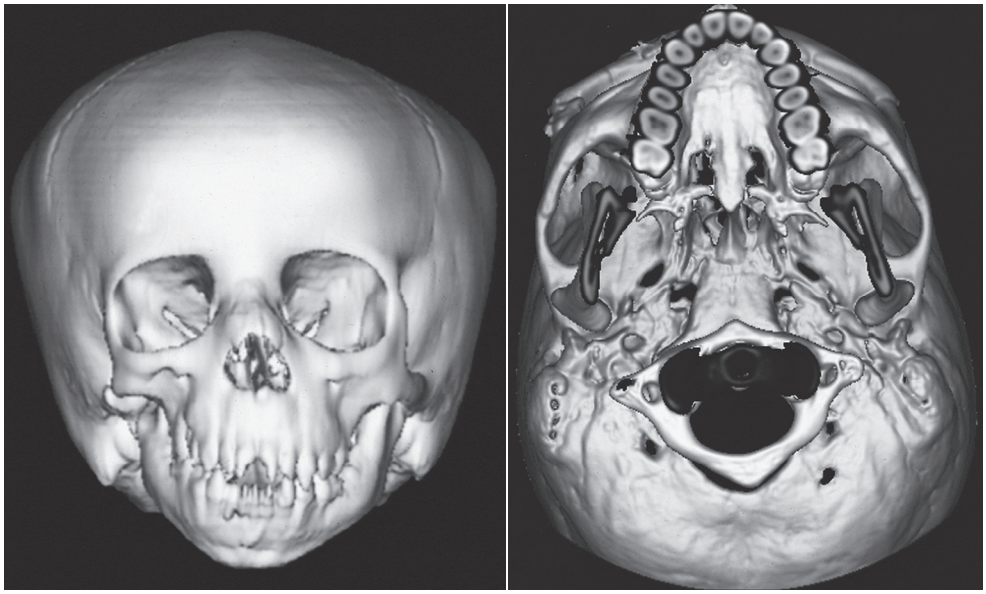

FIGURE 2-13 Three-dimensional surface-rendered CT images. **(A)** Skull of 3-year-old girl with closed sutures (craniosynostosis) and shape deformity. **(B)** Three-dimensional cutaway image illustrating the base of a normal skull. The mandible has been removed from the image.

Magnetic Resonance Imaging

Magnetic resonance imaging (MRI) has become an important clinical tool for a variety of conditions (Figure 2-14) and the modality of choice for imaging the central nervous system and spine. It is also the first choice for imaging most conditions of the musculoskeletal system, and it is a problem solver in the abdomen and pelvis.

Although the physics of MRI is beyond the scope of this book, the basic technique consists of inducing hydrogen atoms (protons) to alternate between a high-energy state and a low-energy state by absorbing and then releasing, or transferring, energy. This absorption of energy is accomplished by placing the anatomic part to be imaged in a strong static magnetic field and directing a **radio frequency (RF) pulse** of a specific frequency at the area. As protons absorb energy (called resonance), they move into a high-energy state. After a predetermined time, the RF pulse is turned off and the protons begin to release, or transfer, their absorbed energy as they move back to a low-energy state. This process is called *relaxation* and it occurs over time. Two types of relaxation, T1 and T2, occur simultaneously. A listening device called a receiver coil, placed near the anatomic site, is able to detect the time it takes for both T1 and T2 relaxation types. A complex computer program uses a mathematical operation called a Fourier transform to translate this information from the receiving coil into a computer-generated, grayscale image.

To generate an MR image, the MRI technologist selects a group of scanning parameters referred to as a *pulse sequence*. A pulse sequence contains a set of RF pulses and their timing, representing a specific echo time (TE) and a repetition time (TR). By varying the TE and TR, the MRI technologist is able to produce an image that is weighted or demonstrates T1 relaxation, T2 relaxation, or proton density. These images display the differences between normal and abnormal tissues. In general, 1.5-Tesla (1.5T) pulse sequences using a short TR (400 to 700 msec) and a short TE (10 to 30 msec) provide a T1-weighted image. A pulse sequence using a long TR (3500 to 4000 msec) and a long TE (80 to 100 msec) provides a T2-weighted image. A pulse sequence using a short TE (15 to 30 msec) and a long TR (3500 msec) provides a proton-density, or spin-density, image.

Although the degree of signal intensity of various substances on MR scans is complex and depends on multiple factors, some generalizations can be made. On **T1-weighted images**, substances causing high signal intensity (i.e., appears bright) include fat, subacute hemorrhage, melanin, slow-flowing blood, and intravenous gadolinium contrast material. Water, such as cerebrospinal fluid, has a low signal intensity and appears dark. Soft tissue has an intermediate level of signal intensity (Figure 2-15A).

On **T2-weighted images**, the opposite is true. Water has a high signal intensity so it appears bright, whereas muscle and other soft tissues (including fat) tend to have lower signal intensity and appear intermediate to dark. Cortical bone, calcium, air, and fast-flowing blood generate no signal, so they appear very dark on most imaging sequences (Figures 2-15B and 2-15C).

Although MRI is used in conjunction with other modalities, it has some unique advantages. MRI produces images in multiple planes without the use of ionizing radiation and receives no signal from bone so that the underlying tissue can be clearly imaged. The ability to image directly in any plane allows the best visualization of normal and abnormal anatomy. Unlike other imaging modalities that depend on information from one parameter (e.g., CT, which depends on electron density), MRI derives information from multiple biologic parameters, such as proton density (Figure 2-16A), T1 and T2 relaxation times, flow, diffusion, and perfusion. MRI provides excellent spatial contrast resolution of soft

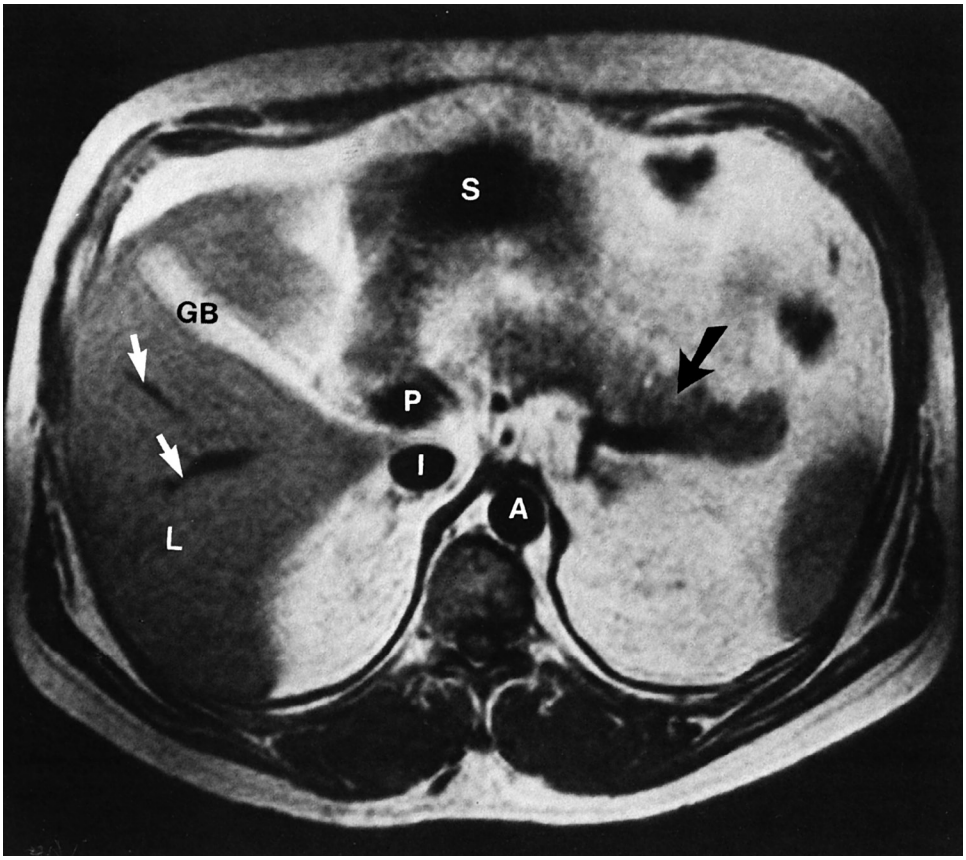

FIGURE 2-14 MRI of normal upper abdomen. Transverse image shows liver (L) and branches of portal veins (*white arrows*). Gallbladder (GB) has high intensity in this fasting person. Pancreas (*black arrow*) and stomach (S) are easily seen. Inferior vena cava (I), aorta (A), and main portal vein (P) are seen with signal void because they contain flowing blood.

tissue, and although it demonstrates improved sensitivity for detection of abnormal tissue, it can lack specificity. In the head, for example, infarction, edema, tumor, infection, and demyelinating disease all produce similar high signal intensity on T2-weighted images. The introduction of intravenous contrast materials, some organ specific, and different types of pulse sequences helps increase specificity.

One disadvantage of MRI is longer scanning times, which can result in image degradation from patient and physiologic motion. This problem is being addressed with new, faster breath-hold techniques. Patient claustrophobia is always a concern due to the small, enclosed space of the MRI scanner. It is also difficult to monitor patients in the MR environment, which requires specialized MRI-compatible equipment. In patients with certain implants, such as brain aneurysm clips, vascular stents, cardiac pacemakers, or other electromechanical devices, MRI may be contraindicated due to the deleterious effects of the magnetic environment.

MR angiography (MRA) produces high-resolution images of the vascular system without the need for intravenous contrast material (Figure 2-17A) using time-of-flight and phase-contrast imaging. Although these techniques acquire images of both arterial and venous systems, they are somewhat slow and lack the ability to cover large areas. The use of a rapidly infused intravenous contrast agent (gadolinium) and very rapid scanning has resulted in larger areas of coverage and diagnostic images that rival those of invasive catheter angiography (Figures 2-17B and 2-17C). The development of newer inflow techniques may one day eliminate the need for contrast material. The use of CT and MR angiography has virtually eliminated conventional contrast angiography for the diagnosis of vascular disease.

The development of magnetic resonance spectroscopy (MRS) has made it possible to analyze the chemical composition of tissues *in vivo*. This sophisticated process produces chemical spectra instead of anatomical images. MRS is helping distinguish benign and malignant lesions in patients in whom breast or prostate carcinoma is suspected. In the brain, MRS is used to discriminate between tumor recurrence and necrotic tissue following radiation therapy, as well to increase specificity in other diseases. Research is also being conducted into other uses of MRS, such as the tracking of adenosine diphosphate/triphosphate (ADP/ATP) in energy metabolism of muscles.

Diffusion imaging relies on fast scanning techniques and rapid gradient switching to image the random movement of water (Brownian motion) molecules within the brain or other organ. Using very strong gradients applied in all directions, disruption of this normal random motion by a disease process can be imaged, resulting in a signal change from normal tissue. Diffusion imaging can pinpoint altered diffusion

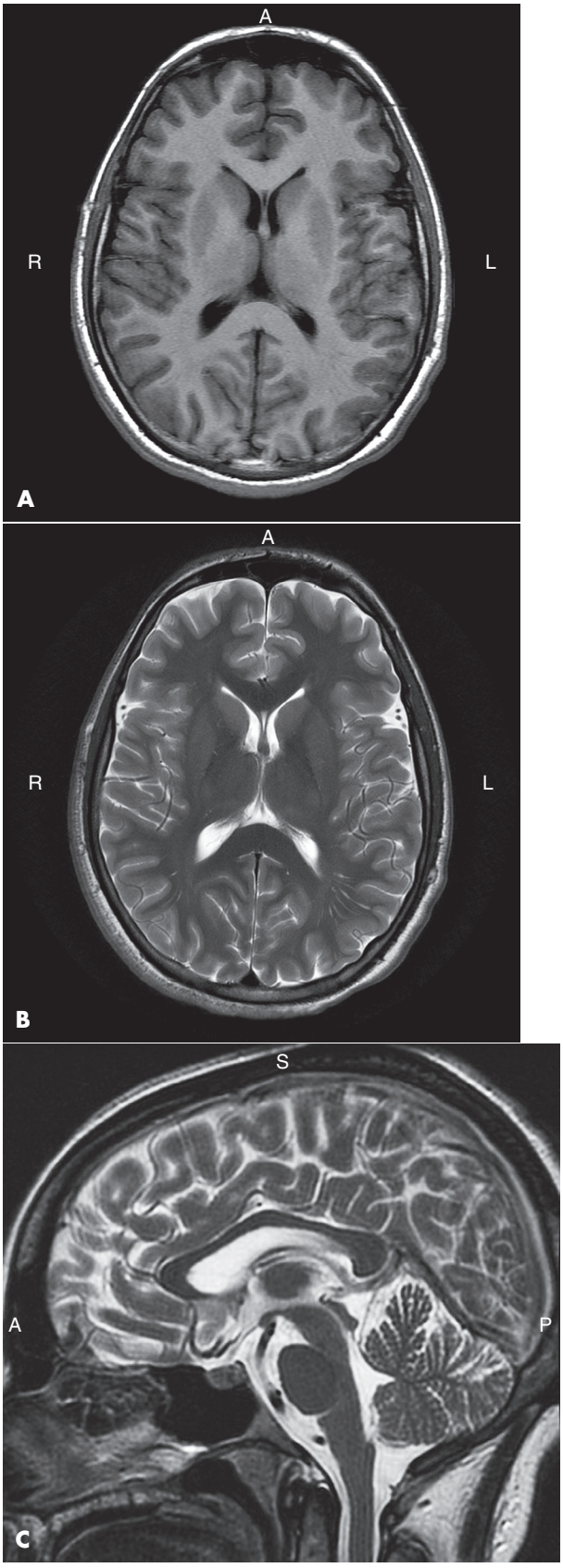

FIGURE 2-15 MRI of normal brain. **(A)** T1-weighted image. The ventricles and cerebrospinal fluid areas appear dark, and the white matter and gray matter are shades of gray. **(B)** T2-weighted image. The cerebrospinal fluid produces a high signal intensity (*white area*) on the image. **(C)** Sagittal T2-weighted image demonstrates cerebral cortex, ventricles, pons, and cerebellum.

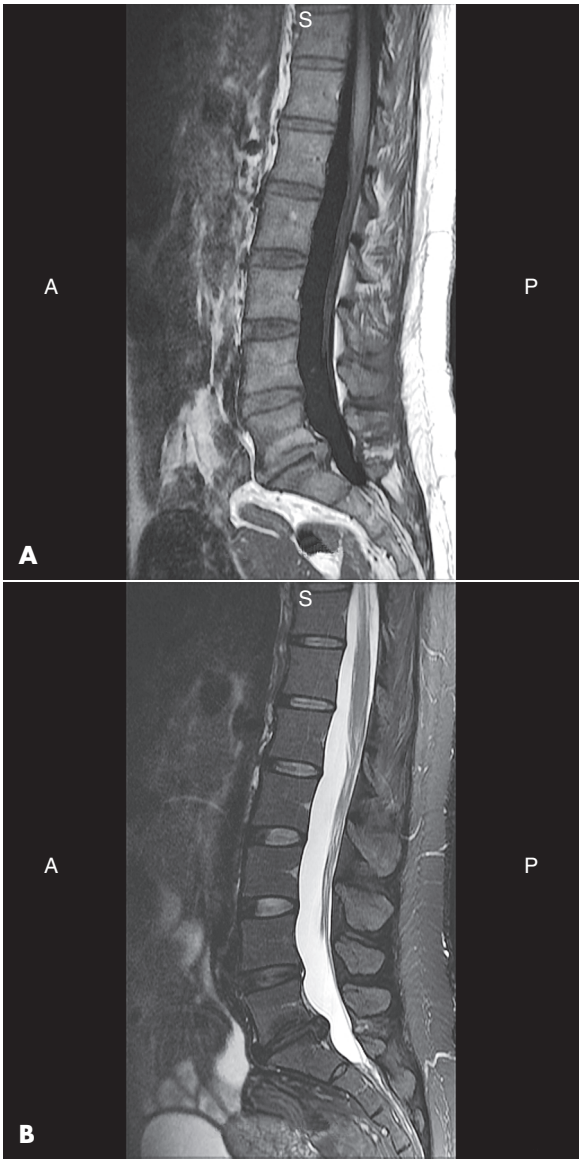

FIGURE 2-16 MRI of sagittal lumbar spine with small disk protrusion at L5–S1 and slightly desiccated disk spaces. **(A)** Proton density fast spin-echo image demonstrating disk protrusion. **(B)** Fat-suppressed image. Spinal fluid has a high-intensity signal, and spinal nerves have a lower-intensity signal.

within minutes of the onset of stroke symptoms. It can also be employed to help differentiate among liver, breast, and prostate lesions and to detect acute compression fractures.

Perfusion imaging, used in conjunction with diffusion imaging, also relies on fast scanning techniques and the rapid infusion of an intravenous contrast agent (gadolinium) to visualize the transit time of blood through a specific area. Perfusion images of the brain, visceral organs (e.g., the liver), and myocardium demonstrate circulation in viable tissue, which helps to distinguish old from new infarctions or ischemic regions. Mismatches in diffusion and perfusion imaging of the brain during a stroke indicate those parts of the brain that are not salvageable (diffusion) and are at further risk (perfusion). Currently, diffusion and perfusion techniques assist in demonstrating strokes early, increasing the possibility of revascularization with immediate treatment. Perfusion imaging also helps delineate

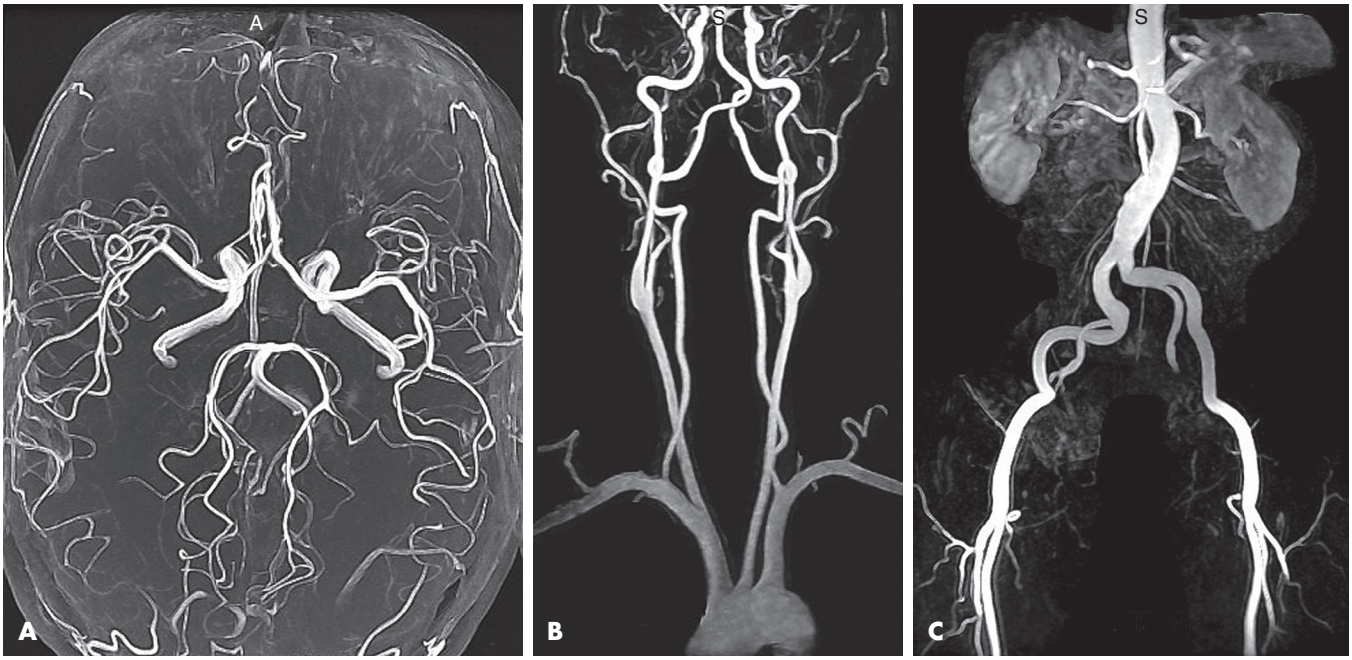

FIGURE 2-17 MR angiography. **(A)** Collapsed view of the cerebrum showing a normal arterial circle (circle of Willis). **(B)** Gadolinium enhancement of the aortic arch demonstrating the brachiocephalic, left common carotid, and left subclavian arteries to the base of the skull. **(C)** Gadolinium enhancement of the abdomen demonstrates renal and mesenteric arteries.

the vascularization of a tumor mass, which is helpful in presurgical planning. In cardiac imaging, perfusion can indicate ischemic or infarcted tissue. One of the unique advantages of MRI is its ability to acquire images with selective tissue suppression. The tissue most often suppressed in routine imaging is fat. **Fat suppression** or fat separation can be acquired on a T1- or T2-weighted image. With these techniques, fat produces little or no signal (see Figure 2-16B). On routine T1-weighted images, both fat- and contrast-enhanced lesions appear bright. This technique effectively suppresses the bright signal from fat, allowing the enhancing lesion to be seen. Fat-suppression images are most often employed for imaging the skull base and the soft tissues of the neck, the abdomen, and the pelvis. When bone marrow is being imaged, fat suppression accentuates marrow edema, such as is found in stress fractures and bone bruises.

Functional MRI (fMRI) is a process that maps specific regions of the brain that correspond to specific functions, such as motor, sensory, memory, vision, and language. The patient is asked to perform a precise function (paradigm), such as finger tapping (motor) or listening to music (sensory). The part of the brain being utilized demonstrates an increase in blood flow. Employing gradient echo pulse sequences, the differing magnetic properties of oxyhemoglobin and deoxyhemoglobin can be imaged using a process called BOLD (blood oxygen level dependent). Prior to the acquisition of the "functional" images, high-resolution "anatomic" images are acquired. These two sets of images are combined, or overlaid, to allow the diagnostician to precisely plan interventions to spare specific functional areas. Future uses of fMRI include the evaluation of stroke, epilepsy, pain, and behavioral problems.

Higher field strengths, coil development, and 3D volumetric imaging hold the future of MRI. Three Tesla (3T) magnets are becoming commonplace and have replaced some of the 1.5T workhorse magnets of prior years due to their increased signal-to-noise ratios and rapid gradients. Coil development is allowing smaller fields of view and thinner slices while preserving anatomic coverage. The acquisition of 3D volumetric data sets and the ability to post-process these data will lead to more complete diagnostic information.

Summary of Magnetic Resonance Imaging—Anatomic and Tissue Imaging

Image creation	Radiofrequency (RF) pulses emitted to change hydrogen atom energy states
Image receptor	Receiver coil to detect energy changes to relaxation times
Pulse sequence	T1-weighted—high signals (bright) include fat, subacute hemorrhage, melanin, slow-flowing blood, and IV contrast T2-weighted—high signals (bright) include water; lower signal intensities (intermediate to dark) include muscle and soft tissue; low signal intensities (dark) may indicate cortical bone, calcium, air, or fast-flowing blood (no signal) Fat suppression—differentiates fat from contrast material to highlight vascular structures Susceptibility weighted—extremely sensitive to products that create changes in magnetic susceptibility; low signal intensity (dark); hemorrhage, calcium Diffusion weighted—high signal intensity (bright) where random movement of water is restricted; stroke, liver lesions

Nuclear Medicine

In radiography, ionizing radiation interacts with tissue to produce an image. In **nuclear medicine**, however, the patient ingests, or receives an injection (intravenous [IV], intramuscular [IM], intrathecal [lumbar puncture], or into a shunt) of, a **radiopharmaceutical**. Each radiopharmaceutical is made up a **radionuclide** (radioactive isotope) and a **pharmaceutical** (R-group) that is united through both chemical and physical reactions. The pharmaceutical emits radiation and localizes in the patient based on the pharmaceutical portion attached. An image is created from the gamma rays radiating from the patient (Figure 2-18). The radiopharmaceutical dose is based on the calculation of the basis of the specific half-life and decay rate of its attached radionuclide. The amount of ionizing radiation given to the patient in a nuclear medicine study may equate to the exposure received from as many as 25 to 1000 radiographic images. The amount of pharmaceutical being used is so small that it has very little or no physiologic effects, allowing for the viewing of naturally occurring physiology and not altered physiology, unless indicated. The injected radionuclide does not produce the pharmacologic side effects or complications seen with radiographic iodinated contrast agents, making the study safer for all patients with an iodine allergy. However, all radiopharmaceuticals have some risk, and allergic reactions have been known to occur.

A **gamma camera** with a sodium iodide crystal detects the ionizing radiation emitted from the patient. The gamma rays interact with the crystal and scintillate light rays. The light is amplified and converted into a digital signal from which an image is created. Because the gamma rays emit from the patient in all directions, they must be filtered. The gamma camera has a **collimator** made of lead that contains multiple parallel channels. These channels only allow rays that are perpendicular to the camera to pass and be detected while attenuating those that are not. Collimation reduces the sensitivity of the camera. Another form of attenuation also occurs when gamma rays interact with the body to cause Compton scattering and the photoelectric effect, which lead to a loss of image spatial resolution. To compensate for this loss, computer reconstruction software corrects for scatter. The scintigraphic image, which defines the distribution of the radiopharmaceutical, represents the physiologic map of the organ and/or system being imaged.

The physiologic map produced by some nuclear medicine procedures allows earlier detection of pathologic issues compared with plain radiographic images. This is because the functional perspective makes it more sensitive, possibly leading to an earlier diagnosis and thus a better prognosis. Abnormal radionuclide images are demonstrated by hot spots (produced by an increase in uptake that is directly proportional to the emission of gamma radiation) and/or by cold spots (which reflect a decreased uptake).

The images obtained using nuclear medicine techniques are excellent for documenting organ physiology, but they can be lacking in anatomic information. Plain radiographic images can therefore be useful for correlative purposes.

New technology has expanded the role of nuclear medicine to include tumor imaging. These studies help determine tumor size, location, and recurrence. Because radiopharmaceuticals differ in their ability to demonstrate various tumors, a choice is made on the basis of the suspected diagnosis and biopsy results (Figure 2-19). The scintigraphic images can be used to document diagnoses and for treatment management.

FIGURE 2-18 Nuclear medicine bone scan (technetium-99m–labeled bone scintigraphy). This normal scan demonstrates the anterior **(A)** and posterior **(B)** perspectives in a patient with hypercalcemia.

Single-Photon Emission Computed Tomography

Single-photon emission computed tomography (SPECT) represents another aspect of nuclear medicine imaging (Figure 2-20). Radiopharmaceuticals used in SPECT are the same as those used in planar nuclear medicine. To gather the tomographic information, a detector array rotates 180 to 360 degrees around the patient, acquiring multiple projections. The equipment is similar to a CT scanner, but in SPECT, instead of the source (the x-ray tube) and the detector array moving simultaneously, the source (the patient) emits the signal while the detector array rotates. The signal, which the computer reconstruction algorithm analyzes, determines the position and strength of the data to create an image. Because the position and attenuation coefficients are unknown, the information must be inferred by the signal detector system, resulting in decreased resolution and sensitivity. SPECT cameras can use a multitude of reconstruction techniques and filters to re-create 3D slices at any level and/or orientation in the body.

A disadvantage of SPECT is the gamma camera, which only allows imaging of a small region of interest that is only the size of the camera. Due to the limited imaging parameters, the length of the exams is increased. As technology improves, the resolution and sensitivity of this modality will increase. Currently,

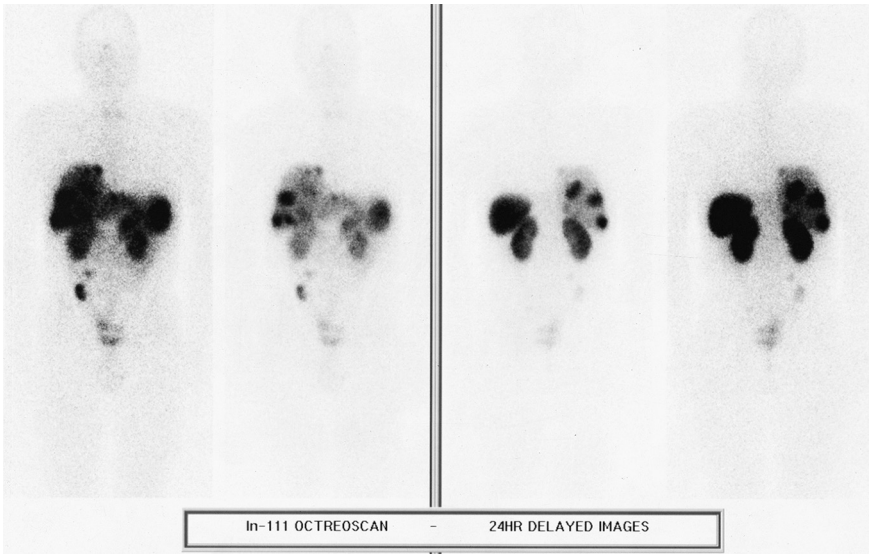

FIGURE 2-19 24-Hour delayed dual-intensity In-111 octreotide scan. The anterior *(left)* and the posterior *(right)* perspective illustrate multiple hepatic carcinoma metastases.

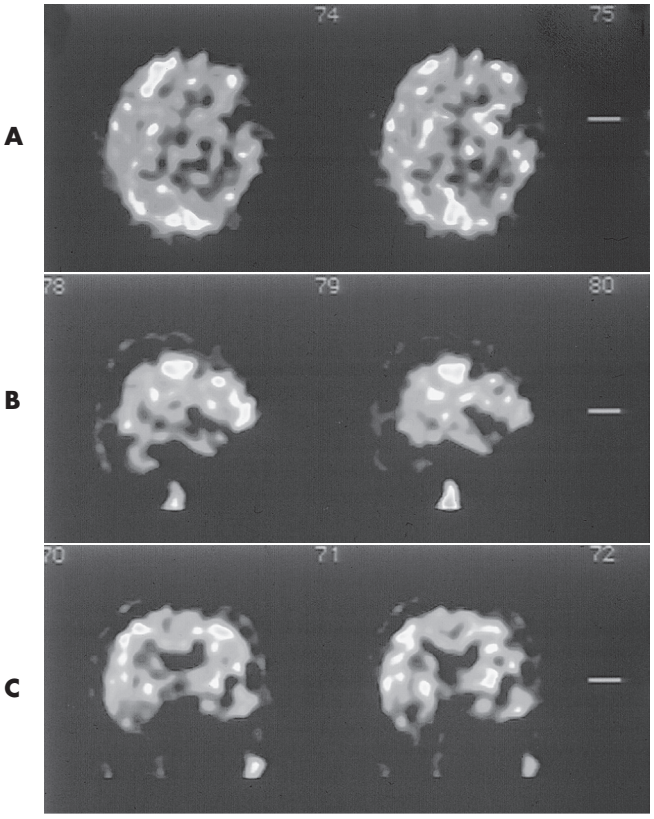

FIGURE 2-20 SPECT images of the brain reconstructed into three planes of view. **(A)** Transverse, **(B)** sagittal, and **(C)** coronal.

the advantage of SPECT is that SPECT imaging provides useful information in evaluating patients with many disease states: coronary artery disease, ventricular function disorders, ventricular wall motion abnormalities (Figure 2-21), infection, tumors (evaluation, staging, and restaging), strokes, focal seizures, and traumatic brain injuries.

Summary of Imaging for Nuclear Medicine (NM) and Single-Photon Emission Computed Tomography (SPECT)—Functional Imaging	
Image creation	Radiopharmaceutical that emits gamma radiation
Image receptor	NM—gamma camera that detects gamma radiation emitted from patient SPECT—rotating gamma camera for multiplanar gamma radiation collection
Imaging descriptors	Hot spot—increased uptake directly proportional to the emission of gamma radiation Cold spot—reflection of decreased uptake directly proportional to the emission of gamma radiation

Positron Emission Tomography

Positron emission tomography (PET) is very similar to general nuclear medicine procedures with one difference—the type of radiation emitted (Figure 2-22). Radionuclides used during general nuclear medicine procedures emit radiation directly from the nucleus of the atom, whereas in PET, a positron (a positively charged electron) is emitted. Upon emission, the positron travels until it interacts with an electron. With enough energy (1.22 MeV), the combination of a positron and an electron causes an annihilation. As a result, the positron and electron are completely converted into energy in the form of two gamma rays (0.511 MeV) emitted in opposite directions (approximately 180 degrees). PET camera systems are designed to detect both photons produced. By detecting both photons, the camera can calculate where the annihilation originally occurred based on the time it took for each ray to reach the camera. The pathway taken by the photons from

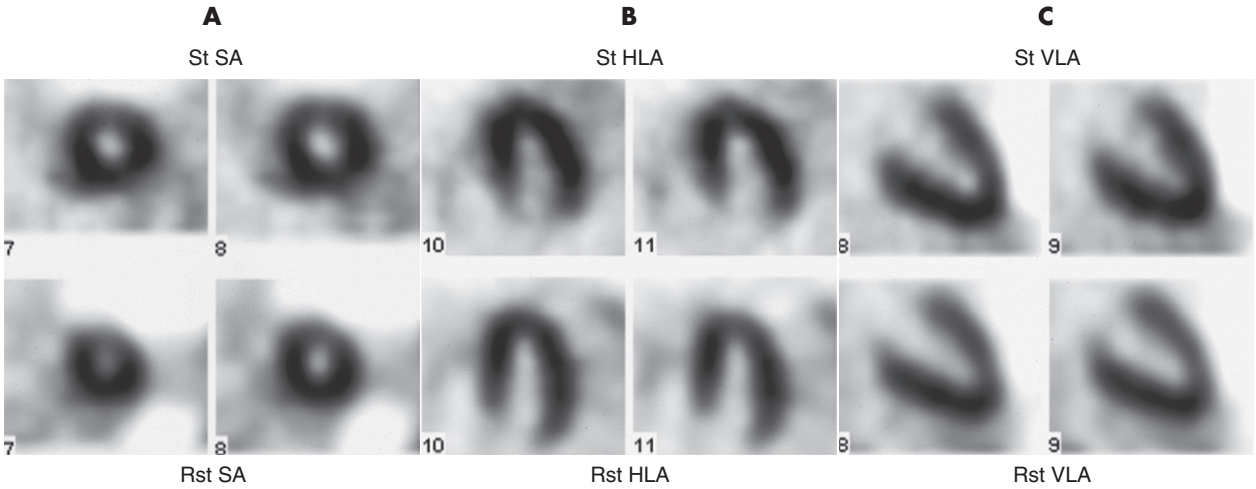

FIGURE 2-21 SPECT images of the normal heart in three planes of view, completed at rest (Rst) and stress (St) levels, with image reconstruction. **(A)** Short axis (SA) shows the coronal heart plane. **(B)** Horizontal long axis (HLA) shows the oblique transaxial plane. **(C)** Vertical long axis (VLA) shows the oblique sagittal plane.

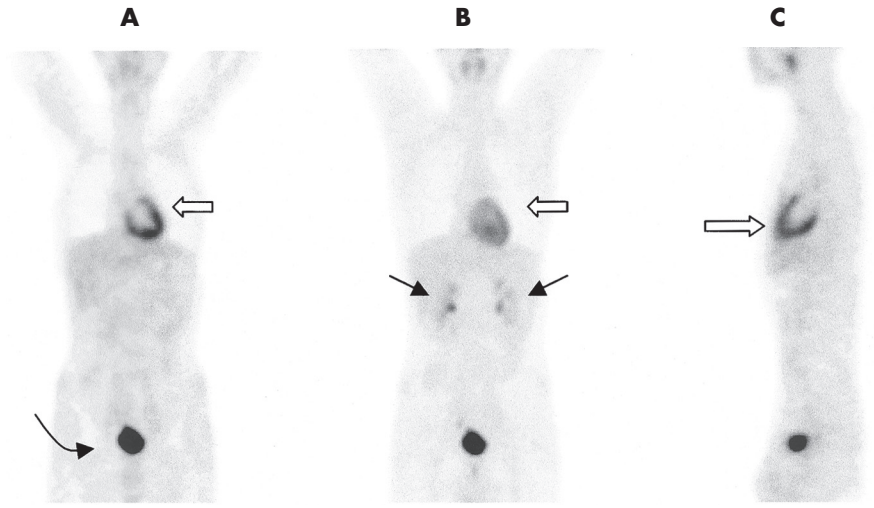

FIGURE 2-22 Normal PET scan with multiplanar body imaging. **(A)** Coronal plane, **(B)** projection plane, and **(C)** sagittal plane. Bladder (*curved arrow*), heart (*open arrows*), and kidney (*solid arrows*) are shown.

the point of the annihilation to interaction with the camera is referred to as the "line of response." When both rays are detected by the camera, it is called a "true" event. Detection of only a single photon is not recorded and is considered a "random" or "scattered" event. The combination of millions to billions of true events can be used to slowly formulate an image.

Radionuclides used in PET are elements that are common within the human body, such as carbon, oxygen, and nitrogen. The most common PET radionuclide is fluorine because in the body its biological and chemical properties are similar to hydrogen. Fluorine is a substituted atom in a glucose molecule to create the most widely used radiopharmaceutical in ^{18}F-fluorodeoxyglucose positron emission tomography (^{18}F-FDG-PET). The imaging distribution of these molecules creates a finely detailed metabolic representation of the area of interest. The body or organ metabolism illustrates the biochemistry of the tissue, distinguishing diseased or dead tissue from healthy or normal tissue and demonstrating tissue viability. Thus, PET images the distribution of the gamma rays in the specific organs of interest and provides diagnosticians with a biologic map.

With PET imaging, multiple detectors (sometimes in excess of 8000) receive the signal, and computerized software converts the raw data to a 3D image in three planes: axial, coronal, and sagittal. In PET imaging, attenuation

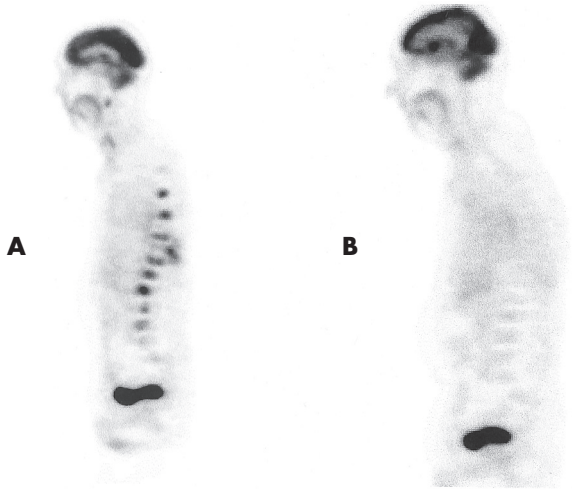

FIGURE 2-23 PET used to assess effectiveness of chemotherapy. **(A)** Image before therapy. **(B)** After chemotherapy, the image demonstrates decreased uptake of ^{18}F-FDG.

correction is required and is resolved by performance of a transmission scan on each patient. The computer reconstruction software then corrects for each patient's individual body contour and attenuation factor. This attenuation correction to the image increases the resolution of PET images and produces higher-quality images than SPECT. Radiation exposure rates to the patient in PET imaging are similar to those in general nuclear medicine exams and similar to that of a diagnostic CT. For the technologist, handling concentrated doses of radiopharmaceuticals and patient care leads to a higher radiation exposure.

PET is especially useful in three medical specialties: oncology, cardiology, and neurology. For oncology patients, this imaging modality can accurately image the whole body (cone of the head to the thigh), permitting the detection of metastases in multiple organs and aiding in tumor staging. Because PET produces a metabolic image, follow-up scans can be used to demonstrate the effectiveness of radiation or chemotherapy treatment by documenting any changes (Figure 2-23). In cardiology patients, PET imaging assists in screening for coronary artery disease by demonstrating myocardial perfusion (flow rates, flow reserves, and viable myocardium) (Figures 2-24 and 2-25).

In neurologic patients, PET can be used to evaluate for a variety of dementias (i.e., Alzheimer's, frontotemporal, and Parkinson's dementia) and to identify epileptic foci for surgical intervention (Figure 2-26). The scanning environment (i.e., sound and light) may influence the scan results because these stimuli can affect the metabolism of the temporal and occipital regions of the brain; therefore, the environment needs to be strictly controlled. ^{18}F-FDG is the tracer that is used in brain imaging to demonstrate different aspects of cerebral metabolic function. Unlike the anatomic map produced by CT and MRI, the physiologic map provided by PET may permit earlier detection of abnormalities by demonstrating pathology before morphologic changes, leading to prompt treatment interventions and a better prognosis.

Summary of Imaging for Positron Emission Tomography—Molecular Imaging

Image creation	Radiopharmaceutical that emits a positron—through the collection following annihilation, two gamma rays are created
Image receptor	Two opposite gamma cameras that detect gamma radiation simultaneously emitted from patient
Imaging descriptors	3D—three planes of colored images to demonstrate the biochemistry of tissue (biologic map) Distinguishes diseased or necrotic tissue from healthy or normal tissue Demonstrates tissue viability

Fusion Imaging

Today, physicians are using top-of-the-line technologies to combine anatomic images with physiologic functional images. This imaging integration provides a high degree of clarity to view the pathophysiologic changes without the need to examine each modality separately. Fusing the morphology and physiology enables the diagnosis to be made much more quickly and with increased accuracy.

Integrated imaging is accomplished with the use of special software designed to overlay or fuse multidimensional computed data from MRI, CT, nuclear medicine, SPECT, or PET into a single set of images. Many angles viewed in this manner provide improved visualization of the anatomic site of interest. Currently, **direct fusion** equipment (also known as hybrid technology) for PET/CT, PET/MR, and SPECT/CT

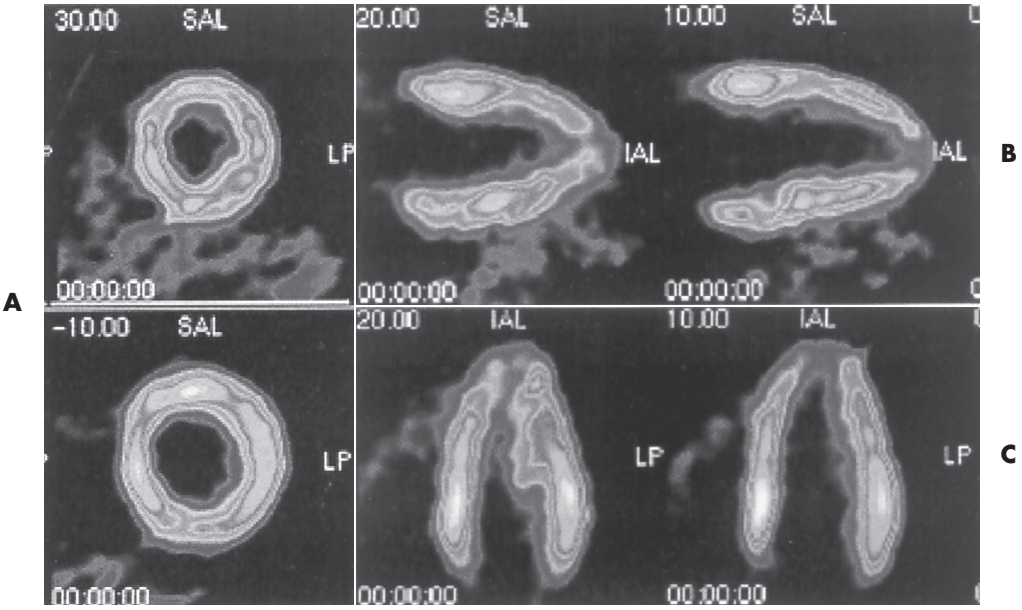

FIGURE 2-24 Normal PET images of the heart. Cardiology procedure demonstrating **(A)** short axis, **(B)** long vertical axis using ^{18}F-FDG, and **(C)** horizontal long axis (HLA) with normal perfusion.

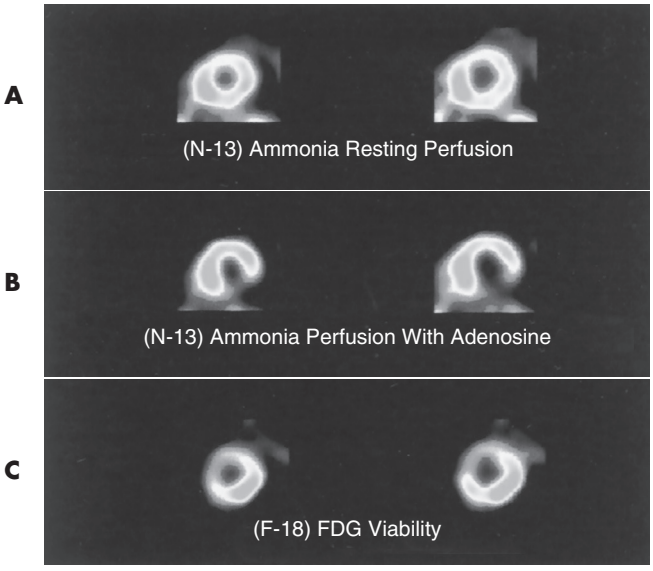

FIGURE 2-25 PET images demonstrating myocardial viability. Cardiac resting and artificial stress (adenosine) perfusion images of the short axis using $^{13}NH_3$ {∑Y}–{/∑Y} ammonia (N-13). **(A)** At rest, perfusion is normal. **(B)** After artificial stress, uptake in the inferolateral wall is decreased. **(C)** Viability scan with ^{18}F-FDG suggests ischemia of the right coronary artery and the left circumflex coronary artery. Perfusion of the region indicates that the myocardium remains viable.

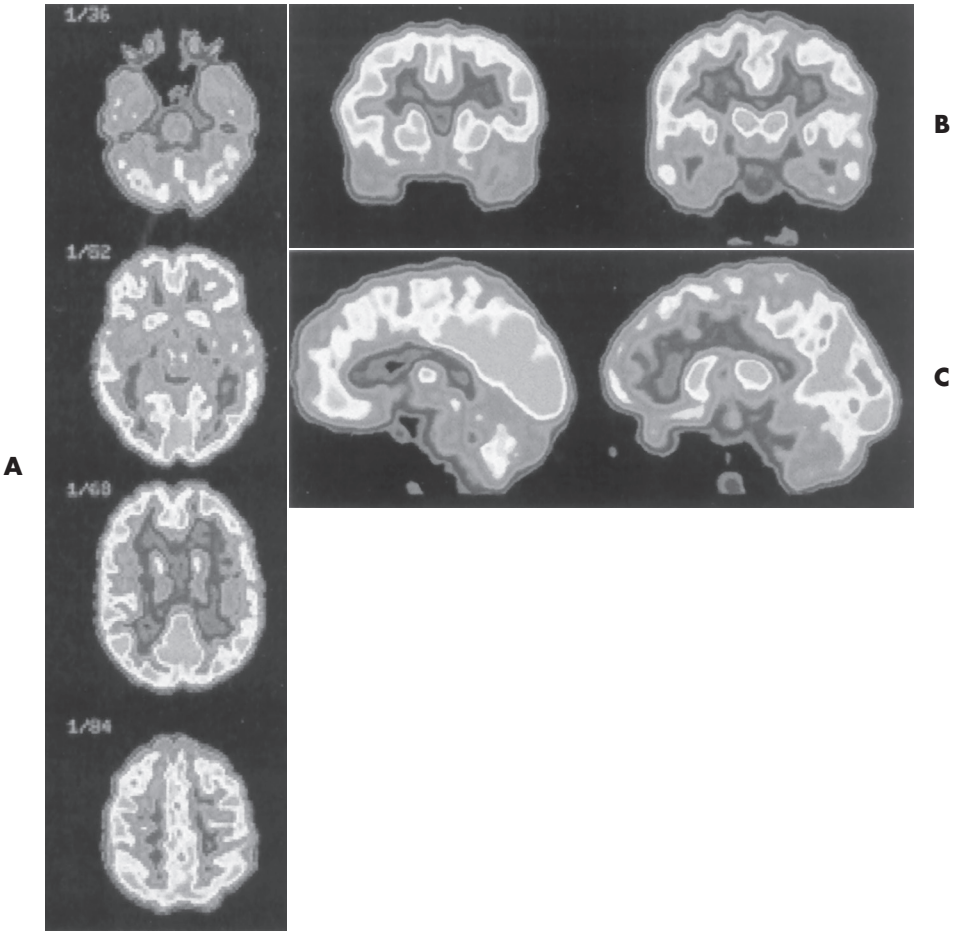

FIGURE 2-26 PET image of the brain. Normal ^{18}F-FDG uptake in the brain is indicated by the symmetric and consistent blood flow and metabolism in three planes: **(A)** axial or transverse, **(B)** coronal, and **(C)** sagittal.

is available (Figure 2-27). The examinations are completed simultaneously (preferred) or separately, and then fusion software puts the data together. PET/CT with hybrid imaging demonstrates increased sensitivity compared with either modality alone, especially for lymph node staging. Additional training and certifications may be required for the technologist responsible for producing these special images to ensure the use of the lowest radiation dose. Also, more education may be required to correctly demonstrate anatomic structures or molecular–physiologic relationships.

Summary of Fusion Imaging—Anatomic and Molecular Imaging	
Image creation	Combination of two imaging modalities—most common PET/CT Integrated imaging—software creates images overlaying modality image data set Direct fusion—simultaneous image creation
Image receptor	Two imaging receptors of modalities employed
Imaging descriptors	Specific to the imaging modalities used to create fused images

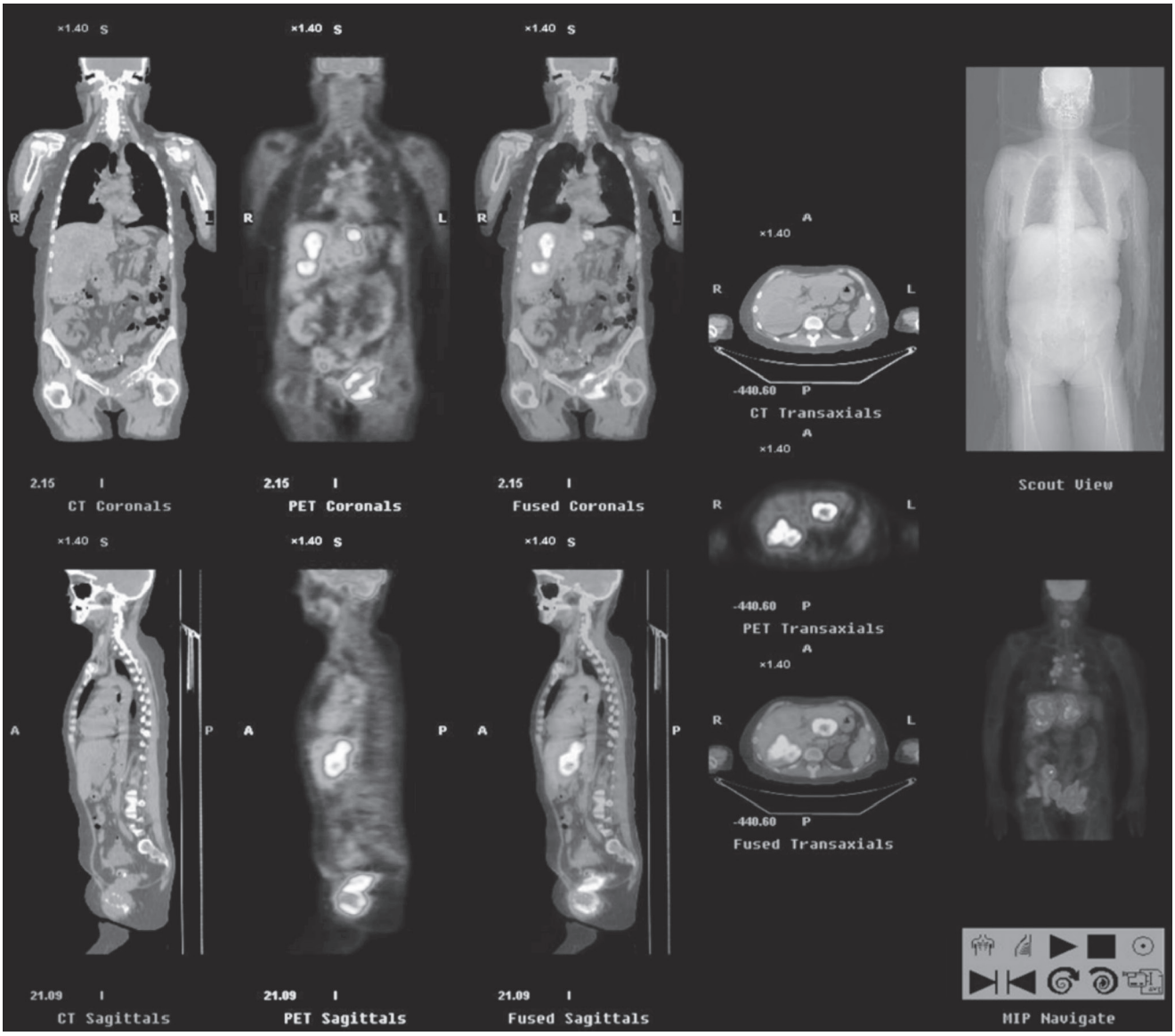

A **B** **C** **D**

FIGURE 2-27 PET/CT of the body. **(A)** This fusion provides the anatomic landmarks in the coronal and sagittal planes using the CT images. **(B)** PET coronal and sagittal images demonstrate increased molecular uptake. **(C)** The fused images provide greater detail by locating the increased uptake in its anatomic position. **(D)** The axial projection through the liver.

REVIEW QUESTIONS

1. The _____ describes where the pathophysiologic changes are visualized in relative position to the other organs or vessels in the body.
2. A pathophysiologic change that appears as a similar tissue structure is termed _____.
   a. heterogeneous
   b. isodense
   c. sharply marginated
   d. hyperdense
3. Pathophysiologic changes described as tubular, nodular, and diffuse are descriptors of _____.
4. Screening mammography recommends that _____ _____ and _____ projections be performed.
   a. craniocaudal, mediolateral oblique
   b. mediolateral oblique, 90-degree mediolateral
   c. craniocaudal, 90-degree mediolateral
   d. craniocaudal, mediolateral oblique, and 90-degree mediolateral
5. Ultrasound depends on the echo of the high-frequency sound waves produced by the transducer. Tissue that produces a strong reflection is known as _____.
   a. hypoechoic
   b. anechoic
   c. isoechoic
   d. hyperechoic or echogenic
6. Ultrasound is limited by acoustic barriers, such as _____.
   a. liver and splenic tissue
   b. air and bone
   c. urine in the bladder
   d. gallstones or kidney stones
7. The modality that views tissue from multiple angles using a narrow x-ray beam is _____.
   a. CT
   b. SPECT
   c. PET
   d. MRI
8. The CT technique using continuous scanning while the table moves the patient through the gantry is _____.
   a. helical scanning
   b. conventional single-slice scanning
   c. high-resolution scanning
   d. CTA
9. Currently, the term multidetector CT indicates _____ _____.
   a. multitransducer crystals
   b. a two-detector array
   c. 16- to 320-multidetector array
   d. 128- to 256-channel array
10. Which of the following is *not* a postprocessing imaging technique for CT?
    a. volume rendering
    b. virtual reality
    c. maximum intensity projection
    d. fat suppression
11. To create an image in MRI, the technology depends on _____.
    a. hydrogen atoms and their response to radiofrequency pulses
    b. x-radiation attenuation
    c. radiopharmaceuticals
    d. electrical stimulation of transducer crystals
12. Multiple-pulse sequences may be required to illustrate pathophysiologic changes. Examples of MRI pulse sequences are _____.
    a. T1- and T2-weighted images
    b. positron emission (gamma)
    c. single-photon emission
    d. 2-MHz to 15-MHz images
13. Nuclear medicine and SPECT imaging rely on scintillation cameras to detect _____.
    a. multiple-photon emission
    b. electron annihilation
    c. gamma rays
    d. photoelectric interaction
14. PET imaging is especially useful to evaluate _____ _____.
    a. chest for pneumothorax
    b. reproductive organs for cysts
    c. preradiation and postradiation or chemotherapy
    d. cerebral ventricle displacement
15. Hybrid imaging equipment combines two _____ _____.
    a. image modalities using software to fuse images
    b. images comparatively viewed side by side
    c. modalities simultaneously to produce one set of images
    d. technologists and a radiologist viewing images

3

Respiratory System

OUTLINE

Physiology of the Respiratory System
Internal Devices
- Endotracheal Tube
- Central Venous Catheters
- Swan–Ganz Catheters
- Transvenous Cardiac Pacemakers

Congenital/Hereditary Diseases
- Cystic Fibrosis
- Hyaline Membrane Disease

Inflammatory Disorders of the Upper Respiratory System
- Croup
- Epiglottitis

Inflammatory Disorders of the Lower Respiratory System
- Pneumonia
- Anthrax
- Lung Abscess
- Tuberculosis
- Pulmonary Mycosis
- Respiratory Syncytial Virus
- Severe Acute Respiratory Syndrome

Diffuse Lung Disease
- Chronic Obstructive Pulmonary Disease
- Sarcoidosis
- Pneumoconiosis

Neoplasms
- Solitary Pulmonary Nodule
- Bronchial Adenoma
- Bronchogenic Carcinoma
- Treatment of Pulmonary Neoplastic Diseases
- Pulmonary Metastases

Vascular Diseases
- Pulmonary Embolism
- Septic Embolism
- Pulmonary Arteriovenous Fistula

Miscellaneous Lung Disorders
- Atelectasis
- Adult Respiratory Distress Syndrome
- Intrabronchial Foreign Bodies
- Mediastinal Emphysema (Pneumomediastinum)
- Subcutaneous Emphysema
- Treatment of Mediastinal and Subcutaneous Emphysema

Disorders of the Pleura
- Pneumothorax
- Pleural Effusion
- Empyema
- Mediastinal Masses

Disorders of the Diaphragm
- Diaphragmatic Paralysis
- Eventration of the Diaphragm
- Other Causes of Elevation of the Diaphragm

KEY TERMS

adenocarcinomas
adult respiratory distress syndrome (ARDS)
alveolar, or air-space, pneumonia
asthma
bronchial adenomas
bronchiectasis
bronchioalveolar carcinoma
bronchiolar (alveolar cell) carcinoma
bronchogenic carcinoma
bullae
chronic bronchitis
emphysema
extrinsic asthma
interstitial pneumonia
intrinsic asthma
pulmonary mycosis
small cell (oat cell) carcinomas
squamous carcinoma
surfactant

OBJECTIVES

After reading this chapter, the reader will be able to:

- Locate placement for an endotracheal tube, central venous catheter, Swan–Ganz catheter, and transvenous cardiac pacemaker
- Recognize the most common complications involved with improper placement of these tubes and catheters and how chest radiography plays an important role in diagnosing them
- Classify the more common diseases in terms of their attenuation of x-rays
- Explain the changes in technical factors required to obtain optimal quality radiographs for patients with various underlying pathologic conditions
- Define and describe all boldface terms in this chapter
- Describe the physiology of the respiratory system
- Identify anatomic structures on both diagrams and radiographs of the respiratory system
- Differentiate the more common pathologic conditions affecting the respiratory system and their radiographic manifestations

RADIOGRAPHER NOTES

Proper positioning and the correct exposure factors are especially important in radiography of the respiratory system because to make a precise diagnosis, radiologists must be able to detect subtle changes in pulmonary and vascular structures. Ideally, follow-up studies should be performed with the same exposure factors used to make the initial radiographs. With the same exposure factors, any density changes can be attributed to true pathologic findings rather than to mere technical differences.

All chest radiography should be performed with the patient in full inspiration (inhalation), except when expiration images are used for those few pathologic conditions requiring expiration images. In an ideal image, the upper 10 posterior ribs should be visualized above the diaphragm. Poor expansion of the lungs may cause a normal-sized heart to appear enlarged and makes it difficult to evaluate the lung bases. To obtain a full-inspiration radiograph, the patient should be instructed to take a deep breath, exhale, and inhale again (thus accomplishing maximal inspiration), at which time the exposure should be made. This technique avoids the Valsalva effect, which is a forced expiration against the closed glottis that increases the intrapulmonary pressure. The Valsalva effect results in compression and a large decrease in the size of the heart and adjacent blood vessels, which make it difficult to evaluate heart size and pulmonary vascularity accurately.

The patient must be precisely positioned for chest radiography to ensure symmetry of the lung fields and a true appearance of the heart and pulmonary vasculature. Whenever possible, all chest radiographs should be taken with the patient in the erect position. The only exception is for the patient with a suspected pathologic condition that requires a lateral decubitus position. Although recumbent radiographs may be necessary in immobile or seriously ill patients, they are less than satisfactory because in this position the abdominal contents tend to prevent the diaphragm from descending low enough to permit visualization of well-expanded lung bases or fluid levels. A 72-inch source-to-image receptor distance should be used when possible to minimize magnification of the heart and mediastinal structures. Correct positioning with absence of rotation in the frontal projection can be demonstrated by symmetry of the sternoclavicular joints. The shoulders must be rolled forward (anteriorly) to prevent the scapulas from overlying the lungs. In large-breasted women, it is often necessary to elevate and separate the breasts to allow good visualization of the lung bases. Nipple shadows of both men and women occasionally appear as soft tissue masses. If the nature of these soft tissue masses is unclear, it may be necessary to repeat the examination using small lead markers placed on the nipples. Collimation of the radiograph is required to reduce scattered radiation, although it is essential that both costophrenic angles be visualized. However, the radiographer obtains a diagnostic image, and it is necessary to label the image appropriately.

Radiographs exhibiting a long scale of contrast are necessary to visualize the entire spectrum of densities within the thoracic cavity (including those of the mediastinum, heart, lung markings, and pulmonary vasculature) and the surrounding bony thorax. Most authorities agree that a minimum of 120 kilovolts-peak (kVp) should be used with an appropriate ratio grid for all adult chest radiography. If it is necessary to decrease the overall density, this should be accomplished by reduction of the milliampere seconds (mAs) rather than of the kVp. Decreasing the kVp tends to enhance the bony thorax, which may obscure vascular details and cause underpenetration of the mediastinal structures. In general, the density and contrast should be such that the thoracic vertebrae and intervertebral disk spaces are faintly visible through the shadow of the mediastinum without obscuring the lung markings and pulmonary vascularity. Many facilities have advanced from an analog imaging system to digital imaging systems, either computed radiography (CR) or direct radiography (DR). With digital systems, density (brightness) and contrast are primarily controlled by the algorithm used to process the image, although the technical factors selected also influence final appearance of the image. When producing radiographs for line placement, the technologist should use the appropriate technical factors to demonstrate the line and possible chest pathology (pneumothorax or hemothorax) that may result from line placement.

Short exposure times (10 msec or less) must be used in chest radiography because longer times may not eliminate the involuntary motion of the heart. Automatic exposure devices are generally recommended, and they help ensure that follow-up studies will have a similar image density. When a digital imaging system is used, the automatic exposure device helps ensure that the exposure index will be within range, thus producing the correct brightness and contrast on the image. An exception is the expiration (exhalation) chest radiograph, which should be exposed with a manual technique because the preset density of an automatic exposure device may cause excessive overexposure of the lungs and thus obscure a small pneumothorax.

Compensatory filters are sometimes needed to overcome the broad range of different tissue densities within the chest. They are especially important to allow good visualization of the mediastinum without overexposing the lungs. The use of compensatory filters generally requires that the radiographic exposure be twice that used when there is no additional filtration.

To demonstrate fluid levels, the patient should be in an erect position for a minimum of 5 minutes (preferably 10 to 15 minutes), and a horizontal x-ray beam must be used. Any angulation of the beam prevents a parallel entrance to the air–fluid interface and obscures the fluid level. In some clinical situations (e.g., when there is a small pneumothorax or pleural thickening as opposed to free pleural fluid), it is necessary to use a horizontal beam with the patient placed in the lateral decubitus position.

Certain pathologic conditions of the respiratory system require that the radiographer alter the routine technical factors. Some disorders produce increased tissue density (fluid), which attenuates more of the x-ray beam, whereas others decrease the tissue density of the lungs (hyperaeration) so there is less attenuation by the pulmonary tissue. It is important to remember that these changes may vary for a single disease because the chest structures attenuate more or less of the x-ray beam depending on the stage of the disease process. Unless the radiographer has access to previous images with recorded techniques, the initial exposures should be made with use of a standard technique chart. Adjustments and technical factors can then be made, if necessary, on subsequent images. (See Box 1-1 for a list of the changes in attenuation factors expected in advanced stages of various disease processes.)

PHYSIOLOGY OF THE RESPIRATORY SYSTEM

The major role of the respiratory system is the oxygenation of blood and the removal of the body's waste products in the form of carbon dioxide. The respiratory system consists of two separate divisions, the upper tract located outside the thorax and the lower tract found within the thoracic cavity (Figure 3-1). The upper respiratory system, which consists of the nasopharynx, oropharynx, and larynx, provides structure for the passage of air into the lower respiratory system. The lower respiratory system, which consists of the trachea, bronchi, and bronchioles, is composed of tubular structures responsible for conducting air from the upper respiratory structures. The smallest unit where gas exchange occurs consists of the terminal bronchiole, alveolar ducts, and alveolar sacs. With the use of the upper and lower respiratory structures, the air from outside the body enters the lungs. The single trachea branches out into two bronchi (one to each lung) at the carina (last segment of the trachea), which in turn branch out into progressively smaller bronchioles to produce a structure termed the bronchial tree because its appearance resembles an inverted tree. The tracheobronchial tree is lined with a mucous membrane (the respiratory epithelium) containing numerous hairlike projections called cilia. During inspiration, the air is moistened and warmed as it enters the lungs. The cilia act as miniature sweepers to prevent dust and foreign particles from reaching the lungs. When the ciliary blanket works correctly, the particles are moved away from the lungs to be coughed up or swallowed. Any damage to the respiratory epithelium and its cilia permits particles (entering with the inspired or inhaled air) to proliferate and produce a disease process.

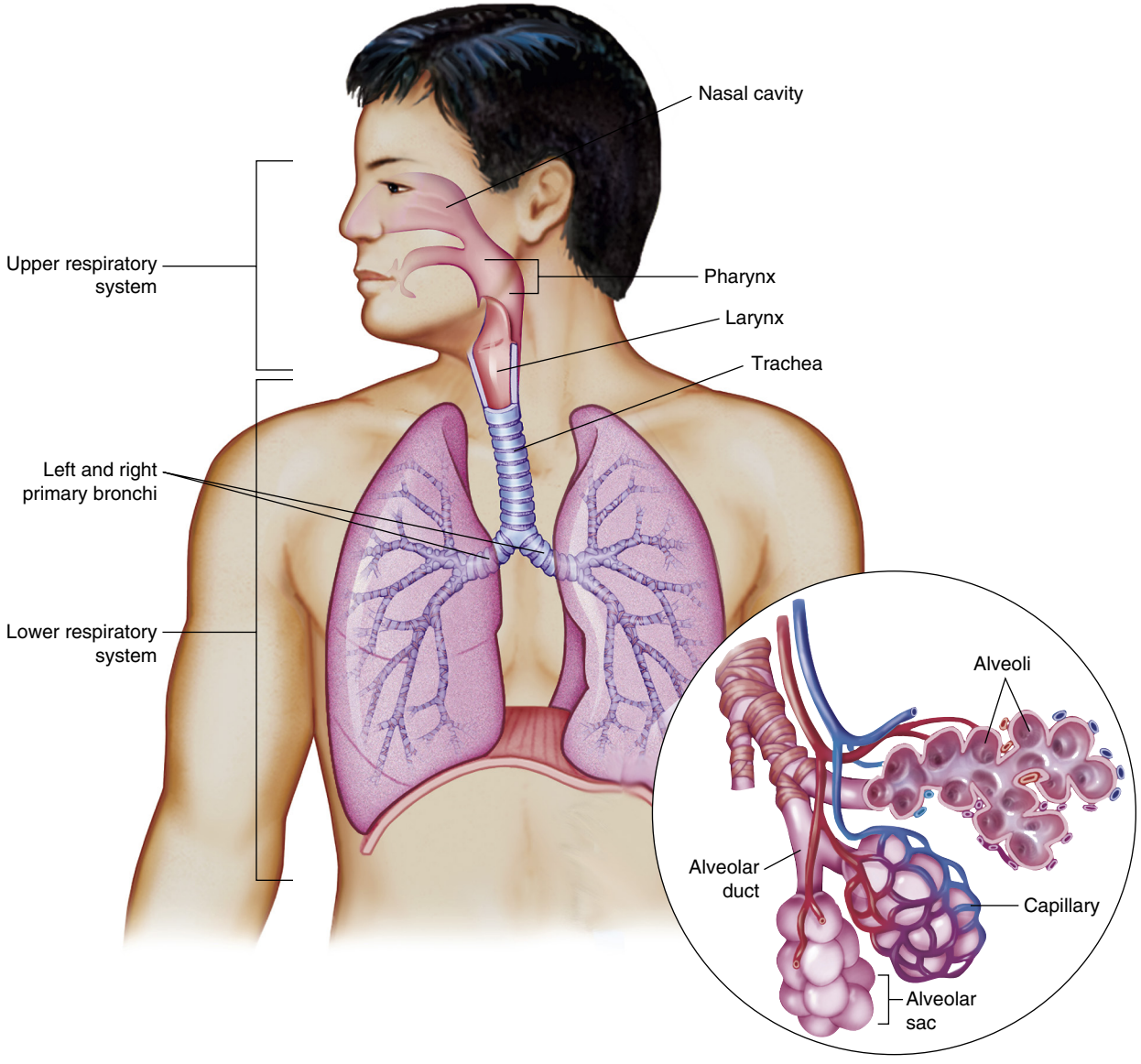

FIGURE 3-1 Structure plan of the respiratory system. The *inset* shows the alveolar sacs where the interchange of oxygen and carbon dioxide takes place through the walls of the grapelike alveoli.

The vital gas exchange within the lung (called external respiration) takes place within the alveoli, extremely thin-walled sacs surrounded by blood capillaries, which represent the true parenchyma of the lung (see Figure 3-1 *inset*). Oxygen in the inhaled air diffuses from the alveoli into the blood capillaries, where it attaches to hemoglobin molecules in red blood cells and circulates to the various tissues of the body (called internal respiration). Carbon dioxide, a waste product of cellular metabolism, diffuses in the opposite direction, passing from the blood capillaries into the alveoli and then exiting the body during expiration (or exhalation). Because individual alveoli are extremely small, chest radiographs can demonstrate only a cluster of alveoli and their tiny terminal bronchioles, which are the basic anatomic units of the lung. A cluster of alveoli is termed the acinus.

Respiration is controlled by a center in the medulla at the base of the brain. The level of carbon dioxide in the blood regulates the respiratory center. Even a slight increase in the amount of carbon dioxide in the blood increases the rate and depth of breathing, such as when an individual exercises. The accumulation of waste gases that must be removed from the body (and the body's need for additional oxygen) causes the respiratory center to stimulate the muscles of respiration—the diaphragm and the intercostal muscles between the ribs. Contraction of the muscles of respiration causes the volume of the chest cavity to increase. This decreases the pressure within the lungs and forces air to move into the lungs through the tracheobronchial tree. As the respiratory muscles relax, the volume of the chest cavity decreases, and air is forced out of the lungs. Special muscles of expiration (abdominal and internal intercostal muscles) may be needed for difficult breathing or in patients with decreased gas exchange, as occurs in emphysema.

Unlike most other organs, the lung has two different blood supplies. The pulmonary circulation is a low-pressure, low-resistance system through which oxygen enters and carbon dioxide exits the circulatory system. The bronchial circulation, which is a part of the high-pressure systemic circulation, supplies oxygenated blood to nourish (or support) the lung tissue.

A double-walled membrane consisting of two layers of pleura encases the lungs (Figure 3-2). The visceral pleura is the inner layer that adheres to the lung, whereas the parietal pleura lines the inner chest wall (the thoracic cavity). Between the two layers of pleura is a potential space (pleural space), which normally contains only a small amount of fluid to lubricate the surfaces to prevent friction as the lungs expand and contract. The airtight space between the lungs and the chest wall has a pressure slightly less than that in the lungs. This difference in pressure acts like a vacuum to prevent the lungs from collapsing. An inflammatory or neoplastic process that involves the pleura may produce fluid within the potential space (a pleural effusion).

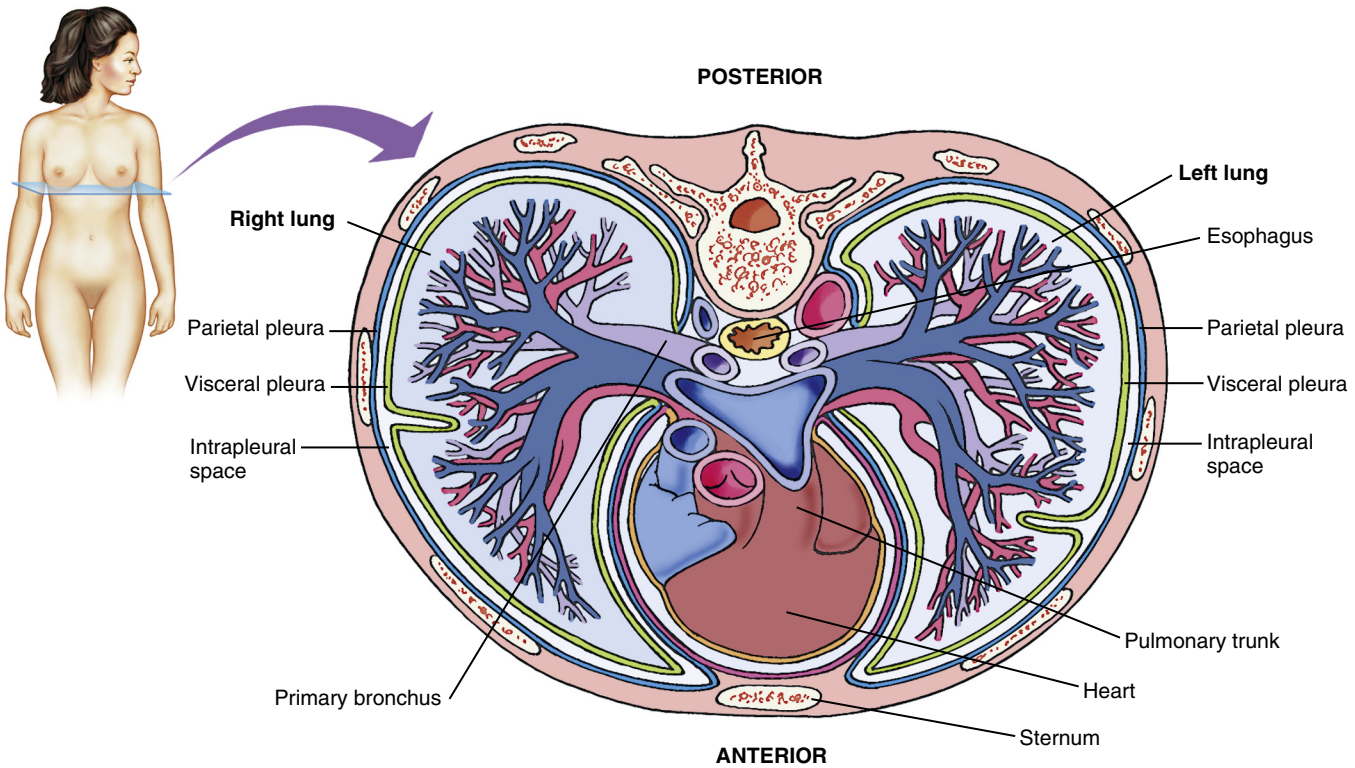

FIGURE 3-2 Lungs and pleura (transverse section). Note the parietal pleura, which lines the right and left pleural divisions of the thoracic cavity before folding inward near the bronchi to cover the lungs as the visceral pleura. The intrapleural space separates the parietal and visceral pleura. The heart, esophagus, and aorta are shown in the central mediastinum.

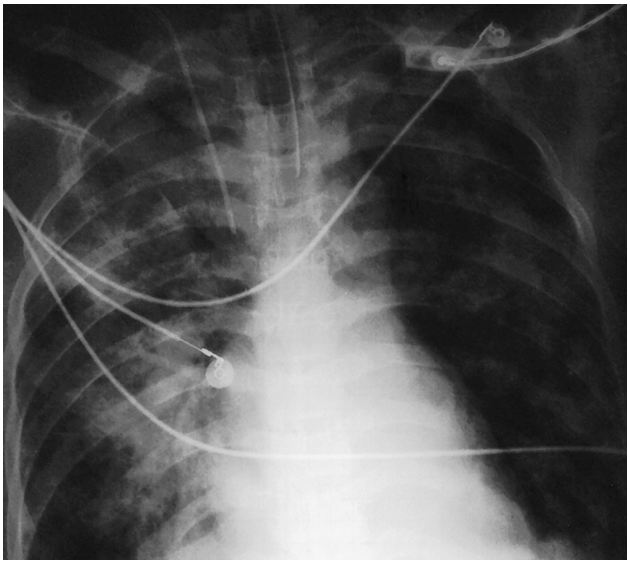

FIGURE 3-3 Endotracheal tube. Proper position.

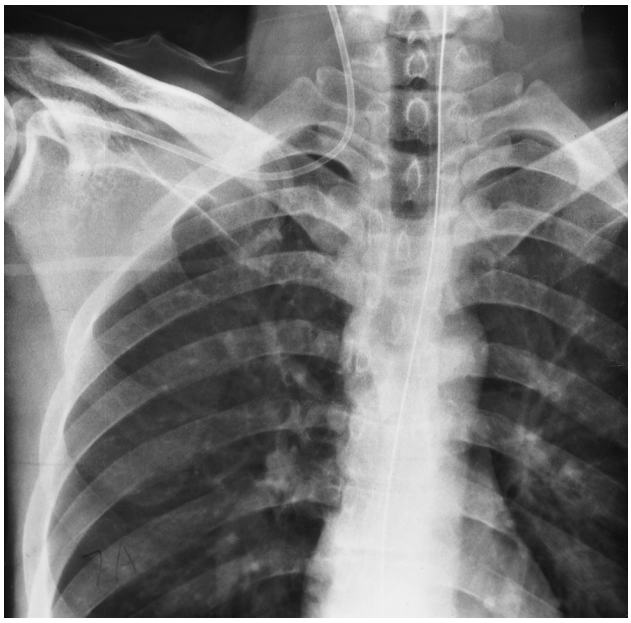

FIGURE 3-4 CVP catheter. Located in the right internal jugular vein.

INTERNAL DEVICES

Endotracheal Tube

A chest radiograph should always be obtained immediately after endotracheal intubation to ensure proper positioning of the tube because clinical evaluation (bilateral breath sounds, symmetric thoracic expansion, and palpation of the tube in the sternal notch) does not allow detection of the majority of malpositioned tubes. Daily radiographs are usually taken to ensure that the tube has not been inadvertently displaced by the weight of the respiratory apparatus, the patient's coughing, or other unforeseen events. In addition, imaging permits prompt detection of complications of intubation and barotrauma (positive-pressure breathing), such as pneumothorax and pneumomediastinum.

The relationship between the tip of the tube and the carina (tracheal bifurcation) must be carefully assessed. When the head and neck are in a neutral position, the endotracheal tube tip ideally should be approximately 5 to 7 cm above the carina (Figure 3-3). With flexion and extension of the neck, the tip of the tube will move approximately 2 cm caudally and cranially, respectively.

Approximately 10% to 20% of endotracheal tubes require repositioning after insertion. A tube positioned too low usually extends into the right mainstem bronchus, where it eventually leads to atelectasis of the left lung (see Figure 3-76). A tube positioned excessively high or in the esophagus causes the inspired air to enter the stomach, causing severe gastric dilation and a high likelihood of regurgitation of gastric contents and aspiration pneumonia.

Central Venous Catheters

Central venous catheters inserted into the subclavian vein or a more peripheral vein in the upper extremity are extremely useful for measurement of the central venous pressure (CVP) and for providing a conduit for the rapid infusion of fluid or chronic hyperalimentation. So that the CVP may be correctly measured, the catheter must be located within the true central venous system, beyond all the valves that interfere with direct transmission of right atrial pressure to the catheter. The optimal location is where the brachiocephalic veins join to form the superior vena cava (medial to the anterior border of the first rib on chest radiographs) or within the superior vena cava itself.

Because up to one-third of CVP catheters are initially inserted incorrectly, the position of the catheter should be confirmed by a chest radiograph. The most common aberrant location of a CVP catheter is the internal jugular vein (Figure 3-4). CVP catheters that extend to the right atrium are associated with an increased risk of cardiac arrhythmias and even perforation. Extension of the catheter into the hepatic veins may result in the infusion of potentially toxic substances (some antibiotics and hypertonic alimentation solutions) directly into the liver. Even after successful placement, CVP catheters may change position as a result of patient motion or medical manipulation. Therefore, periodic radiographic confirmation of the catheter position is often recommended.

The anatomy of the subclavian region may lead to complications when a central catheter is introduced via the subclavian vein. Because the pleura covering the apex of the lung lies just deep to the subclavian vein, a pneumothorax may develop. This problem may be difficult to detect clinically, and thus a chest radiograph (if possible with the patient in an upright position and in expiration) should be obtained whenever insertion of a subclavian catheter has been attempted. Another complication is perivascular CVP catheter placement, which may result in ectopic infusion of fluid into the mediastinum or pleural space. This diagnosis should be suggested if there is rapid development of mediastinal widening or pleural effusion after CVP catheter insertion (Figure 3-5). Other complications include inadvertent puncture of the subclavian artery, air embolism, and injury to the phrenic nerve.

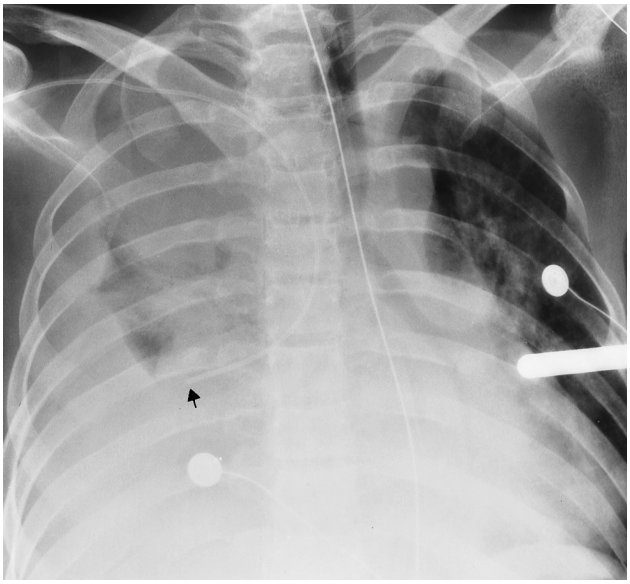

FIGURE 3-5 CVP catheter with its tip in the pleural space. A right subclavian catheter, which was introduced for total parenteral nutrition, perforated the superior vena cava and eroded into the right pleural space. Note the tip of the catheter projecting beyond the right border of the mediastinum (*arrow*). The direct infusion of parenteral fluid into the pleural space has led to a large right hydrothorax.

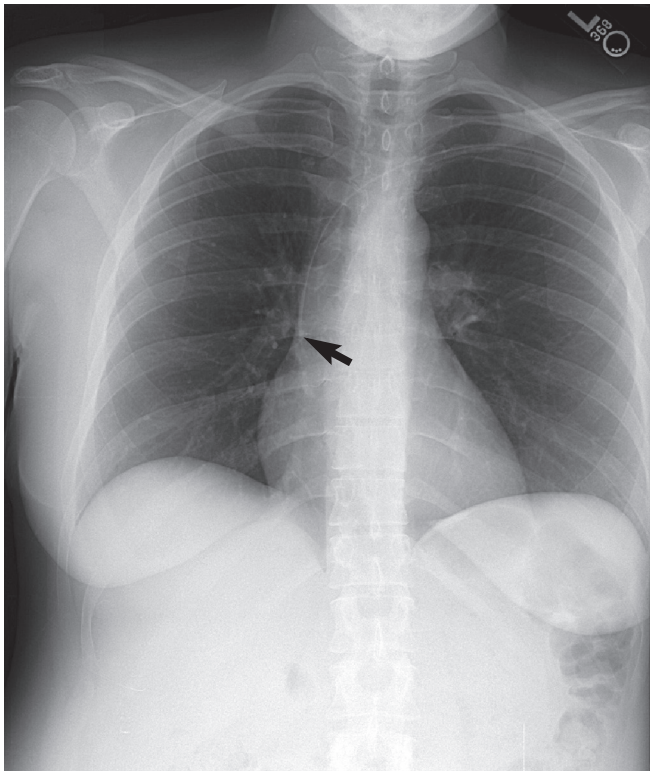

FIGURE 3-6 PICC line placement. The PICC line appears in the superior vena cava.

The peripherally inserted central catheter (PICC) has become the long-term venous access device used for home therapy and for patients undergoing chemotherapy (Figure 3-6).

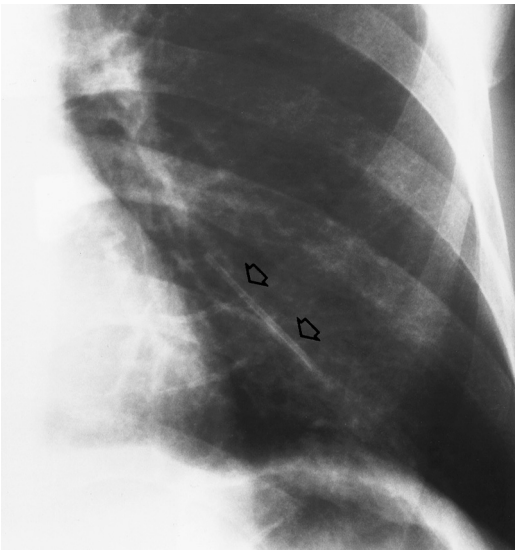

FIGURE 3-7 Broken CVP catheter. The sheared-off portion of the catheter (*arrows*) is located in the left lower lobe.

Catheter breakage and embolization can result from laceration of the catheter by the needle used to insert it, fracture at a point of stress, or detachment of the catheter from its hub. The catheter fragment may lodge in the vena cava, in the right side of the heart, or in branches of the pulmonary artery (Figure 3-7). Adverse results include thrombosis, infection, and perforation.

Swan–Ganz Catheters

The flow-directed Swan–Ganz catheter consists of a central channel for measuring pulmonary capillary wedge (PCW) pressure and a second, smaller channel connected to an inflatable balloon at the catheter tip. Cardiac output and CVP can also be measured using the Swan–Ganz catheter. It can be inserted at the bedside and floated to the pulmonary artery without the need for fluoroscopic monitoring.

Ideally, the catheter is positioned so that it lies within the right or left main pulmonary artery. Inflating the balloon causes the catheter to float downstream into a wedge position; deflating the balloon permits the catheter to recoil into the central pulmonary artery. Unlike standard intravenous catheters, the Swan–Ganz catheter has a radiopaque strip down its center. Radiographically, the tip of the tube is visualized within the borders of the mediastinum when properly placed; this would substantially decrease the likelihood of occlusion of the distal pulmonary vessel.

The most common complication associated with the use of a Swan–Ganz catheter is pulmonary infarction distal to the catheter tip. Infarction may result from occlusion of a pulmonary artery by the catheter itself (if it is wedged in a too peripheral vessel) or from clot formation in or about the catheter. Pulmonary infarction appears as a patchy air-space consolidation involving the area of the lung supplied by the pulmonary artery in which the catheter lies. The appropriate treatment is simply removal of the Swan–Ganz catheter; systemic heparinization is not required once this source of emboli or obstruction has been removed.

Transvenous Cardiac Pacemakers

Transvenous endocardiac pacing is the method of choice for maintaining cardiac rhythm in patients with heart block or bradyarrhythmias. Radiographic evaluation plays an important role in the initial placement of a pacemaker and in the detection of any subsequent complications. An overexposed image can demonstrate both the generator (for permanent pacemakers) and the course of the electrodes.

Ideally, the tip of the pacemaker should be positioned at the apex of the right ventricle. One common aberrant location is the coronary sinus. On a frontal radiograph, the tip often appears to be well positioned. A lateral projection is required to show that the tip is directly posterior in the coronary sinus, rather than in its proper position anterior in the right ventricle.

Although electrode fractures have become less common because of the development of new alloys, they are still a significant cause of pacing failure (Figure 3-8). The usual sites of fracture are near the pulse generator, at sharp bends in the wires, and at the point where the electrodes are inserted into the epicardium. Although most electrode fractures are easily detected on routine chest radiographs, some subtle fractures may be demonstrated only on oblique views or at fluoroscopy.

Perforation of the myocardium by an intravenous electrode usually occurs at the time of insertion or during the first few days thereafter. Perforation should be suspected when the pacemaker fails to sense or elicit a ventricular response. Plain radiographs show the electrode tip lying outside the right ventricular cavity (Figure 3-9).

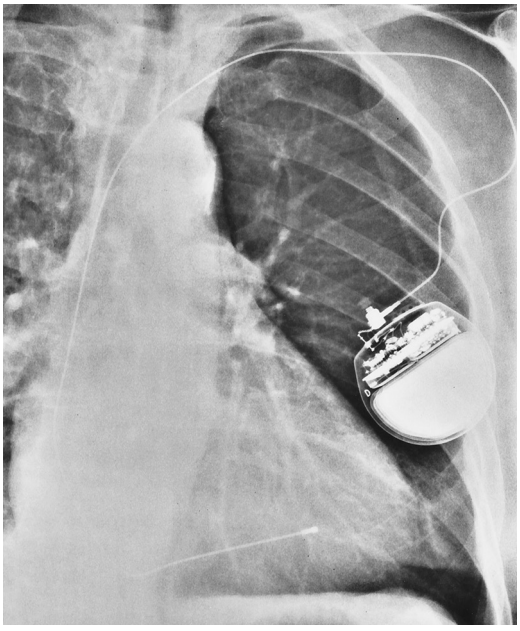

FIGURE 3-8 Pacemaker tip in coronary sinus. On the frontal projection, the tip of the electrode is angled slightly superiorly, traversing the heart in a higher plane than when it is located in the right ventricle.

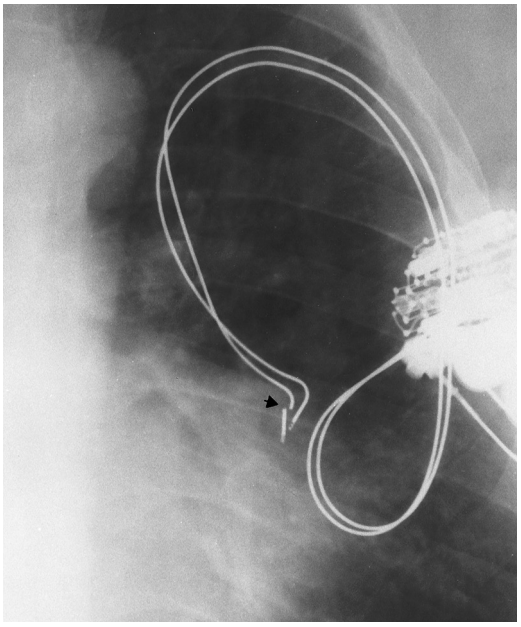

FIGURE 3-9 Cardiac pacemaker. Fracture of a pacemaker wire (*arrow*).

Summary of Findings for Internal Devices

Internal Device	Correct Placement*	Complications
Endotracheal tube	Tip of tube 5–7 cm above the carina	Low placement—atelectasis High placement—air entering the stomach
Central venous pressure catheters	Tip of catheter should be in the superior vena cava	Internal jugular vein placement Right atrium—possible arrhythmias or perforation Pneumothorax with placement Infusion of fluid into mediastinum or pleural space
Swan–Ganz catheters	Right or left main pulmonary artery seen radiographically within the borders of the mediastinum	Pulmonary infarction
Transvenous cardiac pacemakers	Overexpose to demonstrate the tip of the electrode at the apex of the right ventricle	Coronary sinus placement—needs a lateral chest image to distinguish Perforation at initial insertion

*Placement determined by chest radiograph.

CONGENITAL/HEREDITARY DISEASES

Cystic Fibrosis

Cystic fibrosis (mucoviscidosis) is a hereditary disease characterized by the secretion of excessively viscous mucus by all the exocrine glands; it is caused by a defective gene in the middle of chromosome 7. Cystic fibrosis is the most common clinically important genetic disorder among white children. This disorder also affects the pancreas and digestive system. However, 90% of the morbidity and mortality related to cystic fibrosis occurs as a result of respiratory involvement.

In the lungs, thick mucus secreted by mucosa in the trachea and bronchi blocks the air passages. The thick mucus is the result of an imbalance of sodium and chloride production and reabsorption. These mucous plugs lead to focal areas of lung collapse. Recurrent pulmonary infections are common because bacteria that are normally carried away by mucosal secretions adhere to the sticky mucus produced in this condition. Because of the recurring nature of the disease, by age 10 years many children have widespread bronchiectasis with the formation of large cysts and abscesses. In the pancreas, blockage of the ducts by mucous plugs prevents pancreatic enzymes from entering the duodenum. This process impairs the digestion of fat, resulting in failure of the child to gain weight and the production of large, bulky, foul-smelling stools. In approximately 10% of newborns with cystic fibrosis, the thick mucus causes obstruction of the small bowel (meconium ileus) (Figure 3-10). Bowel perforation with subsequent fatal peritonitis may occur.

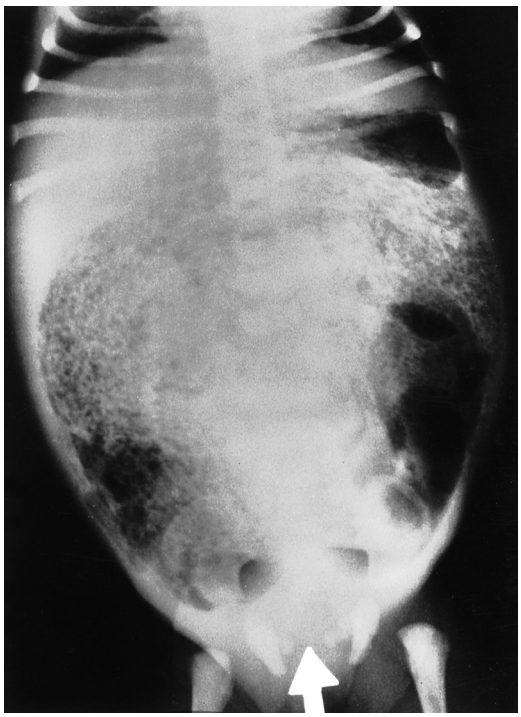

FIGURE 3-10 Meconium ileus in cystic fibrosis. Massive small bowel distention with profound soap-bubble effect of gas mixed with meconium.

Involvement of the sweat glands in cystic fibrosis causes the affected child to perspire excessively. The perspiration excess leads to a loss of large amounts of salt (sodium, potassium, and chloride), two to three times the normal amount. Patients are therefore extremely susceptible to heat exhaustion in hot weather. The presence of excessive chloride on the skin is the basis for the "sweat test," a simple and reliable test for cystic fibrosis.

Imaging appearance. Radiographically, cystic fibrosis causes generalized irregular thickening of linear markings throughout the lungs that, when combined with the almost invariable hyperinflation, produces an appearance similar to that of severe chronic lung disease in adults (Figure 3-11). Computed tomography (CT) screening to detect structural lung damage and assess disease progression is becoming more accepted by clinicians. There is a concern regarding the radiation dose if CT were used on a routine basis (yearly), especially because people with cystic fibrosis are now living into their 30s.

Treatment. Patient well-being depends on the use of prophylactic antibiotics, chest physiotherapy (percussions), and improved airflow. Prophylactic antibiotics reduce the risk of lung infections that may cause permanent lung damage or bronchiectasis. Chest physiotherapy (hand tapping against the chest) prevents lungs from filling with viscous mucus by keeping the mucus moving. Improved airflow depends on the use of bronchodilators. Currently, to help control pulmonary infections, administered by inhalation is recombinant human deoxyribonuclease (DNase), an enzyme that digests the DNA of bacterial and inflammatory cells in the lungs. The newest research trials focus on methods to control the production and reabsorption of sodium and chloride. In the future, gene therapy will be a viable alternative for patients with cystic fibrosis.

FIGURE 3-11 Cystic fibrosis. Multiple small cysts superimposed on diffuse, coarse, reticular pattern.

Hyaline Membrane Disease

Hyaline membrane disease, also known as idiopathic respiratory distress syndrome (IRDS), is one of the most common causes of respiratory distress in the newborn. It occurs primarily in premature infants, especially those who have diabetic mothers or who have been delivered by cesarean section. Hypoxia and increasing respiratory distress may not be immediately evident at birth but almost always appear within 6 hours of delivery.

The progressive underaeration of the lungs in hyaline membrane disease results from a lack of surfactant and immature lungs. **Surfactant** consists of a mixture of lipids, proteins, and carbohydrates that creates a high surface tension, requiring less force to inflate and maintain the alveoli. Normally, the alveolar cell walls produce lipoprotein, which maintains the surface tension within the alveoli. This tension permits the alveoli to remain inflated so that atelectasis does not occur. The disease process results from surfactant deficiency caused by cell immaturity or birth trauma.

Imaging appearance. In addition to pronounced underaeration, the radiographic hallmark of hyaline membrane disease is a finely granular appearance of the pulmonary parenchyma (Figure 3-12). A peripherally extending air bronchogram develops because the small airways dilate and stand out clearly against the atelectasis in the surrounding lung.

Treatment. New treatment advances for this disease include the use of an artificial surfactant, which offers the best therapy to reduce morbidity and mortality from this disease process. The artificial surfactant is administered into the airways via a saline solution.

The treatment of hyaline membrane disease includes the use of positive-pressure ventilators that pump air (often with high concentrations of oxygen) into the lungs through an endotracheal tube. The positive-pressure ventilator ensures satisfactory levels of tissue oxygenation. The high ventilator pressure may cause leakage of air from overinflated alveoli or small terminal bronchioles, leading to interstitial emphysema, pneumothorax, and pneumopericardium, all of which further decrease the expansion of the lungs.

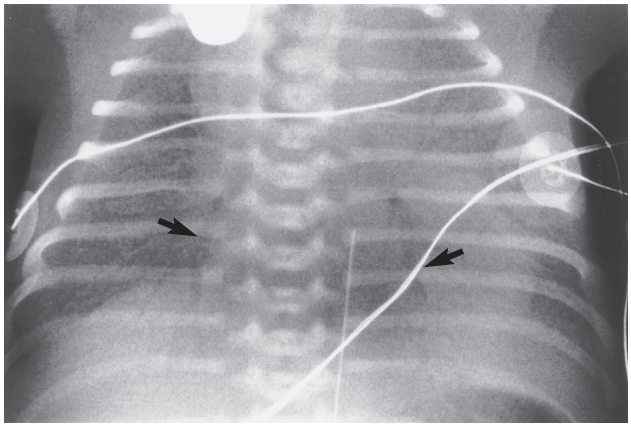

FIGURE 3-12 Hyaline membrane disease. Diffuse granular pattern of pulmonary parenchyma associated with air bronchograms (*arrows*).

INFLAMMATORY DISORDERS OF THE UPPER RESPIRATORY SYSTEM

Croup

Croup is primarily a viral infection of young children that produces inflammatory obstructive swelling localized to the subglottic portion of the trachea. The edema causes inspiratory stridor or a barking cough, depending on the degree of laryngeal obstruction.

Imaging appearance. Frontal radiographs of the lower neck show a characteristic smooth, fusiform, tapered narrowing (hourglass shape) of the subglottic airway caused by the edema (Figure 3-13A), which is unlike the broad shouldering normally seen (Figure 3-13B).

Treatment. A cool mist helps alleviate the breathing difficulty in patients with croup. At home, many patients or parents use the steam from a hot shower for 15- to 20-minute intervals. When breathing continues to be difficult, medical attention should be sought. Corticosteroid treatment is used in severe cases to help reduce swelling.

Epiglottitis

Acute infections of the epiglottis, most commonly caused by *Haemophilus influenzae* in children, cause thickening of

Summary of Findings for Congenital/Hereditary Disorders

Disorder	Location	Imaging Appearance	Treatment
Cystic fibrosis	Bronchi	Irregular thickening of linear markings throughout lung Hyperinflation CT demonstrates structural lung damage and disease progression	Prophylactic antibiotics Chest physiotherapy Bronchodilators
Hyaline membrane disease	Alveoli	Minute granular densities in parenchyma Air bronchogram	Artificial surfactant administered into the lungs via a saline solution Positive-pressure ventilation

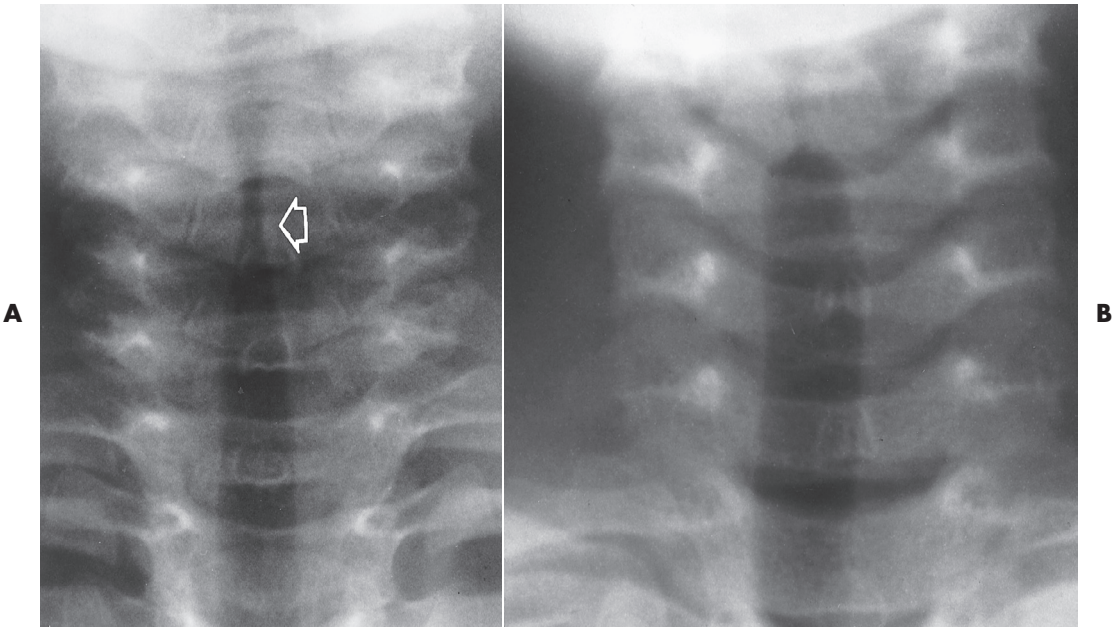

FIGURE 3-13 Croup. **(A)** *Arrow* indicates smooth, tapered narrowing of subglottic portion of trachea (the Gothic arch sign). **(B)** Normal trachea with broad shouldering in subglottic region.

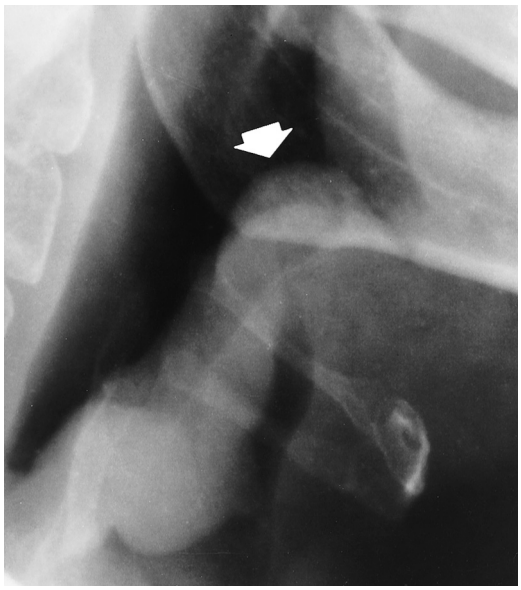

FIGURE 3-14 Epiglottitis. Lateral radiograph of neck demonstrates wide, rounded configuration of inflamed epiglottis (*arrow*).

epiglottic tissue and the surrounding pharyngeal structures. The incidence of epiglottitis has decreased dramatically since the inception of the *Haemophilus influenzae* type B (HiB) vaccine as a routine childhood immunization.

Imaging appearance. On lateral projections of the neck using soft tissue techniques, a rounded thickening of the epiglottic shadow gives it the configuration and approximate size of an adult's thumb (Figure 3-14), in contrast to the normal, narrow epiglottic shadow resembling an adult's little finger.

Treatment. Prompt recognition of acute epiglottitis is imperative because the condition may result in sudden complete airway obstruction. Because of its severity, epiglottitis requires hospitalization so the patient may be monitored. Intubation may become necessary to restore normal respiration. Also, antibiotics may have to be administered to treat the infection, and corticosteroids may have to be administered to reduce the swelling.

Summary of Findings for Inflammatory Disorders of the Upper Respiratory System

Disorder	Location	Imaging Appearance	Treatment
Croup	Subglottic trachea Larynx	Smooth, tapered narrowing	Steam, mist tent, O_2
Epiglottitis	Supraglottic area or supraglottis	Rounded thickening epiglottic shadow	ER—intubation Antibiotic for infection

INFLAMMATORY DISORDERS OF THE LOWER RESPIRATORY SYSTEM

Pneumonia

Acute pneumonia is an inflammation of the lung that can be caused by a variety of organisms, most commonly bacteria and viruses. Regardless of the cause, pneumonias tend to produce one of three basic radiographic patterns.

Alveolar Pneumonia

Alveolar, or air-space, pneumonia, exemplified by pneumococcal pneumonia, is produced by an organism that causes

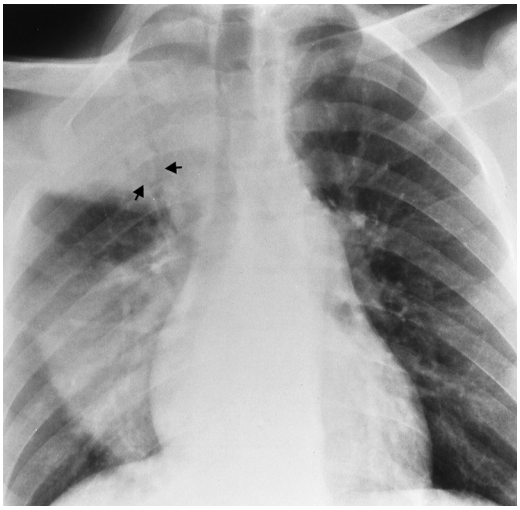

FIGURE 3-15 Alveolar pneumonia (pneumococcal). Homogeneous consolidation of right upper lobe and medial and posterior segments of right lower lobe. Note associated air bronchograms (*arrows*).

an inflammatory exudate that replaces air in the alveoli so that the affected part of the lung is no longer air containing but rather appears solid, or radiopaque (Figure 3-15). The inflammation spreads from one alveolus to the next by way of communicating channels, and it may involve pulmonary segments or an entire lobe (lobar pneumonia).

Imaging appearance. Consolidation of the lung parenchyma with little or no involvement of the airways produces the characteristic air bronchogram sign (Figure 3-16). The sharp contrast between air within the bronchial tree and the surrounding airless lung parenchyma permits the normally invisible bronchial air column to be seen radiographically. The appearance of an air bronchogram requires the presence of air within the bronchial tree, which suggests that the bronchus is not completely occluded at its origin. The presence of an air bronchogram excludes the diagnosis of a pleural or mediastinal lesion because there are no bronchi in these regions. Because air in the alveoli is replaced by an equal or almost equal quantity of inflammatory exudate and because the airways leading to the affected portions of the lung remain open, there is no evidence of volume loss in alveolar pneumonia.

Bronchopneumonia

Bronchopneumonia, typified by staphylococcal infection, is primarily an inflammation that originates in the bronchi or the bronchiolar mucosa and spreads to adjacent alveoli. Because alveolar spread of the infection in the peripheral air spaces is minimal, the inflammation tends to produce small patches of consolidation. Bronchial inflammation causing airway obstruction leads to atelectasis with loss of lung volume.

Imaging appearance. The small patches of consolidation may be seen radiographically as opacifications that are scattered throughout the lungs but are separated by an abundance of air-containing lung tissue (Figure 3-17); air bronchogram is absent. If consolidation causes obstructed airways, atelectasis is evident.

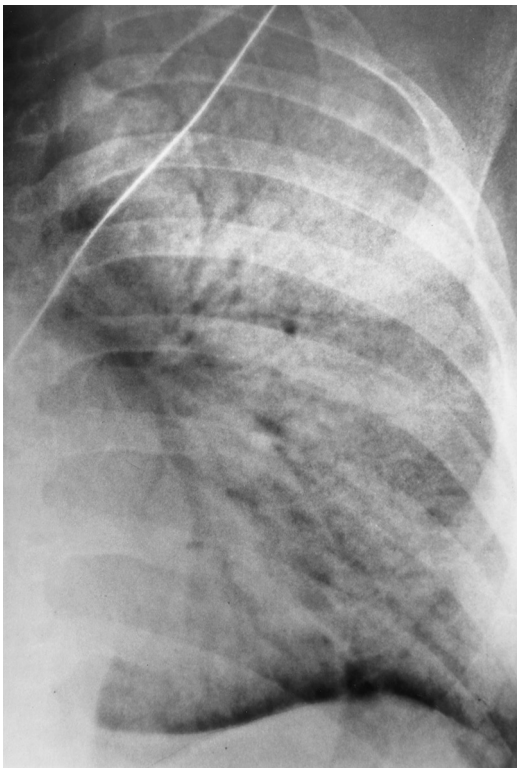

FIGURE 3-16 Air bronchogram sign in pneumonia. Frontal chest radiograph demonstrates air within intrapulmonary bronchi in patient with diffuse alveolar pneumonia of left lung.

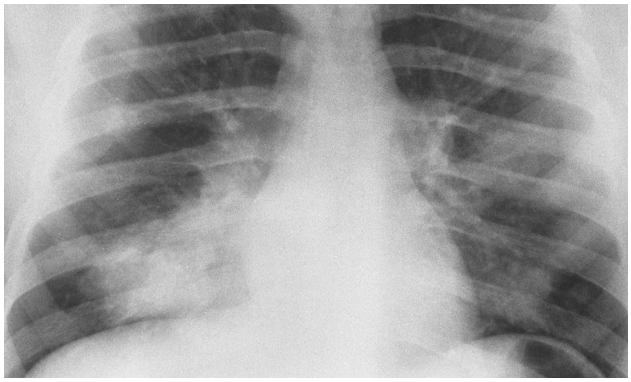

FIGURE 3-17 Bronchopneumonia (staphylococcal). Ill-defined consolidation at right base.

Interstitial Pneumonia

Interstitial pneumonia is most commonly produced by viral and mycoplasmal infections. In this type of pneumonia, the inflammatory process predominantly involves the walls and lining of the alveoli and the interstitial supporting structures of the lung, the alveoli septa.

Imaging appearance. The interstitial dispersal of the infection produces a linear or reticular pattern (Figure 3-18). When seen on end, the thickened interstitium may appear as multiple small nodular densities. Left untreated, interstitial pneumonia may cause "honeycomb lung," which is demonstrated on CT as cystlike spaces and dense fibrotic walls (Figure 3-19).

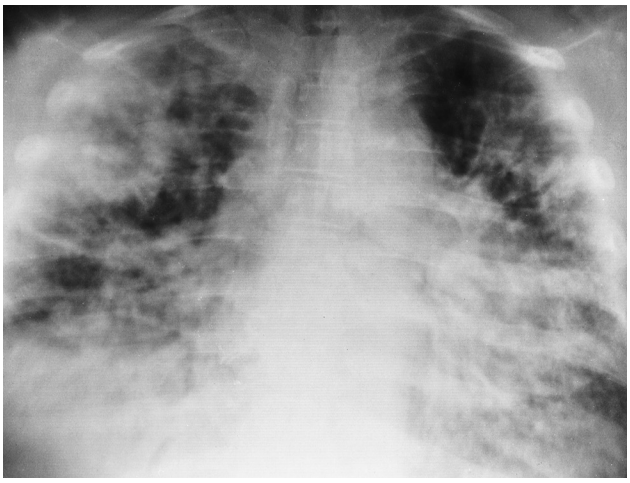

FIGURE 3-18 Interstitial pneumonia (viral). Diffuse peribronchial infiltrate with associated air-space consolidation obscures heart border (shaggy heart sign). Patchy alveolar infiltrate is present in right upper lung.

FIGURE 3-19 Pneumonia. CT scan demonstrates single lobe infiltrate as increased density of lung tissue on the left side.

Treatment. Extensive inflammation of the lung can cause a mixed pattern of alveolar, bronchial, and interstitial pneumonias, and this pattern appears as opacifications representing pulmonary consolidation. Treatment for these types of pneumonias usually includes regimented doses of an antibiotic to eradicate the cause. Rest, hydration, and deep-breathing techniques (supportive therapy) help in treating the infectious process.

Aspiration Pneumonia

The aspiration of esophageal or gastric contents into the lung can lead to the development of pneumonia. Aspiration of esophageal material can occur in patients with esophageal obstruction (e.g., tumor, stricture, and achalasia), diverticula (Zenker's), or neuromuscular swallowing disturbances.

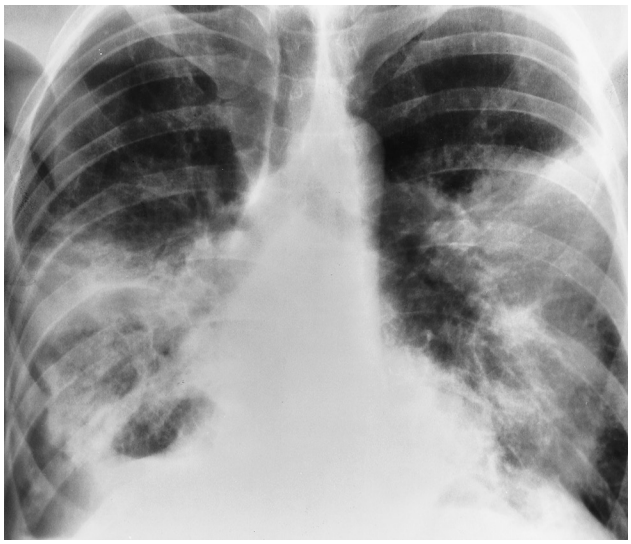

FIGURE 3-20 Aspiration pneumonia. Bilateral, nonsegmental air-space consolidation.

Aspiration of liquid gastric contents is most often related to general anesthesia, tracheostomy, coma, or trauma.

Imaging appearance. Both types of aspiration cause multiple alveolar densities, which may be distributed widely and diffusely throughout both lungs (Figure 3-20). Because the anatomic distribution of pulmonary changes is affected by gravity, the posterior segments of the upper and lower lobes are most commonly affected, especially in debilitated or bedridden patients.

Treatment. For effective treatment, early diagnosis of aspiration pneumonia and the prompt institution of corticosteroid and antibiotic therapy are essential to improve the otherwise grave prognosis.

Anthrax

Anthrax is caused by the sporelike microbe known as *Bacillus anthracis*. From the mid-1970s, there were no cases of anthrax in the United States until the biologic terrorist attacks using the bacillus that occurred in the fall of 2001. Anthrax is considered a highly volatile microbe because of its ease of transmission and high fatality rate. The organism can survive for decades in the soil in extreme conditions (heat and cold), without the need for a host.

There are three ways to contract anthrax: cutaneous, through an opening in the skin; inhalation (lungs), which is usually fatal (75%) if not treated in the early stages; and gastrointestinal. The cutaneous form is the most common type (75%) and is contracted by working with animals or animal by-products (hides). Inhaled *B. anthracis* germinates in the lung tissue and lymph nodes, producing deadly toxins. These toxins cause cellular edema and disruption of normal cell function. Early signs are similar to those of influenza; however, progressive infection may cause labored breathing, shock, or even death. The gastrointestinal type, which causes intestinal inflammation, is usually caused by the consumption of contaminated meat.

Imaging appearance. Inhalation anthrax causes mediastinal widening and often pleural effusion without infiltrates

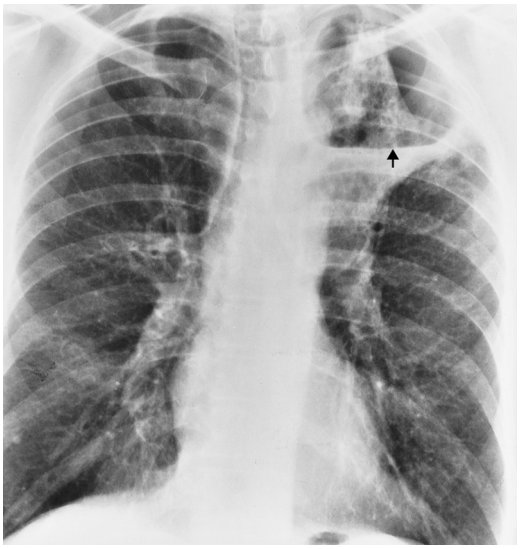

FIGURE 3-21 Lung abscess (bacterial pneumonia). Large, thick-walled left upper lobe abscess with air–fluid level (*arrow*) and associated infiltrate.

on a chest image. Rarely, infiltrates may develop. Gastrointestinal involvement manifests as mesenteric adenopathy on CT.

Treatment. Although high-dose antibiotics in the early stages attack the bacteria, the anthrax toxins are still produced and sometimes cause death. Vaccines are highly effective and available for limited use. They are not employed routinely in the United States because the last known reported incidence was 1976 (until the previously mentioned 2001 attacks).

Lung Abscess

A lung abscess is a necrotic area of pulmonary parenchyma containing purulent (puslike) material. A lung abscess may be a complication of bacterial pneumonia, bronchial obstruction, aspiration, a foreign body, or the hematogenous spread of organisms to the lungs either in a patient with diffuse bacteremia or as a result of septic emboli. Aspiration, which is the most common cause of lung abscesses, frequently occurs in the right lung because the right main bronchus is more vertical and larger in diameter than the left. The necrotic parenchyma becomes encapsulated by a fibrous wall, which encases the necrotic material. Unlike abscesses involving other organs, lung abscesses create an opening into the airway that can expand the extent of the infection.

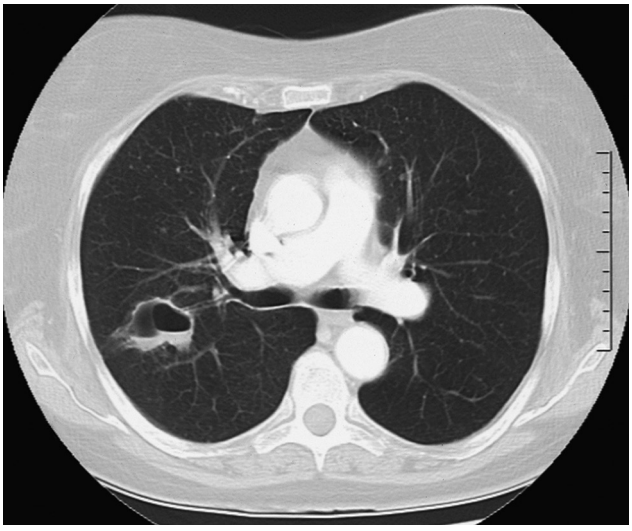

FIGURE 3-22 Lung abscess. CT scan demonstrates multiloculated capsule with air–fluid level.

Clinically, a patient with a lung abscess has a fever and cough and produces copious amounts of foul-smelling sputum. An important complication of lung abscess is the development of a brain abscess, which is produced by infected material carried by the blood from the lung to the left side of the heart and then on to the brain.

Imaging appearance. The earliest radiographic finding in lung abscess is a spherical density that characteristically has a dense center with a hazy, poorly defined periphery. If there is communication with the bronchial tree, the fluid contents of the cavity are partly replaced by air, producing a typical air–fluid level within the abscess (Figure 3-21). A cavitary lung abscess usually has a thickened wall with a shaggy, irregular inner margin. CT can assist in the diagnostic process to demonstrate an ill-defined outer wall and rule out empyema (Figure 3-22).

Treatment. The treatment for lung abscesses varies according to the cause. Specific therapy to control and eradicate the underlying organism is used along with supplemental treatment to alleviate possible complications. The patient also receives supportive therapy to help the lung mobilize the purulent material and to ensure pulmonary volume.

Summary of Findings for Inflammatory Disorders of the Lower Respiratory System

Disorder	Location	Imaging Appearance	Treatment
Pneumococcal pneumonia	Lobar/segment	Lobe/segment opacification	Antibiotic
Staphylococcal pneumonia	Bronchial airway/alveoli	Patchy opacification with air bronchogram	Antibiotic
Viral or mycoplasmic pneumonia	Alveoli/interstitium	Linear or reticular pattern	Antibiotic
Aspiration pneumonia	Alveoli (lobe/segment)	Patchy opacification	Corticosteroid and antibiotic
Anthrax	Throughout both lungs	Mediastinal widening with associated pleural effusions without infiltrates	High-dose antibiotics and vaccination
Lung abscess	Most common in right lung	Encapsulated opaque mass with air–fluid level	Appropriate antibiotic for specific organism, aid in expectoration of purulent material

Tuberculosis

Tuberculosis is caused by *Mycobacterium tuberculosis,* a rod-shaped bacterium with a protective waxy coat that permits it to live outside the body for a long time. Tuberculosis spreads mainly by droplets in the air, which are produced in huge numbers by the coughing of an infected patient. Therefore, it is essential that respiratory precautions be followed by radiographers imaging patients with active disease to prevent spreading of the infection. The organisms may be inhaled from sputum that has dried and turned into dust. They are rapidly killed by direct sunlight but may survive a long time in the dark. Tuberculosis may also be acquired by drinking the milk of infected cows. However, routine pasteurization of milk has virtually eliminated this route of infection.

Unlike most bacteria, mycobacteria do not stain reliably by Gram method. However, once mycobacteria take up the stain, it is difficult to decolorize mycobacteria by either acid or alcohol, and thus the organisms are often called acid-fast bacilli.

Tuberculosis is primarily a disease of the lungs, although it can spread to involve the gastrointestinal, genitourinary, and skeletal systems. In the initial tuberculous infection (the primary lesion), a collection of inflammatory cells collects around a clump of tuberculosis bacilli to form a small mass (tubercle) that is visible to the naked eye. The outcome of this initial infection depends on the number of bacilli and the resistance of the infected tissue. If the resistance is good and the dose is small, the proliferation of fibrous tissue around the tumor limits the spread of infection and produces a mass of scar tissue. In the lung, tuberculous scars are commonly found in the posterior apical segments. They often contain calcium, which is deposited as healing occurs.

A larger dose of bacilli or lower patient resistance tends to permit the disease to progress slowly. Within the center of the tubercle, the bacilli kill inflammatory cells so that the core becomes a necrotic, Swiss cheese–like mass (caseation). The caseous material may eventually become liquefied to form a cavity. Coalescence of several small cavities can result in the formation of a large cavity, which may contain an air–fluid level. Rupture of blood vessels crossing a cavity causes bleeding and the coughing up of blood (hemoptysis). An overwhelming infection with low resistance causes diffuse destruction throughout the lung, with the formation of huge cavities and often a fatal outcome.

The tuberculin skin test can detect previous tuberculous infection. The purified protein derivative (PPD) of the tuberculosis bacillus is injected into the skin, and the injection site is examined 2 or 3 days later. A visible and palpable swelling 10 mm in diameter or larger indicates that the individual has developed antibodies to a previous exposure to the bacilli. If there is no such reaction, the individual has either not been exposed to the tuberculosis bacilli or is anergic (i.e., immunologically nonreacting). The tuberculin test is not positive during an acute infection or for several weeks thereafter. When dealing with a possibly infected patient, one must consider the 3- to 6-week incubation period and the fact that the tuberculin skin test does not become positive until 2 to 10 weeks after infection.

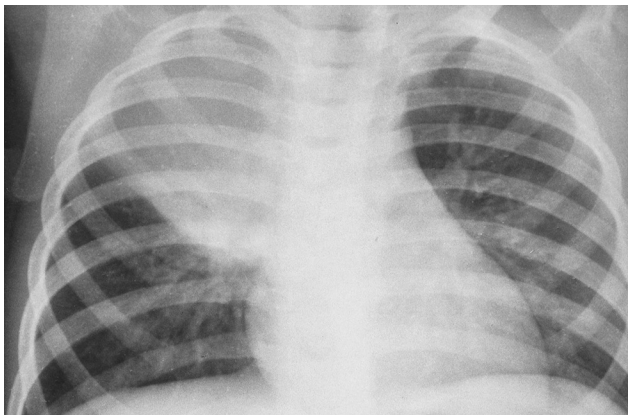

FIGURE 3-23 Primary tuberculosis. Consolidation of right upper lobe.

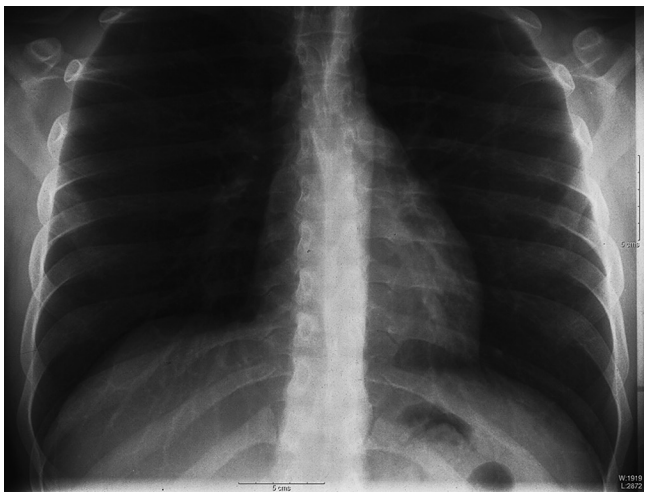

FIGURE 3-24 Apical lordotic projection. Lung apices can be seen without bony superimposition.

Primary Tuberculosis

Primary pulmonary tuberculosis has traditionally been considered a disease of children and young adults. However, with the dramatic decrease in the prevalence of tuberculosis (especially in children and young adults), primary pulmonary disease can develop at any age. The current decline is the result of wider screening and prevention programs.

Imaging appearance. There are four basic radiographic patterns of primary pulmonary tuberculosis, as follows:

1. The infiltrate may be seen as a lobar or segmental air-space consolidation that is usually homogeneous, dense, and well-defined (Figure 3-23). The apical lordotic projection best demonstrates the apices without superimposition of bony structures (Figure 3-24).
2. Associated enlargement of hilar or mediastinal lymph nodes is very common (Figure 3-25).
3. Indeed, the combination of a focal parenchymal lesion and enlarged hilar or mediastinal lymph nodes produces the classic primary complex (the Ghon lesion), an appearance strongly suggestive of primary tuberculosis.
4. Pleural effusion is common, especially in adults (Figure 3-26). Most primary tuberculous pleural effusions are unilateral and clear rapidly with treatment.

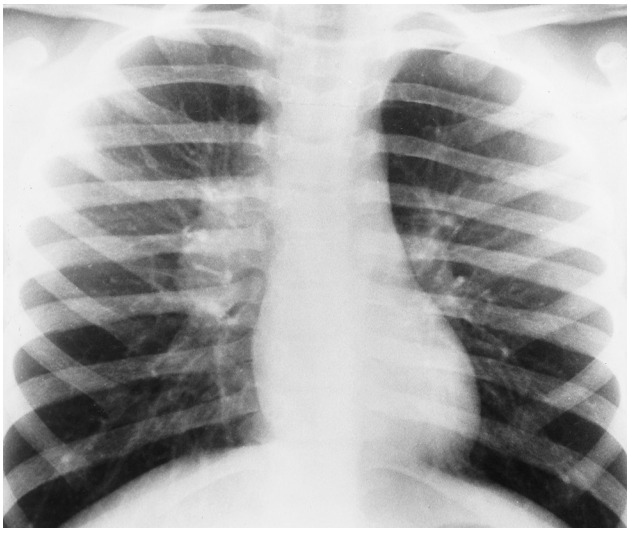

FIGURE 3-25 Primary tuberculosis. Enlargement of right hilar lymph nodes without discrete parenchymal infiltrate.

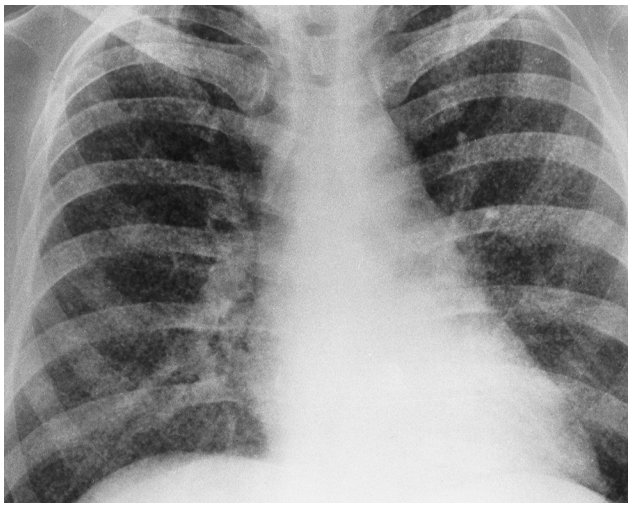

FIGURE 3-27 Miliary tuberculosis. Fine discrete nodules uniformly throughout both lungs.

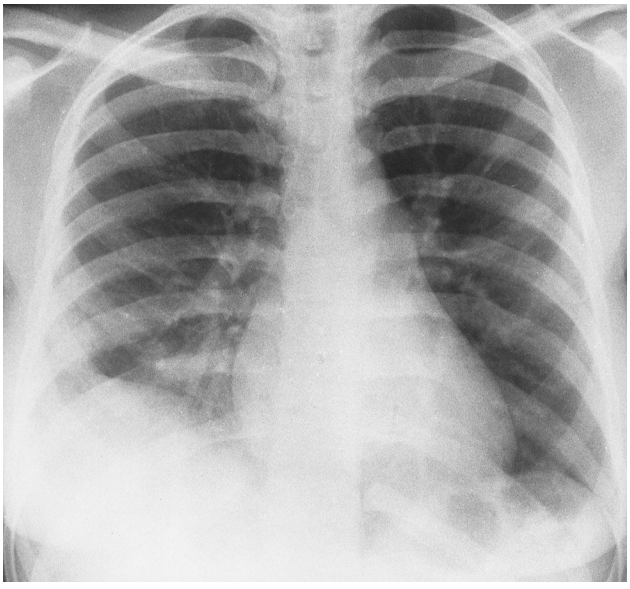

FIGURE 3-26 Primary tuberculosis. Unilateral right tuberculous pleural effusion without parenchymal or lymph node involvement.

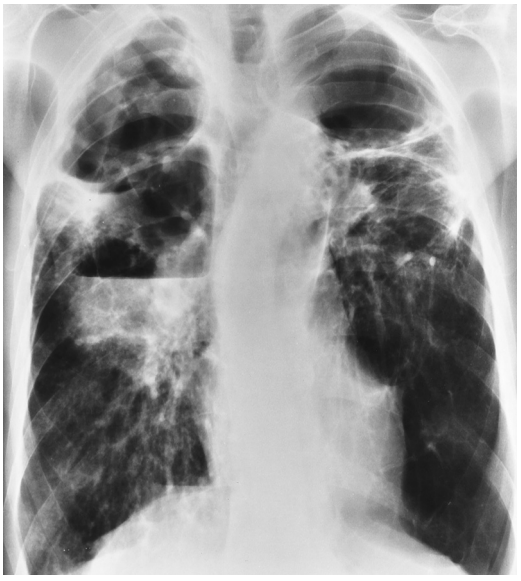

FIGURE 3-28 Tuberculosis. Multiple large cavities with air–fluid levels in both upper lobes. Note chronic fibrotic changes and upward retraction of hila.

Miliary tuberculosis refers to dissemination of the disease by way of the bloodstream. Radiographically, this development produces innumerable fine discrete nodules (granulomas) distributed uniformly throughout both lungs (Figure 3-27).

Tuberculous pneumonia may resolve completely and leave a normal lung. However, if necrosis and caseation develop, some fibrous scarring occurs. Calcification may develop within both the parenchymal and the nodal lesions, and it may be the only residue of primary tuberculous infection on subsequent images. If the disease responds poorly to therapy and continues to progress (especially in patients with immunodeficiency or diabetes and in those receiving steroid therapy), the pneumonia may break down into multiple necrotic cavities or a single large abscess filled with caseous material (Figure 3-28).

Secondary (Reactivation) Tuberculosis

Reactivation of organisms from previously dormant tubercles is termed a secondary lesion or reinfection tuberculosis. At times, the tuberculosis bacillus may remain inactive for many years before a secondary lesion develops, often because of a decrease in the body's immune defense. The diffuse, poorly defined lesion develops areas of caseous necrosis. Necrosis and liquefaction commonly lead to the development of tuberculous cavities, which typically have thick walls with ill-defined inner margins. Secondary pulmonary tuberculosis heals slowly with extensive fibrosis. Contraction of the fibrous scars causes loss of volume of the involved segment or lobe and a decrease in the size of the hemithorax. The trachea and other mediastinal structures are retracted to the involved side; in upper lobe disease, the hilum is elevated.

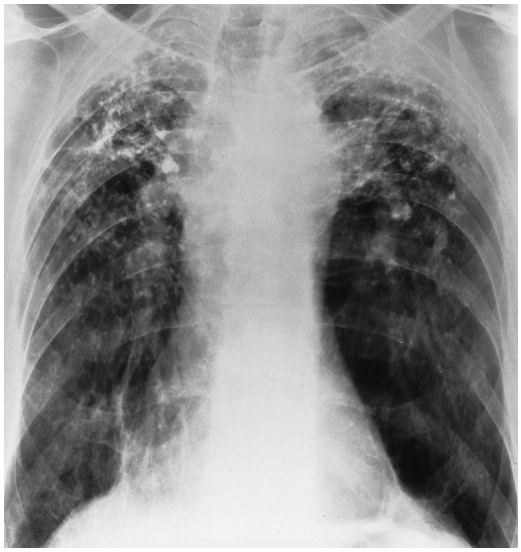

FIGURE 3-29 Secondary tuberculosis. Bilateral fibrocalcific changes at apices. Note upward retraction of hila.

Imaging appearance. Secondary tuberculosis most commonly affects the upper lobes, especially the apical and posterior segments (Figure 3-29). It is initially seen as a nonspecific, hazy, poorly marginated alveolar infiltrate that often radiates outward from the hilum.

Because of the difficulty of radiographically determining the activity of secondary tuberculosis, comparison with previous images is essential. An unchanged appearance of fibrosis and calcification on serial images usually indicates evidence of "healing" of the tuberculous process. Nevertheless, even densely calcified lesions can contain central areas of necrosis in which viable organisms can still be found even after long periods of apparent inactivity. Of course, new cavitation or an increasing amount of pulmonary infiltrate indicates active disease.

Tuberculoma

A tuberculoma is a sharply circumscribed parenchymal nodule, often containing viable tuberculosis bacilli, that can develop in either primary or secondary disease. Although the residual localized caseation may remain unchanged for a long period or permanently, a tuberculoma is potentially dangerous because it may break down at any time and lead to dissemination of the disease.

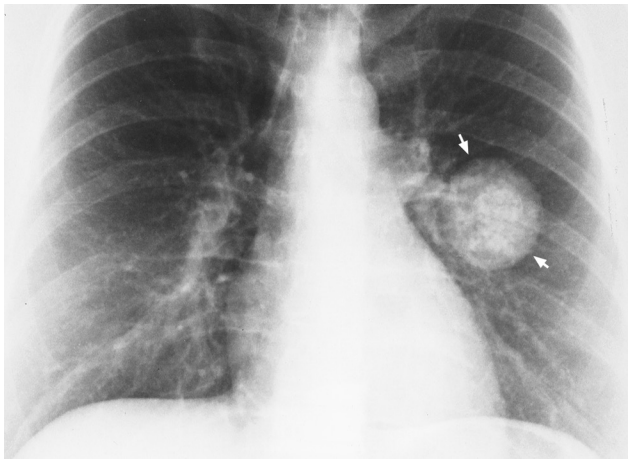

FIGURE 3-30 Calcified tuberculoma. Large soft tissue mass in left lung (*arrows*) that contains dense central calcification.

Imaging appearance. Radiographically, tuberculomas appear as single or multiple pulmonary nodules, usually 1–3 cm in diameter. They can occur in any part of the lung but are most common in the periphery and in the upper lobes. A central nidus of calcification (which may be detectable only on tomograms) is strongly suggestive of the lesion representing a tuberculoma (Figure 3-30). However, the lack of calcification is of no diagnostic value.

Treatment. Currently, two groups of patients receive therapy for tuberculosis. One consists of those who have active tuberculosis; the other is those who have been exposed to active tuberculosis and are at risk. For persons with active tuberculosis, treatment begins with a two-drug regimen to help prevent drug resistance through mutation. The most common drugs used today are isoniazid, rifampin, and pyrazinamide. The effectiveness of the treatment is evaluated regularly to be sure that the patient's strain of *M. tuberculosis* has not become resistant to the drugs of choice. The treatment may take as long as 6 to 12 months. For the second group, prophylactic treatments are determined by the strain of tuberculosis to which the person has been exposed.

Summary of Findings for Tuberculosis

Disorder	Location	Imaging Appearance	Treatment
Primary tuberculosis	Lobar or segmental	Consolidation is homogeneous, dense, and well-defined	For all active cases of tuberculosis, treatment is a two-drug regimen for 2 months or longer (isoniazid, rifampin, and pyrazinamide) For persons exposed to active tuberculosis, prophylactic treatment is suggested
	Hilar and mediastinal lymph nodes	Hilar enlargement without parenchymal involvement	
	Parenchymal, hilar, and mediastinal nodes	Demonstrates Ghon lesion	
	Pleural cavity	Pleural effusion	
Miliary tuberculosis	Throughout lungs, and possible spread to other organs	Innumerable fine discrete nodules uniformly throughout lungs	
Tuberculous pneumonia	Parenchymal and nodal	Necrotic cavities or large abscess	
Secondary tuberculosis	Upper lobes and posterior segments	Extensive fibrotic changes with possible calcification	
Tuberculoma	Any part of lung, commonly in periphery and upper lobes	Single or multiple nodules, 1–3 cm	

Pulmonary Mycosis

The term **pulmonary mycosis** means fungal infection of the lung. The two most common systemic fungal infections found in North America are histoplasmosis (endemic in the Mississippi River and Ohio River valleys) and coccidioidomycosis (seen in the southwestern United States).

Histoplasmosis

Histoplasmosis, caused by the fungus *Histoplasma capsulatum,* is a common disease that often produces a radiographic appearance simulating that of tuberculosis. The primary form of histoplasmosis is usually relatively benign and often passes unnoticed.

Histoplasmosis can incite progressive fibrosis in the mediastinum. This process can cause obstruction of the superior vena cava, pulmonary arteries, and pulmonary veins, as well as severe narrowing of the esophagus.

Diffuse calcification in the liver, spleen, and lymph nodes is virtually diagnostic of histoplasmosis, especially in areas in which the disease is endemic (e.g., the Mississippi River and Ohio River valleys). These calcifications tend to be small, multiple, dense, and discrete, although occasionally they appear as moderately large, solidly calcified granulomas.

Coccidioidomycosis

Coccidioidomycosis is caused by a fungus, *Coccidioides immitis,* which is found in the desert soil of the southwestern United States. Coccidioidomycosis can develop from an acute infection to chronic or disseminated forms. The infection is transmitted through fungal spores in the air. Immunosuppressed patients are more susceptible, and the disease may progress rapidly in those with a compromised immune system.

Acute coccidioidomycosis has few or no symptoms in most cases. The symptoms emulate those of influenza. As with histoplasmosis, people who are infected often remain undiagnosed, and the immune system builds antibodies to fight the infection. In chronic disease, the infection results in lung abscesses, which may rupture and infect the mediastinum and pleural cavity. The disease processes of the chronic and disseminated forms of coccidioidomycosis are similar to and may be indistinguishable from those of chronic histoplasmosis.

Imaging appearance. Chest radiographs may demonstrate single or multiple areas of pulmonary infiltration; these most often appear in the lower lung and are frequently associated with hilar lymph node enlargement in primary histoplasmosis. Although this pattern simulates the primary complex of tuberculosis, pleural effusion rarely occurs with histoplasmosis. In children, striking hilar adenopathy, which may cause bronchial compression, may develop without radiographic evidence of parenchymal disease. Hilar lymph node calcification commonly occurs in adults and produces a "popcorn" radiographic appearance. Pulmonary histoplasmosis frequently manifests as a solitary, sharply circumscribed, granulomatous nodule (histoplasmoma), which is usually less than 3 cm in diameter and found most often in a lower lobe. Central, rounded calcification within the mass (the target lesion) is virtually pathognomonic (characteristic) of this disease (Figure 3-31). Multiple soft tissue nodules scattered throughout both lungs may simulate miliary tuberculosis. These shadows may clear completely or may fibrose and persist, often appearing on subsequent chest radiographs as widespread punctate calcifications (Figure 3-32).

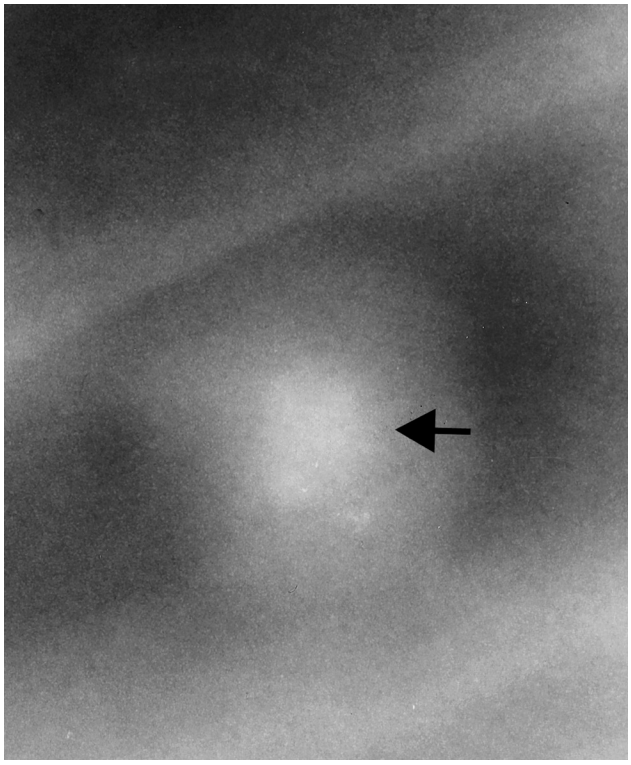

FIGURE 3-31 Histoplasmoma. Central calcification (*arrow*) in solitary pulmonary nodule.

FIGURE 3-32 Histoplasmosis. Diffuse calcifications in lungs produce snowball pattern.

Coccidioidomycosis typically produces small pulmonary consolidations in the periphery of the parenchyma that resemble those in extensive pneumonia (Figure 3-33).

Chronic histoplasmosis and advanced chronic coccidioidomycosis closely simulate the radiographic appearance

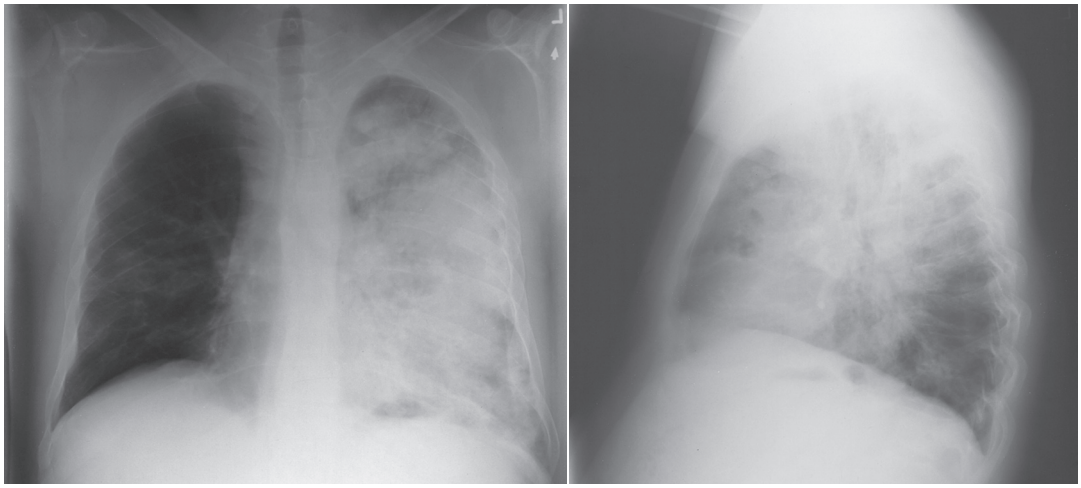

FIGURE 3-33 Coccidioidomycosis. Posteroanterior and lateral views demonstrate consolidation caused by fungus in the left lung.

Summary of Findings for Pulmonary Mycosis

Disorder	Location	Imaging Appearance	Treatment
Primary histoplasmosis	Lower lung	Pulmonary infiltration	<1% require treatment; amphotericin B
	Hilar lymph nodes	Granulomatous nodule	
		Hilar lymph node enlargement and/or calcification	Fluconazole for patients with AIDS
Chronic histoplasmosis	Upper lobe	Zones of parenchymal consolidation	<1% require treatment; amphotericin B
		Cavitation	
		Calcified granulomas	Fluconazole for patients with AIDS
Acute coccidioidomycosis	Peripheral parenchyma	Pneumonia appearance	None needed unless grave; amphotericin B
		Coccidioidoma (granuloma)	
Chronic coccidioidomycosis	Peripheral parenchyma	Lung abscesses	None needed unless grave; amphotericin B

of reinfection tuberculosis because they both commonly exhibit cavitation and are found in an upper lobe.

Treatment. Fewer than 1% of patients with primary or chronic histoplasmosis or with coccidioidomycosis require any drug treatment. Restricted activity and bed rest are encouraged. When drug treatment is required, the drug of choice is amphotericin B.

Respiratory Syncytial Virus

Respiratory syncytial virus (RSV) is estimated to affect almost all children by age 2 years (data as of 2010). Of those affected, fewer than 2% require hospitalization, according to the Centers for Disease Control and Prevention. Of all bronchiolitis cases, 80% occur as a result of a respiratory syncytial virus infection. The virus attacks the lower respiratory tract and causes necrosis of the respiratory epithelium of the bronchi and bronchioles, which leads to bronchiolitis. The necrotic material and edema from the infection cause bronchial obstruction. Bronchiolitis produces bronchial spasm, and interstitial pneumonia occurs as a result of the obstruction. The patient has only coldlike or flulike symptoms and may not be managed with the appropriate infection control procedures, causing a high rate of nosocomial infections. Fomites carry the virus through droplets from the nose or throat, and the virus has the ability to persist for many hours on surfaces. Healthcare workers in contact with an infected patient must use appropriate protective personal devices and dispose of them properly to protect themselves and others.

Imaging appearance. Hyperinflation with diffuse increased interstitial markings is the most common finding on chest images. The necrosis of the respiratory epithelium, if severe, appears radiographically as an interstitial pneumonia (Figure 3-34). In the most severe cases, focal areas of atelectasis are apparent.

Treatment. Many children do not need drug therapy and recover simply through their immune response. Those children who require hospitalization receive antibiotics for infectious complications, and they may also be given the antiviral drug ribavirin aerosol. Children may require oxygen therapy and, in the most severe cases, mechanical ventilation. Most infected adults recover without treatment.

Severe Acute Respiratory Syndrome

Severe acute respiratory syndrome (SARS) caused global concern in 2003 as a result of the 8000 cases diagnosed according to criteria of the World Health Organization. The first cases appeared in China. The SARS virus, a coronavirus of unknown etiology, may survive in the environment many days. Person-to-person or droplet contact causes upper and lower respiratory infections that begin

Summary of Findings for Viruses

Disorder	Location	Imaging Appearance	Treatment
Respiratory syncytial virus (RSV)	Bronchial epithelium	Hyperinflation with diffuse increased interstitial markings Interstitial pneumonia Severe cases demonstrate focal areas of atelectasis	No treatment needed in most cases Antibiotic and antiviral drugs (ribavirin)
Severe acute respiratory syndrome (SARS)	Throughout both lungs	Early focal infiltrates progressing to generalized patchy interstitial infiltrates	Bacterial and antiviral agents, other treatment regimens similar to those for atypical pneumonia

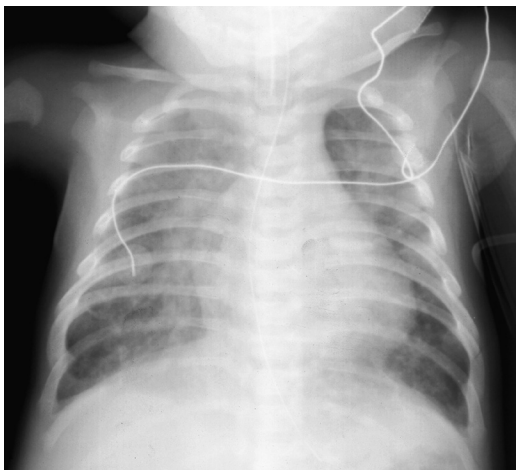

FIGURE 3-34 Respiratory syncytial virus. Bilateral fluffy pulmonary infiltrates associated with hyperinflation, the features being consistent with respiratory syncytial virus pneumonia.

with a nonproductive cough and progress to hypoxemia. Severe SARS requires intubation and mechanical ventilation and is associated with a fatality rate of approximately 3%. Other symptoms are similar to those of community-acquired atypical pneumonia. Since 2004, there has been no evidence of known transmissions of SARS.

Imaging appearance. On chest images, the lungs appear normal in the early stages of disease. As the disease progresses into the lower respiratory region, development of early focal infiltrates may progress to generalized, patchy interstitial infiltrates. Eventually, areas of consolidation may be seen.

Treatment. Most persons with SARS in whom less than 10% of the lung is infected on the seventh day survive the disease. Follow-up images play a vital role in determining whether treatment is appropriate or requires a more aggressive approach. Currently, antibacterial and antiviral agents are used to combat the disease. There is no known curative treatment, and SARS is treated the same as other atypical pneumonia.

DIFFUSE LUNG DISEASE

Chronic Obstructive Pulmonary Disease

Chronic obstructive pulmonary disease (COPD) includes several conditions in which chronic obstruction of the airways leads to an ineffective exchange of respiratory gases and makes breathing difficult. In many cases, two disease processes coexist to cause the obstructive process. **Chronic bronchitis** is characterized by excessive tracheobronchial mucus production, leading to the obstruction of small airways. *Emphysema* refers to the distention of distal air spaces as a result of the destruction of alveolar walls and the obstruction of small airways. Asthma occurs when the bronchioles go into spasm, causing decreased airflow and sometimes obstruction of the airway. Chronic dilation of the bronchi or bronchioles indicates *bronchiectasis*. Factors that predispose to COPD include cigarette smoking, infection, air pollution, and occupational exposure to harmful substances such as asbestos.

Chronic Bronchitis

Chronic inflammation of the bronchi leads to severe coughing with the production of sputum. Bronchitis may be a complication of respiratory infection or the result of long-term exposure to air pollution or cigarette smoking. Of all chronic bronchitis cases, 90% are associated with cigarette smoking. The severity of the disease and how quickly the symptoms can be relieved are directly related to the number of cigarettes smoked.

The walls of the bronchi and bronchioles thicken and produce viscous mucus. Over an extended period, the mucous glands become hyperplastic.

Imaging appearance. Approximately half of patients with chronic bronchial disease demonstrate no changes on chest radiographs. The most common radiographic abnormality in chronic bronchitis is a generalized increase in bronchovascular markings ("dirty chest"), especially in the lower lungs (Figure 3-35). Thickening of bronchial walls and peribronchial inflammation can cause parallel or slightly tapered tubular line shadows ("tram lines") or may appear as thickening of bronchial shadows when viewed end on.

Eventually, excessive production of mucus and swelling of the bronchial mucosa may lead to narrowing of the airways and overinflation of the lungs (emphysema). Chest radiographs demonstrate hyperinflated lungs and a depressed diaphragm.

Treatment. In general, the treatment for chronic bronchitis is designed to improve symptoms, decrease any reversible processes, and prevent progression of the disease. Prophylactic antibiotic therapy reduces infections. Bronchial dilators reduce spasm and open airways. Expectorants assist in keeping the lungs clear. Although currently there is no cure for chronic bronchitis, appropriate therapy can be expected to reduce severe flare-ups and minimize progression of the disease.

Emphysema

Emphysema is a crippling and debilitating condition in which obstructive and destructive changes in small airways (the acini or terminal bronchioles) lead to a dramatic increase in the volume of air in the lungs. In many patients, the development of emphysema is closely associated with heavy cigarette smoking. Other predisposing factors are chronic bronchitis, air pollution, and long-term exposure to irritants of the respiratory tract.

Irritating smoke, fumes, and pollutants injure the fine hairs (cilia) of the respiratory mucosa, which can no longer sweep away foreign particles. The result is mucosal inflammation and the secretion of excess mucus that plugs up the air passages and leads to an increase in airway resistance. Collateral air drift permits the ventilation of lung parenchyma served by the obstructed airways. Continuous bronchial narrowing and loss of elasticity, exacerbated by cigarette smoking, make it very difficult for the patient to exhale the stale air. The resulting air trapping and overinflation of the lung lead to alveolar distention and eventually to the rupture of alveolar septa. As the walls between alveoli are destroyed, these tiny air sacs become transformed into large air-filled spaces called **bullae**. With the loss of alveolar septa, the surface for gas exchange decreases, limiting the transfer of oxygen into the bloodstream. As the lungs become less efficient, the heart tries to compensate. This effort places excessive strain on the heart, which eventually enlarges. The large air sacs (bullae) may rupture, allowing air to enter into the pleural space (spontaneous pneumothorax) and cause collapse of the lung (atelectasis).

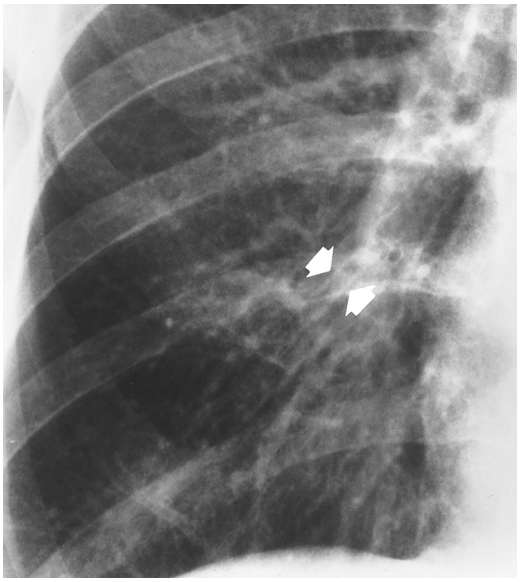

FIGURE 3-35 Chronic bronchitis. Coned view of right lower lung demonstrates an increase in coarseness in interstitial markings. *Arrows* point to characteristic parallel line shadows ("tram lines") outside the boundary of the pulmonary hilum.

Imaging appearance. The major radiographic signs of emphysema are related to pulmonary overinflation, alterations in the pulmonary vasculature, and bullae formation.

The hallmark of pulmonary overinflation is flattening of the domes of the diaphragm (Figure 3-36). Another important sign seen on lateral chest radiographs is an increase in the size and lucency of the retrosternal air space, the distance between the posterior side of the sternum and the anterior wall of the ascending aorta. The anteroposterior (AP) diameter of the chest increases and the chest becomes more barrel shaped as the disease progresses. Air trapping may be detected fluoroscopically as a decrease in the normal movement of the diaphragm during respiration.

The major vascular change in patients with emphysema is a reduction in the number and size of the peripheral arteries. As the pressure in the pulmonary arteries increases, the main and central pulmonary arteries become more prominent, further accentuating the appearance of rapid tapering of peripheral vessels.

Bullae appear as air-containing cystic spaces whose walls are usually of hairline thickness. They range in size from 1 to 2 cm in diameter up to an entire hemithorax (Figure 3-37). These large, radiolucent, air-filled sacs are found predominantly at the apices or at the bases and may become so large that they cause respiratory insufficiency by compressing the remaining relatively normal lung.

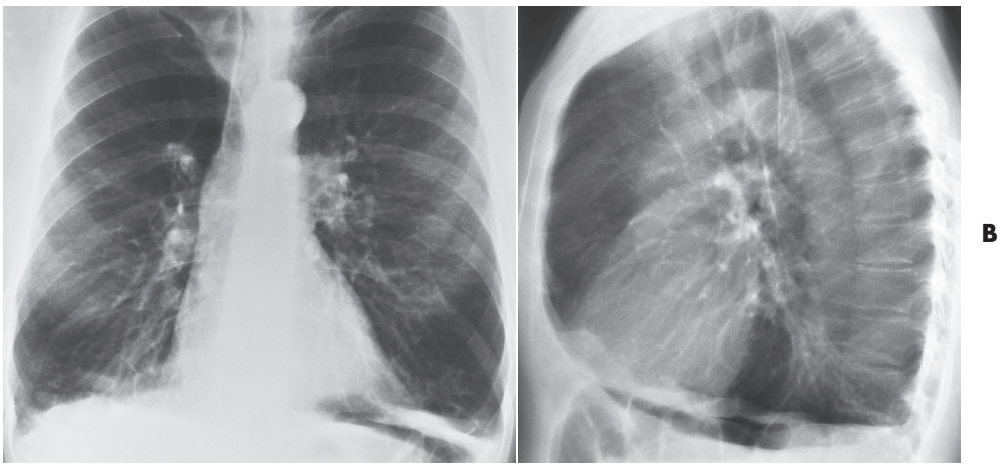

FIGURE 3-36 Emphysema. Frontal (A) and lateral (B) projections of the chest demonstrate severe overinflation of lungs along with flattening and even a superiorly concave configuration of the hemidiaphragms. Also, the size and lucency of the retrosternal air space are increased, the AP diameter of the chest is increased, and the number and caliber of peripheral pulmonary arteries are reduced.

A less common radiographic appearance of emphysema is the increased markings pattern. Instead of being narrowed, the vascular markings in this condition are more prominent than normal and tend to be irregular and indistinct, producing a "dirty chest" appearance.

Emphysema occasionally occurs in young patients who have hereditary disorders of connective tissue (osteogenesis imperfecta). Striking lower lobe predominance develops in young patients who have a deficiency of the enzyme α-antitrypsin, which leads to destruction of elastic and connective tissue in the lungs.

When patients have advanced stages of pulmonary emphysema and have large amounts of air trapped in their lungs (more radiolucent), the radiographer should reduce exposure factors for chest radiography. CT demonstrates large blebs and destruction of the lung parenchyma, and it can detect any spontaneous pneumothorax (Figure 3-38).

FIGURE 3-37 Giant emphysematous bulla. Air-containing mass fills most of the left hemithorax.

FIGURE 3-38 Emphysematous blebs. CT scan shows the destruction of lung parenchyma.

Treatment. Currently, there is no cure for emphysema. Treatment assists only in relieving symptoms and in preventing progressive destruction by the disease.

Asthma

Asthma is a very common disease in which widespread narrowing of the airways develops because of an increased responsiveness of the tracheobronchial tree to various stimuli (allergens). Common allergens are house dust, pollen, molds, animal dander, certain fabrics, and various foods (**extrinsic asthma**). Exercise, heat or cold exposure, and emotional upset can also cause an asthma attack (**intrinsic asthma**). The hypersensitivity reaction to one or more of these allergens leads to swelling of the mucous membranes of the bronchi, excess secretion of mucus, and spasm of the smooth muscle in the bronchial walls, all of which lead to severe narrowing of the airways. This makes breathing (especially expiration) difficult and results in the characteristic wheezing sound that is produced by air passing through the narrowed bronchial tubes. Untreated or uncontrolled asthma permanently scars the bronchial structure, causing progressive disease.

Imaging appearance. Early in the course of the disease, chest radiographs obtained between acute episodes demonstrate no abnormalities. During an acute asthmatic attack, bronchial narrowing and difficulty in expiration lead to an increased volume of the hyperlucent lungs with flattening of the hemidiaphragms and an increase in the retrosternal air space. In asthma, unlike in emphysema, the pulmonary vascular markings remain normal. In patients with chronic asthma, especially those with a history of repeated episodes of superinfection, thickening of bronchial walls can produce prominence of interstitial markings and the "dirty chest" appearance (Figure 3-39). The results of the chest radiograph

FIGURE 3-39 Asthma. Recurrent pulmonary infections have led to the development of diffuse pulmonary fibrosis and prominence of interstitial markings in lungs.

FIGURE 3-40 Chronic bronchiectasis. Severe coarsening of interstitial markings involves the bases and right upper lobe. Oval and circular cystic spaces, which produce a honeycomb-like pattern, are best seen in the right upper lobe.

taken in the emergency room determine whether the asthma has progressed to pneumonia.

Treatment. Patients with allergy-induced asthma can use preventive and rescue (β_2 stimulants) bronchodilators. Allergy shots may build up natural antibodies. Asthmatics with exercise-induced problems may take oral medication to decrease bronchiomuscular spasm in addition to preventive and rescue bronchodilators. Keeping airways open helps prevent infections, to which asthmatic patients are prone. New inhaled steroid drugs help control the inflammatory process and decrease the potential for development of pulmonary infection.

Bronchiectasis

Bronchiectasis refers to permanent abnormal dilation of one or more large bronchi as a result of destruction of the elastic and muscular components of the bronchial wall. Bronchitis, a destructive process, is a common complication of bronchiectasis and is nearly always the result of a bacterial infection. The infection may be either a severe necrotizing pneumonia or a result of a local or systemic abnormality that impairs the body's defense mechanisms and promotes bacterial growth. Since the advent of antibiotic therapy and vaccines, the incidence of bronchiectasis has substantially decreased.

The patient with bronchiectasis typically has a chronic productive cough, often associated with recurrent episodes of acute pneumonia and hemoptysis. The disease usually involves the basal segments of the lower lobes, and it is bilateral in approximately half the cases. Pulmonary function tests assist in the diagnostic process by detecting any evidence of decreased gas exchange.

Imaging appearance. Plain chest radiographs may show coarseness and loss of definition of interstitial markings caused by peribronchial fibrosis and retained secretions (Figure 3-40). In more advanced disease, oval or circular cystic spaces can develop. These cystic dilations can be up to 2 cm in diameter and often contain air–fluid levels. In very severe cases, coarse interstitial fibrosis surrounding local areas of dilation can produce a honeycomb pattern.

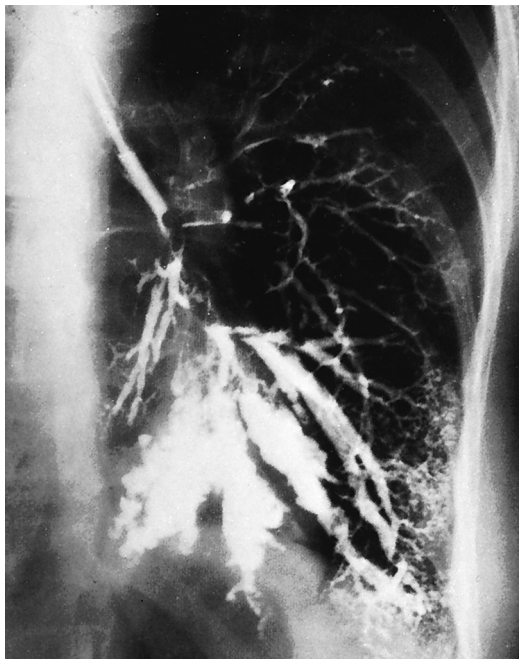

FIGURE 3-41 Chronic bronchiectasis. Bronchogram shows severe dilation of the basal bronchi of the left lower lobe.

Although plain radiographs may strongly indicate bronchiectasis, bronchography is necessary to fill the dilated cystic spaces with contrast material and to establish the diagnosis unequivocally (Figure 3-41).

Treatment. Vaccines prevent many of the bacterial and viral infections that led to bronchiectasis in the past. Treatment of bronchiectasis consists of therapy to decrease the symptoms and an antibiotic chosen on the basis of the specific bacterial cause.

Sarcoidosis

Sarcoidosis is a multisystem granulomatous disease of unknown cause that is most often detected in young adults. Women are affected slightly more often than men, and the disease is far more prevalent among African Americans than among whites. Histopathologic findings include multiple epithelioid granulomas.

Imaging appearance. Approximately 90% of patients with sarcoidosis have radiographic evidence of thoracic involvement. Indeed, in most cases, the presence of the disease is first identified on a screening chest radiograph of an asymptomatic individual.

Bilateral, symmetric hilar lymph node enlargement, with or without diffuse parenchymal disease, is the classic radiographic abnormality in sarcoidosis. Usually, enlargement of the right paratracheal nodes occurs, producing the typical 1-2-3 pattern (Figure 3-42). Conventional tomography frequently reveals additional enlargement of the left paratracheal nodes, which usually cannot be seen on routine frontal radiographs because they are obscured by the superimposed aorta and brachiocephalic vessels. Unilateral hilar enlargement, which is a common manifestation of primary tuberculosis or

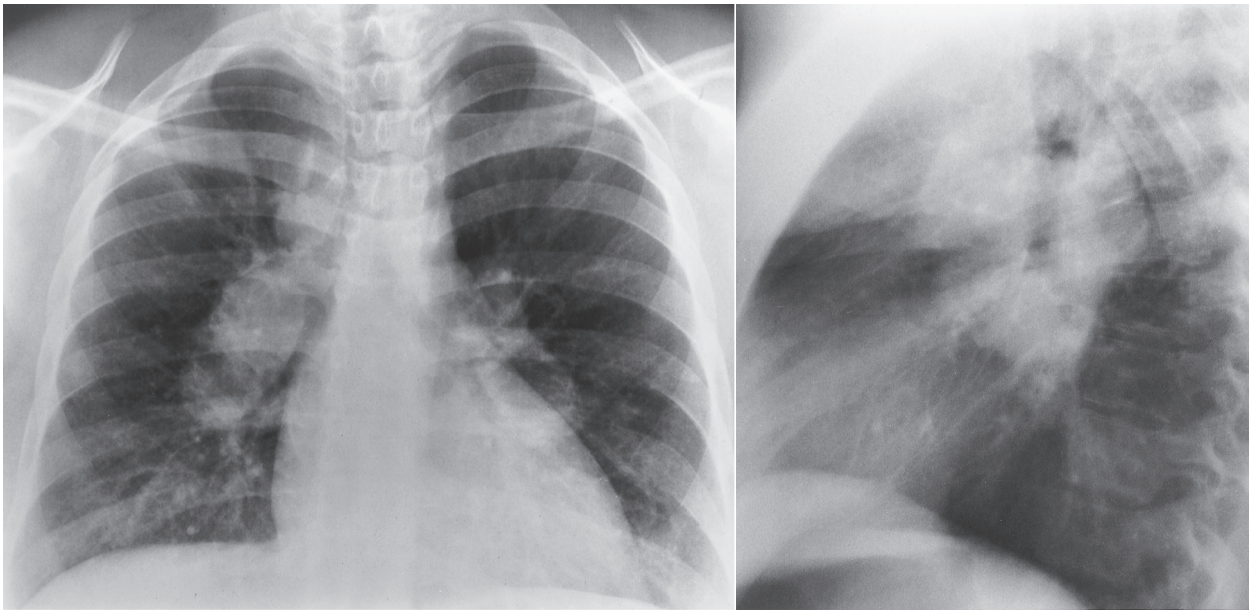

FIGURE 3-42 Sarcoidosis. Frontal (A) and lateral (B) projections of the chest demonstrate enlargement of the right hilar, left hilar, and right paratracheal lymph nodes, producing the classic 1-2-3 pattern of adenopathy.

FIGURE 3-43 Sarcoidosis. Diffuse coarse interstitial pattern.

FIGURE 3-44 Sarcoidosis. Multiple osteolytic lesions throughout the phalanges produce the typical punched-out appearance. The apparent air density in the soft tissues is a photographic artifact.

lymphoma, is rare in sarcoidosis. High-resolution CT (HRCT) is more sensitive than chest radiographs for detecting subtle lymphadenopathy and parenchymal disease (ground-glass attenuation). The anterior mediastinal and left paratracheal nodes, which are obscured on the chest radiograph, are well visualized on HRCT.

Diffuse pulmonary disease develops in most patients with sarcoidosis. Although hilar and mediastinal lymph nodes are often involved, there tends to be an inverse relationship between the degree of lymphadenopathy and the extent of parenchymal disease, with the latter increasing while the adenopathy regresses. The most common appearance is a diffuse interstitial pattern that is widely distributed throughout both lungs (Figure 3-43). An alveolar pattern appears as ill-defined densities that may be discrete or may coalesce into large areas of consolidation. This pattern resembles an acute inflammatory process and may contain an air bronchogram. Infrequently, large, dense, round lesions may simulate metastatic malignancy.

The skeletal lesions in sarcoidosis involve primarily the small bones of the hands and feet. Granulomatous infiltration can cause destruction of the fine trabeculae, producing a mottled to lacelike, coarsely trabeculated pattern. Lytic destruction can produce sharply circumscribed, punched-out areas of lucency (Figure 3-44). Approximately 10% of

Summary of Findings for Diffuse Lung Disease

Disorder	Location	Imaging Appearance	Treatment
Chronic bronchitis	Bronchi/bronchioles Mucous gland hyperplasia	No image change in 50% Increased bronchovascular markings Hyperinflation and depressed diaphragm	Prophylactic antibiotics Bronchial dilators Expectorants No cure
Emphysema	Destroyed alveolar septa	Pulmonary hyperinflation Bulla formation Flattened diaphragm Radiolucent retrosternal space	Treatment for symptoms No cure
Asthma	Bronchi	No evidence unless during acute attack Bronchial narrowing/hyperlucent lungs Radiographic appearance Excludes other processes	Preventive and rescue bronchial dilators
Bronchiectasis	Basal segments of lower lobes	Coarseness and decreased interstitial markings	Vaccines or antibiotic drugs
Advanced bronchiectasis	Basal segments of lower lobes	Oval/circular cystic spaces	Bronchodilator to increase pulmonary function
Sarcoidosis	Nonspecific or unknown cause of multisystem granulomatous disease	Chest radiography—bilateral hilar lymph node enlargement with or without diffuse parenchymal disease High-resolution CT—demonstrates subtle lymphadenopathy in the anterior mediastinal and left paratracheal nodes and parenchymal disease as ground-glass attenuation	No treatment if spontaneous recovery occurs Steroid therapy

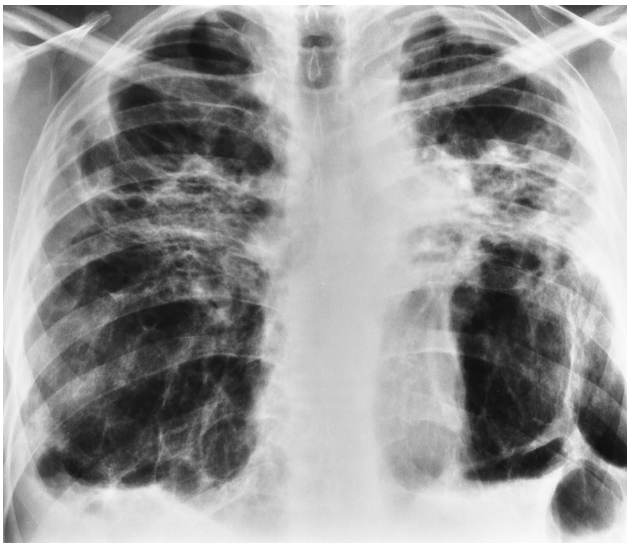

FIGURE 3-45 Sarcoidosis. In end-stage disease, there is severe fibrous scarring, bleb formation, and emphysema.

patients with sarcoidosis have elevated serum calcium values, which may lead to nephrocalcinosis. Sarcoid involvement of the stomach can produce discrete masses or generalized luminal narrowing that predominantly involves the antrum.

Treatment. Although the pulmonary lesions usually regress spontaneously or after steroid therapy, irreversible pulmonary changes develop in up to 20% of cases. Coarse scarring is seen as irregular linear strands extending outward from the hilum toward the periphery, often associated with bulla formation (Figure 3-45). Severe fibrosis and emphysema can cause pulmonary hypertension and right-sided heart failure.

Pneumoconiosis

Prolonged occupational exposure to certain irritating particulates can cause severe pulmonary disease and a spectrum of radiographic findings. Inhaled foreign substances retained permanently in the acini cause irreversible damage. These inhaled particles cause a chronic interstitial inflammation that leads to pulmonary fibrosis and a diffuse nonspecific radiographic pattern of linear streaks and nodules throughout the lungs. The inflammation initially causes injury to the mucosal lining; long-term exposure may injure the pulmonary parenchyma and even lead to the development of a malignant neoplasm. The severity of the pneumoconiosis depends on the size of the particles, the length of exposure, and the concentration of particulates in the atmosphere (type of exposure). The more severe the exposure, the more fibrotic the lung becomes and the greater the resultant shortness of breath. The most common of the pneumoconioses are silicosis, asbestosis, and anthracosis (coal worker's disease). Other causes include exposure to such dusts as tin, iron oxide, barium, and beryllium. As many as 40 minerals cause lung lesions when inhaled, although most do not produce morphologic or functional abnormalities.

Silicosis

Silicosis is the most common and best known work-related lung disease. The inhalation of high concentrations of silicon dioxide (crystalline silica) primarily affects workers engaged in mining, foundry work, and sandblasting. Quartz dust, the most frequent cause of inhalation silicosis, is the second most common element in the earth's crust. The lung reacts to the silica by producing a fibroblast-stimulating factor that results in extensive fibrosis. Acute silicosis can develop within

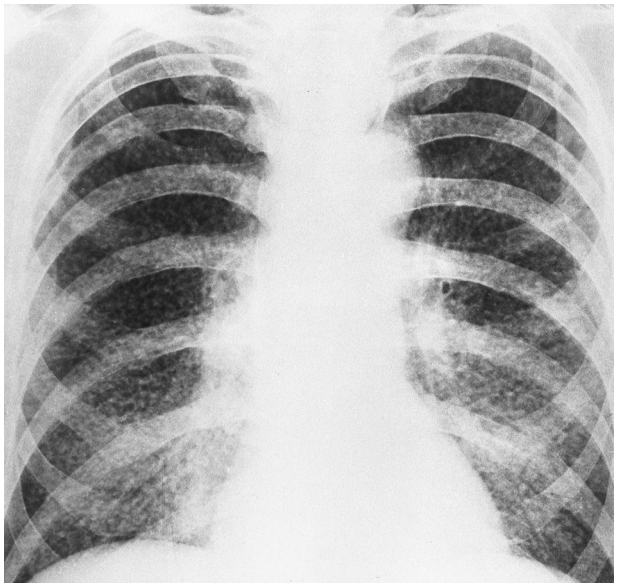

FIGURE 3-46 Silicosis. Calcification in miliary nodules is scattered throughout both lungs.

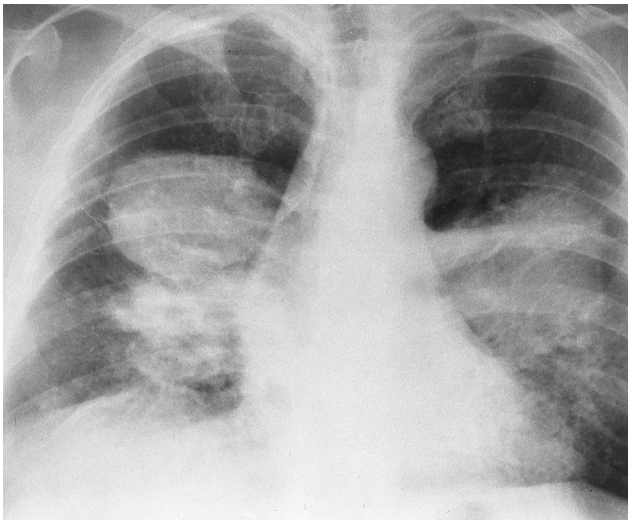

FIGURE 3-47 Progressive massive fibrosis in silicosis. Large, irregular nodules can be seen in both perihilar regions.

10 months of exposure in workers exposed to sandblasting in confined spaces. Most radiographic changes are the result of 15 to 20 years of long-term, less intense exposure. As the disease progresses, death occurs as a result of lung or heart failure.

Imaging appearance. The classic radiographic pattern in silicosis consists of multiple nodular shadows scattered throughout the lungs. These nodules, usually fairly well circumscribed and of uniform density, may become calcified (Figure 3-46). As the pulmonary nodules increase in size, they tend to coalesce and form conglomerates of irregular masses in excess of 1 cm in diameter (progressive massive fibrosis) (Figure 3-47). These masses are usually bilateral and relatively symmetric, and they almost always occur in the upper lobes or segments of the lungs. Occasionally, a single large homogeneous mass in the perihilar area of one lung may closely simulate bronchogenic carcinoma. Hilar lymph node enlargement is common. The deposition of calcium salts in the periphery of enlarged lymph nodes produces the characteristic eggshell appearance (Figure 3-48), which is virtually pathognomonic of silicosis.

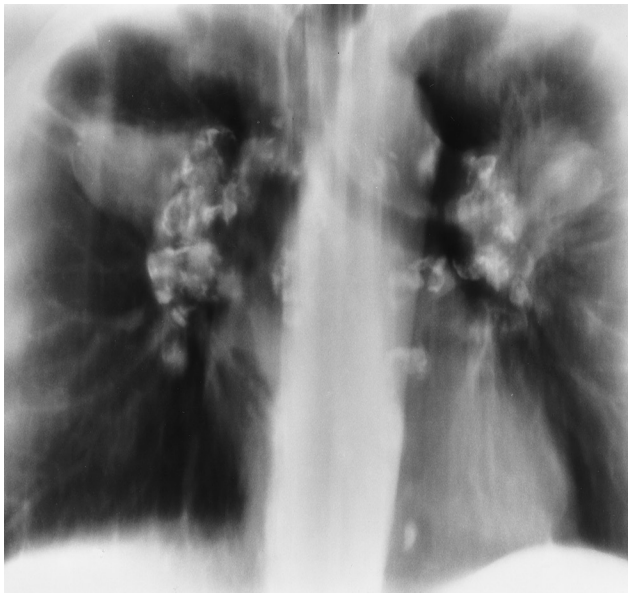

FIGURE 3-48 Silicosis. Chest tomogram demonstrates the characteristic eggshell lymph node calcification associated with bilateral perihilar masses.

Asbestosis

Asbestosis may develop in improperly protected workers engaged in manufacturing asbestos products, in handling building materials, or in working with insulation composed of asbestos. In the 1980s, many public buildings with fireproof plasterboard and ceiling panels containing asbestos, such as schools, were reconstructed, and the asbestos was removed to prevent excessive public exposure to this particulate. Asbestos particles occur as long, thin fibers that cause little dust but produce major fibrosis in the lung. The disease manifests as alveolitis, with asbestos deposits at the bifurcation of the alveolar ducts. These deposits activate the fibrogenic and growth factors, resulting in extensive fibrosis. The major complication of asbestosis is mesothelioma, a highly malignant pleural tumor.

Imaging appearance. The radiographic hallmark of asbestosis is involvement of the pleura. Initially, pleural thickening appears as linear plaques of opacification, which are most often along the lower chest wall and diaphragm. Calcification of the pleural plaques is virtually pathognomonic of asbestosis, especially when the calcified plaques appear in the form of thin, curvilinear densities conforming to the upper surfaces of the diaphragm bilaterally (Figure 3-49). This pleural calcification generally does not develop until at least 20 years after the first exposure to asbestos (Figure 3-50). HRCT best demonstrates the developing pleural plaques.

In the lungs, round or irregular opacities produce a combined linear and nodular pattern that may obscure the heart border, producing the so-called shaggy heart. Pleural mesothelioma appears as an irregular scalloped or nodular density within the pleural space. It is frequently associated with a large pleural effusion that may obscure the underlying tumor. CT demonstrates the precise tumor involvement of

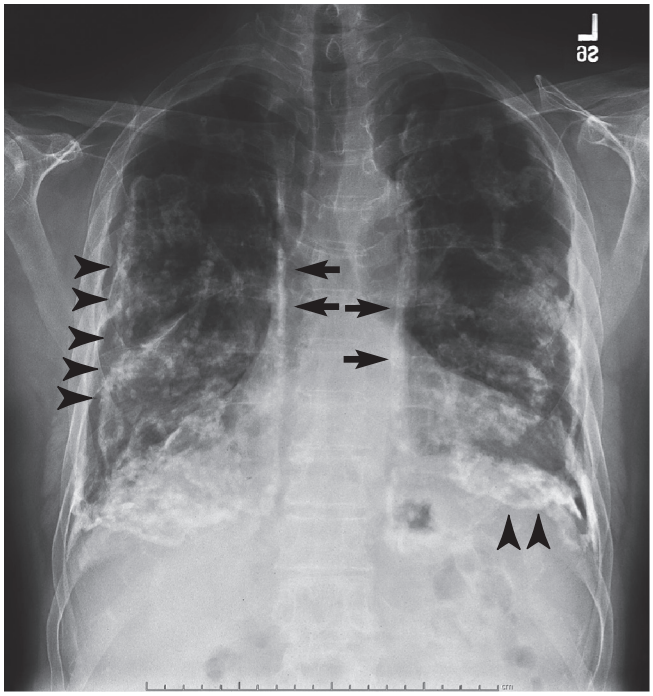

FIGURE 3-49 Asbestosis. PA image shows en face pleural calcifications on right (*horizontal arrowheads*), linear calcifications in profile in mediastinal reflection of pleura on right and on left (*horizontal arrows*), and linear calcification in left diaphragmatic pleura (*vertical arrowheads*).

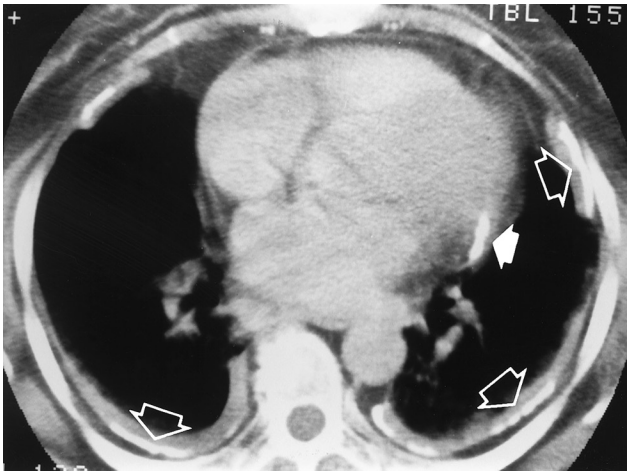

FIGURE 3-50 Asbestosis. CT scan shows calcified pleural plaques along lateral and posterior chest wall (*open arrows*) and adjacent to heart (*solid arrow*).

the lung tissue. In addition to mesothelioma, bronchogenic carcinoma is unusually common in patients with asbestosis, especially those who are cigarette smokers.

Anthracosis (Coal Worker's Pneumoconiosis)

Coal miners, especially those working with anthracite (hard coal), have increased susceptibility to development of pneumoconiosis from inhalation of high concentrations of coal dust. Anthracite collects in the walls of the respiratory bronchioles, causing weakened musculature and dilation. The deposition of anthracite particles changes the lung tissue to a dark color, leading to the name "black lung."

Imaging appearance. Initially, multiple small, irregular opacities produce a reticular pattern similar to that of silicosis (Figure 3-51). However, the nodules tend to be somewhat less well-defined than those of silicosis, and they tend to have a granular density unlike the homogeneous density of silicosis nodules. With advanced disease, the pattern of progressive massive fibrosis can develop. In progressive massive fibrosis, one or more masses of fibrous tissue with smooth, well-defined lateral borders gradually migrate toward the hilum, leaving a zone of hyperinflated emphysematous lung between the fibrous mass and the chest wall. A single large homogeneous mass in the perihilar area of one lung may simulate bronchogenic carcinoma; an occupational history is necessary to make the proper diagnosis of pneumoconiosis.

Treatment. Today, there is no effective treatment for pneumoconiosis. Once the particles have embedded in the pulmonary tissue, the lungs deteriorate and lose the ability to remove them. The best available treatment is simply to avoid further exposure. Breathing clean air may assist in halting progression of the disease and reducing the severity of the symptoms. Treatment is limited to addressing complications of the disease. Patients who progress from asbestosis to mesothelioma may require lung resection to remove the cancerous tissue, radiation therapy to shrink the tumor, or chemotherapy.

Summary of Findings for Pneumoconiosis

Disorder	Location	Imaging Appearance	Treatment
Silicosis	Most often upper lobes Lung parenchyma	Multiple, well-defined, scattered nodules of uniform density	For all cases of pneumoconiosis:
Asbestosis	Pleural lining	Pleural thickening with calcified plaques	Prevent further exposure
Anthracosis	Throughout lungs	Multiple less well-defined nodules of granular density	Breathe clean air Treat complications

NEOPLASMS

Solitary Pulmonary Nodule

The asymptomatic solitary pulmonary nodule seen as an incidental finding on a screening chest radiograph poses a diagnostic dilemma because it could represent a benign granuloma or neoplastic process, a primary bronchogenic carcinoma, or a solitary metastasis. In persons younger than 30 years, a small, round, sharply defined solitary pulmonary nodule is associated with a minimal risk of cancer (<1%). However, this risk increases to approximately 15% in individuals between ages 30 and 45 years and to approximately 50% in those older than 50 years.

Imaging appearance. The presence of central dense or popcorn calcification is diagnostic of a benign process, and a low-kVp technique may be required to demonstrate the calcification to best advantage (Figure 3-52).

FIGURE 3-51 Coal worker's pneumoconiosis. Diffuse reticular pattern throughout both lungs is associated with ill-defined masses of fibrous tissue in the perihilar region that extend to the right base.

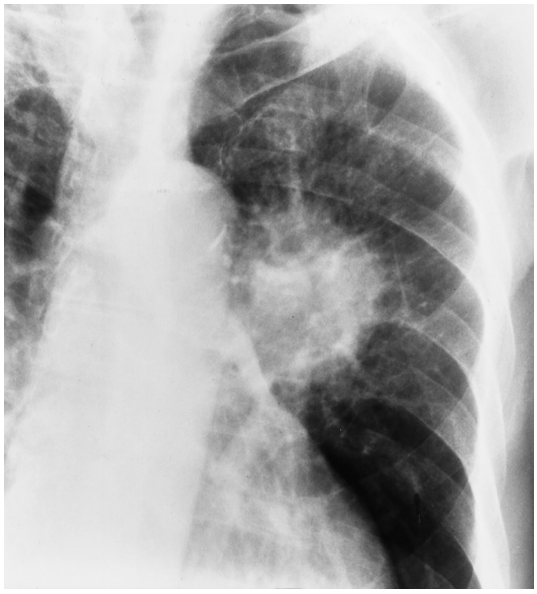

FIGURE 3-53 Malignant solitary pulmonary nodule (bronchogenic carcinoma). Note fuzzy, ill-defined (spiculated) margins.

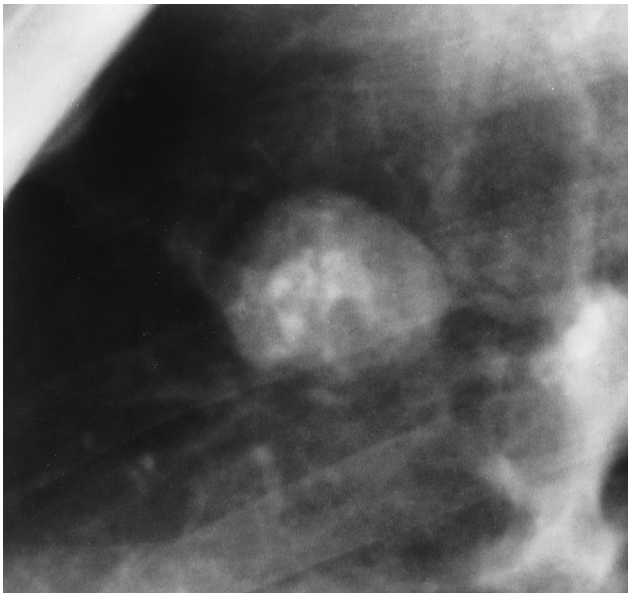

FIGURE 3-52 Benign solitary pulmonary nodule (tuberculoma). Note central calcification characteristic of this benign lesion (smooth surface).

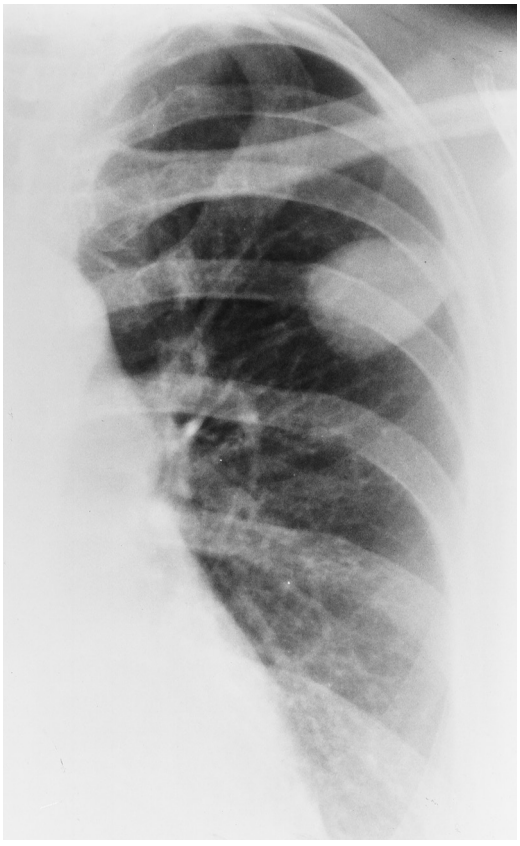

FIGURE 3-54 Benign solitary pulmonary nodule (tuberculoma). Note sharp, well-defined borders of this left upper lobe mass.

Another characteristic of a benign tumor is the absence of growth of the lesion on serial chest images over 2 years (therefore, comparison images must be eagerly sought).

A CT scan can demonstrate the size, density, position, and borders of the lesion, all of which help determine the diagnosis. Although malignant tumors generally have ill-defined, irregular, or fuzzy borders (Figure 3-53) in contrast to the sharp margins of benign lesions (Figure 3-54), there are many exceptions to this rule. CT may best differentiate the smooth, sharp margins of a benign tumor (Figure 3-55) from the spiculated, ill-defined contour of a malignant nodule (Figure 3-56). The growth rate (or doubling time) of a solitary pulmonary nodule has been used to determine the likelihood of its being malignant. A pulmonary nodule that doubles in volume in less than 1 month or more than 18 months is usually benign. However, the overlapping of growth rates of benign and malignant

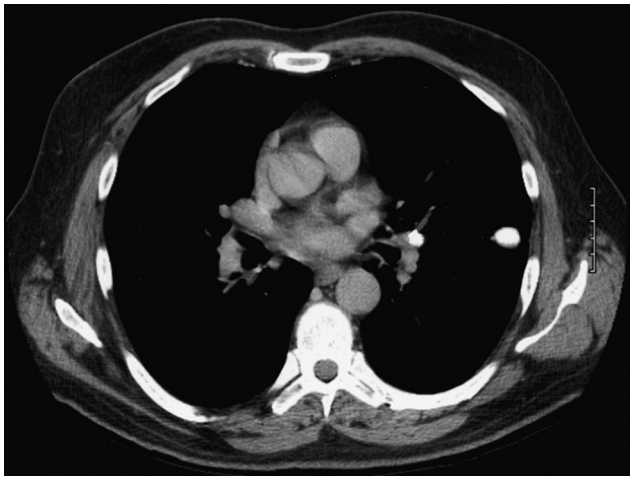

FIGURE 3-55 Benign solitary pulmonary nodule (granuloma). CT scan demonstrates a discrete homogeneous lobulated mass in the left lung periphery.

FIGURE 3-56 Malignant solitary pulmonary nodule (adenocarcinoma). CT scan demonstrates spiculated mass with ill-defined contour.

lesions, particularly among rapidly growing nodules, makes the use of doubling time unreliable as an absolute indicator of malignancy. In the patient older than 35 to 40 years, a solitary pulmonary nodule should be resected unless it can be unequivocally demonstrated to be benign. If the diagnosis is equivocal, CT is required. This modality may demonstrate additional nodules not visible on plain chest radiography (suggesting metastases) or may detect hilar or mediastinal metastases (indicating a malignant process). Positron emission tomography (PET) may be employed to show increased metabolic activity of the lesion suggestive of malignancy (Figure 3-57). At times, percutaneous fine-needle aspiration biopsy (FNAB) may be required to provide a definitive diagnosis (Figure 3-58).

Bronchial Adenoma

Bronchial adenomas are neoplasms of low-grade malignancy that constitute approximately 1% of all bronchial neoplasms. They are equally common in men and women. Bronchial adenomas appear in a younger age group than bronchogenic carcinoma. Hemoptysis and recurring pneumonia are the most common symptoms. They arise in the same glandular structures in the bronchi in which malignant neoplasms develop.

Imaging appearance. Approximately 80% of bronchial adenomas occur centrally in major or segmental bronchi and cause obstruction. The most common radiographic findings are peripheral atelectasis and pneumonitis due to bronchial obstruction. This obstruction characteristically produces a homogeneous increase in density corresponding exactly to a lobe or one or more segments, usually with a substantial loss of volume. If large enough, a central bronchial adenoma causing peripheral atelectasis and pneumonia may be identifiable as a discrete, lobulated, soft tissue mass. A tumor too small to obstruct the lumen may not be detectable on the chest radiograph. Tomography may demonstrate the rounded tumor mass within an air-filled bronchus. Peripheral bronchial adenomas do not cause bronchial obstruction and appear as nonspecific solitary pulmonary nodules (Figure 3-59).

Bronchogenic Carcinoma

Primary carcinoma of the lung arises from the mucosa of the bronchial tree. The most common primary malignant lung neoplasm is **bronchogenic carcinoma**. Although its precise cause remains unknown, bronchogenic carcinoma has been closely linked to smoking and to the inhalation of cancer-causing agents (carcinogens), such as air pollution, exhaust gases, and industrial fumes. A major form of bronchogenic carcinoma is the solitary pulmonary nodule within the lung parenchyma.

The most common type of lung cancer is **squamous carcinoma**, which typically arises in the major central bronchi and causes gradual narrowing of the bronchial lumen. **Adenocarcinomas** usually arise in the periphery of the lung rather than in the larger central bronchi. The least common type of lung tumor is **bronchiolar (alveolar cell) carcinoma**. Non–small cell lung cancers (i.e., the three types of lung cancer just listed) make up 80% of all lung cancers. **Small cell (oat cell) carcinomas** characteristically cause bulky enlargement of hilar lymph nodes, often bilaterally, and are responsible for the remaining 20% of primary pulmonary malignancies.

Although bronchogenic carcinoma may be diagnosed through detection of cancer cells in the sputum, a precise diagnosis usually requires biopsy of the tumor during bronchoscopy (i.e., direct visualization of the tracheobronchial tree using a tube inserted through the nose) or a needle biopsy performed in the radiology department under CT or fluoroscopic guidance.

Imaging appearance. Bronchogenic carcinoma produces a broad spectrum of radiographic abnormalities that depend on the site of the tumor and its relationship to the bronchial tree. The tumor may appear as a discrete mass, or it may be undetectable and identified only by virtue of secondary changes resulting from an obstruction caused by the tumor within or compressing the bronchus.

Airway obstruction by bronchogenic carcinoma may cause atelectasis of a segment of lung and often leads to pneumonia that develops in the lung distal to the obstructed bronchus.

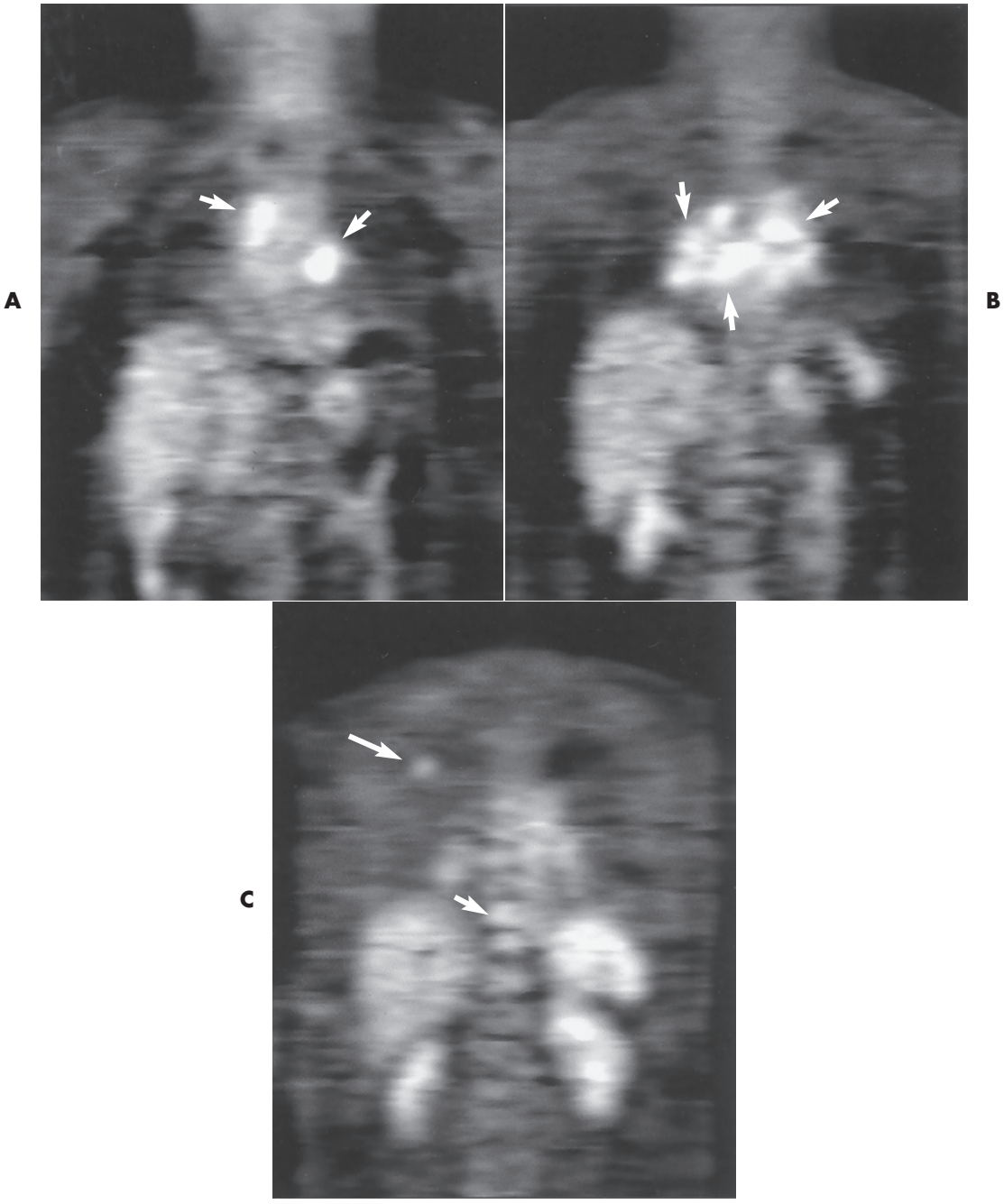

FIGURE 3-57 Pulmonary metastases. Images from PET with fluorodeoxyglucose reveal foci demonstrating metastases. **(A)** Intense radionuclide-labeled foci in each perihilar region. **(B)** The posterior mediastinal focus was identified in conjunction with additional bilateral perihilar radionuclide-labeled foci. **(C)** The thoracic vertebral radionuclide-labeled foci (*short arrow*) were identified in conjunction with a posterior right upper lobe focus (*long arrow*) that demonstrated a positive finding. PET confirmed the presence of metastasis; the patient was referred to the medical oncologist for consideration of chemotherapy.

An important radiographic sign differentiating this postobstructive pneumonia from simple inflammatory disease is the absence of an air bronchogram in the former. The air bronchogram can be detected only if there is an open airway leading to the area of consolidation.

Unilateral enlargement of the hilum, best appreciated on serial chest radiographs, may be the earliest sign of bronchogenic carcinoma. The enlarged hilum represents either a primary carcinoma arising in the major hilar bronchus or metastases to enlarged pulmonary lymph nodes from a small primary lesion elsewhere in the lung (Figure 3-60). CT is far superior to plain radiographs in detecting hilar and mediastinal lymphadenopathy and bronchial narrowing resulting from bronchogenic carcinoma.

Cavitation commonly occurs in bronchogenic carcinoma. It most often involves upper lung lesions and represents

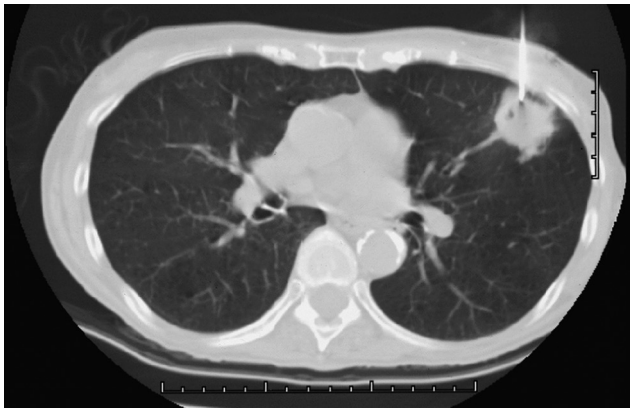

FIGURE 3-58 CT-guided FNAB of peripheral lung nodule in left lower lobe. CT scan demonstrates the needle position. Cells were sent for cytologic testing, and the results indicated infiltrating, poorly differentiated adenocarcinoma.

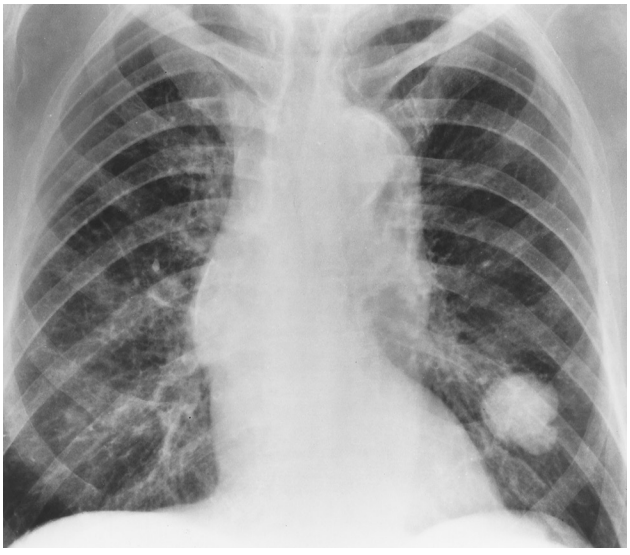

FIGURE 3-59 Peripheral bronchial adenoma. Nonspecific solitary pulmonary nodule at the left base.

central necrosis of the neoplasm. The cavities usually resemble acute lung abscesses and have thick walls with irregular, often nodular, inner surfaces (Figure 3-61).

Bronchiolar (alveolar cell) carcinoma has a spectrum of appearances, which can vary from a well-circumscribed, peripheral solitary nodule to a poorly defined mass simulating pneumonia or multiple nodules scattered throughout both lungs.

Treatment of Pulmonary Neoplastic Diseases

For **bronchial adenomas**, the most common treatment involves surgical resection of the lobe.

The prognosis for bronchogenic carcinoma is poor, except when the tumor is in the form of a solitary pulmonary nodule that can be surgically removed. Direct lymphatic spread of a tumor can cause enlargement of hilar or mediastinal lymph nodes (Figure 3-62). Distant metastases most frequently involve the bones, where they cause osteolytic destruction. Metastases to the liver, brain, and adrenal glands commonly develop.

FIGURE 3-60 Bronchogenic carcinoma. Tomography demonstrates bilateral bulky hilar adenopathy typical of oat cell carcinoma.

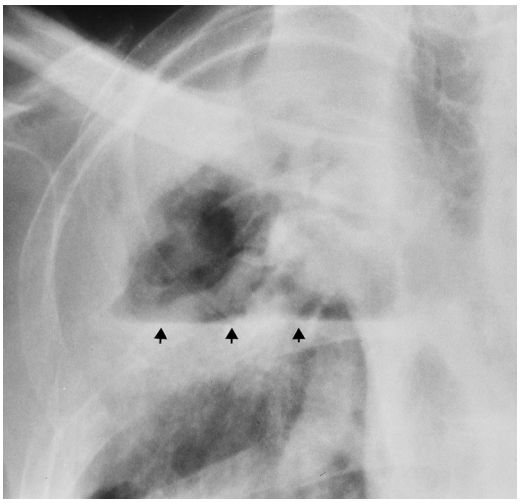

FIGURE 3-61 Bronchogenic carcinoma. Large cavitary right upper lobe mass with air–fluid level (*arrows*) and associated rib destruction.

Squamous carcinoma, adenocarcinoma, and **bronchioalveolar carcinoma** grow more slowly than small cell carcinomas. Surgical resection has a cure rate of approximately 10%. Radiation therapy (which has a low cure rate) and chemotherapy are generally used for palliative treatment.

Pulmonary Metastases

Up to one-third of patients with cancer develop pulmonary metastases; in approximately half of these patients, the only demonstrable metastases are confined to the lungs. Pulmonary metastases may develop from hematogenous or lymphatic spread, most commonly from musculoskeletal sarcomas, myeloma, and carcinomas of the breast, urogenital tract, thyroid, and colon. Carcinomas of the breast, esophagus, or stomach may directly extend to involve the lungs because of anatomic proximity.

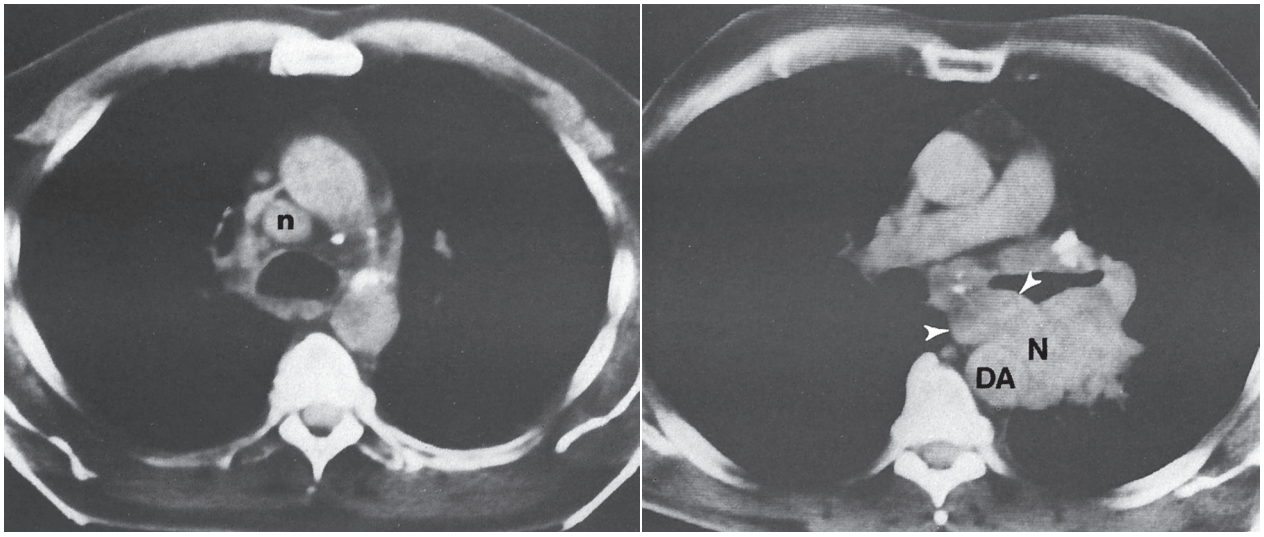

FIGURE 3-62 Spread of bronchogenic carcinoma to mediastinum. **(A)** CT scan shows enlarged lymph node (*n*) in pretracheal region, a finding consistent with the diagnosis of unresectable mediastinal spread. **(B)** In another patient, CT scan shows obliteration of fat plane around descending aorta (*DA*) by adjacent neoplasm (*N*). In addition, tumor extends deep into the mediastinum *(arrowheads)* behind the left mainstem bronchus and in front of the descending aorta.

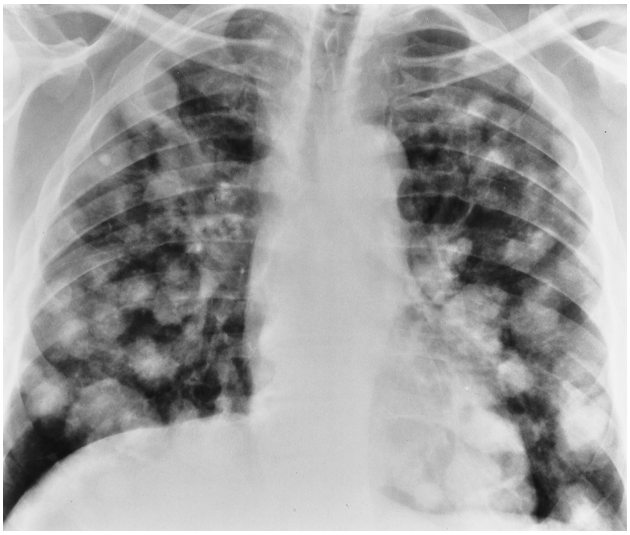

FIGURE 3-63 Hematogenous metastases. Multiple, well-circumscribed nodules scattered diffusely throughout both lungs.

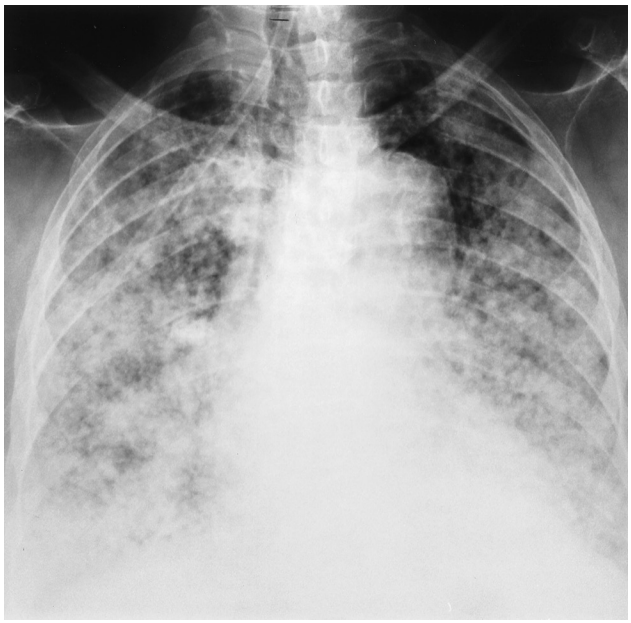

FIGURE 3-64 Metastatic thyroid carcinoma. Multiple fine miliary nodules throughout both lungs.

Primary lung lesions may metastasize by spread through the bronchial tree.

Imaging appearance. Hematogenous metastases typically appear radiographically as multiple, relatively well-circumscribed, round or oval nodules throughout the lungs (Figure 3-63). The pattern may vary from fine miliary nodules (Figure 3-64) produced by highly vascular tumors (e.g., kidney or thyroid gland carcinomas, sarcoma of bone, and trophoblastic disease) to huge, well-defined masses (cannonball lesions) caused by metastatic sarcomas. Carcinoma of the thyroid gland typically causes a snowstorm of metastatic deposits yet radiographically remains unchanged for a prolonged period because of a very low grade of malignancy.

Solitary metastases, which occur in approximately 25% of cases, may be indistinguishable from primary bronchogenic carcinomas or benign granulomas (Figure 3-65). In such cases, CT may permit the detection of additional pulmonary masses that cannot be seen on standard chest radiographs but aid in determining the choice of treatment. The emerging technology of PET, which images cellular activity, has been used in the search for metastases when CT is inconclusive, as well as in determining whether a solitary pulmonary nodule is benign (when PET detects low cellular activity) or malignant (when PET detects high cellular activity) (Figure 3-66).

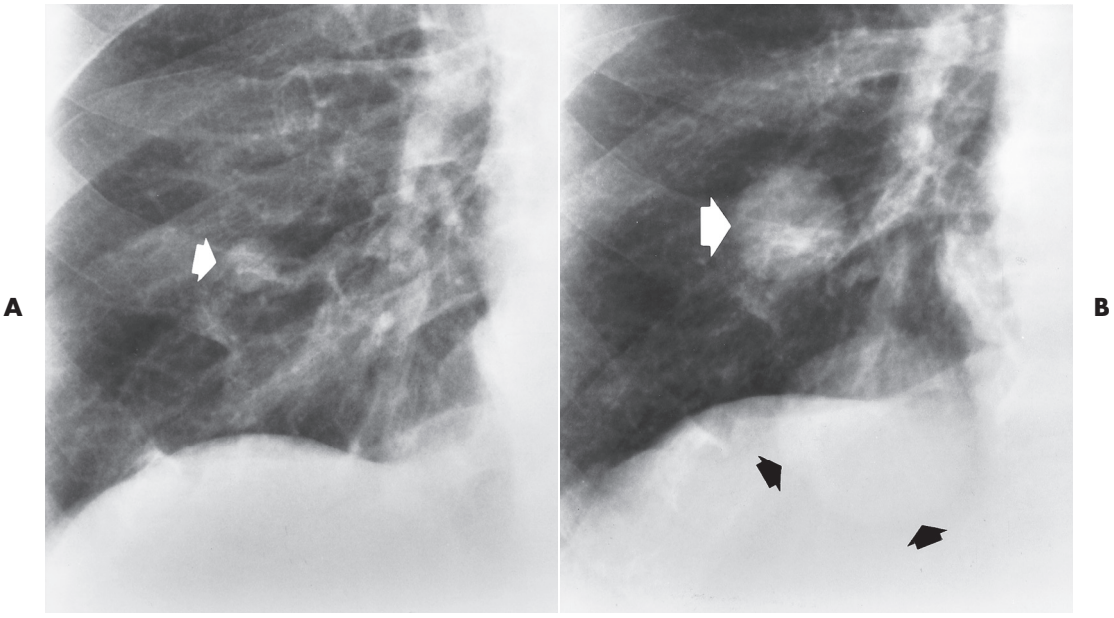

FIGURE 3-65 Pulmonary metastases. (A) Solitary metastasis (*arrow*). (B) Repeat examination 5 months later shows rapid growth of previous solitary nodule (*white arrow*). Second huge nodule (*black arrows*) was not appreciated on previous examination because it projected below the right hemidiaphragm.

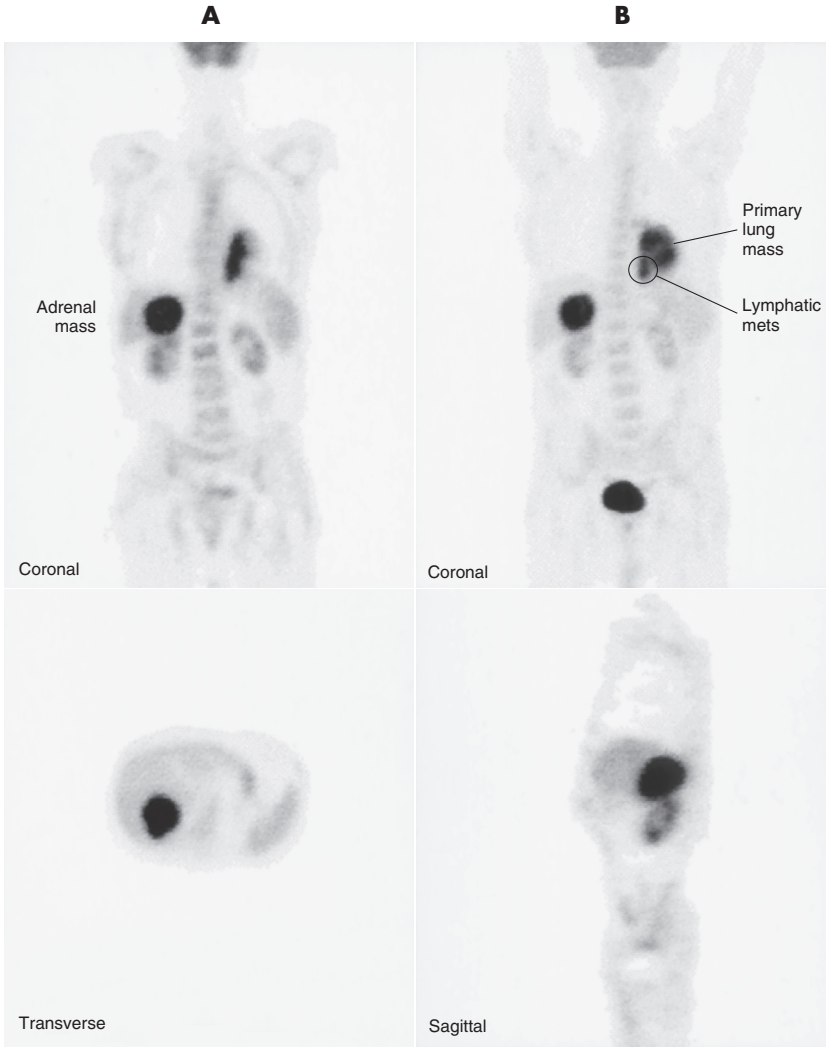

FIGURE 3-66 Non–small cell carcinoma. Muliplanar PET lung scan performed for initial staging. Following the injection of fluorodeoxyglucose, metabolically active metastases are suggested in the left hilum with lymphatic involvement (A) and in the right adrenal gland with hepatic involvement (B) by an increase in uptake (hot spot).

Summary of Findings for Pulmonary Neoplasms

Disorder	Location	Imaging Appearance	Treatment
Solitary pulmonary nodule	Throughout lungs	Solitary nodule Dense or popcorn calcification—benign Continued growth—malignancy	Depends on diagnosis (benign or malignant)
Bronchial adenoma	Glandular structure of major/segmental bronchi	Peripheral atelectasis (obstruction) Obstructive pneumonia	Surgical resection
Bronchogenic carcinoma	Lung parenchyma	Solitary lesion, ill-defined Atelectasis with obstruction Hilar enlargement Cavitation in upper lung	Surgical resection (cure) Radiation therapy (cure and palliative) Chemotherapy (palliative)
Pulmonary metastases	Throughout lungs	Multiple nodules, sharp margins Miliary/snowstorm nodules Solitary nodule Coarsened interstitial markings	All treatments palliative Surgical resection Radiation therapy Chemotherapy

Lymphangitic metastatic spread throughout the lungs is most commonly a complication of carcinoma of the breast, stomach, thyroid, pancreas, larynx, cervix, or prostate. The radiographic appearance consists of coarsened interstitial markings that have an irregular contour and are poorly defined (Figure 3-67). These coarsened markings are most prominent in the lower lobes and may simulate interstitial pulmonary edema.

Treatment. The treatment of pulmonary metastases includes surgical resection, radiation therapy, and chemotherapy; however, these serve only a palliative purpose.

FIGURE 3-67 Lymphangitic metastases. Coarsened bronchovascular markings of irregular contour and poor definition are seen on the chest radiograph in this patient with metastatic carcinoma of stomach.

VASCULAR DISEASES

Pulmonary Embolism

Pulmonary embolism, a potentially fatal condition, is by far the most common pathologic process involving the lungs of hospitalized patients. In approximately 80% of patients with this disorder, the condition does not cause symptoms and thus remains unrecognized because the emboli are too small or too few to occlude blood flow to a substantial portion of the lung. Even when symptomatic, pulmonary embolism may be difficult to diagnose. More than 95% of pulmonary emboli arise from thrombi that develop in the deep venous system of the lower extremities because of venous stasis. The remainder come from thrombi that occur in the right side of the heart or in brachial or cervical veins and are trapped by the capillaries in the pulmonary artery circulation. Thrombi originating in the left side of the heart can embolize to the peripheral systemic arterial circulation, where they are trapped in the arterioles or capillaries before they can return in the venous blood to the heart and the pulmonary circulation. Most embolic occlusions occur in the lower lobes because of the preferential blood flow to these regions.

The physiologic consequences of embolic occlusion of the pulmonary arteries depend on the size of the embolic mass and the general state of the pulmonary circulation. In young persons with good cardiovascular function and adequate collateral circulation, the occlusion of a large central vessel may cause minimal, if any, functional impairment. In contrast, in patients with cardiovascular disease or severe debilitating illnesses, pulmonary vascular occlusion often leads to infarction.

Imaging appearance. For most patients with thromboembolism without infarction, the findings on the chest radiograph are normal. Nevertheless, some subtle yet distinctive abnormalities on plain radiographs can be strongly suggestive of this diagnosis. A large-vessel pulmonary embolism causes a focal reduction in blood volume without a substantial change in air or tissue volume. This leads to focal pulmonary oligemia and relative lucency of the involved portion of lung. Another sign of pulmonary embolism is enlargement of the ipsilateral main pulmonary artery caused by distention of the vessel by the bulk of the thrombus. Serial radiographs may demonstrate progressive enlargement of the affected vessel.

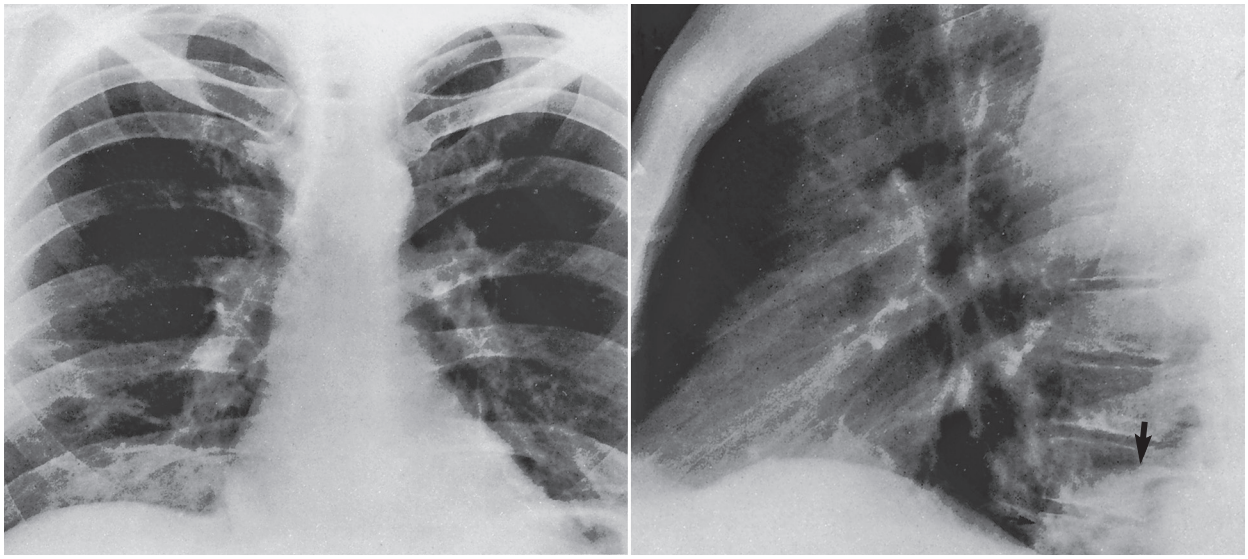

FIGURE 3-68 Pulmonary embolism. Frontal (A) and lateral (B) projections of the chest demonstrate fairly well-circumscribed shadow of homogeneous density occupying the posterior segment of the right lower lobe. On lateral projection, the pleura-based density has the shape of a truncated cone and is convex toward the hilum (Hampton's hump; *arrow*).

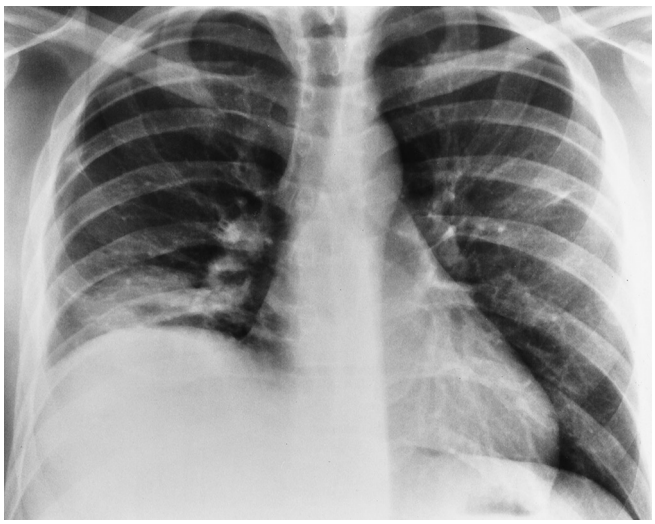

FIGURE 3-69 Pulmonary embolism. Plain chest radiograph demonstrates atelectasis at the right base; this is associated with elevation of the right hemidiaphragm and represents a large subpulmonic effusion.

Pulmonary embolism with infarction appears radiographically as an area of lung consolidation. A highly characteristic, although somewhat uncommon, appearance of pulmonary infarction is the so-called Hampton's hump (Figure 3-68). This pleura-based, wedge-shaped density has a rounded apex and is most commonly seen at the base of the lung, often in the costophrenic sulcus. In many instances, an infarction merely produces a nonspecific parenchymal density that simulates acute pneumonia. A pleural effusion often develops (Figure 3-69).

Because the findings on the chest radiograph are usually either normal or nonspecific, the radionuclide lung scan, or ventilation–perfusion ratio (V/Q) scan has been generally considered the most effective screening procedure for significant pulmonary embolism. On a radionuclide perfusion scan that measures blood flow to the lungs, the area of lung distal to an embolus appears as a filling defect (Figure 3-70). Unfortunately, false-positive scan results may be recorded in portions of the lung that are poorly perfused because of impaired ventilation, even if no obstructing vascular lesion is present. Therefore, ventilation lung scans are also performed to increase the diagnostic accuracy. The results of the ventilation scan are usually relatively normal in patients with pulmonary embolism, whereas they generally demonstrate defects corresponding to areas of decreased perfusion in patients with chronic pulmonary disease.

HRCT has now replaced radionuclide lung scanning in many institutions as the preferred imaging modality for detecting and excluding pulmonary emboli. Following the injection of a contrast agent, cross-sectional images of the lung are obtained from the base of the heart to the top of the aortic arch. CT demonstrates pulmonary embolus either as a filling defect within the pulmonary artery (Figure 3-71) or as an abrupt cutoff indicating complete obstruction of a pulmonary vessel (Figure 3-72).

Pulmonary arteriography is the definitive technique for evaluating the patient with suspected pulmonary embolism (Figure 3-73). However, this invasive procedure carries a small but definite risk of morbidity and mortality. The unequivocal arteriographic diagnosis of pulmonary embolism requires the demonstration of an abrupt occlusion (cutoff) of a pulmonary artery or a persistent intraluminal filling defect within it. Magnetic resonance imaging (MRI) has been used to show a pulmonary embolus either as a moderate- to high-intensity signal within the black flow void of the normal pulmonary artery or as a generalized increased signal intensity caused by slow blood flow in an obstructed pulmonary vessel.

Treatment. The first line of treatment is anticoagulant therapy, which limits the extent of infarction of the affected lung

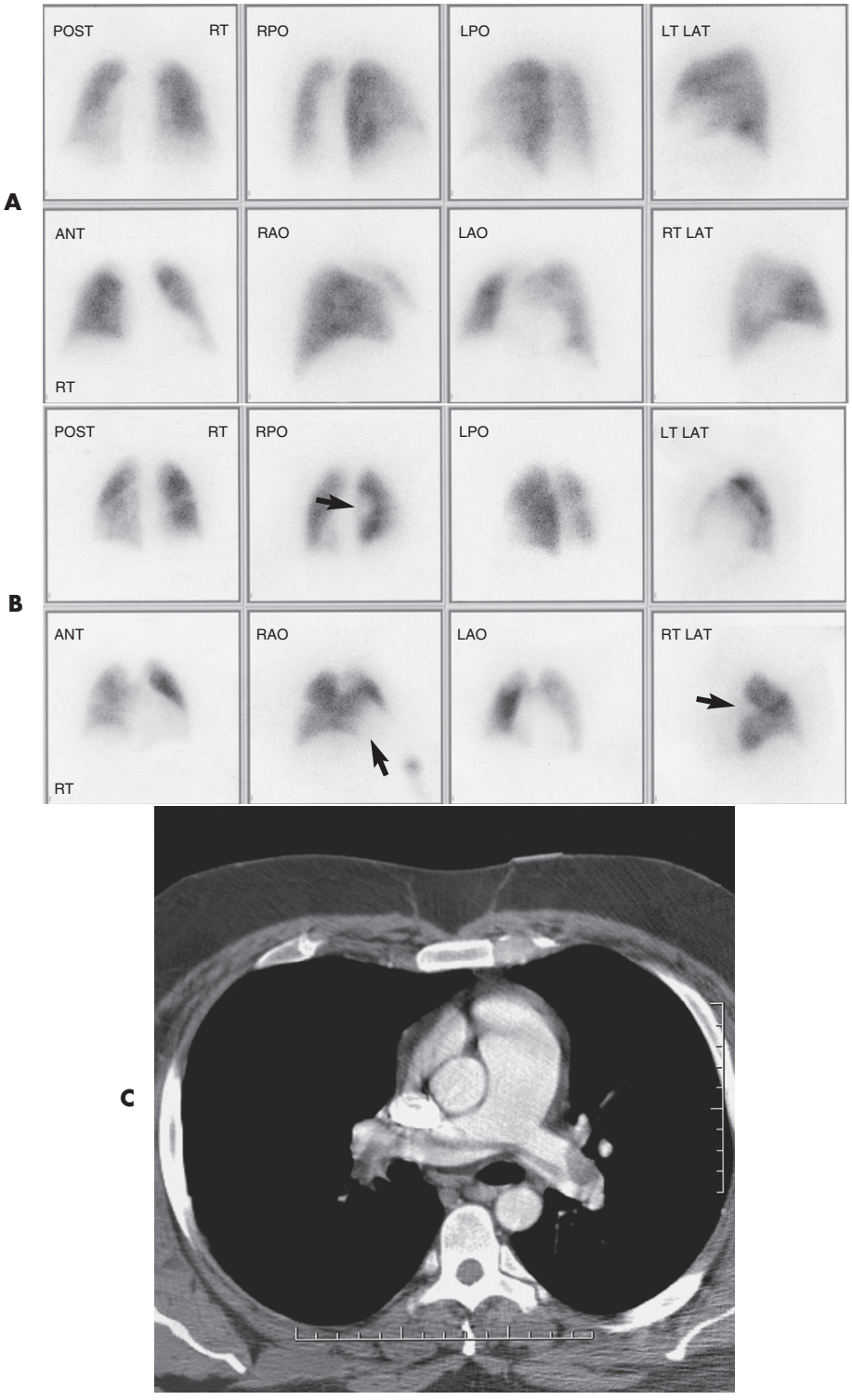

FIGURE 3-70 **Pulmonary embolism.** **(A)** Normal radionuclide perfusion lung scan with uniform uptake in both lungs. **(B)** Radionuclide scan in a different patient showing multiple wedge-shaped areas without isotope uptake (*arrows*). **(C)** CT scan (correlating with lung scan in panel **B**) demonstrates pulmonary emboli in both right and left pulmonary arteries. Note that the emboli are connected—a "saddle" embolus.

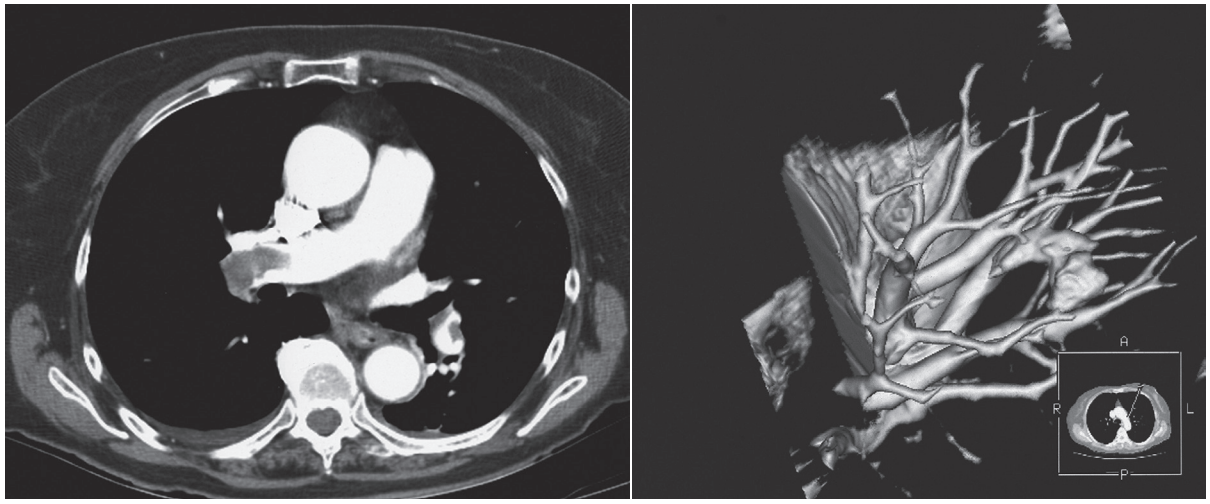

FIGURE 3-71 Pulmonary embolism. (A) A filling defect of the right pulmonary artery demonstrated on a high-resolution spiral CT scan. (B) With use of 3D volume rendering, CT can visualize a smaller pulmonary embolus.

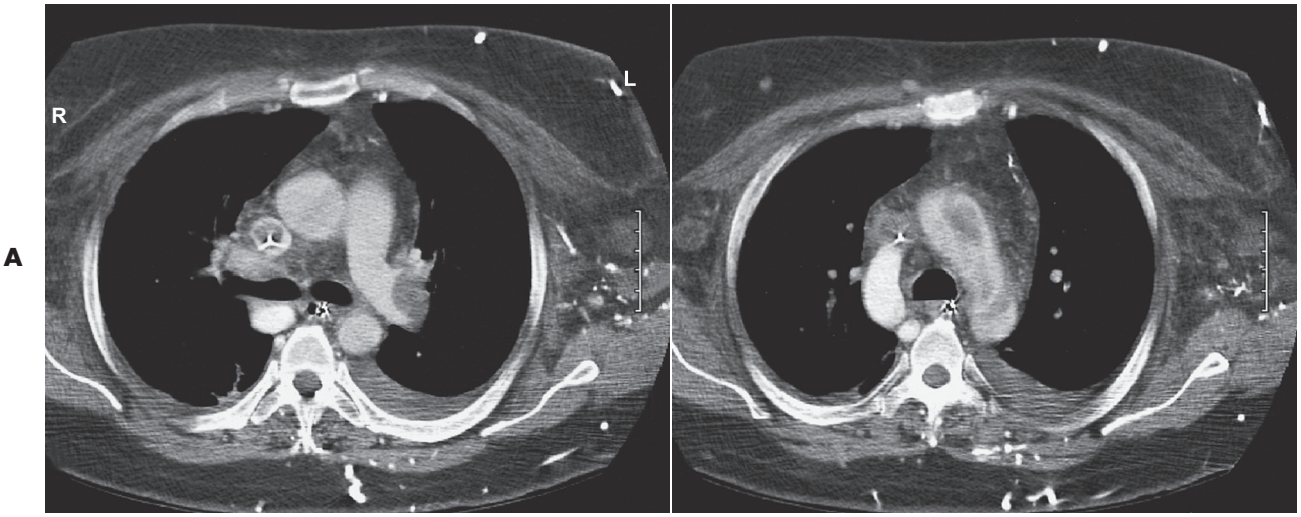

FIGURE 3-72 Pulmonary embolism. (A) CT scan illustrates a filling defect in the left main pulmonary artery in a 41-year-old woman. (B) The patient also has a thrombus, located in the ascending aorta and aortic arch.

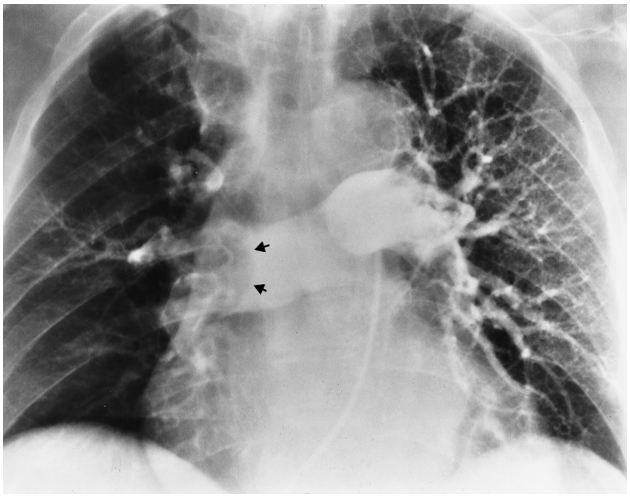

FIGURE 3-73 Pulmonary artery obstruction. Pulmonary arteriogram shows virtually complete obstruction (*arrows*) of the right pulmonary artery.

tissue and decreases the likelihood of more emboli to the lung. The patient may be required to take the anticoagulants for an extended period. If the emboli do not respond to anticoagulant therapy, thrombolytics can assist in dissolving them. In patients with large clot burdens, thrombolytic therapy may be the first line of treatment. The most invasive treatment is the placement of a filter in the vena cava, which is indicated if the anticoagulant or thrombolytic therapy is contraindicated or ineffective.

Septic Embolism

Septic embolism refers to a shower of bacteria that enter the pulmonary circulation and remain trapped within the lung. Septic emboli arise primarily from either the heart (bacterial endocarditis) or the peripheral veins (septic thrombophlebitis). Many patients have a clinical history of intravenous drug abuse.

Imaging appearance. Septic emboli, almost always multiple, appear radiographically as ill-defined, round or wedge-shaped opacities in the periphery of the lung. They often

Summary of Findings for Pulmonary Vascular Diseases

Disorder	Location	Imaging Appearance	Treatment
Pulmonary embolism	Most often lower lobes	Serial images demonstrating progressive enlargement of the affected vessel CT—filling defect in the pulmonary artery Nuclear medicine ventilation study—lobar perfusion defect in one or more regions of the lung with normal ventilation	Anticoagulants Thrombolytics Vena cava filter placement
Septic embolism	Lung periphery	Peripheral opacities	Regimented antibiotics until bacterial infection eradicated
Pulmonary arteriovenous fistula	Most often lower lobes	Defined soft tissue mass	Surgical removal Embolization

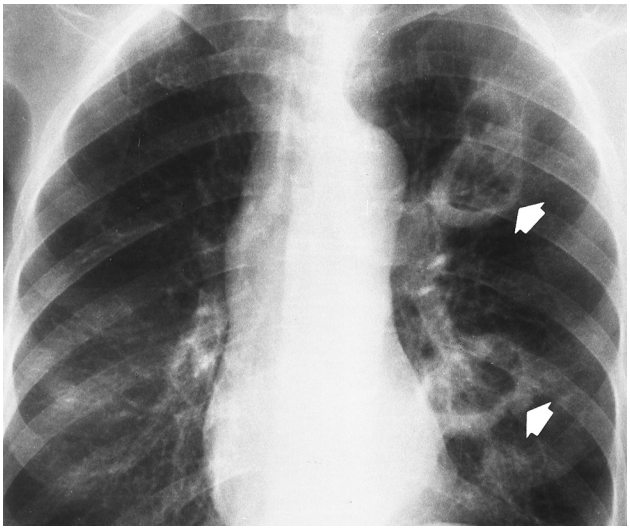

FIGURE 3-74 Septic pulmonary emboli. Large cavitary lesions (*arrows*) in the left lung of an intravenous drug abuser with septic thrombophlebitis.

demonstrate a migratory pattern, first appearing in one area and then in another as the older lesions resolve. Cavitation frequently develops (Figure 3-74).

Treatment. Patients with septic embolism require regimented doses of antibiotics to destroy the underlying bacterial infection.

Pulmonary Arteriovenous Fistula

Pulmonary arteriovenous fistula is an abnormal vascular communication from a pulmonary artery to a pulmonary vein. Pulmonary arteriovenous fistulas are multiple in approximately one-third of patients; up to two-thirds of patients with these pulmonary malformations have similar arteriovenous communications elsewhere (hereditary hemorrhagic telangiectasia). Very large or multiple fistulas can cause so much shunting of blood from the pulmonary arteries to the pulmonary veins that the blood cannot be adequately oxygenated and cyanosis results.

Imaging appearance. A pulmonary arteriovenous fistula typically appears as a round or oval, lobulated soft tissue mass that is most commonly situated in the lower lobes. A pathognomonic finding is a feeding artery and a draining vein (Figure 3-75A). This finding may be difficult to demonstrate on plain radiographs and often requires tomography or angiography (Figure 3-75B).

Treatment. Before surgical removal, a pulmonary angiogram can confirm the diagnosis and detect smaller, unsuspected vascular malformations that cannot be identified on routine radiographs. Another treatment for arteriovenous fistula is the placement of a detachable balloon (embolization) to block the flow of blood through the fistulous connection.

MISCELLANEOUS LUNG DISORDERS

Atelectasis

Atelectasis refers to a condition in which there is diminished air within the lung associated with reduced lung volume. Most commonly this results from bronchial obstruction, which may be attributable to a neoplasm, foreign body (e.g., peanut, coin, or tooth), or mucous plug. Mucoid obstruction may be attributable to an excessive secretion in patients with chronic bronchitis, or it may be a complication of abdominal surgery. As a result of surgery, mucus collects in the bronchi because of the irritative effect of anesthesia. Normal coughing, which would mobilize the secretions, is decreased because of the pain of the abdominal wound. Compression of the lung by pneumothorax, pleural fluid, a tumor, a lung abscess, or a large emphysematous bulla may result in atelectasis. Regardless of the precise cause, air cannot enter that part of the lung supplied by the obstructed bronchus. As the air trapped in the lung is absorbed into the bloodstream, the lung collapses.

An important iatrogenic cause of atelectasis is the improper placement of an endotracheal tube below the level of the tracheal bifurcation. Because of geometric factors, the endotracheal tube tends to enter the right mainstem bronchus, effectively blocking the left bronchial tree and causing collapse of part or all of the left lung (Figure 3-76).

Imaging appearance. The most common radiographic sign of atelectasis is a local increase in density caused by the airless lung, which may vary from thin, platelike streaks (Figure 3-77) to lobar collapse (Figure 3-78). An important direct sign of atelectasis is displacement of interlobar fissures, which shift and become bowed, conforming to the contour of the collapsed segment. Indirect signs of atelectasis reflect an attempt by the remaining lung to compensate for the loss of the collapsed portion. These signs include elevation of the ipsilateral hemidiaphragm; displacement of the heart, mediastinum, and hilum toward the atelectatic segment; and compensatory overinflation of the remainder of the ipsilateral lung.

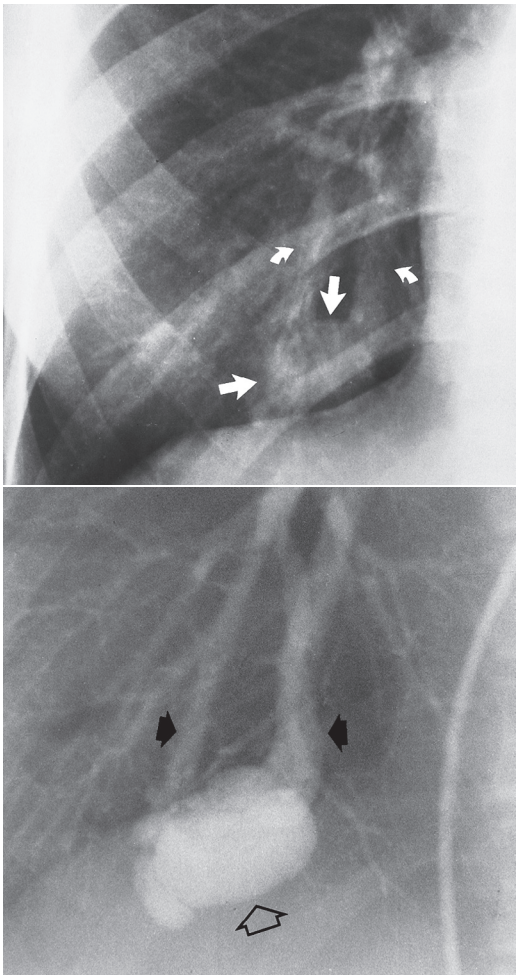

FIGURE 3-75 Pulmonary arteriovenous fistula. (A) Radiographic image of right lung shows round soft tissue mass (*straight arrows*) at the base. Feeding and draining vessels (*curved arrows*) extend to the lesion. (B) Arteriogram clearly shows feeding artery and draining veins (*solid arrows*) associated with arteriovenous malformation (*open arrow*).

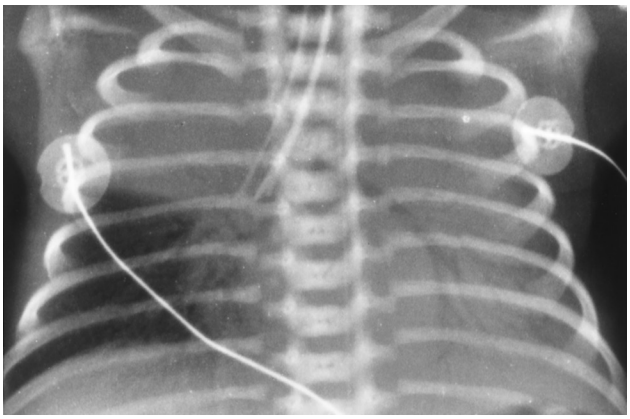

FIGURE 3-76 Malpositioned endotracheal tube. Excessively low position of endotracheal tube in the bronchus intermedius causes collapse of right upper lobe and entire left lung.

Treatment. The goal of the treatment of atelectasis is the removal of pulmonary secretions and reexpansion of the affected lung tissue. To accomplish it, positioning or incentive spirometry (measurement of air capacity in the lungs) is employed. Positioning uses gravity to assist in expanding the affected lung tissue, and incentive spirometry directly increases lung volume by positive pressure.

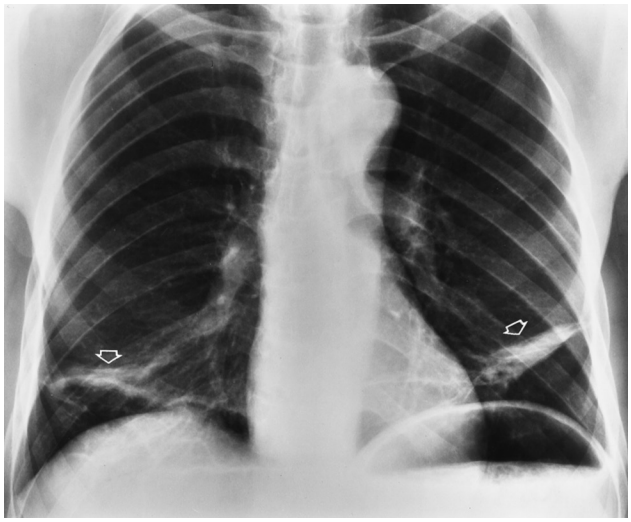

FIGURE 3-77 Platelike atelectasis. Horizontal linear streaks of opacity (*arrows*) can be seen in lower portions of both lungs.

Adult Respiratory Distress Syndrome

The term **adult respiratory distress syndrome (ARDS)** describes a clinical picture of severe, unexpected, and life-threatening acute respiratory distress that develops in patients who have a variety of medical and surgical disorders but no major underlying lung disease. Because it occurs most commonly in patients with nonthoracic trauma in whom hypotension and shock develop, it is often called "shock lung." Other conditions that may lead to ARDS are severe pulmonary infection, aspiration or inhalation of toxins and irritants, and drug overdose. Regardless of the cause, the structure of the lung completely breaks down, leading to massive leakage of cells and fluid into the interstitial and alveolar spaces. The structural breakdown results in severe hypoxemia caused by a pronounced respiratory impairment in the ability to oxygenate blood.

Imaging appearance. Patchy, ill-defined areas of alveolar consolidation are scattered throughout both lungs (Figure 3-79). Unlike in pulmonary edema caused by heart failure, in ARDS the size of the heart usually remains normal, and there is no evidence of redistribution of blood flow to the upper zones.

Treatment. The hypoxemia in ARDS may be fatal, even with intensive medical therapy. Drug treatment may consist of diuretics to decrease the fluid load and possible fluid buildup in the lung tissue. Oxygen therapy and ventilation may assist the patient in breathing, which helps prevent further capillary and alveolar destruction. Continuous positive-pressure ventilation may cause air to enter the interstitium of the lung and lead to pneumothorax and pneumomediastinum. Diffuse interstitial and patchy airspace fibrosis may produce a coarse reticular pattern. If the patient recovers completely, the radiographic abnormalities may clear completely, and there may be only a mild decrease in pulmonary function.

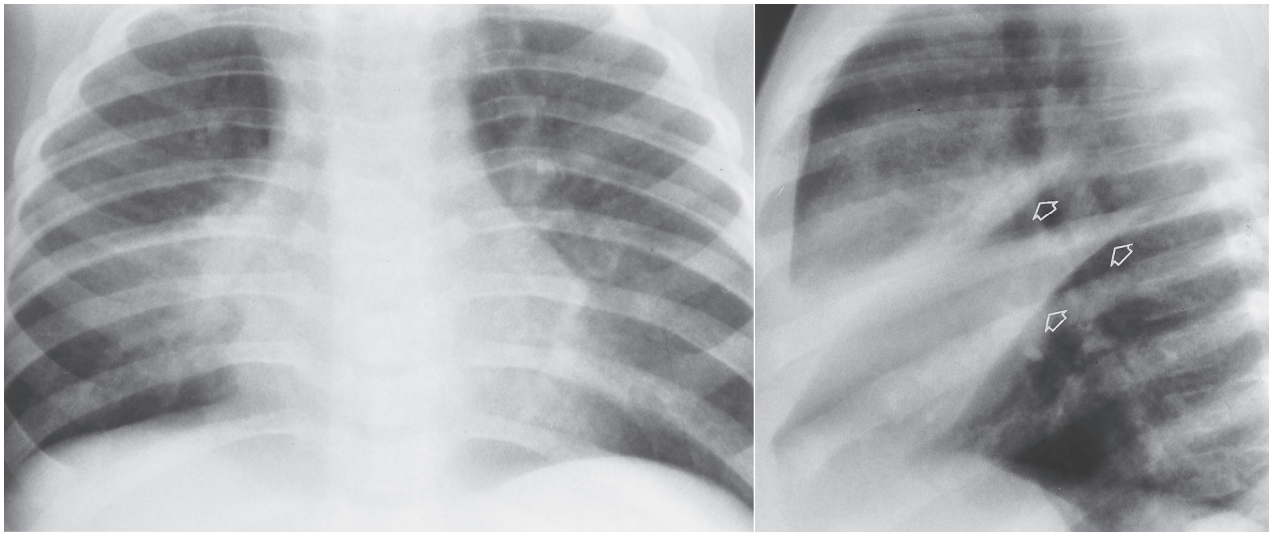

FIGURE 3-78 Right middle lobe and lingular collapse. **(A)** Frontal chest radiograph demonstrates obliteration of right and left borders of the heart. **(B)** Lateral projection demonstrates collapse of right middle lobe and lingula (*arrows*).

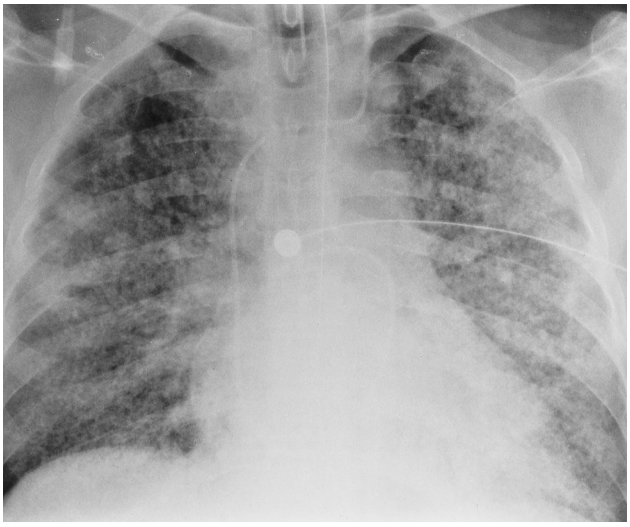

FIGURE 3-79 ARDS. Ill-defined areas of alveolar consolidation scattered throughout the lungs.

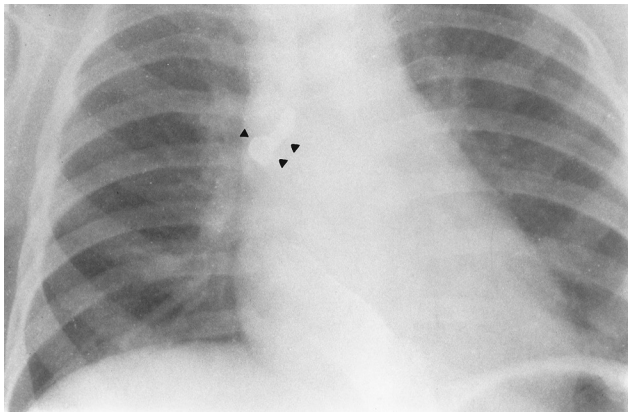

FIGURE 3-80 Intrabronchial foreign body. A nail (*arrows*) lies in the right mainstem bronchus.

Intrabronchial Foreign Bodies

The aspiration of solid foreign bodies into the tracheobronchial tree occurs almost exclusively in young children. Although some foreign bodies are radiopaque and easily detected on plain chest radiographs, most aspirated foreign bodies are not opaque and can be diagnosed only by observation of secondary signs in the lungs caused by partial or complete bronchial obstruction. Obstruction almost always involves the lower lobes, the right more often than the left.

Imaging appearance. The complete obstruction of a major bronchus leads to resorption of trapped air, alveolar collapse, and atelectasis of the involved segment or lobe. Extensive volume loss causes a shift of the heart and mediastinal structures toward the affected side along with elevation of the ipsilateral hemidiaphragm and narrowing of the intercostal spaces.

Partial bronchial obstruction may produce air trapping as a result of a check-valve phenomenon. Air freely passes the partial obstruction during inspiration but remains trapped distally as the bronchus contracts normally during expiration (Figure 3-80). Hyperaeration of the affected lobes causes a shift of the heart and mediastinum toward the normal, contralateral side. This finding is accentuated during forced expiration because the hyperaerated segment does not contract. This classic appearance of partial bronchial obstruction is dramatically demonstrated with fluoroscopy as the mediastinum shifts away from the affected side during deep expiration and returns toward the midline on full inspiration.

A malpositioned endotracheal tube can act as an intrabronchial foreign body. The tube tends to extend down the right mainstem bronchus, causing hyperlucency of the right lung and obstructive atelectasis of the left lung.

Treatment. The treatment of intrabronchial foreign bodies includes expectoration, intervention, and surgery. The simplest is expectoration, which requires the patient to cough hard enough to dislodge the foreign body and spit it out. More invasive interventional techniques employ a bronchoscope to retrieve the object blocking the airway. The most invasive procedure is direct surgical removal of the foreign body.

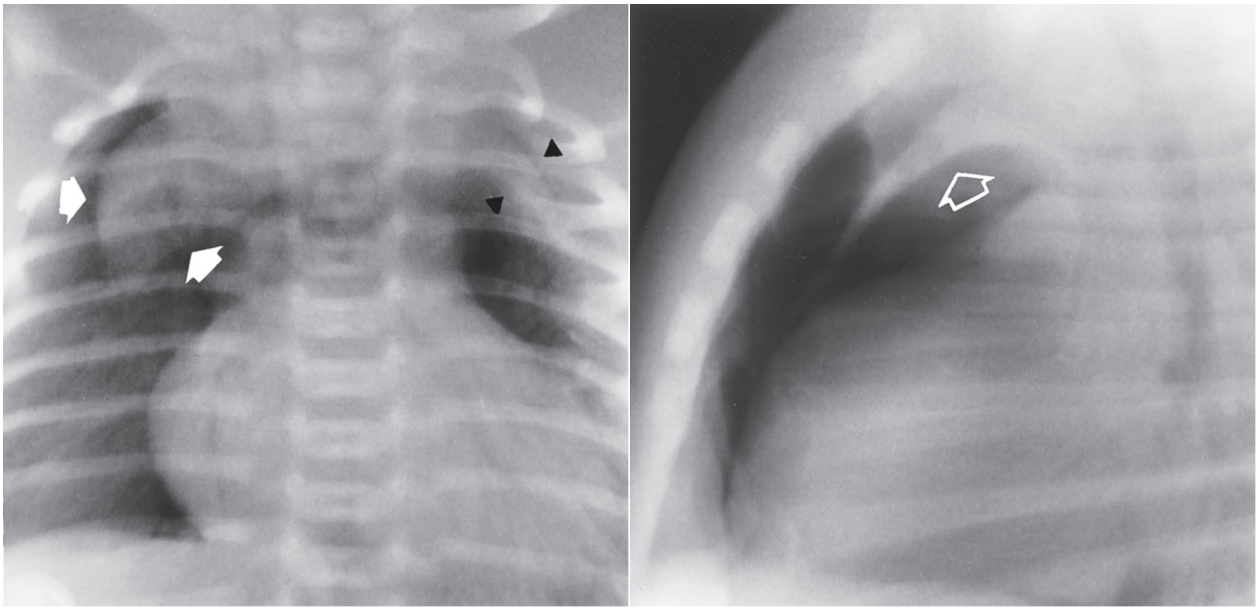

FIGURE 3-82 Mediastinal emphysema in an infant. **(A)** Elevation of both lobes of thymus by mediastinal air (*arrows* and *arrowheads*) produces angel-wings sign. **(B)** Lateral projection shows mediastinal air lifting thymus off pericardium and great vessels (*arrow*).

Mediastinal Emphysema (Pneumomediastinum)

Air within the mediastinal space may appear spontaneously, or it may result from chest trauma, from perforation of the esophagus or tracheobronchial tree, or from the spread of air along fascial planes in the neck, peritoneal cavity, or retroperitoneal space. Spontaneous pneumomediastinum usually results from a sudden rise in intraalveolar pressure (e.g., because of severe coughing, vomiting, or straining) that causes alveolar rupture and the dissection of air along blood vessels in the interstitial space to the hilum and mediastinum. Air may also extend peripherally and rupture into the pleural space, causing an associated pneumothorax.

Imaging appearance. On frontal chest radiographs, air causes lateral displacement of the mediastinal pleura, which appears as a long linear opacity that runs parallel to the heart border but is separated from it by the air (i.e., the bronchovascular sheath) (Figure 3-81). On lateral projections, air is typically seen to have collected behind the sternum, extending in streaks downward and anterior to the heart. Chest radiographs may also demonstrate air outlining the pulmonary arterial trunk and aorta and dissecting into the soft tissue of the neck.

In infants, mediastinal air causes elevation of the thymus. Loculated air confined to one side produces an appearance similar to that of a windblown sail. Bilateral mediastinal air elevates both thymic lobes to produce an angel-wings configuration (Figure 3-82).

Subcutaneous Emphysema

Subcutaneous emphysema is caused by penetrating or blunt injuries that disrupt the lung and parietal pleura and force air into the tissues of the chest wall. When palpating the skin, one might hear or feel crepitation (a crackling sound or sensation).

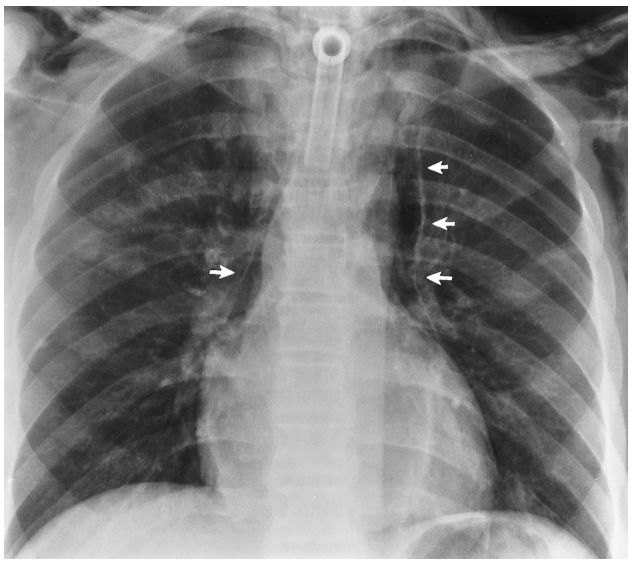

FIGURE 3-81 Mediastinal emphysema. Mediastinal pleura is displaced laterally and appears as a long linear opacity (*arrows*) parallel to the heart border but separated from it by gas. This image also demonstrates subcutaneous emphysema (black streaks in soft tissue) and pneumothorax bilaterally.

Imaging appearance. The radiographic appearance is bizarre, with streaks of lucency outlining muscle bundles (Figure 3-83).

Treatment of Mediastinal and Subcutaneous Emphysema

If the emphysema appears minimal and does not progress, no treatment may be needed. If the air in the mediastinum or subcutaneous tissue does not absorb, or if it increases in amount, surgical resection to block off the source of air may be required.

Summary of Findings for Miscellaneous Lung Disorders

Disorder	Location	Imaging Appearance	Treatment
Atelectasis	Obstruction of segment/lobe or lung collapse	Local increased density; platelike streaks	Positioning of patient Incentive spirometry
Acute respiratory distress syndrome	Lung structure breakdown	Patchy, ill-defined areas of consolidation	Diuretics to decrease fluid buildup Oxygen therapy and ventilation
Intrabronchial foreign body	Lower lobes, most often right	Appears as atelectasis with possible shift	Removal of foreign body Expectoration, intervention, surgery
Mediastinal emphysema	Air in bronchovascular sheath	Radiolucency running parallel to heart border	If minimal, no treatment Surgical resection to prevent more air escape
Subcutaneous emphysema	Air in surrounding muscle bundles	Air streaks in muscle bundles	If minimal, no treatment Surgical resection to prevent more air escape

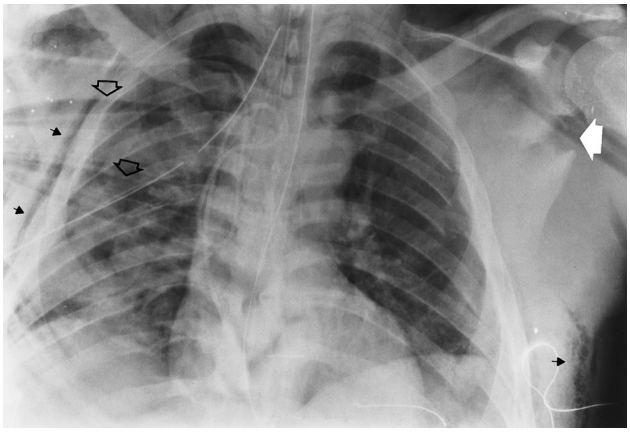

FIGURE 3-83 Subcutaneous emphysema. Frontal chest radiograph of severely injured patient shows streaks and bubbles of subcutaneous air (*black arrows*) in soft tissues along lateral borders of thorax and also broad lucencies outlining muscle bundles (*open arrows*) overlying the anterior chest wall. Note fracture of left scapula (*white arrow*) and multiple rib fractures.

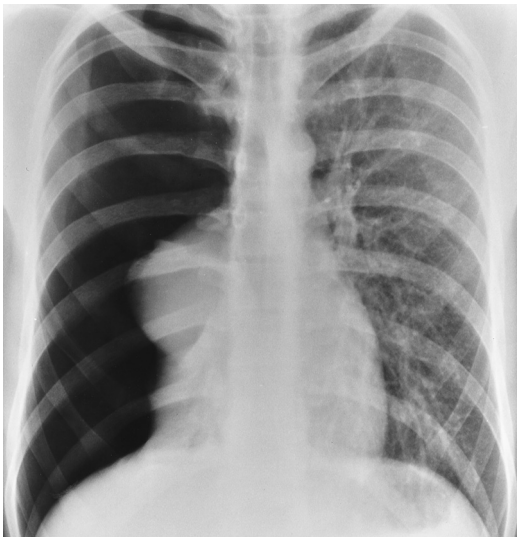

FIGURE 3-84 Spontaneous pneumothorax. Complete collapse of right lung as indicated by an absence of lung markings.

DISORDERS OF THE PLEURA

Pneumothorax

Pneumothorax, the presence of air in the pleural cavity, results in a partial or complete collapse of the lung (Figure 3-84). It most commonly results from rupture of a subpleural bulla, either as a complication of emphysema or as a spontaneous event in an otherwise healthy young adult. Other causes of pneumothorax are traumatic (e.g., stabbing, gunshot, or fractured rib) and iatrogenic (e.g., after lung biopsy or the introduction of a chest tube for thoracentesis); the condition may also be a complication of neonatal hyaline membrane disease and require prolonged assisted ventilation. Regardless of the cause, the increased air in the pleural cavity compresses the lung and causes it to collapse. The collapse may cause the patient to experience sudden, severe chest pain and dyspnea (difficulty breathing).

Imaging appearance. A pneumothorax appears radiographically as a hyperlucent area in which all pulmonary markings are absent. The radiographic hallmark of pneumothorax is the demonstration of the visceral pleural line, which is outlined centrally by air within the lung and peripherally by air within the pleural space. A large pneumothorax can cause collapse of an entire lung. Chest radiographs for pneumothorax should be taken with the patient in the upright position because it may be very difficult to identify this condition in the supine patient. In addition to routine full-inspiration images, a posteroanterior (PA) radiograph, or an anteroposterior radiograph, should be obtained with the lung in full expiration to allow identification of small pneumothoraxes (Figure 3-85). This maneuver causes the lung to decrease in volume and become relatively denser, whereas the volume of air in the pleural space remains constant and is easier to detect. Very small pneumothoraxes may be evident on lateral decubitus images. In this position, air rising to the highest point in the hemithorax is more clearly visible over the lateral chest wall than on erect views, in which a small amount of air in the apical region may be obscured by overlying bony densities. Whenever an expiration radiograph

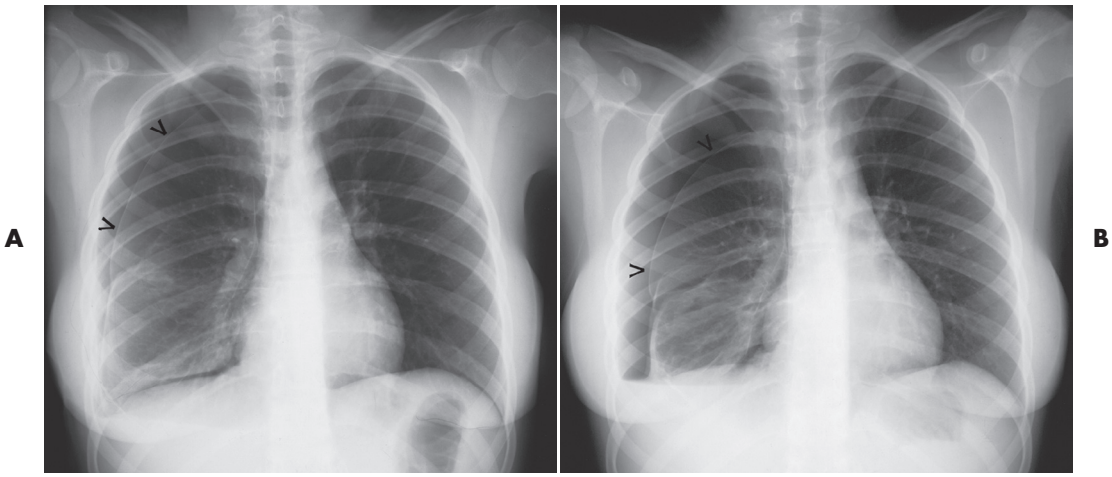

FIGURE 3-85 Pneumothorax. **(A)** On routine frontal chest image, a faint rim of pleura (*arrowheads*) at the right apex is separated from the thoracic wall by an area containing air but no pulmonary vasculature. **(B)** On expiratory image, right pneumothorax (*arrowhead*) is clearly seen.

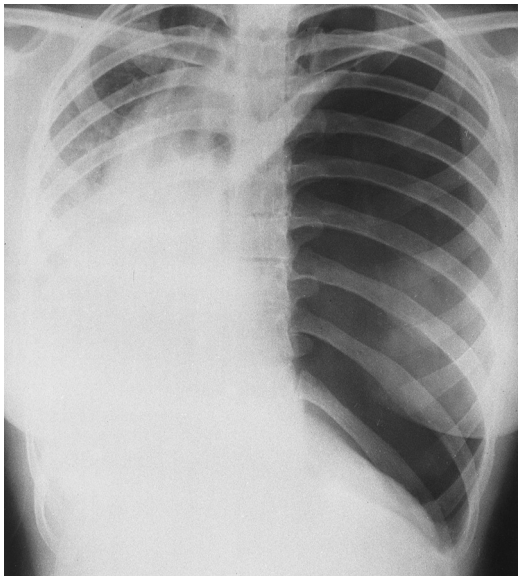

FIGURE 3-86 Tension pneumothorax. Left hemithorax is completely radiolucent and lacks vascular markings. There is a dramatic shift of the mediastinum to the right. Left hemidiaphragm is greatly depressed, and there is spreading of the left ribs.

is being obtained, the use of an automatic exposure control is not recommended because the preset density may produce a radiographic image density capable of concealing a small pneumothorax. With a manual technique, the exposure factor (in milliampere seconds) for an expiration radiograph should be increased approximately one-third of that used for inspiration images.

Treatment. Small pneumothoraxes usually reabsorb spontaneously. Larger pneumothoraxes may require prompt chest tube drainage with suction to remove the air and prevent recurrence. Tension pneumothorax is a medical emergency in which air continues to enter the pleural space but cannot exit. The accumulation of air within the pleural space causes complete collapse of the ipsilateral lung and depression of the hemidiaphragm (Figure 3-86). The heart and mediastinal structures shift toward the opposite side, severely compromising cardiac output because the elevated intrathoracic pressure decreases venous return to the heart. If a tension pneumothorax is not treated promptly, the resulting circulatory collapse may be fatal.

Pleural Effusion

The accumulation of fluid in the pleural space is a nonspecific finding that may be caused by a wide variety of pathologic processes. The most common causes include congestive heart failure, pulmonary embolism, infection (especially tuberculosis), pleurisy, neoplastic disease, and connective tissue disorders. Pleural effusion can also be the result of abdominal disease, such as recent surgery, ascites, subphrenic abscess, and pancreatitis.

Imaging appearance. The earliest radiographic finding in pleural effusion is blunting of the normally sharp angle between the diaphragm and the rib cage (the costophrenic angle) along with an upward concave border of the fluid level (or meniscus) (Figure 3-87). Because the costophrenic angles are deeper posteriorly than laterally, small pleural effusions are best seen on the routine lateral projection posteriorly. As much as 400 mL of pleural fluid may accumulate and still not produce blunting of the lateral costophrenic angles on erect frontal views of the chest. Larger amounts of pleural fluid produce a homogeneous opaque density (or whiteness) that may obscure the diaphragm and adjacent borders of the heart. Massive effusions may compress the adjacent lung and even displace the heart and mediastinum to the opposite side (Figure 3-88).

Small pleural effusions may be difficult to distinguish from pleural thickening and fibrosis, which results from previous pleural inflammation and appears radiographically as a soft tissue density along the lateral chest wall (Figure 3-89). The diagnosis of a small pleural effusion is best made on radiography performed with use of a horizontal x-ray beam and

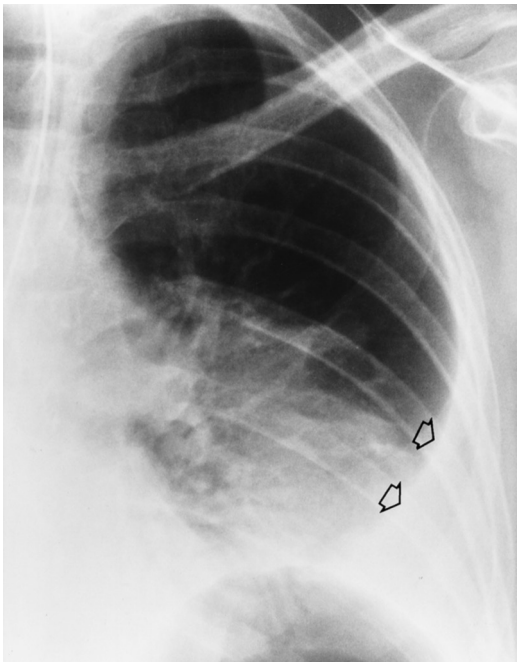

FIGURE 3-87 Pleural effusion. Blunting of normally sharp angle between diaphragm and rib cage (*arrows*) along with characteristic concave-upward fluid level (meniscus).

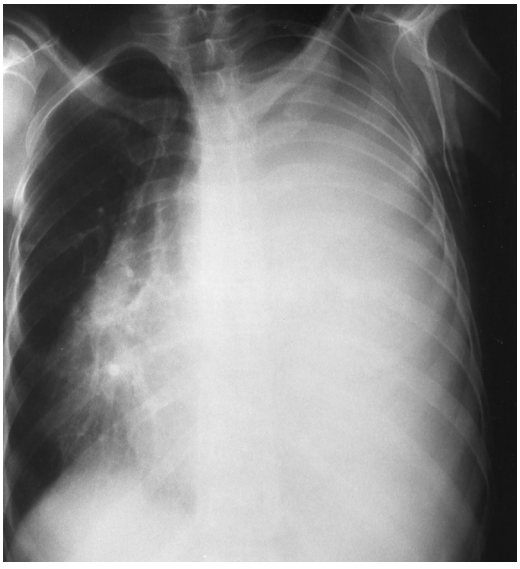

FIGURE 3-88 Pleural effusion causing mediastinal shift. Left hemithorax is virtually opaque, and there is a shift of mediastinal structures to the right.

the patient in a lateral decubitus position with the affected side down (Figure 3-90). With placement of the patient in a slight lateral Trendelenburg position, as little as 5 mL of pleural fluid can be seen as a layer of linear opacification along the dependent chest wall. At times, however, a collection of pleural fluid may be loculated (i.e., fixed in place by fibrous adhesions) and therefore will not form this layer in decubitus views.

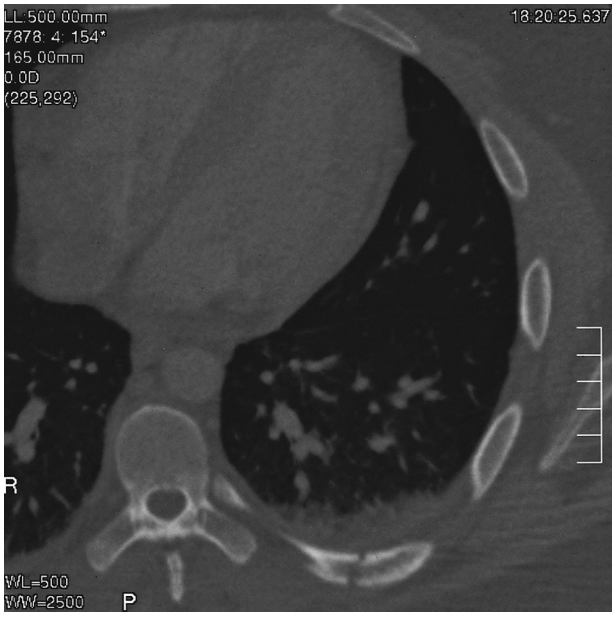

FIGURE 3-89 Pleural effusion. Caused by a left posterior rib fracture demonstrated on a CT scan.

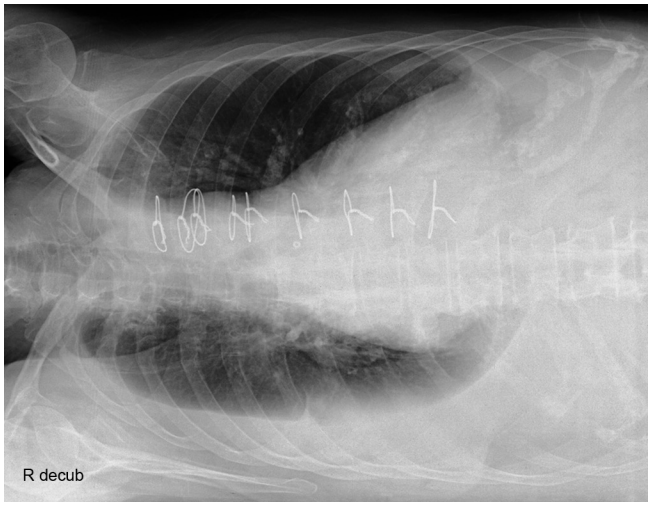

FIGURE 3-90 Right lateral decubitus chest radiograph. Right pleural effusion demonstrated as a fluid level on the right lateral decubitus image.

Pleural effusions may produce less common appearances on chest radiographs. A pleural fluid collection that has become fixed by inflammatory fibrosis may mimic a solid mass. At times, pleural fluid may collect below the inferior surface of the lung (subpulmonic effusion) and give the radiographic appearance of an elevated hemidiaphragm (Figure 3-91). In patients with congestive heart failure, an effusion may develop in an interlobar fissure to produce a round or oval density resembling a solitary pulmonary nodule. As the patient's heart condition improves, repeat examinations demonstrate decreased size or complete resolution of these phantom tumors (see Figure 7-24).

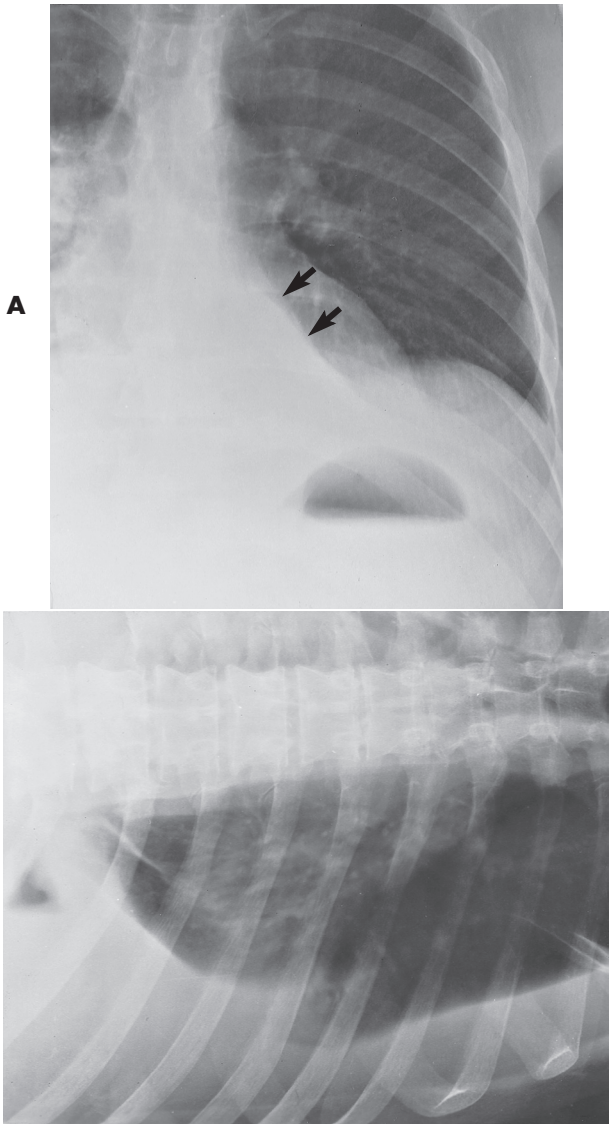

FIGURE 3-91 Pleural effusion. (A) Frontal projection of chest demonstrates long distance between gastric air bubble and top of false left hemidiaphragm in this patient with large subpulmonic effusion. Note retrocardiac paraspinal density (*arrows*) that simulates left lower lobe infiltrate or atelectasis. (B) Left lateral decubitus projection shows that the retrocardiac density represents a large amount of free pleural fluid.

Treatment. Thoracentesis is the procedure for removing fluid from the pleural cavity. Other treatments depend on the cause of the pleural effusion.

Empyema

Empyema refers to the presence of infected liquid or frank pus in the pleural space. Usually the result of the spread of an adjacent infection (e.g., bacterial pneumonia, subdiaphragmatic abscess, lung abscess, and esophageal perforation), empyema may also occur after thoracic surgery, trauma, or instrumentation of the pleural space. Since the development of antibiotics, empyemas have been rare.

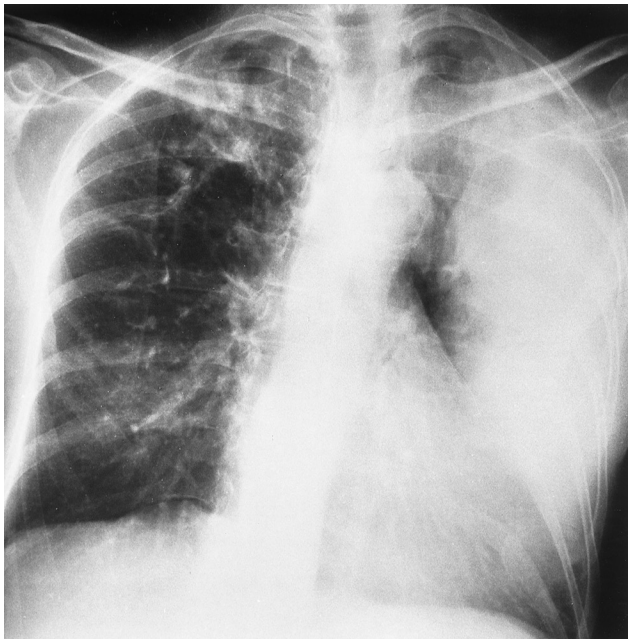

FIGURE 3-92 Empyema. Large soft tissue mass fills much of left hemithorax.

Imaging appearance. Radiographically, an empyema is initially indistinguishable from pleural effusion. As the empyema develops, it becomes loculated and appears as a discrete mass that may vary in size from a large lesion filling much of the hemithorax (Figure 3-92) to a small mass along the chest wall or in an interlobar fissure. Air within a free or loculated empyema causes an air–fluid level, indicating communication with a bronchus or the skin surface.

Treatment. Needle aspiration of an empyema may be performed under fluoroscopic guidance; when the loculated mass is situated adjacent to the chest wall, ultrasound may be used to guide the aspiration needle. A sinus tract or fistula may require drainage tube placement.

Summary of Findings for Pleural Disorders

Disorder	Location	Imaging Appearance	Treatment
Pneumothorax	Air in pleural cavity	Peripheral radiolucency without pulmonary markings	Small—none (reabsorbed) Large—chest tube with suction
Pleural effusion	Fluid in pleural cavity	Fluid level—best seen on lateral decubitus	Thoracentesis to remove fluid
Empyema	Infected fluid in pleural cavity	Lesion—loculated fluid; possible air–fluid level	Needle aspiration with possible drain placement

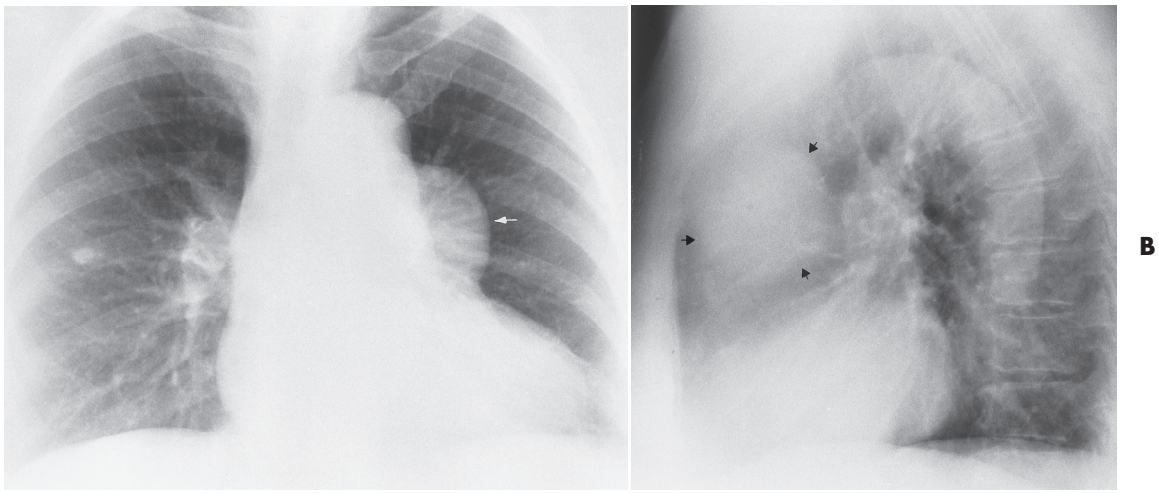

FIGURE 3-93 Anterior mediastinal mass. Frontal (A) and lateral (B) projections of chest demonstrate large mass (thymoma) in anterior mediastinum (*arrows*).

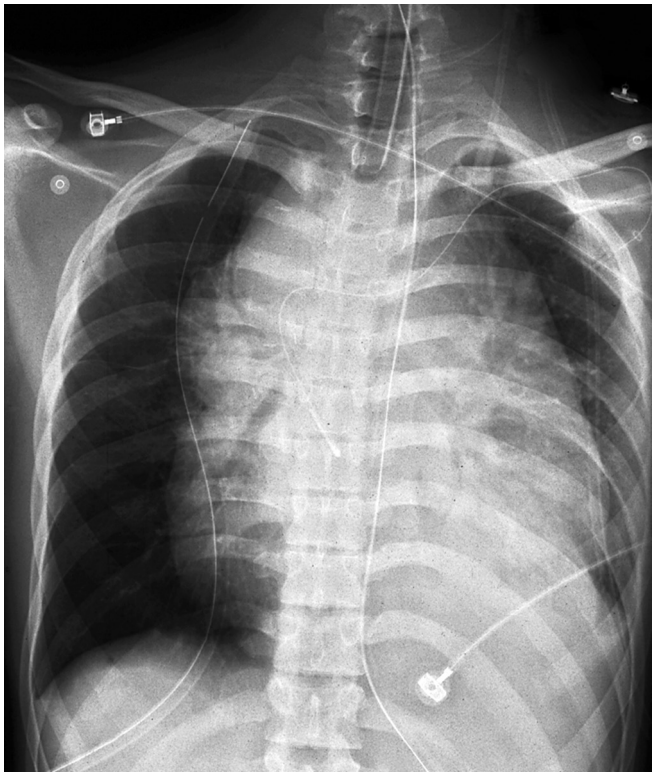

FIGURE 3-94 Anterior mediastinal mass. Mass associated with right hilar adenopathy.

Mediastinal Masses

Because various types of mediastinal masses tend to occur predominantly in specific locations, the mediastinum is often divided into anterior, middle, and posterior compartments. The anterior compartment extends from the sternum back to the trachea and the anterior border of the heart. The middle mediastinum contains the heart and great vessels, the central tracheobronchial tree and lymph nodes, and the phrenic nerves. The posterior compartment consists of the space behind the pericardium.

Major lesions of the anterior mediastinum include thymomas (Figure 3-93), teratomas, thyroid masses, lipomas, and lymphoma (Figure 3-94). The middle mediastinum involves lymph node disorders (e.g., lymphoma, metastatic carcinoma, and granulomatous processes), bronchogenic cysts (Figure 3-95), vascular anomalies, and various masses situated in the anterior costophrenic angle (e.g., pericardial cysts and foramen of Morgagni hernia). The posterior mediastinum is the site of neurogenic tumors, neurogenic cysts (Figure 3-96), aneurysms of the descending aorta, and extramedullary hematopoiesis.

Approximately one-third of patients with mediastinal masses are asymptomatic, and the lesions are detected on routine chest radiographs. Chest pain, cough, dyspnea, and symptoms caused by compression or invasion of structures in the mediastinum (e.g., dysphagia, hoarseness as a result of recurrent laryngeal nerve involvement, and superior vena cava obstruction) are highly suggestive of malignancy.

The configuration of a mediastinal mass depends to a large extent on its consistency. Cystic masses, often compressed between blood vessels and the tracheobronchial tree, produce a multiloculated appearance. In contrast, solid masses tend to compress and displace adjacent structures.

In addition to plain chest radiographs, conventional tomography and contrast studies of the esophagus may be of value in defining the anatomic location and borders of the mass. CT of the chest after the intravenous injection of contrast material may help in distinguishing between vascular and nonvascular lesions and in determining whether a lesion is cystic and thus most probably benign (Figures 3-97 and 3-98).

Treatment. For all masses found in the mediastinal region, surgical excision of the neoplasm is suggested because of the difficulty in differentiating the cause and the possible complications associated with these lesions.

Summary of Findings for Mediastinal Masses

Disorder	Location	Imaging Appearance	Treatment
Thymoma Teratoma Thyroid mass Lipoma Lymphoma	Anterior mediastinum	Cystic masses—compress, producing multiloculated appearance Solid masses—compress and displace adjacent structures	Excision of lesion because of difficult differential diagnosis
Lymph node disorders Bronchogenic cysts Vascular anomalies	Middle mediastinum	Cystic masses—compress, producing multiloculated appearance Solid masses—compress and displace adjacent structures	Excision of lesion because of difficult differential diagnosis
Neurogenic tumors Neurogenic cysts Aneurysms Extramedullary hematopoiesis	Posterior mediastinum	Cystic masses—compress, producing multiloculated appearance Solid masses—compress and displace adjacent structures	Excision of lesion because of difficult differential diagnosis

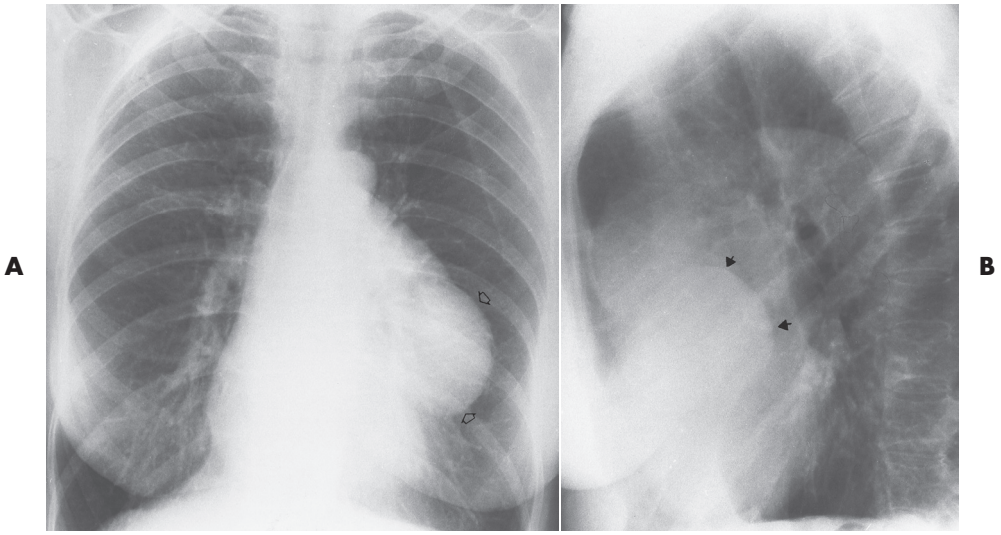

FIGURE 3-95 **Middle mediastinal mass.** Frontal (A) and lateral (B) projections of chest demonstrate a smooth-walled, spherical mediastinal mass (*arrows*) projecting into left lung and left hilum (found to be a bronchogenic cyst).

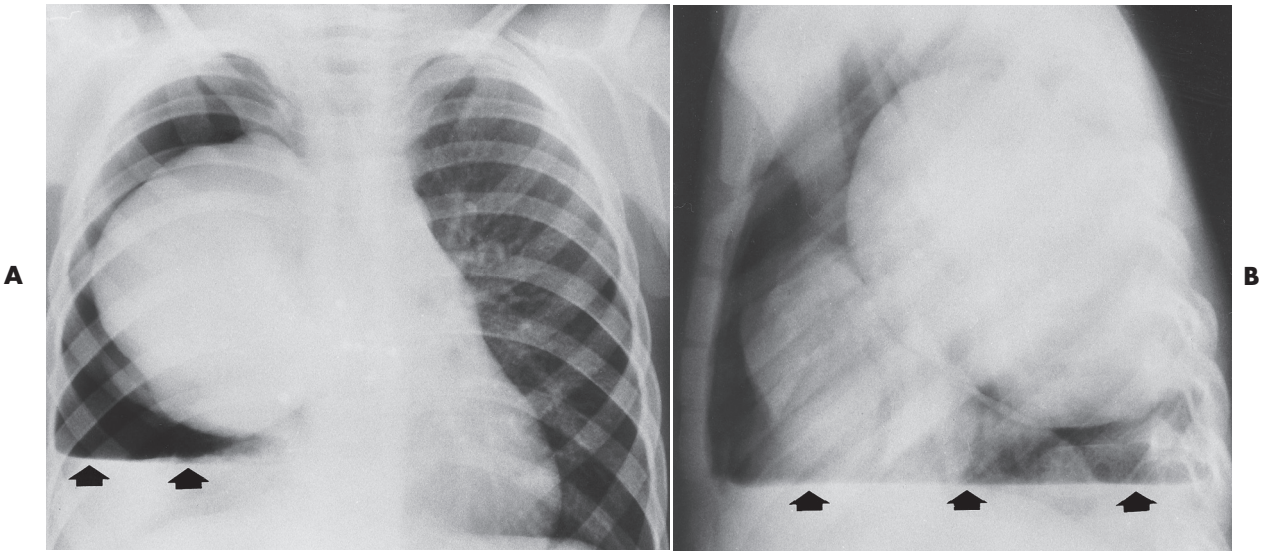

FIGURE 3-96 **Posterior mediastinal mass.** Frontal (A) and lateral (B) projections of chest demonstrate a large, oval, homogeneous mass in posterior mediastinum (neurenteric cyst). Note right hydropneumothorax (*arrows*) with long air–fluid level that developed as a complication of diagnostic needle biopsy.

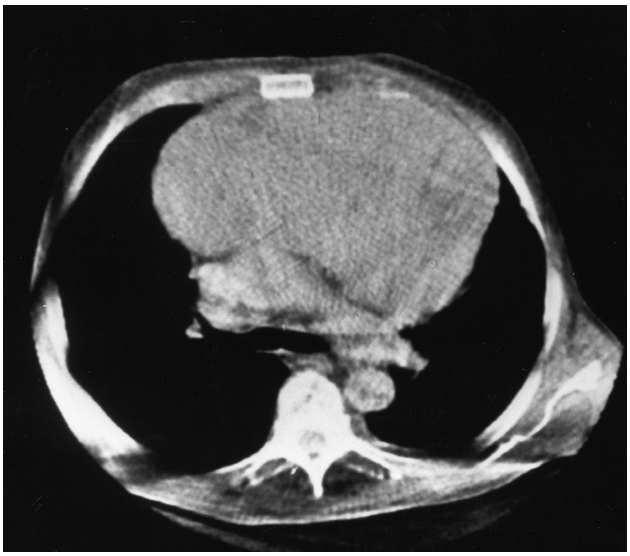

FIGURE 3-97 CT scan of anterior mediastinal mass. Enormous soft tissue mass (thymoma) causes posterior displacement of other mediastinal structures. No difference in density can be seen between the mass and the heart behind it.

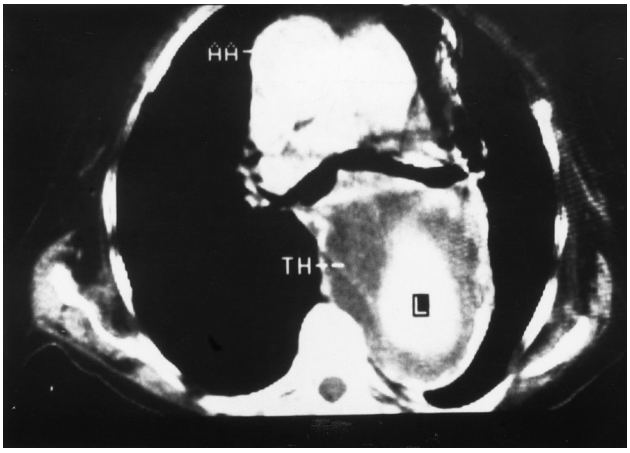

FIGURE 3-98 CT of posterior mediastinal mass. Contrast-enhanced scan at level just below carina shows large aneurysm of descending aorta. Large mural thrombus (TH) surrounds greatly dilated lumen of descending aorta (L). Note also the prominently dilated ascending aorta (AA).

DISORDERS OF THE DIAPHRAGM

The diaphragm is the major muscle of respiration separating the thoracic and abdominal cavities. Radiographically, the height of the diaphragm varies considerably with the phase of respiration. On full inspiration, the diaphragm usually projects at about the level of the tenth posterior intercostal space. On expiration, it may appear two or three intercostal spaces higher. The average range of diaphragmatic motion with respiration is 3 to 6 cm, but in patients with emphysema it may be substantially reduced. The level of the diaphragm falls as the patient moves from a supine to an upright position. In an erect patient, the dome of the diaphragm tends to be approximately half an interspace higher on the right than on the left.

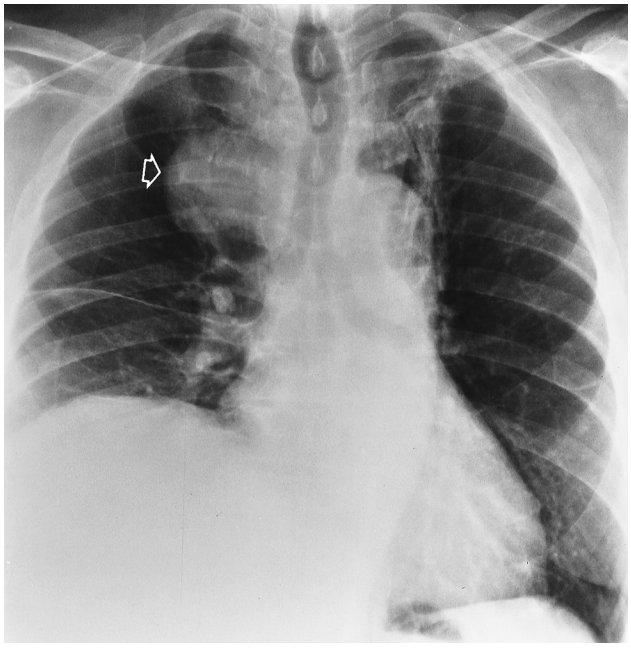

FIGURE 3-99 Diaphragmatic paralysis. Paralysis of right hemidiaphragm caused by involvement of phrenic nerve by primary carcinoma of lung (*arrow*) demonstrating a reduced lung volume.

However, in approximately 10% of normal individuals, the hemidiaphragms are at the same height or the left is higher than the right.

Diaphragmatic Paralysis

Elevation of one or both leaves of the diaphragm can be caused by paralysis resulting from any process that interferes with the normal function of the phrenic nerve. The paralysis may be attributable to accidental surgical transection of the phrenic nerve, involvement of the nerve by primary bronchogenic carcinoma or metastatic malignancy in the mediastinum, or a variety of intrinsic neurologic diseases (Figure 3-99). Reduced lung volume results from this paralysis.

Imaging Appearance. The radiographic hallmark of diaphragmatic paralysis is paradoxical movement of the diaphragm, which is best demonstrated at fluoroscopy by having the patient sniff. This rapid but shallow inspiration causes a quick downward thrust of a normal leaf of the diaphragm, whereas a paralyzed hemidiaphragm tends to rise with inspiration because of the increased intraabdominal pressure. During expiration, the normal hemidiaphragm rises and the paralyzed one descends. The demonstration of a pronounced degree of paradoxical motion is a valuable aid in differentiating paralysis of the diaphragm from limited diaphragmatic motion resulting from intrathoracic or intraabdominal disease.

Treatment. In most cases, diaphragmatic paralysis requires no treatment. If gravity does not provide enough lung volume, insertion of a diaphragmatic pacer may be necessary.

FIGURE 3-100 Diaphragmatic eventration. Lack of movement in a poorly developed diaphragm resulting in generalized elevation of the right hemidiaphragm.

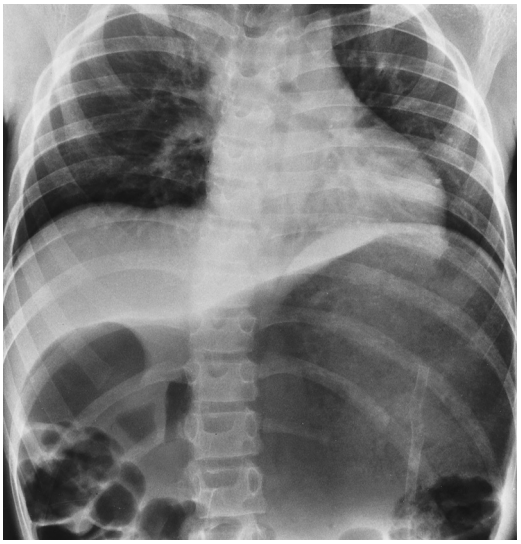

FIGURE 3-101 Diaphragmatic elevation. Diffuse elevation of both leaves of the diaphragm caused by severe, acute gastric dilation.

Eventration of the Diaphragm

Eventration of the diaphragm is a rare congenital abnormality in which one hemidiaphragm (very rarely both) is poorly developed and too weak to permit the upward movement of abdominal contents into the thoracic cage. The condition is usually asymptomatic and occurs more frequently on the left.

Imaging appearance. Eventration produces the radiographic appearance of a localized bulging or generalized elevation of the diaphragm (Figure 3-100). An eventration must be distinguished from a diaphragmatic hernia, through which abdominal contents are displaced into the chest. Oral administration of barium should permit the differentiation between the normal contours of the bowel below a diaphragmatic eventration and the crowding of these structures and narrowing of their afferent and efferent limbs when trapped in a hernia sac.

Treatment. Eventration rarely needs treatment. Infants in distress may require surgical plication to shorten the diaphragm by removal of a fold.

Other Causes of Elevation of the Diaphragm

Diffuse elevation of one or both leaves of the diaphragm can be caused by ascites, obesity, pregnancy, or any other process in which the intraabdominal volume is increased (Figure 3-101). Intraabdominal inflammatory diseases, such as subphrenic abscess, can lead to elevation of a hemidiaphragm with severe limitations of diaphragmatic motion. Cystic or tumor masses arising in the upper quadrants can cause localized or generalized bulging of the diaphragm. Acute intrathoracic processes (e.g., chest-wall injury, atelectasis, and pulmonary embolism) can produce diaphragmatic elevation caused by splinting of the diaphragm.

Imaging appearance. An apparent elevation of a hemidiaphragm may be caused by a subpulmonic pleural effusion, which can be correctly diagnosed on a chest radiograph performed with a horizontal x-ray beam and the patient in a lateral decubitus position.

Summary of Findings for Diaphragmatic Disorders

Disorder	Location	Imaging Appearance	Treatment
Diaphragmatic paralysis	Diaphragm motion	Sniff test to distinguish normal from abnormal	No treatment in most cases Diaphragmatic pacer
Diaphragmatic eventration	Diaphragm poorly developed and elevated	Diaphragm elevation	No treatment in most cases Plication possible
Other causes of diaphragmatic elevation	Elevation due to extrinsic cause	Diaphragm elevation	Treatment varies on the basis of cause

REVIEW QUESTIONS

1. Two common complications of intubation and barotrauma are _____ and _____.
2. A catheter commonly used to measure cardiac output and central venous pressure is the:
3. The optimal location for a central venous catheter is where the brachiocephalic veins join to form the:
4. An overexposed radiograph is often requested for visualizing transvenous endocardiac pacemakers to demonstrate both the _____ and the _____.

5. The most common complication associated with the Swan–Ganz catheter is _____ distal to the catheter tip.
6. Briefly describe why a lateral chest radiograph is very important for determining the correct position of the tip of the electrode of a transvenous cardiac pacemaker.
7. _____ is a disease of newborns characterized by progressive underaeration of the lungs and a granular appearance.
8. _____ is a hereditary disease in which thick mucus is secreted by all the exocrine glands.
9. A viral infection causing inflammatory obstructive swelling of the subglottic portion of the trachea is:
10. *Haemophilus influenzae* most commonly causes _____ _____.
11. When inflammatory exudate replaces air in the alveoli causing the affected area of the lung to appear radiopaque on the image, this is an example of _____.
12. A necrotic area of pulmonary parenchyma containing purulent or puslike material is called a(n) _____.
13. What radiographic procedure is often required to confirm the diagnosis of bronchiectasis when the results of routine chest radiographs are inconclusive?
14. Flattening of the domes of the diaphragm, increased AP diameter of the chest, and increased lucency of the retrosternal air space are suggestive of a diagnosis of _____.
15. The three most common pneumoconioses are _____, _____, and _____.
16. A granulomatous disease of unknown origin that usually affects women more than men and African Americans more than whites, and whose presence is most often identified on screening chest radiographs, is _____.
17. An abnormal vascular communication between a pulmonary artery and a pulmonary vein is termed a(n) _____.
18. What medical emergency has occurred when air continues to enter the pleural space and cannot escape, leading to complete collapse of a lung and shift of the heart and mediastinal structures?
19. Pus in the pleural space is called _____.
20. A lung inflammation caused by bacteria or viruses is called a(n) _____.
21. Name two common types of pulmonary mycoses.
22. For the radiographer's safety, it is important to remember that tuberculosis is spread mainly by _____, which produces infectious _____.
23. What medical term is used to describe the entry of air into the pleural space?
24. An increased volume of air in the lungs is seen in _____.
25. Inhalation of irritating dusts leading to chronic inflammation and pulmonary fibrosis is called _____.
26. A malignant pleural neoplasm that results from asbestosis is _____.
27. The trapping of bacteria in the pulmonary circulation that occurs in patients with a history of intravenous drug abuse is called _____.
28. Reduced air volume within a lung leading to collapse is termed _____.
29. Why do intrabronchial foreign bodies occur more frequently in the lower right lung?
30. Blunt or penetrating trauma to the chest can produce _____, which appears as streaks of air that outline muscles of the thorax and sometimes the neck.
31. At what costal interspace does the diaphragm lie when the lungs are fully inflated?
    a. eighth
    b. ninth
    c. tenth
    d. eleventh
32. Air collecting behind the sternum and dissecting up into the soft tissue of the neck is called _____.
33. An accumulation of fluid in the pleural space, sometimes caused by heart failure or pulmonary embolus, is called _____.
    a. emphysema
    b. edema
    c. effusion
    d. abscess

Skeletal System

OUTLINE

Physiology of the Skeletal System
Congenital/Hereditary Diseases of Bone
- Vertebral Anomalies
- Spina Bifida
- Osteopetrosis
- Osteogenesis Imperfecta
- Achondroplasia
- Congenital Hip Dysplasia (Dislocation)

Inflammatory and Infectious Disorders
- Rheumatoid Arthritis
- Rheumatoid Variants: Ankylosing Spondylitis, Reiter's Syndrome, and Psoriatic Arthritis
- Osteoarthritis (Degenerative Joint Disease)
- Infectious Arthritis
- Treatment of Arthritis
- Bursitis
- Rotator Cuff Tears
- Tears of the Menisci of the Knee
- Bacterial Osteomyelitis
- Tuberculous Osteomyelitis

Metabolic Bone Disease
- Osteoporosis
- Osteomalacia
- Rickets
- Gout
- Paget's Disease
- Lead Poisoning

Fibrous Dysplasia
Ischemic Necrosis of Bone
Benign Bone Tumors
- Treatment of Benign Bone Tumors

Malignant Bone Tumors
- Treatment of Malignant Bone Tumors

Bone Metastases
Fractures
- Types of Fractures
- Fracture Healing
- Pathologic Fractures
- Stress Fractures
- Battered-Child Syndrome
- Common Fractures and Dislocations

Fractures and Dislocations of the Spine
Herniation of Intervertebral Disks
Scoliosis
Spondylolysis and Spondylolisthesis

KEY TERMS

aneurysmal bone cyst
angulation
ankylosing spondylitis
appositional growth
avulsion fractures
bone islands
bowing fracture
boxer's fracture
butterfly fragment
cancellous (spongy) bone
cervical rib
chondrosarcoma
clay shoveler's fracture
closed fractures
Colles' fracture
comminuted fracture
compact bone
complete fracture
compound fracture
compression fracture
depressed fracture
diaphysis
dislocation
displacement
endosteum
epiphyseal cartilage
epiphyses
external fixation
external, or closed, reduction
Galeazzi fracture
giant cell tumor (osteoclastoma)
greenstick fracture
hangman's fracture
incomplete fracture
internal fixation
intramembranous ossification
Jefferson fracture
Jones fracture
lead poisoning
marrow
medullary cavity
meningocele
metaphysis
Monteggia fracture
multiple myeloma
myelomeningocele
navicular
oblique fracture
open fracture
open reduction
ossification
osteoblasts
osteoclasts
osteogenic sarcoma
osteomas
pathologic fracture
periosteum
Pott's disease
psoriatic arthritis
resorption
seat belt fracture
segmental fracture
simple bone cyst (unicameral)
spina bifida occulta
spiral fracture
spondylolisthesis
spondylolysis
stable
stress, or fatigue, fracture
subluxation
torus (buckle) fracture
trabeculae
transitional vertebra
transverse fracture
tuberculous arthritis
undisplaced fracture
unstable

OBJECTIVES

After reading this chapter, the reader will be able to:

- Classify the more common diseases in terms of their attenuation of x-rays
- Explain the changes in technical factors required for obtaining optimal-quality images in patients with various underlying pathologic conditions
- Define and describe all boldface terms in this chapter
- Describe the physiology of the skeletal system
- Identify anatomic structures on both diagrams and radiographs of the skeletal system
- Differentiate the various pathologic conditions affecting the skeletal system and their radiographic manifestations

RADIOGRAPHER NOTES

Three factors are critical in radiography of the skeletal system: (1) proper patient positioning; (2) correct alignment of the radiographic tube, the body part being imaged, and the image receptor; and (3) choice of exposure factors that produce optimal contrast and visibility of detail. In patients with suspected fractures, two projections as close as possible to 90 degrees to each other must always be obtained to demonstrate fracture relationships. A variety of projections (e.g., oblique, tangential, and coned-down) may be required to identify obscure fractures.

At times, the poor condition of a patient may require ingenuity on the part of the radiographer to obtain diagnostic radiographs when routine positioning methods cannot be accomplished. Patients with bone tumors, arthritis, or recent trauma are frequently in severe pain and extremely frightened of further injury or of suffering more discomfort. The radiographer must reassure such patients that positioning will be carefully accomplished with as little pain or discomfort as possible. The radiographer must remember that further injury to the patient can easily occur if the proper moving techniques are not used.

At times, the radiographer may need to perform cross-table or tube-angulation projections to obtain the required images without moving the patient. In such cases, the radiographic tube must be perpendicular to the image receptor and the body part to prevent image distortion. Variations in this relationship can obscure pathologic bone conditions or lead to errors in interpretation of the alignment of fracture fragments.

Bone radiographs require a short scale of contrast to provide maximal visibility of detail. The periosteum, cortex, and internal bone structure (trabeculae) must be well demonstrated to detect the often subtle changes of fractures, demineralization, and bone destruction. For example, periosteal new bone formation may indicate underlying tumor, infection, or prior trauma, whereas minute juxta-articular erosions are often seen in arthritis. The scale of contrast must also allow visualization of the soft tissues and muscles because soft tissue swelling, calcifications, opaque foreign bodies, muscle wasting, and the presence of gas are all important radiographic findings.

It is recommended that lower to middle kVp ranges be used in all skeletal radiography. To achieve the necessary scale of contrast, extremity radiographs should be exposed using an exposure in the 60- to 69-kVp range, whereas a range of 70 to 85 kVp is recommended for studies of the spine, pelvis, thoracic cavity, and shoulder. As radiographers change to digital images, the kVp should be increased slightly to compensate for a slower system with only minimal increase in patient dose. The scale of contrast will be controlled by selection of the correct algorithm during processing of the image. Appropriate ratio grids, or Bucky devices, should be used for all body parts 10 cm or larger to aid in producing images with a higher contrast (by reducing secondary and scatter radiation).

Special techniques, such as magnification or tomography, may be necessary to detect subtle fractures or other pathologic bone conditions. For example, the navicular bone of the wrist typically requires the use of the magnification technique. For 2× linear or 4× area magnification, the object must be an equal distance from the radiographic tube and the image receptor. For 3× linear or 9× area magnification, the body part must be twice as far from the image receptor as from the x-ray tube. Close collimation is extremely important to prevent undercutting the image. A radiographic tube with a fractional focal spot of 0.3 mm or less is mandatory for a magnification factor of 2× or more to compensate for the excessive penumbra (geometric blur) that results from the object image receptor distance. Larger focal spot sizes cause excessive geometric blurred images that appear to have motion and lack recorded detail as a result of excessive geometric blur (penumbra).

Tomography may be required to make a definitive diagnosis if the plain radiographic images are equivocal or to delineate precisely the extent of bone involvement. For example, tomography was frequently needed in the evaluation of fractures of the tibial plateau and spine. Currently, computed tomography (CT) is the modality of choice for evaluation of the bones and spinal injuries. It is used for spinal injury because it best demonstrates the vertebrae and fracture fragments that could impinge on the spinal cord or peripheral nerves. Magnetic resonance imaging (MRI) better demonstrates nontraumatic disk herniation or tumor impingement. In trauma cases, if CT results are inconclusive, MRI may better delineate soft tissue injury.

In most cases, it is essential to prevent motion of the body part being radiographed. To accomplish this, the radiographer should make the patient as comfortable as possible, use immobilization devices when necessary, and use the shortest possible exposure times. However, a few portions of the skeletal system are better visualized using a motion technique. For three such areas (the sternum and the lateral thoracic spine, and to obtain a transthoracic lateral projection of the upper humerus), a shallow breathing technique is used while the patient remains immobilized. A minimum exposure time of approximately 5 seconds and a very low milliamperage should be used. The patient is instructed to breathe rhythmically during the entire exposure to blur out overlying ribs and lung

markings. An additional technique, the Ottonello (or "wagging jaw") method, is used to obtain an AP projection of the cervical spine. Movement of the jaw is used to blur out the image of the mandible, which otherwise would superimpose the upper portion of the cervical spine.

Certain pathologic conditions of the skeletal system require that the radiographer alter routine technical settings. Some disorders produce greater bone density (e.g., sclerosis and increased bone growth), which increases attenuation; others decrease the density of the bony structures (e.g., lytic bone destruction and loss of calcium from bone), and so they will attenuate x-rays less (see Box 1-1). It is important to remember that the necessary technical changes may vary according to the stage of the underlying condition. However, the technical factors should not be changed to obscure or change the interpretation of the pathophysiologic changes.

PHYSIOLOGY OF THE SKELETAL SYSTEM

The skeletal system is composed primarily of two highly specialized connective tissues: bone and cartilage. Bone consists of an organic matrix in which inorganic salts (primarily calcium and phosphate) are deposited. A fibrous membrane termed the **periosteum** covers the outer surfaces of bone, except at joint surfaces, where articular cartilage covers the bone and acts as a protective cushion. The periosteum contains a network of blood vessels from which nutrient arteries penetrate into the underlying bone. The main shaftlike portion is termed the **diaphysis**, and the ends of the bone are called **epiphyses**. The hollow, tubelike structure within the diaphysis, known as the **medullary cavity**, or **marrow**, is lined by an inner membrane termed the **endosteum** (Figure 4-1A).

There are two major types of bone. The outer layer consists of **compact bone**, which to the naked eye appears dense and structureless. Under the microscope, the matrix of compact bone consists of complex structural units called "haversian systems." **Cancellous (spongy) bone** is composed of a web-like arrangement of marrow-filled spaces separated by thin processes of bone, called **trabeculae**, that are visible to the naked eye (Figure 4-1B). The relative amount of each type of bone depends on the strength required and thus varies from bone to bone and in different portions of the same bone. For example, the shafts of long bones, such as the femur and tibia, have a thick outer layer of compact bone, whereas the layer of compact bone is relatively thin in irregular bones, such as vertebral bodies and facial bones, and in short bones, such as the carpal and tarsal bones.

Most bones form from models composed of hyaline cartilage (enchondral ossification). In a typical long bone, a primary ossification center appears in the center of the cartilage precursor in about the eighth week of intrauterine life, and bone formation extends so that the entire shaft is usually ossified before birth. Just before or after birth, secondary ossification centers appear in the epiphyses, the ends of developing long bones. Until the linear growth of bone is complete, the epiphysis remains separated from the diaphysis by a cartilaginous plate called the **epiphyseal cartilage**. The epiphyseal cartilage persists until the growth of the bone is complete. At that time, the epiphyseal plate ossifies, and the epiphysis and diaphysis fuse (at various ages depending on the specific bones). Where the diaphysis meets the epiphyseal growth plate is a slight flaring, known as the **metaphysis**.

The increase in length of a developing long bone occurs by growth of the epiphyseal cartilage followed by ossification. Bones grow in diameter by the combined action of two special types of cells called **osteoblasts** and **osteoclasts**. Osteoclasts enlarge the diameter of the medullary cavity by removing bone from the diaphysis walls. At the same time, osteoblasts from the periosteum produce new bone around the outer circumference. Osteoblasts and osteoclasts thus continuously resorb old bone and produce new bone. This constant process of remodeling occurs until the bone assumes its adult size and shape.

The radiographic determination of bone age is useful for evaluating physiologic age and growth potential and also for predicting adult stature. The best known and most widely accepted method of determining skeletal bone age (skeletal maturation) is that of Greulich and Pyle in their radiographic atlas compiled from thousands of examinations of American children at different ages. This atlas contains standard radiographs for age and sex that permit an assessment of bone age based on the presence or absence of ossification centers and their configuration, and the fusion of epiphyses in various portions of the hand and wrist.

Throughout life, bone formation (**ossification**) and bone destruction (**resorption**) continue to occur. They are in balance during the early and middle years of adulthood. After approximately age 40 years, however, bone loss at the inner or endosteal surface exceeds bone gain at the outer margins. Thus, in long bones, the thickness of compact bone in the diaphyses decreases, and the diameter of the medullary cavity increases. The bone eventually resembles a hollow shell and is less able to resist compressive and bending forces. This process may lead to collapse and loss of height of vertebral bodies as well as to fractures of long bones after relatively mild injury.

Bones can also develop within a connective tissue membrane (**intramembranous ossification**). The clavicles and flat bones of the skull have no cartilaginous stage and begin to take shape when groups of primitive cells differentiate into osteoblasts, which secrete matrix material and collagenous fibrils. Deposition of complex calcium salts in the organic bone matrix produces rodlike trabeculae that join in a network of interconnecting spicules to form spongy or cancellous bone. Eventually, plates of compact or dense bone cover the core layer of spongy bone. Flat bones grow in size by the addition of osseous tissue to their outer surfaces (**appositional growth**). They cannot grow by expansion, as enchondral bone does. Bones perform five basic functions (Box 4-1).

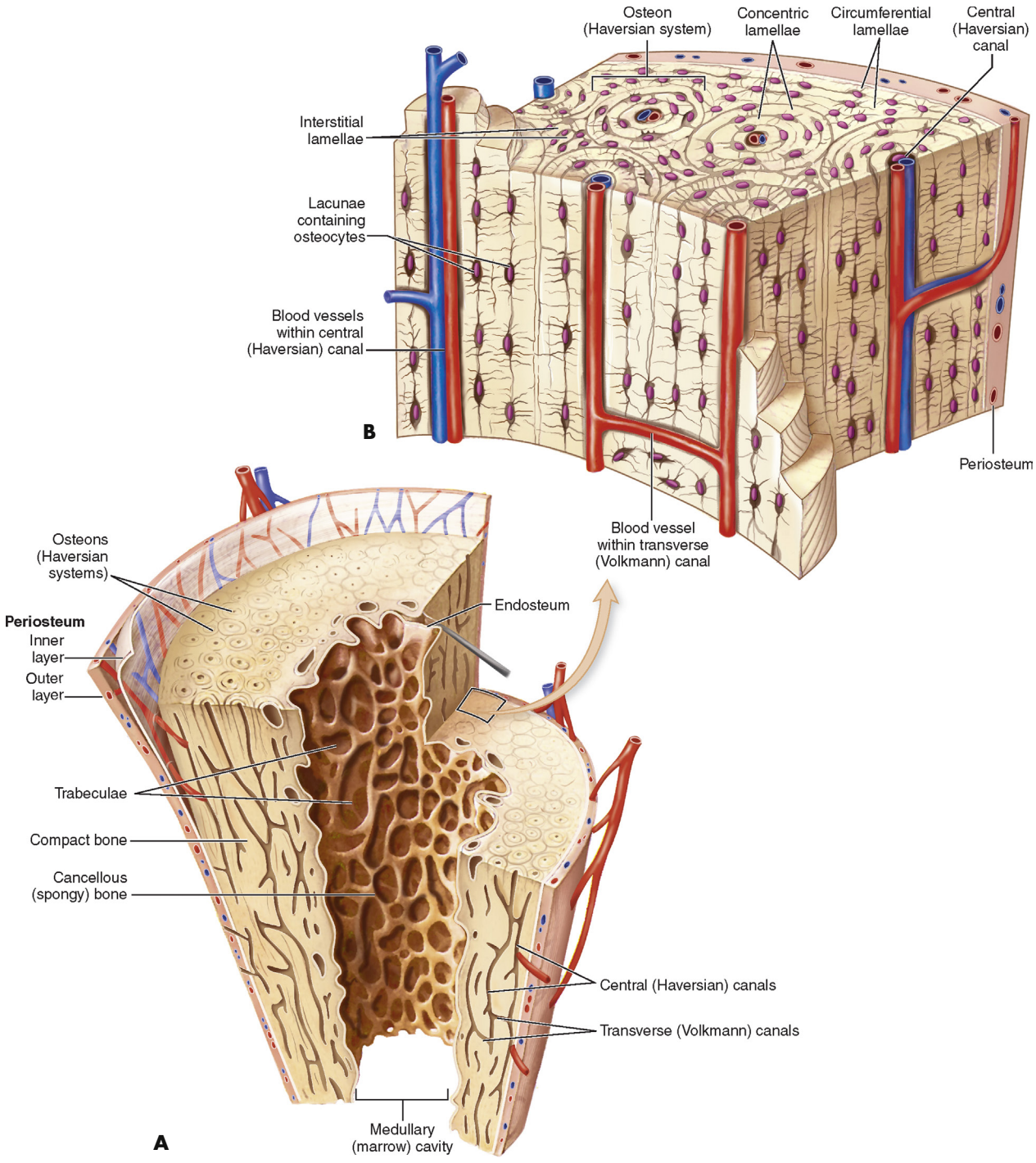

FIGURE 4-1 Long bone. (A) Partial frontal section of a long bone (tibia) showing cancellous and compact bone. (B) Frontal section of a long bone.

BOX 4-1 Five Basic Functions of Bones

1. Bones serve as the supporting framework of the body.
2. Bones protect the vital organs (e.g., the skull protects the brain, and the rib cage protects the heart and lungs).
3. Bones serve as levers on which muscles can contract and shorten and thus produce movement at a joint.
4. Red bone marrow within certain bones (spinal column, upper humerus, and upper femur in the adult) is the major site of production of blood cells.
5. Bone serves as the major storehouse for calcium salts. The maintenance of a normal level of calcium, which is essential for survival, depends on a balance in the rates of calcium movement between the blood and bones.

CONGENITAL/HEREDITARY DISEASES OF BONE

Vertebral Anomalies

A **transitional vertebra** is one that has characteristics of vertebrae on both sides of a major division of the spine.

Imaging appearance. Transitional vertebrae most frequently occur at the lumbosacral junction and contain expanded transverse processes, which may form actual unilateral or bilateral joints with the sacrum (Figure 4-2). When unilateral, this process often leads to degenerative change involving the opposite hip and the intervertebral disk space above it. At the thoracolumbar junction, the first lumbar vertebra may have rudimentary ribs articulating with the transverse processes. The seventh cervical vertebra may also have a rudimentary rib (Figure 4-3).

Treatment. Most vertebral anomalies remain unnoticed and are incidental findings on radiographs. A **cervical rib** may compress the brachial nerve plexus (causing pain or numbness in the upper extremity) or the subclavian artery (decreasing blood flow to the arm) and therefore require surgical removal.

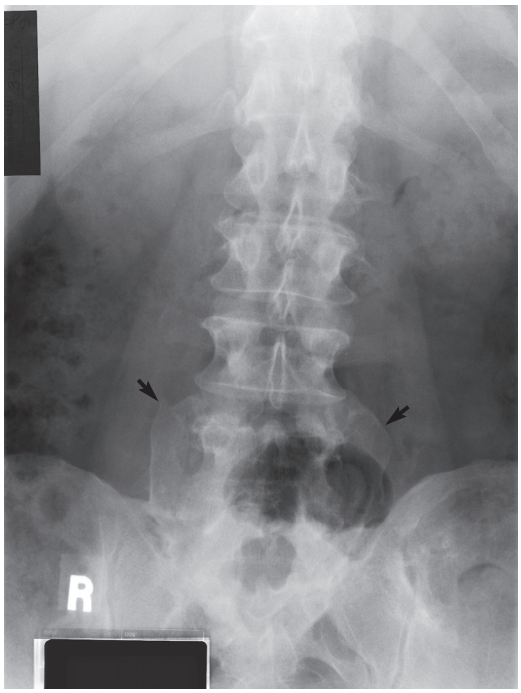

FIGURE 4-2 Transitional vertebrae. Expanded transverse process at the lumbosacral junction.

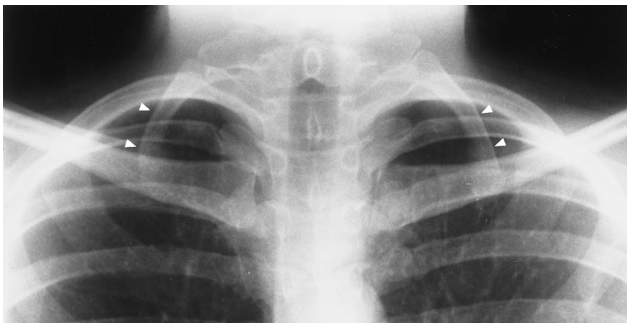

FIGURE 4-3 Transitional vertebrae. Bilateral cervical ribs (*arrowheads*).

Spina Bifida

Spina bifida refers to a posterior defect of the spinal canal, resulting from failure of the posterior elements to fuse properly. A mild, insignificant form is **spina bifida occulta**, in which there is a splitting of the bony neural canal at the L5 or S1 level (Figure 4-4). Large defects are associated with spinal cord abnormalities and may lead to a variety of muscular abnormalities and lack of bladder or bowel control. In many cases, a slight dimpling of the skin or a tuft of hair over the vertebral defect indicates the site of the lesion.

Large defects in the lumbar or cervical spine may be accompanied by herniation of the meninges (**meningocele**) or of the meninges and a portion of the spinal cord or nerve roots (**myelomeningocele**). A patient with a meningocele may be asymptomatic. Other malformations associated with a meningocele are clubfoot, gait disturbances, and bladder incontinence. The myelomeningocele has associated neurologic deficits at and below the site of protrusion. Almost all patients with myelomeningocele have the Chiari II malformation, with caudal displacement of posterior fossa structures into the cervical canal. Hydrocephalus is a frequent complication.

Imaging appearance. Spina bifida lesions are associated with large bony defects, absence of the laminae, and increased interpedicular distance (Figure 4-5). The herniated spinal contents are seen as a soft tissue mass posterior to the spine. Myelography, CT, or MRI can demonstrate the presence of spinal cord or nerve roots within the herniated sac. Prenatal real-time ultrasound can now demonstrate this serious malformation *in utero* on sagittal spine fetal images that determine the location and severity of the deformity.

Treatment. Prenatal intervention involves the daily supplement of folic acid, which has reduced the number of

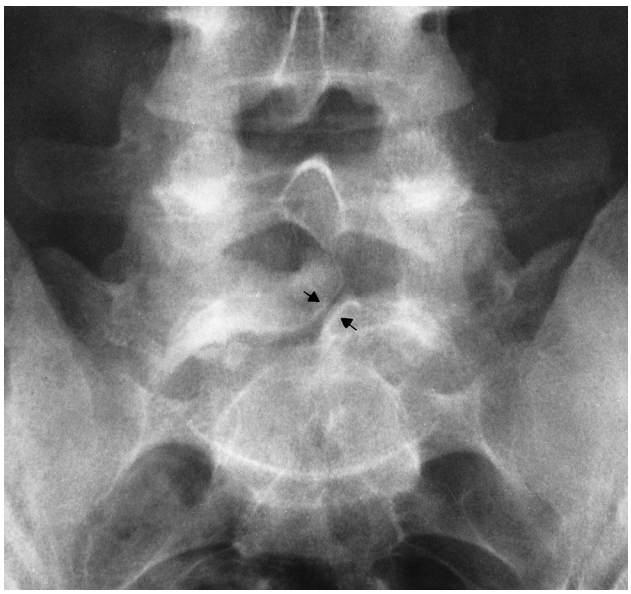

FIGURE 4-4 Spina bifida occulta. Failure of the posterior elements to fuse (*arrows*).

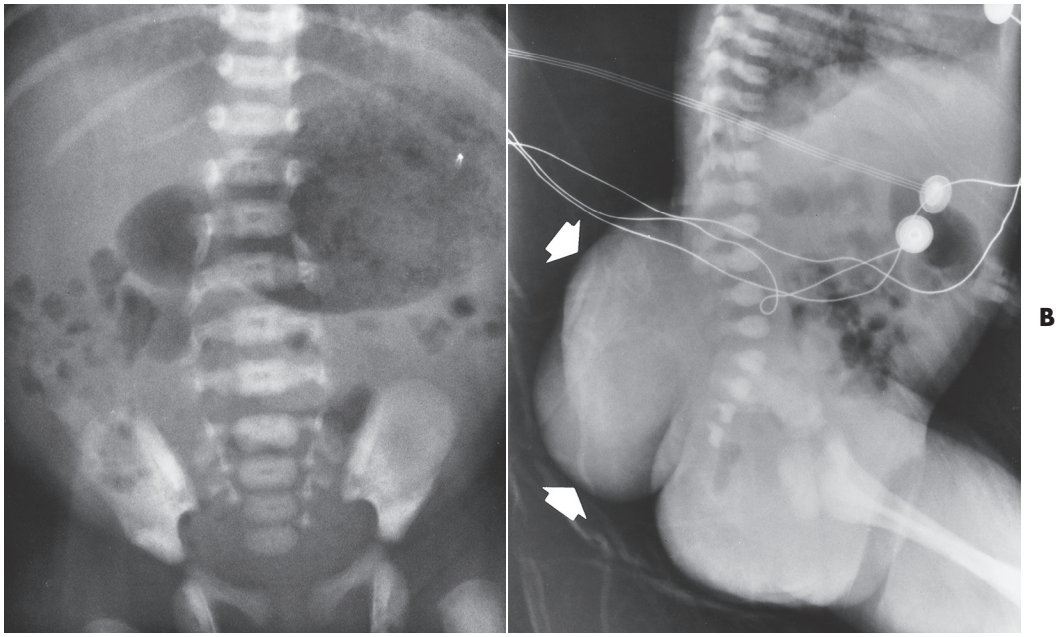

FIGURE 4-5 Meningomyelocele. (A) Frontal projection of the abdomen shows greatly increased interpedicular distance of the lumbar vertebrae. (B) In another patient, lateral projection demonstrates a large soft tissue mass (*arrows*) situated posterior to the spine. Note the absence of the posterior elements in the lower lumbar and sacral regions.

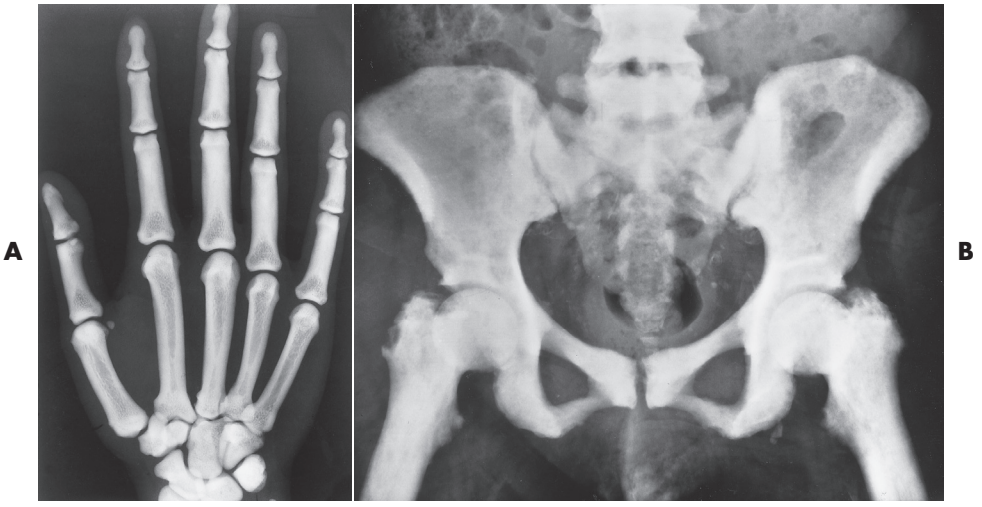

FIGURE 4-6 Osteopetrosis. (A) Striking sclerosis of the bones of the hand and wrist. (B) Generalized increased bone density of the lower spine, pelvis, and hips.

incidences of spina bifida. The ability to diagnose the fetus allows for fetal intervention, experimental surgery that helps minimize nerve deficits. Spina bifida occulta and meningoceles usually require no treatment. Sometimes a meningocele requires surgical repair, depending on the size and location of the protrusion. A myelomeningocele generally requires surgical repair. When this repair is being completed, a shunt is placed to prevent hydrocephalus.

Osteopetrosis

Osteopetrosis (marble bones) is a rare hereditary bone dysplasia in which failure of the resorptive mechanism of calcified cartilage interferes with the normal replacement by mature bone. It prevents the bone marrow from forming so that the bones become very brittle and stress fractures occur often. The patient may also become anemic as a result of the lack of blood-producing bone marrow. Osteopetrosis varies in severity and age at clinical presentation, from a fulminant, often fatal condition involving the entire skeleton at birth or *in utero* to an essentially asymptomatic form that is an incidental radiographic finding.

Imaging appearance. Osteopetrosis results in a symmetric, generalized increase in bone density (Figure 4-6). To produce a diagnostic image, the radiographer must increase the

FIGURE 4-7 Osteogenesis imperfecta of the adult foot. Demineralization and the lack of bony cortices are demonstrated on anteroposterior and lateral projections.

exposure factors (milliampere seconds [mAs] and kilovolts peak [kVp]) to compensate for the increase in bone formation (increased attenuation factor). The image may appear blurred because of the structural changes; in some cases, a good image may be difficult to produce.

Treatment. Currently, no effective treatment exists for osteopetrosis. Medications designed to increase bone resorption and blood cell production may help control the disease. For the most severe cases, bone marrow transplantation is the only way to improve the prognosis of this pathologic disorder. For less severe cases, bone marrow transplants increase the production of blood cells to manage the anemia. Transplantation of osteoclastic precursors may help control the balance of bone formation and resorption.

Osteogenesis Imperfecta

Osteogenesis imperfecta (brittle bones) is an inherited generalized disorder of connective tissue characterized by multiple fractures and an unusual blue color of the normally white sclera of the eye. Due to imperfectly formed or inadequate bone collagen, the adult patient with osteogenesis imperfecta is generally wheelchair bound because the skeletal structure does not support the body weight (Figure 4-7).

Imaging appearance. Patients with this condition suffer repeated fractures caused by the severe osteoporosis and the thin, defective cortices (Figure 4-8A). The fractures often heal with exuberant callus formation (often so extensive as to simulate a malignant tumor), sometimes causing bizarre deformities. Because of the severe cortical bone loss in advanced stages of disease, producing a good radiographic image may require lowering the kilovoltage to compensate for the loss of bone quality. Ossification of the skull progresses slowly, leaving wide sutures and multiple juxtasutural accessory bones within a suture (wormian bones) that produce a mosaic appearance (Figure 4-8B). "Child abuse" may be confused with osteogenesis imperfecta because of the presentation of multiple fractures in different stages of the healing process.

Treatment. The aim of treatment is to reduce fractures by using proper safety measures. Because of defective cortices in severe cases, the long bones become less supportive. Therefore, in some instances, extendable rods are surgically placed to provide more support, help prevent new fractures from occurring, and prevent long bone bowing (Figure 4-9). Currently, drugs are prescribed to regulate the osteoclastic formation, thus keeping the bone density more normal. As research continues, stem cell transplants may become a viable cure.

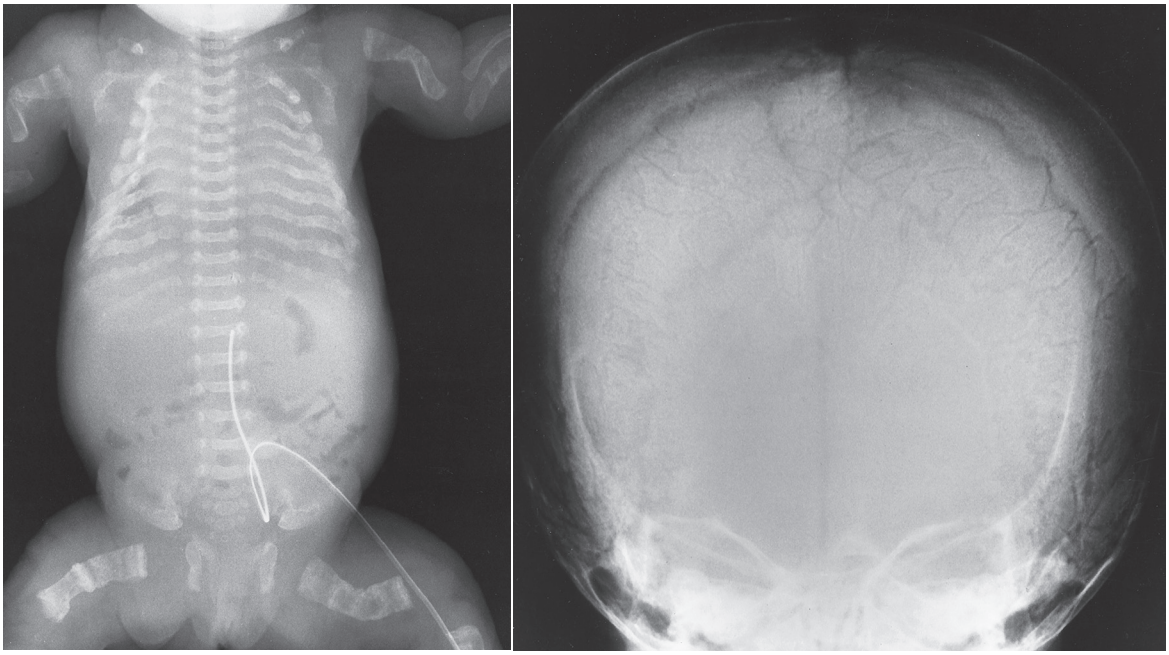

FIGURE 4-8 Osteogenesis imperfecta. **(A)** Generalized flattening of vertebral bodies associated with fractures of multiple ribs and long bones in an infant. **(B)** Multiple wormian bones.

Achondroplasia

Achondroplasia is the most common form of dwarfism; it results from diminished proliferation of cartilage in the growth plate (decreased enchondral bone formation). This autosomal dominant condition does not affect membranous bone formation. Therefore, the individual has short limbs, which contrast with the nearly normal length of the trunk (axial skeleton). Other characteristic physical features are a large head with frontal bulging, saddle nose, a prognathous (jutting) jaw, and prominent buttocks that give the false impression of lumbar lordosis.

Imaging appearance. Typical radiographic findings include progressive narrowing of the interpedicular distances from above downward, which is the opposite of normal, and scalloping of the posterior margins of the lumbar vertebral bodies (Figure 4-10). The decreased enchondral bone formation may make the long bones appear short and thick with a widened metaphysis (Erlenmeyer flask deformity) (Figure 4-11). CT is beneficial in demonstrating the degree of spinal narrowing caused by spondylosis and the changes in the vertebral column.

Treatment. Achondroplasia has no cure, and treatments address complications or deformities associated with the disease process. Patients afflicted with it live normal independent and productive lives. With today's technology, the long bones can be surgically lengthened. Growth hormone treatment for achondroplasia is still considered experimental; however, preliminary reports indicate positive results in increasing bone growth.

Congenital Hip Dysplasia (Dislocation)

Congenital hip dysplasia, also known as developmental hip dysplasia, results from incomplete acetabulum formation caused by physiologic and mechanical factors. Physiologically, the fetus is exposed to increased hormone levels during delivery. Mechanically, as the fetus grows and occupies more space, the amount of amniotic fluid decreases, placing gentle pressure on the infant. Hip dysplasia is more common in females. During pediatric assessment of the hip, when the leg is flexed and abducted, the hip may "pop" out of joint and a "click" is felt or heard. The tendons and ligaments responsible for proper femoral head alignment are affected.

Imaging appearance. Anteroposterior (AP) pelvis and bilateral frog-leg (Cleaves) views are required to make a diagnosis (Figure 4-12). In many cases, the AP image appears almost normal with only a slightly larger joint space. On the bilateral frog-leg view, the hip is usually dislocated superiorly and posteriorly. Because children with this disorder will undergo a multitude of follow-up images to recheck development, it is very important to shield the gonadal anatomy.

Ultrasound imaging (ultrasonography) now provides an alternative imaging method. The sonolucent femoral head can be viewed in relationship to the acetabulum to demonstrate the femoral angles. If sonography is available, its use allows the ionizing radiation dose to the child to be reduced because previously, clinicians relied on two different x-ray projections for each assessment.

Treatment. Treatment depends on the type of femoral head movement: subluxation or dislocation. Children not diagnosed and treated before walking may appear to "waddle like a duck." Immobilization of the femoral head is the most common treatment. To accomplish this, a harness or pelvic cast is used. Such immobilization allows the acetabulum to continue to form correctly before the infant begins to walk.

FIGURE 4-9 Osteogenesis imperfecta. Anteroposterior (A) and lateral (B) projections of the lower leg show extension rod placement to strengthen bone and decrease fracture possibility.

Summary of Findings for Congenital/Hereditary Bone Diseases

Disorder	Location	Imaging Appearance	Treatment
Vertebral anomalies	Lumbar Cervical	Unilateral or bilateral, L5 expanded transverse process Rudimentary C7 rib	Cervical—may require surgical removal for compression of brachial plexus or subclavian artery
Spina bifida	Cervical, thoracic, or lumbar/sacral spine	Splitting of bony neural canal CT/MRI—soft tissue posterior mass with or without spinal cord and nerve roots US—fetal demonstration of location and severity of pathophysiology	Prevention—folic acid supplements during pregnancy Fetal intervention—minimizing nerve damage Nonfusion requires no treatment Myelomeningocele is removed surgically

Continued

Summary of Findings for Congenital/Hereditary Bone Diseases—cont'd

Disorder	Location	Imaging Appearance	Treatment
Osteopetrosis	Entire skeleton	Generalized increased bone density	No efficacious treatment Medications to increase bone resorption Possible transplant—bone marrow or osteoclastic precursors
Osteogenesis imperfecta	Long bones	Pathologic fracture, very thin cortical density	Fracture alignment External fixation—casting or braces Internal fixation—extension rods for long-bone support to reduce deformities Medications to reduce osteoclastic formation Stem cell transplants are on the horizon
Achondroplasia	Vertebrae (short stature), long bones	Progressive interpedicular distance from superior to inferior, and scalloping of posterior vertebral bodies Widened metaphysis (Erlenmeyer flask deformity) CT—demonstrates spinal narrowing due to spondylosis and vertebral column changes	Nonspecific Growth hormone therapy (experimental)
Hip dysplasia	Incomplete acetabulum formation	AP and frog-leg projections of pelvis to demonstrate superior and posterior dislocation US—sonolucent femoral head in relationship to acetabulum (angle determination)	Immobilization by a harness or casting

US, Ultrasound.

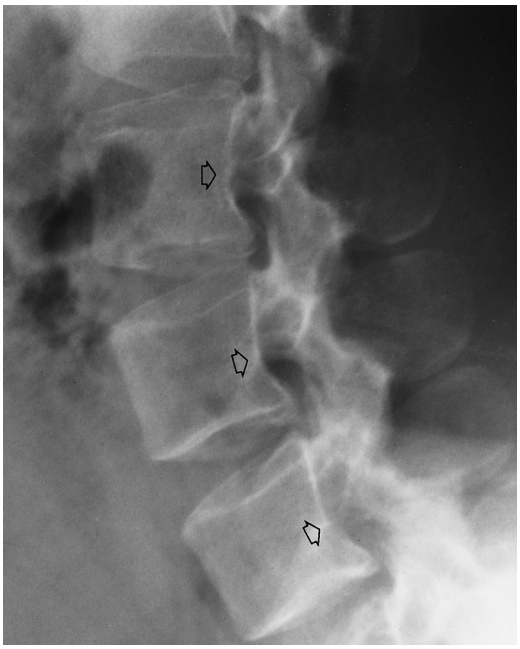

FIGURE 4-10 Achondroplasia. Posterior scalloping of multiple vertebral bodies (*arrowheads*).

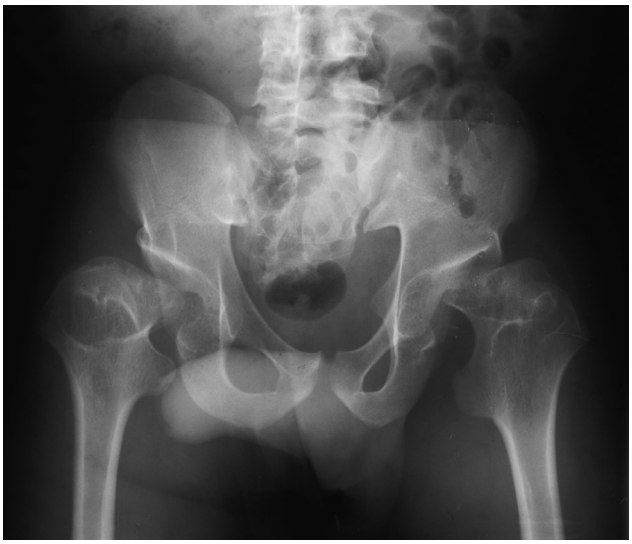

FIGURE 4-11 Achondroplasia. View of the pelvis demonstrates femoral head deformity caused by decreased endochondral bone formation.

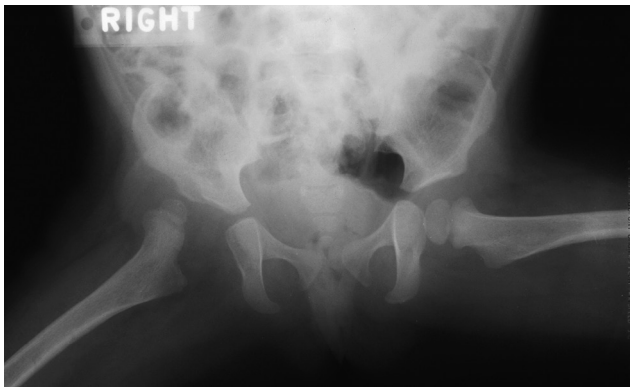

FIGURE 4-12 Hip dysplasia of the right hip in a 2-year-old child. Cleaves (frog-leg) view of the pelvis demonstrates superior and posterior displacement.

INFLAMMATORY AND INFECTIOUS DISORDERS

Rheumatoid Arthritis

Rheumatoid arthritis is a chronic systemic disease of unknown cause that appears primarily as a nonsuppurative (noninfectious) inflammatory arthritis of the small joints of the hands and feet. Women are affected approximately three times more frequently than men, and the average age at onset in adults is 40 years. Rheumatoid arthritis usually has an insidious origin and may either run a protracted and progressive course, leading to a crippling deformity of affected joints, or undergo spontaneous remissions of variable length. There is usually symmetric involvement of multiple joints, and the disease often progresses proximally toward the trunk until practically every joint in the body is involved.

Rheumatoid arthritis begins as an inflammation of the synovial membrane (synovitis) that lines the joints. The excessive exudate, a result of the inflammation, causes proliferation of the synovium. The resulting mass of thickened granulation tissue (*pannus*, meaning "covers like a sheet") causes erosion of the articular cartilage and underlying bony cortex, fibrous scarring, and even the development of ankylosis (bony fusion across a joint). The erosion occurs because the inflammatory cells produce lytic enzymes. A combination of the fusion of joint surfaces and an inflammatory laxity of ligaments leads to the development of crippling deformities in the end stage of the disease (Figure 4-13).

Imaging appearance. The earliest radiographic evidence of rheumatoid arthritis is fusiform periarticular soft tissue swelling caused by joint effusion and hyperplastic synovial inflammation. Disuse and local hyperemia (increased blood flow) lead to periarticular osteoporosis that initially is confined to the portion of bone adjacent to the joint but may extend to involve the entire bone (Figure 4-14). Extension of the pannus from the synovial reflections onto the bone causes characteristic small foci of destruction at the edges of the joint, where articular cartilage is absent. These typical marginal erosions have poorly defined edges without a sclerotic rim and sometimes may be seen only on oblique or magnification projections. Destruction of articular cartilage causes narrowing of the joint space. The laying down of bony trabeculae across a narrow joint space may completely obliterate the joint cavity and produce solid bony ankylosis, which most frequently involves the bones of the wrist (see Figure 4-13).

FIGURE 4-13 Mutilating rheumatoid arthritis. Severe, bilaterally symmetric destructive changes of the hands and wrists with striking subluxations.

FIGURE 4-14 Rheumatoid arthritis. Striking periarticular osteoporosis.

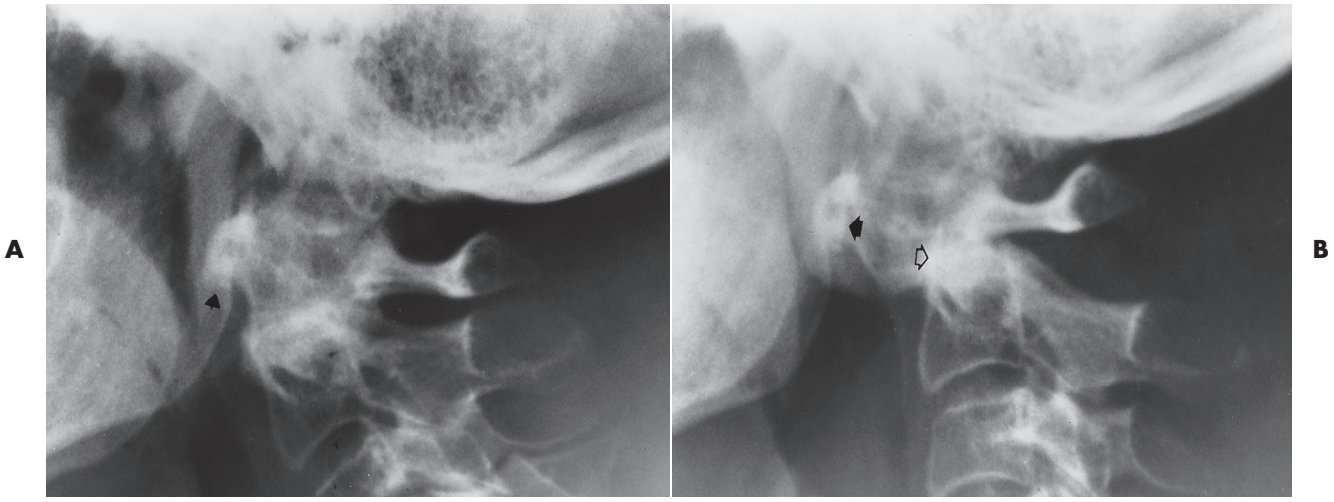

FIGURE 4-15 Subluxation of the atlantoaxial joint in rheumatoid arthritis. **(A)** Routine lateral image of the cervical spine shows a normal relationship between the anterior border of the odontoid process and the superior portion of the anterior arch of the atlas (*arrowhead*). **(B)** With flexion, there is wide separation between the anterior arch of atlas (*solid arrow*) and the odontoid (*open arrow*).

Ligamentous involvement produces a variety of contractures and subluxations causing the common ulnar deviation of the hands (see Figure 4-13). In the cervical spine, rheumatoid arthritis characteristically produces atlantoaxial subluxation (Figure 4-15), an increased distance between the anterior border of the odontoid and the superior border of the anterior arch of the atlas (normally less than 2.5 mm), which results from weakening of the transverse ligaments from synovial inflammation. The synovial inflammation appears as a soft tissue mass that causes a narrowing of the atlantoaxial articulation on CT images. CT also demonstrates associated erosion of the odontoid (in approximately two-thirds of patients).

Rheumatoid nodules are soft tissue masses that usually appear over the extensor surfaces on the ulnar aspect of the wrist or the olecranon but occasionally are seen over other body prominences, tendons, or pressure points. These characteristic nodules, which develop in approximately 20% of patients with rheumatoid arthritis and do not occur in other diseases, aid in making the diagnosis.

Rheumatoid Variants: Ankylosing Spondylitis, Reiter's Syndrome, and Psoriatic Arthritis

Imaging appearance of ankylosing spondylitis. **Ankylosing spondylitis** almost always begins in the sacroiliac joints, causing bilateral and usually symmetric involvement. Blurring of the articular margins and patchy sclerosis generally progress to narrowing of the joint space and may lead to complete fibrous and bony ankylosis (Figure 4-16). The disease typically progresses from the lumbar spine upward.

Ossification in the paravertebral tissues and longitudinal spinal ligaments (poker spine) combines with extensive lateral bony bridges (syndesmophytes) between vertebral bodies to produce the characteristic "bamboo spine" of advanced disease (Figure 4-17; see Figure 4-16). Limitation of activity leads to generalized skeletal osteoporosis and a tendency to fracture in response to the stress of minor trauma (Figure 4-18). CT demonstrates both the fusion due to intra-articular and ligamentous ossification and any spinal stenosis caused by the displacement of the fractures.

FIGURE 4-16 Ankylosing spondylitis. Bilateral, symmetric obliteration of the sacroiliac joints and "bamboo spine."

Imaging appearance of Reiter's syndrome. Reiter's syndrome (reactive arthritis) is characterized by arthritis, urethritis, and conjunctivitis. It primarily affects young adult men and appears to occur after certain types of venereal or gastrointestinal infections. Reiter's syndrome most frequently involves the sacroiliac joints, heel, and toes (Figure 4-19). Unlike in ankylosing spondylitis, the sacroiliac involvement here is usually bilateral but asymmetric, and Reiter's syndrome tends to cause only minimal changes in the spine.

FIGURE 4-17 Lumbar spine. Severe vertebral fusion, or "bamboo spine."

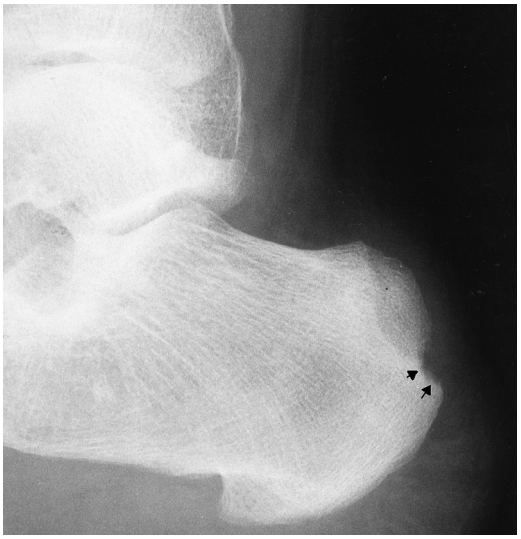

FIGURE 4-19 Reiter's syndrome. Striking bony erosion (*arrows*) at insertion of the Achilles tendon on the posterosuperior margin of calcaneus.

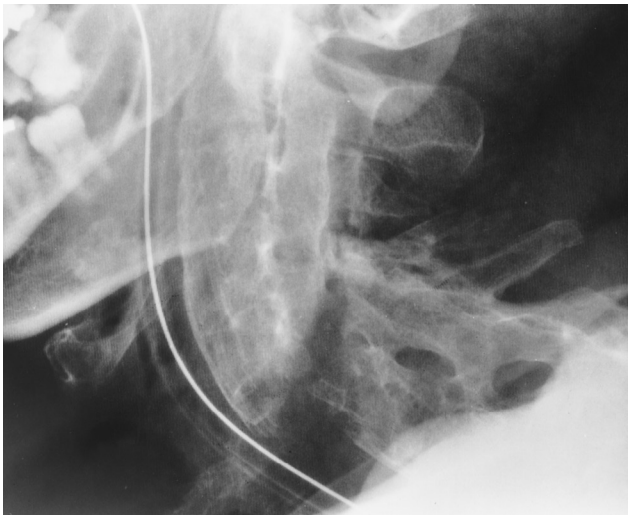

FIGURE 4-18 Ankylosing spondylitis. Oblique fracture of the midcervical spine with anterior dislocation of the superior segment is seen in a patient who fell while dancing and struck his head. Fracture extends through the lateral mass and lamina.

FIGURE 4-20 Reiter's syndrome. Erosive changes about the metatarsophalangeal joint of the fifth digit. Erosions involve juxta-articular region, leaving articular cortex intact.

Although the radiographic changes in peripheral joints often mimic rheumatoid arthritis, Reiter's syndrome tends to be asymmetric and primarily involves the feet rather than the hands (Figure 4-20).

Imaging appearance of psoriatic arthritis. **Psoriatic arthritis** refers to a rheumatoid arthritis–like destructive process involving peripheral joints that develops in patients with typical skin changes of psoriasis (Figure 4-21). Unlike rheumatoid arthritis, psoriatic arthritis predominantly involves the distal rather than the proximal interphalangeal joints of the hands and feet, produces asymmetric rather than symmetric destruction, and causes little or no periarticular osteoporosis.

Characteristic findings include bony ankylosis of the interphalangeal joints of the hands and feet and resorption of the terminal tufts of the distal phalanges (Figure 4-22). Characteristics common to both Reiter's syndrome and psoriatic

FIGURE 4-21 Psoriatic arthritis. Bizarre pattern of asymmetric bone destruction, subluxation, and ankylosis. Note the particularly severe pencil-in-cup deformity of the third proximal interphalangeal joint and also the bony ankylosis involving the wrist and the phalanges of the second and fifth digits.

FIGURE 4-22 Psoriatic arthritis. Severe mutilating arthritis of the foot and ankle. There is extreme pencil-like destruction of the metatarsals and phalanges, with ankylosis of almost all tarsal joints.

arthritis include erosions and hypertrophic changes occurring in the origin and insertion of the tendons and ligaments.

Osteoarthritis (Degenerative Joint Disease)

Osteoarthritis is an extremely common generalized disorder characterized pathologically by loss of joint cartilage and reactive new bone formation. Part of the wear and tear of the aging process, degenerative joint disease tends to affect predominantly the weight-bearing joints (spine, hip, knee, and ankle) and the interphalangeal joints of the fingers. A secondary form of degenerative joint disease may develop in a joint that has been repeatedly traumatized or subjected to abnormal stresses because of orthopedic deformities, or it may be a result of a septic or inflammatory arthritis that destroys cartilage.

Imaging appearance. The earliest radiographic findings in degenerative joint disease are narrowing of the joint space, caused by thinning of the articular cartilage, and development of small bony spurs (osteophytes) along the margins of the articular edges of the bones. In contrast to the smooth, even narrowing of the joint space in rheumatoid arthritis, the joint space narrowing in degenerative joint disease is irregular and more pronounced in that part of the joint where weight-bearing stress is greatest and where degeneration of the articular cartilage is most noticeable. The articular ends of the bones become increasingly dense (periarticular sclerosis). Erosion of the articular cortex may produce typical irregular, cystlike lesions with sclerotic margins in the subchondral bone near the joint. Calcific or ossified loose bodies may develop, especially at the knee. With advanced disease, relaxation of the joint capsule and other ligamentous structures may lead to subluxation. Local osteoporosis does not occur unless pain causes prolonged disuse of the joint.

In the fingers, degenerative joint disease involves primarily the distal interphalangeal joints (Figure 4-23). Marginal spurs produce well-defined bony protuberances that appear clinically as the palpable and visible knobby thickening of Heberden's nodes. In the hip, the most prominent finding is asymmetric narrowing of the joint space that involves predominantly the superior and lateral aspects of the joint, where the greatest stress of weight bearing exists (Figure 4-24). Joint space narrowing is also asymmetric in the knee, where it predominantly involves the medial femorotibial compartment (Figure 4-25).

Infectious Arthritis

Pyogenic (pus-forming) organisms may gain entry into a joint by the hematogenous route, by direct extension from an

FIGURE 4-23 Osteoarthritis of fingers. Note narrowing of the interphalangeal joints with spurring and erosions.

FIGURE 4-24 Osteoarthritis of the hip. Demonstrates sclerotic bone formation in the acetabulum.

adjacent focus of osteomyelitis, or from trauma to the joint (e.g., after surgery). The onset of bacterial arthritis usually occurs abruptly with a high fever, shaking chills, and one or a few severely tender and swollen joints. The most common type today is a migratory arthritis from Lyme disease.

Imaging appearance. Soft tissue swelling is the first radiographic sign of acute bacterial arthritis. In children, fluid

FIGURE 4-25 Osteoarthritis of the knee. Decreased joint space and osteophytes on the femur and tibia.

distention of the joint capsule may cause widening of the joint space and actual subluxation, especially about the hip and shoulder. Periarticular edema displaces or obliterates adjacent tissue fat planes (Figure 4-26A). Rapid destruction of articular cartilage causes joint space narrowing early in the course of the disease. The earliest bone changes, which tend to appear 8 to 10 days after the onset of symptoms, are small focal erosions in the articular cortex. Because of the delay in bone changes, detection of the characteristic soft tissue abnormalities is essential for early diagnosis. Severe, untreated infections cause extensive destruction and a loss of the entire cortical outline (see Figure 4-26). With healing, sclerotic bone reaction results in an irregular articular surface. If the articular cartilage has been completely destroyed, bony ankylosis usually follows.

Imaging appearance of tuberculous arthritis. **Tuberculous arthritis** is a chronic, indolent (organic) infection that has an insidious (gradual) onset and a slowly progressive course (Figure 4-27). It usually involves only one joint, and it affects primarily the spine, hips, and knees. Most patients have a focus of tuberculosis elsewhere in the body, most commonly in the lungs.

A distinctive early radiographic feature of tuberculous arthritis is the extensive juxta-articular (near a joint) osteoporosis that precedes bone destruction—in contrast to bacterial arthritis, in which osteoporosis is a relatively late finding. Joint effusion leads to a nonspecific periarticular soft tissue swelling. Cartilage and bone destruction occur relatively late in the course of tuberculous arthritis and tend to initially involve the periphery of the joint, sparing the maximal weight-bearing surfaces that are destroyed in pyogenic arthritis. Therefore, joint space narrowing occurs late in tuberculous arthritis, in contrast to the early narrowing seen with bacterial infections. As in pyogenic arthritis, the earliest

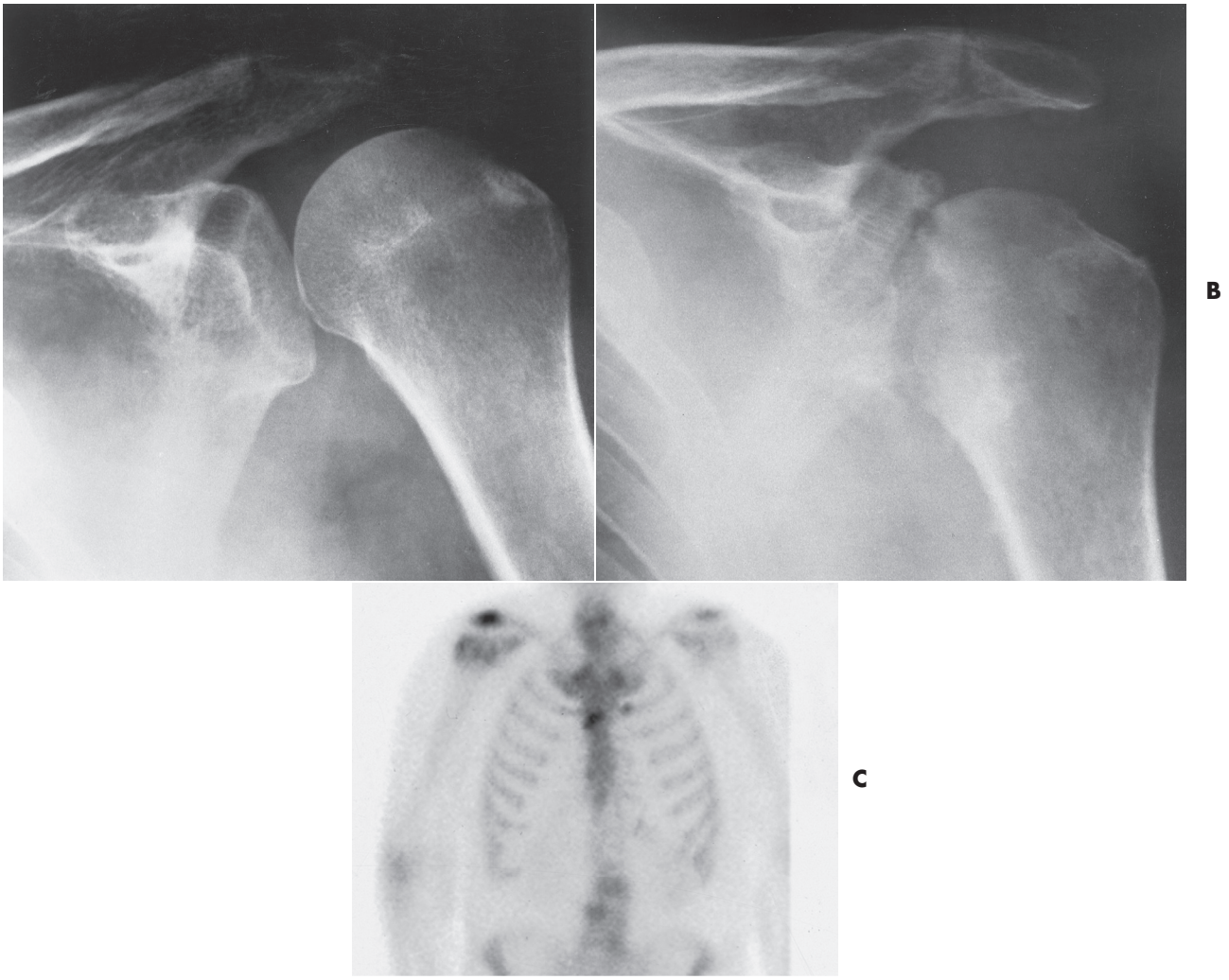

FIGURE 4-26 Acute staphylococcal arthritis. (A) Several days after instrumentation of the shoulder for joint pain, there is separation of the humeral head from the glenoid fossa caused by fluid in the joint space. (B) Six weeks later, pronounced cartilage and bone destruction are evident, with sclerosis on both sides of the glenohumeral joint. (C) Septic arthritis. On a radionuclide bone scan, a focal area of increased activity in the right shoulder correlates with the clinical history of septic arthritis.

FIGURE 4-27 Tuberculous arthritis of the elbow with complete destruction of the joint space. A large chronic granulomatous mass can be seen in the antecubital region.

evidence of bone destruction is usually erosion at the margins of the articular ends of bone. With progressive disease, there is ragged destruction of the articular cartilage and subchondral cortex and disorganization of the joint, often with preservation of necrotic fragments of bone (sequestra) that may involve opposing surfaces ("kissing sequestra").

Treatment of Arthritis

Arthritis therapy should protect affected joints, maintain mobility, and strengthen muscles. For this to occur, lifestyle changes, use of support devices, drugs, and surgery may be necessary. For those with rheumatoid arthritis and osteoarthritis, which make up 90% of all cases diagnosed, rest and exercise are recommended to minimize inflammation and preserve the range of motion. The first-line medications are nonsteroidal anti-inflammatory drugs (NSAIDs), which decrease the inflammatory response but do not affect the disease process. Prostaglandin inhibitors, such as aspirin and ibuprofen (salicylates), fall into this category of drugs

FIGURE 4-28 Rheumatoid arthritis. (A) This posteroanterior image of the hand demonstrates dislocation and joint destruction of the second through fifth metacarpophalangeal joints. (B) Postoperative image, with digits fully extended, illustrates second through fifth metacarpophalangeal joint implants.

that reduce the triggering of inflammation. A more aggressive group of drugs, disease-modifying antirheumatic drugs, are used in advanced stages to reduce symptoms. The antimetabolite methotrexate, a cytotoxic drug, tempers cell division in the synovial joint. Invasive surgery involves replacing joints with new artificial joints (Figure 4-28) to increase joint mobility. For infectious arthritis, antibiotics usually eradicate the infection and cure the arthritis. Aspiration may be needed if fluid accumulates in the bursa.

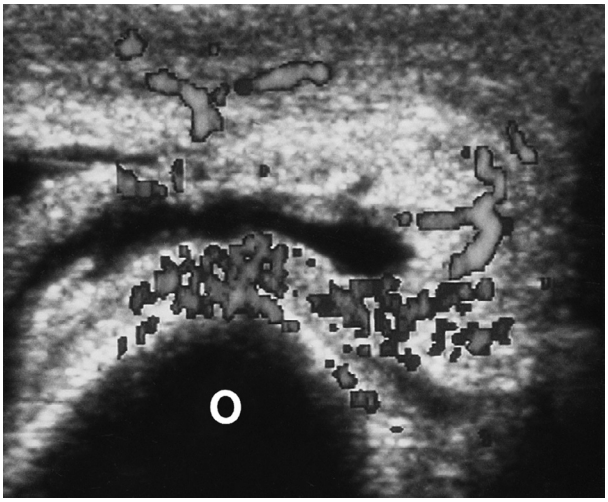

FIGURE 4-29 Bursitis. Transverse scan of the posterior aspect of the elbow shows the thick-walled, fluid-containing olecranon bursa. Power color Doppler imaging shows the bursa's activity.

Bursitis

Bursitis refers to an inflammation of the bursae, small fluid-filled sacs located near the joints that reduce the friction caused by movement. Repeated physical activity commonly causes bursitis, but trauma, rheumatoid arthritis, gout, or infection also can cause this inflammation. Bursitis or tenosynovitis is usually not visualized on plain radiographs, but disorders of the bursa and synovium can be seen on ultrasound images (Figure 4-29). Plain radiographic images may exclude other disorders that cause similar symptoms.

Imaging appearance. The major radiographic manifestation of bursitis is the deposition of calcification in adjacent tendons, which is a common cause of pain, limitation of motion (frozen joints), and disability about a joint. Calcific tendinitis most commonly involves the shoulder, and calcification may be demonstrated radiographically in approximately half the patients with persistent pain and disability in the shoulder region (Figure 4-30). However, calcification may also be detected in asymptomatic persons, and severe clinical symptoms may occur without evidence of calcification. Calcific tendinitis appears as amorphous calcium deposits that most frequently occur about the shoulder in the supraspinatus tendon, where they are seen directly above the greater tuberosity of the humerus. The deposits vary greatly in size and shape, from thin curvilinear densities to large calcific masses.

In the acute early stages of bursitis, ultrasonography demonstrates the bursa filled with synovial fluid and having ill-defined margins. During the acute phase of true tendinitis, the thickened tendon has ill-defined margins. Both bursitis and tendinitis may demonstrate increased vascularity on Doppler ultrasound.

Treatment. First-line treatments for bursitis include application of heat, rest, and immobilization. NSAIDs are taken to reduce inflammation and relieve pain, as necessary. If the inflammation results from an infection, a regimen of

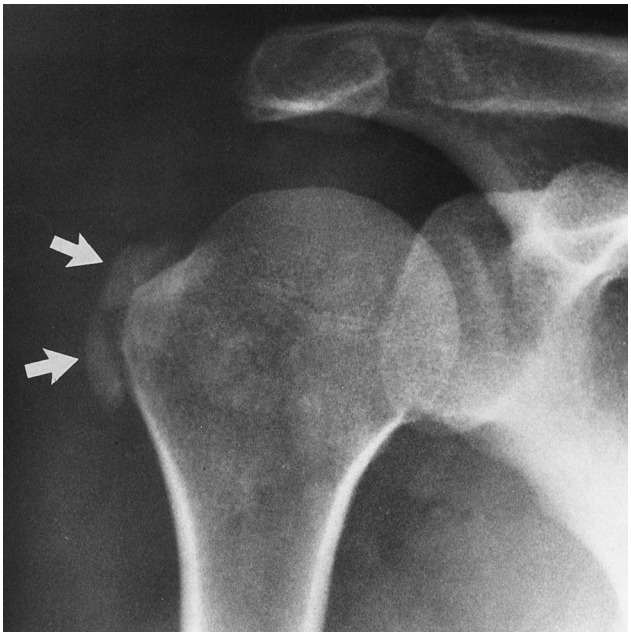

FIGURE 4-30 Calcific tendinitis. Frontal projection of the shoulder demonstrates amorphous calcium deposits (*arrows*) in the supraspinatus tendon.

FIGURE 4-31 Shoulder arthrography of a rotator cuff tear. Opacification of the subacromial and subdeltoid bursae indicates abnormal communication between them and the glenohumeral joint cavity, thus confirming the diagnosis.

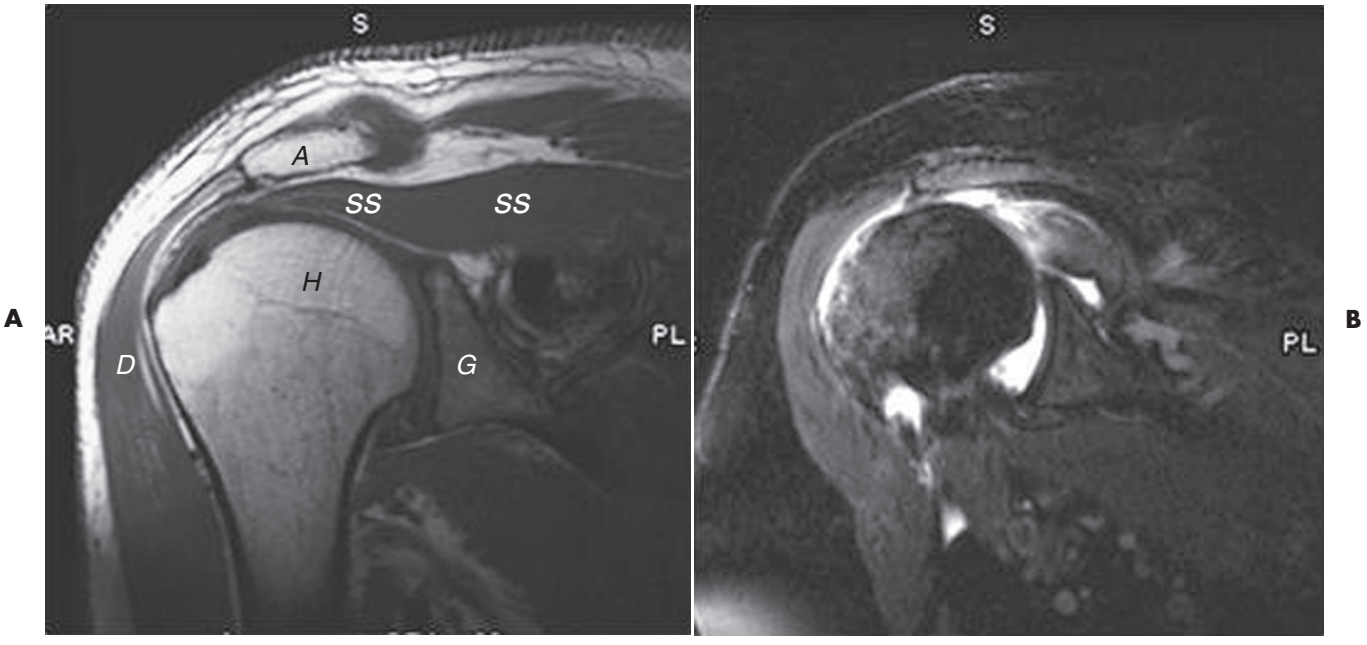

FIGURE 4-32 MRI of rotator cuff tear. (A) Coronal image of normal shoulder. Note the low signal intensity of the supraspinatus tendon (*SS*). *A,* Acromion; *D,* deltoid muscle; *G,* glenoid fossa; *H,* humeral head. **(B)** T2-weighted coronal image with fat saturation with intra-articular contrast. Supraspinatus tendon is torn and retracted.

antibiotics is appropriate. In recurring or severe bursitis, corticosteroid injections into the affected bursa may reduce the inflammation.

Rotator Cuff Tears

The rotator cuff of the shoulder is a musculotendinous structure composed of the teres minor, infraspinatus, supraspinatus, and subscapularis muscles. Rupture of the rotator cuff produces a communication between the shoulder joint and the subacromial bursa that can be demonstrated by arthrography (the injection of contrast material directly into the shoulder joint) (Figure 4-31). Currently, MRI is considered the modality of choice for demonstrating a rotator cuff disorder. The normal rotator cuff appears as a black structure, but tears cause it to have high signal intensity (Figure 4-32). However, ultrasound may be the preferred initial modality to

FIGURE 4-33 Horizontal partial-thickness tear. The longitudinal ultrasound image through the supraspinatus tendons shows a 0.69-cm retraction of the partially torn tendon (the distance between the calipers [+]).

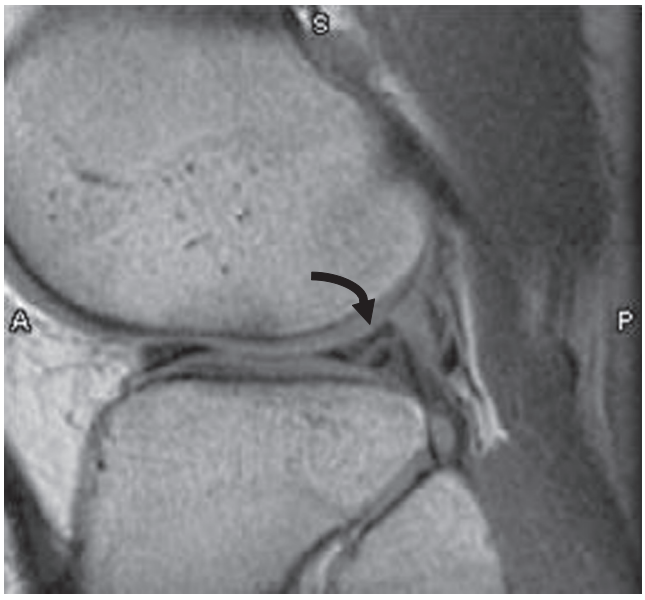

FIGURE 4-34 Meniscal tear. Sagittal proton density MR scan of knee shows bucket handle tear of the lateral meniscus (*curved arrow*).

demonstrate the tear of the tendon (Figure 4-33) because of its wider availability and lower cost.

Tears of the Menisci of the Knee

Meniscal tears are a common cause of knee pain. Although occasionally the result of acute trauma, meniscal tears more frequently reflect a degenerative process caused by the chronic trauma inherent in human knee function. In the past, meniscal tears were best demonstrated by arthrography, which is invasive; now, MRI is clearly the imaging modality of choice because it is noninvasive and has an accuracy of 90% to 98%.

MRI demonstrates a tear as a sharply marginated line of high signal intensity (Figure 4-34) that crosses the normally dark, triangular meniscus. In addition, this modality can show the often-associated tears of the anterior and posterior cruciate ligaments and changes in the underlying

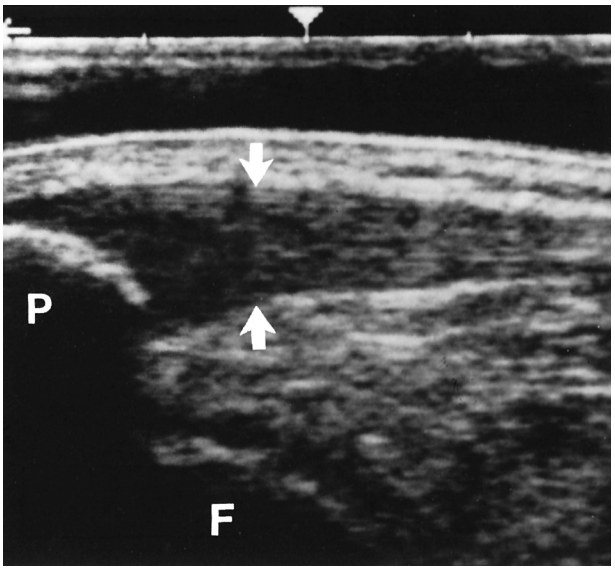

FIGURE 4-35 Acute patellar tendinitis. Longitudinal ultrasound scan shows thickening and decreased echogenicity of the upper two-thirds of the tendon (*arrows*). *F,* Femoral condyle; *P,* patella.

bone. Ultrasound may demonstrate tenosynovitis of related tendons, which appears as a thickened synovial sheath (Figure 4-35).

Treatment for Intra-articular Components

Anti-inflammatory medications and immobilization of the joint are the first line of treatment if the damage will repair itself. When the component is not completely destroyed, this treatment may result in cure (30% to 90% of cases respond to nonsurgical treatment). When irreparable joint damage has occurred, the orthopedist performs arthroscopic surgery to remove a complete or nonhealing tear or to attempt suture repair.

Bacterial Osteomyelitis

Bacterial osteomyelitis is an inflammation of the bone (osteitis) and bone marrow (myelitis) caused by a broad spectrum of infectious (most often gram-positive) organisms that reach bone by hematogenous spread, by extension from an adjacent site of infection, or by direct introduction of organisms (after trauma or surgery). Acute hematogenous osteomyelitis tends to involve bones with rich red marrow. In infants and children, the metaphyses of long bones, especially the femur and tibia, are most often affected; staphylococci and streptococci are the most common organisms. Patients with acute osteomyelitis experience fever and localized warmth, swelling, and tenderness. In adults, acute hematogenous osteomyelitis primarily occurs in the vertebrae, causing localized back pain and muscle spasm, and it rarely involves the long bones. Although the incidence and severity of osteomyelitis have decreased since the advent of antibiotics, this disease has now become more prevalent as a complication of intravenous drug abuse (in which case, gram-negative organisms are found). In diabetic patients and patients with other types

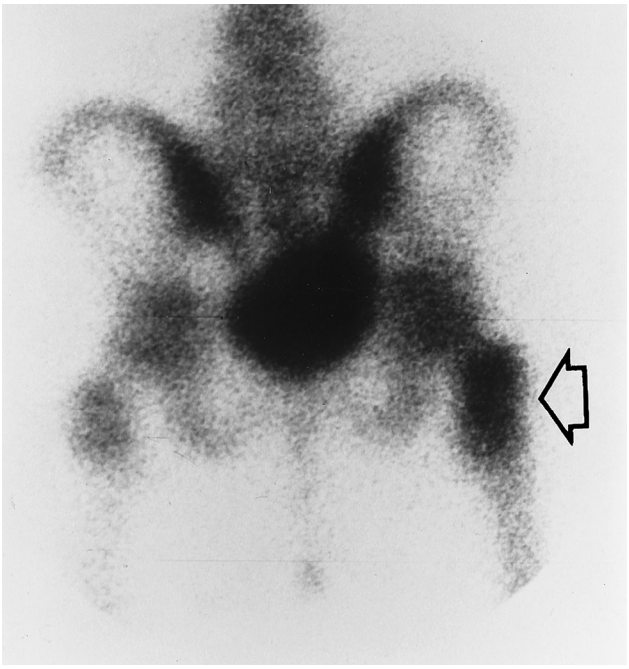

FIGURE 4-36 Osteomyelitis. Radionuclide bone scan (posterior projection) demonstrates increased uptake of radionuclide in the trochanteric portion of the right femur (*arrow*). Plain x-ray of the pelvis and hips obtained at the same time showed no detectable abnormality.

of vascular insufficiency, a soft tissue infection may spread from a skin abscess or a decubitus ulcer, usually in the foot, to cause cellulitis and eventually osteomyelitis in adjacent bones.

Osteomyelitis begins as an abscess of the bone. Pus produced by the acute inflammation spreads down the medullary cavity and outward to the surface. Once the infectious process has reached the outer margin of the bone, it raises the periosteum from the bone and may spread along the surface for a considerable distance.

Because the earliest changes of osteomyelitis are usually not evident on plain radiographic images until approximately 10 days after the onset of symptoms, radionuclide (technetium-99m) bone scanning is the most valuable imaging modality for the early diagnosis of osteomyelitis. Increased nuclide uptake, reflecting the inflammatory process and increased blood flow, is evident within hours of the onset of symptoms (Figure 4-36).

Imaging appearance. On plain radiographs, the earliest evidence of osteomyelitis in a long bone is a localized, deep soft tissue swelling adjacent to the metaphysis. The inflammation causes displacement or obliteration of the normal fat planes adjacent to and between the deep muscle bundles, unlike in skin infections, in which the initial swelling is superficial. The initial bony change appears as subtle areas of metaphyseal lucency reflecting resorption of necrotic bone. Soon, bone destruction becomes more prominent, producing a ragged, moth-eaten appearance (Figures 4-37 and 4-38). The more virulent the organism, the larger the area of destruction. Subperiosteal spread of inflammation elevates

FIGURE 4-37 Osteomyelitis. Patchy pattern of bone destruction involves much of the shaft of the radius. Note the early periosteal new bone formation (*arrows*).

the periosteum and stimulates the deposition of layers of new bone parallel to the shaft. This results in a layered periosteal reaction that is characteristic of benign diseases, especially infection. Eventually, a large amount of new bone surrounds the cortex in a thick, irregular bony sleeve (involucrum). Disruption of cortical blood supply leads to bone necrosis. Segments of avascular dead bone (sequestra) remain as dense as normal bone and are clearly differentiated from the demineralized bone, infected granulation tissue, and pus around them (Figure 4-39). Power Doppler ultrasound demonstrates increased vascularity in the inflammation elevating the periosteum.

After the acute infection has subsided, a pattern of chronic osteomyelitis develops. The bone appears thickened and sclerotic with an irregular outer margin. The cortex may become so dense that the medullary cavity is difficult to demonstrate. Reactivation of infection may appear as the recurrence of deep soft tissue swelling or periosteal calcification, or the

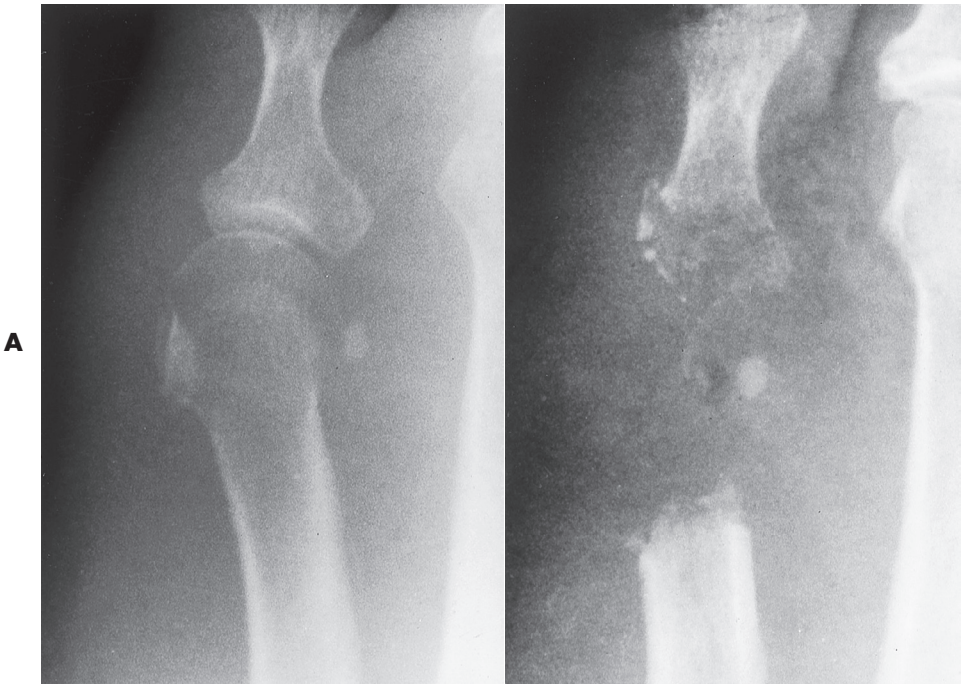

FIGURE 4-38 Staphylococcal osteomyelitis. (A) Initial image of the first metatarsophalangeal joint shows soft tissue swelling and periarticular demineralization caused by increased blood flow to the region. (B) Several weeks later, severe bony destruction about the metatarsophalangeal joint can be seen.

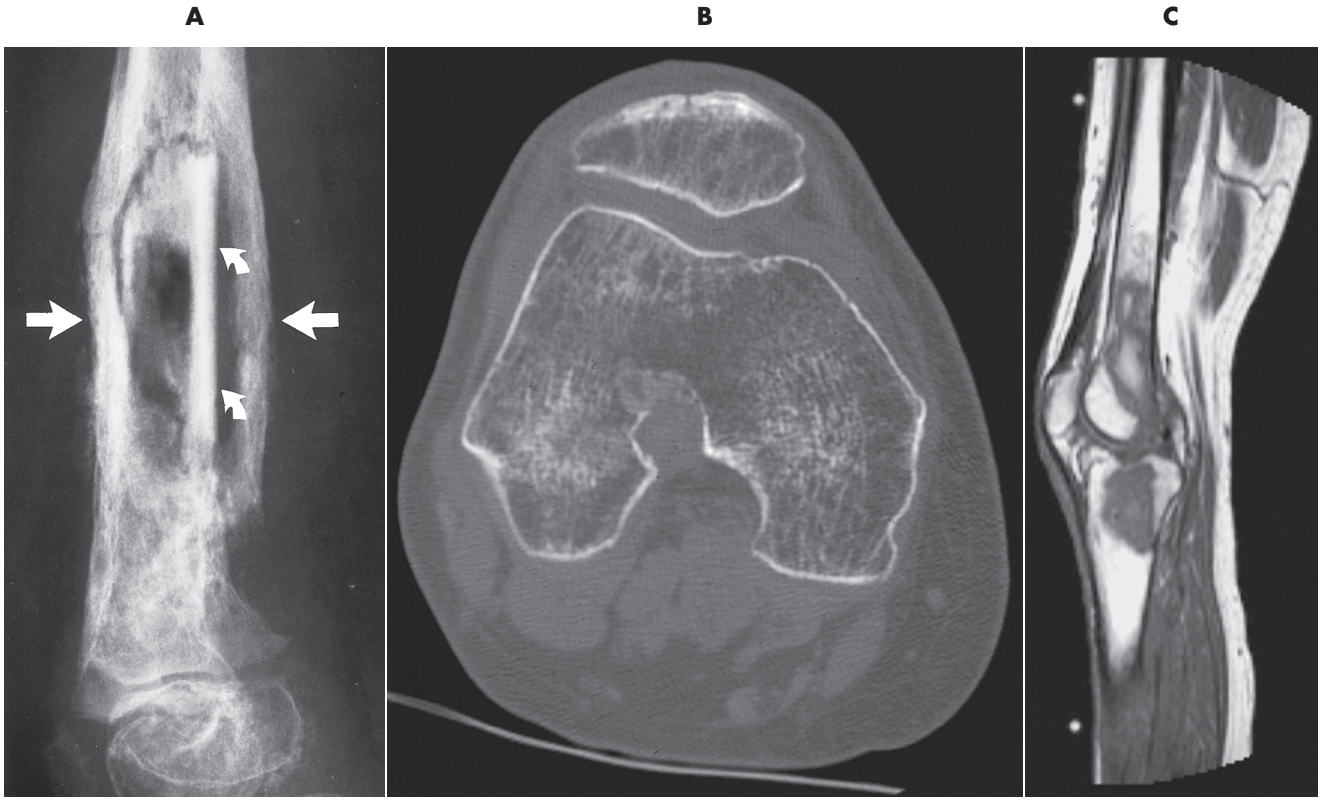

FIGURE 4-39 Chronic osteomyelitis. (A) Involucrum (*straight arrows*) surrounds sequestra (*curved arrows*). (B) After knee surgery, multiple foci can be seen to be lacking trabeculation in both femoral condyles in this 33-year-old woman. (C) Sagittal MR image of the patient in image B shows decreased signal intensity from the femoral condyle extending into the femoral shaft.

FIGURE 4-40 Bacterial vertebral osteomyelitis. Narrowing of the intervertebral disk space with irregularity of the end plates and reactive sclerosis.

development of lytic abscess cavities within the bone. However, plain radiographs are often inadequate to determine whether an active infection is present. A three-phase radionuclide scan demonstrates increased uptake on all phases and is much more sensitive and accurate for establishing recurrence.

The earliest sign of vertebral osteomyelitis is subtle erosion of the subchondral bony plate with loss of the sharp cortical outline. This may progress to total destruction of the vertebral body associated with a paravertebral soft tissue abscess (Figure 4-40). Unlike neoplastic processes, osteomyelitis usually affects the intervertebral disk space and often involves adjacent vertebrae. Depending on the site of disease, anterior extension of osteomyelitis may cause retropharyngeal abscess, mediastinitis, empyema, pericarditis, subdiaphragmatic abscess, psoas muscle abscess, or peritonitis; posterior extension of inflammatory tissue can compress the spinal cord or produce meningitis if the infection penetrates the dura to enter the subarachnoid space.

CT can be of value in the diagnosis of osteomyelitis, especially that involving the spine. This modality can precisely define the size of the surrounding soft tissue mass, its relation to nearby vital structures (aorta and spinal cord), and the presence of abscess cavities requiring surgical drainage (see Figure 4-39B). In acute osteomyelitis of long bones, the bone destruction and periosteal reaction produce a thin laminated periosteal reaction.

MRI can assist in determining whether an abscess has formed and in excluding cellulitis. Bone marrow changes caused by inflammatory exudate result in decreased signal intensity on T1-weighted images and increased signal intensity on T2-weighted images (see Figure 4-39C).

Treatment. Antibiotics to eradicate gram-negative or gram-positive organisms should be given for 4 to 8 weeks to prevent recurrence. Surgery may be required for débridement of necrotic tissue or for placement of a drain into an abscess. Bone grafts, usually of bone marrow, are placed to fill bony defects or to help bones heal. After surgery, the patient must continue to take antibiotics for approximately 3 weeks.

Tuberculous Osteomyelitis

Tuberculous osteomyelitis (which is rare today) most commonly involves the thoracic and lumbar spine. **Pott's disease** (tuberculosis of the spine) occurs in the midthoracic spine and thoracolumbar region. Irregular, poorly marginated bone destruction within the vertebral body is often associated with a characteristic paravertebral abscess, an accumulation of purulent material that produces a fusiform soft tissue mass about the vertebra. The spread of tuberculous osteomyelitis causes narrowing of the adjacent intervertebral disk and the extension of infection and bone destruction across the disk to involve the adjacent vertebral body. Unlike bacterial infection, tuberculous osteomyelitis is rarely associated with periosteal reaction or bone sclerosis.

Imaging appearance. The infection tends to begin in the anterior part of the vertebral body adjacent to the intervertebral disk (Figure 4-41A). Caseous necrosis of the vertebral marrow produces a slow resorption of bony trabeculae, with bone destruction appearing 2 to 5 months after onset of infection. In the untreated patient, progressive vertebral collapse and anterior wedging lead to a characteristic sharp kyphotic angulation (gibbous deformity) (Figure 4-41B). A radionuclide bone scan may demonstrate early activity but cannot distinguish tumors or fractures. The gallium bone scan can help to define the total tissue involvement and determine response to therapy in tuberculous osteomyelitis. CT also may delineate the extent of soft tissue involvement and illustrate osseous destruction. Soft tissue calcifications identified on CT aid in distinguishing tuberculous osteomyelitis from other conditions. MRI demonstrates changes in the bone marrow, but these findings are no more specific than those of radionuclide bone scans.

Tuberculosis can, rarely, involve a low-grade chronic infection of the long bones that appears radiographically as a generally destructive lytic process with minimal or no periosteal reaction. The spectrum of radiographic appearances is wide, varying from localized, well-circumscribed, expansile lesions to diffuse, uniform, honeycomb-like areas of destruction that are often associated with pathologic fractures. Chronic draining sinuses may develop, especially in children.

Treatment. Nonoperative treatments for tuberculous osteomyelitis include a regimen of antibiotics, antituberculous drug therapy, and possible bracing. Antibiotics help prevent abscess development, antituberculous drug therapy eradicates the tuberculosis bacilli, and bracing provides support. With this treatment combination, most patients do not require surgery. If the pain, neurologic deficits, and deformities progress, surgical intervention may be necessary. Spinal fusion or Harrington rod placement for stability may be performed.

Inflammatory and Infectious Disorders

Disorder	Location	Imaging Appearance	Treatment
Rheumatoid arthritis (ankylosing spondylitis, Reiter's syndrome, psoriatic arthritis)	Small joints symmetrically	All rheumatoid variants • Periarticular soft tissue swelling • Symmetric joint destruction and deformity RA–CT–synovial inflammation (soft tissue mass) causes narrowing of atlantoaxial articulation Ankylosing spondylitis–CT–fusion due to intra-articular and ligament ossification and spinal stenosis	NSAIDs Surgery is last resort Possible joint implants or replacements
Osteoarthritis	Weight-bearing joints	Irregular narrowing of joint space with small bony spurs (osteophytes)	NSAIDs (timed-release and coated)
Infectious arthritis	Any joint	Early joint narrowing with focal erosions NM—bone scan shows increased uptake at infected location	Antibiotics
Bursitis	Shoulder most common	Radiograph—calcific tendinitis in 50% US—thickened synovium or dense synovial fluid	Immobilization, heat, rest NSAIDs Antibiotics if infection related Corticosteroid injection for recurring incidences
Rotator cuff tear	Shoulder	US—tear in bursa and inflamed synovium	Nonsurgical: physical therapy, immobilization, and NSAIDs
Meniscal tear of the knee	Knee	MRI—tears have a high signal intensity (normal—black)	Surgery: rotator cuff repair or meniscus removal
Bacterial osteomyelitis	Child—long bones high in red marrow Adult—vertebra or bone associated with decubitus ulcer	Radiograph—soft tissue swelling with periosteal elevation Doppler US—soft tissue vascularity elevating periosteum NM—three-phase bone scan most accurate at localizing process and recurrence by an increased uptake CT—defines tissue involvement and thin laminated periosteal reaction MRI—demonstrates changes in bone marrow signal intensity	Antibiotics first-line treatment Surgery for débridement
Tuberculous osteomyelitis	Vertebra (Pott's disease)—thoracic and lumbar most common	Lytic lesion without periosteal elevation Collapsed vertebra with kyphosis	Nonoperative: antibiotics, antituberculous drug therapy, and bracing Surgical: spinal fusion and Harrington rod placement for stability

NM, Nuclear medicine; *NSAIDs,* nonsteroidal antiinflammatory drugs; *RA,* rheumatoid arthritis; *US,* ultrasound.

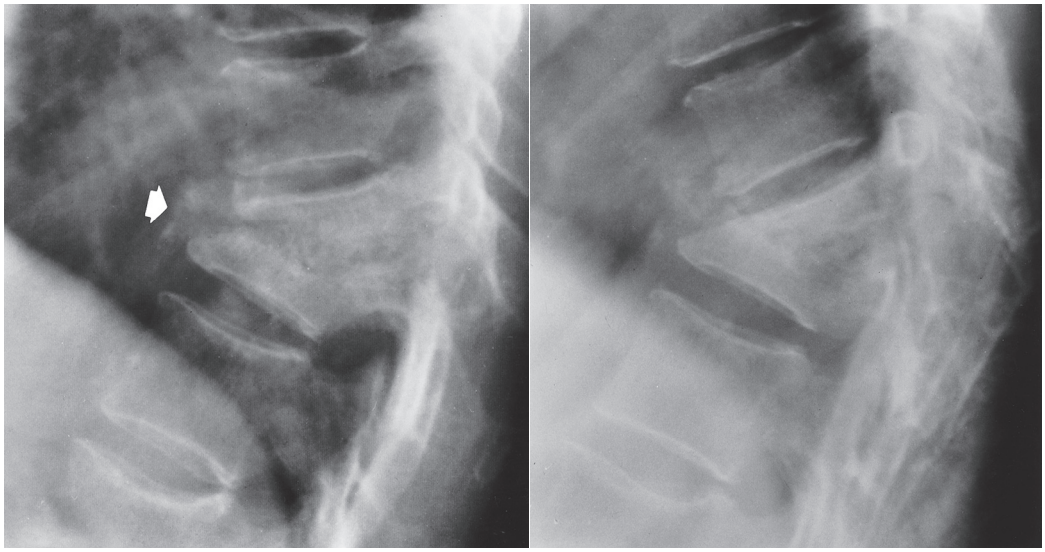

FIGURE 4-41 Tuberculous osteomyelitis. **(A)** Initial image demonstrates vertebral collapse and anterior wedging of adjacent midthoracic vertebrae (*arrow*). Residual intervertebral disk space can barely be seen. **(B)** In an image obtained several months later, there is virtual fusion of the collapsed vertebral bodies, producing the characteristic sharp kyphotic angulation (gibbous deformity).

METABOLIC BONE DISEASE

Osteoporosis

Osteoporosis is a generalized or localized deficiency of bone matrix in which the mass of bone per unit volume is decreased in amount but normal in composition. Bone is a living, constantly changing tissue, and normally a balance exists between the amount of old bone being removed (an osteoclastic process) and the amount of new bone replacement (an osteoblastic process). Osteoporosis is usually caused by accelerated resorption of bone, although decreased bone formation may lead to osteoporosis in some situations—for example, in Cushing's syndrome, after prolonged steroid administration, and after prolonged disuse or immobilization as in a casted extremity (Figure 4-42).

Loss of mineral salts causes osteoporotic bone to become more lucent than normal. This may be difficult to detect because approximately 50% to 70% of the bone density must be lost before it can be demonstrated as a lucent area on routine radiographs. For patients with osteoporosis, it is essential to use the lowest practical kVp. This technique provides the extremely short scale of contrast necessary to visualize the demineralized osteoporotic bones. Today, quantitative CT (QCT), single-photon absorptiometry, and dual-energy x-ray absorptiometry (DEXA bone densitometry–qualitative) provide data that measure bone mineral content. A QCT scan accurately demonstrates levels of bone mass and determines the rate of bone decay, which represents bone quantity. Three-dimensional QCT is considered more sensitive and accurate than the other methods. QCT measurements depend on the trabecular bone, which demonstrates the earliest signs of osteoporosis. CT scans, because of their high radiation dose, are not done as frequently as bone densitometry. DEXA bone densitometry is used to image the hip and spine, assisting in the determination of bone quality.

FIGURE 4-42 Disuse osteoporosis. Severe periarticular demineralization after prolonged immobilization of the hand.

The patient's history is entered into the computer system and two images, usually an AP lumbar spine and an AP hip, are taken (Figure 4-43). The image data are compared with those of other individuals of the same race, age, and weight to determine a bone-quality value. This value indicates whether the patient has normal bone (*T*-score > –1.0 standard deviation [SD]), osteopenia (*T*-score between –1.0 and –2.5 SD), or osteoporosis (*T*-score < –2.5 SD).

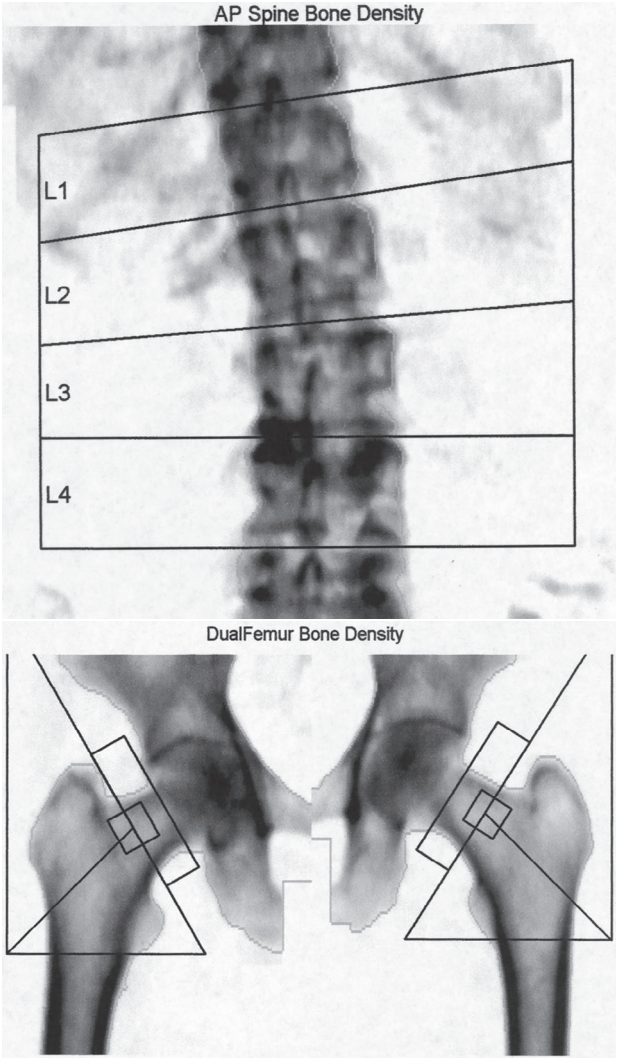

FIGURE 4-43 Osteoporosis. Results of DEXA bone mineral density (BMD) scan of the spine. **(A)** A *T*-score average of 3.3 demonstrates osteoporosis. **(B)** The dual femur of this 65-year-old woman has a *T*-score average of 2.3, indicating osteopenia.

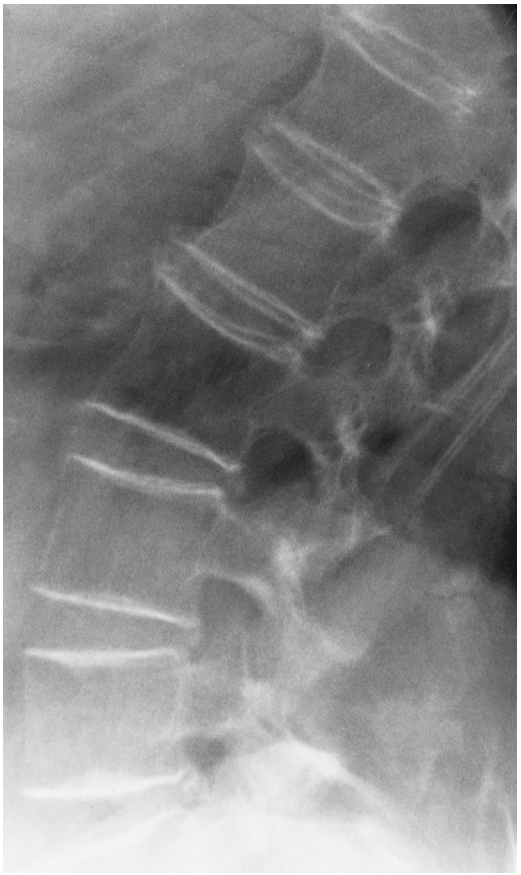

FIGURE 4-44 Osteoporosis of aging. Generalized demineralization of the spine in a postmenopausal woman. The cortex appears as a thin line that is relatively dense and prominent (picture-frame pattern).

The major causes of generalized osteoporosis are aging and postmenopausal hormonal changes. With increasing age, bones lose density and become more brittle, fracturing more easily and healing more slowly. Two factors contribute to this process: Elderly persons may become less active and they may have poor diets, often deficient in protein. In postmenopausal women, there is a deficiency in the gonadal hormonal levels that stimulate bone formation. This decreased bone formation, plus an increase in bone resorption by a factor of three to five times, results in a loss of density.

Imaging appearance. Regardless of the cause, the radiographic appearance is somewhat similar in all conditions producing osteoporosis. The most striking change is cortical thinning, with irregularity and resorption of the endosteal (inner) surfaces (Figure 4-44). These findings are most evident in the spine and pelvis. As the bone density of a vertebral body decreases, the cortex appears as a relatively dense and prominent thin line producing the typical picture-frame pattern. Because of the severe loss of bone density, anterior wedging or compression fractures of one or more vertebral bodies may result, most commonly in the middle and lower thoracic and upper lumbar areas. The intervertebral disk may expand into the weakened vertebral bodies and produce characteristic concave contours of the superior and inferior disk surfaces. In the skull, the calvaria may show a spotty loss of density, and deossification (bone loss) of the floor of the sella turcica and dorsum sellae is commonly seen.

Treatment. To help prevent osteoporosis, weight-bearing exercises help build bone density and muscle mass. For postmenopausal osteoporosis, hormonal replacement therapy and dietary supplements of calcium and vitamin D may reduce development of the disease process. In severe cases, vertebroplasty (kyphoplasty) is performed to prevent vertebral collapse (Figure 4-45).

Osteomalacia

Osteomalacia refers to insufficient mineralization of the adult skeleton. The lack of a balance between osteoid formation and mineralization influencing bone quality results in either excessive osteoid formation or, more frequently, insufficient mineralization. Proper calcification of osteoid requires that adequate amounts of calcium and phosphorus be available at

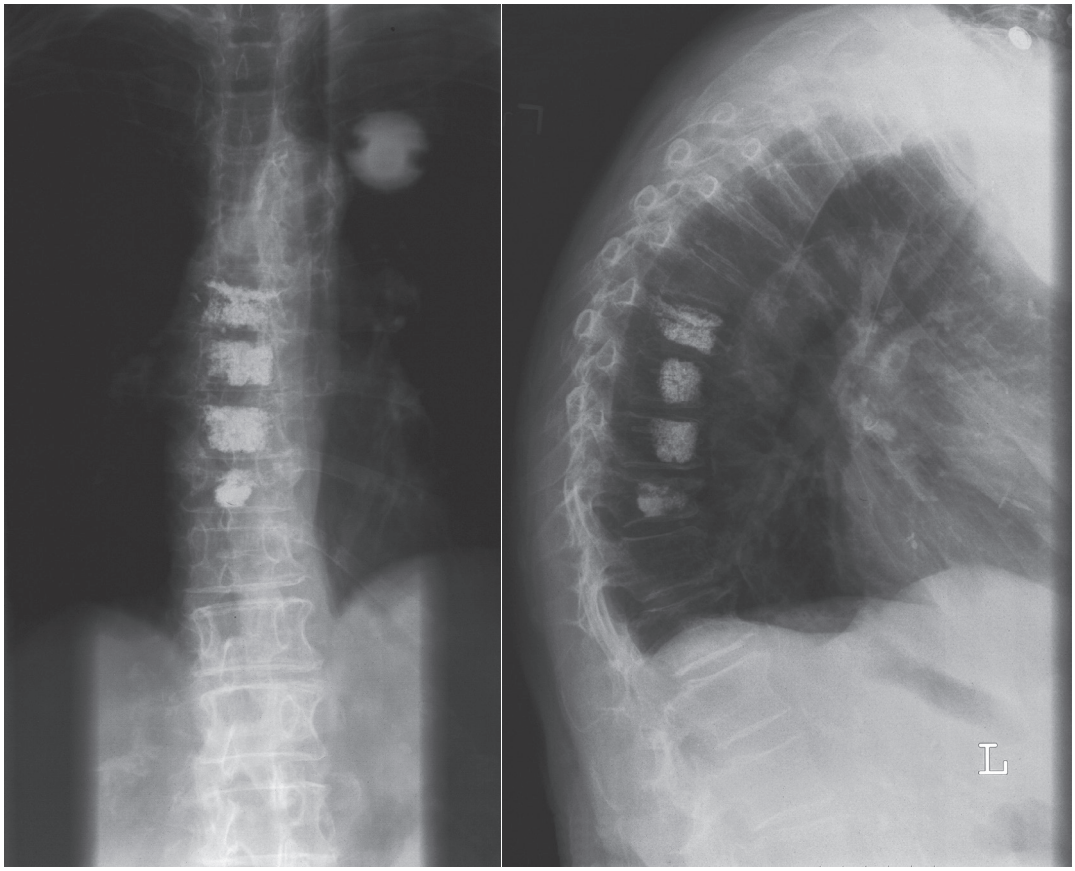

FIGURE 4-45 Thoracic vertebroplasty. Demonstration of a thoracic vertebroplasty on AP (A) and lateral (B) projections performed to prevent vertebral collapse in an 81-year-old woman with osteoporosis.

the mineralization sites. In osteomalacia, failure of calcium and phosphorus deposition in bone matrix may be attributable to an inadequate intake of, or to a failure of absorption of, calcium, phosphorus, or vitamin D. Vitamin D is necessary for intestinal absorption of calcium and phosphorus and may have a direct effect on bone. At times, the level of vitamin D is sufficient but is not used because of resistance to the action of the vitamin at end organs, such as the kidneys. Other, nonnutritional causes of osteomalacia include chronic kidney failure and certain renal diseases in which calcium is lost to the urine and then bone breaks down as the body attempts to maintain a normal calcium level in the blood.

Imaging appearance. Regardless of the cause, osteomalacia appears radiographically as a loss of bone density because of the presence of nonmineralized osteoid. Although the cortex is thinned, it may stand out more prominently than normal because of the uniform deossification of medullary bone (Figure 4-46). In contrast to the situation in osteoporosis, the cortical borders in osteomalacia often appear indistinct. Fine-detail radiographs of the hands in patients with osteomalacia often demonstrate intracortical lines caused by local resorption or lack of mineralization, a finding not seen in osteoporosis.

Bones that are softened by osteomalacia may bend or give way as a result of weight bearing. Bowing deformities primarily involve the pelvis, vertebral column, thorax, and proximal extremities. In the pelvis, there may be a characteristic inward bending of the sidewalls with deepening of the acetabular cavities (protrusio acetabuli) (Figure 4-47).

Rickets

Rickets is a systemic disease of infancy and childhood that is the equivalent of osteomalacia in the mature skeleton. In this condition, calcification of growing skeletal elements is defective because of a deficiency of vitamin D in the diet or a lack of exposure to ultraviolet radiation (sunshine), which converts sterols in the skin into vitamin D. Most common in premature infants, rickets usually develops between ages 6 months and 1 year.

Imaging appearance. The early radiographic changes in rickets are best seen in the fastest-growing portions of bone, such as the sternal ends of the ribs, the proximal ends of the tibia and humerus, and the distal ends of the radius and ulna. An overgrowth of noncalcified osteoid tissue appears radiographically as a characteristic increase in distance between the ossified portion of the epiphysis and the end of the shaft. In response to the pull of muscular and ligamentous attachments, the metaphyseal ends of the bone become cupped and frayed, and the normally sharp metaphyseal lines disappear (Figure 4-48). Lack of calcification leads to a delayed

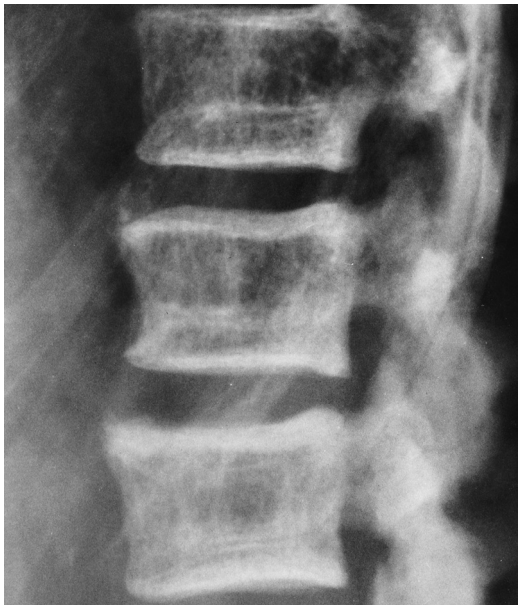

FIGURE 4-46 Osteomalacia. Striking prominence of the cortices of the vertebral bodies with increased trabeculation of spongy bone.

FIGURE 4-47 Protrusio acetabuli. As seen in osteomalacia and also in Paget's disease.

appearance of the epiphyseal ossification centers. Because of poor mineralization, bowing of weight-bearing bones (especially the tibia) develops once the infant begins to stand or walk. Extensive osteoid tissue in the sternal ends of the ribs produces a characteristic beading (rachitic rosary).

Softening of the vertebral bodies leads to the development of kyphosis. In females, narrowing of the pelvic inlet may make normal delivery impossible in later life.

Treatment for Osteomalacia and Rickets

Treatment consists of doses of vitamin D with calcium supplements. Other treatments are required if the calcium loss has a nonnutritional cause.

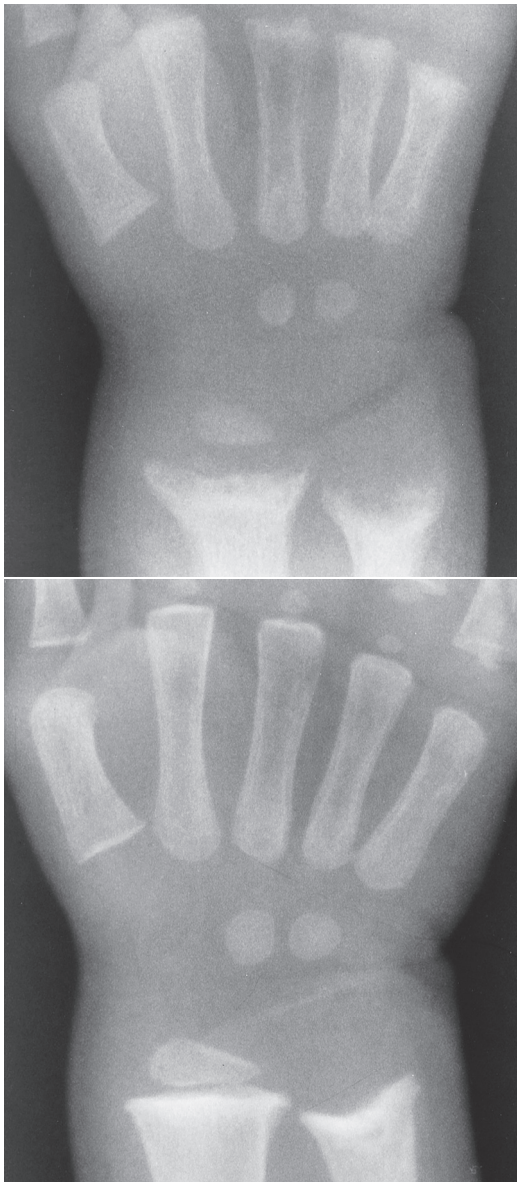

FIGURE 4-48 Rickets. (A) Initial image of this wrist shows characteristic cupping and fraying of the metaphyseal ends of the radius and ulna, with disappearance of normally sharp metaphyseal lines. (B) On an image obtained after therapy with vitamin D, there is remineralization of the metaphyseal ends of the radius and ulna, increased sharpness of metaphyseal lines, and a return of the epiphyseal centers to normal density and sharpness of outline.

Gout

Gout is a disorder in the metabolism of purine (a component of nucleic acids) in which an increase in the blood level of uric acid leads to the deposition of uric acid crystals in the joints, cartilage, and kidney. Several inherited enzyme defects can cause overproduction of uric acid (primary gout). In secondary gout, hyperuricemia can be caused by an overproduction of uric acid, which in turn may be caused by increased turnover of nucleic acids (e.g., as in metastatic carcinoma, myeloma, and hemolytic anemia), drugs (e.g., chemotherapy

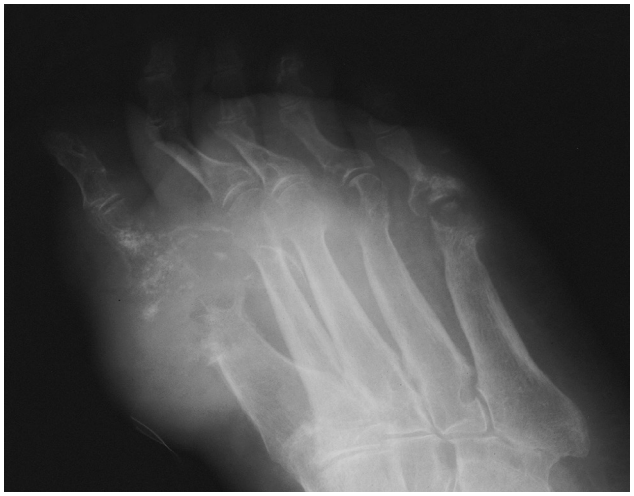

FIGURE 4-49 Gout. Effusion with tophi deposits at the first, fourth, and fifth metatarsophalangeal joints.

and thiazides used to treat hypertension), or a decrease in the excretion of uric acid resulting from kidney failure.

Imaging appearance. Acute gout manifests primarily as an exquisitely painful arthritis that initially attacks a single joint, usually the first metatarsophalangeal joint (Figure 4-49). Radiographic changes develop late in the disease and only after repeated attacks. Therefore, negative radiographic findings do not exclude gout and thus do not aid in early diagnostic evaluation.

Deposition of nonopaque urate crystals in the joint synovial membrane and on the surface of articular cartilage incites an inflammatory reaction that produces the earliest radiographic signs of joint effusion and periarticular swelling (Figure 4-50). Clumps of urate crystals (tophi) form along the margins of the articular cortex and erode the underlying bone, leading to small, sharply marginated, punched-out defects at the joint margins of the small bones of the hand and foot. These erosions often have the appearance of cystlike lesions with thin sclerotic margins and characteristic overhanging edges ("rat bite" erosions) (Figure 4-51). In advanced disease, severe destructive lesions are associated with joint space narrowing and even fibrous ankylosis. Because patients are relatively free of symptoms between acute exacerbations of the disease, the bone density remains relatively normal, and diffuse osteoporosis is not part of the radiographic appearance.

Continued deposition of urate crystals in the periarticular tissues causes the development of the characteristic large, lumpy soft tissue swellings representing gouty tophi. In addition to the first metatarsophalangeal joints, other common sites of tophi are the ear, the olecranon bursa, and the insertion of the Achilles tendon. Tophi consisting of only sodium urate appear as soft tissue densities. Deposition of calcium in these urate collections causes the tophaceous periarticular masses to become radiopaque (Figure 4-52).

Although some renal dysfunction occurs in almost all patients with gouty arthritis, no radiographic abnormalities in the urinary tract can be demonstrated unless uric

FIGURE 4-50 Gout. Severe joint effusion and periarticular swelling of the proximal interphalangeal joint of the finger. Note the associated erosion of the articular cartilage.

acid stones form. Nonradiopaque pure uric acid stones can be demonstrated only on excretory urograms, where they appear as filling defects in the pelvicalyceal system or ureter. Stones containing the calcium salts of uric acid can be detected on plain abdominal radiographs, on which they appear radiopaque.

MRI of gout produces various patterns, although regions of persistent low signal intensity are characteristic.

Treatment. Patients receiving doses of antihyperuricemic drugs rarely experience tophi. Untreated gout may lead to decreased renal excretion because of renal damage resulting from crystal deposits in the interstitial tissue. Eventually, this process causes obstruction of the renal tubules and renal failure.

Paget's Disease

Paget's disease (osteitis deformans) is one of the most common chronic metabolic diseases of the skeleton. Destruction of bone, followed by a reparative process, results in weakened, deformed, and thickened bony structures that tend to fracture easily. The disease, seen most commonly

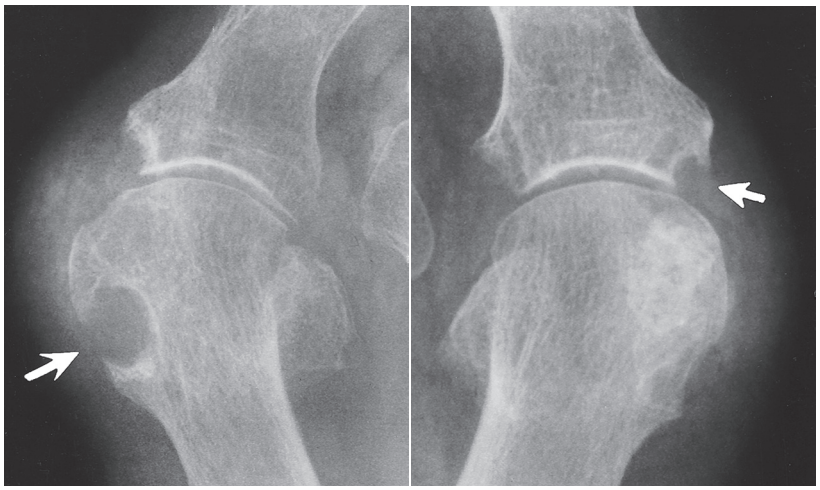

FIGURE 4-51 Gout—two examples of typical "rat bite" erosions about the first metatarsophalangeal joint (*arrows*). The cystlike lesions have thin sclerotic margins and characteristic overhanging edges.

FIGURE 4-52 Gout. Massive deposition of calcium in a long-standing tophaceous lesion about the elbow.

during middle life, affects men twice as often as women and has been reported to occur in approximately 3% of all persons older than 40 years. Although the destructive phase often predominates initially, there is more frequently a combination of destruction and repair in the pelvis and weight-bearing bones of the lower extremities. The reparative process may begin early and may be the prominent feature, often involving multiple bones. Paget's disease affects particularly the pelvis, femurs, skull, tibias, vertebrae, clavicles, and ribs. The radionuclide bone scan is the most efficient method to visualize multicentric lesions (Figure 4-53A).

Imaging appearance. In the skull, Paget's disease begins as an area of sharply demarcated radiolucency (osteoporosis circumscripta) that represents the destructive phase of the disease (Figure 4-53B). During the reparative process, the development of irregular islands of sclerosis and cortical thickening results in a mottled, cotton-wool appearance (Figure 4-53C). A bone scan demonstrates "cold spots" representing the initial destructive phase and "hot spots" as a result of the reparative process (see Figure 4-53A). In the spine, Paget's disease characteristically causes enlargement of the vertebral body. Increased trabeculation, which is most prominent at the periphery of the bone, produces a rim of thickened cortex and a picture-frame appearance. Uniform dense sclerosis of one or more vertebral bodies (ivory vertebrae) may occur.

The pelvis is the most common and often the initial site of Paget's disease. A distinctive early sign is coarsening of the trabeculae along the iliac margins, which causes thickening of the pelvic brim (Figure 4-54).

In the long bones, the destructive phase almost invariably begins at one end of the bone and extends along the shaft for a variable distance before ending in a typical, sharply demarcated, V-shaped configuration (blade of grass appearance). In the reparative stage, the bone is enlarged with an irregularly widened cortex and coarse, thickened trabeculae (Figure 4-55). Although dense, the bones are soft and weakened, and deformities are common. On CT, the lytic stage produces a washed-out appearance with cortical bone deformity. During the reparative process, the sclerosis appears as increased irregular cortical thickening and enlargement.

Paget's disease may have severe clinical complications. The downward thrust of the heavy head on the softened bone of the skull base may compress the brainstem and cause numerous cranial nerve deficits. Expansion and distortion of softened vertebral bodies, sometimes with pathologic fractures, may compress the spinal cord and produce nerve root deficits. Multiple microscopic arteriovenous malformations in pagetoid bone may result in high-output

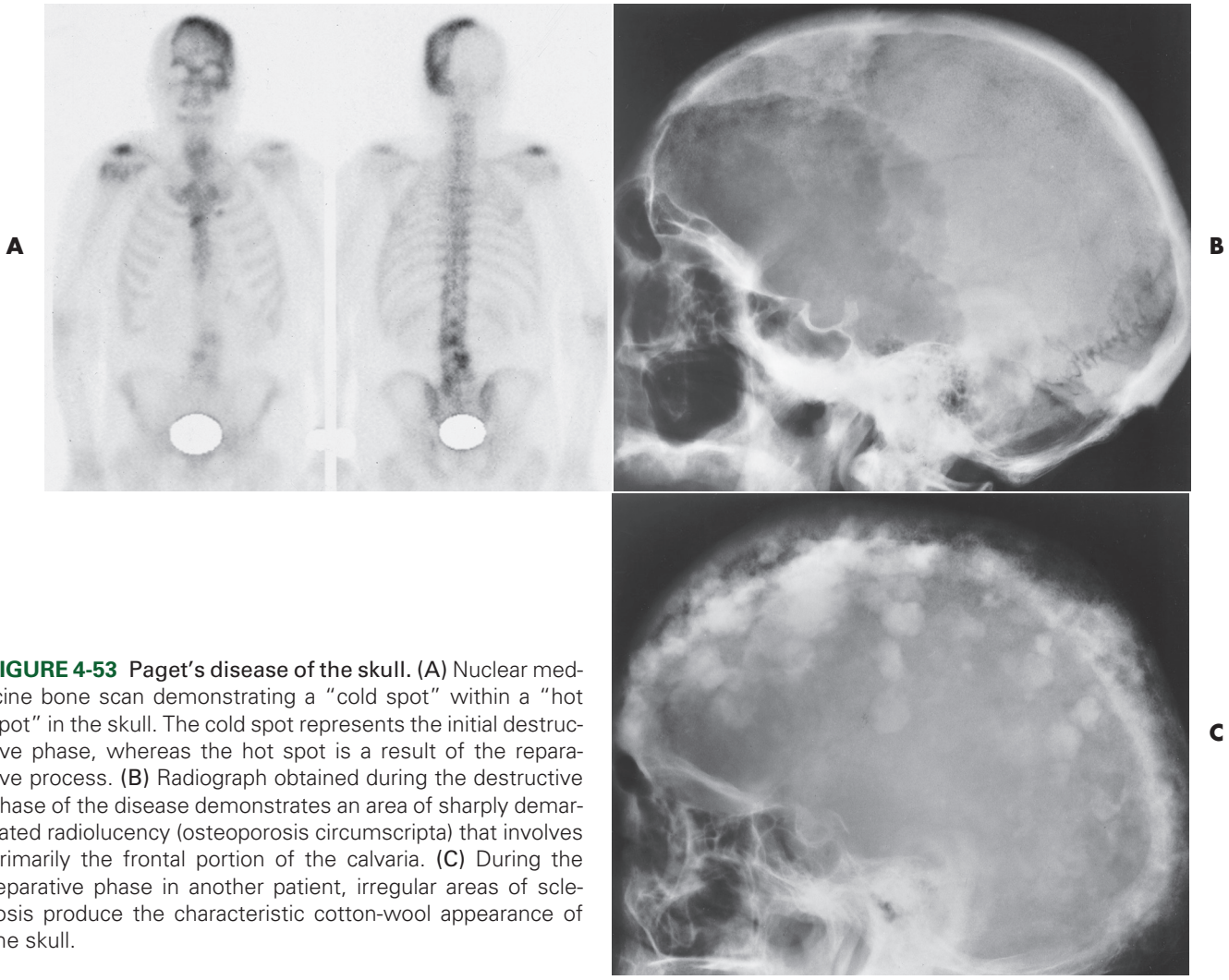

FIGURE 4-53 Paget's disease of the skull. **(A)** Nuclear medicine bone scan demonstrating a "cold spot" within a "hot spot" in the skull. The cold spot represents the initial destructive phase, whereas the hot spot is a result of the reparative process. **(B)** Radiograph obtained during the destructive phase of the disease demonstrates an area of sharply demarcated radiolucency (osteoporosis circumscripta) that involves primarily the frontal portion of the calvaria. **(C)** During the reparative phase in another patient, irregular areas of sclerosis produce the characteristic cotton-wool appearance of the skull.

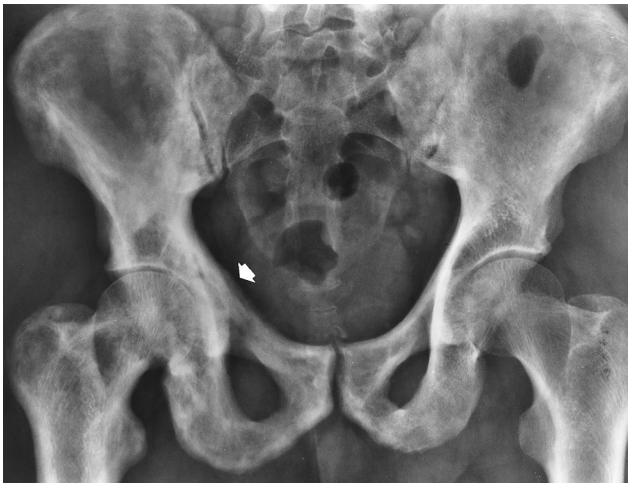

FIGURE 4-54 Paget's disease of the pelvis. Diffuse sclerosis with cortical thickening involves the right femur and both iliac bones. Note the characteristic thickening and coarsening of the iliopectineal line (*arrow*) on the involved right side.

cardiac failure. The most serious complication of Paget's disease, the development of osteosarcoma, fortunately occurs in less than 1% of patients with this condition. MRI and CT provide the most accurate imaging if osteosarcoma is suspected.

Treatment. No known cure exists for Paget's disease; however, the process may be slowed by the administration of bisphosphonates, which bind to the bone to minimize the resorption, and calcitonin, which inhibits the activity of the osteoclasts (resorption cells). Sometimes anti-inflammatory drugs reduce the inflammation caused by cell breakdown.

Lead Poisoning

Lead poisoning results from the ingestion of lead-containing materials (especially paint) or from the occupational inhalation of lead fumes. Environmental exposure occurs in the drinking of water (leaded pipes) or the eating of food that is processed, preserved, or stored in containers made with lead. Currently, lead is the number one environmental

FIGURE 4-55 Paget's disease of the knee. Note the characteristic cortical thickening, destruction of fine trabeculae, and accentuation of secondary trabeculae.

pollutant worldwide; however, the incidence in the United States has decreased as a result of public education and governmental restrictions of its use. In the past decade, the United States has experienced concern about imported toys that contain lead. The chronic form of lead poisoning may cause mental retardation, seizures, behavioral disorders, or delayed development. Ingested lead affects all systems of the body. Children are more susceptible to lower doses, and the effect on their central nervous system is more severe, causing interference in the cognitive thought process.

Imaging appearance. In children, because lead and calcium are used interchangeably by bone, high concentrations of lead are deposited in the most rapidly growing portions of the skeleton, especially the metaphyses at the distal ends of the femur. This results in classic lead lines, dense transverse bands extending across the metaphyses of the long bones (Figure 4-56) and along the margins of flat bones, such as the iliac crest. In young children who eat lead-containing paint (pica), plain abdominal radiographs may show extensive mottled opacities, which are suggestive of intestinal barium, even though no contrast material has been administered (Figure 4-57). CT is the modality of choice for demonstrating cerebral edema and structural changes.

Treatment. First, the source must be eliminated. If the drop in the body's lead content is not quick enough, chelation therapy to aid in the urinary excretion of lead is prescribed for those who do not have kidney or liver disease. The objective is to keep the blood lead level lower than 60 μg/dL to prevent potential encephalopathy.

Metabolic Bone Disease

Disorder	Location	Imaging Appearance	Treatment
Osteoporosis	Loss of bone mass in entire skeleton (accelerated bone resorption)	Cortical thinning appears as a relatively dense and prominent thin line	Weight-bearing exercise
		DEXA BMD *T*-scores • Normal, ≥ –1.0 SD • Osteopenia, –1.0 to –2.25 SD • Osteoporosis, ≤ –2.5 SD	Postmenopausal—hormonal replacement therapy Vitamin D and calcium supplements
Osteomalacia	Insufficient mineralization of adult skeleton (deossification of medullary bone)	Loss of bone density Cortex becomes thin and often indistinct	Vitamin D supplements with calcium
Rickets	Insufficient mineralization of immature skeleton	Cupped and frayed metaphysis in long bones	Vitamin D with calcium supplements
Gout	First metatarsophalangeal joint May attack any joint	Joint inflammation (effusion) and destruction Urate crystals (tophi) in joint space	Antihyperuricemic drugs
Paget's disease	Destruction and reparative process in pelvis, weight-bearing bones, and skull	Radiolucencies in destructive (lytic) phase Cotton-wool appearance in reparative phase NM–lytic phase—"cold spot"; reparative phase—"hot spot" CT–lytic phase—washed out lesions with bone deformity and sclerosis with irregularity in the reparative stage	No known cure Bisphosphonates and calcitonin to slow bone resorption Anti-inflammatory drugs

BMD, Bone mineral density; *DEXA,* dual-energy x-ray absorptiometry; *SD,* standard deviation.

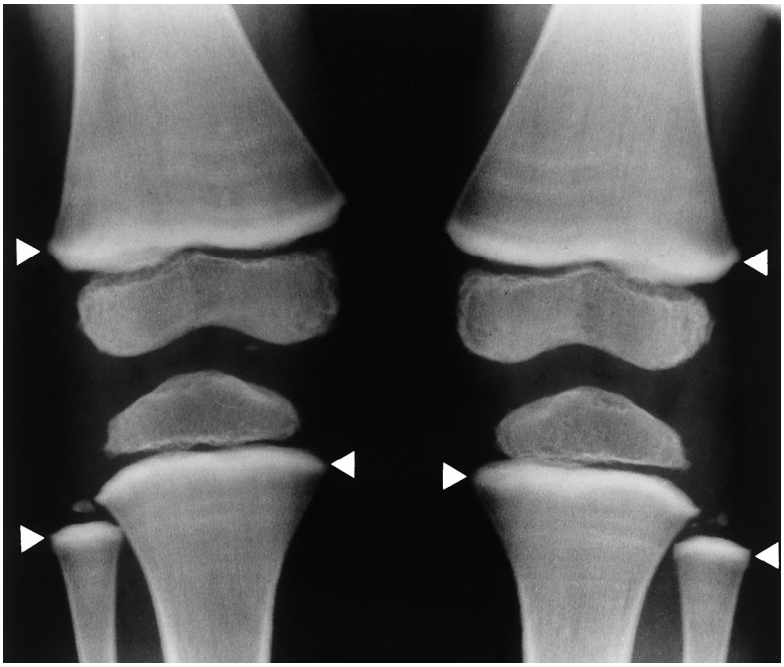

FIGURE 4-56 Lead poisoning lead lines. Dense transverse bands of sclerosis (*arrowheads*) extend across the metaphyses of the distal femurs and the proximal tibias and fibulas.

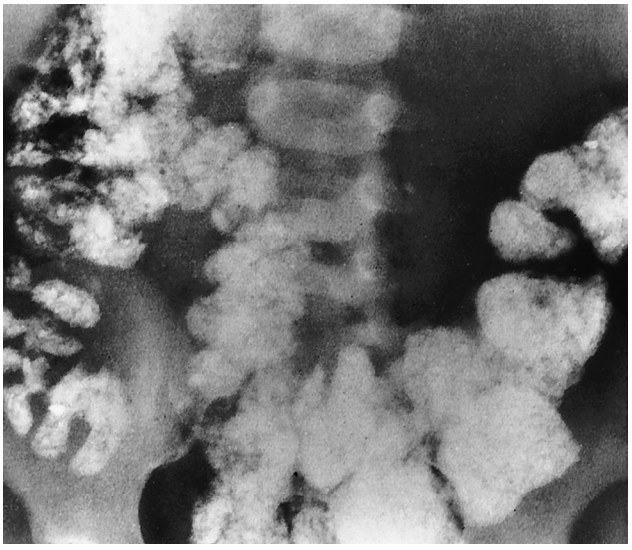

FIGURE 4-57 Pica. Large amounts of lead-containing material ingested by a young child who had received no contrast material.

FIBROUS DYSPLASIA

Fibrous dysplasia, a disorder that usually begins during childhood, is characterized by the proliferation of fibrous tissue within the medullary cavity. This proliferation causes loss of trabecular markings and widening of the bone. The disease may be confined to a single bone (monostotic) or the bones of one extremity, which is the most common form when it occurs in adults. The other form, in which the disease is widely distributed throughout the skeleton (polyostotic—among patients with this form, 25% have involvement of half the skeleton with more than 25% involvement of the skull), is present in children and occurs most often in girls. Fibrous dysplasia involves primarily the long bones (especially the femur and tibia), ribs, and facial bones.

Imaging appearance. Fibrous replacement of the medullary cavity typically produces a well-defined radiolucent area, which may vary from completely radiolucent to a homogeneous ground-glass density, depending on the amount of fibrous or osseous tissue deposited in the medullary cavity (Figure 4-58). Irregular bands of sclerosis may cross the cyst-like lesion, giving it a multilocular appearance (Figure 4-59). The bone is often locally expanded (suggesting a balloon), and the cortex may be eroded from within, predisposing to pathologic fractures. In severe and long-standing disease, affected bones may become bowed or deformed. CT images have a similar appearance to that of diagnostic x-rays, a cross-sectional perspective demonstrating sclerotic formation with radiolucent lesions. CT better demonstrates the location of the lesion, the cause (tissue type—lucent or sclerotic), and the degree of expansion. For the most definitive diagnosis, CT complements radiographic findings.

Fibrous dysplasia is the most common cause of an expansile focal rib lesion, which usually has a ground-glass or soap-bubble appearance.

Treatment. Treatment of fibrous dysplasia consists of curettage, repair of fractures, and prevention of deformities.

ISCHEMIC NECROSIS OF BONE

Ischemic necrosis of bone is caused by loss of the blood supply, which in turn can result from such varied conditions as thrombosis, vasculitis, disease of surrounding bone, and

FIGURE 4-58 Fibrous dysplasia. Note the smudgy, ground-glass appearance of the medullary cavities with failure of normal modeling.

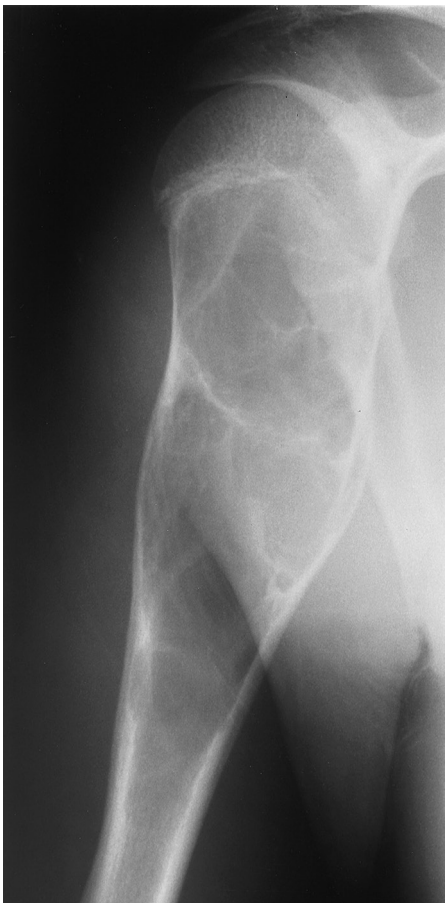

FIGURE 4-59 Fibrous dysplasia. An expansile lesion of the humerus contains irregular bands of sclerosis, giving it a multilocular appearance.

single or repeated episodes of trauma. Among the many conditions associated with ischemic necrosis are acute trauma (fracture or dislocation), steroid therapy and Cushing's disease, hemolytic anemia (especially sickle cell disease), chronic alcoholism and chronic pancreatitis, Gaucher's disease, radiation therapy, and caisson disease (a complication of underwater diving, the so-called bends).

Imaging appearance. The femoral head is the most common site of ischemic necrosis. Initially, the ischemic bone may appear denser than adjacent viable bone. The first sign of structural failure is the development of a radiolucent subcortical band (the crescent sign) representing a fracture line (Figure 4-60A). As the disorder progresses, fragmentation, compression, and resorption of dead bone, along with proliferation of granulation tissue, revascularization, and production of new bone, produce a pattern of lytic and sclerotic areas with flattening of the femoral head and periosteal new bone formation (Figure 4-60B). Mechanical distortion about the hip leads to uneven weight bearing and accelerated secondary osteoarthritis.

It is often necessary to obtain two radiographs in patients with ischemic necrosis. The first is taken with normal density, whereas the second is made with an increased kVp to allow for adequate penetration of the more opaque sclerotic ischemic bone.

Radionuclide bone scanning is more sensitive than plain radiography for detecting changes of ischemic necrosis. In the initial stages of infarction, radionuclide activity is absent in the area of involvement. As the disease progresses, this area of decreased activity may become rimmed by a zone of increased activity as a result of the reparative process.

MRI may be even more sensitive than radionuclide bone scanning for detecting ischemic necrosis. Infarction at the end of a bone causes changes in the fatty marrow, sharply reducing the normally intense T1-weighted signal from the marrow so that the infarcted area becomes gray or black (Figure 4-61).

In addition to ischemic changes in the subchondral areas of bone, infarction may involve the shaft of a long bone. In many cases, this type of bone infarction is asymptomatic and is detected only on radiographs obtained for another purpose. A mature infarct in the shaft of a bone appears as a densely calcified area in the medullary cavity (Figure 4-62). It may be sharply limited by a dense sclerotic zone or associated with dense streaks extending from the central region. Bone infarction must be differentiated from a calcified enchondroma, which contains amorphous, spotty calcific densities; is not surrounded by a sclerotic rim; and may expand the bone.

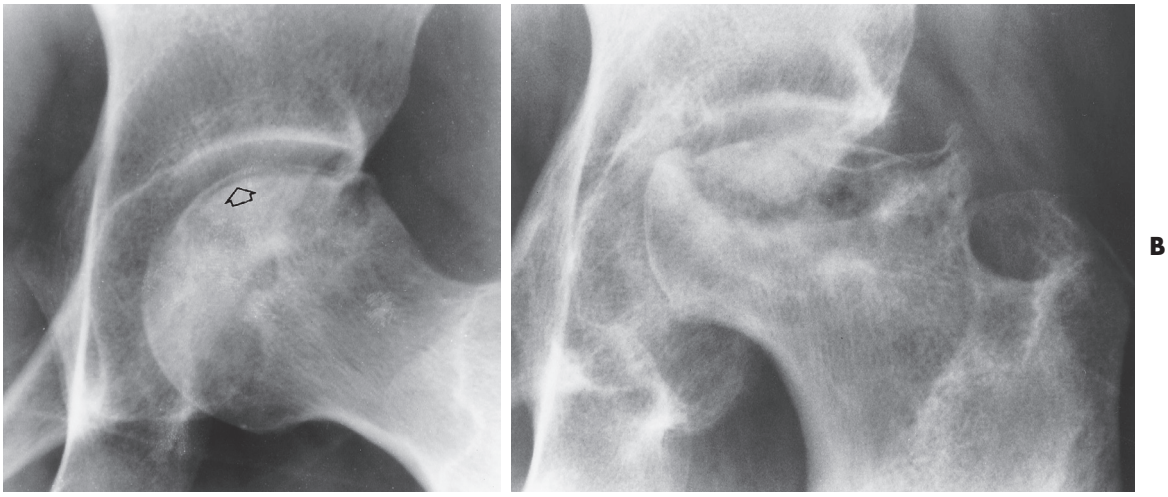

FIGURE 4-60 Ischemic necrosis of the femoral head. (A) An arclike radiolucent cortical band (the crescent sign) (*arrow*) in the femoral head represents the fracture line. (B) Eventually, there is combination of lytic and sclerotic areas with severe flattening of the femoral head.

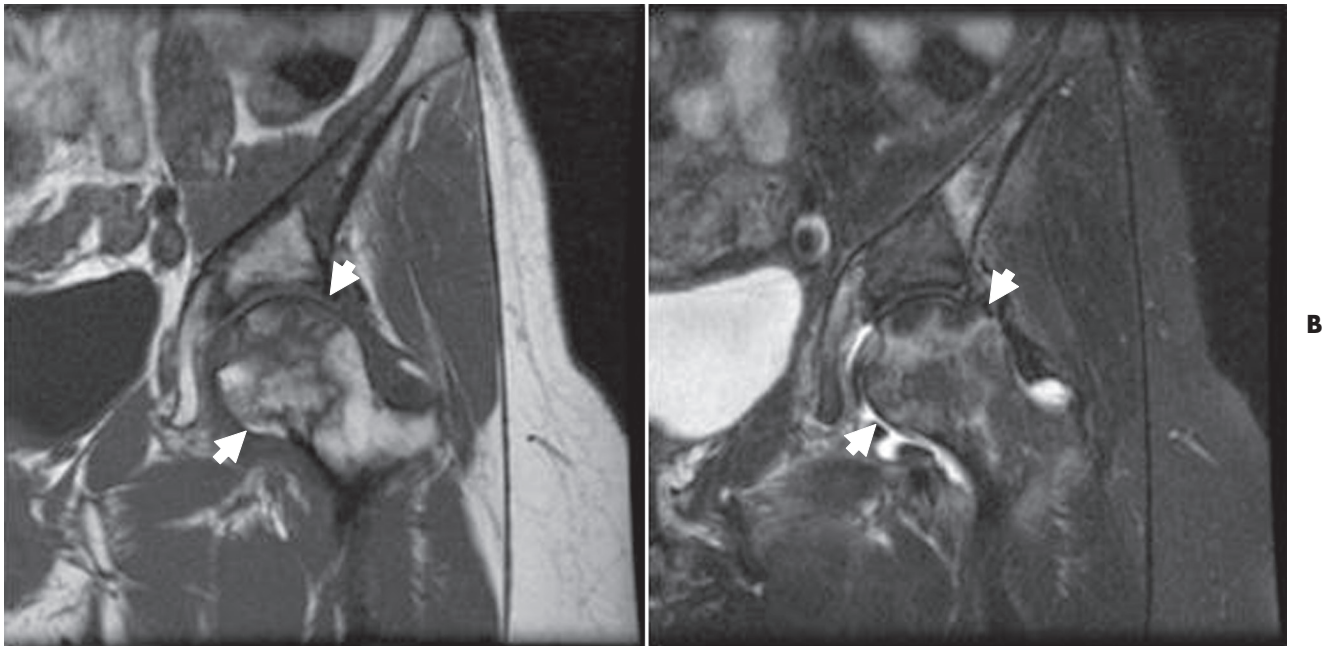

FIGURE 4-61 Ischemic necrosis. (A) On this T1-weighted image, the ischemic right femoral head has lost its normal bright homogenous signal intensity and appears dark and mottled (*arrows*), and (B) on this T2-weighted image of the affected area, it appears as a bright signal intensity, representing edema.

Lead Poisoning, Fibrous Dysplasia, and Ischemic Necrosis

Disorder	Location	Imaging Appearance	Treatment
Lead poisoning	Ingestion of lead-containing materials	Classic lead lines (dense transverse bands extending across the metaphyses of long bones)	Eliminate source Chelation therapy to aid in elimination
Fibrous dysplasia	Monostotic—single bone or entire extremity Polyostotic—widely distributed	Well-defined radiolucent area, homogeneous ground-glass density or soap-bubble appearance CT—demonstrates the degree of sclerotic regions and radiolucent areas	Curettage Repair of fractures Prevention of deformities
Ischemic necrosis	Femoral head most common	Crescent sign, lytic/sclerotic areas with flattening of femoral head NM—bone scan—cold spot in lytic phase; cold spot rimmed by increased activity in reparative phase MRI—in T1-weighted images, infarcted marrow appears gray or black	Immobilization Antibiotics Analgesics

FIGURE 4-62 Bone infarct. Densely calcified area in the medullary cavity of the humerus with dense streaks extending from the central region.

Treatment. Immobilization is accomplished with braces (pelvic for femoral head necrosis) to prevent further erosion and necrosis. Antibiotics may be useful if the necrosis results from infection. Analgesics are appropriate if inflammation is caused by vasculitis or trauma.

BENIGN BONE TUMORS

Benign bone neoplasms generally displace soft tissue, whereas malignant bone tumors produce true soft tissue swelling. When there is bone expansion, an intact cortex with a sclerotic margin usually indicates a benign lesion. Benign bone neoplasms occur much less often than bone metastases.

Osteochondromas

Osteochondroma (exostosis) is a benign projection of bone with a cartilaginous cap that arises in childhood or the teen years, especially about the knee. The exostosis occurs in the epiphyseal plate (the ring of Ranvier) and grows laterally from the epiphysis. A true osteochondroma must exhibit the cortex and medullary portion (spongiosa) as continuous bone growth. The cartilaginous cap of the lesion may convert to a malignancy if the cartilage cap becomes thicker and contains disorganized calcifications (chondrosarcoma or osteosarcoma). Ultrasound is a safe, quick, and inexpensive method to evaluate the thickness of the cartilaginous cap. A hereditary form of osteochondroma (autosomal dominant) produces multiple lesions and has an increased risk of malignancy.

Imaging appearance. A radiograph is the preferred method to demonstrate that the cortex of an osteochondroma blends with that of normal bone. The long axis of the tumor characteristically runs parallel to the parent bone and points away from the nearest joint (Figure 4-63). The best modality to demonstrate the thickness of the cartilaginous cap and thus rule out malignant conversion is MRI with long TR pulses (increased signal). On T2-weighted spin-echo images, the cartilaginous cap produces a high signal intensity.

FIGURE 4-63 Osteochondroma. The long axis of the tumor is parallel to that of the femur and points away from the knee joint.

Enchondromas

Enchondroma begins as a slow-growing benign cartilaginous tumor arising in the medullary canal (ectopic cartilaginous growth). This tumor destroys normal bone by erupting as a mixture of calcified and uncalcified hyaline cartilage. Enchondromas are most frequently found in children and young adults, and they involve primarily the small bones of the hands and feet. These tumors are often multiple.

Imaging appearance. As the well-demarcated tumor grows, it expands bone locally, causing thinning and endosteal scalloping of the cortex. This process often leads to a pathologic fracture with only minimal trauma (Figure 4-64). A characteristic finding in enchondroma is stippled, speckled, and ringlike or arclike calcifications within the lucent matrix because of the tumor composition. This radiographic appearance is also seen on CT images.

T2-weighted MR images demonstrate a lesion having lobulated borders from the endosteal scalloping and containing focal areas of high signal intensity. On T1-weighted

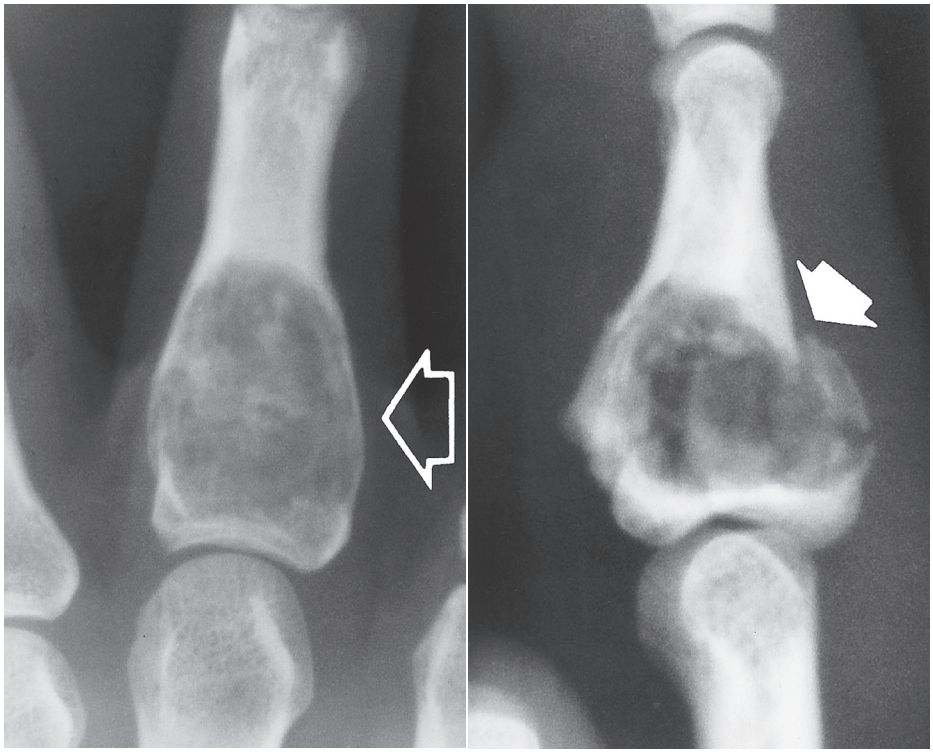

FIGURE 4-64 Enchondroma. **(A)** A well-demarcated tumor (*arrow*) expands the bone and thins the cortex. **(B)** Pathologic fracture (*arrow*).

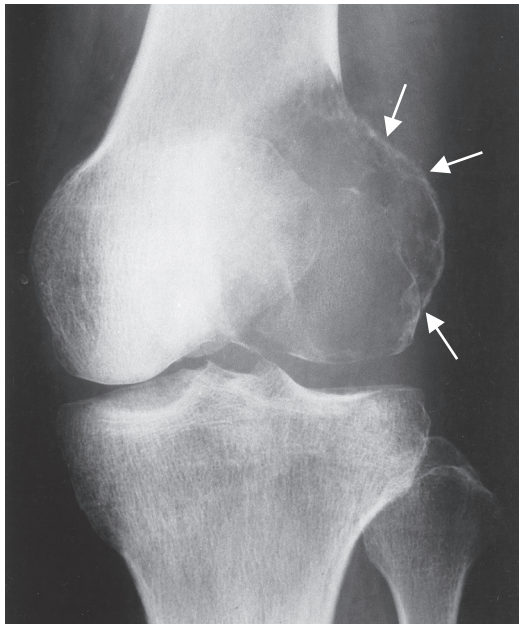

FIGURE 4-65 Giant cell tumor. Typical eccentric lucent lesion (*arrows*) in distal femoral metaphysis extends to the immediate subarticular cortex. Surrounding cortex, although thinned, remains intact.

images, enchondromas have low to intermediate signal intensity.

Nuclear medicine bone scan findings are usually negative in cases of enchondromas, ruling out the possibility of malignancy.

Giant Cell Tumors

Giant cell tumor (osteoclastoma) typically arises at the end of the distal femur or proximal tibia of a young adult after epiphyseal closure (20 to 40 years old). It begins as an eccentric lucent lesion in the metaphysis, and it characteristically extends to the immediate subarticular cortex of the bone but does not involve the joint (Figure 4-65).

Imaging appearance. MRI is used to determine intra-articular extension, soft tissue involvement, and bone marrow changes. When these results are combined with radiographic images, the accuracy is especially high. A few giant cell tumors may be premalignant or actually malignant.

As the tumor expands toward the shaft, it produces the characteristic radiographic appearance of multiple large bubbles separated by thin strips of bone.

Osteomas

Osteomas most often arise in the outer table of the skull, the paranasal sinuses (especially frontal and ethmoid), and the mandible. Detection of these tumors may be incidental on radiographs taken because of the pain produced by bone expansion.

Imaging appearance. Osteomas appear radiographically as well-circumscribed, extremely dense, round lesions that are rarely more than 2 cm in diameter (Figure 4-66).

Osteoid Osteomas

Osteoid osteoma usually develops in teenagers or young adults and produces the classic clinical symptom of local pain

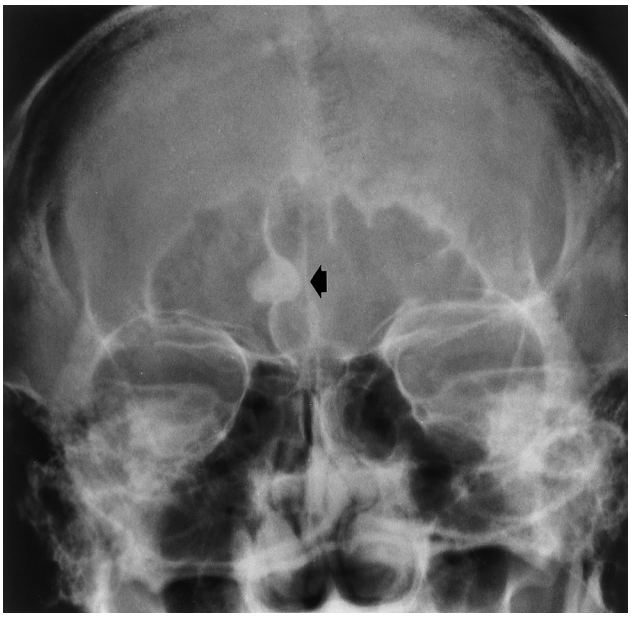

FIGURE 4-66 Osteoma. Radiopaque density (*arrow*) in a frontal sinus.

that is worse at night and is dramatically relieved by aspirin. Most osteoid osteomas occur in the femur and tibia, originate from osteoblastic cells, and are less than 1.5 cm in diameter.

Imaging appearance. A radionuclide bone scan can help differentiate osteoid osteoma from osteomyelitis; osteoid osteoma has a double density, whereas osteomyelitis demonstrates only an outline because of the avascularity of the inner structure. Preoperatively, nuclear medicine studies localize the tumor for complete excision.

The tumor is typically seen as a small, round or oval, lucent center (the nidus), less than 1 cm in diameter, that is surrounded by a large, dense sclerotic zone of cortical thickening (Figure 4-67). The nidus may not be visualized, depending on the bone structure involved (cortical versus cancellous). Because this dense reaction may obscure the nidus on conventional radiographs, overpenetrated images or tomography (conventional or computed) may be necessary to demonstrate it. CT is commonly used if there is the need to demonstrate the central radiolucent nidus for percutaneous ablation. The nidus enhances following administration of contrast material. T1-weighted MR images demonstrate the

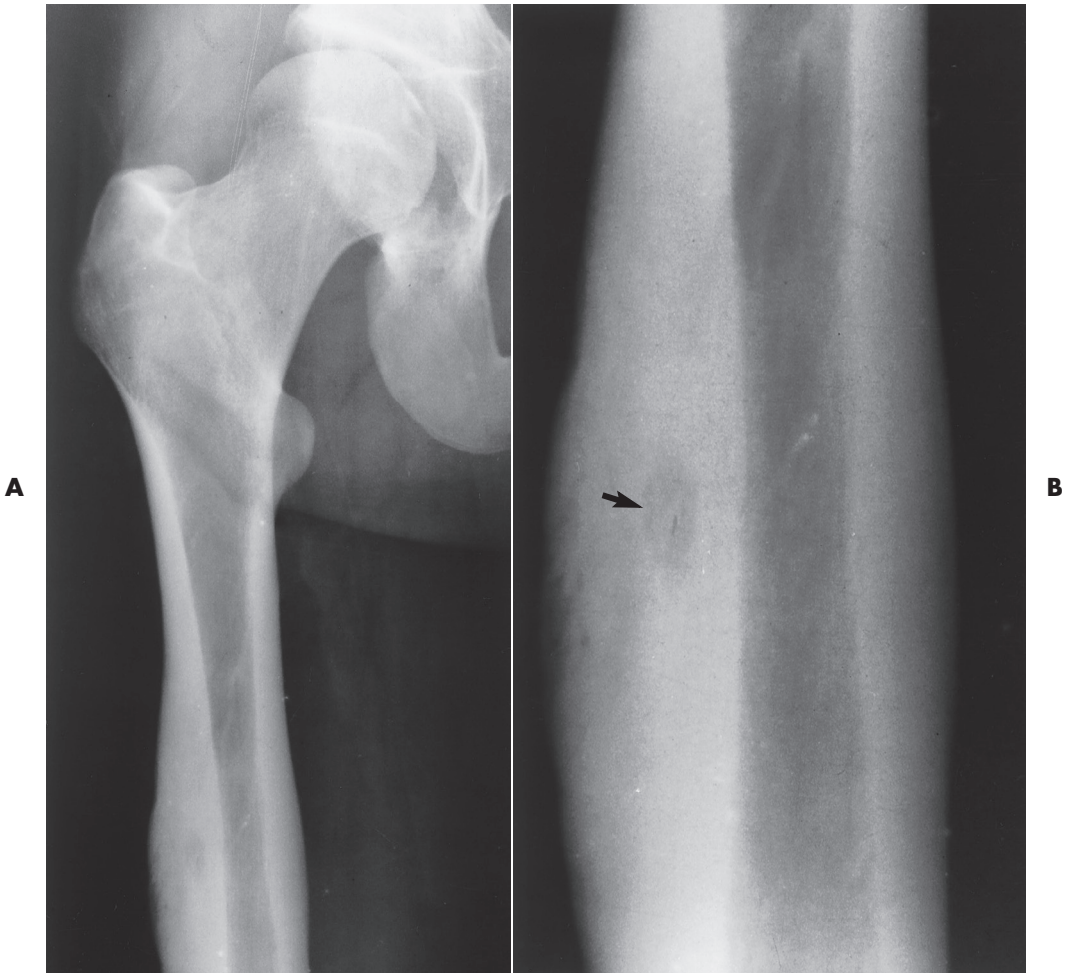

FIGURE 4-67 Osteoid osteoma. Full (A) and coned-down (B) projections of the midshaft of the femur demonstrate a dense sclerotic zone of cortical thickening laterally, which contains a small oval lucent nidus (*arrow*).

FIGURE 4-68 Simple bone cyst. This cyst in the proximal humerus has an oval configuration, with its long axis parallel to that of the host bone.

nidus as isoechoic to muscle (same intensity as muscle). CT is considered the definitive diagnostic modality.

Simple Bone Cysts

A **simple bone cyst (unicameral)** is a true fluid-filled cyst with a wall of fibrous tissue that most often occurs in the proximal humerus or femur at the metaphysis. Although not a true neoplasm, a simple bone cyst may resemble one radiographically and clinically. Solitary bone cysts are asymptomatic and often discovered either incidentally or after pathologic fracture.

Imaging appearance. The simple bone cyst appears as an expansile lucent lesion that is sharply demarcated from adjacent normal bone and may have a thin rim of sclerosis around it. It has an oval configuration, with its long axis parallel to that of the host bone, and may cause cortical bone thinning (Figure 4-68). Its appearance on CT is very similar to that on radiographs, so CT is usually unnecessary. Simple bone cysts produce low signal intensity on T1-weighted MR images (high signal intensity on T2-weighted images). To aid in determining proper treatment, MRI determines whether septations exist that may not be visible on the radiograph.

FIGURE 4-69 Aneurysmal bone cyst. This expansile, eccentric, cystic lesion of the tibia has multiple fine internal septa. Because severely thinned cortex is difficult to detect, the tumor resembles a malignant process.

Aneurysmal Bone Cysts

An **aneurysmal bone cyst,** rather than being a true neoplasm or cyst, consists of numerous blood-filled arteriovenous communications thought to be caused by trauma.

Imaging appearance. In long bones, an aneurysmal bone cyst is an expansile, eccentric, cystlike lesion that causes pronounced ballooning of the thinned cortex (Figure 4-69). In some cases, the cystlike lesion may have internal separations. At times, the cortex may be so thin that it is invisible on plain radiographs, and thus this benign lesion may be mistaken for a malignant bone tumor. A CT scan may assist in defining the well-lobulated lesion, but MRI better shows the internal loculations and fluid levels that produce low signal intensity on T2-weighted images. On T1-weighted images, the cyst has a low to intermediate signal intensity but contains high signal intensity if there has been acute hemorrhage.

Bone islands are solitary, sharply demarcated areas of dense compact bone that occur most commonly in the pelvis and upper femur. They appear in every bone except the skull (Figure 4-70). Although almost half of the bone islands enlarge over a period of years and many show activity on radionuclide scans, bone islands are asymptomatic and completely benign and must be distinguished from osteoblastic metastases.

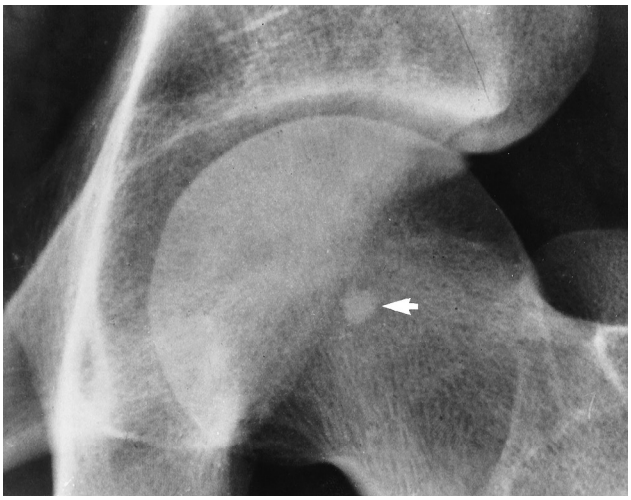

FIGURE 4-70 Bone island. Radiopaque density (*arrow*) in the femoral head.

Treatment of Benign Bone Tumors

An osteochondroma requires treatment only when mechanical friction (joint mobility) impinges on nerves, blood vessels, or muscles. For an enchondroma, curettage of the lesion is the common treatment. The treatment for giant cell tumor includes curettage of the bone and local resection. Approximately 50% of giant cell tumors recur. Surgical excision of the nidus of an osteoid osteoma is essential for cure; it is not necessary to remove the reactive calcification, although it may form the major part of the lesion. CT-guided percutaneous radiofrequency ablation (destruction) may provide the best treatment. Simple bone cyst treatment depends on the size and location of the cyst. If the cyst continues to develop, surgical curettage and implantation of bone chips is performed. Aneurysmal bone cysts require curettage to prevent further destruction from occurring. Bone islands require no treatment.

Summary of Findings for Benign Bone Tumors (Neoplasia)

Disorder	Location	Imaging Appearance	Treatment
Osteochondroma	Epiphyseal plate growing laterally in long bones	Tumor runs parallel to long bone and points away from nearest joint US—determines cartilage cap thickness MRI—cartilage cap produces a high signal intensity on T2-weighted spin-echo images	Surgical removal only when mechanical impingement occurs
Enchondroma	Arises in the medullary canal of hands and feet	Cortical thinning and endosteal scalloping Calcifications within lesion appear stippled, speckled, ringlike, or arclike MRI—T2-weighted image shows lobulated endosteal scalloping with focal high-intensity signals	Curettage of lesion
Giant cell tumor (osteoclastoma)	Metaphysis extends into subarticular cortex; does not involve the joint	Multiple large bubbles separated by strips of bone MRI—demonstrates tumor extension with soft tissue involvement and bone marrow changes	Curettage and local resection
Osteoma	Outer table of the skull	Well-circumscribed, extremely dense, round lesions <2 cm in diameter	No treatment required
Osteoid osteoma	Femur and tibia, osteoblastic cells	Round or oval lesion with lucent center (nidus), sometimes surrounded by dense sclerotic zone; <1 cm CT—contrast enhancement to demonstrate nidus	Surgical removal must include nidus to be successful Percutaneous ablation
Simple bone cyst	Most common in proximal humerus and femur at the metaphysis	Expansile lucent lesion with a thin rim of sclerosis MRI—low signal intensity on T1-weighted images; demonstrates septations within the cyst	Many require no treatment Curettage with implantation of bone chips
Aneurysmal bone cyst	Metaphysis or long bones	Pronounced ballooning with thinned cortex (internal separations) MRI—T2-weighted image demonstrates loculated lesions producing low signal intensity; T1-weighted image shows high signal intensity if cyst is hemorrhagic in nature	Curettage
Bone island	Every bone except the skull	Sharply defined, dense compact lesion	No treatment required

US, Ultrasound.

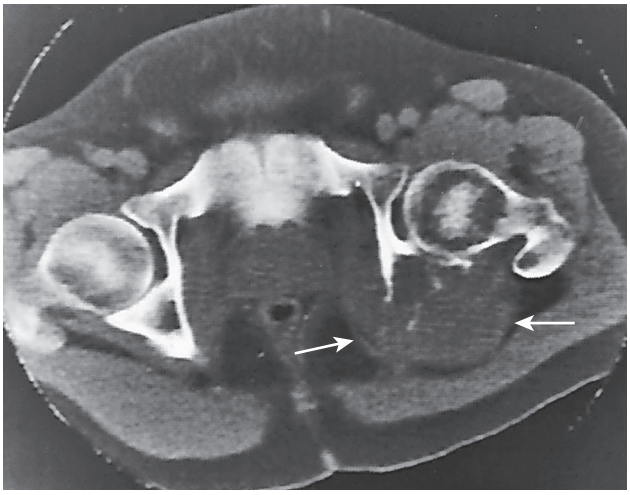

FIGURE 4-71 Osteogenic sarcoma. CT scan through the level of the femoral head shows destruction of the left ischium, which was seen on plain radiographs. In addition, the CT scan demonstrates a large soft tissue mass (*arrows*) in the area covered by gluteus maximus muscle and separated from rectum. The mass was not clinically palpable.

MALIGNANT BONE TUMORS

Malignant bone neoplasms generally cause soft tissue swelling and cortical bone erosion with a margin that is poorly defined or absent. The neoplasm extends into the soft tissue through spiculations (finger-like projections). Plain radiographs may identify a single lesion. A radionuclide bone scan or positron emission tomography (PET) scan can detect silent lesions when minimal cellular destruction has occurred. Discovering additional lesions determines the treatment and prognosis. CT and MRI can precisely define the location of a malignant bone tumor and its extension into the medullary cavity and spread to surrounding structures (Figures 4-71 and 4-72).

Osteogenic Sarcoma

Osteogenic sarcoma generally occurs in the end of a long bone in the metaphysis (especially about the knee). This tumor consists of osteoblasts, which produce osteoid and spicules of calcified bone. Most osteogenic sarcomas arise in persons between 10 and 25 years old, although a smaller peak incidence is seen in older persons who have a preexisting bone disorder, particularly Paget's disease. The usual initial complaints are local pain and swelling, sometimes followed by fever, weight loss, and secondary anemia. Pulmonary metastases develop early, and a plain chest radiograph should be obtained to exclude this unfavorable prognostic sign. If no metastases to the lung are detected by this modality, CT or PET should be performed.

Imaging appearance. The typical radiographic appearance of osteogenic sarcoma is a mixed destructive and sclerotic lesion associated with a soft tissue mass, irregular periosteal reaction, and reactive new bone formation (Figure 4-73A). In the classic sunburst pattern, horizontal bony spicules extend in radiating fashion into the soft tissue mass (Figure 4-73B). A characteristic finding is elevation of the periosteum at the periphery of a lesion, with subsequent new bone formation

FIGURE 4-72 MRI of osteogenic sarcoma. A coronal image shows destruction of the intramedullary bone and soft tissue extent of the mass.

(Codman's triangle) (Figure 4-74). CT scans are beneficial in demonstrating this finding in flat bones, where periosteal change is more difficult to visualize. MRI of the entire length of the bone is important to rule out skip lesions, and this modality is more accurate to visualize the tissue extension and medullary involvement. To determine the longitudinal involvement, specifically in the medullary cavity, T1-weighted images using a spin-echo sequence are best. The short-tau inversion recovery (STIR) sequence produces high-intensity signals. Both signal sequences are required because the T1-weighted images are slightly more specific, whereas the STIR sequence produces images that are slightly more sensitive.

Chondrosarcoma

Chondrosarcoma is a malignant tumor of cartilaginous origin that may originate anew or within a preexisting cartilaginous lesion (e.g., osteochondroma and enchondroma). Tumor grading of this particular neoplasm depends on the maturity and differentiation of the cells. Chondrosarcomas commonly occur in long bones, but they often originate in a rib, scapula, or vertebra. The tumor is approximately half as common as osteogenic sarcoma; it develops at a later age (peak incidence in 35- to 60-year-olds), grows more slowly, and metastasizes later.

Imaging appearance. In addition to the bone destruction seen with all malignant tumors, chondrosarcoma often contains punctate or amorphous calcification within its cartilaginous matrix (Figure 4-75). On CT, as on radiographs, chondrosarcomas demonstrate endosteal scalloping and cortical destruction. To evaluate for possible pulmonary metastases, CT is the modality of choice. On T2-weighted MR images,

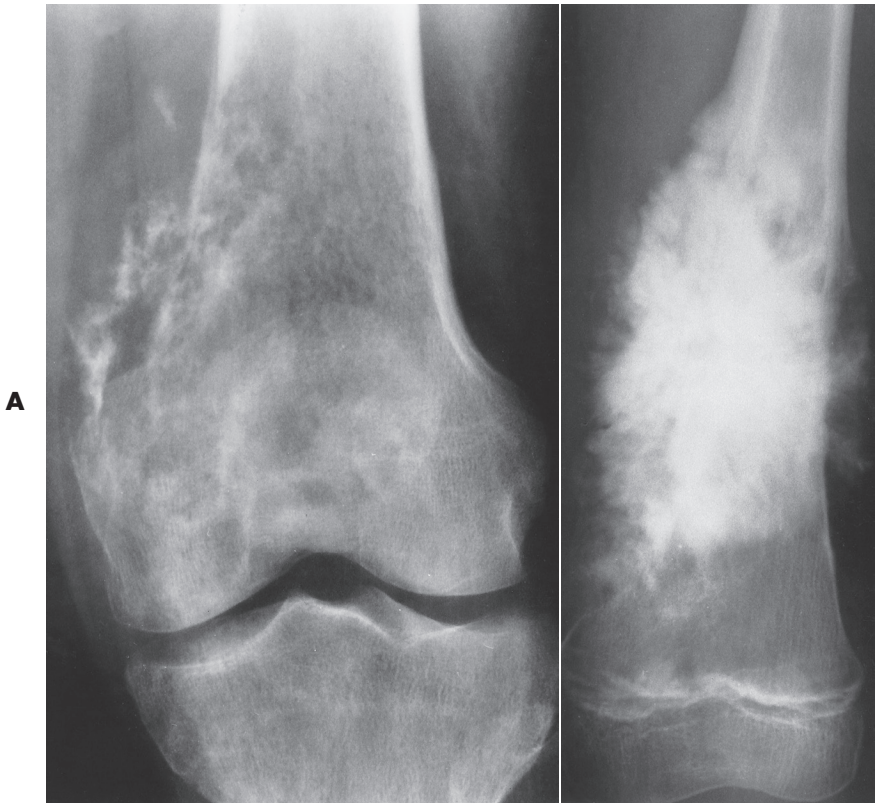

FIGURE 4-73 Osteogenic sarcoma. (A) A predominantly destructive lesion with an irregular periosteal reaction. (B) Classic sunburst pattern with bony spicules extending outward in radiating fashion.

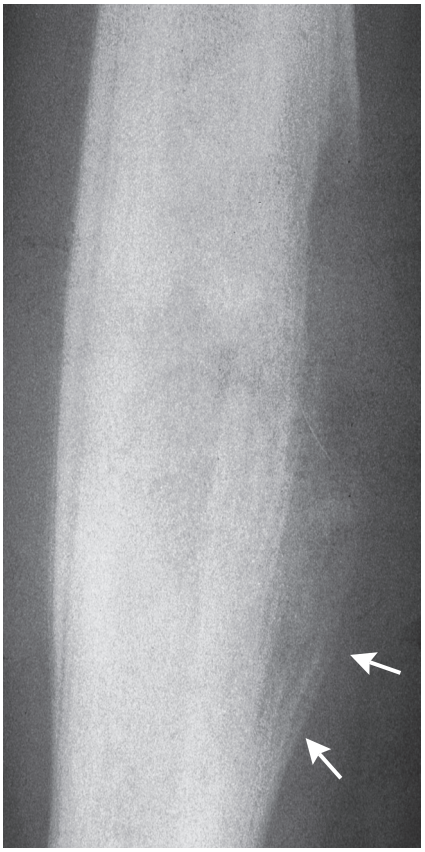

FIGURE 4-74 Codman's triangle. Thin periosteal elevation (*arrows*) and subsequent new bone formation at periphery of this neoplastic lesion.

FIGURE 4-75 Chondrosarcoma. Prominent dense calcification in large neoplastic mass.

the lobulated lesions have high signal intensity, whereas the septations appear as low signal intensity.

Ewing's Sarcoma

Ewing's sarcoma is a primary malignant tumor arising in the bone marrow of long bones. A tumor of children and young adults, Ewing's sarcoma has a peak incidence in the mid-teens and is rare in persons older than age 30 years. The major clinical complaint is local pain, often of several months' duration, that persistently increases in severity and may be associated with a tender soft tissue mass. Patients with this tumor characteristically have malaise and appear sick, often with fever and leukocytosis, suggestive of osteomyelitis.

FIGURE 4-76 Ewing's sarcoma. Diffuse permeative destruction with mild periosteal response involving the distal half of the femur.

Imaging appearance. The classic radiographic appearance of Ewing's sarcoma is an ill-defined permeative area of bone destruction that involves a large central portion of the shaft of a long bone (underlying medullary destruction) and is associated with a fusiform layered periosteal reaction (onionskin appearance) parallel to the shaft (Figure 4-76). Tumor cells invade the cortical bone and spread into the soft tissue. For staging and follow-up, MRI is the modality of choice. MRI best demonstrates the soft tissue involvement on T1-weighted images, where the tumor has a low signal intensity when compared with normal bone marrow. On T2-wighted imaging, the tumor has a higher signal intensity than muscle, so fat-saturation sequences are best (STIR sequences provide an alternative when fat saturation is unavailable).

Multiple Myeloma

Multiple myeloma is a disseminated (widespread) malignancy of plasma cells that may be associated with bone destruction, bone marrow failure, hypercalcemia, renal failure, and recurrent infections. The disease affects primarily persons between 40 and 70 years of age. This frequently occurring primary bone tumor attacks the intramedullary canal of the diaphysis. Typical laboratory findings include an abnormal spike of monoclonal immunoglobulin and the presence of Bence Jones protein in the urine.

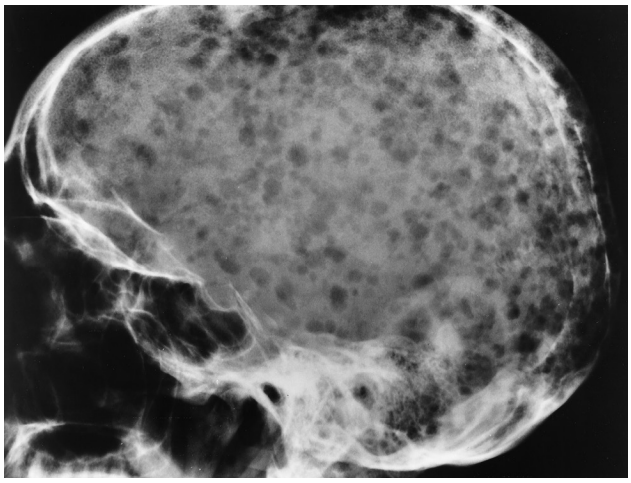

FIGURE 4-77 Multiple myeloma. Diffuse punched-out osteolytic lesions scattered throughout the skull.

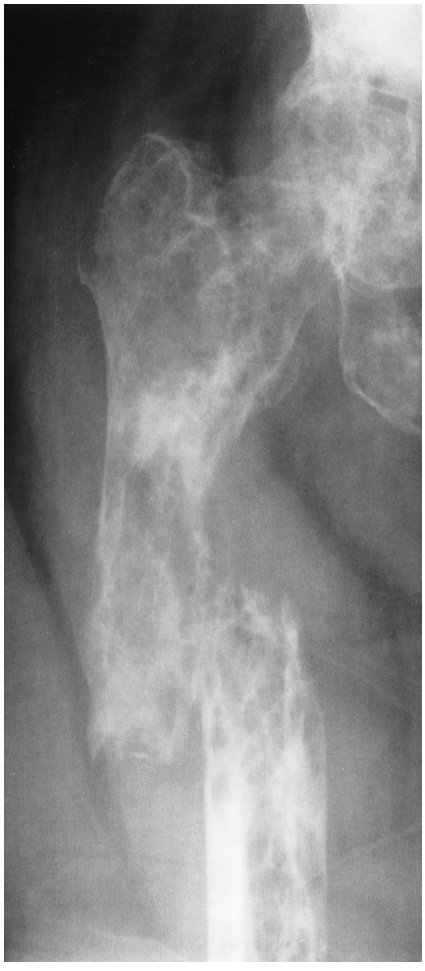

FIGURE 4-78 Multiple myeloma. A diffuse destructive bone lesion that has led to a pathologic fracture of the femur.

Imaging appearance. The classic radiographic appearance of multiple myeloma is multiple punched out osteolytic lesions scattered throughout the skeletal system and best seen on lateral views of the skull (Figures 4-77 and 4-78).

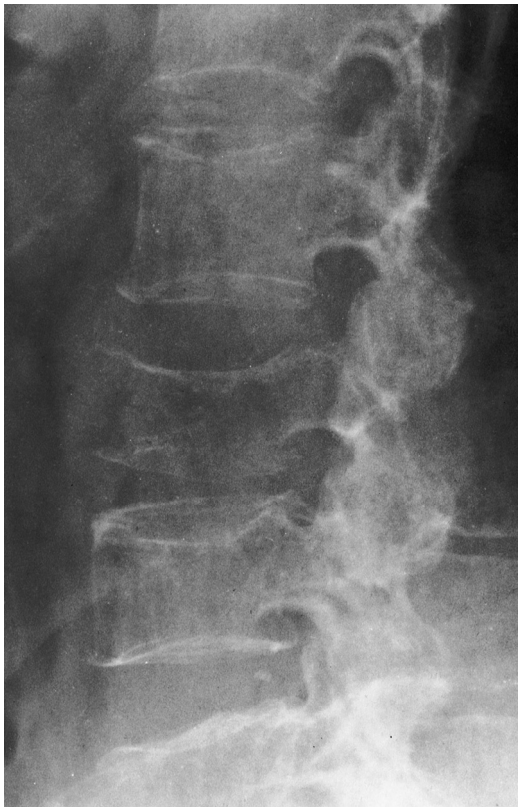

FIGURE 4-79 Multiple myeloma. Diffuse myelomatous infiltration has caused generalized demineralization of the vertebral bodies and compression fracture of L2.

Because the bone destruction is attributable to the proliferation of plasma cells distributed throughout the bone marrow, the flat bones containing red marrow (vertebrae, skull, ribs, and pelvis) are primarily affected. The appearance may be indistinguishable from that of a metastatic carcinoma, although the lytic defects in multiple myeloma tend to be more discrete and uniform in size. Extensive plasma cell proliferation in the bone marrow with no tendency to form discrete tumor masses may produce generalized skeletal deossifications simulating postmenopausal osteoporosis. In the spine, decreased bone density and destructive changes in multiple myeloma are usually limited to the vertebral bodies, sparing the pedicles (which lack red marrow and are frequently destroyed by metastatic disease). The severe loss of bone substance in the spine often results in multiple vertebral compression fractures (Figure 4-79).

Because multiple myeloma causes little or no stimulation of new bone formation, radionuclide bone scans may be normal even with extensive skeletal infiltration. On T1-weighted MR images, low-intensity tumor tissue replaces the normal high-intensity fatty marrow.

Treatment of Malignant Bone Tumors

The treatment of osteogenic sarcoma includes surgical removal with or without chemotherapy and/or radiation therapy. Although osteogenic sarcoma is usually fatal, approximately 30% of patients receiving chemotherapy are cured. For chondrosarcoma lesions, the treatment usually includes surgical excision. Because of poor response, chemotherapy and radiation therapy are not suggested. The more differentiated the involved cells, the higher the survival rate. Chondrosarcoma tumors are not sensitive to chemotherapy. Ewing's sarcoma and multiple myeloma are treated with radiation therapy and chemotherapy. Chemotherapy for Ewing's sarcoma increases the survival rate to approximately 30%. Multiple myeloma patients have a grim prognosis, with most dying within 3 or 4 years. PET imaging helps to determine therapy effectiveness by demonstrating active tumor metastases in multiple myeloma (Figure 4-80).

BONE METASTASES

Metastases are the most common malignant bone tumors, spreading by means of the bloodstream or lymphatic vessels or by direct extension. The most common primary tumors are carcinomas of the breast, lung, prostate, kidney, and thyroid. Favorite sites of metastatic spread are bones containing red marrow, such as the spine, pelvis, ribs, skull, and the upper ends of the humerus and femur. Metastases distal to the knees and elbows are infrequent but do occur, especially with bronchogenic (lung) tumors.

Summary of Findings for Malignant Bone Tumors (Neoplasia)

Disorder	Location	Imaging Appearance	Treatment
Osteogenic sarcoma	Metaphysis of long bone Most common in knee	Mixed destructive/sclerotic lesion with soft tissue mass "Sunburst" pattern Codman's triangle CT—best to visualize periosteal changes in flat bones MRI—T1-weighted spin-echo and STIR sequences demonstrate longitudinal medullary bone involvement	Surgical excision, with/without chemotherapy or radiation therapy
Chondrosarcoma	Metaphysis of long bone or flat bones	Punctate or amorphous calcification in cartilaginous matrix CT—endosteal scalloping and cortical destruction MRI—T1-weighted image produces high signal intensity with low signal intensity of septations	Surgical excision

Continued

Summary of Findings for Malignant Bone Tumors (Neoplasia)—cont'd

Disorder	Location	Imaging Appearance	Treatment
Ewing's sarcoma	Bone marrow of long bones	Medullary destruction with "onionskin" periosteal reaction MRI—on T1-weighted image, lesion produces lower intensity signal than bone marrow; on T2-weighted image, lesion produces higher signal intensity than muscle	Radiation therapy Chemotherapy
Multiple myeloma	Intramedullary canal of the diaphysis	Multiple punched-out lesions MRI—tumor tissue has a low signal intensity (replacing high signal intensity of fatty marrow) PET—metabolically active tumor metastases appear as hot spots on the full body scan	Radiation therapy Chemotherapy
Bone metastases	Entire skeleton	Irregular, poorly defined lucent lesions or poorly defined increased densities depending on site of origin Nuclear medicine—bone scan demonstrates multiple focal areas of radionuclide uptake	Radiopharmaceuticals to reduce bone pain Radiation therapy Chemotherapy

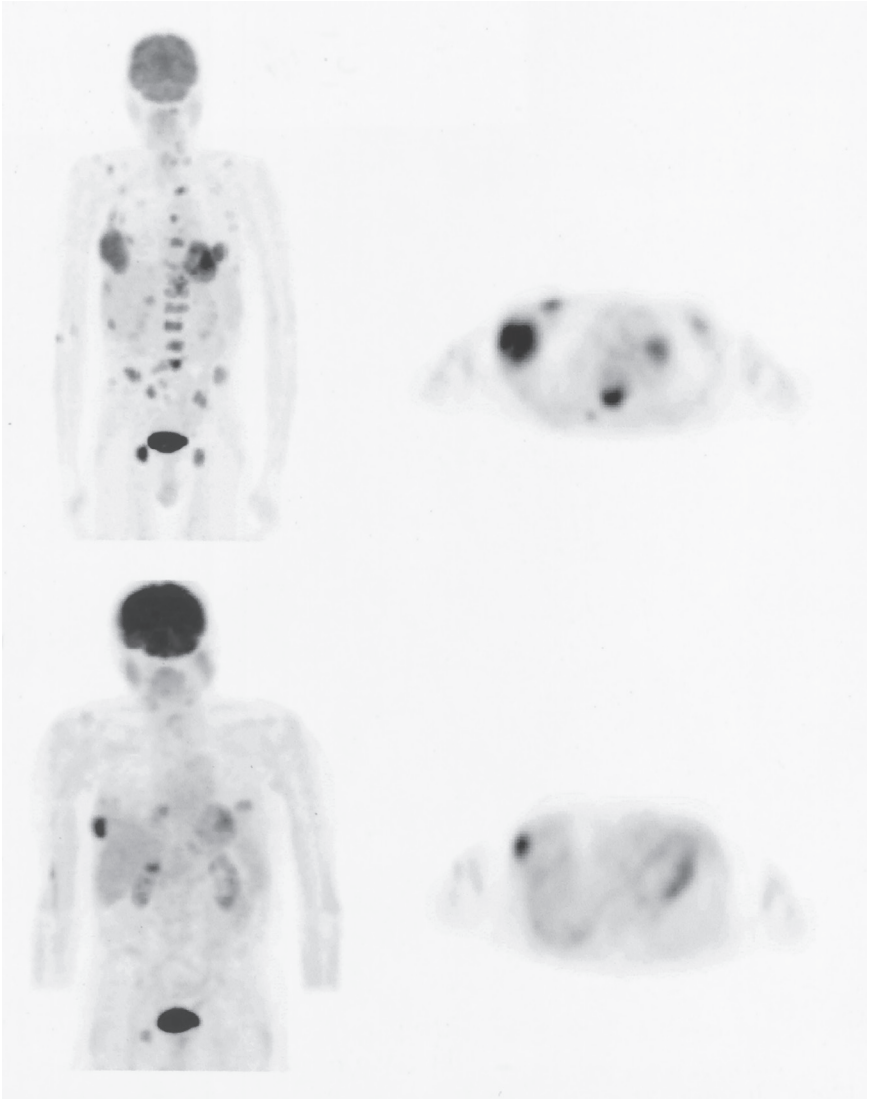

FIGURE 4-80 Multiple myeloma. The PET oncologic survey findings are positive, with a pattern of extensive metabolically active tumor metastases demonstrated throughout the axial skeleton and in both lower lung fields on coronal (A) and transverse (B) images. After 4 months, when the patient is in his last cycle of chemotherapy, the survey images (C and D) still demonstrate persistent, viable, metabolically active neoplasm. However, a dramatic improvement in the overall pattern in comparison with the earlier scan is seen.

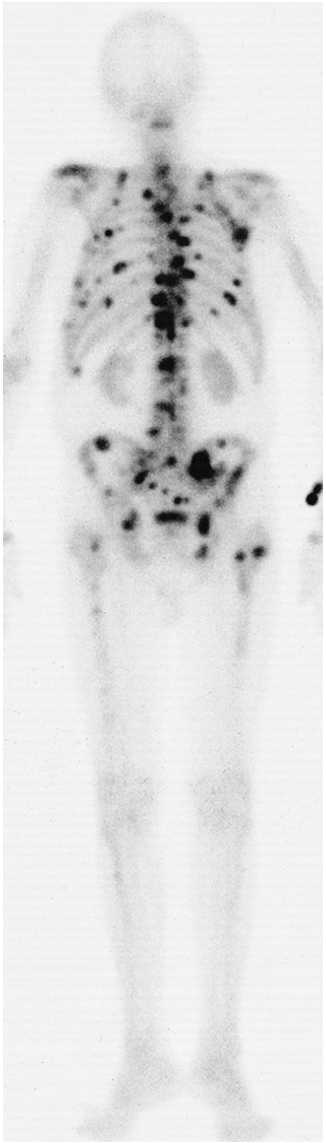

FIGURE 4-81 Screening radionuclide bone scan. Multiple focal areas of radionuclide uptake in the axial skeleton, representing metastases from prostate carcinoma.

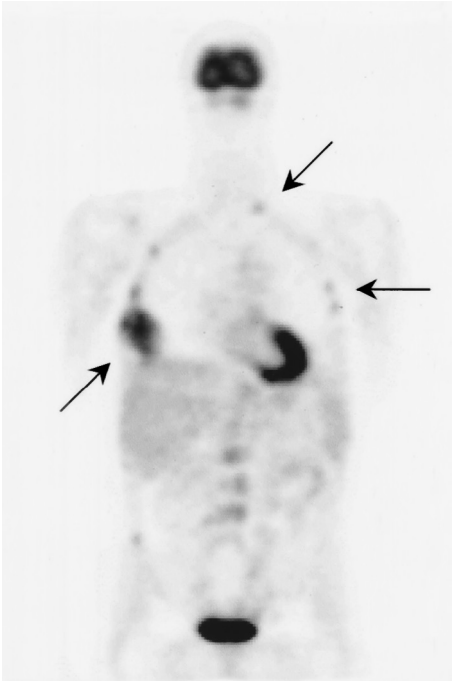

FIGURE 4-82 Fluorodeoxyglucose-PET scan showing metastases. *Arrows* point to metabolic activity in the skeletal system (ribs).

The detection of skeletal metastases is critical in the management of patients with known or suspected neoplastic disease, both at the time of initial staging and during the period of continuing follow-up care. The presence of metastases may exclude some patients from the radical "curative" therapy that is offered to those without disseminated disease, thus sparing them from fruitless, high-morbidity procedures for a nonremediable condition.

The best screening examination for the detection of asymptomatic skeletal metastases is the radionuclide bone scan (Figure 4-81) or the PET scan (Figure 4-82), which is unquestionably more sensitive than the radiographic skeletal survey. Because almost half the mineral content of a bone must be lost before the loss is detectable on plain radiographs, the skeletal survey should be abandoned as a general screening examination for the detection of asymptomatic skeletal metastases. False-negative findings on bone scans occur only with aggressively osteolytic lesions, especially in patients with multiple myeloma. The role of plain radiographs in screening for metastases is to further evaluate focal abnormalities detected on radionuclide scanning because a variety of lesions (e.g., infections, benign tumors, fibrous dysplasia, and bone islands) can also show positive findings on bone scans. Because the presence of multiple focal abnormalities is typical of metastatic disease, it is necessary to radiographically examine only a single lesion or area to confirm the diagnosis. In addition, because of the occasional false-negative results on a bone scan, it is imperative that all symptomatic sites in patients with neoplastic disease be examined by plain radiographs unless the radionuclide bone scan unequivocally demonstrates diffuse metastatic disease.

Imaging appearance. Metastatic disease may produce a broad spectrum of radiographic appearances: osteolytic, sclerotic, or mixed. Osteolytic metastases cause destruction without accompanying bone proliferation. They develop from tumor embolic deposits in the medullary canal and eventually extend to destroy cortical bone. The margins of the lucent lesions are irregular and poorly defined, rarely sharp and smooth. The most common primary lesions causing osteolytic metastases are carcinomas of the breast, kidney, and thyroid. Metastases from carcinomas of the kidney and thyroid typically produce a single large metastatic focus that may appear as an expansile trabeculated lesion (a "blowout") (Figure 4-83). Metastases from breast carcinoma are most often multiple when first detected.

In the spine, osteolytic metastases tend to involve not only the vertebral bodies but also the pedicles and posterior arches. Destruction of one or more pedicles may be the earliest sign

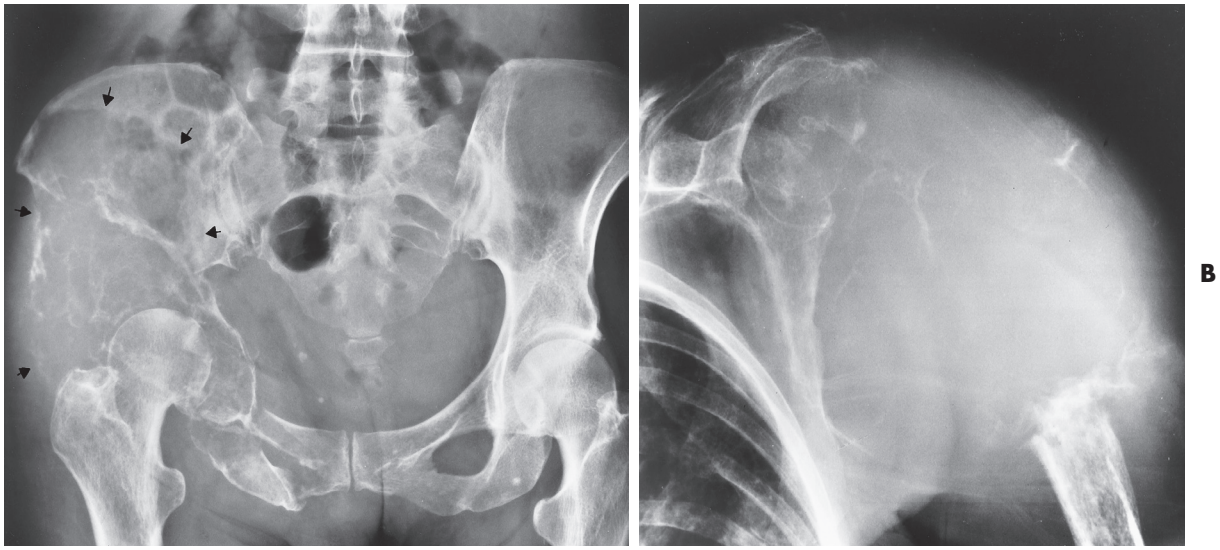

FIGURE 4-83 Blowout metastases. (A) Lytic expansile destruction of the left ilium (*arrows*) in a patient with metastatic thyroid carcinoma. (B) Osteolytic metastasis to the humerus from carcinoma of the kidney.

FIGURE 4-84 Osteoblastic metastases. Multiple areas of increased density involving the pelvis and proximal femurs, representing metastases from carcinoma of the urinary bladder.

FIGURE 4-85 Ivory vertebra. Diffuse sclerosis of the L4 vertebral body from metastatic carcinoma of the prostate.

of metastatic disease and may help in differentiating this process from multiple myeloma, in which the pedicles are much less often involved. Because cartilage is resistant to invasion by metastases, preservation of the intervertebral disk space may help to distinguish metastases from an inflammatory process. Pathologic collapse of vertebral bodies frequently occurs in advanced disease.

Osteoblastic metastases are generally considered evidence of slow growth in a neoplasm that has allowed time for a proliferation of reactive bone. In men, osteoblastic metastases are usually a result of carcinoma of the prostate gland; carcinoma of the breast is the most common primary site of osteoblastic metastases in women. These lesions initially appear as ill-defined areas of increased density that may progress to complete loss of normal bony architecture. They may vary from small, isolated round foci of sclerotic density to a diffuse sclerosis involving most or all of a bone (Figure 4-84). In the spine, this may produce the characteristic uniform density of an "ivory" vertebral body (Figure 4-85).

The combination of destruction and sclerosis in the mixed type of metastasis causes the affected bone to have a mottled appearance, with intermixed areas of lucency and increased density.

Bone destruction by metastases and associated extension of tumor in the adjacent soft tissues can be well demonstrated by CT and MRI (Figure 4-86). A PET scan can quickly determine whether the patient has a solitary metastatic lesion or multiple lesions. New fusion technology (superimposition of two imaging modality scans, such as PET and MRI) can further

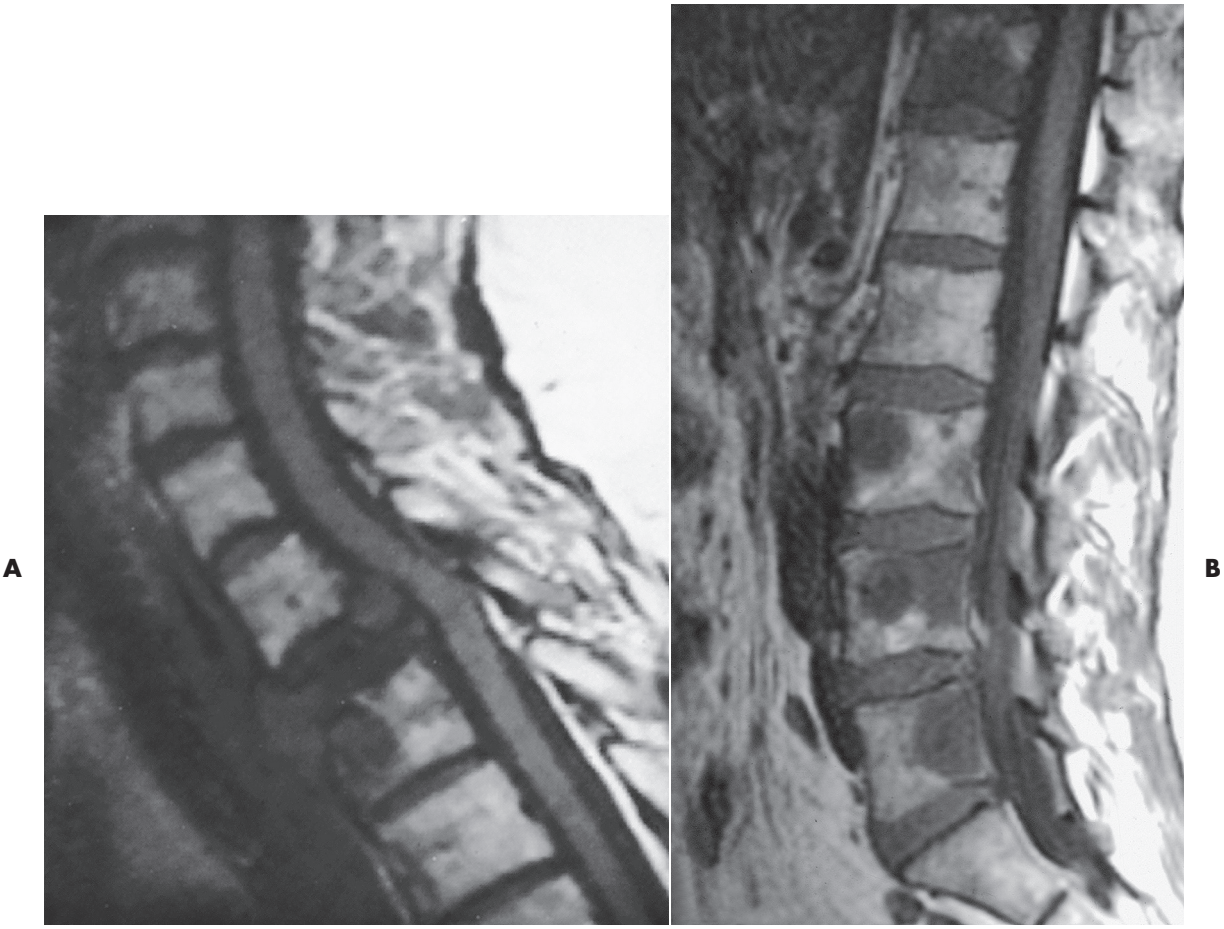

FIGURE 4-86 MR image of vertebral metastases. **(A)** Sagittal image shows gross metastatic destruction and replacement of the body of T2, which has collapsed. The metastasis has a lower signal intensity than that of vertebral marrow or the spinal cord. The spinal cord is focally indented and displaced posteriorly by the tumor. Also, a low-signal-intensity lytic metastasis involves the anterior portion of T3. **(B)** Vertebral metastasis from breast carcinoma. Many lytic lesions are evident on this MR image of the lumbar region.

define the number, size, and location of metastatic lesions, influencing the type of treatment best suited for the patient.

Treatment. Radiopharmaceuticals are increasing in use to reduce painful bone metastases. Radiation therapy and chemotherapy are the most common types of treatment, but they are generally only palliative because patients diagnosed with bone metastasis have a poor prognosis.

FRACTURES

Fractures are the most common skeletal abnormality seen in a general radiology practice. A *fracture* is defined as a disruption of bone caused by mechanical forces applied either directly to the bone or transmitted along the shaft of a bone. Although often obvious, some fractures are subtle and difficult to detect. A fracture typically appears as a radiolucent line crossing the bone and disrupting the cortical margins. However, the fracture line may be thin and easily overlooked, whereas overlap of fragments may produce a radiopaque line. Secondary signs of an underlying fracture include joint effusion, soft tissue swelling, and interruption of the normal pattern of bony trabeculae.

Types of Fractures

Fractures are described and classified by their extent, direction, and position; the number of fracture lines; and the integrity of the overlying skin (Figure 4-87). A fracture that results in discontinuity between two or more fragments is a **complete fracture**; an **incomplete fracture** causes only partial discontinuity, with a portion of the cortex remaining intact. In **closed fractures**, the overlying skin is intact; if the overlying skin is disrupted, the fracture is open, or **compound**. Although it is a clinical distinction, the radiographic demonstration of bone clearly protruding through the skin and the presence of air in soft tissues about the fracture site on radiographs obtained immediately after the injury are highly suggestive of an **open fracture**.

The direction of a fracture is determined by its relationship to the long axis of long and short bones and to the longest axis of irregular bones (e.g., the talus or carpal navicular).

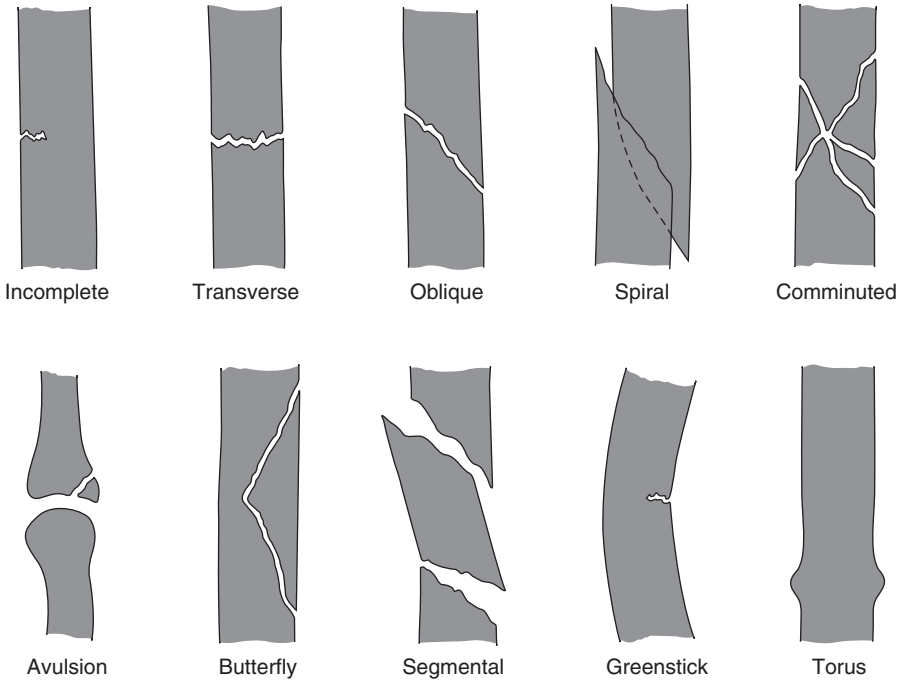

FIGURE 4-87 Classification of fractures.

A **transverse fracture** runs at a right angle to the long axis of a bone and most commonly results from a direct blow or is a fracture within pathologic bone. An **oblique fracture** runs a course of approximately 45 degrees to the long axis of the bone and is caused by angulation or by both angulation and compression forces. A **spiral fracture** encircles the shaft, is generally longer than an oblique fracture, and is caused by torsional forces. **Avulsion fractures** are generally small fragments torn from bony prominences; they are usually the result of indirectly applied tension forces within attached ligaments and tendons rather than direct blows.

A **comminuted fracture** is composed of more than two fragments. A **butterfly fragment** is an elongated triangular fragment of cortical bone generally detached from two other larger fragments of bone. A **segmental fracture** consists of a segment of the shaft isolated by proximal and distal lines of fracture.

A **compression fracture** results from a compression force that causes compaction of bone trabeculae and results in decreased length or width of a portion of a bone. Compression fractures most commonly occur in the vertebral body as a result of flexion of the spine; they may also be seen as impacted fractures of the humeral or femoral heads. A **depressed fracture** occurs in the skull or tibial plateau. In the skull, a small object with great force can produce a comminuted fracture, with portions of the fracture fragments driven inward. In the knee, the relatively hard lateral femoral condyle may impact on the relatively soft lateral tibial plateau with sufficient force to push the cortical surface of the tibia into the underlying cancellous bone.

A **stress, or fatigue, fracture** is the response of bone to repeated stresses, none of which is sufficient to cause a fracture. The earliest pathologic process in a stress fracture is osteoclastic resorption, followed by the development of periosteal callus in an attempt to repair and strengthen the bone. A **pathologic fracture** occurs in bone at an area of weakness caused by a process such as tumor, infection, or metabolic bone disease.

A **greenstick fracture** is an incomplete fracture with the opposite cortex intact. Greenstick fractures are found almost exclusively in infants and children because of the softness of their cancellous bone. A **torus (buckle) fracture** is one in which one cortex is intact with buckling or compaction of the opposite cortex. A **bowing fracture** is a plastic deformation caused by a stress that is too great to permit a complete recovery of normal shape but is less than the stress required to produce a fracture.

An **undisplaced fracture** occurs when a plane of cleavage exists in the bone without angulation or separation. **Displacement** refers to separation of bone fragments; the direction of displacement describes the relationship of the distal fragment with respect to the proximal fragment and is usually measured in terms of the thickness of the shaft. **Angulation** indicates an angular deformity between the axes of the major fragments and also describes the position of the distal fragment with respect to the proximal one. **Dislocation** refers to the displacement of a bone that is no longer in contact with its normal articulation. If there is only partial loss of continuity of the joint surfaces, the displacement is called a **subluxation**.

Imaging appearance. Radiographs are essential in the diagnosis and management of fractures. Initially, a radiograph documents the clinically suspected fracture and determines whether the underlying bone is normal or whether the fracture is pathologic and has occurred in abnormal bone. After the orthopedic reduction of a fracture, a second set of radiographs determines whether the fracture fragments are in

anatomic position. During the next several weeks or months, additional radiographs are obtained to assess fracture healing and to exclude possible complications.

In all cases of trauma, it is essential to have at least two projections of the injured part, preferably taken at 90 degrees to each other, to determine fracture continuity or displacement in the anterior or posterior, medial or lateral, and superior or inferior direction. It is also important to demonstrate the joint above and below the fracture to search for a dislocation or a second fracture that may have resulted from transmission of the mechanical force. An example of this mechanism is the fracture or dislocation of the head of the fibula that frequently occurs with a fracture of the distal part of the tibia at the ankle.

Treatment. The overall goal of fracture treatment is to restore function and stability with an acceptable cosmetic result and a minimum of residual deformity. In **external, or closed, reduction**, the fracture is treated by manipulation of the affected body part without surgical incision. **Open reduction** is a surgical procedure using direct or indirect manipulation of the fracture fragments and usually involving the application or insertion of some type of appliance or device to achieve and maintain the reduction (Figure 4-88). **External fixation** is accomplished with the use of splints, external reduction devices, or casts (Figure 4-89); **internal fixation** uses metal plates and screws, wires, rods, and nails, either alone or in combination, to maintain the reduction (Figure 4-90).

FIGURE 4-88 Open reduction with internal fixation. An intramedullary rod has been placed across a fracture of the femoral shaft. Note the extensive callus formation about the fracture site.

FIGURE 4-89 AP and lateral radiographs of the lower leg with external fixation of a comminuted fracture.

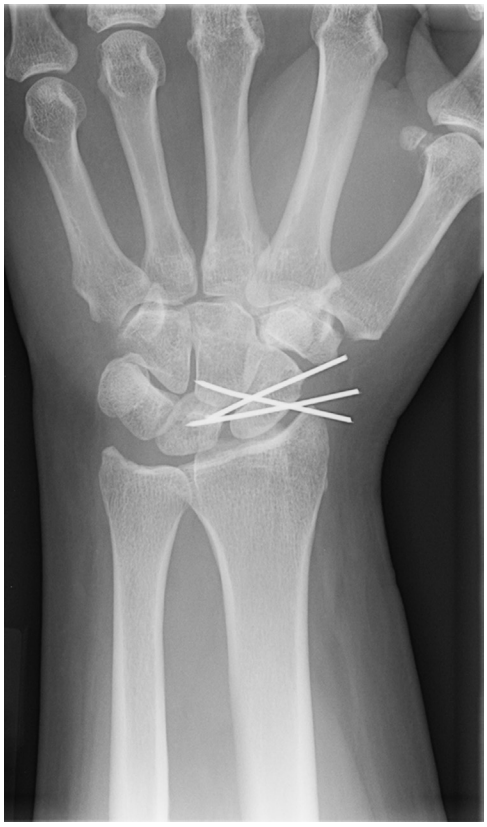

FIGURE 4-90 Scaphoid fracture post reduction. Internal fixation with pins.

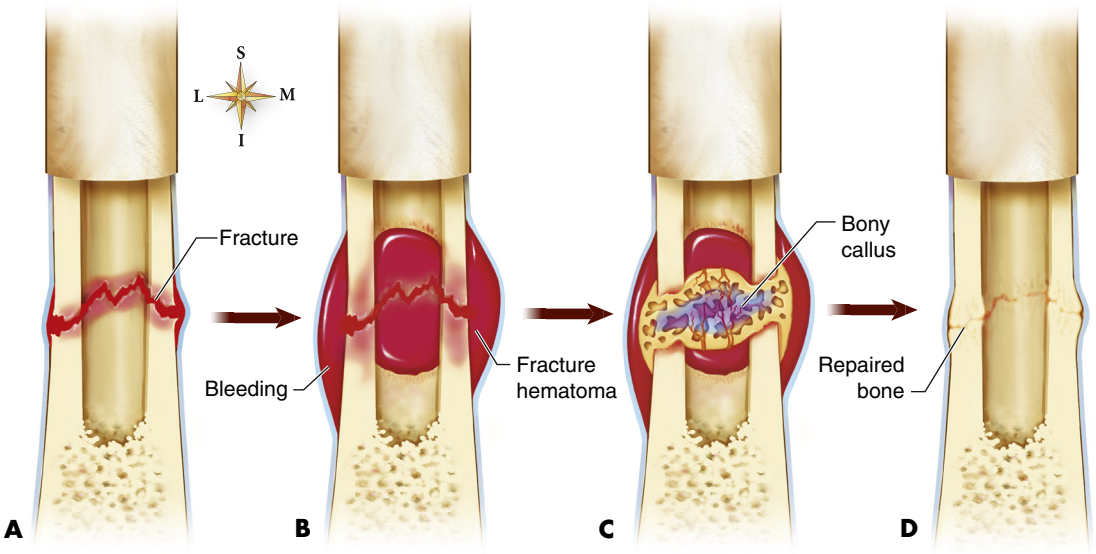

FIGURE 4-91 Bone fracture healing. (A) Fracture of the femur. (B) Formation of a fracture hematoma. (C) Formation of internal and external bony callus. (D) Bone remodeling complete.

FIGURE 4-92 Normal union of a fracture. There is dense callus formation bridging the previous fracture of the midshaft of the femur. The original fracture line is completely obliterated.

Most reduced fractures are immobilized or protected by an overlying cast. Fiberglass casting material causes less attenuation than plaster and thus produces less artifact. The radiopaque cast causes some obscuration of fine bony detail and, in severely osteoporotic bone, may make it difficult to visualize the fracture site. Therefore, if there is a question of healing that requires the demonstration of early callus formation or if there is a possibility of osteomyelitis, it is essential that the cast be removed by the physician before radiographs are obtained so that there is sufficient visibility of bone detail to resolve the questions. The radiographer must increase exposure factors to compensate for the use of plaster or fiberglass casting and whether the cast is wet or dry. Depending on the resource, some authorities recommend an increase in mAs, whereas others indicate an increase in kVp; it is recommended that one follow department protocol to produce the best images possible.

Fracture Healing

The radiographic evidence of fracture healing is a continuous external bridge of callus (calcium deposition) (Figure 4-91) that extends across the line of fracture and unites the fracture fragments (Figures 4-92 and 4-93). The callus uniformly ossifies and approaches the density of normal bone. It is essential that at least two views be taken (preferably 90 degrees to each other) to ensure that there is callus about the fracture line in all directions. Proper exposure of the radiograph is required because underexposed images may produce the illusion of obliteration of the fracture line by bony trabeculae, whereas a properly exposed image would demonstrate the continued presence of the fracture line and a lack of healing. If the findings are equivocal, either CT or conventional tomography may be required to determine the degree of union. "Stress" images, a series of radiographs obtained with the injured part in the neutral position and during the application of stress

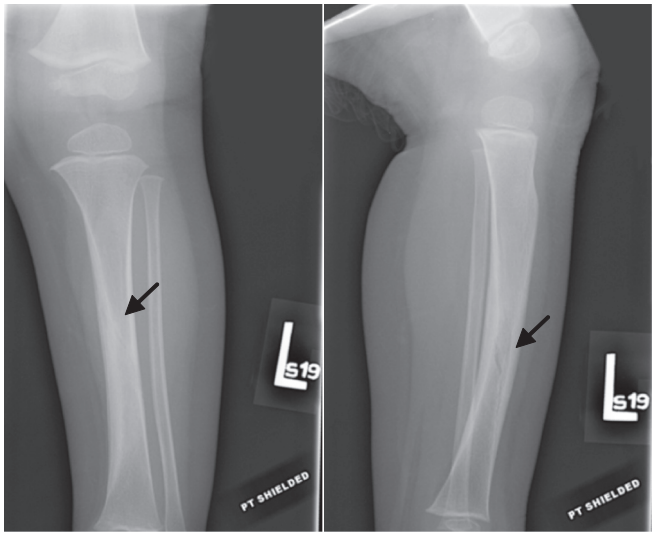

FIGURE 4-93 Healed fracture. Lower leg image demonstrating a healed fracture located in tibia (*arrow*).

by a physician or designated assistant on the distal fragment or part in the plane of suspected motion, may demonstrate a change in the alignment of the fragment, which indicates a lack of union.

Malunion is the healing of fracture fragments in a faulty position. It leads to impairment of normal function or a cosmetic appearance that may require surgical correction (Figure 4-94).

Delayed union is an ill-defined term arbitrarily applied to any fracture that takes longer to heal than the average fracture at that anatomic location. Delayed union may result from infection, inadequate immobilization, limited blood supply, or loss of bone at the fracture site.

Nonunion refers to a condition in which the fracture healing process has completely stopped and the fragments remain ununited even with prolonged immobilization. Radiographically, nonunion characteristically appears as smooth, well-defined sclerosis about the fracture margins with occlusion of the medullary canal by sclerotic bone (Figure 4-95). A persistent defect, consisting of fibrous tissue and cartilage, appears between the fragments. Nonunion occurs predominantly in adults, is rare in children, and requires operative intervention to reinitiate the healing process.

Pathologic Fractures

Pathologic fractures are those occurring in bone that has been weakened by a preexisting condition. The most common underlying process is metastatic malignancy or multiple myeloma. In children, developmental diseases, such as osteogenesis imperfecta and osteopetrosis, and nutritional deficiencies (rickets and scurvy) may result in pathologic fractures. Pathologic fractures also may occur when there is a benign cause of weakened bone, such as simple bone cyst, enchondroma, aneurysmal bone cyst, or fibrous dysplasia. Metabolic disorders causing a diffuse loss of bone substance (osteoporosis, osteomalacia, and hyperparathyroidism) also make the skeleton more susceptible to injury.

FIGURE 4-94 Malunion. Healing of proximal phalangeal fracture in poor position led to impairment of normal function.

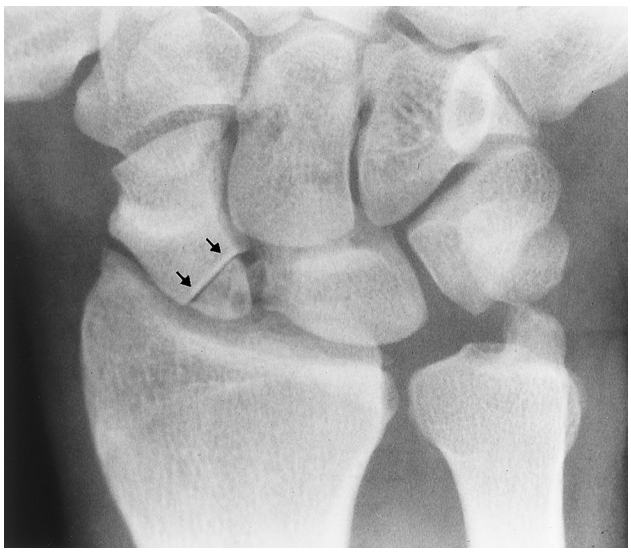

FIGURE 4-95 Nonunion of fracture of carpal navicular bone. Twenty years after initial injury, there is a smooth, well-defined line of sclerosis (*arrows*) about the fracture margin.

Imaging appearance. Clinically, pathologic fractures arise from minor trauma that would not affect normal bone. Radiographically, the fracture crosses an area of abnormal thinning, expansion, or bone destruction (Figure 4-96). The most common sites of pathologic fractures are the spine, femur, and humerus—areas in which metastatic disease is most common. In the spine, a pathologic fracture results in collapse of the vertebral body; indeed, a compressed vertebra in a patient older than 40 years should indicate underlying myeloma or metastatic disease.

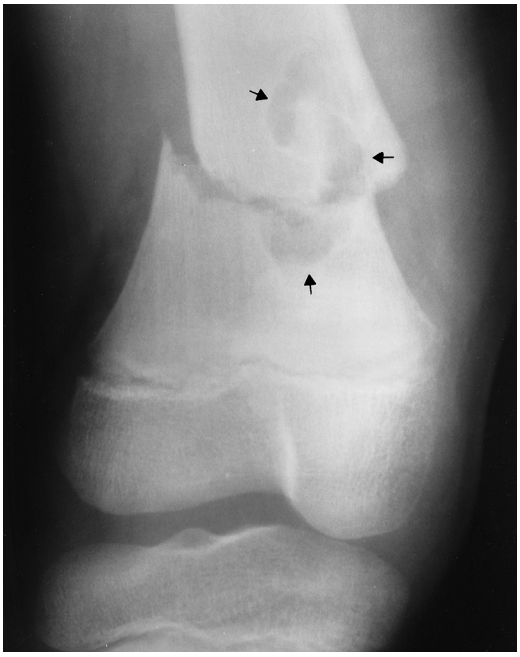

FIGURE 4-96 Pathologic fracture. A transverse fracture crosses the large benign tumor (*arrows*) of the distal femur.

CT or MRI may detect a subtle change in the abnormal bone that is obscured by an abnormal lytic area or by sclerotic changes on plain radiographs.

The radiographer must remember that patients with suspected pathologic fractures must be handled with extreme care to avoid causing either further injury to the bone in question or an additional pathologic fracture in another area.

Treatment. Treatment of a pathologic fracture varies depending on the cause. Patients with malignant causes of fracture receive palliative therapy with possible surgery to place an orthotic fixation device, joint replacement, or amputation. For benign lytic lesions (cysts), surgical bone grafts or implantation of bone chips may be required to increase bone strength and structure.

Stress Fractures

Stress (fatigue) fractures are the result of repeated stresses to a bone that would not be injured by isolated forces of the same magnitude. The type of stress fracture and the site where it occurs vary with the activity. Regardless of location, the activities resulting in stress fractures are usually strenuous, often new or different, and repeated with frequency before producing pain. Stress fracture frequently occurs in soldiers during basic training ("march" fracture). The most common sites are the shafts of the second and third metatarsals, the calcaneus, the proximal and distal shafts of the tibia and fibula, the shaft and neck of the femur, and the ischial and pubic rami.

Imaging appearance. Initially, findings on plain radiographs of the symptomatic area are within normal limits (Figure 4-97). The stress fracture is first visualized 10 to 20 days after the onset of symptoms as either a thin line of transverse or occasionally oblique radiolucency or as fluffy periosteal callus formation without evidence of a fracture line. When

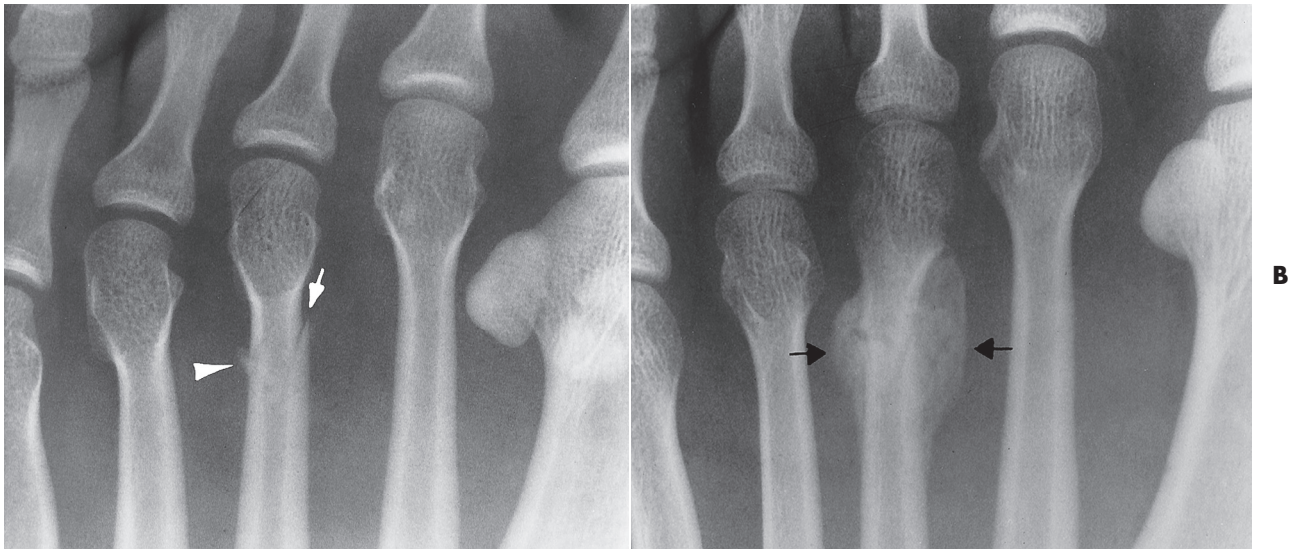

FIGURE 4-97 Stress fracture of the third metatarsal. Initial radiographic findings were within normal limits. **(A)** Radiograph obtained 14 days after onset of symptoms demonstrates thin oblique lucency (*arrow*) interrupting one cortex and a small amount of fluffy periosteal callus formation (*arrowhead*) along the opposite cortex. There is no evidence of complete fracture line. **(B)** Second radiograph obtained 3 weeks later shows dense callus formation (*arrows*) about the fracture site.

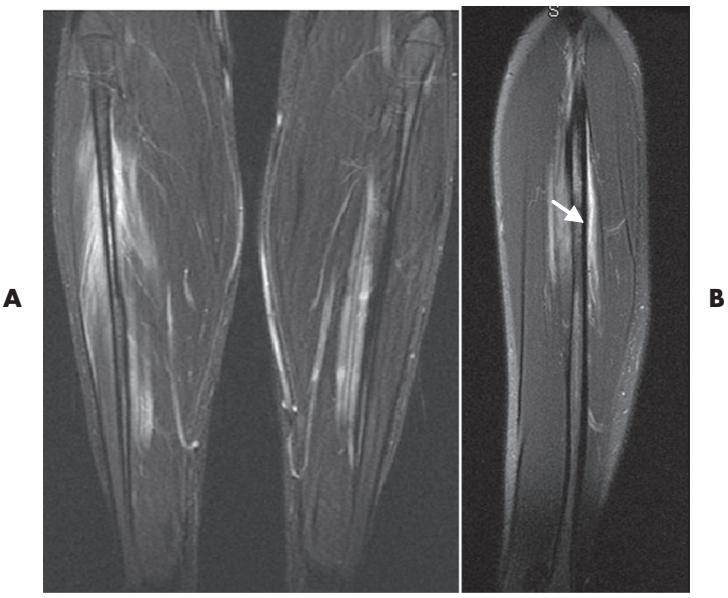

FIGURE 4-98 **Tibial stress fracture.** T2-weighted MR image with fat saturation, coronal **(A)** and sagittal **(B)**, showing increased signal within the bone and the surrounding periosteum. The fracture line demonstrates on the sagittal image (*arrow*).

this radiographic appearance is detected at a site common to stress fractures, a history of athletic or other unusual activity should be elicited as the underlying cause.

Radionuclide bone scans using a triple-phase technique to maximize specificity can demonstrate a stress fracture before it can be detected on plain radiographs. MRI, used only for cases with indeterminate radiographic findings, is highly sensitive for detecting stress fractures (Figure 4-98). In some cases, MRI has higher specificity than radionuclide bone scans. Early stress fractures produce low signal intensity on T1-weighted images; there is a progressive increase in signal intensity with increased T2 weighting. A fat-saturation (fat-suppressing) technique may demonstrate associated medullary edema or hemorrhage, which produces a high signal compared with the fat-suppressed background.

Treatment. Immobilization of the injured area prevents further injury and gives the stressed area time to heal.

Battered-Child Syndrome

Battered-child syndrome refers to multiple, repeated, physically induced injuries in young children caused by parents or guardians. The facility treating the suspected battered child, also known as suspected non-accidental trauma (SNAT), has a legal responsibility to report suspicious cases to child protective services. While the child is being evaluated, diagnosed, and treated, the environment must be protective for the child.

Shaken-baby syndrome, Munchausen syndrome by proxy, and sudden infant death syndrome are all situations investigated to prove or disprove abusive injury. A skeletal radiographic series is performed in such instances and includes an AP view of each extremity and the pelvis. AP and lateral projections of the chest and skull are also required.

Imaging appearance. The radiographic findings in this syndrome include multiple fractures of varying age in various stages of healing, fractures of the corners of metaphyses with or without associated epiphyseal displacement, and exuberant subperiosteal new bone formation along the shafts of long bones (Figure 4-99). Skull fractures or widening of the cranial sutures are commonly associated. Another highly suggestive finding is one or more fractures at otherwise unusual sites (usually fractured only by direct blows), such as the ribs, scapula, sternum, spine, or lateral ends of the clavicles (Figure 4-100).

Treatment. Prompt and accurate diagnosis of battered-child syndrome is essential to minimize the extent of physical and psychological damage and sometimes to prevent a fatal injury.

Common Fractures and Dislocations

Colles' fracture is a transverse fracture through the distal radius with dorsal (posterior) angulation and often overriding of the distal fracture fragment (Figure 4-101). In more than half the cases, there is an associated avulsion fracture of the ulnar styloid process. Colles' fracture is usually caused by a fall on the outstretched hand and is the most common fracture of the wrist.

Navicular (scaphoid) fractures are the most common fractures involving the carpal bones. They are usually transverse and occur through the central part (the waist) of the bone. Although most navicular fractures can be identified on routine frontal projections of the wrist, subtle fractures may require specific oblique and angulated projections or images made using magnification techniques. In some cases, a navicular fracture cannot be detected on the initial examination despite strong clinical suspicion (Figure 4-102A). In this situation, the wrist should be placed in a cast or plaster splint and reexamined (without the cast or splint) in 7 to 10 days. At this time, resorption of bone at the margins of the

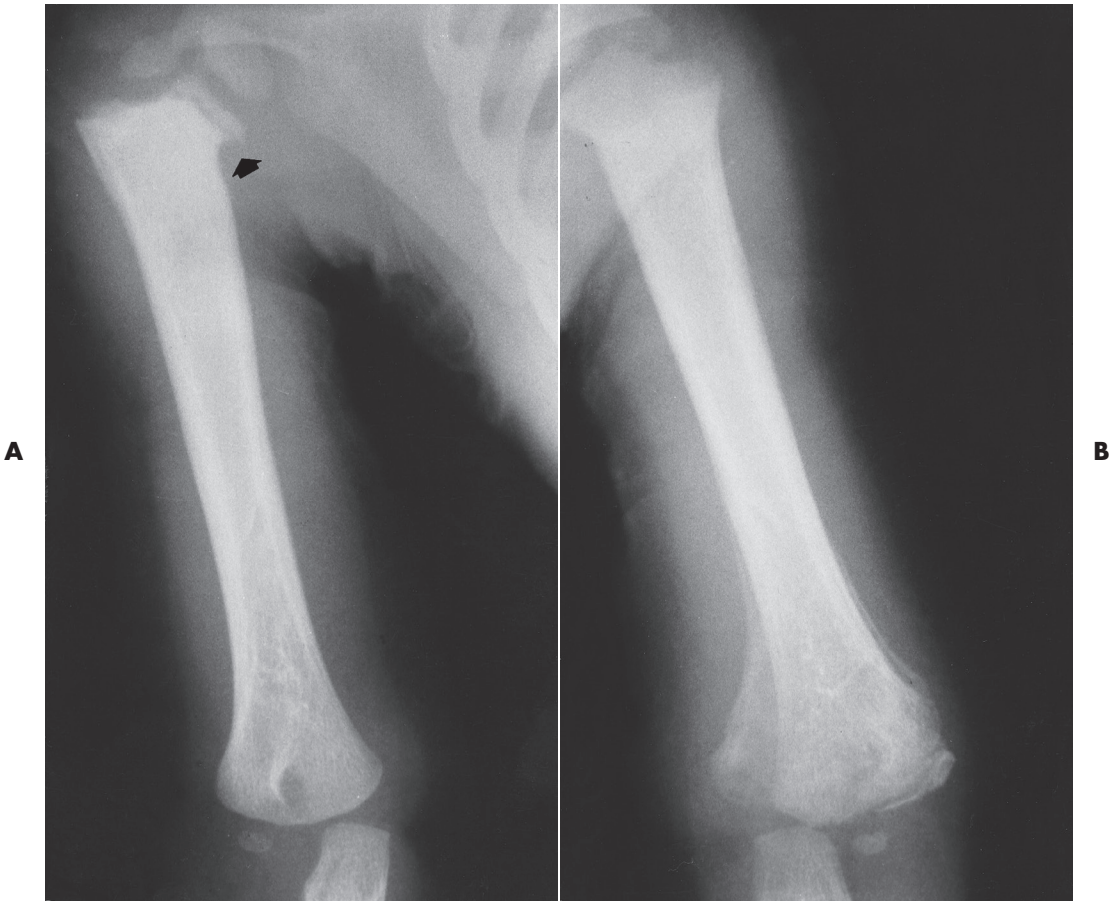

FIGURE 4-99 Battered-child syndrome. (A) Frontal radiograph of right arm demonstrates a corner fracture (*arrow*) of the proximal humerus. (B) Frontal radiograph of the left arm shows a healing displaced fracture of the distal humerus.

FIGURE 4-100 Bone scan of the upper body. Demonstrates multiple hot spots indicating fracture sites in the humerus, clavicle, and scapula.

fracture widens the fracture line and makes it more apparent radiographically (Figure 4-102B).

Nonunion is a serious complication of navicular fractures (see Figure 4-95). Its incidence increases with motion or displacement of the fracture fragments resulting from either poor immobilization or neglect. Because the blood supply to the navicular bone comes primarily from the distal portion, the proximal fragment may become avascular and undergo ischemic necrosis. This condition is seen as an increase in bone density associated with collapse of bone or loss of volume in the affected fragment (Figure 4-103).

A **boxer's fracture** is a transverse fracture of the neck of the fifth metacarpal with volar (palmar) angulation of the distal fragment (Figure 4-104). This injury is typically the result of a blow struck with the fist.

In the detection of fractures about the elbow, a valuable clue is displacement of the normal elbow fat pads (the fat pad sign). On lateral projections of the elbow, the anterior fat pad normally appears as a radiolucency closely applied to the anterior surface of the distal end of the humerus. The posterior fat pad, normally hidden in the depths of the olecranon fossa, should not be visible on standard lateral projections of the elbow. Any process producing synovial or hemorrhagic

FIGURE 4-101 Colles' fracture. Frontal (A) and lateral (B) projections of the wrist show overriding and dorsal displacement of distal fragment. There is also a displaced fracture of the distal ulna.

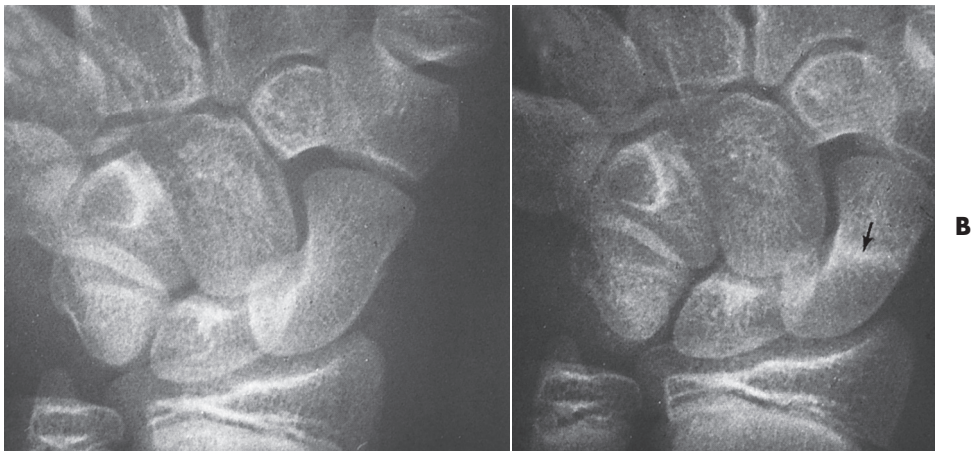

FIGURE 4-102 Navicular fracture. (A) On a radiograph obtained immediately after injury, fracture cannot be detected. (B) On a second radiograph obtained 3 weeks later, fracture is clearly signified by a sclerotic band (*arrow*) of opaque internal callus.

effusion within the elbow joint displaces the fat pads. The normally hidden posterior fat pad, when posteriorly displaced, becomes visible as a crescentic lucency behind the lower end of the humerus (Figure 4-105). The anterior fat pad becomes more rounded and further separated from the underlying bone. The posterior fat pad is by far the more sensitive indicator of an elbow joint effusion. Its presence on the lateral projection of the patient with elbow trauma strongly suggests an underlying fracture, especially of the radial head, and indicates the need for oblique projections if no fracture is seen on standard projections. If no fracture is identified, a second radiograph obtained 2 weeks or more after appropriate immobilization often shows a fracture by demonstrating a fracture line or callus formation indicating healing.

Most fractures of the forearm involve both the radius and the ulna. If only one bone fractures, it is essential to examine both the elbow and the wrist to exclude the possibility of proximal or distal joint dislocation. A **Monteggia fracture** (Figure 4-106) is an isolated fracture of the shaft of the ulna associated with anterior dislocation of the radius at the

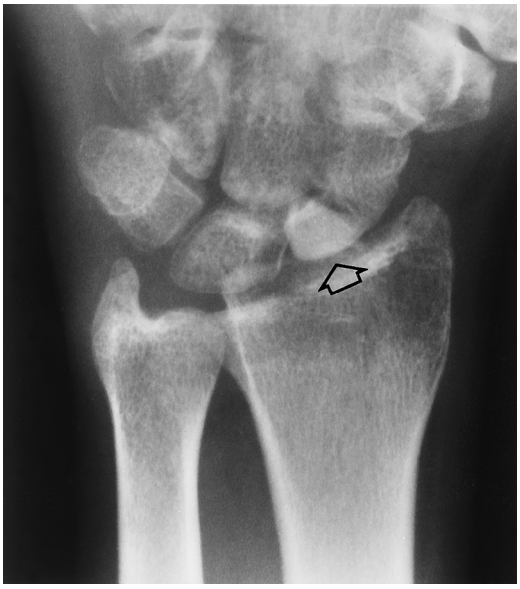

FIGURE 4-103 Avascular necrosis of a navicular fracture. Increased bone density is seen in the avascular proximal fragment (*arrow*).

FIGURE 4-104 Boxer's fracture. There is a fracture at the neck of the fifth metacarpal (*arrow*) with volar angulation of the distal fragment.

elbow. A **Galeazzi fracture** is the combination of a fracture of the shaft of the radius and a dorsal (posterior) dislocation of the ulna at the wrist.

Pott's fracture involves both malleoli (i.e., of tibia and fibula) with dislocation of the ankle joint. A bimalleolar fracture

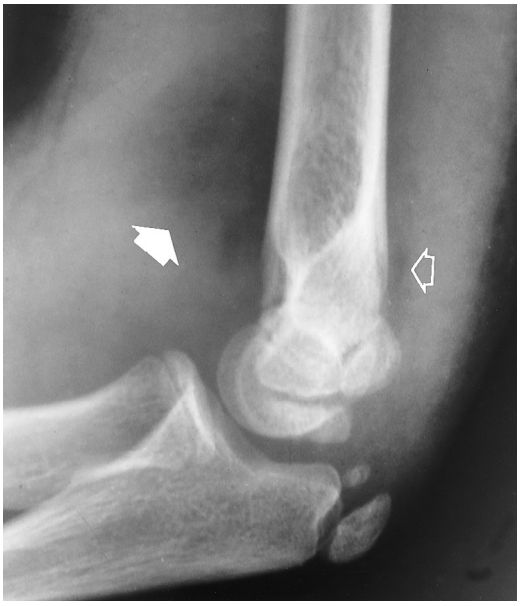

FIGURE 4-105 Fat pad sign in the elbow. The anterior fat pad (*solid arrow*) is clearly lifted from its fossa as a result of a large joint effusion in this child with a supracondylar fracture of the distal humerus. The normally hidden posterior fat pad is posteriorly displaced by effusion (*open arrow*).

is one involving both the medial and the lateral malleoli (Figure 4-107). Because of the mechanism of injury, the fracture on one side is transverse, whereas the fracture on the other side is oblique or spiral. Trimalleolar fractures involve the posterior lip of the tibia in addition to the medial and lateral malleoli and usually represent fracture–dislocations.

One of the most frequent injuries to the foot is a transverse fracture at the base of the fifth metatarsal (a **Jones fracture**) (Figure 4-108). This fracture represents an avulsion injury that results from plantar flexion and inversion of the foot, as occurs when stepping off a curb or falling while walking on stairs. It is important to distinguish this fracture from the longitudinally oriented apophysis that is normally found in children at the lateral margin of the base of the fifth metatarsal.

The shoulder is by far the most commonly dislocated joint in the body (Figure 4-109). Approximately 95% of shoulder dislocations are anterior, resulting from external rotation and abduction of the arm. As the anterior displacement occurs, the posterolateral surface of the humeral head impacts against the anterior or anteroinferior surface of the glenoid fossa, possibly resulting in a compression fracture of the humeral head, a fracture of the glenoid rim, or both. In most cases, the humeral head is displaced medially and anteriorly and comes to rest beneath the coracoid process.

Dislocations of the hip, with or without associated fracture of the acetabulum, are caused by severe injuries, such as automobile collisions, pedestrian accidents, or falls from a great height. Unlike in the shoulder, posterior dislocations of the hip are far more common than anterior dislocations, accounting for 85% to 90% of the cases (Figure 4-110).

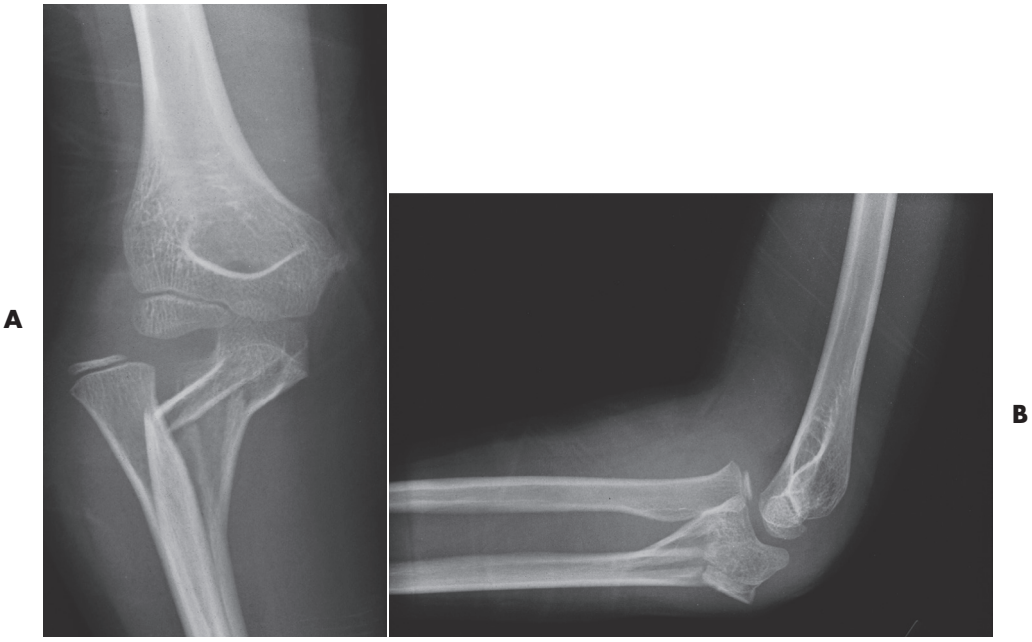

FIGURE 4-106 Monteggia fracture. (A) The anteroposterior projection demonstrates lateral radial head dislocation with a proximal ulna fracture. (B) The lateral projection demonstrates a displaced fracture of the proximal ulna with associated anterior dislocation of radial head.

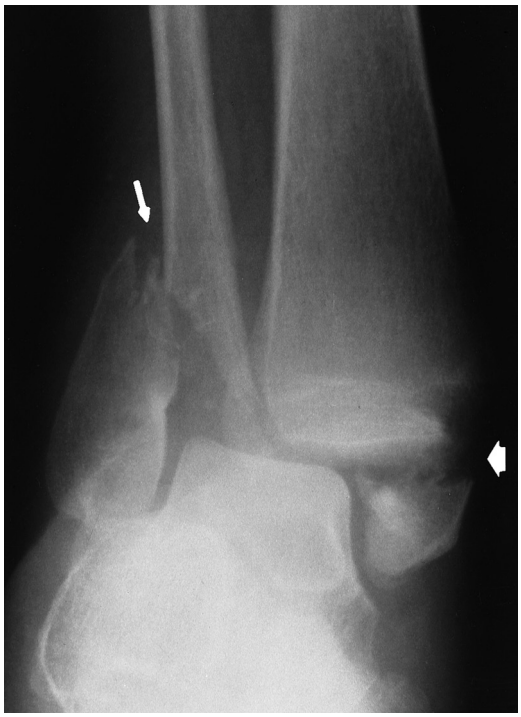

FIGURE 4-107 Bimalleolar fracture of the ankle. A transverse fracture of the medial malleolus (*wide arrow*) is associated with a low oblique fracture of the distal fibula (*thin arrow*).

FIGURE 4-108 Jones fracture of the base of the fifth metatarsal. Note that the fracture line is transverse (*black arrow*) on the base of the fifth metatarsal, whereas the normal apophysis in this child has vertical orientation (*white arrow*).

FRACTURES AND DISLOCATIONS OF THE SPINE

Fractures and dislocations of the spine may be the result of direct trauma, hyperextension–flexion injuries (whiplash), or normal stresses in abnormal bone (osteoporosis and metastatic destruction). In the patient with spinal injury, the major goal of the radiographic evaluation is to determine whether a fracture or dislocation is present and whether the injury is stable or unstable. The spine can be regarded

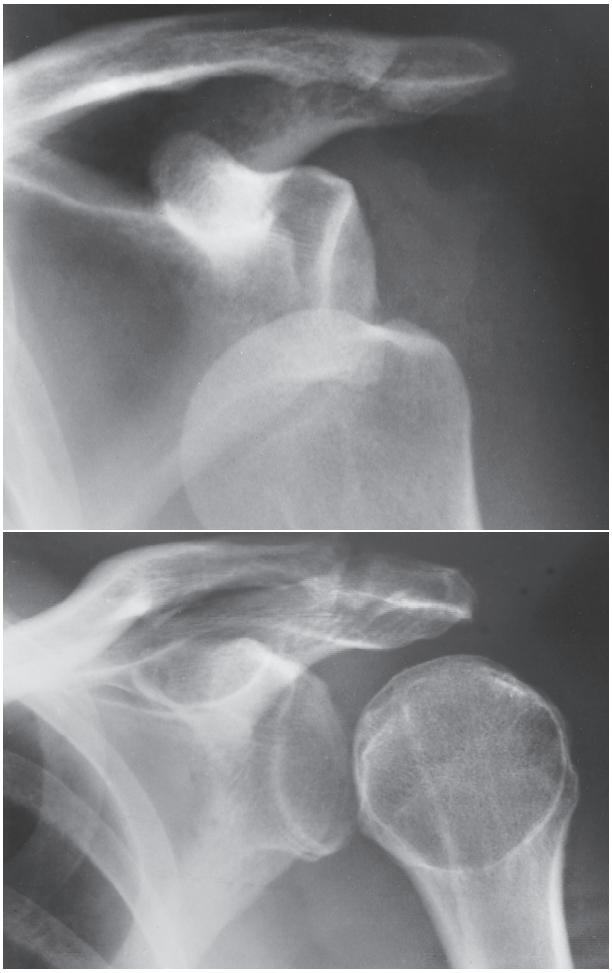

FIGURE 4-109 Dislocation of the shoulder. (A) Anterior dislocation seen with inferior and medial displacement of the humeral head. (B) Posterior dislocation demonstrated by the increased distance between the anterior glenoid rim and the humeral head.

FIGURE 4-110 Dislocations of the hip. Frontal radiograph of teenage girl injured in motor vehicle collision demonstrates right posterior dislocation and left anterior dislocation of the hip. Right posterior dislocation is characterized by typical superolateral displacement of the femoral head, fixed adduction, and internal rotation (lesser trochanter superimposed on the femoral shaft). Left anterior dislocation is manifested by the characteristic inferomedial displacement of the femoral head, which has come to overlie the obturator foramen; fixed abduction; and external rotation (lesser trochanter depicted in profile).

as consisting of two major columns. The anterior column consists of the vertebral bodies, intervertebral disks, and anterior and posterior longitudinal ligaments. The facets, apophyseal joints, pedicles, laminae, spinous processes, and all the intervening ligaments form the posterior column. If one of the two columns remains intact, the injury is considered **stable**. If both columns are disrupted, the injury is considered **unstable**.

If there is a strong suspicion of injury to the cervical spine, the initial radiograph should be a horizontal-beam lateral projection with the patient supine. This cross-table

Summary of Findings for Fractures

Fracture Type	Location	Imaging Appearance	Treatment
Trauma	All skeletal bones	Fragments, bone separation, and/or discontinuity	Reduction with immobilization—external/cast, internal/surgical fixation
Pathologic	Diseased bone	Vertebral collapse Bone destruction—radiolucency due to underlying cause	Treatment of cause Immobilization
Stress	Site of increased stress activity	Bone discontinuity Radiolucent, transverse, or oblique line Fluffy periosteal callus formation without fracture line Nuclear medicine—three-phase technique; hot focal region in affected area MRI—low signal intensity on T1-weighted images; progressively increased signal intensity on T2-weighted images	Immobilization Reduce cause of stress
Battered-child syndrome	Skull, long bones, flat bones	Multiple fractures of varying age in various stages of healing	Minimize physical and psychological damage

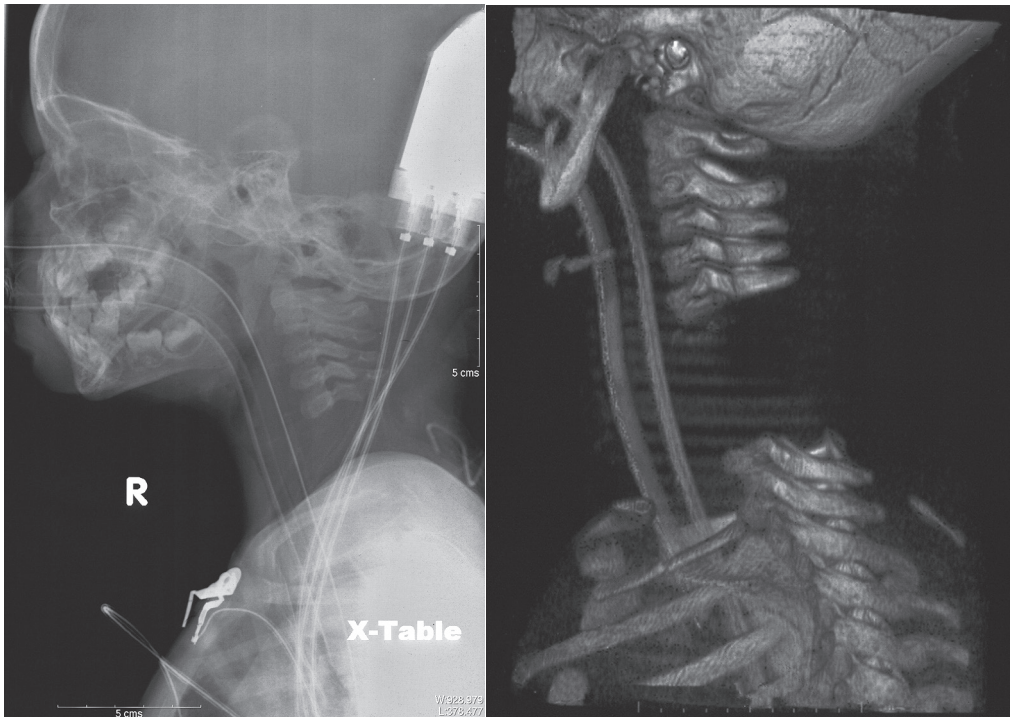

FIGURE 4-111 Cervical spine separation. **(A)** Cross-table C-spine radiograph of a 23-month-old demonstrating internal decapitation. **(B)** Volume-rendered CT scan better delineates the separation of C5–C6.

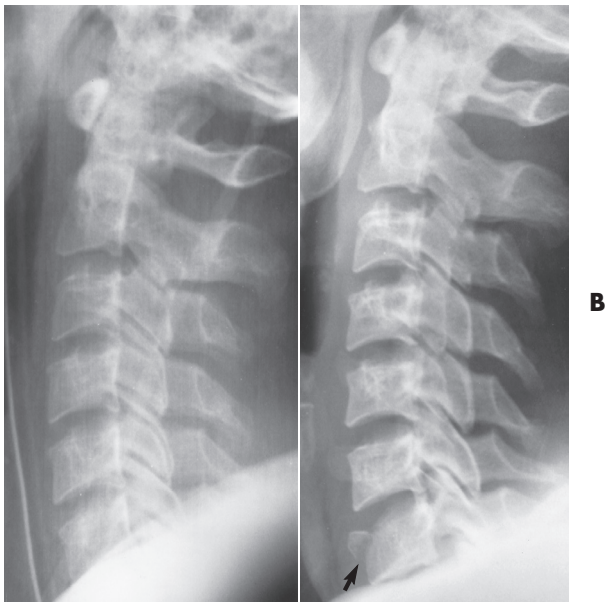

FIGURE 4-112 Fracture of the C7 vertebral body. **(A)** On the initial lateral radiograph, only the upper six cervical vertebrae can be seen. The patient's shoulders overlie the seventh cervical vertebra. **(B)** With shoulders pulled down to expose the seventh cervical vertebra, the anterosuperior fracture (*arrow*) is clearly identified.

lateral radiograph must be checked by the physician before any other projections are obtained (Figure 4-111). It is essential to include all seven cervical vertebrae on the image, lest the relatively common injuries of C6 and C7 be overlooked (Figure 4-112). This requirement may require supine oblique projections or images made in the swimmer's position, in which one arm of the patient is extended over the head while the other arm remains by the side so as to slightly oblique the upper torso and permit visualization of the cervicothoracic junction. A frontal projection of the spine and an open-mouth projection of the atlas and axis (C1 and C2) should be obtained next. In an acutely injured patient, oblique or flexion and extension projections should be performed only under the direct supervision of the attending physician. CT or even conventional tomography may be used to confirm the presence or absence of a fracture (especially of the posterior elements) and to visualize otherwise obscured areas of the spine, such as the craniovertebral and cervicothoracic junctions. CT can precisely localize fracture fragments in relation to the spinal canal and detect otherwise obscure fractures of the posterior elements. Myelography may be performed in patients with a spinal cord injury in the absence of an obvious fracture or dislocation to identify a condition amenable to surgical removal or repair (e.g., a herniated disk fragment or an epidural hematoma of the spinal cord).

Several types of fractures are peculiar to the cervical spine. A **Jefferson fracture**, a comminuted fracture of the ring of the atlas, involves both anterior and posterior arches and causes displacement of the fragments. The characteristic appearance on frontal radiographs or tomograms is a bilateral offset or spreading of the lateral articular masses of C1 in relation to the opposing articular surfaces of C2 (Figure 4-113).

Fractures of the odontoid process are usually transverse and located at the base of the dens at its junction with the

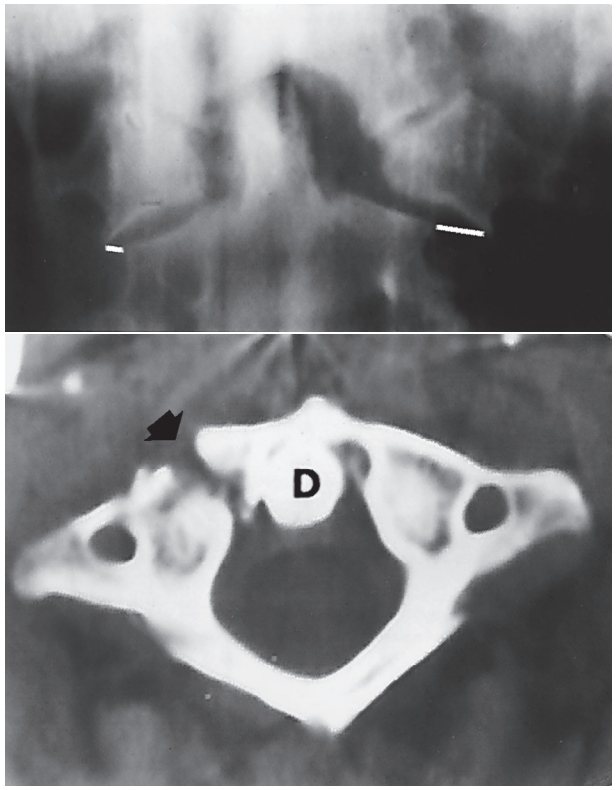

FIGURE 4-113 Jefferson fracture. **(A)** On frontal projection, there is lateral displacement of the lateral masses of C1 bilaterally (*white lines*). **(B)** CT scan in another patient shows a unilateral break in the arch of C1 (*arrow*). *D,* Dens.

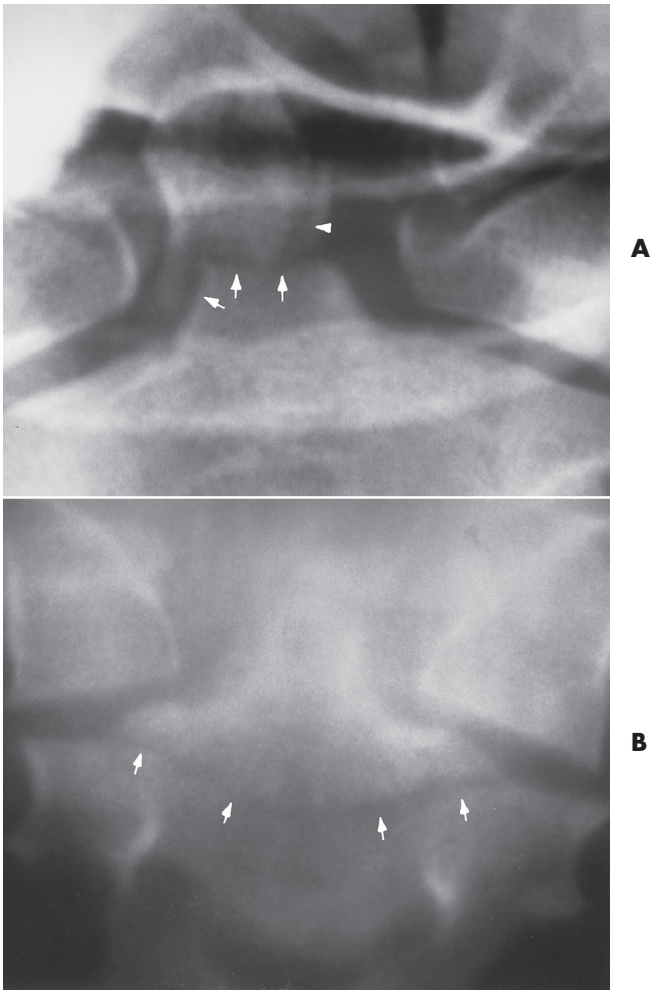

FIGURE 4-114 Fracture of the odontoid process. **(A)** Open-mouth frontal projection shows combined oblique and transverse fracture at the base of the dens (*arrows*). There is also a separate cortical fragment on left (*arrowhead*), which most likely remains attached to the alar ligament. **(B)** In another patient, a frontal tomogram shows a low fracture (*arrows*) through the body of C2.

body (Figure 4-114). On an open-mouth view, a lucency between the upper central incisor teeth often overlaps the dens; this must be differentiated from a rare vertical fracture of the dens.

The **hangman's fracture** is the result of acute hyperextension of the head on the neck. It appears as a fracture of the arch of C2 anterior to the inferior facet and is usually associated with anterior subluxation of C2 on C3 (Figure 4-115). Although originally described in patients who had been hanged, this injury is now far more commonly the result of motor vehicle collisions.

Clay shoveler's fracture is an avulsion fracture of a spinous process in the lower cervical or upper thoracic spine. The fracture is difficult to demonstrate on emergency cross-table lateral radiographs because the shoulders frequently obscure the lower cervical region. The diagnosis can be made from the frontal view by noting the double shadow of the spinous processes caused by the caudal displacement of the avulsed fragment (Figure 4-116). This double spinous process sign must be differentiated from a bifid spinous process, which usually lies at a higher level and on a more horizontal plane.

Most fractures of the thoracolumbar spine are attributable to compressive forces that cause anterior wedging or depression of the superior end plate of a vertebral body (Figure 4-117). The **seat belt fracture** is a transverse fracture of a lumbar vertebra that is often associated with significant visceral injuries (Figure 4-118). In this condition, a horizontal fracture of the vertebral body extends to involve some or all of the posterior elements.

HERNIATION OF INTERVERTEBRAL DISKS

The intervertebral disks act as shock absorbers between the vertebrae, cushioning the movements of the spine. Each disk consists of a fibrous outer cartilage (annulus) surrounding a central nucleus pulposus, which is the essential part of the disk. The nucleus pulposus is a highly elastic, semifluid mass compressed like a spring between the vertebral surfaces. In youth, it contains a large amount of fluid to cushion the motion of the spine. With increasing age, the fluid and

elasticity gradually diminish, leading to degenerative changes and back pain. Protrusion, or herniation, of a lumbar intervertebral disk is the major cause of severe acute, chronic, or recurring low back and leg pain. It most frequently involves the L4–L5 and L5–S1 levels in the lumbar region, where it often causes sciatica, pain that radiates down the sciatic nerve to the back of the thigh and lower leg. Other major sites are the C5–C6 and C6–C7 levels in the neck and the T9–T12 levels in the thoracic region.

Imaging appearance. Although plain radiographs show characteristic narrowing of the intervertebral disk spaces with hypertrophic spur formation, bony sclerosis, spurs impinging on the neural foramina, and the vacuum phenomenon (lucent collections overlying the intervertebral disks), these findings are nonspecific and frequently occur in patients with minimal symptoms (Figure 4-119). The diagnosis of herniation of an intervertebral disk requires CT, MRI, or myelography

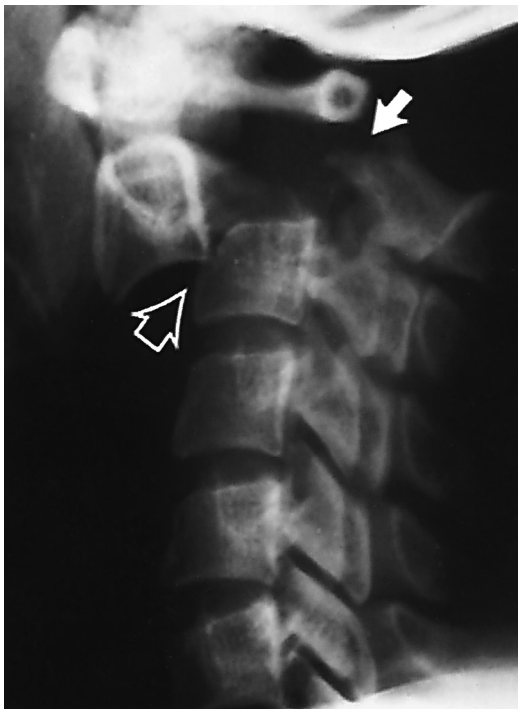

FIGURE 4-115 Hangman's fracture. Neural arch fracture (*solid arrow*) associated with complete C2–C3 subluxation (*open arrow*).

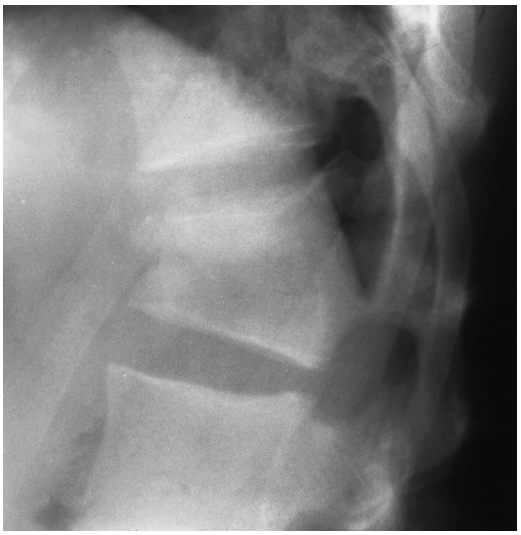

FIGURE 4-117 Vertebral body fracture. Characteristic anterior wedging of superior end plate of the L1 vertebral body.

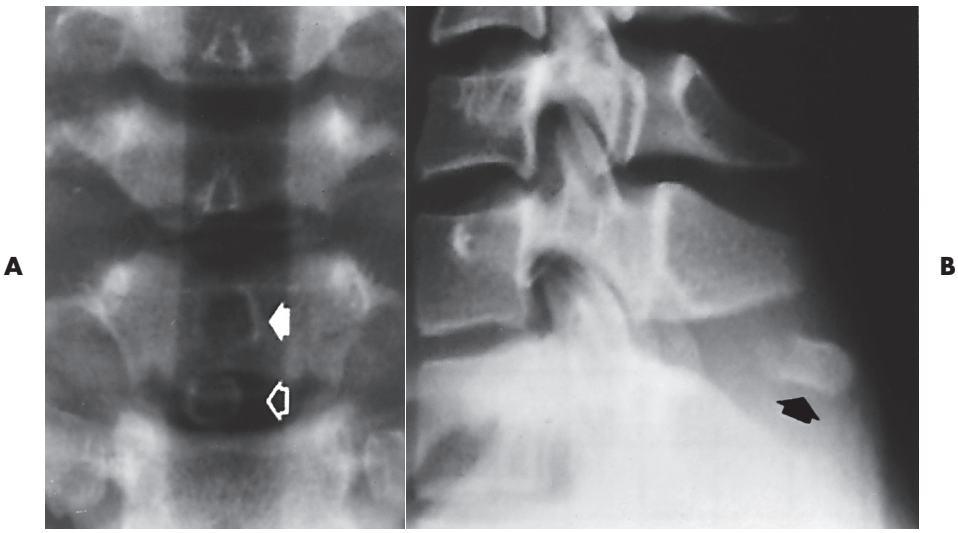

FIGURE 4-116 Clay shoveler's fracture. **(A)** Frontal projection of the cervical spine shows the characteristic double spinous process sign resulting from caudal displacement of an avulsed fragment (*open arrow*) with respect to the normal position of the major portion of the spinous process (*solid arrow*). **(B)** Lateral projection clearly shows the avulsed fragment (*arrow*).

FIGURE 4-118 Seat belt fracture. CT scan shows fracture of the lumbar vertebral body (*black arrows*) associated with a laminar fracture at the same level (*white arrow*).

FIGURE 4-119 Degenerative disk disease. Hypertrophic spurring, intervertebral disk space narrowing, and reactive sclerosis. Note the linear lucent collections (vacuum phenomenon) overlying several intervertebral disks.

to demonstrate impression of the disk on the spinal cord or individual nerve roots (Figures 4-120 to 4-125).

Treatment. Patients with symptoms suggestive of disk herniation are initially treated conservatively with bed rest, muscle relaxants, and analgesics before being subjected to radiographic studies. If conservative treatment is unsuccessful, surgery may be necessary to remove the cause of impingement and alleviate the pain and symptoms.

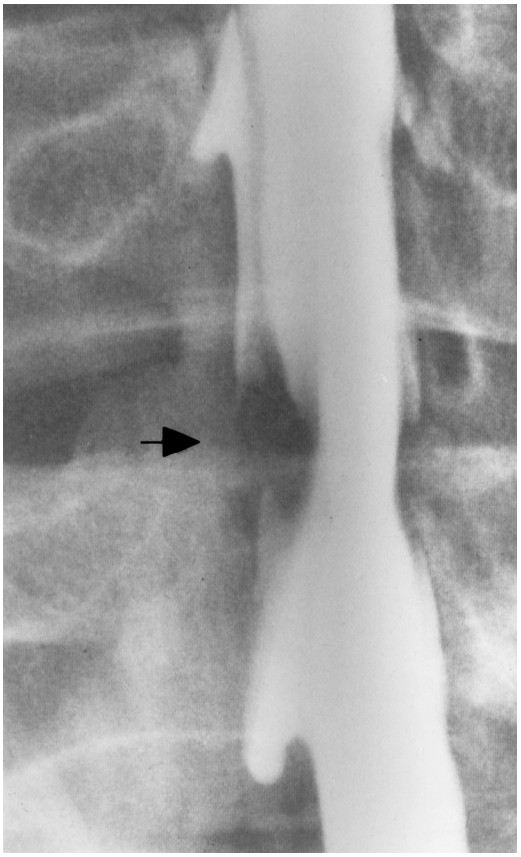

FIGURE 4-120 Lumbar disk herniation. Myelogram shows an extradural lesion (*arrow*) at the level of the intervertebral disk space. Note the amputation of the nerve root by disk compression.

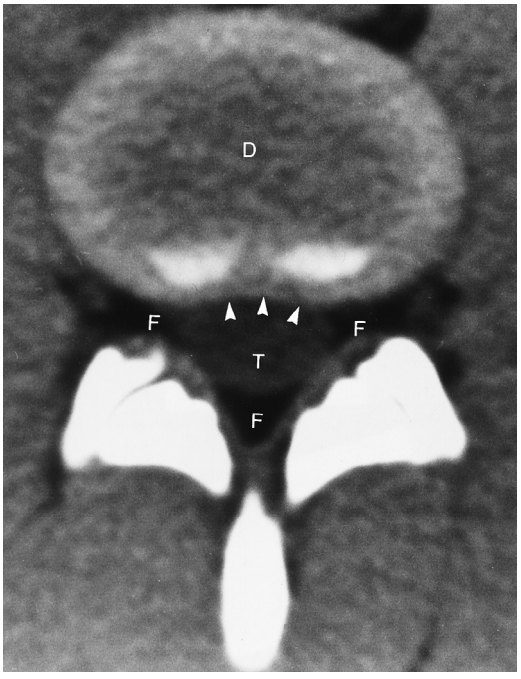

FIGURE 4-121 CT of a normal lumbar disk (*D*). The normal lumbar intervertebral disk has a concave posterior border (*arrowheads*). Note the normal epidural fat (*F*) surrounding the thecal sac (*T*).

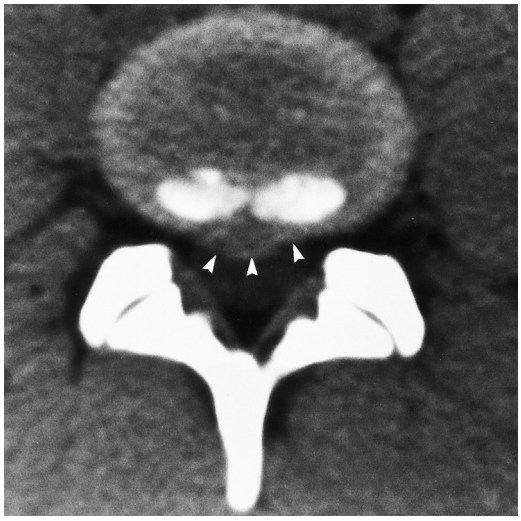

FIGURE 4-122 Central bulging of an intervertebral disk. CT scan shows convex posterior border of the disk (*arrowheads*). Note the preservation of epidural fat.

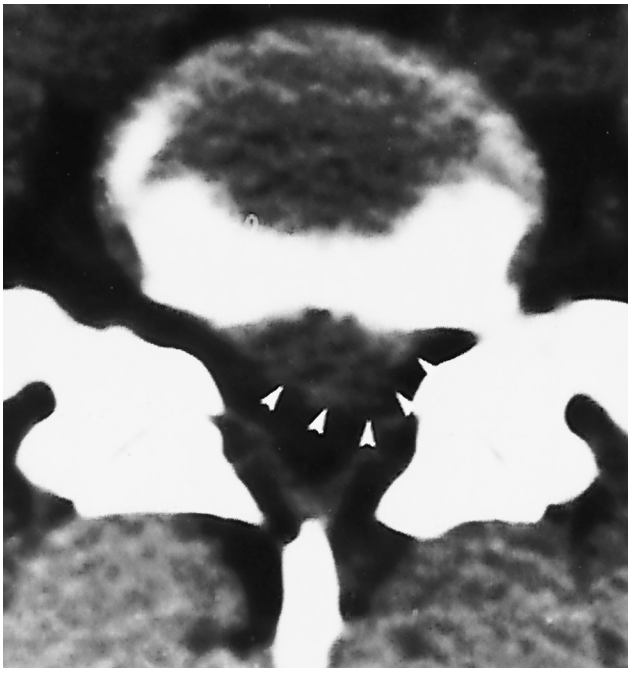

FIGURE 4-123 Disk herniation at the L5–S1 level. CT shows herniation of the disk (*arrowheads*) to the left with obliteration of epidural fat.

FIGURE 4-124 Disk herniation of the cervical spine. T2-weighted sagittal MR image shows an extradural impression on spinal cord.

SCOLIOSIS

Scoliosis is a twisting and curvature in the lateral perspective, somewhat like an S curve. The most common types of scoliosis can be classified as idiopathic, functional, neuromuscular, and degenerative. Idiopathic, the most common in young females, can be divided into infantile, juvenile, and adolescent. Adolescent scoliosis occurs in people 10 years old or older with an abnormal curvature from an unknown cause. Functional scoliosis occurs because of a problem outside of the spine, such as one leg being shorter than the other for which the body compensates naturally. Neuromuscular scoliosis occurs when the vertebra fails to form completely or fails to separate appropriately. Adult-type scoliosis is degenerative in form and is usually caused by arthritis.

Imaging appearance. Full spine images should be acquired in the upright position with the patient standing using normal stance and weight distribution. The technologist must include the iliac crest while shielding the gonad region and the breast tissue; some even suggest removing the shoes for the most accurate images. The spinal curvature will be measured each clinic visit to determine whether the curvature is progressing or remaining constant (Figure 4-126). This evaluation is important in helping to determine the treatment necessary. Curvatures that are considered normal are less than 20 degrees, whereas curvatures of 40 to 50 degrees and greater need the most extensive treatment. To obtain more extensive information of the bony development, a CT scan demonstrates the vertebral structure. In some cases, an MRI is used to ensure that the spinal cord and spinal canal are within normal limits in preparation for surgical treatments.

Treatment. For curvatures of 25 to 40 degrees, bracing technology is the treatment of choice. The brace is custom fitted and is most effective if worn more than 12 hours a day. For the more severe cases, curvatures 40 degrees or greater, surgery is most often recommended and has a high success rate. Surgery possibly includes a spinal fusion and rods to provide as much correction as possible.

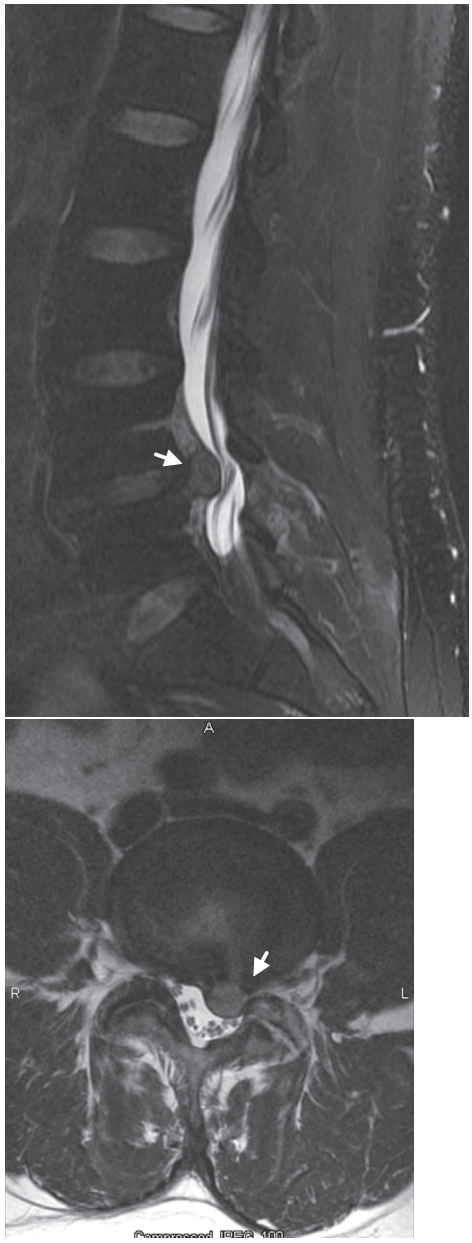

FIGURE 4-125 Lumbar disk herniation. T2-weighted MR images illustrating a torn annulus fibrosis and nucleus pulposus of L4–L5 (*arrow*) in sagittal (A) and transverse (B) planes.

SPONDYLOLYSIS AND SPONDYLOLISTHESIS

Spondylolysis refers to a cleft in the pars interarticularis that is situated between the superior and inferior articular processes of a vertebra. Occurring in approximately 5% of the population, such clefts are usually bilateral, most commonly involve the fifth lumbar vertebra, and predispose to the forward displacement of one vertebra on the other that may cause chronic back pain. *Spondylolysis* is the term for a defect in the pars interarticularis without displacement; if displacement occurs, the condition is called **spondylolisthesis**.

Imaging appearance. A plain lateral radiograph of the lower lumbar spine clearly shows any spondylolisthesis and may demonstrate the lucent cleft in the pars interarticularis even if no displacement has occurred (Figure 4-127). In the grading of spondylolisthesis of the lumbosacral junction on the lateral projection, the superior surface of the sacrum is divided into four equal parts. A forward

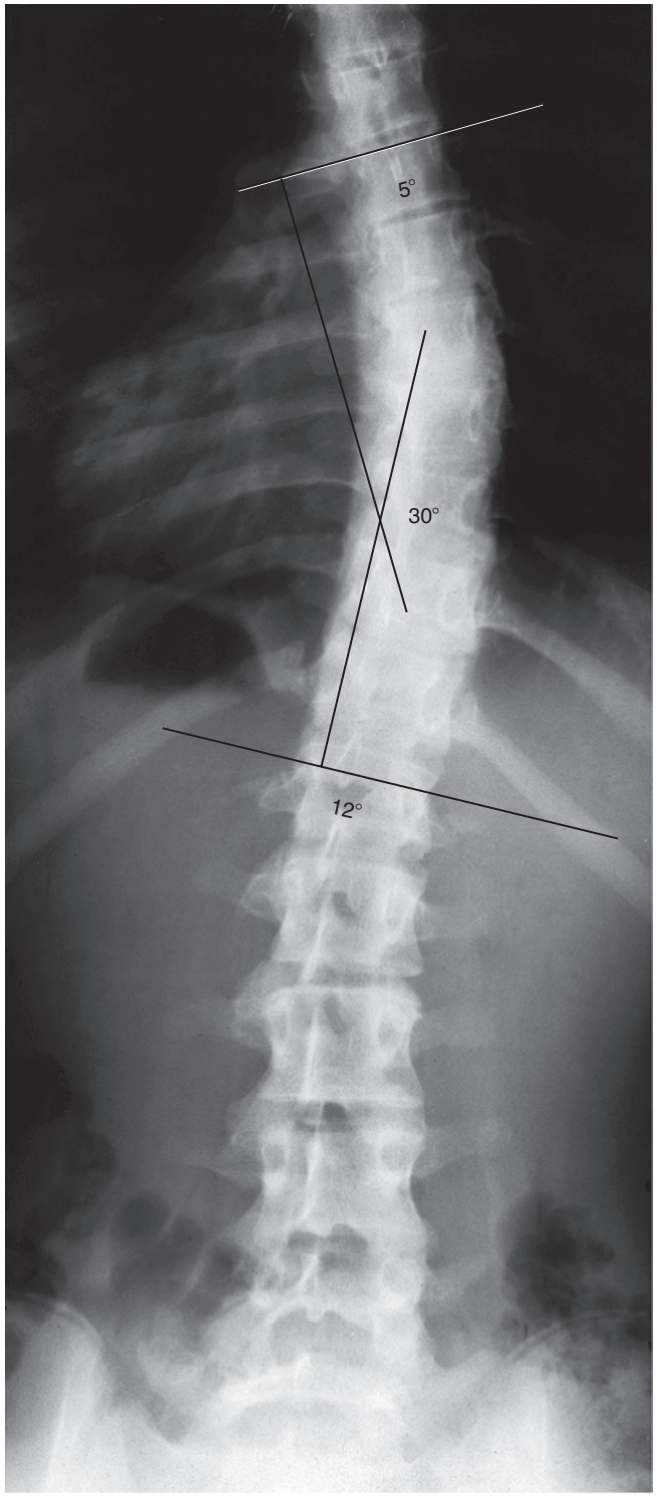

FIGURE 4-126 Scoliosis. Anteroposterior spine image with curvature measurements—cervicothoracic 5 degrees, thoracic 30 degrees, and thoracolumbar 12 degrees.

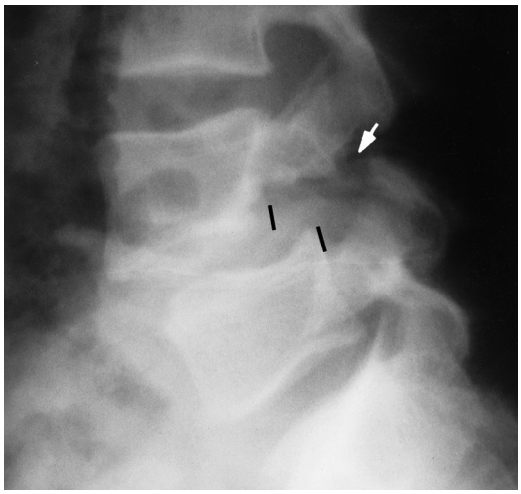

FIGURE 4-127 Spondylolisthesis. Lateral view of the lower lumbar spine shows a break in the pars interarticularis (*arrow*), with resultant anterior slippage of L4 with respect to L5. *Black lines* indicate the posterior margins of the vertebral bodies.

displacement of the fifth lumbar vertebra up to one-fourth the thickness of the sacrum is called a first-degree spondylolisthesis; half the thickness, a second-degree spondylolisthesis; and so on.

The diagnosis of spondylolysis without displacement may require an oblique projection of the lumbar spine, in which the appearance of the posterior elements has been likened to that of a Scotty dog (Figure 4-128). The pedicle and transverse process form the eye and nose; the superior and inferior articular processes form the ear and leg; and the pars interarticularis forms the neck, which is "fractured" in a patient with spondylolysis.

Treatment. Passive treatment for spondylosis or spondylolisthesis includes bracing, physical therapy, restricted activity, and nonnarcotic analgesics to control pain to a tolerable level. Conservative therapy works for the majority of patients. Surgical treatment is necessary only when passive treatment is unsuccessful for controlling pain. A complete laminectomy, usually with spinal fusion, is performed to free the peripheral nerves and stabilize spinal movement.

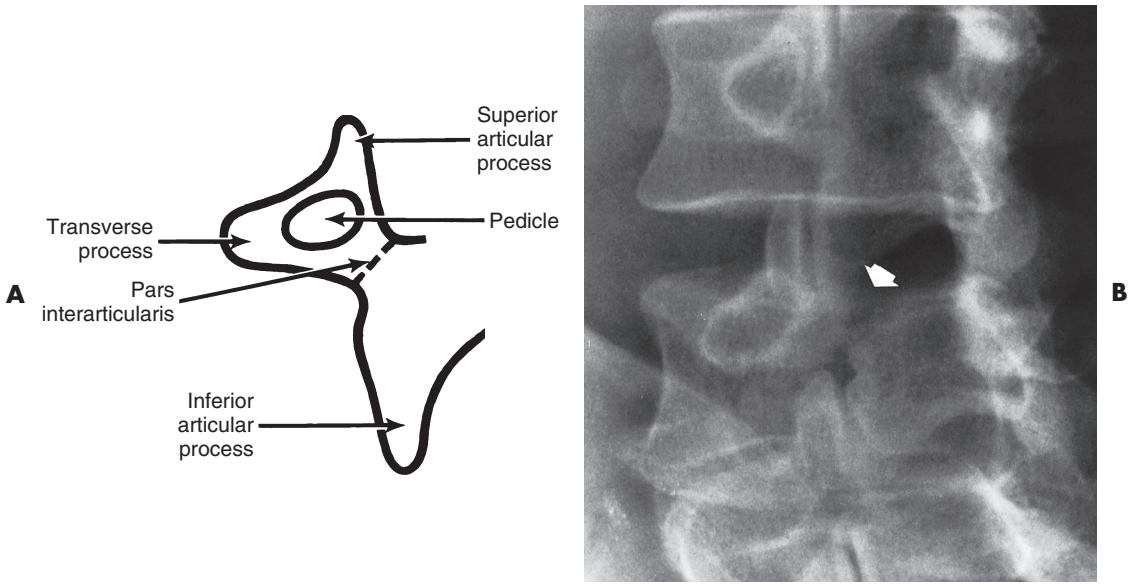

FIGURE 4-128 Spondylolysis. **(A)** Diagram of the "Scotty dog" sign. **(B)** Oblique projection of the lumbar spine demonstrates a defect in the pars interarticularis, which appears as a fracture through the neck of the Scotty dog (*arrow*).

Summary of Findings for Common Spinal Disorders

Disorder	Location	Imaging Appearance	Treatment
Disk herniation	Cervical and lumbar spine regions	CT and MRI—disk impingement on nerve or spinal cord	Conservative—bed rest, muscle relaxants, and analgesics Aggressive—surgical removal of disk
Scoliosis	Lateral curvature of any of the spine	Curvature of the spine from side to side	Nonoperative—bracing, physical therapy, and possibly restricted activity Surgical—posterior spinal fusion with rod placement
Spondylolysis Spondylolisthesis	Fifth lumbar vertebra, lumbosacral junction	Defect in pars interarticularis without displacement Forward displacement with pars interarticularis defect	Nonoperative—bracing, physical therapy, restricted activity, and nonnarcotic analgesics Surgical—complete laminectomy with spinal fusion

REVIEW QUESTIONS

1. The shaft of any long bone is termed the _____.
   a. epiphysis
   b. diaphysis
   c. metaphysis
   d. periosteum
2. The end of a long bone is referred to as the _____.
   a. epiphysis
   b. diaphysis
   c. metaphysis
   d. periosteum
3. The special types of cells responsible for the diameter growth of bones are _____.
   a. osteoblasts
   b. chondroblasts
   c. osteoclasts
   d. both a and b
4. The common area(s) of the body radiographed to determine bone age is/are _____.
   a. skull
   b. wrist
   c. hand
   d. both b and c
5. What pathologic condition is present if the posterior elements of one or more vertebrae fail to unite?
   a. meningocele
   b. spina bifida
   c. myelomeningocele
   d. spondylolisthesis
6. A vertebra that has characteristics of two divisions of the spine is called a(n) _____.
7. Osteopetrosis causes the bone to _____ in bone density.
8. Aging and postmenopausal hormonal changes are the major causes of generalized _____.
   a. osteogenesis imperfecta
   b. osteoporosis
   c. osteopetrosis
   d. osteomalacia
9. An inherited generalized disorder of connective tissue characterized by multiple fractures and a bluish color of the sclera of the eye is _____.
   a. osteogenesis
   b. osteoporosis
   c. osteopetrosis imperfecta
   d. osteomalacia
10. Lack of vitamin D in the diet of infants and children can cause a systemic disease called _____.
    a. achondroplasia
    b. rickets
    c. osteomalacia
    d. osteopetrosis
11. A disorder of metabolism causing an increased blood level of uric acid is called _____.
    a. achondroplasia
    b. rickets
    c. gout
    d. uremia
12. On a radiographic image, dense transverse bands extending across the metaphyses of the long bones are commonly seen in _____.
    a. achondroplasia
    b. gout
    c. lead poisoning
    d. rickets
13. A benign projection of bone with a cartilage-like cap occurring around the knee in children or adolescents is _____.
    a. osteochondroma
    b. enchondroma
    c. achondroplasia
    d. osteoma
14. An example of a malignant bone tumor is _____.
    a. osteogenicsarcoma
    b. chondrosarcoma
    c. Ewing's sarcoma
    d. all of the above
15. The form of noninfectious arthritis characterized by osteoporosis, soft tissue swelling, and erosions of the metacarpophalangeal joints and ulnar styloid processes is _____.
    a. Reiter's syndrome
    b. rheumatoid arthritis
    c. psoriatic arthritis
    d. osteoarthritis
16. The extremely common form of arthritis that is characterized by loss of joint cartilage and reactive new bone growth and that is part of the normal wear of aging is _____.
    a. Reiter's syndrome
    b. rheumatoid arthritis
    c. psoriatic arthritis
    d. osteoarthritis
17. Inflammation of the small fluid-filled sacs that are located around joints and that reduce friction is termed _____.
    a. tendinitis
    b. arthritis
    c. bursitis
    d. both a and c
18. The most common metabolic skeletal disease is _____.
    a. osteomalacia
    b. rickets
    c. osteopetrosis
    d. Paget's

19. In what type of fracture is the skin broken?
    a. butterfly
    b. compound
    c. comminuted
    d. both a and c
20. What type of fracture consists of more than two fragments?
    a. open
    b. compound
    c. comminuted
    d. both a and b
21. What term applies to the new calcium deposits that unite fracture sites?
    a. bone
    b. callus
    c. periosteum
    d. both a and c
22. What type of fracture occurs in bone weakened by some preexisting condition, such as a metastatic lesion or multiple myeloma?
    a. stress
    b. Colles'
    c. Pott's
    d. pathologic
23. What is the name for the type of fracture that can occur from falling on the outstretched hand and that involves the distal portion of the radius?
    a. stress
    b. Colles'
    c. Pott's
    d. pathologic
24. What name is applied to a fracture involving both malleoli?
    a. stress
    b. Colles'
    c. Pott's
    d. pathologic
25. What is the name applied to the fracture resulting from acute hyperextension of the head on the neck that usually affects C2 and C3?
    a. hangman's
    b. Jefferson
    c. boxer's
    d. Monteggia
26. What area of the spine does a clay shoveler's fracture involve?
    a. lower thoracic and upper lumbar
    b. lumbar only
    c. lower cervical and upper thoracic
    d. cervical only
27. Ischemic necrosis can be caused by?
    a. thrombosis
    b. proliferation of fibrous tissue within the medullary cavity
    c. vasculitis
    d. a and c
28. Diagnosis of an intervertebral disk herniation requires which radiographic procedure(s)?
    a. myelography
    b. CT
    c. MRI
    d. a or b or c
29. An abnormal lateral curvature of the spine (more than 20 degrees) is known as _____.
    a. scoliosis
    b. spondylolysis
    c. spondylitis
    d. spondylolisthesis
30. What medical term refers to a cleft in the pars interarticularis commonly involving the fifth lumbar vertebra?
    a. spondylolisthesis
    b. spondylolysis
    c. spondylitis
    d. a or b or c
31. What pathologic condition sometimes occurs after trauma, causing an interrupted blood supply to a bone?
    a. vasculitis
    b. ischemic necrosis
    c. Cushing's disease
    d. stress fracture

5

Gastrointestinal System

OUTLINE

Physiology of the Digestive System
Esophagus
- Tracheoesophageal Fistula
- Esophagitis
- Ingestion of Corrosive Agents
- Esophageal Cancer
- Esophageal Diverticula
- Esophageal Varices
- Hiatal Hernia
- Achalasia
- Foreign Bodies
- Perforation of the Esophagus

Stomach
- Gastritis
- Pyloric Stenosis
- Peptic Ulcer Disease
- Cancer of the Stomach

Small Bowel
- Crohn's Disease (Regional Enteritis)
- Small Bowel Obstruction
- Adynamic Ileus
- Intussusception
- Malabsorption Disorders

Colon
- Appendicitis
- Diverticulosis
- Diverticulitis
- Ulcerative Colitis
- Crohn's Colitis
- Ischemic Colitis
- Irritable Bowel Syndrome
- Cancer of the Colon
- Large Bowel Obstruction
- Volvulus of the Colon
- Hemorrhoids

Gallbladder
- Gallstones (Cholelithiasis)
- Acute Cholecystitis
- Emphysematous Cholecystitis
- Porcelain Gallbladder

Liver
- Hepatitis
- Cirrhosis of the Liver
- Hepatocellular Carcinoma
- Hepatic Metastases

Pancreas
- Acute Pancreatitis
- Chronic Pancreatitis
- Pancreatic Pseudocyst
- Cancer of the Pancreas

Pneumoperitoneum
Spleen
- Enlargement
- Rupture

KEY TERMS

alcoholic gastritis
bacterial (phlegmonous) gastritis
chronic atrophic gastritis
chyme
colonic ileus
congenital tracheoesophageal (TE) fistulas
constipation
corrosive gastritis
deglutition
diarrhea
diarrheogenic islet cell tumors
emulsifier
epiphrenic diverticula
gastrinomas
glycogen
hepatitis
infectious gastritis
infiltrating
insulinoma
irritable bowel syndrome
localized ileus
malabsorption disorder
Mallory–Weiss syndrome
mastication
pancreatitis
peristalsis
polypoid
pyloric stenosis
traction
ulceration
ulcerogenic islet cell tumors (gastrinomas)
villi
Zenker's diverticula

OBJECTIVES

After reading this chapter, the reader will be able to:

- Classify the more common diseases in terms of their attenuation of x-rays
- Explain the changes in technical factors required for obtaining optimal quality radiographs in patients with various underlying pathologic conditions
- Define and describe all boldface terms in this chapter
- Describe the physiology of the gastrointestinal system
- Identify anatomic structures on both diagrams and radiographs of the gastrointestinal system
- Differentiate the various pathologic conditions affecting the gastrointestinal system and their radiographic manifestations

As in other body systems, certain pathologic conditions in the gastrointestinal (GI) system require alterations in the technical factors chosen for imaging. In patients with ascites, a common complication of advanced cirrhosis, an increased kilovolt peak (kVp) is required to penetrate the additional fluid content of the abdomen. On the other hand, a decreased kVp is needed in patients with suspected large or small bowel obstruction because of the excessive amount of gas in the abdominal cavity. When using a computed radiography or a direct digital imaging system, the radiographer should still consider the pathology condition in relationship to its attenuation factor.

The radiographer is usually called on to assist the radiologist during fluoroscopic examinations of the GI tract. Indeed, it is generally the radiographer's task to coerce the patient into drinking (and not vomiting) the rather unpleasant-tasting contrast material and to urge the patient to turn around several times to provide adequate mucosal coating for the double-contrast upper GI series. Similarly, the radiographer may have to persuade the patient to retain barium and air during the often uncomfortable barium enema examinations. It is frequently time well spent for the radiographer to explain fully to the patient both the mechanics of the procedure and the extreme importance of patient cooperation.

RADIOGRAPHER NOTES

Plain abdominal radiographs and contrast studies of the digestive tract remain the most common imaging examinations of the gastrointestinal system. Ultrasound and computed tomography (CT) are the major imaging modalities for the pancreas and biliary tract, and magnetic resonance imaging (MRI) is now being used in some institutions to screen for hepatic metastases.

Plain abdominal radiographs must illustrate an appropriate scale of contrast to demonstrate the many different tissue densities in the abdominal cavity. When using a screen–film combination, this goal requires the use of a middle to high kVp range (70 to 80 kVp). The use of digital imaging does allow for a slight increase in the kVp range as the contrast is controlled by the digital processing parameters. Bony structures, such as the lumbar spine and its transverse processes, must be well demonstrated along with soft tissue shadows of the liver, kidney, and psoas muscle. For barium studies of the gastrointestinal tract, adequate penetration of the dense barium solution requires a high kVp range (~120 kVp). For double-contrast (air–barium) studies, a kVp range of 90 to 100 kVp is needed to allow penetration of the barium combined with excellent visualization of mucosal detail. Gallbladder studies require a shorter scale of contrast than other abdominal examinations and therefore are usually performed with a kVp in the low to middle range (~70 kVp). Computed radiography and direct imaging systems utilize the computer algorithm to control the image contrast, so the use of slightly higher kVp ranges (~10 kVp higher) to produce the same images as obtained on screen–film systems aids in reducing the patient radiation dose. The radiographer must select the proper algorithm (combination of procedure and position) to obtain an image with the proper contrast and density.

PHYSIOLOGY OF THE DIGESTIVE SYSTEM

The basic function of the digestive system is to alter the chemical and physical composition of food so that it can be absorbed and used by body cells. This process depends on secretions of the endocrine and exocrine glands and on the controlled movement of ingested food through the tract so that absorption can occur (Figure 5-1).

Digestion begins in the mouth with chewing (**mastication**), the mechanical breakdown of food. The secretion of saliva moistens the food in preparation for swallowing. Swallowing (**deglutition**) is a complex process that requires coordination of many muscles in the head and neck and the precise opening and closing of esophageal sphincters. Digestion continues in the stomach with the churning movement of gastric contents that have become mixed with hydrochloric acid and the proteolytic enzyme pepsin (Figure 5-2). The resulting milky white **chyme** is propelled through the pyloric sphincter into the duodenum by rhythmic smooth muscle contractions called **peristalsis**.

The greatest amount of digestion occurs in the duodenum, the first part of the small bowel. In addition to intestinal secretions containing mucus and enzymes, secretions of the pancreas and liver enhance digestion in this region. The pancreas secretes enzymes for the digestion of proteins (trypsin and chymotrypsin), fat (lipase), and carbohydrates (amylase). It also secretes an alkaline solution to neutralize the acid carried into the small intestine from the stomach. Bile is secreted by the liver, stored in the gallbladder, and enters the duodenum through the common bile duct. Bile is an **emulsifier**, a substance that acts like soap by dispersing the fat into very small droplets that permit it to mix with water.

When digestion is complete, the nutrients are absorbed through the intestinal mucosa into blood capillaries and lymph vessels of the wall of the small bowel. The inner surface area of the small bowel is increased by the formation of numerous finger-like projections (**villi**), which provide the largest amount of surface area possible for digestion and absorption.

Material that has not been digested passes into the colon, where water and minerals are absorbed, and the remaining matter is excreted as feces (Figure 5-3). If the contents of the lower colon and rectum move at a rate that is slower than normal, extra water is absorbed from the fecal mass to produce a hardened stool and **constipation**. **Diarrhea** results from increased motility of the small bowel, which floods the colon with an excessive amount of water that cannot be completely absorbed.

The vermiform (worm-shaped) appendix arises from the inferomedial aspect of the cecum approximately 3 cm below the ileocecal valve. Although the appendix has no functional importance in digestion, it is often classified as an accessory digestive organ merely because of its location.

The liver is the largest gland in the body and is responsible for several vital functions. Liver cells detoxify (make harmless) a variety of poisonous substances that enter the blood from the intestines. Toxic chemicals that are changed to nontoxic compounds in the liver include ammonia (converted to urea and excreted by the kidneys), alcohol, and barbiturates.

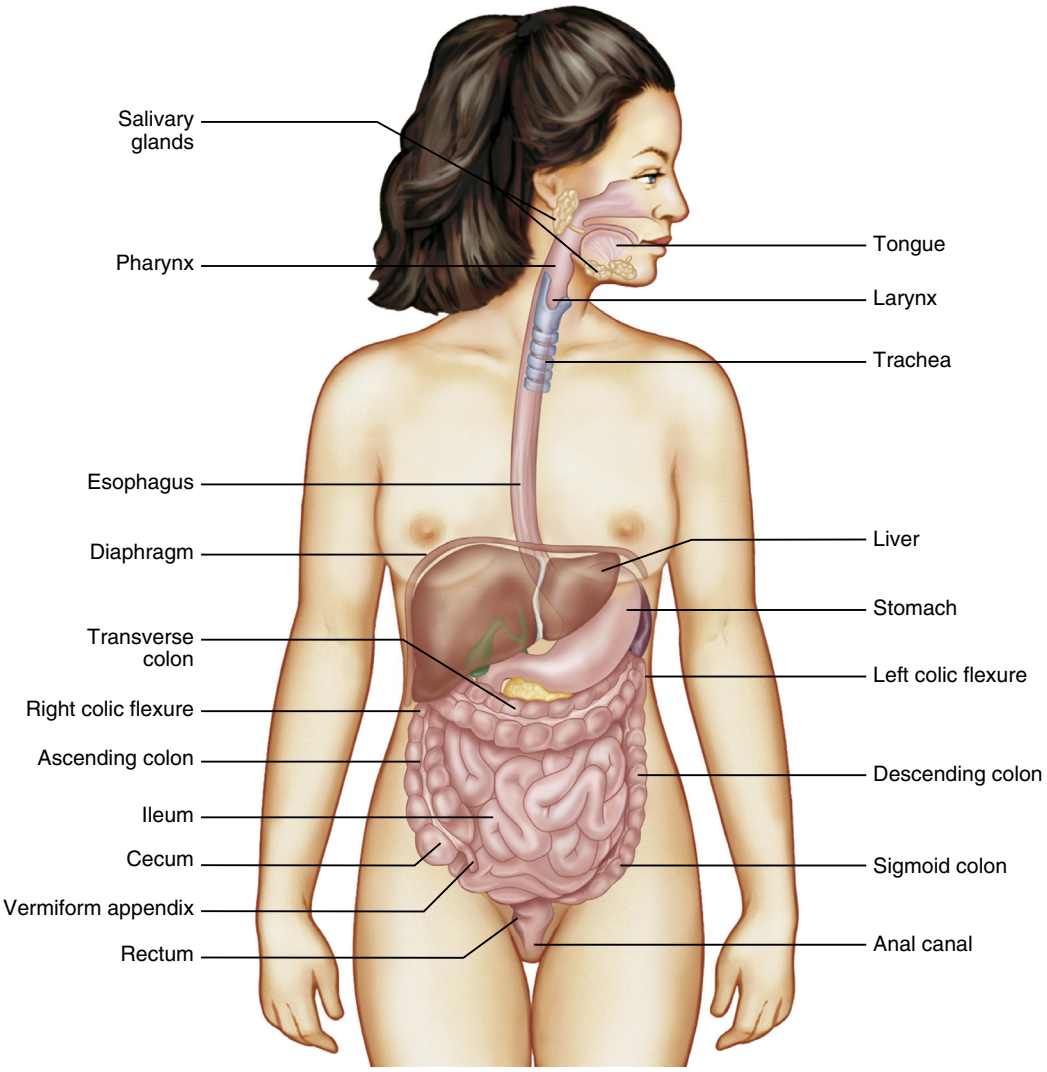

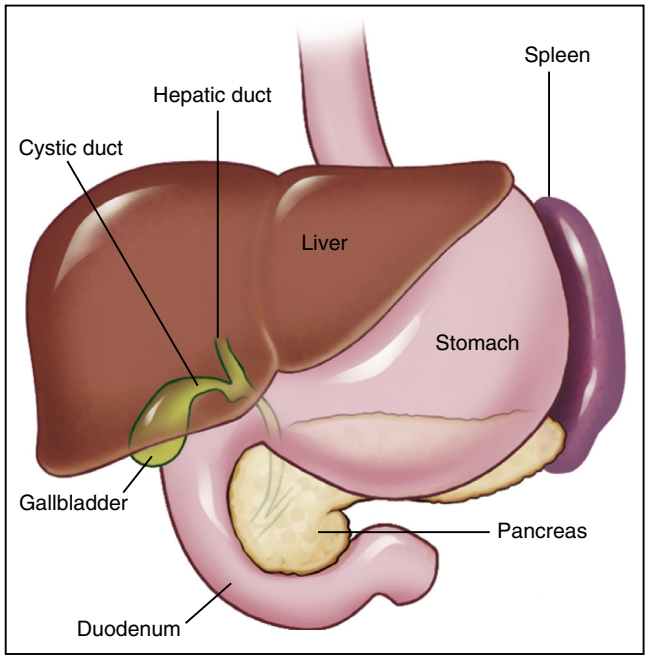

FIGURE 5-1 Location of the digestive organs.

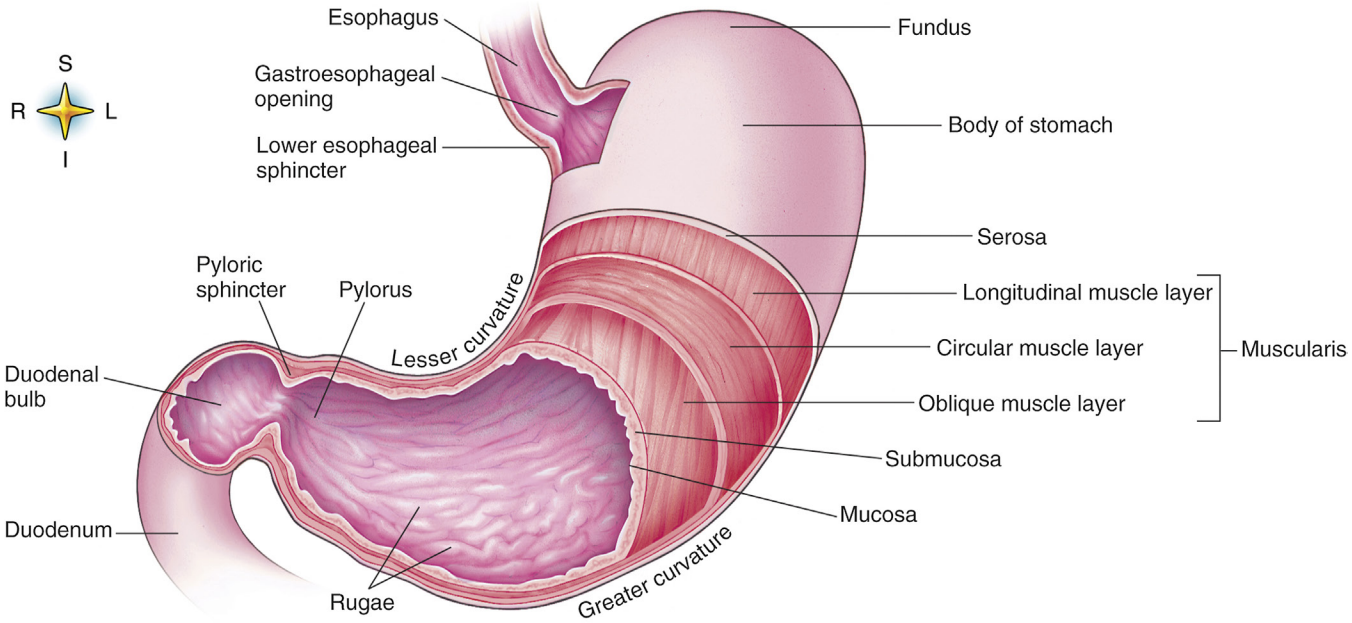

FIGURE 5-2 Stomach.

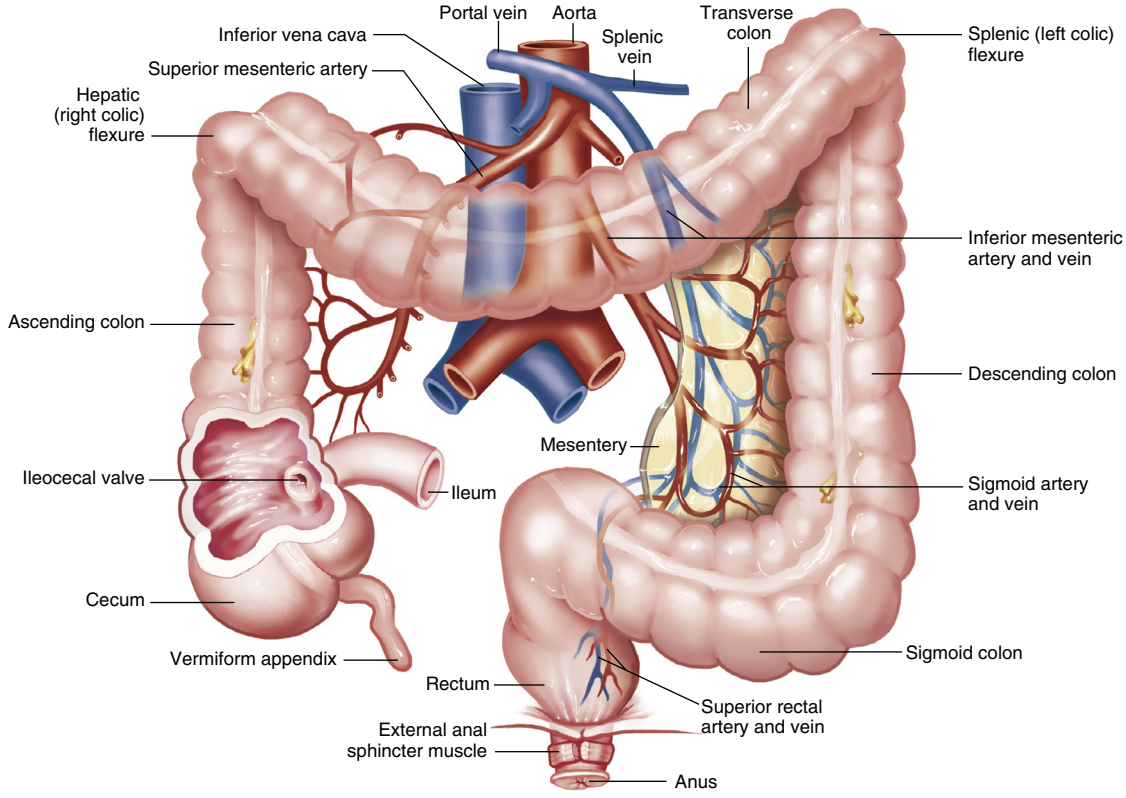

FIGURE 5-3 Divisions of the large intestine.

Liver cells secrete approximately 1 pint of bile each day. As mentioned previously, bile is an emulsifier; it is essential for the digestion and absorption of dietary fat and the fat-soluble vitamins A, D, E, and K. Bile is a greenish liquid consisting of water, bile salts, cholesterol, and bilirubin (a breakdown product of hemoglobin).

Liver cells play a vital role in the metabolism of proteins, fats, and carbohydrates. The liver is the major site of synthesis of the enzymes necessary for various cellular activities throughout the body. Liver cells also synthesize blood proteins such as albumin, which maintains the correct amount of fluid within blood vessels, and the essential proteins required

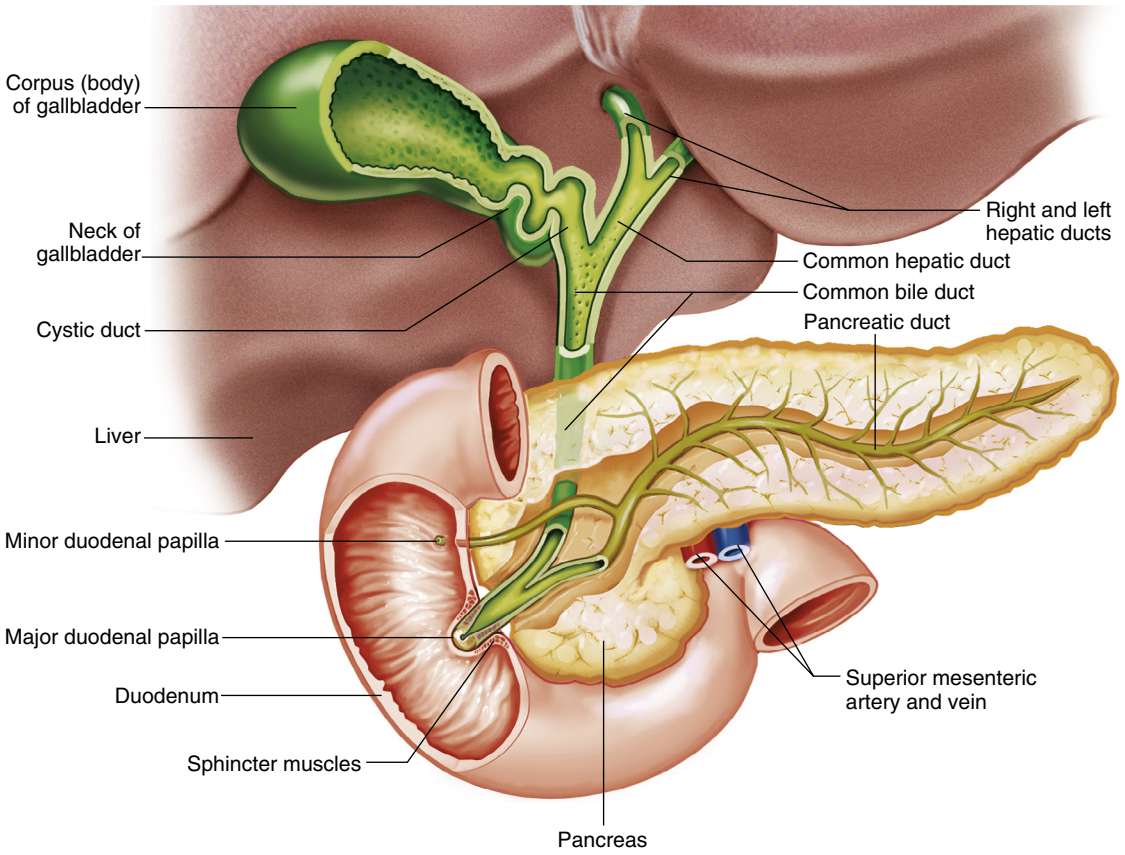

FIGURE 5-4 Ducts that carry bile from the liver and gallbladder.

for blood clotting (fibrinogen and prothrombin). Therefore, liver damage may result in edema (excess water in the soft tissues) and a serious bleeding tendency. The liver plays an important role in maintaining the proper level of glucose in the blood by taking up excess glucose absorbed by the small intestine and storing it as **glycogen**. When the level of circulating glucose falls below normal, the liver breaks down glycogen and releases glucose into the bloodstream. Liver cells also store iron and vitamins A, B_{12}, and D.

The gallbladder is a pear-shaped sac that lies on the undersurface of the liver (Figure 5-4). Its function is to store bile that enters by way of the hepatic and cystic ducts and to concentrate the bile by absorbing water. In response to the presence of dietary fat in the small bowel, the gallbladder contracts and ejects the concentrated bile into the duodenum.

The pancreas controls the level of circulating blood glucose by secreting insulin and glucagon in the islets of Langerhans. An increased concentration of glucose in the blood stimulates the beta cells to increase secretion of insulin, which decreases the blood glucose level probably by accelerating the transport of glucose into cells. A blood glucose concentration less than normal triggers the alpha cells to secrete glucagon, which accelerates the breakdown of glycogen into glucose by the liver.

As discussed previously, pancreatic secretions are vital for digestion. Pancreatic enzymes that pass through the pancreatic duct into the duodenum are necessary for the breakdown of proteins, carbohydrates, and fats.

ESOPHAGUS

Tracheoesophageal Fistula

Congenital Type

Congenital tracheoesophageal (TE) fistulas result from the failure of a satisfactory esophageal lumen to develop completely separate from the trachea. The lack of the development of the esophageal lumen resulting in a blind pouch describes congenital esophageal atresia. Esophageal atresia and TE fistulas are often associated with other congenital malformations involving the skeleton, cardiovascular system, and GI tract.

Imaging appearance. In the second most common type of esophageal anomaly, type I, both upper and lower segments of the esophagus are blind pouches. This anomaly can be differentiated from the type III lesion (the most common type) only by plain abdominal radiographs, which demonstrate the absence of air below the diaphragm in the type I lesion and the presence of air below the stomach in the type III lesion.

In the type II form of TE fistula, the upper esophageal segment communicates with the trachea, whereas the lower segment ends in a blind pouch. Because there is no connection between the trachea and the stomach, there is no radiographic evidence of gas within the abdomen. Oral administration of contrast material in this condition immediately outlines the tracheobronchial tree.

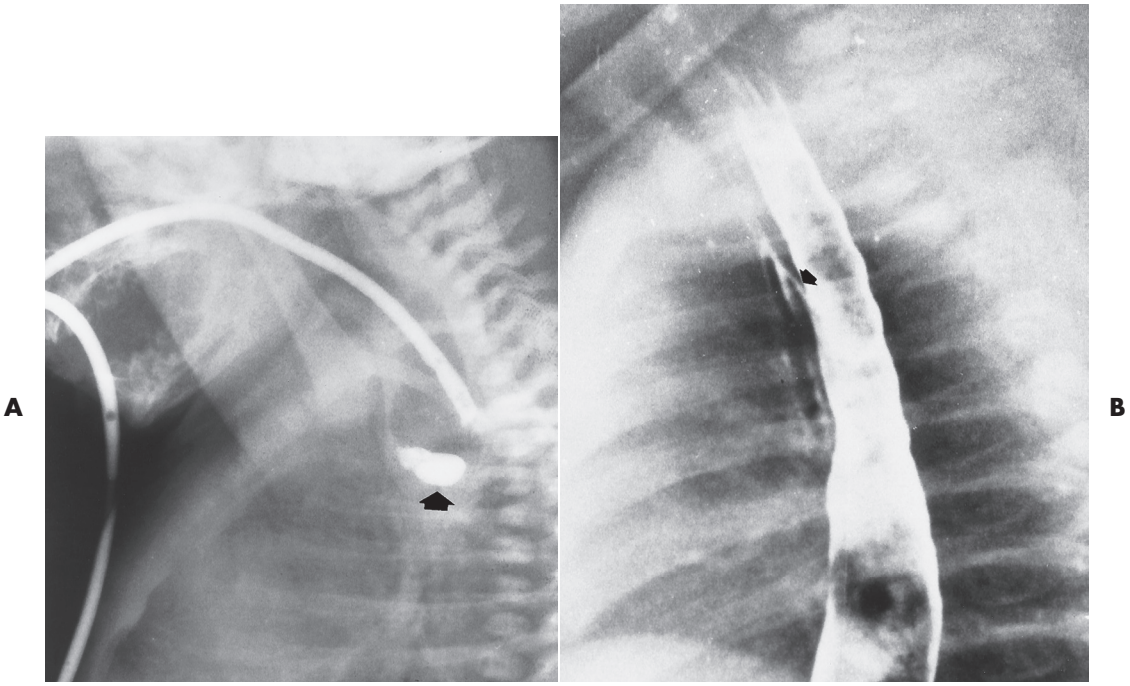

FIGURE 5-5 Congenital tracheoesophageal fistula. **(A)** Type III fistula (*arrow*), in which contrast material (injected through a feeding tube) demonstrates occlusion of proximal esophageal pouch. **(B)** Type IV, or H, fistula (*arrow*).

The type III TE fistula (seen in 85% to 90% of cases) consists of an upper segment that ends in a blind pouch at the level of the bifurcation of the trachea or slightly above it, and a lower segment attached to the trachea by a short fistulous tract. Radiographic demonstration of the looping of a small esophageal feeding tube indicates that the proximal esophagus ends in a blind pouch (Figure 5-5A). Plain radiographs of the abdomen demonstrate the presence of air in the bowel that has freely entered the stomach through the fistulous connection between the trachea and the distal esophagus.

There are two forms of type IV TE fistula. In one, the upper and lower esophageal segments end in blind pouches, both of which are connected to the tracheobronchial tree. In this form, gas is seen in the stomach, and oral contrast material outlines both fistulas and the bronchial tree. In the other form of type IV TE fistula (called an H fistula), both the trachea and the esophagus are intact. These two structures are connected by a single fistulous tract that can be found at any level from the cricoid cartilage of the trachea to the tracheal bifurcation (Figure 5-5B). Unlike the other forms of TE fistula, the H fistula may not be identified in infancy and, if it is small and only occasionally causes emptying of material into the lungs, can permit survival into adulthood.

Computed tomography (CT) esophagography without use of a contrast agent that is performed using a multidetector CT scanner with three-dimensional reconstructions demonstrates TE fistulas. CT is less invasive than contrast radiography and provides clinicians with critical surgical planning information.

Treatment. Immediate surgical repair keeps the infant from dying of starvation. If a fistula exists, delayed surgical repair may result in aspiration pneumonia.

Acquired Type

Approximately 50% of acquired fistulas between the trachea and esophagus are caused by malignancy in the mediastinum. Almost all the rest result from infectious processes or trauma.

Fistulization between the esophagus and the respiratory tract is a major late complication of esophageal carcinoma and is often a terminal event (Figure 5-6). A fistula can also be a complication of erosion into the esophagus either by carcinoma of the lung arising near or metastasizing to the middle mediastinum or by mediastinal metastases from other primary sites. Regardless of therapy, the overall prognosis of malignant TE fistulas is dismal, and more than 80% of patients with this complication die within 3 months from uncontrollable hemorrhage or from pulmonary infection caused by repeated episodes of aspiration pneumonia.

Fistulous communications between the esophagus and the tracheobronchial tree can be the result of esophageal instrumentation and perforation (Figure 5-7). It is most common after esophagoscopy but may also occur after instrumental dilation of strictures by bougienage, pneumatic dilation of the esophagus for the treatment of achalasia, or even the insertion of a nasogastric tube. Blunt or penetrating trauma to the chest, especially after crush injury, can result in esophageal perforation and fistulization.

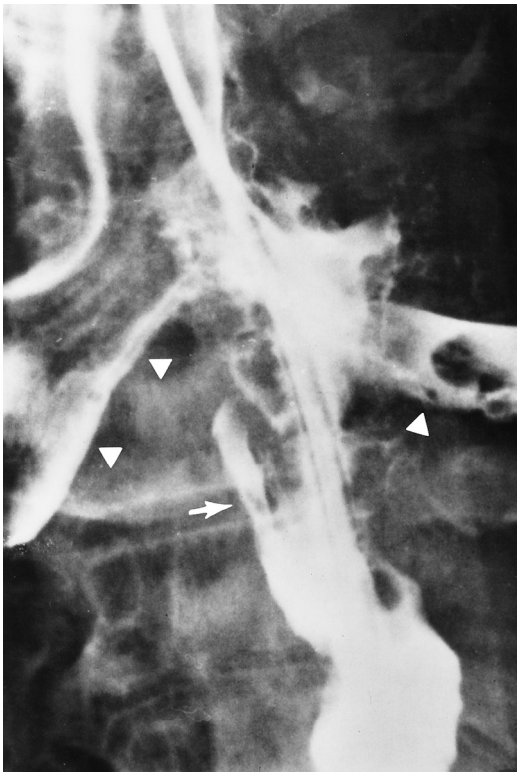

FIGURE 5-6 Esophagorespiratory fistula. Communication between esophagus (*arrow*) and bronchial tree (*arrowheads*), seen as complication of esophageal carcinoma.

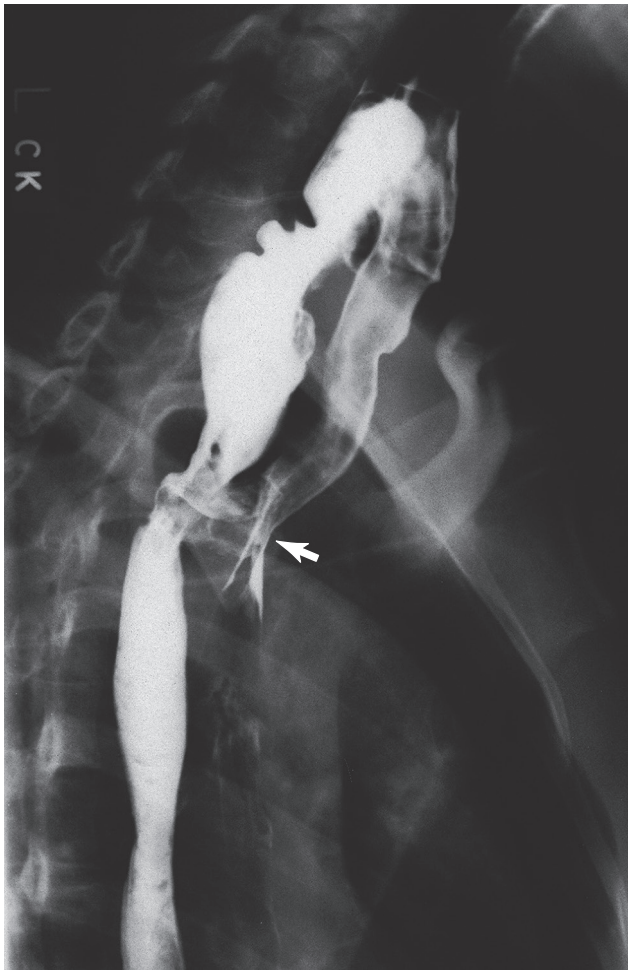

FIGURE 5-7 Acquired tracheoesophageal fistula. A 23-year-old female aspirated her dentures, causing an erosion through the esophagus. The esophagram demonstrates the fistula (*arrow*) between the esophagus and trachea.

Types of Findings for Tracheoesophageal (TE) Fistula

Congenital TE fistula	Type I—second most common	Pure esophageal atresia—upper and lower esophagus blind pouches
	Type II	Upper esophagus communicates with trachea; lower segment blind pouch
	Type III—most common	Upper esophagus forms blind pouch (esophageal atresia) with a distal esophagus communicating with the trachea
	Type IV—third most common	(1) Upper and lower esophageal segments blind pouches with both connected to the bronchial tree (2) H fistula is a connection at the midesophagus and trachea
Acquired TE fistula	Fistula caused by:	(1) Mediastinal malignancy (2) Infection process (3) Trauma

Imaging appearance. After traumatic perforation of the thoracic esophagus, chest radiographs may demonstrate air dissecting within the mediastinum and soft tissue, often with pleural effusion or hydropneumothorax. The introduction of an oral contrast agent may demonstrate the site of perforation and the extent of fistulization.

Treatment. For patients with unresectable metastases or esophageal malignancies, using an interventional technique to place a stent to maintain the lumen may be the best palliative treatment available. Surgery may be performed if the benefit outweighs the risk.

Esophagitis

Reflux (Gastroesophageal Reflux Disease)

Although the reflux of gastric acid contents is the most common cause of acute esophagitis, infectious and granulomatous disorders, physical injury (caustic agents and radiation injury), and medication may produce a similar inflammatory response. *Gastroesophageal reflux disease* (GERD) describes any symptomatic condition or structural changes caused by reflux of the stomach contents into the esophagus. Alcohol,

chocolate, caffeine, and fatty foods tend to decrease the pressure of the esophageal sphincter, allowing reflux to occur. Regardless of the cause, acute esophagitis produces burning chest pain that may simulate the pain of heart disease. Superficial ulcerations are most typical of reflux. The esophagus is often dilated, with a loss of effective peristalsis. Nonpropulsive peristaltic waves, ranging from mild tertiary contractions to severe segmental spasms, are an early finding.

Reflux esophagitis develops when the lower esophageal sphincter fails to act as an effective barrier to the entry of gastric acid contents into the distal esophagus. Although there is a higher-than-normal likelihood of gastroesophageal reflux in patients with sliding hiatal hernias, reflux esophagitis can be endoscopically demonstrated in only approximately one fourth of these patients. On the other hand, esophagitis is often encountered in patients in whom no hiatal hernia can be demonstrated.

Several radiographic approaches have been suggested for the demonstration of gastroesophageal reflux. One procedure is to increase intra-abdominal pressure by straight-leg raising or manual pressure on the abdomen, often with Valsalva maneuver (forced expiration with the glottis closed). Having the patient turn from prone to supine or vice versa may demonstrate reflux of barium from the stomach into the esophagus. It must be remembered, however, that the failure to demonstrate reflux radiographically does not exclude the possibility that a patient's esophagitis is related to reflux. As long as typical radiographic findings of reflux esophagitis are noted, there is little reason to persist in strenuous efforts to actually demonstrate retrograde flow of barium from the stomach into the esophagus.

Imaging appearance. The earliest radiographic findings in reflux esophagitis are detectable on double-contrast studies. They consist of superficial ulcerations or erosions that appear as streaks or dots of barium superimposed on the flat mucosa of the distal esophagus. In single-contrast studies of patients with esophagitis, the outer borders of the barium-filled esophagus are not sharply seen but, rather, have a hazy, serrated appearance with shallow, irregular protrusions indicating erosions of varying length and depth. Widening and coarsening of edematous longitudinal folds can simulate filling defects. In addition to diffuse erosion, reflux esophagitis can result in large, discrete, penetrating ulcers in the distal esophagus (Figure 5-8) or in a hiatal hernia sac (Figure 5-9). Fibrotic healing of diffuse reflux esophagitis or a localized penetrating ulcer may cause narrowing of the distal esophagus. Strictures resulting from reflux esophagitis tend to be smooth and tapering with no demonstrable mucosal pattern (Figure 5-10).

FIGURE 5-8 Penetrating ulcer. Large ulcer (*arrow*) in reflux esophagitis.

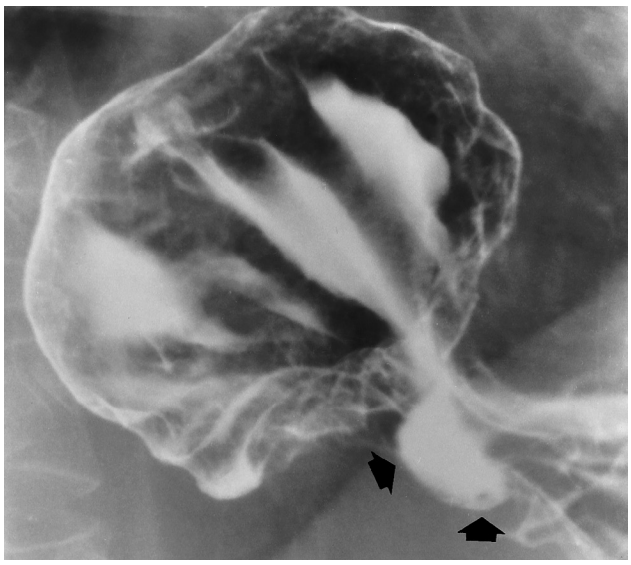

FIGURE 5-9 Ulcer. Large hiatal hernia sac with an ulcer (*arrows*).

Barrett's Esophagus

Barrett's esophagus is a condition related to severe reflux esophagitis in which the normal squamous lining of the lower esophagus is destroyed and replaced by columnar epithelium similar to that of the stomach. Ulceration in Barrett's esophagus typically occurs at the squamocolumnar junction (Z-line). In addition to exhibiting postinflammatory stricture, Barrett's esophagus has an unusually high propensity for development of malignancy in the columnar cell–lined portion. These tumors are almost always adenocarcinomas, which are otherwise very rare in the esophagus (accounting for approximately 5% of esophageal cancers).

Imaging appearance. Although a hiatal hernia with gastroesophageal reflux is commonly demonstrated, Barrett's ulcer is usually separated from the hiatal hernia by a variable length of normal-appearing esophagus (Figure 5-11), in contrast to reflux esophagitis, in which the distal esophagus is abnormal down to the level of the hernia. As in reflux esophagitis, fibrotic healing of the ulceration in Barrett's esophagus often leads to a smooth, tapered stricture (Figure 5-12).

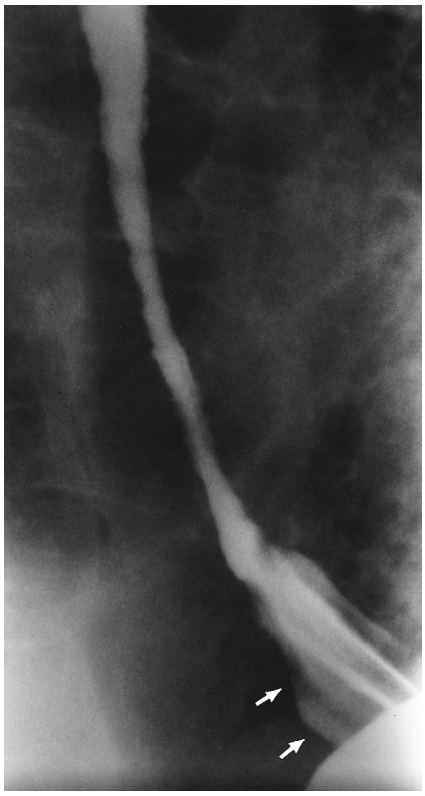

FIGURE 5-10 Long esophageal stricture caused by reflux esophagitis. Note the associated hiatal hernia (*arrows*).

Because the distal esophagus consists of a gastric type of mucosa in Barrett's esophagus, it actively takes up the intravenously injected radionuclide pertechnetate. The demonstration of a continuous concentration of the isotope from the stomach into the distal esophagus to a level that corresponds approximately to that of the ulcer or stricture is indicative of Barrett's esophagus.

Candida and Herpesvirus

Candida (fungal) and herpesvirus are the organisms most often responsible for infectious esophagitis, which usually occurs in patients with widespread malignancy who are receiving radiation therapy, chemotherapy, corticosteroids, or other immunosuppressive agents. It also can develop in patients with acquired immunodeficiency syndrome (AIDS) and even in otherwise healthy adults who have received antibiotics (especially tetracycline) for upper respiratory infection.

Imaging appearance. The classic radiographic appearance of infectious esophagitis is an irregular cobblestone pattern with a shaggy marginal contour of the esophagus caused by deep ulcerations and sloughing of the mucosa (Figure 5-13). *Candida* infection manifests as plaques and nodules resulting from a superficial collection of fungi. Characteristics of herpetic esophagitis include small mucosal ulcers or plaques.

Treatment for esophagitis. Modifications to lifestyle, including weight loss, changes in diet to prevent decreased esophageal sphincter control, and medications to reduce acidity, are the first line of treatment. One technique, called proton pump inhibitor therapy (using esomeprazole), can help control progression in reflux disease and Barrett's esophagus. Other techniques used are photodynamic therapy and thermal ablation to destroy the Barrett's tissue. If these therapies do not work, surgical fundoplication (tucks in the stomach fundus and distal esophagus) is an option. Infectious esophagitis caused by *Candida* or herpesvirus may require a regimen of antifungal or antiviral drugs to eradicate the cause.

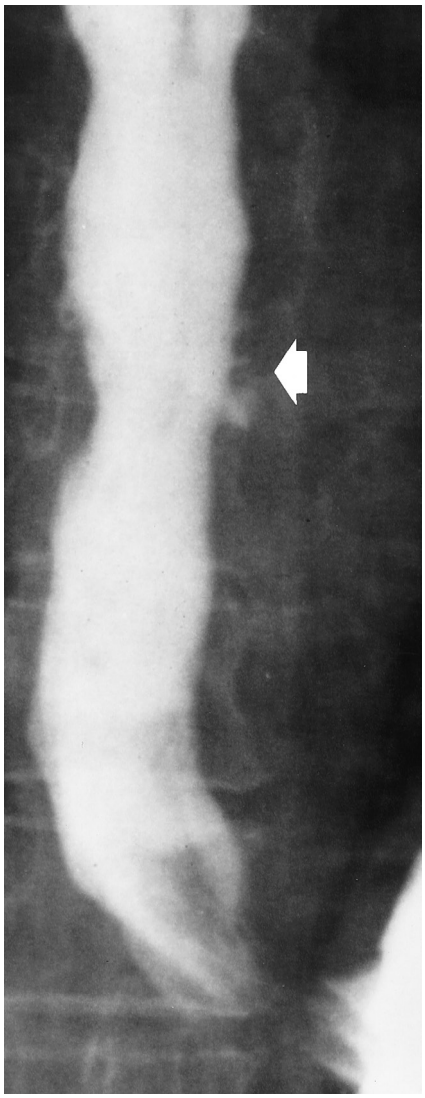

FIGURE 5-11 Barrett's esophagus. Ulcerations (*arrow*) have developed at a distance from esophagogastric junction.

Ingestion of Corrosive Agents

The ingestion of alkaline or acidic corrosive agents produces acute inflammatory changes in the esophagus. Superficial penetration of the toxic agent results in only minimal ulceration. Deeper penetration of the submucosa and muscular layers causes sloughing of destroyed tissue and deep ulceration. Ingestion of strong alkaline agents causes deeper lesions than ingestion of strong acids, and only half of those who ingest an acid suffer severe injury. Drug-induced esophagitis may occur in patients who have delayed esophageal transit time, which permits prolonged mucosal contact with the ingested substance. The most common drug causing esophageal ulceration

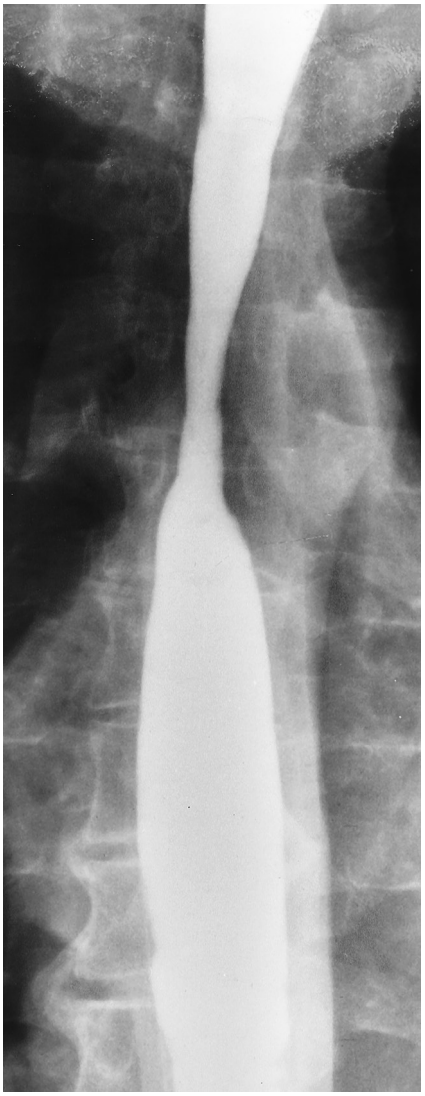

FIGURE 5-12 Barrett's esophagus. Note the smooth, tapered stricture in the upper thoracic esophagus.

is potassium chloride in tablet form. Other medications that can cause esophagitis are weak caustic agents that are harmless when they pass rapidly through the esophagus.

Imaging appearance. Healing of the intense mucosal and intramural inflammation of acute esophagitis may lead to pronounced fibrosis and stricture formation. These benign strictures tend to be long lesions with tapered margins and relatively smooth mucosal surfaces (Figure 5-14), in contrast to the irregular narrowing, mucosal destruction, and overhanging margins that are generally associated with malignant processes.

Treatment. The type of agent ingested determines the therapy. The local or state poison control service is usually called for specific treatments if the situation is not drug induced. Vomiting is generally not induced because this would cause a second exposure of the esophagus to the agent. Dilution by administration of milk or water is appropriate unless the corrosive agent is acidic (in this case, water should not be used because it would produce excessive heat).

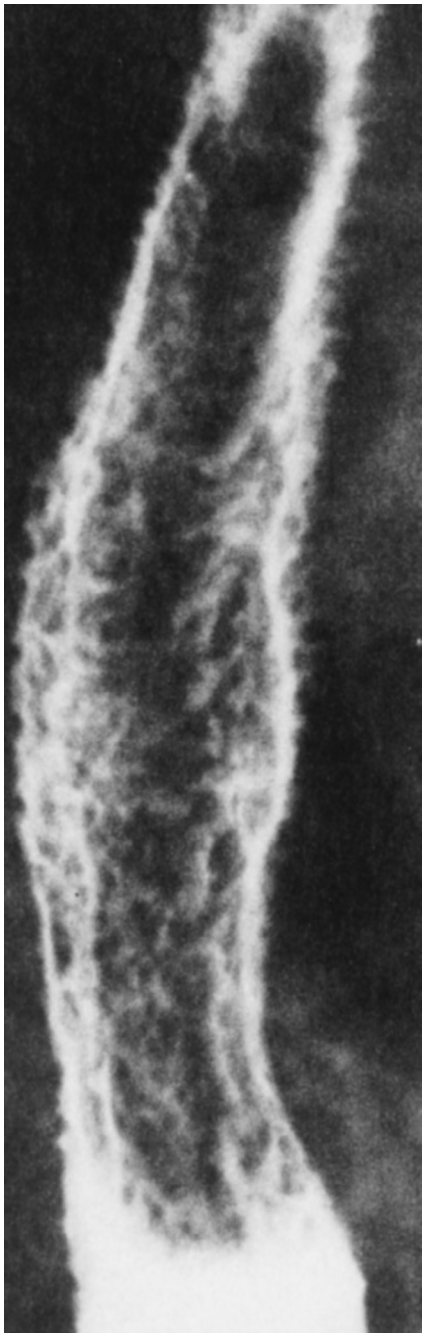

FIGURE 5-13 *Candida* esophagitis. Multiple ulcers and nodular plaques produce the grossly irregular contour of shaggy esophagus. This manifestation of far-advanced candidiasis has become infrequent because of earlier and better treatment of the disease.

Esophageal Cancer

Progressive difficulty in swallowing (dysphagia) in a person older than 40 years must be assumed to be caused by cancer until demonstrated otherwise. Because the symptoms of esophageal carcinoma tend to appear late in the course of the disease, and because the lack of a limiting outer layer (serosa) commonly permits direct extension of the tumor by the time of the initial diagnosis, carcinoma of the esophagus has a dismal prognosis. Most carcinomas of the esophagus are of the squamous cell

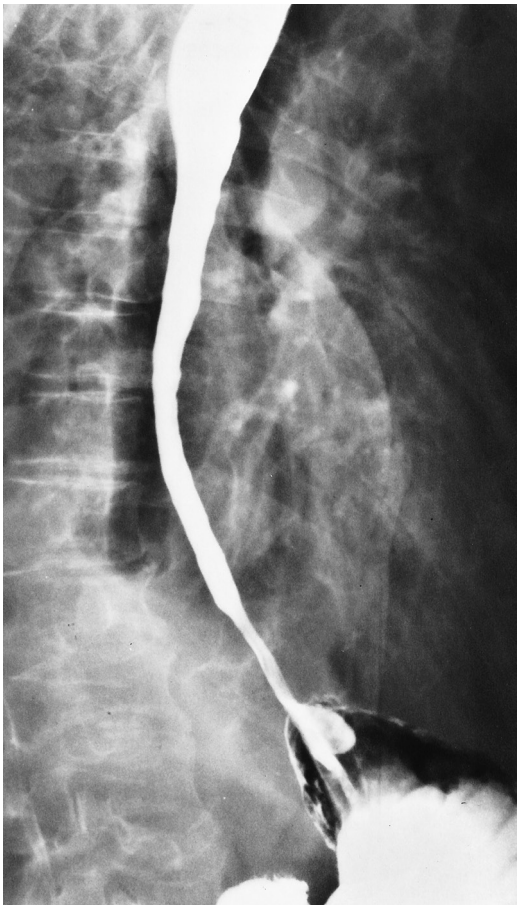

FIGURE 5-14 Corrosive stricture. Caused by the ingestion of lye.

type, and they occur most often at the esophagogastric junction. The incidence of carcinoma of the esophagus is far higher in men than in women. There is a strong correlation between excessive alcohol intake, smoking, and esophageal carcinoma.

Imaging appearance. The earliest radiographic evidence of infiltrating carcinoma of the esophagus appears on a double-contrast barium swallow image as a flat, plaquelike lesion, occasionally with central **ulceration**, that involves one wall of the esophagus (Figure 5-15). At this stage, there may be minimal reduction in the caliber of the lumen. Unless the patient is carefully examined in various positions, this earliest form of esophageal carcinoma can be missed. As the **infiltrating** cancer progresses, irregularity of the wall is seen, indicating mucosal destruction. Advanced lesions encircle the lumen completely, causing annular constrictions with overhanging margins and often some degree of obstruction. The lumen through the stenotic area is irregular, and mucosal folds are absent or severely ulcerated (Figure 5-16). Less commonly, carcinoma of the esophagus can appear as a localized **polypoid** mass, often with deep ulceration and a fungating appearance.

Luminal obstruction as a result of carcinoma causes proximal dilation of the esophagus and may result in aspiration pneumonia. Extension of the tumor to adjacent mediastinal structures may lead to fistula formation, especially between the esophagus and the respiratory tract (see Figure 5-20).

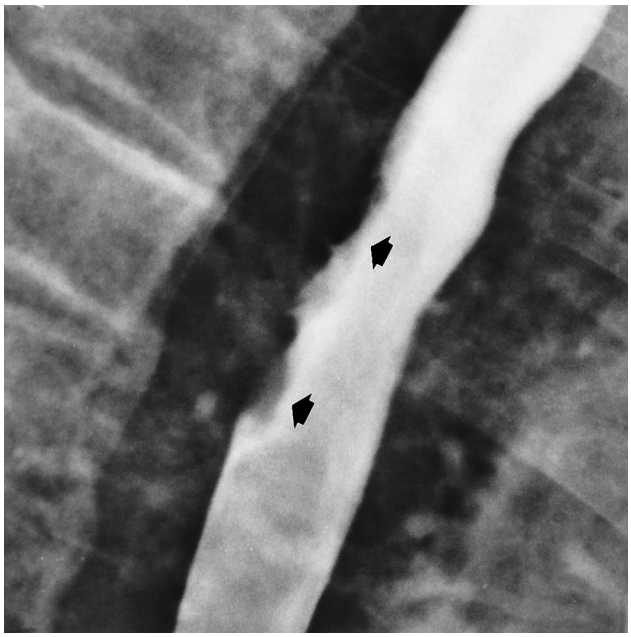

FIGURE 5-15 Early carcinoma of the esophagus. Flat, plaquelike lesion (*arrows*) involves the posterior wall of the esophagus.

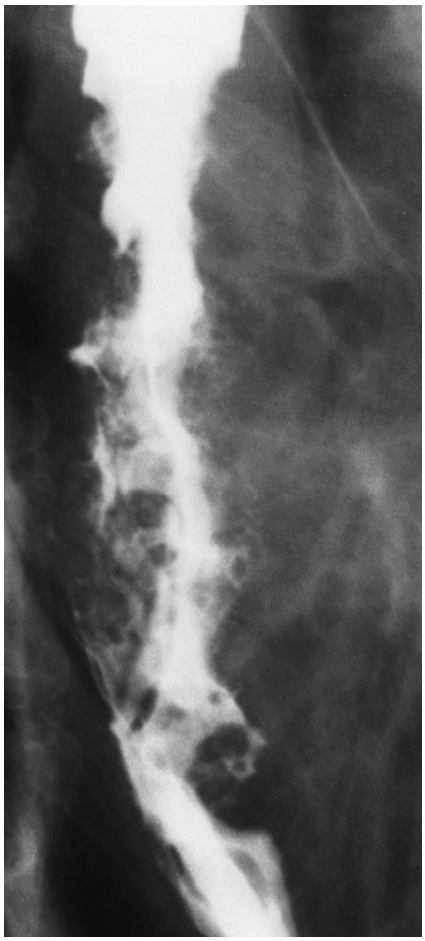

FIGURE 5-16 Carcinoma of the esophagus. Irregular narrowing with ulceration involves an extensive segment of the thoracic portion of the esophagus.

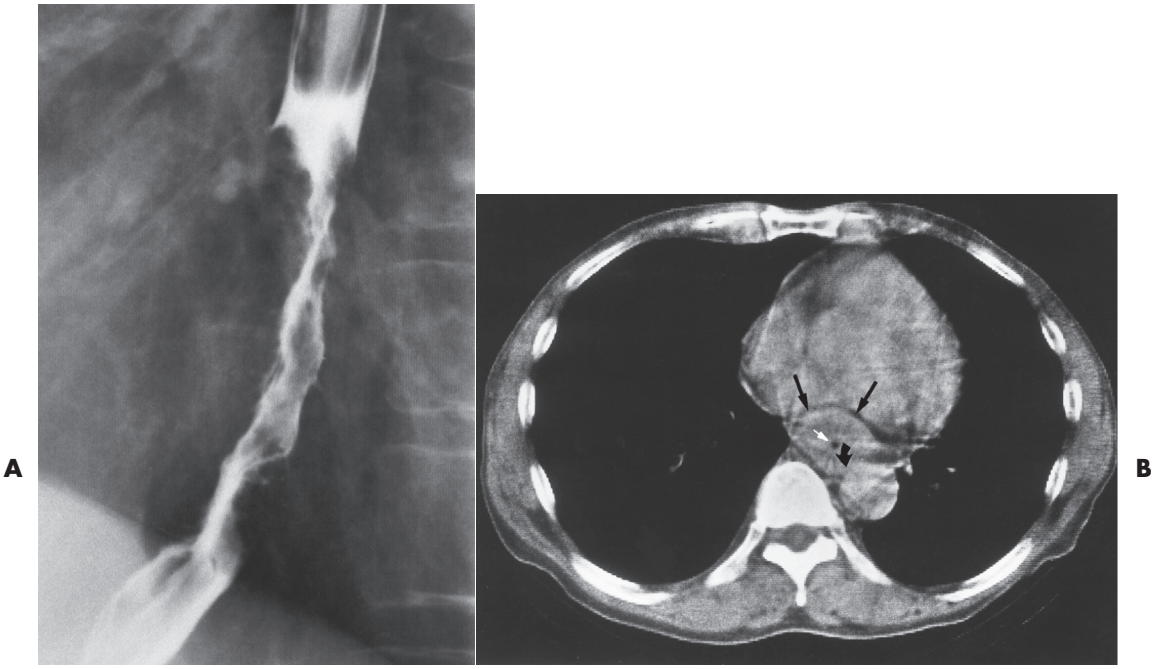

FIGURE 5-17 CT staging of esophageal carcinoma. (A) Esophagram demonstrates infiltrating lesion causing irregular narrowing of the distal part of the esophagus. (B) CT scan shows a mass of bulky carcinoma (*black arrows*) filling most of the lumen (*white arrow*). Obliteration of the fat plane adjacent to the aorta (*curved arrow*) indicates mediastinal invasion.

Wall thickening greater than 3 to 5 mm on a CT scan is suggestive of esophageal cancer. CT has become a major method of staging patients with esophageal carcinoma (with 90% accuracy), providing information on tumor size, extension, and resectability that was previously available only at thoracotomy (Figure 5-17). Evidence of tumor spread includes the obliteration of fat planes between the esophagus and adjacent structures (left atrium and aorta), the formation of a fistula to the tracheobronchial tree, and recognition of metastatic disease (e.g., low-density masses in the liver and enlargement of draining lymph nodes). Use of contrast enhancement improves the detail of tumor delineation.

Treatment. If the cancerous lesion has not extended into surrounding tissue, surgical resection may result in cure. When the cancerous lesion involves surrounding tissue, treatment becomes palliative surgery together with radiation therapy or chemotherapy. If the esophagus is severely narrowed, a technique known as *bougienage* can be employed; this is the introduction of a long instrument to dilate and help maintain an adequate lumen. Laser therapy aids in treating the dysphagia in patients with unresectable lesions. A newer technique, photodynamic therapy using laser-activated chemicals, is a method of destroying tumor tissue. The prognosis of the patient who is diagnosed in the late stages of esophageal cancer is extremely poor.

Esophageal Diverticula

Esophageal diverticula (outpouchings) are common lesions that either contain all layers of the wall (traction or true diverticula) or are composed of only mucosa and submucosa herniating through the muscular layer (pulsion or false diverticula). Small diverticula do not retain food or secretions and are asymptomatic. When a diverticulum fills with food or secretions, aspiration pneumonia may result.

Imaging appearance. **Zenker's diverticula** arise from the posterior wall of the upper (cervical) esophagus (Figure 5-18). Occasionally, they can become so large that they almost occlude the esophageal lumen. CT prominently demonstrates the cricopharyngeal muscle, which aids in locating the origin of Zenker's diverticula at the pharyngoesophageal junction. Diverticula of the thoracic portion of the esophagus are primarily found opposite the bifurcation of the trachea, in the region of the hilum of the lung (Figure 5-19). These **traction** diverticula reflect motor function disturbance and develop in response to the pull of fibrous adhesions after infection of the mediastinal lymph nodes. **Epiphrenic diverticula** arise in the distal 10 cm of the esophagus (Figure 5-20). They are associated with incoordination of esophageal peristalsis and sphincter relaxation, which increases the intraluminal pressure in this segment.

Treatment. Diverticula do not require treatment unless they interfere with swallowing. In Zenker's diverticulum, surgery consists of excision of the diverticulum and correction of any motility issues.

Esophageal Varices

Esophageal varices are dilated veins in the wall of the esophagus that are most commonly the result of increased pressure in the portal venous system (portal hypertension), which is in turn usually a result of cirrhosis of the liver. In patients with portal hypertension, much of the portal blood cannot flow along its normal pathway through the liver to the inferior vena cava and then on to the heart. Instead, it must go by a circuitous collateral route, and increased blood flow through

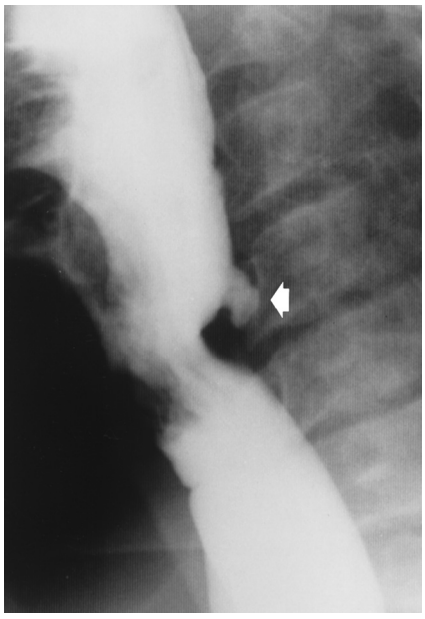

FIGURE 5-18 Small Zenker's diverticulum. Saccular outpouching (*arrow*) arising posteriorly just proximal to an impression produced by the cricopharyngeal muscle.

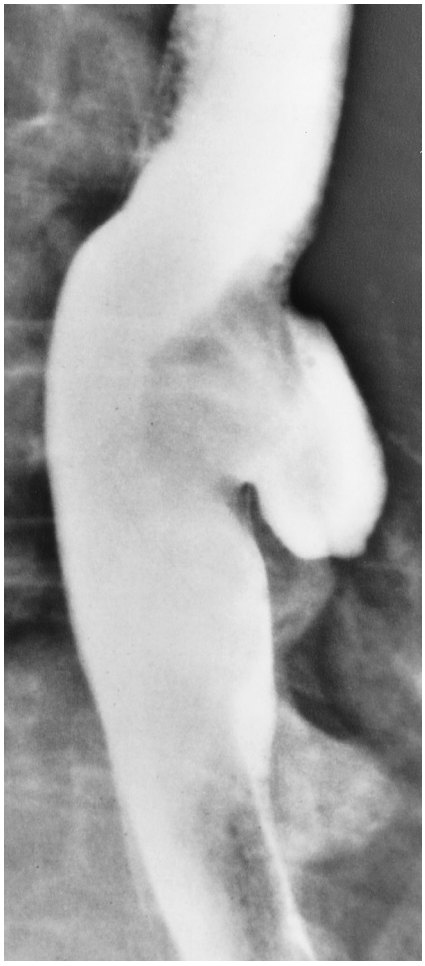

FIGURE 5-19 Traction diverticulum. Diverticulum in the midthoracic portion of the esophagus.

FIGURE 5-20 Epiphrenic diverticulum. Diverticulum in the distal portion of the esophagus near the lower esophageal sphincter.

these dilated veins causes the development of esophageal (and gastric) varices. Esophageal varices are infrequently demonstrated in the absence of portal hypertension. "Downhill" varices are produced when venous blood from the head and neck cannot reach the heart because of an obstruction of the superior vena cava caused by tumors or inflammatory disease in the mediastinum. In this situation, blood flows "downhill" through the esophageal veins before eventually entering the portal vein, through which it flows to the inferior vena cava and the right atrium.

Imaging appearance. The characteristic radiographic appearance of esophageal varices is serpiginous (wavy border) thickening of folds, which appear as round or oval filling defects resembling the beads of a rosary (Figure 5-21). Precise technique is required to demonstrate esophageal varices. A double-contrast barium swallow study best demonstrates the serpiginous and wormlike filling defect. Complete filling of the esophagus with barium may obscure varices, and powerful contractions of the esophagus may squeeze blood out of the varices and make them

FIGURE 5-21 Esophageal varices. Note the diffuse round and oval filling defects, which resemble rosary beads.

impossible to detect. Upright and recumbent imaging may best demonstrate the varices dilated and empty, respectively.

Varices can be demonstrated with endoscopic ultrasound imaging (ultrasonography) as compressible hypoechoic or cystic masses in the GI tract from the outer to the submucosal layers.

The major complication of esophageal varices is bleeding. Their appearance in patients with cirrhotic liver disease implies significant portal venous hypertension and is an ominous sign because up to 90% of the deaths from liver disease in patients with cirrhosis occur within 2 years of the diagnosis of varices.

Treatment. Vasoconstrictor drugs to constrict the dilated vessels are commonly used to treat esophageal varices. Active bleeding can be controlled by a technique called *balloon tamponade*, which creates pressure to stop the bleeding. If bleeding cannot be controlled, surgery is performed to tie off collateral vessels.

Hiatal Hernia

Hiatal hernia is the most common abnormality (occurring in 50% of the population) detected on upper GI examination. Its broad radiographic spectrum ranges from large esophagogastric hernias, in which much of the stomach lies within the thoracic cavity and there is a predisposition to volvulus (twisting), to small hernias that emerge above the diaphragm only in certain circumstances (related to changes in intra-abdominal or intrathoracic pressure) and easily slide back into the abdomen through the hiatus (sliding hiatal hernia). The symptoms associated with hiatal hernia and its complications (esophagitis, esophageal ulcer, and esophageal stenosis) are related to the presence of esophageal reflux rather than to the hiatal hernia itself. Most hiatal hernias do not produce symptoms and are clinically of no importance.

Imaging appearance. Although the diagnosis of hiatal hernia generally requires a barium study (Figure 5-22), at times a large hiatal hernia may appear on plain chest radiograph as a

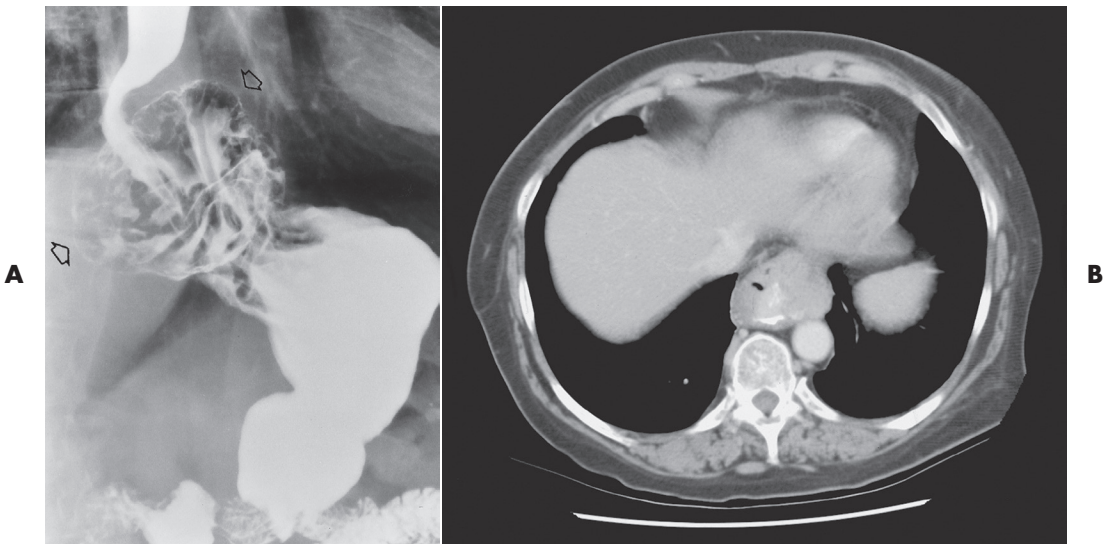

FIGURE 5-22 Large hiatal hernia. **(A)** GI shows a large hiatal hernia (*arrows*). **(B)** This 65-year-old woman had right lower quadrant pain. Hiatal hernia was an incidental finding on CT scanning of the abdomen with oral contrast agent. The stomach was shown to be in the retrocardiac area.

soft tissue mass in the posterior mediastinum, often containing a prominent air–fluid level (Figure 5-23). The esophagus and stomach are distinguished by their appearance; mucosal folds are linear and parallel in the esophagus, whereas in the stomach the folds appear numerous and thicker without a parallel orientation.

Treatment. In most cases, a hiatal hernia requires no treatment. If surgical intervention is necessary, the hiatus is tightened, and the stomach is secured below the diaphragm.

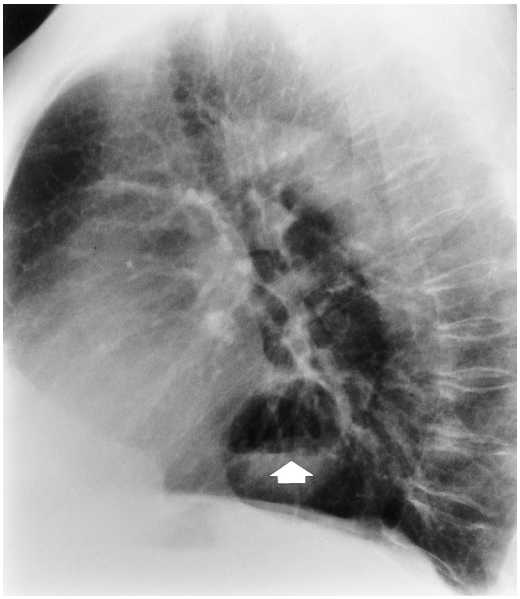

FIGURE 5-23 Hiatal hernia. Prominent air–fluid level (*arrow*) in a hiatal hernia seen on a lateral chest radiograph.

Achalasia

Achalasia is a functional obstruction of the distal section of the esophagus with proximal dilation caused by incomplete relaxation of the lower esophageal sphincter. It is related to a paucity or absence of ganglion cells in the myenteric neural plexuses of the distal esophageal wall.

Imaging appearance. On plain chest radiographs, the dilated, tortuous esophagus may produce a widened mediastinum (often with an air–fluid level) on the right side adjacent to the cardiac shadow (Figure 5-24). The hallmark of achalasia, seen on barium studies, is a gradually tapered, smooth, conical, 1- to 3-cm narrowing of the distal esophageal segment (rat-tail or beak appearance) (Figure 5-25). On sequential radiographs, especially with the patient upright, only small spurts of barium are seen to pass through the narrowed distal segment to enter the stomach.

Treatment. Medications are given before meals to assist in relaxing the esophageal sphincter. If these do not control the symptoms, endoscopic balloon dilation with a bougienage may be helpful. A last resort is surgery (Heller's myotomy) to open the sphincter.

Foreign Bodies

A wide spectrum of foreign bodies can become impacted in the esophagus, usually in the cervical esophagus at or just above the level of the thoracic inlet (Figure 5-26). Symptomatically, the patient is unable to swallow without regurgitation. Most metallic objects, such as pins, coins, and small toys, are radiopaque and are easily visualized on radiographs or during fluoroscopy. Objects made of aluminum and some light alloys may be impossible to detect

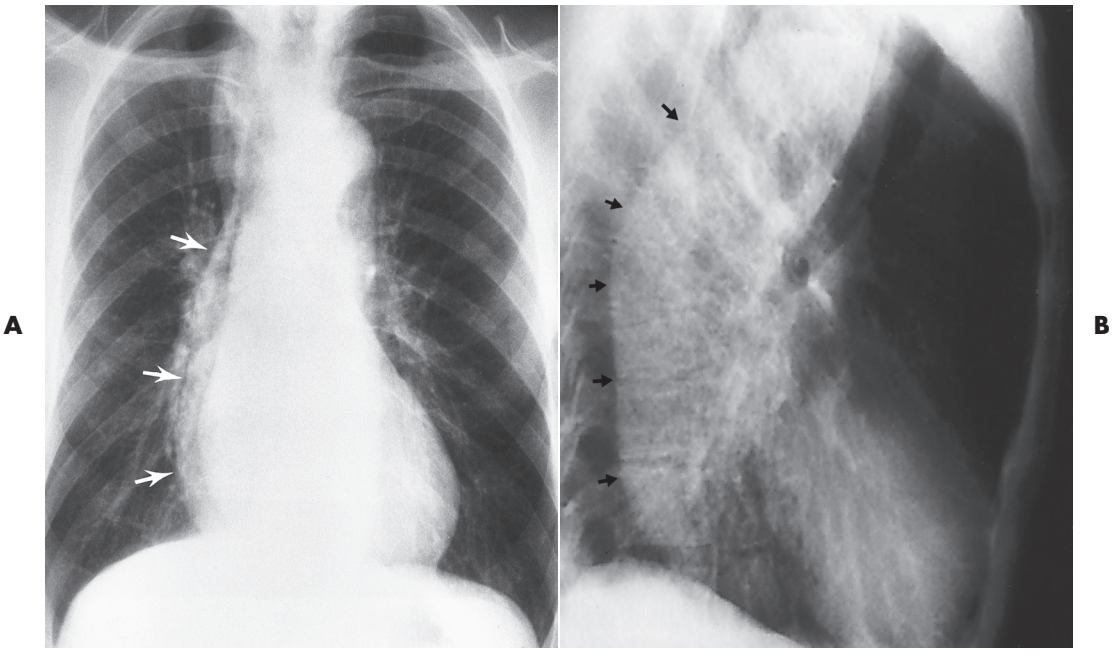

FIGURE 5-24 Achalasia. **(A)** Frontal chest radiograph demonstrates the margin of a dilated tortuous aorta (*arrows*) parallel with the right border of the heart, producing a widened mediastinum. **(B)** The lateral image demonstrates posterior widening of the mediastinum (*arrows*).

radiographically because the density of these metals is almost equal to that of soft tissue. It is essential that any suspected foreign body be evaluated on two projections to be certain that the object projected over the esophagus truly lies within it.

Imaging appearance. Nonopaque foreign bodies in the esophagus, especially pieces of poorly chewed meat (masticated food bolus), can be demonstrated only after the ingestion of barium (Figure 5-27). Such a foreign body usually becomes impacted in the distal esophagus just above the level of the diaphragm and is often associated with a distal stricture. The intraluminal filling defect usually has an irregular surface and may resemble a completely obstructing carcinoma.

Treatment. Medications are the first line of treatment to relax the esophagus and allow the foreign body to move naturally into the stomach. In some instances, especially for a sharper-pointed object, retrieval of the foreign body using

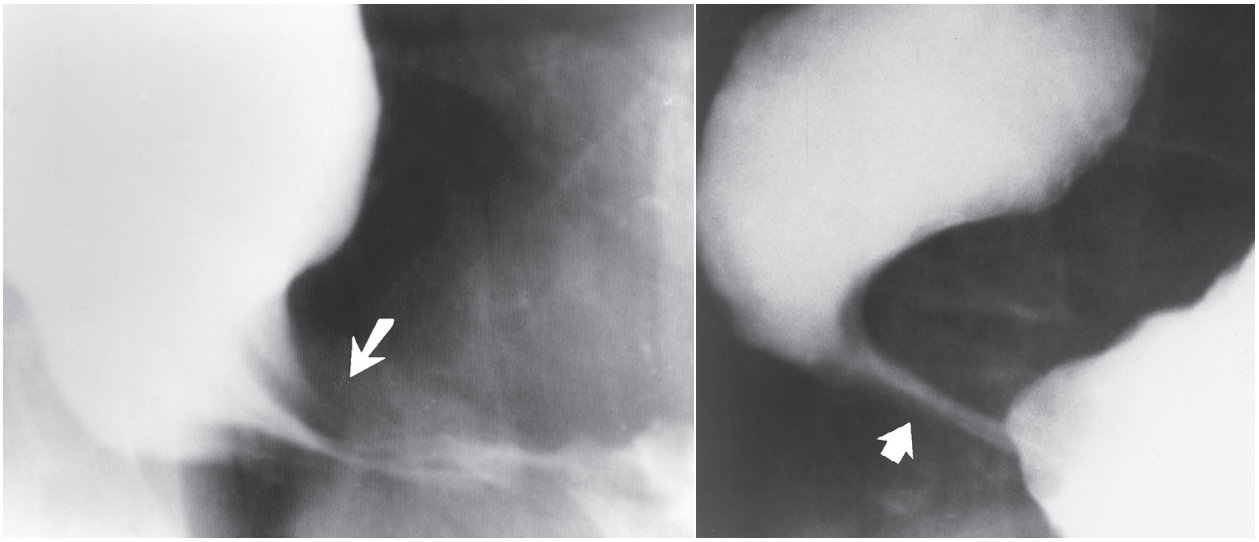

FIGURE 5-25 Achalasia. **(A)** Rat-tail narrowing of the distal part of the esophagus (*arrow*). **(B)** Small spurt of barium (*arrow*) enters the stomach through the narrowed distal segment (the jet effect).

FIGURE 5-26 Foreign body. Fish bone (*arrow*) impacted in the lower cervical portion of the esophagus.

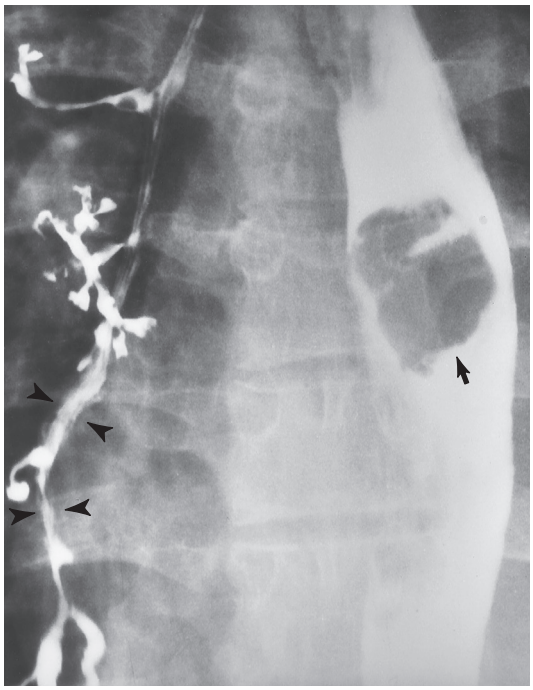

FIGURE 5-27 Meat impaction in the esophagus. Large bolus of hot dog (*arrow*) is trapped in the midesophagus of a patient with quadriplegia. Note barium in the bronchial tree (*arrowheads*) caused by aspiration.

endoscopy may be appropriate. Interventional approaches are attempted before the patient is taken to surgery to remove the obstruction. If the esophageal foreign body causes obstruction for more than 12 hours, there is an increased risk of perforation.

Perforation of the Esophagus

Perforation of the esophagus may be a complication of esophagitis, peptic ulcer, neoplasm, external trauma, or instrumentation. At times, perforation of a previously healthy esophagus can result from severe vomiting (the most common cause) or coughing, often from dietary or alcoholic indiscretion. Complete rupture of the wall of the esophagus may cause the sudden development of severe upper gastric pain simulating that of myocardial infarction. In the **Mallory–Weiss syndrome**, an increase in intraluminal and intramural pressures associated with vomiting (severe retching) after an alcoholic bout causes superficial mucosal laceration or fissures near the esophagogastric junction that produce severe hemorrhage. Endoscopy is required to best demonstrate lacerations, especially those close to the sphincter.

Imaging appearance. A perforation that extends throughout the entire esophageal wall can lead to free air in the mediastinum or periesophageal soft tissues. The administration of radiopaque contrast material may demonstrate extravasation through the perforation (Figure 5-28) or an intramural dissection channel separated by an intervening lucent line from the normal esophageal lumen. CT is the preferred modality to define the extent of the process.

Treatment. An expandable stent is placed, and then the complications are treated (chest tube for pneumothorax; antibiotics to prevent infection). A surgical procedure (band ligation) can be performed to close the perforation.

Summary of Findings for the Esophagus

Disorder	Location	Imaging Appearance	Treatment
Congenital tracheoesophageal fistula	Blind pouch superiorly Blind pouch distally or tracheal fistula	Blind pouch filled with contrast agent or NG tube Fistula track (if one exists), NG tube injection CT demonstrates fistula location and size for presurgical planning	Surgical repair—connect esophagus (anastomosis), fistula repair
Tracheoesophageal fistula—acquired	Usually at level of the carina or more proximal	Demonstration of connection between esophagus and tracheobronchial tree	Palliative—interventional stent placement Surgical—fistula repair
Reflux esophagitis	Distal esophagus	Streaks or dots superimposed on flat mucosa	Lifestyle modifications Weight-reduction diet Medication
Barrett's esophagus	Middle to lower esophagus	Smooth tapered stricture(s)	Photodynamic therapy and thermal ablation Surgery—fundoplication
Candida (fungal) and herpesvirus esophagitis	Entire esophagus	Cobblestone pattern Shaggy marginal contour Small mucosal ulcers or plaques	Same treatment as for Barrett's, with addition of antifungal or antiviral medication
Ingestion of corrosive agents	Alkaline ingestion	Deeper ulceration Stricture formation	Call poison control
	Acidic ingestion	Superficial minimal ulceration Stricture formation	Call poison control Water or milk dilution—alkaline
Esophageal cancer	Distal esophagus, esophagogastric junction	Double-contrast barium swallow study: Flat plaquelike lesion Infiltrating lesion (irregular wall) Polypoid mass (deep ulceration) CT with contrast enhancement—wall thickening greater than 3–5 mm	Surgical resection—possible cure Palliative therapy—chemotherapy or radiation Laser-activated chemical photodynamic therapy
Esophageal diverticula	Traction—all layers of wall Epiphrenic—distal portion of the esophagus	Esophagram—an outpouching or pocket filling with barium CT—an outpouching at the pharyngoesophageal junction	Usually no treatment Surgery if diverticulum interferes with swallowing

Summary of Findings for the Esophagus—Cont'd

Disorder	Location	Imaging Appearance	Treatment
Esophageal varices	Distal esophagus and stomach	Esophagram—serpiginous thickening of folds—resembles rosary beads Endoscopic ultrasound—compressible hypoechoic mass in the outer or submucosal layer	Medication—vasoconstrictor drugs Active bleeding—interventional balloon tamponade or surgery to tie off collateral vessels
Hiatal hernia	Esophagogastric region	GI series—numerous thicker folds of the stomach above the diaphragm	No treatment in most instances Surgical intervention includes tightening the hiatus
Achalasia—functional obstruction	Distal esophagus with proximal dilation	Chest radiograph—dilated esophagus GI series—narrowing of distal esophageal segment	Medication to relax sphincter Endoscopic balloon dilation Surgical myotomy
Foreign bodies—food bolus or nonopaque objects Foreign bodies—non–food-related (coin) or opaque	Any region of the esophagus	Barium swallow to demonstrate the level of impaction causing the obstruction Intraluminal filling defect with an irregular surface	Medication to relax esophagus Endoscopy to retrieve foreign body Surgical retrieval if all interventional approaches fail
Esophageal perforation—inflammatory, neoplastic, or traumatic	Any region of the esophagus	Perforation through entire wall—air in the mediastinum Extravasation of contrast material through perforation	Interventional—expandable stent Treatment of complications Surgical band ligation

GI, gastrointestinal; *NG*, nasogastric.

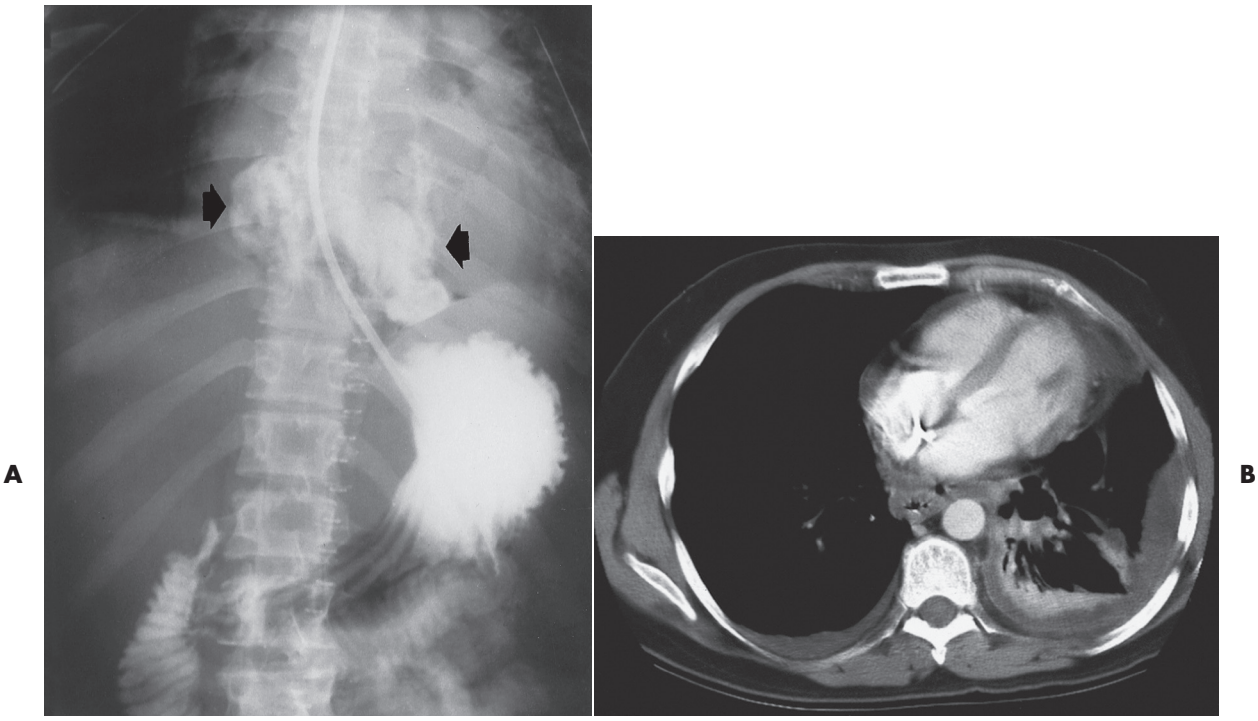

FIGURE 5-28 Esophageal perforation. (A) Extravasation of contrast material (*arrows*) is seen in a previously healthy patient who experienced severe vomiting after excessive ingestion of alcohol. (B) CT scan of the chest of a 41-year-old man illustrates perforation of the esophagus with drainage into the thoracic cavity.

FIGURE 5-29 Gastritis. Note the pronounced thickening of rugal folds throughout the stomach.

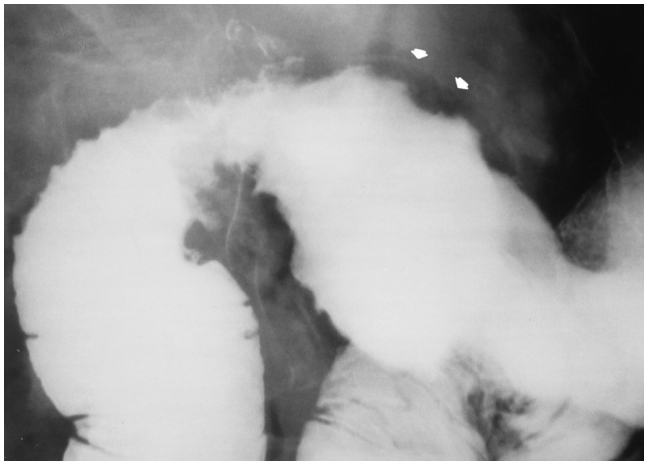

FIGURE 5-30 Phlegmonous emphysematous gastritis. Note the severe, irregular ulceration of the distal stomach, with air in the wall (*arrows*).

STOMACH

Gastritis

Inflammation of the stomach can be the result of a variety of irritants including alcohol, corrosive agents, and infection. Gastritis changes the normal surface pattern of the gastric mucosa. *Helicobacter pylori* can cause chronic gastritis that may lead to peptic ulcer disease.

Imaging appearance. **Alcoholic gastritis** may produce thickening of gastric folds (Figure 5-29), multiple superficial gastric erosions, or both. In **corrosive gastritis**, the acute inflammatory reaction heals by fibrosis and scarring, which result in severe narrowing of the antrum and may cause gastric outlet obstruction. In **bacterial (phlegmonous) gastritis**, inflammatory thickening of the gastric wall causes narrowing of the stomach that may mimic gastric cancer. The diagnosis of **infectious gastritis** can be made if there is evidence of gas bubbles (produced by the bacteria) in the stomach wall (Figure 5-30). These types of gastritis are known as erosive or acute gastritis.

Chronic atrophic gastritis (nonerosive) refers to severe mucosal atrophy (wasting) that causes thinning and a relative absence of mucosal folds, with the fundus or entire stomach having a bald appearance. This is a nonspecific radiographic pattern that can be related to such factors as age, malnutrition, medication, and complications of alcoholism. Chronic atrophic gastritis also occurs in patients with pernicious anemia, who cannot absorb vitamin B_{12} because of an inability of the stomach to secrete intrinsic factor (or hydrochloric acid).

Treatment. The causative agent in erosive gastritis determines treatment. Eliminating the causative agent, such as alcohol, reduces the changes in the mucosal lining as well as the symptoms because production of the protecting mucus is not inhibited. If overproduction of stomach acid produces the changes, acid-reduction medications are used to help maintain the mucous defense barrier. Antibiotics are the appropriate medication for bacterial or infectious gastritis. Patients with *H. pylori* gastritis receive a regimen of multiple antibiotics because this infection may be antibiotic resistant. Use of a combination of antibiotics has resulted in an 80% to 90% cure rate.

Pyloric Stenosis

Pyloric stenosis, also known as infantile hypertrophic pyloric stenosis (IHPS), occurs when the two muscular layers of the pylorus become hyperplastic and hypertrophic. Environmental and hereditary factors are believed to cause this process in 2 to 4 per 1000 live births. The gastric antrum and the pyloric canal become lengthened, whereas the mucosa is usually edematous and thickened. This causes a complete or near-complete obstruction, preventing food from entering into the duodenum. The edematous and thickened pylorus may be palpated and is described as a mobile, hard "olive."

Imaging appearance. In today's imaging arena, ultrasound is the modality of choice due to its high sensitivity and specificity, an accuracy approaching 100%. Pyloric stenosis appears as a thickened pyloric muscle (width >3 mm) and an elongated pyloric canal (>1.2 cm) on the longitudinal sonogram (Figure 5-31). The palpable olive appears as a "doughnut" or "target" sign in the cross-sectional image. When ultrasonographic findings are inconclusive, an upper GI series may aid in confirming the diagnosis by demonstrating the shouldering caused by a filling defect at the antrum as a result of the hypertrophic pyloric sphincter and delayed gastric emptying.

Treatment. Immediate diagnosis and pyloromyotomy (an incision of the circular muscles the pylorus) have decreased the mortality rates for pyloric stenosis, which are relatively low. Death results from delayed diagnosis, caused by possible dehydration and shock.

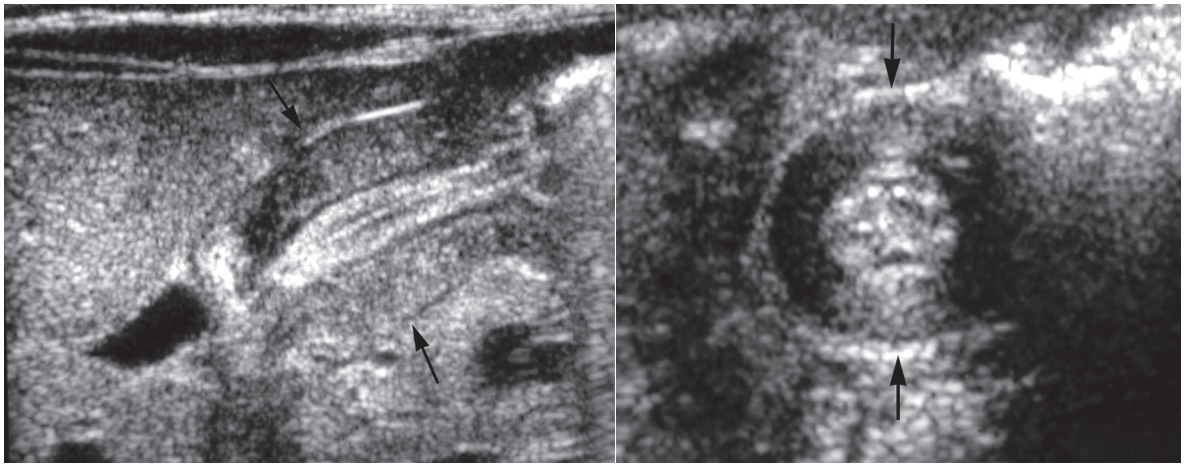

FIGURE 5-31 Hypertrophic pyloric stenosis. (A) Longitudinal sonogram demonstrates a markedly thickened, hypoechoic gastric antral muscle (*arrow*) with an elongated canal nearly 2 cm in length. (B) Transverse image demonstrates the typical hypoechoic doughnut (*arrows*).

Peptic Ulcer Disease

Peptic ulcer disease is a group of inflammatory processes involving the stomach and duodenum. It is caused by the action of acid and the enzyme pepsin secreted by the stomach and occurs most frequently on the lesser curvature. The spectrum of peptic ulcer disease varies from small and shallow superficial erosions to huge ulcers that may perforate through the bowel wall.

The major complications of peptic ulcer disease are hemorrhage (20%), gastric outlet obstruction (5% to 10%), and perforation (<5%). Peptic ulcer disease is the most common cause of acute upper GI bleeding. Free perforation of a peptic ulcer located in the anterior wall of the stomach or duodenum is the most common cause of pneumoperitoneum with peritonitis (see later discussion "Pneumoperitoneum"). Narrowing of the lumen of the distal stomach or duodenal bulb caused by peptic ulcer disease is by far the most common cause of gastric outlet obstruction.

Duodenal Ulcer

Duodenal ulcer is the most common manifestation of peptic ulcer disease. More than 95% of duodenal ulcers occur in the first portion of the duodenum (the duodenal bulb).

Imaging appearance. An unequivocal diagnosis of active duodenal ulcer requires the demonstration of an ulcer crater, which appears in profile as a small collection of barium projecting from the lumen. When seen en face, the ulcer niche appears as a rounded or linear collection of contrast material surrounded by lucent folds that often radiate toward the crater (Figure 5-32). Secondary signs of duodenal ulcer disease include thickening of the mucosal folds and a deformity of the duodenal bulb. Acute ulcers incite muscular spasm, leading to deformity of the margins of the duodenal bulb that may be inconsistent and varied during the examination. With chronic ulceration, fibrosis and scarring cause a fixed deformity that persists even though the ulcer heals. Symmetrical narrowing of the duodenal bulb in its midportion may produce the typical cloverleaf deformity of chronic duodenal ulcer disease (Figure 5-33). CT demonstrates an irregularity or collection of contrast material in the gastric wall; however, as with barium studies, this appearance may be difficult to differentiate from that of malignancy.

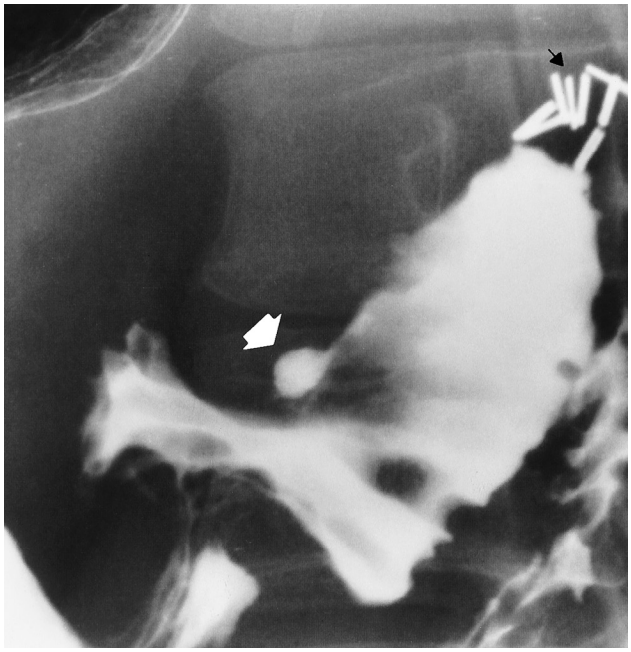

FIGURE 5-32 Duodenal ulcer. An ulcer niche appears as a rounded collection of barium (*white arrow*) surrounded by lucent edema. Multiple surgical clips are shown incidentally (*black arrow*).

Gastric Ulcer

Gastric ulcers, another form of peptic ulcer disease, usually occur on the lesser curvature of the stomach. Unlike duodenal ulcers, which are virtually always benign, up to 5% of gastric ulcers are malignant.

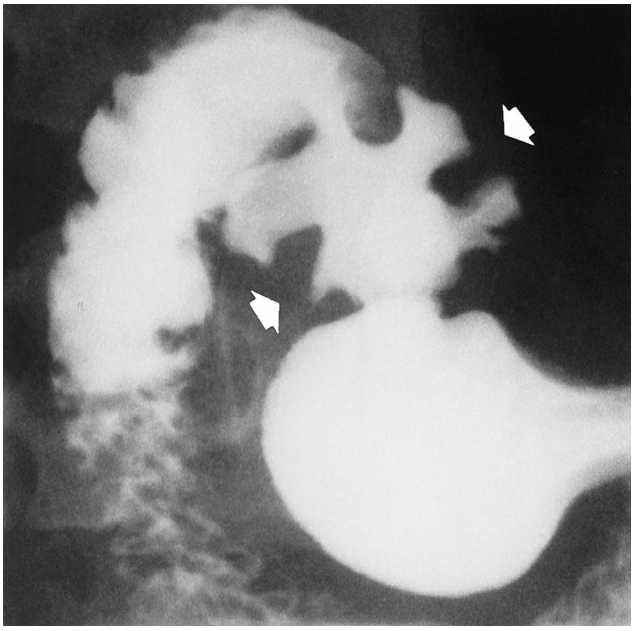

FIGURE 5-33 Chronic duodenal ulcer disease. Typical cloverleaf deformity is visible (*arrows*).

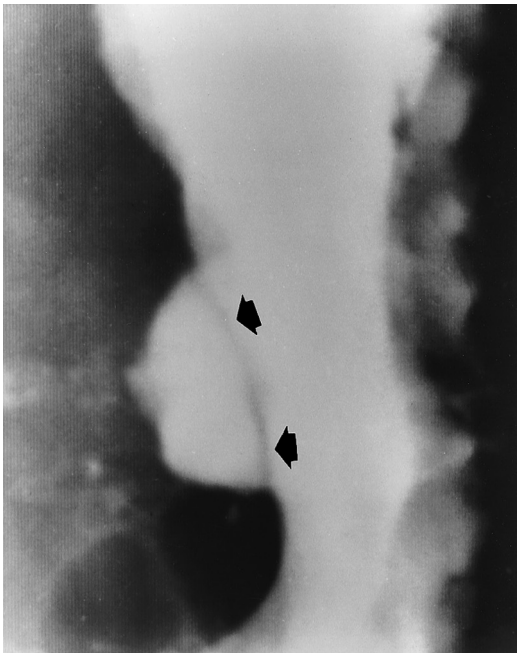

FIGURE 5-34 Benign gastric ulcer. Penetration of contrast material outside the normal, barium-filled gastric lumen associated with a thin, sharply demarcated, lucent line with parallel straight margins (*arrows*), representing edema at the base of the ulcer crater.

Imaging appearance. Radiographic signs that indicate whether a gastric ulcer is more likely to be benign or malignant have been described. The classic sign of a benign gastric ulcer in profile is penetration, with clear projection of the ulcer outside the normal barium-filled gastric lumen because the ulcer represents an excavation in the wall of the stomach (Figure 5-34). A thin lucency at the base of the ulcer, reflecting mucosal edema caused by inflammatory exudate, is another sign of benignancy. When viewed en face, a gastric ulcer appears as a persistent collection of barium surrounded by a halo of edema (the ulcer collar) (Figure 5-35).

FIGURE 5-35 Benign gastric ulcer. On en face projection, prominent radiating folds extend directly to the ulcer. Lucency around the ulcer (*arrows*) represents inflammatory mass effect.

A hallmark of benign gastric ulcer is radiation of mucosal folds to the edge of the crater. However, because radiating folds can be identified in both malignant and benign ulcers, the character of the folds must be carefully assessed. If the folds are smooth and slender and appear to extend into the edge of the crater, the ulcer is most likely benign (Figure 5-36A). In contrast, irregular folds that merge into a mound of polypoid tissue around the crater are suggestive of malignancy (Figure 5-36B).

Although the size, shape, number, and location of gastric ulcers have been suggested as criteria for distinguishing between benign and malignant lesions, these findings are of little practical value. One exception is ulcers in the gastric fundus above the level of the esophagogastric junction—essentially all of which are malignant.

An abrupt transition between the normal mucosa and the abnormal tissues surrounding a gastric ulcer is characteristic of a malignant lesion (Figure 5-37), in contrast to the diffuse and almost imperceptible transition between the normal gastric mucosa and the mound of edema surrounding a benign ulcer. Neoplastic tissue surrounding a malignant ulcer is usually nodular, unlike the smooth contour of the edematous mound around a benign ulcer. A malignant ulcer does not penetrate beyond the normal gastric lumen but remains within it because the ulcer merely represents a necrotic area within an intramural or intraluminal mass.

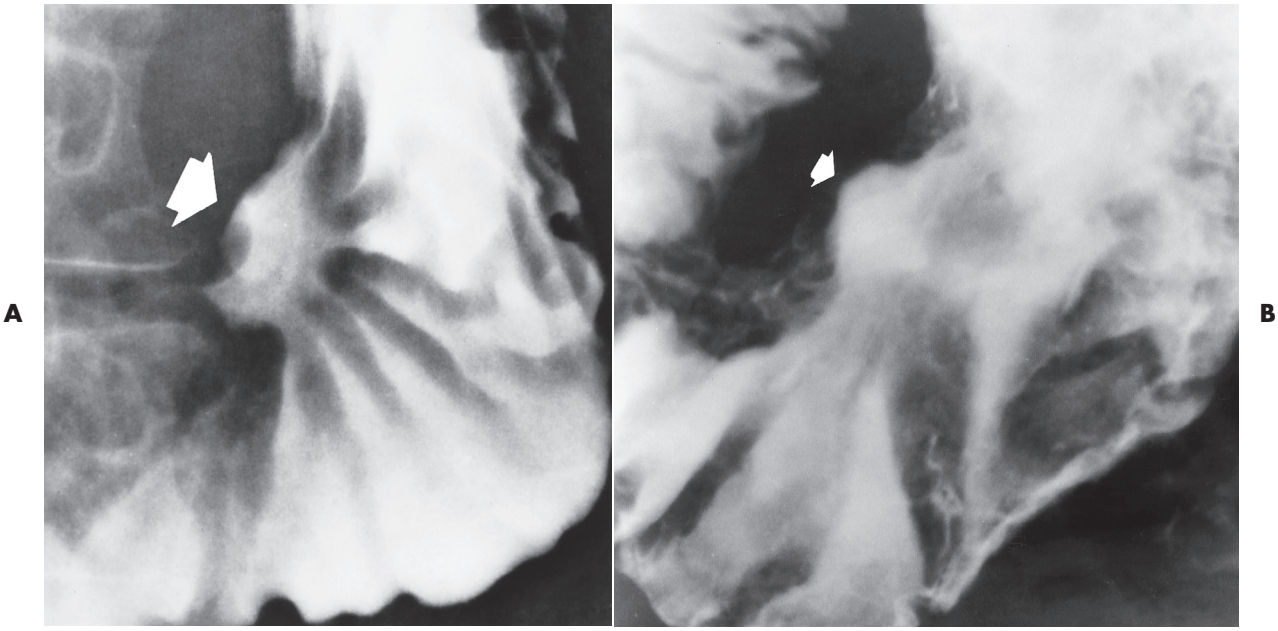

FIGURE 5-36 Radiating folds in gastric ulcers. (A) Small, slender folds extending to the edge of the crater (*arrow*) indicate the benign nature of this ulcer. (B) In this malignant gastric ulcer, thick folds radiate to an irregular mound of tissue around the ulcer (*arrow*).

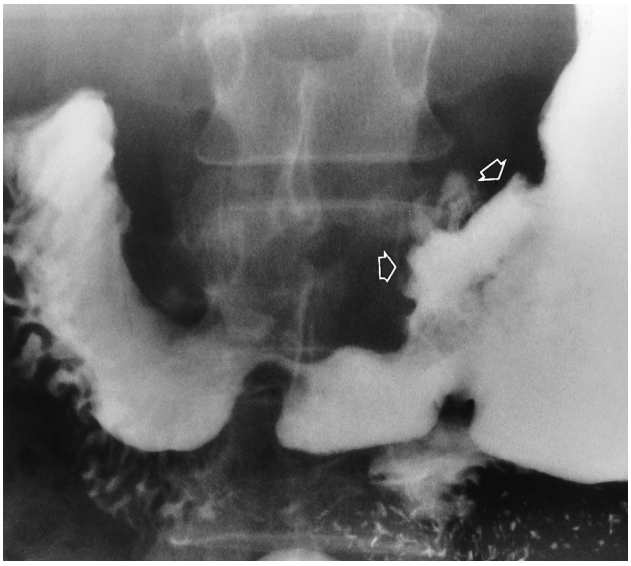

FIGURE 5-37 Malignant gastric ulcer. An abrupt transition occurs between normal mucosa and abnormal tissue surrounding an irregular gastric ulcer (*arrows*).

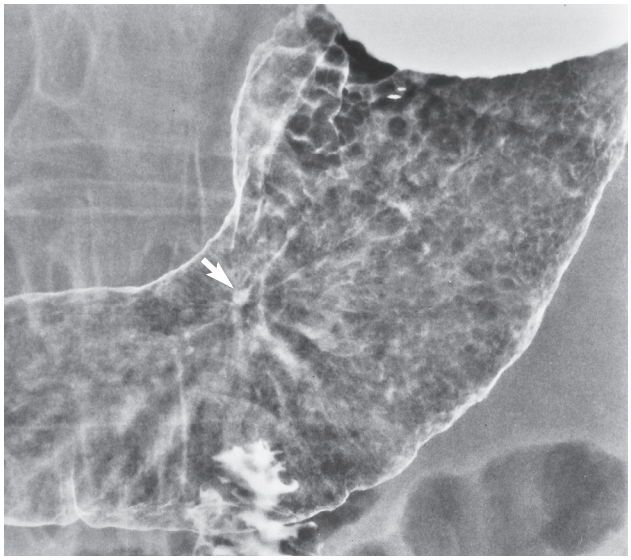

FIGURE 5-38 A healing gastric ulcer. Folds converge to a residual central depression (*arrow*).

Most benign gastric ulcers heal completely with medical therapy (see "Treatment of Ulcers") (Figure 5-38). Complete healing does not necessarily mean that the stomach returns to an absolutely normal radiographic appearance; bizarre deformities can result from fibrotic retraction and stiffening of the stomach wall. Although many malignant ulcers show significant healing, there is almost never complete disappearance of the ulcer crater.

The role of endoscopy in evaluating patients with gastric ulcers is controversial. Currently, endoscopy is indicated only when the radiographic findings are not typical for a benign ulcer, when healing of the ulcer does not progress at the expected rate, or when the mucosa surrounding a healed ulcer crater has a nodular surface or any other feature suggestive of an underlying early gastric cancer.

Superficial Gastric Erosions

Superficial gastric erosions are ulcerations that are so small and shallow that they are rarely demonstrated on conventional single-contrast upper GI examinations. With the increasing use of double-contrast techniques, a superficial gastric erosion typically appears radiographically as a tiny fleck of barium, which represents the erosion, surrounded by a radiolucent halo, which represents a mound of edematous mucosa (Figure 5-39).

FIGURE 5-39 Superficial gastric erosions in a patient with gastritis. Collection of barium represents a shallow erosion surrounded by a radiolucent halo (*arrow*).

Possible factors implicated in the production of superficial gastric erosions include alcohol, anti-inflammatory drugs (aspirin and steroids), Crohn's disease (see later discussion), and candidiasis (see previous discussion, "*Candida* and Herpesvirus").

Treatment of Ulcers

Lifestyle modifications are the first line of treatment for ulcers. First, the patient should avoid foods that cause an increase in the acid secretions (i.e., alcohol and caffeine). Antacids aid in neutralizing stomach acid. If stress is the cause of the increase in acidic secretions, stress management is appropriate. When the ulceration is caused by an infection (*H. pylori*), antibiotics are given to kill the bacteria. If the acidic secretions cannot be controlled by these methods, histamine H_2 antagonists help in reducing stomach acids and protecting the stomach lining. When more aggressive treatment is required, proton pump inhibitors may be used. Surgical treatment for management of complications may be necessary when ulcers do not respond to other treatments.

Cancer of the Stomach

Because pain is infrequently an early symptom, carcinoma of the stomach is rarely noted until the disease is far advanced and thus has a dismal prognosis (survival rate, 10%). The incidence of gastric cancer varies widely throughout the world. It is very high in Japan, Chile, and areas of Eastern Europe. It is low in the United States, where for reasons unknown it has been decreasing.

Several conditions appear to predispose persons to the development of carcinoma of the stomach. There is an increased risk of gastric cancer in patients with atrophic gastric mucosa, as in pernicious anemia, and in persons 10 to 20 years after a partial gastrectomy for peptic ulcer disease. A suggestive laboratory sign is *achlorhydria,* the absence of hydrochloric acid in gastric secretions obtained by means of a stomach tube. Most carcinomas occur in the distal stomach and are adenomatous in nature.

Imaging appearance. Gastric carcinoma can have a broad spectrum of radiographic appearances. Tumor infiltration of the gastric wall may stimulate intense fibrosis, which produces

FIGURE 5-40 Gastric carcinoma. Linitis plastica pattern demonstrated.

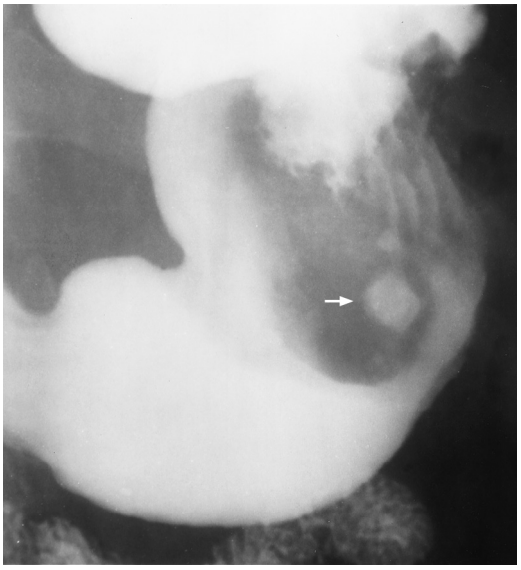

FIGURE 5-41 Gastric carcinoma. Carcinoma produced a large polypoid mass with associated ulceration (*arrow*).

diffuse thickening, narrowing, and fixation of the stomach wall (a linitis plastica pattern) (Figure 5-40). The stomach is contracted into a tubular structure without normal pliability. This fibrotic process usually begins near the pylorus and progresses slowly upward; the fundus is the area least involved.

Another major form of gastric carcinoma is a large irregular polypoid mass (approximately one third of cancers). Irregularity and ulceration within the mass are suggestive of malignancy, whereas the presence of a stalk and normal-appearing gastric folds extending to the tumor are sign of benignancy. Ulceration can develop in any gastric carcinoma and occurs in approximately one third. It varies from shallow erosions in relatively superficial mucosal lesions to huge excavations within fungating polypoid masses (Figure 5-41).

CT is of major value in the staging of gastric carcinoma, in planning its treatment, in assessing the response to therapy, and in detecting tumor recurrence (Figure 5-42). Carcinoma of the stomach may appear as thickening of the gastric wall or as an intraluminal mass. The earliest stage (stage I) demonstrates as an intraluminal mass without wall thickening. Stage II consists of wall thickening of greater than 1 cm without invasion of other tissue or organs. As the disease progresses, the stomach wall thickens and invades adjacent organs (stage III). Obliteration of the fat planes (the covering layers of fat) around the stomach is a reliable indicator of the extragastric spread of tumor (stage IV). CT can demonstrate direct tumor extension to intra-abdominal organs and distant metastases, especially to the liver.

Gastric carcinoma may also be demonstrated using endoscopic ultrasound. The gastric mucosa produces an increased echogenicity and demonstrates vertical invasion through the gastric wall. If diagnosed at a late stage, the lesion may extend into the perigastric lymph nodes.

Treatment. In most cases, treatment of stomach cancer consists of surgical resection of all or part of the stomach.

Summary of Findings for the Stomach

Disorder	Location	Imaging Appearance	Treatment
Gastritis	Alcohol—gastric folds	Thickened gastric folds Gastric outlet obstruction	Depends on cause: Avoidance of long-term irritants Acid-reduction medications Antibiotics for infections Treatment of cause
	Corrosive—narrowing of antrum		
	Bacterial or infectious—gastric wall	Thickened gastric wall causing narrowing of stomach and gas in the stomach wall	
	Chronic atrophic—mucosal folds	Thinning and absence of mucosal folds ("bald")	
Pyloric stenosis	Two muscular layers of the pylorus	US—thickened pyloric muscle (>3 mm in width) and an elongated pyloric canal (>1.2 cm) on the longitudinal sonogram UGI—demonstrating shouldering caused by a filling defect at the antrum	Pyloromyotomy (an incision of the circular muscles of the pylorus)
Peptic ulcer	Inflammatory process	Small shallow erosions to perforations—bleeding ulcer	Avoidance of foods causing increased acid secretion (alcohol and caffeine) Antibiotics for infectious process Histamine H_2 antagonist to reduce acidic secretions Proton pump inhibitors
	Duodenal ulcer	CT—irregular collection of contrast material in the gastric wall Rounded or linear collection of contrast material surrounded by lucent folds that often radiate toward the crater	
	Gastric ulcer	Benign—mucosal folds are smooth and slender and appear to extend into the edge of the crater Malignant—irregular folds merge into a mound of polypoid tissue around the crater	
	Superficial gastric erosions	Fleck of barium with radiolucent halo	
Cancer	Gastric wall infiltration	Diffuse thickening, narrowing, and fixation of stomach wall	Surgical resection of all or part of stomach
	Polypoid mass	Irregularity and ulceration suggest malignancy CT: Intraluminal mass without wall thickening: stage I Wall thickening <1 cm without invasion outside the organ: stage II Thickened wall with extension into adjacent organs: stage III Wall thickening and obliteration of perigastric fat planes: stage IV Endoscopic ultrasound—increased echogenicity of gastric mucosa with vertical invasion through the wall	

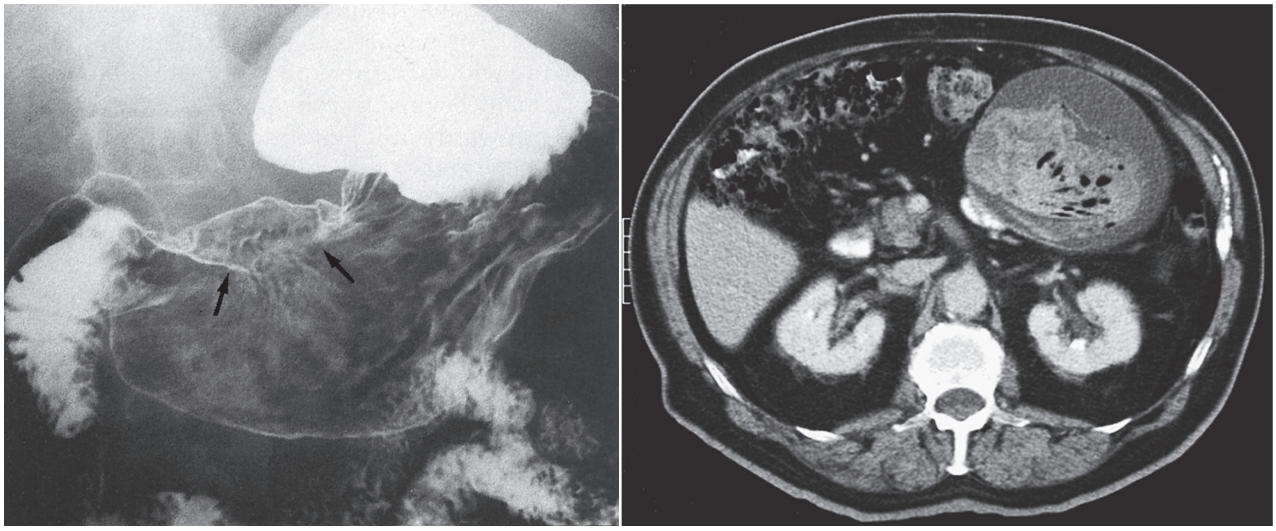

FIGURE 5-42 CT staging of gastric carcinoma. **(A)** Double-contrast study demonstrates large lesser-curvature mass (*arrows*) with a thickened wall. **(B)** CT scan shows a thickened gastric wall; the contrast agent demonstrates the lumen of the stomach.

SMALL BOWEL

Crohn's Disease (Regional Enteritis)

Crohn's disease is a chronic inflammatory disorder of unknown cause that most often involves the terminal area of the ileum but can affect any part of the GI tract. Although it can occur at any age, Crohn's disease is most common in young adults. The underlying cause is unknown, although there appears to be some psychogenic element; stress or emotional upsets are frequently related to the onset or relapse of the disease.

The granulomatous inflammatory process in Crohn's disease is frequently discontinuous, with diseased segments of bowel separated by apparently healthy portions (skip areas). Diffuse inflammation with edema involves all layers of the intestinal wall. Ulceration is common, and fistulas running in the bowel wall or extending to other organs are not infrequent.

The clinical spectrum of Crohn's disease is broad, ranging from a relatively benign course with unpredictable acute attacks and remissions to severe diarrhea and an acute condition in the abdomen. Although acute Crohn's disease may produce right lower quadrant pain simulating that of appendicitis, there is often blood in the stools that has come from the intensely congested mucous membranes. Small bowel obstruction and fistula formation occur in up to half of patients. Rectal fissures and perirectal abscesses occur in approximately one third.

Imaging appearance. In the small bowel, the earliest radiographic changes of Crohn's disease include irregular thickening and distortion of mucosal folds caused by submucosal inflammation and edema. Transverse and longitudinal ulcerations can separate islands of thickened mucosa and submucosa, leading to a characteristic rough cobblestone appearance (Figure 5-43). Rigid thickening of the entire bowel wall produces pipelike narrowing. Continued inflammation and fibrosis can result in a severely narrowed, rigid segment of small bowel in which the mucosal pattern is lost (string sign) (Figure 5-44). When several areas of small bowel are diseased, involved segments of varying length are often sharply separated from radiographically normal segments (skip lesions). On CT images, there is thickening of the wall of the small bowel, and the mesentery has an appearance that is described as "dirty fat." The new technology of CT enterography demonstrates subtle findings, such as mild wall thickening and mucosal vascular changes. CT is recommended for a patient with active Crohn's disease to determine the nature of the mass (Figure 5-45).

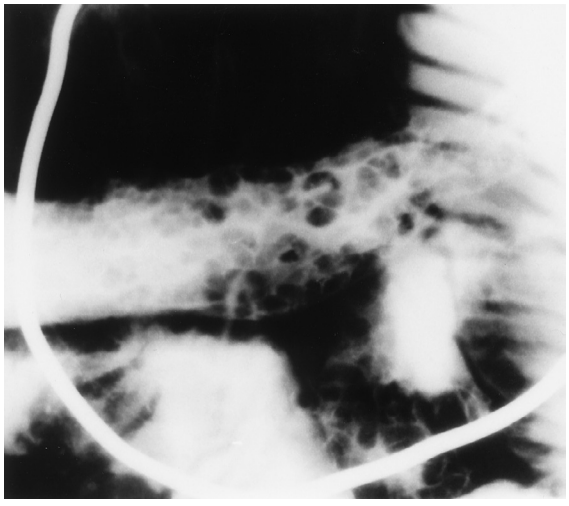

FIGURE 5-43 Crohn's disease. Cobblestone appearance is produced by transverse and longitudinal ulcerations separating islands of thickened mucosa and submucosa.

Fistula formation, a hallmark of chronic Crohn's disease, is found in at least half of all patients with this condition (Figure 5-46). The diffuse inflammation of the serosa and mesentery

in Crohn's disease causes involved loops of bowel to be firmly matted together by fibrous peritoneal and mesenteric bands. Fistulas apparently begin as ulcerations that burrow through the bowel wall into adjacent loops of small bowel and colon. In addition to fistulas between loops of bowel, a characteristic finding in Crohn's disease is the appearance of fistulous tracts ending blindly in abscess cavities surrounded by dense inflammatory tissue. These abscess cavities can produce palpable masses, persistent fever, or pain. Although less common than bowel-to-bowel fistulas, internal fistulas extending from the bowel to the bladder or vagina can occur. A common complication is the development of external gastrointestinal fistulas, which usually extend to the perianal area and may be associated with fissures and perirectal abscesses.

Treatment. Whenever possible, Crohn's disease is treated with medications, and surgery is performed only if complications require it. Surgical resection of an involved segment of small bowel is associated with a high incidence of recurrence of Crohn's disease adjacent to the anastomosis.

FIGURE 5-44 Crohn's disease. *Arrows* point to widely separated areas of disease (skip lesions). The lesions are greatly narrowed segments of small bowel (string sign).

Small Bowel Obstruction

Fibrous adhesions caused by previous surgery or peritonitis account for almost 75% of all small bowel obstructions. External hernias (inguinal, femoral, umbilical, and incisional) are the second most common cause. Other general causes of mechanical small bowel obstruction include luminal occlusion (gallstone and intussusception) and intrinsic lesions of the bowel wall (neoplastic or inflammatory strictures and vascular insufficiency).

Imaging appearance. Distended loops of small bowel containing gas and fluid can usually be recognized radiographically within 3 to 5 hours of the onset of complete obstruction. Almost all gas proximal to a small bowel obstruction represents swallowed air. On upright or lateral decubitus projections, the interface between gas and fluid forms a straight horizontal margin (Figure 5-47). Although the presence of gas–fluid levels at different heights in the same loop has traditionally been considered evidence for mechanical obstruction, an identical pattern can also be demonstrated in some patients with adynamic ileus (see later discussion). The air-filled bowel appears as a dilated proximal bowel and a collapsed distal bowel. On upright images, a string-of-beads sign appears. In adynamic ileus, the bowel has no caliber change.

As time passes, the small bowel may become so distended as to be almost indistinguishable from the colon. To make the critical differentiation between small and large bowel obstruction, it is essential to determine which loops of bowel contain abnormally large amounts of air. Small bowel loops generally occupy the more central portion of the abdomen, whereas colonic loops are positioned laterally around the periphery of the abdomen or inferiorly in the pelvis (Figure 5-48). Gas within the lumen of the small bowel outlines the thin valvulae conniventes, which completely encircle the bowel. In contrast, colonic haustral markings are thicker and

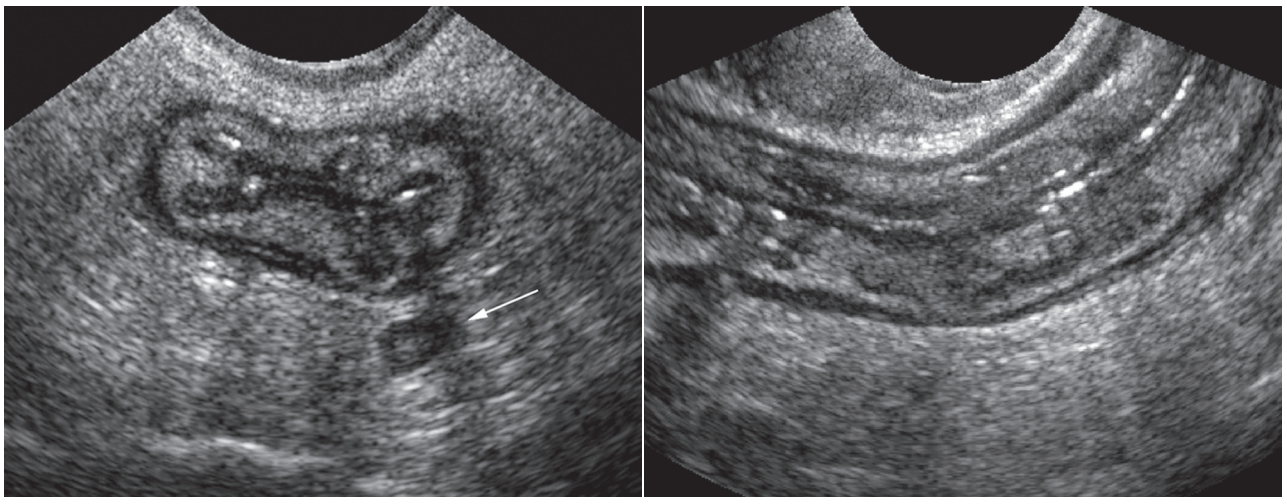

FIGURE 5-45 Crohn's disease. Ultrasound: Images A (sagittal) and B (in long axis) demonstrate the ileum with a very thick wall and that wall layering is preserved.

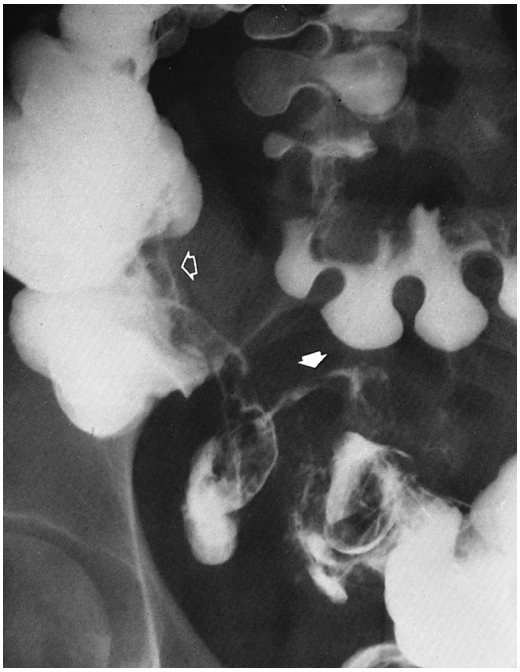

FIGURE 5-46 Crohn's disease. Note fistulization between the terminal ileum and the sigmoid colon (*solid arrow*) and along the cecum (*open arrow*).

farther apart and occupy only a portion of the transverse diameter of the bowel.

The site of obstruction can usually be predicted with considerable accuracy if the number and position of dilated bowel loops are analyzed. The presence of a few dilated loops of small bowel located high in the abdomen (in the center or slightly to the left) indicates an obstruction in the distal duodenum or jejunum. The involvement of additional small bowel loops is suggestive of a lower obstruction. As more loops are affected, they appear to be placed one above the other upward and to the left, producing a characteristic step-ladder appearance (Figure 5-49). The point of obstruction is always distal to the lowest loop of dilated bowel.

Patients with complete mechanical small bowel obstruction demonstrate little or no gas in the colon. This is a valuable point in the differentiation between mechanical obstruction and adynamic ileus, in which gas is seen within distended loops throughout the bowel. Although a small amount of gas or fecal accumulation may be present at an early stage of a small bowel obstruction (see Figure 5-48), the detection of a large amount of gas in the colon effectively eliminates this diagnosis.

The bowel proximal to an obstruction may contain no gas but be completely filled with fluid. This may produce a confusing picture of a normal-appearing abdomen or a large soft tissue abdominal mass.

Plain abdominal radiographs are occasionally insufficient for a distinction to be made between small and large bowel obstructions. In these instances, a carefully performed barium enema examination can document or eliminate the possibility of large bowel obstruction. If it

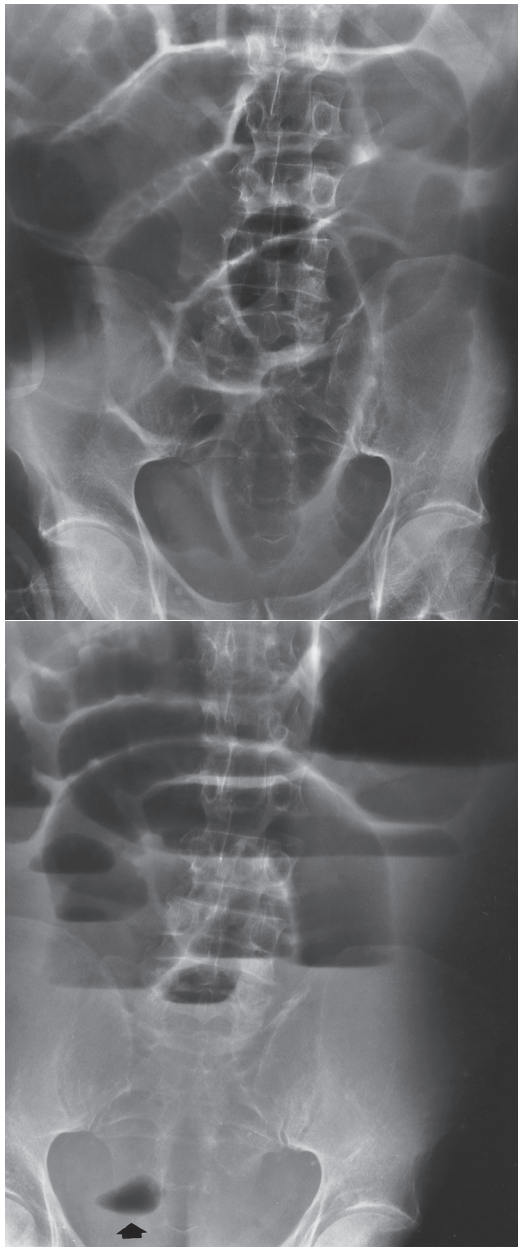

FIGURE 5-47 Small bowel obstruction. Supine (A) and upright (B) projections demonstrate large amounts of gas in dilated loops of small bowel. Image B, which was taken with the patient in the upright position and using a horizontal beam, demonstrates multiple prominent air–fluid levels. A single, small collection of gas (*arrow*) remains in colon.

is necessary to determine the precise site of small bowel obstruction, barium can be administered in either a retrograde (by means of an enema) or an antegrade (by way of the mouth) manner. Orally administered barium (not water-soluble agents) is the most effective contrast material for demonstrating the site of small bowel obstruction (Figure 5-50). The large amount of fluid proximal to a small bowel obstruction prevents any trapped barium from hardening or increasing the degree of obstruction. The density of barium permits excellent visualization far

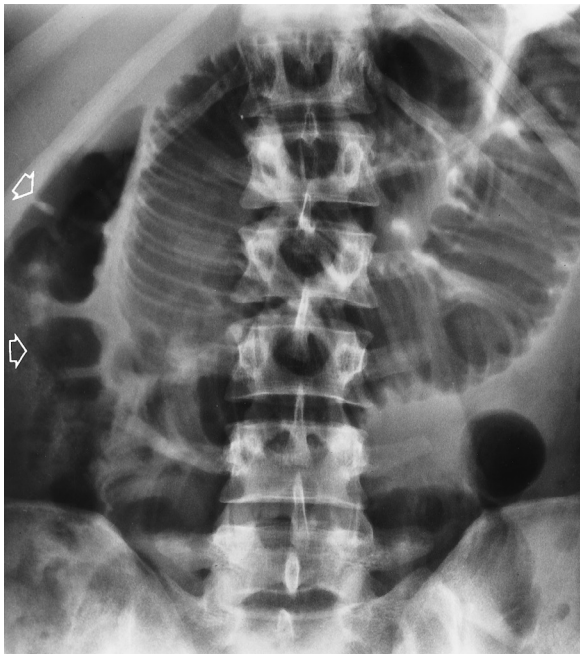

FIGURE 5-48 Small bowel obstruction. Dilated loops of small bowel occupy the central portion of the abdomen, with the nondilated cecum and ascending colon positioned laterally around the periphery of the abdomen (*arrows*).

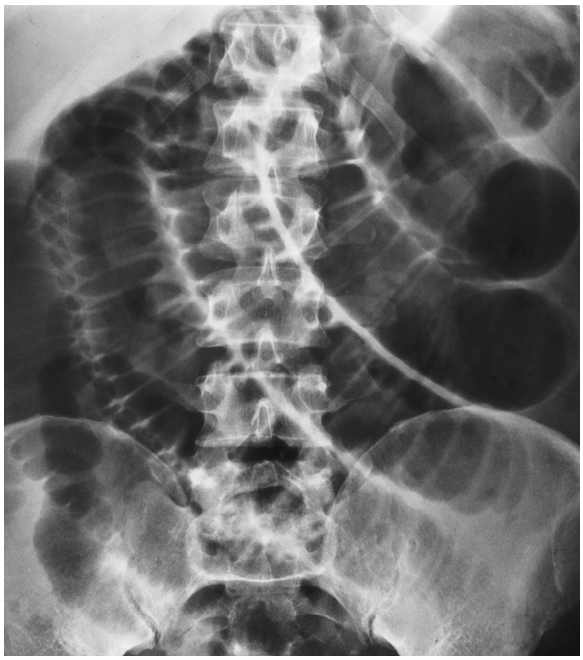

FIGURE 5-49 Low small bowel obstruction. Dilated loops of gas-filled bowel appear to be placed one above the other, upward and to the left, producing the characteristic stepladder appearance.

into the intestine; water-soluble agents, however, are lost to sight because of dilution and absorption. It must be emphasized that if plain radiographs clearly demonstrate a mechanical small bowel obstruction, a contrast examination is unnecessary.

FIGURE 5-50 Barium upper gastrointestinal series. An impacted bezoar (*arrows*) causing a small bowel obstruction.

Strangulation of bowel caused by interference with the blood supply is a serious complication of small bowel obstruction. In a closed-loop obstruction (e.g., volvulus and incarcerated hernia) (Figure 5-51), the loops going both toward (afferent) and away from (efferent) the area of narrowing become obstructed. The involved segments usually fill with fluid and appear radiographically as a tumor-like soft tissue mass. A closed loop is a clinically dangerous form of obstruction because the continuing outpouring of fluid into the enclosed space can raise intraluminal pressure and rapidly lead to occlusion of the blood supply to that segment of bowel. Because venous pressure is normally lower than arterial pressure, blockage of venous outflow from the strangulated segment occurs before obstruction of the mesenteric arterial supply. Ischemia can rapidly cause necrosis of the bowel with sepsis, peritonitis, and a potentially fatal outcome.

CT may aid in demonstrating small bowel obstruction when the plain abdominal radiographs are normal or nonspecific. In addition to showing the site, level, and cause of the obstruction, this modality may indicate whether there is strangulation of the involved loops of bowel. Specifically, herniation causes slight wall thickening that appears as a "target sign" as a result of engorgement of the superior and inferior mesenteric vessels. CT appears to be the most valuable modality for patients with a history of abdominal malignancy

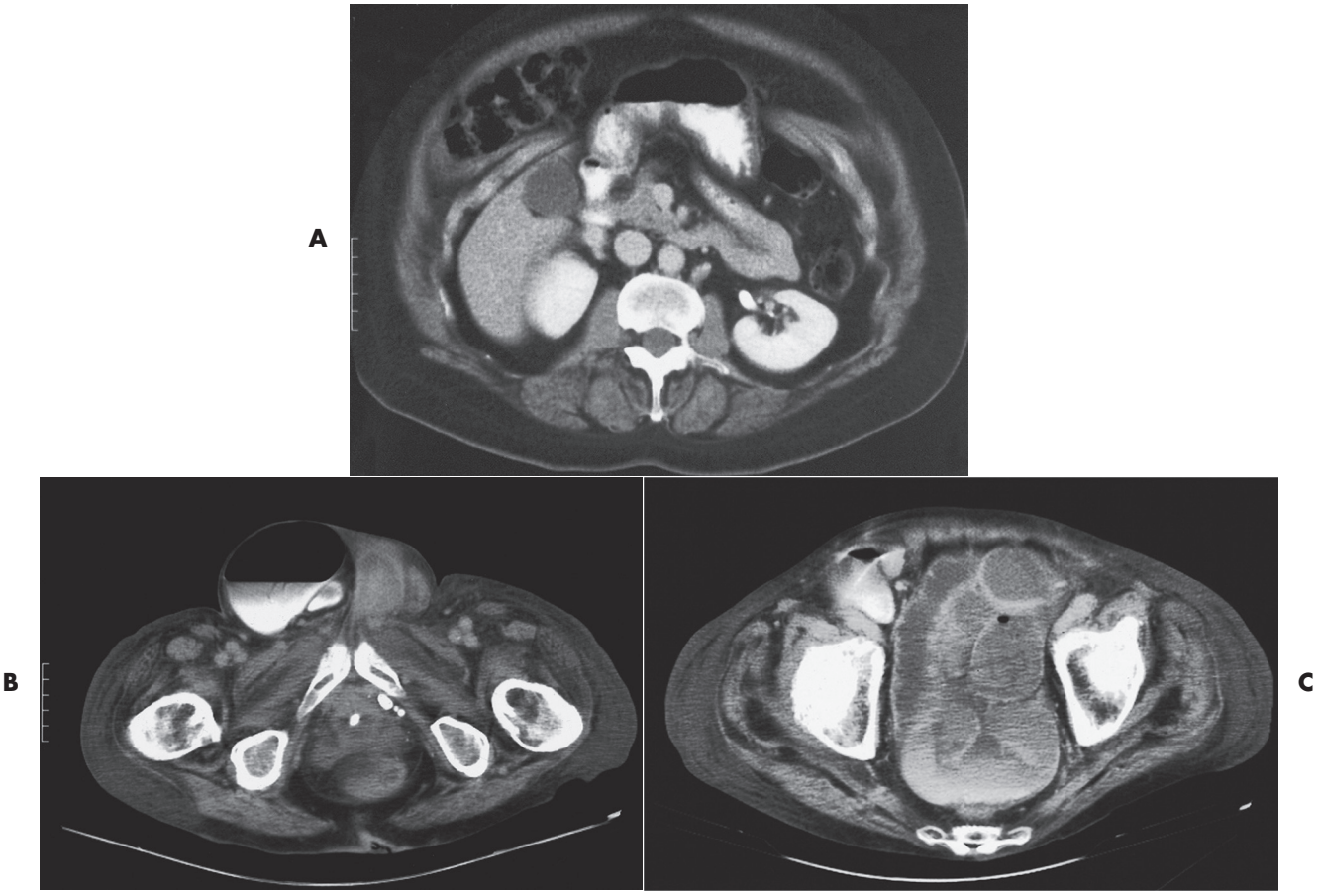

FIGURE 5-51 CT scans of bowel obstructions. **(A)** Herniation of the small bowel and stomach through anterior abdominal wall. **(B)** Scrotal herniation of the large bowel causing bowel obstruction. **(C)** Dilated sigmoid colon caused by obstruction.

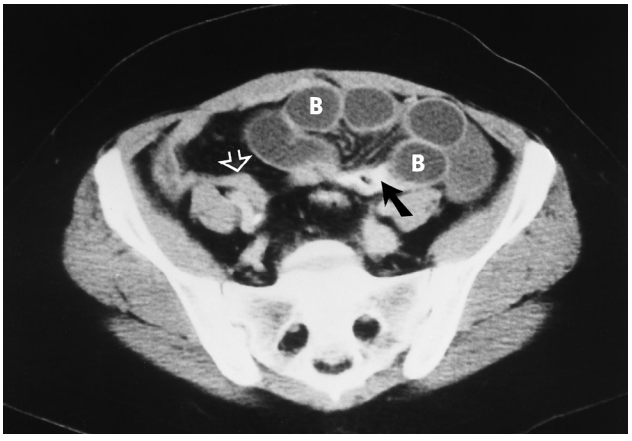

FIGURE 5-52 CT diagnosis of clinically unsuspected small bowel obstruction caused by adhesions. Note the transition point between the dilated loops of small bowel (B) and the collapsed ileum (*black arrow*). Note also the collapsed terminal ileum (*open arrow*).

and for those who have signs of infection, bowel infarction, or a palpable abdominal mass (Figure 5-52).

Treatment. Surgery is usually required to decompress the bowel as soon as possible to prevent necrosis or bowel perforation from occurring.

Adynamic Ileus

Adynamic ileus is a common disorder of intestinal motor activity in which fluid and gas do not progress normally through a nonobstructed small and large bowel. A variety of neural, hormonal, and metabolic factors can precipitate reflexes that inhibit intestinal motility. Adynamic ileus occurs to some extent in almost every patient who undergoes abdominal surgery. Other causes of adynamic ileus are peritonitis, medications that decrease intestinal peristalsis (those with an atropine-like effect), electrolyte and metabolic disorders, and trauma. Adynamic ileus (or paralytic ileus) occurs more often than mechanical bowel obstruction. The clinical findings in patients with adynamic ileus vary from minimal symptoms to generalized abdominal distention with a sharp decrease in the frequency and intensity of bowel sounds.

Imaging appearance. The radiographic hallmark of adynamic ileus is the retention of large amounts of gas and fluid in dilated small and large bowel. The entire small and large bowel in adynamic ileus, unlike in mechanical small bowel obstruction, appears almost uniformly dilated with no demonstrable point of obstruction (Figure 5-53).

There are two major variants of adynamic ileus. **Localized ileus** refers to an isolated distended loop of small or

FIGURE 5-53 Adynamic ileus. Large amounts of gas and fluid are retained in loops of dilated small and large bowel. The entire bowel, small and large, appears almost uniformly dilated with no demonstrable point of obstruction.

FIGURE 5-55 Colonic ileus. Massive distention of large bowel without obstruction in a patient with severe diabetes and electrolyte abnormalities.

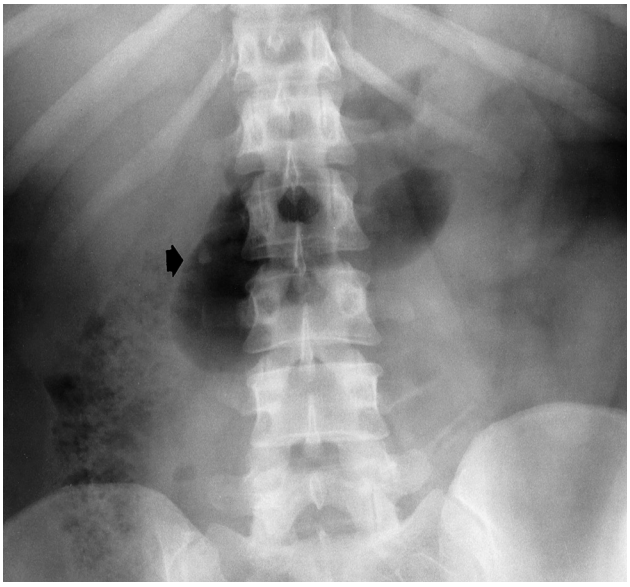

FIGURE 5-54 Localized ileus in patient with acute ureteral colic. *Arrow* points to impacted ureteral stone.

large bowel (the sentinel loop), which is often associated with an adjacent acute inflammatory process. The portion of the involved bowel can offer a clue to the underlying disease. Localized segments of the jejunum or transverse colon are frequently dilated in patients with acute pancreatitis. Similarly, the hepatic flexure of the colon can be distended in acute cholecystitis, the terminal ileum can be dilated in acute appendicitis, the descending colon can be distended in acute diverticulitis, and dilated loops can be seen along the course of the ureter in acute ureteral colic (Figure 5-54). Unfortunately, isolated segments of distended small bowel are commonly seen in patients with abdominal pain and thus the sentinel loop may be found "guarding" the wrong area.

Colonic ileus refers to selective or disproportionate gaseous distention of the large bowel without an obstruction (Figure 5-55). Massive distention of the cecum, which is often horizontally oriented, characteristically dominates the radiographic appearance. Colonic ileus usually accompanies or follows an acute abdominal inflammatory process or abdominal surgery. The clinical presentation and the findings on plain abdominal radiographs simulate those in mechanical obstruction of the colon. A barium enema examination is usually necessary to exclude an obstructing lesion.

Treatment. Adynamic ileus caused by surgery usually resolves itself spontaneously in 36 to 48 hours if no complications are involved. Treatment involves insertion of a nasogastric tube to aspirate the stomach, decompress the bowel, and allow the intestine to rest. Electrolyte and fluid imbalances are corrected by intravenous (IV) injection.

Intussusception

Intussusception is a major cause of bowel obstruction in children; it is much less common in adults. *Intussusception* is the telescoping of one part of the intestinal tract into another because of peristalsis, which forces the proximal segment of bowel to move distally within the ensheathing outer portion. Once such a lead point has been established, it gradually progresses forward and causes increased obstruction. This process can compromise the vascular supply and produce ischemic necrosis of the intussuscepted bowel.

In children, intussusception is most common in the region of the ileocecal valve. The clinical onset tends to be abrupt, with severe abdominal pain, blood in the stool ("currant jelly" stool), and often a palpable right-sided mass. If the diagnosis is made early and therapy instituted promptly, the mortality of intussusception in children is less than 1%. However, if treatment is delayed more than 48 hours after the onset of symptoms, the mortality increases dramatically. In adults, intussusception is often chronic or subacute and is characterized by irregular recurrent episodes of colicky pain, nausea, and vomiting. A specific cause of intussusception often cannot be detected in children. In adults, however, the leading edge is frequently a polypoid tumor with a stalk (pedunculated) or an inflammatory mass.

Imaging appearance. Radiographically, an intussusception produces the classic coiled-spring appearance of barium trapped between the intussusceptum and the surrounding portions of bowel (Figure 5-56A). Reduction of a colonic intussusception can sometimes be accomplished by a barium enema examination (Figures 5-56B and 5-56C), although great care must be exercised to prevent excessive intraluminal pressure, which may lead to perforation of the colon. On CT images, intussusception appears as three concentric circles forming a soft tissue mass.

Ultrasound, used especially in children, demonstrates the obstructive mass as a doughnut-shaped lesion on the transverse scan and as a "pseudokidney" on the longitudinal scan (Figure 5-57).

Treatment. Reduction of intussusceptions by rectal insufflation of air (instead of barium) has been reported to be an effective technique in children. In older children and adults, a second barium enema examination after reduction is necessary to determine whether an underlying polyp or a tumor caused the intussusception.

Malabsorption Disorders

Malabsorption disorder refers to a multitude of conditions in which there is defective absorption of carbohydrates, proteins, and fats from the small bowel. Regardless of the cause, malabsorption results in *steatorrhea*—the passage of bulky, foul-smelling, high-fat-content stools that float.

Imaging appearance. Many of the diseases that cause malabsorption produce radiographic abnormalities in the small bowel, although malabsorption can exist without any detectable small bowel changes. The two major radiographic appearances are (1) small bowel dilation with normal folds (Figure 5-58) and (2) a pattern of generalized, irregular, distorted small bowel folds (Figure 5-59).

Treatment. Patients afflicted with malabsorption disorders take medications to assist in absorbing key nutrients to keep the body's systems in good health. *Probiotics* are live microbial food supplements that aid in improving the intestinal microbial balance. These supplements enhance the bioavailability of nutrients to the body.

FIGURE 5-56 Intussusception. **(A)** Obstruction of the colon at the hepatic flexure produces the characteristic coiled-spring appearance of intussuscepted bowel. Partial **(B)** and complete **(C)** reduction of intussusception by careful barium enema examination.

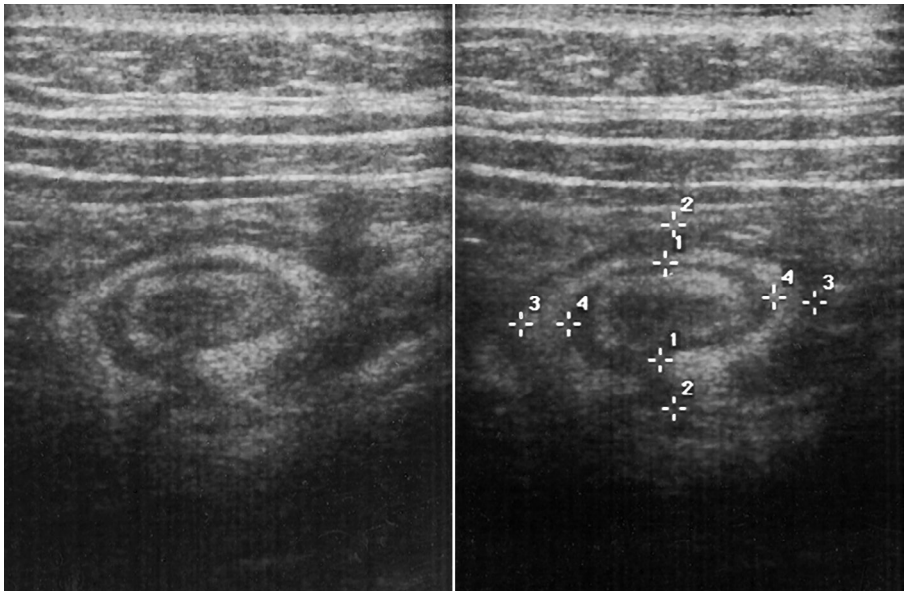

FIGURE 5-57 **Intussusception.** Ultrasound image illustrates doughnut-shaped lesion marked for measurement.

Summary of Findings for the Small Bowel

Disorder	Location	Imaging Appearance	Treatment
Crohn's disease (regional enteritis)	Most often in terminal ileum	Small bowel series: • Irregular thickened mucosal folds • Cobblestone appearance • String sign and skip lesions CT—thick mucosal walls and "dirty fat" mesenteric appearance CT enterography—subtle wall thickening and mucosal vascular changes Ulcerations—fistula formation	Medications Surgery if complications occur
Small bowel obstruction	Mechanical	Abdomen • Caliber of the air-filled bowel appears as a dilated proximal bowel and a collapsed distal bowel • Stepladder appearance CT—herniation illustrates as a "target sign" as a result of slight wall thickening with mesenteric engorgement	Decompression as soon as possible Usually surgery
Adynamic ileus	Loss of motility in small bowel	Large amounts of gas and fluid in small and large bowel	Usually resolves itself in 36–48 hr Place nasogastric tube and balance fluids
Intussusception	Children—ileocecal valve	Radiograph—coiled spring appearance on contrast enema CT—three concentric circles forming a soft tissue mass Ultrasound—doughnut-shaped lesion	Reduction of telescoping bowel (rectal insufflation) Therapeutic enema of air or barium
Malabsorption disorders	Throughout small bowel	Dilation with normal folds Irregular distorted folds	Medications to increase nutrient absorption

COLON

Appendicitis

Acute appendicitis develops when the neck of the appendix becomes blocked by a fecalith or by postinflammatory scarring that creates a closed-loop obstruction within the organ. Because of inadequate drainage, fluid accumulates in the obstructed portion and serves as a breeding ground for bacteria. High intraluminal pressure causes distention and thinning of the appendix distal to the obstruction, which interferes with the circulation and may lead to gangrene and perforation. If the process evolves slowly, adjacent organs (terminal ileum, cecum, and omentum) may wall off the appendiceal area so that a localized abscess

FIGURE 5-58 Malabsorption patient. Diffuse dilation of entire small bowel with excessive intraluminal fluid in a patient with malabsorption caused by sprue.

FIGURE 5-59 Malabsorption patient. Diffuse, irregular thickening of small bowel folds in a patient with malabsorption secondary to Whipple's disease.

FIGURE 5-60 Appendicolith. Laminated calcification in the appendix.

develops; rapid vascular compromise may permit free perforation with the spilling of fecal material into the peritoneal cavity and the development of generalized peritonitis. Appendicitis occurs in all age groups but is more common in children and adolescents.

The clinical symptoms (and laboratory results) of acute appendicitis are usually so characteristic that there is no need for routine radiographs to make the correct diagnosis. The presence of severe right lower quadrant pain, low-grade fever, and slight leukocytosis, especially in younger adults, is presumed to be evidence of appendicitis. However, in some patients, especially the elderly, the clinical findings may be obscure or minimal. In addition, because the appendix is mobile and may be in an unusual location, the pain of acute appendicitis may mimic that of cholecystitis, diverticulitis, or pelvic inflammatory disease. When the symptoms are confusing, an imaging examination may be necessary for prompt diagnosis and surgical intervention before perforation occurs.

Imaging appearance. Plain abdominal radiographs demonstrate a round or oval, laminated calcified fecalith in the appendix (appendicolith) (Figure 5-60) in approximately one third of patients. Surgical experience indicates that the presence of an appendicolith in combination with symptoms of acute appendicitis usually implies that the appendix is

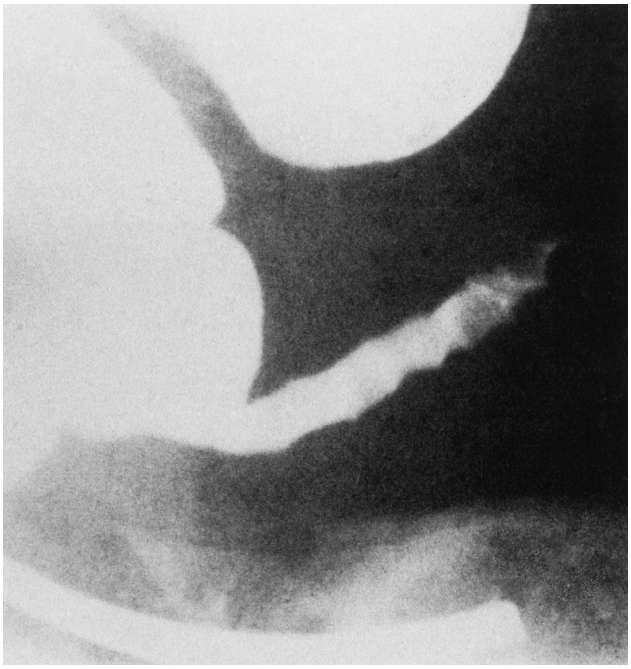

FIGURE 5-61 Acute appendicitis. Spot radiograph from barium enema examination shows incomplete filling of appendix.

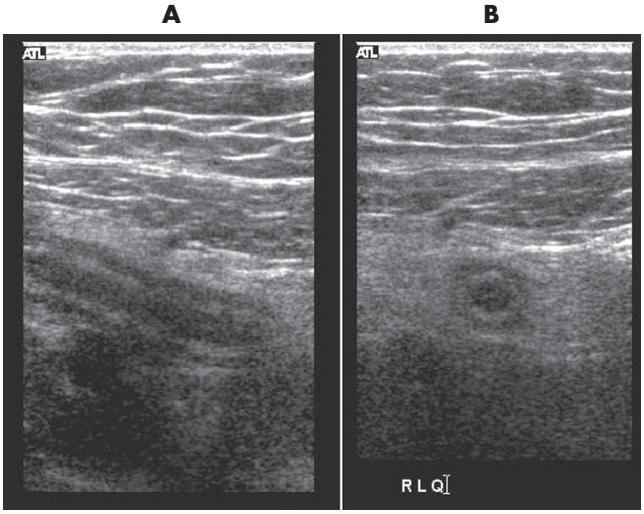

FIGURE 5-62 Ultrasound images of appendicitis. The sagittal scan (A) illustrates an inflamed appendix that is elongated and hypoechoic. The transverse scan (B) demonstrates the appendiceal lumen surrounded by hypoechoic hypoechoic inflamed tissue.

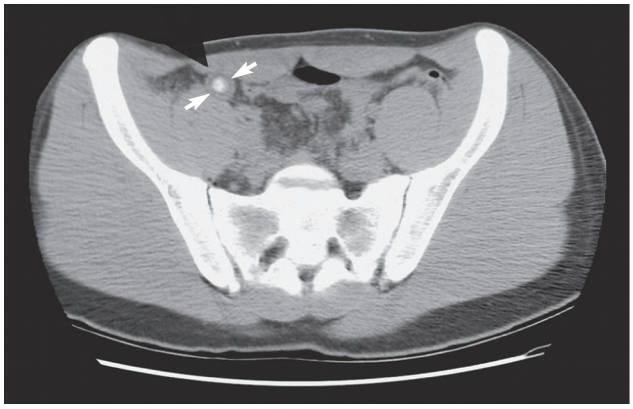

FIGURE 5-63 CT scan of the upper pelvis. Shows an appendix with an enlarged thickened wall indicating inflammation. An appendicolith can be seen in the appendix (*arrows*).

gangrenous (necrotic) and likely to perforate. Most appendicoliths are located in the right lower quadrant overlying the iliac fossa. Depending on the length and position of the appendix, however, an appendicolith can also be seen in the pelvis or in the right upper quadrant (retrocecal appendix), where it can simulate a gallstone.

Because of the danger of perforation, barium enema examination is usually avoided in acute appendicitis. If it is performed, an irregular impression of the base of the cecum (caused by inflammatory edema), in association with failure of barium to enter the appendix, is a characteristic finding. Nevertheless, failure of barium to fill the appendix is not a reliable sign of appendicitis because the normal appendix does not fill with barium in approximately 20% of cases. Partial filling of the appendix with distortion of its shape or caliber strongly suggests acute appendicitis (Figure 5-61), especially if there is a cecal impression. In contrast, a patent (open) appendiceal lumen effectively excludes the diagnosis of acute appendicitis, especially when barium extends to fill the rounded appendiceal tip.

When the clinical presentation is unclear, high-resolution ultrasound with graded compression is the imaging modality of choice for diagnosing acute appendicitis, especially when use of ionizing radiation is contraindicated in the patient. A noncompressible appendix measuring 7 mm or more in maximal outer diameter is considered virtually pathognomonic of acute appendicitis (Figure 5-62).

CT, the gold standard, shows an appendiceal abscess as a round or oval mass of soft tissue density that may contain gas. After administration of IV contrast material, the appendix appears as a dilated structure with a thickened, circumferentially enhancing wall (Figure 5-63). This modality provides a more precise evaluation of the nature, extent, and location of the pathologic process and can detect intra-abdominal disease unrelated to appendicitis that may explain the patient's clinical presentation.

Treatment. When a patient is diagnosed with appendicitis, an immediate appendectomy should be performed before perforation occurs to prevent complications (e.g., peritonitis, gangrene, and abscess formation). If perforation occurs, a regimen of antibiotics helps reduce the risk of peritonitis and sepsis.

Diverticulosis

Colonic diverticula are outpouchings that represent acquired herniations of mucosa and submucosa through the muscular layers at points of weakness in the bowel wall. The incidence of colonic diverticulosis increases with age. Rare in persons younger than 30 years, diverticula can be demonstrated in up to half of persons older than 60 years. Diverticular disease is presumed to occur in individuals who frequently exert high

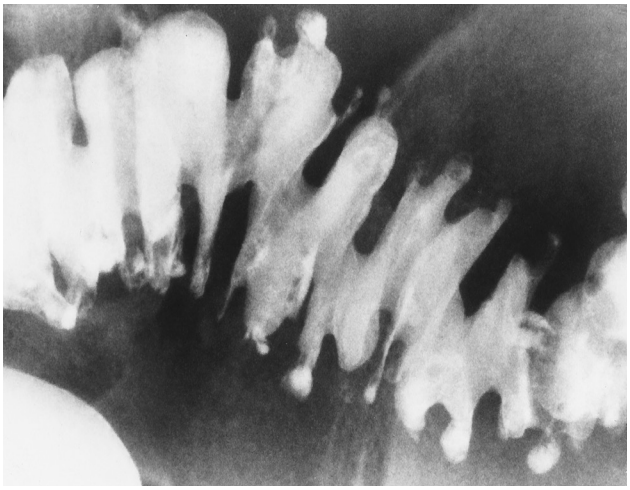

FIGURE 5-64 Diverticulosis. The typical sawtoothed configuration is produced by thickened circular muscle and is associated with multiple diverticula.

pressures in the lumen while straining to pass a large bulk of stool. Those consuming low-fiber and low-bulk meals are more susceptible. Diverticula occur most commonly in the sigmoid colon and decrease in frequency in the proximal colon. Although most patients with diverticulosis have no symptoms, a substantial number have chronic or intermittent lower abdominal pain, frequently related to meals or emotional stress, and alternating bouts of diarrhea and constipation. Bleeding may be caused by inflammatory erosion of penetrating blood vessels at the base of the diverticulum. The leading cause of massive lower GI bleeding in adults and guaiac-positive (indicating occult blood) stools in the elderly is diverticular disease.

Imaging appearance. Colonic diverticula appear radiographically as round or oval outpouchings of barium projecting beyond the confines of the lumen. They vary in size from barely visible dimples to saclike structures 2 cm or more in diameter. Giant sigmoid diverticula up to 25 cm in diameter, which probably represent slowly progressing chronic diverticular abscesses, may appear as large, well-circumscribed, lucent cystic structures in the lower abdomen.

Diverticula are usually multiple and tend to occur in clusters, although a solitary diverticulum is occasionally found. When diverticula are multiple, deep crisscrossing ridges of thickened circular muscle (sawtoothed configuration) can produce a characteristic series of sacculations (Figure 5-64).

Diverticula also commonly occur in the esophagus and duodenum and infrequently may develop in the jejunum and ileum.

Diverticulitis

Diverticulitis is a complication of diverticular disease of the colon (necrosing inflammation in the diverticula), especially in the sigmoid region, in which perforation of a diverticulum leads to the development of a peridiverticular abscess. It is estimated that up to 20% of patients with diverticulosis eventually develop acute diverticulitis. Retained fecal material trapped in a diverticulum by the narrow opening of the

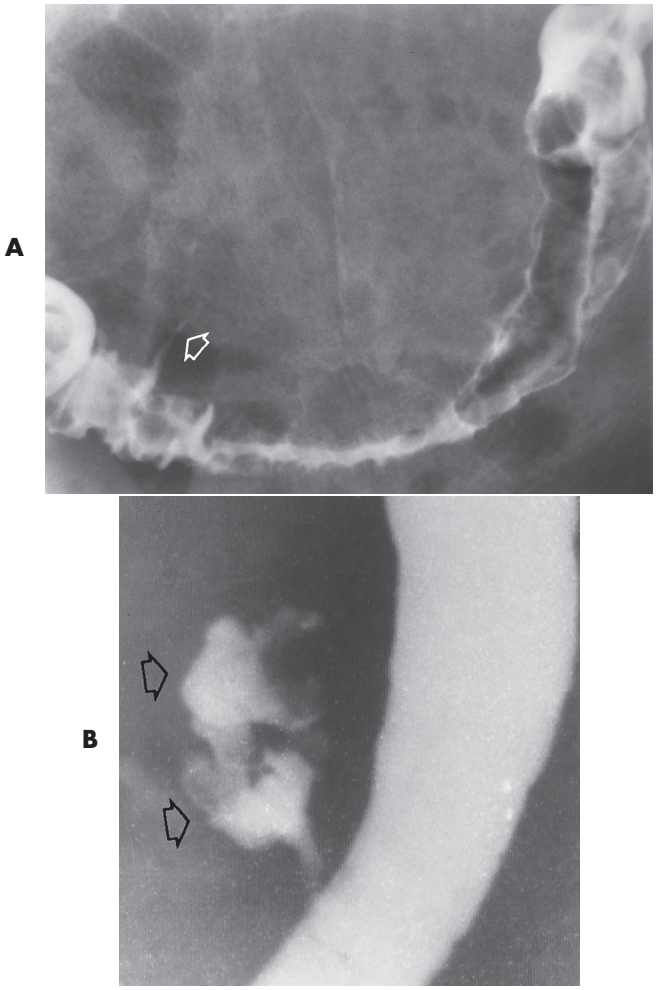

FIGURE 5-65 Diverticulitis. **(A)** Thin projection of contrast material (*arrow*) implies extravasation from colonic lumen. Note severe spasm of the sigmoid colon caused by intense adjacent inflammation. **(B)** The pericolic abscess is clearly filled with contrast material (*arrows*).

diverticular neck causes inflammation of the mucosal lining, which then leads to perforation of the diverticulum. This usually results in a localized peridiverticular abscess that is walled off by fibrous adhesions. The inflammatory process may localize within the wall of the colon and produce an intramural mass, or it may dissect around the colon, causing segmental narrowing of the lumen. Extension of the inflammatory process along the colon wall can involve adjacent diverticula, resulting in a longitudinal sinus tract along the bowel wall. A common complication of diverticulitis is the development of fistulas to adjacent organs (bladder, vagina, ureter, and small bowel).

Imaging appearance. The radiographic diagnosis of diverticulitis requires direct or indirect evidence of diverticular perforation. The most specific sign is extravasation, which can appear either as a tiny projection of contrast material from the tip of a diverticulum (Figure 5-65A) or as an obvious filling of a pericolic abscess (Figure 5-65B). A more common, although somewhat less specific, sign of diverticulitis is the demonstration of a pericolic soft tissue mass that

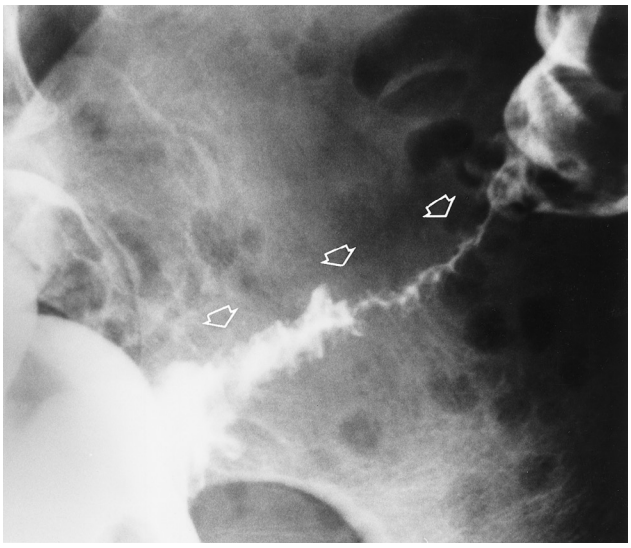

FIGURE 5-66 Sigmoid diverticulitis. Severe narrowing of the long involved portion of the sigmoid colon (*arrows*) in a patient with no radiographically detectable diverticula.

is attributable to a localized abscess and represents a walled-off perforation. This extraluminal mass appears as a filling defect causing eccentric narrowing of the bowel lumen. The adjacent diverticula are spastic, irritable, and attenuated and frequently seem to drape over the mass. It is important to remember, however, that a peridiverticular abscess caused by diverticulitis can occur without radiographically detectable diverticula (Figure 5-66).

Severe spasm or fibrotic healing of diverticulitis can cause a rigidity and progressive narrowing of the colon that simulates annular carcinoma. Although radiographic distinction from carcinoma may be impossible, findings favoring the diagnosis of diverticulitis include the involvement of a relatively long segment, a gradual transition from diseased to normal colon, a relative preservation of mucosal detail, and fistulous tracts and intramural abscesses. At times, colonoscopy or surgery may be required to make a definitive diagnosis.

Acute diverticulitis on ultrasound appears as a hypoechoic projection that arises from the wall of the bowel and is surrounded by inflamed fat. CT demonstrates pericolic fluids or gas collections, usually with nonspecific colonic wall thickening that produces narrowing of the bowel lumen (Figure 5-67). Inflammatory stranding may appear in the adjacent fat.

Treatment of diverticulosis and diverticulitis. Noninvasive treatment is the first choice for diverticulosis, with use of dietary modifications (nothing with seeds, nuts, popcorn, etc.) and exercise (to increase peristalsis). If diverticulitis has developed, antibiotics and diet adjustments (liquids) are given until the bowel heals. Perforation requires surgical repair and a regimen of antibiotics.

Ulcerative Colitis

Ulcerative colitis is one of the two major inflammatory bowel diseases (the other is Crohn's colitis; see later discussion).

FIGURE 5-67 Diverticulitis. CT scan illustrates thickened small bowel wall. The tissue has a "dirty" appearance (*arrow*).

It primarily affects young adults and is highly variable in severity, clinical course, and ultimate prognosis. The cause is unknown, although an autoimmune cause has been suggested and a psychogenic factor may be involved because the condition is often aggravated by stress. The onset of the disease and subsequent exacerbations can be insidious or abrupt. The main symptoms are bloody diarrhea, abdominal pain, fever, and weight loss. A characteristic feature of ulcerative colitis is alternating periods of remission and relapse. Most patients have intermittent episodes of symptoms, with complete remission between attacks. In fewer than 15% of patients, ulcerative colitis is an acute severe process with a far higher incidence of serious complications, such as toxic megacolon (extreme dilation of a segment of colon with systemic toxicity) and free perforation into the peritoneal cavity. Usually, ulcerative colitis involves only the mucosal layer of the colon.

Imaging appearance. In the radiographic evaluation of a patient with known or suspected ulcerative colitis, plain abdominal radiographs are essential. Large nodular protrusions of hyperplastic mucosa, deep ulcers outlined by intraluminal gas, or polypoid changes along with a loss of haustral markings (normal indentations in the wall of the colon) may indicate the diagnosis. Plain abdominal radiographs can also demonstrate evidence of toxic megacolon, a dramatic and ominous complication of ulcerative colitis that is characterized by extreme dilation of a segment of colon (Figure 5-68), or evidence of an entire diseased colon, combined with systemic toxicity (abdominal pain and tenderness, tachycardia, fever, and leukocytosis). Toxic megacolon can lead to spontaneous perforation of the colon, which can be dramatic and sudden and can cause irreversible shock. Because there is such a high danger of spontaneous perforation, barium enema examination is absolutely contraindicated during a recognized attack of toxic megacolon.

Ulcerative colitis has a strong tendency to begin in the rectosigmoid area. Although by radiographic criteria alone the rectum appears normal in approximately 20% of patients with ulcerative colitis, true rectal sparing is infrequent, and

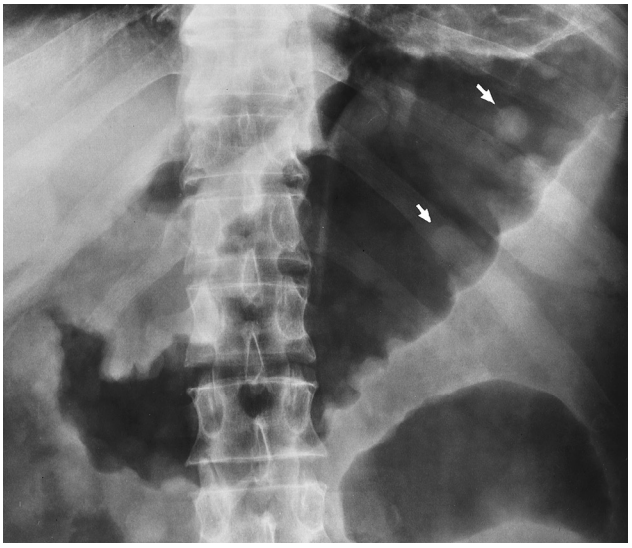

FIGURE 5-68 Toxic megacolon in ulcerative colitis. Note dilation of the transverse colon with multiple pseudopolypoid projections extending into the lumen (*arrows*).

FIGURE 5-69 Ulcerative colitis involving primarily the rectosigmoid. Distal rectosigmoid mucosa (*white arrow*) is finely granular compared with the normal-appearing mucosa (*black arrow*) in the more proximal colon.

there is usually evidence of disease on sigmoidoscopy or rectal biopsy. Isolated right colon disease with a normal left colon does not occur, and ulcerative colitis may spread to involve the entire colon (pancolitis). The disease is almost always continuous, without evidence of the skip areas seen in Crohn's disease. Except for "backwash ileitis" (minimal inflammatory changes involving a short segment of terminal ileum), ulcerative colitis does not involve the small bowel, a feature distinguishing it from Crohn's disease, which may involve both the large and the small intestines.

On double-contrast studies, the earliest detectable radiographic abnormality in ulcerative colitis is fine granularity of the mucosa corresponding to the hyperemia and edema seen endoscopically (Figure 5-69). Once superficial ulcers develop, small flecks of adherent barium produce a stippled mucosal pattern. As the disease progresses, the ulcerations become deeper. Extension into the submucosa may produce broad-based ulcers with a collar-button appearance (Figure 5-70). Perirectal inflammation can cause widening of the soft tissue space between the anterior sacrum and the posterior rectum (retrorectal space).

When the disease is chronic, fibrosis and muscular spasm cause progressive shortening and rigidity of the colon (Figure 5-71). The haustral pattern is absent, and the bowel contour is relatively smooth because of ulcer healing and subsequent reepithelization. Eventually, the colon may appear as a symmetric, rigid, tubular structure (lead-pipe colon).

Carcinoma of the colon is approximately 10 times more frequent in patients with ulcerative colitis than in the general population. During the first 10 years of disease, there is only a small risk of malignancy. Thereafter, it is estimated that there is a 20% chance per decade that carcinoma will develop in a patient with ulcerative colitis. Malignant lesions in patients with ulcerative colitis generally occur at a much younger age than they occur in the general population, and they tend to be extremely virulent.

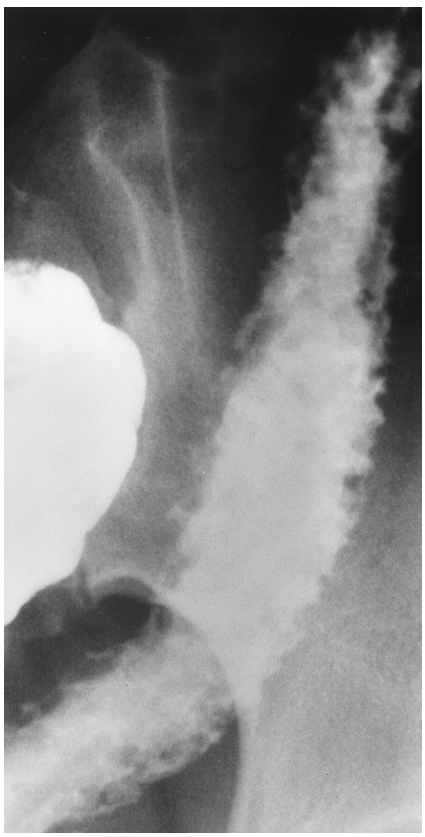

FIGURE 5-70 Ulcerative colitis. Progression of disease results in deep ulcerations (collar-button ulcers) extending into the submucosal layer.

Carcinoma of the colon in patients with chronic ulcerative colitis often appears as a bizarre stricture rather than with the more characteristic polypoid or apple-core appearance of a primary colonic malignancy (Figure 5-72). The tumor typically produces a narrowed segment with an eccentric lumen, irregular

contours, and margins that are rigid and tapered. Because it is frequently difficult to distinguish carcinoma from benign stricture in patients with ulcerative colitis, colonoscopy or surgery is often required for an unequivocal diagnosis.

Crohn's Colitis

Crohn's disease of the colon, the second major cause of inflammatory bowel disease, is identical to Crohn's disease in the small bowel and must be distinguished from ulcerative colitis. The proximal portion of the colon is most frequently involved in Crohn's disease; associated disease of the terminal ileum is seen in up to 80% of affected patients. Unlike in ulcerative colitis, in Crohn's colitis the rectum is often spared, and isolated rectal disease very rarely occurs. Crohn's disease usually has a patchy distribution, with involvement of multiple noncontiguous segments of colon (skip lesions), unlike the continuous colonic involvement in ulcerative colitis. Perirectal abnormalities (fissures, abscesses, and fistulas) occur at some point during the course of disease in half of patients with Crohn's colitis but are rare in those with ulcerative colitis. Crohn's disease involves all layers of the GI tract.

FIGURE 5-71 Chronic ulcerative colitis (lead-pipe colon). Muscular hypertrophy and spasm cause shortening and rigidity of the colon with loss of haustral markings.

Imaging appearance. The earliest radiographic findings in Crohn's disease of the colon are seen on double-contrast examinations. Isolated tiny, discrete erosions (aphthous ulcers) appear as punctate collections of barium with a thin halo of edema around them (Figure 5-73). Aphthous ulcers in Crohn's disease have a patchy distribution against a background of normal mucosa, unlike the blanket of abnormal granular mucosa seen in ulcerative colitis.

As Crohn's colitis progresses, the ulcers become deeper and more irregular, with a great variation in size, shape, and overall appearance. Deep linear, transverse, and longitudinal ulcers often separate intervening mounds of edematous but nonulcerating mucosa, producing a characteristic cobblestone appearance (see Figure 5-43). If the penetrating ulcers extend beyond the contour of the bowel, they can coalesce (grow together) to form long tracts running parallel to the long axis of the colon (Figure 5-74). The penetration of ulcers into adjacent loops of bowel or into the bladder, vagina, or abdominal wall causes fistulas, which can often be demonstrated radiographically. Inflammatory and fibrotic thickening of the bowel wall leads to narrowing of the lumen and stricture formation. Occasionally, an eccentric stricture with a suggestion of overhanging edges can be difficult to distinguish from annular carcinoma (Figure 5-75). In most instances, however, characteristic features of Crohn's disease elsewhere in the colon (deep ulcerations, pseudopolyps, skip lesions, sinus tracts, and fistulas) clearly indicate the correct diagnosis.

CT demonstrates the mesenteric and extraintestinal extent of the disease and also any abscess formation or colonic wall

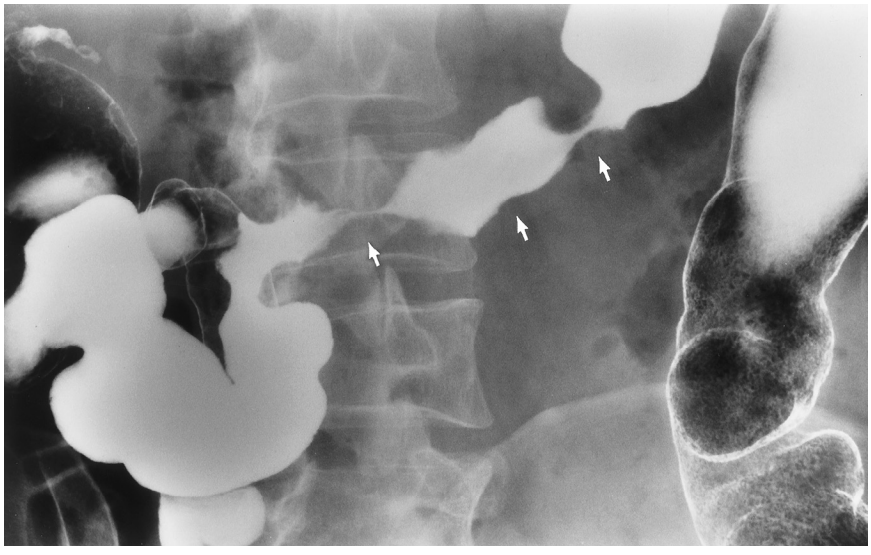

FIGURE 5-72 Carcinoma of the colon developing in a patient with long-standing chronic ulcerative colitis. A long, irregular lesion with a bizarre pattern is visible in the transverse colon (*arrows*).

FIGURE 5-73 Crohn's colitis. Diffuse aphthous ulcers (*arrowheads*) in early Crohn's colitis.

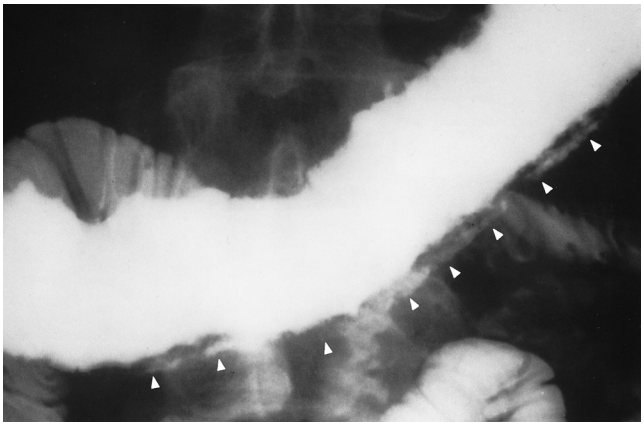

FIGURE 5-74 Crohn's colitis. Note long intramural fistula (*arrowheads*) in the transverse colon.

thickening. Magnetic resonance (MR) spectroscopy is currently under investigation as a way to help distinguish ulcerative colitis from Crohn's colitis. Preliminary results indicate that this technique is able to differentiate between the two inflammatory bowel diseases in more than 90% of cases.

Patients with Crohn's colitis appear to have a higher incidence of developing colon cancer than the general population, although this association is less striking than that between colon cancer and ulcerative colitis. Carcinoma complicating Crohn's colitis is most common in the proximal portion of the colon and usually appears radiographically as a fungating mass with typical malignant features, unlike the mildly irregular stricture characteristic of colon cancer in patients with ulcerative colitis. A small bowel examination may be necessary to demonstrate the terminal ileum.

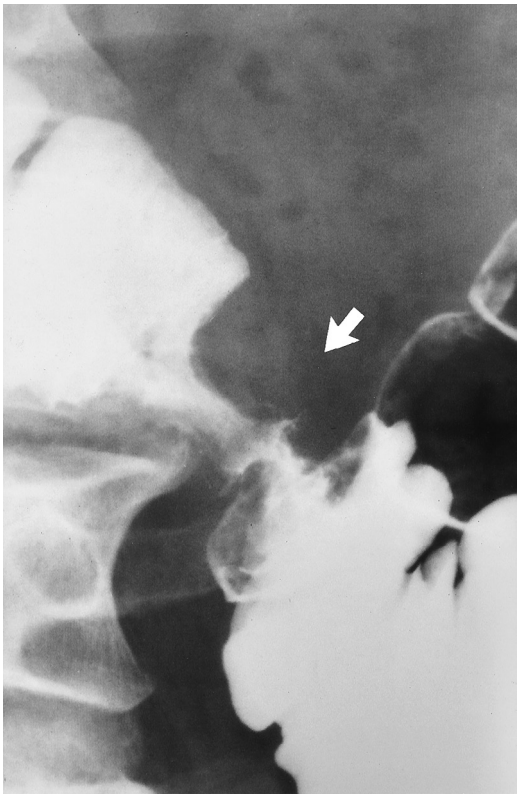

FIGURE 5-75 Chronic Crohn's colitis. Benign stricture with overhanging edges in the transverse colon simulates carcinoma (*arrow*).

Summary of Findings for Inflammatory Disease—Colitis

Disorder	Location	Involvement	Layers
Ulcerative	Rectal involvement in 95% of cases; moves proximally	Continuous	Only mucosal layer
Crohn's	Proximal colon (terminal ileum in 80% of cases)	Patchy	All intestinal wall layers (Mucosal through serosal layer)

Treatment of Ulcerative Colitis and Crohn's Colitis

The initial treatments for ulcerative colitis and Crohn's disease are identical because both are inflammatory bowel diseases. First, nutritional supplements and dietary modifications (decrease bulk to reduce stool frequency) begin to diminish the inflammatory process. A regimen of anti-inflammatory drugs interrupts the inflammatory cycle. Stress-related conditions require psychological support to control episodes. For ulcerative colitis, surgical resection may be necessary to prevent the spread of the condition. With proper treatment or spontaneous remission, many of the radiographic changes in this disease are reversible. In Crohn's colitis, surgery is usually ineffective

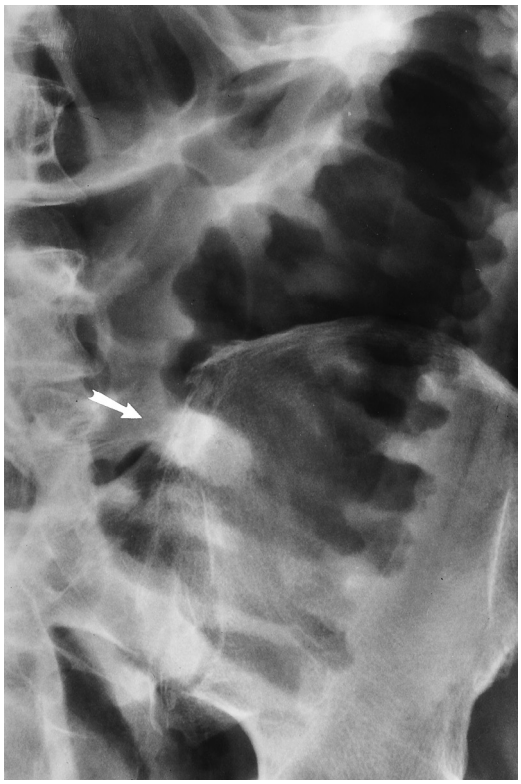

FIGURE 5-76 Ischemic colitis. Soft tissue polypoid densities (*arrow*) protrude into the lumen of the descending colon in a patient with acute abdominal pain and rectal bleeding.

because the area adjacent to the anastomosis becomes involved as a result of the resection. For severe cases of the disorder, parenteral (IV) nutrition allows the intestine time to heal.

Ischemic Colitis

Ischemic colitis is characterized by the abrupt onset of lower abdominal pain and rectal bleeding. Diarrhea is common, as is abdominal tenderness on physical examination. Most patients are older than 50 years, and many have a history of prior cardiovascular disease.

Imaging appearance. The initial radiographic appearance of ischemic colitis is fine superficial ulceration caused by inflammatory edema of the mucosa. As the disease progresses, deep penetrating ulcers, pseudopolyps, and characteristic thumbprinting can be demonstrated. *Thumbprinting* refers to sharply defined, finger-like indentations along the margins of the colon wall (Figure 5-76). In most cases, the radiographic appearance of the colon returns to normal within 1 month if good collateral circulation is established. Extensive fibrosis during the healing phase can cause tubular narrowing and a smooth stricture. If blood flow is insufficient, acute bowel necrosis and perforation may result.

Treatment. In some cases, no intervention is needed because the bowel heals itself. Patients taking vasoconstricting drugs are most susceptible, and when the diagnosis is ischemic colitis, these medications are discontinued and supportive care is given. Immediate surgical intervention is required for bowel infarctions and other complications.

Irritable Bowel Syndrome

Irritable bowel syndrome refers to several conditions that have an alteration in intestinal motility as the underlying pathophysiologic abnormality. Most consider these conditions to be functional disorders because there is a disruption of the food sequence breakdown in the stomach and intestines. Patients with irritable bowel syndrome may complain primarily of chronic abdominal pain and constipation (spastic colitis); chronic intermittent watery diarrhea, often without pain; or alternating bouts of constipation and diarrhea.

Imaging appearance. Although there are no specific radiographic findings in irritable bowel syndrome, patients with this condition usually undergo a barium enema examination to exclude another chronic disorder as the cause of the symptoms. When the patient is symptomatic, a barium enema may demonstrate areas of irritability and spasticity and accentuated haustration, although similar radiographic findings may be observed in normal asymptomatic persons, especially those who have received laxatives and enemas.

Treatment. No cure exists for irritable bowel syndrome. Because the precise cause of this functional disorder has not been determined, symptomatic relief is provided. It is necessary to identify trigger foods so that they can be avoided, thus decreasing the spasms and pain. Alternative therapies, relaxation, meditation, and physical exercise have value if the patient can use them to help ease some of the spasms and pain.

Cancer of the Colon

Carcinoma of the colon and rectum is the third leading cause of death from cancer in the United States. Even though colon and rectal cancer can be more easily diagnosed than most other malignant neoplasms, it remains a leading cause of death. Approximately half of colon carcinomas occur in the rectum and sigmoid, where they can be felt by rectal examination or seen with a sigmoidoscope. Carcinoma of the colon and rectum is primarily a disease of older persons, with a peak incidence in the 50- to 70-year range, and twice as common in men. Two diseases predispose to the development of cancer of the colon: long-standing ulcerative colitis and familial polyposis, a hereditary disease in which innumerable polyps develop in the colon and elsewhere in the intestinal tract.

Imaging appearance. Because cancer of the colon is curable if discovered early in its course, delay in diagnosis is the most significant factor in the poor prognosis. There is considerable evidence to indicate that many, if not most, carcinomas of the colon arise in preexisting polyps. Therefore, the early diagnosis of colonic cancer depends on polyp detection. Malignant polyps (Figure 5-77) tend to be sessile lesions (without stalks) with an irregular or lobulated surface, unlike benign polyps, which are usually smooth and often have a stalk (are pedunculated). Other radiographic criteria suggestive that a polyp is malignant include large size (especially if more than 2 cm in diameter), retraction or indentation (puckering) of the colon wall seen on profile view at the site of origin of a sessile polyp, and evidence of interval growth of a polyp on sequential examinations.

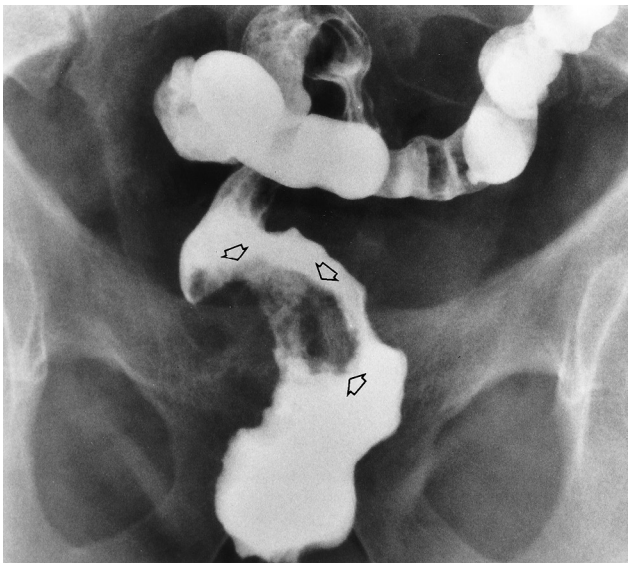

FIGURE 5-77 Carcinoma of the rectum. Bulky lesion (*arrows*) could be felt on rectal examination.

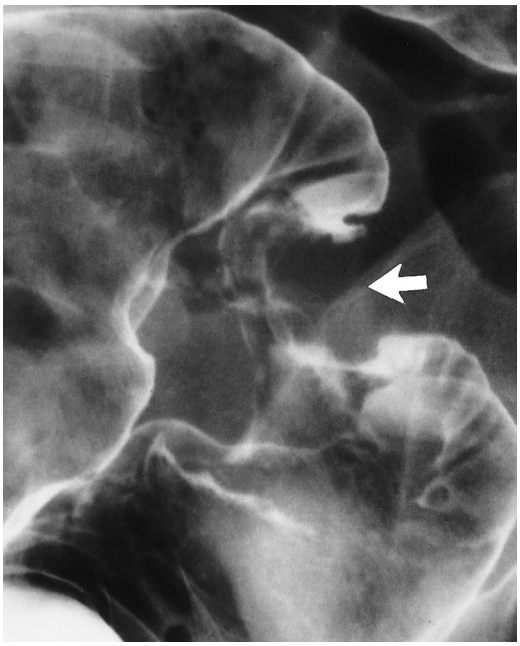

FIGURE 5-78 Annular carcinoma of the sigmoid colon. Note the sharply defined proximal and distal margins of this relatively short, apple-core lesion (*arrow*).

Annular carcinoma (described as apple-core or napkin-ring carcinoma) is one of the most typical forms of primary colonic malignancy (Figure 5-78). Annular carcinomas appear to arise from flat plaques of tumor (saddle lesions) that involve only a portion of the circumference of the colon wall. Unless meticulous care is taken to search for an area of minimal straightening or slight contour defects, the small and subtle, but lethal, saddle carcinoma can be easily overlooked. As the tumor grows, it characteristically infiltrates the bowel wall rather than forming a bulky intraluminal mass. This produces a classic bilateral contour defect with ulcerated mucosa,

FIGURE 5-79 CT scan of a patient with rectal carcinoma. Shows a soft tissue mass on the lateral wall of the rectum containing a central ulceration (*straight arrows*). Thickening of the perirectal fascia (*curved arrow*), the presence of multiple lymph nodes (on the more cephalic images), and increased soft tissue density of perirectal fat were suggestive of tumor extension beyond the bowel wall, which was confirmed at surgery.

eccentric and irregular lumen, and overhanging margins. Progressive constriction of the bowel can cause complete colonic obstruction, most commonly in the sigmoid region.

Ulceration is common in carcinoma of the colon. It can vary from an excavation within a large fungating mass to mucosal destruction within an annular apple-core tumor.

A patient with carcinoma of the colon has a 1% risk of having multiple synchronous (occurring simultaneously) colon cancers. Therefore, it is essential to carefully examine the rest of the colon once an obviously malignant lesion has been detected. In addition, such a patient has a 3% risk of developing additional metachronous cancers later.

CT virtual colonoscopy has become more frequently used as a screening tool for colon cancer. Today, two- or three-dimensional CT colonoscopy can demonstrate lesions of 8 to 10 mm with an accuracy similar to that obtained with traditional colonoscopy. CT virtual colonoscopy is an alternative for incomplete or equivocal results of traditional colonoscopy. CT is also the modality of choice for staging carcinoma of the colon and for assessing tumor recurrence (Figure 5-79). Carcinoma causes asymmetrical or circumferential thickening of the bowel wall with narrowing and deformity of the lumen. CT can demonstrate local extension of tumor to the pelvic organs as well as lymphadenopathy and metastases to the adrenal glands or liver (Figure 5-80).

Transrectal ultrasound produces the most accurate images for staging of local rectal cancer by demonstrating the depth of invasion within the bowel wall. Ultrasound also may determine the presence of a tumor in adjacent, normal-size lymph nodes.

FIGURE 5-80 Lymphadenopathy. CT scan shows retroperitoneal and periaortic lymphadenopathy (*arrows*) in a 51-year-old woman with colon cancer.

Positron emission tomography (PET) with ^{18}F-fluorodeoxyglucose (FDG–PET), although less specific than CT and ultrasound, has a higher accuracy for detecting distant nodular metastases. Fusion imaging, which superimposes the functional (PET) and anatomic (CT) studies, provides more specific detail to localize and evaluate the severity of the disease process.

Treatment. Surgical resection is required to remove a solitary carcinoma. Postoperative treatment may involve chemotherapy or radiation therapy. Following resection, FDG–PET in combination with a CT scan helps rule out recurrence. FDG–PET images can differentiate recurrence of the tumor from adhesions or scar tissue resulting from the resection. The presence of multiple lesions requires irradiation and chemotherapy.

Large Bowel Obstruction

Approximately 70% of large bowel obstructions result from primary colonic carcinoma. Diverticulitis and volvulus account for most other cases. Colonic obstructions tend to be less acute than small bowel obstructions; the symptoms develop more slowly, and fewer fluid and electrolyte disturbances are produced.

Imaging appearance. The radiographic appearance of colonic obstruction depends on the competency of the ileocecal valve. If the ileocecal valve is competent, obstruction causes a large, dilated colon with a greatly distended, thin-walled cecum and little small bowel gas (Figure 5-81). The colon distal to the obstruction is usually collapsed and free of gas. If the ileocecal valve is incompetent, there is distention of gas-filled loops of both colon and small bowel, which may simulate an adynamic ileus.

The major danger in colonic obstruction is perforation. If the ileocecal valve is competent, the colon behaves like a closed loop, and the increased pressure caused by the obstruction cannot be relieved. Because the cecum is spherical and has a large diameter, it is the most likely site for perforation. In acute colonic obstruction, perforation is very likely if the

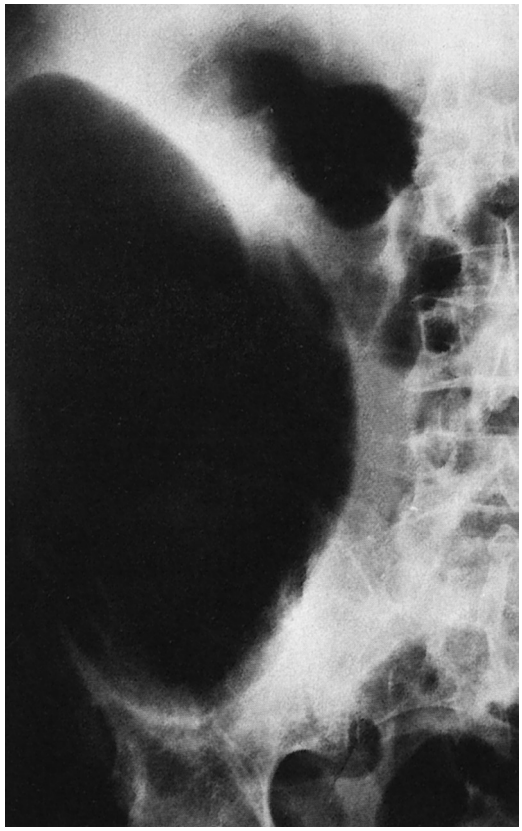

FIGURE 5-81 Large bowel obstruction. Huge dilation of cecum (up to 13 cm in diameter) without perforation.

cecum distends to more than 10 cm; in intermittent or chronic obstruction, however, the cecal wall can become hypertrophied, and the diameter of the cecum can greatly exceed 10 cm without perforation (see Figure 5-81). In the patient with suspected large bowel obstruction, a low-pressure barium enema can be safely performed (Figure 5-82) and demonstrates the site and often the cause of the obstruction (Figure 5-83).

Some professionals recommend an abdominal/pelvic CT scan as an initial examination, especially for patients without a surgical history who have symptomatic signs suggesting infection, bowel infarction, or a palpable mass. CT can demonstrate causes of an obstruction, such as diverticulitis or appendicitis.

Volvulus of the Colon

Volvulus refers to a twisting of the bowel on itself that may lead to intestinal obstruction. Because twisting of the bowel usually requires a long, movable mesentery, volvulus of the large bowel most frequently involves the cecum and sigmoid colon. The transverse colon, which has a short mesentery, is rarely affected by volvulus. A sigmoid volvulus, more commonly found in the elderly, results from a low-fiber diet causing constipation.

Cecal Volvulus

The ascending colon and the cecum may have a long mesentery as a fault of rotation and fixation during the embryonic

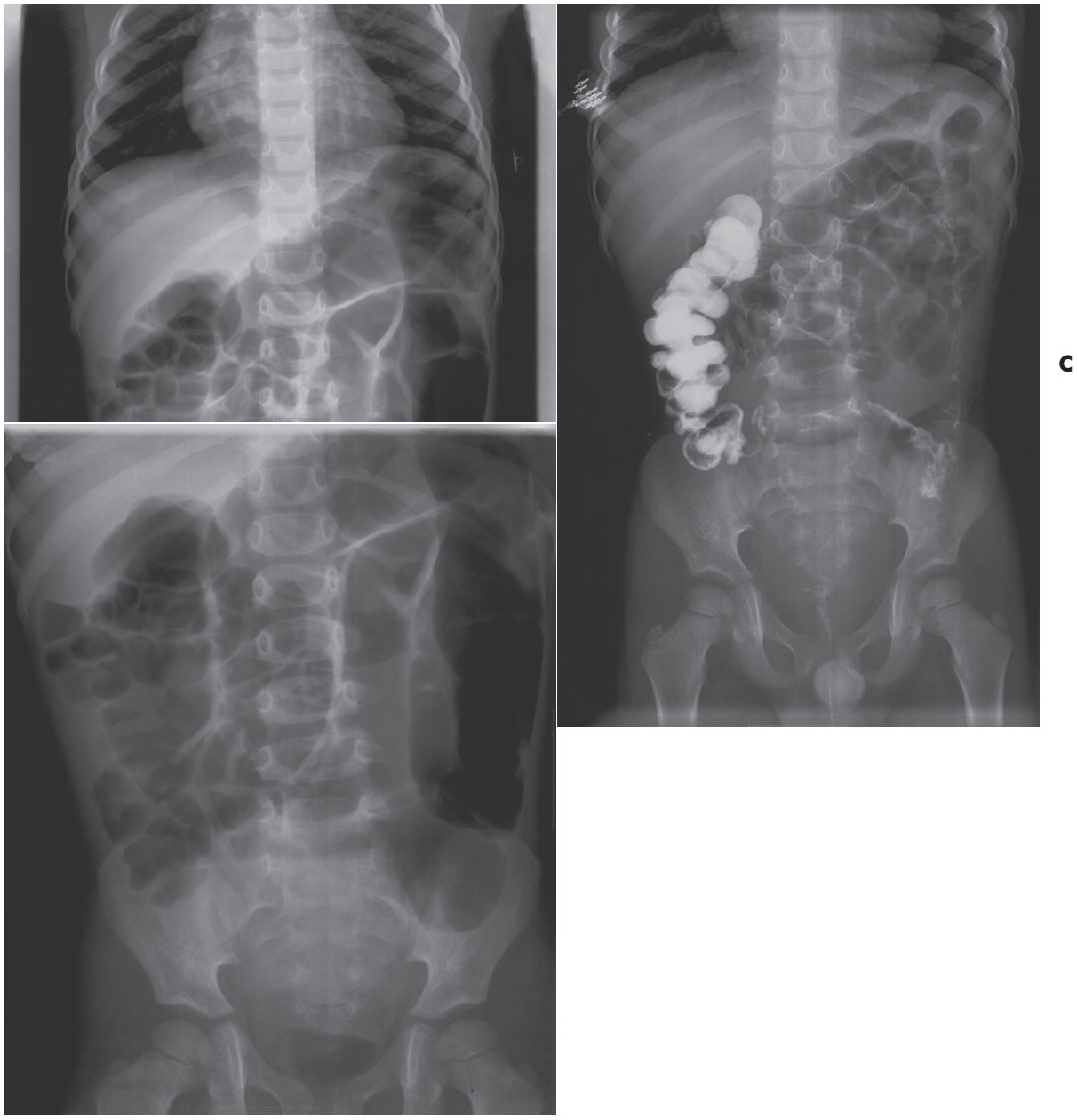

FIGURE 5-82 Large bowel obstruction. Upper (A) and lower (B) abdominal radiographs in a 4-year-old illustrate a gas pattern indicating a large bowel obstruction. A low-pressure barium enema was performed to relieve the obstruction, as seen on the post-evacuation view. (C) As barium is seen in the cecum.

development of the gut. This situation predisposes to volvulus, with the cecum twisting on its long axis. It should be stressed, however, that cecal volvulus develops in only a few patients with an extremely mobile cecum.

Imaging appearance. In cecal volvulus, the distended cecum tends to be displaced upward and to the left, although it can be found anywhere within the abdomen. A pathognomonic sign of cecal volvulus is a kidney-shaped mass (representing the twisted cecum) with the twisted and thickening mesentery mimicking the renal pelvis (Figure 5-84A). A barium enema examination is usually required for definite confirmation of the diagnosis. This study demonstrates obstruction of the contrast column at the level of the stenosis, with the tapered edge of the column pointing toward the site of the twist (Figure 5-84B).

Sigmoid Volvulus

A long, redundant loop of sigmoid colon can undergo a twist on its mesenteric axis and form a closed-loop obstruction. In sigmoid volvulus, the greatly inflated sigmoid loop appears as an inverted U-shaped shadow that rises out of the pelvis in a vertical or oblique direction and can even reach the level of the diaphragm. The affected loop appears devoid of haustral markings and has a sausage or balloon shape.

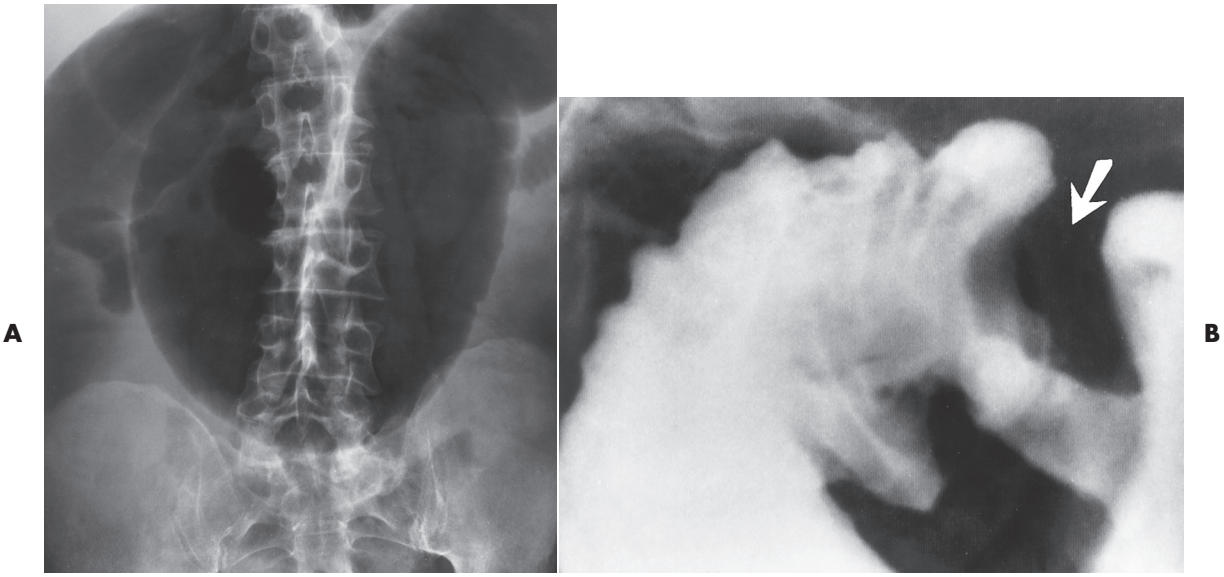

FIGURE 5-83 Large bowel obstruction caused by annular carcinoma of the sigmoid. **(A)** Plain abdominal radiograph demonstrates pronounced dilation of the gas-filled transverse and ascending colon. **(B)** Barium enema demonstrates typical apple-core lesion (*arrow*) producing the colonic obstruction.

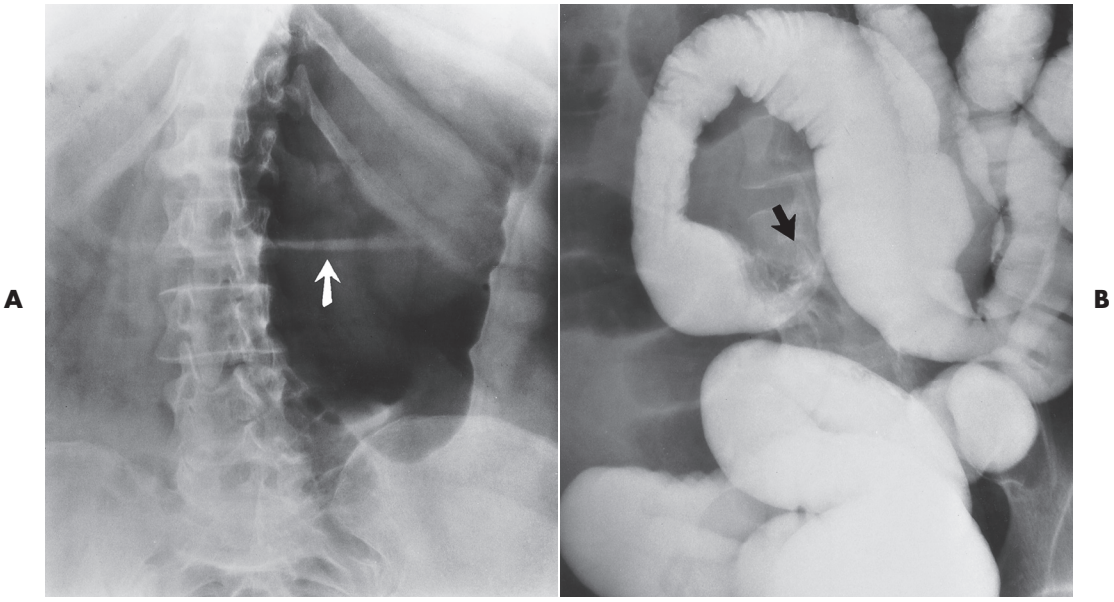

FIGURE 5-84 Cecal volvulus. **(A)** The dilated, gas-filled cecum appears as a kidney-shaped mass with twisted and thickening mesentery (*arrow*) mimicking the renal pelvis. **(B)** Barium enema examination demonstrates obstruction of the contrast column at the level of the stenosis (*arrow*); the tapered edge of the column points toward the torsion site.

Imaging appearance. A barium enema examination demonstrates an obstruction to the flow of contrast material at the site of volvulus and considerable distention of the rectum. The lumen of the sigmoid tapers toward the site of stenosis, and a pathognomonic bird's-beak appearance is produced (Figure 5-85).

Treatment for large bowel obstruction or volvulus. Surgical detorsion is usually required for large bowel obstruction or volvulus, although a water-soluble enema may be therapeutic and resolve the obstruction.

Hemorrhoids

Hemorrhoids are varicose veins of the lower end of the rectum that cause pain, itching, and bleeding. Like varicose veins in the leg, hemorrhoids are caused by increased venous pressure. The most common cause of increased pressure is chronic constipation with resulting excessive muscular straining needed to empty the bowel. Increased venous pressure can also be produced by a pelvic tumor or a pregnant uterus.

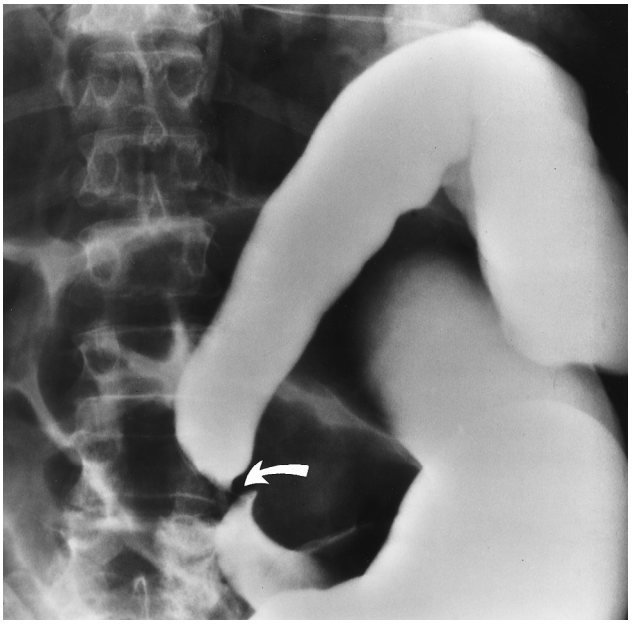

FIGURE 5-85 Sigmoid volvulus. Luminal tapering at site of stenosis produces characteristic bird's beak configuration.

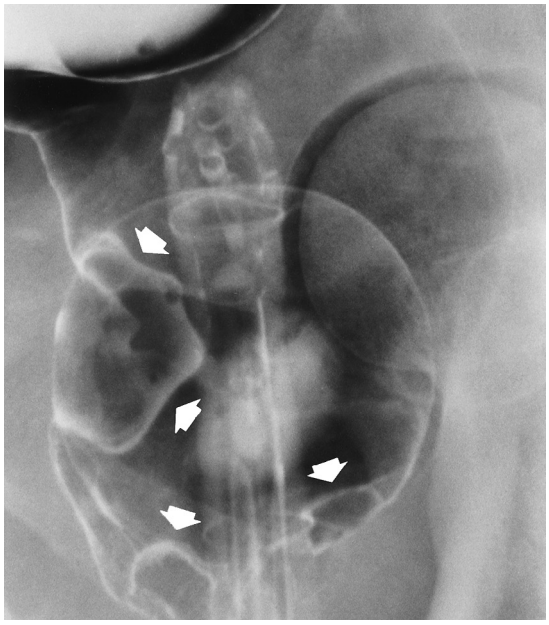

FIGURE 5-86 Hemorrhoids. Multiple rectal filling defects (*arrows*) simulate polyps.

Imaging appearance. On barium enema examinations, hemorrhoids occasionally can produce single or multiple rectal filling defects that simulate polyps (Figure 5-86). The proper diagnosis can easily be made by inspection, digital examination, or direct vision through the anoscope.

Treatment. Hemorrhoids may be treated nonsurgically and surgically. The nonsurgical approach consists of rubber band ligation. The surgical intervention consists of circumferential mucosectomy, which is a stapled hemorrhoidectomy, a safe and effective procedure for advanced stages (third- and fourth-degree hemorrhoidal prolapse).

Summary of Findings for the Colon

Disorder	Location	Imaging Appearance	Treatment
Appendicitis	Appendix	KUB—appendicolith US—noncompressible 7-mm or larger outer diameter CT—round or oval mass, possibly containing gas; dilated lumen with thickened, circumferentially enhancing wall	Appendectomy should be performed before perforation
Diverticulosis	Most common in sigmoid	Round or oval outpouching projecting beyond lumen; usually multiple	Noninvasive: Dietary modifications and exercise Antibiotics for diverticulitis
Diverticulitis	Inflammation of diverticula	Diverticular perforation with possible abscess US—hypoechoic projection surrounded by inflamed fat CT—nonspecific wall thickening with a narrowed bowel lumen	Invasive: surgery for perforated diverticula
Ulcerative colitis	Superficial and acute; beginning in rectosigmoid area with continuous involvement throughout colon	KUB—deep ulcers with intraluminal gas or polypoid changes, loss of haustral markings BE (double contrast)—fine granularity of mucosa; submucosa with broad-based ulcers having a collar-button appearance	Nutritional supplements Dietary modifications (to decrease bulk) Anti-inflammatory drugs Surgical resection for severe ulcerative colitis
Crohn's disease	Terminal ileum and proximal colon most often	BE (double contrast)—patchy distribution, noncontiguous segments (skip lesions) CT—colonic wall thickening and abscess formation	Nutritional supplements Dietary modifications (to decrease bulk) Anti-inflammatory drugs

Summary of Findings for the Colon—Cont'd

Disorder	Location	Imaging Appearance	Treatment
Ischemic colitis	Entire colon	Fine superficial ulceration Characteristic "thumbprinting" Tubular narrowing and a smooth stricture	Many cases resolve spontaneously Restrict vasoconstrictor drugs and give supportive care Immediate surgery for infarctions and complications
Irritable bowel syndrome	Alteration of intestinal motility	No specific findings Rule out other disorders	No cure exists; treatments aid in alleviating the symptoms Identification and avoidance of trigger foods to reduce pain Alternative therapies: relaxation, meditation to reduce stress
Cancer	50% in rectum and sigmoid region	Sessile lesion: irregular, lobulated surface Larger than 2 cm: "apple-core" or "napkin-ring" appearance CT: • Circumferential bowel wall thickening, metastasis, lymphadenopathy • Virtual colonoscopy demonstrates 8- to 10-mm lesions US—transrectal; depth of tumor invasion into bowel wall PET—detection of distant nodular metastasis Fusion (PET/CT) imaging provides the most specific detail	Solitary lesion: surgical resection, with or without chemotherapy Multiple or distant lesions: chemotherapy and/or radiation therapy
Large bowel obstruction	Large bowel	Ileocecal valve competent: large dilated colon, thin-walled cecum, little small-bowel gas Ileocecal valve incompetent: gas-filled loops of colon and of small bowel	Surgical detorsion
Volvulus	Cecal or sigmoid colon	Distended cecum, displaced upward and to the left Distended rectum, devoid of haustral markings, and a sausage or balloon shape Bird's-beak appearance	Water-soluble enema may be therapeutic
Hemorrhoids	Distal rectum	Single or multiple rectal filling defects simulating polyps	Nonsurgical—rubber-band ligations Surgical—circumferential mucosectomy

BE, barium enema examination; *KUB,* kidney–ureter–bladder radiograph; *US,* ultrasound.

GALLBLADDER

Gallstones (Cholelithiasis)

Gallstones consist of two major types: cholesterol stones and pigment stones. Cholesterol stones are predominant (75%) in the United States, whereas pigment stones occur more frequently in the tropics and Asian countries. Genetic predispositions associated with higher incidence include family history of the disorder, age older than 40 years, excess weight, and female sex. Gallstones can develop whenever bile contains insufficient bile salts and lecithin in proportion to cholesterol to maintain the cholesterol in solution. This situation can result from a decrease in the amount of bile salts present (because of decreased reabsorption in the terminal ileum as a result of inflammatory disease or surgical resection), or it can be caused by increased hepatic synthesis of cholesterol.

Imaging appearance. Because cholesterol is not radiopaque, most gallstones are radiolucent and visible only on contrast examinations or ultrasound. In up to 20% of patients, however, gallstones contain sufficient calcium to be detectable on plain abdominal radiographs (Figure 5-87). Gallstones can have a central nidus (or focus) of calcification, a laminated appearance (with alternating opaque and lucent rings), or calcification around the periphery. Occasionally, a nonopaque stone may contain gas-filled fissures that produce the Mercedes-Benz sign, a characteristic triradiate pattern similar to the German automobile trademark (Figure 5-88).

Oral cholecystography (OCG) was the traditional technique for the diagnosis of gallstones. It is rarely used today because it has been replaced in most institutions by ultrasound (discussed later). Gallstones appear as freely movable filling defects in the opacified gallbladder. They fall by gravity

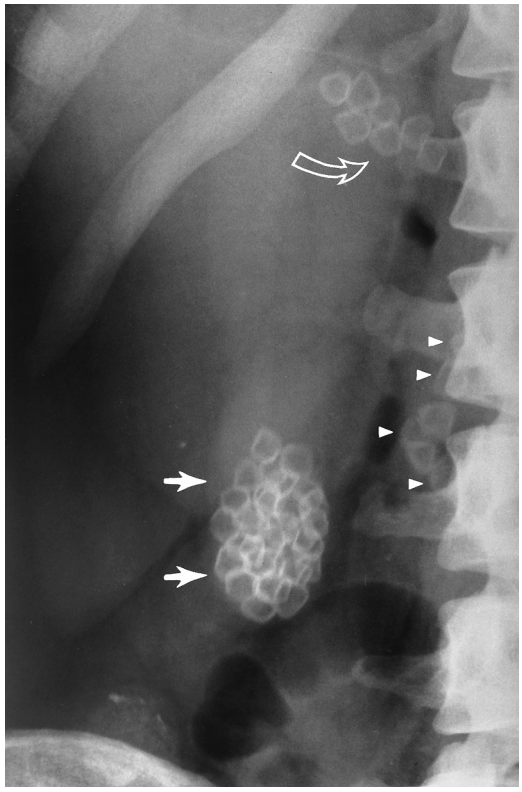

FIGURE 5-87 Cholelithiasis. Calculi in the gallbladder (*solid arrows*) and bile ducts (*open arrow*). Calculi (*arrowheads*) lie in common bile duct, some of which overlie the spine and are difficult to detect.

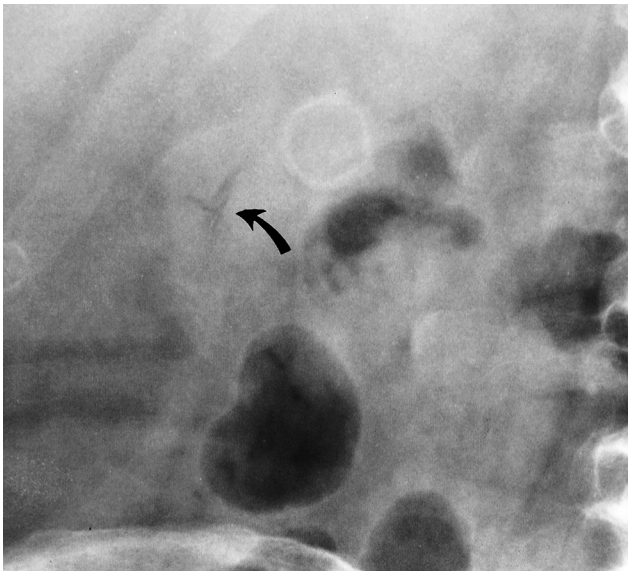

FIGURE 5-88 Cholelithiasis. Mercedes-Benz sign of fissuring in a gallstone (*arrow*). Note the adjacent gallstone with a radiopaque rim.

to the dependent portion of the gallbladder and frequently layer out at a level that depends on the relationship of the specific gravity of the stone to that of the surrounding bile (Figure 5-89). Solitary gallstones are usually rounded; multiple stones are generally faceted. Large numbers of stones can

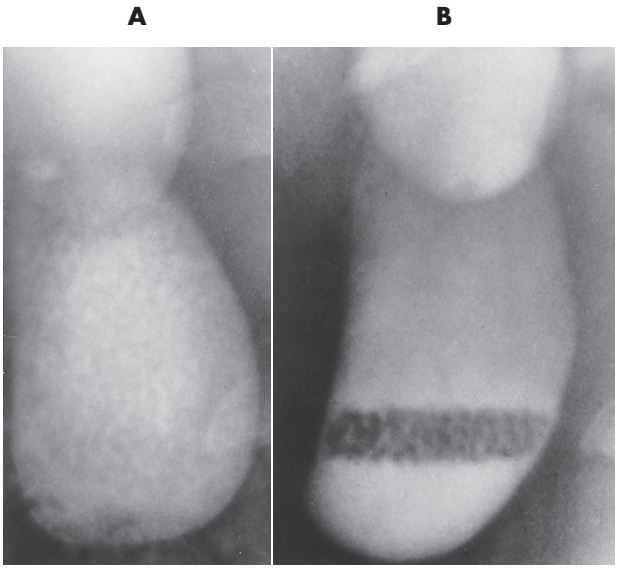

FIGURE 5-89 Oral cholecystogram showing multiple gallstones. **(A)** With the patient supine, the stones are poorly defined and have a gravel-like consistency. **(B)** On an erect image taken with a horizontal beam, the innumerable gallstones layer out and are easily seen.

have a sandlike or gravel-like consistency and be visible only when they layer out on radiographs obtained using a horizontal beam and with the patient in an erect or lateral decubitus position. Infrequently a gallstone is coated with tenacious mucus and adheres to the gallbladder wall.

Malabsorption of the radiopaque contrast material, hepatocellular dysfunction (serum bilirubin value ≥2 mg/dL), and intrinsic disease of the gallbladder (cystic duct obstruction and chronic cholecystitis) can lead to nonvisualization of the gallbladder on OCG. If these causes can be excluded, failure of the gallbladder to opacify after the administration of two doses of orally administered cholecystographic contrast material is highly reliable evidence of gallbladder disease.

Ultrasound is now the imaging modality of choice for demonstrating gallstones. This noninvasive technique is as accurate as OCG, is independent of hepatic function, and does not rely on patient compliance in taking oral contrast agents. In addition to imaging the gallbladder, ultrasound can provide important additional information by effectively demonstrating the biliary tree and hepatic parenchyma. Gallstones appear on ultrasound as foci of high-amplitude echoes associated with posterior acoustic shadowing (Figure 5-90). The mobility of free-floating gallstones may be demonstrated by performing the examination with the patient in various positions.

Acute Cholecystitis

Acute cholecystitis (inflammation of the gallbladder) usually (in 95% of cases) occurs after obstruction of the cystic duct by an impacted gallstone. Gallstones may injure the mucosal wall, allowing bacteria to enter.

Imaging appearance. Either ultrasound or radionuclide scanning can be used. The ultrasonographic diagnosis of

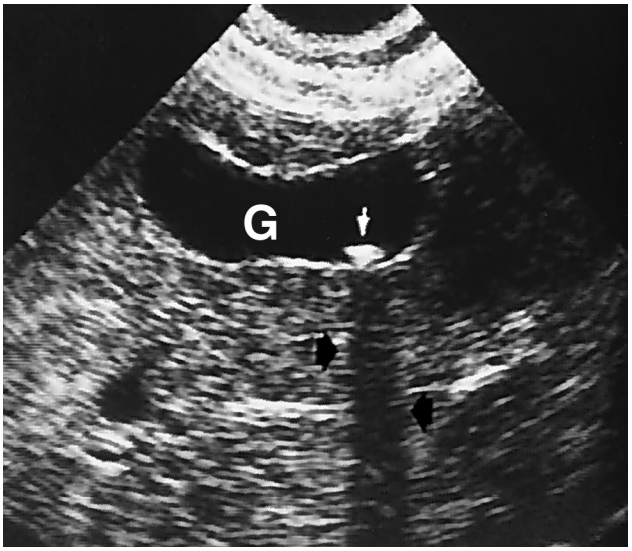

FIGURE 5-90 Ultrasound image of gallstones. Echogenic focus (*white arrow*) in otherwise sonolucent gallbladder (G) represents a large gallstone. Note the acoustic shadowing immediately inferior to the stone (*black arrows*).

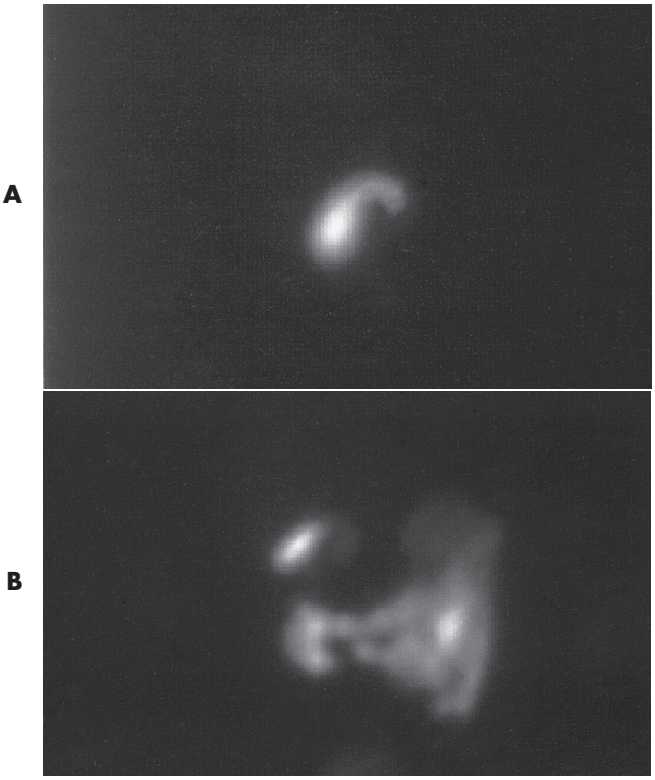

FIGURE 5-91 Acute cholecystitis. (A) Radionuclide hepatobiliary study using technetium-99m disofenin in a 51-year-old woman with right upper quadrant pain demonstrates an engorged gallbladder at 1 hour after injection. **(B)** At 28 minutes after injection of cholecystokinin (CCK), the gallbladder can be seen emptying into the small bowel with an ejection fraction of 83%, which is normal.

acute cholecystitis requires the demonstration of a distended gallbladder containing gallstones. Important additional findings include edema of the gallbladder wall and focal tenderness elicited directly over the gallbladder. A normal gallbladder ultrasound image virtually excludes the diagnosis of acute cholecystitis. Because many disorders may mimic acute cholecystitis, ultrasound can also be used to evaluate the remainder of the right upper quadrant for any other acute abnormality.

When the results of a radionuclide cholescintigram are normal, they demonstrate the bile ducts, the gallbladder, and early excretion of radionuclide into the duodenum and proximal jejunum, within 30 minutes after the IV injection of the radionuclide (technetium-99m) (Figure 5-91). Failure to accumulate radioactivity (after 4 hours) in the gallbladder is highly sensitive (98%) and specific for cystic duct obstruction. If associated with appropriate symptoms, this finding is virtually diagnostic of acute cholecystitis.

When ultrasound findings are inconclusive, MR cholangiopancreatography can demonstrate the cystic duct and any obstructing calculi located in the gallbladder neck. MR imaging (MRI) does not, however, evaluate the gallbladder wall thickness as well as ultrasound.

Emphysematous Cholecystitis

Emphysematous cholecystitis is a rare condition in which the growth of gas-forming organisms in the gallbladder is facilitated by stasis and ischemia caused by cystic duct obstruction (most often by stones). Emphysematous cholecystitis occurs most frequently in elderly men and in patients with poorly controlled diabetes mellitus.

Imaging appearance. Plain abdominal radiographs demonstrate gas in the gallbladder lumen that dissects into the wall or pericholecystic tissues. This produces the pathognomonic appearance of a rim of lucent bubbles or streaks of gas outside of and roughly parallel to the gallbladder lumen (Figure 5-92).

Treatment for cholecystitis. No treatment is necessary for asymptomatic patients. For acute impaction and biliary colic, prompt treatment using an antispasmodic and an analgesic helps alleviate symptoms. Interventional treatments available today include extracorporeal shock wave therapy (lithotripsy), stone removal by endoscopic retrograde cholangiopancreatography (ERCP), and chemical dissolution. The most common surgical approach used currently is laparoscopic cholecystectomy. The radiographer may be requested to obtain images during operative cholangiography to determine ductal blockage and identify remaining stones. Imaging must be performed at the appropriate medium-to-low kVp (70 to 80) at the completion of contrast injection. The contrast agent should be free of air bubbles, which would otherwise simulate stones.

Porcelain Gallbladder

Porcelain gallbladder refers to extensive calcification in the wall of the gallbladder, which forms an oval density that corresponds to the size and shape of the organ (Figure 5-93).

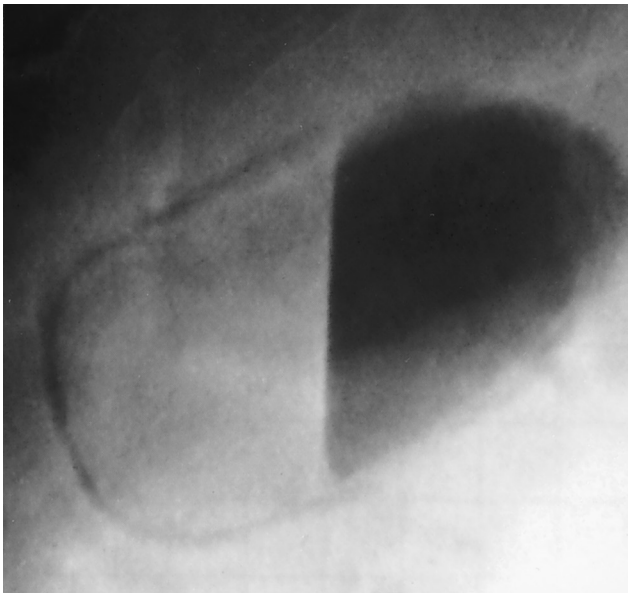

FIGURE 5-92 Emphysematous cholecystitis. Gas is found in both the lumen and the wall of gallbladder.

Because chronic cholecystitis produces a loss of wall function, the gallbladder becomes fibrotic and calcified. The term reflects the blue discoloration and brittle consistency of the gallbladder wall.

Imaging Appearance. The calcification in a porcelain gallbladder can appear as a broad continuous band in the muscular layers, or it may be multiple and punctate and occur in the glandular spaces of the mucosa.

The detection of extensive calcification in the wall of the gallbladder should indicate the possibility of carcinoma. Although a porcelain gallbladder is uncommon in cases of carcinoma of the gallbladder, there is a striking incidence of carcinoma in patients with porcelain gallbladder (up to 60% of the cases).

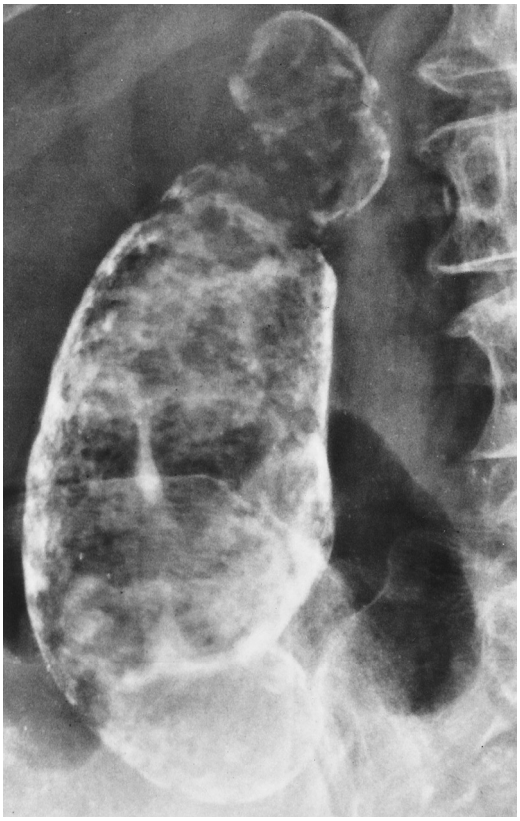

FIGURE 5-93 Porcelain gallbladder. Note the extensive mural calcification around the perimeter of the gallbladder.

Treatment. Because of the high incidence of associated carcinoma, patients with porcelain gallbladder usually undergo prophylactic cholecystectomy even if they are asymptomatic.

Summary of Findings for the Gallbladder

Disorder	Location	Imaging Appearance	Treatment
Gallstones	Gallbladder and biliary tree	KUB—cholelithiasis evident if calcified US—foci of high-amplitude echoes associated with acoustic shadowing	
Acute cholecystitis	Gallbladder and biliary tree	US—demonstrates distended gallbladder containing gallstones and possibly edema of the gallbladder wall NM cholescintigram—failure to accumulate radioactivity after 4 hr MR cholangiopancreatography—demonstrates the cystic duct and obstructing calculi located in gallbladder neck	Asymptomatic: no treatment Noninvasive—lithotripsy; chemical dissolution Invasive—ERCP for stone retrieval; laparoscopic cholecystectomy
Emphysematous cholecystitis	Gallbladder	KUB—demonstrates gas in the gallbladder lumen that dissects into the wall to produce appearance of a rim of lucent bubbles or streaks of gas outside of and roughly parallel to the gallbladder lumen	
Porcelain gallbladder	Extensive calcification in the wall	Broad continuous band of calcification in the muscular layers, or multiple and punctate calcifications in the glandular spaces of mucosa	Prophylactic cholecystectomy

ERCP, endoscopic retrograde cholangiopancreatography; *KUB,* kidney–ureter–bladder radiograph; *NM,* nuclear medicine; US, ultrasound.

LIVER

Hepatitis

Hepatitis is the most prevalent inflammatory disease of the liver. The most common causes are viral infection and reactions to drugs and toxins. The viral types of hepatitis are hepatitis A virus (HAV), hepatitis B virus (HBV), hepatitis C virus (HCV), and hepatitis E virus (HEV).

Hepatitis A virus, previously known as *infectious hepatitis,* is transmitted in the digestive tract from oral or fecal contact. In most cases, HAV is self-contained and has a favorable prognosis.

Hepatitis B virus, previously known as *serum hepatitis,* is contracted by exposure to contaminated blood or blood products, or through sexual contact. Healthcare workers are more susceptible to this virus and are usually required to have been vaccinated or to prove immunity. Ninety percent of patients with HBV recover without incident; however, because of the high incidence (200,000 to 300,000 new cases/year), the vaccine is required as part of the childhood immunization process.

Hepatitis C virus, formerly known as *non-A, non-B hepatitis,* is the common cause of chronic hepatitis, cirrhosis, and hepatocellular carcinoma. Because it is contracted by blood transfusion or sexual contact, some authorities believe that healthcare workers are more susceptible; however, in the general population, the source of 40% of cases is unknown. It is estimated that 50% of patients with HVC-related cirrhosis will develop cancer. In the United States and Western Europe, HCV cirrhosis is the principal cause of liver transplantation.

Hepatitis E virus is self-limited and is acquired by the ingestion of food or water that has been contaminated with fecal material.

Imaging appearance. Viral hepatitis in the earliest stages is not visible on diagnostic images. As the disease progresses, complications of cirrhosis or hepatocellular carcinoma can be demonstrated on ultrasound, CT, and MRI. On ultrasound, cirrhosis due to viral hepatitis usually manifests as macronodules (Figure 5-94), which may vary in size from 3 mm to 5 cm. The liver has an internal coarse texture with increased echogenicity, and the surface may have a nodular appearance representing fibrosis (Figure 5-95). Portal hypertension, due to enlargement or blockage of the portal system, can also be detected. CT demonstrates hepatocellular necrosis with scattered inflammatory cells and evidence of a fatty liver. Normally, the density of the liver is similar to that of the spleen. In fatty liver, infiltrates of fat appear as discrete or diffuse areas of low density within the liver. Contrast-enhanced CT in the portal venous phase is best for demonstrating a lobulated liver. Due to atrophy, the intrahepatic fissures appear more prominent. T1-weighted contrast MR images show the liver to have irregular diffuse enhancement with ill-defined margins; there may be rim enhancement in the venous phase. T2-weighted fat-suppressed MR images demonstrate a heterogeneous mass appearance with moderate elevation of the signal intensity. MRI enhancement with gadolinium is superior to that produced by iodinated contrast agents on CT for distinguishing abnormalities.

Treatment. At this time, prevention is the best method to control hepatitis. Standard precautions for healthcare workers should include the use of personal protective equipment for all patients. Vaccines exist for HAV and HBV. For short-term immunization, immune globulin is used.

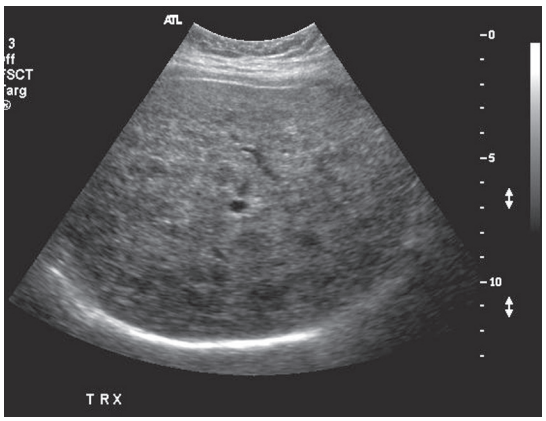

FIGURE 5-94 Hepatitis B. The liver sonogram illustrates multiple nodules and has an internal coarse texture with increased echogenicity.

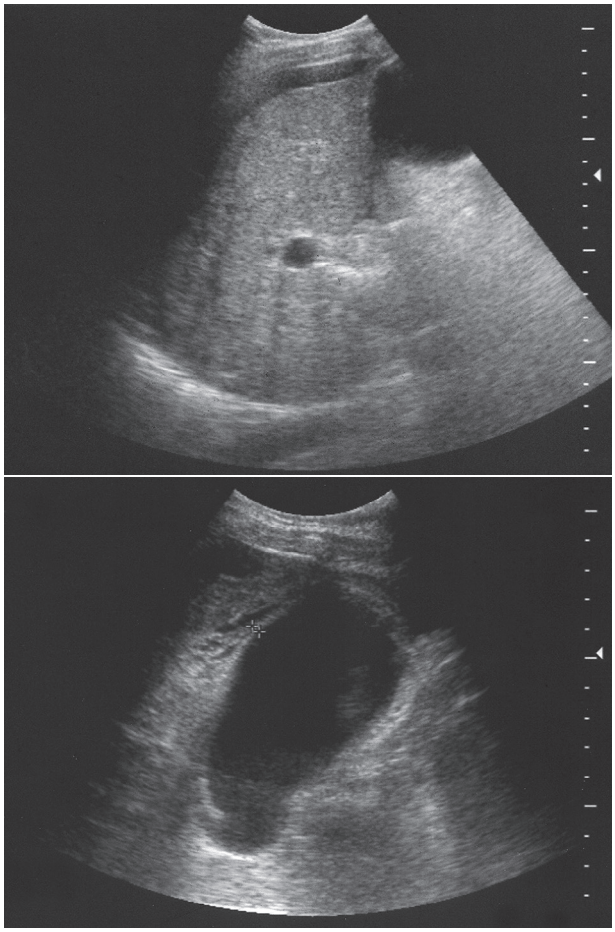

FIGURE 5-95 Autoimmune hepatitis in an 18-year-old female with end-stage liver disease. On ultrasound images, the liver demonstrates an internal coarse texture (A) and a lobulated surface (B), which is consistent with severe cirrhosis.

Cirrhosis of the Liver

Cirrhosis refers to the chronic destruction of liver cells and structure, with nodular regeneration of liver parenchyma and fibrosis; it is an end-stage liver disease. The major cause of cirrhosis is chronic alcoholism (i.e., 10 to 20 years of alcohol abuse), in which damage to the liver is related either to the toxic effect of alcohol or to the malnutrition that frequently accompanies chronic alcoholism. Other causes of liver destruction leading to cirrhosis are postnecrotic viral hepatitis, hepatotoxic drugs and chemicals that destroy liver cells, disease of the bile ducts (primary and secondary biliary cirrhosis), and excessive deposition of iron pigment within the liver (hemochromatosis).

Regardless of the cause, fibrous connective tissue replaces the destroyed liver cells with cells that have no liver cell function. Initially, the liver enlarges because of regeneration, but it eventually becomes smaller as the fibrous connective tissue contracts, and the surface becomes bumpy and nodular.

Imaging appearance. Cirrhosis causes many physiologic changes that can be detected clinically or radiographically. In alcoholic cirrhosis, a large amount of fat accumulates within the liver. This fatty infiltration is well demonstrated on CT. In normal individuals, the liver always appears brighter than the spleen, whereas in patients with cirrhosis the liver is much darker because of the large amount of fat (Figure 5-96). The portal veins appear as high-density structures surrounded by a background of low density caused by hepatic fat; this is the opposite of the normal pattern of portal veins, which are low-density channels on noncontrast scans. Ultrasound images of the liver demonstrate coarse echogenicity, which results from diffuse liver disease. Multiple hyperechoic micronodules (0.1 to 1 cm) or macronodules (varying up to 5 cm) cause a nodular surface pattern.

Nodular regeneration of the liver combined with fibrosis causes obstruction of the portal vein, which drains blood from the GI tract through the liver before emptying into the inferior vena cava near the heart. Increased pressure within this vessel causes pronounced enlargement of the spleen (splenomegaly). Because blood cannot flow through the obstructed portal vein, it must find an alternative route to bypass the liver. This leads to the development of collateral circulation, with large dilated veins becoming prominent on the abdominal wall in the area of the umbilicus. Another alternative route for blood to take in its return to the heart is the periesophageal veins, which dilate to become esophageal varices, which then can rupture and result in fatal hemorrhage (see Figure 5-21). Destruction of liver cells substantially decreases the ability of the organ to synthesize proteins, such as albumin, and several of the factors required for blood clotting. A deficiency of albumin (hypoalbuminemia) results in fluid leaking out of the circulation and the development of generalized edema, which is evidenced by swelling of the lower extremities. When edema involves the wall of the intestinal tract, it can produce regular, uniform thickening of small bowel folds.

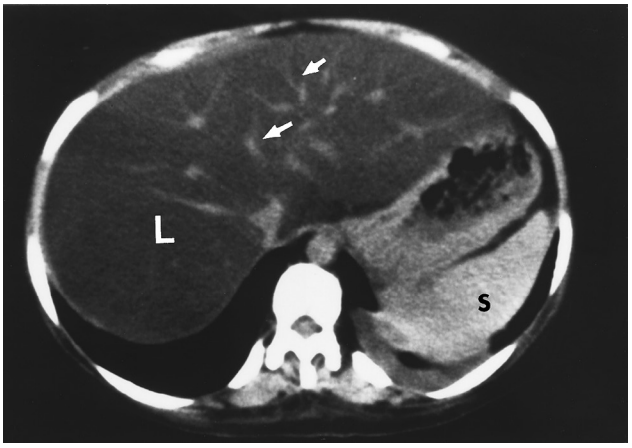

FIGURE 5-96 Fatty infiltration of the liver in cirrhosis. CT scan shows generalized decrease in the attenuation value of the liver (L), which is far less than that of the spleen (S). Portal veins appear as high-density structures (*arrows*) surrounded by a background of low-density hepatic fat.

One of the most characteristic symptoms of cirrhosis is the accumulation of fluid in the peritoneal cavity (ascites), which causes characteristic abdominal distention. The abdomen is tight and quite hard, and an increase in exposure factors is required if a large amount of fluid has accumulated. Ascites develops because of a combination of albumin deficiency and increased pressure within obstructed veins, which permits fluid to leak into the abdominal cavity. Large amounts of ascitic fluid are easily detectable on plain abdominal radiographs as a general abdominal haziness (ground-glass appearance) (Figure 5-97A). With the patient in a supine position, the peritoneal fluid tends to gravitate to dependent portions of the pelvis and accumulate within the pelvic peritoneal reflections, thus filling the recesses on both sides of the bladder and producing a symmetrical density resembling a dog's ears. Smaller amounts of fluid (300 to 1000 mL) may widen the flank stripe and obliterate the right lateral inferior margin of the liver (the hepatic angle). Ascites is exquisitely shown on ultrasound as a mobile, echo-free fluid region shaped by adjacent structures (Figure 5-97B) or on CT as an extravisceral collection of fluid with a low attenuation value (Figure 5-97C).

Cirrhosis may lead to the development of jaundice, either from destruction of liver cells or from obstruction of bile ducts. Because the liver cannot perform its usual task of inactivating the small amounts of female sex hormones secreted by the adrenal glands in both men and women, men with cirrhosis often have breast enlargement (gynecomastia). The inability of necrotic liver cells to detoxify harmful substances leads to an accumulation of ammonia and other poisonous material in the circulation. The patient becomes confused and disoriented, demonstrates a typical flapping tremor or shaking, becomes abnormally sleepy (exhibits somnolence), and may lapse into a potentially fatal hepatic coma. Ascites occurs in advance stages of cirrhosis; of those afflicted, only 20% survive 5 years.

Treatment. The damage caused by cirrhosis is irreversible and incurable except by liver transplantation. Most patients without a liver transplant die within 15 years of diagnosis. The patient may control the process by choosing a nutritional diet that decreases the metabolic load on the liver, stopping

alcohol consumption, resting, and managing the complications of liver failure.

Hepatocellular Carcinoma

In the United States, primary liver cell carcinoma most commonly occurs in patients with underlying diffuse hepatocellular disease, especially alcoholic or postnecrotic cirrhosis. The clinical presentation varies from mild right upper quadrant discomfort and weight loss to hemorrhagic shock from massive intraperitoneal bleeding, which reflects rupture of the tumor into the peritoneal cavity. Invasion of the biliary tree may produce obstructive jaundice.

Imaging appearance. CT is the modality of choice in the diagnosis of hepatocellular carcinoma. The tumor appears as a large mass, with an attenuation value close to that of normal parenchyma, that tends to alter the contour of the liver by projecting beyond its outer margin (Figure 5-98). After the rapid administration of IV contrast material, there is usually dense, diffuse, and nonuniform enhancement of the tumor. Unlike metastases, hepatocellular carcinoma tends to be a solitary mass or to produce a small number of lesions (thus appearing multinodular). Hepatocellular carcinoma tends to invade the hepatic and portal venous systems, and tumor thrombi within these veins are well demonstrated on CT. Currently, a three-phase contrast helical CT study is performed to image the arterial phase, the portal circulation, and the contrast-staining tumor in the venous or excretory phase (Figure 5-99).

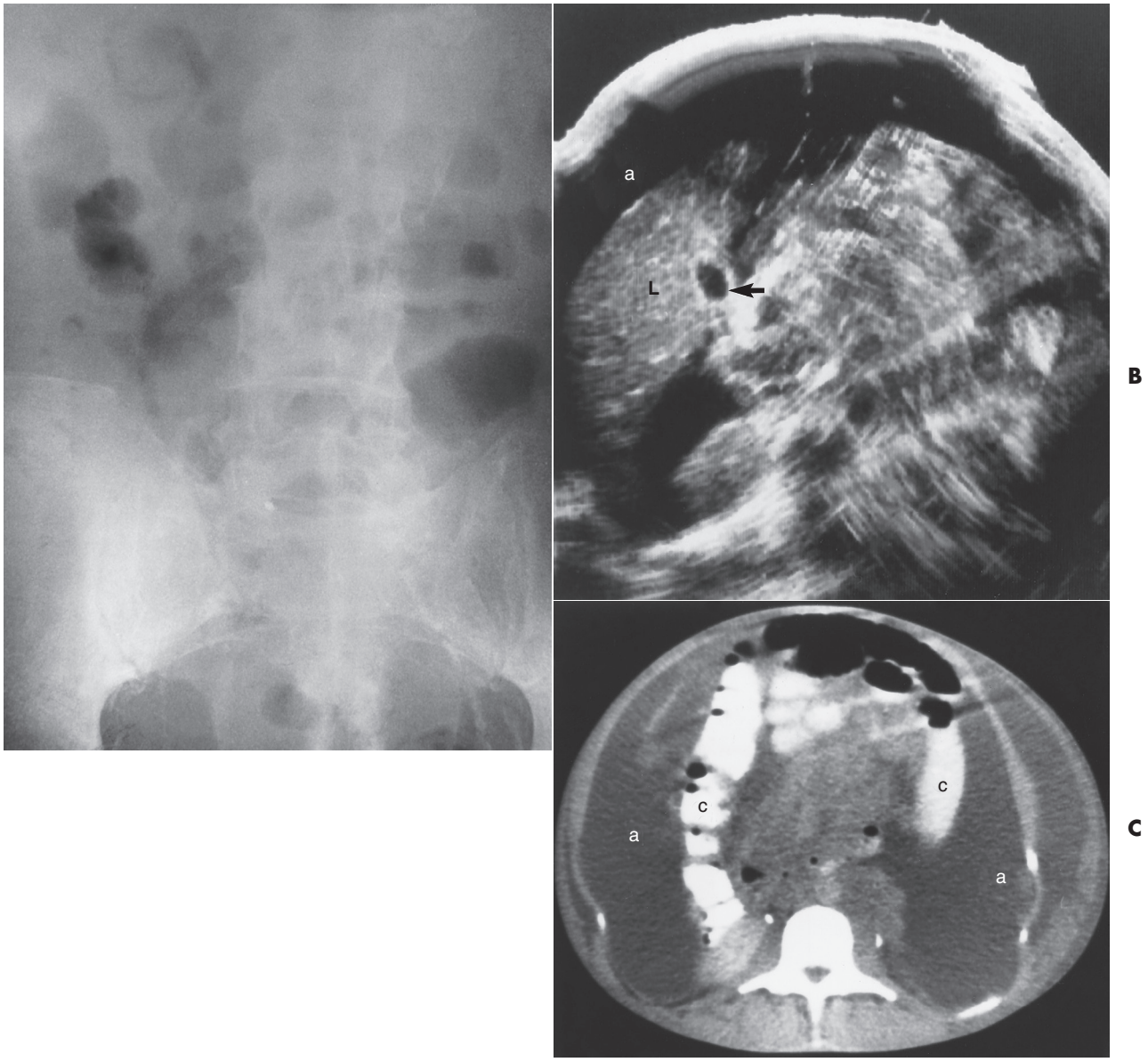

FIGURE 5-97 Ascites. **(A)** Plain radiograph shows general abdominal haziness (ground-glass appearance). **(B)** On an ultrasound image, a large amount of sonolucent ascitic fluid (a) separates the liver (L) and other soft tissue structures from the anterior abdominal wall. Note the relative thickness of the gallbladder wall (*arrow*). **(C)** CT scan through the lower abdomen shows a huge amount of low-density ascitic fluid (a) with medial displacement of ascending and descending colon (c).

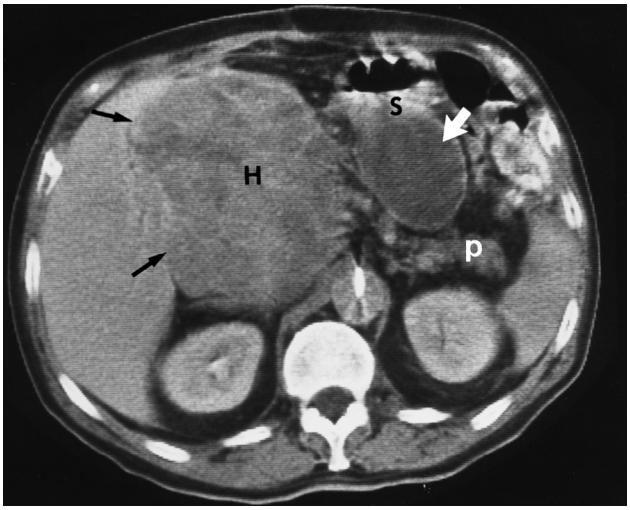

FIGURE 5-98 Hepatocellular carcinoma. CT scan shows huge mass (H) with an attenuation value slightly less than that of normal liver. *Black arrows* point to the interface between the tumor and normal liver. Incidentally shown is a pancreatic pseudocyst (*white arrow*) in the lesser sac between the stomach (S) and pancreas (p).

Ultrasonography is used to screen chronic hepatitis B virus carriers. With the use of microbubble contrast agents, Doppler ultrasound imaging demonstrates lesion vascularity through the use of phasing techniques similar to those used in CT. MRI may permit a specific diagnosis by demonstrating (during the arterial phase, after gadolinium injection) a characteristic capsule of compressed liver tissue, an accumulation of fat within the tumor, and the propensity of the tumor to spread into the hepatic and portal venous system.

Treatment. Although the overall prognosis for patients with hepatocellular carcinoma remains bleak, radiographic studies can determine whether the tumor can be successfully removed surgically. If the tumor is confined to one lobe of the liver and there is no evidence of metastases, arteriography is usually indicated to demonstrate the precise surgical anatomy and to detect small, staining tumor nodules that cannot be identified with noninvasive imaging techniques. Surgery and chemotherapy are the treatments of choice. Metastases occur late and are usually not the cause of death. A common cause of death is catastrophic bleeding into the peritoneal cavity from hepatic failure or esophageal varices.

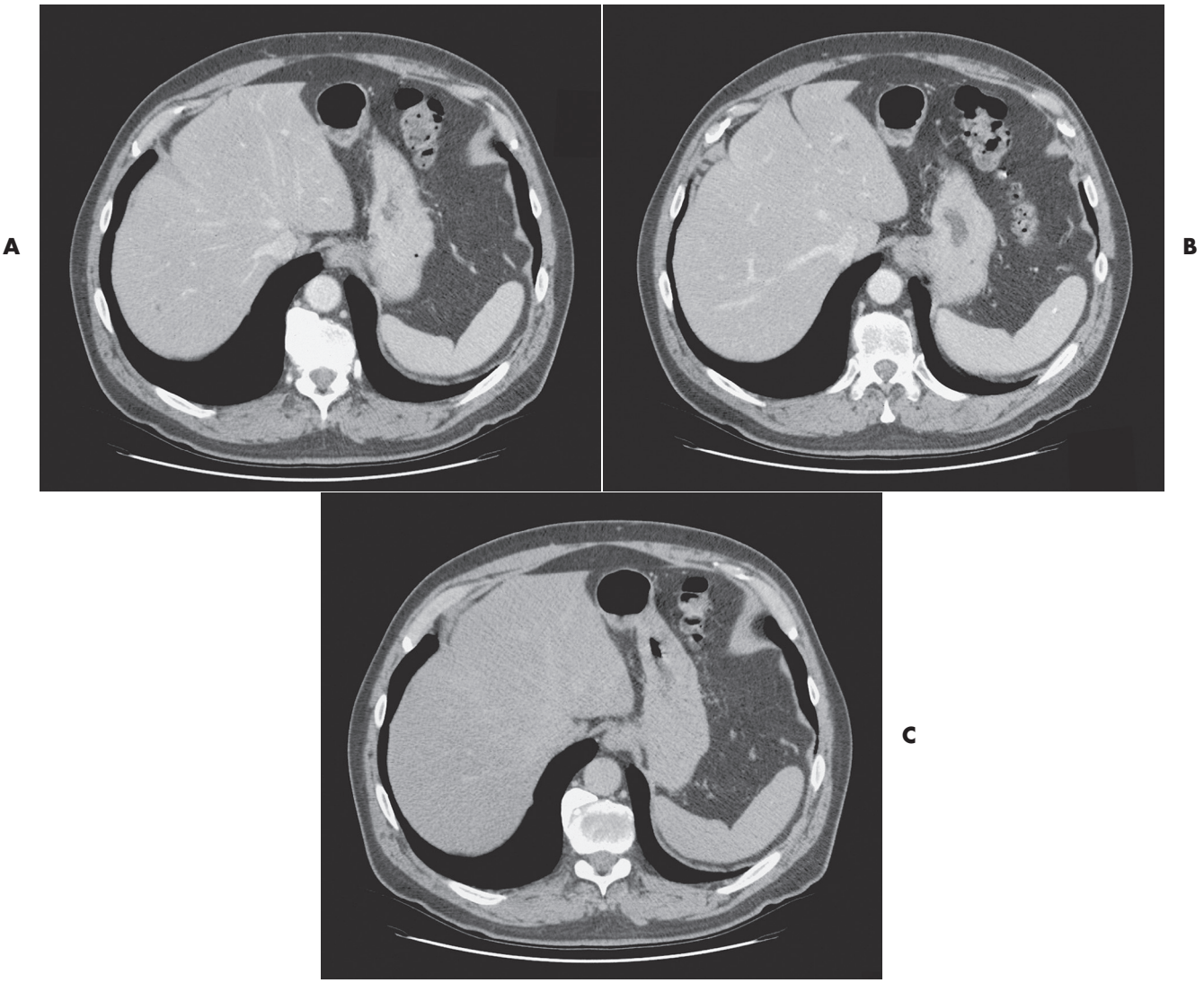

FIGURE 5-99 Three-phase CT scanning of the normal liver. **(A)** Hepatic arteries. The bolus of contrast material is in the abdominal aorta. **(B)** The inferior vena cava and the portal system are visible. **(C)** The liver parenchyma is homogeneous, indicating normal study.

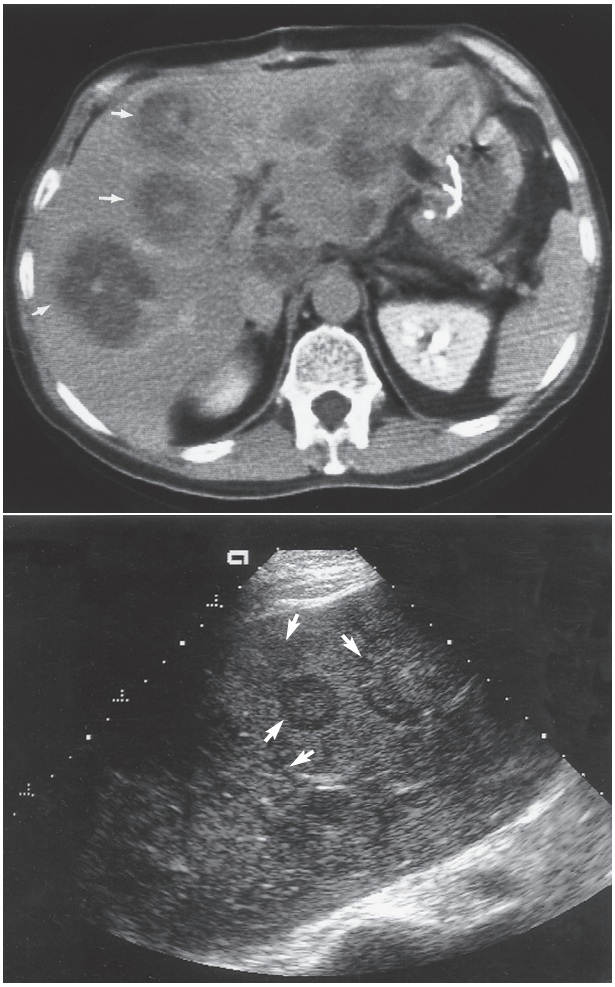

FIGURE 5-100 Hepatic metastases. **(A)** CT scan shows multiple low-density metastases with high-density centers (*arrows*). **(B)** Ultrasound image of the liver demonstrates a diffuse, patchy, nodular appearance (*arrows*).

Hepatic Metastases

Metastases are by far the most common malignant tumors involving the liver. Although some types of metastases (especially mucinous carcinoma of the colon or rectum) may produce diffuse, finely granular calcifications that can be seen on plain radiographs, the diagnosis of hepatic metastases usually requires CT, ultrasound, MRI, or radionuclide studies.

Imaging appearance. CT and MRI are probably the most sensitive techniques for detecting hepatic metastases. On CT, most metastases are relatively well marginated and appear less dense than normal liver parenchyma (Figure 5-100A). Although frequently detectable on noncontrast scans, most metastatic lesions are best seen as areas of increased density adjacent to normally enhancing hepatic parenchyma after the administration of IV contrast material. CT-guided fine-needle aspiration biopsy can be used to obtain cells that can be studied for a definitive diagnosis. MRI demonstrates liver metastases as areas of low signal intensity on T1-weighted sequences and bright lesions on T2-weighted sequences. This modality is especially important for patients who cannot receive IV iodinated contrast agents.

Ultrasound (Figure 5-100B) and radionuclide scans can demonstrate hepatic metastases, but these modalities are slightly less sensitive than CT. CT has the additional advantage of being able to detect extrahepatic metastases, such as those to abdominal lymph nodes.

Treatment. Once diagnosed with hepatic metastases, most patients face imminent death (within months).

Summary of Findings for the Liver

Disorder	Location	Imaging Appearance	Treatment
Hepatitis	Liver cells and function	US—macronodules measuring >5 mm; enlargement of the portal venous system CT—hepatocellular necrosis with fatty liver; contrast enhancement for portal venous system to see lobulated liver MRI—irregular diffuse enhancement with ill-defined margins	Prevention most effective Vaccines for hepatitis A and B; immune globulin for short-term immunization
Cirrhosis	Liver cells and structure	KUB—haziness in ascites US—coarse echogenicity, multiple nodules of varying size and a nodular liver surface CT—fatty infiltration in liver, portal vein involvement/obstruction, ascites, extravisceral fluid collection	Dietary modifications Cessation of alcohol consumption Irreversible; curable only by liver transplant
Hepatocellular carcinoma	Previously injured liver cells are most susceptible	CT—diffuse infiltrate, solitary multinodular mass	Poor prognosis Surgery and chemotherapy are treatments of choice
Hepatic metastases	Liver	CT—increased density adjacent to normal parenchyma when IV contrast administered MRI—low signal intensity on T1-weighted images; high signal intensity on T2-weighted images	Terminal Treatment palliative only

KUB, Kidney–ureter–bladder radiograph; *US,* ultrasound.

PANCREAS

Acute Pancreatitis

Acute **pancreatitis** is an inflammatory process in which protein- and lipid-digesting enzymes become activated within the pancreas and begin to digest the organ. Occasionally, this necrotic process extends into blood vessels, causing bleeding (acute hemorrhagic pancreatitis), which may be life threatening.

The most common cause of acute pancreatitis is excessive alcohol consumption. Less frequently, acute pancreatitis is related to gallstones, which may enter the common bile duct and obstruct the ampulla of Vater, forcing bile to reflux into the pancreas and causing an inflammatory reaction.

The first symptom of acute pancreatitis usually is the sudden onset of severe, steady abdominal pain that radiates to the back; this may indicate a perforated ulcer. Nausea and vomiting are common, and jaundice may develop if inflammatory edema of the head of the pancreas sufficiently obstructs the common bile duct. If a large area of the pancreas is affected, the absence of lipid enzymes from the pancreas prevents the proper absorption of fat, leading to the malabsorption syndrome. Blood tests and urinalysis typically show a high level of the pancreatic enzyme amylase, which confirms the diagnosis of acute pancreatitis.

Imaging appearance. The findings on plain abdominal radiographs are often normal in the patient with acute pancreatitis; even when abnormal, they are usually nonspecific and consistent with any intra-abdominal inflammatory disease. The most common abnormalities include a localized adynamic ileus, usually involving the jejunum (the "sentinel loop"); generalized ileus with diffuse gas–fluid levels; isolated distention of the duodenal sweep (C-loop); and localized distention of the transverse colon to the level of the left colonic flexure (the colon cutoff sign). Pancreatic calcifications indicate that the patient has chronic pancreatitis, and moreover they may indicate an exacerbation of the inflammatory disease.

Ultrasound and CT are the imaging modalities that most precisely define the degree of pancreatic inflammation and the pathways of its spread throughout the abdomen. They are also of great clinical importance in the early diagnosis of complications of acute pancreatitis, such as abscess, hemorrhage, and pseudocyst formation.

CT in acute pancreatitis demonstrates diffuse or focal enlargement of the gland. The margins of a normal pancreas are sharply delineated by surrounding peripancreatic fat. Spread of inflammation and edema beyond the confines of the pancreas obscures the peripancreatic soft tissues and often thickens the surrounding fascial planes (Figure 5-101), making CT superior to ultrasound.

Acute pancreatitis may alter both the size and the parenchymal echogenicity of the gland on ultrasound examination. Although the pancreas usually enlarges symmetrically and retains its initial shape, nonspecific enlargement of the pancreatic head or tail can simulate focal pancreatic carcinoma. Gallstones causing pancreatitis can be demonstrated. The accompanying interstitial inflammatory edema causes the pancreas to appear relatively sonolucent in comparison with the adjacent liver (Figure 5-102). One limitation of ultrasound in patients with acute pancreatitis is the frequent occurrence of adynamic ileus with excessive intestinal gas, which may prevent adequate visualization of the gland.

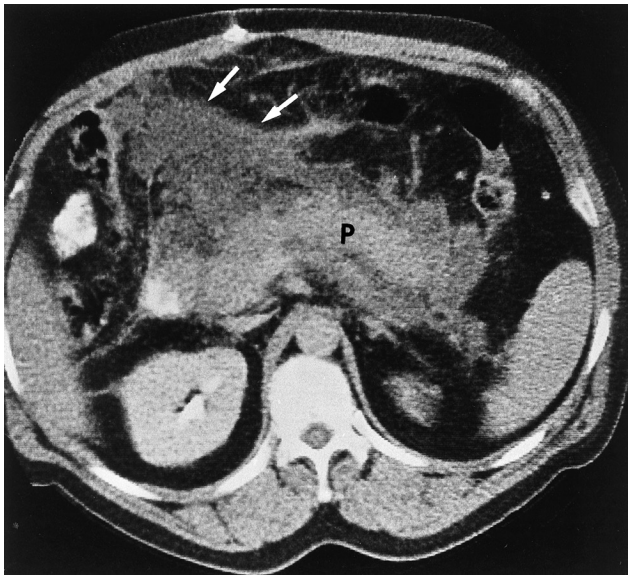

FIGURE 5-101 Acute pancreatitis. CT scan demonstrates diffuse enlargement of the pancreas (P) with obliteration of peripancreatic fat planes by an inflammatory process. Extension of the inflammatory reaction into the transverse mesocolon (*arrows*) is shown.

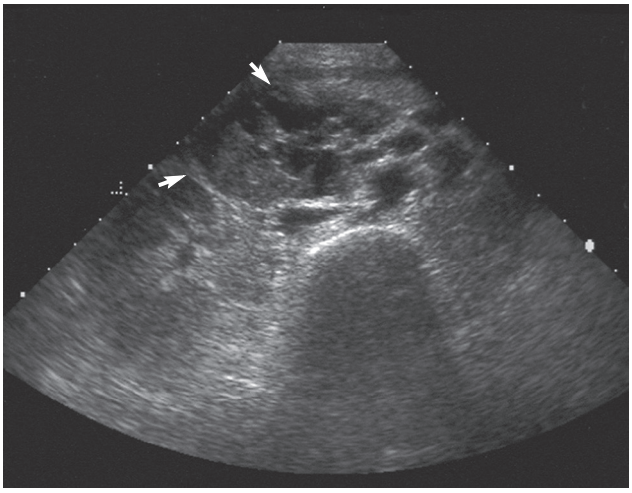

FIGURE 5-102 Acute pancreatitis. Transverse sonogram illustrates multiple hypoechoic areas in the head of the pancreas (*arrows*), which cause biliary tree dilation.

Chronic Pancreatitis

Chronic pancreatitis results when frequent intermittent injury to the pancreas causes increasing damage that produces scar tissue. Recurring episodes usually result from chronic alcohol abuse, which may cause the gland to lose its ability to produce digestive enzymes, insulin, and glucagon. Three symptoms that help identify chronic pancreatitis are pain, malabsorption

FIGURE 5-103 Chronic pancreatitis. Diffuse pancreatic calcifications.

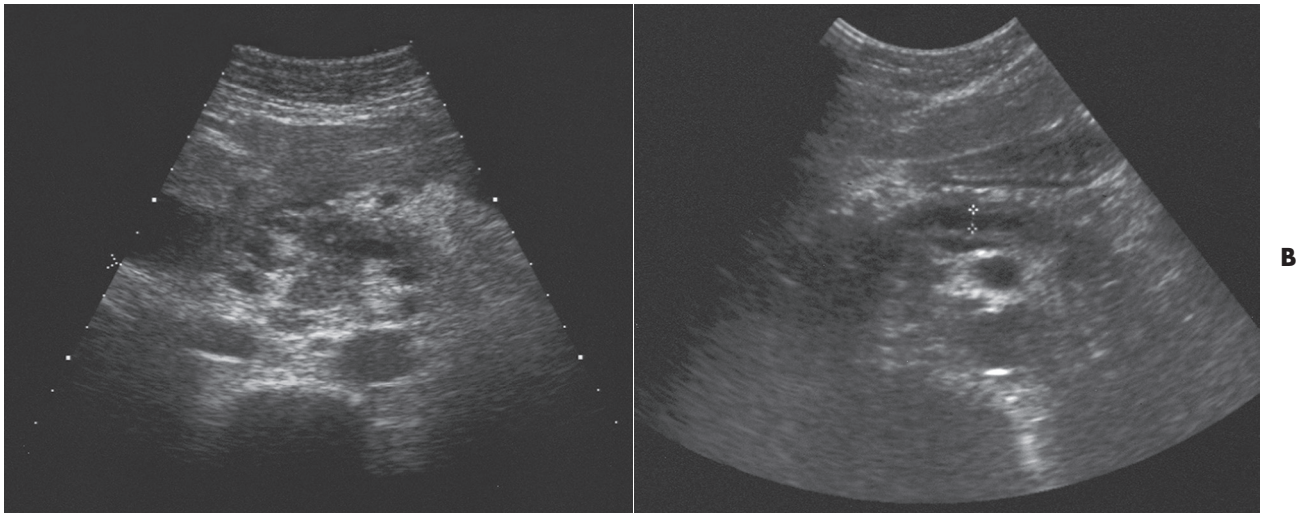

FIGURE 5-104 Chronic pancreatitis in a 40-year-old man with abdominal pain. History of chronic alcoholism. **(A)** An ultrasound image obtained in April shows the pancreas to be inhomogeneous with a patchy appearance. **(B)** On the follow-up scan obtained in May, the pancreatic ducts are considerably dilated (*cursors*).

causing weight loss (exocrine failure—digestive enzymes), and diabetes (endocrine failure—insulin and glucagon).

Imaging appearance. Pancreatic calcifications are a pathognomonic finding in chronic pancreatitis, developing in approximately one third of patients with this disease (Figure 5-103). The small, irregular calcifications are seen most frequently in the head of the pancreas and can extend upward and to the left to involve the body and tail of the organ.

On ultrasound examination, the major feature of chronic pancreatitis is an alteration of the intrinsic echo pattern caused by calcification and fibrosis (Figure 5-104). The pancreas may be atrophic as a result of fibrous scarring or may appear significantly enlarged during recurrences of acute inflammation. Dilation of the pancreatic duct as a result of gland atrophy and obstruction can be seen, although a similar pattern can be produced by the ductal obstruction in pancreatic cancer. CT can also demonstrate ductal dilation, calcification, and atrophy of the gland in patients with chronic pancreatitis. However, because similar information can be obtained less expensively and without ionizing radiation with the use of ultrasound, CT is usually reserved for patients with chronic pancreatitis in whom technical factors make ultrasound suboptimal.

Enlargement of the pancreatic head can cause widening and pressure changes on the inner aspect of the duodenal

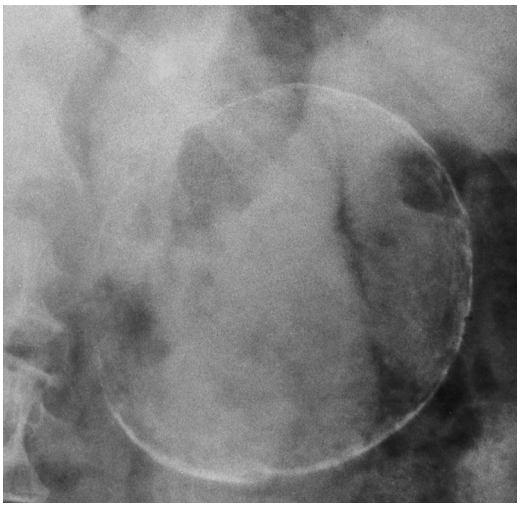

FIGURE 5-105 Calcified pancreatic pseudocyst.

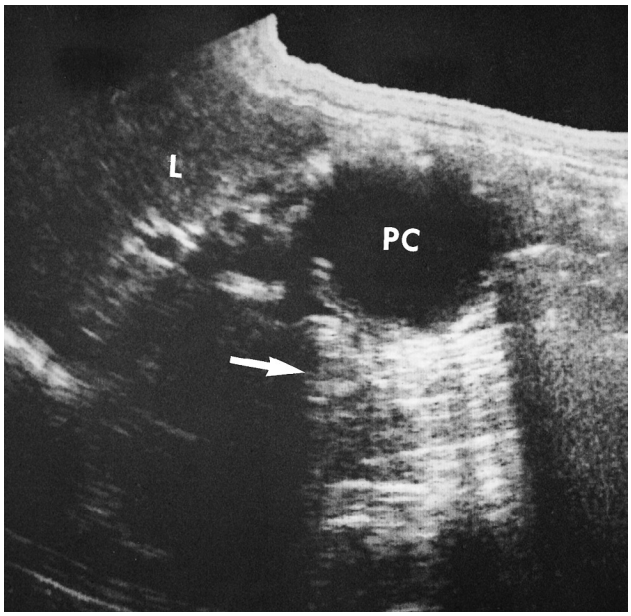

FIGURE 5-106 Ultrasound image of pancreatic pseudocyst. Longitudinal sonogram of the right upper quadrant demonstrates irregularly marginated pseudocyst (PC) with acoustic shadowing (*arrow*). *L,* Liver.

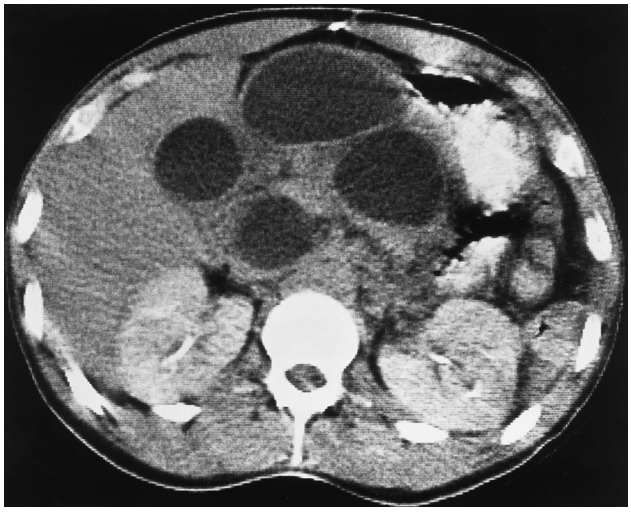

FIGURE 5-107 Multiple pancreatic pseudocysts. CT scan after IV administration of contrast material demonstrates four sharply marginated, fluid-filled collections.

sweep on barium studies. These changes produce narrowing of the lumen (the double-contour effect) and spiny protrusions of mucosal folds (spiculation) that can be indistinguishable from those of pancreatic carcinoma.

Treatment of acute and chronic pancreatitis. Most cases of acute pancreatitis require supportive treatment only (e.g., IV fluids and pain and nausea medications) because the pancreas will heal itself. If acute pancreatitis is caused by stone blockage, procedures to remove the stone (e.g., ERCP) or possibly surgery to remove the gallbladder should be performed. In some cases, IV antibiotics are given to help reduce the inflammatory process and prevent infection.

In chronic pancreatitis, treatment is directed toward controlling pain and managing nutritional and metabolic problems. Consumption of alcohol must cease. Dietary changes are made to reduce fat and protein intake; supplements containing pancreatic enzymes are taken to aid in digestion. If the blood sugar becomes uncontrolled, insulin is prescribed. Most patients who follow their prescribed treatment do well.

Pancreatic Pseudocyst

Pancreatic pseudocysts are loculated (walled-off) fluid collections arising from inflammation, necrosis, or hemorrhage associated with acute pancreatitis or trauma (Figure 5-105). When the infected or traumatized pancreas continues to release enzymes, pseudocysts are commonly formed. The pseudocyst has a shaggy lining surrounded by dense white scar tissue and may or may not connect with the pancreatic duct.

Imaging appearance. On ultrasound examination, a pseudocyst typically appears as an echo-free cystic structure with a sharp posterior wall (Figure 5-106). Hemorrhage into the pseudocyst produces a complex fluid collection containing septations of echogenic areas. CT demonstrates pseudocysts as sharply marginated, fluid-filled collections that are often best delineated after the administration of IV contrast material (Figure 5-107).

Large pseudocysts are visible on plain radiographs of the abdomen when they displace the gas-filled stomach and bowel. Similarly, pseudocysts in the head of the pancreas can cause pressure defects and widening of the duodenal sweep, whereas those arising from the body or tail of the pancreas can displace and deform the stomach, proximal jejunum, or colon. However, because ultrasound is highly accurate in diagnosing pancreatic pseudocysts, it has completely replaced plain abdominal radiographs and barium studies, which display only indirect signs.

Treatment. Pseudocysts may undergo spontaneous resolution or persist as chronic collections that may require surgical

intervention. Because ultrasound is relatively inexpensive and does not involve ionizing radiation, serial sonograms are usually used to monitor the progression of a pancreatic pseudocyst. Percutaneous drainage of a pseudocyst and endoscopic drainage of cysts extending into the stomach are interventional therapies used today.

Cancer of the Pancreas

The most common pancreatic malignancy is adenocarcinoma (90%), which often is far advanced and has metastasized before it is detected and thus has an extremely poor survival rate. Of these malignancies, 60% occur in the head of the pancreas. Less common pancreatic tumors are hormone-secreting neoplasms of the islet cells of the islets of Langerhans. Production of insulin by an **insulinoma** can lower the blood glucose level, leading to attacks of weakness, unconsciousness, and insulin shock. This tumor occurs most frequently in the tail and is usually benign. **Ulcerogenic islet cell tumors** (**gastrinomas**—usually malignant) produce the Zollinger–Ellison syndrome, which is characterized by intractable ulcer symptoms, hypersecretion of gastric acid, and diarrhea. **Diarrheogenic islet cell tumors** produce the WDHA syndrome—watery diarrhea, hypokalemia (low serum potassium), and achlorhydria (low serum chloride), which are major features of the clinical picture. Adrenocorticotropic hormone (ACTH) production by pancreatic islet cell tumors causes Cushing's syndrome; the release of serotonin by pancreatic tumors may cause the carcinoid syndrome. Because these functional islet cell tumors usually become apparent through their hormonal effects rather than from the consequences of tumor bulk, they are often small and difficult to detect.

Imaging appearance. Because it is noninvasive and relatively inexpensive, ultrasound is often the initial screening modality for a patient with suspected pancreatic carcinoma. Ultrasound can demonstrate most tumors larger than 2 cm in diameter that lie in the head of the pancreas, but lesions in the body and tail of the pancreas are more difficult to detect. Pancreatic carcinoma typically causes the gland to have an irregular contour and a semisolid pattern of intrinsic echoes (Figure 5-108).

CT is the most effective modality for detecting pancreatic cancer in any portion of the gland and for defining its extent. CT can demonstrate the mass of the tumor, ductal dilation, and invasion of neighboring structures. After the administration of IV contrast material, the relatively avascular tumor appears as an area of decreased attenuation in comparison with the normal pancreas (Figure 5-109). CT is the best procedure for staging pancreatic carcinoma and may prevent needless surgery in patients with nonresectable lesions. This technique may permit detection of hepatic metastases or involvement of regional vessels and adjacent retroperitoneal lymph nodes.

Cytologic examination of tissue obtained by percutaneous fine-needle aspiration under ultrasound or CT guidance can often provide the precise histologic diagnosis of a neoplastic mass, thus making surgical intervention unnecessary.

Carcinoma of the head of the pancreas often causes obstructive jaundice and the appearance of narrowing of

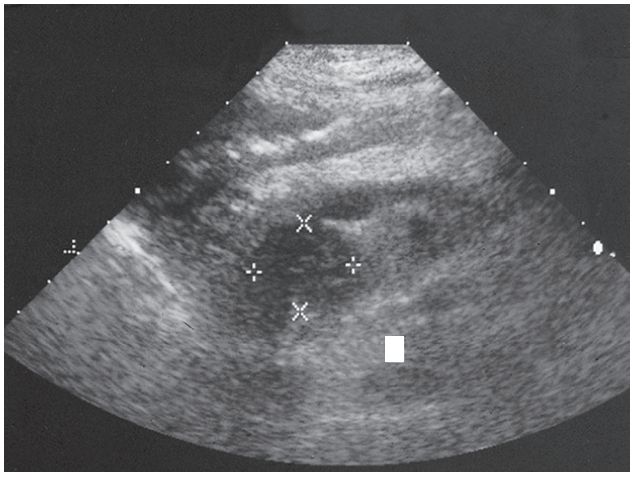

FIGURE 5-108 Pancreatic adenocarcinoma in a 66-year-old man with a 10-day history of painless jaundice and weight loss. Ultrasound image demonstrates a heterogeneous hypoechoic mass (dark area with measurement *cursors*) in the pancreatic head and uncinate process; the mass is obstructing the pancreatic and common bile ducts.

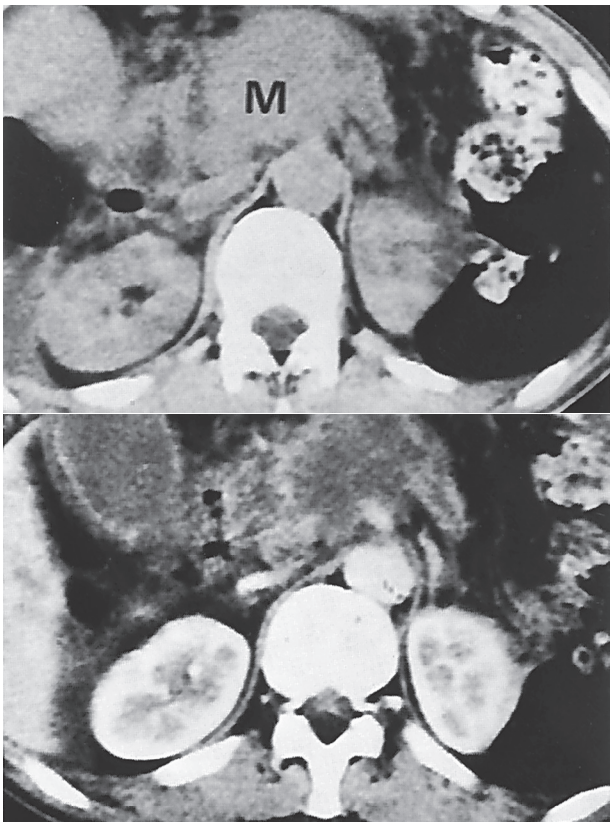

FIGURE 5-109 Carcinoma of the pancreas. **(A)** Noncontrast CT scan demonstrates a homogeneous mass (M) in the body of the pancreas. **(B)** After IV injection of a bolus of contrast material, there is enhancement of the normal pancreatic parenchyma and the surrounding vascular structures. The pancreatic carcinoma remains unchanged and thus appears as a low-density mass.

Summary of Findings for the Pancreas

Disorder	Location	Imaging Appearance	Treatment
Pancreatitis	Acute—pancreatic ducts Chronic—pancreatic parenchyma	US—altered echogenicity CT—diffuse or focal enlargement KUB—pancreatic calcifications US—intrinsic echo pattern, alteration by calcification and fibrosis CT—ductal dilation, calcification, atrophy, and pseudocyst formation	Supportive treatment IV antibiotics Reduction of fat/protein intake Pancreatic enzyme supplements Insulin for uncontrolled blood glucose levels
Pseudocyst	Cyst walled off from ductal system	US—echo-free cyst with sharp posterior wall CT—sharply marginated fluid-filled collection(s) best seen with IV contrast agent	Spontaneous resolution Drainage (percutaneous or endoscopic) Surgical correction
Cancer	Adenocarcinoma Head of pancreas in 60% of cases	US—tumor 2 cm or greater, irregular contour, and semisolid pattern of intrinsic echoes CT (most effective)—tumor mass, ductal dilation, and invasiveness	Survival, 2% Surgery Radiation therapy Chemotherapy Biologic therapy

KUB, Kidney–ureter–bladder radiograph; *US,* ultrasound.

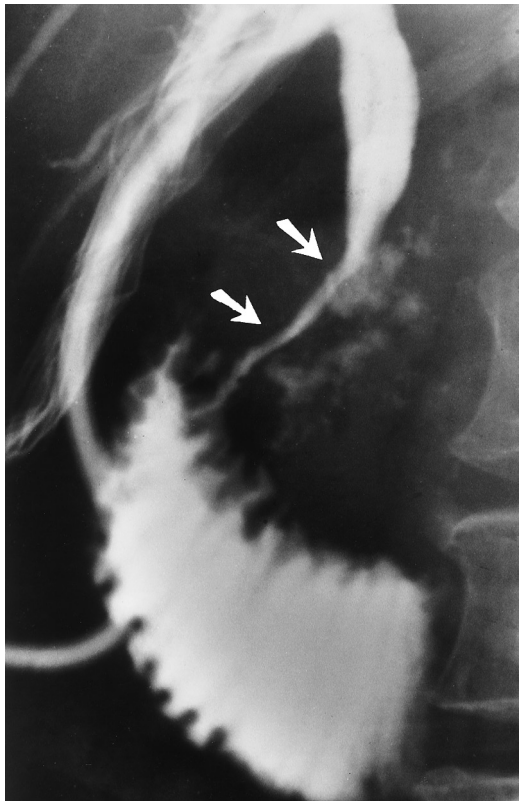

FIGURE 5-110 Carcinoma of the head of the pancreas. A transhepatic cholangiogram shows irregular narrowing of the common bile duct (*arrows*). Calcifications reflect the underlying chronic pancreatitis.

the distal common bile duct on transhepatic cholangiography (Figure 5-110) or ERCP. Percutaneous biliary drainage may represent an alternative to surgical intervention for relieving biliary obstruction in patients with pancreatic carcinoma who cannot be cured. Although the transhepatic insertion of biliary drainage tubes does not alter the dismal prognosis, it can reduce patient morbidity and the need for hospitalization.

A barium upper GI series demonstrates distortion of the mucosal pattern and configuration of the duodenal sweep in approximately half of patients with carcinoma of the head of the pancreas. Early or small lesions, however, rarely produce detectable radiographic abnormalities; tumors of the body or tail of the pancreas must be quite large to be visible on barium examinations.

Treatment. Finding pancreatic cancer in the earliest stages can result in a cure (the 5-year survival rate is 2%). In most cases, the diagnosis of the disease occurs after metastasis, and most patients die within 12 to 24 months of diagnosis. Nevertheless, treatment can improve the quality of life. Surgical resection, radiation therapy, chemotherapy, and biologic therapy help alleviate the patient's symptoms.

Surgical resection (total pancreatectomy) involves the removal of the entire pancreas, duodenum, common bile duct, gallbladder, spleen, and surrounding lymph nodes. The Whipple procedure consists of removing only the head of the pancreas, the duodenum, a portion of the stomach, and other nearby tissue. If a distal pancreatectomy is performed, only the body and tail of the pancreas are removed. In most cases, the purpose of the surgery is to alleviate biliary and small bowel obstruction. Surgery and chemotherapy are most effective for islet cell cancers.

PNEUMOPERITONEUM

Free air in the peritoneal cavity associated with significant abdominal pain and tenderness is often caused by perforation of a gas-containing viscus and indicates a surgical emergency. Less frequently, pneumoperitoneum results from abdominal, gynecologic, intrathoracic, or iatrogenic causes and does not require operative intervention.

Imaging appearance. The radiographic demonstration of free air in the peritoneal cavity is a valuable sign in the diagnosis of perforation of the GI tract. As little as 1 mL of free intraperitoneal gas can be identified. Free air is best demonstrated by examination of the patient in the upright position with a horizontal beam (Figure 5-111). Because the gas rises to the highest point in the peritoneal cavity, it accumulates beneath the domes of the diaphragm. Free intraperitoneal gas appears as a sickle-shaped lucency that is easiest to recognize on the right side between the diaphragm and the homogeneous density of the liver. On the left side, the normal gas and fluid shadows present in the fundus of the stomach can be confusing. The free air is shown to best advantage if the patient remains in an upright (or lateral decubitus) position for 10 minutes before a radiograph is obtained.

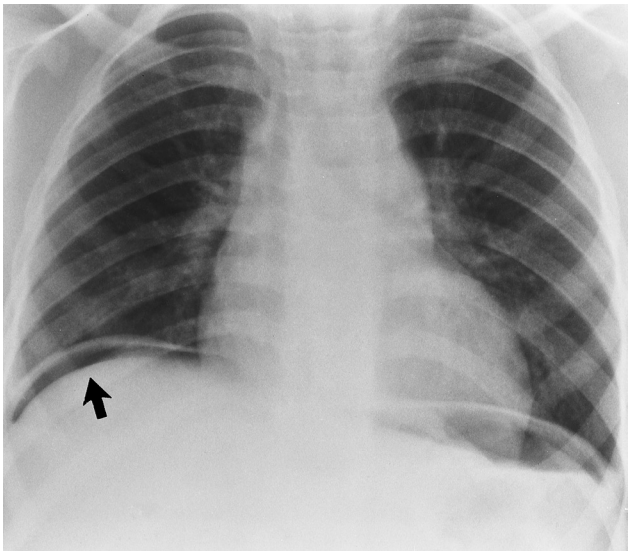

FIGURE 5-111 Pneumoperitoneum. Gas accumulating beneath the dome of the right hemidiaphragm (*arrow*) appears as a sickle-shaped lucency on this erect chest radiograph obtained with a horizontal beam.

If the patient is too ill to sit or stand, a lateral decubitus view (preferably with the patient on the left side) can be used. In this position, free air moves to the right side and collects between the lateral margin of the liver and the abdominal wall (Figure 5-112). Some gas also collects in the right iliac fossa and, when large amounts are involved, can be seen along the flank down to the pelvis.

When the patient is in the supine position, free intraperitoneal gas accumulates between the intestinal loops and is much more difficult to demonstrate. However, a large quantity of gas can be diagnosed indirectly because the outer margins of the intestinal wall can be visualized (Figure 5-113). The demonstration of distinct inner and outer contours of the bowel wall is often the only sign of pneumoperitoneum in patients who are in such poor condition that they cannot be turned on their side or be examined while upright.

In children, pneumoperitoneum can manifest as a generalized greater-than-normal lucency of the entire abdomen. An important sign of pneumoperitoneum on the supine radiograph is demonstration of the falciform ligament. This almost vertical, curvilinear, water-density shadow in the upper abdomen to the right of the spine is outlined only when there is gas on both sides of it, as in pneumoperitoneum (Figure 5-114).

The most common cause of pneumoperitoneum with associated inflammation is perforation of a peptic ulcer, either gastric or duodenal. Colonic perforations, especially those involving the cecum, give the most abundant quantities of free intraperitoneal gas. Septic infection of the peritoneal cavity by gas-forming organisms can result

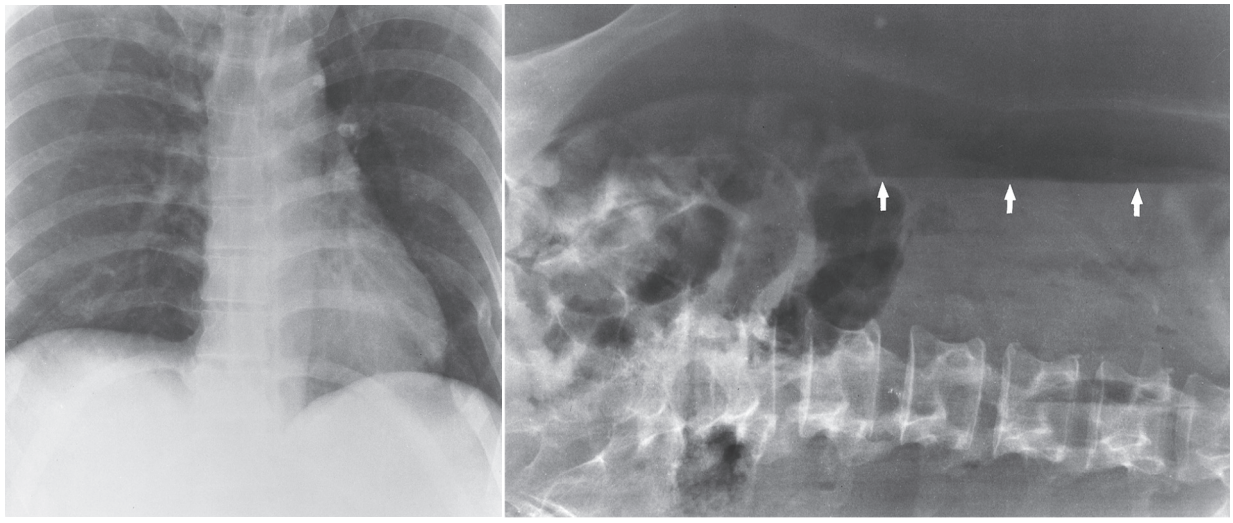

FIGURE 5-112 Pneumoperitoneum. **(A)** Semierect projection obtained without a horizontal beam shows no evidence of free intraperitoneal gas beneath the domes of the diaphragm. **(B)** On a lateral decubitus projection obtained with a horizontal beam in the same patient, free intraperitoneal gas is clearly shown collecting under the right side of the abdominal wall (*arrows*). Gas can even be seen extending down the flank to the region of the pelvis.

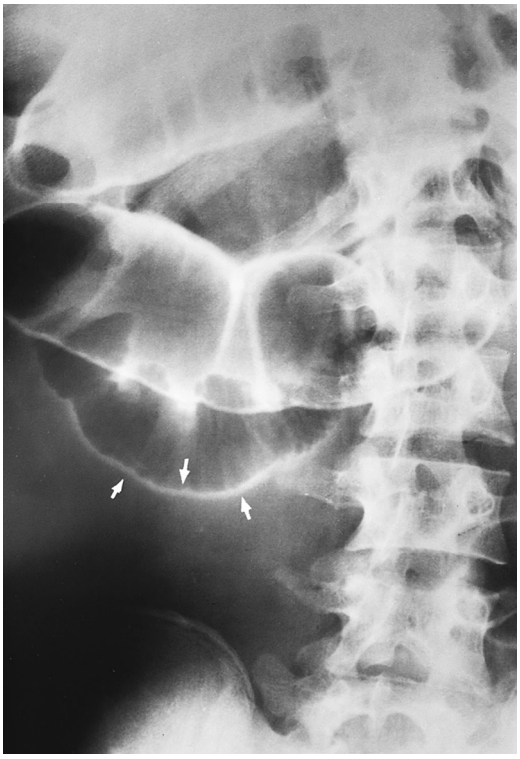

FIGURE 5-113 Double-wall sign of pneumoperitoneum demonstrated on supine projection. Large quantities of free intraperitoneal gas may be diagnosed indirectly because gas permits visualization of both inner and outer margins of the intestinal wall (*arrows*).

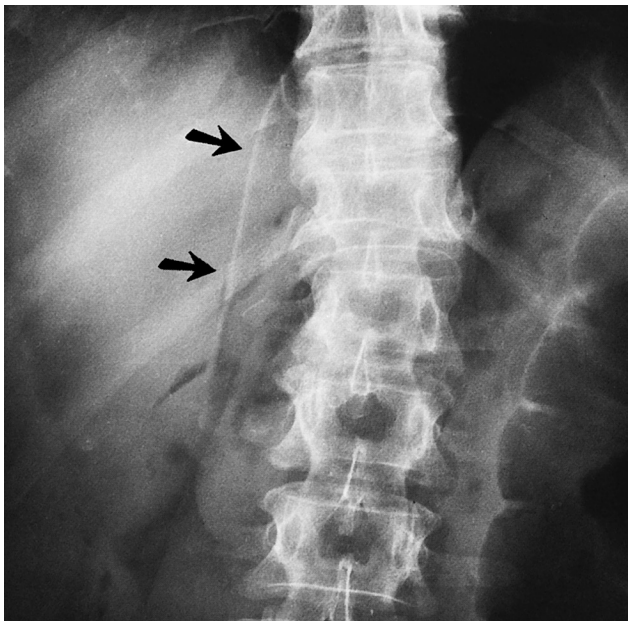

FIGURE 5-114 Falciform ligament sign of pneumoperitoneum. On a supine projection, the falciform ligament appears as a curvilinear water-density shadow (*arrows*) in the upper abdomen to the right of the spine. This finding implies that pneumoperitoneum with gas is on both sides of the ligament.

Summary of Findings for Pneumoperitoneum

Disorder	Location	Imaging Appearance	Treatment
Pneumoperitoneum	Abdominal cavity	Upright abdominal radiographic image (first choice)—1 mL free intraperitoneal gas (air) under diaphragm Left lateral decubitus view (second choice)—air collection between lateral margin of liver and outer abdominal wall	Immediate surgery for visceral perforation IV antibiotics

in the production of a substantial amount of gas and the radiographic appearance of pneumoperitoneum. Pneumoperitoneum can also develop after penetrating injuries of the abdominal wall and after blunt trauma causing rupture of a hollow viscus.

Iatrogenic pneumoperitoneum is generally asymptomatic and usually follows abdominal surgery. Postoperative pneumoperitoneum can be radiographically detectable for up to 3 weeks after surgery, but usually it can no longer be demonstrated after the first postoperative week. Rarely, free air in the peritoneal cavity may be the result of perforation during an endoscopic procedure.

Treatment. Immediate surgical repair of a perforation is required to reduce the risk of peritonitis and sepsis. IV antibiotics help control infection.

SPLEEN

Enlargement

Enlargement of the spleen (splenomegaly) is associated with numerous conditions, including infections (subacute bacterial endocarditis, tuberculosis, infectious mononucleosis, and malaria), connective tissue disorders, neoplastic hematologic disorders (lymphoma and leukemia), hemolytic anemia and hemoglobinopathies, and portal hypertension (cirrhosis).

Imaging appearance. Plain abdominal radiographs can demonstrate the inferior border of the enlarged spleen well below the costal margin. An enlarged spleen can elevate the left hemidiaphragm, impress the greater curvature of the barium-filled stomach, and displace the entire stomach toward the midline. Splenomegaly can also cause downward

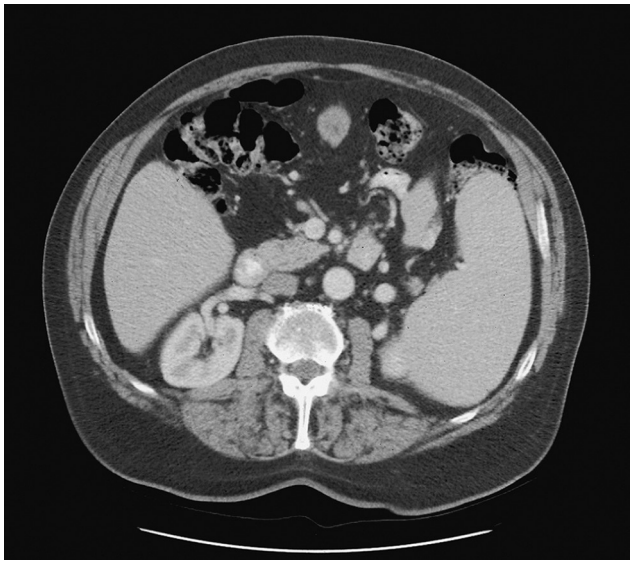

FIGURE 5-115 Splenomegaly. CT scan demonstrates a homogeneous and extremely enlarged spleen.

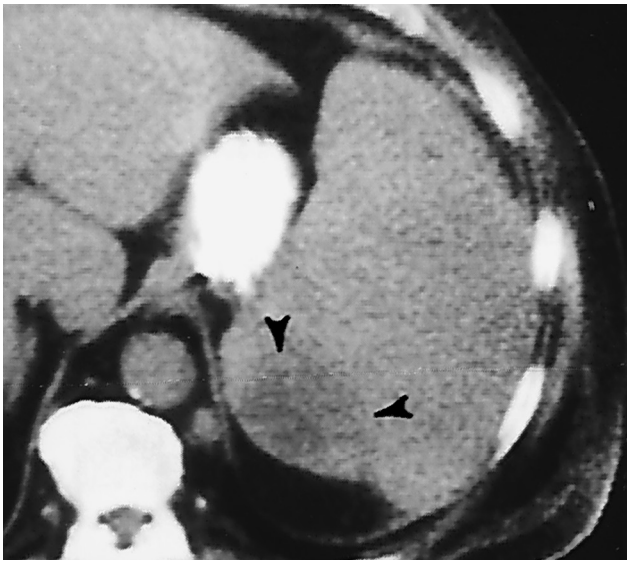

FIGURE 5-116 Lymphoma of the spleen. CT scan shows focal low-attenuation lesion (*arrowheads*) posteriorly in this greatly enlarged spleen.

displacement of the left kidney and the splenic flexure of the colon.

CT is of value when it is unclear whether a mass palpated in the left upper quadrant represents an enlarged spleen or a separate abdominal mass. When splenomegaly is present (Figure 5-115), CT findings may indicate the cause of the splenic enlargement by demonstrating a tumor (Figure 5-116), abscess, or cyst. Associated abdominal lymph node enlargement is suggestive of lymphoma; characteristic alterations in the size and shape of the liver and prominence of collateral venous structures in the splenic hilum indicate that splenomegaly may be a result of cirrhosis and portal hypertension.

FIGURE 5-117 Splenic rupture and hematoma. CT scan in a patient who was ejected from a motor vehicle. Traumatic splenic rupture and hematoma are illustrated by the decreased attenuation surrounding the spleen.

Rupture

Rupture of the spleen is usually caused by trauma. Infrequently, it may be a complication of the palpation of a spleen enlarged by infection (especially infectious mononucleosis) or leukemia. In many patients suffering traumatic rupture of the spleen, the severity of clinical symptoms and the rapid loss of blood into the abdominal cavity require immediate surgery without radiographic investigation. However, in patients in whom bleeding stops temporarily or in whom there is slow bleeding over several days, radiographic studies may be of diagnostic value.

Imaging appearance. CT is the best imaging procedure for screening patients with blunt abdominal trauma for the presence of splenic injury. Indeed, its almost 100% sensitivity in detecting splenic injury has substantially decreased the need for abdominal arteriography and exploratory surgery. Subcapsular hematomas appear on CT as crescentic collections of fluid that flatten or indent the lateral margin of the spleen (Figure 5-117). Splenic lacerations, which may occur with or without an accompanying subcapsular hematoma, produce a CT appearance of splenic enlargement, an irregular cleft or defect in the splenic border, and free blood in the peritoneal cavity.

Before the advent of CT, splenic arteriography was the procedure of choice for demonstrating splenic rupture. Major positive findings include extravasation of contrast material into the splenic parenchyma, obstruction of a major splenic artery, and—in an enlarged spleen—vascular defects that indicate sites of rupture and hematoma.

Treatment of splenic disorders. Treatment depends on the causative factors. A very enlarged spleen has a higher incidence of rupture and thus the patient should limit physical activity to avoid trauma. In most cases, the patient with splenomegaly does well with conservative treatment. Aggressive treatment would include possible embolization of the splenic artery to stop the bleeding in a splenic rupture. Surgical procedures include laparoscopic splenectomy and distal pancreatectomy, if necessary.

Summary of Findings for Splenic Disorders

Disorder	Location	Imaging Appearance	Treatment
Splenomegaly	Enlarged spleen	Abdominal radiographic image—elevated left diaphragm, stomach displacement CT—demonstrates tumor, abscess, or cyst causing splenomegaly	Treat cause Limited physical activity to prevent traumatic rupture
Splenic rupture	Fracture by trauma	CT—subcapsular hematoma appears as a crescentic fluid collection; splenic laceration appears as enlargement with an irregular splenic border	Aggressive treatment Embolization of splenic artery Laparoscopic splenectomy

REVIEW QUESTIONS

1. Visualization of which of the following structures indicate that the correct contrast scale has been used for a plain abdominal radiograph?
   1. Liver, kidneys, and psoas muscle shadows
   2. Lumbar spine and transverse processes
   3. Kidneys and psoas muscle shadows
   4. Lumbar spine and psoas shadows
   - **a.** both 1 and 4
   - **b.** both 1 and 2
   - **c.** 1 only
   - **d.** 4 only
2. The rhythmic smooth muscle contractions found in the upper gastrointestinal system are called _____ _____.
   - **a.** chyme
   - **b.** digestion
   - **c.** peristalsis
   - **d.** mastication
3. The greatest amount of digestion occurs in which portion of the intestines?
   - **a.** duodenum
   - **b.** jejunum
   - **c.** ileum
   - **d.** colon
4. Detoxification of poisonous substances takes place in which organ?
   - **a.** kidneys
   - **b.** liver
   - **c.** pancreas
   - **d.** spleen
5. Which organ controls the level of glucose in the circulating blood?
   - **a.** kidneys
   - **b.** liver
   - **c.** pancreas
   - **d.** spleen
6. The telescoping of one part of the intestinal tract into another is termed _____.
   - **a.** intussusception
   - **b.** volvulus
   - **c.** Crohn's disease
   - **d.** ileus
7. Twisting of the bowel upon itself is termed _____ _____.
   - **a.** intussusception
   - **b.** volvulus
   - **c.** Crohn's disease
   - **d.** ileus
8. What is now considered to be the major imaging modality for the demonstration of gallstones?
   - **a.** OCG
   - **b.** MRI
   - **c.** CT
   - **d.** ultrasound
9. What is the major cause of cirrhosis in the United States and Europe?
   - **a.** hepatitis
   - **b.** elevated cholesterol
   - **c.** alcoholism
   - **d.** cholecystitis
10. Rupture of the spleen as a result of blunt abdominal trauma can be best demonstrated by what imaging procedure?
    - **a.** OCG
    - **b.** MRI
    - **c.** CT
    - **d.** ultrasound
11. If a patient is too ill to stand, what position can be used to demonstrate pneumoperitoneum?
    - **a.** right lateral decubitus, patient on left side
    - **b.** right lateral decubitus, patient on right side
    - **c.** left lateral decubitus, patient on left side
    - **d.** left lateral decubitus, patient on right side
12. Extensive calcification in the wall of the gallbladder is termed _____.
    - **a.** cholelithiasis
    - **b.** porcelain gallbladder
    - **c.** cholecystitis
    - **d.** a or b
13. Varicose veins of the rectum are termed _____ _____.
    - **a.** polyps
    - **b.** hemorrhoids
    - **c.** ulcerations
    - **d.** carcinomas

14. "Apple-core" and "napkin-ring" are common descriptive terms for annular carcinoma of the _____.
    a. small intestine
    b. stomach
    c. jejunum
    d. colon
15. Crohn's disease occurs in which organ(s)?
    a. colon
    b. small bowel
    c. stomach
    d. all of the above
16. The presence of large amounts of gas and fluid in uniformly dilated loops of small and large bowel, often seen after abdominal surgery, is termed _____.
    a. adynamic ileus
    b. localized ileus
    c. colonic ileus
    d. ileus
17. What medical term is used to denote difficulty in swallowing?
    a. mastication
    b. dysphagia
    c. deglutition
    d. b and c
18. Gastric contents that are mixed with hydrochloric acid and pepsin are called _____.
    a. chyme
    b. digest
    c. enzyme
    d. emulsifier
19. To demonstrate esophageal reflux, the patient is often asked to perform the _____.
    a. Trendelenburg maneuver
    b. Sims maneuver
    c. Fowler maneuver
    d. Valsalva maneuver
20. An abnormal connection between the esophagus and trachea is termed a(n) _____.
    a. intussusception
    b. volvulus
    c. fistula
    d. abscess
21. The most common TE fistula is _____, described as esophageal atresia.
    a. type I
    b. type II
    c. type III
    d. type IV
22. An abnormal accumulation of fluid in the peritoneal cavity is termed _____.
    a. pneumoperitoneum
    b. ascites
    c. volvulus
    d. hydroperitoneum
23. Herniations, or outpouchings, of the walls of a hollow organ are termed _____.
    a. ulcers
    b. diverticula
    c. hemorrhoids
    d. polyps
24. A colonic intussusception can sometimes be reduced by what radiographic procedure?
    a. upper gastrointestinal series
    b. small bowel series
    c. enteroclysis series
    d. barium enema
25. Patients older than 40 years with a history of difficulty in swallowing are usually assumed, until demonstrated otherwise, to have what pathologic condition?
    a. esophageal fistula
    b. esophageal hernia
    c. esophageal varices
    d. esophageal carcinoma
26. What is the most common manifestation of peptic ulcer disease?
    a. gastric ulcer
    b. esophageal ulcer
    c. duodenal ulcer
    d. peritoneal ulcer
27. If loops of bowel are distended by abnormally large amounts of air and are occupying the central portion of the abdomen, the patient most likely has _____ _____.
    a. small bowel obstruction
    b. large bowel obstruction
    c. gastric obstruction
    d. a and b
28. The muscle becomes hypertrophic preventing the normal emptying of the stomach in cases of _____.
    a. gastric carcinoma
    b. duodenal ulcers
    c. peptic ulcerations
    d. pyloric stenosis
29. When loculated fluid collections arise in the pancreas, these formations are called _____.
    a. simple cysts
    b. pseudocysts
    c. pancreatic masses
    d. pancreatitis
30. The most prevalent inflammatory disease of the liver most commonly caused by a viral infection or a reaction to drugs and toxins is _____.
    a. hepatitis
    b. necrotic cirrhosis
    c. alcoholic cirrhosis
    d. hepatocellular carcinoma

6

Urinary System

OUTLINE

Physiology of the Urinary System
Congenital/Hereditary Diseases
- Anomalies of Number and Size
- Anomalies of Rotation, Position, and Fusion
- Anomalies of Renal Pelvis and Ureter
- Treatment of Congenital/Hereditary Anomalies
- Ureterocele
- Posterior Urethral Valves

Inflammatory Disorders
- Glomerulonephritis
- Pyelonephritis
- Tuberculosis
- Papillary Necrosis
- Cystitis

Urinary Calculi
Urinary Tract Obstruction
Cysts and Tumors
- Renal Cyst
- Polycystic Kidney Disease
- Renal Carcinoma
- Wilms' Tumor (Nephroblastoma)
- Carcinoma of the Bladder

Renal Vein Thrombosis
Acute Renal Failure
Chronic Renal Failure

KEY TERMS

acid–base balance
Bowman's capsule
collecting tubules
complete fusion
crossed ectopia
duplication
ectopic kidney
electrolyte balance
glomerulus
horseshoe kidney
hydronephrosis
hydroureter
hypernephroma
hypoplastic kidney
incontinence
intrathoracic kidney
loop of Henle
micturate
nephrocalcinosis
pelvic kidney
proximal convoluted tubule
staghorn calculus
supernumerary kidney
trigone
unilateral renal agenesis
uremia
ureterocele

OBJECTIVES

After reading this chapter, the reader will be able to:

- Classify the more common diseases in terms of their attenuation of x-rays
- Explain the changes in technical factors required for obtaining optimal-quality radiographs in patients with various underlying pathologic conditions
- Define and describe all boldface terms in this chapter
- Describe the physiology of the urinary system
- Identify anatomic structures on both diagrams and radiographs of the urinary system
- Differentiate the various pathologic conditions affecting the urinary system and their radiographic manifestations

PHYSIOLOGY OF THE URINARY SYSTEM

The urinary system consists of the kidneys, ureters, and bladder (Figure 6-1). The functional unit of the kidney is the nephron. Each kidney contains more than 1 million nephrons, which filter waste products from the blood, reabsorb water and nutrients (e.g., glucose and amino acids) from the tubular fluid, and secrete excess substances in the form of urine. In an average person, the nephron filters approximately 190 L of water out of glomerular blood each day. This enormous amount is many times the total volume of blood in the body. However, only a small proportion of this water (1 to 2 L) is excreted in the urine. Therefore, more than 99% of water is reabsorbed into tubular blood.

The formation of urine begins in the **glomerulus**, a tuft of capillaries with very thin walls and a large surface area. The blood pressure within the glomerulus is higher than that in Bowman's capsule, which surrounds it. This difference causes the filtration of fluid into **Bowman's capsule** that is equivalent

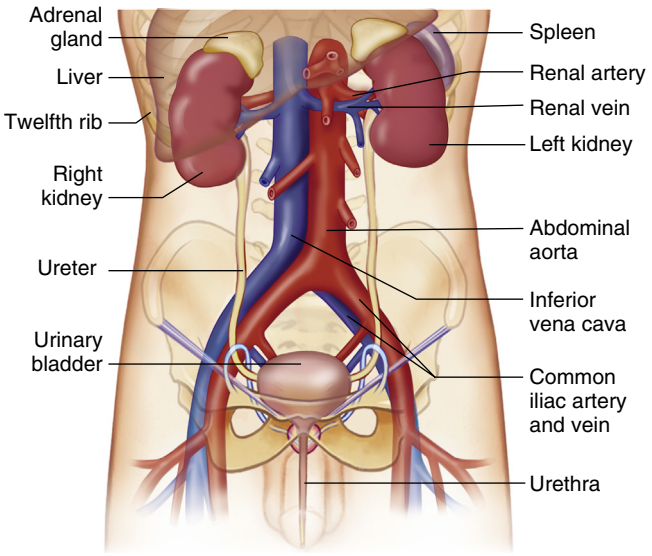

FIGURE 6-1 Location of urinary system organs.

to plasma containing neither protein nor red blood cells (if the nephron is healthy). The initial urine proceeds into the **proximal convoluted tubule**, where a large amount of water and virtually all nutrients are reabsorbed into the blood capillaries surrounding the tubules. The amount of sodium and chloride reabsorbed is determined by the concentration of these substances in the body, and it occurs at a variable rate designed to keep the osmotic pressure of the body constant. This process is greatly influenced by two hormones: antidiuretic hormone (ADH), secreted by the posterior pituitary gland, and aldosterone, secreted by the adrenal glands.

RADIOGRAPHER NOTES

Ultrasound and computed tomography (CT) are being used with increasing frequency, and plain radiography with contrast material introduced intravenously or by means of a catheter has become a less frequently used technique for imaging the urinary system. In intravenous urography, the radiographer is responsible for preparing sterile injections of contrast material and for operating the equipment properly and positioning the patient. In some instances, the radiographer may have to perform these functions in an operating room using sterile technique.

All radiographic studies begin with a "scout" image that is obtained before the injection of any contrast material. The radiographer should evaluate this image for proper technique and positioning so that any required alterations can be made on subsequent radiographs during the procedure. An image with correct density and contrast should demonstrate the kidney and psoas major muscle shadows, and the lumbar vertebrae and their transverse processes. A correctly positioned image should demonstrate from the superior portion of both kidneys and include the superior portion of the pubic bones (to ensure that the entire bladder is included). The radiograph must be in a true anteroposterior position with the pelvis appearing symmetric and the spinous processes of the lumbar vertebrae projected over the central portions of the vertebral bodies. The radiologist evaluates the scout radiograph to make certain that the technique and positioning are appropriate for the clinical history and to confirm proper patient preparation. The radiographic image is also checked for any radiopaque calculi or other abnormality that might be obscured after the injection of contrast material.

The radiographer must be alert to the possibility of any reaction, specifically an allergic reaction, whenever contrast agents are used. It is essential that the radiographer be aware of the proper procedures to follow in the event of any reaction and be able to initiate and maintain basic life support until advanced life-support personnel have arrived. Depending on departmental policy, it is usually the radiographer's responsibility to assist during resuscitation procedures. Therefore, it is essential that the radiographer be familiar with the contents of the emergency cart and take responsibility for ensuring that the cart is completely stocked with appropriate medications.

All radiographs of the urinary system must be made with the patient in full exhalation so that the diaphragm assumes its highest position and does not compress the abdominal contents. Depending on the specific area being evaluated, the radiographer may have to perform oblique or erect projections, coned-down views of the kidneys or bladder, tomograms, or images made with abdominal compression. In certain pathologic conditions, radiographs must be obtained at precisely timed intervals, and delayed images may be necessary.

After passing through the proximal tubule, the fluid flows through the **loop of Henle**, a complex structure consisting of a descending limb, a loop, and an ascending limb. Following the reabsorption of salt and water in the loop of Henle, the distal convoluted tubules permit the excretion of concentrated urine by actively secreting substances such as potassium ions (K^+), hydrogen ions (H^+), and some drugs. In this way, the kidney plays an essential role in maintaining salt or **electrolyte balance** and **acid–base balance** of blood and body fluids.

To maintain a healthy metabolism, the pH must be kept in the very limited range of 7.35 to 7.45. If the pH of blood is lower than this (i.e., too acidic), the kidney excretes an acid urine to remove H^+; if the pH of blood is higher than 7.5 (i.e., too alkaline), the kidney preserves H^+ and secretes an alkaline urine.

Eventually, urine passes from the **collecting tubules**, whose openings are in the papillae, into the calyces and on to the funnel-shaped renal pelvis and tubular ureters (Figure 6-2). Peristaltic waves (approximately 1 to 5 per minute) force the urine down the ureters and into the bladder. The ureters enter the bladder through an oblique tunnel that functions as a valve to prevent backflow of urine into the ureters (vesicoureteral reflux) during bladder contraction.

The bladder acts as a reservoir for the urine before it leaves the body (Figure 6-3). The openings of the two ureters lie at the posterior corners of the triangle-shaped floor (the **trigone**), and the urethral opening is situated at the anterior lower corner. Filling of the bladder (approximately 250 mL in the average person) stimulates autonomic nerve endings in the wall that are perceived as a distended sensation and the desire to void (**micturate**). A complicated sequence of bladder contractions and relaxation of the sphincter muscles permits the bladder to expel urine from the body through the urethra. Voluntary contraction of the external sphincter

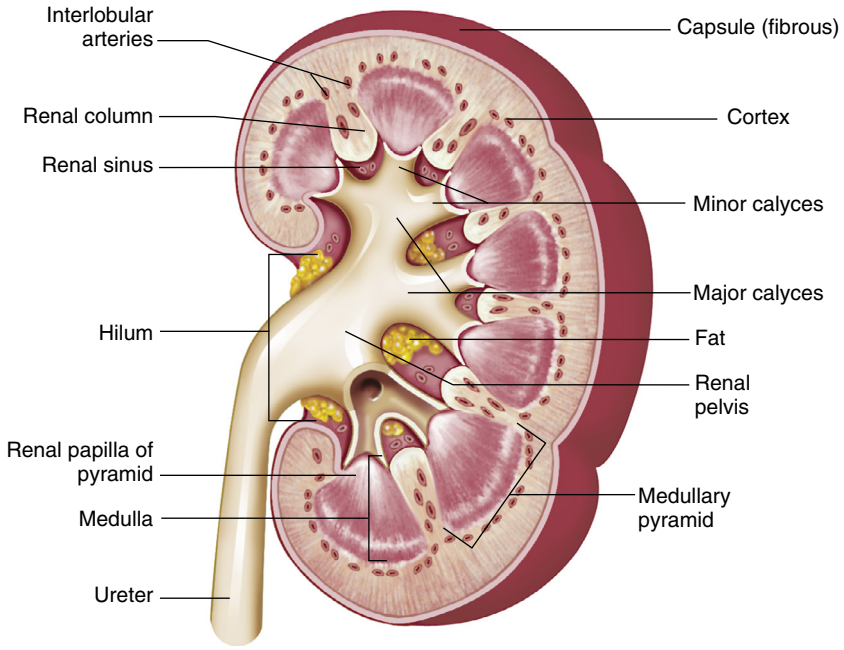

FIGURE 6-2 Internal structure of the kidney.

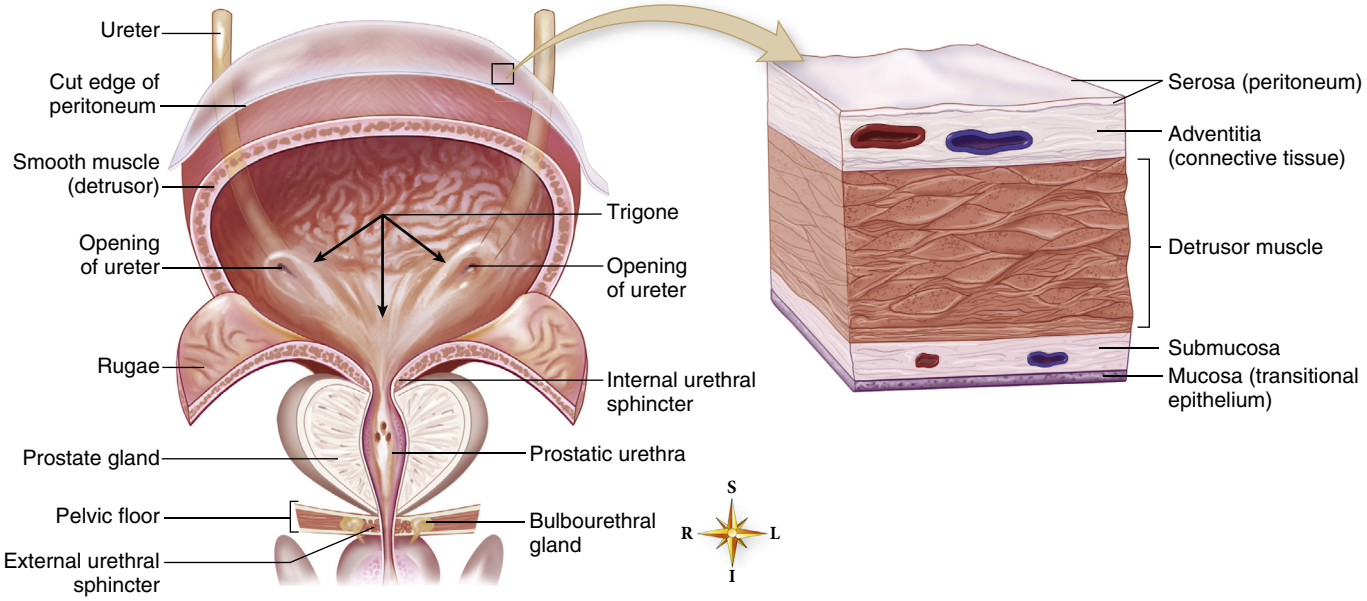

FIGURE 6-3 Structure of the bladder. Frontal view of a dissected urinary bladder (male) in a fully distended state. Inset detail shows a cross section of the bladder wall, which has layers similar to those in other hollow abdominopelvic organs.

to prevent or terminate micturition is learned and is possible only if the motor system is intact. Nervous system injury (cerebral hemorrhage and spinal cord injury) results in involuntary emptying of the bladder at intervals (**incontinence**).

The kidney is also important in the production of red blood cells and in the control of blood pressure. Erythropoietin, a substance produced by the kidney, stimulates the rate of production of red blood cells. Therefore, renal failure is often associated with a severe anemia. *Juxtaglomerular apparatus* refers to specialized cells within renal arterioles that secrete renin, an enzyme that acts with one of the plasma proteins to produce angiotensin. Decreased blood flow through these arterioles increases the secretion of renin and thus the blood level of angiotensin, which constricts peripheral arterioles throughout the body and elevates the blood pressure.

CONGENITAL/HEREDITARY DISEASES

Anomalies of Number and Size

Unilateral renal agenesis (solitary kidney) is a rare anomaly that may be associated with a variety of other congenital malformations (Figure 6-4). Before the diagnosis can be made, it

is essential to exclude a nonfunctioning, diseased kidney and prior nephrectomy. Unilateral renal agenesis results from a failure of the embryonic renal bud or renal vascular system to form. In true renal agenesis, the ureter and corresponding half of the trigone are missing also. Ultrasound (ultrasonography) or CT can demonstrate the absence of renal tissue. A solitary kidney tends to be larger than expected, reflecting compensatory hypertrophy.

A **supernumerary kidney** is also a rare anomaly. The third kidney is usually small and rudimentary and possesses a separate pelvis, ureter, and blood supply. Although supernumerary kidneys function normally, they tend to cause secondary infections that eventually may require their removal.

A small, **hypoplastic kidney** often appears as a miniature replica of a normal kidney, with good function and a normal relationship between the amount of parenchyma and the size of the collecting system (Figure 6-5). Renal hypoplasia must be differentiated from an acquired atrophic kidney, which is small and contracted because of vascular or inflammatory disease that has reduced the volume of renal parenchyma.

Compensatory hypertrophy is an acquired condition that develops when one kidney is forced to perform the function normally carried out by two kidneys (see Figure 6-5). This phenomenon may follow unilateral renal agenesis, hypoplasia, atrophy, or nephrectomy. The ability of the kidney to undergo compensatory hypertrophy is greatest in children and diminishes in adulthood. Ultrasound demonstrates the size of the renal parenchyma, calyces, and pelvis without the use of a contrast agent or ionizing radiation to provide a diagnosis.

Anomalies of Rotation, Position, and Fusion

Malrotation of one or both kidneys may produce a bizarre appearance of the renal parenchyma, calyces, and pelvis that suggests a pathologic condition when in reality the kidney is otherwise entirely normal (Figure 6-6). Abnormally positioned kidneys (**ectopic kidney**) may be found in various locations, from the true pelvis (**pelvic kidney**) (Figure 6-7) to above the diaphragm (**intrathoracic kidney**) (Figure 6-8). Pelvic kidneys occur much more frequently than intrathoracic kidneys. Whenever only one kidney is seen on intravenous urography, a full view of the abdomen is essential to search for an ectopic kidney. Although the ectopic kidney usually functions, the nephrogram and the pelvicalyceal system may be obscured by overlying bone and fecal contents. Patient history can distinguish a true pelvic kidney from a kidney transplant, which typically is located in the right pelvis. **Crossed ectopia** refers to a situation in which an ectopic kidney lies on the same side as the normal kidney and is very commonly fused with it.

Horseshoe kidney is the most common type of fusion anomaly. In this condition, both kidneys are malrotated, and their lower poles are joined by a band of normal renal parenchyma (isthmus) or connective tissue (Figure 6-9). The ureters arise from the kidneys anteriorly instead of medially, and the lower pole calyces point medially rather than laterally. The pelves are often large and flabby and may simulate obstruction. Obstruction at the ureteropelvic junction may occur because of the anterior position of the ureters. **Complete fusion** of the

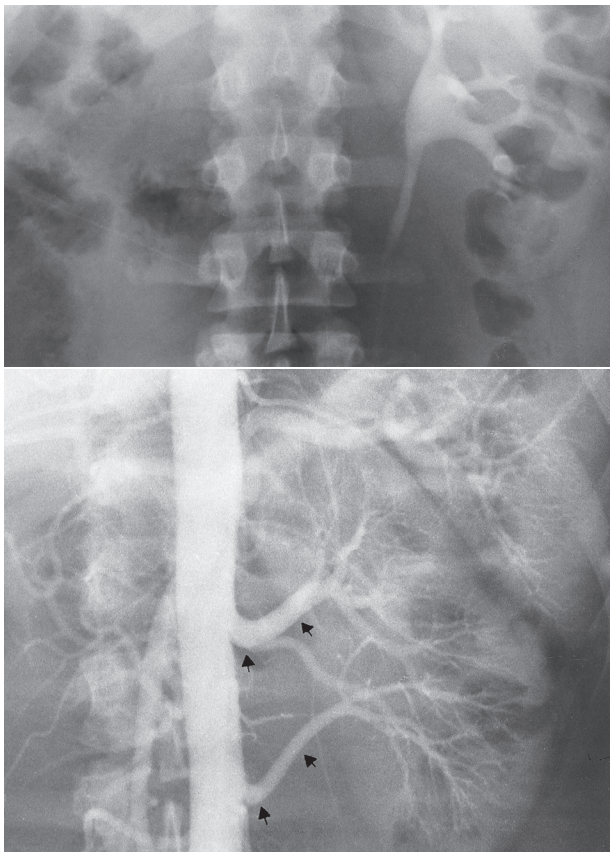

FIGURE 6-4 Solitary kidney. (A) Intravenous urogram demonstrates normal left kidney with no evidence of right renal tissue. (B) Aortogram shows two renal arteries leading to the left kidney (*arrows*) and no evidence of a right renal artery, thus confirming the diagnosis of unilateral renal agenesis.

FIGURE 6-5 Hypoplastic kidney with compensatory hypertrophy. Small left kidney (miniature replica of a normal kidney) has good function with a normal relationship between the amount of parenchyma and the size of the collecting system. Greatly enlarged right kidney represents compensatory hypertrophy.

kidneys is a rare anomaly that produces a single irregular mass that has no resemblance to a renal structure. The resulting bizarre appearance has been given such varied names as disk, cake, lump, and doughnut kidney.

Anomalies of Renal Pelvis and Ureter

Duplication (duplex kidney) is a common anomaly that may vary from a simple bifid pelvis (Figure 6-10) to a completely double pelvis ureter (Figure 6-11) and ureterovesical orifice. The ureter draining the upper renal segment enters the bladder below the ureter draining the lower renal segment. Complete duplication can be complicated by obstruction or by vesicoureteral reflux with infection. Vesicoureteral reflux and infection more commonly involve the ureter draining the lower renal segment; obstruction more frequently affects the upper pole, where it can cause

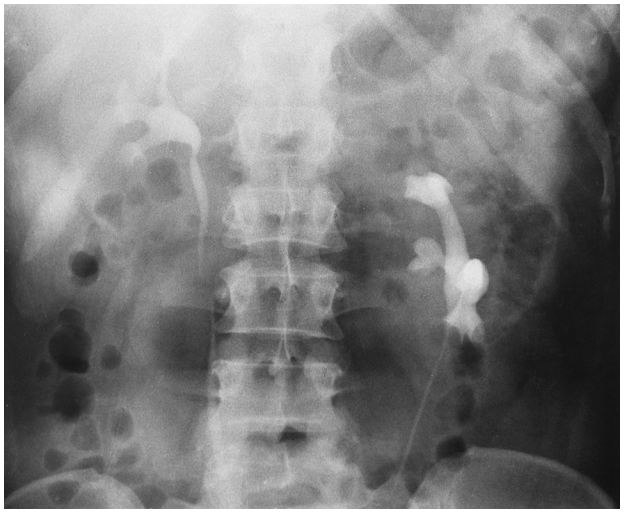

FIGURE 6-6 Malrotation of the left kidney. Note the apparent lateral displacement of the upper ureter and elongation of pelvis.

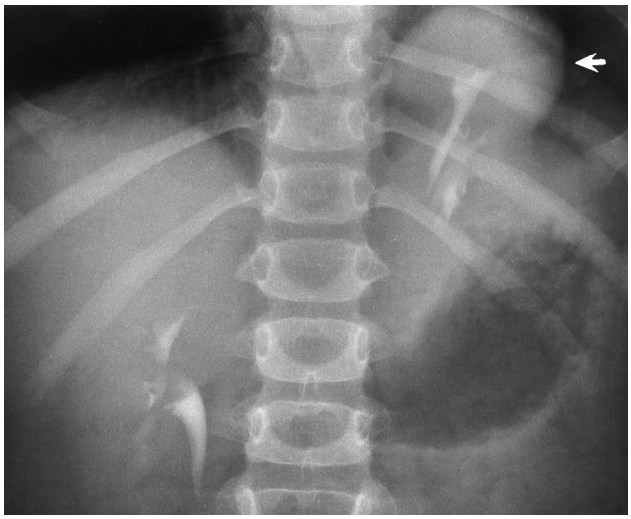

FIGURE 6-8 Intrathoracic kidney (*arrow*).

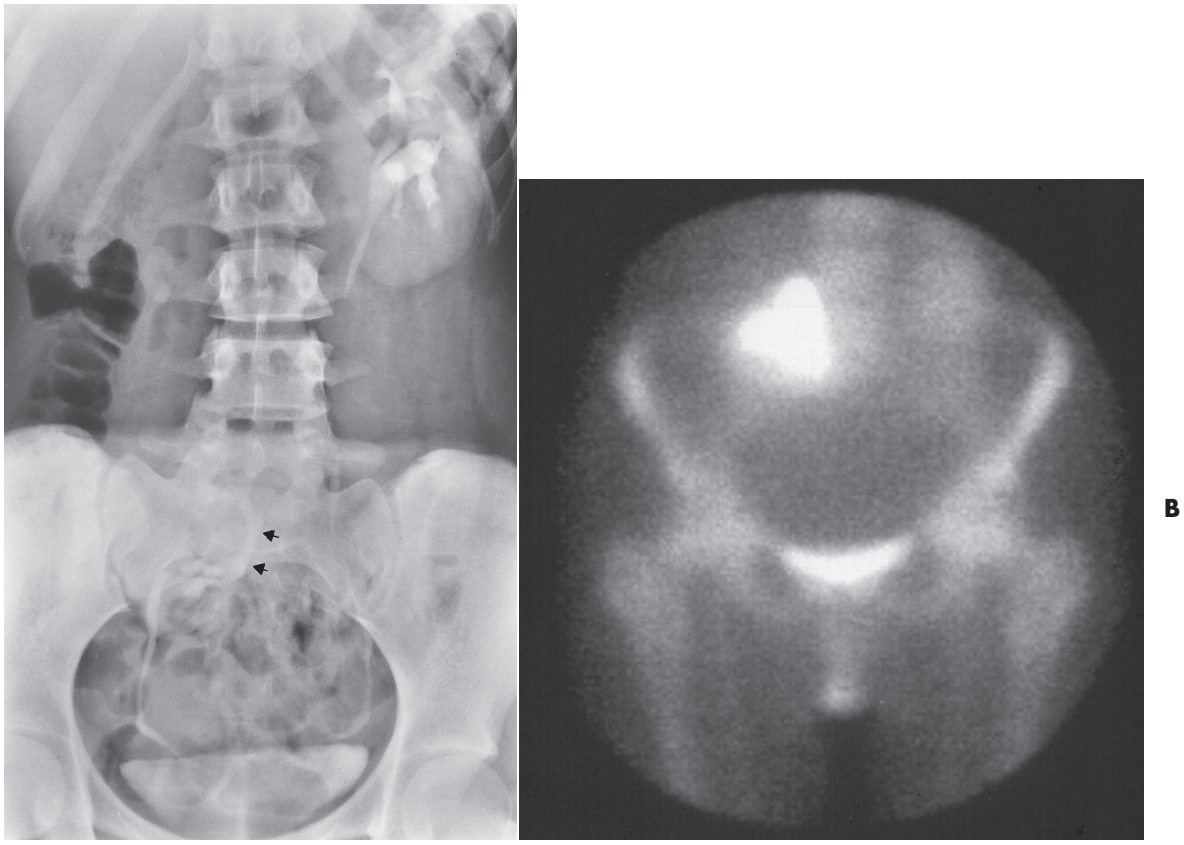

FIGURE 6-7 Pelvic kidney. (A) *Arrows* point to the collecting system, a right pelvic kidney. (B) Right-sided pelvic kidney, an incidental finding on a bone scan.

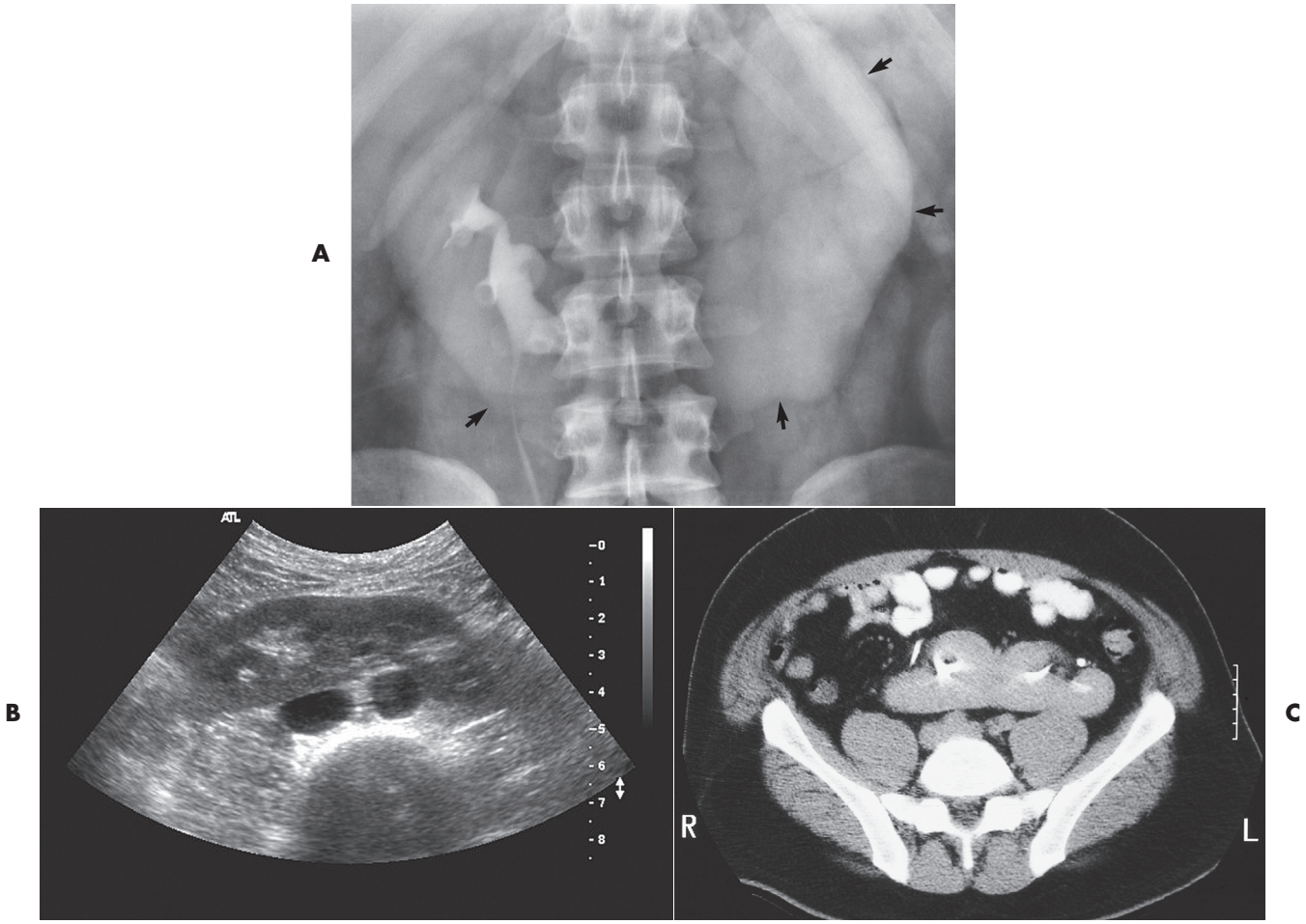

FIGURE 6-9 Horseshoe kidney (*arrows*). **(A)** Prolonged nephrogram and delayed calyceal filling on *left* are caused by an obstructing stone at the ureteropelvic junction on that side. **(B)** Transverse ultrasound shows fused lower poles of a horseshow kidney. The patient had flank pain, which was caused by a stone in the ureterovesicle junction. **(C)** CT scan shows the lower pole connection.

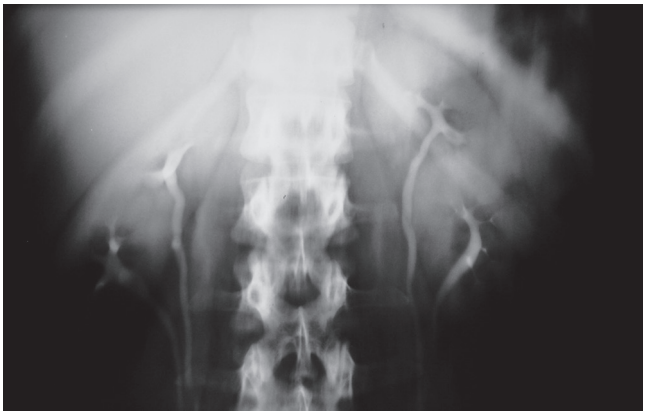

FIGURE 6-10 Bifid renal pelvis. Both kidneys have two separate renal collecting systems (*arrows*) that unite to form a single renal pelvis and ureter.

a hydronephrotic mass that displaces and compresses the lower calyces.

In cases of renal congenital anomalies, to minimize radiation exposure to the patient, ultrasound and plain radiography are the first imaging modalities performed, rather than CT.

Treatment of Congenital/Hereditary Anomalies

Most cases of congenital/hereditary anomalies of the urinary tract require no treatment. If obstruction occurs as a result of the anomaly (because of twisting or angulation of the ureter), therapy (stent placement or surgery) is necessary to maintain normal urine flow. In cases of infection, which occurs more frequently in renal or ureteral duplication because of vesicoureteral reflux, antibiotics are required and it is necessary to determine whether there is an anatomic cause that can be corrected surgically. The large pelvis in a horseshoe kidney makes this anomaly more prone to infection.

Ureterocele

A **ureterocele** is a cystic dilatation of the distal ureter near its insertion into the bladder. In the simple (adult) type, the opening in the ureter is situated at or near the normal position in the bladder, usually with stenosis of the ureteral orifice and with varying degrees of dilatation of the proximal ureter. The stenosis leads to prolapse of the distal ureter into the bladder and dilatation of the lumen of the prolapsed segment. Ectopic ureteroceles are found almost exclusively in infants and children; most are associated with ureteral duplication.

FIGURE 6-11 Renal pelvis and ureters. Note the two separate renal collecting systems with independent renal pelvis and double ureters.

Imaging appearance. The appearance of a ureterocele on intravenous urography depends on whether opaque medium fills it. If it is filled, the lesion appears as a round or oval density surrounded by a thin radiolucent halo representing the wall of the prolapsed ureter and the mucosa of the bladder (cobra head sign) (Figure 6-12A). When the ureterocele is not filled with contrast material, it appears as a radiolucent mass within the opacified bladder in the region of the ureteral orifice (Figure 6-12B). Ultrasound is the modality of choice to evaluate infants and children. Children with ureteral duplication have an 80% incidence of an associated ureterocele. On ultrasound images, a ureterocele appears as a round cystlike structure within the bladder (Figure 6-12C).

On intravenous urography, an ectopic ureterocele typically appears as a large, eccentric filling defect impressing the floor of the bladder (Figure 6-13). The ureterocele arises from the ureter draining the upper segment of the duplicated collecting system. A mass effect, representing hydronephrosis, often involves the upper pole of the kidney and causes downward and lateral displacement of the lower portion of the collecting system.

Treatment. Ureteroceles may need to be treated to preserve kidney function and to reduce the risk of infection. An endoscopic incision of the ureterocele (at the vesicoureteral junction) allows normal urine drainage into the bladder. More aggressive treatment includes surgical resection of the ureterocele with bladder reconstruction.

Posterior Urethral Valves

Posterior urethral valves are thin, transverse membranes, found almost exclusively in males, that cause bladder outlet obstruction and may lead to severe hydronephrosis, hydroureter, and renal damage. The thin, transverse membranes work as a reverse valve, meaning that catheterization is normal but the valve prevents antegrade flow. They are best demonstrated on a voiding cystourethrogram (Figure 6-14). The proximal urethra is dilated, and the thin, lucent, transverse membrane of the valve can be identified.

Treatment. Surgical intervention to correct the anatomic relationships and allow normal urine flow is required to prevent any kidney or ureteral destruction.

Summary of Findings for Congenital/Hereditary Diseases

Disorder	Location/ Description	Imaging appearance	Treatment
Renal agenesis	Solitary kidney	IVU—hypertrophic single functioning kidney US—size of renal parenchyma, calyces, and pelves	Usually no treatment Obstruction: alleviate cause of obstruction Infection: antibiotics, and determine cause, if any
Supernumerary kidney	More than two kidneys	IVU—hypoplastic third kidney, may or may not be fused	
Malrotation	Abnormal position of kidney	Bizarre appearance of renal parenchyma, calyces, and pelvis	
Ectopic kidney		Solitary kidney—second kidney seen in another location (pelvis or thorax)	
Horseshoe kidney	Lower-pole parenchymal fusion	IVU—kidney malrotation and possible nephrogram demonstrating parenchymal fusion US/CT—demonstration of renal fusion	
Duplication	More than one renal pelvis or ureter	IVU—double renal pelvis in single kidney; two ureters exiting kidney and emptying into bladder	
Ureterocele	Distal ureter (vesicoureteral junction)	Round or oval dilated ureter with radiolucent halo US—round, cystlike structure within the bladder	Endoscopic incision of vesicoureteral junction Surgical resection with bladder reconstruction
Posterior urethral valves	Transverse membranes in urethra	VCUG—stricture or narrowing of urethra and a thin radiolucency representing the membrane	Surgical intervention to correct anatomic function

IVU, Intravenous urography; *US,* ultrasound; *VCUG*, voiding cystourethrography.

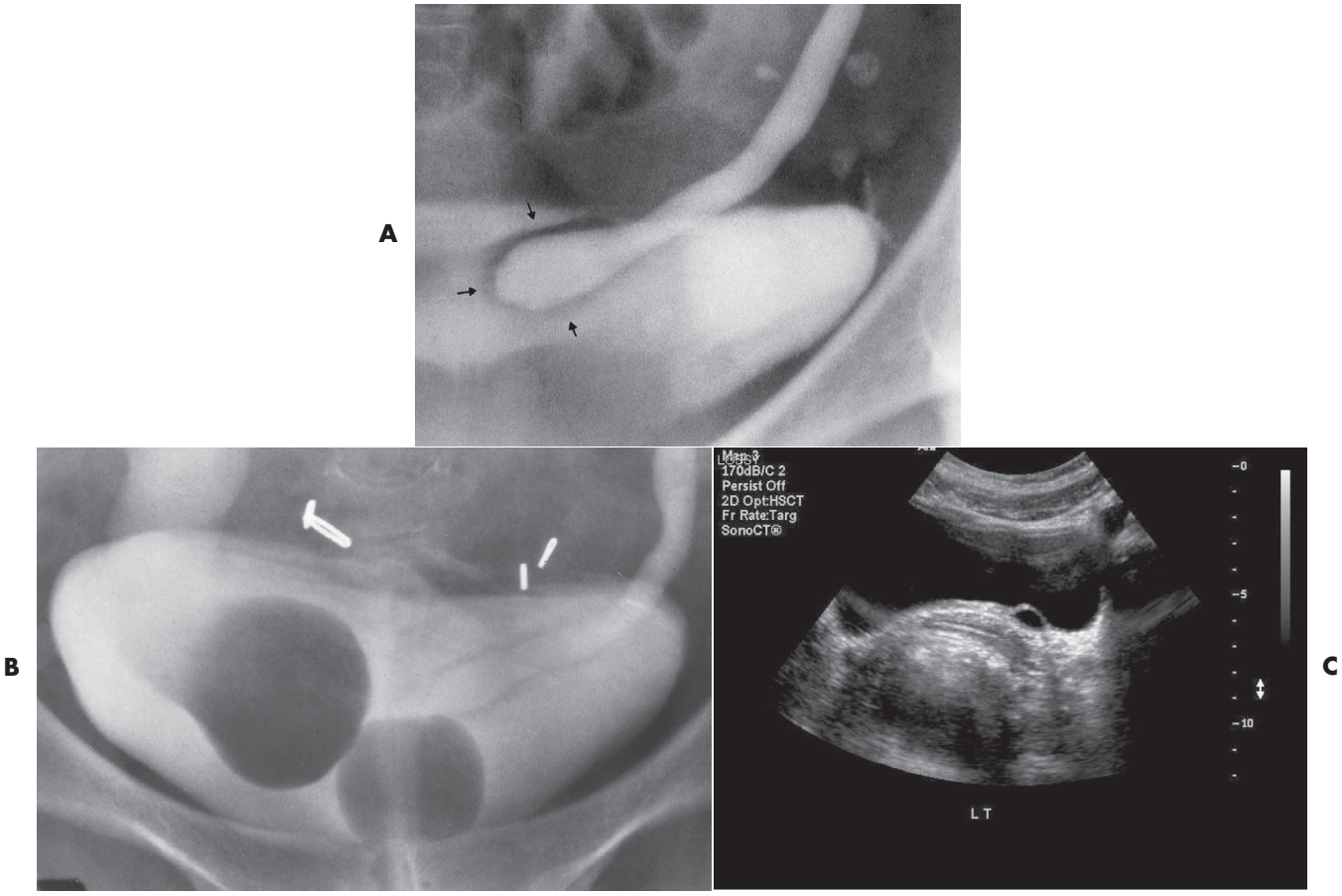

FIGURE 6-12 Simple ureteroceles. (A) Unilateral ureterocele (*arrows*) filled with contrast material. (B) Bilateral ureteroceles without contrast material appear as radiolucent masses in the bladder. (C) Transabdominal ultrasound demonstrates a uterocele (*arrow*) on the left with dilatation.

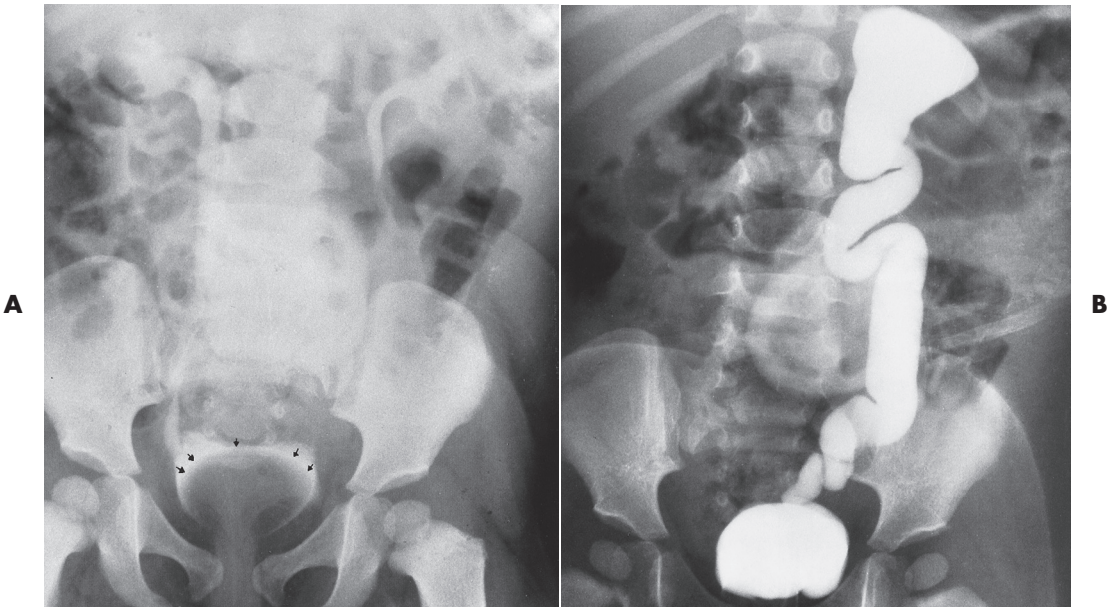

FIGURE 6-13 Ectopic ureteroceles. (A) Intravenous urogram demonstrates large lucency (*arrows*) filling much of the bladder. A slight downward and lateral displacement of the pelvicalyceal system can be seen on the left. (B) Cystogram shows contrast material undergoing reflux to fill the greatly dilated collecting system draining the upper pole of the left kidney. Note the severe dilatation and tortuosity of the ureter.

FIGURE 6-14 Posterior urethral valve. Voiding cystourethrogram shows the characteristic thin transverse membrane of the valve (*arrow*). Distally, the caliber of the bulbous urethra is normal.

FIGURE 6-15 Chronic glomerulonephritis. Nephrotomogram shows bilateral small smooth kidneys. Uniform reduction in parenchymal thickness is particularly apparent in the right kidney. Note that the pelvicalyceal system is well opacified and without the irregular contours and blunted calyces seen in chronic pyelonephritis.

INFLAMMATORY DISORDERS

Glomerulonephritis

Glomerulonephritis is a nonsuppurative inflammatory process involving the tufts of capillaries (glomeruli) that filter the blood within the kidney. It represents an antigen–antibody reaction that most commonly occurs several weeks after an acute upper respiratory or middle ear infection with certain strains of hemolytic streptococci. In recent years, Western countries have seen a decrease in acute glomerulonephritis caused by streptococci. More frequently, the inflammatory process is due to a chronic autoimmune disorder. The inflammatory process makes the glomeruli extremely permeable, allowing albumin and red blood cells to leak into the urine (resulting in proteinuria or hematuria). A decreased glomerular filtration rate results in *oliguria,* a smaller-than-normal amount of urine.

Imaging appearance. The intravenous urographic findings in glomerulonephritis depend on the duration and severity of the disease process and on the level of renal function. In patients with acute glomerulonephritis, the kidneys may be normal or diffusely increased in size with smooth contours and normal calyces. A loss of renal substance in chronic glomerulonephritis produces bilateral small kidneys (Figure 6-15). The renal outline remains smooth and the collecting system is normal, unlike the irregular contours and blunted calyces seen in chronic pyelonephritis. Ultrasound may demonstrate these findings more efficiently without contrast enhancement or radiation exposure.

Treatment. Most cases of acute glomerulonephritis resolve completely, and the kidney returns to normal. In some patients, however, chronic inflammation with periods of remission and exacerbation (increased severity) leads to a fibrotic reaction that results in shrinkage of the kidneys with loss of renal function and the development of uremia. Before therapy is implemented, a renal biopsy may be required to determine the specific cause. If there is an underlying antigen–antibody reaction, corticosteroids for immunosuppression would be appropriate. Infectious processes are treated with antibiotics.

Pyelonephritis

Pyelonephritis is a suppurative inflammation of the kidney and renal pelvis caused by pyogenic (pus-forming) bacteria. Unlike glomerulonephritis, which primarily involves the parenchyma (glomeruli and tubules) of the kidney, the inflammatory process of pyelonephritis affects the interstitial tissue between the tubules. The infection is patchy in distribution, often involves only one kidney, and is asymmetric if both kidneys are involved. Although it may spread from the bloodstream or lymphatics, the infection usually originates in the bladder and ascends by means of the ureter to involve the kidneys. Pyelonephritis often occurs in women and children. The disease frequently develops in patients with obstruction of the urinary tract (due to enlarged prostate gland, kidney stone, or congenital defect), which causes stagnation of the urine and provides a breeding ground for infection. Instrumentation or catheterization of the ureter is also an important contributing factor to the development of pyelonephritis.

Patients with pyelonephritis have high fever, chills, and sudden back pain that spreads over the abdomen. Painful urination (dysuria) usually occurs. Large amounts of pus may be

FIGURE 6-16 Chronic pyelonephritis. Diffuse rounded clubbing of multiple calyces with atrophy and thinning of the overlying renal parenchyma. *Arrows* indicate the outer margin of the kidney.

FIGURE 6-17 Emphysematous pyelonephritis.

detected in the urine (pyuria), and bacteria can be cultured from the urine or observed in the urinary sediment.

Imaging appearance. In most patients with acute pyelonephritis, the intravenous urogram findings are normal. Occasional abnormalities include generalized enlargement of the kidney on the symptomatic side, delayed calyceal opacification, and decreased density of the contrast material. A characteristic finding is linear striation in the renal pelvis, which probably represents mucosal edema.

The urographic hallmark of chronic pyelonephritis is patchy calyceal clubbing with overlying parenchymal scarring (Figure 6-16). Initially, there is blunting of the calyces, which then become rounded or clubbed. Fibrotic scarring causes a cortical depression overlying the dilated calyx. Progressive cortical atrophy and thinning may be so extensive that the tip of the blunted calyx appears to lie directly beneath the renal capsule. The urographic findings may be unilateral or bilateral and are often most pronounced at the poles. If calyceal changes are minimal, the overlying cortical depressions may simulate lobar infarctions or normal kidney lobulations. However, in chronic pyelonephritis, the cortical depression lies directly over a calyx rather than between calyces as in lobar infarctions or congenital lobulation. Chronic pyelonephritis may progress to end-stage renal disease with small, usually irregular, poorly functioning kidneys.

CT has become the imaging modality of choice for this disease. Contrast-enhanced CT demonstrates the cortical changes and may show an associated abscess. Ultrasound also can demonstrate an abscess but is less sensitive. Both CT and ultrasound can detect hydronephrosis, which would indicate that urinary tract obstruction is a predisposing factor. In chronic nephritis, ultrasound shows loss of renal parenchyma as an increase in echogenicity in the area of the scar and extension of the central renal sinus echoes to the periphery of the affected area. Dimercaptosuccinic acid scintigraphy (nuclear medicine study) can demonstrate inflammation and scarring of the kidney and determine the distribution of function in the renal cortex. Some clinicians prefer this study to CT because of the lower radiation dose.

Treatment. With the availability of antibiotic therapy, pyelonephritis generally heals without complication. However, fibrous scarring can cause irregular contraction of the kidney. Severe infection can destroy large amounts of renal tissue, leading to uremia or septicemia as a result of diffuse spread of infection throughout the body. In cases of chronic pyelonephritis, a long-term regimen of antibiotics is appropriate. If this is ineffective, more aggressive therapy may be required. Some investigators consider percutaneous drain placement an acceptable alternative to surgery in such cases.

Emphysematous Pyelonephritis

Emphysematous pyelonephritis is a severe form of acute parenchymal and perirenal infection with gas-forming bacteria that occurs virtually only in diabetic patients and causes an acute necrosis of the entire kidney.

Imaging appearance. The presence of radiolucent gas shadows within and around the kidney is pathognomonic of emphysematous pyelonephritis (Figure 6-17). CT is the preferred modality for localizing the gas patterns within and around (perinephric) the kidney. The affected region appears as mottled areas of low attenuation.

Treatment. When the gas pattern is within the kidney—a finding associated with a mortality rate of 60%—antibiotics and drainage are necessary. This condition is a surgical emergency requiring nephrectomy, which lowers the mortality rate to 20%. In most cases, this disease process is fatal if the patient is treated with just medications.

Tuberculosis

The hematogenous spread of tuberculosis may lead to the development of small granulomas scattered in the cortical

FIGURE 6-18 Tuberculosis. Early stage of papillary destruction (*arrows*).

FIGURE 6-19 Tuberculous autonephrectomy. Plain image shows coarse, irregular calcification that retains a kidney-like shape (*solid arrow*). Note also the tuberculous calcification of the right distal ureter (*open arrow*).

portion of the kidneys. Renal tuberculosis usually occurs as a secondary infection from lung involvement but can evolve from other sites. It typically becomes manifest 5 to 10 years following the primary infection.

Imaging appearance. Spread of infection to the renal pyramid causes an ulcerative, destructive process in the tips of the papillae with irregularity and enlargement of the calyces (Figure 6-18). Fibrosis and stricture formation lead to cortical scarring and parenchymal atrophy, which may simulate the appearance of chronic bacterial pyelonephritis. Flecks of calcification may develop in multiple tuberculous granulomas. With progressive disease, gross amorphous and irregular calcifications can form. Eventually, the entire nonfunctioning renal parenchyma may be replaced by massive calcification (autonephrectomy) (Figure 6-19).

Tuberculosis can also involve the ureter and bladder. Initially, there are multiple ulcerations that result in a ragged, irregular appearance of the ureteral wall. As the disease heals, there are usually multiple areas in which the ureteral strictures alternate with dilated segments, producing a beaded or corkscrew appearance. In advanced cases, the wall of the ureter may become thickened and fixed with no peristalsis; this results in a pipestem ureter that runs a direct course toward the bladder (Figure 6-20). Tuberculous involvement of the urinary bladder may produce mural irregularities simulating carcinoma or, more commonly, a small, contracted bladder with a thickened wall.

Treatment. A regimen (6 to 8 months) of a combination of powerful tuberculostatic drugs is required for a cure. If the tuberculostatic drugs are not used in combination, a drug resistance can develop, making the treatment ineffective.

Papillary Necrosis

Papillary necrosis refers to a destructive process involving a varying amount of the medullary papillae and the terminal portion of the renal pyramids. Common predisposing factors include diabetes, pyelonephritis, urinary tract infection or obstruction, sickle cell disease, and phenacetin abuse.

Imaging appearance. The necrotic process causes cavitation of the central portion of the papillae or complete sloughing of the papillary tip (Figure 6-21). When a piece of medullary tissue has been completely separated from the rest of the renal parenchyma, an intravenous urogram shows a characteristic ring of contrast material surrounding a triangular lucent filling defect representing the sloughed necrotic tissue. The remaining calyx has a round, saccular, or club-shaped configuration. The sloughed papilla may stay in place and become calcified, or it may pass down the ureter, where it may simulate a stone and even cause obstruction. Ultrasound images show sloughing as an echogenic, nonshadowing structure in the collecting system.

Treatment

In most cases, the treatment is supportive. If the condition is induced by medication, the offending agent must be

discontinued. Any predisposing condition (diabetes or sickle cell anemia) should be controlled. If obstruction occurs as a result of medullary tissue separation, removal of the obstruction endoscopically or surgically is necessary to prevent renal failure. Ureteral tamponade placement can control papillary bleeding caused by the separation.

Cystitis

Inflammation of the urinary bladder is more common in women because the urethra is shorter. The major cause is the inadvertent spread of bacteria present in fecal material, which reaches the urinary opening and travels upward to the bladder. Instrumentation or catheterization of the bladder is another important cause of cystitis, which is the most common infection in hospitalized patients (nosocomial infection). The radiographer needs to keep the urine bag below the patient to prevent retrograde flow that may cause cystitis. Cystitis can also develop from sexual intercourse, with the spread of infecting organisms from around the vaginal opening. Urinary frequency, urgency, and a burning sensation during urination are typical clinical findings.

Imaging appearance. Although acute inflammation of the bladder generally does not produce changes detectable on intravenous urography, chronic cystitis causes a decrease in bladder size that is often associated with irregularity of the bladder wall (Figure 6-22). In candidal cystitis, fungus balls may produce lucent filling defects in the opacified bladder. Similar lucent filling defects in the bladder may reflect blood clots in patients with hemorrhagic cystitis and may complicate chemotherapy in the treatment of leukemia and lymphoma. Sonographic images demonstrate a thickened bladder wall.

A dramatic radiographic appearance is produced by emphysematous cystitis, an inflammatory disease of the bladder that most often occurs in diabetic patients and is caused by gas-forming bacteria. Characteristic plain image findings are a ring of lucent gas outlining all or a part of the bladder wall and the presence of gas within the bladder lumen (Figure 6-23). The CT demonstration of gas within the bladder wall aids in determining the extent of the inflammation.

Treatment. With the use of antibiotic and sulfa drug therapy, cystitis generally heals without complication.

FIGURE 6-20 Ureteral tuberculosis. Irregular and enlarged calyces.

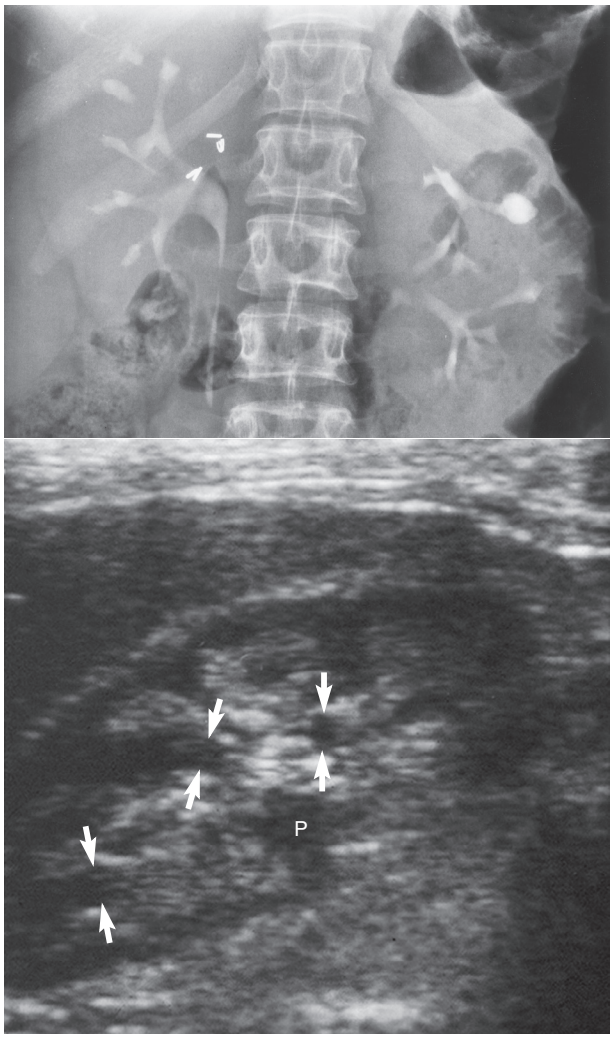

FIGURE 6-21 Papillary necrosis. (A) Generalized saccular or club-shaped configuration of most calyces bilaterally in patient with sickle cell disease. Note the surgical clips. **(B)** Ultrasound illustrates sloughed papilla causing shadowing and swollen pyramids (*arrows*). *P,* renal pelvis.

Summary of Findings for Inflammatory Disorders

Disorder	Location	Imaging appearance	Treatment
Glomerulonephritis (nonsuppurative)	Parenchyma (glomeruli and tubules)	Normal contour Acute: normal to increased kidney size Chronic: small kidney	Most cases resolve completely Corticosteroids for immunosuppression Antibiotics for infection
Pyelonephritis (suppurative)	Interstitial tissue between tubules	IVU—acute produces striation in renal pelvis; chronic blunting to clubbing of calyces CT—changes in cortex and associated abscesses US—large pelvis with loss of parenchyma NM—inflammation, scarring and renal distribution function	Conservative—antibiotics, fluid management Aggressive—percutaneous drainage, antibiotics, surgery
Emphysematous pyelonephritis	Parenchymal and perirenal	Radiolucent gas CT—mottled areas of low attenuation	Acute medical emergency—nephrectomy
Tuberculosis	Cortex	Irregularity and enlargement of calyces, calcifications	Regimen of combination of tuberculostatic drugs
Papillary necrosis	Medullary papillae and terminal portion of renal pyramids	Cavitation of central portion of papillae US—sloughing appears as an echogenic nonshadowing structure in the collecting system	Medication-induced: discontinuation of offending agent Predisposing conditions: control of conditions to reduce risk Obstruction: removal, endoscopic or surgical
Cystitis	Bladder	Irregularity of bladder wall US—thickened bladder wall CT—bladder wall filled with gaseous material	Antibiotics or sulfa drugs

IVU, Intravenous urography; *NM,* nuclear medicine; *US,* ultrasound.

FIGURE 6-22 Cystitis. Intravenous urogram shows irregular, lobulated filling defects (representing intense mucosal edema) at the base of the bladder.

URINARY CALCULI

Urinary calculi most commonly form in the kidney. They are asymptomatic until they lodge in the ureter and cause partial obstruction, resulting in extreme pain that radiates from the area of the kidney to the groin (Figure 6-24). The cause of kidney stones varies and often reflects an underlying metabolic abnormality, such as hypercalcemia (resulting from hyperparathyroidism) or any cause of increased calcium excretion in the urine. Urinary stasis and infection are also important factors in promoting stone formation.

Imaging appearance. More than 80% of symptomatic renal stones contain enough calcium to be radiopaque and detectable on plain abdominal radiographs (Figure 6-25 and Figure 6-26A). Completely radiolucent calculi contain no calcium and are composed of a variety of substances (e.g., oxalates, mineral magnesium, or uric acid) that are in excessive concentration in the urine. Plain abdominal radiographs miss approximately 34% of the stones because of their size or location or because they are obscured by bowel or bone. Noncontrast helical CT is used most frequently to best demonstrate the stone without anatomically obscuring the area (Figure 6-26B). This modality is safer, easier, and more accurate (95%) than intravenous urography. CT demonstrates the hydroureter or hydronephrosis that results from

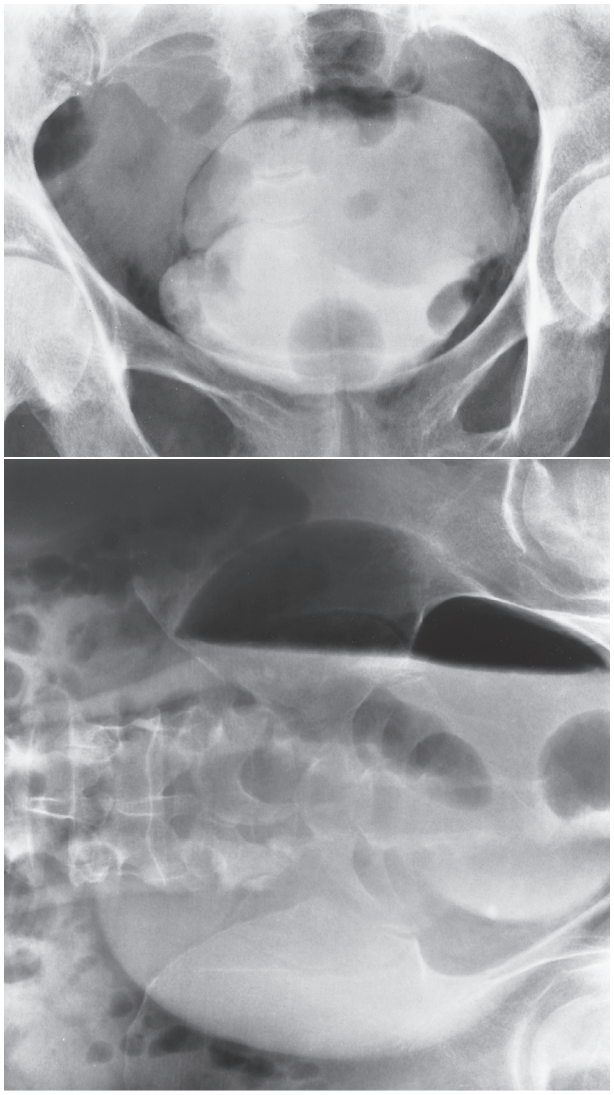

FIGURE 6-23 Emphysematous cystitis. (A) Image from a cystogram shows a thin rim of lucency surrounding much of the bladder, which is filled with contrast material. (B) Right lateral decubitus view clearly shows a long air–fluid level.

FIGURE 6-24 Contrast extravasation. Fifteen-minute intravenous urogram demonstrates a stricture on the left ureter (*straight black arrow*) and a filling defect in the right ureter (*white arrow*). Both renal pelves are dilated, and the right demonstrates extravasation of contrast material (*curved black arrows*).

the obstruction, and density readings help determine the type of stone.

Ultrasound demonstrates an echogenic region with acoustic shadowing of the stone with hydroureter or hydronephrosis; however, a stone smaller than 3 mm may not produce a detectable acoustic shadow. This modality is used when ionizing radiation is contraindicated.

When CT is unavailable, intravenous urography is used to detect these otherwise invisible, nonopaque stones, which appear as filling defects in the contrast agent–filled collecting system. In patients with acute renal colic caused by an obstructing stone in the ureter, intravenous urography may demonstrate the point of cutoff and dilatation of the proximal ureter and pelvicalyceal system. With acute obstruction, the intrapelvic pressure may increase to such an extent that there is little or no glomerular filtration, resulting in a delayed and prolonged nephrogram and a lack of calyceal filling on the affected side.

Small renal stones (3 mm or less) may pass spontaneously in the urine. At times, a stone may completely fill the renal pelvis (**staghorn calculus**) (see Figure 6-26A), blocking the flow of urine. Figure 6-26C shows nephrostomy placement to drain the kidney to aid in preventing renal failure.

Calcium can also deposit within the renal parenchyma (**nephrocalcinosis**) (Figure 6-27). This calcification varies from a few scattered punctate densities to very dense and extensive calcifications throughout both kidneys. The most common causes of nephrocalcinosis are hyperparathyroidism, increased intestinal absorption of calcium (sarcoidosis, hypervitaminosis D, and milk-alkali syndrome), and renal tubular acidosis, a disorder in which the kidney is unable to excrete an acid urine (below pH 5.4).

Stones can also form in other portions of the genitourinary tract. Ureteral calculi almost invariably result from the downward movement of kidney stones (Figure 6-28). They are usually small, irregular, and poorly calcified and are therefore easily missed on abdominal radiographs that are not of good quality. Calculi most commonly lodge in the lower portion of the ureter, especially at the ureterovesical junction and at the pelvic brim (Figure 6-29). They are often oval, with their long axes paralleling the course of the ureter. Ureteral calculi must be differentiated from the far

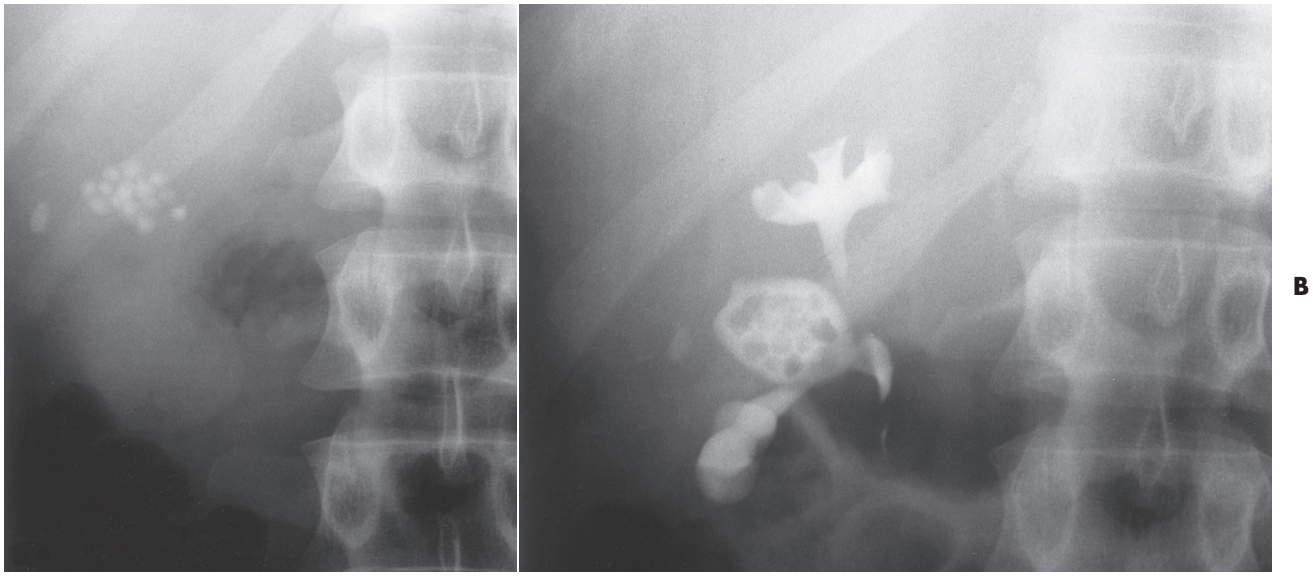

FIGURE 6-25 Cystine stones. (A) Plain image shows multiple radiopaque calculi. (B) Intravenous urogram demonstrates stones as lucent filling defects in the opacified renal pelvis.

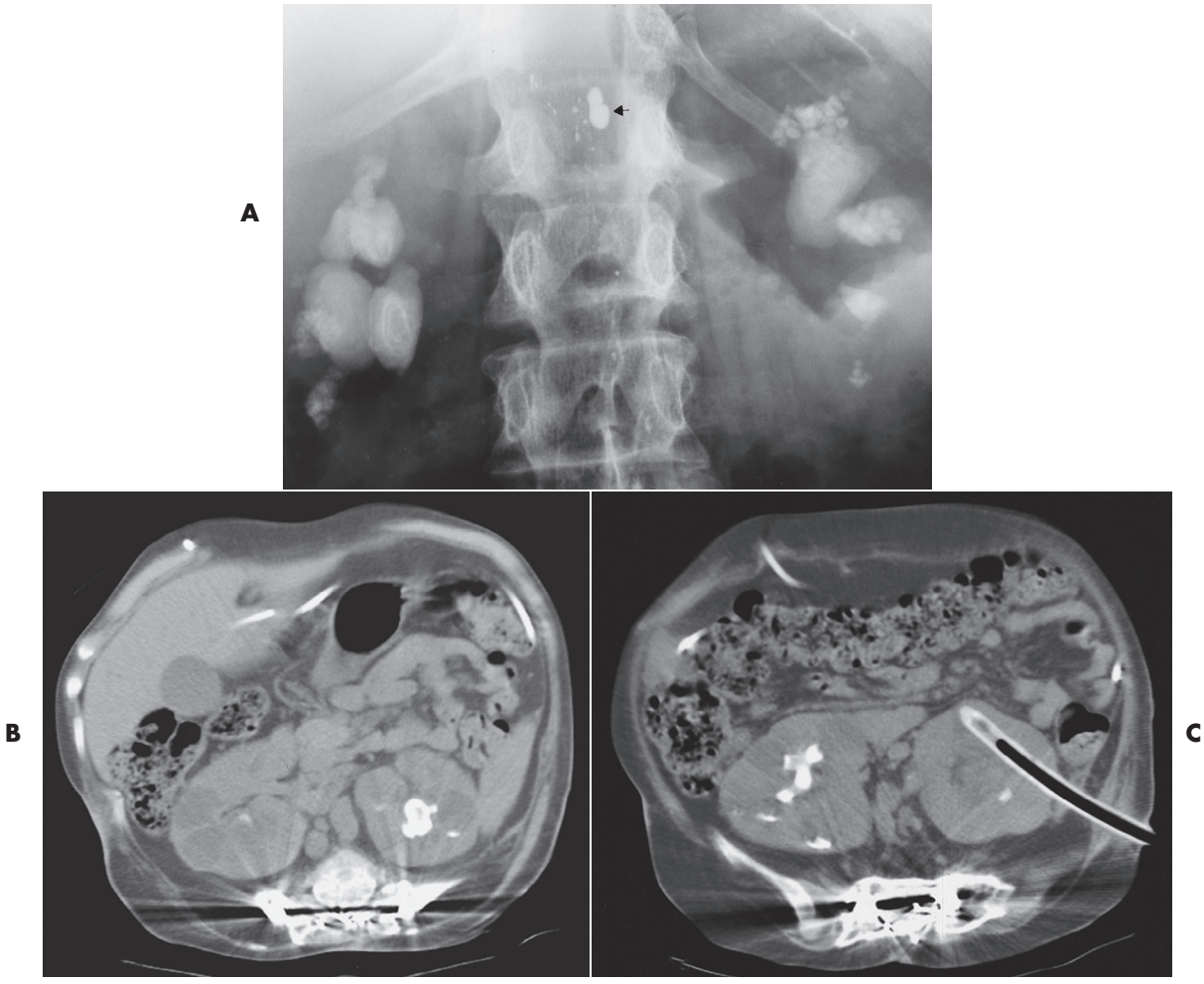

FIGURE 6-26 Urinary calculi. (A) Staghorn calculi fill the renal pelves bilaterally. Of incidental note is residual contrast material (*arrow*) from prior myelogram. (B) Spiral CT scanning obtained at 5-mm intervals on an 11-year-old boy, demonstrating bilateral renal calculi with caliectasis (dilated calyces) and kidney enlargement. (C) Nephrostomy tube placement in the left renal pelvis to drain the kidney.

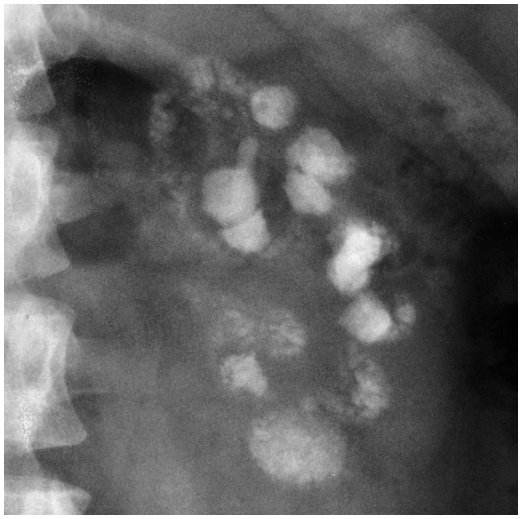

FIGURE 6-27 Nephrocalcinosis. Multiple deposits are scattered throughout the parenchyma of the left kidney.

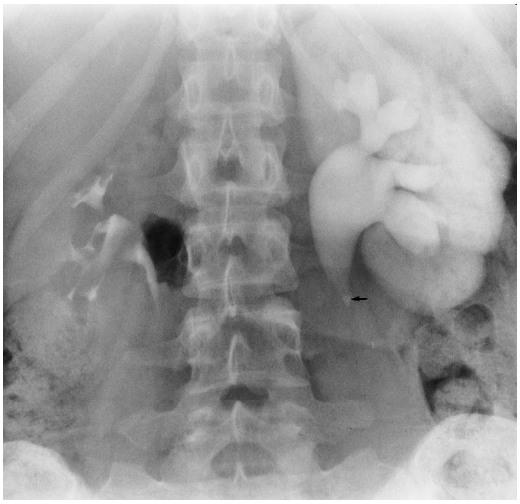

FIGURE 6-28 Obstructing ureteral calculus. Intravenous urogram demonstrates prolonged nephrogram and pronounced dilatation of collecting system and pelvis proximal to the obstructing stone (*arrow*).

more common phleboliths, which are spherical and located in the lateral portion of the pelvis below a line joining the ischial spines. In contrast, ureteral stones are situated medially above the interspinous line.

Stone formation in the bladder is a disorder primarily of elderly men with obstruction or infection of the lower urinary tract (Figure 6-30A). Frequently associated lesions include bladder-outlet obstruction, urethral strictures, neurogenic bladder, and bladder diverticula (Figure 6-30B). At times, upper urinary tract stones migrate down the ureter and are retained in the bladder. Bladder calculi can be single or multiple. They vary in size from tiny concretions, each the size of a grain of sand, to an enormous single calculus occupying the entire bladder lumen. Most bladder calculi are circular or oval; however, almost any shape can be encountered. They can be amorphous, laminated (layered), or even spiculated. One unusual type with a characteristic radiographic appearance is the hard burr, or jackstone, variety, which gets its name from the many irregular prongs that project from its surface and simulate the child's toy jack.

Treatment. Preventive measures for kidney stones include increasing fluid intake and decreasing the intake of the stone-forming substances. In the past, surgery was frequently necessary to remove large kidney stones. Recently, medication introduced into the upper urinary tract by means of a percutaneous catheter has been used to dissolve large kidney stones into smaller pieces that pass easily (chemolysis). Lithotripsy is a technique to break up the stone using an external source of shock waves that shatter the hard stones into sand-sized particles, which are then excreted in the urine. This technique works well for stones in the kidney or the upper ureter (above the pelvic brim). For stones in the lower ureter (in the pelvis), cystoscopic retrieval (ureteroscopy basket) or laser destruction is an option. The last resort is performing surgery because it traumatizes the patient and requires a longer recovery period.

URINARY TRACT OBSTRUCTION

Urinary tract obstruction produces anatomic and functional changes that vary with regard to rapidity of onset, degree of occlusion, and distance between the kidney and the obstructing lesion. In adults, urinary calculi, pelvic tumors, urethral strictures, and enlargement of the prostate gland are the major causes. In children, congenital malformations (ureteropelvic junction narrowing, ureterocele, retrocaval ureter, and posterior urethral valve) are usually responsible for mechanical obstruction. Normal points of narrowing, such as the ureteropelvic and ureterovesical junctions, the bladder neck, and the urethral meatus, are common sites of obstruction. Blockage above the level of the bladder causes unilateral dilatation of the ureter (**hydroureter**) and renal pelvicalyceal system (**hydronephrosis**); if the lesion is at or below the level of the bladder, as in prostatic hypertrophy or tumor, bilateral involvement is the rule.

Imaging appearance. Noncontrast helical CT scanning detects mass effects, stones, and other causes of obstruction better than intravenous urography. A contrast agent may be used to demonstrate renal function and the renal vascular structures if needed. In acute urinary tract obstruction, diminished filtration of urographic contrast material results in parenchymal opacification that is delayed in comparison with that of the nonobstructed kidney. The nephrogram eventually becomes more dense than normal because of a decreased rate of flow of fluid through the tubules, which results in enhanced water reabsorption by the nephrons and greater concentration of the contrast material (Figure 6-31). There is delayed and decreased pelvicalyceal filling because of dilatation and elevated pressure in the collecting system. The radiographic study may have to be prolonged for up to 48 hours after the administration of contrast material to determine the precise site of obstruction.

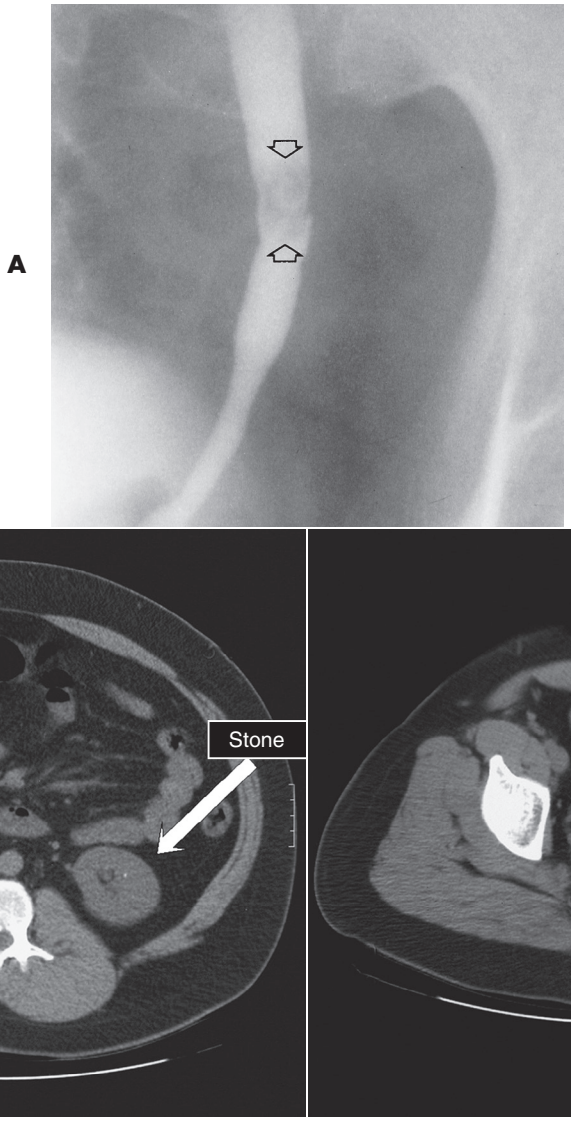

FIGURE 6-29 **Ureteral calculus.** (A) A stone appears as a nonopaque filling defect (*arrows*) in the distal portion of the ureter. (B) CT scanning performed at 5-mm intervals without contrast material demonstrates a stone in the right kidney. (C) A scan of the lower pelvis demonstrates a second stone in the distal portion of the ureter.

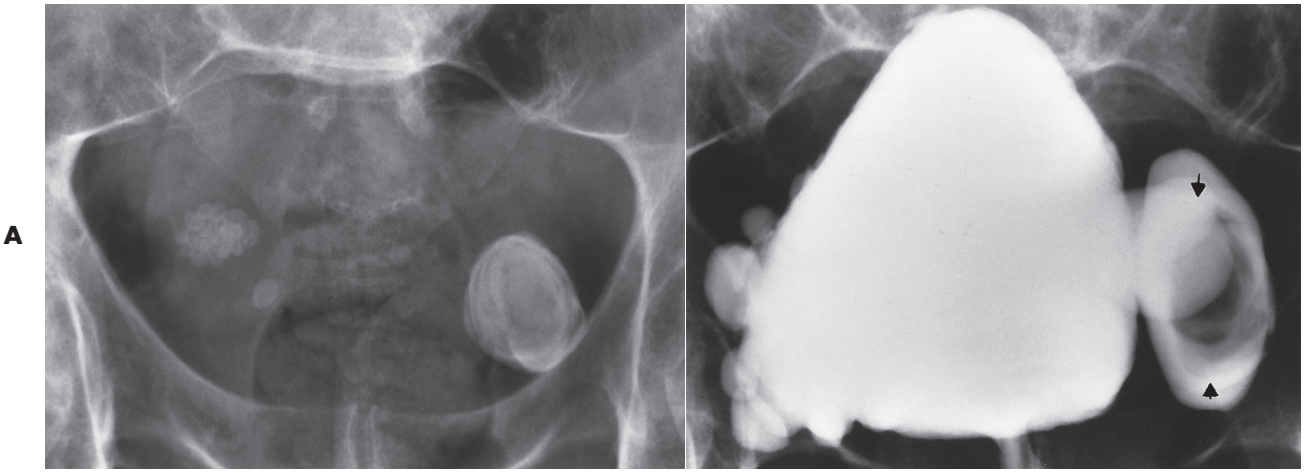

FIGURE 6-30 **Bladder calculi.** (A) Plain radiograph of the pelvis shows a large laminated stone on the left and multiple smaller calculi on the right. (B) Intravenous urogram demonstrates a large stone (*arrows*) in the bladder diverticulum on the left side. Multiple smaller calculi on the right have been obscured by overlying contrast material.

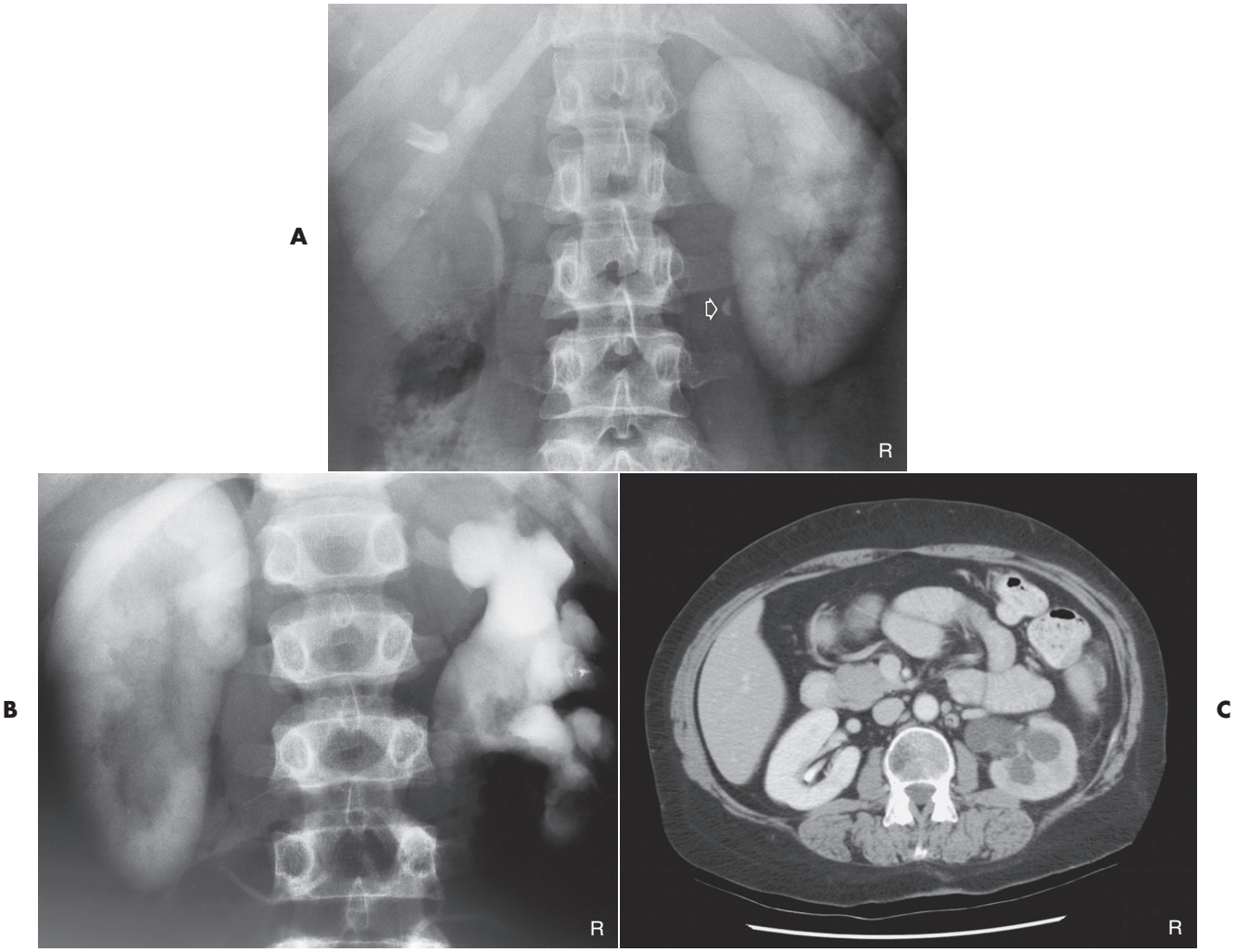

FIGURE 6-31 Urinary tract obstruction. **(A)** Intravenous urogram demonstrates prolonged nephrogram on the left and no calyceal filling. *Arrow* points to the obstructing stone in the proximal left ureter. **(B)** In another patient, there is a prolonged and intensified obstructive nephrogram of the right kidney. On the left, there is pronounced dilatation of the pelvicalyceal system but no persistent nephrogram, reflecting intermittent chronic obstruction on this side. **(C)** CT scan of a different patient shows large renal calyces, hydronephrosis, and a hydroureter on the left.

In the patient with acute urinary tract obstruction, the kidney is generally enlarged, and the calyces are moderately dilated. An uncommon but pathognomonic urographic finding in acute unilateral obstruction (usually caused by a ureteral stone) is opacification of the gallbladder 8 to 24 hours after the injection of contrast material. This "vicarious excretion" is related to increased liver excretion of contrast material that cannot be promptly excreted by the kidneys.

As an obstruction becomes more chronic, the predominant urographic finding is a greatly dilated pelvicalyceal system and ureter proximal to the obstruction (Figure 6-32). A prolonged increase in pressure causes progressive papillary atrophy, leading to calyceal clubbing. Gradual enlargement of the calyces and renal pelvis with progressive destruction of renal parenchyma may continue until the kidney becomes a nonfunctioning hydronephrotic sac in which its normal anatomy is obliterated.

Whenever possible, the site of obstruction should be demonstrated. Although intravenous urography with delayed images may accomplish this purpose, antegrade pyelography is often required. In this procedure, a catheter or needle is placed percutaneously into the dilated collecting system under ultrasound or fluoroscopic guidance, and contrast material is then introduced. This approach has the added advantage of providing immediate and certain decompression of a unilateral obstructing lesion.

Ultrasound is of particular value in detecting hydronephrosis in patients with such severe urinary tract obstruction and renal dysfunction that there is no opacification of

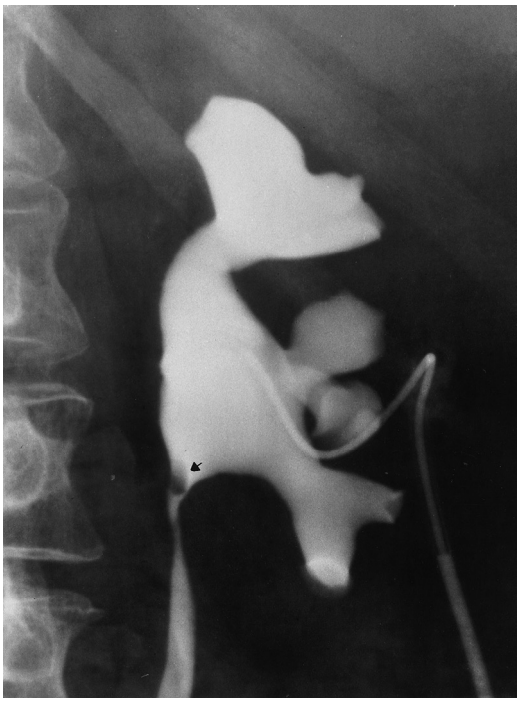

FIGURE 6-32 Hydronephrosis. Dilatation of the entire pelvicalyceal system proximal to an obstructing *Cryptococcus* fungus ball (*arrow*) at the ureteropelvic junction.

the kidneys and collecting systems on intravenous urograms. The dilated calyces and pelvis become large, hydronephrotic, echo-free sacs separated by septa of compressed tissue and vessels (Figure 6-33A). With increased duration and severity of hydronephrosis, the intervening septa may disappear, leaving a large fluid-filled sac with no evidence of internal structure and no normal parenchyma apparent at its margins (Figure 6-33B).

A physiologic form of hydronephrosis often develops during pregnancy. The enlarging uterine mass and physiologic hormonal changes cause extrinsic pressure on the ureter, leading to progressive dilatation of the proximal collecting systems (Figure 6-34). Often bilateral, the dilatation usually is more prominent and develops earlier on the right side. After delivery, the urinary tract returns to normal within several weeks. In some women, however, persistent dilatation of the ovarian vein can compress the ureter and result in prolonged postpartum hydronephrosis.

Treatment. Appropriate treatment requires decompression of the urinary tract to prevent parenchymal damage and possible ureteral rupture due to the blockage. Percutaneous nephrostomy provides drainage and may help demonstrate the site of obstruction (see Figure 6-26C). Once the cause of the obstruction is determined, therapy for the specific cause can be initiated.

Summary of Findings for Urinary Obstructions

Disorder	Location	Imaging appearance	Treatment
Calculi	Most commonly form in the kidney	KUB—radiopaque calcium renal stones CT—demonstrates location of stone IVU—noncalcium stones cause filling defects US—an echogenic region with acoustic shadowing	Medications to dissolve stone Lithotripsy to break up the stone Cystoscopy for retrieval or laser destruction Surgery
Obstruction	Internal or external pressure prevents normal urine flow	CT—mass effects, stones, or other causes of obstruction IVU: Dense nephrogram, delayed or decreased pelvicalyceal filling Chronic obstruction has calyceal clubbing US—chronic hydronephrosis with echo-free sacs	Decompression of urinary tract to prevent damage Percutaneous nephrostomy to demonstrate obstruction and provide drainage Treatment of cause of obstruction

IVU, Intravenous urography; *KUB,* kidney–ureter–bladder radiograph; *US,* ultrasound.

CYSTS AND TUMORS

Renal Cyst

Simple renal cysts are the most common unifocal masses of the kidney. They are fluid filled and usually unilocular, although septa sometimes divide the cyst into chambers, which may or may not communicate with each other. Cysts vary in size, and they may occur at single or multiple sites in one or both kidneys. Thin, curvilinear calcifications can be demonstrated in the wall of approximately 3% of simple cysts. However, this peripheral type of calcification is not pathognomonic of a benign process because malignant kidney lesions can produce a similar pattern.

Imaging appearance. As a simple renal cyst slowly increases in size, its protruding portion elevates the adjacent edges of the cortex. The cortical margin appears on nephrotomography as a very thin, smooth, radiopaque rim about the bulging lucent cyst (beak sign) (Figure 6-35). Although the beak sign is generally considered characteristic of benign renal cysts, it merely reflects a slow expansion of a mass and thus may occasionally be seen in slow-growing solid lesions, including carcinoma. Thickening of the rim about a lucent mass is suggestive of bleeding into a cyst, cyst infection, or a malignant lesion. Renal cysts cause focal displacement of adjacent portions of the pelvicalyceal system. The displaced, attenuated collecting structures remain smooth, unlike the shagginess

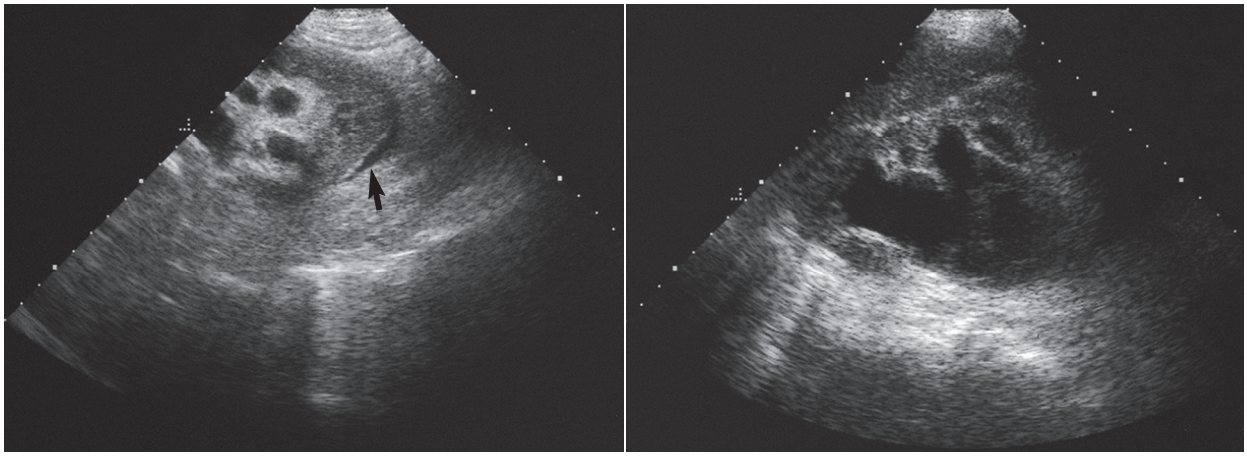

FIGURE 6-33 Hydronephrosis. Longitudinal ultrasound images demonstrating dilatation of renal collecting system appearing as echo-free sacs (dark areas) in this 73-year-old patient. **(A)** Left kidney with perirenal fluid (*arrow*). **(B)** Right kidney demonstrates more severe dilatation.

FIGURE 6-34 Hydronephrosis of pregnancy. Intravenous urogram performed 3 days postpartum demonstrates bilateral large kidneys with dilatation of ureters and pelvicalyceal systems, especially on the right. The large pelvic mass (*arrows*) indenting the superior surface of the bladder represents the uterus, which is still causing extrinsic pressure on the ureters.

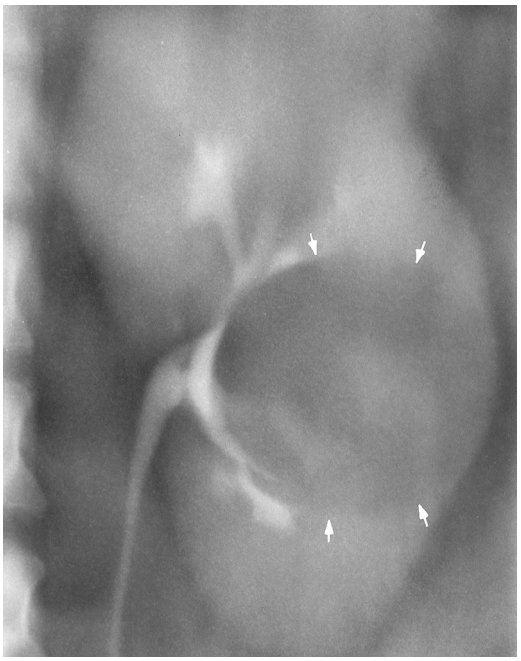

FIGURE 6-35 Renal cyst. Nephrotomogram shows smooth-walled mass with characteristic "beak sign" (*arrows*).

and obliteration that often occur when focal displacement is caused by a malignant neoplasm.

Ultrasound is the modality of choice for distinguishing fluid-filled simple cysts from solid mass lesions. Fluid-filled cysts classically appear as echo-free structures with strongly enhanced posterior walls (Figure 6-36), in contrast to solid or complex lesions, such as tumors, that appear as echo-filled masses without posterior wall enhancement. CT is also highly accurate in detecting and characterizing simple renal cysts. On unenhanced scans, the cyst has a uniform attenuation value near that of water. After the injection of contrast material,

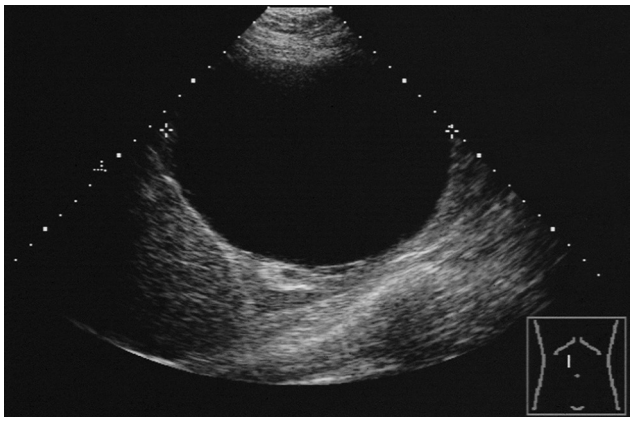

FIGURE 6-36 Huge renal cyst. Anechoic lesion (dark round area) with a well-defined posterior wall.

a simple cyst becomes more apparent as the contrast material is concentrated by the normal surrounding parenchyma (Figure 6-37). The cyst itself shows no change in attenuation value, unlike a solid renal neoplasm, which always shows a small but definite increase in density. Because of the accuracy of CT and ultrasound, percutaneous cyst puncture is rarely necessary if these imaging modalities provide unequivocal evidence of a simple cyst.

However, because abscesses, cystic or necrotic tumors, and inflammatory or hemorrhagic cysts can mimic simple cysts, cyst puncture should be performed if there is an atypical appearance or a strong clinical suspicion of abscess, or if the patient has hematuria or hypertension. Fluid aspirated from a renal cyst can be clearly differentiated from that obtained from an abscess or a renal tumor. The introduction of contrast material or air after the cyst fluid has been removed demonstrates the smooth inner wall of the cyst and further decreases the possibility of missing a malignant neoplasm (Figure 6-38).

Treatment. Following needle puncture, a catheter can be placed for drainage if needed. An injection of iodine or alcohol may obliterate the cyst.

Polycystic Kidney Disease

Polycystic kidney disease is an inherited disorder in which multiple cysts of varying size cause lobulated enlargement of the kidneys and progressive renal impairment, which presumably results from cystic compression of nephrons, which in turn causes localized intrarenal obstruction. One-third of patients with this condition have associated cysts of the liver, which do not interfere with hepatic function. Approximately 10% have one or more saccular (berry) aneurysms of cerebral arteries, which may rupture and produce a fatal subarachnoid hemorrhage. Many patients with polycystic disease are hypertensive, a condition that may cause further deterioration of renal function and increase the likelihood that a cerebral aneurysm will rupture. Because patients with this disorder tend to be asymptomatic during the first three decades of life, early diagnosis is made either by chance or as a result of a specific search prompted by the discovery of findings in the family history.

Imaging appearance. Intravenous urography in a patient with polycystic kidney disease demonstrates enlarged kidneys with a multilobulated contour. The pelvic and infundibular structures are elongated, effaced, and often displaced around larger cysts, producing a crescentic outline. The nephrogram typically has a distinctive mottled or Swiss cheese pattern caused by the presence of innumerable lucent cysts of varying size throughout the kidneys (Figure 6-39). Plaques of calcification occasionally occur in cyst walls.

Ultrasound demonstrates grossly enlarged kidneys containing multiple cysts that vary considerably in size and are randomly distributed throughout the kidney (Figure 6-40). The renal parenchyma becomes hyperechoic because of small cysts that do not appear as fluid filled but are large

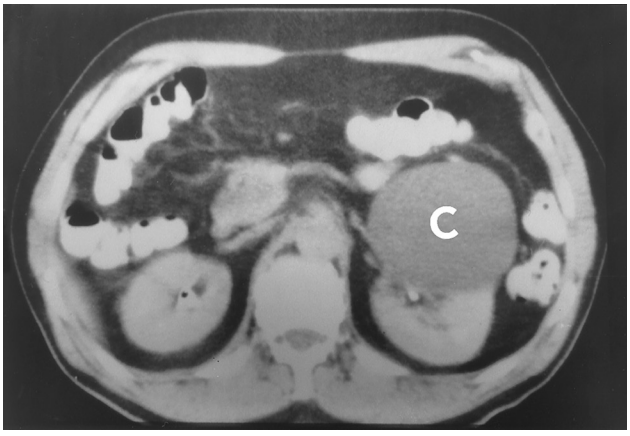

FIGURE 6-37 Abdominal CT for renal cyst. Renal cyst appears as a nonenhancing left renal mass (C) with sharply marginated border and thin wall.

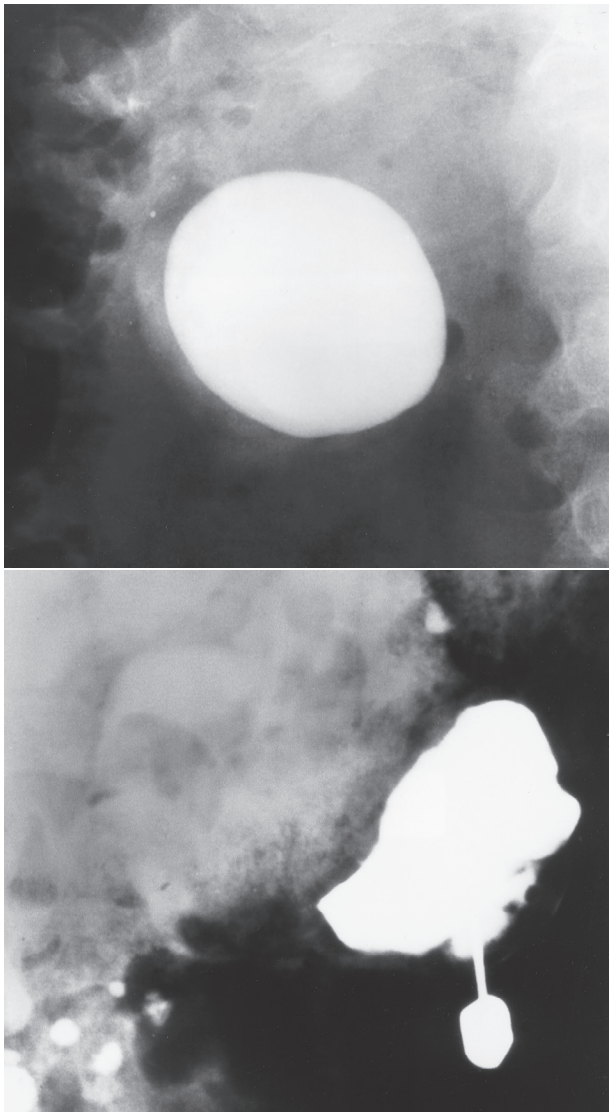

FIGURE 6-38 Renal cyst puncture. (A) Instillation of contrast material shows a smooth inner wall characteristic of a benign cyst. **(B)** In another patient, injection of contrast material reveals a highly irregular inner border of a necrotic renal cell carcinoma.

enough to cause echoes. The demonstration of similar hepatic cysts further strengthens the diagnosis. Ultrasound is also of value in screening family members of a patient known to have this hereditary disorder. In patients with bilateral kidney enlargement and poor renal function, ultrasound permits the differentiation of polycystic kidney disease from multiple solid masses.

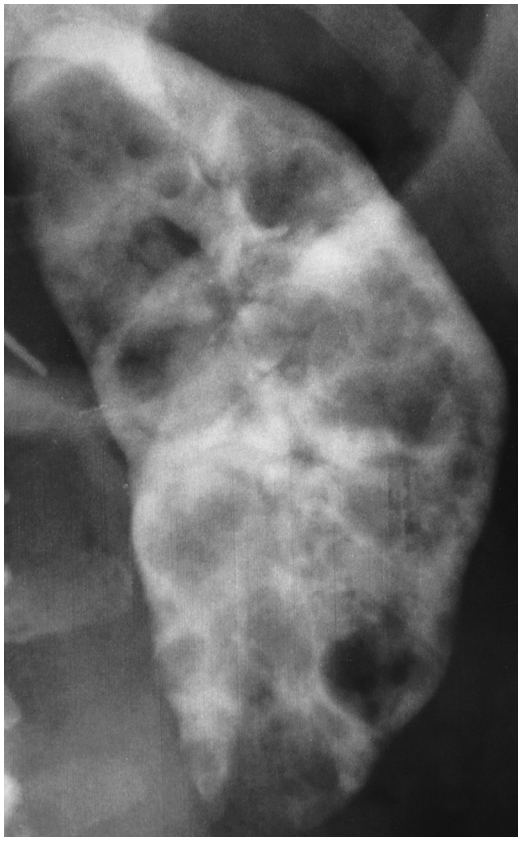

FIGURE 6-39 Polycystic kidney disease. Nephrogram phase from selective arteriography of left kidney demonstrates innumerable cysts ranging from pinhead size to 2 cm. The opposite kidney had an identical appearance.

The multiple cysts in polycystic kidney disease can also be detected on CT scans (Figure 6-41) and magnetic resonance imaging (MRI). Although most individual cysts are histologically identical to simple cysts, intracystic hemorrhage is common. Unlike simple renal cysts, which demonstrate low attenuation on CT scan, hemorrhagic cysts have high attenuation values. On MRI, a hemorrhagic cyst has high signal intensity on both T1- and T2-weighted images, unlike simple renal cysts, which have low signal intensity on T1-weighted images.

A rare, usually fatal form of polycystic disease can manifest at birth; it involves diffusely enlarged kidneys, renal failure, and maldevelopment of intrahepatic bile ducts. The margins of the kidneys are smooth in infantile polycystic disease, unlike the irregular renal contours in the adult form of polycystic disease that are attributable to the protrusion of innumerable cysts from the kidney surface. When renal function is sufficient, intravenous urography results in a striking nephrogram in which a streaky pattern of alternating dense and lucent bands reflects contrast material puddling in elongated cystic spaces that radiate perpendicular to the cortical surface (Figure 6-42). Ultrasound shows distortion of the intraparenchymal architecture, although the individual cysts are too small to be visualized.

Treatment. No cure is available for polycystic kidney disease. Medications are prescribed to control pain, high blood pressure, and infection related to the disease. Renal failure due to the loss of functioning kidney tissue requires dialysis, and renal transplantation may be considered.

Renal Carcinoma

Renal cell carcinoma (**hypernephroma**) is the most common renal neoplasm, occurring predominantly in patients older than 40 years and often with painless hematuria. The tumor usually originates in the tubular epithelium of the renal cortex. Approximately 10% of hypernephromas involve calcification, usually located in reactive fibrous zones about areas of tumor necrosis. In the differentiation of a solid tumor from fluid-filled benign cysts, the location of calcium within the mass is more important than the pattern

A

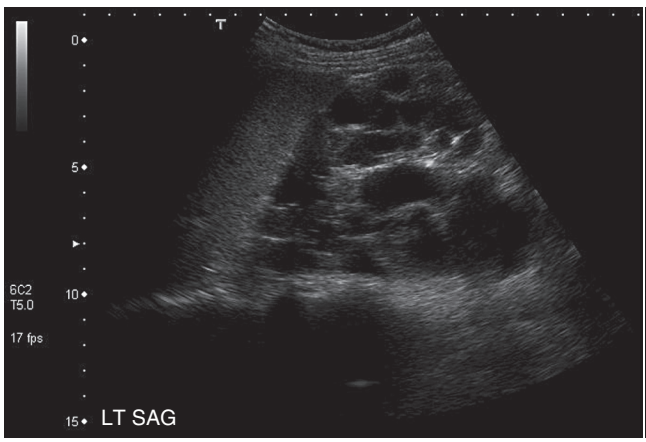

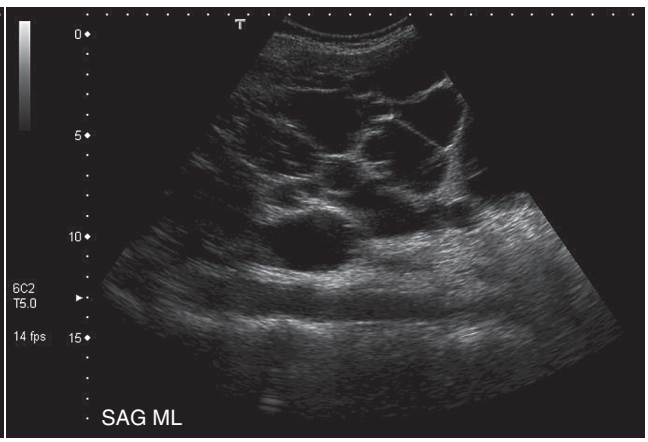

B

FIGURE 6-40 Polycystic kidney disease. **(A)** Left kidney sagittal ultrasound image demonstrates multiple cysts (dark areas). **(B)** Sagittal image of the liver in the same patient shows the destruction of the liver parenchyma due to cystic disease.

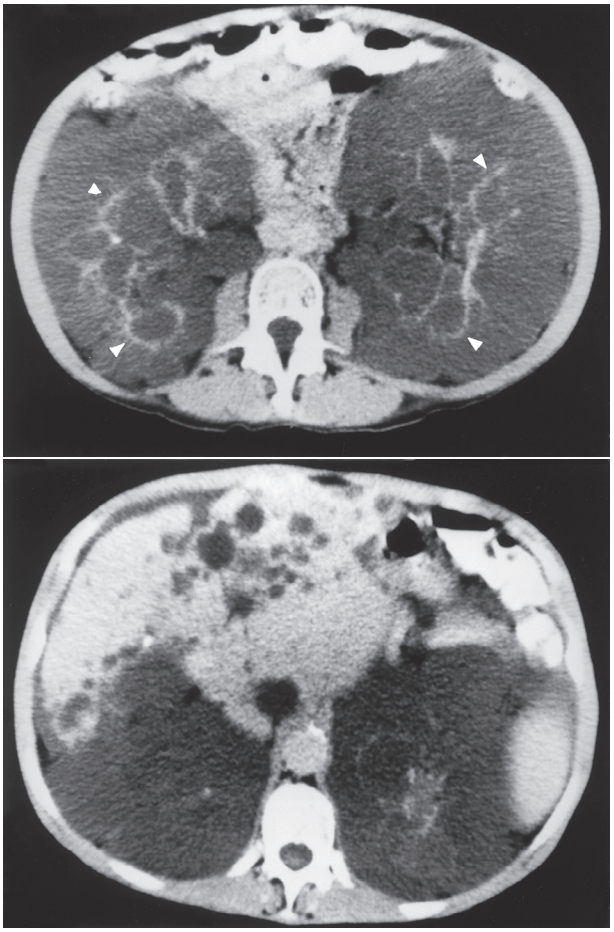

FIGURE 6-41 Polycystic kidney disease. (A) CT scan shows contrast-enhancing rims (*arrowheads*) in severely thinned renal parenchyma around innumerable large renal cysts. (B) A CT scan at a higher level also shows diffuse cystic involvement of the liver.

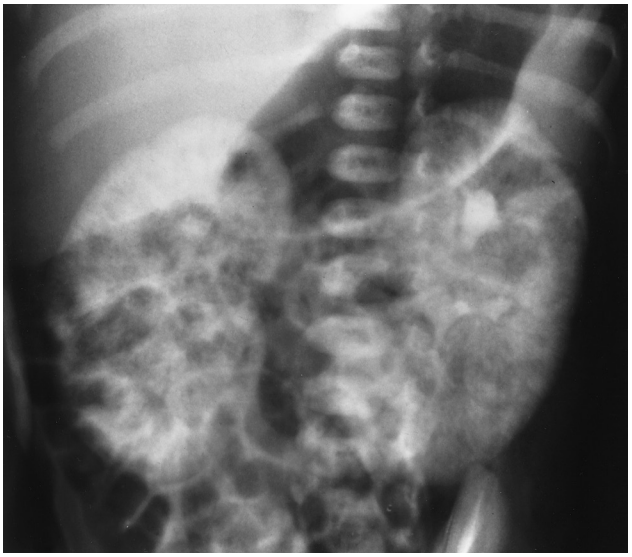

FIGURE 6-42 Infantile polycystic kidney disease. Intravenous urogram in a young boy with large, palpable abdominal masses demonstrates renal enlargement with characteristic streaky densities leading to calyceal tips. There is only minimal distortion of the calyces.

of calcification. Of all masses containing calcium in a nonperipheral location, almost 90% are malignant. The classic triad of symptoms (seen in approximately 10% of cases) consists of hematuria, flank pain, and a palpable abdominal mass. Although peripheral curvilinear calcification is much more suggestive of a benign cyst, hypernephromas can have a calcified fibrous pseudocapsule that results in an identical radiographic appearance.

Imaging appearance. Hypernephromas typically produce urographic evidence of localized bulging or generalized renal enlargement. The tumor initially causes elongation of adjacent calyces; progressive enlargement and infiltration lead to distortion, narrowing, or obliteration of part or all of the collecting system (Figure 6-43). Large tumors may partially obstruct the pelvis or upper ureter and cause proximal dilatation. Complete loss of function on intravenous urography usually indicates tumor invasion of the renal vein.

On nephrotomography, a hypernephroma generally appears as a mass with indistinct outlines and a density similar to that of normal parenchyma, unlike the classic radiolucent mass with sharp margins and a thin wall that represents a benign cyst. Necrotic neoplasms can also appear cystic, although they are usually surrounded by thick, irregular walls (Figure 6-44).

Ultrasound reveals a renal carcinoma as a solid mass with numerous internal echoes and no evidence of the acoustic enhancement seen with renal cysts (Figure 6-45). On unenhanced CT scans, a hypernephroma appears as a solid neoplasm that is often not homogeneous and has an attenuation value near that of normal renal parenchyma, unlike a simple cyst, which has a uniform attenuation value near that of water. After the injection of contrast material, a simple

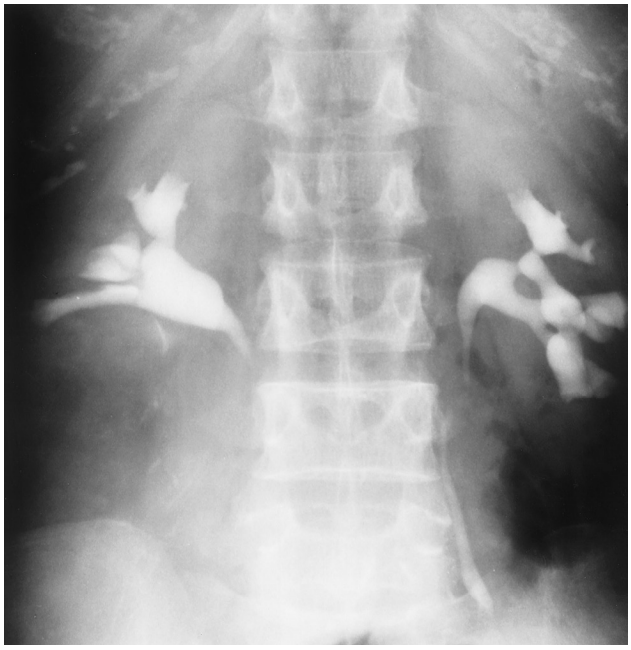

FIGURE 6-43 Renal cell carcinoma. Upward displacement of the right kidney and distortion of the collecting system by a large lower pole mass.

FIGURE 6-44 Renal cell carcinoma. Nephrotomogram demonstrates a lucent, well-demarcated renal mass with thick wall (*arrows*).

cyst shows no change in attenuation value, whereas a solid renal neoplasm demonstrates a small but definite increase in density that is probably attributable primarily to vascular perfusion. However, this increased density is much less than that of surrounding normal parenchyma, which also tends to concentrate the contrast material, and thus renal neoplasms become more apparent on contrast-enhanced scans (Figure 6-46). Helical three-phase CT aids in evaluation of arterial anatomy, which is of value in determining the type of treatment.

Currently, CT is considered the most accurate method for detecting local and regional spread of hypernephroma. It can usually distinguish between neoplasms confined to the renal capsule and those that have extended beyond it. CT is also the most accurate method for detecting enlargement of paraaortic, paracaval, and retrocrural lymph nodes and spread to the ipsilateral renal vein and inferior vena cava (Figure 6-47). When CT findings are equivocal or contrast enhancement is contraindicated, MRI can be useful.

MRI allows detailed demonstration of the renal anatomy and approaches the accuracy of CT in staging the abdominal extent of tumor in the patient with renal cell carcinoma (Figure

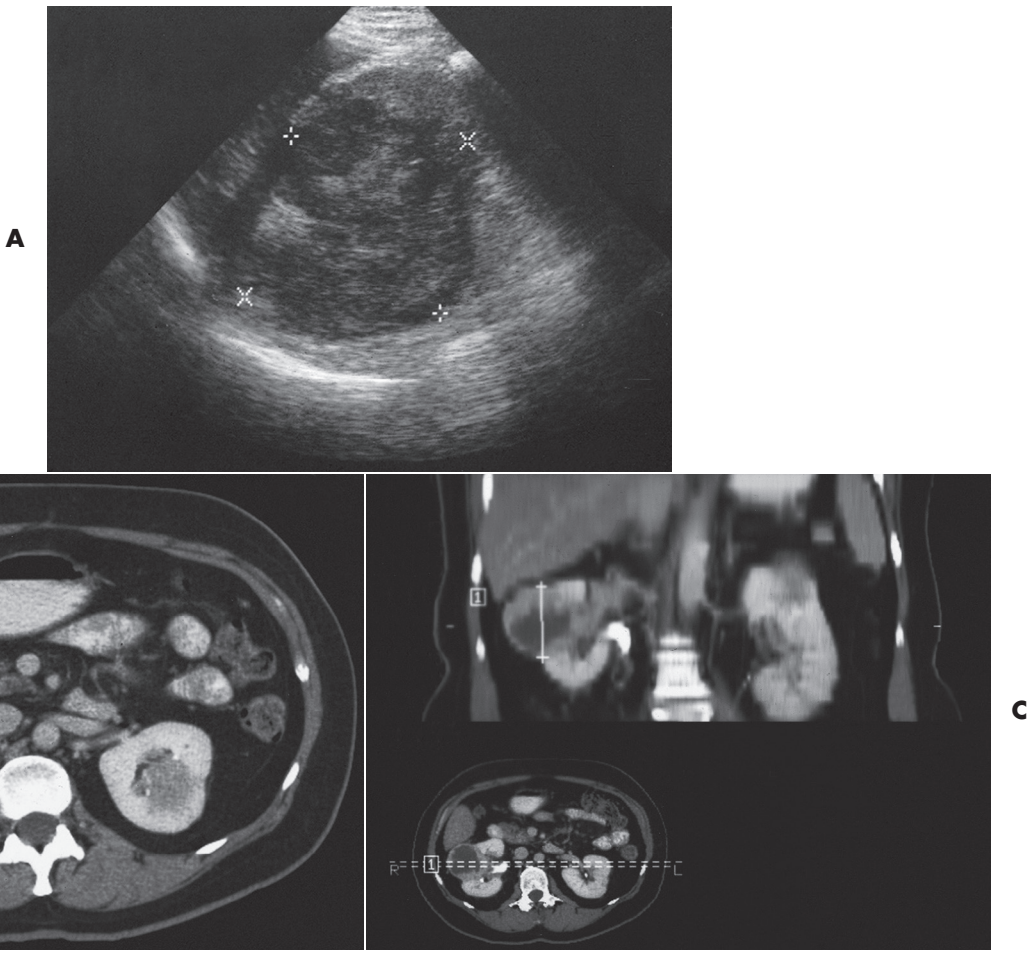

FIGURE 6-45 Renal cell carcinoma. Ultrasound image **(A)** shows a solid echo-filled mass measuring approximately 10 × 9 cm in a 55-year-old woman with hematuria. Axial **(B)** and coronal **(C)** CT scans demonstrate an inhomogeneous mass in the middle pole of the right kidney. The left kidney mass in the superior pole exhibits inhomogeneous attenuation and a decreased central density, indicating areas of necrosis.

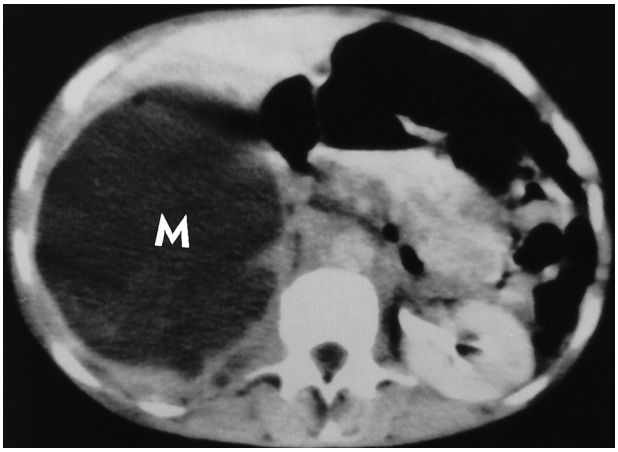

FIGURE 6-46 Necrotic renal cell carcinoma. CT scan shows a huge, nonenhancing, cystlike mass (M) with irregular margins (especially on its medial and posterior aspects).

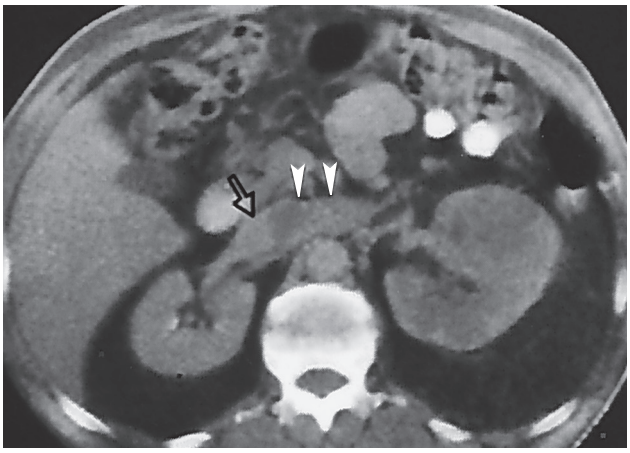

FIGURE 6-47 Renal cell carcinoma with left renal vein invasion. CT scan after administration of a contrast agent shows a dilated left renal vein filled with tumor thrombus (*arrowheads*). The thrombus extends to the inferior vena cava (*arrow*).

6-48A). Advantages of MRI include its ability to determine the origin of the mass, to detect perihilar and perivascular lymph node metastases, and to demonstrate tumor invasion of adjacent organs. On T1-weighted images, the tumor appears isointense or hypointense in relation to normal kidney tissue; on T2-weighted images, the tumor is usually hyperintense and heterogeneous. The superb delineation of blood vessels with MRI permits evaluation of tumor thrombus extension into the renal veins (a common occurrence) and into the inferior vena cava without the need for intravenous contrast material (Figure 6-48B). MRI is more definitive than CT only if contrast enhancement cannot be used.

The most common sites of metastasis from renal cell carcinoma are the lungs, liver, bones, and brain.

Treatment. Nephrectomy, the most common treatment for renal neoplasm, is associated with a 40% survival rate. Irradiation and chemotherapy are ineffective in treating renal cell carcinoma. Radiofrequency ablation is suggested for patients with bilateral lesions and those for whom surgery poses a high risk.

Wilms' Tumor (Nephroblastoma)

Wilms' tumor is the most common abdominal neoplasm of infancy and childhood. The lesion arises from embryonic renal tissue, it may be bilateral, and it tends to become very large and appear as a palpable mass.

Wilms' tumor, which is highly malignant, must be differentiated from neuroblastoma, a tumor of adrenal medullary origin that is the second most common malignancy in children. Peripheral cystic calcification occurs in approximately 10% of Wilms' tumors, in contrast to the fine, granular, or stippled calcification seen in approximately half of the cases of neuroblastoma.

Imaging appearance. At intravenous urography, the intrarenal Wilms' tumor causes pronounced distortion and displacement of the pelvicalyceal system (Figure 6-49). The major effect of the extrarenal neuroblastoma is to displace the entire kidney downward and laterally. Because the kidney itself is usually not invaded, there is no distortion of the pelvicalyceal system.

Ultrasound is of value in distinguishing Wilms' tumor from hydronephrosis, another major cause of a palpable renal mass in a child. Wilms' tumors typically have a solid appearance with gross distortion of the renal structure (Figure 6-50), which is not like the precise organization of symmetrically positioned, fluid-filled spaces in hydronephrosis. Ultrasound can also demonstrate the intrarenal location of Wilms' tumor, which is different from the extrarenal origin of a neuroblastoma.

Although it entails the use of ionizing radiation, CT can demonstrate the full extent of the tumor (including invasion of the inferior vena cava) and can detect any recurrence of the neoplasm after surgical removal (Figure 6-51). Coronal T1-weighted MR images can accurately differentiate Wilms' tumor from renal and hepatic lesions (Figure 6-52). This modality is also extremely useful in defining the extent of the lesion and showing possible tumor thrombus within the renal vein or the inferior vena cava. Because MRI uses no ionizing radiation, it is an ideal modality for follow-up evaluation after surgical removal of the tumor.

Treatment. Surgery, radiation therapy, and chemotherapy result in an 85% cure rate in patients with Wilms' tumor.

Carcinoma of the Bladder

Bladder carcinoma most commonly originates in the epithelium and is called urothelial carcinoma (previously known as transitional cell carcinoma). Bladder carcinoma is usually seen in men older than age 50 years and is the fourth most common cancer in men. Many industrial chemicals have been implicated as factors in the development of carcinoma of the bladder. Cigarette smoking has also been associated with bladder tumors, presumably because of carcinogenic metabolites being excreted in the urine. Internationally, the incidence of bladder cancer is especially high in Egypt, most likely related to the high

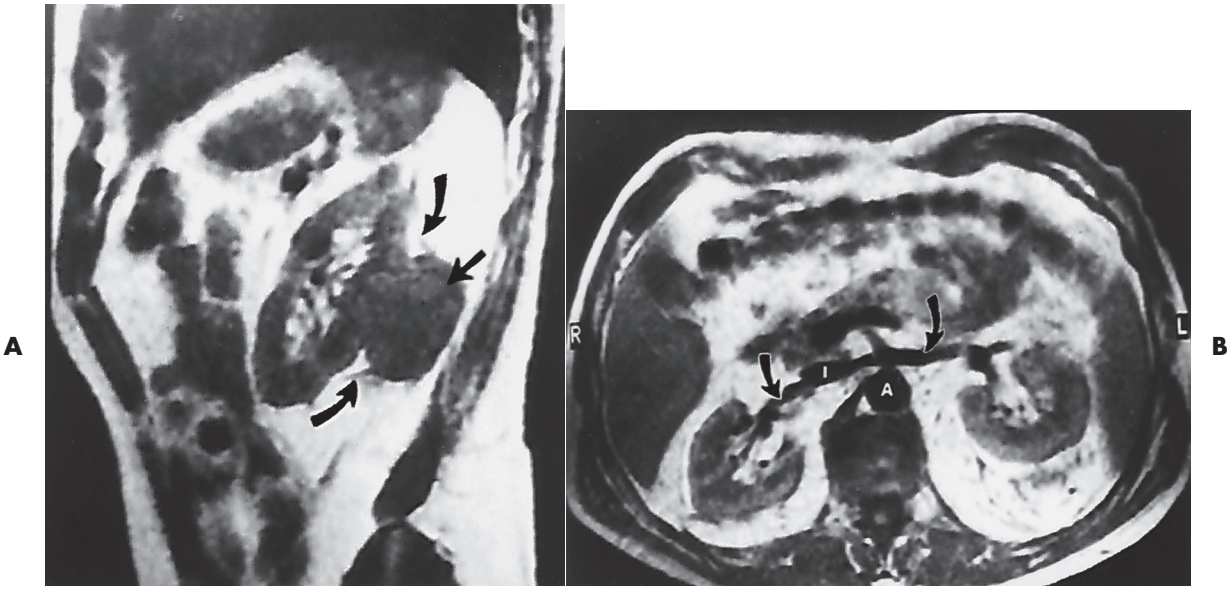

FIGURE 6-48 Renal cell carcinoma. (A) Sagittal T1-weighted MR image through the left kidney demonstrates a large renal cell carcinoma (*straight arrow*) arising from the posterior aspect of the kidney and displacing Gerota's fascia outward (*curved arrows*). (B) Transverse MR image at the level of the renal veins (*arrows*) and inferior vena cava (I) demonstrates normal signal from flowing blood without evidence of a tumor thrombus. This modality is especially useful for staging renal cell carcinoma because of its multiplanar capability and its ability to allow assessment of vascular invasion. *A*, Aorta.

FIGURE 6-49 Wilms' tumor. Huge mass in right kidney distorts and displaces the pelvicalyceal system.

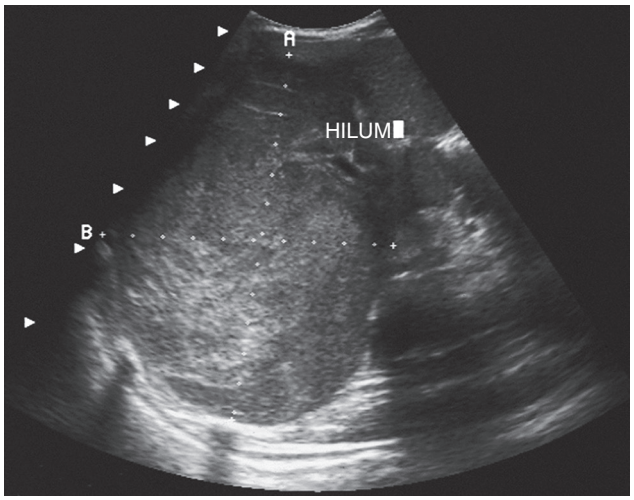

FIGURE 6-50 Wilms' tumor. Ultrasound image of the right kidney shows a large, complex mass measuring 12.6 × 9.95 cm. The kidney hilum is pushed medially.

prevalence of the parasitic infection schistosomiasis in that country.

Imaging appearance. Carcinoma of the bladder may produce finger-like projections into the lumen, or it may infiltrate the bladder wall. Plain radiographs may demonstrate punctate, coarse, or linear calcifications that are usually encrusted on the surface of the tumor but occasionally lie within it. On intravenous urograms, bladder cancer appears as one or more polypoid defects arising from the bladder wall or as focal bladder wall thickening (Figure 6-53). However, urography can detect only approximately 60% of bladder carcinomas because most are small when first symptomatic and are located on the trigone, where they can be difficult to visualize. Therefore, all patients with lower urinary tract hematuria should undergo cystoscopy to exclude a bladder neoplasm.

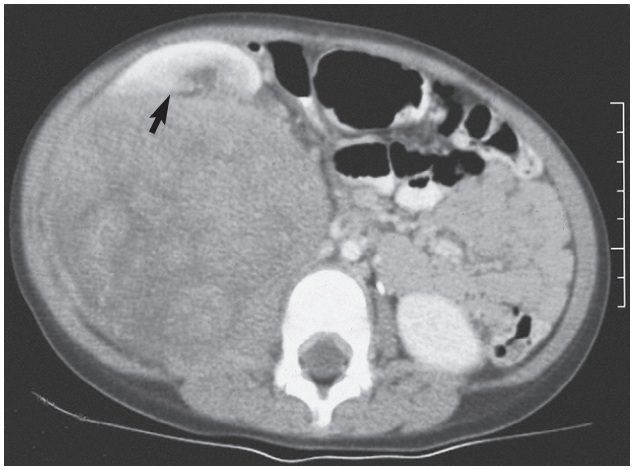

FIGURE 6-51 Wilms' tumor. CT scan of a 3-year-old child with a large nonfunctioning mass pushing the functioning right kidney anteriorly (*arrow*).

CT performed with full distention of the bladder demonstrates a neoplasm as a mass projecting into the bladder lumen (Figure 6-54) or as focal thickening of the bladder wall (Figure 6-55A). This modality is excellent when MRI is not available for preoperative staging, because CT can determine the presence and degree of extravesical extension, involvement of the pelvic sidewalls (Figure 6-55B), and enlargement of pelvic or para-aortic lymph nodes.

MRI can demonstrate the depth of bladder wall invasion by showing a high-signal-intensity tumor disruption on T2-weighted images. The extension in the perivesical fat appears as a low signal intensity on T1-weighted images. MRI is equal to or better than CT for this purpose.

Treatment. Many carcinomas of the bladder have a low grade of malignancy, although they tend to recur repeatedly after surgical removal. More invasive tumors require removal of the entire bladder with transplantation of the ureters into a loop of ileum.

Summary of Findings for Cysts and Tumors

Disorder	Location	Imaging appearance	Treatment
Renal cyst	Renal parenchyma	US—fluid-filled cyst, echo free with enhanced posterior wall CT—region with lack of contrast enhancement IVU—radiopaque rim surrounding lucent cyst ("beak sign")	Percutaneous drainage; if indicated, an injection to collapse the cyst
Polycystic kidney	Renal parenchyma	IVU—mottled presence of multiple lucent lesions US—enlarged and hyperechoic kidneys, multiple anechoic lesions CT—hemorrhagic cyst with increased attenuation MRI—hemorrhagic cyst with increased signal intensity on both T1- and T2-weighted images	No cure Loss of kidney function—dialysis and renal transplantation
Renal carcinoma	Kidney	Nephrotomogram—indistinct outlines; tumor density similar to that of normal tissue; cystic type surrounded by thick irregular walls US—solid mass with numerous internal echoes CT—solid mass with heterogeneous attenuation values that increase with contrast MRI—determines extent of involvement and staging of tumor; on T1-weighted images, tumor appears isointense or hypointense; on T2-weighted images, tumor is usually hyperintense and most often heterogeneous	Nephrectomy Radiofrequency ablation
Wilms' tumor	Embryonic renal tissue	IVU—inferior and lateral displacement of kidney US—solid structure with gross distortion of the renal structure CT—tumor and extent of invasion MRI—differentiates Wilms' from other renal or hepatic tumors; demonstrates vascular involvement	Surgical removal, with chemotherapy and radiation therapy
Bladder carcinoma	Wall of bladder (epithelium)	KUB—punctate, coarse, or linear calcifications IVU—polypoid defects with wall thickening CT—mass projecting into bladder lumen, focal thickening of bladder wall MRI—predicts depth of wall invasion	Surgical removal of tumor Surgical removal of bladder and redirection of ureters into the ileum

IVU, Intravenous urography; *KUB,* kidney–ureter–bladder radiograph; *US,* ultrasound.

RENAL VEIN THROMBOSIS

Renal vein thrombosis occurs most frequently in children who are severely dehydrated. In the adult, thrombosis is most often a complication of another renal disease (e.g., chronic glomerulonephritis, amyloidosis, and pyelonephritis), trauma, the extension of a thrombus from the inferior vena cava, or direct invasion or extrinsic pressure resulting from renal tumors.

Imaging appearance. Renal vein thrombosis may be unilateral or bilateral. The clinical and radiographic findings are greatly influenced by the rapidity with which venous occlusion occurs. Sudden total occlusion causes striking kidney

FIGURE 6-52 Wilms' tumor. T1-weighted coronal MR image shows sharply marginated infrahepatic mass (W) that is clearly distinct from the liver (L). The inferior vena cava (*arrowheads*), although displaced by the mass, shows no evidence of tumor extension into it.

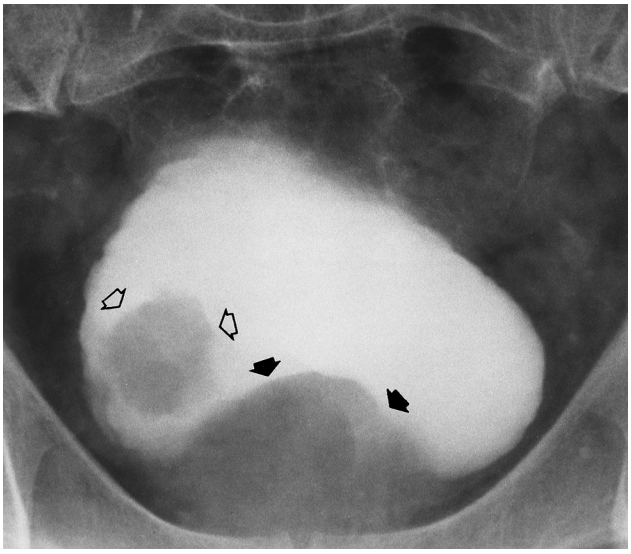

FIGURE 6-53 Bladder carcinoma. An irregular tumor (*open arrows*) is associated with a large filling defect (*solid arrows*), representing benign prostatic hypertrophy, at the base of the bladder.

enlargement with minimal or no opacification on intravenous urograms (Figure 6-56). If unresolved, this acute venous occlusion leads to the urographic appearance of a small, atrophic, nonfunctioning kidney.

When venous occlusion is partial or is accompanied by adequate collateral formation, the kidney enlarges and appears smooth, and there is some excretion of contrast material. The collecting system is stretched and thinned as a result of surrounding interstitial edema. Enlargement of collateral pathways (e.g., gonadal and ureteric veins) for renal venous outflow produces characteristic notching of the upper ureter.

Diagnostic ultrasound, currently the initial modality of choice, shows enlarged kidneys that have decreased echogenicity because of diffuse edema in acute renal vein thrombosis; the kidneys become increasingly atrophic as the disease slowly progresses. Doppler ultrasonography may permit direct visualization of the clot within the renal vein. CT does not allow visualization of a clot-filled renal vein on contrast-enhanced images. Magnetic resonance angiography (MRA) can detect an abnormally strong signal from the renal veins, suggesting stasis (no flow) of blood. A renal vein with a slow flow caused by partial obstruction by a clot produces a lower signal. Ultrasound and MRI are the modalities used more frequently because they do not require an iodinated contrast agent to demonstrate the anatomy.

The confirmation of renal vein thrombosis requires venographic demonstration of vessel occlusion or a localized filling defect (Figure 6-57). An examination of the inferior vena cava with a catheter placed well below the renal veins is often performed initially to exclude caval thrombosis with proximal extension before the renal veins are catheterized directly.

Treatment. Anticoagulants are generally given to prevent new clots from forming. To reduce the possibility of emboli, the patient assumes bed rest and limited activity. Medications can be given intravenously or can be directly injected into the clot to lyse it. Renal vein thrombosis usually resolves without permanent damage to the kidneys.

ACUTE RENAL FAILURE

Acute renal failure refers to a rapid deterioration in kidney function that is sufficient to result in the accumulation of nitrogen-containing wastes in the blood and a characteristic odor of urine-like or "fishy" breath. In prerenal failure, blood flow to the kidneys is decreased as a result of low blood volume (e.g., because of hemorrhage, dehydration, or surgical shock), cardiac failure, or obstruction of both renal arteries. Postrenal failure is caused by obstruction of the urine outflow from both kidneys, most commonly a result of prostatic disease or functional obstruction of the bladder neck. Acute renal failure may also be the result of specific kidney diseases, such as glomerulonephritis, bilateral acute pyelonephritis, and malignant (severe) hypertension. Other causes of acute renal failure include nephrotoxic agents (antibiotics, radiographic contrast material, anesthetic agents, heavy metals, and organic solvents), intravascular hemolysis, and large amounts of myoglobin (muscle protein) in the circulation resulting from muscle trauma or ischemia. Urine output may decrease to less than 400 mL per 24-hour period (oliguria).

Imaging appearance. Because it is independent of renal function, ultrasound is especially useful in the evaluation of patients with acute renal failure. In addition to demonstrating dilatation of the ureters and pelves caused by postobstructive

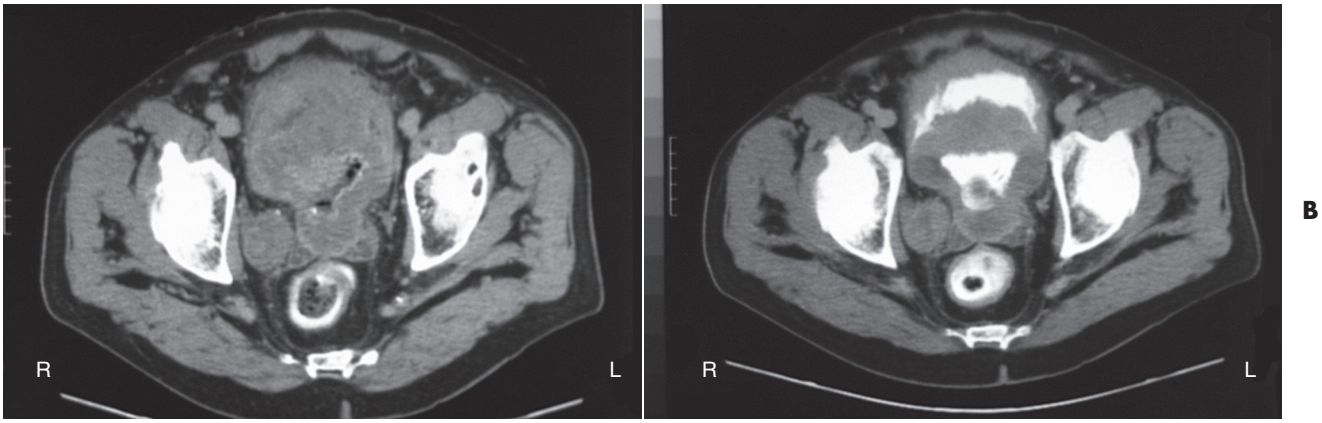

FIGURE 6-54 Bladder carcinoma. **(A)** CT scan of the upper bladder demonstrates wall thickening and mixed attenuation, with no contrast agent visible. **(B)** CT scan of the same patient demonstrates a contrast agent–filled bladder with finger-like projections into the lumen demonstrating the erratic and speculated bladder wall.

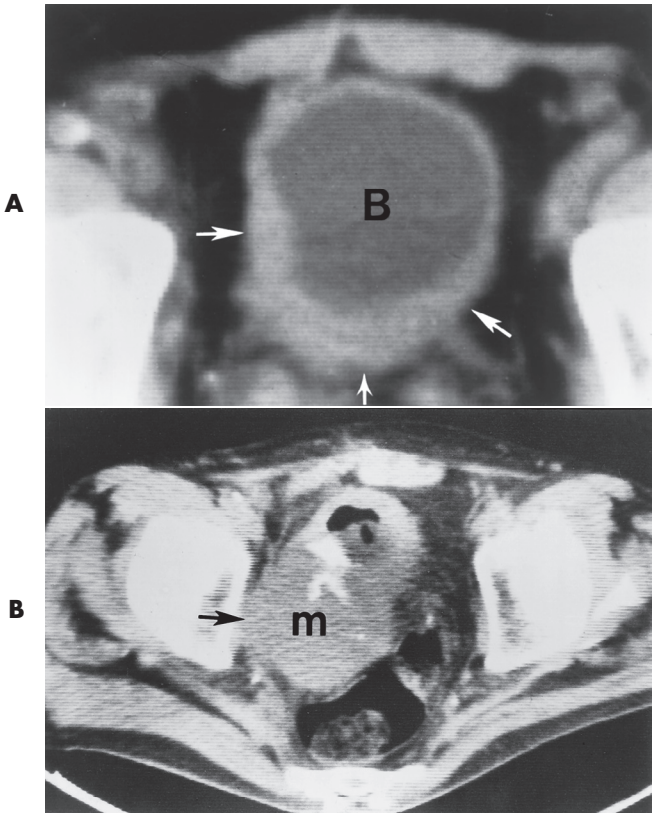

FIGURE 6-55 CT scan of bladder carcinoma. **(A)** Focal thickening of the posterior wall (*arrows*). **(B)** Extensive bladder cancer (m) has extended to involve the sidewall of the pelvis (*arrow*).

hypernephrosis, ultrasound can assess renal size and the presence of focal kidney lesions or diffuse renal cystic disease. In the patient with prerenal failure, ultrasound can aid in distinguishing low blood volume from right-sided heart failure. In the latter, there is dilatation of the inferior vena cava and hepatic veins that does not occur in patients with low circulating blood volume.

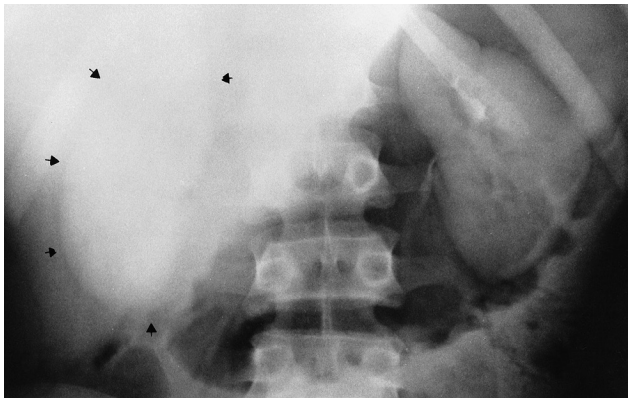

FIGURE 6-56 Acute renal vein thrombosis. Radiograph of the right kidney taken 5 minutes after injection of contrast material shows a dense nephrogram (*arrows*) and an absence of calyceal filling.

Conventional tomography can often demonstrate renal size and contours. Bilaterally enlarged, smooth kidneys are suggestive of acute renal parenchymal dysfunction; small kidneys usually indicate chronic, preexisting renal disease. Plain image tomograms can also demonstrate bilateral renal calcification, which may indicate either secondary hyperparathyroidism caused by chronic renal disease or bilateral stones that have obstructed both ureters to produce postrenal failure.

Intravenous urography in the patient with acute renal failure demonstrates bilateral renal enlargement with a delayed and prolonged nephrogram (Figure 6-58); vicarious excretion of contrast material by the liver occasionally results in opacification of the gallbladder. However, in most instances, intravenous urography is unnecessary in the patient with acute renal failure, especially because many authors believe that intravenous contrast material can cause further damage to the kidneys in this condition.

Ultrasonography is the modality of choice because it does not require the use of intravenous contrast agents. It can assess

FIGURE 6-57 Renal vein thrombosis. Renal venogram demonstrates a large filling defect in the left renal vein (*arrows*) that extends into the vena cava.

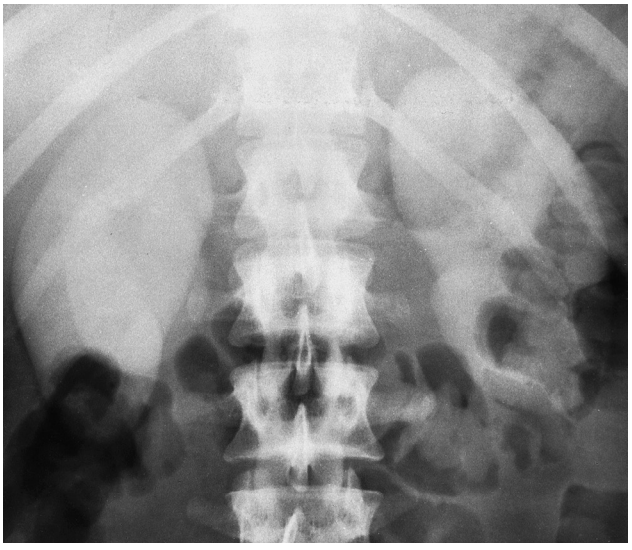

FIGURE 6-58 Acute renal failure. Intravenous urogram obtained 20 minutes after injection of contrast material shows bilateral persistent nephrograms with no calyceal filling.

renal size, identify renal parenchymal disease, and exclude hydronephrosis. Renal parenchymal disease appears as a diffuse increase in echogenicity, with loss of corticomedullary differentiation. If a vascular cause is suggested clinically, color Doppler studies enable visualization of patency or occlusion. If this procedure is unsuccessful, a radionuclide scan or an MRI study may show these vessels without the use of an intravenous contrast agent.

Treatment. Treatment of predisposing conditions reduces the risk that acute renal failure will become chronic or continue. Some physicians use diuretics to increase urine flow and vasodilators to increase renal blood flow to help prevent the likelihood of more severe renal failure. Dietary modifications, including decreasing potassium and protein intake and increasing carbohydrates, can reduce the load on the kidneys. Antibiotics may be used to prevent or treat infections because of the high risk of sepsis associated with renal failure. In some cases, renal dialysis provides time for the kidneys to recover.

CHRONIC RENAL FAILURE

Like acute renal failure, chronic kidney dysfunction may reflect prerenal, postrenal, or intrinsic kidney disease. Therefore, underlying causes of chronic renal failure include bilateral renal artery stenosis; bilateral ureteral obstruction; and intrinsic renal disorders, such as chronic glomerulonephritis, pyelonephritis, and familial cystic diseases.

A failure to clear nitrogen-containing wastes adequately from the circulation leads to the accumulation of excessive blood levels of urea and creatinine (waste products of protein metabolism) in the blood. This condition, called **uremia**, has toxic effects on many body systems. Irritation of the gastrointestinal tract produces nausea, vomiting, and diarrhea. In the nervous system, uremia causes drowsiness, dim vision, decreased mental ability, convulsions, and eventually coma. A decreased ability of the kidney to synthesize erythropoietin, which helps regulate the production of red blood cells, leads to the development of anemia. In the skin, uremia causes intense itching (pruritus) and a sallow (yellowish) coloring resulting from the combined effects of anemia and retention of a variety of pigmented metabolites (urochromes).

Because of the kidney's role in maintaining water balance and regulating acid–base balance and electrolyte levels, chronic renal failure causes abnormalities involving all these vital functions. Retention of sodium leads to increased water retention and the development of generalized edema and congestive heart failure. An elevated serum potassium value is potentially life threatening because of its direct effect on cardiac muscle contractility and the possibility of causing an arrhythmia or cardiac arrest. A reduction of serum calcium can produce the muscle twitching commonly seen in uremic patients. Low calcium levels also lead to increased activity of the parathyroid glands, which results in the removal of calcium from bones and a high incidence of renal stones.

Imaging appearance. Because it is independent of renal function, ultrasound is most often the initial procedure in the evaluation of patients with chronic renal failure and demonstrates a small echogenic kidney (Figure 6-59). This modality is of special value in diagnosing treatable diseases, such as hydronephrosis and intrarenal or perirenal infections. It can also allow assessment of renal size and the presence of focal kidney lesions or diffuse renal cystic disease, and it can be used to localize the kidneys for percutaneous renal biopsy.

Even in patients with chronic renal failure and uremia, intravenous urography with tomography may produce sufficient opacification of the kidneys to be of diagnostic value. However, intravenous urography is infrequently required because similar information can be provided by ultrasound or retrograde pyelography. An initial plain abdominal

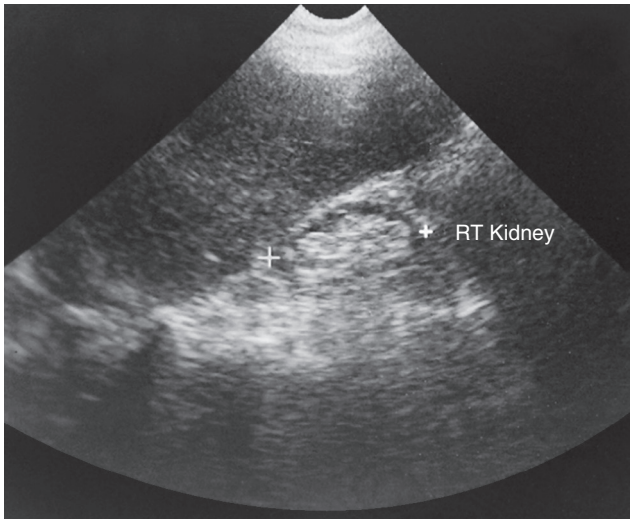

FIGURE 6-59 Chronic renal failure. Ultrasound image of a patient with a very small right kidney, measuring less than 6 cm, suggesting irreversible end-stage renal disease.

radiograph may demonstrate bilateral renal calcifications (nephrocalcinosis) or obstructing ureteral stones (see Figure 6-28). Small kidneys with smooth contours are suggestive of chronic glomerulonephritis (see Figure 6-15), nephrosclerosis, or bilateral renal artery stenosis. Small kidneys with irregular contours, thin cortices, and typical clubbing of the calyces are consistent with chronic pyelonephritis (see Figure 6-16). Large kidneys are suggestive of obstructive disease, infiltrative processes (lymphoma, myeloma, and amyloidosis), renal vein thrombosis (see Figure 6-56), or polycystic kidney disease (see Figure 6-41).

Treatment. The initial goal of treatment is to slow the nephron loss and minimize complications. Antihypertensive drugs assist in preventing the continuation of this process. It is essential to properly balance intake and output of fluids and electrolyte levels. The inevitable occurrence of kidney failure requires dialysis to maintain the balance of body fluids. At this point, kidney transplantation may be suggested.

Summary of Findings for Renal Disorders

Disorder	Location	Imaging appearance	Treatment
Renal vein thrombosis	Renal vein	IVU—kidney enlarged, appearing smooth with some contrast excretion; collecting system stretches and thins; notching of upper ureter US—acute: enlarged kidneys; chronic: atrophic kidneys with increased echogenicity Doppler—visualization of clot MRA—abnormally high signal intensity, suggesting stasis	Prevention of new clots—anticoagulants Bed rest and limited activity to reduce risk of clot travel Medications to lyse clot Usually resolves without permanent injury
Acute renal failure	Nephron function	Tomography—acute: enlarged smooth kidneys; chronic: small kidneys IVU—delayed and prolonged nephrogram US—renal size; identifies parenchymal disease and excludes hydronephrosis	Prevention—treatment of predisposing conditions Drug and dietary intervention Short-term dialysis
Chronic renal failure	Renal parenchyma	US—small echogenic kidney size, lesions, and cysts; hydronephrosis, intrarenal or perirenal infections	Slowing of destructive process Correction of fluid imbalances Dialysis and transplantation

IVU, Intravenous urography; *US,* ultrasound.

REVIEW QUESTIONS

1. The imaging criteria for pyelography are the same as for an abdominal radiograph but must include the area from the _____ to the _____.
   a. diaphragm; kidneys
   b. kidneys; pelvis
   c. kidneys; superior pubis
   d. diaphragm; inferior bladder
2. What organ of the body plays an essential role in maintaining the acid–base balance of the blood and body fluids, and also the electrolyte balance?
   a. nephron
   b. glomerulus
   c. bladder
   d. kidney
3. A bacterial inflammation of the kidney and renal pelvis is termed _____.
   a. renitis
   b. pyelonephritis
   c. glomerulitis
   d. none of the above

4. The medical term used to describe dilated calyces and renal pelvis is _____.
   a. hydronephrosis
   b. pyelonephritis
   c. nephrosis
   d. none of the above
5. What is the name for the most common abdominal neoplasm of infants and children?
   a. polycystic disease
   b. pyelonephritis
   c. Wilms' tumor
   d. hypernephroma
6. What is the name of the most common fusion anomaly of the kidneys?
   a. complete fusion
   b. crossed ectopia
   c. pelvic kidney
   d. horseshoe kidney
7. What is the name for a cystic dilatation of the distal ureter near the bladder?
   a. compensatory hypertrophy
   b. renal agenesis
   c. ureterocele
   d. hypoplasty
8. Name the first portion of the kidney to become visible after injection of a contrast agent.
   a. nephron
   b. glomerulus
   c. Bowman's capsule
   d. calyces
9. What term is used to describe a kidney not in the normal area of the abdomen?
   a. horseshoe
   b. duplex
   c. ectopic
   d. ectopic ureterocele
10. The medical term for painful urination is _____ _____.
    a. dysuria
    b. anuria
    c. micturition
    d. exacerbation
11. A hypoplastic kidney _____.
    a. is of normal size
    b. functions normally
    c. has a reduced volume of parenchyma due to disease
    d. both a and b
12. Cystitis can be caused by (select as many as apply) _____ _____.
    a. nosocomial infection
    b. dysuria
    c. bacteria
    d. diabetes
    e. sexual relations
13. Name the two most common causes of urinary tract obstruction.
14. The term used to describe dilatation of the ureter is _____.
15. Name the disease process in which multiple cysts develop and will eventually reduce the kidney parenchyma.

7

Cardiovascular System

OUTLINE

Physiology of the Cardiovascular System
Congenital Heart Disease
- Left-to-Right Shunts
- Tetralogy of Fallot
- Coarctation of the Aorta

Acquired Vascular Disease
- Coronary Artery Disease
- Congestive Heart Failure
- Pulmonary Edema
- Hypertension
- Hypertensive Heart Disease
- Aneurysm
- Traumatic Rupture of the Aorta
- Dissection of the Aorta
- Atherosclerosis
- Thrombosis and Embolism

Valvular Disease
- Rheumatic Heart Disease
- Mitral Stenosis
- Mitral Insufficiency
- Aortic Stenosis
- Aortic Insufficiency
- Infective Endocarditis

Pericardial Effusion
Venous Disease
- Deep Venous Thrombosis
- Varicose Veins

KEY TERMS

aortic valve
atrial septal defect
coeur en sabot
diastole
ectopic pacemakers
Eisenmenger's syndrome
embolus
fibromuscular dysplasia
fusiform aneurysm
insufficiency
intrinsic rhythm
left-to-right shunts
mitral valve (bicuspid valve)
myocardial infarction
patent ductus arteriosus
pericardium
pulmonary valve
right-to-left shunting
saccular aneurysm
stenosis
systemic circulation
systole
thrombus
tricuspid valve
vegetations
ventricular septal defect

OBJECTIVES

After reading this chapter, the reader will be able to:

- Define and describe all boldface terms in this chapter
- Describe the physiology of the cardiovascular system
- Identify anatomic structures on both diagrams and radiographs of the cardiovascular system
- Differentiate the various pathologic conditions affecting the cardiovascular system and their radiographic manifestations
- Provide a description of the special procedures that are used when imaging particular pathologic conditions

PHYSIOLOGY OF THE CARDIOVASCULAR SYSTEM

The function of the cardiovascular system is to maintain an adequate supply of blood to all the tissues of the body. This is accomplished by the rhythmic contractions of the heart, the rate of which is controlled by the autonomic nervous system. The vagus nerve slows heart action by transmitting the chemical acetylcholine, whereas the sympathetic nervous system stimulates the release of epinephrine that accelerates the heart rate and increases the force of its contractions.

The heart consists of four chambers whose walls are composed of striated muscle (myocardium), and it is lined with a smooth delicate membrane (endocardium), which is continuous with the inner surface of the blood vessels (Figure 7-1). The heart consists of two atria and two ventricles, with a partition (the septum) separating the right and left sides of the heart. The ventricles are considerably larger and thicker walled than the atria because they have a substantially heavier pumping load. Between each atrium and its associated ventricle are the atrioventricular valves (one on the right and one on the left side of the heart), which permit blood to flow in only one direction (Figure 7-2).

These valves consist of flaps (or cusps) of endocardium that are anchored to the papillary muscles of the ventricles by cordlike structures called the chordae tendineae. The **mitral valve** (**bicuspid valve**) (left atrioventricular) between the left atrium and the left ventricle has two cusps, whereas the **tricuspid valve** (right atrioventricular) between the right atrium and the right ventricle has three cusps. The semilunar valves separate the ventricles from the great vessels leaving the heart. The **pulmonary valve** lies between the right ventricle and the pulmonary artery, whereas the **aortic valve** separates the aorta from the left ventricle.

RADIOGRAPHER NOTES

Plain chest radiography and fluoroscopy of the cardiovascular system are used to identify abnormalities in the size and shape of the heart and to detect calcification of heart valves, coronary arteries, or the pericardium. The presence and extent of functional disorders are better demonstrated using angiography, computed tomography (CT), ultrasound (US), radionuclide imaging, and magnetic resonance imaging (MRI).

As for all chest radiographs, it is essential that the radiographer perform cardiovascular studies with the patient positioned correctly and using proper technical factors. To this end, it would be helpful for the reader to review the radiographer notes at the beginning of the chapter on the respiratory system. An abnormality identified on a chest radiograph may be the first evidence of cardiovascular disease in an asymptomatic patient.

Radiographers can specialize in invasive diagnostic and therapeutic cardiovascular procedures, gain advanced certification in cardiovascular interventional technology, and be employed by cardiac or vascular catheterization laboratories. Angiocardiography is a diagnostic procedure performed to identify the exact anatomic location of an intracardiac disorder. Coronary angioplasty is a therapeutic procedure in which a narrowed coronary artery is dilated by inflation of a balloon, which is attached to a catheter and manipulated fluoroscopically to the site of the stenosis. Because both angiocardiography and angioplasty involve the use of contrast material in patients who often have severe preexisting medical conditions, it is essential that the radiographer be always alert to the possibility of cardiac or respiratory arrest and prepared to immediately assist with basic and advanced life support.

The injection of contrast material into arteries (arteriograms) and veins (venograms) can be performed in almost any portion of the body. As in the heart, these invasive studies use potentially dangerous substances, so the radiographer must be alert for possible complications and prepared to assist in cardiorespiratory emergencies. In addition, these examinations require that the radiographer be trained in sterile technique, be able to use specialty equipment, and be familiar with the various types of catheters that are inserted into the vascular system for the delivery of contrast material.

Ultrasound, Doppler US, CT, and MRI are quickly becoming preferred initial modalities for imaging the vascular system.

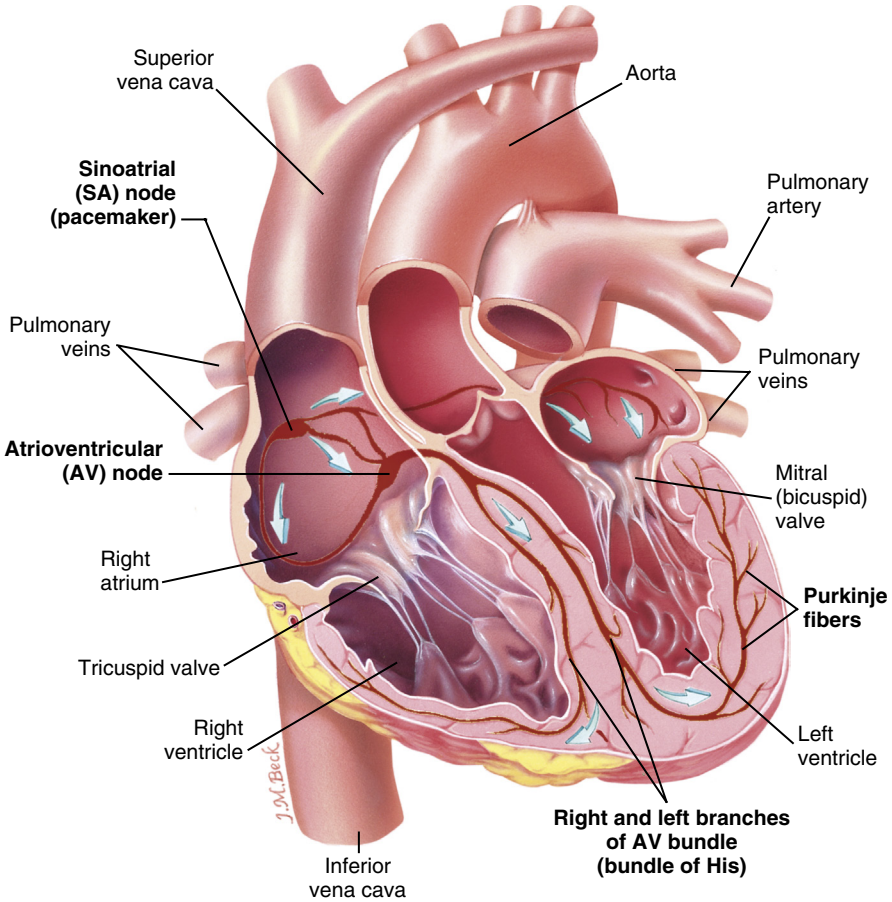

FIGURE 7-1 Conduction system of the heart and vascular anatomy.

Deoxygenated venous blood is returned to the heart from the body through the superior and inferior venae cavae, which empty into the right atrium. Blood flows from the right atrium across the tricuspid valve into the right ventricle, which then pumps blood through the pulmonary valve into the pulmonary artery. Within the capillaries of the lungs, the red blood cells take up oxygen and release carbon dioxide. The freshly oxygenated blood then passes through the pulmonary veins into the left atrium, from which it flows across the mitral valve into the left ventricle. Contraction of the left ventricle forces oxygenated blood through the aortic valve into the aorta and the rest of the arterial tree to provide oxygen and nourishment to tissues throughout the body. The general circulation of the body is termed the **systemic circulation** (Figure 7-3), whereas the circulation of blood through the lungs is the pulmonary circulation. Because greater pressure is needed to pump blood through the systemic circulation than through the pulmonary circulation, the wall of the left ventricle is considerably thicker than that of the right ventricle.

The atria and ventricles alternately contract and relax. The contraction phase is called **systole**; the heart chambers relax and fill with blood during **diastole** (the relaxation phase). The normal cardiac impulse that stimulates mechanical contraction of the heart arises in the sinoatrial (SA) node, or pacemaker, which is situated in the right atrial wall near the opening of the superior vena cava. The impulse passes slowly through the atrioventricular (AV) node, which is located in the right atrium along the lower portion of the interatrial septum, and then spreads quickly throughout the ventricles by way of a band of atypical cardiac muscle fibers called the bundle of His. The bundle of His terminates in

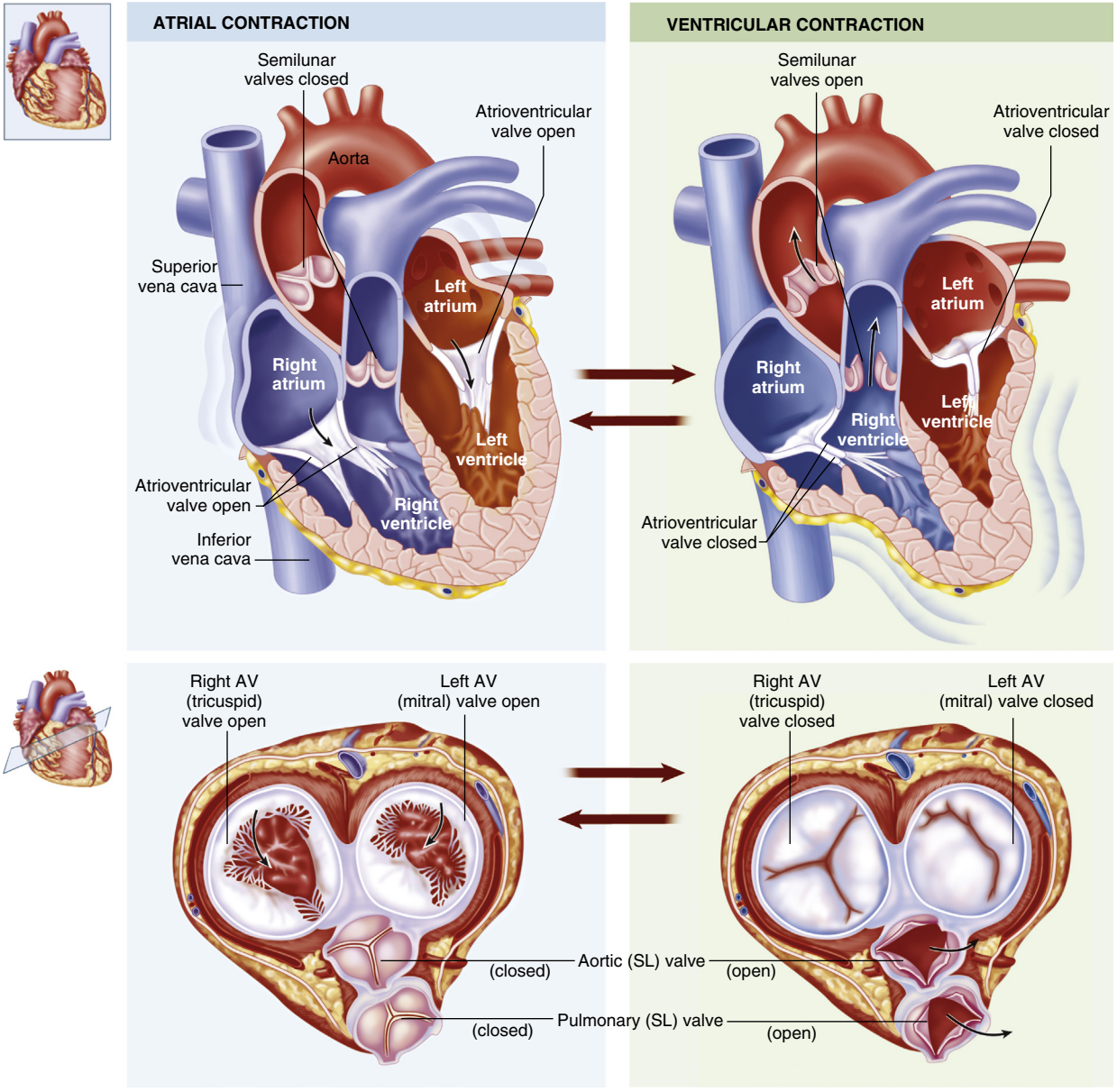

FIGURE 7-2 Structure of the heart valves.

Purkinje fibers, which can conduct impulses throughout the muscle of both ventricles and stimulate them to contract almost simultaneously. Specialized pacemaker cells in the SA node possess an **intrinsic rhythm** so that even without any stimulation by the autonomic nervous system, the node itself initiates impulses at regular intervals (approximately 60 to 75 beats per minute).

If the SA node for some reason is unable to generate an impulse, pacemaker activity shifts to another excitable component of the conduction system. These **ectopic pacemakers** also generate impulses rhythmically, although at a much slower rate. For example, if the AV node were to control pacemaker activity, the heart would beat 40 to 60 times per minute. If the conduction system of the heart is unable to maintain

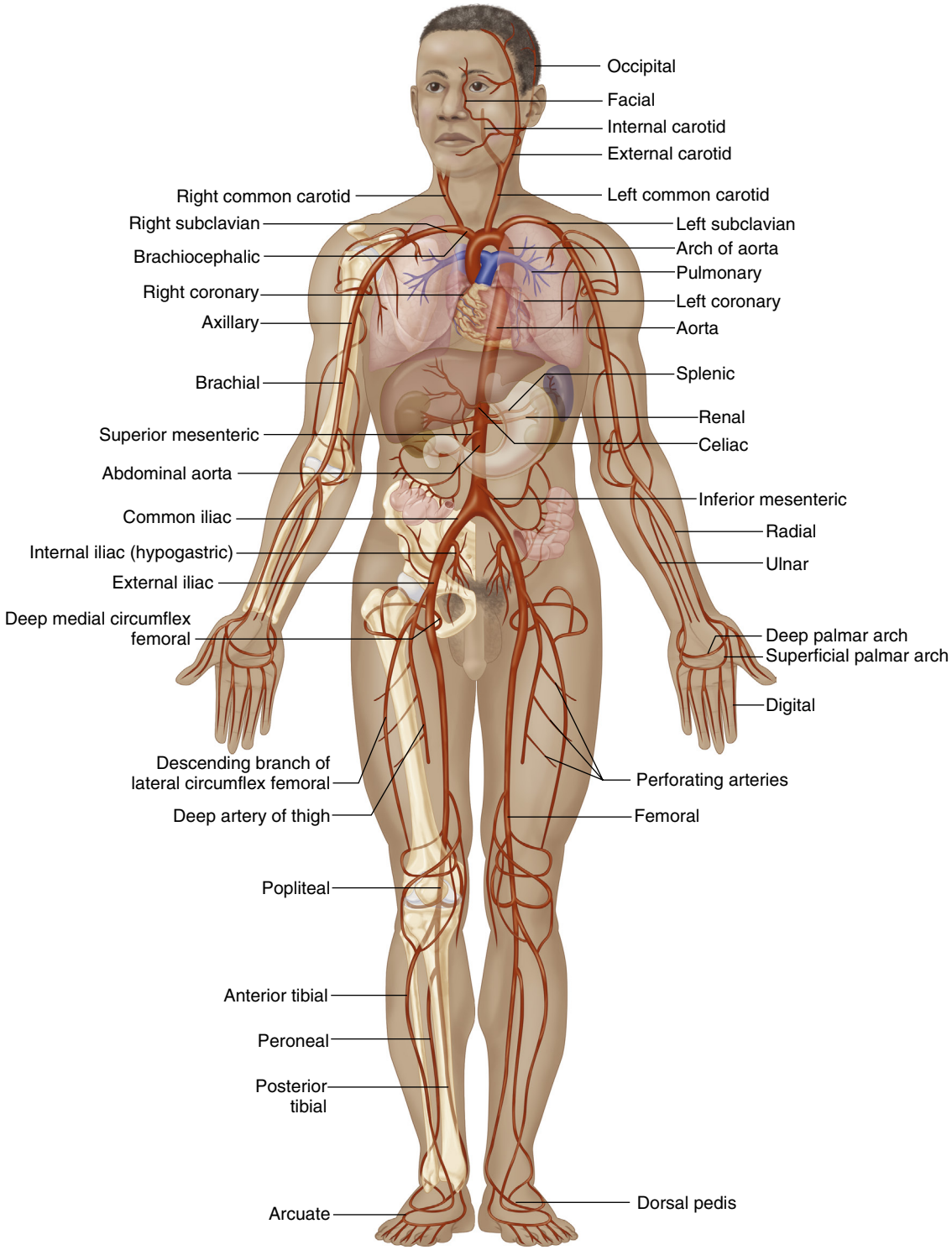

FIGURE 7-3 Systemic arterial system.

an adequate rhythm, the patient may receive an artificial pacemaker that electrically stimulates the heart, either at a set rhythm or only when the heart rate decreases below a preset minimum.

The heart muscle is supplied with oxygenated arterial blood by way of the right and left coronary arteries. These small vessels arise from the aorta just above the aortic valve. Unoxygenated blood from the myocardium drains into the coronary veins, which lead into the coronary sinus before opening into the right atrium.

The heart is surrounded by a double membranous sac termed the **pericardium**. The pericardium has a well-lubricated lining that protects against friction and permits the heart to move easily during contraction.

CONGENITAL HEART DISEASE

Left-to-Right Shunts

The most common congenital cardiac lesions are **left-to-right shunts**, which permit mixing of blood in the systemic and pulmonary circulations. Because blood is preferentially shunted from the high-pressure systemic circulation to the relatively low-pressure pulmonary circulation, the lungs become overloaded with blood. The magnitude of the shunt depends on the size of the defect and the differences in pressure on the two sides. An increased load on the heart produces enlargement of specific cardiac chambers, depending on the location of the shunt. The size of the defect determines the hemodynamic consequence for the systemic cardiac output.

The most common congenital cardiac lesion is **atrial septal defect**, which permits free communication between the two atria as a result of either lack of closure of the foramen ovale after birth or its improper closure during gestation. Because the left atrial pressure is usually higher than the pressure in the right atrium, the resulting shunt is from left to right and causes increased pulmonary blood flow and overloading of the right ventricle. This produces the radiographic appearance of enlargement of the right ventricle, the right atrium, and the pulmonary outflow tract (Figure 7-4).

In a patient with a **ventricular septal defect**, the resulting shunt is also from left to right because the left ventricular pressure is usually higher than the pressure in the right ventricle. The shunt causes increased pulmonary blood flow and consequently increased pulmonary venous return (Figure 7-5). This leads to diastolic overloading and enlargement of the left atrium and left ventricle. Because shunting occurs primarily in systole and any blood directed to the right ventricle immediately goes into the pulmonary artery, there is no overloading of the right ventricle and radiographically no right ventricular enlargement is seen.

The third major type of left-to-right shunt is **patent ductus arteriosus**. The ductus arteriosus is a vessel that extends from the bifurcation of the pulmonary artery to join the aorta just distal to the left subclavian artery. It serves to shunt blood from the pulmonary artery into the systemic

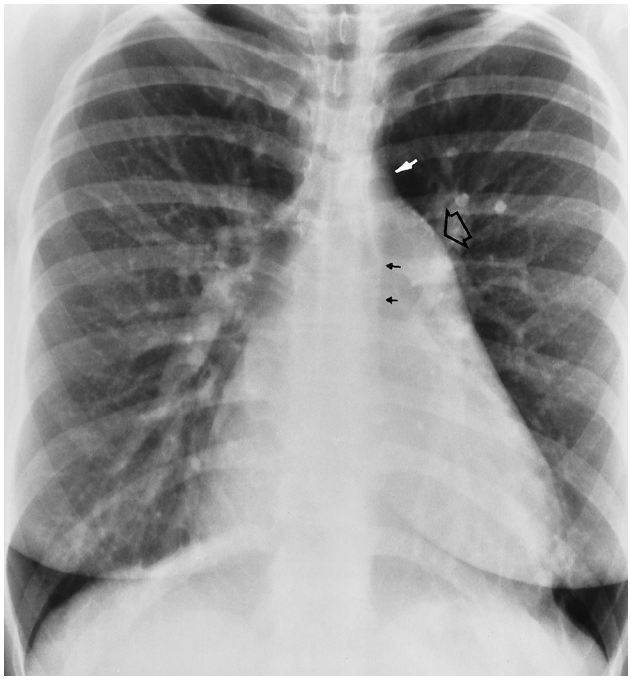

FIGURE 7-4 Atrial septal defect. Frontal projection of the chest demonstrates cardiomegaly along with an increase in pulmonary vascularity reflecting a left-to-right shunt. Small aortic knob (*white arrow*) and descending aorta (*small arrows*) are dwarfed by enlarged pulmonary outflow tract (*open arrow*).

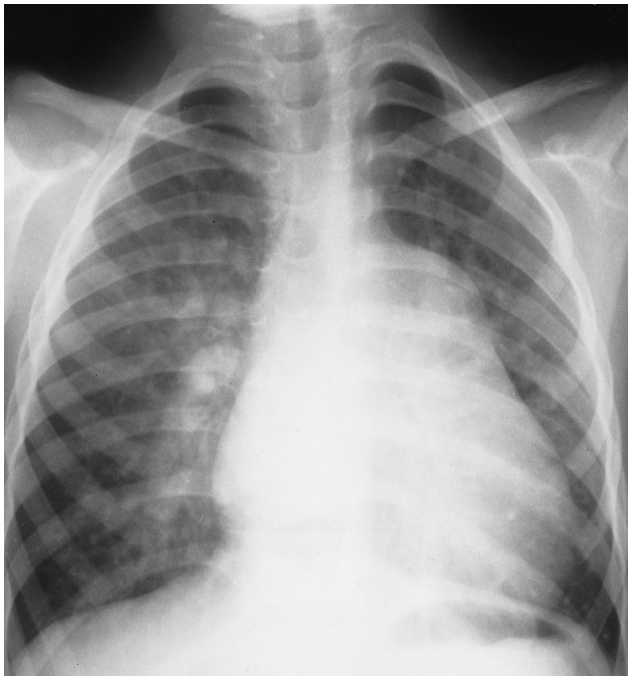

FIGURE 7-5 Ventricular septal defect. Heart is enlarged and somewhat triangular, and there is increased pulmonary vascular volume. Pulmonary trunk is very large and overshadows the normal-sized aorta, which seems small by comparison.

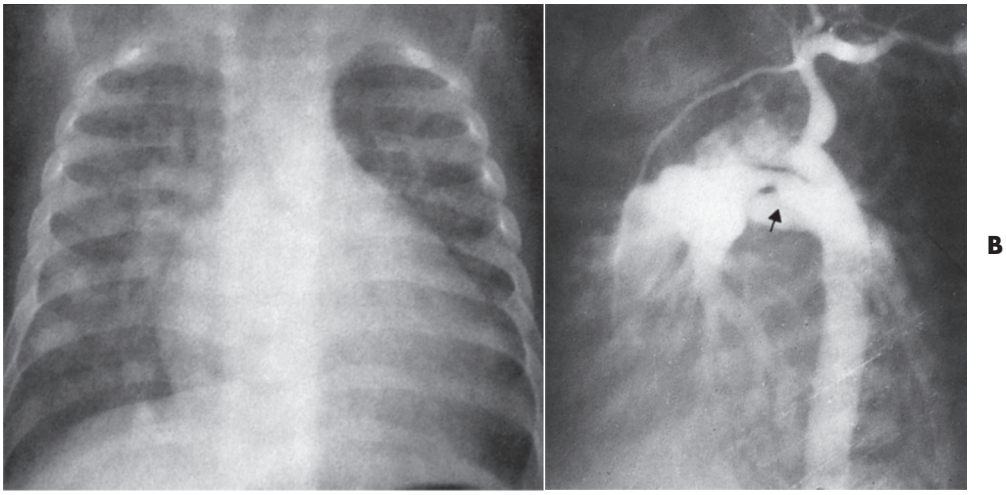

FIGURE 7-6 Patent ductus arteriosus. (A) Frontal chest radiograph demonstrates cardiomegaly with enlargement of the left atrium, left ventricle, and central pulmonary arteries. There is diffuse increase in the pulmonary vascularity. (B) In another patient, an aortogram shows patency of the ductus arteriosus (*arrow*).

circulation during intrauterine life. Persistence of the ductus arteriosus, which normally closes soon after birth, results in a left-to-right shunt. The flow of blood from the higher-pressure aorta to the lower-pressure pulmonary artery causes increased pulmonary blood flow, and an excess volume of blood is returned to the left atrium and left ventricle. Radiographically, there is enlargement of the left atrium, the left ventricle, and the central pulmonary arteries, along with a diffuse increase in pulmonary vascularity (Figure 7-6). The increased blood flow through the aorta proximal to the shunt produces a prominent aortic knob in contrast to the small- or normal-size aorta seen in atrial and ventricular septal defects.

All left-to-right shunts can be complicated by the development of pulmonary hypertension (**Eisenmenger's syndrome**). This is caused by increased vascular resistance within the pulmonary arteries related to chronic increased flow through the pulmonary circulation. Pulmonary hypertension appears radiographically as an increased fullness of the central pulmonary arteries with abrupt narrowing and pruning of peripheral vessels (Figure 7-7). The elevation of pulmonary arterial pressure tends to balance or even reverse the left-to-right shunt, thus easing the volume overloading of the heart.

Imaging appearance. Chest radiographs provide an initial assessment of pulmonary vasculature, size of the main pulmonary arteries, size and position of the aorta, and size and contour of the cardiac silhouette. In the preceding paragraphs, specific descriptions appear with each septal defect.

Doppler echocardiography can identify atrial and ventricular defects and extent of blood flow to determine the severity of the left-to-right shunting (Figure 7-8). Pressures can be measured to determine cardiac output from both the atria and the ventricles. Dilation of the ventricles implies patent ductus arteriosus.

Spin-echo magnetic resonance imaging (MRI), breath-hold magnetic resonance angiography (MRA), and cine MRI studies are being used to demonstrate congenital heart disease in cases in which ultrasonography is not diagnostic or feasible. MRI demonstrates both the morphologic and the functional anomalies in multiple planes. Patent ductus arteriosus appears as a signal loss on cine MRI and MRA images.

Angiocardiography is the most definitive imaging technique for demonstrating the atria and ventricles of the heart, but it is also the most invasive.

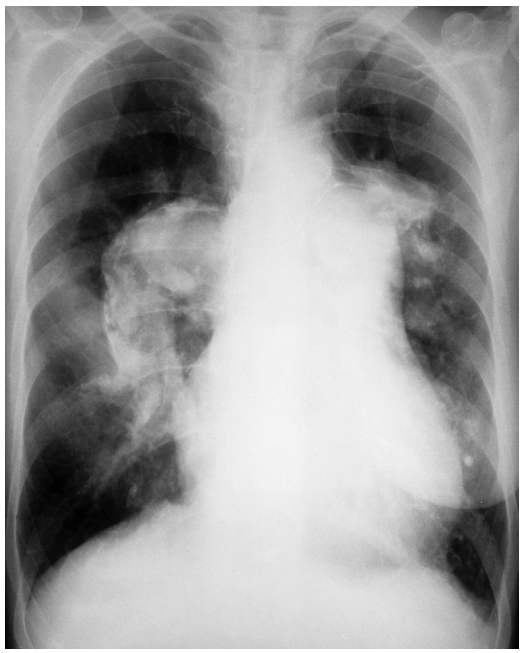

FIGURE 7-7 Eisenmenger's syndrome in atrial septal defect. There is slight but definite cardiomegaly and a great increase in the size of the pulmonary trunk. Right and left pulmonary artery branches are huge, but the peripheral pulmonary vasculature is relatively sparse. Long-standing pulmonary hypertension has produced degenerative changes in the walls of the pulmonary arteries, which have become densely calcified.

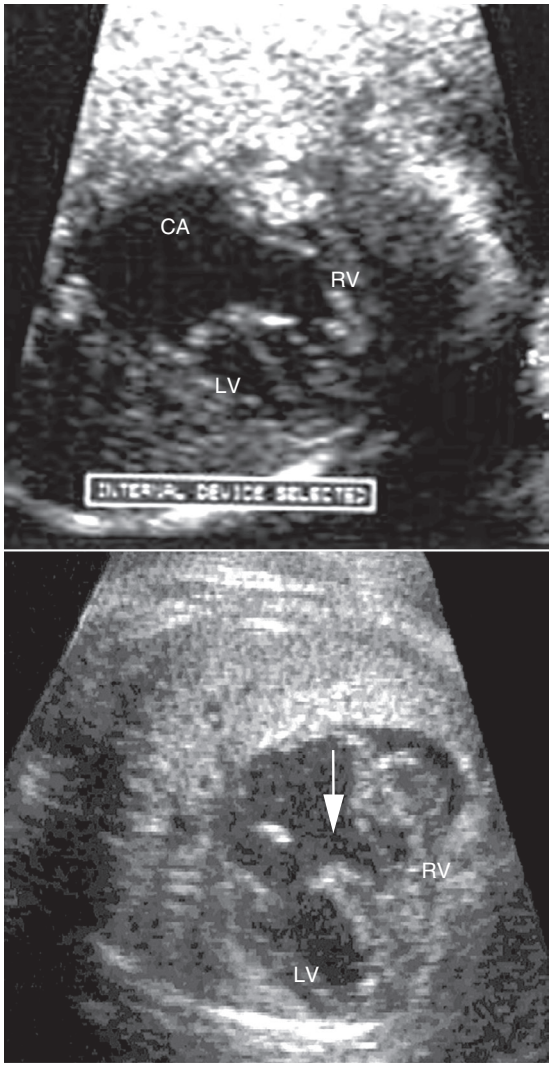

FIGURE 7-8 Atrial septal defect and ventricular septal defect. **(A)** Right (RV) and left (LV) ventricles are demonstrated with a common atrium (CA). **(B)** Right (RV) and left (LV) ventricles are seen without septal closure (*arrow*), allowing shunting of the blood.

Treatment. Small defects may not require treatment and may spontaneously close. The use of prostaglandin synthetase inhibitors may achieve closure. Surgery may be necessary to correct a large defect.

Tetralogy of Fallot

Tetralogy of Fallot is the most common cause of cyanotic congenital heart disease. It consists of four (thus "tetra") abnormalities: (1) high ventricular septal defect, (2) pulmonary stenosis, (3) overriding of the aortic orifice above the ventricular defect, and (4) right ventricular hypertrophy. Pulmonary stenosis causes an elevation of pressure in the right ventricle and hypertrophy of that chamber. Because of the narrow opening of the pulmonary valve, an inadequate amount of blood reaches the lungs to be oxygenated. The ventricular septal defect and the overriding of the aorta produce **right-to-left shunting** of unoxygenated venous blood into the left ventricle and then into the systemic circulation, thus increasing the degree of cyanosis.

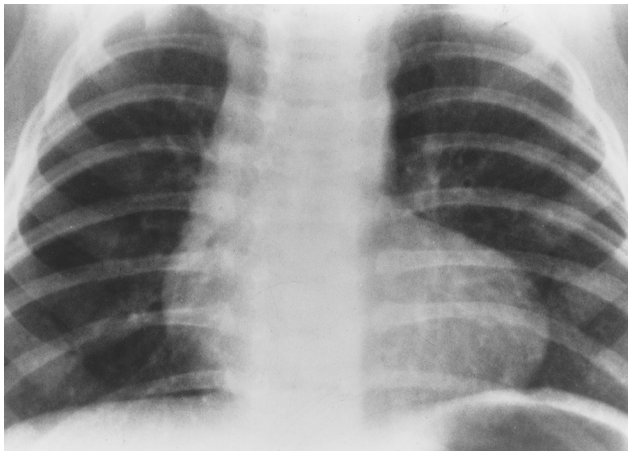

FIGURE 7-9 Tetralogy of Fallot. Plain chest radiograph demonstrates the characteristic lateral displacement and upward tilting of the prominent cardiac apex. There is also decreased pulmonary vascularity and a flat pulmonary outflow tract.

Imaging appearance. Enlargement of the right ventricle causes upward and lateral displacement of the apex of the heart (Figure 7-9). This results in the classic **coeur en sabot** appearance, in which the heart resembles the curved-toe portion of a wooden shoe. In approximately one-fourth of patients with tetralogy of Fallot, the aorta is on the right side.

Currently, echocardiography is the modality of choice to demonstrate the four abnormalities constituting tetralogy of Fallot. Spin-echo MRI best demonstrates the ventricular septal defect, right ventricular outflow (pulmonary stenosis), overriding aorta, and right ventricular hypertrophy. Cine MRI shows pulmonary stenosis as a flow void, for demonstrating it better than echocardiography.

Treatment. Without surgical repair, most patients with tetralogy of Fallot die before reaching puberty. Although operative repair provides some chance of recovery, the outcome depends on the severity of the defect and other extenuating circumstances. In some cases, surgery has only a palliative, supportive role.

Coarctation of the Aorta

Coarctation refers to a narrowing, or constriction, of the aorta that most commonly occurs just beyond the branching of the blood vessels to the head and arms. The blood supply and the pressure to the upper extremities are higher than normal. As a result, there is decreased blood flow through the constricted area to the abdomen and legs. Classically, the patient has normal blood pressure in the arms but very low blood pressure in the legs. Coarctation of the aorta is the most frequent cause of hypertension in children.

The relative obstruction of aortic blood flow leads to the progressive development of collateral circulation—the enlargement of normally tiny vessels in an attempt to

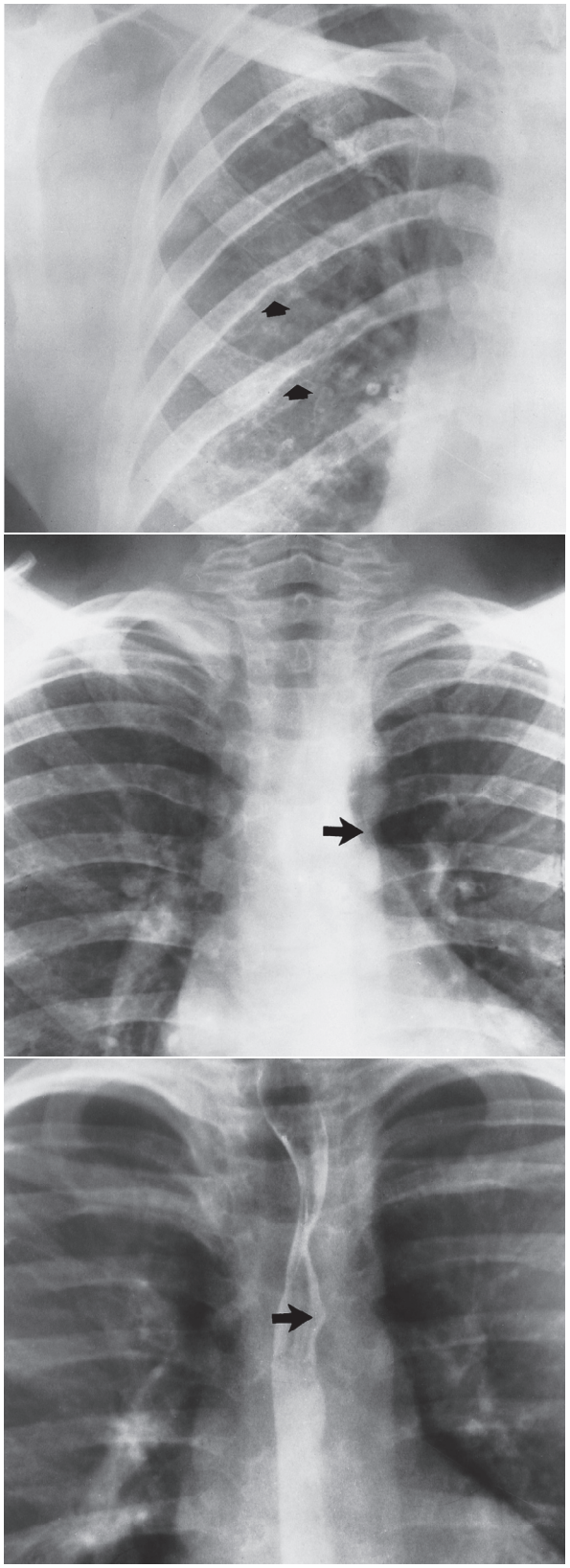

FIGURE 7-10 Coarctation of the aorta. **(A)** There is notching of the fourth through eighth posterior ribs (*arrows*). **(B)** Plain chest radiograph demonstrates a figure-3 sign (*arrow* pointing to its center). Upper bulge represents prestenotic dilation; lower bulge represents poststenotic dilation. **(C)** Esophagram demonstrates reverse figure-3 sign (*arrow* pointing to its center).

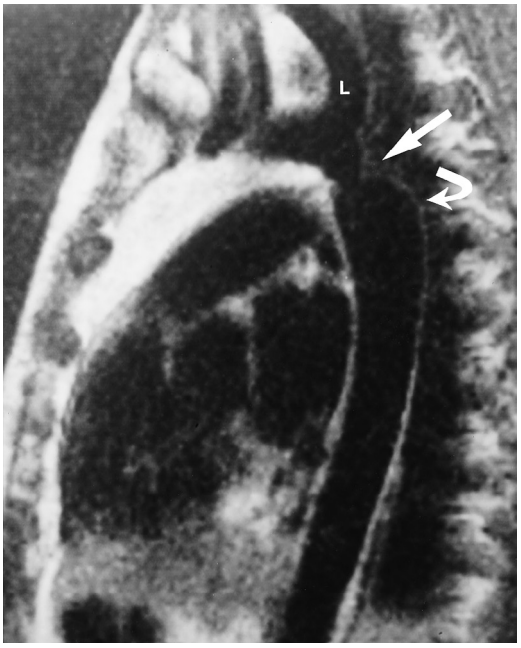

FIGURE 7-11 Coarctation of the aorta. Sagittal MR image demonstrates coarctation (*straight arrow*) of the thoracic aorta with associated poststenotic dilation of the proximal descending thoracic aorta (*curved arrow*). *L,* Left subclavian artery.

compensate for the inadequate blood supply to the lower portion of the body.

Imaging appearance. Coarctation of the aorta is often seen radiographically as rib notching (usually involving the posterior fourth to eighth ribs) resulting from pressure erosion by dilated and pulsating intercostal collateral vessels, which run along the inferior margins of these ribs (Figure 7-10A). Notching of the posterior border of the sternum may be produced by dilation of mammary artery collaterals.

Coarctation of the aorta often causes two bulges in the region of the aortic knob that produce a characteristic figure-3 sign on plain chest radiographs (Figure 7-10B) and a reverse figure-3 (or figure-E) impression on the barium-filled esophagus (Figure 7-10C). The more cephalic bulge represents dilation of the proximal aorta and the base of the subclavian artery (prestenotic dilation); the lower bulge reflects poststenotic aortic dilation.

With use of echocardiography to evaluate the aortic arch, the severity of the coarctation can be determined. Doppler echocardiography measures the gradient flow at the stenosis, and the diastolic runoff can be demonstrated.

Aortography can accurately localize the site of obstruction, determine the length of the coarctation, and identify any associated cardiac malformations. More recently, MRI has been used to demonstrate aortic narrowing (Figure 7-11) and to evaluate the appearance of the aorta after corrective surgery.

Treatment. Uncorrected aortic coarctation has a dismal prognosis, and surgical repair is required for patient survival. Currently, three surgical repairs are being used: (1) end-to-end anastomosis, (2) patch aortoplasty, and (3) left subclavian flap aortoplasty (surgical reformation of the aorta).

Summary of Findings for Congenital Heart Disease

Disorder	Location	Imaging Appearance	Treatment
Atrial septal defect	Communication between atria	PA chest—enlarged right ventricle, right atrium, and pulmonary outflow tract	Small defects may spontaneously close and not require treatment Medical treatment to achieve closure Large defects require surgical repair
Ventricular septal defect	Communication between ventricles	PA chest: Pulmonary trunk enlargement No right ventricular enlargement	
Patent ductus arteriosus	Vascular connection between pulmonary artery and aorta	PA chest—enlargement of left atrium, left ventricle, and pulmonary arteries with an increase in pulmonary vascularity MRI—spin-echo MRA breath-hold and cine to investigate morphologic and functional anomalies when US is not feasible or not diagnostic US—atrial defect has a common atria; ventricular defect demonstrates lack of septal closure	
Tetralogy of Fallot	High ventricular septal defect Pulmonary stenosis Overriding of the aortic orifice above the ventricular defect Right ventricular hypertrophy	PA chest—enlarged right ventricle causes upward and lateral displacement of the heart apex Echocardiography—demonstrates the four abnormalities of the disease MRI—demonstrates the morphologic conditions: Spin-echo scans to identify abnormalities Cine to demonstrate flow void in pulmonary stenosis	Operative repair
Coarctation of the aorta	Constriction of aorta at the distal arch	PA chest—rib notching, figure-3 Barium-filled esophagus—reverse figure-3 or figure-E Echocardiography—demonstrates the severity of stricture Doppler echo—determines flow gradient and possible collateral vessels Aortography—localizes obstruction, determines length of coarctation, and identifies an associated malformation MRI—demonstrates narrowing; used for follow-up of corrective surgery	Surgical repair

PA chest, Posteroanterior image of the chest; *US,* ultrasound.

ACQUIRED VASCULAR DISEASE

Coronary Artery Disease

Narrowing of the coronary arteries causes oxygen deprivation of the myocardium and ischemic heart disease. In most patients, narrowing of the lumen of one or more of the coronary arteries is attributable to the deposition of fatty material on the inner arterial wall (atherosclerosis). Factors predisposing to the development of coronary artery disease include hypertension, obesity, smoking, a high-cholesterol diet, and lack of exercise.

The speed and degree of luminal narrowing determine whether an atherosclerotic lesion causes significant and clinically evident ischemia. Temporary oxygen insufficiency causes *angina pectoris,* a feeling of severe chest pain that may radiate to the neck, jaw, and left arm (sometimes both arms) and that is often associated with the sensation of chest tightness or suffocation. Attacks of angina pectoris are often related to a sudden increase in the demand of the myocardium for oxygen, such as after strenuous exercise or a heavy meal or with emotional stress or exposure to severe cold. The placing of a nitroglycerin tablet under the tongue causes venous dilation, thus decreasing preload and myocardial oxygen demand.

Occlusion of a coronary artery deprives an area of myocardium of its blood supply and leads to the death of muscle cells (**myocardial infarction**) in the area of vascular distribution. The size of the coronary artery that is occluded and the myocardium that it supplies determines the extent of heart muscle damage. The greater the area affected, the poorer the prognosis because of the increased loss of pumping function that may result in congestive heart failure (CHF). A favorable prognostic factor is the development of collateral circulation, through which blood from surrounding vessels is channeled into the damaged tissue. If the patient survives, the infarcted

region heals with fibrosis. Long-term complications include the development of thrombi on the surface of the damaged area and the production of a local bulge (ventricular aneurysm) at the site of the weakness of the myocardial wall.

Imaging appearance. Radionuclide thallium perfusion scanning is the major noninvasive study for assessment of regional blood flow to the myocardium. Focal decreases in thallium uptake that are observed immediately after exercise but are no longer identified on delayed scans usually indicate transient ischemia associated with significant coronary artery stenosis or spasm. After exercise, focal defects that remain unchanged on delayed scans more frequently reflect scar formation. A normal thallium exercise scan makes the diagnosis of myocardial ischemia unlikely, although in approximately 10% of patients with significant obstructive disease, the presence of sufficient collateral vessels can prevent the radionuclide demonstration of regional ischemia.

Radionuclide CT scanning (single-photon emission computed tomography [SPECT]), using technetium pyrophosphate or other compounds that are taken up by acutely infarcted myocardium, is a noninvasive technique for detecting, localizing, and classifying myocardial necrosis (Figure 7-12). Newer CT technology (spiral multidetector) provides visualization of the coronary arteries in a noninvasive approach. CT quantifies the artery calcification, evaluates stenosis, measures cardiac function, and analyzes plaque. To best demonstrate the coronary arteries, electrocardiography-synchronized scanning is completed in the diastolic phase (Figure 7-13). On CT, areas of myocardial ischemia appear as regions of decreased attenuation because of the higher water content resulting from intramyocardial cellular edema. Multidetector helical CT scans provide calcium screening for detecting hard plaque. To evaluate soft plaque, CT angiography (CTA) is required. Studies have indicated that MRI is also of value in detecting early signs of muscular necrosis in myocardial infarction (Figure 7-14) and may help determine whether the infarction is acute or remote.

Plain chest radiographs are usually normal or nonspecific in most patients with ischemic heart disease. Calcification of a coronary artery, although infrequently visualized on routine chest radiographs and usually requiring cardiac fluoroscopy, strongly suggests the presence of hemodynamically significant coronary artery disease (Figure 7-15). Plain chest radiographs are also entirely normal in many, if not most, patients after myocardial infarction. The images are primarily of value in detecting evidence of pulmonary venous congestion in patients in whom CHF develops as a result of an inability of the remaining heart muscle to propel blood through the circulation adequately.

Coronary arteriography is generally considered the definitive test for determining the presence and assessing the severity of coronary artery disease. Approximately 30% of significant stenoses involve a single vessel, most commonly the anterior descending artery. Another 30% involve two vessels, and significant stenosis of the three main vessels can be demonstrated in the remaining 40%. Approximately 50% of coronary artery disease occurs in the left coronary artery,

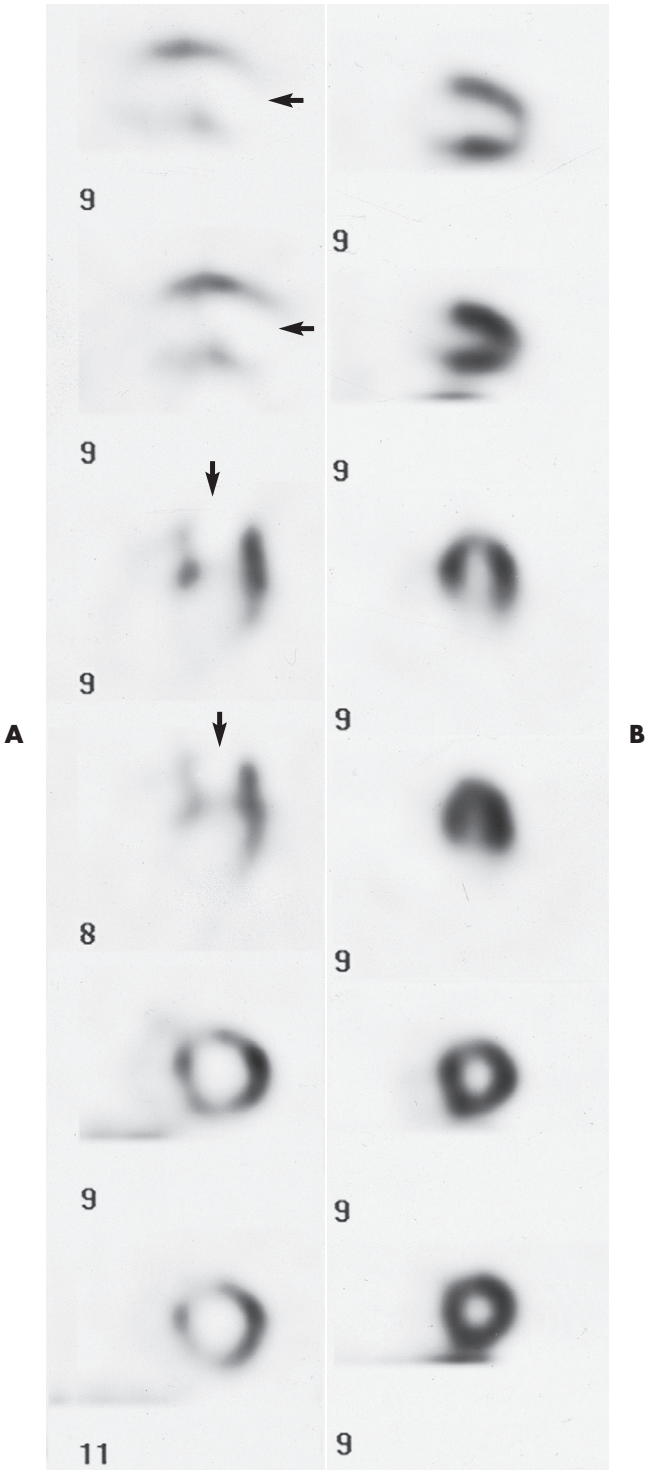

FIGURE 7-12 Myocardial stress/rest perfusion single-photon emission computed tomography scan. **(A)** Apical defect is demonstrated on the stress images because of the lack of uptake in the cardiac apex (*arrows*). **(B)** The defect on rest images shows perfusion to the apex of the heart, indicating ischemia.

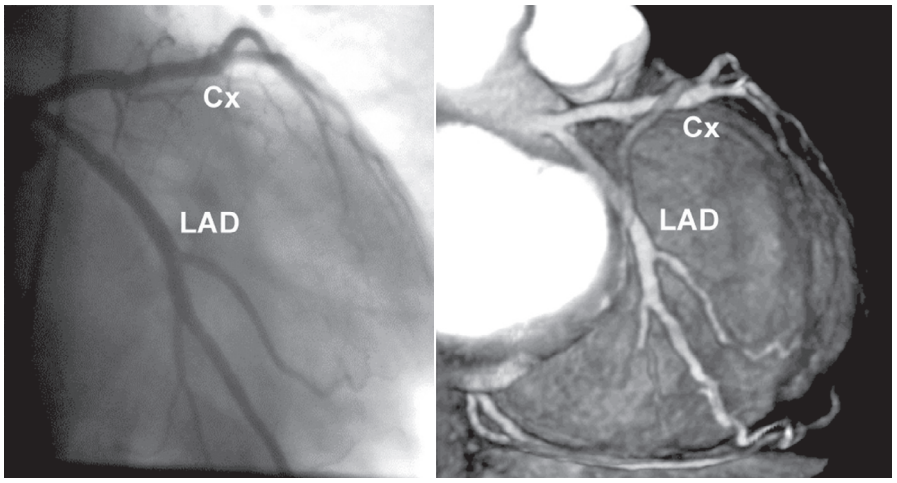

FIGURE 7-13 Comparison of conventional angiography and contrast-enhanced CT coronary angiography in one patient. **(A)** Anteroposterior cranial projection from conventional selective coronary angiography shows the left anterior descending (LAD) and circumflex (Cx) coronary arteries. **(B)** CT volume rendering in anteroposterior cranial projection shows the left main coronary artery with its branches, the left anterior descending (LAD) and left circumflex (Cx) coronary arteries.

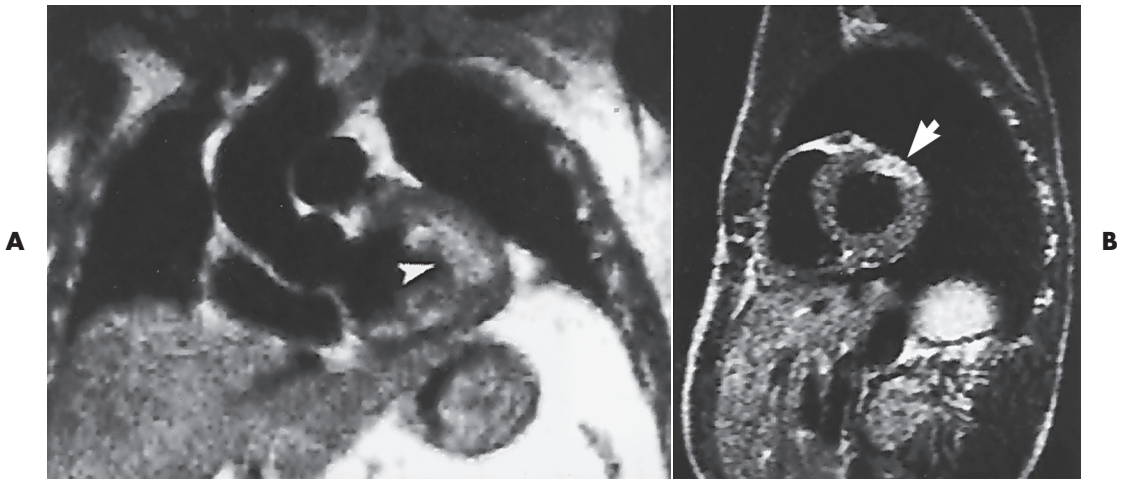

FIGURE 7-14 MRI of acute myocardial infarction. **(A)** T2-weighted coronal image obtained in a patient 10 days after acute myocardial infarction demonstrates an area of increased signal intensity (indicating edema associated with muscle necrosis) in subendocardial regions of the lateral wall (*arrowhead*). **(B)** Short-axis view of another patient shows acute transmural infarction (*arrow*) of the anterolateral wall.

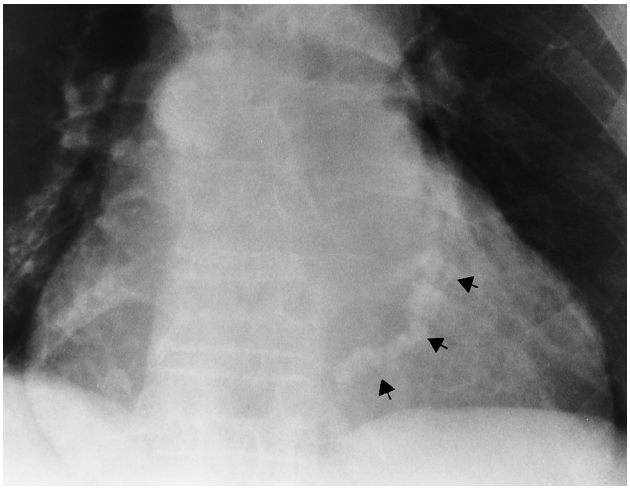

FIGURE 7-15 Ischemic heart disease. Frontal projection of chest demonstrates cardiomegaly with the typical linear calcification in coronary artery (*arrows*).

35% in the right coronary artery, and 15% in the left circumflex artery (Figure 7-16).

Intravascular ultrasound (IVUS) provides the most precise anatomic information to guide interventional procedures. The severity of arterial stenosis, measurement of lesion length, lumen dimension, and any unusual morphology can be determined. This modality is especially helpful in demonstrating the origin of the left main coronary artery, which may be obscured by the catheter in angiography. However, this equipment is not readily available in most institutions because of its expense.

Treatment. Aortocoronary bypass grafting, usually using sections of saphenous vein, is an increasingly popular procedure in patients with ischemic heart disease. Arteriography has been the procedure of choice for demonstrating the patency and functional efficiency of aortocoronary bypass grafts. Patent functioning grafts demonstrate prompt clearing of contrast material and adequate filling of the grafted artery.

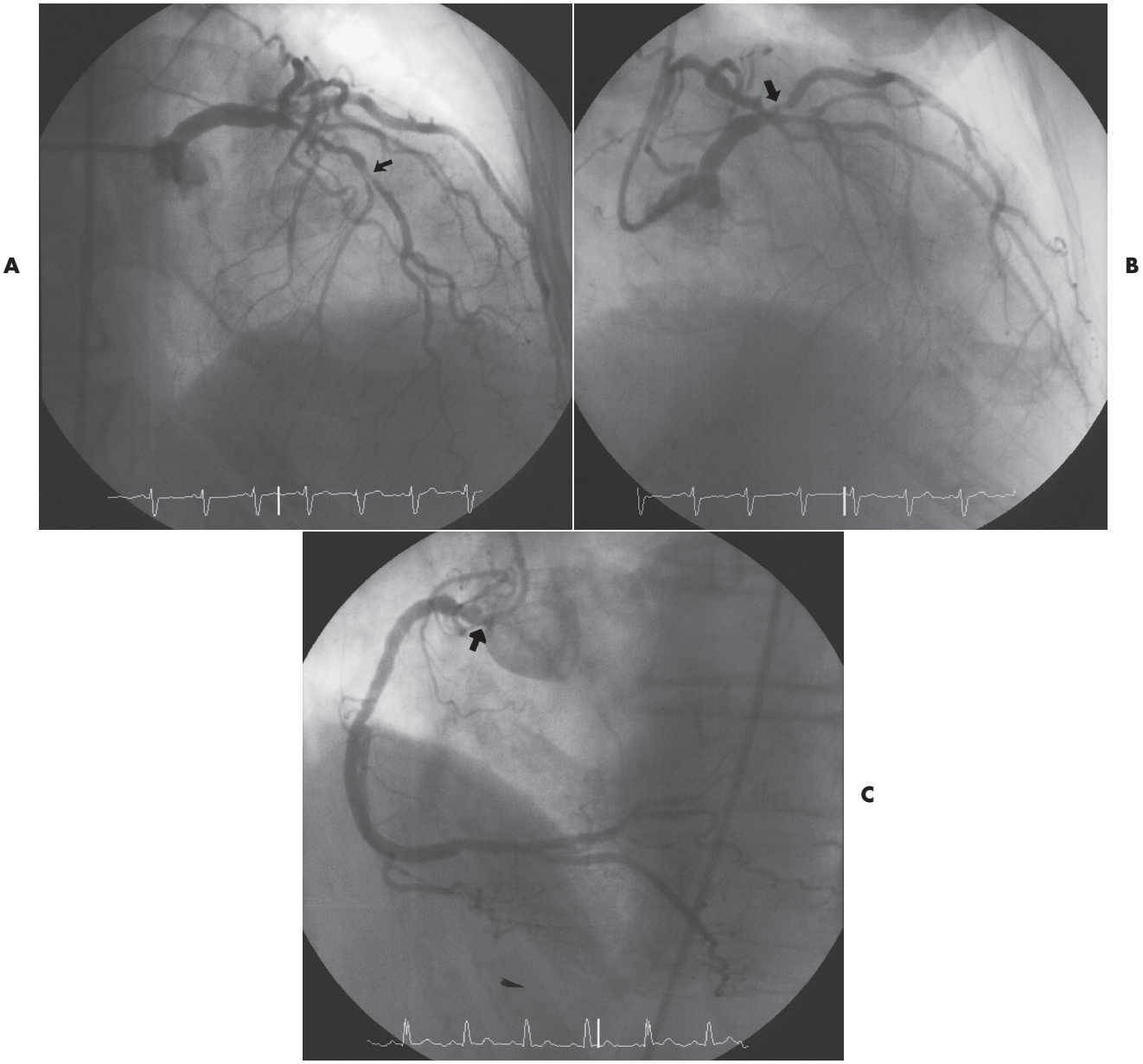

FIGURE 7-16 Coronary angiography. **(A)** Posteroanterior cranial projection of the left main coronary artery shows a lesion involving the left anterior descending artery. **(B)** Right anterior oblique cranial projection of the left main coronary artery shows a lesion in the diagonal artery. **(C)** Left anterior oblique projection of the right coronary artery demonstrates an ostial lesion at the origin.

Stenotic or malfunctioning grafts demonstrate areas of narrowing, filling defects, and slow flow with delayed washout of contrast material.

Percutaneous transluminal coronary angioplasty (PTCA) using a balloon catheter is now a recognized procedure for the treatment of patients with narrowing of one or more coronary arteries (Figure 7-17). As in other types of PTA, a catheter is placed under fluoroscopic guidance into the affected coronary artery, and an arteriogram is performed for localization. The angioplasty balloon is then positioned at the level of the stenosis and inflated. After dilation, coronary arteriography is repeated to illustrate the resulting appearance of the stenosis and to detect any complications of the procedure. Symptomatic improvement occurs in 50% to 70% of dilations. Approximately 3% to 8% of patients who undergo PTCA experience either persistent coronary insufficiency or sudden occlusion of a coronary artery at the site of dilation at the time of the procedure. Therefore, the procedure should be performed at a time when an operating room, an anesthetist, and a cardiac surgeon are available so that immediate coronary bypass surgery can be performed if necessary. The percentage of deaths from coronary angioplasty is less than 1%. In conjunction with PTCA, deployment of a drug-eluting stent helps in many cases to maintain the open lumen (Figure 7-18). Other interventional procedures are endovascular stenting, atherectomy, and laser-assisted angioplasty.

Congestive Heart Failure

Congestive heart failure (CHF) refers to the inability of the heart to propel blood at a rate and volume sufficient to provide an adequate supply to the tissues. Causes of CHF include an intrinsic cardiac abnormality, hypertension, and any obstructive process that abnormally increases the peripheral resistance to blood flow. Intrinsic cardiac abnormalities include insufficient or defective cardiac filling and impaired contractions for emptying.

Imaging appearance. Left-sided heart failure produces a classic radiographic appearance of cardiac enlargement, redistribution of pulmonary venous blood flow (enlarged superior pulmonary veins and decreased caliber of the veins draining the lower lungs), interstitial edema, alveolar edema (irregular, poorly defined patchy densities), and pleural effusions (Figure 7-19). In acute left ventricular failure resulting from coronary thrombosis, however, there may be severe pulmonary congestion and edema with very little cardiac

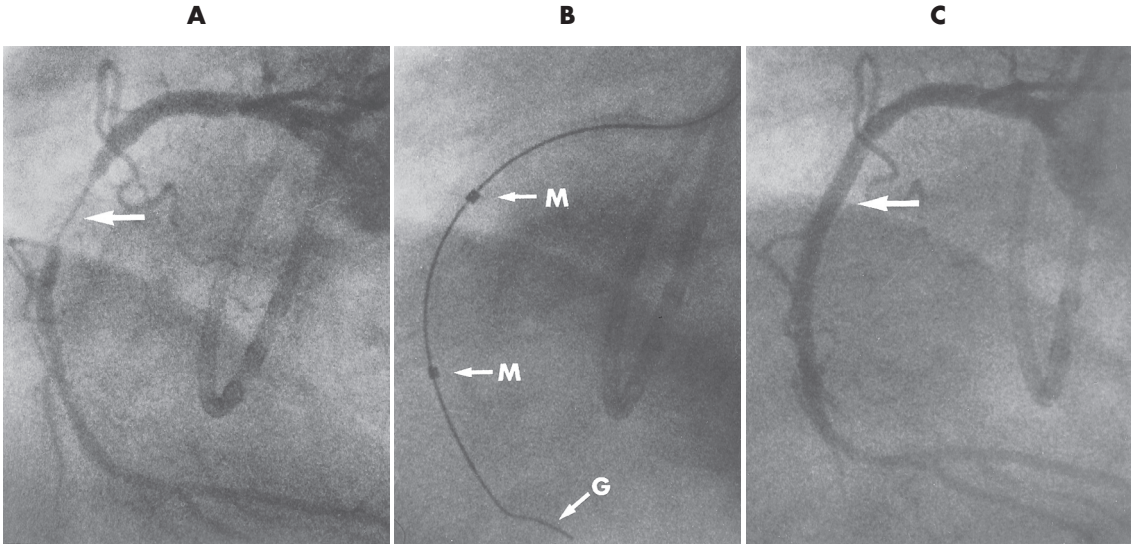

FIGURE 7-17 Percutaneous transluminal coronary angioplasty. (A) Initial right coronary angiogram shows severe narrowing (*arrow*) of the midportion of the right coronary artery. (B) During percutaneous transluminal coronary angioplasty, a steerable guidewire (G) is passed down the coronary artery and through the coronary stenosis. The tip lies within the distal right coronary artery. Radiopaque markers (M) identify the balloon portion of the dilating catheter that has been advanced over the guidewire through the coronary stenosis. (C) Immediately after angioplasty, the previous site of stenosis (*arrow*) is now patent.

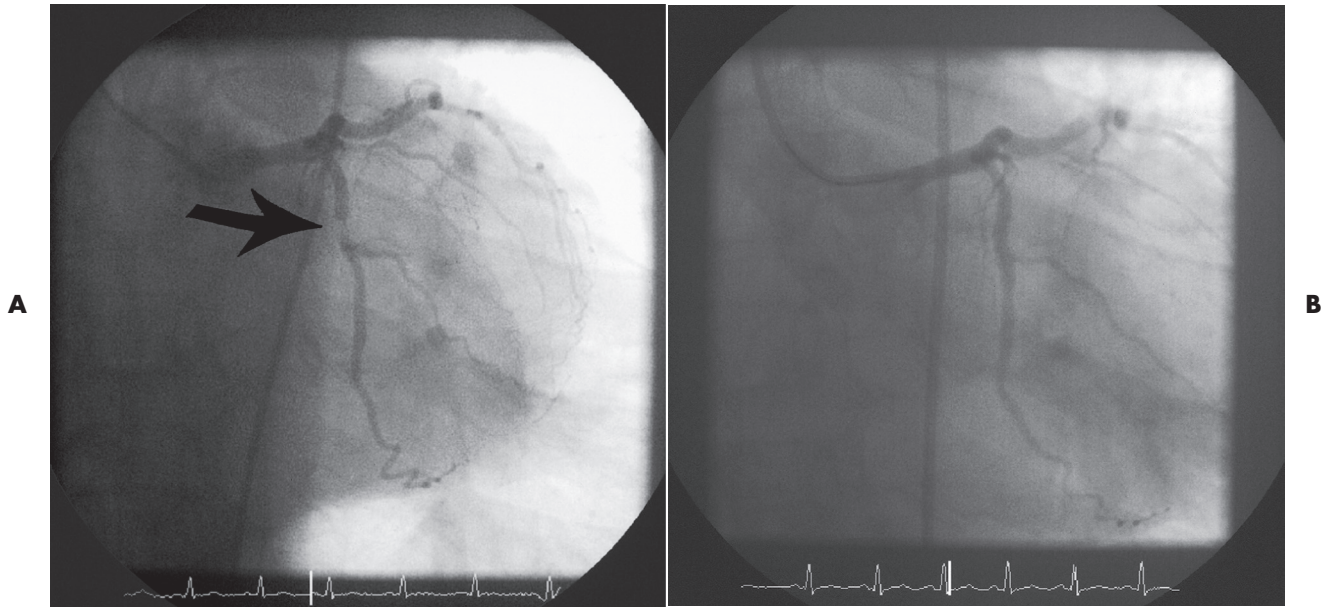

FIGURE 7-18 Coronary angiography. (A) Angiogram of the left coronary artery with a stenotic lesion in the circumflex artery (*arrow*). (B) Angiogram demonstrating the left circumflex artery after PTA and stent placement with no evidence of a stenotic lesion.

enlargement. Pulmonary congestion and edema may require a change in radiographic technique to compensate for the increased fluid in the lungs. The major causes of left-sided heart failure include coronary heart disease, valvular disease, and hypertension.

In right-sided heart failure, dilation of the right ventricle and right atrium is present (Figure 7-20). The transmission of increased pressure may cause dilation of the superior vena cava, widening of the right superior mediastinum, and edema of the lower extremities. The enlargement of a congested liver may elevate the right hemidiaphragm. Common causes of right-sided heart failure are pulmonary valvular stenosis, emphysema, and pulmonary hypertension resulting from pulmonary emboli.

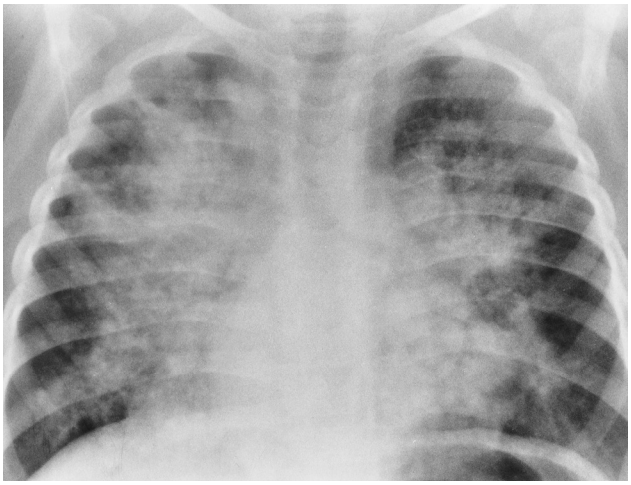

FIGURE 7-19 Left-sided heart failure. Diffuse perihilar alveolar densities.

Many patients with CHF have cardiomegaly. A simple measurement made on a posteroanterior (PA) chest radiograph to evaluate the heart size is the cardiothoracic ratio (C/T ratio), with a value greater than 50% indicating cardiomegaly. In these cases, the radiologist relies on information provided by the radiographer about the images: erect versus recumbent, PA versus anteroposterior (AP), and source-to-image receptor distance—all of which influence the heart size. Lack of (or inaccurate) information can result in misdiagnosis.

Echocardiography is the modality of choice for measuring left ventricle performance, ejection fraction, and filling pressures in the pulmonary artery and ventricles.

Pulmonary Edema

Pulmonary edema refers to an abnormal accumulation of fluid in the extravascular pulmonary tissues. The most common cause of pulmonary edema is an elevation of the pulmonary venous pressure. This pressure is most often attributable to left-sided heart failure but may also be caused by pulmonary venous obstruction (mitral valve disease and left atrial tumor) or lymphatic blockade (fibrotic, inflammatory, or metastatic disease involving the mediastinal lymph nodes). Other causes of pulmonary edema include uremia, narcotic overdose, exposure to noxious fumes, excessive oxygen, high altitudes, fat embolism, adult respiratory distress syndrome, and various neurologic abnormalities.

Imaging appearance. Transudation of fluid into the interstitial spaces of the lungs is the earliest stage of pulmonary

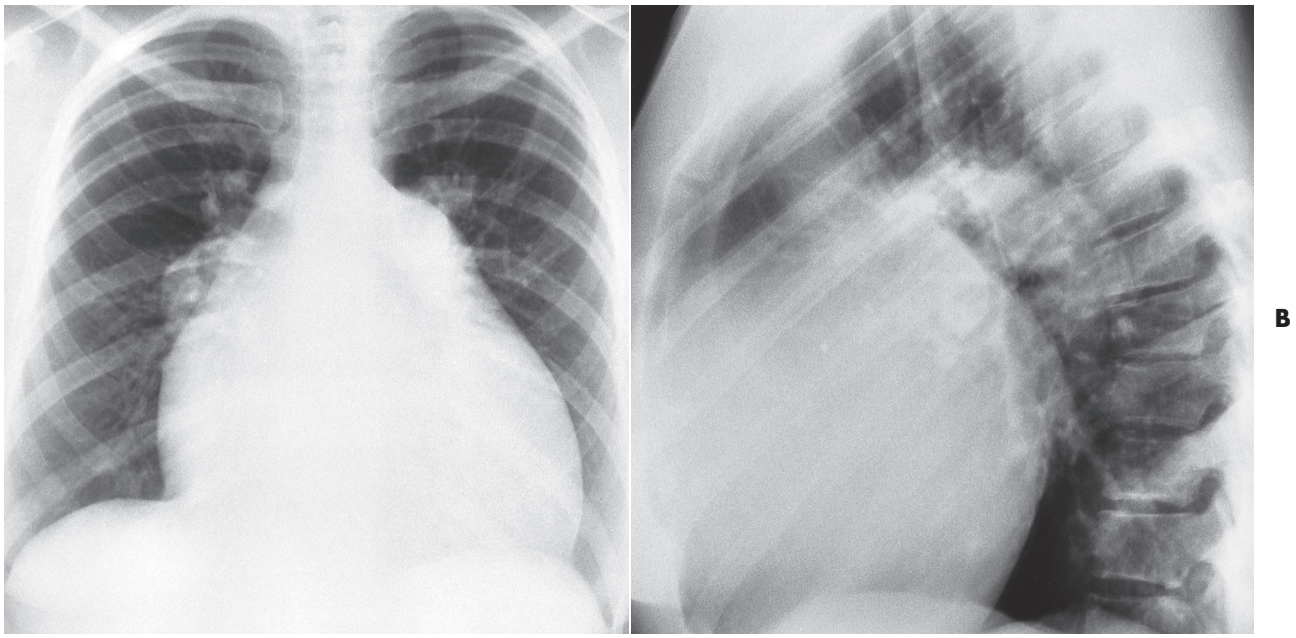

FIGURE 7-20 Right-sided heart failure. Frontal (A) and lateral (B) projections of the chest in a patient with primary pulmonary hypertension show pronounced globular cardiomegaly with prominence of the pulmonary trunk and central pulmonary arteries. Peripheral pulmonary vascularity is strikingly reduced. Right ventricular enlargement has obliterated retrosternal air space on the lateral projection.

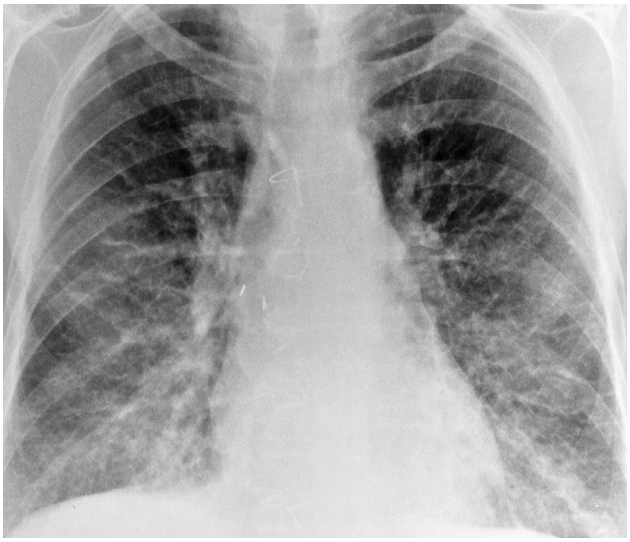

FIGURE 7-21 Interstitial pulmonary edema. Edema fluid in the interstitial space causes loss of the normal sharp definition of pulmonary vascular markings and a perihilar haze. At the bases, notice the thin, horizontal lines of increased density (Kerley B lines), which represent fluid in interlobular septa.

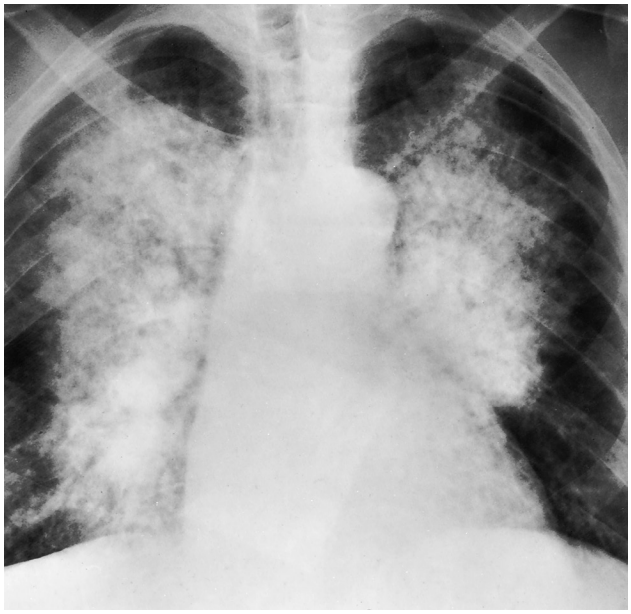

FIGURE 7-22 Butterfly pattern of severe pulmonary edema. Diffuse bilateral symmetric infiltration of the central portion of lungs along with relative sparing of the periphery produces a butterfly pattern.

edema. However, in patients with CHF or pulmonary venous hypertension, increased pulmonary venous pressure first appears as a redistribution of blood flow from the lower to the upper lung zones. This phenomenon, probably caused by reflex venous spasm, causes prominent enlargement of the superior pulmonary veins and decreases the caliber of the veins draining the inferior portions of the lung. Edema fluid in the interstitial space causes a loss of the normal sharp definition of pulmonary vascular markings (Figure 7-21). Accentuation of the vascular markings about the hila produces a perihilar haze. Fluid in the interlobular septa produces characteristic thin, horizontal lines of increased density at the axillary margins of the lung inferiorly (Kerley B lines).

A further increase in pulmonary venous pressure leads to the development of alveolar or pleural transudates. Alveolar edema appears as irregular, poorly defined patchy densities scattered throughout the lungs. The classic radiographic finding of alveolar pulmonary edema is the butterfly (or bat's wing) pattern, a diffuse, bilaterally symmetric, fan-shaped infiltration that is most prominent in the central portion of the lungs and fades toward the periphery (Figure 7-22).

Pleural effusion associated with pulmonary edema usually occurs on the right side (Figure 7-23). When bilateral, the effusion tends to be more noticeable on the right. There is often an associated thickening of the interlobar fissures. Pleural effusions are best demonstrated radiographically with use of a horizontal beam and the patient in a lateral decubitus position.

After adequate treatment of pulmonary edema, the interstitial, alveolar, and pleural abnormalities may disappear within several hours. Loculated pleural fluid within a fissure (especially the minor fissure) may resorb more slowly and

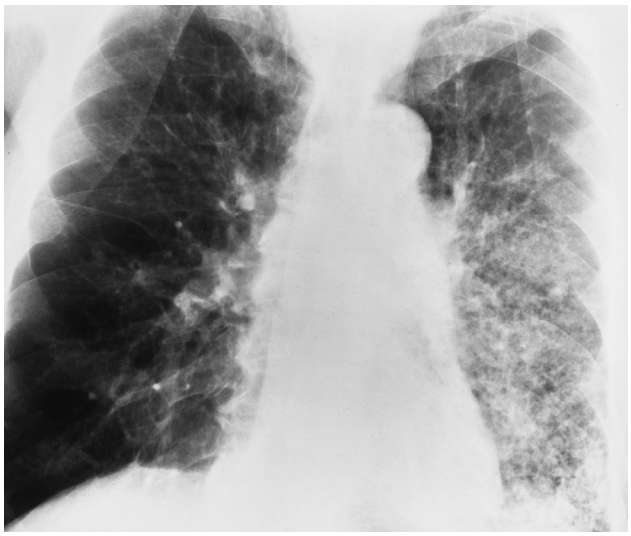

FIGURE 7-23 Unilateral pulmonary edema. Diffuse alveolar pattern limited to the left lung because of the effect of gravity on the patient lying on the left side.

appear as a sharply defined, elliptical, or circular density that simulates a solid parenchymal mass (Figure 7-24).

Most patients with pulmonary edema caused by CHF or other heart disease have evidence of cardiomegaly. When the cause of the pulmonary edema is noncardiogenic, the heart often remains normal in size (Figure 7-25).

Treatment of Congestive Heart Failure and Pulmonary Edema

The nonpharmacologic approach to the treatment of CHF and pulmonary edema involves avoiding excessive physical

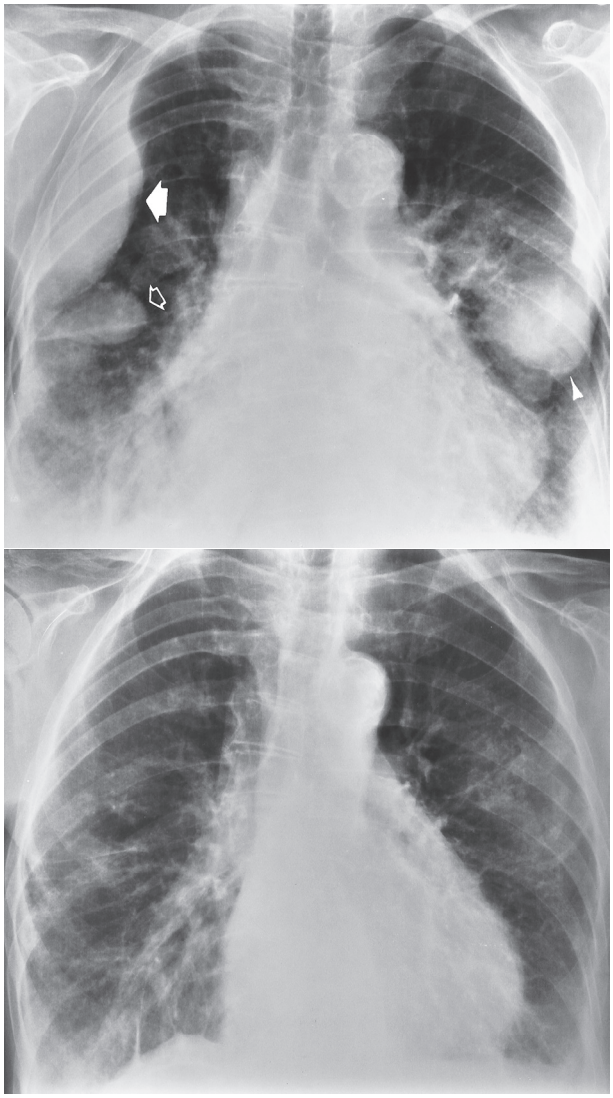

FIGURE 7-24 Loculated pleural fluid (phantom tumors). (A) Frontal chest radiograph taken during an episode of CHF demonstrates pronounced cardiomegaly with bilateral pleural effusions. Note the fluid collections along the lateral chest wall (*solid arrow*), in a minor fissure (*open arrow*), and in a left major fissure (*arrowhead*). (B) With improvement in the patient's cardiac status, phantom tumors have disappeared. Bilateral small pleural effusions persist.

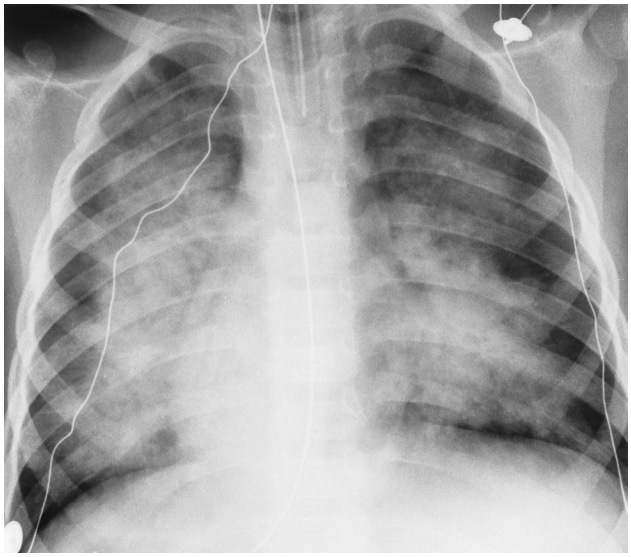

FIGURE 7-25 Pulmonary edema. After a near-drowning event, the patient has a normal-size heart and a pattern of diffuse pulmonary edema.

stress, decreasing dietary salt, and wearing compressive stockings to decrease the incidence of deep vein thrombosis (DVT). Pharmacologic therapy includes some combination of the following drugs: diuretics, angiotensin-converting enzyme inhibitors, digoxin (digitalis), parenteral inotropic agents, calcium channel blockers, beta-blockers, and antithrombotic therapy.

Hypertension

Hypertension, or high blood pressure, is the leading cause of strokes and CHF. The blood pressure is a function of cardiac output (the amount of blood pumped per minute by the heart) and the total peripheral resistance, which reflects the condition of the walls of the blood vessels throughout the body. Although the peripheral resistance and cardiac output may fluctuate rapidly, depending on such factors as whether a person sits or stands and is quiet or excited, the systemic blood pressure remains remarkably constant in a healthy person.

A blood pressure reading consists of two parts. The systolic pressure is the highest pressure in the peripheral arteries that occurs when the left ventricle contracts. The diastolic pressure is the pressure in the peripheral arteries when the left ventricle is relaxing and filling with blood from the left atrium. *High blood pressure* is defined as elevation of the systolic pressure above 140 millimeters of mercury (mm Hg) and of the diastolic pressure above 90 mm Hg. In patients older than 40 years, the systolic pressure may be somewhat higher and still be considered within normal limits. As a rough rule of thumb, a person is allowed an additional 10 mm Hg in systolic pressure for each decade over 40 years of age.

Most patients with elevated blood pressure have essential, or idiopathic, hypertension. The benign form of essential hypertension is characterized by a gradual onset and a prolonged course, often of many years. In the much less common malignant form, the elevated blood pressure has an abrupt onset, runs a rapid course, and often leads to renal failure or cerebral hemorrhage.

Approximately 6% of patients have secondary hypertension resulting from another disease. Although some patients in this group have adrenal abnormalities (Cushing's syndrome, primary aldosteronism, and pheochromocytoma) in which there is an abnormality of the regulation of salt and water content (and thus the blood volume), and others have an abnormality involving the secretion of a substance that increases vascular tone and peripheral arterial resistance, most have renal parenchymal or vascular disease as the underlying cause of hypertension.

Imaging appearance. Arteriography is the most accurate screening examination for detecting renovascular lesions. If a noninvasive screening test is desired, a radionuclide renogram

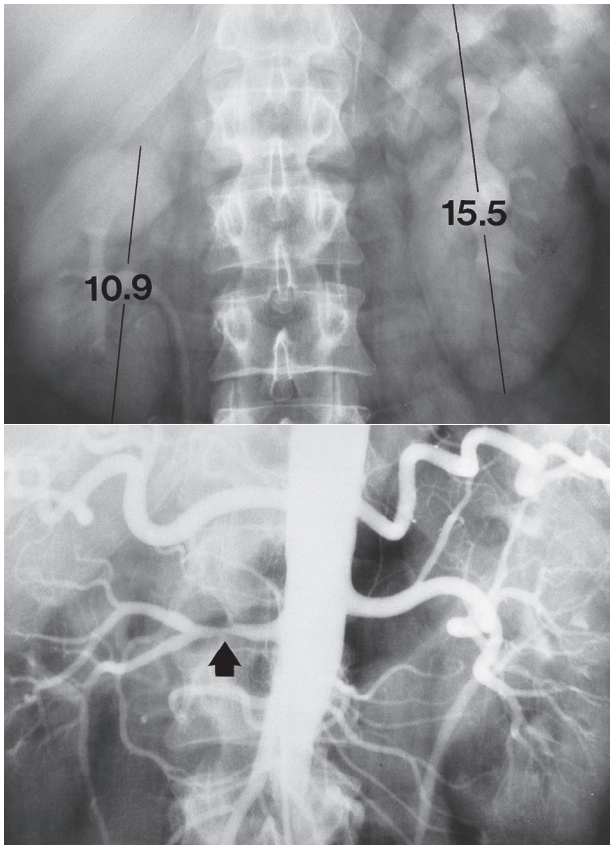

FIGURE 7-26 Renovascular hypertension. **(A)** Radiograph shows diminished size of the right kidney. **(B)** Arteriography demonstrates that the cause is renal artery stenosis (*arrow*).

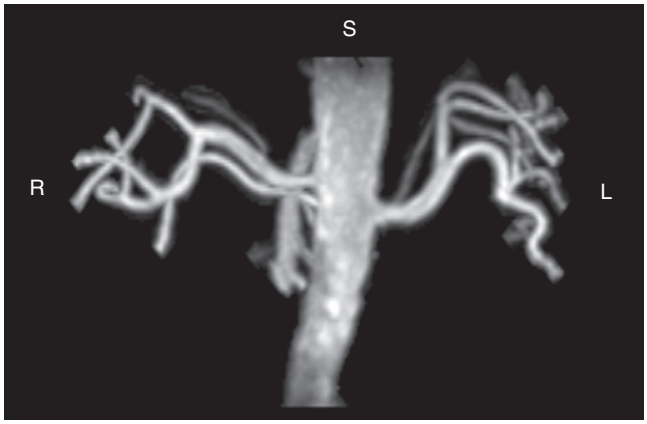

FIGURE 7-27 Abdominal aorta MRA. Normal appearance on noncontrast renal MRA.

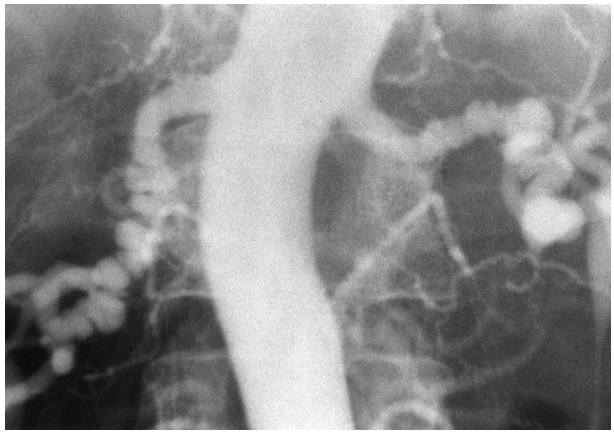

FIGURE 7-28 Renovascular hypertension. String-of-beads pattern of fibromuscular dysplasia bilaterally.

with captopril is performed. The most common cause of renal artery obstruction is arteriosclerotic narrowing, which usually occurs in the proximal portion of the vessel close to its origin from the aorta (Figure 7-26). Bilateral renal artery stenoses are noted in up to one-third of patients with this disorder. Oblique projections, which demonstrate the vessel origins in profile, are often required to demonstrate renal artery stenosis. CTA can detect renal artery stenosis, including fibromuscular dysplasia. MRA can detect stenosis, but the resolution is still inadequate to visualize segmental renal branches (Figure 7-27). The sensitivity and specificity of this modality for proximal renal disease are higher than 90%. One of the advantages of MRA is that iodinated contrast agents are not required to visualize the vessel anatomy; however, kidney function is of concern if a contrast agent (gadolinium) is used.

The other major cause of renovascular hypertension is **fibromuscular dysplasia**. This disease is most common in young adult women and is often bilateral. The most common radiographic appearance of fibromuscular dysplasia is the string-of-beads pattern, in which there are alternating areas of narrowing and dilation (Figure 7-28). Smooth, concentric stenoses occur less frequently.

The mere presence of a renovascular lesion does not mean that it is the cause of hypertension; indeed, many patients with normal blood pressure have severe renal artery disease. Therefore, bilateral renal vein catheterization for the measurement of plasma renin activity is used to assess the functional significance of any stenotic lesion. A renal vein renin concentration on the abnormal side that is more than 50% greater than the renin level in the renal vein on the normal side indicates the functional significance of a lesion with an accuracy rate of approximately 85%.

Prolonged high blood pressure forces the heart to overwork, causing the left ventricle to enlarge and eventually fail. Because high blood pressure affects all arteries of the body, including the coronary and carotid vessels, this condition increases the risk of coronary occlusion, myocardial infarction, and carotid narrowing leading to a stroke.

Decreased function of the kidneys leads to the retention of water and salt, which increases the blood volume and elevates the blood pressure. Long-standing hypertension causes atherosclerosis of the renal artery, which reduces blood flow to the kidneys and causes further damage.

Treatment. Medical treatment involves some combination of diuretics and beta-, alpha-, and calcium-blockers to control blood pressure. Surgery has traditionally been the treatment for a patient with arteriographically demonstrated renal artery lesions and confirmatory renal vein renin study findings. PTA, with stent placement, has been

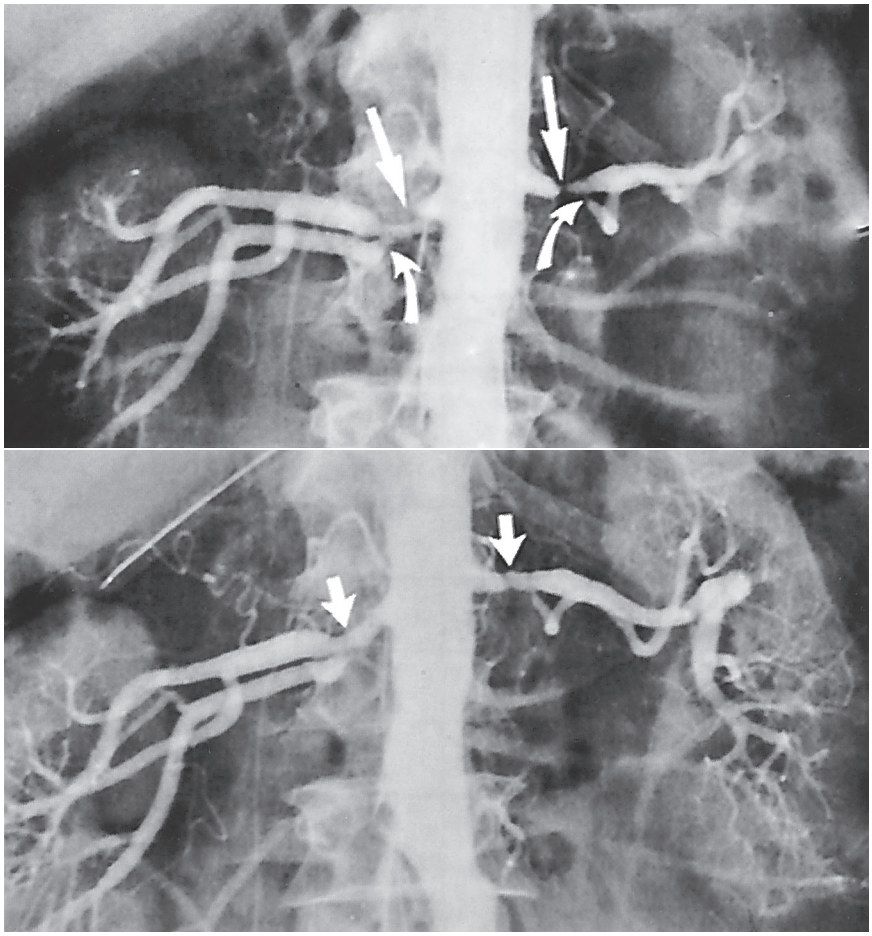

FIGURE 7-29 PTA for renovascular hypertension. (A) Abdominal aortogram demonstrates severe bilateral stenoses of the main renal arteries (*straight arrows*) and stenoses at the origins of early bifurcations (*curved arrows*). (B) Aortogram after angioplasty of both renal arteries shows irregularities in areas of previous atherosclerotic narrowing (*arrows*) but an improved residual lumen in both main renal arteries. After the procedure, the patient's previous severe hypertension was controllable to normal levels with only minimal dosages of diuretic medication.

shown to be effective in dilating renal artery stenoses (Figure 7-29). Although insufficient time has elapsed to compare the long-term results of renal transluminal angioplasty with those of corrective surgical procedures, initial studies demonstrate the improvement or cure of hypertension in approximately 80% of patients treated with angioplasty. Stenosis recurs in 10% to 20%, usually because of incomplete dilation.

Hypertensive Heart Disease

Long-standing high blood pressure causes narrowing of systemic blood vessels and an increased resistance to blood flow. The left ventricle is forced to assume a larger workload, which initially causes hypertrophy (double thickness of normal wall) and little if any change in the radiographic appearance of the cardiac silhouette.

Imaging appearance. Eventually, the continued strain on the heart leads to dilation and enlargement of the left ventricle (Figure 7-30), along with downward displacement of the cardiac apex, which often projects below the left hemidiaphragm. Aortic tortuosity with prominence of the ascending portion commonly occurs (Figure 7-31). Notching of the undersurface of the ribs may become evident. Failure of the left ventricle leads to increased pulmonary venous pressure and CHF (in 40% of cases).

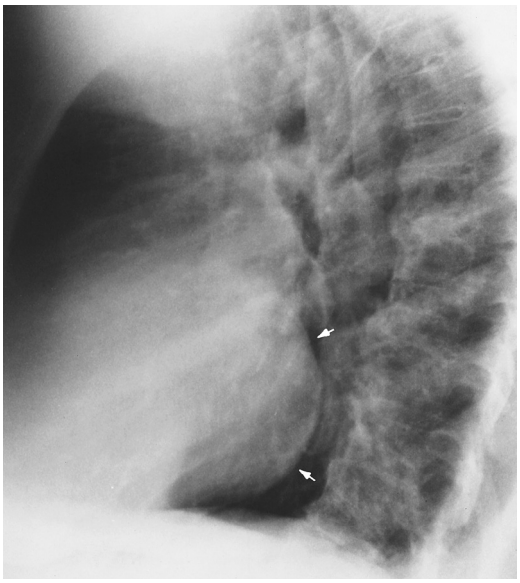

FIGURE 7-30 Hypertensive heart disease. Lateral projection of chest shows prominence of left ventricle (*arrows*).

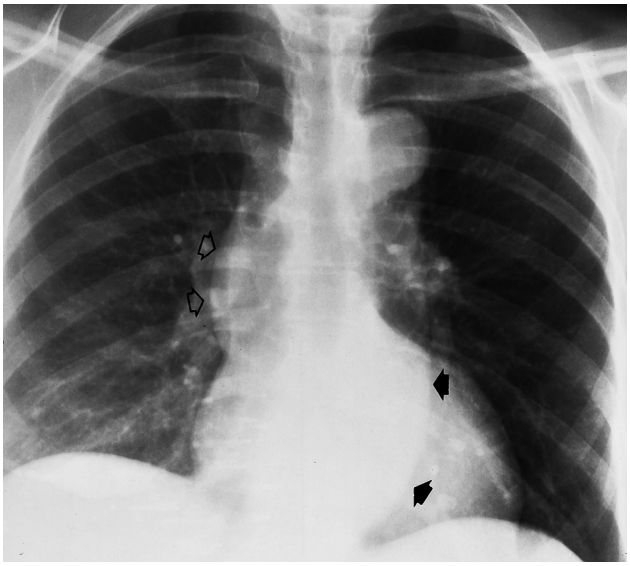

FIGURE 7-31 Hypertensive heart disease. Generalized tortuosity and elongation of the ascending aorta (*open arrows*) and descending aorta (*solid arrows*).

Treatment. Therapy of hypertensive heart disease consists of treating the high blood pressure and any complications, such as CHF.

Aneurysm

An *aneurysm* is a localized dilation of an artery that most commonly involves the aorta, especially its abdominal portion. A **saccular aneurysm** involves only one side of the arterial wall, whereas bulging of the entire circumference of the vessel wall is termed a **fusiform aneurysm**. An aneurysm represents a weakness in the wall (decreased elastin and increased collagen production) of a blood vessel caused by atherosclerosis, syphilis or other infection, trauma, or a congenital defect such as Marfan's syndrome. The presence of multiple small aneurysms is suggestive of a generalized arterial inflammation (arteritis). In the abdominal aorta, most aneurysms occur below the origin of the renal arteries, and thus the aneurysm can be surgically replaced by a prosthetic graft without injuring the kidneys. The danger of an aneurysm is its tendency to enlarge and rupture, leading to massive hemorrhage, which may be fatal if it involves a critical organ, such as the brain.

Imaging appearance. Although plain abdominal radiographs can demonstrate curvilinear calcification in the wall of an aneurysm (Figure 7-32), ultrasound (ultrasonography) is the modality of choice for detection of an abdominal aortic aneurysm. The ultrasonographic definition of aneurysmal dilation of the abdominal aorta is an enlargement of the structure to a diameter greater than 3 cm. Ultrasound can demonstrate an intraluminal clot as a hypoechoic or anechoic lesion (Figure 7-33A), and the noninvasive nature of the modality permits an evaluation of the enlargement of an aneurysm on serial studies. Ultrasound is the best imaging modality for defining the abdominal aortic aneurysm; CTA and MRA are superior for demonstrating aortic rupture.

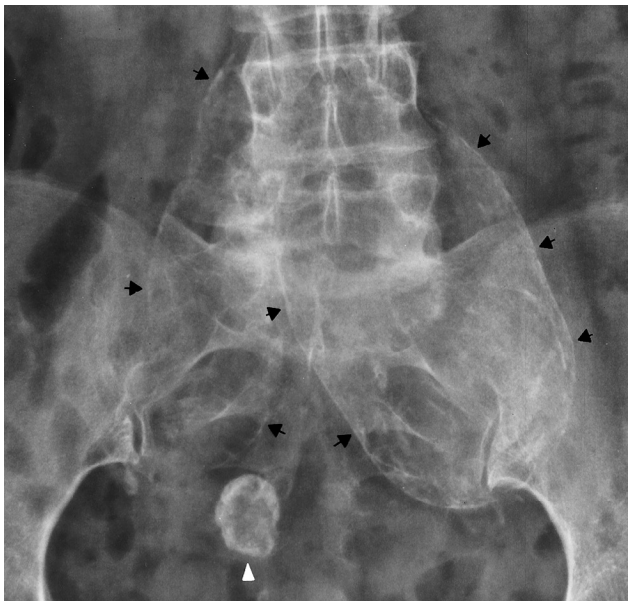

FIGURE 7-32 Fusiform aneurysm. Calcification in the walls of aneurysms of the lower abdominal aorta and both common iliac arteries (*black arrows*). Of incidental note is a calcified uterine fibroid (*white arrowhead*) in the pelvis.

CTA and MRA also can demonstrate the location and extent of an aneurysm, and these modalities have begun to replace catheter angiography. CTA can identify a retroperitoneal hematoma secondary to leaking or acute rupture of the aneurysm. With helical CT, three-dimensional reformation permits demonstration of the abdominal aorta in multiple planes, improving visualization of the origin of the aneurysm and its relationship to the renal arteries (see Figure 7-33B). When a thrombus is demonstrated on CT, the attenuation values (Hounsfield units) can be used to determine whether the rupture and/or thrombus is fresh or weeks old. A new bleed has a high attenuation value, whereas older blood causes isoattenuation or hypoattenuation. MRA may be the better choice if the patient has depressed renal function because the contrast agent it uses is less nephrotoxic.

The major value of arteriography in patients with abdominal aortic aneurysm is as a presurgical road map to define the extent of the lesion and whether the renal arteries or other major branches are involved. Because the lumen of an aneurysm may be filled with clot, aortography often produces an underestimation of the extent of aneurysmal dilation.

In the chest, CT after the intravenous injection of contrast material is the most efficient technique for demonstrating the size and extent of an aortic aneurysm and for differentiating this vascular lesion from a solid mediastinal mass. Unlike aortography, CT is relatively noninvasive and can directly identify an intraluminal thrombus (seen as a soft tissue density separating the contrast agent–filled portion of the lumen from the aortic wall), which can only be inferred on contrast examination (see Figures 7-33B and 7-33C). CT can also demonstrate aortic mural calcification and the effects of the aneurysm on adjacent structures, such as displacement of the mediastinum and bone erosion. Because of its ability to

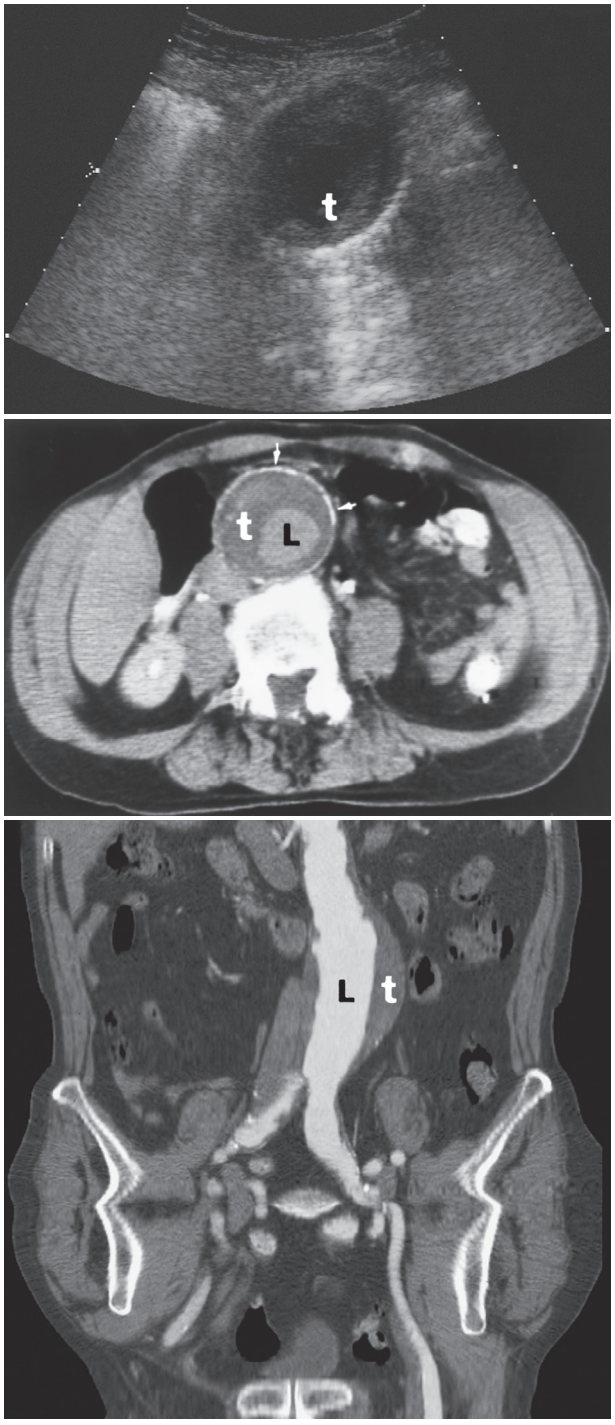

FIGURE 7-33 Abdominal aortic aneurysm. (A) Ultrasound shows a large aneurysm with an echogenic thrombus (t) filling the outer margins of the aorta, creating a false lumen 2.25 cm in diameter. (B) CT axial scan of an abdominal aortic aneurysm in another patient shows a low-density thrombus (t) surrounding a blood-filled lumen (L). The wall of the aneurysm contains high-density calcification (*arrows*). (C) CT coronal reconstruction in a third patient shows an abdominal aortic aneurysm beginning below the renal arteries and extending below the iliac bifurcation.

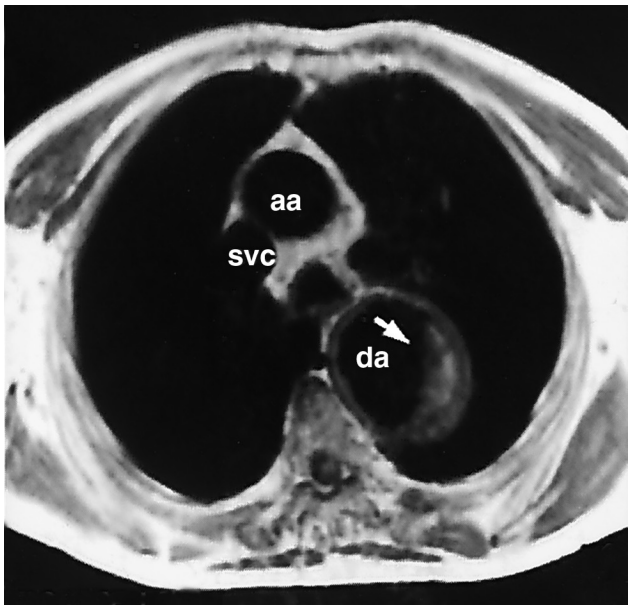

FIGURE 7-34 MR image of an aortic aneurysm. Transverse scan with cardiac gating permits differentiation of a large mural thrombus (*arrow*) from the signal void of rapidly flowing intraluminal blood. aa, ascending aorta; da, descending aorta; svc, superior vena cava.

demonstrate flowing blood as a signal void and clot as a heterogeneous collection of signal intensities, MRI can provide information about an aneurysm that is comparable to that obtained from CT without the need for intravenous contrast material (Figure 7-34).

Treatment. An abdominal aortic aneurysm may require surgical graft placement to maintain circulation to the inferior part of the abdomen and lower extremity. Currently, a patient may be a candidate for percutaneous stent placement (Figure 7-35) to strengthen the abdominal aorta and prevent rupture and growth of the aneurysm.

Traumatic Rupture of the Aorta

Traumatic rupture of the aorta is a potentially fatal complication of closed-chest trauma (rapid deceleration, blast, and compression). In almost all cases, the aortic tear occurs just distal to the left subclavian artery at the site of the ductus arteriosus.

Imaging appearance. On plain chest radiographs, hemorrhage into the mediastinum causes widening of the mediastinal silhouette and loss of a discrete aortic knob shadow. Associated rib or sternal fractures may be apparent. However, because nonspecific mediastinal widening is a frequent finding, especially on the supine anteroposterior portable radiographs taken after trauma, other plain image signs are of diagnostic importance (Figure 7-36). These include displacement of an opaque nasogastric tube to the right (because of a hematoma that displaces the esophagus), widening of the right paratracheal stripe (Figure 7-37), and a collection of blood over the apex of the left lung (apical pleural cap sign).

CT and emergency aortography are the definitive examinations for the evaluation of possible laceration or rupture

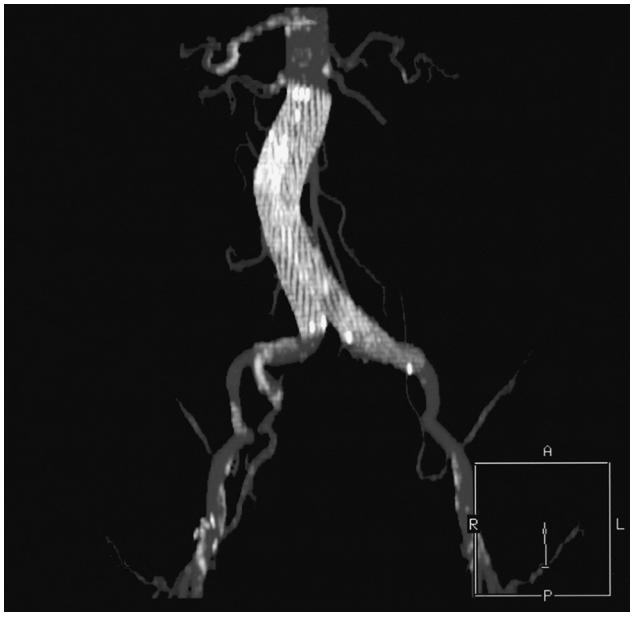

FIGURE 7-35 CTA of an abdominal aortic stent placed for an abdominal aortic aneurysm. Posterior perspective demonstrates the stent placed in the aorta and a second stent placed in the right iliac artery.

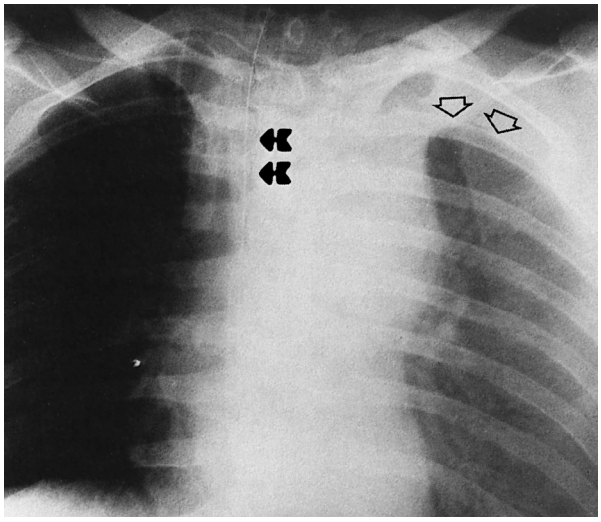

FIGURE 7-36 Traumatic aneurysm of the aorta. There is widening of the mediastinum and deviation of the nasogastric tube to the right (*solid arrows*). *Open arrows* point to the collection of fluid over the left apex (apical pleural cap) in this patient, who suffered severe blunt chest trauma.

of the aorta. The patient's condition and facility preferences determine the modality of choice. CTA using multidetector helical scanners to scan in thin slices and reconstruct in multiplanar dimensions provides extremely detailed images in a very short time. If the patient has multiple traumatic injuries for which CT is needed, then CT is the modality of choice to evaluate a traumatic rupture of the aorta. In aortography, right anterior oblique and left anterior oblique projections are best to demonstrate both the contours of the aortic arch and any rupture.

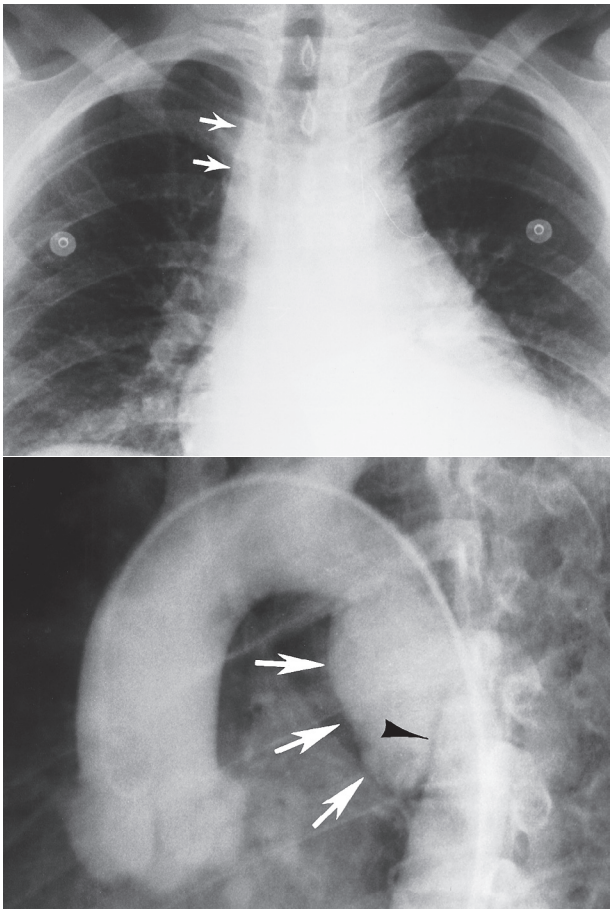

FIGURE 7-37 Traumatic aneurysm of the aorta. (A) Supine chest radiograph in a patient with blunt chest trauma shows thickening of the right paratracheal stripe (*arrows*), which measures 1 cm in width. (B) Aortogram demonstrates a pseudoaneurysm at the level of the aortic isthmus (*arrows*). *Arrowhead* indicates intimal flap.

Treatment. Immediate surgical intervention to repair the aortic laceration or rupture is required to prevent morbidity and mortality.

Dissection of the Aorta

Dissection of the aorta is a potentially life-threatening condition in which disruption of the intima (the inner layer) permits blood to enter the wall of the aorta and separate its layers. As a result of the disruption, the aorta is divided into true and false lumens. The false lumen may form an aneurysm as a result of the high pressure in the systemic vascular system. Most aortic dissections occur in patients with arterial hypertension. Some are a result of trauma, whereas others are attributable to a congenital defect, such as Marfan's syndrome. An acute dissection typically causes sudden sharp or excruciating pain in the chest or abdomen. Although the pain passes, death frequently occurs some days later from rupture of the aneurysm into the chest or abdominal cavity.

Most aortic dissections begin as a tear in the intima immediately above the aortic valve. In two-thirds of these (type I), the dissection continues into the descending aorta, often extending as far as the level of the iliac

bifurcation. In the remainder (type II), the dissection is limited to the ascending aorta and stops at the origin of the innominate artery. In type III disease, the dissection begins in the thoracic aorta distal to the subclavian artery and extends for a variable distance proximally and distally to the original site.

Imaging appearance. On plain chest radiographs, aortic dissection causes progressive widening of the aortic shadow, which may have an irregular or wavy outer border (Figure 7-38) that most likely represents the site of origin of the dissection. However, this is a nonspecific appearance, and a definitive diagnosis of dissection must be made on the basis of aortography or CT. CT, MRI, and transesophageal echocardiography (TEE) can demonstrate aortic dissection. The modality of choice depends on the patient's status, including such factors as overall physical condition, degree of renal function, suspected complications, and equipment availability. Spiral multidetector CT has become the modality of choice. CT, nonenhanced scans followed with enhanced images, is the protocol recommended for demonstrating acute rupture and hemorrhage. The detection of an intimal flap identifies the true and false lumens.

In the patient in whom nonacute aortic dissection is being considered in the differential diagnosis of chest pain, CT and MRI offer low-risk alternative diagnostic methods to arteriography. The emergence of spiral multidetector CT has enhanced the ability to demonstrate aortic dissection as a double channel with an intimal flap. With dynamic scanning and the rapid injection of a bolus of contrast material, differential filling of the true and false channels can be observed as with aortography (Figure 7-39). The major limitation of conventional CT in the patient with suspected acute dissection is that only a single level can be evaluated on a given slice, as opposed to the rapid series of images covering a large portion of the aorta that can be obtained with aortography. With the development of helical CT, however, multiplane images are available to quickly visualize the classic double-barrel aorta and the linear filling defect within the aortic lumen. With the new technology, CT has a sensitivity of approximately 90% and specificity of 96%.

The high contrast between rapidly flowing blood, vessel wall, and adjacent soft tissue structures permits identification of vessels by MRI without the need for intravenous injection of contrast material. This technique can demonstrate aortic dissections and show their extent. The intimal flap is usually detected as a linear structure of medium signal intensity separating the true and false lumina (Figure 7-40). Rapidly flowing blood in these lumina appears as a signal void. If the false lumen is thrombosed, or even if it is open but the flow is slow, the intimal flap may not be visualized. In this situation, aortic dissection is difficult to differentiate from an aortic aneurysm with mural thrombus, and aortography may be required to make this distinction. A new MR sequence is available to evaluate aortic dissection. Cardiac-gated gradient-echo sequences demonstrate the intimal flap as a dark line against the high signal intensity of

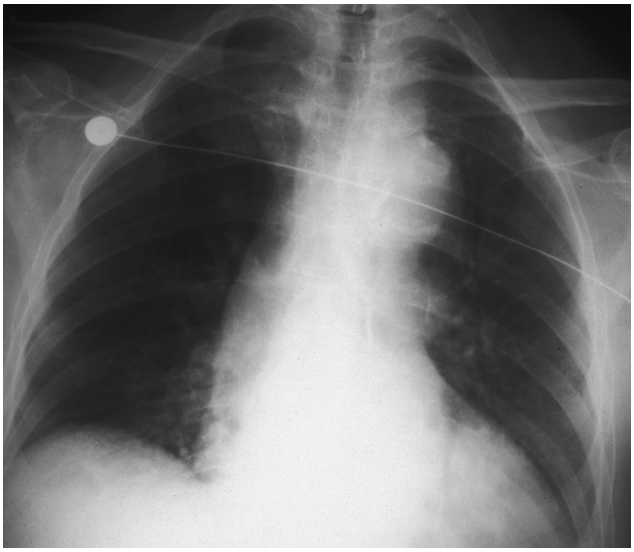

FIGURE 7-38 Aortic dissection. Plain chest radiograph shows diffuse widening of the descending aorta with an irregular, wavy outer border.

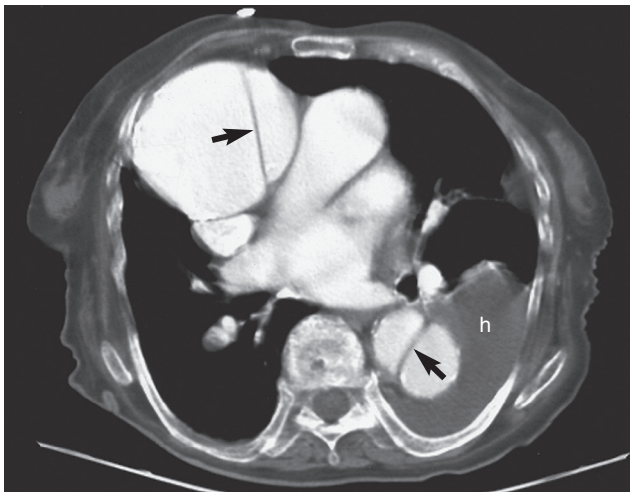

FIGURE 7-39 CT image of aortic dissection. The ascending aorta is dilated and has a radiolucent intimal flap (*arrows*). The descending aorta demonstrates a much larger tear and hemorrhage (h) surrounding the aorta.

FIGURE 7-40 MR image of aortic dissection. Axial image at the level of the main and right pulmonary arteries clearly shows the intimal flap (*arrow*) in the descending aorta.

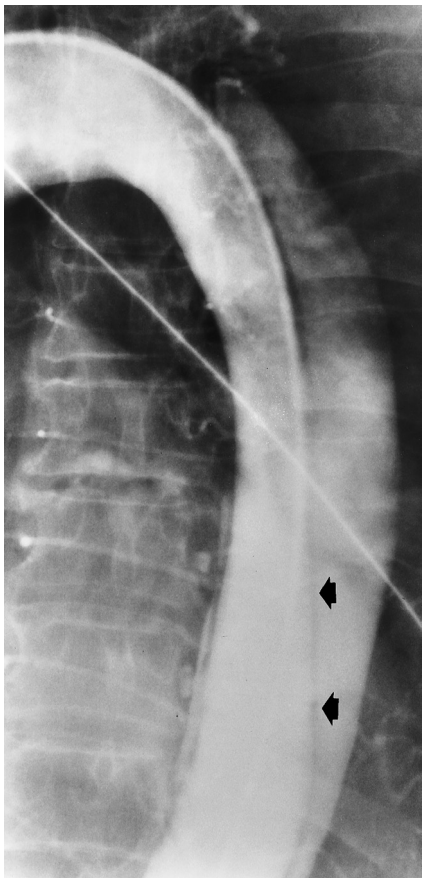

FIGURE 7-41 Aortic dissection. Aortogram demonstrates a thin radiolucent intimal flap (*arrows*) separating the true and false aortic channels.

flowing blood. MRA has largely replaced conventional angiography. MR is the modality of choice for follow-up and for evaluating treatment.

TEE is another modality available to provide images of the ascending aorta to demonstrate an intimal tear, the extension of the dissection, and pleural effusion.

In aortography, the diagnosis of aortic dissection depends on the demonstration of two channels separated by a thin radiolucent intimal flap (Figure 7-41). The false channel may be filled with clot and impossible to opacify with contrast material. In this case, the diagnosis can be made by demonstration of narrowing and compression of the true channel. When both true and false lumina fill with contrast material, it is important to demonstrate the distal reentry point where the false lumen joins the true lumen. If the dissection extends below the diaphragm, arteriography can provide presurgical information about which major vessel branches from the aorta are blocked and which remain patent.

Treatment. Proximal aortic dissections are fatal if not immediately treated surgically (by graft placement). Interventional treatment involves creating an opening (fenestration) between the true and false lumina to provide blood supply to the descending aortic vascular system. As an alternative, an aortic stent may be placed in the true lumen to allow blood to flow freely. The stent provides the same results as surgery; however, this is a new technique, and its long-term effectiveness is unknown. Many other dissections require only medical management (80% survival rate).

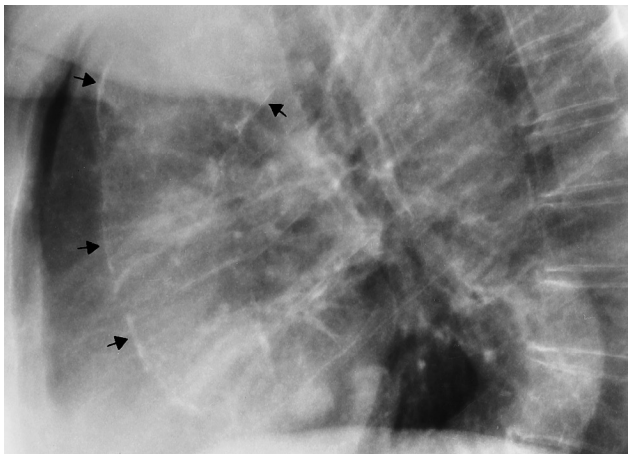

FIGURE 7-42 Atherosclerosis. Lateral projection of the chest demonstrates calcification of the anterior and posterior walls of the ascending aorta (*arrows*). The descending thoracic aorta is tortuous.

Atherosclerosis

Arteriosclerosis occurs when arteries become marked by thickening, hardening, and loss of elasticity in the arterial wall. Atherosclerosis is one form of arteriosclerosis. The major cause of vascular disease of the extremities is atherosclerosis, in which fatty deposits called plaques develop in the intima and produce progressive narrowing and often complete occlusion of large and medium-size arteries. In the abdomen, the disease primarily involves the aorta and the common iliac arteries, often sparing the external iliac vessels. In the lower extremities, atherosclerotic narrowing most commonly affects the superficial femoral artery just above the knee. Plaque formation and luminal narrowing often involve the coronary and cerebral arteries, thus decreasing the blood flow to the heart muscle and the brain and leading to a myocardial infarction or stroke (cerebrovascular accident).

Imaging appearance. Atherosclerotic plaques often calcify and appear on plain radiographs as irregularly distributed densities along the course of an artery (Figure 7-42). Small vessel calcification, especially in the hands and feet, is often seen in patients with accelerated arteriosclerosis, especially those with diabetes mellitus.

Doppler ultrasound is an effective and preferred noninvasive technique for screening patients with clinically suspected peripheral arteriosclerotic disease. Color Doppler ultrasonography demonstrates the presence of atherosclerotic plaques and assesses the degree of luminal stenosis. Definitive diagnosis requires arteriographic demonstration of the peripheral vascular tree. Evidence of arteriosclerosis includes diffuse vascular narrowing, irregularity of the lumen, and filling defects. In patients with severe stenosis or obstruction,

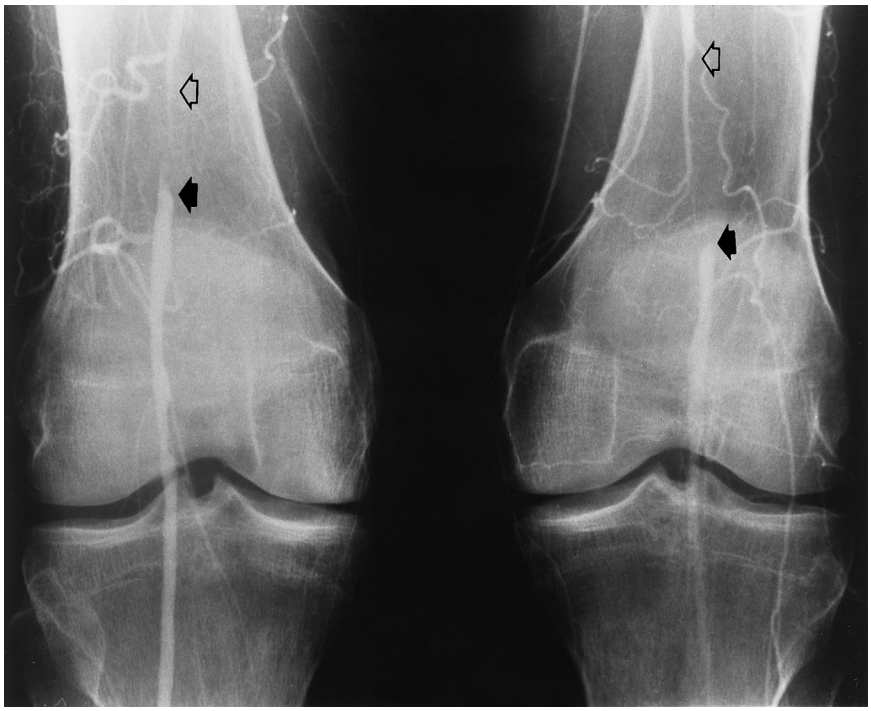

FIGURE 7-43 Bilateral atherosclerotic occlusion of the superficial femoral arteries. Arteriogram demonstrates occlusion of both distal superficial femoral arteries (*open arrows*) with reconstitution by collateral vessels (*solid arrows*).

FIGURE 7-44 Abdomen and pelvis MRA. Normal appearance of the abdomen and pelvis on contrast-enhanced MRA.

arteriography demonstrates the degree and source of collateral circulation and the status of the vessels distal to an area of narrowing (Figure 7-43). With spiral CT scanning ability, the vessels of the lower extremity can be visualized. As MRA has evolved, three-dimensional (3D) MRA has become the method of choice, replacing catheter angiography (Figure 7-44). The two-dimensional time-of-flight method is preferred for evaluating the infrapopliteal vessels. MRA images illustrate areas of narrowing and occlusion as an absence of signal intensity.

Treatment. PTA using a balloon catheter is now a recognized procedure for the alleviation of symptoms of peripheral ischemia in patients with arteriosclerosis (Figure 7-45). In addition, a stent may be placed to aid in keeping the vessel open if the vessel is not too small or not too distal. The results of this interventional approach (95% success for the iliac artery and 50% to 60% for the thigh and calf) are similar to those of bypass grafting but with a much lower morbidity rate. It is of special value in patients who are extremely ill and in those who would not benefit from reconstructive arterial surgery. Other treatments available are atherectomy, cryotherapy, and laser to aid in salvaging the extremity.

Thrombosis and Embolism

The blood-clotting mechanism is the major protective device of the body in response to the escape of blood from a vessel (hemorrhage). This same mechanism can occur in intact blood vessels, leading to the development of an intravascular clot called a **thrombus**. Three factors lead to the development of intravascular thrombosis. Clots tend to form where blood flow is slow and thus develop much more commonly in veins than in arteries. Thrombi occur especially in areas of stasis (slow circulation) in patients who are inactive or immobilized, as after abdominal surgery.

The second factor is a change in the wall of blood vessels that leads to thrombosis. Normally, the inner wall of a blood vessel has a very smooth lining (endothelium), and platelets

cannot stick, or adhere, to it. However, when the endothelium is destroyed by injury or inflammation, platelets rapidly adhere to the rough spot, and a clot begins to form from the blood as it flows past. Arteriosclerosis is the major cause of endothelial irregularity and subsequent thrombosis. Nodules of vegetation on heart valves caused by rheumatic heart disease are also important predisposing factors for thrombus formation.

The third factor is a change in the blood itself, which leads to thrombosis. A low level of oxygen within the blood, as in some forms of heart disease, forces the body to compensate by increasing the number of red blood cells (polycythemia). This causes the blood to become more viscous and increases the risk of thrombosis. Changes in the clotting and fibrinolytic mechanisms also may increase the risk of thrombus formation.

Once a thrombus is formed, it may follow one of three courses. The thrombus may contract or become canalized so that blood can once again flow through the lumen. The thrombus may continually enlarge or become converted into fibrous tissue, resulting in permanent occlusion of the vessel. A potentially catastrophic event is the production of an **embolus**—part or all of a thrombus that becomes detached from the vessel wall and enters the bloodstream. Embolization is especially likely to occur if there is infected tissue around the thrombus or if there is a sudden movement caused by rough handling of the involved area. An embolism may lodge at any of several points, depending on the size of the vessels through which it travels. Because veins become larger as they approach the heart, an embolism arising from a thrombus in a leg vein flows easily to the heart and typically gets stuck in a pulmonary artery (pulmonary embolism). An embolism arising from a mitral valve damaged by rheumatic heart disease flows through the left ventricle and aorta and lodges in a smaller artery in the brain, kidney, or other organ. A septic embolism contains infected material from pyogenic bacteria, whereas tumor emboli are groups of cancer cells that have invaded a vein, become detached, and are then carried to the lungs or other organs where they form metastases. Fat emboli are the result of trauma, especially leg fractures, in which marrow fat enters torn peripheral veins and is trapped by the pulmonary circulation. *Air embolism* refers to bubbles of air introduced into a vein during surgery, trauma, or an improperly administered intravenous injection.

Regardless of its type or source, an embolism blocks the vascular lumen and cuts off the blood supply to the organ or parts supplied by that artery. The effect of an embolism depends on the size of the embolus; the extent of collateral circulation, which can bring blood to an affected part by an alternate route; and the location of the embolus.

Imaging appearance. Acute embolic occlusion of an artery most commonly affects the lower extremities. The success of therapy depends on the rapid recognition of the clinical problem and the institution of appropriate treatment. Arteriography is the procedure of choice to confirm the clinical diagnosis and to demonstrate the extent of occlusion, the degree of collateral circulation, and the condition of the distal vessels. Embolic occlusion typically appears as an abrupt termination of the contrast agent column, along with a proximal curved margin reflecting the nonopaque embolus protruding into the contrast agent–filled lumen (Figure 7-46). In acute

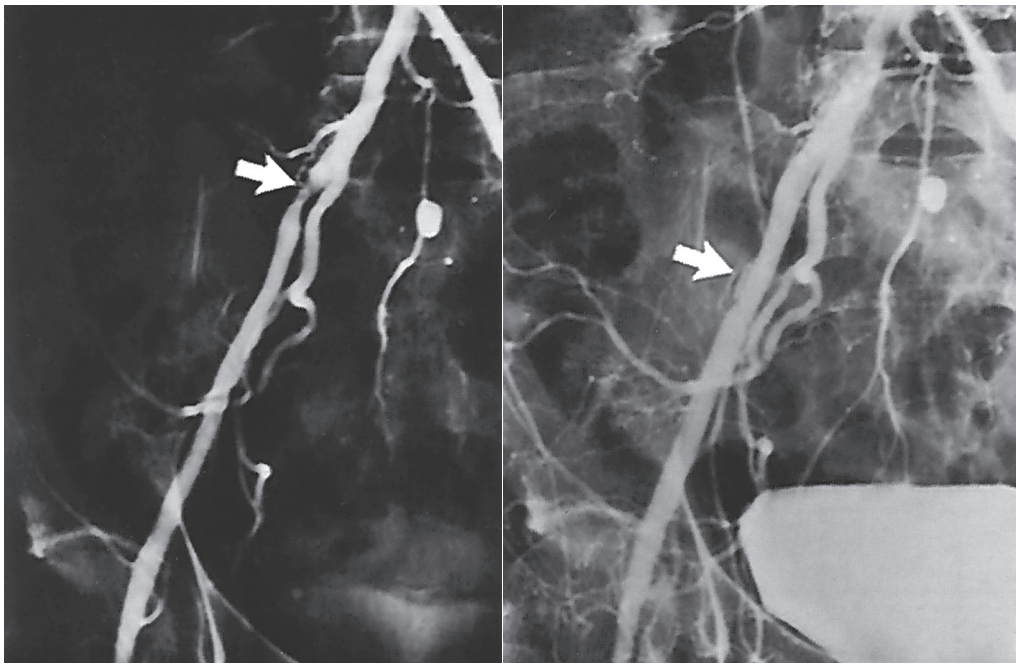

FIGURE 7-45 PTA of the right external iliac artery stenosis. **(A)** Initial image in a patient with claudication demonstrates narrowing of the proximal right external iliac artery (*arrow*). **(B)** After angioplasty, there is relief of stenosis (*arrow*) and of symptoms.

occlusion, there is usually little, if any, evidence of collateral circulation. Further discussion can be found in the later section "Deep Venous Thrombosis."

Treatment. Anticoagulants, such as heparin and warfarin (Coumadin), are often used to prevent intravascular clotting.

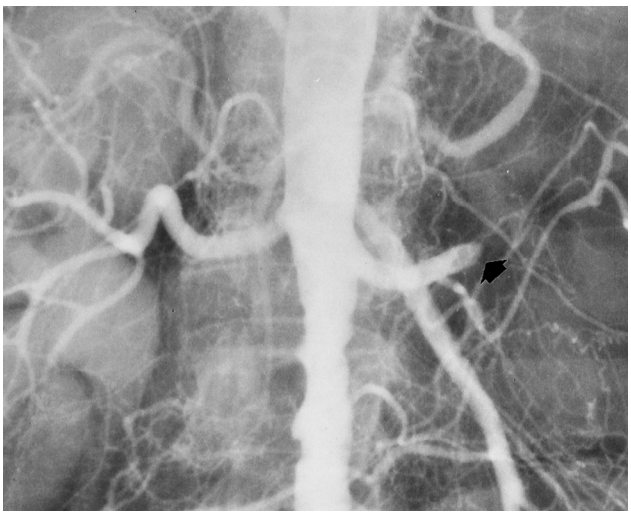

FIGURE 7-46 Acute embolic occlusion of the left renal artery. There is abrupt termination of the contrast column (*arrow*). Note the irregular infrarenal aortic contour, which represents atherosclerotic disease.

Heparin deactivates coagulation proteins by stimulation of antithrombin, helping prevent thrombus formation. Warfarin acts by antagonizing the action of vitamin K, which is necessary for blood clotting. However, these medications also interfere with the person's normal ability to stop bleeding and may lead to severe hemorrhage from relatively minor trauma or to potentially fatal bleeding in the brain and gastrointestinal tract. Reports have now described the value of aspirin in preventing intravascular clotting because of its inhibition of platelet aggregation.

Interventional treatment has become more popular because the recovery time for the patient is much less. This technique utilizes a thrombectomy catheter (AngioJet catheter, MEDRAD, Inc., Warrendale, PA) to remove the thrombus or an export catheter for manual evacuation of the thrombi.

Although emergency surgery to remove the embolus (embolectomy) has been the traditional treatment for acute arterial occlusion, the intra-arterial infusion of streptokinase by means of a catheter placed immediately proximal to the occlusion is becoming a more common alternative therapy, especially in patients who are poor surgical candidates (Figure 7-47). The tissue plasminogen activator (TPA) alteplase (Activase), produced by recombinant DNA technology, has been administered intravenously to lyse thrombi obstructing coronary arteries for the treatment of acute myocardial infarction.

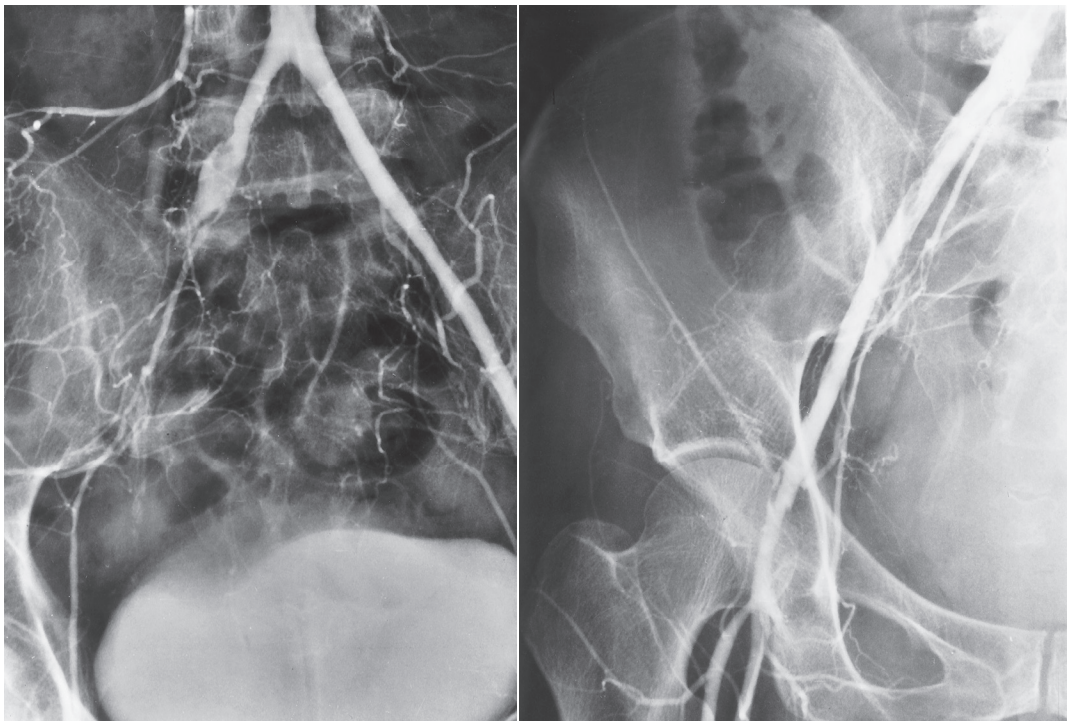

FIGURE 7-47 Streptokinase therapy for acute arterial occlusion. **(A)** After angioplasty of the right external iliac artery, there was loss of the right common femoral pulse. Repeat arteriogram from the left femoral approach shows complete occlusion of the external iliac artery at its origin. **(B)** After 8 hours of streptokinase administration, arteriogram demonstrates lysis of the thrombus and reestablishment of the lumen. One year after angioplasty, the patient had a normal femoral pulse and a patent artery.

Summary of Findings for Acquired Vascular Disease

Disorder	Location	Imaging Appearance	Treatment
Coronary artery disease	Blood vessels supplying the heart	PA chest—vessel calcifications SPECT—classifies myocardial necrosis CT—decreased attenuation in affected myocardial tissue; calcium scoring to visualize hard plaque; CTA to visualize soft plaque MRI—increased T2-weighted signal intensity in affected myocardial tissue NM—focal defects (cold spots) after exercise with filling at rest indicates stenosis IVUS—vessel size and length of lesion Angiogram—strictures or narrowings are filling defects	Surgery—bypass graft Interventional—PTCA, PTCA with stent placement, percutaneous atherectomy
Congestive heart failure	Insufficient cardiac output	PA chest—C/T ratio > 50% Left-sided: cardiac enlargement, pulmonary edema, and pulmonary effusion Right-sided: widened mediastinum and elevated right hemidiaphragm Echocardiography—measuring left ventricular performance, ejection fraction, and filling pressures of the pulmonary artery and ventricles	Diuretics Digoxin
Pulmonary edema	Extravascular fluid in the lungs	PA chest—vascular markings not sharp; severe edema produces a butterfly pattern	Treatment of cause of edema
Hypertension	Increased pressure in the systemic vascular system	Arteriography—detects renovascular lesions Radionuclide renogram—noninvasive screening to demonstrate lesions	Drug therapy to control vascular volume and heart rates Interventional—PTA with or without stent
Hypertensive heart disease	Left ventricle enlargement	PA chest—enlarged left ventricle, inferior displacement of cardiac apex, aortic tortuosity	Therapy for high blood pressure and/or CHF
Aneurysm	Dilation of artery; fusiform or saccular	Radiograph—calcification outlining vessel US—abdominal aortic enlargement, of a diameter >3 cm CTA—aneurysm extent and size, evidence of leak or rupture by retroperitoneal hematoma MRA—same as CTA, but used when iodinated contrast agents are contraindicated	Surgical graft placement Percutaneous stent placement
Traumatic aortic rupture	Aortic tear distal to left subclavian artery	PA chest—widened mediastinum; deviation of NG tube to right; apical pleural cap CTA/aortography—demonstrates tear and hemorrhage	Surgical repair
Aortic dissection	Disruption of aortic intima	PA chest—widening of aortic shadow, which may be irregular CT—double-barrel channel with linear filling defect within lumen (intimal flap) MRI—intimal flap causes medium-intensity signal separating true and false lumina; blood flow causes signal void TEE—demonstrates intimal tear, extension of dissection and pleural effusion Aortography—extent of true and false lumina	Proximal or continuous dissection—immediate surgical repair Intervention—fenestration and stenting Other dissections—medical management
Atherosclerosis	Plaques develop in the intima of the artery	Radiograph—calcification demonstrating "hardening" of the artery Color Doppler—demonstrates plaque and degree of luminal stenosis MRA—two-dimensional time-of-flight view demonstrates narrowing and flow changes in infrapopliteal vessels; 3D images demonstrate narrow occlusions as signal absences	PTA with or without stent placement Surgical arterial bypass
Thrombus and embolism	Blockage of a vessel	Arteriography—extent of occlusion, degree of collateral circulation, and distal vessel condition	Interventional catheter removal Surgical removal Medical treatment to reduce thrombus or emboli

IVUS, Intravascular ultrasound; *NG,* nasogastric; *NM,* nuclear medicine; *PTCA,* percutaneous transluminal coronary angioplasty; *SPECT,* single-photon emission computed topography; *US,* ultrasound.

VALVULAR DISEASE

The valves of the heart permit blood to flow in only one direction through the heart. There are four heart valves. As previously described, the tricuspid valve separates the right atrium and the right ventricle, and the mitral valve separates the left atrium and the left ventricle. These two atrioventricular valves must open for the heart chambers to fill. The pulmonary valve lies between the right ventricle and the pulmonary artery, and the aortic valve is situated between the left ventricle and the aorta. When any of these valves is closed, the heart chamber fills with blood; when the valve opens, blood can move forward and leave the chamber.

The malfunction of a heart valve alters the normal blood flow through the heart. Too small an opening (stenosis) does not permit sufficient blood flow. In contrast, too large an opening or failure of the valve to properly close permits backflow of blood (regurgitation) and the condition of valvular insufficiency. Both stenosis and insufficiency of valves cause heart murmurs with characteristic sounds that indicate the nature of the defect. Two-dimensional and Doppler echocardiography have become the modalities of choice to demonstrate valvular diseases. Although valvular heart disease once invariably forced a patient to restrict activity and was associated with a limited life span, surgical reconstruction or replacement of a diseased valve (Figure 7-48) can offer a patient the prospect of a normal life.

Rheumatic Heart Disease

Rheumatic fever is an autoimmune disease that results from a reaction of the patient's antibodies against antigens from a previous streptococcal infection. The disease is much less common today because of the frequent use of antibiotics to treat streptococcal throat or ear infections. The symptoms of rheumatic fever (fever, inflamed and painful joints, and rash) typically develop several weeks after the streptococcal infection.

The major damage of rheumatic fever is to the valves of the heart, most frequently the mitral and aortic valves. Indeed, it is the major cause of acquired cardiac valvular disease. The allergic response causes inflammation of the valves. Deposits of blood platelets and fibrin from blood flowing over the valve produce small nodules (**vegetations**) along the margin of the valve cusps. The thickened valves may stick together so that the valvular opening remains permanently narrowed (**stenosis**) rather than opening properly when blood flows through. In contrast, fibrous scarring may cause retraction of the valve cusps so that the cusps are unable to meet when the valve tries to close; this is **insufficiency**, and blood leaks through the valve when it should be closed. Doppler echocardiography is used to best identify and quantify the insufficiencies and determine the degree of ventricular dysfunction.

Treatment. Prevention of rheumatic fever and subsequent heart disease by treatment of the streptococcal infection with a full course of antibiotic therapy is the best approach. If the infection progresses into rheumatic heart disease, antibiotics, anti-inflammatory drugs, and restricted activity are the appropriate interventions.

Mitral Stenosis

Stenosis of the mitral valve, almost always a complication of rheumatic disease, results from diffuse thickening of the valve by fibrous tissue, calcific deposits, or both.

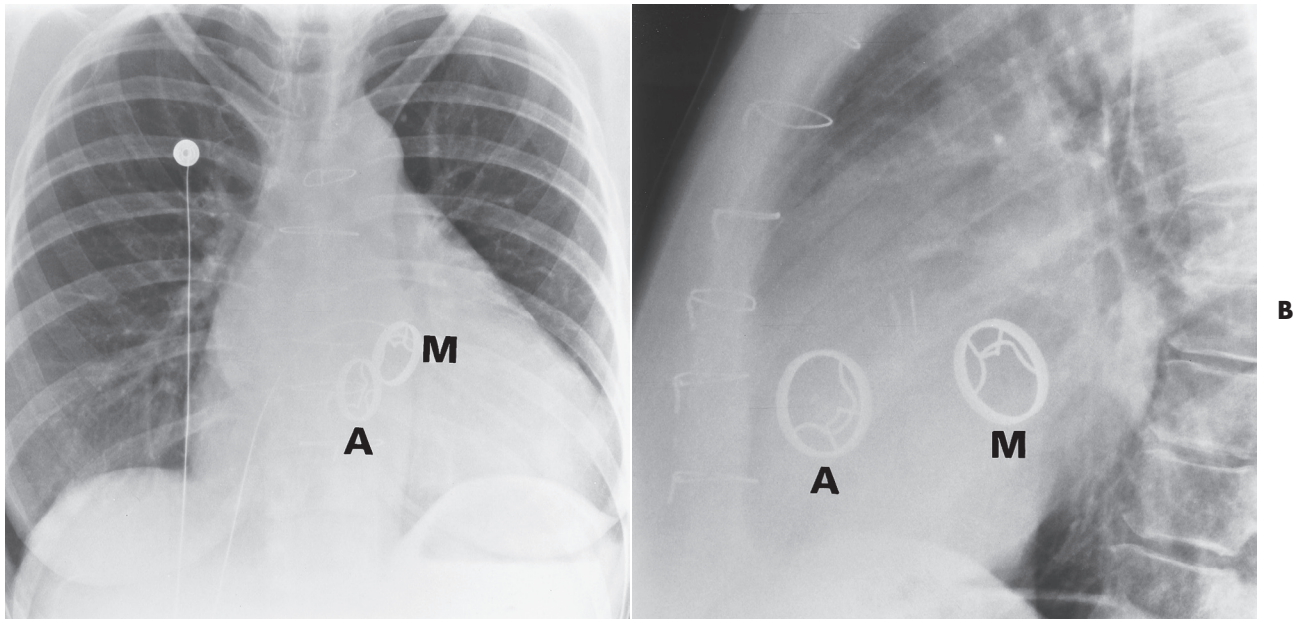

FIGURE 7-48 Prosthetic aortic and mitral valves. Frontal (A) and lateral (B) projections of the chest show an anteromedially located prosthetic aortic valve (A) and a posterolaterally situated prosthetic mitral valve (M).

Imaging appearance. The obstruction of blood flow from the left atrium into the left ventricle during diastole causes increased pressure in the left atrium and enlargement of this chamber (Figure 7-49). The enlarged left atrium produces a characteristic anterior impression on and posterior displacement of the barium-filled esophagus that is best seen on lateral and right anterior oblique projections. Other radiographic signs of left atrial enlargement include posterior displacement of the left mainstem bronchus, widening of the tracheal bifurcation (carina), and a characteristic "double-contour" configuration caused by the projection of the enlarged left atrium through the normal right atrial silhouette. The increased left atrial pressure is transmitted to the pulmonary veins and produces the appearance of chronic venous congestion.

Calcification of the mitral valve or left atrial wall (Figure 7-50), best demonstrated by fluoroscopy, can develop in patients with long-standing severe mitral stenosis. A thrombus may form in the dilated left atrium and be the source of emboli to the brain or elsewhere in the systemic circulation.

Echocardiography is the most sensitive and most specific, noninvasive method for diagnosing mitral stenosis (Figure 7-51). Echocardiography demonstrates chamber enlargement or wall thickening and permits measurement of the valvular orifices. Cine MRI has now been used to demonstrate and quantitate the abnormal pattern of flow between the left atrium and the left ventricle in mitral stenosis without the use of contrast agents.

Mitral Insufficiency

Although most often caused by rheumatic heart disease, mitral insufficiency may also be caused by the rupture of the chordae tendineae or by the dysfunction of the papillary muscles that are attached to the underside of the valve cusps and normally prevent them from swinging up into the atrium when the ventricles contract. Regurgitation of blood into the left atrium during ventricular systole causes overfilling and

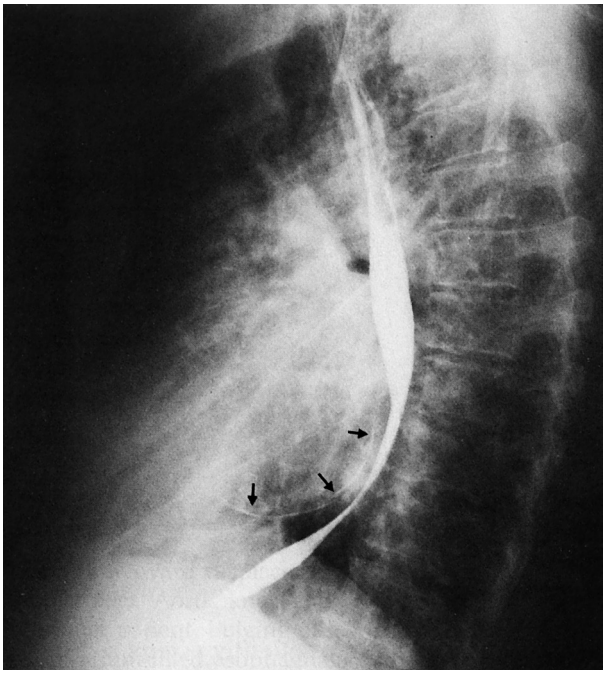

FIGURE 7-50 Left atrial calcification in mitral stenosis. Lateral projection with barium in the esophagus shows enlargement of the left atrium and calcification of the wall of its chamber (*arrows*).

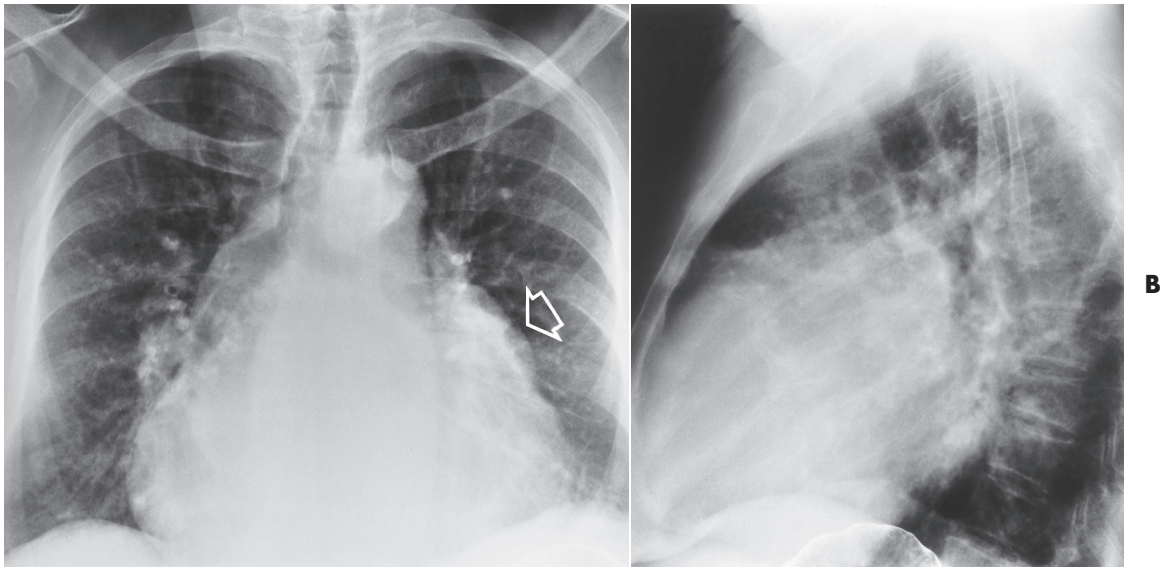

FIGURE 7-49 Mitral stenosis. Frontal (A) and lateral (B) projections of the chest demonstrate cardiomegaly with enlargement of the right ventricle and left atrium. Right ventricular enlargement causes obliteration of the retrosternal air space, whereas left atrial enlargement produces convexity of the upper left border of the heart (*arrow*).

dilation of this chamber, which lead to a decrease in ventricular stroke volume and cardiac output.

In most cases, the left atrium is considerably larger in mitral insufficiency than in mitral stenosis (Figure 7-52); occasionally, an enormous left atrium can form both the right and the left borders of the heart on frontal projections. An increased volume of blood flowing from the dilated left atrium to the left ventricle in diastole increases the left ventricular workload and leads to dilation and hypertrophy of this chamber. CHF, pulmonary congestion, and pulmonary hypertension may result, causing downward displacement of the cardiac apex and rounding of the lower left border of the heart.

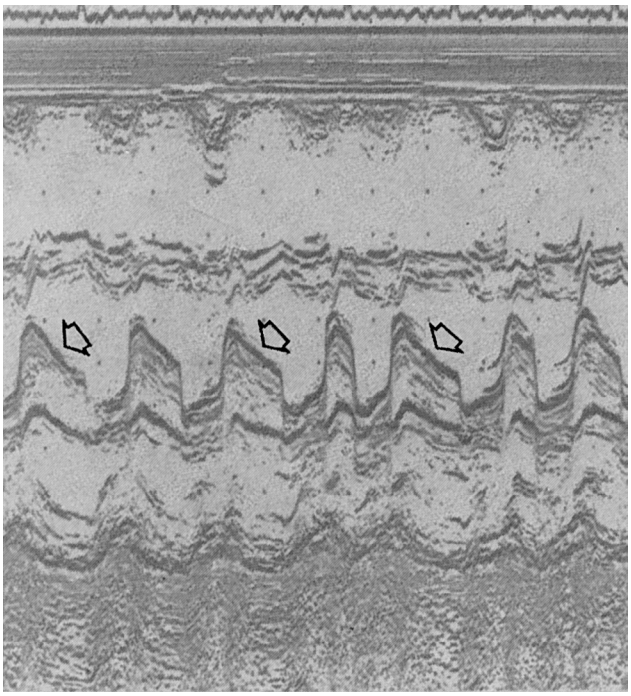

FIGURE 7-51 Echocardiogram of mitral stenosis. There is thickening of the mitral valve with decreased slope (*arrows*).

Treatment of Mitral Stenosis and Mitral Insufficiency

Surgical valvular replacement or correction of the stenosis may be performed to correct flow insufficiency. CHF resulting from stenosis or insufficiency may require treatment.

Aortic Stenosis

Aortic stenosis may be caused by rheumatic heart disease, a congenital valvular deformity (especially of a bicuspid valve), or a degenerative process of aging (idiopathic calcific stenosis). The obstruction to left ventricular outflow in aortic stenosis increases the workload of the left ventricle.

Imaging appearance. Initially, this condition causes left ventricular hypertrophy without dilation, which produces only some rounding of the cardiac apex on frontal chest radiographs and slight backward displacement on lateral projections. The overall size of the heart remains within normal limits until left ventricular failure develops. Significant aortic stenosis is usually associated with lateral bulging (poststenotic dilation) of the ascending aorta caused by the jet of blood forced under high pressure through the narrowed valve (Figure 7-53). Aortic valve calcification, best demonstrated on fluoroscopic examination, is

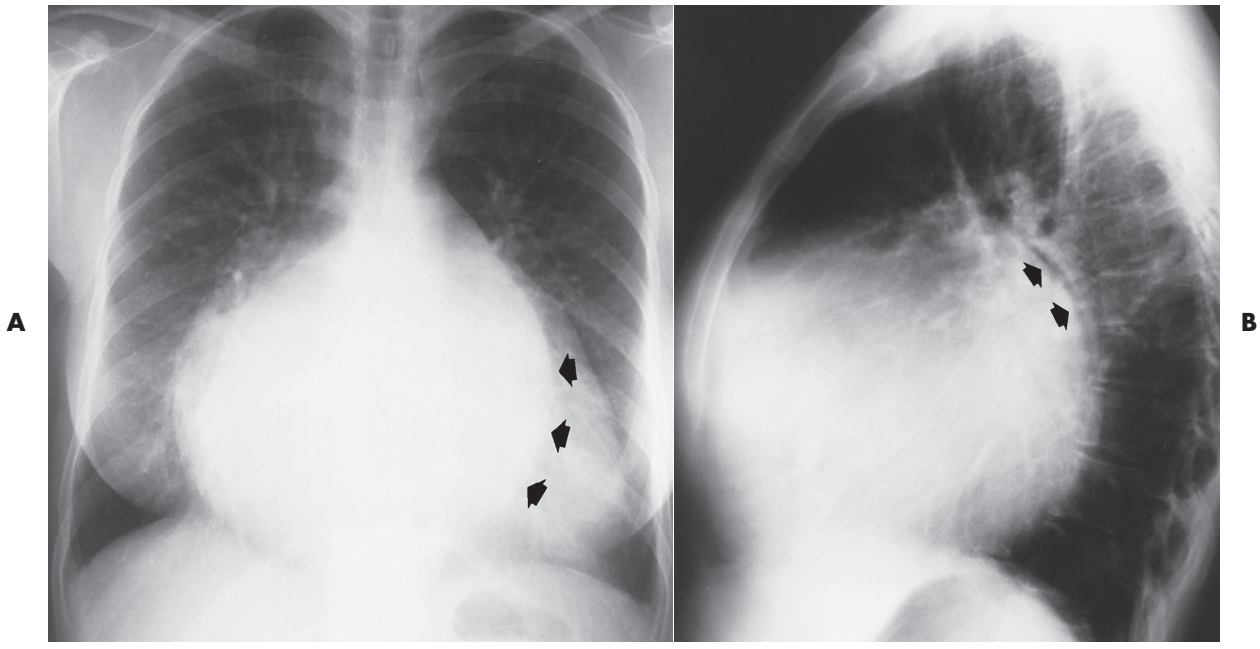

FIGURE 7-52 Mitral insufficiency. Frontal (A) and lateral (B) projections of the chest demonstrate gross cardiomegaly with enlargement of the left atrium and left ventricle. Note the striking double-contour configuration (*arrows*) on the frontal image and elevation of the left mainstem bronchus (*arrows*) on the lateral image, characteristic signs of left atrial enlargement.

a common finding and indicates that the aortic stenosis is severe (Figure 7-54).

Aortic Insufficiency

Although most commonly caused by rheumatic heart disease, aortic insufficiency may be attributable to syphilis, infective endocarditis, dissecting aneurysm, or Marfan's syndrome. Reflux of blood from the aorta during diastole causes volume overloading of the left ventricle and dilation of this chamber.

Imaging appearance. Aortic insufficiency causes downward, lateral, and posterior displacement of the cardiac apex (Figure 7-55). Pronounced left ventricular dilation causes relative mitral insufficiency, which leads to left atrial enlargement and signs of pulmonary edema.

Treatment of Aortic Stenosis and Aortic Insufficiency

CHF should be treated if the patient is symptomatic. Surgical valvular replacement or repair to correct stenosis can reestablish correct pressures and flow.

Infective Endocarditis

Infective endocarditis refers to the formation of nodules or vegetations on heart valves by deposits of bacteria or fungi. Unlike the smaller nodules in rheumatic fever, the vegetations of infective endocarditis are filled with bacteria and tend to break apart easily (they are friable) to enter the bloodstream and form septic emboli that travel to the brain, kidney, lung, or other vital organs. Emboli lodging in the skin may cause rupture of small blood vessels and characteristic tiny hemorrhagic red spots (petechiae).

Imaging appearance. Plain radiography is of little value in patients with infective endocarditis. The cardiac silhouette may be normal or may demonstrate evidence of previous valvular heart disease or CHF. Echocardiography is the only noninvasive procedure that can detect the valvular vegetations that are the hallmark of infective endocarditis. On the echocardiogram, these vegetations appear as masses of shaggy echoes producing an irregular thickening of the affected valves (Figure 7-56). Electron-beam CT demonstrates the vegetations and the valvular calcifications, distorted orifices, and possible aneurysms.

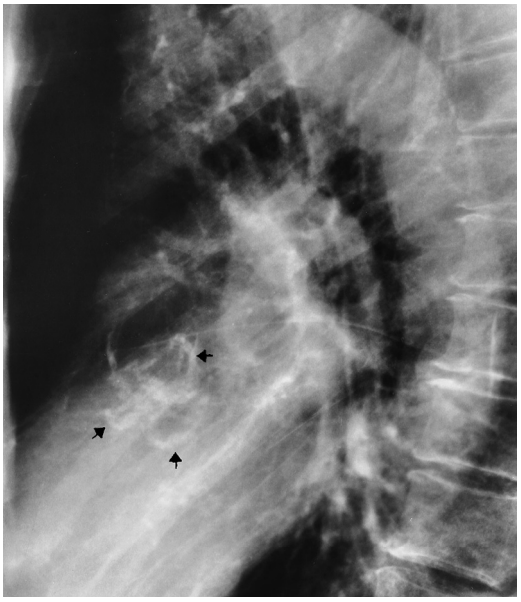

FIGURE 7-54 Aortic stenosis. Calcification in three leaflets of the aortic valve (*arrows*).

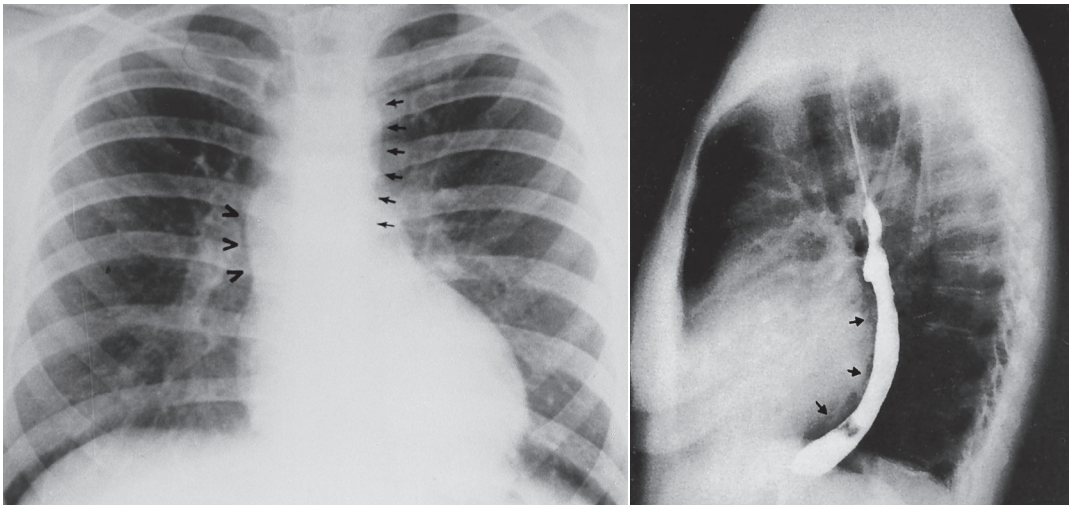

FIGURE 7-53 Aortic stenosis. **(A)** Frontal projection shows downward displacement of the cardiac apex with poststenotic dilation of the ascending aorta (*arrowheads*). The aortic knob and descending aorta (*arrows*) are normal. **(B)** On lateral projection in another patient, bulging of the lower half of the posterior cardiac silhouette causes a broad indentation on the barium-filled esophagus (*arrows*).

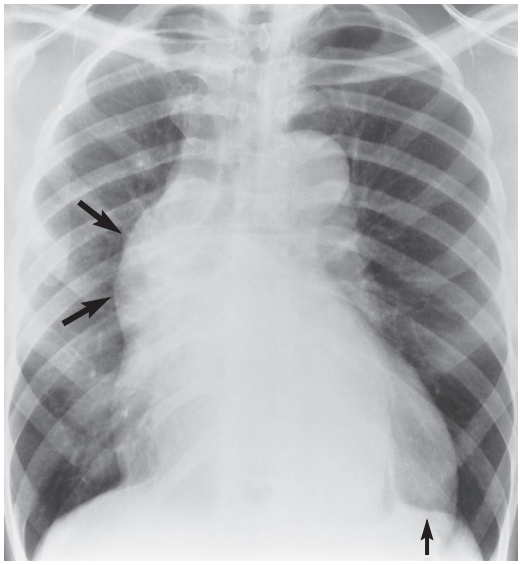

FIGURE 7-55 **Aortic insufficiency.** Frontal chest radiograph shows left ventricular enlargement with downward and lateral displacement of the cardiac apex. Notice that the cardiac shadow extends below the dome of the left hemidiaphragm (*small arrow*). The ascending aorta is strikingly dilated (*large arrows*), suggestive of some underlying aortic stenosis.

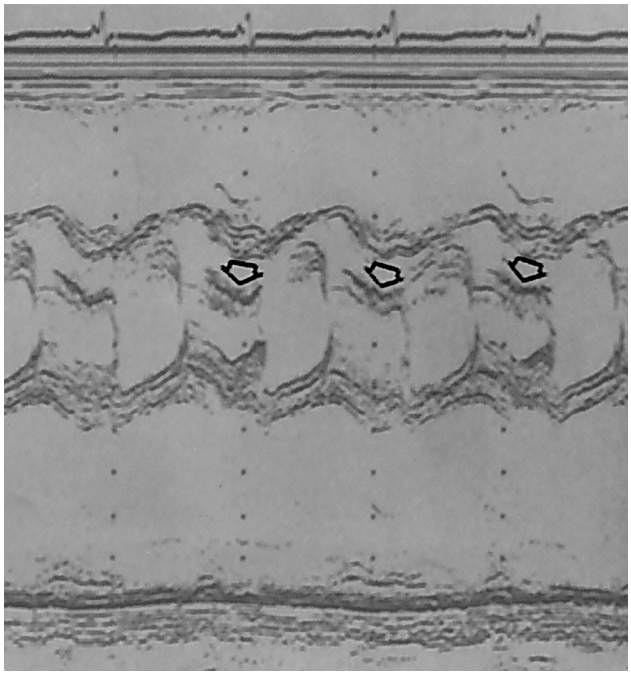

FIGURE 7-56 **Infective endocarditis.** Echocardiogram demonstrates vegetations as masses of shaggy echoes producing irregular thickening of the aortic valve (*arrows*).

Summary of Findings for Valvular Disease

Disorder	Location	Imaging Appearance	Treatment
Rheumatic heart disease	Most frequently in mitral and aortic valves	Doppler echocardiography—quantify valvular insufficiencies	Prevention—antibiotics for streptococcal infections Therapy—antibiotics, anti-inflammatory drugs, and restricted activity
Mitral stenosis	Mitral valve	PA chest—left atrium enlargement Lateral, RAO—posterior displacement of esophagus, posterior displacement of left main bronchus, calcification of valves Echocardiography—chamber enlargement, wall thickness, and size of valvular orifices Cine MRI—demonstrates and quantitates abnormal flow pattern	Surgical—valvular replacement, correction of stenosis Treat for CHF if needed
Mitral insufficiency	Valve dysfunction, rupture, or muscular dysfunction	PA chest—cardiomegaly—enlarged left atrium and left ventricle	
Aortic stenosis	Obstruction of flow exiting the heart	PA chest—enlargement of left ventricle; rounding of cardiac apex Posterior displacement of cardiac apex in lateral projection Lateral—posterior displacement of a cardiac apex; bulging of ascending aorta Aortic valve calcification	
Aortic insufficiency	Reflux of blood, causing volume overload of left ventricle	PA chest—cardiac apex—inferior, lateral, and posterior displacement	
Infective endocarditis	Nodules on heart valves	Echocardiography—shaggy echoes produced by irregular thickening of affected valves Electron-beam CT—vegetations in valve, valvular calcifications, distorted orifices	Bacterial—treatment with antibiotics Surgically replace severely damaged valves

PA chest, Posteroanterior image of the chest; *RAO,* right anterior oblique.

Treatment. Antibiotics are taken until there is complete eradication of the bacterial infections. Severely damaged valves must be surgically replaced with artificial valves.

PERICARDIAL EFFUSION

Pericardial effusion refers to the accumulation of fluid within the pericardial space surrounding the heart. The effusion may result from bacteria, viruses, or neoplastic involvement. In some cases, the cause cannot be determined (idiopathic pericardial effusion). Rapid accumulation of effusion interferes with cardiac function because of an increase in pericardial pressure. A slow accumulation of fluid allows the pericardium to expand so that the pericardial pressure usually remains within the normal range.

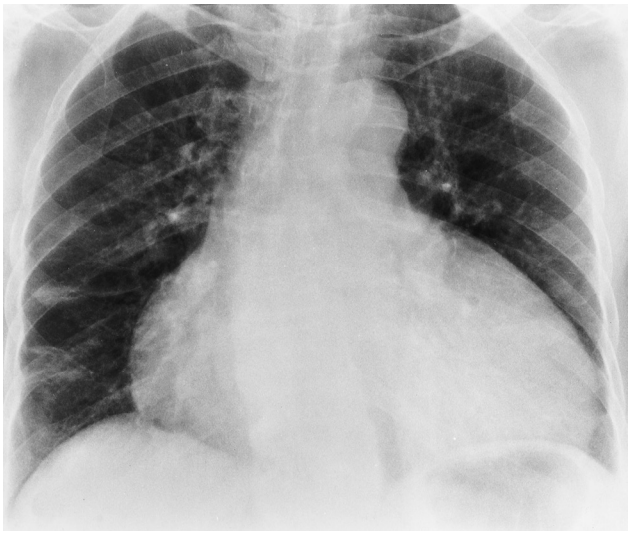

FIGURE 7-57 Pericardial effusion. Globular enlargement of the cardiac silhouette.

Imaging appearance. Echocardiography is the most effective imaging technique for demonstrating pericardial effusions and has largely replaced other methods. With this modality, a pericardial effusion is seen as a posterior sonolucent collection, and as little as 50 mL of fluid can be detected as an echo-free space between the visceral and parietal pericardium. On plain chest radiographs, on the other hand, at least 200 mL of fluid must be present before it is possible to detect an effusion, which appears as an enlargement of the cardiac silhouette (Figure 7-57). Rapid enlargement of the cardiac silhouette, especially in the absence of pulmonary vascular engorgement indicating CHF, is highly suggestive of pericardial effusion.

Angiocardiography, intravenous carbon dioxide injection, and a pericardial tap with air injection have been used in the past to demonstrate pericardial effusion by showing an excessive distance (>5 mm) between the contrast agent– or air-filled atrium and the outer border of the cardiac silhouette. CT can detect loculated pericardial effusions as small as 50 mL (Figure 7-58), whereas MRI may be able to characterize the fluid as serous or hemorrhagic by characteristic changes in the signal intensity and identify an accumulation of as little as 30 mL. Gated MRI (Figure 7-59) demonstrates a pericardial effusion as a region of decreased signal intensity between the myocardium and the fat on the surface of the parietal pericardium (which is usually invisible when it is in direct contact with the heart). However, echocardiography has effectively replaced these invasive techniques (Figure 7-60).

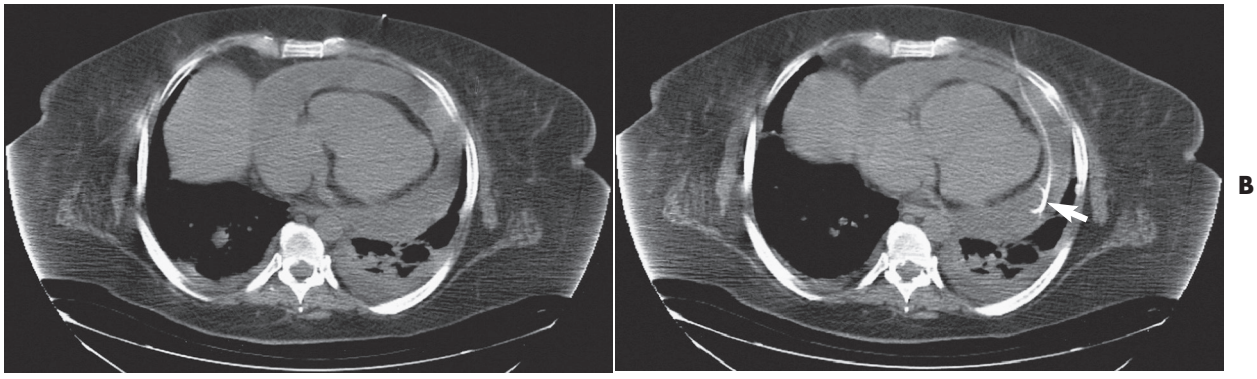

FIGURE 7-58 CT scans demonstrating pericardial effusion. **(A)** The heart is seen with a dark halo surrounded by fluid. **(B)** A CT-guided catheter was placed in this patient for drainage (*arrow*).

Summary of Findings for Pericardial Effusion

Disorder	Location	Imaging Appearance	Treatment
Pericardial effusion	Increased fluid accumulation in pericardial sac	PA chest—enlargement of cardiac silhouette Echocardiography—posterior sonolucent fluid collection CT—loculated fluid accumulations MRI—differentiates serous from hemorrhagic fluid as a decreased signal intensity	Pericardiocentesis Pericardiectomy Administration of drugs into pericardial sac

PA chest, Posteroanterior image of the chest.

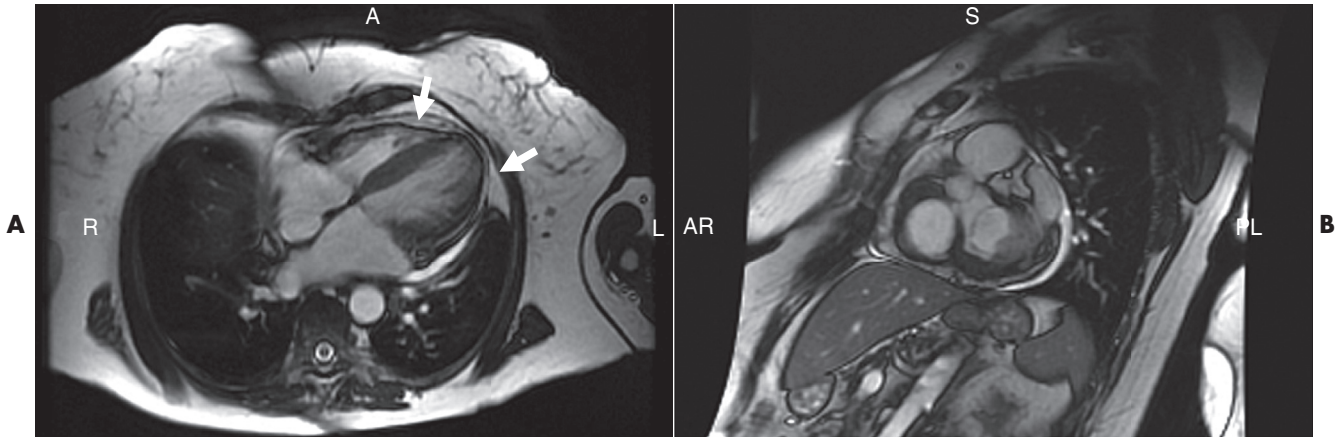

FIGURE 7-59 MRI of pericardial effusion. Transverse (A) and sagittal (B) images demonstrate the pericardium (*arrows*) displaced away from the heart by a huge pericardial effusion that has a very low signal intensity.

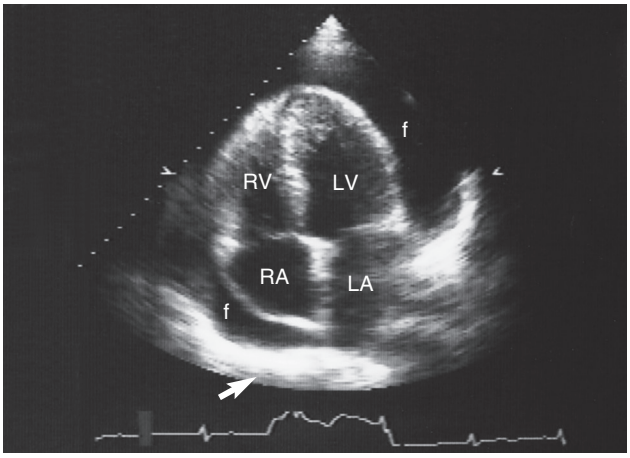

FIGURE 7-60 Pericardial effusion. Echocardiogram demonstrates an apical four-chamber heart image with fluid around the heart (f) producing back-wall enhancement (*arrow*). LA, left atrium; LV, left ventricle; RA, right atrium; RV, right ventricle.

Treatment. The treatment depends on the cause. Pericardiocentesis is performed to remove fluid buildup, and insertion of a drain may be required. If the pericardial effusion recurs, a pericardiectomy may be necessary. An interventional technique includes administration of drugs into the pericardial sac.

VENOUS DISEASE

Deep Venous Thrombosis

DVT, which primarily involves the lower extremities, is the major source of potentially fatal pulmonary embolism. Precipitating factors in the development of venous thrombosis include trauma, bacterial infection, prolonged bed rest, and oral contraceptives. At times, DVT may be the earliest symptom of an unsuspected malignancy of the pancreas, lung, or gastrointestinal system.

Imaging appearance. A precise diagnosis of DVT requires contrast venography, which can demonstrate the major venous channels and their tributaries from the foot to the inferior vena cava. During venography, the patient's leg should not be massaged to decrease edema. If DVT exists, the pressure applied could cause a thrombus to break free, becoming an embolus. The identification of a constant filling defect, representing the actual thrombus, is conclusive evidence of DVT (Figure 7-61). Venographic findings that are highly suggestive of, although not conclusive for, the diagnosis of DVT include the abrupt ending of the opaque column in a vein, the nonfilling of one or more veins that are normally opacified, and extensive collateral venous circulation.

Because venography is an invasive technique, other modalities have been developed for detecting DVT. Duplex color Doppler ultrasound, which demonstrates changes in the velocity of venous blood flow with 95% accuracy, is now the preferred initial imaging modality. It is of special value in demonstrating thrombotic occlusion of major venous pathways in the popliteal and femoral regions. Ultrasound demonstrates lack of compressibility of the vein, an indication of the presence of a thrombus (Figure 7-62). Color Doppler allows visualization of the intraluminal thrombus itself and the characteristic changes in spontaneous flow that occur because of obstruction. However, abnormal Doppler ultrasound findings are not specific for thrombosis because similar changes in venous blood flow may be caused by CHF, extensive leg edema, local soft tissue masses, and decreased inflow of arterial blood into the extremity.

Treatment. An anticoagulant drug is prescribed to prevent the formation of more thrombi. The patient receives an intravenous thrombolytic agent to lyse the already formed clot. For DVT involving the lower extremity, many authorities recommend bed rest to reduce the possibility of emboli.

Varicose Veins

Varicose veins are dilated, elongated, and tortuous vessels that most commonly involve the superficial veins of the leg just under the skin (Figure 7-63). If the venous dilation becomes extreme, the valves that normally prevent backflow of blood

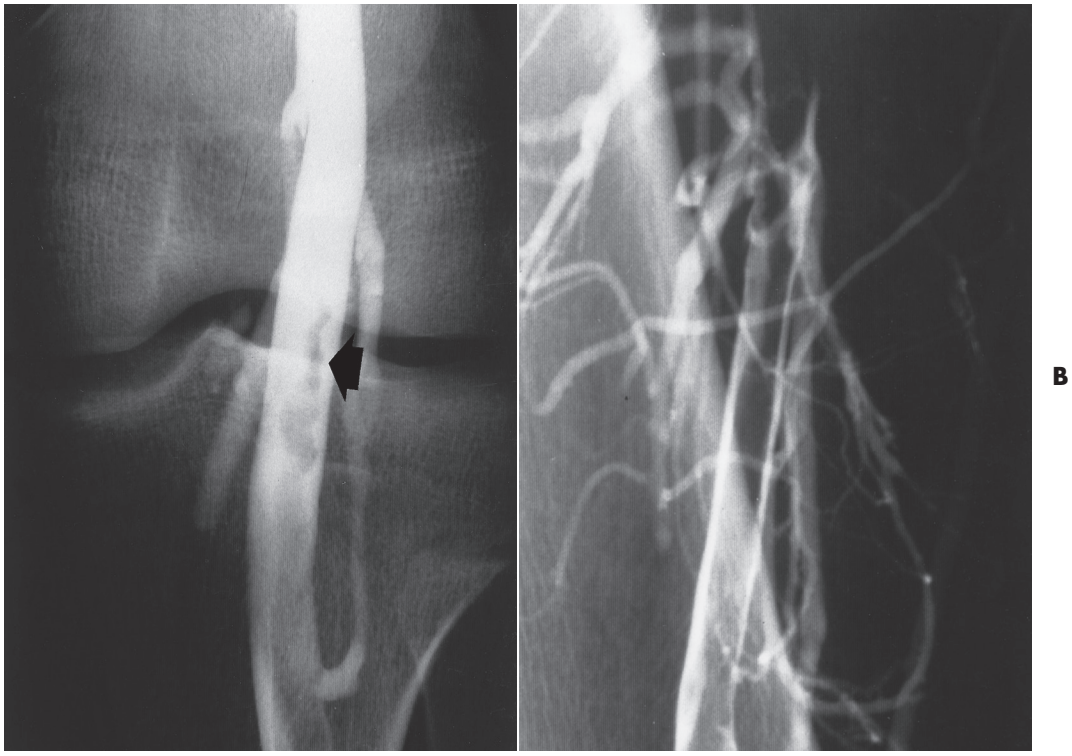

FIGURE 7-61 DVT. (A) Initial contrast venogram demonstrates early nonocclusive thrombus extending from the valve cusp. *Arrow* points to the thrombus tail, the portion most likely to embolize. (B) Subsequent contrast venogram demonstrates growth and proximal extension of the thrombus, which has resulted in occlusion of the popliteal vein at the adductor hiatus.

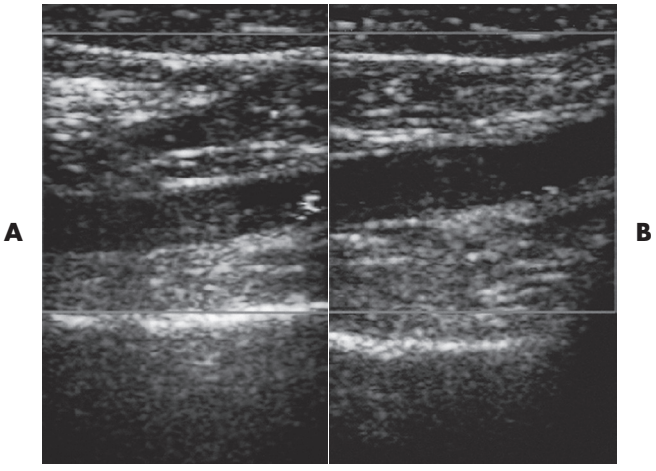

FIGURE 7-62 Doppler image of DVT. The left leg was swollen with some discoloration. The deep venous system shows abnormal intraluminal echoes involving the distal superficial femoral vein (A) and the popliteal vein (B); both areas show no compressibility, a finding consistent with a diagnosis of thrombosis.

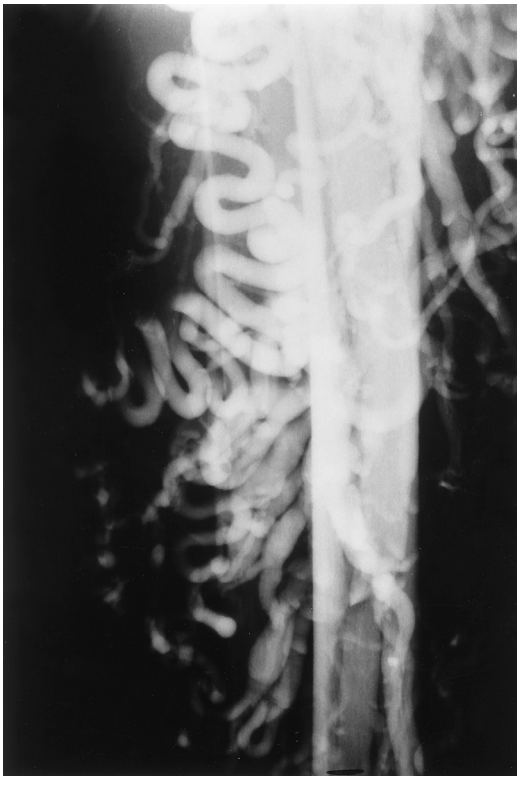

FIGURE 7-63 Varicose veins. Lower extremity venogram shows multiple tortuous, dilated venous structures.

due to gravity become incompetent and cease to function, thus increasing the volume of blood in these slow-flowing vessels.

Although heredity plays some role in the development of varicose veins, the underlying cause is increased pressure in an affected vein. Varicose veins can be an occupational hazard for people who stand or sit for long periods. Normally, the action of leg muscles helps move blood upward toward the heart from one venous valve to the next. If this "milking action" of the muscles is absent, the blood puts pressure on the closed valves and the thin walls of the veins, resulting in venous dilation, incompetence of the valves, and stasis of blood in the stagnant lower extremity veins. Increased pressure on a vein can also be attributable to a pregnant uterus or a pelvic tumor.

Stasis of blood within varicose veins may lead to the development of phleboliths, calcified clots within a vein that appear radiographically as rounded densities, which often contain lucent centers (Figure 7-64). Chronic venous stasis may also lead to periosteal new bone formation along the tibial and fibular shafts and the development of plaquelike calcifications in the chronically congested subcutaneous tissues. The poor venous flow can lead to the development of superficial ulcers, and the distended veins can rupture, causing hemorrhage into the surrounding tissues.

Imaging appearance. Although the diagnosis of varicose veins is primarily based on the clinical observation of the multiple bluish nodules just under the skin, venography is of value in demonstrating the patency of the deep venous system and the degree of collateral circulation from the superficial to the deep veins, especially if surgical intervention (tying off and removing the superficial veins) is being considered. After the application of a tourniquet to occlude superficial flow, the peripheral injection of contrast material opacifies the deep venous system. Filling of the superficial veins indicates that the perforating veins above the level of the tourniquet are incompetent.

Treatment. Treatment consists of various ways to decrease the pressure in the lower extremities. If the varices are related to excess weight, weight reduction helps alleviate symptoms; if they are related to standing all day, then elevating the legs to assist blood flow return is recommended. Support hose and exercise to strengthen contractibility of the leg muscles may also aid in blood flow return. When nonsurgical treatment is not successful, vein stripping or cauterization may be performed.

FIGURE 7-64 Varicose veins. Multiple round and oval calcifications in soft tissues (phleboliths) represent calcified thrombi, some of which have characteristic lucent centers (*black arrows*). Extensive new bone formation along the medial aspect of the tibial shaft (*white arrows*) is caused by long-standing venous stasis.

Summary of Findings for Venous Disease

Disorder	Location	Imaging Appearance	Treatment
Deep venous thrombosis	Primarily involves the lower extremities	Venography—constant filling defect or abrupt ending of the opaque column in a vein; nonfilling of one or more veins; extensive collateral venous circulation Color Doppler—visualization of thrombus and flow changes due to obstruction	Anticoagulants to prevent new thrombus formation Thrombolytic to lyse clot Bed rest to decrease possible emboli
Varicose veins	Commonly involve superficial veins of the leg	Venography—demonstrates patency of the deep venous system and degree of collateral circulation from the superficial to deep veins	Therapeutic—weight reduction; elevation of legs; support hose and exercise Surgical—vein stripping or cauterization; removal of superficial veins

REVIEW QUESTIONS

1. Heart rate is controlled by the _____ nervous system.
   a. psychogenic
   b. central
   c. peripheral
   d. autonomic
2. The _____ valve is located between the left atrium and the left ventricle, whereas the _____ valve is located between the right atrium and the right ventricle.
   1. tricuspid
   2. mitral
   3. pulmonary
   4. aortic

   a. 2, 1
   b. 3, 1
   c. 4, 1
   d. 1, 2
3. The general circulation of the body is termed the _____ circulation.
   a. pulmonary
   b. systemic
   c. general
   d. autonomic
4. The contracting phase of the heart is termed _____, whereas the relaxation phase is termed _____.
   1. autonomic
   2. diastole
   3. systemic
   4. systole

   a. 1, 3
   b. 2, 4
   c. 2, 3
   d. 4, 2
5. Contraction of which chamber of the heart forces oxygenated blood into the aorta?
   a. right atrium
   b. right ventricle
   c. left atrium
   d. left ventricle
6. Oxygenated blood reaches the heart muscle by way of the _____ and _____.
   1. right coronary artery
   2. left coronary artery
   3. left coronary vein
   4. right coronary vein

   a. 1, 3
   b. 4, 1
   c. 2, 1
   d. 2, 3
7. The heart has a specialized pacemaker named the _____.
   a. bundle of His
   b. sinoatrial node
   c. Purkinje fibers
   d. atrioventricular node
8. Which of the following factors leads to coronary artery disease?
   a. lack of exercise
   b. obesity, hypertension
   c. smoking, high-cholesterol diet
   d. all of above
9. Temporary oxygen insufficiency to the heart muscle causes severe chest pain termed _____.
   a. angina pectoris
   b. myocardial occlusion
   c. myocardial pectoris
   d. angina occlusion
10. Arterial disease caused by fatty deposits on the inner arterial wall is termed _____.
    a. arteriosclerosis
    b. myocardial infarction
    c. aneurysm
    d. myocardial ischemia
11. What radiographic procedure is used to determine the presence of coronary artery disease?
    a. angioplasty
    b. chest image
    c. coronary arteriogram
    d. CT
12. The procedure in which a balloon is used to dilate narrowed coronary arteries is named _____.
    a. aortocoronary bypass
    b. coronary arteriography
    c. percutaneous transluminal angioplasty
    d. fluoroscopy
13. Which term refers to an inability of the heart to propel blood at a sufficient rate and volume?
    a. congestive heart failure
    b. pulmonary edema
    c. valvular disease
    d. valvular stenosis
14. An elevation of the pulmonary venous pressure is the most common cause of _____.
    a. congestive heart failure
    b. pulmonary edema
    c. valvular disease
    d. valvular stenosis
15. The leading cause of strokes and CHF is _____ _____.
    a. hypertension
    b. low blood pressure
    c. hypotension
    d. cor pulmonale
16. A localized bulging or dilation of an artery is termed _____.
    a. edema
    b. effusion
    c. aneurysm
    d. fat emboli

17. What is the modality of choice for demonstration of an abdominal aortic aneurysm?
    a. MRI
    b. ultrasonography
    c. CT
    d. plain image radiography
18. A congenital narrowing or constriction of the thoracic aorta is referred to as _____.
    a. embolism
    b. plaque
    c. coarctation
    d. tetralogy
19. The _____ of the heart is/are the major site of damage from rheumatic fever.
    a. myocardium
    b. valves
    c. septum
    d. endocardium
20. The most sensitive and specific noninvasive method of diagnosing mitral stenosis is _____.
    a. ultrasonography
    b. echocardiography
    c. cardiac arteriography
    d. CT
21. The accumulation of fluid within the pericardial space surrounding the heart is termed _____.
    a. pericardial thrombosis
    b. pericardial effusion
    c. pulmonary edema
    d. pulmonary effusion
22. The invasive procedure for determining deep venous thrombosis is _____.
    a. Doppler ultrasound
    b. venography
    c. CT
    d. arteriography
23. The most accurate screening procedure for assessing renovascular lesions is _____.
    a. Doppler ultrasound
    b. venography
    c. CT
    d. arteriography
24. A potentially life-threatening condition that usually begins as a tear in the intima above the aortic valve is an _____.
    a. aortic stenosis
    b. aortic coarctation
    c. aortic thrombosis
    d. aortic dissection

8

Nervous System

OUTLINE

Physiology of the Nervous System
Infections of the Central Nervous System
- Meningitis
- Encephalitis
- Brain Abscess
- Subdural Empyema
- Epidural Empyema
- Treatment of Subdural and Epidural Empyemas
- Osteomyelitis of the Skull

Tumors of the Central Nervous System
- Glioma
- Meningioma
- Acoustic Neuroma
- Pituitary Adenoma
- Craniopharyngioma
- Pineal Tumors
- Chordoma
- Metastatic Carcinoma

Traumatic Processes of the Brain and Skull
- Skull Fracture
- Epidural Hematoma
- Subdural Hematoma
- Cerebral Contusion
- Intracerebral Hematoma
- Subarachnoid Hemorrhage
- Carotid Artery Injury
- Facial Fractures

Vascular Disease of the Central Nervous System
- Cerebrovascular Disease
- Stroke Syndrome
- Transient Ischemic Attacks
- Intraparenchymal Hemorrhage
- Subarachnoid Hemorrhage

Multiple Sclerosis
Epilepsy and Convulsive Disorders
Degenerative Diseases
- Normal Aging
- Alzheimer's Disease
- Huntington's Disease
- Parkinson's Disease
- Cerebellar Atrophy
- Amyotrophic Lateral Sclerosis (Lou Gehrig's Disease)

Hydrocephalus
Sinusitis

KEY TERMS

arachnoid membrane
arachnoid villi
astrocytomas
autonomic nervous system
bacterial meningitis
basal ganglia
blowout fracture
central nervous system (CNS)
cerebellum
cerebrovascular disease
cerebrum
choroid plexuses
chromophobe adenomas
communicating hydrocephalus
corpus callosum
cortex
depressed fractures
diastatic fracture
diencephalon
dura mater
dysarthria
ependymomas
fissures
glioblastomas
gliomas
grand mal
gyri
hemiparesis
hemiplegia
hypothalamus
linear skull fracture
mandibular fractures
medulla
medulloblastomas
meninges
meningitis
midbrain
myelin sheath
nasal bone fractures
neuron
noncommunicating (obstructive) hydrocephalus
normal-pressure hydrocephalus
oligodendrocytomas
peripheral nervous system (PNS)
petit mal
pia mater
pituitary adenomas
pons
reflex arc
releasing hormones
somatic nervous system
stroke
subarachnoid space
sulci
synapse
thalamus
tripod fracture
vermis
viral meningitis
zygomatic arch fractures

OBJECTIVES

After reading this chapter, the reader will be able to:

- Define and describe all boldface terms in this chapter
- Describe the physiology of the nervous system
- Identify anatomic structures on both diagrams and radiographs of the skull and nervous system
- Differentiate the various pathologic conditions affecting the skull and nervous system, and their radiographic manifestations

RADIOGRAPHER NOTES

Proper positioning is critical in skull and spine radiography to ensure bilateral symmetry and to permit an evaluation of the complex anatomy and structural relationships. The demonstration of asymmetry or a shift in the normal location of a structure in a patient who is positioned correctly may be indicative of an underlying pathologic condition. Proper positioning and correct angulation of the central ray may allow visualization of otherwise superimposed structures. When evaluating anatomic areas such as the sinuses or facial bones, it is often necessary to place the patient in the erect position (either standing or sitting) and to use a horizontal beam to demonstrate an air–fluid level indicative of underlying inflammatory disease or fracture. If the patient's condition prohibits placement in an erect position, air–fluid levels can be demonstrated only by obtaining a cross-table lateral projection using a horizontal beam with the patient in a dorsal decubitus position.

Exposure factors should produce a scale of contrast that provides maximal detail (definition), especially when imaging vascular structures and when looking for subtle changes in bone density, such as those resulting from fractures of the skull or spine. Advanced stages of certain pathologic conditions may require changes in technique to maintain the proper level of density, contrast, and visibility of detail (see Box 1-1 in Chapter 1). If contrast material is used, the kilovolts-peak level must remain in the low to mid-range (70–85 kVp) to provide enough radiographic contrast to properly show the contrast-filled vessels. In digital imaging, the technologist must process the digital image to provide the greatest contrast resolution by selecting the proper processing algorithm.

The administration of radiographic contrast material is an essential component of many examinations of the skull and nervous system. Therefore, it is essential that the radiographer be familiar with the use of these agents and be extremely alert to the development of possible allergic reactions. Currently, the radiographic scope of practice includes venous access and pharmacology of contrast agents. Some facilities may require the radiographer to inject agents intravenously, especially for computed tomography (CT) and magnetic resonance imaging (MRI). After contrast administration, the radiographer is often left alone in the room with the patient and must be able to immediately recognize an allergic reaction to contrast material and be able to initiate and maintain basic life-support techniques until advanced life-support personnel have arrived. Although departmental policy varies, it is usually the radiographer's responsibility to assist during resuscitation procedures. Therefore, it is essential that the radiographer be familiar with the contents of the emergency cart and be responsible for ensuring that the cart is completely stocked with all appropriate medications.

PHYSIOLOGY OF THE NERVOUS SYSTEM

The divisions of the nervous system can be classified by location or by the type of tissue supplied by the nerve cells in the division. The **central nervous system (CNS)** consists of the brain and spinal cord. The remaining neural structures, including 12 pairs of cranial nerves, 31 pairs of spinal nerves, autonomic nerves, and ganglia, make up the **peripheral nervous system (PNS)**. The PNS consists of afferent and efferent neurons. Afferent (sensory) neurons conduct impulses from peripheral receptors to the CNS. Efferent (motor) neurons conduct impulses away from the CNS to the peripheral effectors. The **somatic nervous system** supplies the striated skeletal muscles, whereas the **autonomic nervous system** supplies smooth muscle, cardiac muscle, and glandular epithelial tissue.

The basic unit of the nervous system is the **neuron**, or nerve cell (Figure 8-1). A neuron consists of a cell body and two types of long, threadlike extensions. A single axon leads from the nerve cell body, and one or more dendrites lead toward it. Axons are insulated by a fatty covering called the **myelin sheath**, which increases the rate of transmission of nervous impulses. Deterioration of this fatty myelin sheath (demyelination) is a characteristic abnormality in multiple sclerosis.

In involuntary reactions, the impulse conduction route to and from the CNS is termed a **reflex arc**. Voluntary actions are commonly a reaction due to stimulation of a combination of sensors. The basic reflex arc consists of an afferent, or sensory, neuron, which conducts impulses to the CNS from the periphery; and an efferent, or motor, neuron, which conducts impulses from the CNS to peripheral effectors (muscles or glandular tissue).

Impulses pass from one neuron to another at a junction called the **synapse**. Transmission at the synapse is a chemical reaction in which the termini of the axon release a neurotransmitter substance that produces an electrical impulse in the dendrites of the next axon. Once the neurotransmitter has accomplished its task, its activity rapidly terminates so that subsequent impulses pass along this same route.

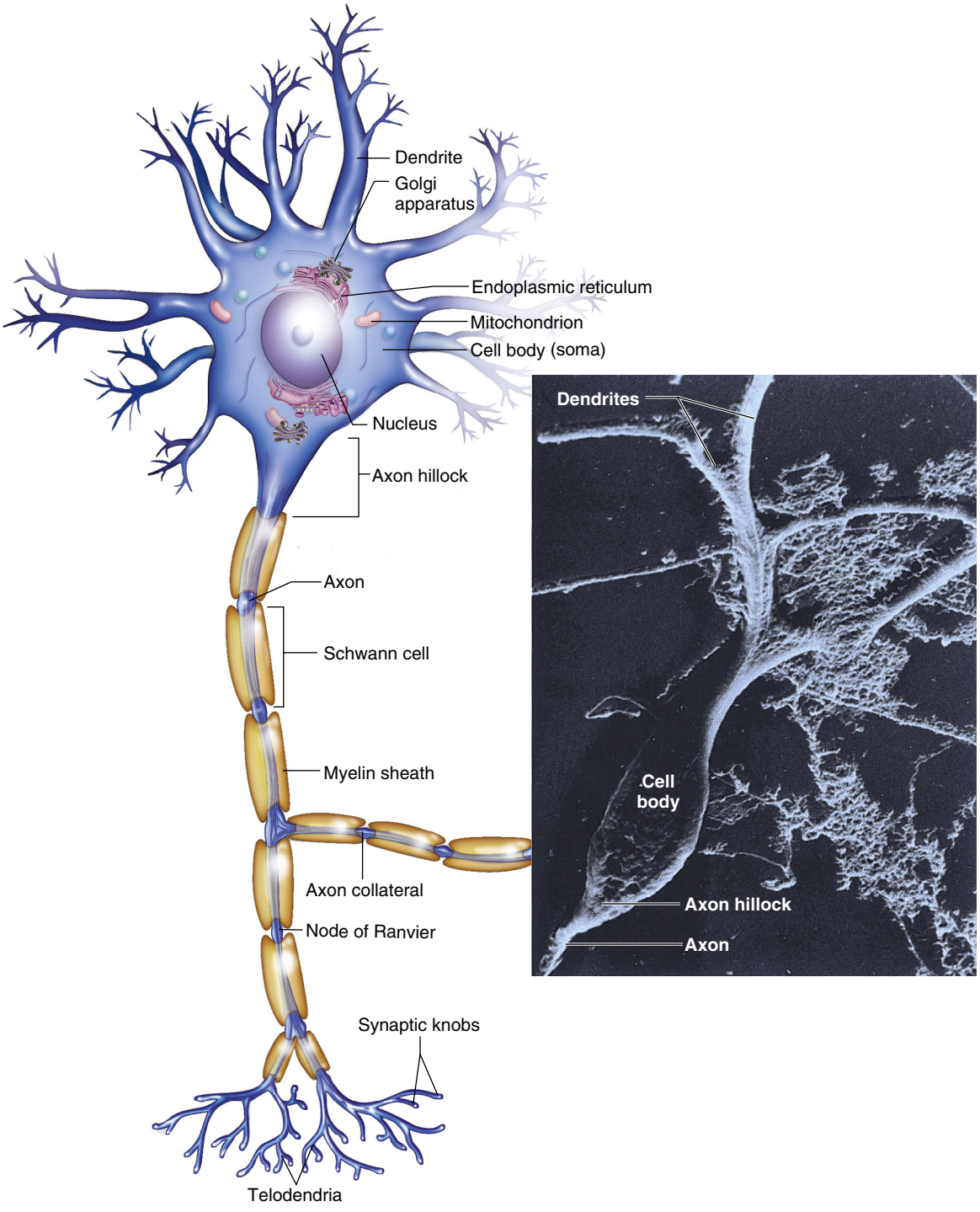

FIGURE 8-1 Structure of a neuron.

The largest part of the brain is the **cerebrum**, which consists of two cerebral hemispheres (Figure 8-2). The surface of the cerebrum is highly convoluted with elevations called **gyri** and shallow grooves called **sulci**. Deeper grooves called **fissures** divide each cerebral hemisphere into lobes. The outer portion of the cerebrum, termed the **cortex**, consists of a thin layer of gray matter where the nerve cell bodies are concentrated. The inner area consists of white matter, which is composed of the nerve fiber tracts.

The cerebral cortex is responsible for receiving sensory information from all parts of the body and for triggering impulses that govern all motor activity. Just posterior to the central sulcus, the cerebral cortex has specialized areas to receive and precisely localize sensory information from the PNS. Visual impulses are transmitted to the posterior portion of the brain; olfactory (smell) and auditory impulses are received in the lateral portions. The primary motor cortex is just anterior to the central sulcus. Because efferent motor

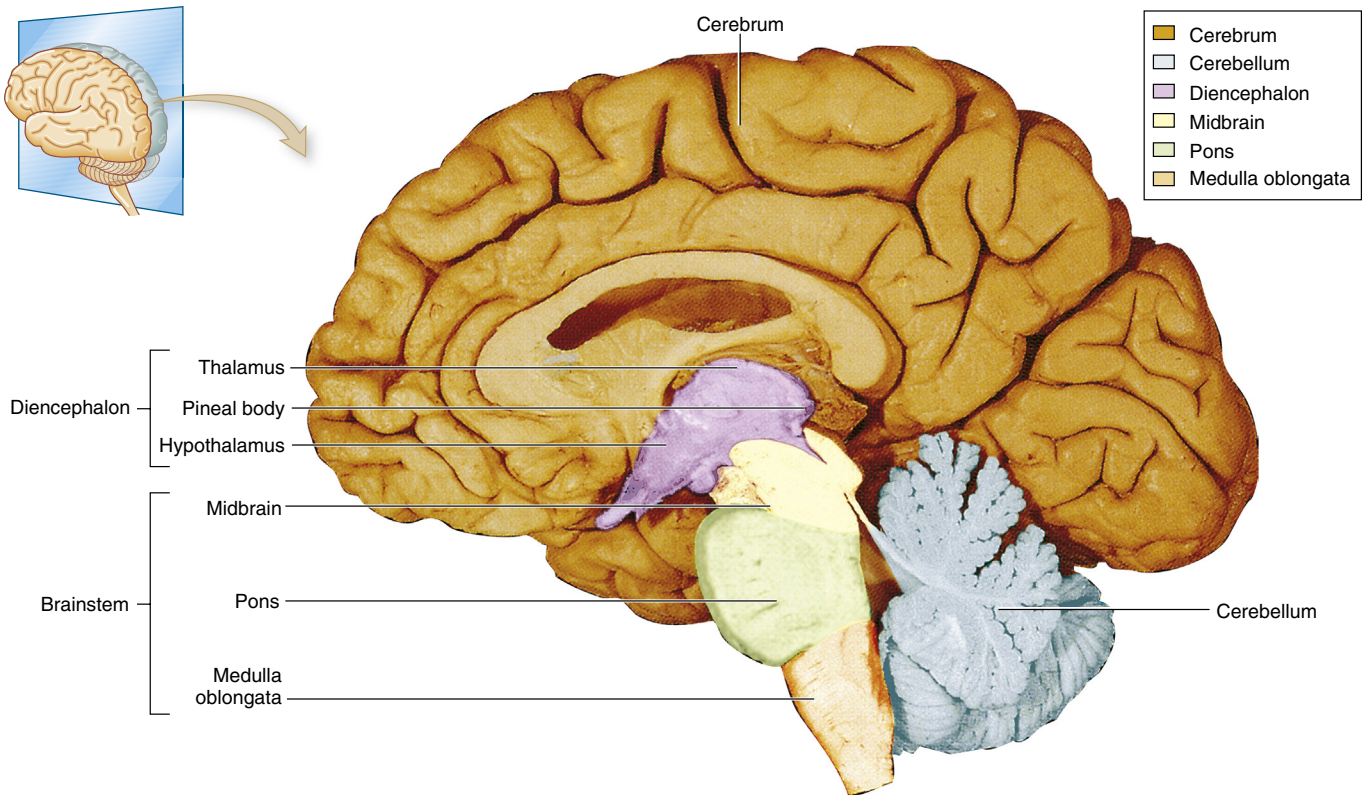

FIGURE 8-2 Divisions of the brain.

fibers cross over from one side of the body to the other at the level of the medulla and spinal cord, stimulation on one side of the cerebral cortex causes contraction of muscles on the opposite side of the body. The premotor cortex, which lies anterior to the primary motor cortex, controls movements of muscles by stimulating groups of muscles that work together. This region also contains the portion of the brain responsible for speech, which is usually on the left side in right-handed people. In addition, the cerebral cortex is the site of all higher functions, including memory and creative thought.

The two cerebral hemispheres are connected by a mass of white matter called the **corpus callosum**. These extensive bundles of nerve fibers lie in the midline just above the roofs of the lateral ventricles.

Deep within the white matter are a few islands of gray matter that are collectively called the **basal ganglia**. These structures help control position and automatic movements and consist of the caudate nuclei, the globus pallidus, and the putamen.

Between the cerebrum and spinal cord lies the brainstem, which is composed of (from top down) the **midbrain** (mesencephalon), the **pons**, and the **medulla** (see Figure 8-2). In addition to performing sensory, motor, and reflex functions, the brainstem contains the nuclei of the 12 cranial nerves and the vital centers controlling cardiac, vasomotor, and respiratory function. Centers in the medulla are responsible for such nonvital reflexes as vomiting, coughing, sneezing, hiccupping, and swallowing.

The **cerebellum**, the second largest part of the brain, is located just below the posterior portion of the cerebrum (see Figure 8-2). It is composed of two large lateral masses: the cerebellar hemispheres and a central section (**vermis**) that resembles a worm coiled on itself. The cerebellum acts with the cerebral cortex to produce skilled movements by coordinating the activities of groups of muscles. It coordinates skeletal muscles used in maintaining equilibrium and posture by functioning below the level of consciousness to make movements smooth rather than jerky, steady rather than trembling, and efficient and coordinated rather than ineffective and awkward. Therefore, cerebellar disease produces such characteristic symptoms as ataxia (muscle incoordination), tremors, and disturbances of gait and equilibrium.

The **diencephalon** lies between the cerebrum and the midbrain (see Figure 8-2). It consists of several structures located around the third ventricle, primarily the thalamus and hypothalamus. The **thalamus** primarily functions as a relay station that receives and processes sensory information of almost all kinds of sensory impulses before sending this information on to the cerebral cortex. The tiny **hypothalamus** is an extremely complex structure that functions as a link between the mind and body and is the site of "pleasure" or "reward" centers for such primary drives as eating, drinking, and mating. It plays a major role in regulating the body's internal environment by coordinating the activities of the autonomic nervous system and secreting the **releasing hormones** that control the secretion of hormones by the anterior and posterior portions of

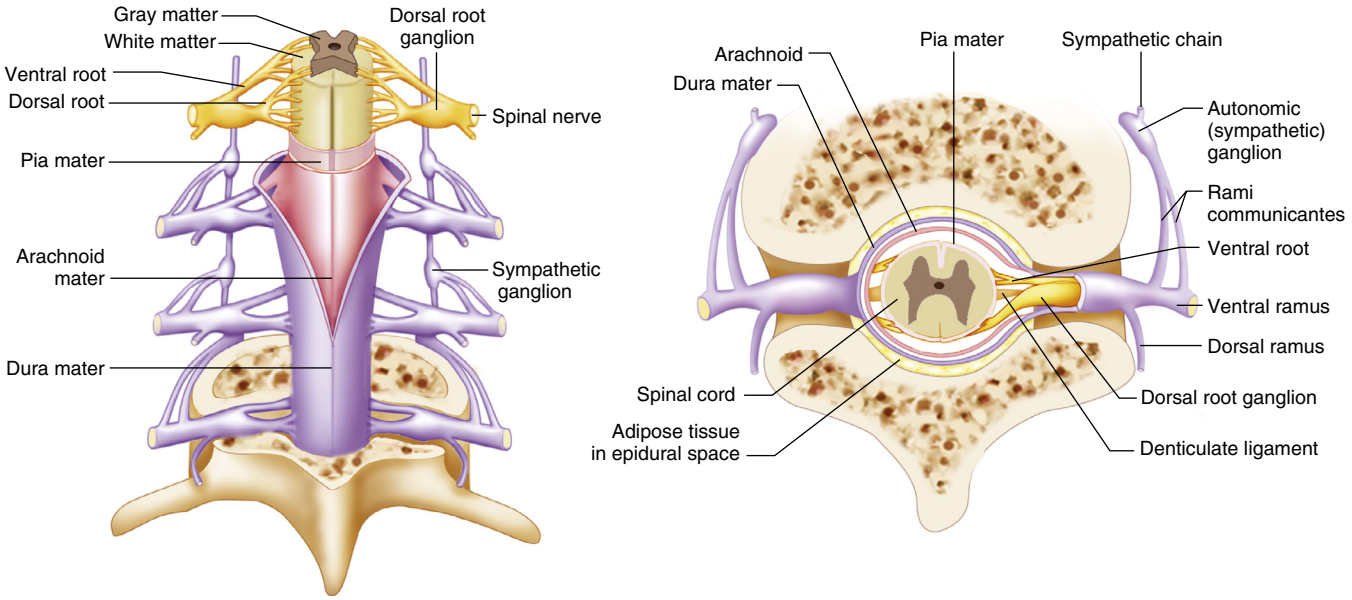

FIGURE 8-3 Structures covering the central nervous system.

the pituitary gland. The hypothalamus is also important in helping to maintain a normal body temperature and in keeping the individual in a waking state.

The spinal cord lies within the vertebral column and extends from its junction with the brainstem at the foramen magnum to approximately the lower border of the first lumbar vertebra. It consists of an inner core of gray matter surrounded by white matter tracts. The basic function of the spinal cord is to conduct impulses up the cord to the brain (ascending tracts) and down the cord from the brain to spinal nerves (descending tracts). It also serves as the center for spinal reflexes and involuntary responses, such as the knee jerk (patellar reflex).

The delicate, yet vital, brain and spinal cord are protected by two layers of coverings. The outer bony coverings are the cranial bones of the skull encasing the brain and the vertebrae surrounding the spinal cord. The inner coverings consist of three distinct layers of **meninges** (Figure 8-3). The innermost layer adhering to the outer surface of the brain and spinal cord is the transparent **pia mater**, and the tough outermost covering is termed the **dura mater**. Between these layers is the delicate, cobweb-like **arachnoid membrane**. Inflammation of these three protective layers is called meningitis.

Three extensions of the dura mater separate portions of the brain. The falx cerebri projects downward into the longitudinal fissure to separate the cerebral hemispheres. Similarly, the falx cerebelli separates the two cerebellar hemispheres. The tentorium cerebelli forms a tentlike covering over the cerebellum that separates it from the occipital lobe of the cerebrum.

In addition to bony and membranous coverings, the brain and spinal cord are further protected by a cushion of fluid both around them and within them. The ventricles are four spaces within the brain that contain cerebrospinal fluid (CSF). There are two large lateral ventricles, one located in each cerebral hemisphere. The slitlike third ventricle lies between the right and left thalamus. The anterior parts of the lateral ventricles (frontal horns) are connected by a Y-shaped canal that extends downward to open into the upper part of the third ventricle at the foramen of Monro. The fourth ventricle is a diamond-shaped space between the cerebellum posteriorly and the medulla and pons anteriorly. It is continuous inferiorly with the central canal of the spinal cord. The third and fourth ventricles are connected by the aqueduct of Sylvius (cerebral aqueduct), a narrow canal that runs through the posterior part of the midbrain.

CSF is formed by the filtration of plasma from blood in the **choroid plexuses**, networks of capillaries that project from the pia mater into the lateral ventricles and into the roofs of the third and fourth ventricles. After flowing through the ventricular system, the fluid circulates in the **subarachnoid space** (between the pia mater and the arachnoid) around the brain and spinal cord before being absorbed into venous blood through **arachnoid villi**. Obstruction of CSF circulation results in hydrocephalus.

INFECTIONS OF THE CENTRAL NERVOUS SYSTEM

The incidence of infectious diseases of the CNS has decreased with the widespread availability of antibiotics. Nevertheless, bacterial, fungal, viral, and protozoal organisms can infect the brain parenchyma, meningeal linings, and bones of the skull.

Meningitis

Meningitis is an acute inflammation of the pia mater and arachnoid, two of the membranes covering the brain and spinal cord. Infecting organisms can reach the meninges from a middle ear, the upper respiratory tract, or a frontal sinus

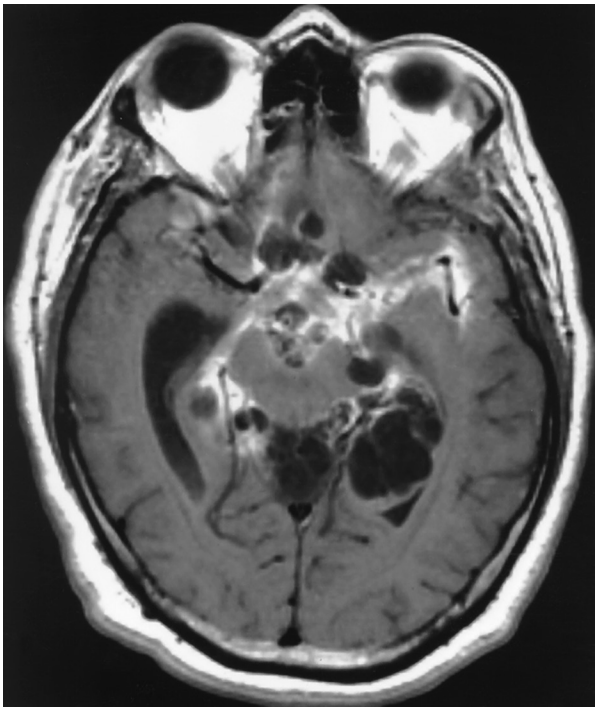

FIGURE 8-4 Meningitis. Subarachnoid enhancement in the basal cisterns and left sylvian fissure in a patient with cysticercosis.

infection, or they can be spread through the bloodstream (hematogenously) from an infection in the lungs or other site. **Bacterial meningitis** (pyogenic) is most commonly caused by *Haemophilus influenzae* in neonates and young children and by meningococci and pneumococci in adolescents and adults. **Viral meningitis** may be caused by mumps, poliovirus, and occasionally herpes simplex. A chronic form of meningitis can be caused by tuberculous infection. Bacterial meningitis is the most common form. The bacteria release toxins that destroy the meningeal cells, thus stimulating immune and inflammatory reactions.

Imaging appearance. Although the meninges initially demonstrate vascular congestion, edema, and minute hemorrhages, the underlying brain remains intact. MRI and CT scans are normal during most acute episodes of meningitis and remain normal if appropriate therapy is promptly instituted. If the infection extends to involve the cortex of the brain and the ependymal lining of the ventricles, contrast studies may show characteristic meningeal enhancement in the basal cisterns, interhemispheric fissure, and choroid plexus (Figure 8-4). Diffuse brain swelling may symmetrically compress the lateral and third ventricles. MRI and CT are also of value in the early detection of such complications of acute meningitis as arterial or venous vasculitis or thrombosis with infarction, hydrocephalus caused by adhesions or thickening of the arachnoid at the base of the brain, subdural effusion or empyema, and brain abscess. A spinal tap is necessary to determine the cause of meningitis. CT is the modality of choice to rule out contraindications to lumbar puncture (cerebral hemorrhage or increased ventricular pressure).

Although MRI and CT are best for evaluating acute bacterial meningitis, plain images of the sinuses and skull can demonstrate cranial osteomyelitis, paranasal sinusitis, or a skull fracture as the underlying cause of meningitis. In approximately 50% of patients, chest radiographs may show a silent area of pneumonia or a lung abscess. Contrast-enhanced MRI is the most sensitive modality for demonstrating enhancement of the two innermost layers of the meninges (pia mater and arachnoid membrane) and subarachnoid distention with interhemispheric widening that is consistent with early findings in severe meningitis. On T2-weighted MR images, edema produces cortical hyperintensities.

Treatment. A sample of CSF is collected for culture, and when the organism is identified, specific antibiotics are given to eradicate the bacteria. Even before these results are available, treatment with a broad-spectrum antibiotic is begun to prevent morbidity. If secondary encephalitis develops, the patient receives antiviral drugs. Any increased intracranial pressure is appropriately treated.

Encephalitis

Encephalitis, a viral inflammation of the brain and meninges (meningoencephalitis), produces symptoms ranging from mild headache and fever to severe cerebral dysfunction, seizures, and coma. Approximately 30% of cases occur in children. Encephalitis caused by herpes simplex is an often fatal, fulminant (sudden severe infection, fever, or hemorrhage) process.

Imaging appearance. The earliest and predominant findings in herpetic encephalitis are poorly marginated areas (with a patchy parenchymal pattern) in the temporal lobes and inferior frontal gray matter, which have high signal intensity on T2-weighted MR images and demonstrate low density on CT scans. These changes probably represent a combination of tissue necrosis and focal brain edema. A mass effect is common and may be seen as a midline shift or as a focal mass compressing the ventricles or the sylvian cisterns. Compromise of the blood–brain barrier in areas of rapid, more progressive hemorrhagic necrosis results in a nonhomogeneous pattern of contrast enhancement. CT reveals abnormalities 3 to 5 days after the onset of symptoms, when the patient may be comatose. In toxoplasmosis, nodular lesions demonstrate ring enhancement on contrast CT. MRI is the preferred modality, even though in acute cases a contrast-enhanced image may appear normal. Follow-up CT scans typically demonstrate widespread low-density encephalomalacia (sponginess) involving the temporal and frontal lobes.

Treatment. In addition to confirming the clinical diagnosis of herpes simplex encephalitis and excluding the presence of an abscess or a tumor, MRI and CT are important because they can indicate the best site for biopsy. A definitive diagnosis of herpes infection is essential before the start of treatment with adenine arabinoside, a chemotherapeutic agent that may be neurotoxic, mutagenic, and carcinogenic. Acyclovir, an antiviral drug used in treating herpes infection, interferes with the deoxyribonucleic acid (DNA) synthesis and inhibits viral replication.

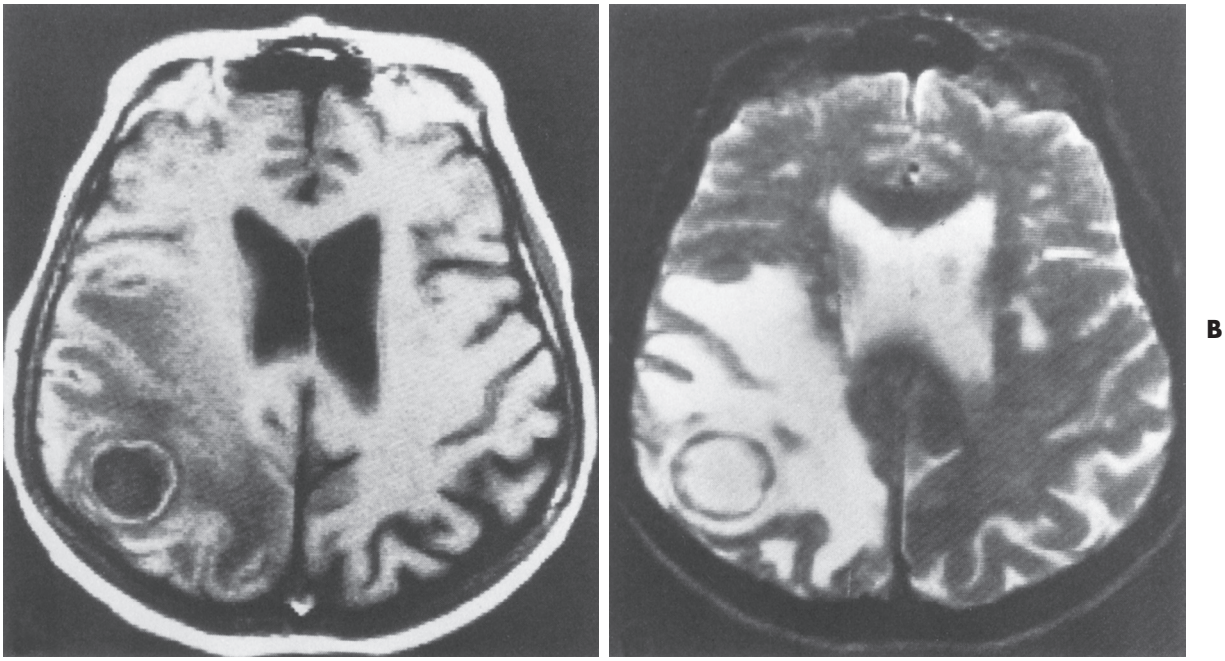

FIGURE 8-5 Brain abscess. (A) T1-weighted MR image shows a central hypointense necrotic mass with an isointense capsule surrounded by low-signal intensity edema. (B) On the T2-weighted image, the hypointense capsule is highlighted by increased signal centrally and peripherally.

Brain Abscess

Brain abscesses are usually a result of chronic infections of the middle ear, paranasal sinuses, or mastoid air cells or of systemic infections (pneumonia, bacterial endocarditis, and osteomyelitis). The organisms that most commonly cause brain abscesses are streptococci. In patients with AIDS, unusual infections such as toxoplasmosis and cryptococcosis often cause brain abscesses. The microorganisms lodge preferentially in the gray matter and spread to the adjacent white matter.

Imaging appearance. The earliest sign of brain abscess on MRI or CT is an area of abnormal density with poorly defined borders and a mass effect reflecting vascular congestion and edema. Further progression of the inflammatory process leads to cerebral softening, which may undergo necrosis and liquefaction, resulting in a true abscess. MRI is considered superior for demonstrating a brain abscess, although CT can be employed when MRI is unavailable. On T1-weighted MR images, an abscess appears as a hypointense mass with an isointense capsule surrounded by low–signal intensity edema (Figure 8-5A). Both the mass and the edema are hyperintense on proton density and T2-weighted images (Figure 8-5B). After the intravenous administration of contrast material, an oval or circular peripheral ring of contrast enhancement outlines the abscess capsule. Although the wall is usually thin and of uniform thickness, an irregularly thick wall, resulting from the formation of granulation tissue, may mimic a malignant glioma. Diffusion MRI can distinguish necrotic tumors from abscesses by demonstrating a reduced diffusion coefficient. Multiple abscesses indicate the possibility of septic emboli from a systemic infection (Figure 8-6).

Plain skull radiographs may show evidence of underlying sinusitis, mastoiditis, or osteomyelitis, although these

FIGURE 8-6 Pyogenic brain abscesses. CT scan shows one frontal and two occipital lesions (*arrows*) with relatively thin, uniform rings of enhancement.

conditions are better evaluated by CT scanning with bone-window settings. Infection by gas-forming organisms occasionally produces an air–fluid level within the abscess cavity.

Treatment. A broad-spectrum antibiotic is given to fight the infection. A craniotomy to totally excise the abscess is most successful in cases of a multiloculated abscess. Image-directed stereotactic aspiration to provide a specimen for microbial evaluation is better because it is less invasive. In some cases, the patient may require medication to reduce increased intracranial pressure.

MRI and CT can be used to assess the results of therapy for a brain abscess and to document complications. These modalities can demonstrate the often fatal intraventricular rupture of an abscess and the development of increased intracranial pressure, which may lead to brain herniation.

Subdural Empyema

Subdural empyema is a suppurative process in the space between the inner surface of the dura and the outer surface of the arachnoid. Approximately 25% of intracranial infections are subdural empyemas. The most common cause of subdural empyema is the spread of infection from the frontal or ethmoid sinuses. Less frequently, subdural empyema may result from mastoiditis, middle ear infection, purulent meningitis, penetrating wounds to the skull, craniectomy, or osteomyelitis of the skull. Subdural empyema is often bilateral and associated with a high mortality even if properly treated. The most common location of a subdural empyema is over the cerebral convexity; the base of the skull is usually spared.

Imaging appearance. MRI is the procedure of choice in evaluating the patient with suspected subdural empyema. Unlike CT, MRI is free from bony artifacts adjacent to the inner table of the skull. In addition, signal characteristics may permit differentiation between benign effusions and infected empyemas. Noncontrast scans demonstrate a crescentic or lentiform (lenslike), extra-axial fluid collection (representing pus) adjacent to the inner border of the skull or the falx (Figure 8-7). There is compression and displacement of the ipsilateral ventricular structures. After the intravenous administration of contrast material, a narrow zone of enhancement of relatively uniform thickness separates the extracerebral collection from the brain surface. MRI can also demonstrate involvement of the adjacent parenchyma by means of retrograde thrombophlebitis with resultant infarction or abscess formation, both of which are signs associated with a poor prognosis.

Epidural Empyema

Epidural empyema (Figure 8-8) is almost invariably associated with osteomyelitis in a cranial bone originating from an infection in the ear or paranasal sinuses. The infectious process is localized outside the dural membrane and beneath the inner table of the skull. The frontal region is most frequently affected because of its close relationship to the frontal sinuses and the ease with which the dura can be stripped from the bone.

Imaging appearance. Noncontrast CT scans demonstrate the epidural infection as a poorly defined area of low density adjacent to the inner table of the skull. An adjacent area of bone destruction or evidence of paranasal sinus or mastoid infection (fluid and soft tissue thickening) can often be demonstrated on CT or plain skull radiographs. After the intravenous administration of contrast material, the inflamed dural membrane appears as a thickened zone of enhancement on the convex inner side of the lesion. If the collection lies in the midline, the attachment of the falx is displaced inward and separated from the adjacent skull, thus identifying its extradural location.

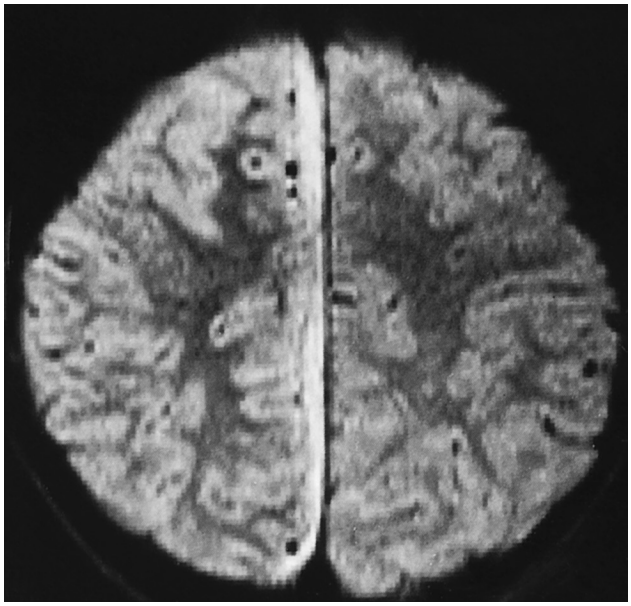

FIGURE 8-7 Subdural empyema. T2-weighted MR image demonstrates high signal intensity of the fluid collections along the falx.

FIGURE 8-8 Epidural empyema. Black rim of the dura delineates the epidural fluid collection in the right frontal region.

Treatment of Subdural and Epidural Empyemas

Subdural and epidural empyemas should be treated as medical emergencies. Immediate surgical drainage of an empyema and the underlying sinus infection aids in preventing recurrence. Craniotomy provides the most complete evacuation. The broad-spectrum antibiotic regimen used for a brain abscess is used here also.

Osteomyelitis of the Skull

Osteomyelitis of the skull is most commonly caused by direct extension of a suppurative process from the paranasal sinuses, mastoid air cells, or scalp. As with osteomyelitis elsewhere in the skeleton, the radiographic changes often develop 1 or 2 weeks after the onset of clinical symptoms and signs.

Imaging appearance. Acute osteomyelitis first appears radiographically as multiple small, poorly defined areas of lucency (Figure 8-9). During the next several weeks, the lucencies enlarge and coalesce centrally with an expanding perimeter of small satellite foci. As the infection becomes more chronic (especially with syphilis, tuberculosis, or fungal infections), attempts at bone regeneration produce multiple areas of poorly defined reactive sclerosis.

Treatment. Refer to the discussion on bacterial osteomyelitis in Chapter 4.

Summary of Findings for Infections of the Central Nervous System

Disorder	Location	Imaging Appearance	Treatment
Meningitis	Acute inflammation of meninges	CT/MRI—arterial or venous vasculitis or thrombosis, hydrocephalus, subdural effusion, and brain abscess MRI—enhancement of the two innermost layers of the meninges and subarachnoid distention with interhemispheric widening Radiographs—osteomyelitis, sinusitis, or fracture	Immediate broad-spectrum antibiotics followed by specific antibiotics determined by culture results
Encephalitis	Viral inflammation of brain and meninges	MRI—hyperintensity on T2-weighted images with mass effect CT—low-attenuation regions without focal enhancement; mass effect	For herpes infection: adenine arabinoside
Brain abscess	Microorganism infection of gray and white matter	MRI—T1-weighted images show hypointense mass with isointense capsule; proton-density and T2-weighted images show hyperintensity of both the mass and surrounding edema; diffusion MRI distinguishes necrotic tumors from abscesses CT—contrast-enhanced scan identifies a high-attenuation capsule surrounding a hypodense necrotic center	Broad-spectrum antibiotics Craniotomy to totally excise the multiloculated abscess Image-directed stereotactic aspiration provides a specimen for microbial evaluation Medication to reduce increased intracranial pressure if symptoms occur
Subdural empyema	Infection located between the dura and the arachnoid	MRI—characteristic crescentic or lentiform extra-axial fluid collection that is mildly hyperintense to cerebrospinal fluid on T2-weighted images	Craniotomy for immediate surgical drainage of empyema and underlying sinus empyema; aids in preventing recurrence Same broad-spectrum antibiotic regimen as for brain abscess
Epidural empyema	Infectious process above the dura and beneath the inner skull table	CT (noncontrast)—shows low-density area adjacent to the inner table of the skull, with possible bone destruction CT (contrast enhanced)—dural membrane appears as a thickened zone of enhancement on the convex inner side of the lesion	
Osteomyelitis of the skull	Cranial bones	Radiograph—multiple, small, poorly defined areas of lucency, 1–2 weeks after onset of symptoms	See Chapter 4

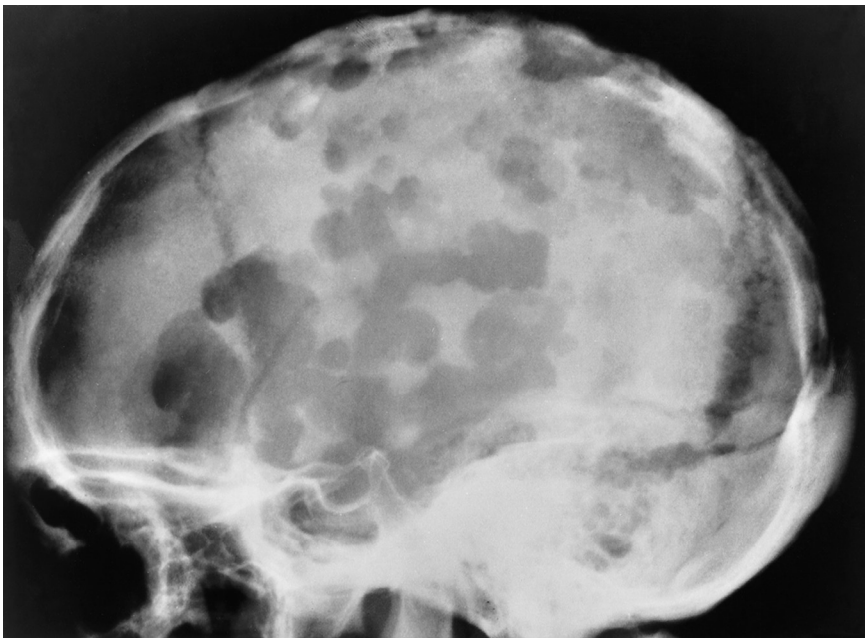

FIGURE 8-9 Osteomyelitis of the skull. Diffuse areas of osteolytic destruction affect most of the calvaria resulting from blastomycosis.

TUMORS OF THE CENTRAL NERVOUS SYSTEM

Intracranial neoplasms manifest clinically as seizure disorders or gradual neurologic deficits (difficulty thinking, slow comprehension, weakness, and headache). Approximately 50% of CNS tumors are primary lesions, and the others represent metastases.

Imaging appearance. The clinical presentation and radiographic appearance depend on the location of the tumor and the site of the subsequent mass effect. MRI is generally considered the most sensitive technique for detecting most suspected brain tumors. In general, both the tumor and its surrounding edema demonstrate high signal intensity on T2-weighted images. After the intravenous injection of contrast material, the enhancing tumor can usually be distinguished from nonenhancing edema on T1-weighted images (Figure 8-10). In addition to its exquisite sensitivity in detecting pathologic alteration of normal tissue constituents, MRI provides excellent delineation of tumor extent and can show associated abnormalities, such as hydrocephalus. This modality is of special value in imaging neoplasms of the brainstem and posterior fossa, which may be poorly demonstrated on CT due to bone artifact. CT with contrast enhancement is an excellent examination for evaluating a patient with suspected brain tumor. It is of special value for detecting punctate or larger calcification that cannot be shown by MRI. Although skull radiographs were used in the past to demonstrate tumoral calcification, bone erosion, and displacement of the calcified pineal gland, plain images are no longer indicated because this information can be more effectively obtained on CT scans.

Before the advent of CT, cerebral arteriography was used to demonstrate evidence of brain tumors, such as mass effect, contralateral displacement of midline arteries and veins, abnormal vessels with tumor staining, and early venous filling. Currently, the major use of arteriography is for precise delineation of the arterial and venous anatomy. This delineation provides a surgical map before operative therapy and for evaluation of those cases in which a vascular anomaly is a strong consideration in the differential diagnosis of a tumor. Radionuclide brain scans have a relatively high rate of detection of cerebral tumors but are far less specific than CT or MRI. Positron emission tomography (PET) scans demonstrate metabolic activity and specific location of a lesion for presurgical planning (Figure 8-11).

Treatment. Therapy of a CNS tumor depends on its location and histology. If possible, the tumor is surgically resected, followed by radiation therapy if the tumor is not completely removed. Radiation therapy and chemotherapy are used when the tumor is inoperable.

Glioma

Gliomas, the most common primary malignant brain tumors, consist of glial cells (supporting connective tissues in the CNS) that still have the ability to multiply. They spread by direct extension and can cross from one cerebral hemisphere to the other through connecting white matter tracts, such as the corpus callosum. Gliomas have a peak incidence in middle adult life and are infrequent in persons younger than 30 years of age.

Glioblastomas are highly malignant lesions that are predominantly cerebral, although similar tumors may occur in the brainstem, cerebellum, or spinal cord. **Astrocytomas** (70% of all gliomas) are slow-growing tumors that have an

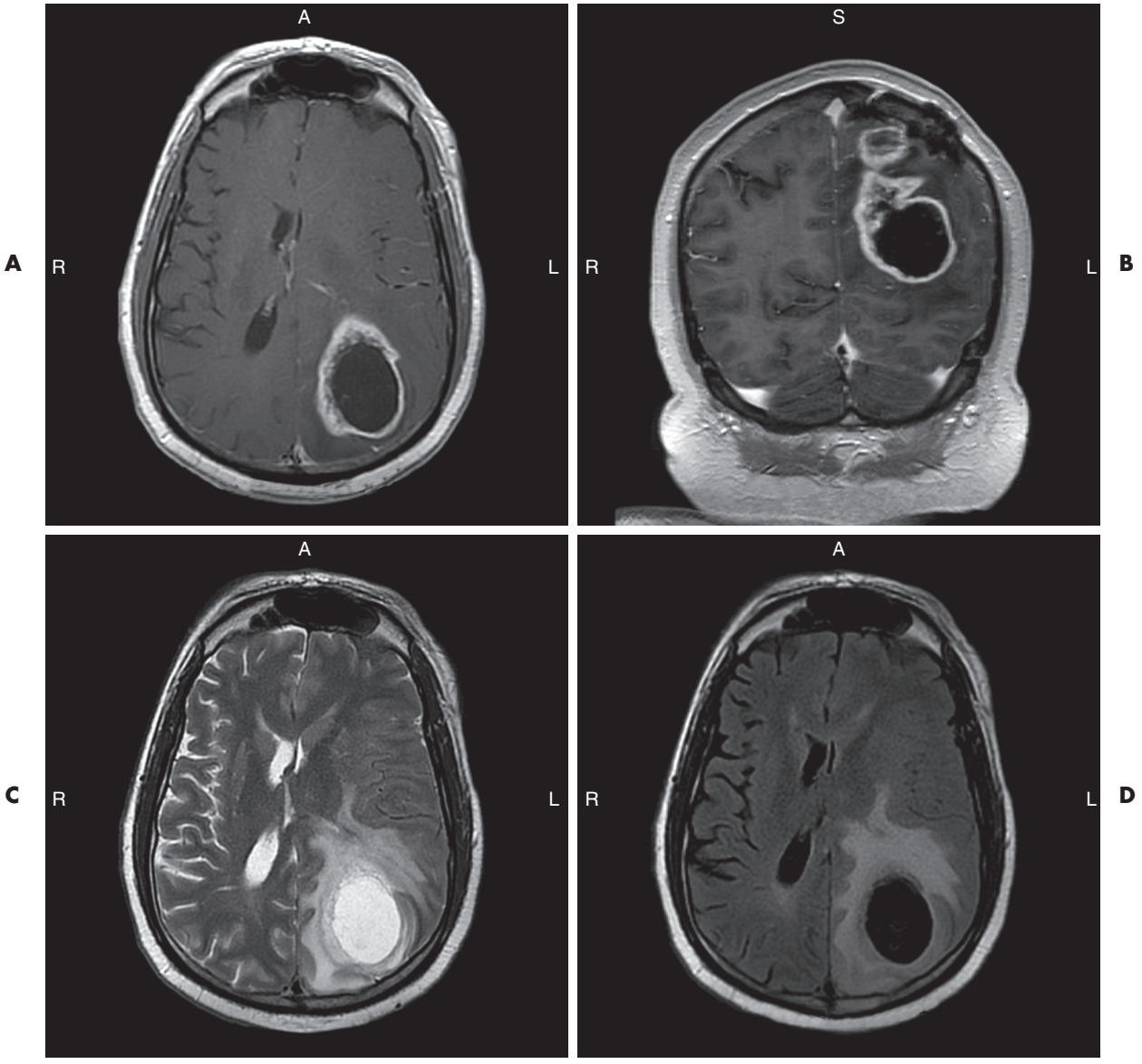

FIGURE 8-10 **Glioblastoma multiforme.** The T1-weighted axial **(A)** and coronal **(B)** MR images after intravenous injection of contrast material demonstrate an irregular ring of contrast enhancement, representing solid vascularized tumor, surrounding a central low-density area of necrosis. **(C)** The tumor and its surrounding edema demonstrate high signal intensity on a T2-weighted axial image. **(D)** On a FLAIR axial image, the tumor demonstrates low signal intensity and the edema appears as high signal intensity, demonstrating the extent of involvement and a ventricular shift to the right.

infiltrative character and can form large cavities or pseudocysts. Favored sites are the cerebrum, cerebellum, thalamus, optic chiasm, and pons.

Less frequent types of gliomas are ependymoma, medulloblastoma, and oligodendrocytoma. **Ependymomas** most commonly arise from the walls of the fourth ventricle, especially in children, and usually from the lateral ventricles in adults. **Medulloblastomas** are rapidly growing tumors, disseminating throughout the spinal fluid, which develop in the posterior portion of the vermis in children and rarely in the cerebellar hemisphere in adults. The tumor tends to spread through the subarachnoid space, with metastatic deposits occurring anywhere within the brain or spinal column. **Oligodendrocytomas** are slow-growing lesions that usually arise in the cerebrum and have a tendency to calcify.

Imaging appearance. On MR images (Figure 8-12), gliomas typically appear as masses of high signal intensity on T2-weighted images. They may be of low intensity or isointense on T1-weighted sequences. MR spectroscopy has a typical spectral pattern with a strongly increased choline peak, which indicates myelin or the breakdown of myelin (the chemical structure that goes into making white matter).

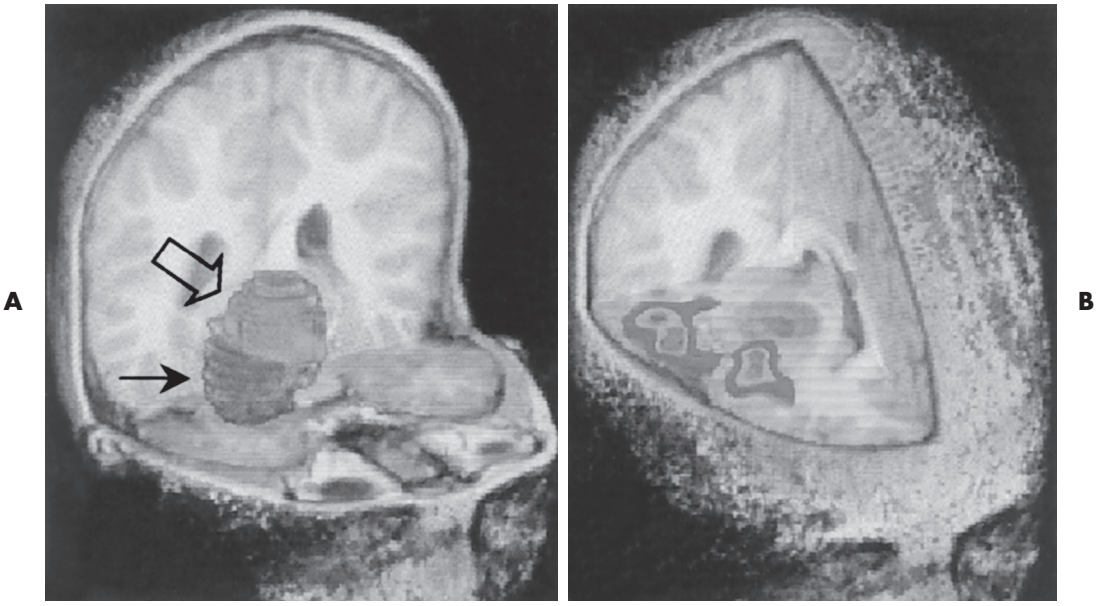

FIGURE 8-11 Low-grade brain tumor studied by three-dimensional reconstruction of a PET cerebral study using ^{11}C-methionine. **(A)** Mass effect near the thalamus is evident when the increased uptake (*open arrow*) is compared with a cystic component showing lack of uptake (*solid arrow*). **(B)** The greatest activity is noted in the right temporal lobe, corresponding to receptive and expressive language areas.

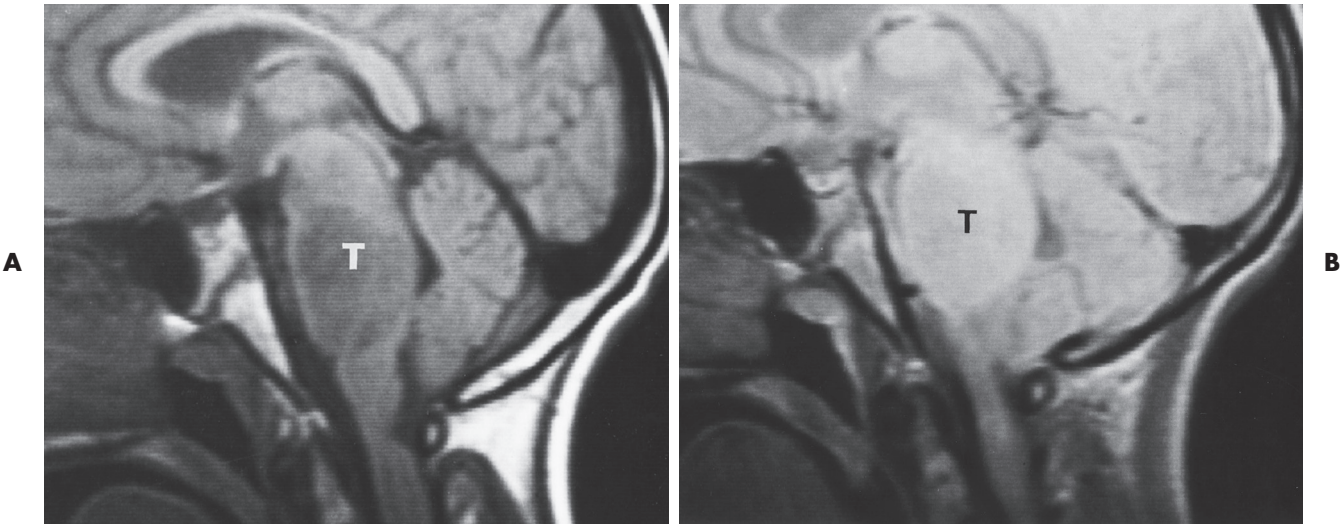

FIGURE 8-12 **Brainstem glioma.** Sagittal MR images show enlargement of brainstem involving the pons and midbrain. Note that various imaging techniques alter the appearance of the tumor (T). **(A)** On a T1-weighted image, the tumor is gray (low-intensity signal). **(B)** On a T2-weighted image, the tumor appears white (high-intensity signal).

In MR spectroscopy, a highly elevated choline level, a drastically lower level of *N*-acetylaspartate (a neuronal marker), and a drastically lower creatine/phosphocreatine ratio confirm an infiltrating glioma (Figure 8-13). Ependymomas, often partially calcified and cystic, have a heterogeneous signal intensity and show enhancement.

On noncontrast CT scans, gliomas are most commonly seen as single, nonhomogeneous masses. Low-grade astrocytomas tend to be low-density lesions showing little or no enhancement (Figure 8-14); glioblastomas most frequently contain areas of both increased and decreased density, although a broad spectrum of CT appearances can occur.

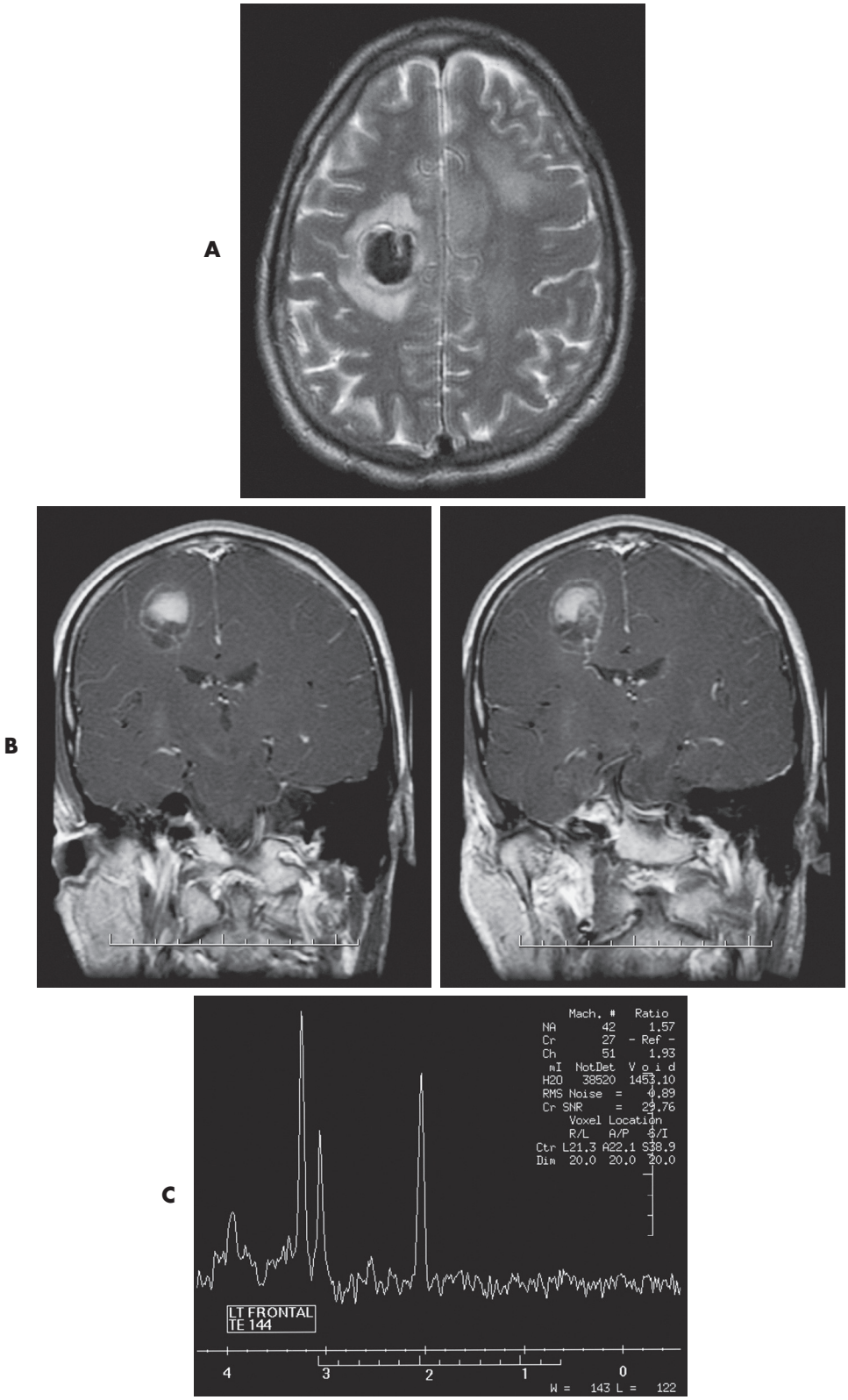

FIGURE 8-13 Infiltrating glioma. (A) T2-weighted MR image demonstrates a 3-cm hypointense lesion in the deep right parietal lobe with a hyperintense peripheral rim. A poorly defined hyperintense lesion is seen within the deep white matter of the left temporal and parietal lobes. (B) On the T1-weighted coronal image, the hyperintense periphery is seen surrounding a low-signal intensity and a high-signal intensity lesion. (C) On MR spectroscopy, the left frontal lobe demonstrates an elevated choline (first) peak, a slightly lower creatine/phosphocreatine (second) peak, and a mildly depressed *N*-acetylaspartate (third) peak. These findings help confirm a low-grade, diffuse infiltrating glioma.

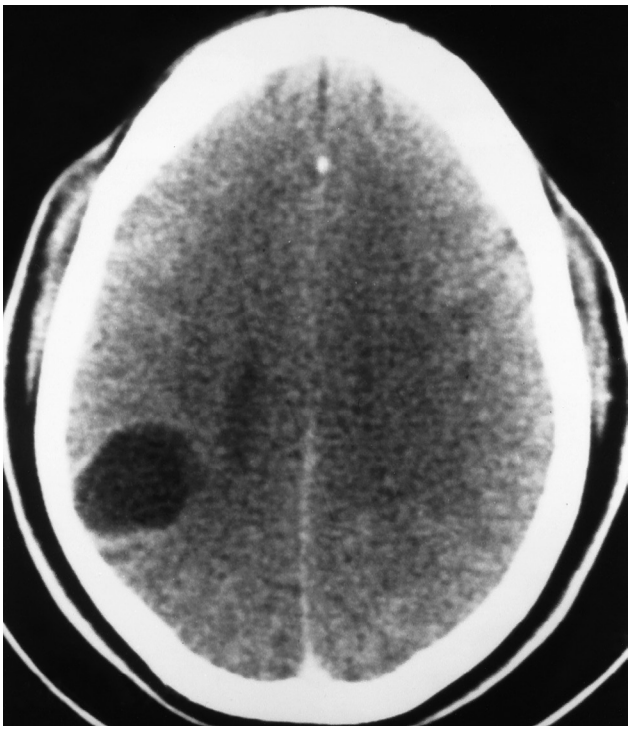

FIGURE 8-14 Cystic astrocytoma. CT scan shows a hypodense mass with a thin rim of contrast enhancement.

Edema is often seen in the adjacent subcortical white matter. After the intravenous injection of contrast material, virtually all gliomas show enhancement, with the most malignant lesions tending to be enhanced to the greatest degree (see Figure 8-10). In MR spectroscopy, an elevated choline/creatine ratio suggests a malignant neoplasm. The most common pattern is an irregular ring of contrast enhancement, representing solid vascularized tumor, surrounding a central low-density area of necrosis. Contrast enhancement also can appear as patches of increased density distributed irregularly throughout a low-density lesion or as rounded nodules of increased density within the mass.

Treatment. Therapy depends on the location and histology of the tumor. Astrocytomas have a good 5-year survival rate after surgery and radiation therapy. For ependymomas of the filum terminale, surgical removal provides a favorable prognosis.

Meningioma

Meningiomas are benign tumors that arise from arachnoid lining cells and are attached to the dura. The most common sites of meningioma are the convexity of the calvaria, the olfactory groove, the tuberculum sellae, the parasagittal region, the sylvian fissure, the cerebellopontine angle, and the spinal canal. Of all spinal tumors, 25% are meningiomas. Seizures and neurologic defects are most often caused by mass effect.

Imaging appearance. Because meningiomas tend to be isointense with brain on both T1- and T2-weighted images, anatomic distortion is the key to the MRI diagnosis (Figure 8-15). A thin rim of low intensity, consisting of a CSF cleft, the vascular rim, or dura, may separate the tumor from the adjacent brain. Calcification within a meningioma may produce nonuniform signal or focal signal void. Surrounding edema may make the lesion easier to identify. Just as the detection of meningiomas by CT is facilitated by the use of iodinated contrast material, paramagnetic contrast agents can enhance the detection of meningiomas on MRI. MR spectroscopy has a typical spectral pattern with a strongly increased choline peak; creatine is a marker of energy metabolism. Alanine is another specific amino acid marker producing a unique peak in meningiomas. CT typically shows a meningioma as a rounded, sharply delineated, isodense (25%) or hyperdense (75%) tumor abutting a dural surface. Calcification often is seen within the mass on noncontrast scans. After the intravenous injection of contrast material, there is intense homogeneous enhancement, which reflects the highly vascular nature of the tumor (Figure 8-16).

Pronounced dilation of meningeal and diploic vessels, which provide part of the blood supply to the tumor, may produce prominent grooves in the calvaria on plain images of the skull. Calvarial hyperostosis (increased density) may develop because of invasion of the bone by tumor cells that stimulate osteoblastic activity. Dense calcification or granular psammomatous deposits may be seen within the tumor (Figure 8-17).

Arteriography can demonstrate the feeding arteries, which most commonly arise from both the internal and the external carotid artery circulation. Preoperative embolization of the external carotid artery supply can decrease the amount of blood loss at surgery.

Spinal meningiomas are best demonstrated on T1- or T2-weighted MR images using gadolinium enhancement as a homogeneous intense lesion. CT myelography demonstrates the location of the mass, which is usually intradural extramedullary (Figure 8-18).

Treatment. Surgical resection is very successful because of the superficial position of the tumor and the lack of tumor infiltration. Incomplete resection results in a lobulated and mushroom pattern of tumor growth.

Acoustic Neuroma

Acoustic neuromas are slowly growing benign tumors that may occur as solitary lesions or as part of the syndrome of neurofibromatosis. Such a tumor arises from Schwann cells in the vestibular portion of the auditory (eighth cranial) nerve. It usually originates in the internal auditory canal and extends into the cerebellopontine angle cistern.

Imaging appearance. MR images (T1-weighted), the preferred modality, exquisitely show an acoustic neuroma as a focal or generalized enlargement of the eighth cranial nerve (Figure 8-19). This technique can even demonstrate small intracanalicular tumors confined to the internal auditory canal, which may be impossible to show on CT unless contrast material (nonionic water-soluble material or air) is administered into the ventricular system. CT scans demonstrate enlargement and erosion of the internal auditory

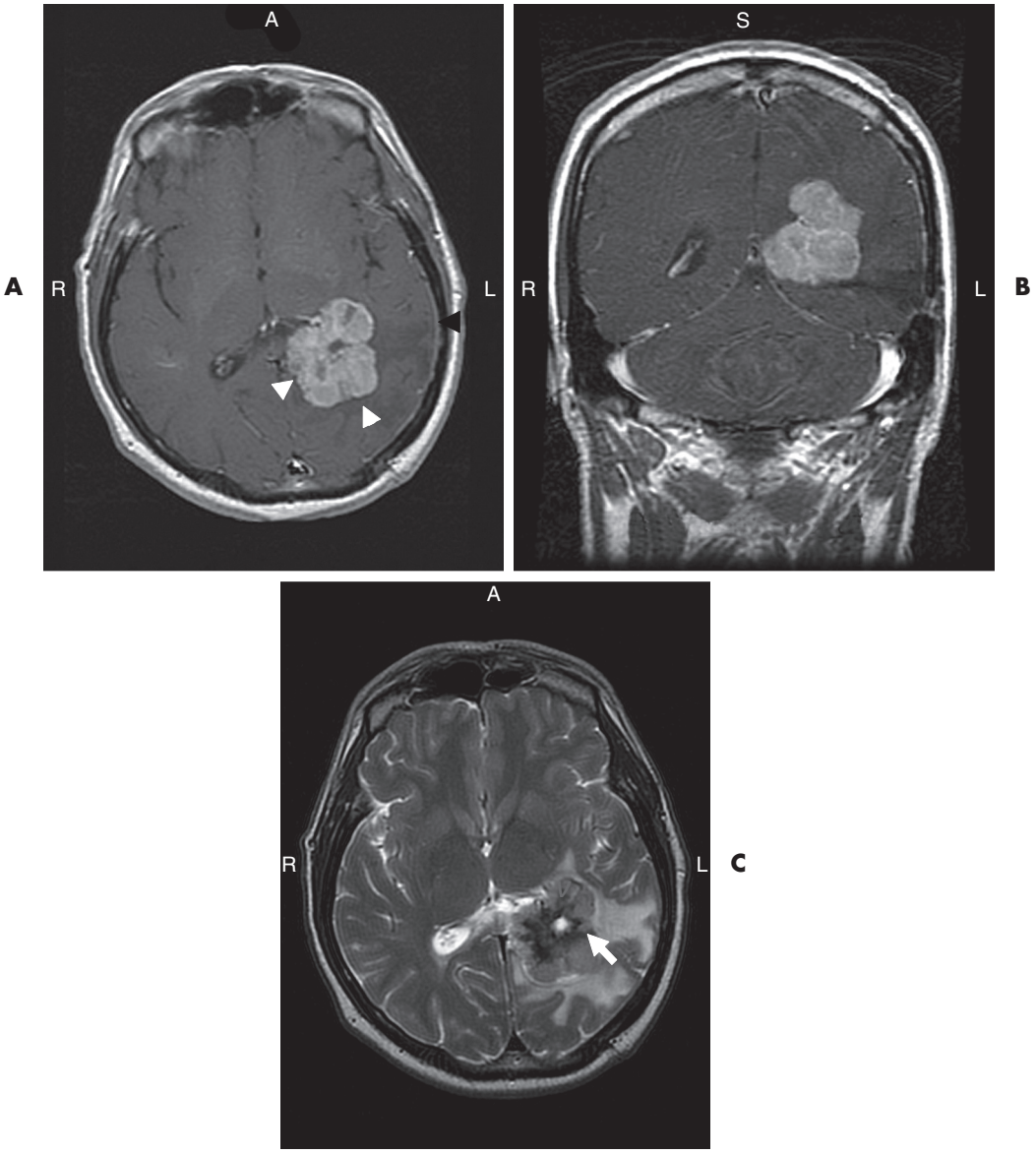

FIGURE 8-15 Meningioma on MRI after intravenous injection of contrast material. A large mass (*arrowheads*) appears hyperintense on T1-weighted axial **(A)** and coronal **(B)** MR images. **(C)** The mass appears hypointense on a T2-weighted image. Note the dramatic shift of the ventricle (v) caused by the mass effect of the tumor. *White arrow* points to areas of hemorrhage within the neoplasm.

canal and a uniformly enhancing mass in the cerebellopontine angle (Figure 8-20). Very large tumors may compress the fourth ventricle and lead to the development of hydrocephalus.

Treatment. Surgical excision of the lesion or gamma knife radiosurgery improves symptoms.

Pituitary Adenoma

Pituitary adenomas, almost all of which arise in the anterior lobe, constitute more than 10% of all intracranial tumors. Most are nonsecreting **chromophobe adenomas**. As chromophobe tumors enlarge, the adjoining secreting cells within the sella turcica are compressed, leading to diminished secretion and decreased levels of growth hormone, gonadotropins, thyrotropic hormone, and adrenocorticotropic hormone (ACTH). Large chromophobe adenomas can extend upward to distort the region of the optic chiasm, whereas lateral expansion of tumor can compress the cranial nerves passing within the cavernous sinus.

A hormone-secreting pituitary tumor can cause clinical symptoms even if it is too small to have a mechanical mass effect. Hypersecretion of growth hormone results in gigantism in adolescents (before the epiphyses have closed) and acromegaly in adults (after the epiphyses have closed). Excess secretion of adrenocorticotropic hormone by a pituitary tumor results in the hypersecretion of steroid hormones

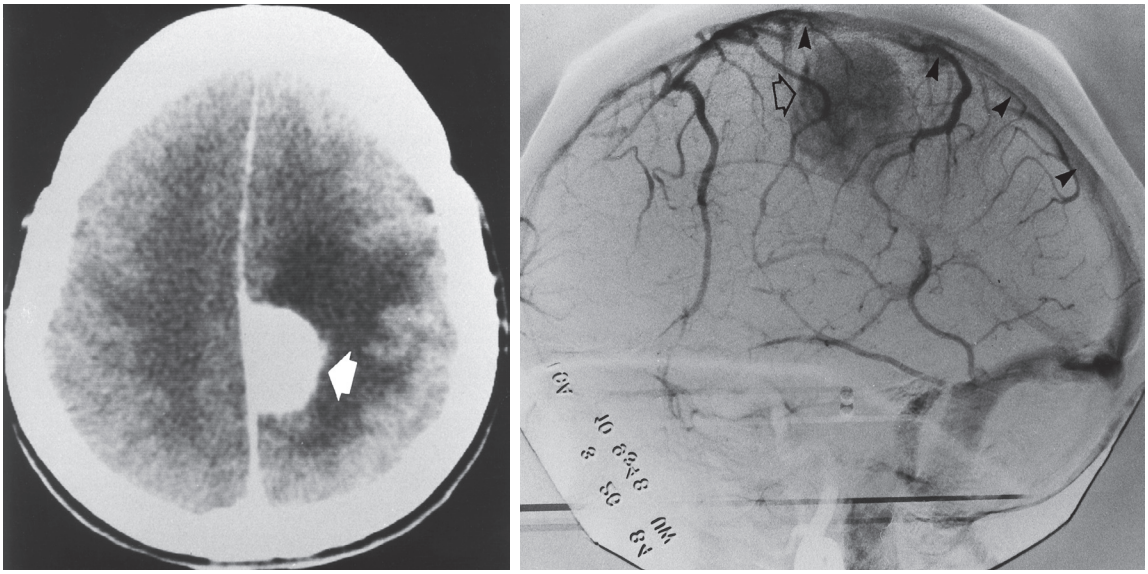

FIGURE 8-16 Meningioma. (A) CT scan after intravenous injection of contrast material shows uniformly enhancing mass (*arrow*) with surrounding low-density edema attached to the falx. (B) Venous phase of carotid arteriogram shows the characteristic prominent vascular blush (*arrow*) of meningioma. Note that the superior sagittal sinus (*arrowheads*) is patent.

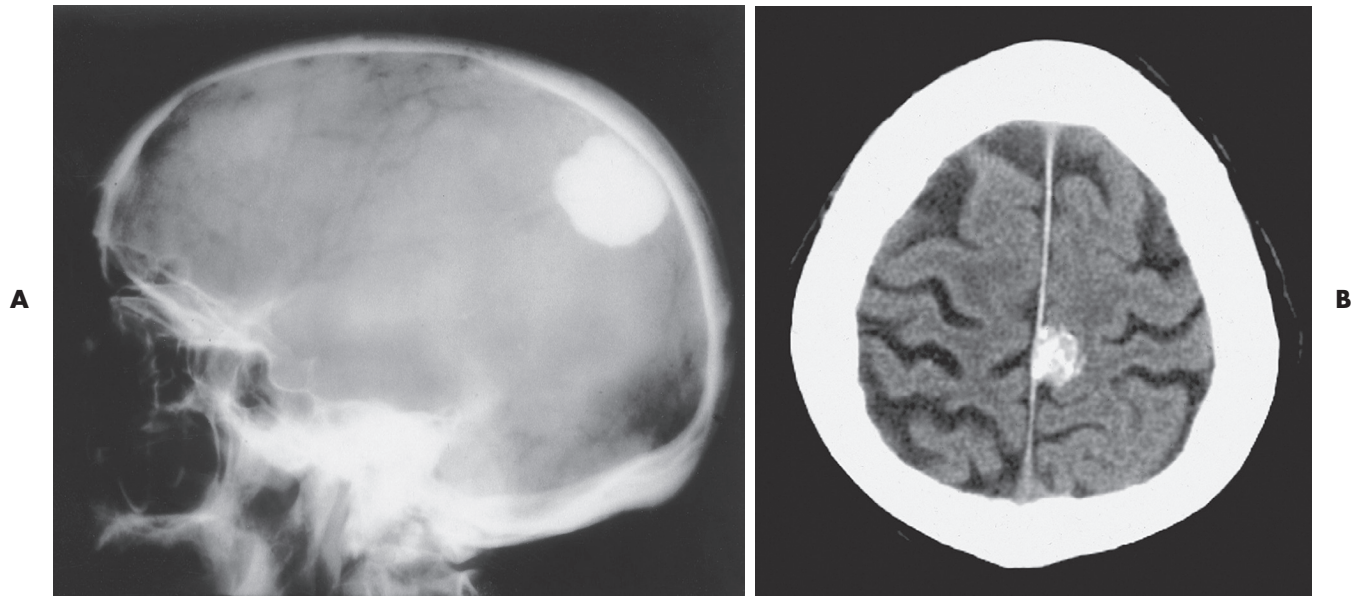

FIGURE 8-17 Parietal meningioma. (A) Plain skull image shows dense calcification in the tumor. (B) CT scan of another patient demonstrating a midline calcified meningioma.

from the adrenal cortex and symptoms of Cushing's disease. Hypersecretion of thyroid-stimulating hormone (TSH) leads to hyperthyroidism; excess secretion of prolactin by a pituitary tumor in women causes the galactorrhea–amenorrhea syndrome.

Imaging appearance. Thin-section CT and MRI are the examinations of choice for evaluating a patient with a suspected pituitary tumor. After the intravenous administration of contrast material, large pituitary tumors are typically homogeneous and hyperdense with respect to surrounding brain tissue. Most pituitary microadenomas are of lower density than the normal pituitary gland. CT can also demonstrate adjacent bone erosion, tumor extension beyond the confines of the sella, and impression on nearby structures, such as the third ventricle, optic nerves, or optic chiasm (Figure 8-21).

The preferred modality for detecting and defining the extent of a pituitary tumor is MRI because of its superior sensitivity and multiplanar capability. Thin-section coronal and sagittal T1-weighted MR images show a microadenoma as a low–signal intensity focal lesion associated with contralateral deviation of the pituitary stalk and an upwardly convex contour of the gland (Figure 8-22). The intravenous injection

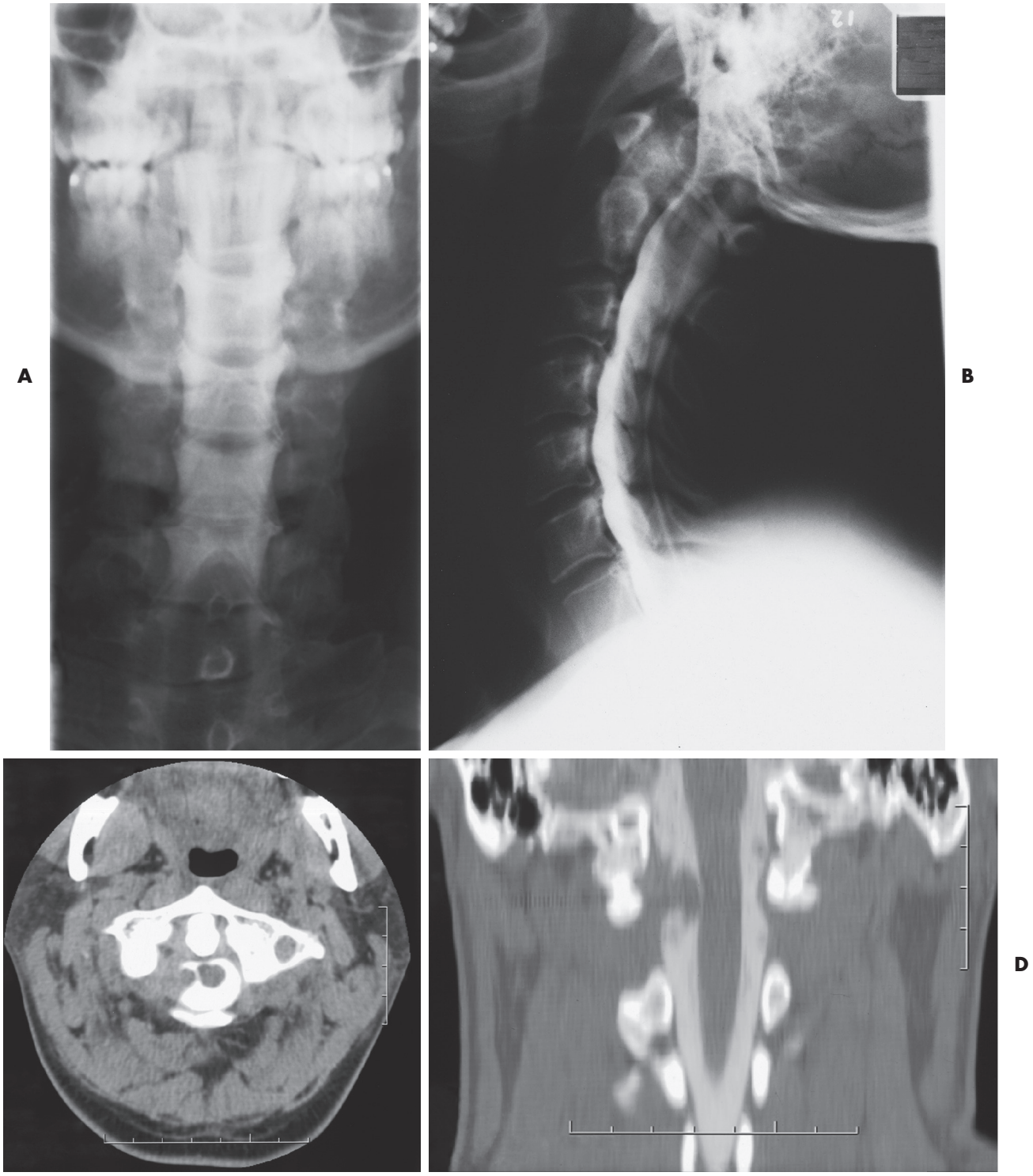

FIGURE 8-18 Spinal meningioma. On anteroposterior (A) and lateral (B) myelogram images, the spine appears normal. Axial (C) and coronal (D) CT scans obtained after the subarachnoid injection of contrast material demonstrate a meningioma as a filling defect at the level of C1–C2.

of paramagnetic contrast material significantly improves diagnostic sensitivity in patients with tiny secreting pituitary tumors. Immediately after injection, small microadenomas appear hypointense relative to the normally enhancing pituitary gland. On delayed scans, the neoplasm may become hyperintense relative to the normal gland.

Although plain skull radiographs can show enlargement of the sella turcica, erosion of the dorsum sellae, and a double floor resulting from the unequal downward growth of the mass, this imaging modality is now of value only in the incidental detection of sellar enlargement on images taken for other purposes.

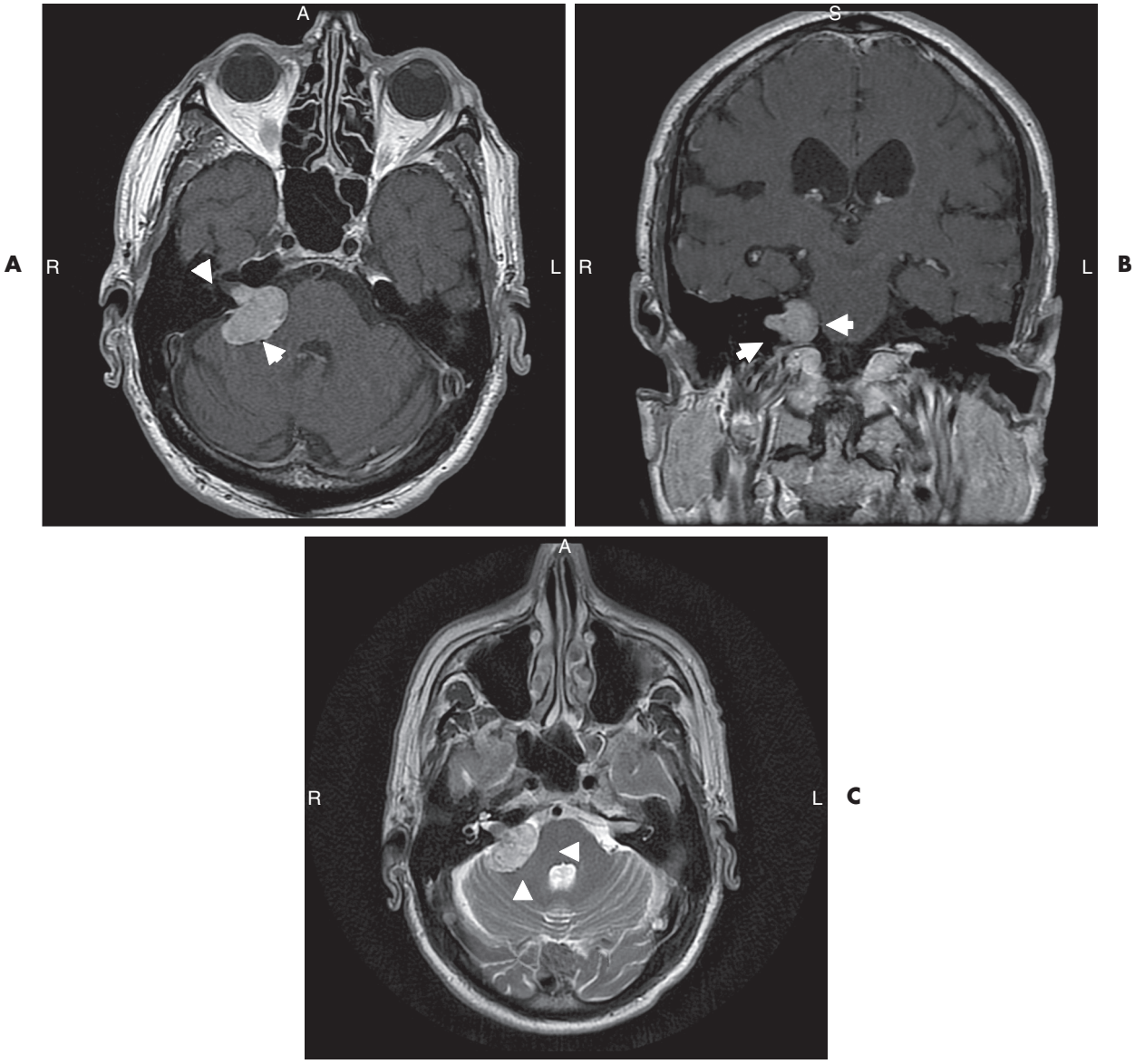

FIGURE 8-19 Acoustic neuroma. MR T1-weighted axial **(A)** and coronal **(B)** and T2-weighted axial **(C)** images show considerable contrast enhancement of the right-sided lesion (*arrows*). Note the normal neural structures on the left.

Treatment. The size of the pituitary adenoma determines the extent of the treatment. For pituitary tumors not extending beyond the gland, surgical transsphenoidal resection has a good prognosis. Adenomas extending beyond the pituitary require surgical resection followed by radiation therapy for best results. The new stereotactic radiosurgery (Gamma Knife®) is another therapeutic alternative which requires no incision. Multiple gamma radiation beams are directed at the target.

Craniopharyngioma

Craniopharyngiomas are benign tumors that contain both cystic and solid components and usually occur in patients younger than 20 years. They generally originate above the sella turcica, from embryonic remnants, depressing the optic chiasm and extending up into the third ventricle. Less commonly, a craniopharyngioma lies within the sella, where it compresses the pituitary gland and may erode adjacent bony walls.

Imaging appearance. Most craniopharyngiomas have calcification that can be detected on plain skull images or CT scans (Figure 8-23). In cystic lesions, the shell-like calcification lies along the periphery of the tumor; in mixed or solid lesions, the calcification is nodular, amorphous, or cloudlike. CT clearly demonstrates the cystic and solid components (isoattenuating) of the multilobulated mass. After the intravenous administration of contrast material, there is variable enhancement, depending on the type of calcification within the tumor and the size of its cystic component (Figure 8-24). CT can also demonstrate hydrocephalus if the tumor has expanded to obstruct one or both of the foramina of Monro.

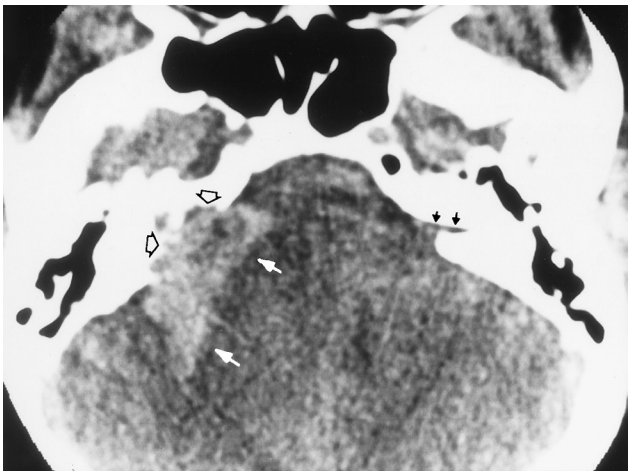

FIGURE 8-20 Acoustic neuroma. CT scan shows widening and erosion of the right internal auditory canal (*open arrows*) associated with a large extra-axial mass (*white arrows*) in the right cerebellopontine angle. *Small black arrows* point to the normal internal auditory canal on the left.

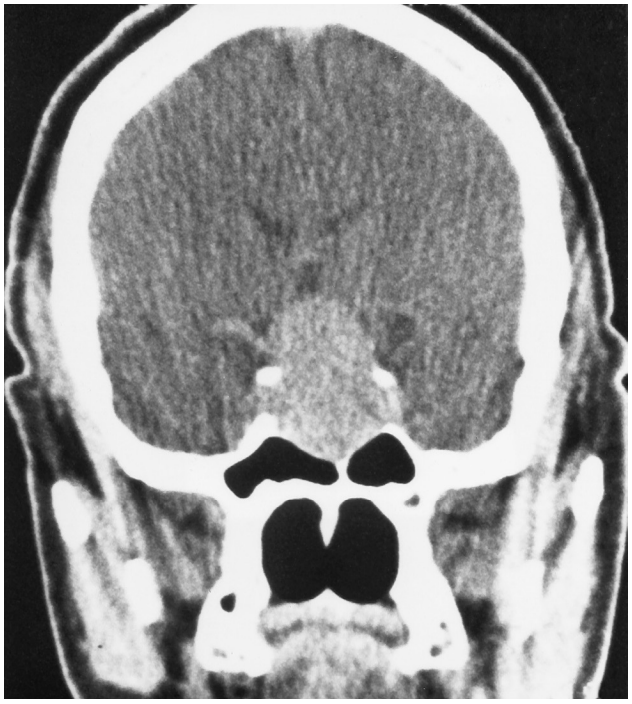

FIGURE 8-21 Pituitary adenoma. Coronal CT scan shows enhancing mass filling and extending out from pituitary fossa. Note the erosion of the base of the sella.

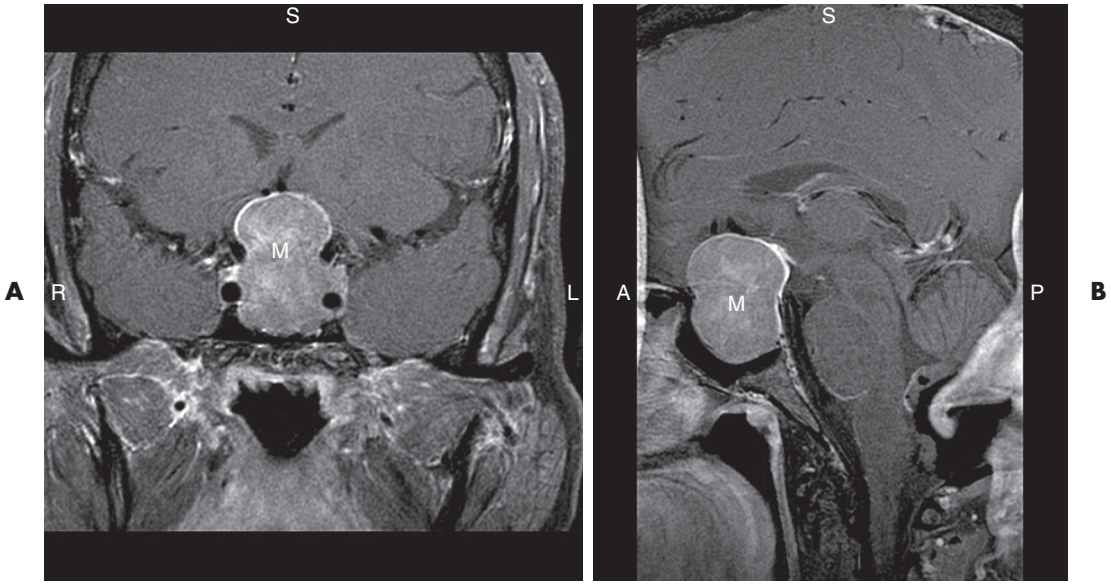

FIGURE 8-22 Pituitary adenoma. Sagittal **(A)** and coronal **(B)** T1-weighted contrast-enhanced MR images demonstrate a large mass (M) that arises from sella turcica and extends upward to fill the suprasellar cistern.

The MRI appearance of craniopharyngioma depends on the tissue components of the tumor. Cystic areas have low signal intensity on T1-weighted images and high signal intensity on T2-weighted images; fat-containing regions have high signal intensity on T1-weighted images and show moderate signal intensity on T2-weighted images (Figure 8-25). Large areas of calcification appear dark on all imaging sequences. Newer MR sequences—gradient-echo, fluid-attenuated inversion recovery, spectroscopy, and diffusion imaging—assist in differentiating tumor consistency.

Treatment. One current treatment is MR-guided stereotactic resection via microsurgery. Some tumors are completely resectable; for others, surgical debulking and radiation therapy are performed. Surgery and radiation therapy, either alone or in combination, may provide long-term control in many patients.

FIGURE 8-23 Craniopharyngioma. Plain skull radiograph shows a large suprasellar calcified mass in a child.

FIGURE 8-24 Craniopharyngioma. CT scan shows rim-enhancing tumor that contains dense calcification (*straight arrows*) and has a large cystic component (*curved arrows*) that extends into the posterior fossa. Note the associated hydrocephalus.

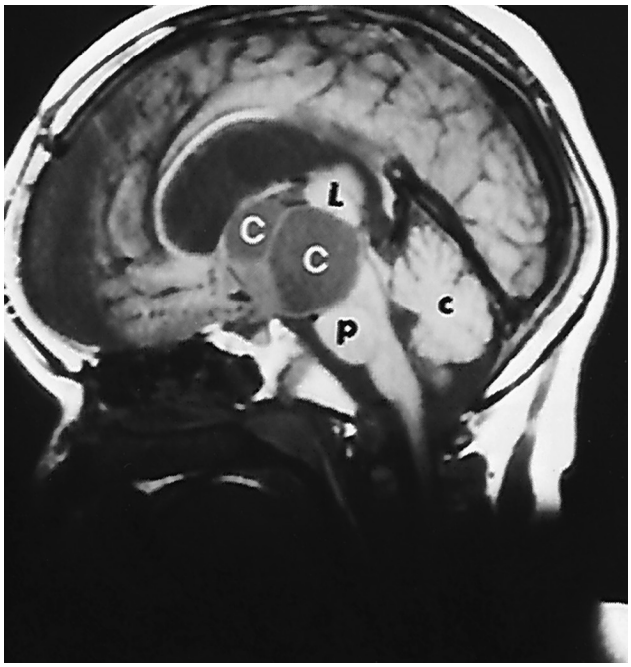

FIGURE 8-25 Craniopharyngioma. Sagittal MR image demonstrates a large multiloculated suprasellar mass with cystic (C) and lipid (L) components. *c,* Cerebellum; *p,* pons.

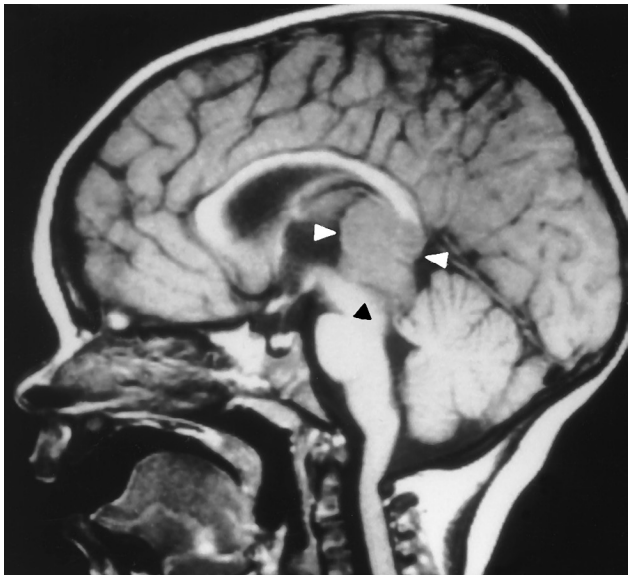

FIGURE 8-26 Pineal germinoma. Sagittal T1-weighted MR image shows a large isointense mass (*white arrowheads*) that compresses the midbrain (*black arrowhead*) and elevates the splenium of the corpus callosum.

Pineal Tumors

The most common tumors of the pineal gland are germinomas and teratomas, rapidly growing germ cell tumors, both of which occur predominantly in males younger than 25 years and may be associated with precocious puberty.

Imaging appearance. Sagittal MR images are ideal for showing pineal tumors, which typically compress the midbrain from above and lift up the splenium of the corpus callosum (Figure 8-26). Although most germinomas are isointense to brain on both T1- and T2-weighted images, teratomas may have mixed signal intensity because they have cystic components and contain fat.

On CT, germinomas appear as hyperdense or isodense masses that tend to deform or displace the posterior aspect of the third ventricle and often obliterate the quadrigeminal cistern. Punctate calcification can often be detected within the mass. Intense enhancement of the tumor occurs after the injection of contrast material. Teratomas in the pineal

region typically appear as hypodense masses with internal calcification (Figure 8-27). Occasionally, other formed elements (e.g., teeth) are seen. Contrast enhancement is usually much less pronounced than with germinomas. Large pineal tumors may cause obstructive hydrocephalus with ventricular dilation.

A small number of tumors with the histologic appearance of pinealomas appear elsewhere in the brain at some distance from the normal pineal gland. These "ectopic pinealomas" generally occur in the anterior aspect of the third ventricle or within the suprasellar cistern. They may produce the clinical triad of bitemporal hemianopsia, hypopituitarism, and diabetes insipidus that simulates a craniopharyngioma.

Treatment. Surgery is the initial therapy of choice for pineal tumors. Radiation therapy following surgery may be helpful. Chemotherapy is used with radiation therapy if surgery is not a viable option.

Chordoma

Chordomas are tumors that arise from remnants of the notochord (the embryonic neural tube). Although any part of the vertebral column and base of the skull can be involved, the most common sites are the clivus and the lower lumbosacral region. The tumors are locally invasive but do not metastasize. Chordomas arising at the base of the skull produce the striking clinical picture of multiple cranial nerve palsies on one or both sides combined with a retropharyngeal mass and erosion of the clivus.

FIGURE 8-27 Pineal teratoma. Nonenhanced CT scan shows an inhomogeneous mass containing a large amount of calcification.

Imaging appearance. On plain radiographs, a chordoma tends to be a bulky mass, causing ill-defined bone destruction or cortical expansion. Flocculent (fluffy or cloudlike) calcification may develop within a large soft tissue mass (Figure 8-28A). On CT scans, chordomas at the base of the skull tend to appear as lesions that are slightly denser than brain tissue and often demonstrate moderate contrast enhancement (Figure 8-28B). Sagittal MR images best demonstrate the clival origin of the mass and its effect on surrounding structures (Figure 8-29). Three-dimensional gradient-echo T1-weighted sequences are best for demonstrating the clival region. With gadolinium enhancement, chordomas have heterogeneous intensity and ring enhancement.

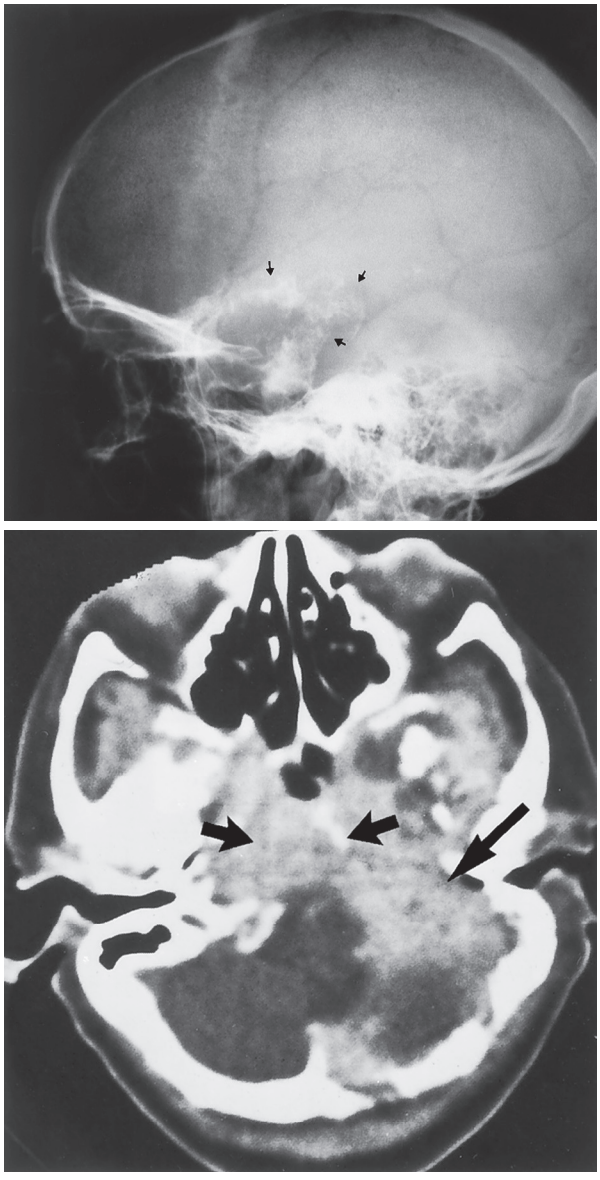

FIGURE 8-28 Chordoma. (A) Plain skull radiograph shows dense calcification (*arrows*) within a large soft tissue mass that has eroded the dorsum sellae and the upper portion of the clivus. **(B)** In another patient, a CT scan shows an enlarging mass with destruction of the entire clivus (*short arrows*) and only small bone fragments remaining. The left petrous pyramid is also destroyed (*long arrow*).

Treatment. Chordomas of the clivus region are difficult to completely remove surgically, and thus the patient usually is also treated with radiation. For chordomas of the lumbar region, complete surgical resection is usually possible.

Metastatic Carcinoma

Carcinomas usually reach the brain by hematogenous spread. Infrequently, epithelial malignancies of the nasopharynx can spread into the cranial cavity through neural foramina or by direct invasion through bone. The most common neoplasms that metastasize to the brain arise in the lung and breast. Melanomas, colon carcinomas, and testicular and kidney tumors also cause brain metastases.

Imaging appearance. On T2-weighted MR images, metastases appear as single or multiple masses of high signal intensity that are most commonly situated at the junction between gray matter and white matter (Figure 8-30). Additional lesions can often be demonstrated after the injection of a paramagnetic contrast agent. On CT, brain metastases typically appear as multiple enhancing lesions of various sizes surrounded by different amounts of low-density edema (Figures 8-31 and 8-32). On noncontrast scans, metastatic deposits may be hypodense, hyperdense, or similar in density

FIGURE 8-29 Clival chordoma. Sagittal MR image shows a low-intensity multilobulated mass deforming and displacing the brainstem, destroying the clivus, and extending into the sella turcica (*upper arrowhead*) and nasopharynx (two lower *arrowheads*).

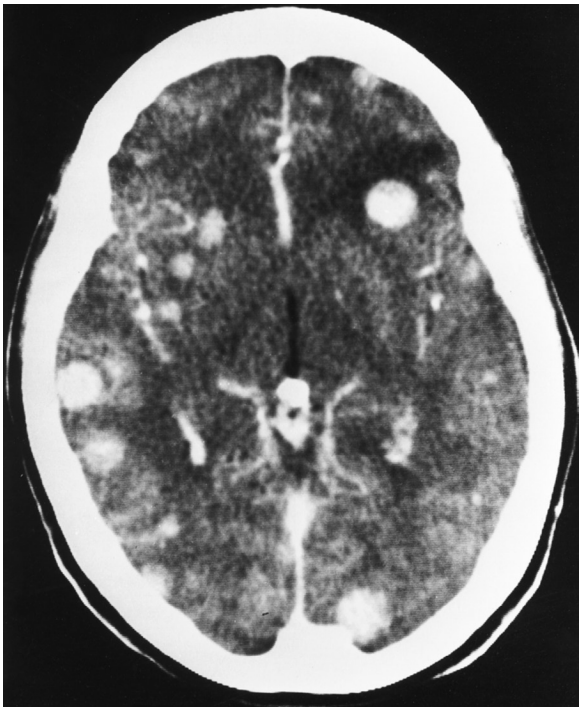

FIGURE 8-31 Brain metastases. CT scan shows multiple enhancing masses of various shapes and sizes representing hematogenous metastases from carcinoma of the breast.

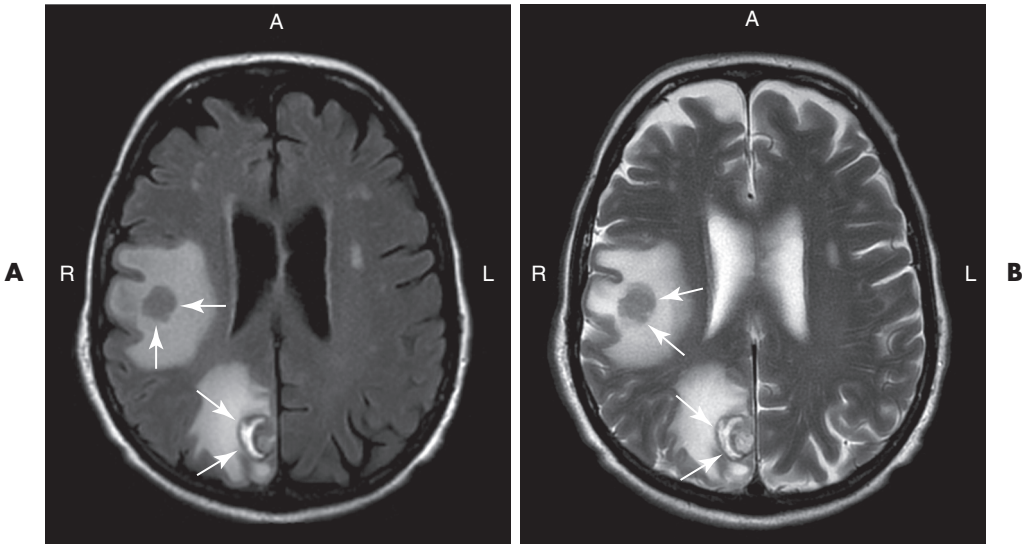

FIGURE 8-30 Brain metastases. Axial T2-weighted **(A)** and FLAIR **(B)** MR images demonstrate two large masses (*arrows*) surrounded by extensive high–signal intensity edema.

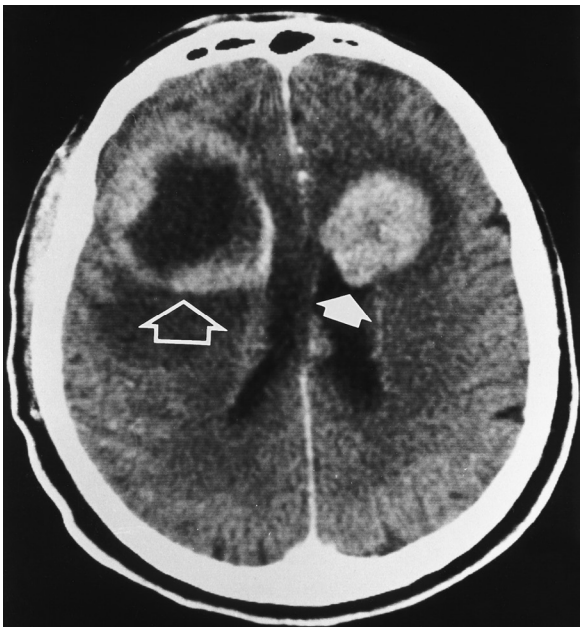

FIGURE 8-32 Brain metastases. CT scan shows enhancing metastases from squamous cell carcinoma of lung that are both ring enhancing (*open arrow*) and solid (*solid arrow*).

to normal brain tissue, depending on such factors as cellular density, tumor neovascularity, and degree of necrosis. In general, metastases from lung, breast, kidney, and colon tend to be hypodense or isodense; hyperdense metastases often reflect hemorrhage or calcification within or adjacent to the tumor.

Single metastatic deposits in the brain may be indistinguishable from primary tumors. However, because primary brain neoplasms are unusual in older patients, single lesions in this population should suggest metastatic disease.

Treatment

The number of lesions determines the choice of therapy. Single metastatic lesions or second-year postprimary (residual or regrowth) lesions require surgical intervention, which may provide relief from symptoms. Multiple metastases require irradiation or chemotherapy. Radiation therapy can be applied to the whole brain or by the gamma knife. Systemic chemotherapy is used if metastasis occurs after radiation treatment. Surgery combined with whole-brain radiation therapy is the most successful treatment.

Summary of Findings for Tumors of the Central Nervous System

Disorder	Location	Imaging Appearance	Treatment
Glioma	Glial cells in CNS	MRI—masses of high signal intensity on T2-weighted images, and of low signal intensity or isointensity on T1-weighted images CT (noncontrast)—a single heterogeneous mass (isodense to hypodense) CT (contrast enhanced)—a homogeneous lesion with an irregular ring of enhancement	Depends on location and histology Astrocytomas: good 5-year survival rate with surgery and radiation therapy Ependymomas of the filum terminale: surgical removal provides the most favorable prognosis
Meningioma	Arises from arachnoid lining and is attached to the dura Spinal	MRI—isointense lesion on T1- and T2-weighted images; hyperintense on contrast-enhanced T1- and T2-weighted images CT—rounded, sharply delineated, hyperdense (75%) tumor MRI—T1- and T2-weighted images that have been contrast enhanced appear as homogenous intense lesions CT myelography—location of mass as a filling defect	Surgical resection is very successful because of the superficial position of the tumor and the lack of tumor infiltration
Acoustic neuroma	Schwann's cells of cranial nerve VIII	MRI—T1-weighted images show focal or generalized enlargement of cranial nerve VIII CT—best demonstrates bone involvement	Surgical excision of the lesion, or gamma knife radiosurgery, to improve symptoms
Pituitary adenoma	Most commonly from anterior lobe of the pituitary gland	CT—large tumor typically homogeneous and hyperdense in comparison with normal brain tissue, bone erosion, and tumor extension MRI—T1-weighted images show hypointense mass associated with contralateral deviation MRI (contrast enhanced)—the microadenoma becomes hypointense initially; delayed scans demonstrate hyperintensity of the tumor	Surgical resection by transsphenoidal approach Radiation therapy if tumor extends beyond pituitary gland Gamma Knife radiosurgery an alternative

Summary of Findings for Tumors of the Central Nervous System—cont'd

Disorder	Location	Imaging Appearance	Treatment
Craniopharyngioma	Usually superior to sella turcica	CT—possible calcification in mass with cystic and solid components MRI—cystic regions produce low signal intensity on T1-weighted images, high signal intensity on T2-weighted images; fatty regions produce hyperintense signals on T1-weighted images	MR-guided stereotactic microsurgery for resection For unresectable tumors, surgical debulking followed by radiation therapy
Pineal tumor	Germ cell tumors of the pineal gland	MRI—sagittal images demonstrate compression of midbrain; germinomas are isointense on T1- and T2-weighted images; teratomas produce a mixed signal intensity because of their cystic components and fat CT—germinomas hyperdense or isodense, displacing third ventricle, and show intense contrast enhancement; teratomas are hypodense masses with internal calcifications	Surgery (first choice) followed by radiation therapy Chemotherapy with radiation therapy when surgery is not an option
Chordoma	Arises from the embryonic neural tube	Radiograph—ill-defined bone destruction or cortical expansion CT—base-of-skull mass is slightly denser than brain tissue and only moderately enhanced MRI—three-dimensional gradient-echo T1-weighted sequences in the sagittal plane best demonstrate the clival area and surrounding structures; gadolinium enhancement produces heterogeneous intensities with border-ring enhancement	Clival region—surgical resection followed by radiation therapy Lumbar area—complete surgical resection
Metastatic carcinoma	Carcinoma reaching the brain by hematogenous spread	MRI—single or multiple masses of high signal intensity; additional lesions often seen with paramagnetic contrast agent CT—multiple enhancing lesions of various sizes with areas of low density surrounding edema	Single lesion: surgical resection Multiple lesions: whole-brain radiation; chemotherapy if metastasis occurs after radiation therapy

TRAUMATIC PROCESSES OF THE BRAIN AND SKULL

In the patient with head trauma, the purpose of radiographic imaging is to detect a surgically correctable hematoma. Emergency CT has virtually replaced all other radiographic investigations in patients with suspected neurologic dysfunction resulting from head injury. Because the presence or absence of a skull fracture does not correlate with intracranial abnormalities, plain radiographs of the skull are no longer indicated in the patient with head trauma.

Because of medicolegal reasons and the fear of missing a skull fracture, CT scans (and plain skull radiographs) are often overused. The following indications have been established for the use of radiographic procedures in the patient with head trauma:

1. Unexplained focal neurologic signs
2. Unconsciousness (including the unarousable alcoholic)
3. Documented decreasing level of consciousness or progressive mental deterioration
4. History of previous craniotomy with shunt tube in place
5. Skull depression or subcutaneous foreign body palpable or identified by a probe through a laceration or puncture wound
6. Hemotympanum or fluid discharge from the ear
7. Discharge of CSF from the nose
8. Ecchymosis over the mastoid process (Battle's sign)
9. Bilateral orbital ecchymoses (raccoon eyes)

Skull Fracture

Imaging appearance. A **linear skull fracture** appears on a plain radiograph as a sharp lucent line that is often irregular or jagged and occasionally branches (Figure 8-33). The fracture must be distinguished from suture lines, which generally have serrated edges and tend to be bilateral and symmetrical, and vascular grooves, which usually have a smooth curving course and are not as sharp or distinct as a fracture line. The location of a linear skull fracture can indicate possible complications. A fracture that crosses a dural vascular groove may cause vessel laceration, leading to an epidural hematoma.

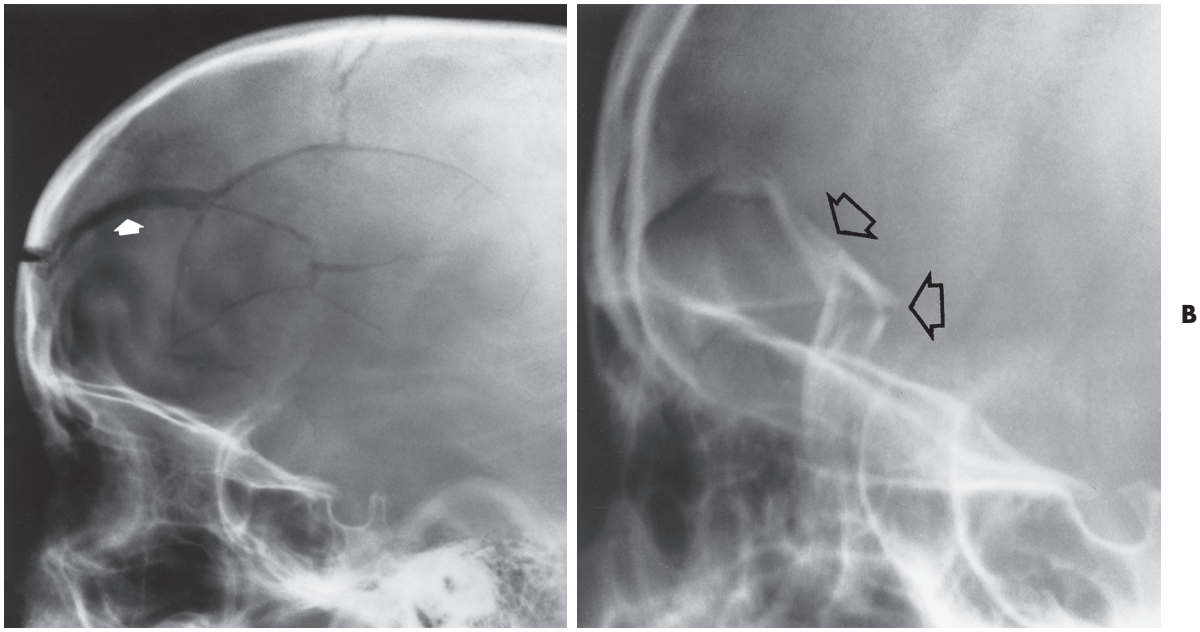

FIGURE 8-33 Skull fracture. (A) Lateral projection of the skull shows a widely separated fracture (*arrow*) extending to a star-shaped array of linear fractures. (B) In another patient, lateral projection shows a severely depressed skull fracture (*arrows*).

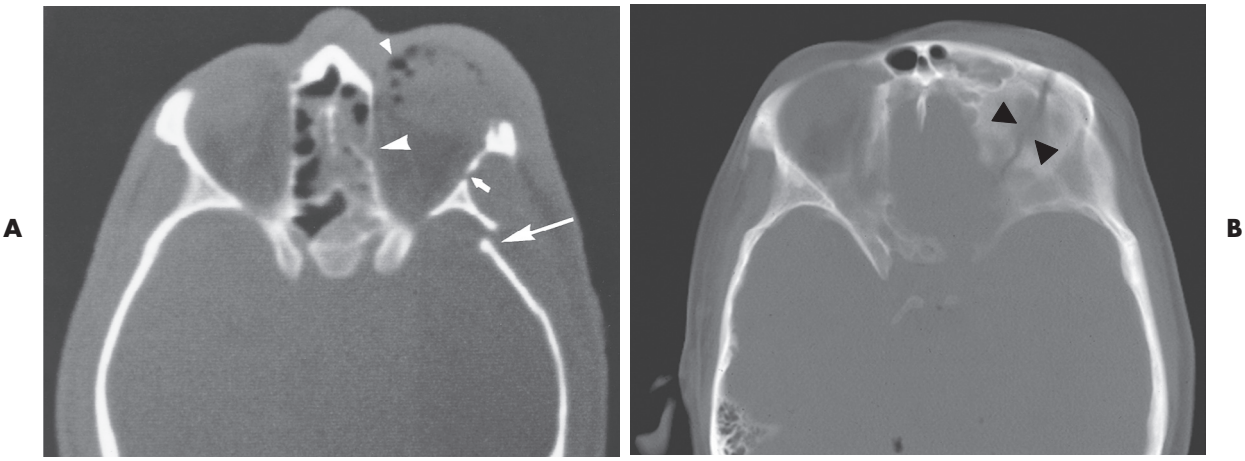

FIGURE 8-34 Skull fracture. (A) CT bone-window image demonstrates depressed temporal fracture (*long arrow*). Note the lateral orbital wall fracture (*short arrow*), the medial orbital wall fracture (*large arrowhead*), and the ethmoid opacification caused by hemorrhage. Also, air can be seen in the orbital soft tissues (*small arrowhead*), resulting from medial fracture into the ethmoids. (B) Trauma resulted in a nondisplaced fracture in the supraorbital plate (*black arrowheads*) in this 24-year-old woman.

A fracture involving the sinuses or mastoid air cells may result in post-traumatic pneumocephalus, with air seen in the ventricles on plain radiographs. A **diastatic fracture** is a linear fracture that intersects a suture and courses along it, causing sutural separation.

More severe trauma, especially if localized to a small area of the skull, may force a fragment of bone to be separated and depressed into the cranial cavity (Figure 8-34). The underlying dura is frequently torn, and there is a relatively high incidence of cerebral parenchymal injury. **Depressed fractures** are often stellate (star shaped), with multiple fracture lines radiating outward from a central point. When the fracture is viewed en face, the overlap of fragments makes the fracture line appear denser than the normal bone. Tangential views are required to determine the amount of depression.

Fractures limited to the base of the skull are often hidden by the complex basal anatomy and may be very difficult to visualize on plain radiographs. A finding suggestive of a basilar skull fracture is an air–fluid level in the sphenoid sinus seen on an erect or cross-table lateral projection of the skull obtained with a horizontal x-ray beam. CT can demonstrate the presence of blood or fluid in the basilar cisterns and show

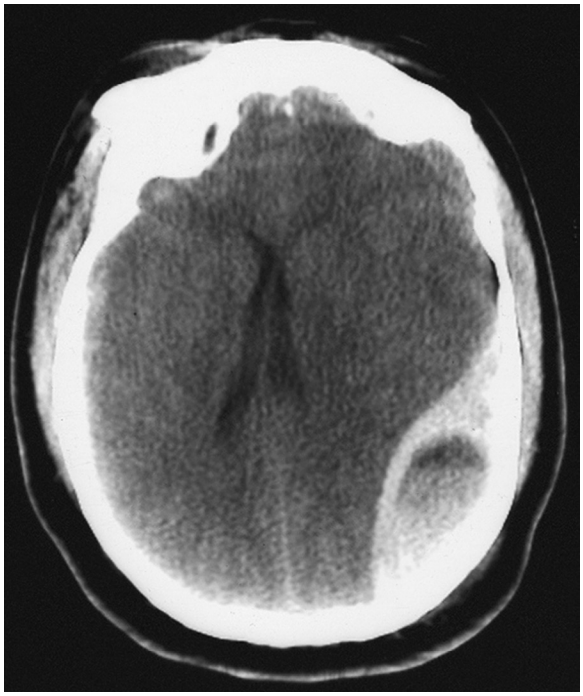

FIGURE 8-35 Acute epidural hematoma in a trauma patient. CT scan illustrates the characteristic lens-shaped epidural hematoma. The mass effect associated with the hematoma causes midline shift.

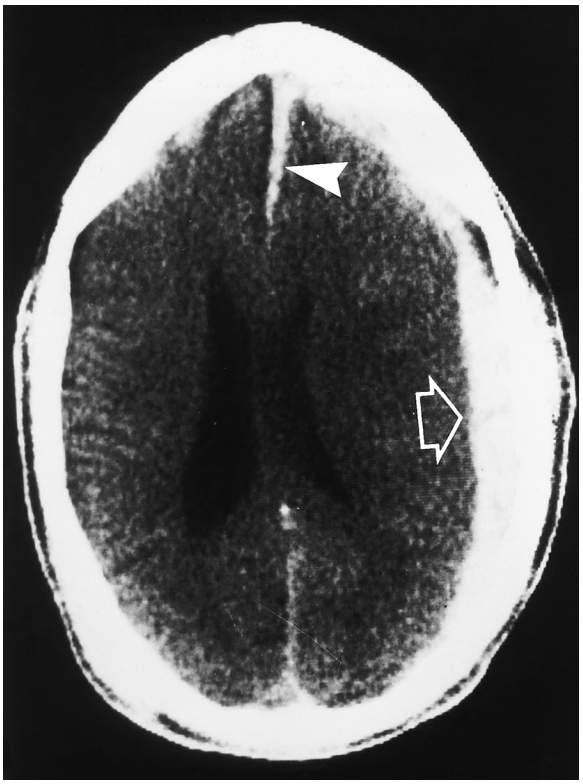

FIGURE 8-36 Acute subdural hematoma. A high-density, crescent-shaped lesion (*arrow*) is adjacent to the inner table of the skull. Hematoma extends into interhemispheric fissure (*arrowhead*).

some basilar skull fractures (using bone windows) that are not visible on routine skull radiographs. Potential complications of basal skull fractures include leakage of CSF, meningitis, and damage to the facial nerve or auditory apparatus within the petrous bone.

It must be emphasized that the presence or absence of a skull fracture does not correlate with intracranial abnormalities. Indeed, serious treatable intracranial hematomas can be present without skull fractures.

Treatment. The severity and location of the fracture and the complications resulting from the trauma determine the treatment.

Epidural Hematoma

Epidural hematomas are caused by acute arterial bleeding and most commonly form over the parietotemporal convexity. Acute arterial bleeding is usually caused by laceration of the medial meningeal artery. Because of a high arterial pressure, epidural hematomas rapidly cause significant mass effect and acute neurologic symptoms.

Imaging appearance. Because the dura is very adherent to the inner table of the skull, an epidural hematoma typically appears as a biconvex (lens-shaped), peripheral, high-density lesion (Figure 8-35). There is usually a shift of the midline structures toward the opposite side unless a contralateral balancing hematoma is present. If not promptly recognized, an epidural hematoma can lead to rapid progressive loss of consciousness, dilation of the ipsilateral pupil, compression of the upper midbrain, and eventually compression of the entire brainstem and death.

Treatment. To prevent death, emergency surgical decompression is required to relieve intracranial pressure.

Subdural Hematoma

Subdural hematomas reflect venous bleeding, most commonly from ruptured veins between the dura and meninges. Symptoms may occur within the first few minutes; however, because of the low pressure of venous bleeding, patients with subdural hematomas tend to have a chronic course with symptoms of headache, agitation, confusion, drowsiness, and gradual neurologic deficits.

Imaging appearance. An acute subdural hematoma typically appears on CT scans as a peripheral zone of increased density that follows the surface of the brain in a crescentic shape adjacent to the inner table of the skull (Figure 8-36). On CT, the finding of isodense to hypodense areas within a hyperdense hematoma indicates rapid bleeding with an accumulation of unclotted blood. There is usually an associated mass effect with displacement of midline structures and obliteration of sulci over the affected hemisphere. The absence of displacement away from the side of a lesion may indicate the not infrequent presence of bilateral subdural hematomas. On MR images, a subdural hematoma is detectable within a few days as an extra-axial mass of high signal intensity representing the accumulation of methemoglobin (Figure 8-37).

Serial CT scans demonstrate a gradual decrease in the attenuation value of a subdural hematoma over a period of weeks.

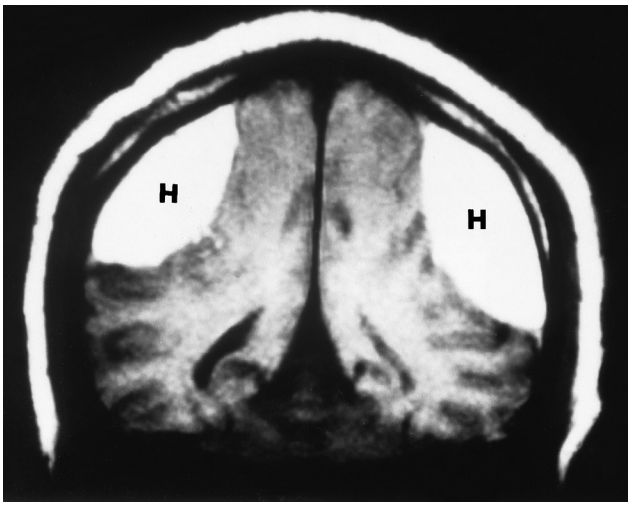

FIGURE 8-37 Bilateral subdural hematoma. Coronal MR image shows the high signal intensity of bilateral subdural collections (H).

With absorption and lysis of the blood clot, the hematoma becomes isodense with normal brain tissue, and the lesion may be identified only because of its mass effect. At this stage, scanning after the administration of contrast material may be of value because of enhancement of the membrane around the subdural hematoma and identification of the cortical veins. MR imaging of a lesion that is isodense on CT may show medial displacement of the superficial cerebral veins, an indication of an extracerebral mass and the entire extent of the hematoma over the cerebral convexity. A chronic subdural hematoma has a density similar to that of spinal fluid (Figure 8-38). Occasionally, the small bridging veins associated with a chronic subdural hematoma may bleed and produce the difficult problem of an acute subdural hematoma superimposed on a chronic one.

Treatment. In small subdural hematomas without any inclination to rebleed, the hemorrhage resorbs naturally, and no treatment is necessary. Severe subdural hematomas require surgical ligation and evacuation of the hematoma to prevent transtentorial herniation. Less invasive methods of decreasing intracranial pressure include drug therapy and placement of an intraventricular catheter to remove CSF, which may prevent herniation.

Cerebral Contusion

Cerebral contusion is an injury to brain tissue caused by movement of the brain within the calvaria after blunt trauma to the skull. Contusions occur when the brain contacts rough skull surfaces, such as the superior orbital roof and petrous ridges. The patient loses consciousness and cannot remember the traumatic event.

Imaging appearance. Cerebral contusions typically appear on CT scans as low-density areas of edema and tissue necrosis, with or without nonhomogeneous density zones, reflecting multiple small areas of hemorrhage (Figure 8-39). The frontal and anterior temporal regions are the most common sites of injury. After the administration of intravenous contrast material, contusions generally enhance for several weeks after the injury because of a breakdown of the blood–brain barrier (BBB). On MR images, the cerebral edema causes high signal intensity on T2-weighted images; associated areas of hemorrhage may produce high–signal intensity regions on T1-weighted scans.

FIGURE 8-38 CT scan of chronic left subdural hematoma. Crescent-shaped high- and low-density regions in the left parietal area. The anterior is isodense (chronic hygroma); posteriorly, a hyperdense crescent shape resulting from acute bleeding can be seen. Midline shift and dilated right lateral ventricle are evident.

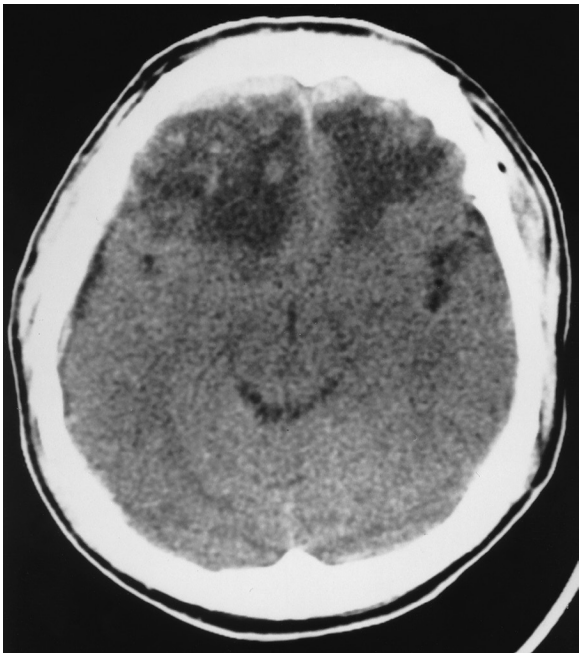

FIGURE 8-39 Cerebral contusion. CT scan shows small punctate hemorrhages (high density) within extensive areas of edema (low density).

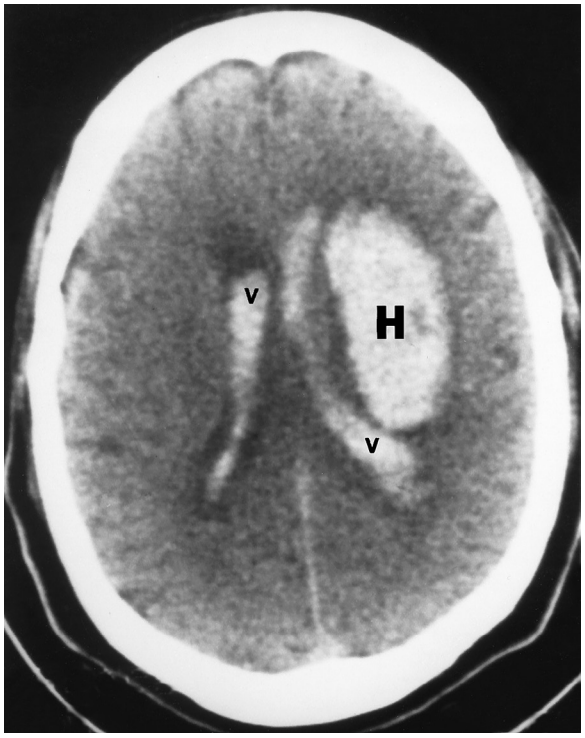

FIGURE 8-40 Intracerebral hematoma. Note the large, homogeneous, high-density area (H) with acute bleeding into lateral ventricles (v).

Treatment. The patient with a cerebral contusion is hospitalized to allow observation of any changes in neurologic function. If the contusion causes swelling, medications to decrease intracranial pressure are prescribed. Surgery is usually not necessary.

Intracerebral Hematoma

Traumatic hemorrhage into the brain parenchyma can result from shearing forces to intraparenchymal arteries, which tend to occur at the junction of the gray and white matter. Injury to the intima of intracranial vessels can cause the development of traumatic aneurysms, which can rupture.

Imaging appearance. On CT scans, an intracerebral hematoma appears as a well-circumscribed, homogeneous, high-density region that is usually surrounded by areas of low-density edema (Figure 8-40). As the blood components within the hematoma disintegrate, the lesion eventually becomes isodense with normal brain (usually 2 to 4 weeks after injury). On MR images, the hematoma shows high signal intensity. A chronic hematoma filled with hemosiderin appears black on T2-weighted images.

Treatment. Although most intracerebral hematomas develop immediately after head injury, delayed hemorrhage is common. This is especially frequent after the evacuation of acute subdural hematomas that are compressing (tamponading) potential bleeding sites. Therefore, repeat CT or MRI is often performed within 48 hours in patients who have undergone decompressive surgery.

Subarachnoid Hemorrhage

Injury to surface veins, cerebral parenchyma, or cortical arteries can produce bleeding into the ventricular system, known as subarachnoid hemorrhage.

Imaging appearance. On a CT scan, a subarachnoid hemorrhage appears as increased density within the basilar cisterns, cerebral fissures, and sulci. Identification of the falx cerebri, straight sinus, or superior sagittal sinus on noncontrast CT scans is often considered an indication of subarachnoid blood in the interhemispheric fissure. However, with high-resolution scanners this appearance may be seen in patients with a normal or calcified falx. MRI does not demonstrate the acute subarachnoid hemorrhage well unless a fluid-attenuated inversion recovery (FLAIR) sequence is used to demonstrate the increased signal intensity. However, T1-weighted scans can show subacute hemorrhage as a high signal intensity because of the conversion of fresh blood to methemoglobin.

Treatment. Subarachnoid hemorrhage may require surgical evacuation and vessel repair if bleeding continues. Less invasive methods of decreasing intracranial pressure include drug therapy and the placement of an intraventricular catheter to remove CSF.

Carotid Artery Injury

The extracerebral carotid arteries can be injured by penetrating trauma to the neck, such as from gunshot wounds or stabbing. Trauma to the internal carotid artery is associated in 50% of traumatic fistulas.

Imaging appearance. Angiography can demonstrate laceration of the artery or intimal damage, which may result in either dissection or thrombotic occlusion (Figure 8-41). Hyperextension injuries from motor vehicle collisions can cause intimal damage to the carotid or vertebral arteries, which may result in pseudoaneurysm formation. Traumatic arteriovenous fistulas usually arise between the internal carotid artery and the cavernous sinus. In this condition, carotid arteriography demonstrates opacification of the cavernous sinus during the arterial phase. Reverse flow from the cavernous sinus may rapidly opacify a greatly dilated ophthalmic vein. The cavernous sinus and superior ophthalmic vein appear enlarged on a CT scan. MRI normally demonstrates strong enhancement of normal venous spaces (cavernous sinus). A fistula produces a signal void as a result of high flow.

Treatment. The placement of a detachable balloon catheter within the fistula using angiographic guidance may eliminate the need for surgical intervention.

Facial Fractures

Although it is padded by overlying skin, fat, and the muscles of expression, the face consists of thin and poorly supported bone, which can easily break in response to a traumatic force. The purpose of radiographic imaging in the patient with a facial injury is to demonstrate major disruptions of the facial skeleton and displacement of fracture fragments that will affect the surgical reduction and stabilization of the fracture.

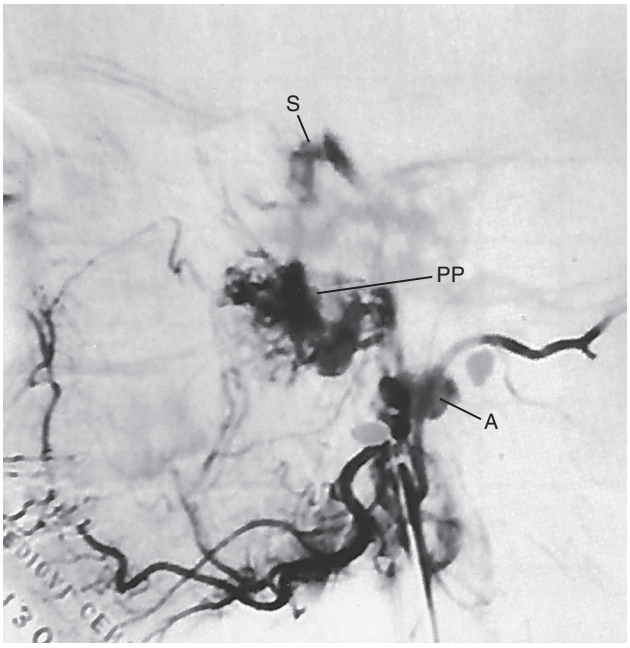

FIGURE 8-41 Post-traumatic carotid–cavernous fistula. A lateral projection of an external carotid artery angiogram shows a pseudoaneurysm (A) and rapid filling of the cavernous sinus (S) and pterygoid plexus (PP). There is total interruption of the external carotid artery trunk beyond the takeoff of the facial artery.

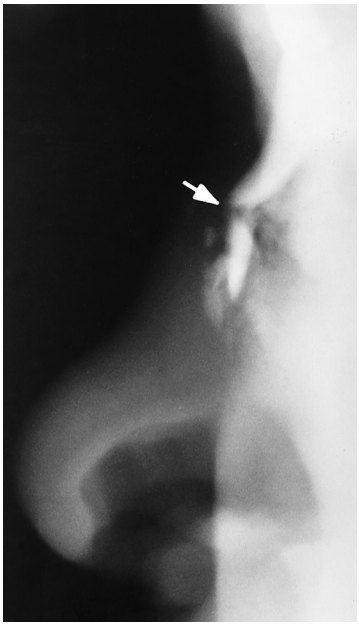

FIGURE 8-42 Nasal bones. Depressed nasal fracture (*arrow*).

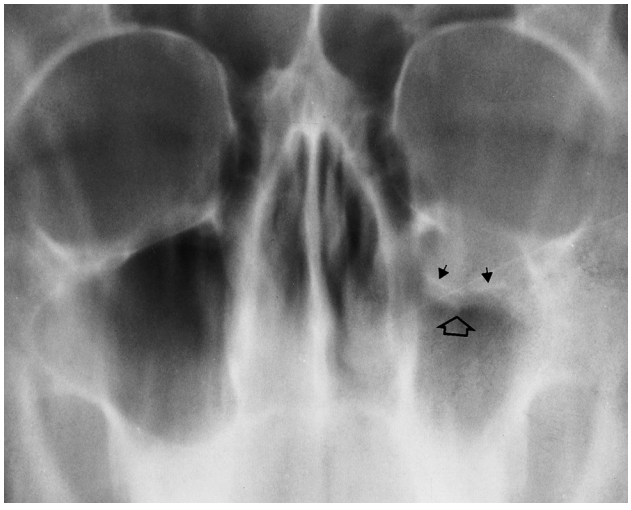

FIGURE 8-43 Blowout fracture. Conventional tomogram shows a comminuted fracture of the floor of the left orbit with inferior displacement of fracture fragments (*solid arrows*). Note the characteristic soft tissue shadow (*open arrow*) protruding through the floor into the superior portion of the maxillary sinus.

Imaging appearance. Plain radiographs of the face are usually performed as an initial screening procedure, especially in a severely traumatized patient with substantial injuries to multiple organ systems. Whenever possible, images should be obtained with the patient in the erect position to demonstrate any air–fluid levels within the sinuses that could indicate recent hemorrhage and raise the suspicion of an underlying fracture. When erect images cannot be obtained, a cross-table lateral projection using a horizontal x-ray beam will demonstrate air–fluid levels. Complex-motion (pluridirectional) tomography can blur unrelated overlying structures and thus display details of injury that are obscure or only suspected on plain radiographs. CT can demonstrate soft tissue abnormalities, such as intraorbital or retrobulbar hematomas, that are impossible to detect by conventional means. In addition, bone detail and displacement can be exquisitely demonstrated when CT window and level settings are adjusted to optimize bony structures.

Nasal bone fractures are the most common facial fractures. Isolated nasal fractures vary from simple, nondisplaced linear fractures to comminuted lesions with depression of the septum and lateral splaying of the fracture fragments (Figure 8-42). These fractures are best demonstrated on right and left (underexposed) soft tissue lateral projections, which also can define interruption of the anterior nasal spine—the anterior projection of the maxilla at the base of the cartilaginous nasal septum. Most fractures are transverse and tend to depress the distal portion of the nasal bones.

A **blowout fracture** is caused by a direct blow to the front of the orbit that causes a rapid increase in intraorbital pressure. The fracture occurs in the thinnest, weakest portion of the orbit, which is the orbital floor just above the maxillary sinus. Plain radiographs (modified Waters' method), the preferred screening study, and thin-section tomography can demonstrate most blowout fractures (Figure 8-43), although CT may be necessary for better visualization and for detecting entrapment of the extraocular muscles in the upper portion of the adjacent maxillary sinus (Figure 8-44). The fracture segment can be comminuted, with a sagging, hammock-like appearance, or can be of the trapdoor variety, with a displaced segment hanging into the antrum by a periosteal

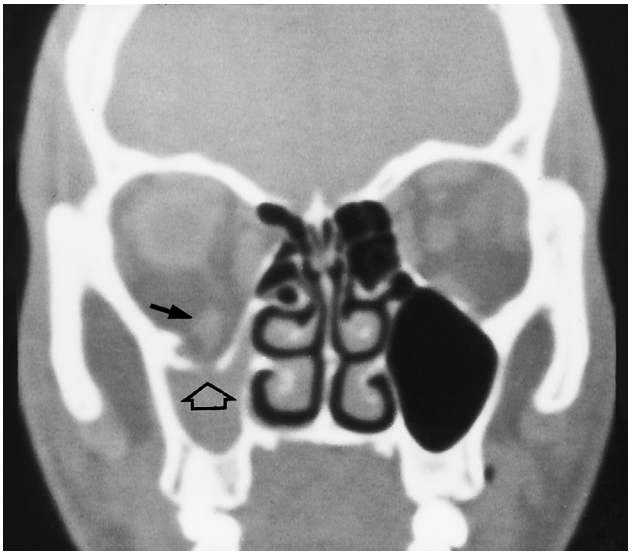

FIGURE 8-44 CT of orbital floor fracture. Coronal CT scan using bone window shows the fractured orbital floor as a double-hinged trap door with a separation in the center (*open arrow*). There is opacification of the right maxillary sinus. Note the displacement of the inferior rectus muscle (*solid arrow*) in this patient, who had limited upward gaze.

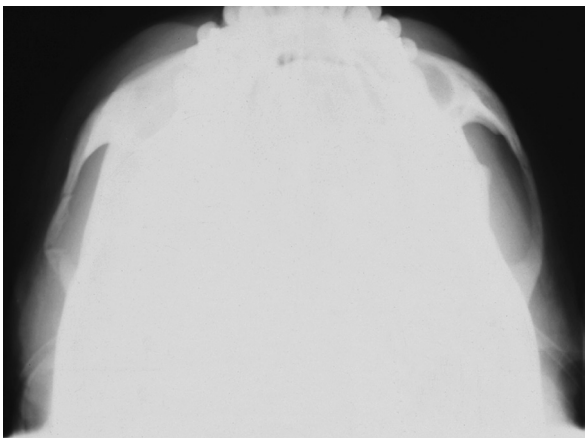

FIGURE 8-45 Zygomatic arch fracture. Submentovertex projection demonstrates two fractures on the right with depression of the zygomatic arch.

hinge. Herniation of orbital fat and extraocular muscles into the fractured orbital floor produces a characteristic soft tissue shadow protruding through the floor into the superior portion of the maxillary sinus. Opacification of the sinus caused by hemorrhage and mucosal edema is an indirect sign of orbital floor fracture. The presence of air within the orbit (orbital emphysema) indicates that there is a communication with a paranasal sinus, usually the ethmoid, as a result of an associated fracture of the medial wall of the orbit through the lamina papyracea.

The zygomatic arch is vulnerable to a blow from the side of the face, which can produce a fracture with inward displacement of the central fragments and outward displacement of

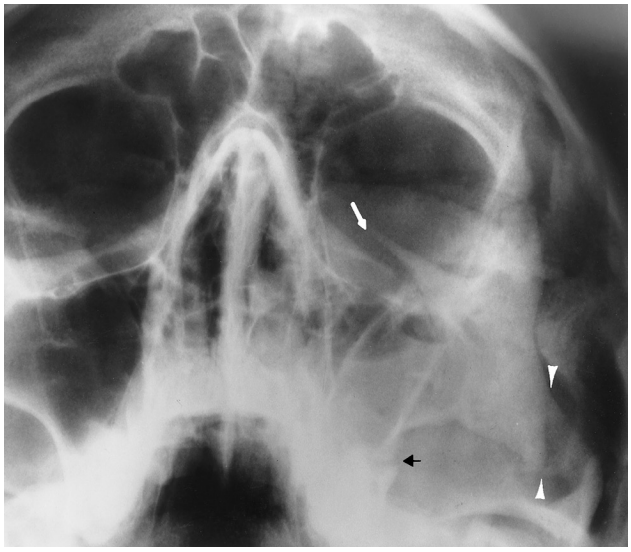

FIGURE 8-46 Tripod fracture. Interruption of the orbital rim (*white arrow*), lateral maxillary fracture (*black arrow*), and nondisplaced zygomatic arch fracture (*arrowheads*) are demonstrated.

the fragments at the zygomatic and temporal ends of the arch (Figure 8-45). **Zygomatic arch fractures** are best demonstrated on underexposed images taken in the basal (submentovertex) projection ("jug-handle" view).

A **tripod fracture** consists of fractures of the zygomatic arch and the orbital floor or rim combined with separation of the zygomaticofrontal suture (Figure 8-46). It is so named because it reflects separation of the zygoma from its three principal attachments. The resulting free-floating zygoma may cause facial disfigurement if the fracture is not diagnosed and properly treated.

The mandible is a prominent, exposed segment of the facial skeleton and is thus a common site for both intentional and accidental trauma. Plain radiographs with oblique views, combined with panoramic tomography, can demonstrate most **mandibular fractures** (Figure 8-47). The angle of the mandible is the most common site of fracture, although fractures can involve any portion of the body and the condylar and coronoid processes. Because the mandible functions essentially as a bony ring, bilateral fractures are common.

Le Fort fractures are severe injuries in which separation at the fracture site results in the formation of a large, complex, detached fragment that is unstable and may have its position altered relative to its site of origin. Le Fort fractures involve bilateral and horizontal fractures of the maxillae and are classified as type I, II, or III, depending on the extent of injury (Figure 8-48).

Treatment. Treatment for nasal bone fractures varies depending on the amount of bony displacement. Reduction is required for fractures causing deviation of the nasal septum. More severe facial fractures require surgical reconstruction, possibly using internal or external fixation devices to prevent disfigurement.

Summary of Findings for Traumatic Processes of the Brain and Skull

Disorder	Location	Imaging Appearance	Treatment
Skull fracture	Any cranial bone	Linear fracture is an irregular or jagged, sharp lucent line Depressed fracture has stellate (star-shaped) fracture lines radiating outward CT—demonstrates fracture and associated intracranial complications	Treat associated complications
Epidural hematoma	Most commonly over parietotemporal convexity	CT—biconvex peripheral high-density lesion, showing midline shift	Emergency surgery to relieve increased intracranial pressure and to stop bleeding
Subdural hematoma	Most commonly from ruptured veins between dura and meninges	CT—acute: crescent-shaped peripheral high-density lesion; chronic: isodense lesion MRI—chronic: extracerebral mass with high signal intensity	Resorption in small hematomas Surgical ligation and evacuation of hematoma Control intracranial pressure with drugs or intraventricular drainage catheter
Cranial contusion	Injury to brain tissue Frontal and anterior temporal most common	CT—low-density areas that usually enhance for several weeks MRI—increased signal intensity on both T2-weighted (cerebral edema) and T1-weighted images (if hemorrhage)	Observation for neurologic change Surgery not usually required
Intracerebral hematoma	Hemorrhage into brain parenchyma	CT—well-circumscribed, homogeneous, high-density region surrounded by low-density regions of edema MRI—high–signal intensity region; chronic hematoma is black on T2-weighted image	Surgical evacuation of hematoma
Subarachnoid hemorrhage	Injury to surface veins or cortical arteries bleeding into the ventricles	CT—increased density within the basilar cisterns, cerebral fissures, and sulci MRI—acute hemorrhage on FLAIR imaging shows as an increased signal intensity; subacute hemorrhage shows high intensity on T1-weighted images	Surgical evacuation of the hemorrhage and vessel repair Drug therapy or an intraventricular catheter to decrease intracranial pressure
Carotid artery injury	Extracerebral carotid arteries	Angiography—demonstrates laceration of artery or intimal damage CT—large cavernous sinus and superior ophthalmic vein MRI—signal void caused by large cavernous vein resulting from high flow	Placement of detachable balloon within fistula Surgical intervention to eliminate fistula
Facial fracture	Nasal bone (most common) Blowout (orbit) Tripod (zygoma separation from other facial and cranial bones) Mandible Le Fort (bilateral and horizontal fracture of maxillae)	Plain images—cranial and facial bones (upright or horizontal beam image shows fluid levels in the sinuses) CT—soft tissue abnormality and bone detail; three-dimensional imaging used for surgical planning	Reduction of fracture Some require surgery to place internal or external fixation device

FLAIR, Fluid-attenuated inversion recovery.

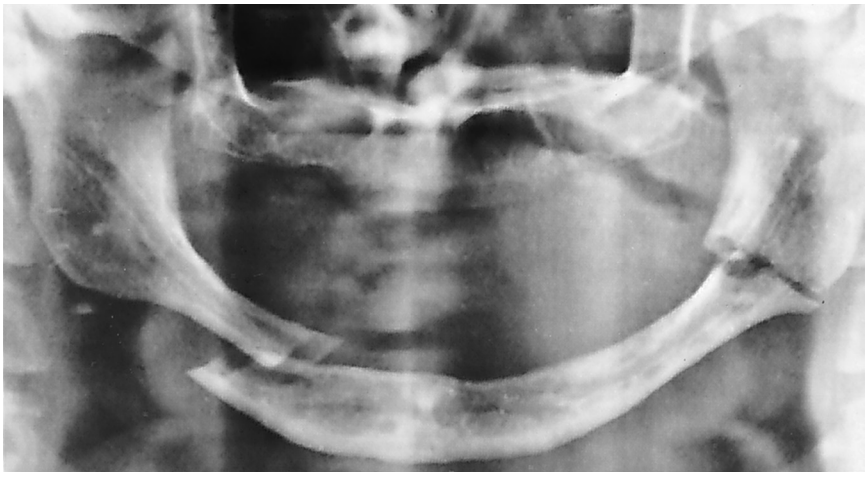

FIGURE 8-47 Mandibular fracture. Panoramic examination in edentulous (without teeth) patient shows fractures of the left angle and the right body of the mandible.

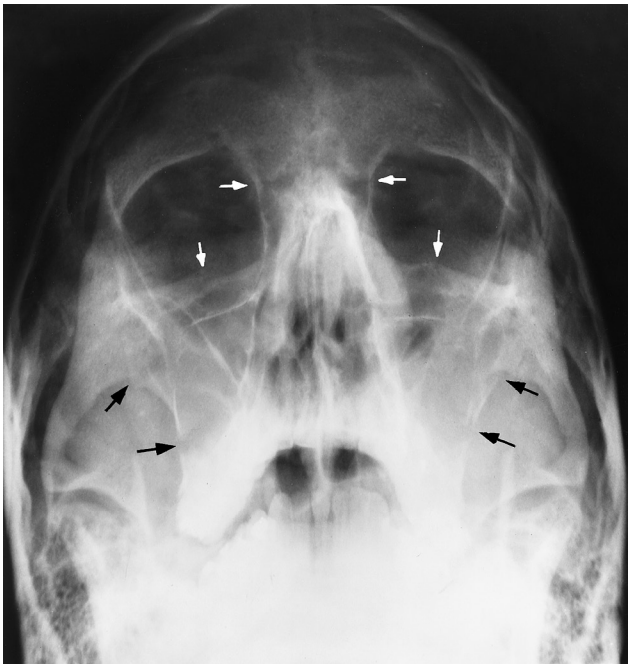

FIGURE 8-48 Le Fort II fracture. Waters' projection shows a large separated fragment produced by multiple fractures (*arrows*).

VASCULAR DISEASE OF THE CENTRAL NERVOUS SYSTEM

Cerebrovascular Disease

The term **cerebrovascular disease** refers to any process that is caused by an abnormality of the blood vessels or blood supply to the brain. Pathologic processes causing cerebrovascular disease include abnormalities of the vessel wall, occlusion by thrombus or emboli, rupture of blood vessels with subsequent hemorrhage, and decreased cerebral blood flow caused by lowered blood pressure or narrowed lumen caliber. Cerebrovascular diseases include arteriosclerosis, hypertensive hemorrhage, arteritis, aneurysms, and arteriovenous malformations (AVMs).

Imaging appearance. The radiographic evaluation of cerebrovascular disease depends on the symptoms and the most likely diagnosis. For ease of classification, cerebrovascular disease can be divided into three categories: completed stroke, transient ischemic attacks (TIAs), and intracranial hemorrhage. Imaging modalities used today include duplex color-flow Doppler ultrasound (ultrasonography), MR angiography (MRA), CT angiography (CTA), conventional angiography, and digital subtraction angiography (DSA).

Stroke Syndrome

Stroke denotes the sudden and dramatic development of a focal neurologic deficit, which may vary from dense **hemiplegia** (paralysis on one side of the body) and coma to only a trivial neurologic disorder. The specific neurologic defect depends on the arteries involved. A stroke, also known as an acute brain infarction, most commonly involves the circulation of the internal carotid arteries and is seen with symptoms that include acute **hemiparesis** (weakness of one side of the body) and **dysarthria** (difficulty speaking).

The purpose of radiographic evaluation in the patient with acute stroke is not to confirm the diagnosis of a stroke but to exclude other processes that can simulate the clinical findings (e.g., parenchymal hemorrhage and subdural hematoma). Although the abrupt onset of a stroke may permit differentiation from other conditions that have a more gradual onset of symptoms, patients with focal neurologic deficits of various causes may initially be found comatose so that the history of gradual onset is not elicited. Clearly, it is essential to exclude an intracranial hemorrhage before considering the possibility of using anticoagulant therapy in a patient with stroke.

Imaging appearance. Noncontrast CT (or MRI, if available) is the examination of choice for the evaluation of the patient with stroke. Intravenous contrast material is contraindicated because it is a toxic substance that can cross the disrupted blood–brain barrier in the region of a cerebral infarct

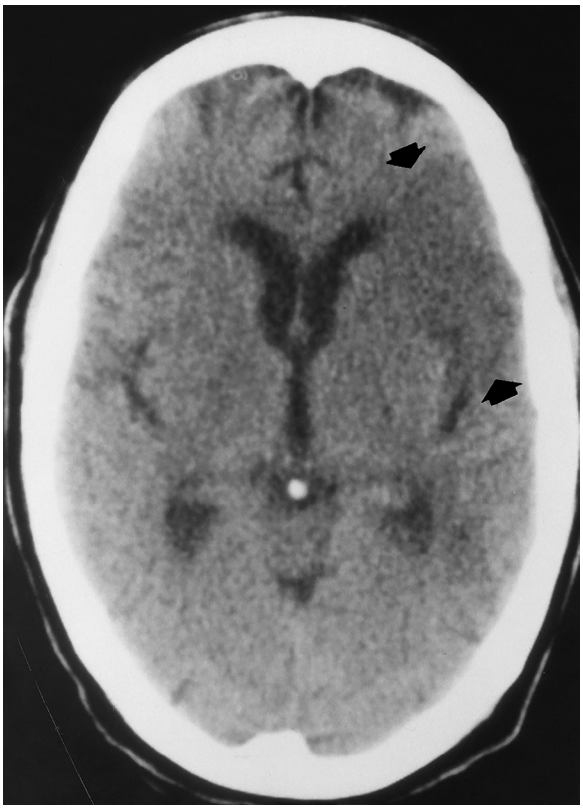

FIGURE 8-49 Acute left middle cerebral artery infarct. CT scan obtained 20 hours after onset of acute hemiparesis and aphasia shows obliteration of normal sulci (*arrows*) in the involved hemisphere. The gray matter and white matter in the distribution of the left middle cerebral artery demonstrate low density.

and lead to increased edema and a slower recovery for the patient. CT and MRI findings are normal in patients with small infarctions and in the early hours of large infarctions. The initial appearance (within 8 to 24 hours) of a cerebral infarction is a triangular or wedge-shaped area of hypodensity on CT (Figure 8-49) and high signal intensity on T2-weighted MRI sequences involving both the cortex and the underlying white matter down to the ventricular surface. The abnormality is confined to the vascular territory of the involved artery. Although little or no mass effect is evident during the first day, progressive edema produces a mass effect that is maximal 7 to 10 days after the acute event (Figure 8-50). As an infarct ages, brain tissue atrophies, and the adjacent sulci and ventricular system enlarge (Figure 8-51). A combination of nonenhanced MRI and MRA is more sensitive than CT in detecting an infarct or ischemic edema, especially involving the brainstem. Occlusion or stenosis of an artery or vein can be demonstrated along with the associated hemorrhage as a result of ischemic infarction. A diffusion-weighted MR image usually demonstrates a positive hyperintense signal within 2 hours of the incident and plays a critical role in diagnosing and determining the age of the stroke (Figure 8-52). There is only a small window of 2 or 3 hours after the onset of a stroke during which fibrinolytic agents are effective in decreasing the risk of permanent neurologic deficits. A T2-weighted image

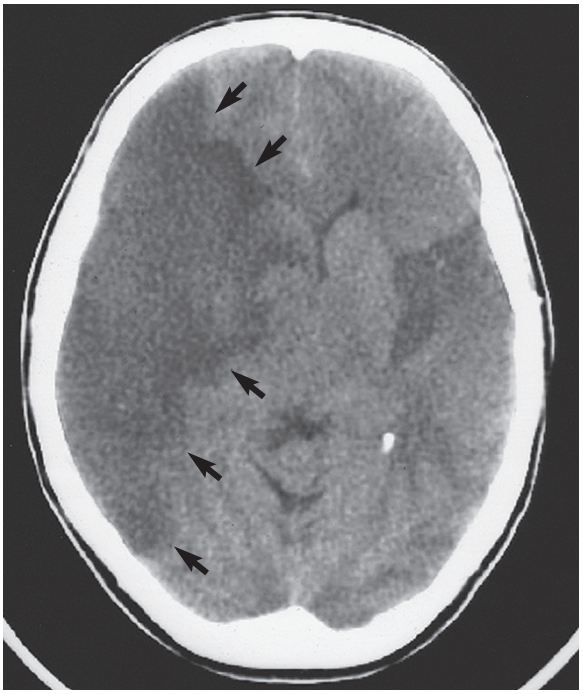

FIGURE 8-50 Chronic right middle cerebral artery infarct. Low-attenuation region (*arrows*) shows sharply defined borders and some midline shift.

FIGURE 8-51 Chronic right middle cerebral artery infarct. Low-attenuation region shows sharply defined borders (*arrows*) and some dilation of the adjacent ventricle.

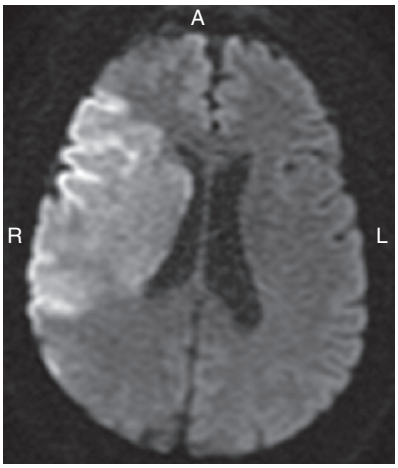

FIGURE 8-52 Right middle cerebral artery infarct. Diffusion-weighted MR image shows a high signal intensity involving both the cortex and the underlying white matter down to the ventricular surface.

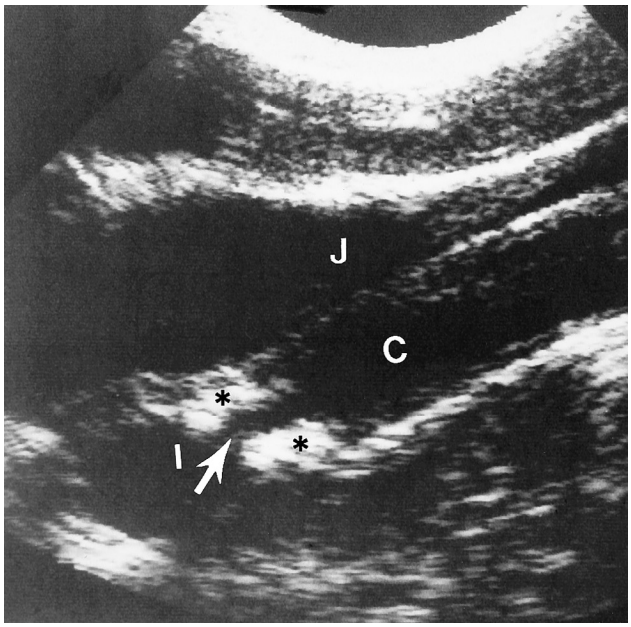

FIGURE 8-53 Ultrasound scan of carotid arteriosclerotic occlusive disease. There is severe narrowing (*arrow*) of the origin of the internal carotid artery (I) by densely echogenic arteriosclerotic plaque (*asterisks*). *C,* Common carotid artery; *J,* jugular vein.

detects edema sooner than CT and thus is considered more sensitive. In patients with classic stroke symptoms, follow-up CT or MRI is not indicated.

Treatment. All patients with stroke are started on bed rest with reduced external stimuli to lower cerebral oxygen demands. Medications may be used to decrease intracranial pressure and intracranial edema. Patients with thrombotic strokes receive anticoagulants and possibly thrombolytic agents.

Transient Ischemic Attacks

TIAs manifest as focal neurologic deficits that completely resolve within 24 hours. They may result from emboli originating from the surface of an arteriosclerotic, ulcerated plaque (embolic stroke), which causes temporary occlusion of cerebral vessels, or from stenosis of an extracerebral artery, which leads to a reduction in critical blood perfusion. Because almost two-thirds of arteriosclerotic strokes are preceded by TIAs and the 5-year cumulative risk of stroke in patients with TIAs may be as high as 50%, accurate diagnosis and appropriate treatment are essential.

Imaging appearance. The most common location of surgically treatable arteriosclerotic disease causing TIAs is the region of the carotid bifurcation in the neck. In patients with an asymptomatic bruit (a rumbling noise heard by a stethoscope) or an unclear history of a TIA, carotid duplex color-flow Doppler scanning is often the initial screening study (Figure 8-53). This technique combines high-resolution ultrasound imaging and Doppler ultrasound with spectral analysis into a "duplex" unit that avoids many of the problems associated with each of these modalities used alone. In most cases, carotid duplex scanning, when combined with MRA, can reliably determine whether the extent of the disease is sufficient to warrant more invasive procedures (angiography). Patients with a normal or near-normal carotid duplex scan do not need to undergo more invasive diagnostic procedures for assessment of the carotid bifurcation. Limitations of the usefulness of carotid duplex scanning include its extreme operator dependence and the fact that 10% of patients cannot be successfully imaged with carotid duplex scanning because of anatomic factors (extremely high carotid bifurcations and short, thick necks). High-resolution, real-time ultrasound techniques provide hemodynamic information about blood flow velocity. With use of ultrasound techniques, it may be impossible to differentiate a total occlusion of the internal carotid artery from a tiny residual lumen. This is an important clinical distinction because the patient with even a small remaining lumen can undergo a successful carotid endarterectomy (surgical removal of atherosclerotic plaque).

Noninvasive MRA provides accurate imaging of the carotid bifurcation and demonstrates narrowing of the vertebral arteries (Figure 8-54). The reconstitution sign (flow gap) confirms a stenosis greater than 60%, indicating advanced disease requiring surgical intervention. Contrast-enhanced MRA also facilitates visualization of the aortic arch and the origins of the carotid and vertebral arteries.

Patients with a clear-cut episode of a TIA or a neurologic deficit usually are subjected to an angiographic study for evaluating the carotid arteries. Either intravenous or intra-arterial digital subtraction angiography or selective intra-arterial carotid arteriography can be used to demonstrate TIA-producing stenotic or ulcerative lesions that may be amenable to surgical therapy (Figures 8-55 to 8-57). Angiographic evaluation of the aortic arch and vertebral arteries is infrequently indicated in the evaluation of patients with TIAs because surgery on the origins of the great vessels and posterior circulation is both difficult and not commonly performed and also because of the higher morbidity from arch and vertebral angiograms reported in some studies.

FIGURE 8-54 Normal MRA of the carotid artery. The anteroposterior perspective of the neck demonstrates vessels from the subclavian arteries to the origin of the basilar artery, and the bifurcation of the common carotid arteries.

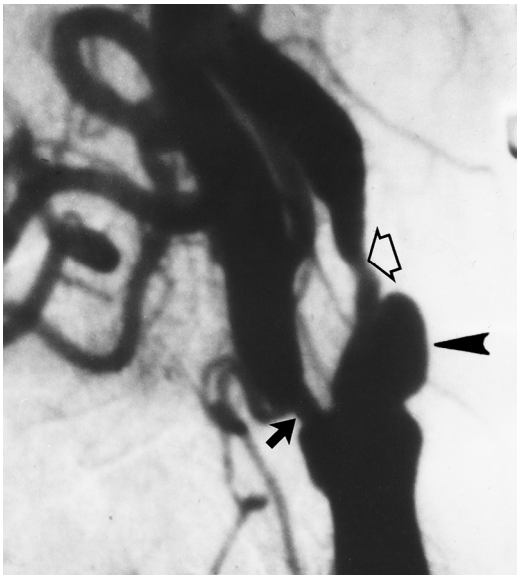

FIGURE 8-56 Ulceration of the internal carotid artery. Common carotid arteriogram shows an ulcerated lesion (*arrowhead*) at the origin of the internal carotid artery, with severe stenosis of the internal carotid (*open arrow*) and external carotid (*black arrow*) arteries.

FIGURE 8-55 Normal carotid artery bifurcation. Common carotid arteriogram shows the bulbous origin of the internal carotid artery (*solid arrow*) and multiple branches of the external carotid artery (*open arrows*).

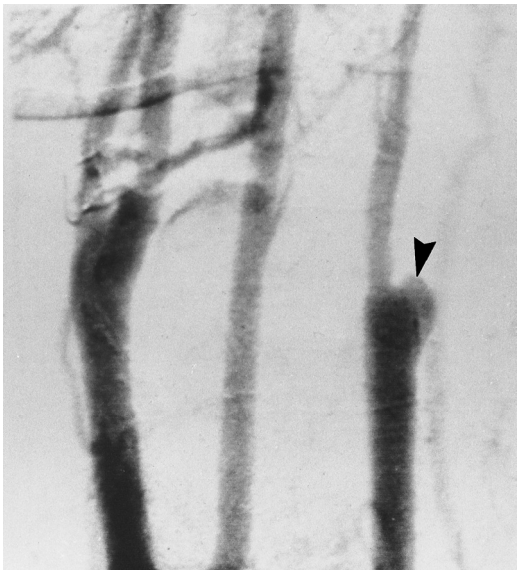

FIGURE 8-57 Occluded internal carotid artery. Intravenous DSA shows occlusion of the left internal carotid artery at its origin (*arrowhead*).

Treatment. Accurate diagnosis and appropriate treatment (antiplatelet therapy, anticoagulation therapy, or carotid endarterectomy) are essential to prevent permanent deficits. Thrombolytic agents may also be used.

Intraparenchymal Hemorrhage

Aside from head trauma, the principal cause of intraparenchymal hemorrhage (hemorrhagic stroke) is hypertensive vascular disease. Less common causes are rupture of a congenital berry aneurysm and AVM. Hypertensive hemorrhages result in oval or circular collections that displace the surrounding brain and can have significant mass effect. Although they can occur at any location within the brain, hypertensive hemorrhages are most frequent in the basal ganglia, white matter, thalamus, cerebellar hemispheres, and pons. A common complication is rupture of the hemorrhage into the ventricular system or subarachnoid space. Intraparenchymal hemorrhages resulting from congenital berry (saccular) aneurysms are usually associated with subarachnoid hemorrhage and

FIGURE 8-58 Intracerebral hematoma. Noncontrast CT scan shows a homogeneous, high-density area in the left thalamus. The low-density area (*arrowheads*) adjacent to the hematoma represents associated ischemia and edema. Hematoma has entered the ventricular system, and a prominent cerebrospinal fluid–blood level can be seen in the dependent lateral ventricle (*arrow*). Such extension of blood into the ventricular system is an extremely poor prognostic sign. Mass effect due to the hematoma has compressed the third ventricle and the foramen of Monro and has resulted in obstructive enlargement of the lateral ventricles.

tend to develop in regions where these congenital vascular anomalies most commonly occur. They include the sylvian fissure (middle cerebral artery) and the midline subfrontal area (anterior communicating artery). AVMs occur throughout the brain and tend to bleed into the white matter.

Imaging appearance. Patients with a suspected intraparenchymal hemorrhage should be evaluated with MRI or noncontrast CT. A fresh hematoma appears on CT as a homogeneously dense, well-defined lesion with a round to oval configuration (Figure 8-58). Hematomas produce ventricular compression and, when large, considerable midline shift and brain herniation. A hematoma that is not homogeneously dense is suggestive of hemorrhage occurring within a tumor, an inflammatory process, or an infarction. As the hematoma ages, its density changes. On CT, after passing through an isodense stage, the hematoma becomes hypodense; by 6 months, it appears as a well-defined, low-density region that is often considerably smaller than the original lesion. Contrast enhancement usually develops around the periphery of a hematoma after 7 to 10 days. On MRI, the preferred study, the high signal intensity within a hematoma (caused by the conversion of normal hemoglobin to methemoglobin) arises after a few days and continues for several months (Figure 8-59). Once the methemoglobin is completely converted to paramagnetic hemosiderin, the hematoma demonstrates very low signal intensity on T2-weighted sequences.

Arteriography is not indicated in patients with classic hypertensive hematomas. However, arteriography remains the gold standard for those patients in whom an aneurysm or AVM is suspected as the underlying cause of the hematoma. In patients with a suspected aneurysm, it is important to determine the number of aneurysms, which aneurysm has ruptured, the location of the neck of the aneurysm, and the patency of the circle of Willis. Statistically, the largest of multiple aneurysms is the one that has ruptured; it is rare for an aneurysm less than 5 mm in diameter to rupture. Because an aneurysm generally ruptures at its apex, an irregular, multiloculated dome is suggestive of a prior rupture. Spasm in adjacent vessels and adjacent hematomas also assist in identifying which of several aneurysms has bled. Noncontrast CT demonstrates an aneurysm as a slightly hyperdense region. The intravenous injection of contrast material produces a strong uniform enhancement. On MRI, an aneurysm produces a flow void on both T1- and T2-weighted images. Imaging has improved the ability to detect an aneurysm. CTA and MRA can visualize large and medium aneurysms, along with feeding and draining vessels associated with an AVM. However, angiography remains the gold standard for demonstrating abnormalities involving small vessels.

In patients younger than 20 years of age, AVM is the most common cause of nontraumatic intraparenchymal hemorrhage. On MRI, a cerebrovascular malformation appears as a mass of vascular structures of varying intensity, depending on whether there is rapid flow (black) or slow flow (white) (Figure 8-60). On CT, the malformation consists of an irregular tangle of vessels (best seen after the intravenous injection of contrast material) and greatly dilated veins draining from the central tangle (Figure 8-61A). Arteriography demonstrates an irregular, racemose tangle of abnormal vessels that are fed by dilated cerebral or cerebellar arteries (Figure 8-61B). There is rapid shunting of blood into dilated, tortuous draining veins. Because of the often multiple sources of blood flow to an AVM, the arteriographic evaluation should include selective injections of contrast material into both internal and external carotid arteries.

Treatment. Steroid therapy, especially in nontraumatic hematomas, usually controls the edema that produces much of the mass effect. In cases of hemorrhagic strokes, the first line of treatment consists of stopping the bleeding (i.e., correct any coagulopathy), and the second is to try to prevent a recurrence of bleeding (control blood pressure), and finally surgery is performed to correct pathology (aneurysm or AVM). For aneurysms, surgical placement of a clip at the neck of the lesion is required to close the pouch. AVMs require surgery or neurointerventional procedures.

Subarachnoid Hemorrhage

A major cause of subarachnoid hemorrhage (hemorrhagic stroke) is rupture of a berry aneurysm (Figure 8-62). Patients

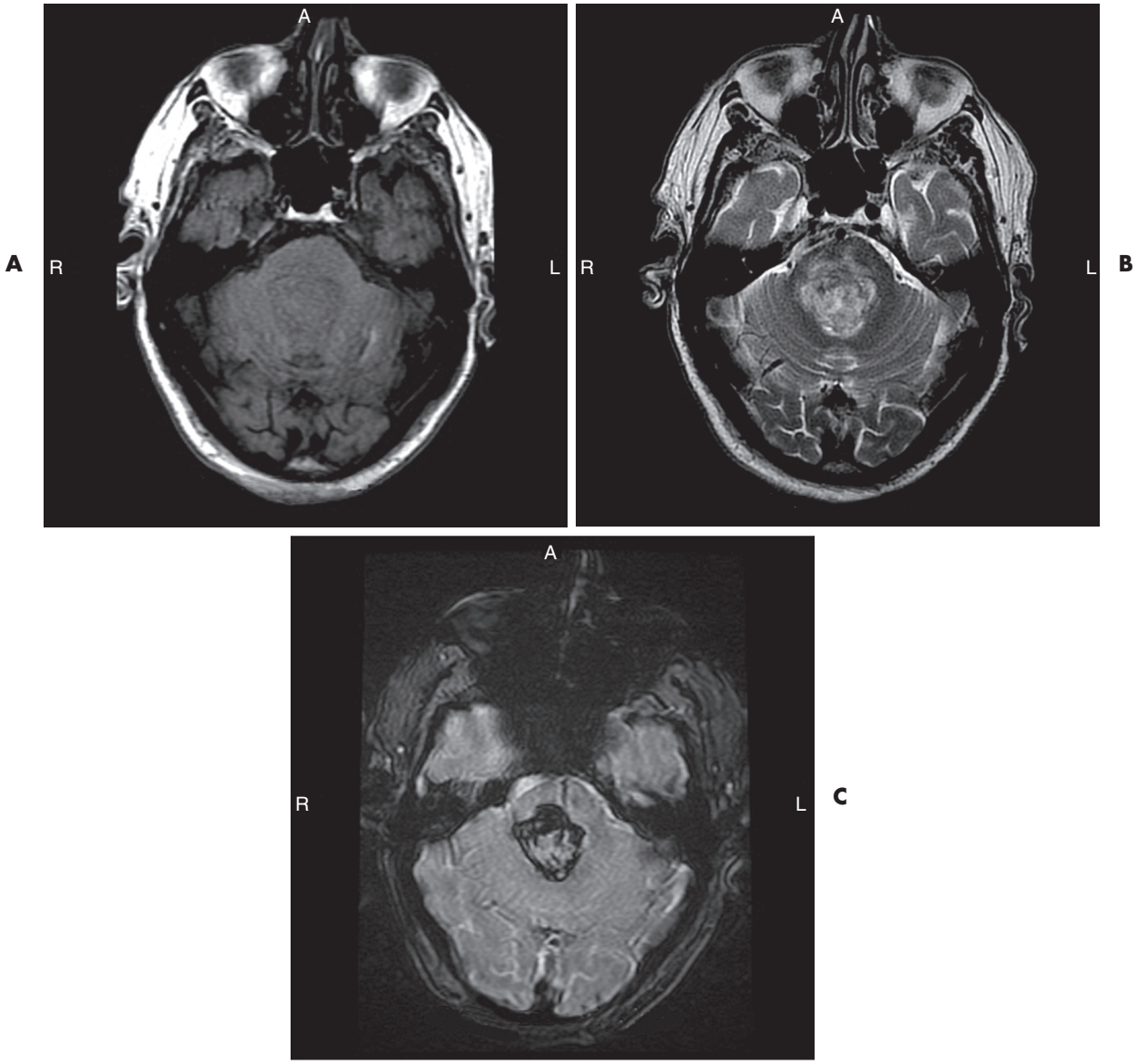

FIGURE 8-59 Intracerebral brainstem hematoma. High signal intensity demonstrated within the hematoma on image B.

with this condition usually have a generalized excruciating headache followed by unconsciousness. The most common locations for berry aneurysms are the origins of the posterior cerebral and anterior communicating arteries and the trifurcation of the middle cerebral artery. Because of the 20% incidence of multiple aneurysms, the angiographic procedure should include evaluation of the internal carotid and vertebral arteries bilaterally.

Imaging appearance. The radiographic procedure of choice is a noncontrast CT scan, which can demonstrate high-density blood in the subarachnoid spaces of the basal cisterns in more than 95% of cases (Figure 8-63). Bleeding may extend into the brain parenchyma adjacent to the aneurysm. Contrast-enhanced CT scans are not indicated in subarachnoid hemorrhage because the surgeon will not operate for a suspected aneurysm without an angiogram, and the patient would thus be exposed to the risk of an excessive load of contrast material. MRI is relatively insensitive for identifying acute subarachnoid bleeds, but it does demonstrate chronic blood staining of the meninges by a marked hypointensity on T2-weighted images. High-resolution CTA can demonstrate aneurysms larger than 3 mm and is becoming more accepted for presurgical planning.

The timing of angiography in subarachnoid hemorrhage depends on the philosophy of the surgeon. Blood in the subarachnoid space is an irritant that causes vasospasm of the vessels of the circle of Willis and the middle cerebral artery. This vasospasm, which can lead to cerebral ischemia and frank infarction, is greatest 3 to 14 days after the acute episode.

Treatment. If emergency surgery within the first 72 hours after the hemorrhage is planned, emergency selective angiography is indicated. If surgical intervention is to be delayed, angiography should be postponed until just before surgery.

Summary of Findings for Vascular Disease of the Central Nervous System

Disorder	Location	Imaging Appearance	Treatment
Stroke syndrome	Neurologic deficit due to lack of circulation; internal carotid artery most common site	CT (initial exam)—a triangular or wedge-shaped hypodensity on noncontrast scan MRI—T2-weighted image produces high signal intensity of vascular territory involved Diffusion-weighted MRI—hyperintense signals within 2 hours of onset CT/MRI—mass effect seen 7–10 days after onset	Bed rest and reduced external stimuli for all stroke victims Medications to treat increased intracranial pressure if symptoms arise
Transient ischemic attack	Embolic stroke originating from arteriosclerotic ulcerated plaque	Duplex color-flow Doppler US—provides hemodynamic information including flow velocity (total occlusion vs. tiny residual flow) MRA—size and shape of diseased carotid and vertebral arteries; contrast-enhanced scan shows aortic arch and origins of vessels DSA—invasive study provides the highest resolution of intraluminal vascular pathology	Anticoagulants and/or thrombolytic agents to treat cause Surgical endarterectomy
Intraparenchymal hemorrhage	Hemorrhage into brain tissue	CT—new hematoma appears as homogeneously dense, well-defined, round or oval lesion, becoming isodense over time; 6-month-old hematoma appears as a well-defined, low-density lesion MRI—high signal intensity after a few days on T1- and T2-weighted images; with time, a low signal intensity is seen on T2-weighted images CTA/MRA—shows arteriovenous malformations in large and medium vessels and can detect an aneurysm Arteriography—used for small vessels	Steroid therapy Surgical clipping of aneurysm Surgery or neurointerventional procedures to correct arteriovenous malformation
Subarachnoid hemorrhage	Bleed beneath arachnoid layer of meninges	CT—noncontrast scan initially shows high attenuation of blood in the subarachnoid space MRI—best demonstrates chronic hemorrhages as hypointense areas on T2-weighted image CTA—high resolution demonstrates aneurysms greater than 3 mm MRA—shows large and medium vessels for detecting an aneurysm Arteriography—to localize and characterize small-vessel anatomy	Stop bleeding Prevent recurrence Surgical intervention to correct pathology

CTA, CT angiography; *DSA,* digital subtraction angiography; *MRA,* MR angiography; *US,* ultrasound.

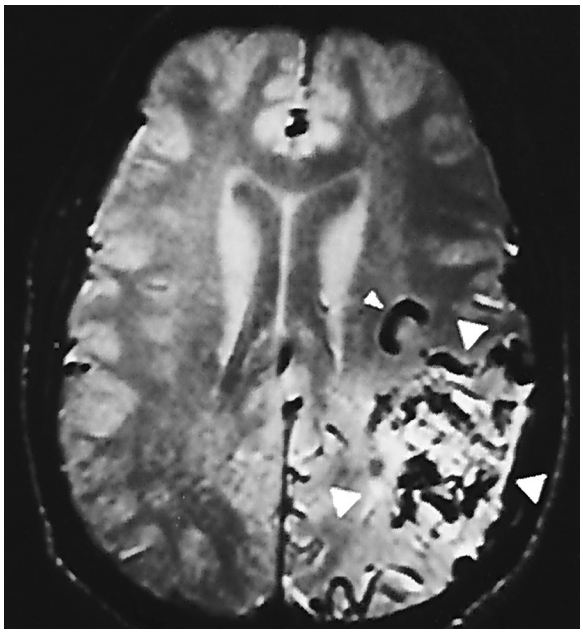

FIGURE 8-60 Arteriovenous malformation. Axial MR image shows large left parietal mass (*large arrowheads*) consisting of vascular structures of varying intensity, depending on whether there is rapid flow (black) or slow flow (white). Note the greatly dilated vessel (*small arrowhead*) that feeds the malformation.

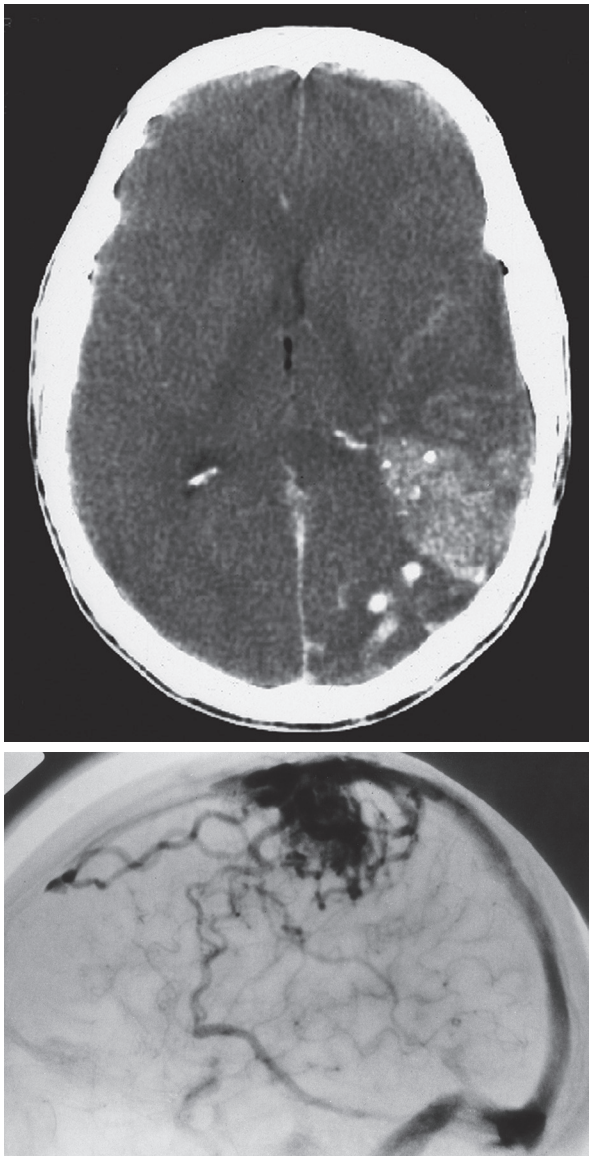

FIGURE 8-61 Arteriovenous malformation with hemorrhage. **(A)** CT scan shows an irregular tangle of vessels in the parietal lobe, seen without a contrast injection. **(B)** In another patient, a carotid arteriogram shows dilated blood vessels constituting an arteriovenous malformation.

FIGURE 8-62 Ruptured berry aneurysm. Left carotid arteriogram demonstrates a left supraclinoid aneurysm of the internal carotid artery. The posterior bulge of the aneurysm (*arrow*) represents the site of rupture.

FIGURE 8-63 Berry aneurysm with subarachnoid hemorrhage. CT scan demonstrates subarachnoid bleed into the cisterns and ventricles (hyperdense) from a ruptured left middle cerebral aneurysm (*arrow*).

MULTIPLE SCLEROSIS

Multiple sclerosis is the most common demyelinating disorder; it manifests as recurrent attacks of focal neurologic deficits that primarily involve the spinal cord, optic nerves, and central white matter of the brain. The disease has a peak incidence between 20 and 40 years of age, a strong preponderance in women, and a clinical course characterized by multiple relapses and remissions. Impairment of nerve conduction caused by the degeneration of myelin sheaths leads to such symptoms as double vision, nystagmus (involuntary, rapid movement of the eyeball in all directions), loss of balance and poor coordination, shaking tremor and muscular weakness, difficulty in speaking clearly, and bladder dysfunction.

Imaging appearance. MRI is the modality of choice for demonstrating the scattered plaques of demyelination that are characteristic of multiple sclerosis. The plaques appear as multiple areas of increased signal intensity on

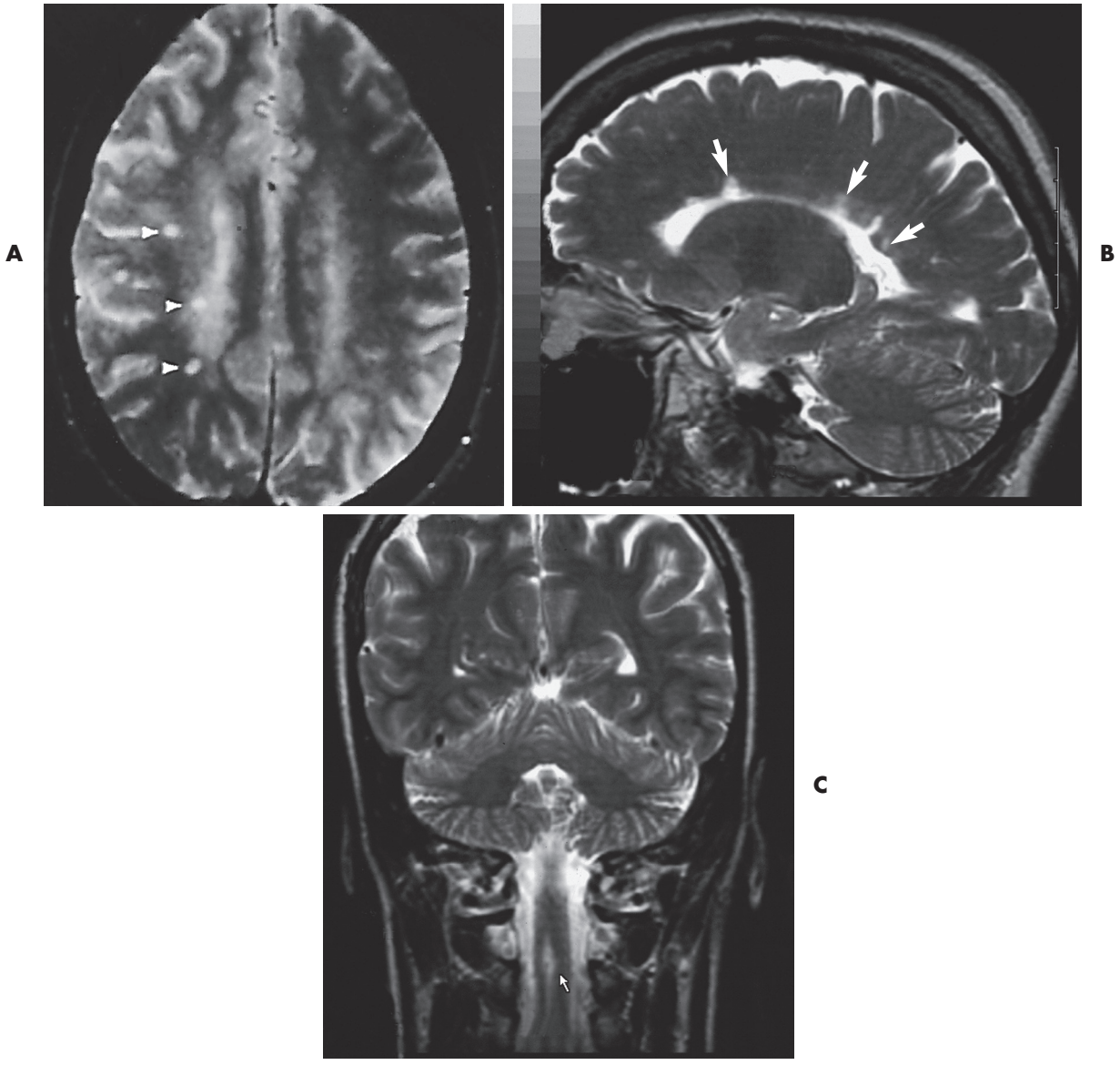

FIGURE 8-64 Multiple sclerosis. **(A)** Axial T2-weighted MR image in a 35-year-old woman shows characteristic areas of increased signal intensity (*arrowheads*) in deep white matter. **(B)** Sagittal image demonstrates periventricular plaques (*arrows*). **(C)** Coronal image shows increased intensity of cervical cord plaque (*arrow*).

T2-weighted images; these areas involve primarily the periventricular white matter, cerebellum, brainstem, and spinal cord (Figure 8-64). Lesions involving the optic nerve or chiasm require contrast enhancement and fat-suppression imaging (which increases the contrast difference between fat and water) to improve their detectability. On T1-weighted images, the plaques appear as isointense or hypointense lesions that may have a beveled edge. The use of MRI sequences using fluid-attenuated inversion recovery and fast-spin echo as well as MR spectroscopy aid in determining the extent of the disease. CT shows old inactive disease as well-defined areas of decreased attenuation in the deep white matter and periventricular regions. In the acute phase, CT performed after intravenous administration of contrast material demonstrates a mixture of nonenhancing focal areas of decreased density (representing old areas of demyelination) and enhancing regions that represent active foci.

Treatment. As the disease progresses and the symptoms increase in severity, immunosuppressive agents may help limit the autoimmune attack. Antiviral drugs may slow the progress of the disease. To reduce the number and severity of attacks, some patients receive subcutaneous injections of disease-modifying immunomodulatory agents (interferon-β). The treatments can only aid in slowing the progress of multiple sclerosis; however, there is no cure.

Summary of Findings for Multiple Sclerosis

Disorder	Location	Imaging Appearance	Treatment
Multiple sclerosis	Most common demyelinating disorder of the CNS	MRI—plaques appear as a hyperintense signal on T2-weighted images and isointense to hypointense, possibly with beveled edges, on T1-weighted images MRI with contrast enhancement and fat suppression best demonstrates plaques involving the optic nerve and chiasm MRI—FLAIR imaging, fast-spin echo imaging, and MR spectroscopy—aid in determining extent of disease	Immunosuppressive agents Antiviral drugs Subcutaneous injections of interferon-β

CNS, Central nervous system; *FLAIR,* fluid-attenuated inversion recovery.

EPILEPSY AND CONVULSIVE DISORDERS

Epilepsy is a condition in which brain impulses are temporarily disturbed, resulting in a spectrum of symptoms ranging from loss of consciousness for a few seconds to violent seizures (shaking and thrashing movements of all extremities). Although most cases of epilepsy are idiopathic, the disorder can be a result of injury (penetrating or nonpenetrating trauma and depressed skull fracture), birth trauma, or infection.

The mildest type of epilepsy, which occurs primarily in children, is called **petit mal**. This results in brief episodes of loss of consciousness, which may be associated with mild muscular twitching. Petit mal epilepsy usually disappears in young adulthood.

Grand mal epilepsy refers to generalized convulsions in which the patient falls to the floor, hypersalivates (foams at the mouth), and loses control of urine and sometimes feces. In many cases, an approaching seizure is heralded by an aura, such as a ringing in the ears, a tingling sensation in the fingers, or spots before the eyes. After a seizure, the patient tends to be groggy and unaware of what has happened (i.e., in a postictal state).

Imaging appearance. Whenever possible, the radiographic evaluation of a patient with a seizure disorder should be performed when the patient is clinically stable. The appropriate procedure is MRI to search for an unsuspected brain tumor, AVM, or hippocampal sclerosis (Figure 8-65). *Hippocampal sclerosis* (mesial temporal sclerosis) refers to neuronal loss and gliosis that occur in the temporal region. High-resolution, thin-section, coronal T2-weighted images are the most specific for diagnosis of this disorder. It is the most common cause of seizures that do not respond to medical therapy.

Because most seizure disorders are attributable to small areas of cortical brain injury resulting from trauma or infarction, CT or MRI findings are usually normal. If the MRI findings are normal, PET using ^{18}F-fluorodeoxyglucose (^{18}F-FDG-PET) may localize the seizure focus in a patient with hippocampal sclerosis. PET has a 70% to 80% sensitivity and a very low rate of false-positive results (Figure 8-66).

Summary of Findings for Epilepsy and Convulsive Disorders

Disorder	Location	Imaging Appearance	Treatment
Epilepsy and convulsive disorders	Brain impulses temporarily disrupted	MRI—high-resolution, thin-section T2-weighted image is most specific PET—localizes seizure foci	Stabilize patient for safety Reverse chemical causes Medications to decrease number of seizures Surgical resection

PET, Positron emission tomography.

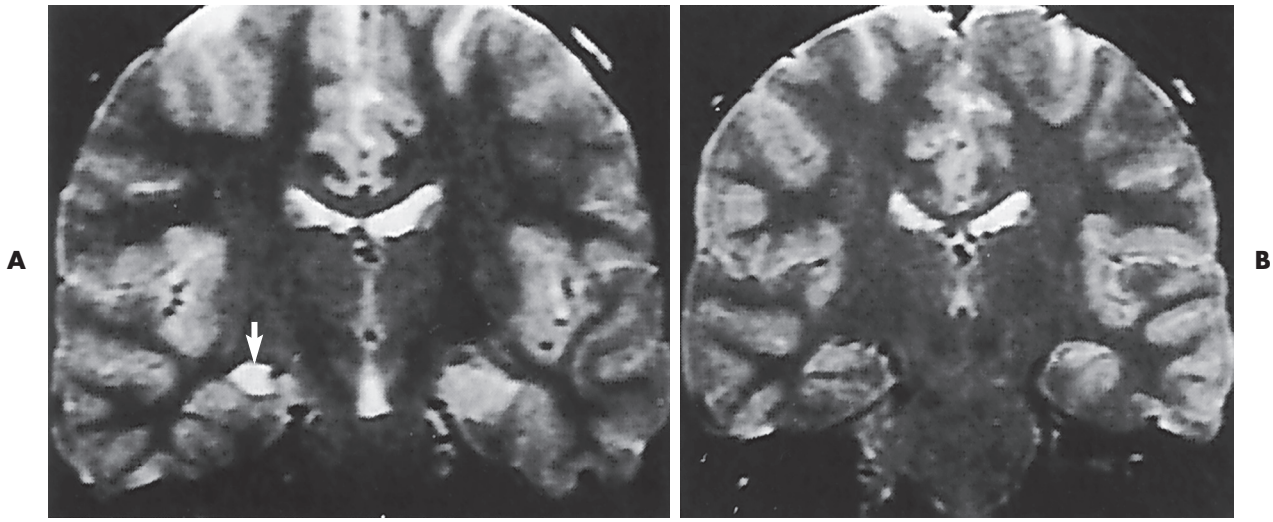

FIGURE 8-65 Seizure disorder caused by hippocampal sclerosis. **(A)** Coronal T2-weighted MR image shows high-intensity signal in the left hippocampal region (*arrow*). **(B)** Image in a normal patient for comparison.

Treatment. For the patient who has an acute seizure, initial efforts are directed toward stabilizing the patient (securing adequate ventilation and perfusion) and stopping the seizure. Subsequently, a careful history, physical examination, and appropriate laboratory studies should be performed to exclude reversible chemical causes of seizures, such as hypoglycemia, hyponatremia (decreased concentration of sodium in the blood) or hypernatremia, and hypocalcemia or hypercalcemia. If the patient shows no response to routine anticonvulsive treatment, CT may be indicated to search for causes of an acute seizure disorder (e.g., subdural hematoma and intracerebral hematoma), which may be amenable to surgical intervention. These conditions can be adequately assessed with a noncontrast CT scan; plain skull radiographs are not required. Medications may help decrease the number of seizures a patient experiences. Surgical resection of the lesion is associated with a very good outcome.

DEGENERATIVE DISEASES

Normal Aging

During normal aging, a gradual loss of neurons results in enlargement of the ventricular system and sulci (Figure 8-67).

Imaging appearance. Demyelination, which is also a part of normal aging, leads to the development of low density in the periventricular regions on CT scans and high signal intensity on T2-weighted MR images (Figure 8-68).

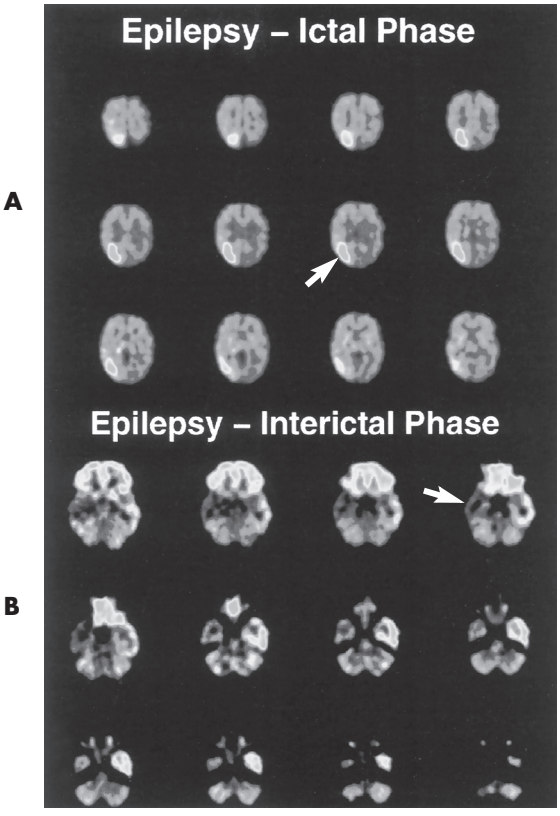

FIGURE 8-66 Epilepsy. **(A)** In a patient with a history of epileptic seizures (ictal phase), FDG–PET brain images demonstrate an area of increased activity: the highlighted region in the posterior portion of the cerebrum (*arrow*). **(B)** The interictal phase (postseizure activity phase in the same patient) illustrates decreased activity in the temporal lobe (*arrow*) resulting from reduced blood flow during the seizure.

Alzheimer's Disease

Alzheimer's disease (presenile dementia) is a diffuse form of progressive cerebral atrophy that develops at an earlier age than the senile period.

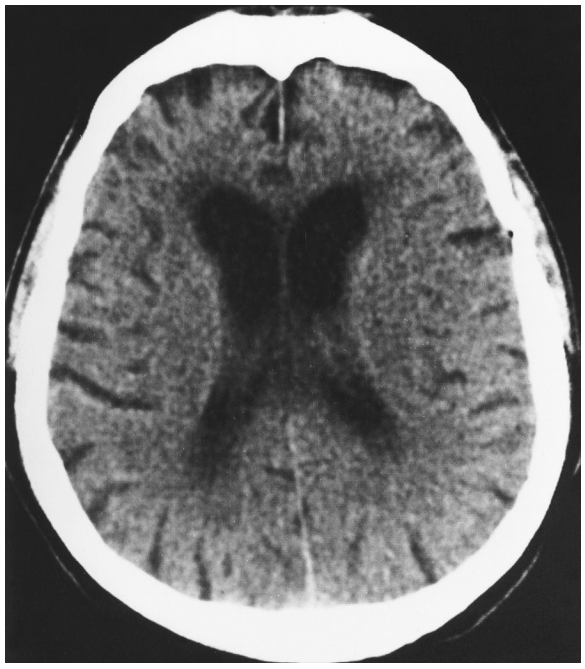

FIGURE 8-67 Normal aging. CT scan of 70-year-old man shows generalized ventricular dilation with prominence of sulci over the surfaces of the cerebral hemisphere.

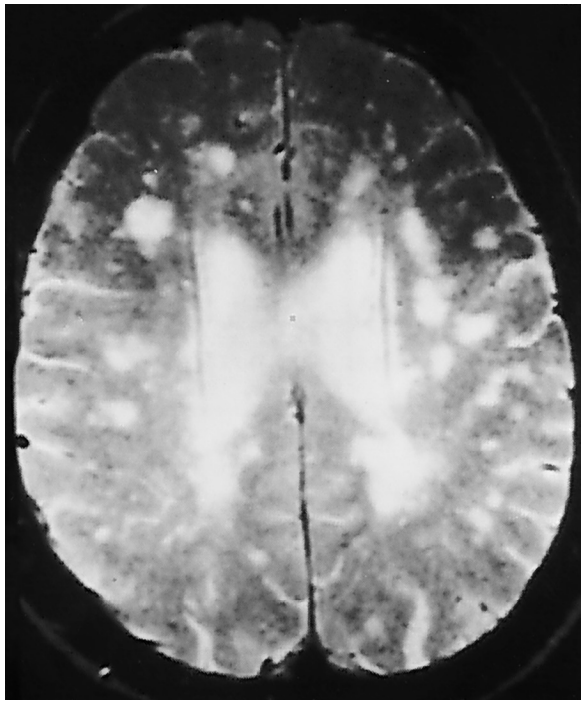

FIGURE 8-68 Degenerative changes of aging. Axial MR image demonstrates multiple areas of increased signal intensity around the ventricles and in the deep white matter, consistent with cerebral ischemia or infarction.

Imaging appearance. CT and MRI demonstrate nonspecific findings of cerebral atrophy, including symmetrically enlarged ventricles with prominence of the cortical sulci (Figure 8-69). T2-weighted MR images show periventricular hyperintensities. FDG–PET metabolic brain imaging used in conjunction with automated brain mapping can help distinguish changes associated with progressive neurodegenerative processes, such as Alzheimer's dementia. When this map is superimposed on an Alzheimer's database, areas of significantly reduced glucose metabolism correspond with Alzheimer's regions (Figure 8-70).

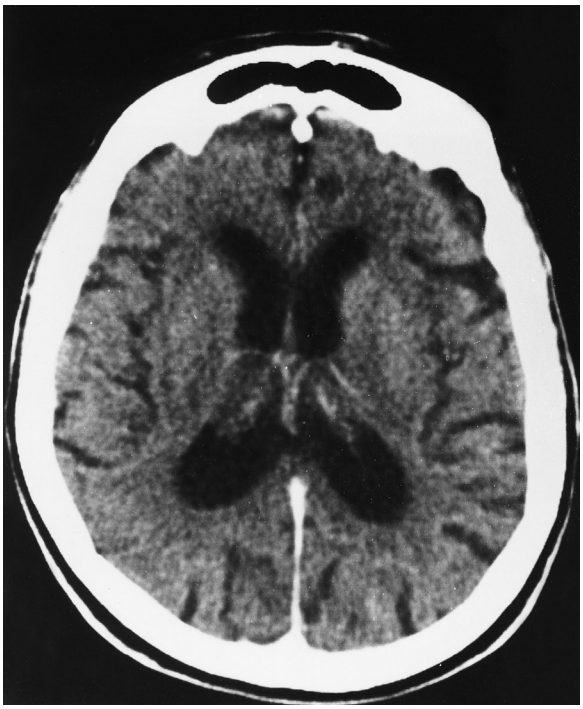

FIGURE 8-69 Alzheimer's disease. Noncontrast CT scan of a 56-year-old woman with progressive dementia shows generalized enlargement of the ventricular system and sulci.

Treatment. Diet, education, memory aids, and safety issues may slow the progression of dementia, but there is no cure at this time. Medications available today help to slow the progression of the disease and may reverse early symptoms to some degree.

Huntington's Disease

Huntington's disease is an inherited (autosomal dominant) condition that predominantly involves men and appears in the early to middle adult years as dementia and typical choreiform movements (involuntary movements that are rapid, jerky, and continuous).

Imaging appearance. The pathologic hallmark of Huntington's disease is atrophy of the caudate nucleus and putamen, which produces the typical CT appearance of focal dilation of the frontal horns and a loss of their normal concave shape (Figure 8-71) as a result of caudate nucleus atrophy. Generalized enlargement of the ventricles and dilation of the cortical sulci can also occur.

Single-photon emission computed tomography (SPECT) images demonstrate a decrease in glucose metabolism, specifically in the caudate, in comparison with the putamen. On PET scans, a decrease in the dopamine receptor sites provides an opportunity to track the condition before its clinical onset.

Treatment. Currently, there is no cure for Huntington's disease. Treatment with acetylcholinesterase inhibitors increases

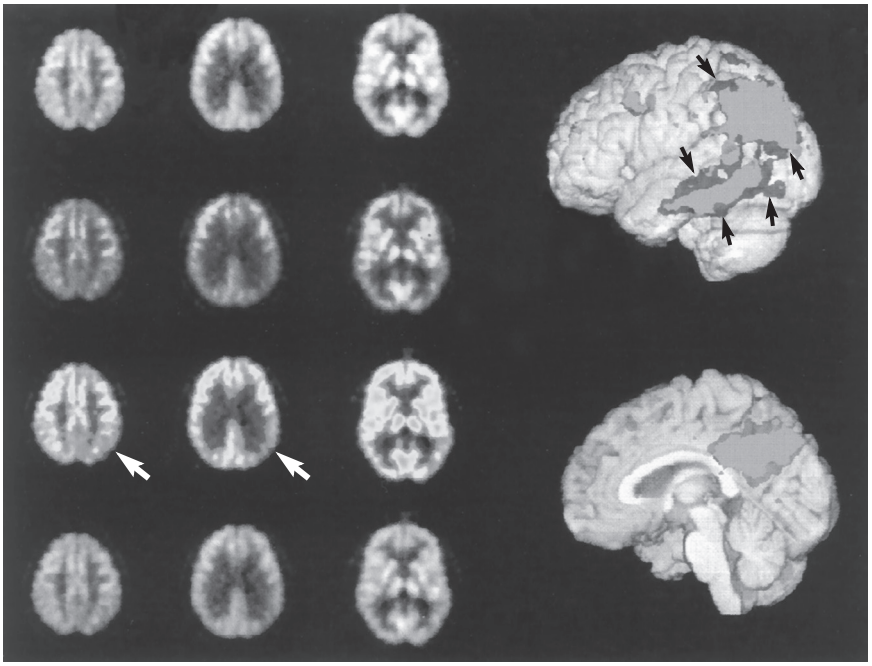

FIGURE 8-70 Alzheimer's dementia. **(A)** FDG–PET metabolic brain images demonstrate significantly reduced glucose metabolism in the left cerebrum on transverse images (*arrows*). **(B)** When the brain map was superimposed, the area of reduced uptake (represented by the *medium gray* area) superimposed the Alzheimer's control data (represented by the *dark gray* area [*black arrows*]). Significantly reduced glucose metabolism can be seen on the patient's left, a finding consistent with a diagnosis of Alzheimer's dementia.

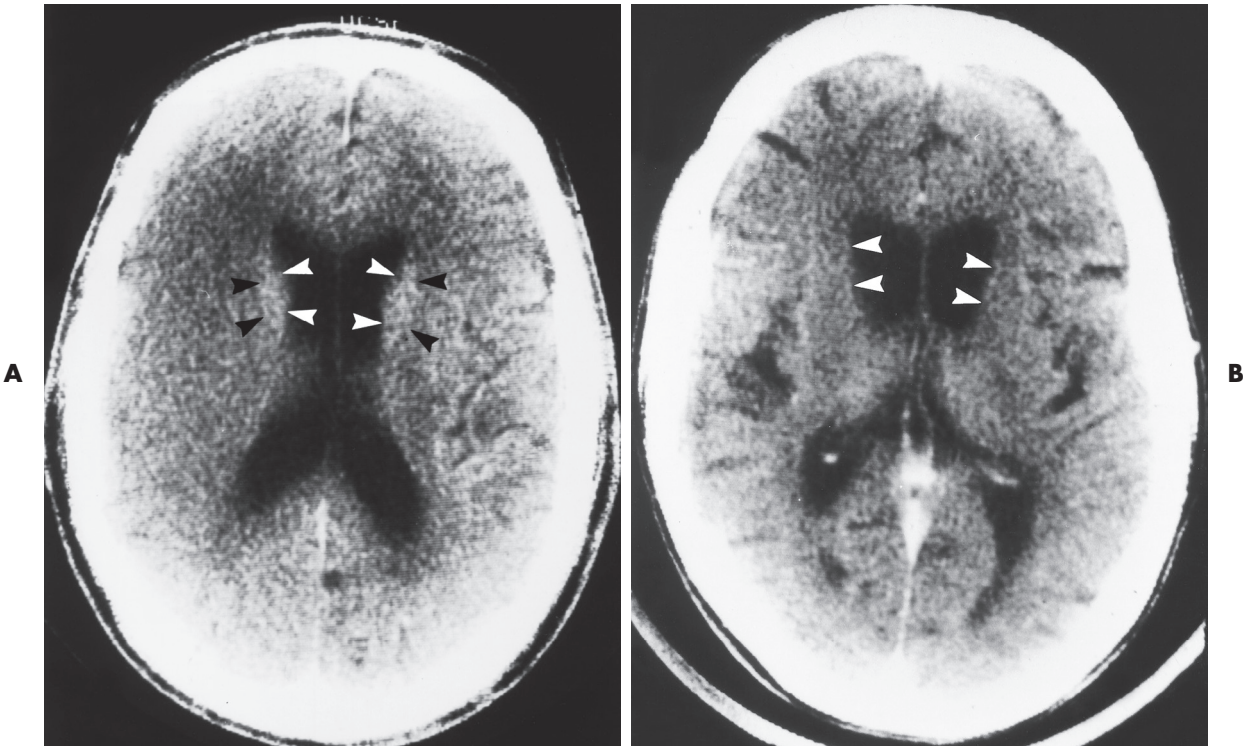

FIGURE 8-71 Huntington's disease. (A) CT scan in a normal patient shows the heads of the caudate nucleus (*black arrowheads*) producing a normal concavity of the frontal horns (*white arrowheads*). **(B)** In a patient with Huntington's disease, atrophy of the caudate nucleus causes a characteristic loss of the normal concavity (*white arrowheads*) of the frontal horns.

cognition but does not halt progression of the disease. Counseling is essential because of the hereditary genetic relationship.

Parkinson's Disease

Parkinson's disease (shaking palsy) is a progressive degenerative disease characterized by stooped posture, stiffness and slowness of movement, fixed facial expression, and involuntary rhythmic tremor of the limbs that disappears with voluntary movement. A disorder of middle or later life, Parkinson's disease is very gradually progressive and has a prolonged course.

The major degenerative changes in nerve cells in Parkinson's disease occur in the basal ganglia, especially the globus pallidus, the substantia nigra, and the fibers of the corpus striatum. The essence of the condition seems to be an enzyme defect that results in an inadequate production of the neuronal transmitter substance dopamine. The newest method of treatment is the administration of L-dopa, a substance that is converted to dopamine in the brain. Although this drug therapy does not stop the neuronal degeneration, it dramatically improves both the appearance and the behavior of the patient.

Imaging appearance. CT scans in patients with Parkinson's disease often demonstrate cortical atrophy. However, because this condition is usually seen in older individuals, the ventricular enlargement and prominent cortical sulci found on CT scans may be indistinguishable from those caused by the normal aging process. SPECT and PET are the most useful imaging modalities to demonstrate degenerative changes. The basal ganglia have decreased uptake and retention of ^{18}F-DOPA (L-dihydroxyphenylalanine) in cases of Parkinson's disease.

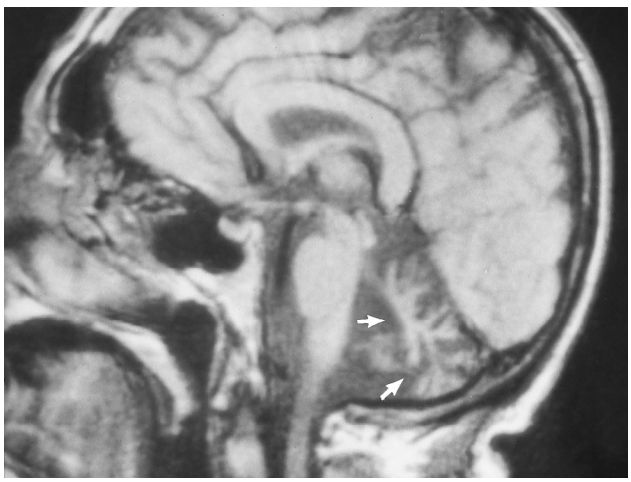

FIGURE 8-72 Cerebellar atrophy. Sagittal MR image shows dramatic loss of substance of the vermis of the cerebellum (*arrows*) in a patient with severe alcoholism.

Treatment. Drug treatment is the first choice for controlling symptoms because no cure currently exists. Stereotactic pallidotomy is a surgical option for some cases and may aid in long-term reduction of symptoms by creating lesions that destroy the globus pallidus.

Cerebellar Atrophy

Isolated atrophy of the cerebellum may represent an inherited disorder, a degenerative disease, or the toxic effect of prolonged use of such drugs as alcohol and phenytoin (Dilantin) (Figure 8-72).

Summary of Findings for Degenerative Diseases of the Central Nervous System

Disorder	Location	Imaging Appearance	Treatment
Normal aging	Cerebral atrophy, enlarged ventricular system, demyelination	CT—low-density periventricular regions MRI—high signal intensity of periventricular regions on T2-weighted images	None in normal aging process
Alzheimer's disease	Cerebral atrophy before senile period	CT—cerebral atrophy with enlarged ventricles and prominent cortical sulci MRI—similar to CT; periventricular high-intensity on T2-weighted images PET—reduced glucose metabolism consistent with Alzheimer's regions	No cure Diet, education, and safety factors to slow progression Medications to slow progression
Huntington's disease	Atrophy of caudate nucleus and putamen	CT—focal ventricular dilation; loss of normal shape of frontal horns SPECT—demonstrates a decrease in glucose metabolism, specifically in the caudate, compared with the putamen PET—dopamine receptor sites decrease, providing early onset tracking prior to clinical onset	No treatment at present Acetylcholinesterase inhibitors increase cognition but do not halt the disease progression Genetic counseling of families
Parkinson's disease	Degeneration of basal ganglia	CT—appearance similar to that of normal aging process SPECT/PET—demonstrates degenerative changes in the basal ganglia as decreased uptake and retention of ^{18}F-DOPA	Drug treatment No cure known Stereotactic pallidotomy
Cerebellar atrophy	Degeneration of cerebellum	MRI—size changes in cerebellum	Discontinue prolonged use of drugs (alcohol and phenytoin)
Amyotrophic lateral sclerosis	Upper and lower motor neurons	CT/MRI/myelography—inconclusive for diagnostic purposes; can demonstrate other causes of similar symptoms	Incurable Psychological support Education

^{18}F-DOPA, L-Dihydroxyphenylalanine; *PET,* positron emission tomography; *SPECT,* single-photon emission CT.

Amyotrophic Lateral Sclerosis (Lou Gehrig's Disease)

In amyotrophic lateral sclerosis, a relentlessly progressive condition of unknown cause, there is widespread selective atrophy and loss of motor nerve cells leading to extensive paralysis and death from respiratory weakness or aspiration pneumonia.

Imaging appearance. Although this disease cannot be diagnosed radiographically, CT, MRI, or myelography is often performed to exclude a spinal malignancy, which could produce a similar clinical appearance.

Treatment. Amyotrophic lateral sclerosis is uniformly fatal because there currently is no cure. Psychological support and education can be provided.

HYDROCEPHALUS

Hydrocephalus refers to dilation of the ventricular system that is usually associated with increased intracranial pressure. In **noncommunicating (obstructive) hydrocephalus**, there is an obstruction to the flow of CSF somewhere along the ventricular pathways from the lateral ventricles to the outlets of the fourth ventricle. Enlargement of the lateral ventricles with normal-sized third and fourth ventricles indicates an obstruction at the level of the foramen of Monro. This is most commonly attributable to a colloid cyst (Figure 8-73) or a suprasellar tumor, especially craniopharyngioma. Enlargement of the

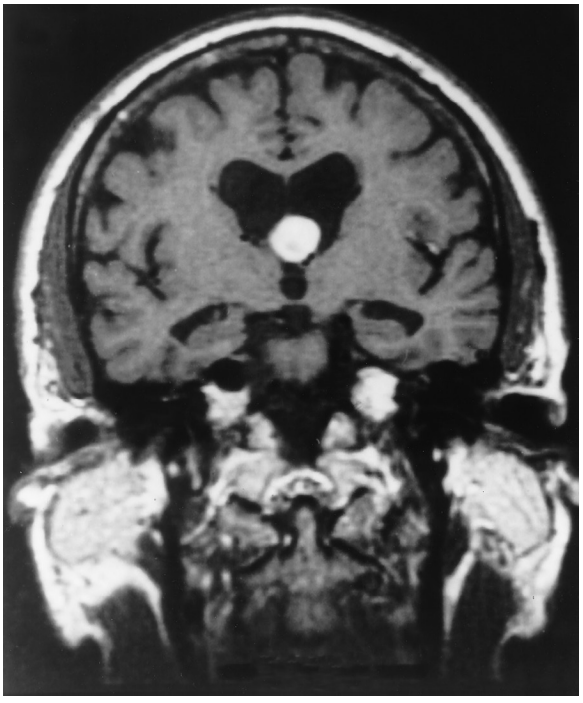

FIGURE 8-73 Hydrocephalus with obstruction at the level of the foramen of Monro. T1-weighted MR image shows a hyperintense colloid cyst causing bilateral enlargement of the frontal horns.

lateral and third ventricles with a normal-sized fourth ventricle indicates an obstruction at the level of the aqueduct of Sylvius (Figures 8-74 and 8-75). The most common causes of this appearance are congenital aqueduct stenosis or occlusion and neoplasm (pinealoma and teratoma). Enlargement of the entire ventricular system (with the fourth ventricle often dilated out of proportion [Dandy–Walker cyst]) indicates an obstruction at the level of the outlet of the fourth ventricle (Figure 8-76), a condition that may reflect congenital atresia, infection, neoplasm, or downward herniation of the cerebellar tonsils through the foramen magnum.

In the much more common **communicating hydrocephalus**, the ventricular fluid passes freely into the extraventricular subarachnoid space. There is generalized ventricular enlargement, and the sulci are normal or absent. Obstruction of the normal CSF pathway distal to the fourth ventricle usually involves the subarachnoid space at the basal cisterns, cerebral convexity, or foramen magnum. Causes include infection (meningitis and empyema), subarachnoid or subdural hemorrhage, congenital anomalies, neoplasm, and dural venous thrombosis. A similar radiographic pattern is seen in **normal-pressure hydrocephalus**, a syndrome of gait ataxia, urinary incontinence, and dementia associated with ventricular dilation and relatively normal CSF pressure.

Imaging appearance. CT clearly shows ventricular dilation. MRI is more specific than CT in demonstrating the underlying cause of obstruction or in excluding obstruction (communicating hydrocephalus). Contrast-enhanced MRI may assist in distinguishing a congenital posterior fossa cyst from an enhancing cystic neoplasm. Ultrasound can demonstrate the ventricular dilation either *in utero* or after birth as long as the sound waves can traverse the open fontanels.

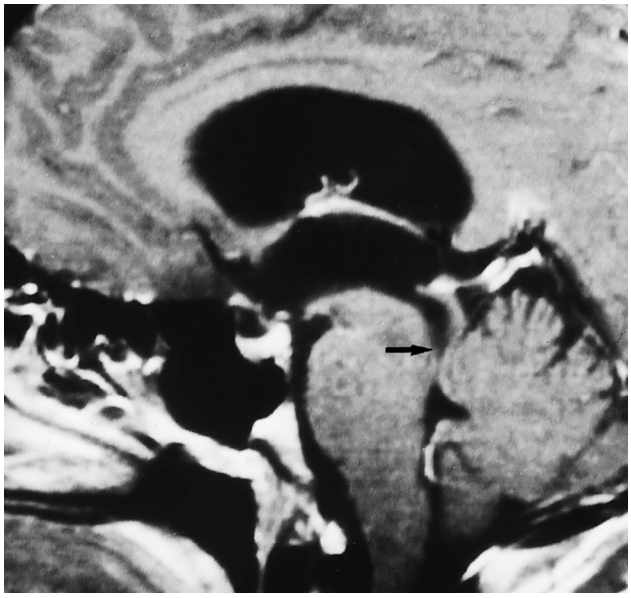

FIGURE 8-75 Aqueductal stenosis. T1-weighted sagittal MR image shows pronounced narrowing of the inferior portion of the aqueduct (*arrow*). There is flaring of the upper portion of the aqueduct and considerable enlargement of the third and lateral ventricles. Note that the fourth ventricle is of normal size.

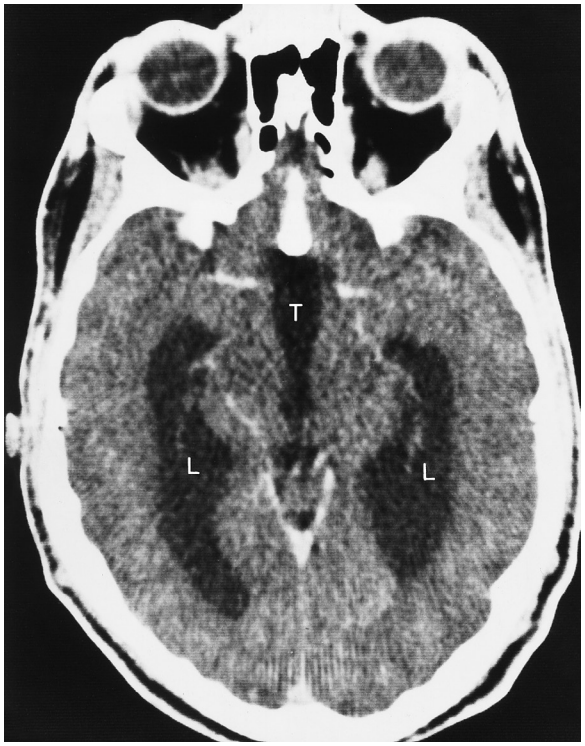

FIGURE 8-74 Hydrocephalus caused by obstruction at the level of the cerebral aqueduct. Dilation of the lateral (L) and third (T) ventricles can be seen in this patient with congenital hydrocephalus. Symptoms of headache and papilledema resolved after ventricular shunting.

FIGURE 8-76 Hydrocephalus caused by obstruction at the level of the outlet of the fourth ventricle. A huge low-density cyst (a Dandy–Walker cyst) occupies most of the enlarged posterior fossa and represents an extension of the dilated fourth ventricle.

Generalized enlargement of the ventricular system can also be attributed to the overproduction of CSF by a papilloma (Figure 8-77) or by carcinoma arising in the choroid plexus (CSF-secreting vascular tissue in the ventricles). These rare tumors usually occur in the fourth ventricle in adults and the lateral ventricles in children.

Treatment. Hydrocephalus can often be treated by the placement of a shunt between the dilated ventricles and the heart or the peritoneal cavity. Successful shunting causes a decrease in the intracranial pressure and ventricular size; the latter can be monitored by CT or MRI. If radiation exposure is of concern (because of patient age or pregnancy), MRI is the modality of choice.

SINUSITIS

The paranasal sinuses (maxillary, ethmoid, frontal, and sphenoid) are paired, air-filled cavities that are lined with a mucous membrane that is directly continuous with the nasal mucosa. The size and shape of the sinuses vary in different age periods, in different individuals, and on the two sides of the same individual. At birth, the maxillary sinus is only a slitlike space that later expands to fill the maxilla and is thus responsible for the growth of the face. The ethmoid sinuses can be seen radiographically by 6 years of age, whereas the frontal sinuses usually are not well demonstrated until approximately 10 years of age. The sphenoid sinuses begin to develop at approximately 2 or 3 years of age and are fully developed by late adolescence.

Viral infection of the upper respiratory tract may lead to obstruction of drainage of the paranasal sinuses and the development of localized pain, tenderness, and fever.

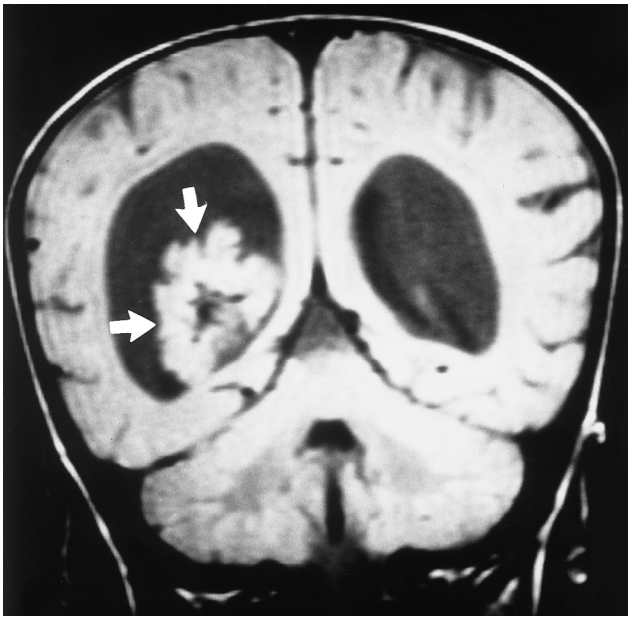

FIGURE 8-77 Choroid plexus papilloma. T1-weighted MR image shows a lobulated isointense mass (*arrows*) in a greatly dilated right lateral ventricle.

Imaging appearance. Radiographically, acute or chronic sinusitis causes mucosal thickening, which appears as a soft tissue density lining the walls of the involved sinuses (Figure 8-78). The maxillary antra are most commonly affected and are best visualized on the Waters' projection. An air–fluid level in a sinus is usually considered a manifestation of acute inflammatory disease (Figure 8-79). To demonstrate this finding, it is essential that all sinus images be obtained with the patient erect and with the use of a horizontal beam. The destruction of the bony wall of a sinus is an ominous sign indicating secondary osteomyelitis (Figure 8-80). CT, the procedure of choice, demonstrates bony sinonasal anatomy; coronal images can show air–fluid levels (Figure 8-81). Coronal MRI provides

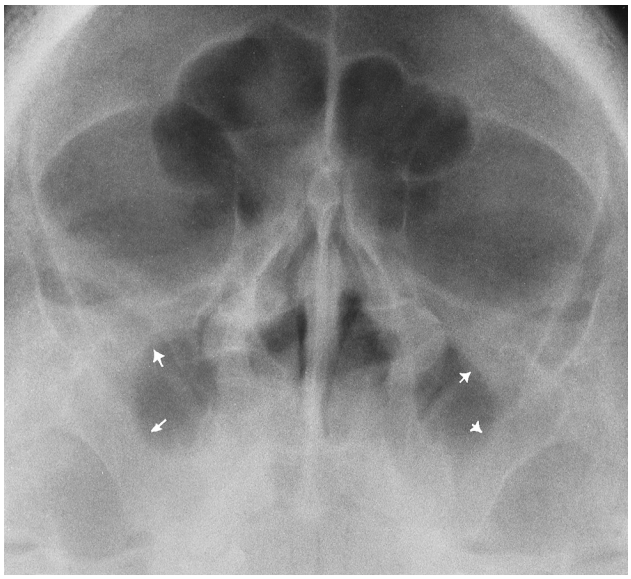

FIGURE 8-78 Chronic sinusitis. Mucosal thickening appears as soft tissue density (*arrows*) lining the walls of the maxillary antra.

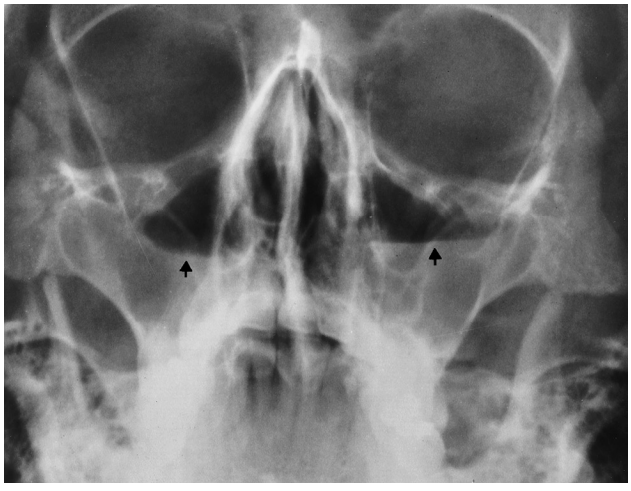

FIGURE 8-79 Acute sinusitis. Mucosal thickening involves most of the paranasal sinuses, and air–fluid levels (*arrows*) are present in both maxillary antra.

FIGURE 8-80 Mucormycosis causing pansinusitis with osteomyelitis. Destruction of the roof of the right orbit and outer margins of the right frontal sinus can be seen.

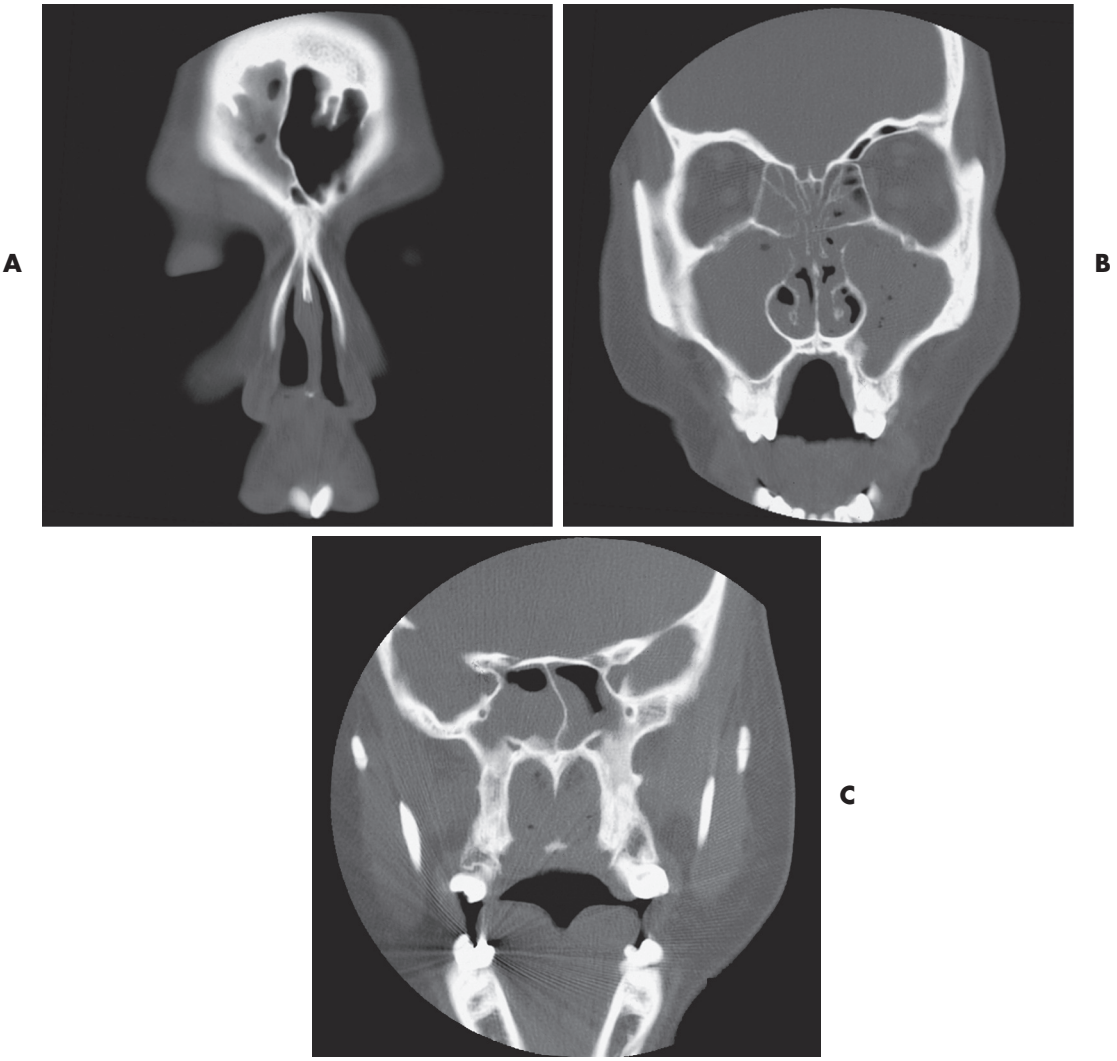

FIGURE 8-81 Pansinusitis in a 29-year-old woman with headache. Coronal CT scans show fluid in the frontal sinus **(A)**, in the maxillary and ethmoid sinuses **(B)**, and in the sphenoid sinus **(C)**.

Summary of Findings for Other Diseases of the Central Nervous System

Disorder	Location	Imaging Appearance	Treatment
Hydrocephalus	Cerebral ventricular system	CT—demonstrates ventricular dilation MRI—may also show underlying cause	Shunt placement
Sinusitis	Paranasal sinuses; maxillary most common	Sinus radiograph—mucosal thickening and fluid levels CT—demonstrates sinonasal anatomy and fluid levels on coronal imaging MRI—suspected complications	Antibiotics for bacterial infection Decongestants Surgery

the best method to detect suspected complications, such as mucocele, osteomyelitis, and underlying intracranial disease.

Treatment. Sinusitis caused by bacteria is treated with antibiotics to eradicate the infection. Decongestants may be used to relieve symptoms and aid in sinus drainage. Steroid nasal sprays help reduce mucosal inflammation. Chronic sinusitis may require surgery to clean and drain the sinus and to repair a deviated septum or nasal obstruction that may be the cause of recurrent inflammation.

REVIEW QUESTIONS

1. The imaging modality of choice to evaluate patients with suspected neurologic dysfunction caused by head trauma is _____.
   a. ultrasound
   b. MRI
   c. CT
   d. skull radiographs
2. Arterial bleeding sometimes associated with head trauma can cause _____ hematomas.
   a. intracranial
   b. subdural
   c. epidural
   d. acute
3. Venous bleeding sometimes associated with head trauma can cause _____ hematomas.
   a. intracranial
   b. subdural
   c. epidural
   d. acute
4. Movement of the brain within the calvaria following blunt trauma to the skull sometimes results in a cerebral _____.
   a. subdural hematoma
   b. epidural hematoma
   c. acute hematoma
   d. contusion
5. Bleeding into the ventricular system caused by injury to surface veins, cerebral parenchyma, or cortical arteries can cause _____ hemorrhage.
   a. epidural
   b. subdural
   c. epiarachnoid
   d. subarachnoid
6. Plain radiographs of the facial bones should always be made with the patient in the _____ position if possible.
   a. supine
   b. erect
   c. lateral decubitus
   d. anterior
7. The most common primary brain tumor is a _____ _____.
   a. glioma
   b. glioblastoma
   c. meningioma
   d. neurinoma
8. A benign tumor that arises from arachnoid lining cells and is attached to the dura is called a _____.
   a. glioma
   b. glioblastoma
   c. meningioma
   d. neurinoma
9. The most common neoplasms that metastasize to the brain arise in the _____ and _____ _____.
   a. lung, stomach
   b. lung, breast
   c. stomach, breast
   d. breast, prostate
10. A viral inflammation of the brain and meninges is called _____.
    a. meningitis
    b. hydrocephalus
    c. encephalitis
    d. encephalomalacia
11. The best imaging modality to evaluate brain abscesses is _____.
12. The two imaging procedures of choice to evaluate the extent of a stroke in the brain are _____ and _____.
13. The acronym TIA stands for _____.
14. The imaging modality of choice to demonstrate the plaques of demyelination that are characteristic of multiple sclerosis is _____.
15. A condition in which brain impulses are temporarily disturbed, the results of which range from loss of consciousness to violent seizures, is termed _____.

16. A diffuse form of progressive cerebral atrophy that develops at an earlier age than the senile period is called _____.
17. A progressive degenerative disease characterized by involuntary tremors of the extremities that disappear with voluntary movement is named _____.
18. Sinus radiographs should be taken using a(n) _____ _____ beam and with the patient in the _____ _____ position.
19. The pathologic condition that refers to dilation of the ventricular system and is usually associated with increased intracranial pressure is _____.
20. If a patient needing facial or sinus radiographs is unable to stand or sit erect, a(n) _____ using a(n) _____ beam may be performed to demonstrate any air–fluid levels that may be present.

9

Hematopoietic System

OUTLINE

Physiology of the Blood
Diseases of Red Blood Cells
- Anemia
- Polycythemia
- Treatment of Polycythemias

Diseases of White Blood Cells
- Leukemia
- Lymphoma
- Infectious Mononucleosis

Diseases of Platelets (Bleeding Disorders)
- Hemophilia
- Purpura (Thrombocytopenia)

KEY TERMS

anemia
basophil
coagulation factors
eosinophils
erythrocytes
hemoglobin
leukocytes
lymphatic leukemia
monocytes
myelocytic leukemia
neutrophils (polymorphonuclear leukocytes)
pernicious anemia
platelets
sickle cell anemia
spherocytosis
thalassemia

OBJECTIVES

After reading this chapter, the reader will be able to:

- Define and describe all boldface key terms in this chapter
- Describe the physiology of the hematopoietic system
- Identify the basic blood structures on diagrams
- Differentiate the various pathologic conditions affecting the hematopoietic system as well as their radiographic manifestations

RADIOGRAPHER NOTES

Although the hematopoietic system cannot be directly imaged, many blood disorders result in abnormalities that can be demonstrated radiographically. It may be necessary to increase or decrease exposure factors when imaging patients who manifest advanced stages of these diseases (see Box 1-1). The radiographer must be aware of the severe pain experienced by patients undergoing a sickle cell crisis. Patients with advanced leukemia or lymphoma who have an altered immune status may require protective isolation. Because many hematopoietic system diseases cause significant demineralization of bone, the radiographer must be alert to the possibility of pathologic fracture and thus must exercise caution when moving and positioning patients with these diseases.

Radiographers need to be aware of the importance of using proper radiation safety shielding, pelvic shielding for patients, and aprons for technologists to prevent possible lack of blood cell formation in the pelvis, which could ultimately result in anemia.

PHYSIOLOGY OF THE BLOOD

Blood and the cells within it are vital to life. An adequate blood supply to all body tissues is necessary to bring oxygen, nutrients, salts, and hormones to the cells and to carry away the waste products of cellular metabolism. The components of blood are also a major defense against infection, toxic substances, and foreign antigens.

Red bone marrow (found in vertebrae, proximal femurs, and flat bones such as the sternum, ribs, skull, and pelvis) and lymph nodes are the blood-forming tissues of the body. Red blood cells (**erythrocytes**) and platelets (thrombocytes) (Figure 9-1) are made in red bone marrow, whereas white blood cells (**leukocytes**) (Figure 9-2) are produced in both red marrow and lymphoid tissue. If a bone marrow puncture is necessary for diagnostic testing, the iliac rim and sternum are good sites.

Erythrocytes are biconcave disks without a nucleus that contain **hemoglobin**, an iron-based protein that carries oxygen from the respiratory tract to the body's tissues. In a normal

person, there are 4.5 million to 6 million red blood cells in each cubic millimeter of blood. The amount of hemoglobin per deciliter is approximately 14 g in women and 15 g in men.

Leukocytes, or white blood cells, normally number from 5000 to 10,000/mm^3 of blood (see Figure 9-2). Unlike erythrocytes, there are several types of white blood cells. **Neutrophils (polymorphonuclear leukocytes)**, which make up 55% to 75% of white blood cells, defend the body against bacteria by ingesting these foreign organisms and destroying them (phagocytosis). The number of polymorphonuclear leukocytes in the blood increases enormously in acute infections because the bone marrow rapidly releases into the bloodstream the large numbers of these cells kept in reserve. **Eosinophils** (1% to 4%) are red-staining cells whose number greatly increases in allergic and parasitic conditions. The third type of leukocyte is the **basophil** (0% to 1%), which contains granules that stain blue. These three types of cells are formed in the sinusoids of bone marrow, and they, like red blood cells, go through immature stages before reaching the adult form.

Lymphocytes represent approximately 25% to 40% of white blood cells. They play a major role in the immune system and aid in the synthesis of antibodies and the production of immunoglobulins.

The final type of white blood cell is the monocyte, which is actively phagocytic and plays an important role in the inflammatory process. **Monocytes** are formed in the bone marrow and represent approximately 2% to 8% of white blood cells.

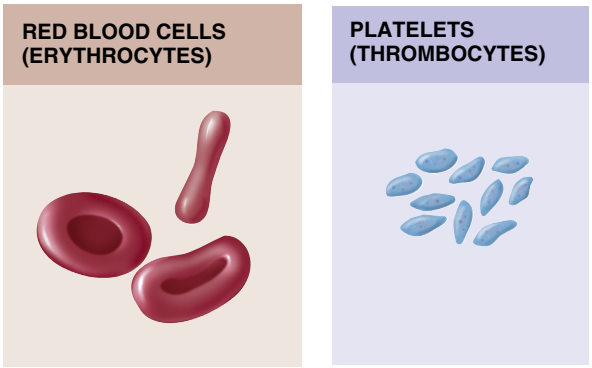

FIGURE 9-1 Red blood cells (erythrocytes) and platelets (thrombocytes).

Platelets, the smallest blood cells, are essential for blood clotting (see Figure 9-1). Normally, there are approximately 150,000 to 400,000 platelets in every cubic millimeter of blood.

DISEASES OF RED BLOOD CELLS

Anemia

Anemia refers to a decrease in the amount of oxygen-carrying hemoglobin in the peripheral blood. This reduction can be attributable to improper formation of new red blood cells, an increased rate of red blood cell destruction, or a loss of red blood cells as a result of prolonged bleeding. Regardless of the cause, a hemoglobin deficiency causes the anemic person to appear pale. This is best appreciated in the mucous membranes of the mouth and conjunctiva, and in the nail beds. A decrease in the oxygen-carrying hemoglobin impairs the delivery of an adequate oxygen supply to the cells and tissues, leading to fatigue and muscular weakness and often to shortness of breath on exertion (dyspnea). To meet the body's need for more oxygen, the respiratory rate increases and the heart beats more rapidly.

Iron Deficiency Anemia

Iron deficiency is the most common cause of anemia. It most frequently results from chronic blood loss, such as from an ulcer, a malignant tumor, or excessive bleeding during menstruation (menorrhagia). Other causes of iron deficiency anemia are inadequate dietary intake of iron and increased iron loss caused by intestinal parasites. Iron deficiency anemia also may develop during pregnancy because the mother's iron supply is depleted by red blood cell development in the fetus.

Treatment. If chronic blood loss causes the iron deficiency, the cause must be determined and treated. The first choice of treatment is for the patient to change dietary habits to include more foods rich in iron. The second option is an oral iron supplement: ferrous sulfate. When a patient is taking an iron supplement, it is important to remember that other products influence iron absorption. For example, increasing vitamin C intake enhances iron absorption. Iron deficiency can be treated successfully in most cases.

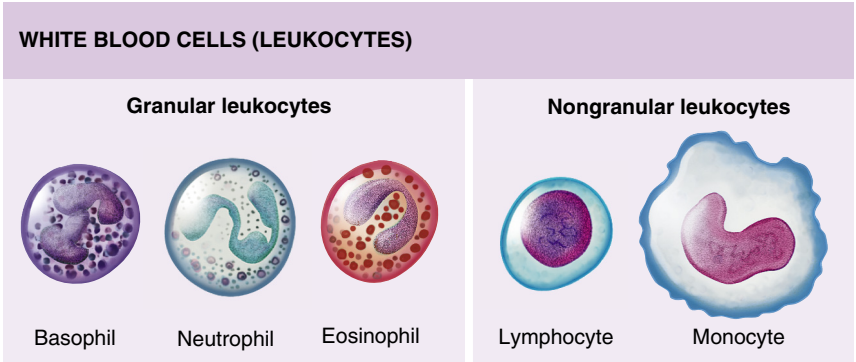

FIGURE 9-2 White blood cells (leukocytes).

Hemolytic Anemia

The underlying abnormality in hemolytic anemia is a shortened life span of the red blood cells with resulting hemolysis and the release of hemoglobin into the plasma. Most hemolytic anemias are caused by a hereditary defect that may produce abnormal red blood cells or abnormal hemoglobin. Less commonly, hemolytic anemia is acquired and related to circulating antibodies from autoimmune or allergic reactions (e.g., drugs such as sulfonamide) or the malarial parasite.

Spherocytosis, **sickle cell anemia**, and **thalassemia** are the major hereditary hemolytic anemias. In spherocytosis, the erythrocytes have a circular rather than a biconcave shape, making them fragile and susceptible to rupture. In sickle cell anemia, which is generally confined to African Americans, the hemoglobin molecule is abnormal and the red blood cells are crescentic or sickle shaped and tend to rupture. A defect in hemoglobin formation is also responsible for thalassemia, which occurs predominantly in persons living near the Mediterranean Sea, especially those of Italian, Greek, or Sicilian descent.

The breakdown of hemoglobin produces bilirubin, a pigmented substance that is normally detoxified by the liver and converted into bile. The accumulation of large amounts of this orange pigment in plasma causes the tissues to have a yellow appearance (jaundice).

Hemolytic anemia of the newborn (erythroblastosis fetalis) can result when the mother is Rh negative and the fetus has Rh-positive blood inherited from the father. Although the fetal and maternal circulations are separate, fetal blood can enter the mother's blood through ruptures in the placenta that occur at delivery. The mother thus becomes sensitized to the Rh factor of the fetus and makes antibodies against it. Any antibodies reaching the fetal blood through the placenta in future pregnancies cause hemolysis of the fetal red blood cells. The severity of the disease ranges from mild anemia with jaundice to fetal death.

Imaging appearance. The hemolytic anemias produce a variety of radiographic abnormalities. Although the radiographic findings are similar in the various types of hemolytic anemia, they tend to be most severe in thalassemia and least prominent in spherocytosis. Extensive marrow hyperplasia, the result of ineffective erythropoiesis and rapid destruction of newly formed red blood cells, causes generalized osteoporosis with pronounced widening of the medullary spaces and thinning of the cortices in long and tubular bones (Figure 9-3). As the fine secondary trabeculae are resorbed, new bone is laid down on the surviving trabeculae, thickening them and producing a coarsened pattern. Normal modeling of long bones does not occur because the expanding marrow flattens or even bulges the normally concave surfaces of the shafts.

In the skull, there is widening of the diploic space and thinning or complete obliteration of the outer table. When the hyperplastic marrow perforates or destroys the outer table, it proliferates under the invisible periosteum, and new bone spicules are laid down perpendicular to the inner table. This produces the characteristic hair-on-end appearance of vertical striations in a radial pattern (Figure 9-4).

FIGURE 9-3 Thalassemia. Pronounced widening of medullary spaces with thinning of cortical margins. Note the absence of normal modeling caused by the pressure of expanding marrow space. Localized radiolucencies simulating multiple osteolytic lesions represent tumorous collections of hypoplastic marrow.

FIGURE 9-4 Thalassemia. Lateral projection of the skull demonstrates hair-on-end appearance. Note the normal appearance of the calvaria inferior to the internal occipital protuberance, an area in which there is no red marrow, and poor pneumatization of the visualized paranasal sinuses.

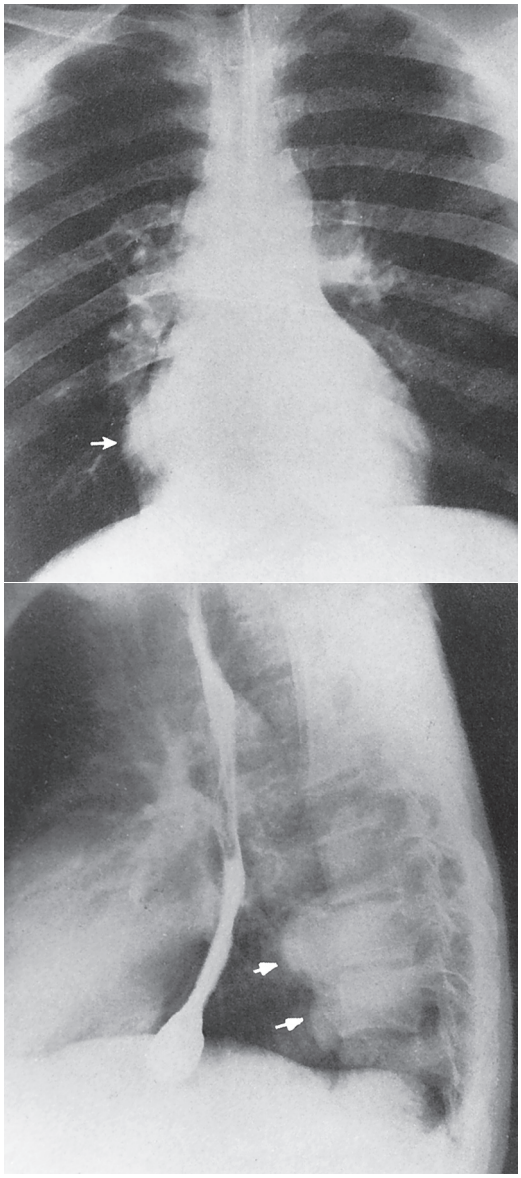

FIGURE 9-5 Extramedullary hematopoiesis in thalassemia. A lateral projection of the chest demonstrates lobulated posterior mediastinal masses of hematopoietic tissue (*arrows*) in the lower thoracic region.

Extramedullary hematopoiesis is a compensatory mechanism of the reticuloendothelial system (liver, spleen, and lymph nodes) in patients with prolonged erythrocyte deficiency resulting from the destruction of red blood cells or the inability of normal blood-forming organs to produce them. Paravertebral collections of hematopoietic tissue may appear on chest radiographs as single or multiple, smooth or lobulated, posterior mediastinal masses that are usually located at the lower thoracic levels (Figure 9-5).

In sickle cell anemia, expansile pressure of the adjacent intervertebral disks produces characteristic biconcave indentations on both the superior and the inferior margins of the softened vertebral bodies, giving the appearance of fish vertebrae (Figure 9-6A). Another typical appearance is the result of the development of localized steplike central depressions of multiple vertebral end plates (Figure 9-6B). This is most often caused by circulatory stasis and ischemia, which retard growth in the central portion of the vertebral cartilaginous growth plate. The periphery of the growth plate, which has a different blood supply, continues to grow at a more normal rate.

Bulging of the abnormally shaped red blood cells in sickle cell anemia typically causes focal ischemia and infarction in multiple tissues. Bone infarcts commonly occur in infants and children. They most frequently involve the small bones of the hands and feet, producing an irregular area of bone destruction with overlying periosteal calcification, which may be indistinguishable from osteomyelitis. In older children and adults, bone infarction may initially appear as an ill-defined lucent area that becomes irregularly calcified.

Acute osteomyelitis, often caused by *Salmonella* infection, is a common complication in sickle cell disease. The resulting lytic destruction and periosteal reaction may be extensive, often involving the entire shaft and multiple bones (Figure 9-7). Radiographically, it may be impossible to distinguish between osteomyelitis and bone infarction without infection (Figure 9-8).

Throughout their lives, patients with sickle cell anemia are plagued by recurrent painful crises. These episodes are attributable to recurrent vaso-occlusive phenomena and may appear with explosive suddenness and attack various parts of the body, especially the abdomen, chest, and joints. It is often difficult to distinguish between a painful sickle cell crisis and some other type of acute process, such as biliary colic, appendicitis, or a perforated viscus. In the extremities, a sickle cell crisis may mimic osteomyelitis or an acute arthritis, such as gout or rheumatoid arthritis.

The most common extraskeletal abnormality in the hemolytic anemias is cardiomegaly caused by severe anemia and increased cardiac output. The heart has a globular configuration, reflecting enlargement of all chambers. Increased pulmonary blood flow produces engorgement of the pulmonary vessels, giving a hypervascular appearance to the lungs. Pulmonary infarction, pulmonary edema with congestive failure, and pneumonia are frequent complications.

Renal abnormalities can be demonstrated by excretory urography in approximately two-thirds of patients with sickle cell disease. A serious complication is renal papillary necrosis (see Figure 6-21), which is probably related to vessel obstruction within the papillae and may produce sinuses or cavity formation within one or more papillae.

Treatment. The cause and type of hemolytic anemia must be determined to successfully begin treatment. For spherocytosis, a splenectomy is curative.

For sickle cell anemia, no cure currently exists. Therefore, treatment consists of management and control of symptoms. The most invasive treatment, bone marrow transplantation, offers a possible cure. During a crisis, bed rest, maintenance of oxygen levels to prevent sickling, folic acid to aid in red blood cell production, maintenance of fluids to keep electrolyte balance stable, and possible blood transfusion (of packed

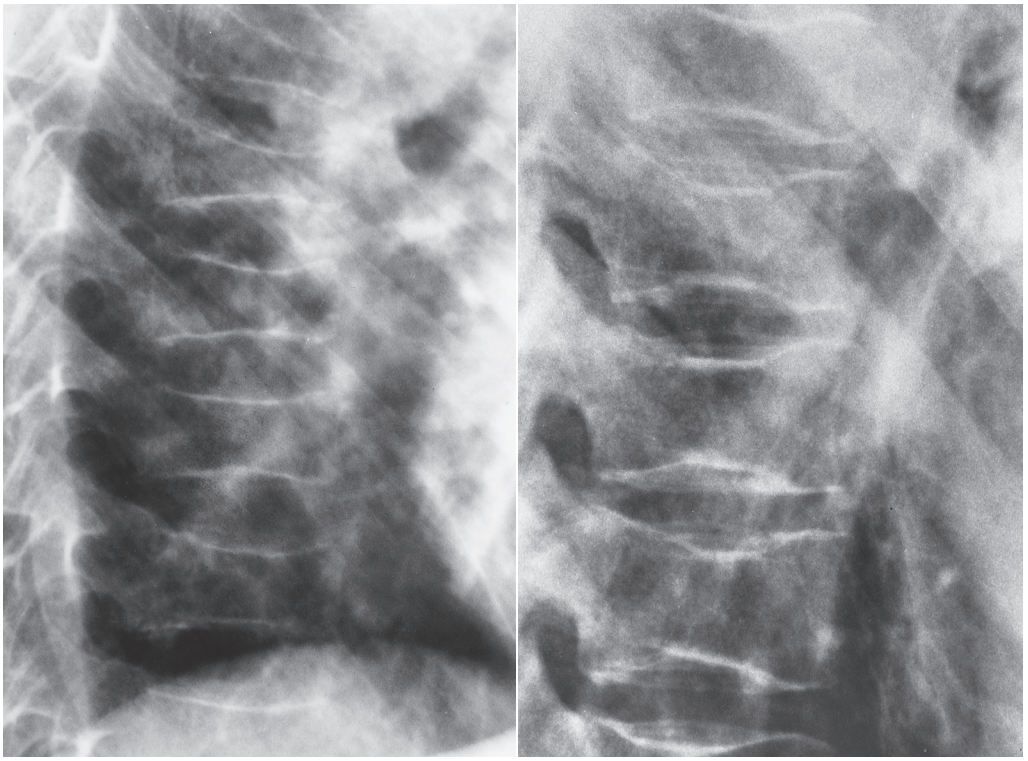

FIGURE 9-6 Sickle cell anemia. (A) Biconcave indentations on both the superior and the inferior margins of the soft vertebral bodies produce a characteristic fish vertebrae appearance. (B) Localized steplike central depressions of multiple vertebral end plates.

FIGURE 9-7 Acute osteomyelitis in sickle cell anemia. Diffuse lytic destruction of the proximal humerus can be seen along with extensive periosteal reaction (*arrows*).

FIGURE 9-8 Aseptic necrosis of the femoral head in sickle cell anemia. Mottled areas of increased and decreased density reflect osteonecrosis without collapse. Trabeculae in the neck and intertrochanteric region are thickened by the apposition of new bone. A solid layer of new bone along the inner aspect of the cortex of the femoral shaft causes narrowing of the medullary canal.

red blood cells) are appropriate. In some cases, prophylactic antibiotics are given. Gene therapy requires removing a defective cell, fixing the gene, and replanting the new cell into the bone marrow. This procedure may help manage and control symptoms and, in some cases, may even provide a cure.

If an Rh-negative mother delivers or aborts an Rh-positive infant, she is given a vaccine of Rh immunoglobulin within 24 hours to prevent the production of antibodies against the Rh factor. Blood testing to determine whether Rh incompatibility exists is now an essential part of prenatal care. An Rh-positive infant born to an Rh-negative mother receives a blood transfusion within 24 hours after birth.

Megaloblastic Anemia

A deficiency of vitamin B_{12} or of folic acid leads to defective deoxyribonucleic acid (DNA) synthesis and an anemia in which there is a decreased number of red blood cells, although each cell contains the normal amount of hemoglobin. The most common cause of vitamin B_{12} deficiency is **pernicious anemia**, in which there is inadequate intrinsic factor secretion related to atrophy of the gastric mucosa. Intrinsic factor acts as a carrier in the small bowel absorption of vitamin B_{12}, which is essential for erythrocyte development.

A deficiency of folic acid (and vitamin B_{12}) may also be related to intestinal malabsorption. This in turn may be related to intestinal parasites or bacterial overproduction, especially in patients with stasis of bowel contents, such as in blind loop syndrome and multiple jejunal diverticula. Other causes of megaloblastic anemia include a poor diet, such as strict vegetarianism, in which there are no sources of vitamin B_{12}, and long-term alcoholism, in which no folic acid is available.

Imaging appearance. Gastric atrophy is seen radiographically as a tubular stomach with a bald appearance that reflects a decrease or absence of the usually prominent rugal folds (Figure 9-9). It must be emphasized, however, that the radiographic findings of atrophic gastritis are often seen in older persons with no evidence of pernicious anemia.

Treatment. The treatment of megaloblastic anemia consists of correcting the deficiency of vitamin B_{12} or folic acid. Vitamin B_{12} deficiency requires an injection because taking vitamin B_{12} orally does not reverse the process. Folic acid deficiency can be treated with an oral supplement. If needed, a blood transfusion is given.

Aplastic Anemia

A generalized failure of the bone marrow to function (aplastic anemia) results in decreased levels of erythrocytes, leukocytes, and platelets. In addition to anemia, the patient cannot fight infection (a white blood cell function) and has a bleeding tendency (platelet depletion). Causes of aplastic anemia include exposure to chemical agents or drugs, infections, and invasion of the bone marrow by cancer.

Treatment. Patient prognosis depends on the severity and duration of the bone marrow aplasia. Regular blood transfusions are generally necessary for survival and to reduce symptoms. Because the patient has a suppressed immune response, preventive antibiotics are sometimes prescribed. Situations exposing the patient to an infection or a viral illness should be avoided. Some clinicians recommend medications to stimulate the bone marrow to produce more blood cells. Bone marrow transplantation is a new technique for treating patients with aplastic anemia.

Myelophthisic Anemia

Infiltration of bone marrow with nonhematopoietic cells, such as tumor cells, or encroachment on marrow cavities

FIGURE 9-9 Megaloblastic anemia. A patient with chronic atrophic gastritis, which is signified by the tubular stomach with a striking decrease in the usually prominent rugal folds.

caused by cortical thickening can result in severe myelophthisic anemia and pancytopenia (decreases in red and white blood cells and platelets). Tumors may arise from cells that are normally found in the bone marrow (leukemia, lymphoma, and myeloma), or the marrow may be invaded by extensive metastases to bone (from carcinomas of the breast, prostate, lung, and thyroid). Less common causes of marrow replacement include lipid storage disorders (Gaucher's disease), osteopetrosis (marble bones), and myelofibrosis.

Imaging appearance. Skeletal images may demonstrate lytic or blastic lesions, depending on the progression of metastases. A radionuclide bone scan detects bone marrow abnormalities and skeletal metastases. Magnetic resonance imaging (MRI) can demonstrate the extent of bone marrow infiltration.

Treatment. Treatment is focused on the underlying cause of the myelophthisic anemia. A packed red blood cell transfusion is used to treat the anemia and help stabilize the patient.

Polycythemia

Primary Polycythemia (Polycythemia Vera)

Polycythemia vera is a hematologic disorder characterized by hyperplasia of the bone marrow (neoplastic) that results in increased production of erythrocytes, granulocytes, and platelets. The disease is slowly progressive and produces symptoms associated with increased blood volume and viscosity. Cerebrovascular and peripheral vascular insufficiencies are common, and many patients give a history of some thrombotic or hemorrhagic event during the course of their disease. There is an increased incidence of peptic ulcer disease, and the excessive cellular proliferation often results in increased levels of uric acid with secondary gout and the formation of urate stones. The spleen is often massively enlarged and may be seen as a left upper quadrant mass.

Imaging appearance. Increased blood volume in polycythemia vera can lead to prominence of the pulmonary vascular shadows, usually without the cardiomegaly associated with the increased pulmonary vascularity that occurs in patients with congenital heart disease (Figure 9-10). Intravascular thrombosis may cause pulmonary infarctions that appear as focal areas of consolidation or as bands of fibrosis.

Secondary Polycythemia

Secondary polycythemia may be the result of long-term inadequate oxygen supply in patients with severe chronic pulmonary disease or congenital cyanotic heart disease, or it may develop in persons living at high altitudes. An elevated hemoglobin concentration may also be caused by certain neoplasms (renal cell carcinoma, hepatoma, and cerebellar hemangioblastoma) that result in an increased production of erythropoietin, which stimulates red blood cell formation.

Imaging appearance. Because secondary polycythemia is a compensatory phenomenon, the pulmonary vasculature is normal in appearance and there is no evidence of the disease on chest radiographs. In children with severe secondary polycythemia due to cyanotic heart disease, the skull may show thickened tables and a hair-on-end appearance, similar to the findings in congenital hemolytic anemias. Computed tomography (CT) may be used to investigate the kidneys and their function if a suspicion of tumor exists.

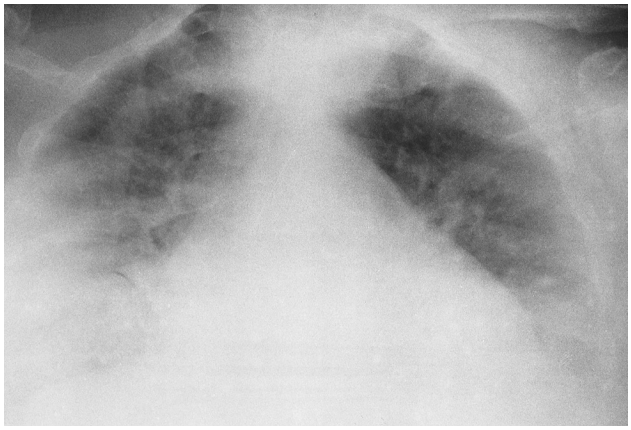

FIGURE 9-10 Primary polycythemia. Severe hypoventilation caused by profound obesity causes engorgement of pulmonary vessels. Although cardiomegaly is uncommon in polycythemia, in this case it reflects pronounced elevation of the diaphragm as a result of a huge abdominal girth and some underlying cardiac decompensation.

Treatment of Polycythemias

Treatment for both primary and secondary polycythemias starts with bloodletting to remove excessive cellular elements. This maneuver improves circulation by lowering blood viscosity and is continued until the hemoglobin and hematocrit levels become normal. Chemotherapy helps lower the platelet count and suppresses production of blood elements by the marrow. For primary polycythemia, clinicians may consider a splenectomy to alleviate painful enlargement of the organ and for patients with repeated episodes of thrombosis causing splenic infarction. Patients who receive these treatments can expect to live approximately 15 to 20 years after their condition is diagnosed.

DISEASES OF WHITE BLOOD CELLS

Leukemia

Leukemia is a neoplastic proliferation of white blood cells. The two major types of leukemia are named for the site of malignancy. **Myelocytic leukemia** is a cancer of the bone marrow (myelocytes are the primitive white blood cells in bone marrow). In this condition, a huge increase in the number of circulating granulocytes occurs, and the production of red blood cells and platelets is decreased. **Lymphatic leukemia** is a malignancy of the lymph nodes; in lymphocytic leukemia, the only white blood cells that dramatically increase are lymphocytes.

Leukemia may be chronic or acute. Acute lymphocytic leukemia, which has an abrupt onset and progresses rapidly, is the most common form in children. Acute myelocytic leukemia is more common in adults. Chronic leukemias run a more prolonged course and may involve either cell type.

Summary of Findings for Diseases of Red Blood Cells

Disorder	Location	Imaging Appearance	Treatment
Hemolytic anemias	Shortened life span of red blood cells	Long bones—osteoporosis, widened medullary spaces with thinning of cortices; in later stages: thickened, coarsened trabecular patterns Skull—thinning of outer table; vertical striation results from new bone formation	Spherocytosis—splenectomy curative Rh-negative mother and Rh-positive fetus—blood transfusion for baby and Rh immunoglobulin vaccine for mother
	Sickle cell anemia—hemoglobin molecule abnormal; red blood cells crescentic or sickle shaped	Spine—characteristic biconcave indentations superiorly and inferiorly on vertebral body Chest—cardiomegaly IVU/US—renal papillary necrosis	Sickle cell anemia—no cure exists Most invasive treatment—bone marrow transplantation offers possible cure Crisis—bed rest, maintenance of oxygen, folic acid, maintenance of fluids, possible blood transfusion
Megaloblastic anemia	Lack of small bowel absorption of vitamin B_{12} or folic acid	GI series—tubular stomach with bald appearance (decreased or absence of rugal folds)	Vitamin B_{12} deficiency requires an injection Folic acid deficiency can be treated with an oral supplement Possible blood transfusion
Polycythemia	Primary (neoplastic)—increased production of erythrocytes, granulocytes, and platelets	Chest image—prominent vascular markings without cardiomegaly	Bloodletting Chemotherapy Splenectomy
	Secondary (nonneoplastic)—elevated hemoglobin concentration	Chest image—normal Skull (of child)—thickened tables, hair-on-end appearance; similar to congenital hemolytic anemia	

GI, Gastrointestinal; *IVU,* intravenous urography; *US,* ultrasound.

Because of the exuberant white blood cell production, there is generally a decrease in the number of circulating red blood cells and platelets. This decrease in red blood cells results in a typical clinical appearance of weakness, shortness of breath, and cardiac palpitations. A decrease in the number of platelets interferes with the blood-clotting mechanism and results in a bleeding tendency. Even though there are more circulating white blood cells than normal, most are immature, and thus the patient becomes highly susceptible to infection. Diffuse infiltration of white blood cells into the spleen and liver may cause massive enlargement of these organs (hepatosplenomegaly).

Imaging appearance. In childhood leukemia, radiographically detectable skeletal involvement is extremely common as a result of the infiltration of leukemic cells into the marrow. The earliest radiographic sign of disease is usually transverse radiolucent bands at the metaphyseal ends of the long bones, most commonly about the knees, ankles, and wrists (Figure 9-11). In infancy, this appearance is nonspecific because it also occurs with malnutrition or systemic disease. The presence of these transverse lucent metaphyseal bands after 2 years of age is strongly suggestive of acute leukemia.

As the proliferation of neoplastic cells in the marrow becomes more extensive, actual destruction of bone may occur. This may cause patchy lytic lesions, a permeative moth-eaten appearance, or diffuse destruction with cortical erosion (Figure 9-12). A reactive response to proliferating leukemic cells can cause patchy or uniform osteosclerosis; subperiosteal proliferation incites the formation of periosteal new bone. Diffuse skeletal demineralization may result in vertebral compression fractures.

Enlargement of mediastinal and hilar lymph nodes is the most common abnormality on chest radiographs. Diffuse bilateral reticular changes may simulate lymphangitic spread of carcinoma. The nonspecific pulmonary infiltrates seen in patients with acute leukemia are usually attributable to hemorrhage or secondary infection.

The radiographic abnormalities in chronic leukemia are often similar to those in the acute disease, although their frequency and degree may vary. Skeletal changes are much

FIGURE 9-11 Acute leukemia. In addition to radiolucent metaphyseal bands, there is frank bone destruction with cortical erosion involving many metatarsals and proximal phalanges.

FIGURE 9-12 Acute leukemia. Proliferation of neoplastic cells in the marrow has caused extensive destruction of bone in both femurs.

less common and are usually limited to generalized demineralization in the flat bones, where active marrow persists in adulthood. The demonstration of focal areas of destruction or periosteal new bone formation indicates probable transformation into an acute phase of the disease.

Hilar and mediastinal adenopathy are common, especially in chronic lymphocytic leukemia. Congestive heart failure commonly results from the associated severe anemia.

Splenomegaly is an almost constant finding in patients with chronic leukemia (Figure 9-13). Leukemic infiltration of the gastrointestinal tract can produce single or multiple intraluminal filling defects, and the infiltrative process may be indistinguishable from carcinoma. Renal infiltration can cause bilateral enlargement of the kidneys. In chronic lymphocytic leukemia, enlargement of retroperitoneal or mesenteric lymph nodes can cause displacement or obstruction of structures in the genitourinary or gastrointestinal tracts.

Treatment. Leukemia treatment may require multidrug chemotherapy, bone marrow transplantation, antibiotics to aid in preventing infections, or a transfusion to reverse the blood cell imbalance. Interferon therapy is a drug regimen to help the body produce antiviral proteins that decrease the production of leukemia cells, resulting in an increase in the effectiveness of the immune system. Stem cell transplantation, although controversial and very expensive, helps by increasing the production of normal cells to replace cells damaged or destroyed by radiotherapy and chemotherapy.

Lymphoma

Lymphomas are neoplasms of the lymphoreticular system, which includes the lymph nodes, the spleen, and the lymphoid tissues of parenchymal organs, such as the gastrointestinal tract, lung, and skin. They are usually divided into two major types, Hodgkin's and non-Hodgkin's lymphomas. Ninety percent of cases of Hodgkin's disease originate in the lymph nodes; 10% are of extranodal origin. In contrast, parenchymal organs are more often involved in non-Hodgkin's lymphomas, approximately 40% of which are of extranodal origin.

Imaging appearance. Mediastinal lymph node enlargement is the most common radiographic finding in lymphoma (Figure 9-14). It is seen on initial chest radiographs of approximately half the patients with Hodgkin's disease and approximately one-third of those with non-Hodgkin's lymphoma. Mediastinal lymph node enlargement is usually bilateral but asymmetric.

Involvement of anterior mediastinal and retrosternal nodes is common, a major factor in differentiating lymphoma from sarcoidosis, which rarely produces radiographically visible enlargement of nodes in the anterior compartment. Calcification may develop in intrathoracic lymph nodes after mediastinal irradiation.

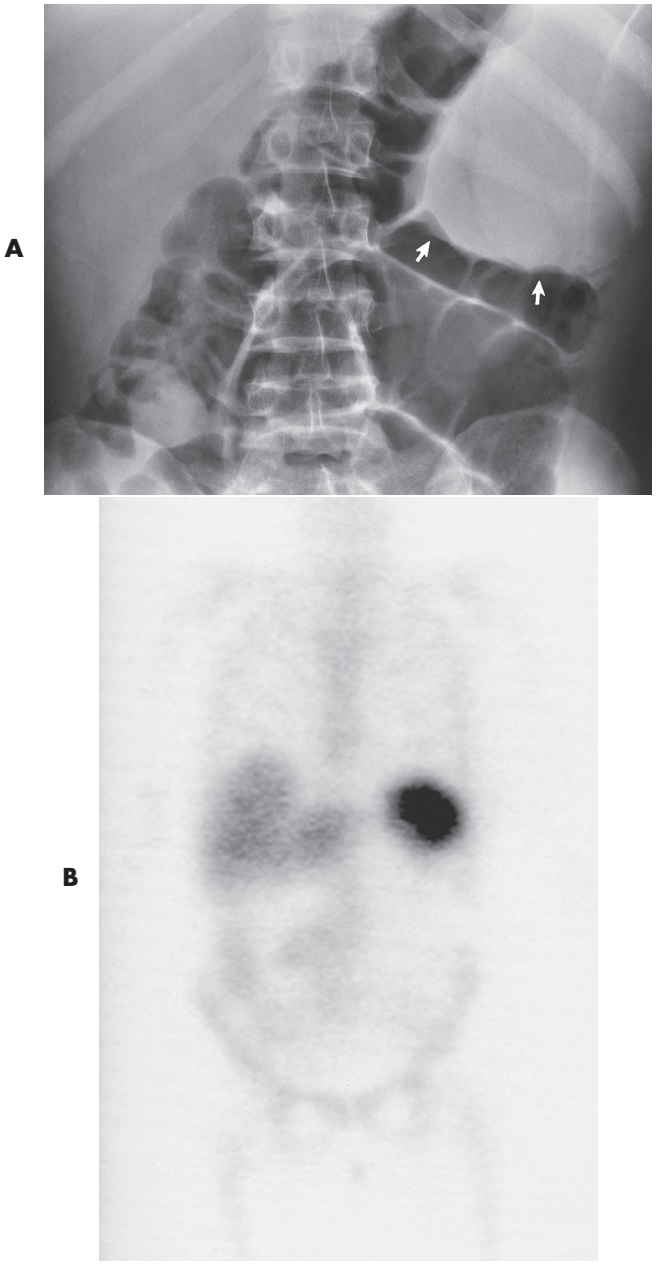

FIGURE 9-13 Chronic leukemia. (A) Massive splenomegaly causes downward displacement of splenic flexure of colon on an upper abdomen image. *Arrows* point to the inferior margin of the spleen. (B) Indium-111 whole-body scan. Indium-111 tagged to white blood cells illustrates a grossly enlarged spleen on images taken 27 hours after injection.

Involvement of the pulmonary parenchyma and pleura usually occurs by direct extension from mediastinal nodes along the lymphatic vessels of the bronchovascular sheaths. Radiographically, this may appear as a coarse interstitial pattern (Figure 9-15), as solitary or multiple ill-defined nodules, or as patchy areas of parenchymal infiltrate that may coalesce to form a large homogeneous mass. At times, it may be difficult to distinguish a superimposed infection after radiation therapy or chemotherapy from the continued spread of lymphomatous tissue. Pleural effusion occurs in up to one-third

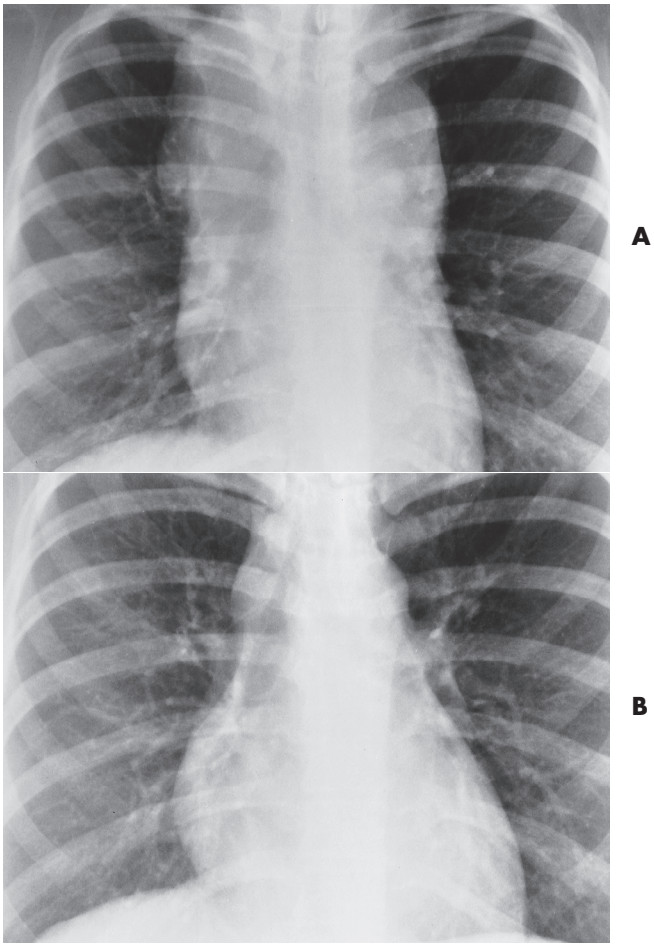

FIGURE 9-14 Lymphoma. (A) Initial chest image demonstrates considerable widening of upper half of the mediastinum caused by pronounced lymphadenopathy. (B) After chemotherapy, there is a dramatic decrease in the width of the upper mediastinum.

FIGURE 9-15 Lymphoma. Diffuse reticular and reticulonodular changes causing prominence of interstitial lung markings. Note the enlargement of the left hilar region.

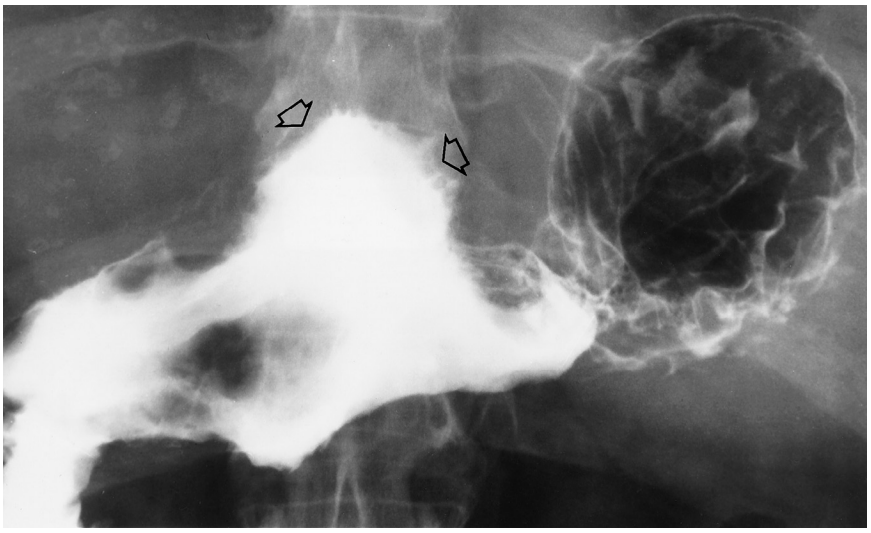

FIGURE 9-16 Lymphoma manifesting as a large mass almost filled by a huge ulcer (*arrows*).

of patients with thoracic lymphoma. Extension of the tumor to the pericardium can cause pericardial effusion.

Approximately 5% to 10% of patients with lymphoma have involvement of the gastrointestinal tract, primarily of the stomach and small bowel. Gastric lymphoma is often seen as a large, bulky polypoid mass, usually irregular and ulcerated, that may be indistinguishable from a carcinoma (Figure 9-16). A multiplicity of malignant ulcers or an aneurysmal appearance of a single huge ulcer (the diameter of which exceeds that of the adjacent gastric lumen) is characteristic of lymphoma. Additional findings suggestive of lymphoma include relative flexibility of the gastric wall, enlargement of the spleen, and associated prominence of retrogastric and other regional lymph nodes that cause extrinsic impressions on the barium-filled stomach. Other manifestations of gastric lymphoma are thickening, distortion, and nodularity of rugal folds (Figure 9-17) and generalized gastric narrowing caused by a severe fibrotic reaction.

Lymphoma can produce virtually any pattern of abnormality in the small bowel. The disease may be localized to a single intestinal segment, it may be multifocal, or it may cause diffuse involvement. The major radiographic appearances include irregular thickening of mucosal folds, large ulcerating masses, and multiple intraluminal or intramural filling defects simulating metastatic disease.

Skeletal involvement can be demonstrated in approximately 15% of patients with lymphoma (Figure 9-18). Direct extension from adjacent lymph nodes causes bone erosion, especially of the anterior surface of the upper lumbar and lower thoracic spine. Paravertebral soft tissue masses may occur. The hematogenous spread of lymphoma produces a mottled pattern of destruction and sclerosis, which may simulate metastatic disease. Dense vertebral sclerosis (ivory vertebra) may develop in Hodgkin's disease (Figure 9-19).

Diffuse lymphomatous infiltration may cause renal enlargement, with distortion, elongation, and compression of the calyces (Figure 9-20). Single or multiple renal nodules or perirenal masses may displace or distort the kidney. Diffuse

FIGURE 9-17 Lymphoma of the stomach. Note the diffuse thickening, distortion, and nodularity of the gastric folds.

retroperitoneal lymphoma can displace the kidneys or ureters and obliterate one or both psoas margins.

Staging. Once the diagnosis of lymphoma is made, it is essential to determine the status of the abdominal and pelvic lymph nodes. This step is necessary both for the initial staging and treatment planning and for assessing the efficacy of treatment and detecting tumor recurrence.

Although lymphography was the procedure of choice in the past, MRI and positron emission tomography (PET) are now the noninvasive techniques employed to demonstrate lymphomatous involvement of the abdominal and pelvic

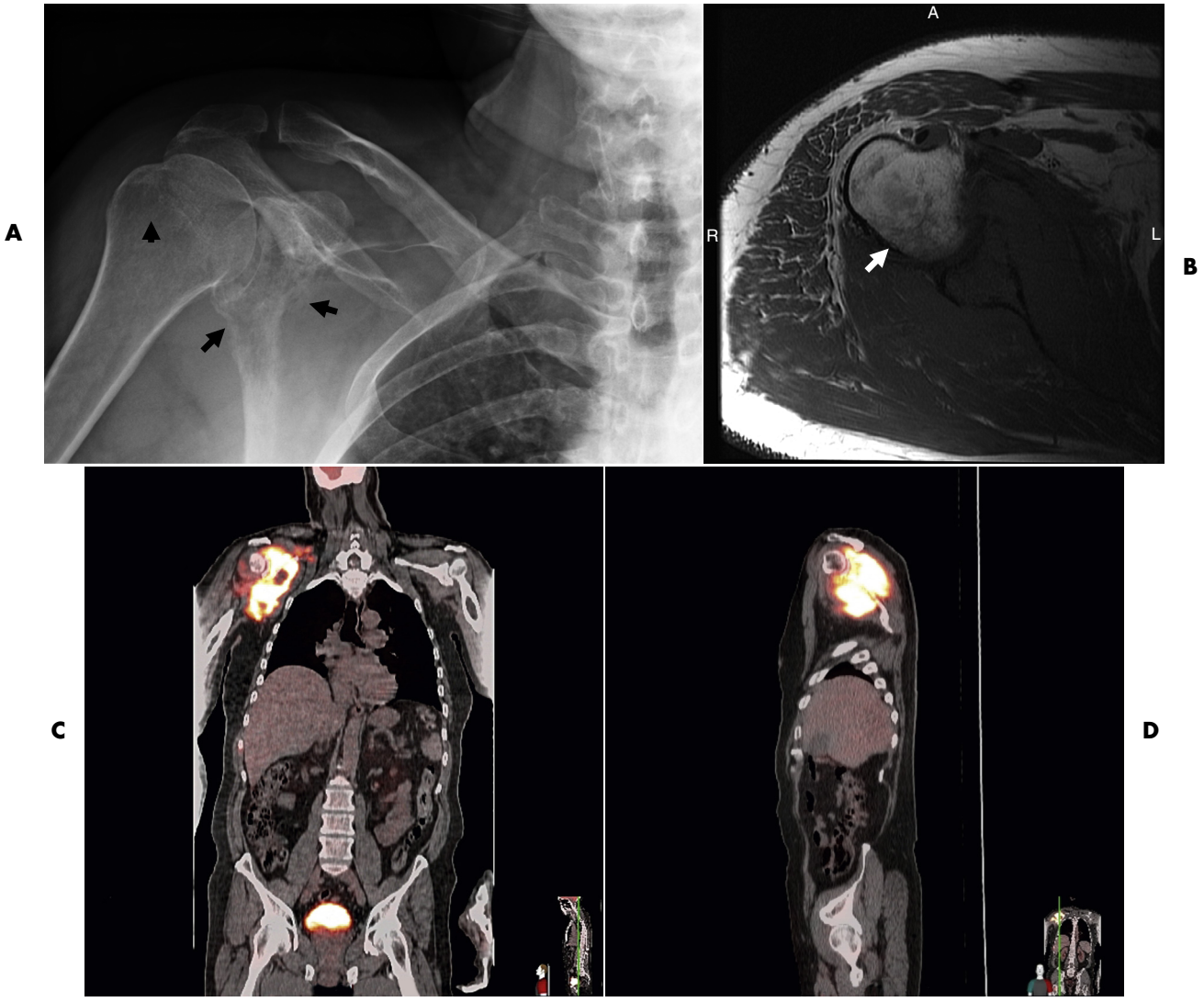

FIGURE 9-18 **Skeletal lymphoma.** Right shoulder radiograph and T1-weighted axial MR image demonstrate multiple lytic lesions with a moth-eaten appearance of the scapula **(A)** (*black arrows*) and humeral head **(B)** (*white arrow*). The coronal **(C)** and sagittal **(D)** PET-CT fusion images appear with increased uptake demonstrating the extent of shoulder girdle involvement.

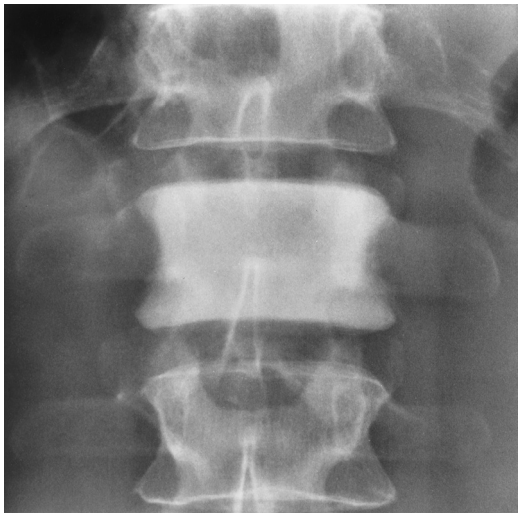

FIGURE 9-19 **Lymphoma.** Ivory vertebra.

FIGURE 9-20 **Lymphoma.** Right kidney is completely replaced by a lymphomatous mass (*L*). Note the extensive involvement of lymph nodes (*M*).

nodes. In practice, CT of the chest, abdomen, and pelvis is generally the first imaging procedure used in staging lymphoma, especially non-Hodgkin's lymphoma, which tends to produce bulky masses in the mesenteric and high retrocrural areas. Abnormal CT scans may eliminate the need for more invasive procedures (Figure 9-21); normal CT scans obtained at 2-cm intervals can exclude retroperitoneal adenopathy with a high degree of confidence. CT is usually used because of standardization and repeatability for patients. Malignant nodes appear round or oval, and their transverse-to-longitudinal ratio is greater than 2. Narrowing or absence of the hilus of the node also suggests malignancy.

Ultrasound (ultrasonography) can detect enlarged retroperitoneal nodes, characterize them, and measure them accurately. For retroperitoneal adenopathy, ultrasound is 80% to 90% accurate, and it has the ability to detect extranodal disease, which typically produces discrete hyperechoic masses. MRI is considered the superior technique because it can detect subtle detail with the use of multiple sequences. Tumor involvement on T1-weighted MR images appears as a relatively homogeneous mass with a low signal intensity that is similar to that of muscle. Edema, inflammation, immature fibrosis, or granulomatous tissue produces high signal intensity equal to or slightly greater than that of fat on T2-weighted MR images.

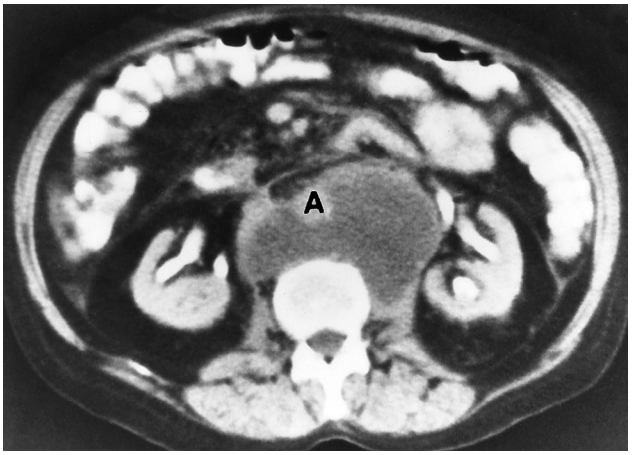

FIGURE 9-21 Lymphoma. CT scan demonstrates anterior displacement of abdominal aorta (*A*) away from the spine, caused by lymphomatous involvement of the retroaortic and para-aortic nodes.

Gallium scanning may illustrate increased nodal uptake (indicating swelling or inflammation) and can assess the response to treatment and detect early recurrence of tumor tissue. PET using fluorodeoxyglucose (FDG) uptake (FDG–PET) is considered superior to gallium scanning and CT because it can detect microscopic tumor foci and alterations in function within normal-size nodes (see Figure 9-18). PET also has the ability to distinguish large nodes that contain tumor from those that have only benign reactive changes. PET can also be used to monitor the effectiveness of the therapy and to identify tumor recurrence (Figure 9-22).

To ensure proper diagnosis and staging of both Hodgkin's and non-Hodgkin's lymphomas, biopsies are performed to extract cell and tissue samples. Free-hand fine-needle aspiration biopsy works best for superficial nodes, whereas CT-guided or ultrasound-guided biopsy is required for deep node evaluation. Patients unable to tolerate surgical procedures may undergo a large-needle core biopsy to determine the extent of the disease before treatment is begun.

Treatment. The best treatment available for Hodgkin's lymphoma consists of multidrug chemotherapy and high-dose radiation therapy. For non-Hodgkin's lymphoma, more aggressive chemotherapy is required if the disease process is diffuse (Figure 9-23), whereas conservative chemotherapy is used for low-level disease. Bone marrow transplantation may be necessary.

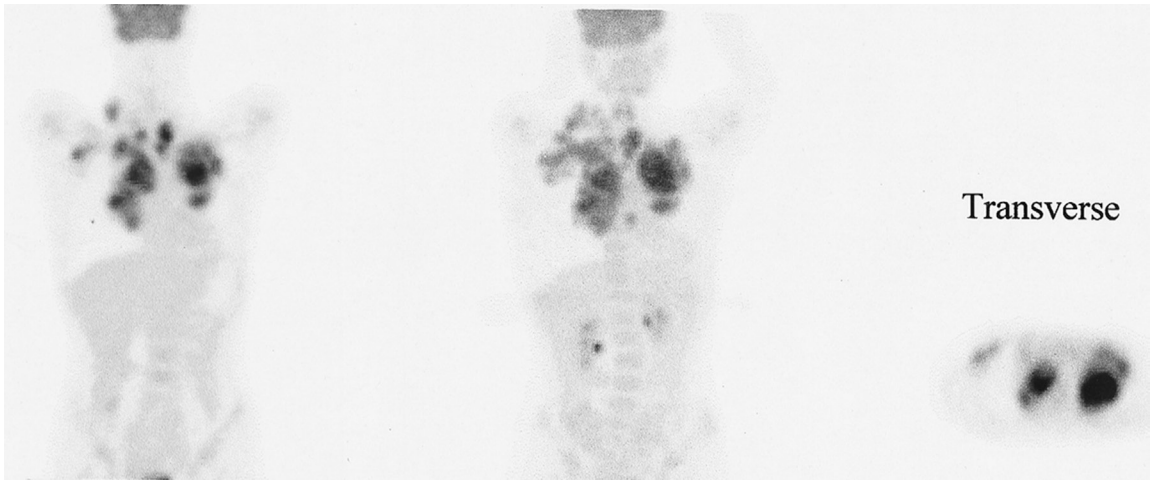

FIGURE 9-22 Lymphoma in a 16-year-old girl with a 3-week history of supraclavicular adenopathy. The PET body scan demonstrates FDG uptake in the supraclavicular fossae, the mediastinum, and the lungs; this finding indicates a metabolically active neoplasm, which is consistent with the clinically suspected lymphoma.

Summary of Findings for Diseases of White Blood Cells

Disorder	Location	Imaging Appearance	Treatment
Leukemia	Neoplastic proliferation of white blood cells	Skeletal radiograph in child—radiolucent bands at metaphyses on long bones after 2 years of age, bone destruction (moth-eaten appearance with resulting osteosclerosis), possible pathologic fractures Chest image—enlarged mediastinal and hilar lymph nodes, bilateral reticular changes; congestive heart failure KUB/US—splenomegaly With organ infiltration there is displacement or obstruction of GI or GU system	Multidrug chemotherapy Bone marrow transplantation Antibiotics Blood transfusion
Lymphoma	Neoplasm of lymphoreticular system	Chest image—asymmetrical, bilaterally enlarged mediastinal lymph nodes GI series—irregular and ulcerated polypoid mass (multiple ulcers or a huge single ulcer); thickening of rugal folds Skeletal radiograph—bone erosion of thoracolumbar spine with mottled pattern and sclerosis (ivory vertebra) CT—detects increased node size PET—metabolically active neoplasm	Hodgkin's lymphoma—multidrug chemotherapy and radiation therapy Non-Hodgkin's lymphoma—aggressive chemotherapy for diffuse disease; conservative chemotherapy for low-level disease Bone marrow transplantation
Infectious mononucleosis	Viral disease of lymphoreticular system	Generalized lymphadenopathy and splenomegaly	Self-limited—supportive treatment, bed rest, and hydration

GI, Gastrointestinal; *GU,* genitourinary; *KUB,* kidney–ureter–bladder radiograph; *PET,* positron emission tomography; *US,* ultrasound.

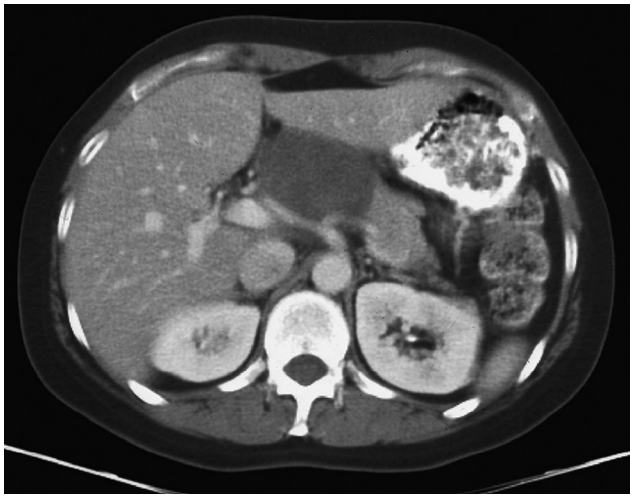

FIGURE 9-23 CT scan of patient with non-Hodgkin's lymphoma. The patient was diagnosed 8 months earlier with a pancreatic tumor measuring 4 × 6 × 4 cm. After chemotherapy, this scan shows a smaller tumor (3 × 5 × 3 cm) and no mass in the tail.

Infectious Mononucleosis

Mononucleosis is a self-limited viral disease of the lymphoreticular system characterized by vague symptoms of mild fever, fatigue, sore throat, and swollen lymph nodes caused by an intense increase of lymphoid cells. The Epstein–Barr virus may cause this disease process. It primarily infects young adults and, although often termed the "kissing disease," is not particularly contagious. Blood tests show an elevated white blood cell count with an abnormally high percentage of atypical lymphocytes, which resemble monocytes. The diagnosis is based on the presence of antibodies to the virus in the blood.

Imaging appearance. Generalized lymphadenopathy and splenomegaly are characteristic clinical and radiographic findings in infectious mononucleosis. Hilar lymph node enlargement, which is usually bilateral, can be demonstrated in approximately 15% of cases (Figure 9-24). Pneumonia is a rare complication that can appear as a diffuse reticular pattern, indicating interstitial disease, or as a patchy, nonspecific air-space consolidation.

Treatment. Because infectious mononucleosis is a self-limited disease, the usual treatment involves supportive therapy, adequate bed rest, and hydration.

DISEASES OF PLATELETS (BLEEDING DISORDERS)

Blood coagulation (clotting) is a complicated mechanism requiring platelets, calcium, and 12 coenzymes and proteins called **coagulation factors**. A deficiency in quantity or activity of any of these elements may lead to an inability to control hemorrhage or even to spontaneous bleeding.

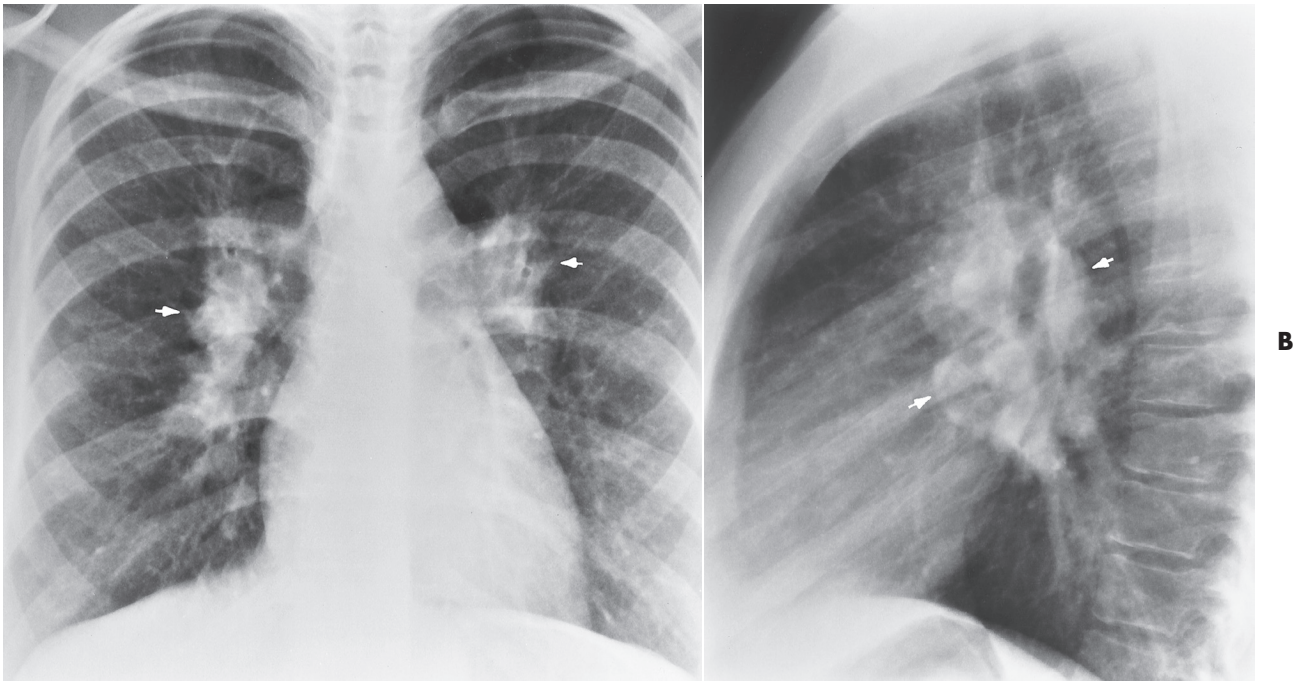

FIGURE 9-24 Infectious mononucleosis. Frontal (A) and lateral (B) projections of the chest demonstrate pronounced enlargement of hilar lymph nodes bilaterally (*arrows*).

Hemophilia

Hemophilia is an inherited (by a sex-linked recessive gene) anomaly of blood coagulation that appears clinically only in males. Patients with this disease have a decreased serum concentration or absence of antihemophilic globulin (factor VIII) and suffer a lifelong tendency to spontaneous hemorrhage or severe bleeding from even minor cuts or injuries.

Imaging appearance. The major radiographic changes in hemophilia are complications of recurrent bleeding into the joints, most commonly involving the knees, elbows, and ankles. Initially, the hemorrhage produces a generalized nonspecific soft tissue prominence of the distended joint. Deposition of iron pigment may produce areas of cloudy, increased density in the periarticular soft tissues. Although complete resorption of intra-articular blood may leave no residual change, subsequent episodes of bleeding result in synovial hypertrophy. In chronic disease, the hyperplastic synovium causes cartilage destruction and joint space narrowing and often leads to the development of multiple subchondral cysts of varying sizes in the immediate juxta-articular bone (Figure 9-25A). Destruction of articular cartilage and continued use of the damaged joint lead to subchondral sclerosis and collapse, extensive and bizarre spur formation, and often pronounced soft tissue calcification. Hemorrhage extending into the adjacent bony structures may cause extensive destruction (pseudotumor of hemophilia), which can mimic a malignant tumor (Figure 9-25B).

Repeated joint hemorrhages lead to increased blood flow in the region of the epiphysis and growth plate. These structures may ossify prematurely, become abnormally large, or fuse prematurely with the metaphysis. The increased blood flow and atrophy of bone and muscle that may follow an episode of joint bleeding result in severe osteoporosis. Common signs suggestive of, although not pathognomonic for, hemophilia include widening and deepening of the intercondylar notch of the femur (Figure 9-26) and "squaring" of the inferior border of the patella. Asymmetric growth of the distal tibial epiphysis may result in "slanting" of the talotibial joint. Hemarthrosis can cause occlusion of epiphyseal vessels and result in avascular necrosis. This process most commonly involves the femoral and radial heads, both of which have a totally intracapsular epiphysis and are therefore especially vulnerable to deprivation of their vascular supply from compression by a tense joint effusion.

As in the other bleeding disorders, submucosal bleeding into the wall of the gastrointestinal tract may develop in patients with hemophilia. It most commonly involves the small bowel and produces a short or long segment with regular thickening of folds. In the colon, bleeding may produce the thumbprint pattern of sharply defined, finger-like, marginal indentations along the contours of the colon wall.

Treatment. Hemophilia is usually treated with transfusions and factor VIII replacement.

Purpura (Thrombocytopenia)

Purpura refers to a deficiency in the number of platelets, and it results in spontaneous hemorrhages in the skin, mucous membranes of the mouth, and internal organs. The reduced number of platelets results from decreased production, increased destruction, or splenic sequestration of platelets. In the skin, purpura leads to the development of small, flat, red spots (petechiae) or larger hemorrhagic areas (ecchymoses).

Acute idiopathic thrombocytopenic purpura typically involves the sudden onset of severe purpura 1 to 2 weeks after a sore throat or upper respiratory infection in an otherwise

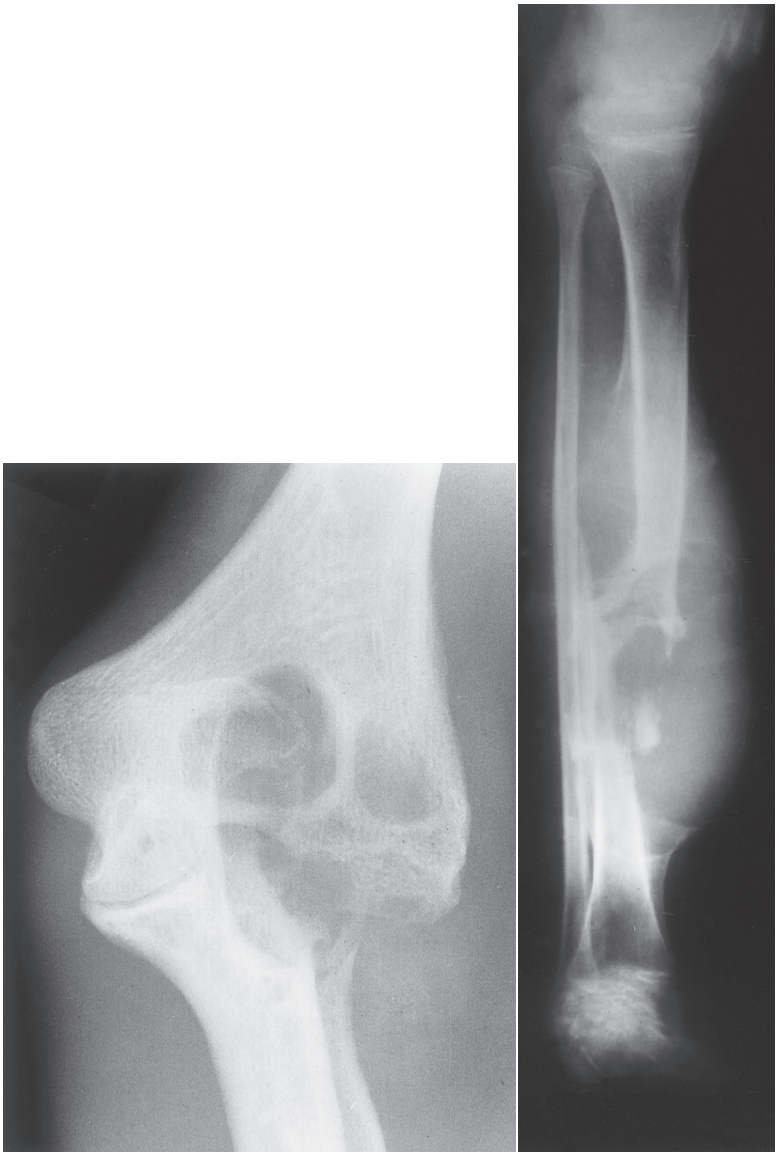

FIGURE 9-25 Hemophilia. (A) Large subchondral cysts about the elbow. (B) Destructive, expansile lesion of the lower tibial shaft.

healthy child. In most patients, the disorder is self-limited and clears spontaneously within a few weeks. Unlike the acute form, chronic idiopathic thrombocytopenic purpura occurs primarily in young women and has an insidious onset with a relatively long history of easy bruising and menorrhagia. This condition is generally considered to be an autoimmune disorder because most patients have a circulating platelet autoantibody that develops without underlying disease or significant exposure to drugs.

Purpura can also be a complication of conditions that suppress the bone marrow (aplastic anemia) or infiltrate the bone marrow with tumor cells (leukemia, lymphoma, myeloma, and metastases).

Imaging appearance. The radiographic changes caused by either acute or chronic idiopathic thrombocytopenic purpura primarily involve the gastrointestinal tract. Hemorrhage into the small bowel produces characteristic uniform, regular thickening of mucosal folds in the affected intestinal segment (Figure 9-27). Splenomegaly is commonly present; splenectomy is often required to remove this important site of platelet destruction and major source of platelet antibody synthesis.

Treatment. Blood platelet transfusions are being used to increase low platelet counts. Anti–human immunodeficiency virus (anti-HIV) drugs are effective in slowing or stopping the production of autoantibodies that attack the platelets. Drug-induced thrombocytopenia responds well to discontinuation of the offending drug. Virus-induced thrombocytopenia shows improvement following a cure of the infection.

FIGURE 9-26 Hemophilia. The intercondylar notch is greatly widened, and coarse trabeculae, narrowing of joint space, and hypertrophic spurring can be seen.

FIGURE 9-27 Chronic idiopathic thrombocytopenic purpura. Hemorrhage into the wall of the small bowel causes regular thickening of the mucosal folds.

Summary of Findings for Bleeding Disorders

Disorder	Location	Imaging Appearance	Treatment
Hemophilia	Anomaly of blood coagulation	Joint images—cloudy increased density in periarticular soft tissues Chronic—cartilage destruction with joint narrowing, multiple subchondral cysts; widening and deepening of intracondylar notch	Blood transfusion Factor VIII replacement
Purpura	Deficiency in number of platelets	Small bowel—uniform regular thickening of mucosal folds Splenomegaly	Self-limited—spontaneous recovery Drug-induced—discontinuation of drug Virus-induced—improves with cure of infection Splenectomy

REVIEW QUESTIONS

1. When diseases of the hematopoietic system result in demineralization of bone, the radiographer must be alert to the possibility of _____.
   a. patient infection
   b. self-infection
   c. pathologic fracture
   d. syncope
2. Red blood cells are called _____.
   a. erythrocytes
   b. leukocytes
   c. thrombocytes
   d. hemoglobin
3. Platelets are called _____.
   a. erythrocytes
   b. leukocytes
   c. thrombocytes
   d. lymphocytes
4. White blood cells are called _____.
   a. erythrocytes
   b. leukocytes
   c. thrombocytes
   d. pericytes
5. The smallest blood cells, platelets, are essential for what process?
   a. immunity
   b. clotting
   c. carrying oxygen
   d. fighting infection
6. Lymphocytes play a major role in the _____ system.
   a. endocrine
   b. hematopoietic
   c. immune
   d. metabolic

7. Which term refers to a decrease in the amount of oxygen-carrying hemoglobin in the blood?
   a. spherocytosis
   b. thalassemia
   c. anemia
   d. hematopoiesis
8. What type of anemia can cause painful bone infarcts and is generally confined to African Americans?
   a. spherocytosis
   b. thalassemia
   c. sickle cell
   d. Salmonella
9. A hematologic disorder characterized by an increase in the production of erythrocytes, granulocytes, and platelets is _____.
   a. polycythemia vera
   b. erythrocytosis
   c. sickle cell anemia
   d. hemolytic anemia
10. A cancerous disease of the hematopoietic system characterized by an increase in white blood cells is _____.
   a. anemia
   b. thrombocytopenia
   c. leukemia
   d. hemophilia
11. What is the name of an inherited anomaly of blood coagulation?
   a. sickle cell anemia
   b. hemophilia
   c. leukemia
   d. leukocytosis
12. What pathologic condition consists of a deficiency in the number of platelets resulting in spontaneous hemorrhages in the skin, internal organs, and mucous membranes of the mouth?
   a. hemophilia
   b. purpura
   c. leukemia
   d. sickle cell anemia

10

Endocrine System

OUTLINE

Physiology of the Endocrine System
Adrenal Glands
- Physiology of the Adrenal Glands
- Diseases of the Adrenal Cortex
- Diseases of the Adrenal Medulla

Pituitary Gland
- Physiology of the Pituitary Gland
- Diseases of the Pituitary Gland

Thyroid Gland
- Physiology of the Thyroid Gland
- Diseases of the Thyroid Gland

Parathyroid Glands
- Physiology of the Parathyroid Glands
- Diseases of the Parathyroid Glands

Diabetes Mellitus

KEY TERMS

acromegaly
androgens
follicular carcinoma
gigantism
glucocorticoids
hyperactive
hyperglycemia
hypoactive
medullary carcinoma
mineralocorticoids
papillary carcinoma
parathormone
primary hyperparathyroidism
primary hypoparathyroidism
secondary hyperparathyroidism
tertiary hyperparathyroidism
thyroxine
triiodothyronine

OBJECTIVES

After reading this chapter, the reader will be able to:

- Define and describe all boldface terms in this chapter
- Describe the physiology of the endocrine system
- Identify anatomic structures on both diagrams and images of the endocrine system
- Differentiate the various pathologic conditions affecting the endocrine system and their radiographic manifestations

RADIOGRAPHER NOTES

Imaging modalities are used to diagnose both the underlying endocrine disorder and the secondary changes that may occur in various areas of the body. Disorders of the endocrine glands themselves are usually evaluated by ultrasound, computed tomography (CT), magnetic resonance imaging (MRI), and radionuclide scanning, including positron emission tomography (PET). Secondary pathologic manifestations elsewhere in the body are generally evaluated on plain radiographs, for which the routine exposure techniques may have to be altered (see Box 1-1). For example, Cushing's syndrome causes extensive osteoporosis, which requires a decrease in kilovolts-peak for adequate visualization of the demineralized bones. Also note that patients with this condition can easily sustain pathologic fractures and thus should always be handled with caution.

PHYSIOLOGY OF THE ENDOCRINE SYSTEM

The endocrine system is a biochemical communication network through which several small glands control a broad range of vital body activities. The endocrine glands secrete chemical messengers called *hormones,* which circulate in the blood and may affect a single target organ or the entire body. Hormones may be proteins (growth hormone), steroids (cortisone), peptides (antidiuretic hormone [ADH]), amino acids (thyroxine), or amines (epinephrine). They range from small to large molecules and have chemical structures of various complexities.

The major endocrine glands are the pituitary, adrenal, thyroid, and parathyroid glands. Inadequate (**hypoactive**) or excess (**hyperactive**) production of hormones from these endocrine glands can give rise to a wide variety of clinical symptoms and radiographic abnormalities.

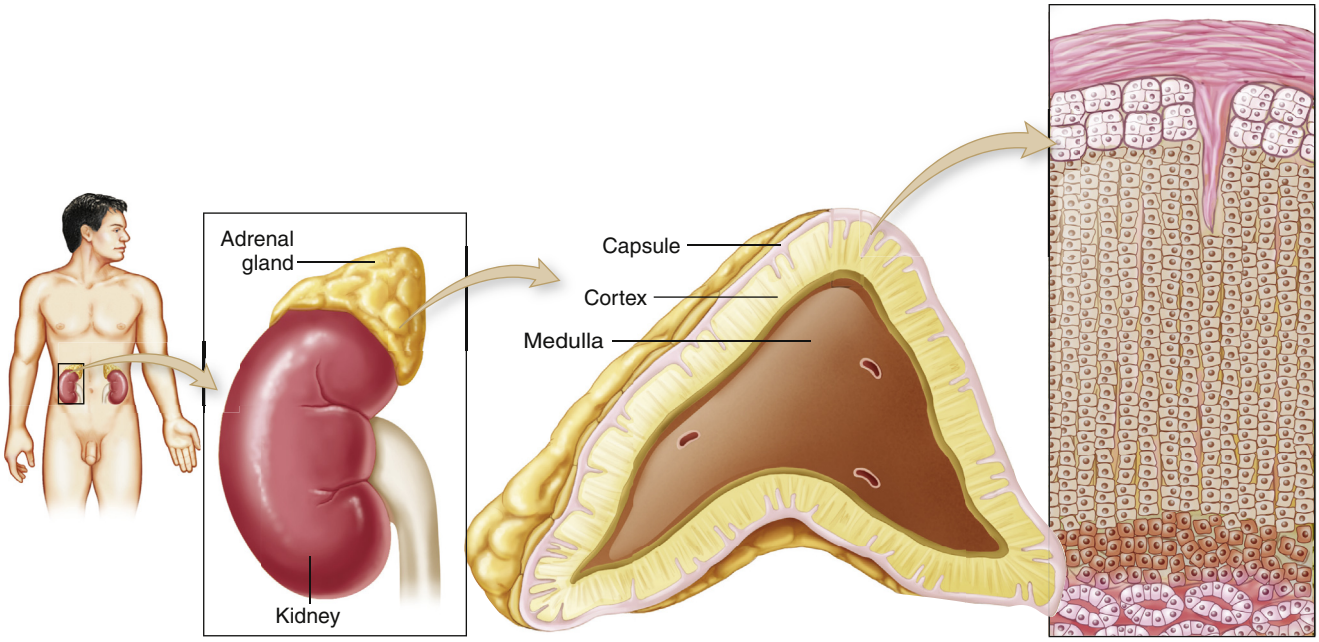

FIGURE 10-1 Structure of the adrenal gland.

Because hormones are powerful chemicals, it is essential that their circulating levels be carefully controlled. One type of control is called the *negative feedback mechanism*. In this system, an adequate level of a hormone in the blood automatically stops the release of additional hormone (somewhat like a thermostat). As the blood level of the hormone decreases, the gland is stimulated to secrete more of it. Another control mechanism is the production of two different hormones whose actions are opposite to each other. For example, insulin is secreted by the pancreas when the blood glucose level rises. When the blood glucose level falls below normal, a second hormone, glucagon, is secreted by the pancreas to raise the blood glucose level. Thus, these two hormones are balanced so that a proper blood glucose level is continually maintained.

ADRENAL GLANDS

Physiology of the Adrenal Glands

Each of the adrenal glands, which are situated at the top of each kidney, consists of an outer cortex and an inner medulla (Figure 10-1). The adrenal cortex secretes several different types of steroid hormones, which can be divided into three general groups. The **mineralocorticoids** (primarily aldosterone) regulate salt and water balance by controlling sodium retention and potassium excretion by the kidneys. The production of aldosterone is regulated primarily by the secretion of renin from specialized cells (the juxtaglomerular apparatus) in the kidney. Reduced blood volume (as in hemorrhage) causes low blood pressure, which is detected by the juxtaglomerular apparatus and eventually results in increased aldosterone secretion from the adrenal cortex.

Glucocorticoids (especially cortisone) regulate carbohydrate metabolism and are under the regulation of adrenocorticotropic hormone (ACTH) from the anterior pituitary gland. Cortisone also depresses the inflammatory response to almost all forms of injury, thus leading to its use in the treatment of trauma, rheumatoid arthritis, bursitis, and asthma and as an immunosuppressive agent to help limit rejection after organ transplantation.

Androgens are sex hormones that tend to masculinize the body, to retain amino acids, and to enhance protein synthesis. These hormones are used both illegally and unwisely by athletes in an attempt to increase body strength.

The adrenal medulla secretes epinephrine (adrenaline) and norepinephrine. These fight-or-flight hormones are secreted in stress situations when additional energy and strength are needed. Epinephrine stimulates heart activity, raises blood pressure, and increases the level of blood glucose. By constricting some blood vessels and dilating others, epinephrine shunts blood to active muscles where oxygen and nutrients are urgently needed.

Diseases of the Adrenal Cortex

Cushing's Syndrome

The excess production of glucocorticoid hormones in Cushing's syndrome may be attributable to generalized bilateral hyperplasia of the adrenal cortex, or it may be a result of a functioning adrenal or even nonadrenal tumor. It can also be the result of the exogenous administration of cortisone. Excess secretion of glucocorticoid hormones mobilizes lipids and increases their level in the blood. This increase produces a characteristic obesity that is confined to the trunk of the body and is associated with a round, moon-shaped face and a pathognomonic fat pad that forms behind the shoulders (buffalo hump). Retention of salt and water results in hypertension.

Imaging appearance. Generalized enlargement of the adrenal glands is best demonstrated by CT, which shows

FIGURE 10-2 Cushing's syndrome caused by large adrenal adenoma. Nephrotomogram demonstrates a huge suprarenal mass (*arrows*) causing indentation and downward displacement of left kidney.

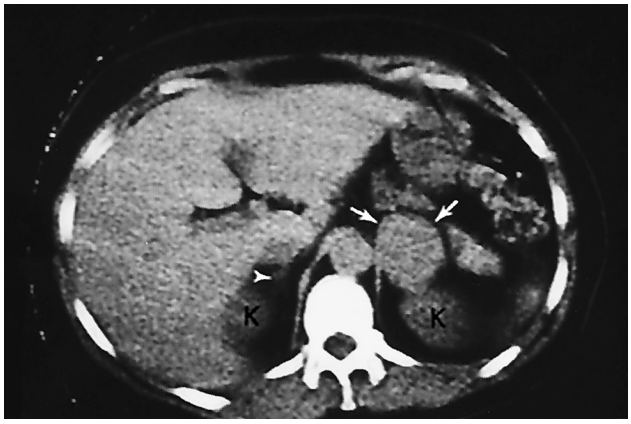

FIGURE 10-3 Cushing's syndrome caused by functioning cortical adenoma. A 4-cm mass in the left adrenal gland (*arrows*) can be seen posterior to the tail of the pancreas and anterior to the kidney (*K*). *Arrowhead* points to the normal right adrenal gland.

thickening of the wings of the adrenal gland; the wings appear to have a stellate or Y-shaped configuration in cross section. Ultrasound can also show diffuse adrenal gland enlargement.

Benign and malignant tumors of the adrenal cortex are less common causes of Cushing's syndrome than is nontumorous adrenal hyperfunction. As a general rule, the larger the adrenocortical tumor and the more abrupt the onset of clinical symptoms and signs, the more likely the tumor is to be malignant (Figure 10-2). However, the differentiation between adenoma and carcinoma may be impossible at the time of histologic examination, and the nature of the tumor may have to be defined by the clinical course alone. Both CT and ultrasound can demonstrate an adrenal tumor (Figure 10-3), but CT is often more valuable because the abundance of retroperitoneal fat may prevent an optimal ultrasound examination. Adrenal venography has been widely used to demonstrate adrenal masses, and it also permits the aspiration of blood samples for assessment of the level of adrenal hormones.

Cushing's syndrome produces radiographic changes in multiple systems. Diffuse osteoporosis causes generalized skeletal demineralization, which may lead to the collapse of vertebral bodies, spontaneous fractures, and aseptic necrosis of the head of the femur or humerus. Widening of the mediastinum as a result of excessive fat deposition sometimes develops in Cushing's syndrome and can be confirmed by CT. Hypercalciuria caused by elevated steroid values can lead to renal calculi and nephrocalcinosis.

Imaging of the sella turcica by conventional tomography or CT is important in the routine assessment of a patient with Cushing's syndrome. Most patients with nontumorous adrenal hyperfunction are found at surgery to have an intrasellar lesion. It is important to emphasize, however, that small pituitary microadenomas may be present in asymptomatic patients. The modality of choice to detect a functioning microadenoma causing adrenal hyperplasia is contrast-enhanced MRI. A pituitary adenoma develops in up to one-third of patients after adrenal surgery and produces progressive sellar enlargement. For this reason, yearly follow-up sellar tomograms may be indicated after adrenalectomy.

Nonpituitary tumors producing ACTH may cause adrenal hyperfunction and Cushing's syndrome. The most common sites of origin are the lung, thymus, and pancreas; approximately half of these tumors can be demonstrated on chest radiographs. Octreotide scintigraphy (a nuclear medicine examination) detects ectopic ACTH tumors on the basis of increased uptake of tumor cell surface receptors for somatostatin.

Treatment. Treatment for Cushing's syndrome depends on the cause of the excess production of glucocorticoid hormones. Surgical resection is the treatment of choice to eliminate the excess hormone production. Medical suppression of abnormal endocrine stimulation and radiation therapy directed to the hyperfunctioning tumor are alternatives if the tumor is inoperable.

Aldosteronism

An overproduction of mineralocorticoid hormones produced by the most superficial layer of the adrenal cortex causes retention of sodium and water and abnormal loss of potassium in the urine. This condition results in hypertension, muscular weakness or paralysis, and excessive thirst (polydipsia). Aldosteronism may be attributable to an adrenocortical adenoma (Conn's syndrome) or to bilateral hyperplasia of the superficial cortical layer. Aldosteronism may also be the result of renin-secreting tumors, renal artery stenosis, malignant hypertension, and bilateral chronic renal disease. The biochemical assay is the basis for diagnosing aldosteronism, and CT or MRI is used for adrenal identification.

Imaging appearance. The role of diagnostic imaging is to demonstrate the location of adenomas that may otherwise be difficult to detect during exploratory surgery.

Noncontrast CT, the most widely used imaging modality, demonstrates the small adrenocortical adenoma as a contour

FIGURE 10-4 Aldosteronoma. Note the small mass (*arrow*) anterior to the left kidney.

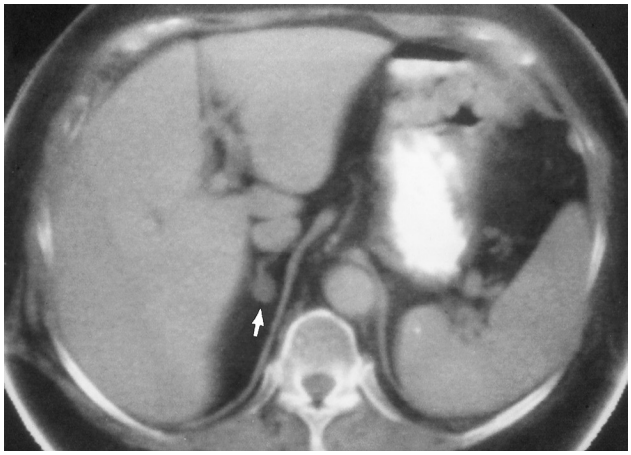

FIGURE 10-5 Adrenogenital syndrome. Caused by a functioning adrenocortical tumor (*arrow*).

abnormality of the gland (Figure 10-4). With use of CT or MRI, the adrenal gland can be measured quite accurately; the normal adrenal measures 3 to 6 mm thick, 4 to 6 mm long, and 2 to 3 cm wide. However, the scan or image may not demonstrate any abnormal findings. With newer CT scanners, specificity has increased to 75%, and tumors larger than 1 cm can be consistently identified. Adenomas may be isointense or hypointense relative to the liver on T1-weighted MR images. On T2-weighted images, they have slight hyperintensity. Chemical-shift imaging can aid in identifying and characterizing an adrenal mass. In adenomas smaller than 1 cm, nuclear medicine studies using ^{131}I attached with a cholesterol binder can differentiate a normal gland from hyperplasia on the basis of the time course of radionuclide uptake. Early uptake (less than 5 days) in both adrenal glands indicates hyperplasia, whereas unilateral early uptake implies an adrenal adenoma. Adrenal venography with biochemical assay of a sample of adrenal blood is another important technique for localizing aldosteronomas and determining whether the hyperaldosteronism is primary or secondary.

Treatment. Hypertension and other clinical manifestations of aldosteronism can be cured by the resection of an adenoma but are little affected by the removal of both adrenal glands in the patient with bilateral hyperplasia. Medical antihypertensive agents, especially long-acting calcium channel blockers, are available if the adenoma is inoperable.

Adrenogenital Syndrome

The adrenogenital syndrome (adrenal virilism) is caused by the excessive secretion of androgenically active substances by the adrenal gland. In the congenital form, a specific enzyme deficiency that prevents the formation of androgenic hormones causes continuous ACTH stimulation and bilateral hyperplasia. The elevated levels of androgens result in accelerated skeletal maturation along with premature epiphyseal fusion, which may lead to dwarfism.

In women, the syndrome causes masculinization, with the development of hair on the face (hirsutism). The breasts diminish, the clitoris enlarges, and ovulation and menstruation cease.

Imaging appearance. Most cases of acquired adrenogenital syndrome are caused by adrenocortical tumors, which can be detected by CT (Figure 10-5), ultrasound, or adrenal venography. CT is currently the imaging modality of choice.

Treatment. Surgical resection of a hyperfunctioning tumor with replacement therapy allows normal development. Medical suppression of abnormal stimuli prevents the excessive release of ACTH, allowing female features to develop normally. If not treated, a masculinized woman may require reconstructive surgery.

Hypoadrenalism

The clinical manifestations of adrenal insufficiency vary from those of a chronic insidious disorder (easy fatigability, anorexia, weakness, weight loss, and increased melanin pigmentation) to those of an acute collapse with hypotension, rapid pulse, vomiting, and diarrhea.

The most common cause of adrenal insufficiency is the excessive administration of steroids. Primary adrenocortical insufficiency (Addison's disease) results from progressive cortical destruction, which must involve more than 90% of the glands before clinical signs of adrenal insufficiency appear. In the past, Addison's disease was usually attributed to tuberculosis; currently, most cases reflect idiopathic atrophy, probably on an autoimmune basis. In areas where the disease is endemic, histoplasmosis is an occasional cause of adrenal insufficiency.

Imaging appearance. Acute inflammatory disease causes generalized enlargement of the adrenal glands, which can be demonstrated by a variety of imaging techniques (Figure 10-6). MRI can differentiate adrenal masses better than CT, but MRI cannot distinguish a tumor from an inflammatory process. Other radiographic findings occasionally seen in patients with adrenal insufficiency include a small heart and calcification of the cartilage of the ear.

Treatment. Corticosteroids produce a fast recovery and must be administered regularly for the patient's survival. Morbidity and mortality are high without treatment.

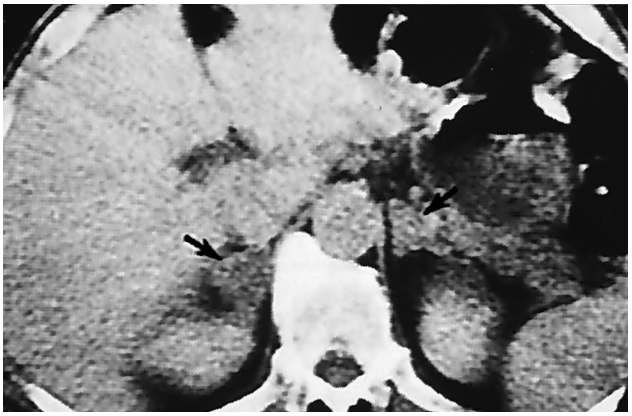

FIGURE 10-6 Adrenocortical insufficiency. Caused by disseminated histoplasmosis. CT scan demonstrates bilateral adrenal enlargement (*arrows*).

Adrenal Carcinoma

Approximately half of adrenal carcinomas are functioning tumors that cause Cushing's syndrome, virilization, feminization, or aldosteronism. The tumors grow rapidly and are usually large necrotic masses at the time of clinical presentation.

Imaging appearance. Ultrasound demonstrates the tumor as a complex mass that may be difficult to separate from an upper pole renal tumor (Figure 10-7). CT demonstrates an adrenal carcinoma as a large unilateral mass with an irregular edge that often contains low-density areas resulting from central necrosis or prior hemorrhage (Figure 10-8) and high-density calcifications. On contrast-enhanced CT, the tumor enhancement is irregular and greatest on the periphery. For adrenal examinations, spiral CT with 3- to 5-cm section reconstructions offers the best resolution and may identify tumors 1 cm or smaller.

Because lymphatic and hepatic metastases are common at the time of clinical presentation, CT scans at multiple abdominal levels are necessary to define the extent of the primary tumor and to detect metastases before surgical resection is attempted. Extension of the tumor into the renal vein and inferior vena cava can also be detected by CT, especially after the injection of intravenous contrast material, or by MRI (Figure 10-9). On MR images, the higher signal intensity of the tumor in comparison with the liver on T2-weighted images (lower signal intensity on T1-weighted images) may distinguish adrenal carcinoma from nonfunctioning adenomas and pheochromocytomas.

Treatment. The treatment of choice for adrenal carcinoma is surgical resection by open laparotomy or laparoscopy. Chemotherapy using mitotane, an adrenocortical cytotoxin and adrenal inhibitor, may improve symptoms if resection is not an option.

Metastases to the Adrenal Gland

The adrenal gland is one of the most common sites of metastatic disease. The primary tumors that most frequently metastasize to the adrenal gland are carcinomas of the lung, breast, kidney, ovary, and gastrointestinal tract, and melanomas.

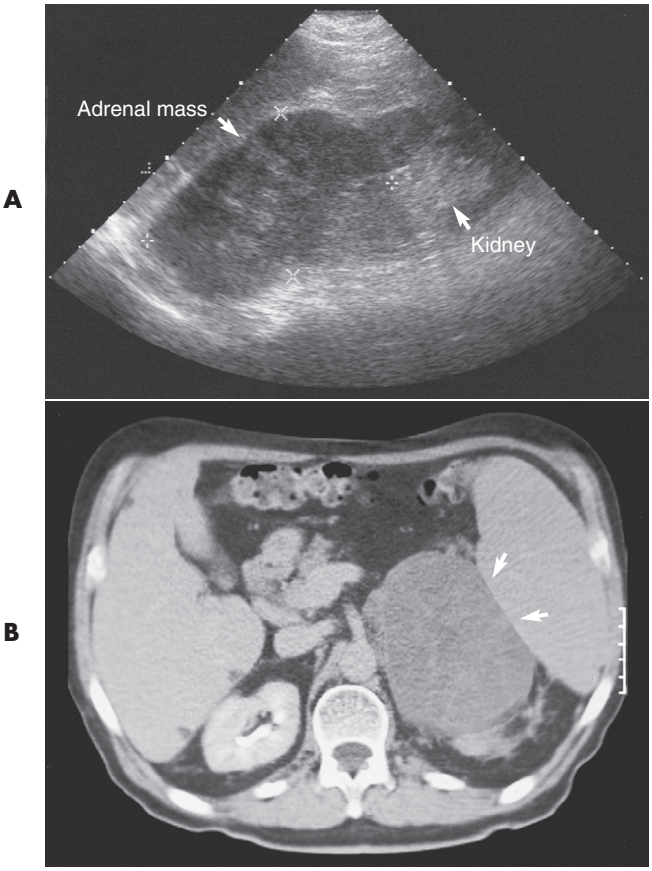

FIGURE 10-7 Adrenal carcinoma. (A) Ultrasound image identifies a heterogeneous lobulated mass (12 × 7 × 11 cm) involving the upper pole of the left kidney. (B) CT scan 1 month later shows diffuse inhomogeneous enhancement with the appearance of some low-density areas suggesting necrosis.

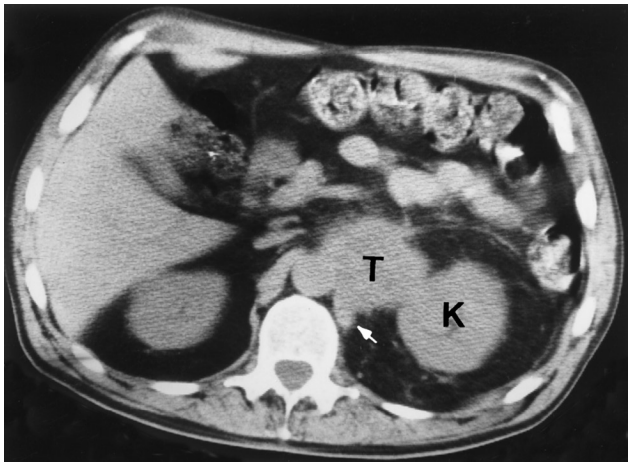

FIGURE 10-8 Adrenal carcinoma. Large soft tissue tumor (*T*) invades the anteromedial aspect of the left kidney (*K*) and the left crus of the diaphragm (*arrow*).

Imaging appearance. Metastatic enlargement of an adrenal gland can cause downward displacement of the kidney with flattening of the upper pole. Ultrasound and CT demonstrate adrenal metastases as solid, soft tissue masses that vary considerably in size and are frequently bilateral (Figure 10-10). However,

the ultrasound (hypoechoic lesions) and CT patterns are indistinguishable from those of primary malignancies of the gland. Therefore, when a known primary tumor exists elsewhere, it is usually assumed that an adrenal mass is metastatic.

On MRI, metastases typically have higher signal intensity on T2-weighted images than do benign adenomas, and they also demonstrate increased contrast enhancement on T1-weighted, fat-suppressed images. In-phase and out-of-phase pulse sequences (also known as chemical-shift imaging) are highly accurate for distinguishing between adrenal adenomas and metastases. Lipid-laden adenomas show low signal intensity on out-of-phase images and intermediate to high signal intensity on in-phase images.

If necessary, a needle biopsy using ultrasound or CT guidance may be of value to determine whether the adrenal lesion is primary or metastatic.

Treatment. The most common form of treatment for adrenal metastases is an adrenalectomy, followed by replacement therapy; however, because metastasis has occurred, the prognosis is unfavorable.

Summary of Findings for Diseases of the Adrenal Cortex

Disorder	Location	Imaging Appearance	Treatment
Cushing's syndrome	Bilateral adrenal hyperplasia, cortical Adrenal tumor	CT (noncontrast)—thickening of adrenal wings, which appear stellate or in a Y shape US—diffuse adrenal gland enlargement CT—to evaluate sella turcica MRI—detects functioning pituitary microadenoma causing adrenal hyperplasia	Surgical resection for erosive hormone production Medical suppression of endocrine stimulation if tumor is inoperable Radiation therapy if tumor is inoperable
Aldosteronism	Overproduction of mineralocorticoid hormones	CT—locates small adrenocortical adenoma as a contour abnormality of the gland MRI—lesion is hypointense or isointense to liver on T1-weighted images, and hyperintense on T2-weighted images NM—unilateral early uptake of the affected gland Venography (adrenal)—to acquire material for biochemical assay	Resection of altered adrenal gland Therapeutic option: antihypertensive drugs
Adrenogenital syndrome	Excessive secretion of androgenically active substances	CT/US—demonstrates underlying adrenal neoplasm or hyperplasia Venography (adrenal)—to acquire material for biochemical assay	Surgical resection Medical suppression Reconstructive surgery if necessary
Hypoadrenalism	Adrenal insufficiency	CT—enlarged or atrophic adrenal glands	Corticosteroids Morbidity and mortality high without treatment
Adrenal carcinoma	Tumor of adrenal cortex	US—complex tabulated mass above upper pole of kidney; homogeneous when small; heterogeneous when large, with central necrosis or hemorrhage CT—irregular mass containing low-density areas often with calcifications; periphery enhances with contrast agent; metastasis also detected MRI—has higher signal intensity than liver on T2-weighted images	Surgical resection Chemotherapy
Adrenal metastases	Adrenal gland	US/CT—demonstrates type of mass and whether bilateral MRI—metastases have high signal intensity on T2-weighted images; greater contrast enhancement with metastases than with benign adenoma Chemical-shift imaging—lipid-laden adenoma produces low signal intensity on an out-of-phase image US/CT—guided biopsy	Adrenalectomy with replacement therapy

NM, Nuclear medicine study; *US,* ultrasound.

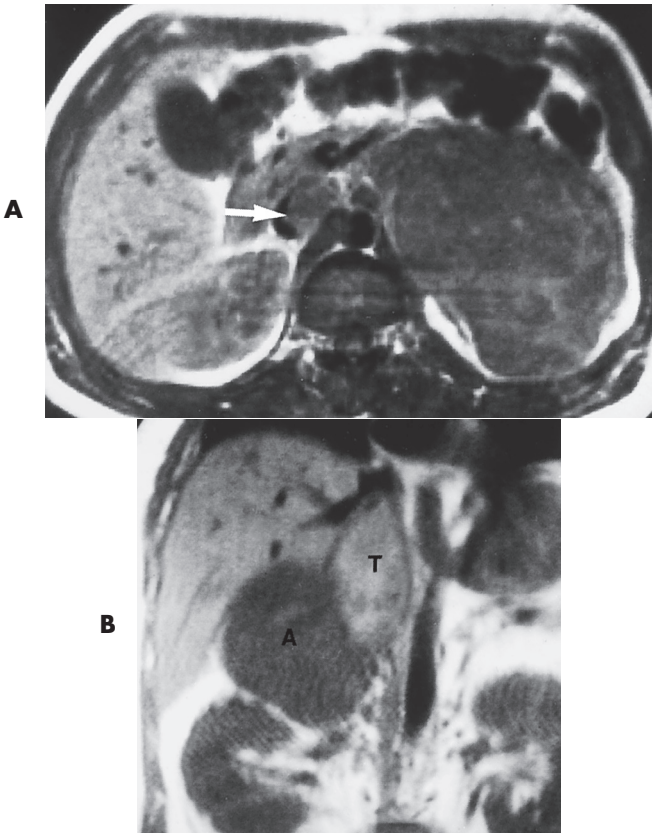

FIGURE 10-9 Adrenal carcinoma. (A) Axial MR image demonstrates a large left adrenal tumor invading the left renal vein and inferior vena cava (*arrow*). (B) In another patient, a coronal MR image shows an adrenal mass (*A*) above the kidney with a tumor thrombus of slightly higher signal intensity filling the inferior vena cava (*T*).

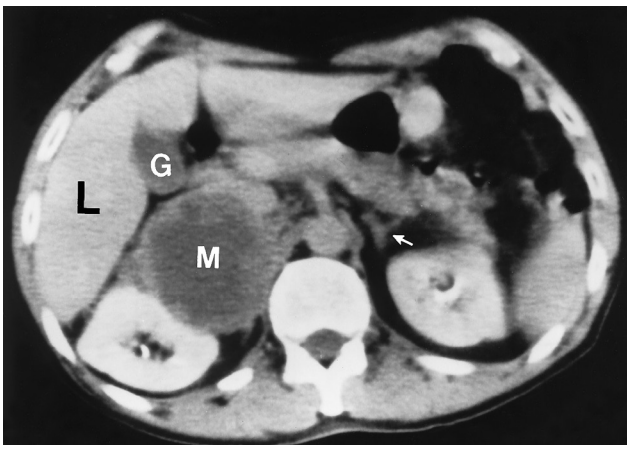

FIGURE 10-10 Adrenal metastases. Note the huge irregular low-attenuation mass (*M*) representing adrenal metastasis from oat cell carcinoma of the lung. The left adrenal gland (*arrow*) is normal. *G,* Gallbladder; *L,* liver.

Diseases of the Adrenal Medulla

Pheochromocytoma

A pheochromocytoma is a tumor that most commonly arises in the adrenal medulla and produces an excess of vasopressor substances (epinephrine and norepinephrine), which can cause an uncommon but curable form of hypertension. Approximately 10% of pheochromocytomas are extra-adrenal in origin. Approximately 10% of patients with pheochromocytoma have bilateral tumors, and a similar percentage of pheochromocytomas are malignant.

Because in almost all patients the diagnosis of a pheochromocytoma can be made with biochemical tests, radiographic imaging serves as a confirmatory study and as a means of localizing the tumor. Excretory urography, even with nephrotomography, may be of limited value because the kidney is often not displaced even when the adrenal pheochromocytoma is large.

Imaging appearance. CT and ultrasound (Figure 10-11) are very useful in the localization of pheochromocytomas. The cross-sectional images not only detail the extent of the adrenal lesion but also define the status of adjacent structures and can demonstrate bilateral or multiple pheochromocytomas, extra-adrenal tumors, and metastases. Pheochromocytomas generally appear as round, oval, or pear-shaped masses, often greater than 3 cm, that are slightly less echogenic than liver and kidney parenchyma on ultrasound and have an attenuation value less than these organs on CT (Figure 10-12). Necrosis, hemorrhage, and fluid levels are common findings in larger lesions. Most extra-adrenal pheochromocytomas arise in the abdomen (Figure 10-13); a few are found in the chest or neck. The tumor may be located anywhere along the sympathetic nervous system, in the organ of Zuckerkandl, and in chemoreceptor tissues such as the carotid body and the glomus jugulare, in the wall of the urinary bladder, or even in the kidney or ureter. Masses may displace the ureter or kidney or may appear as filling defects in the bladder.

MRI can demonstrate the relationship of the tumor to surrounding structures in the coronal plane (Figure 10-14) and has a higher sensitivity than CT. On T2-weighted spin-echo images, the extreme hyperintensity of the tumor (because of its water content) makes it stand out from the surrounding structures. When CT and MRI findings are inconclusive, a radionuclide scan using meta-iodobenzylguanidine is highly sensitive for localizing ectopic pheochromocytomas, but this agent is not readily available.

In patients with pheochromocytomas, the arterial injection of contrast material causes a sharp elevation in blood pressure, which must be controlled by α-adrenergic blocking agents. Therefore, arteriography is hazardous in these patients.

Treatment. Surgical removal of the tumor results in stabilizing the blood pressure and curing the hypertension. Most tumors are benign and well encapsulated, enabling their successful removal.

Neuroblastoma

Neuroblastoma, a tumor of adrenal medullary origin, is the second most common malignancy in children. Approximately 10% of these tumors arise outside the adrenal gland,

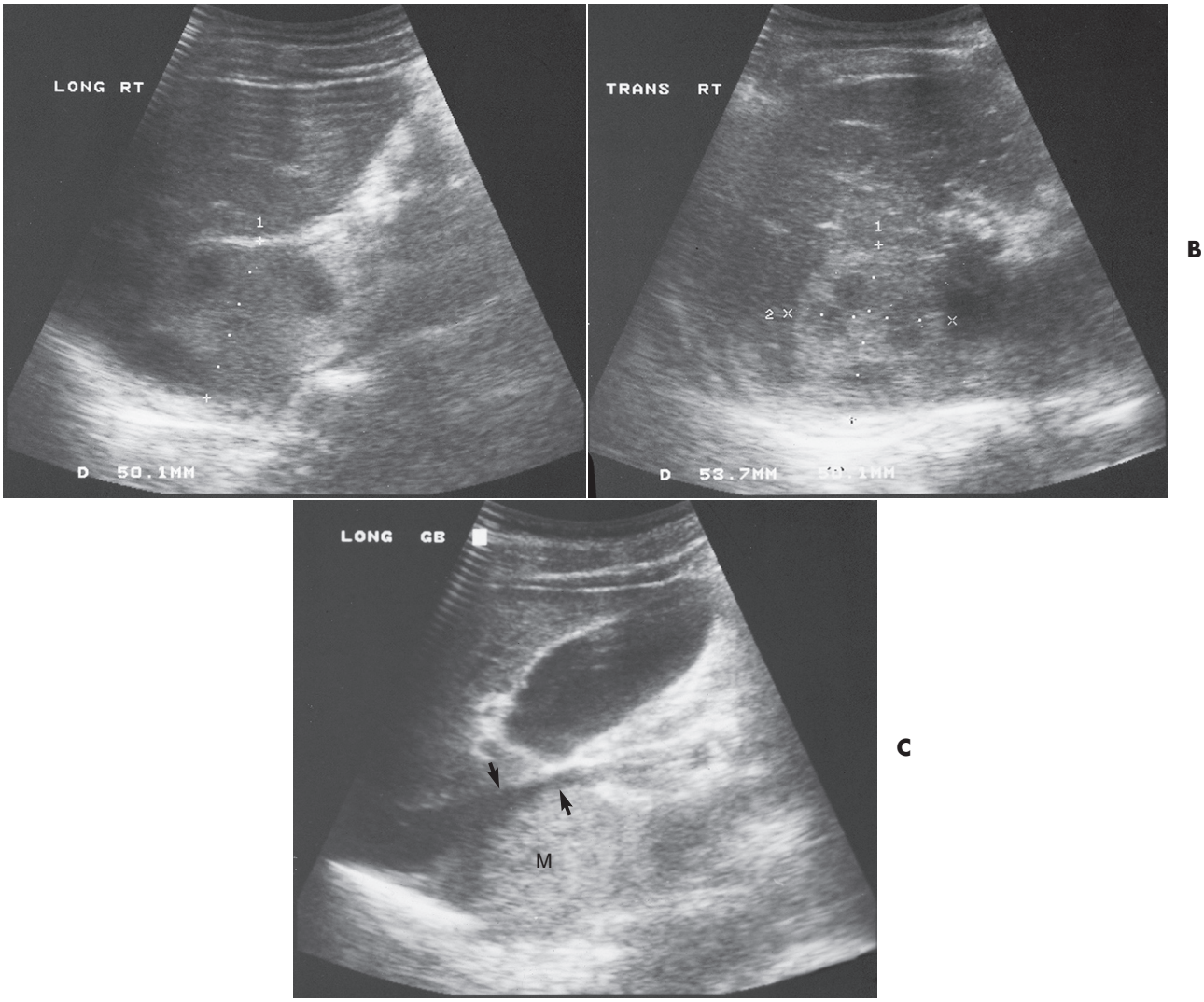

FIGURE 10-11 Pheochromocytoma. Longitudinal (A) and transverse (B) ultrasound images show a cystic and necrotic mass superior to the right kidney (note the measuring markers). (C) The mass (*M*) elevates the inferior vena cava (*arrows*). The patient's history of increased heart rate (up to 200 beats per minute) and elevated blood pressure are consistent with a diagnosis of pheochromocytoma.

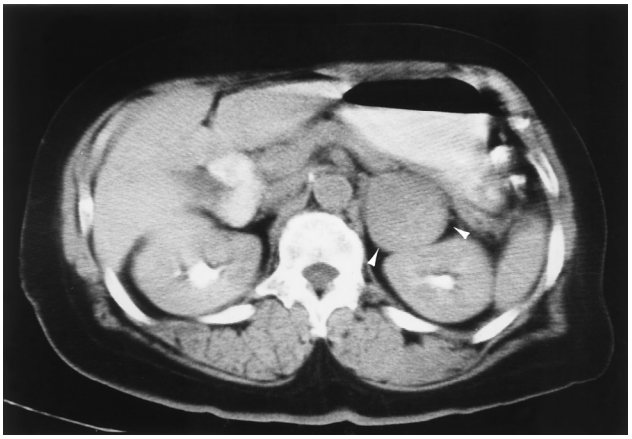

FIGURE 10-12 Pheochromocytoma. Large, pear-shaped mass (*arrows*) is shown anterior to left kidney.

primarily in sympathetic ganglia in the neck, chest, abdomen, or pelvis. The tumor is highly malignant and tends to attain great size before its detection.

Imaging appearance. Calcification is common in neuroblastoma (occurring in approximately 50% of cases), in contrast to the relatively infrequent calcification in Wilms' tumor, from which neuroblastoma must be differentiated. Calcification in a neuroblastoma has a fine granular or stippled appearance (Figure 10-15A). Occasionally, there may be a single mass of amorphous calcification. Calcification can also develop in metastases of neuroblastoma in the paravertebral lymph nodes and the liver.

Intravenous urography usually demonstrates downward and lateral renal displacement by the tumor mass (Figure 10-16). Neuroblastoma tends to cause the entire kidney and its collecting system to be displaced as a unit, unlike Wilms'

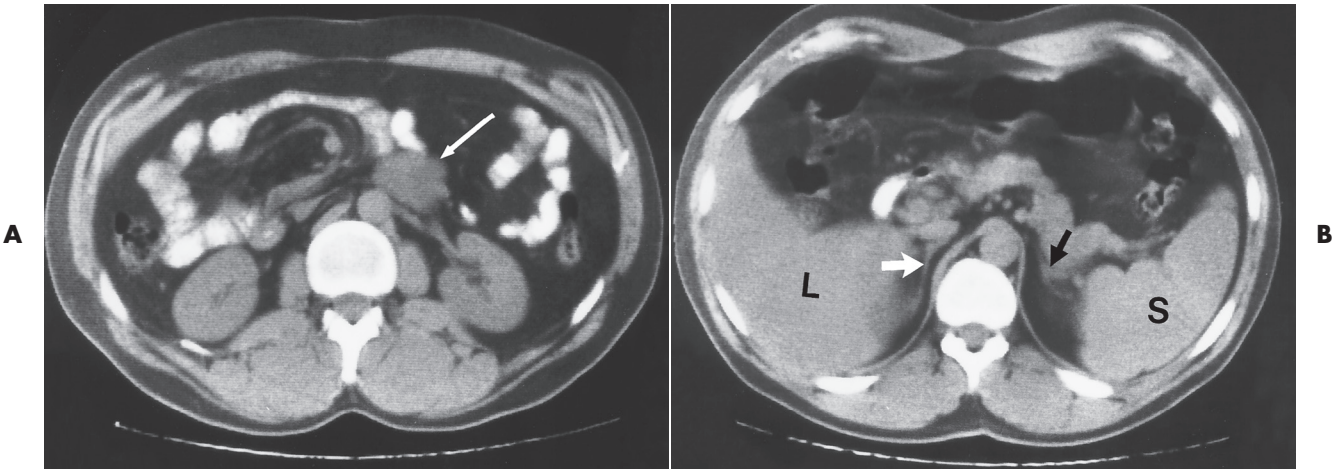

FIGURE 10-13 Ectopic pheochromocytoma. **(A)** Soft tissue mass (*arrow*) can be seen adjacent to the aorta and in front of the left renal vein. **(B)** CT scan taken at a higher level demonstrates that both right and left adrenal glands are normal (*arrows*). *L,* Liver; *S,* spleen.

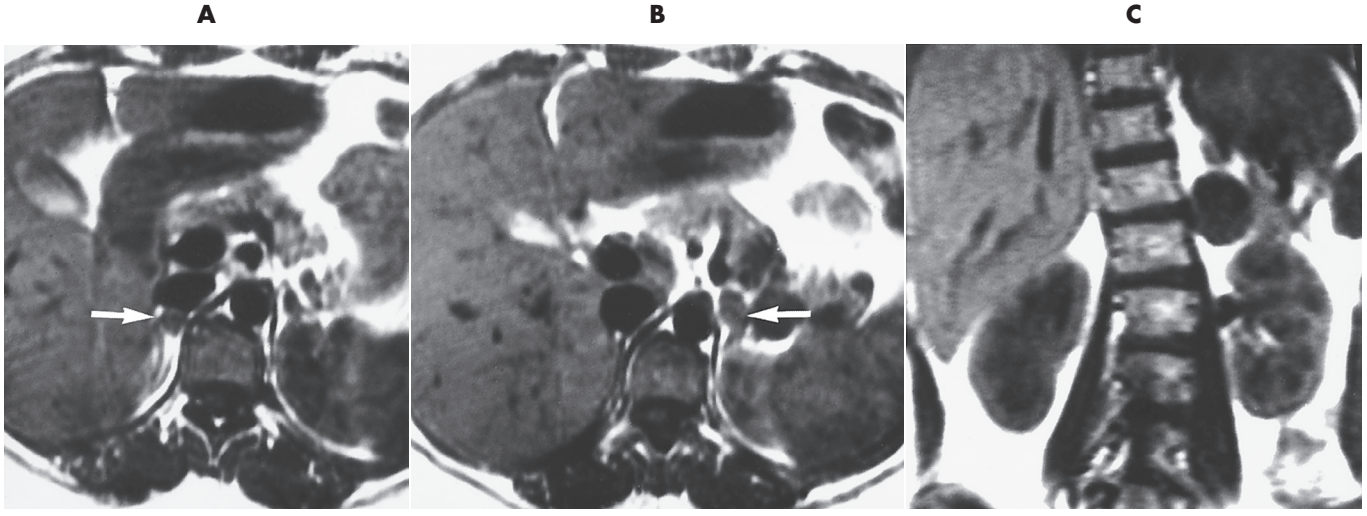

FIGURE 10-14 Pheochromocytoma. **(A** and **B)** Axial MR images at two levels demonstrate bilateral low-intensity lesions (*arrows*). **(C)** Coronal MR image (in a different patient) shows a left suprarenal mass.

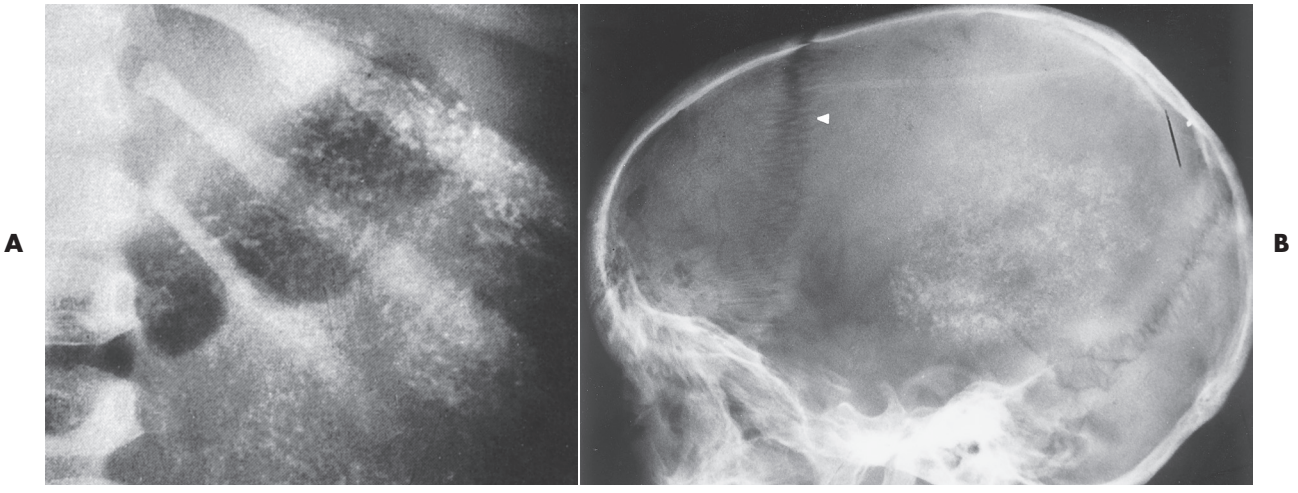

FIGURE 10-15 Neuroblastoma metastatic to bone. **(A)** Plain image of the upper abdomen shows a diffuse granular calcification within a large primary tumor. **(B)** Lateral projection of the skull shows similar calcified deposits within a metastatic lesion in the calvaria. Note the sutural widening (*arrowhead*) consistent with increased intracranial pressure.

FIGURE 10-16 Neuroblastoma. Nephrotomogram demonstrates downward and lateral displacement of the upper pole of the left kidney.

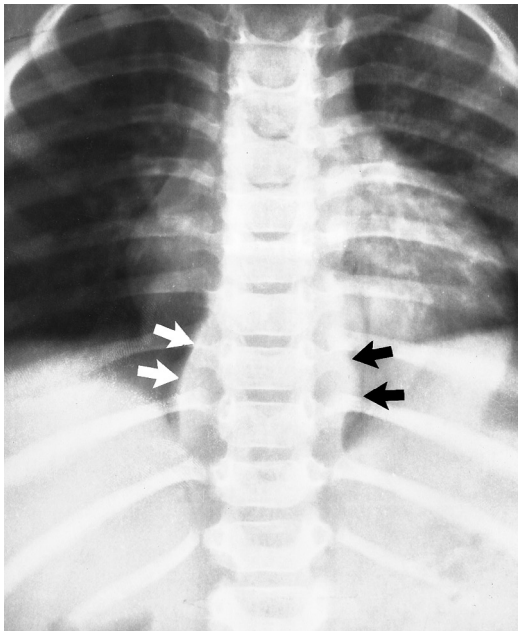

FIGURE 10-17 Neuroblastoma. Bilateral widening of the paravertebral stripes (*arrows*) represents metastatic deposits.

tumor, which has an intrarenal origin and thus tends to distort and widen the pelvicalyceal system.

Because of its nonionizing character, ultrasound is a superb modality for evaluating abdominal masses in children. A neuroblastoma appears as a solid or semisolid mass that is separate from the kidney. It appears as a poorly defined heterogenic mass, unlike the well-defined and relatively homogeneous Wilms' tumor. A neuroblastoma is often diffusely hyperechogenic, probably because of necrosis, calcification, and hemorrhage. On contrast-enhanced CT, necrosis and hemorrhage cause the tumor to appear heterogeneous

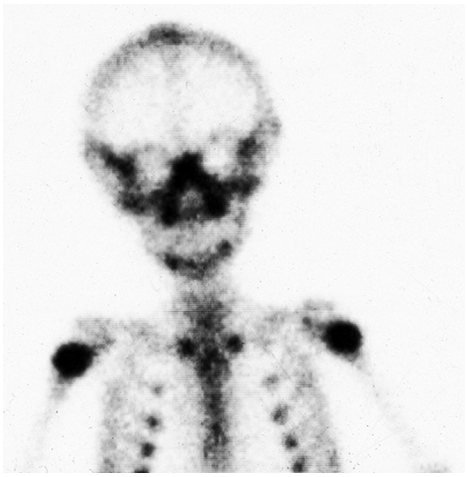

FIGURE 10-18 Neuroblastoma. Bone scan performed in a 1-year-old boy with left adrenal neuroblastoma to evaluate for osseous involvement. Temporal bones and orbital zygomatic region demonstrate increased uptake appearing as "raccoon eyes."

and often lobulated. Because CT can demonstrate evidence of tumor spread to lymph nodes and the sympathetic chain, widening of the paravertebral stripe (also seen on plain images) (Figure 10-17), and metastases to the liver and chest, it has become the most commonly used imaging study to diagnose neuroblastomas. This modality is also used to assess the response to treatment. MRI, which like ultrasound does not use ionizing radiation, may offer a safer approach to demonstrating characteristics typical of tumor tissue. Neuroblastomas usually produce a hypointense signal on T1-weighted images and are hyperintense on T2-weighted images. On contrast-enhanced T1-weighted images, hemorrhage appears as a hyperintense signal.

Metastases to bone, liver, and lungs are common in neuroblastoma. Metastases to the skull typically cause spreading of cranial sutures because of plaques of tumor tissue growing along the surface of the brain (Figure 10-18). Bone destruction leads to a granular pattern of osteoporosis that is often associated with thin, whisker-like calcifications coursing outward and inward from the tables of the skull (see Figure 10-15B). Metastases in long tubular bones are often multiple and relatively symmetric and present a permeative destructive pattern. On T2-weighted MR images, bone metastases appear as hyperintense (bright) and heterogeneous signals.

Neuroblastomas arising in the chest appear as posterior mediastinal masses. Metastases to the chest most commonly cause asymmetric enlargement of mediastinal nodes; metastases to the pulmonary parenchyma are infrequent.

Treatment. Combining surgery, multiple-agent chemotherapy, and radiation therapy for treatment of neuroblastoma has dramatically improved the prognosis to approximately a 90% cure rate. Infants tend to have a more favorable outcome when chemotherapy and surgery are the combined treatment.

Summary of Findings for Diseases of the Adrenal Medulla

Disorder	Location	Imaging Appearance	Treatment
Pheochromocytoma	Adrenal medulla—excessive epinephrine and norepinephrine	CT—round, oval, or pear-shaped mass with lower attenuation than liver or kidney parenchyma; larger lesions may manifest as necrosis; hemorrhage and fluid levels may be apparent US—mass shows lower echogenicity than normal liver and kidney parenchyma MRI— has hyperintense signal on T2-weighted spin-echo sequences NM meta-iodobenzylguanidine scan—supersensitive for localizing lesions ectopic	Surgical resection
Neuroblastoma	Adrenal medullary origin	Radiograph—calcification of tumor; destructive metastatic bone lesions IVU—inferior and lateral kidney displacement US—solid to semisolid mass separate from kidney; poorly defined, heterogeneous mass with irregular hyperechoic areas CT—heterogeneous and lobulated appearance MRI—lesion is hypointense on T1-weighted images; with contrast enhancement, the lesion's T1 signal becomes hyperintense	Combination treatment: surgical resection, chemotherapy, and radiation therapy

IVU, Intravenous urography; *NM,* nuclear medicine; *US,* ultrasound.

PITUITARY GLAND

Physiology of the Pituitary Gland

The pituitary gland is often called the master gland because the many hormones it secretes control the level of most glandular activity throughout the body. The hormone secretion of the pituitary gland itself is controlled by the hypothalamus.

The pituitary is a tiny gland, about the size of a pea, that is suspended from the base of the brain by a slender stalk (infundibulum) and sits in the bony depression of the sella turcica. It is divided into anterior and posterior portions, each of which secretes different hormones (Figure 10-19).

The anterior lobe of the pituitary gland secretes growth hormone, thyroid-stimulating hormone (TSH), ACTH, and a group of hormones that affect the sex organs, or gonads. These gonadotropins include follicle-stimulating hormone (FSH) and luteinizing hormone (LH), which regulate the menstrual cycle and secretion of male and female sex hormones, and prolactin, which stimulates the production of milk during pregnancy and after delivery.

Growth hormone affects all parts of the body by promoting the growth and development of the tissues. Before puberty, it stimulates the growth of long bones (increasing the child's height) and the size of such organs as the liver, heart, and kidneys. After adolescence, growth hormone is secreted in lesser amounts but continues to function in promoting tissue replacement and repair. TSH controls the secretion of thyroid hormone, which regulates the body's metabolism (production and use of energy). ACTH controls the level of activity of the adrenal cortex.

The posterior lobe of the pituitary gland (neurohypophysis) produces two hormones: vasopressin (ADH) and oxytocin. ADH increases the rate of reabsorption of water and electrolytes by the renal tubules, thus decreasing the output of urine and protecting the individual from excessive water loss. Oxytocin causes contraction of smooth muscle, especially in the uterus, and thus strengthens contractions during labor and helps prevent hemorrhage after delivery.

Diseases of the Pituitary Gland

Hyperpituitarism

Hyperpituitarism results from an excess of growth hormone produced by a tumor (see Figures 8-21 and 8-22) or generalized hyperplasia of the anterior lobe of the pituitary gland. The development of this condition before enchondral bone growth has ceased results in **gigantism**; hyperpituitarism beginning after bone growth has stopped produces **acromegaly**.

Generalized overgrowth of all the body tissues is the underlying abnormality in acromegaly. Although the long bones can no longer grow because the epiphyses are closed, the bones of the hands, feet, and face enlarge, and there is excessive growth of soft tissues. Proliferation of cartilage may cause joint space widening, especially of the metacarpophalangeal and hip joints. The slight increase in length of each of the seven articular cartilages for each digit leads to perceptible lengthening of the fingers. Overgrowth of the tips of the distal phalanges produces thick bony tufts with pointed lateral margins. The associated hypertrophy of the soft tissues produces the characteristic square, spade-shaped hand of acromegaly. Degenerative changes develop early and are associated with prominent hypertrophic spurring. Unlike typical osteoarthritis, acromegaly results in joint spaces that remain normal or are even widened.

Imaging appearance. Thickening of the heel pads (the soft tissue inferior to the plantar aspect of the calcaneus) to

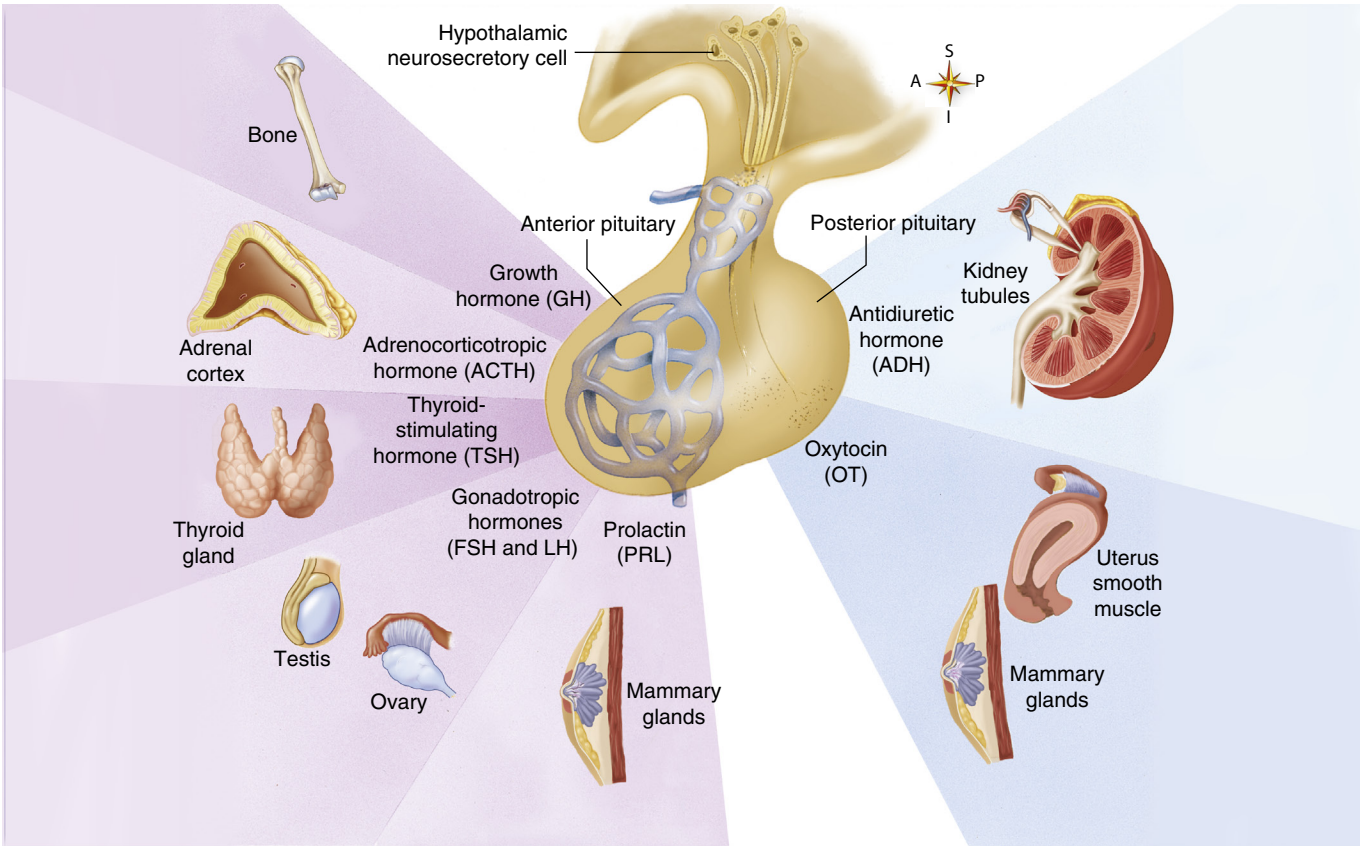

FIGURE 10-19 Pituitary gland and hormones.

FIGURE 10-20 Acromegaly. Prominent thickening of the heel pad measuring 32 mm, which is highly suggestive of acromegaly.

more than 23 mm is highly suggestive of acromegaly (Figure 10-20). However, a similar appearance may also be seen in a patient with obesity, myxedema, or generalized edema.

The bones of the skull become thickened and have increased density, often with obliteration of the diploic space. This bone thickening is especially prominent in the frontal and occipital regions, leading to characteristic frontal bossing and enlargement of the occipital protuberance (Figure 10-21). The paranasal sinuses (especially the frontal) become enlarged, and the mastoid processes are usually overpneumatized. Lengthening of the mandible and an increased mandibular angle produce prognathism, one of the typical clinical features of acromegaly. Thickening of the tongue may lead to slurred speech. Pituitary enlargement causes expansion and erosion of the sella turcica (Figure 10-22).

In the spine, hypertrophy of cartilage causes an increased width of the intervertebral disk spaces. An increase in the size of the vertebral bodies is best seen on lateral projections. Hypertrophy of soft tissues may produce an increased concavity of the posterior aspect of the vertebral bodies (scalloping) that is most prominent in the lumbar spine (Figure 10-23).

Extraskeletal manifestations of acromegaly include visceral enlargement, especially of the heart and kidney; enlargement of the tongue; and calcification of cartilage in the pinna of the ear.

Gigantism is manifested as an excessively large skeleton. If hypersecretion of growth hormone continues after epiphyseal closure, the soft tissue and bony changes of acromegaly are superimposed.

For diagnosis of the pituitary tumor causing the excessive growth, MRI provides the most exact definition of the sella turcica and the tissue contained within. Its superior sensitivity and multiplanar capabilities make MRI the modality of choice. Thin-section coronal and sagittal T1-weighted

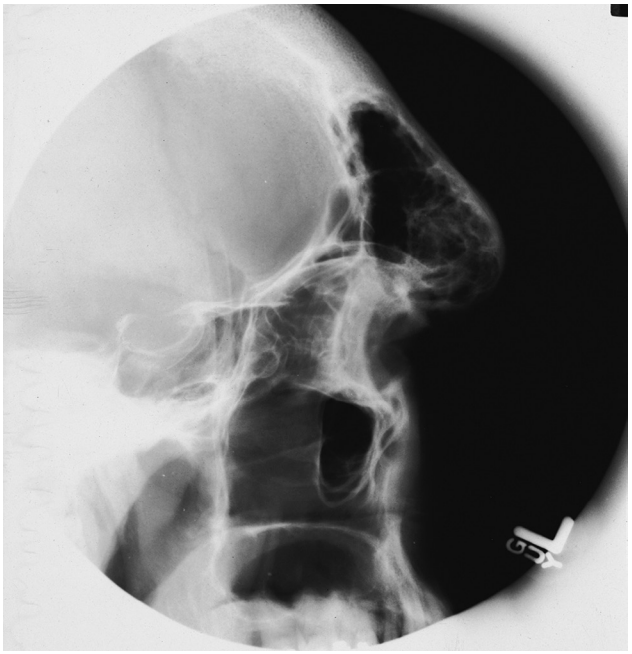

FIGURE 10-21 Acromegaly. Lateral skull projection demonstrating a thickened frontal bone with characteristic frontal bossing.

FIGURE 10-22 Pituitary adenoma causing acromegaly. Ballooning of the sella turcica with downward displacement of the floor is demonstrated.

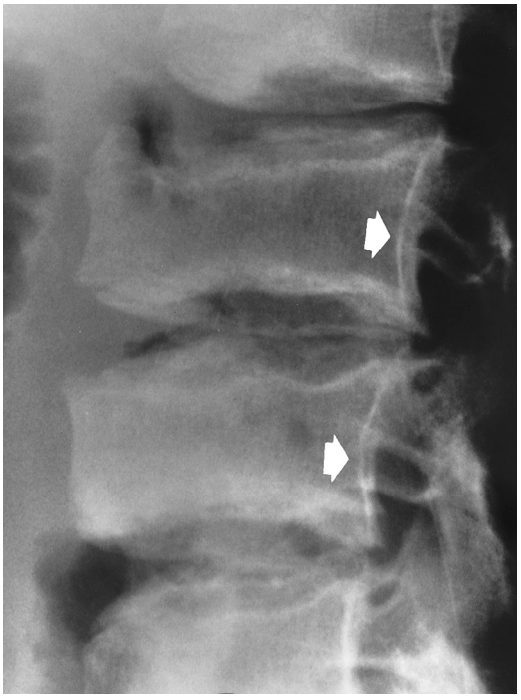

FIGURE 10-23 Acromegaly. Posterior scalloping (*arrows*) associated with enlargement of vertebral bodies (especially in anteroposterior dimension).

spin-echo images permit clear distinction of the sphenoid sinus and carotid artery for surgical planning. After gadolinium injection, normal pituitary tissue enhances more than an adenoma, which appears as a hypoenhancing lesion.

Treatment. Surgical resection of the tumor remains the treatment of choice. Even with treatment, any changes or damage in the skeleton will remain unchanged. Radiation therapy or medications to decrease growth hormone levels may provide some relief if resection is not a viable option for the patient.

Hypopituitarism

Because the pituitary gland controls the level of secretion of gonadal and thyroid hormones and the production of growth hormone, decreased function of the pituitary gland causes profound generalized disturbances in bone growth and maturation. In children, hypopituitarism typically leads to a type of dwarfism in which the delayed appearance of epiphyseal centers causes the failure of bones to grow normally in length or width. This results in a person who is small in stature and sexually immature, although well proportioned and of normal mentality. In many patients, there is a delay in the eruption of the teeth, which tend to become impacted because their size is not affected. The arrest in the growth of the skeleton occurs during childhood, when the cranial vault is proportionally greater in relation to the facial bones than in the adult. Because this discrepancy remains into adulthood in hypopituitary dwarfism, the relatively large skull may be mistakenly believed to result from hydrocephaly.

Hypopituitarism occurring after adolescence results in hypofunction of the thyroid gland, adrenal glands, and gonads but usually causes few radiologic findings. The heart and kidneys are often small, and calcification or ossification may develop in the articular cartilages.

Imaging appearance. MRI is the preferred imaging modality because it has superb sensitivity and can directly image the sellar and parasellar regions in multiple planes. The use of contrast enhancement may help define a microadenoma or detect sarcoidosis in an older patient with Addison's disease.

Treatment. For children, a subcutaneous injection of recombinant growth hormone several times per week during puberty and earlier is recommended to prevent the arrest in growth. Tumor location and type will determine whether surgery is needed. In adults, usually no treatment is required.

Diabetes Insipidus

The impaired ability of the kidneys to conserve water in diabetes insipidus results from low blood levels of ADH, reflecting deficient vasopressin release by the posterior lobe of the pituitary gland in response to normal physiologic stimuli. In response to excessive water loss in the urine (polyuria), the body compensates by developing an insatiable thirst (polydipsia). Another type of diabetes insipidus occurs when the kidneys fail to respond to circulating ADH; this is known as *nephrogenic* diabetes insipidus. It must be stressed that diabetes insipidus is completely unrelated to diabetes mellitus.

Imaging appearance. On T1-weighted MR images, an absence of signal in the posterior pituitary indicates diabetes insipidus. Severe polyuria can lead to massive dilation of the renal pelves, calyces, and ureters. This dilation probably represents a compensatory alteration to accommodate the huge volume of excreted urine.

Treatment. Treatment for diabetes insipidus consists of taking drugs that mimic ADH, delivered most commonly in a nasal spray. For the nephrogenic type, treatment with thiazide diuretics allows the kidney to resorb an increased amount of fluid.

Summary of Findings for Diseases of the Pituitary Gland

Disorder	Location	Imaging Appearance	Treatment
Hyperpituitarism	Excessive growth hormone—anterior pituitary	Radiograph—widened joints, thickened heel pad, thickened skull tables with frontal bossing, paranasal sinus enlargement, mandibular changes, vertebral enlargement with scalloping, hypertrophy of cartilage MRI—superior sensitivity and multiplanar imaging to evaluate the pituitary gland; after contrast enhancement, adenoma appears as a hypoenhancing lesion on T1-weighted spin-echo images	Surgical resection of pituitary tumor
Hypopituitarism	Loss of secretion of any anterior pituitary hormone	Radiograph—skeletal changes in size; dwarfism MRI—detects pituitary tumor by multiplanar imaging; loss of signal of posterior pituitary on T1-weighted images	Children—subcutaneous injection of growth hormone Adults—usually no treatment required
Diabetes insipidus	Deficient release of hormones from the posterior lobe of the pituitary	MRI—detection of pituitary tumor by multiplanar imaging as an absence of signal in the posterior pituitary gland	Drugs to mimic antidiuretic hormone

THYROID GLAND

Physiology of the Thyroid Gland

The thyroid is a butterfly-shaped gland located in the neck at the level of the larynx. It consists of two lobes, one on each side of the trachea, and a connecting strip (the isthmus) that runs anterior to the trachea and connects the lower portions of the two lobes (Figure 10-24). The thyroid lies just below the Adam's apple, the protrusion formed by the cricoid cartilage of the larynx. Microscopically, the thyroid gland consists of innumerable follicles surrounding a central core of colloid, the storage form of the active material known as **thyroxine**, which is the only natural iodine-containing substance in the body.

The thyroid gland picks up iodine from the bloodstream and combines it with the amino acid tyrosine to synthesize thyroid hormones, which are stored in the gland until released into the bloodstream when stimulated by TSH from the anterior lobe of the pituitary gland. The active hormone, **thyroxine**, is a small molecule that may contain either three iodine molecules (**triiodothyronine** [T_3]) or four iodine molecules (T_4). These substances stimulate cellular metabolism in response to the body's need for increased energy production. The higher cellular metabolism requires that additional oxygen be circulated to the cells and that more waste materials be removed, which in turn requires increased blood flow and greater cardiac output. The increased demand for oxygen stimulates the respiratory center and results in a faster rate and greater depth of breathing. Increased cellular metabolism produces heat, which is dissipated by perspiration and by increased blood flow through dilated vessels in the skin, giving the person a flushed appearance. Thyroid hormone also increases the secretion of digestive juices and the movement of ingested material through the intestinal tract.

The release of thyroid hormone is controlled by TSH, which is secreted by the anterior lobe of the pituitary gland. This process is a negative feedback mechanism, in which a high blood level of thyroxine inhibits the anterior pituitary and TSH release, whereas a low level of thyroxine forces the anterior pituitary to release TSH again.

Diseases of the Thyroid Gland

Radioactive Iodine Scanning

Scanning after the administration of radioactive iodine is the superior imaging modality for demonstrating both functioning and nonfunctioning thyroid tissue. This technique is used to localize palpable nodules, to determine the function of nodules, to detect nonpalpable lesions (especially in patients with a history of neck irradiation), and to evaluate the extent of residual tissue after surgical or radioisotopic thyroid ablation. Radionuclide

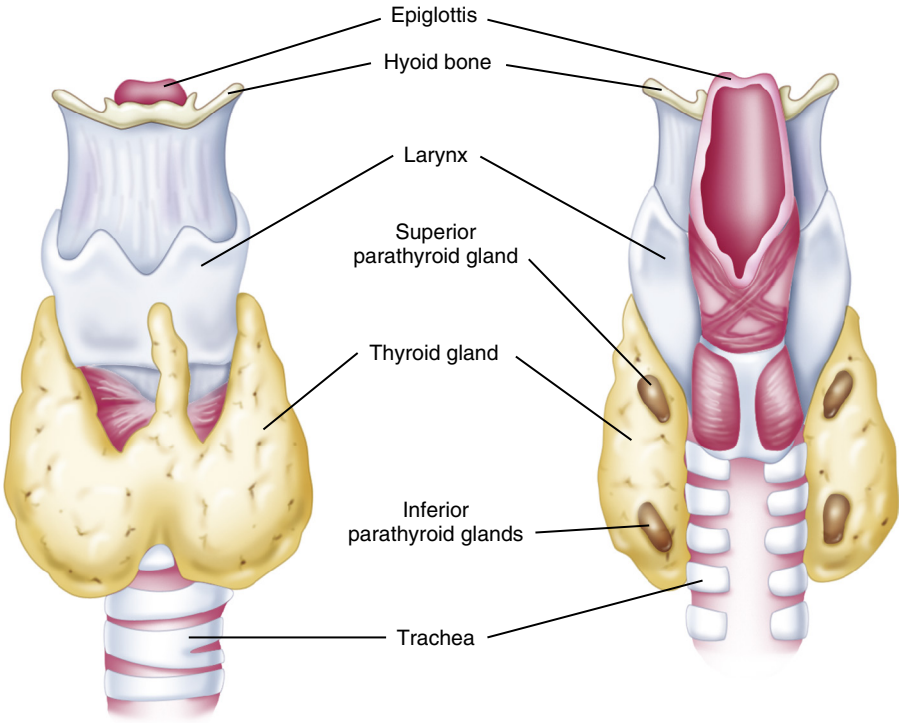

FIGURE 10-24 Thyroid and parathyroid glands.

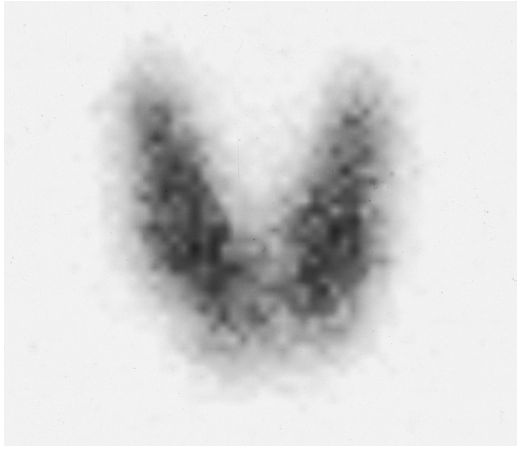

FIGURE 10-25 Normal radioactive iodine scan. There is uniform distribution of nuclide activity throughout the thyroid gland.

scanning may be combined with uptake, stimulation, or suppression techniques to better characterize the thyroid lesions.

Imaging appearance. The distribution of radioactivity is uniform throughout the normal thyroid gland (Figure 10-25). Diffuse thyroid enlargement without hyperthyroidism most frequently represents a multinodular goiter of Hashimoto's thyroiditis. In a patient with hyperthyroidism, diffuse thyroid enlargement is suggestive of Graves' disease.

Masses within the thyroid gland appear as hyperfunctioning ("hot") or poorly functioning ("cold") nodules. A hot nodule demonstrates greater radionuclide uptake than surrounding thyroid tissue (Figure 10-26). Hot nodules usually represent autonomously functioning thyroid tissue and are rarely malignant, although malignancy is sometimes reported elsewhere in the same gland. Large hyperfunctioning nodules may completely suppress the remaining thyroid tissue so that only the nodule itself is visualized. An autonomous nodule may eventually develop central hemorrhage or cystic change and evolve into a nonfunctioning (cold) nodule.

Cold thyroid nodules contain less radionuclide per unit tissue mass than adjacent normal thyroid tissue (Figure 10-27). Most cold nodules represent poorly functioning adenomas. Thyroid cysts, carcinoma, and thyroiditis can also produce this appearance. In a young patient, the absence of uptake in the region of a solitary cold thyroid nodule is associated with a 10% to 25% probability that the nodule is malignant. Ultrasound can establish the precise location of the palpable mass and determine whether it is within the thyroid or in adjacent tissue. In patients who are at risk because of irradiation of the neck during their youth or because of a family history, but who have no palpable lesion, ultrasound may detect an occult thyroid nodule. Although ultrasound can distinguish a thyroid cyst from the other causes of cold nodules, this modality is of little value in further characterizing noncystic thyroid masses.

Hyperthyroidism

Hyperthyroidism results from the excessive production of thyroid hormone, either from the entire gland (Graves' disease) or from one or more functioning adenomas. Graves' disease is a relatively common disorder that most often develops in the third and fourth decades and has a strong female predominance. The major clinical symptoms include nervousness, emotional lability, an inability to sleep, tremors, rapid pulse rate (tachycardia), palpitations, excessive sweating, and heat intolerance. Weight loss is common, usually despite an

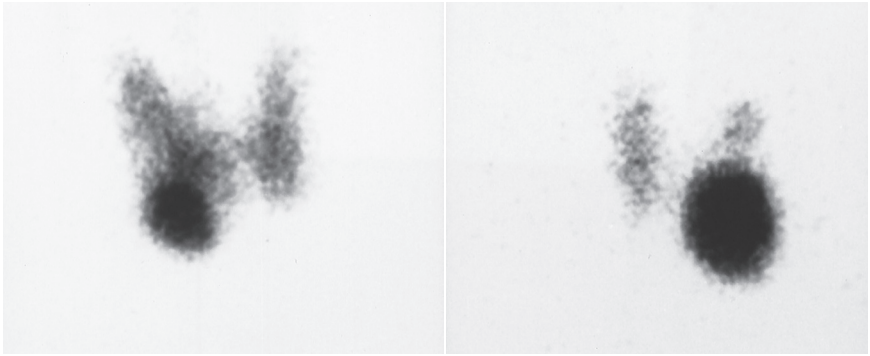

FIGURE 10-26 Hyperfunctioning (hot) nodules. Radioactive iodine scans in two patients, with increased uptake representing nodules. Note the variable amount of suppression in the remainder of the thyroid gland.

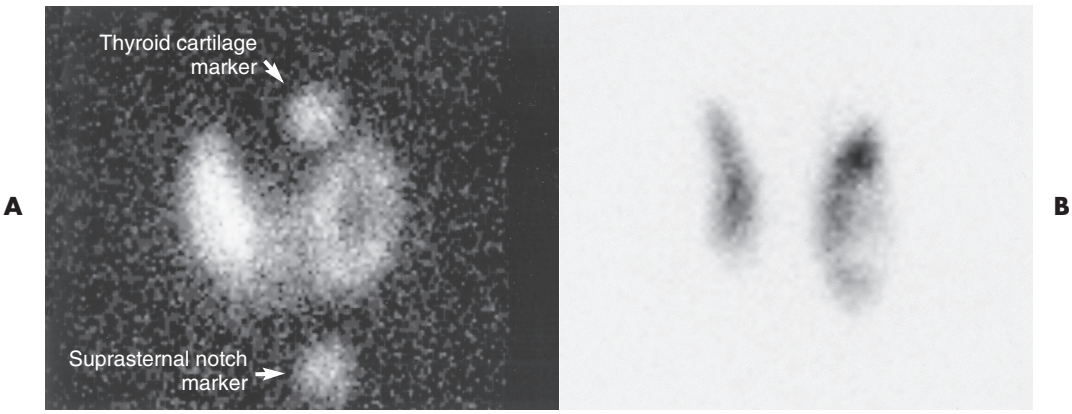

FIGURE 10-27 Nonfunctioning (cold) nodules on radioactive iodine scans in two patients. **(A)** Uptake within the gland is normal. A cold nodule in the left lobe of the thyroid corresponds to the nodule that was seen on ultrasound. **(B)** Inhomogeneous right and left lobes demonstrate multiple cold nodules. There is a dominant cold nodule in the inferior left pole.

increased appetite. A characteristic physical finding is exophthalmos, outward protrusion of the eyeball caused by edema in the tissue behind the eyes.

Imaging appearance. Radioactive iodine scans in patients with Graves' disease typically demonstrate diffuse enlargement of the thyroid gland with increased radioiodine uptake (Figure 10-28), which rules out a single toxic adenoma. The extent of increased uptake on the scan helps to determine the dose of radioactive iodine for treatment.

In severe cases, high-output cardiac failure may develop along with generalized cardiomegaly and pulmonary congestion. Unilateral or bilateral exophthalmos as a result of Graves' disease can be demonstrated by CT as thickening of the extraocular muscles. Ultrasound imaging helps determine the size and location of the thyroid (Figure 10-29), and the image can be correlated with the radioactive scans.

Treatment. Antithyroid drugs are used to decrease thyroid response. Destruction of thyroid cells by radioactive iodine (^{131}I) or total thyroidectomy results in hypothyroidism.

Hypothyroidism

Hypothyroidism can result from any structural or functional abnormality that leads to an insufficient synthesis of thyroid hormone. Hypothyroidism dating from birth (cretinism) results in multiple developmental abnormalities. Children with cretinism typically have a short stature; coarse features with a protruding tongue, a broad, flattened nose, and widely set eyes; sparse hair; dry skin; and a protuberant abdomen with an umbilical hernia.

Adult hypothyroidism has an insidious onset with nonspecific symptoms including lethargy, somnolence (sleeping up to 16 hours a day), constipation, cold intolerance, slowing of intellectual and motor activity, and weight gain despite a decreased appetite. Dry skin; stiff, aching muscles; and a deepening voice with hoarseness often occur. The facial features are thickened, and there is a doughy thickening of the skin (myxedema).

Imaging appearance. The major radiographic abnormalities in children with hypothyroidism include a delay in the appearance and subsequent growth of ossification centers and retarded bone age. Skull changes are common and include an increase in the thickness of the cranial vault, underpneumatization of the sinuses and mastoid air cells, widened sutures with delayed closure, and a delay in the development and eruption of the teeth (Figure 10-30).

Radiographically, the heart in adults is typically enlarged because of pericardial effusion. Soft tissue thickening is often seen on images of the extremities, and adynamic ileus is a common finding on abdominal radiographs.

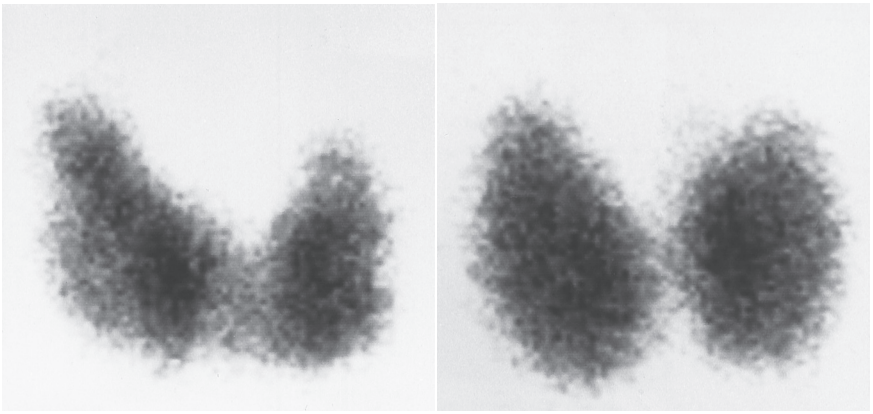

FIGURE 10-28 Hyperthyroidism. Radioactive iodine scans in two patients with Graves' disease show symmetrically enlarged thyroid glands with homogeneously increased iodine uptake.

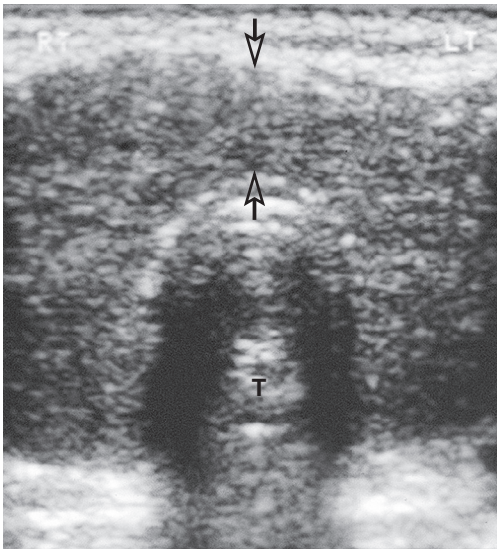

FIGURE 10-29 Thyroid goiter. Ultrasound image shows a thickened isthmus (*arrows*) and enlarged bilateral lobes. *T,* Trachea.

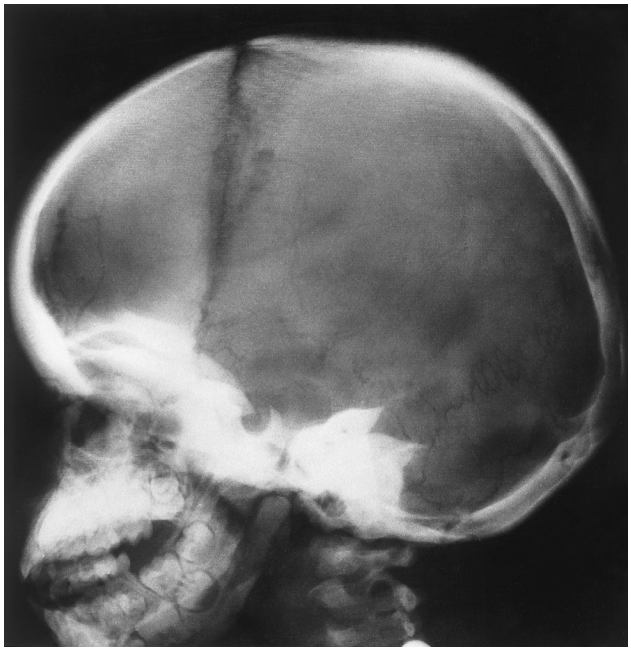

FIGURE 10-30 Cretinism. Lateral projection of the skull shows an increased density at the base, small underdeveloped sinuses, and hypoplasia of teeth with delayed eruption. Retardation of facial maturation makes face appear small relative to size of calvaria.

Treatment. If a tumor is the cause of hypothyroidism, a combination of surgery, chemotherapy, and radiation therapy is the treatment of choice. For functional hypothyroidism, the thyroid hormone is replaced with a synthetic product (thyroxine).

Goiter

A goiter is an enlargement of the thyroid gland that does not result from an inflammatory or neoplastic process and is not initially associated with hyperthyroidism or myxedema. A simple (nontoxic) goiter results when one or more factors impair the capacity of the thyroid gland in the basal state to secrete the quantities of active hormones necessary to meet the needs of the body. Because the blood level of thyroid hormone is low, there is nothing to inhibit the anterior pituitary, which continues to secrete TSH, causing the thyroid gland to enlarge. In most cases, there is a sufficient increase in both the functioning thyroid mass and the cellular activity to overcome the mild or moderate impairment of hormone synthesis, permitting the patient to remain metabolically normal although goitrous.

Although goiters were once endemic in areas where there was insufficient iodine in the diet, this situation is now rare because iodine is added commercially to salt and bread.

Imaging appearance. On a radioactive iodine scan, a nontoxic goiter usually appears as a symmetric or an asymmetric enlargement of the thyroid gland. Plain radiographs and esophagrams often show the enlarged thyroid gland impressing on or displacing the trachea and esophagus (Figure 10-31).

A toxic multinodular goiter may be a consequence of a long-standing nontoxic goiter. In this condition, one or more areas of the gland become independent of TSH stimulation. Radioactive iodine scans most commonly show accumulation of iodine in diffuse but patchy foci throughout the gland (Figure 10-32). Another pattern consists of iodine accumulation in one or more discrete nodules within

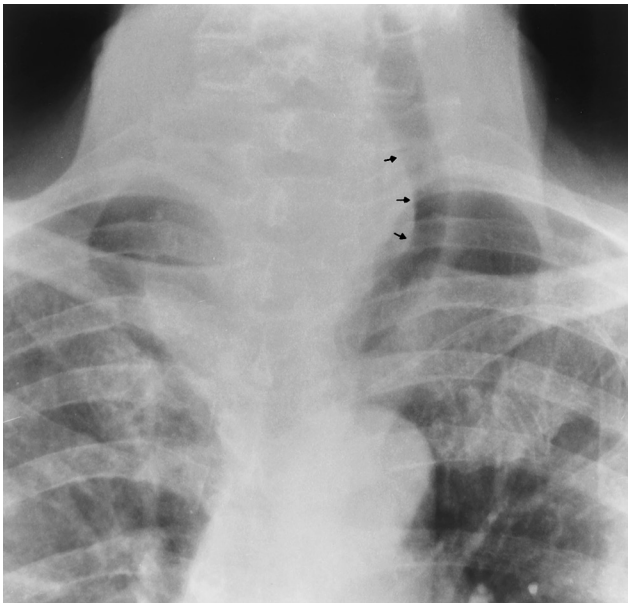

FIGURE 10-31 Goiter. Greatly enlarged thyroid gland appears as a soft tissue mass impressing the trachea (*arrows*) and displacing it to the left.

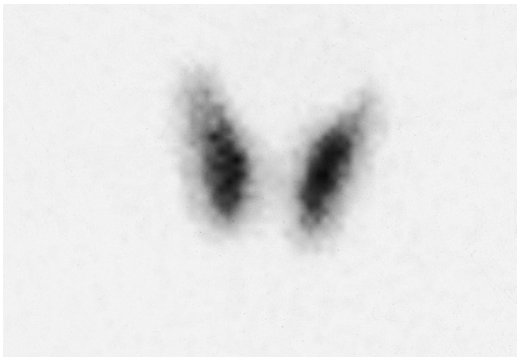

FIGURE 10-32 Multinodular goiter. Radioactive iodine scan shows patchy uptake of the nuclide caused by increased and decreased uptake by the thyroid.

the gland, with the remainder of the gland being essentially nonfunctional.

Ultrasound is indicated to determine whether a nonfunctioning mass detected on a radioactive iodine scan is cystic or solid (Figure 10-33). Ultrasound may be used to monitor growth of thyroid nodules. CT or MRI is employed only when there is a substernal thyroid that cannot be seen with ultrasound.

Treatment. The first-line treatment of small goiters is to control the nodule size with oral thyroxine. If the goiter continues to enlarge, the thyroid is surgically resected to relieve the compression of anatomic structures in the neck (trachea and esophagus).

Benign Thyroid Adenomas

Benign thyroid adenomas are encapsulated tumors that vary greatly in size and usually compress adjacent tissue. They may be located within the neck, where they tend to cause deviation or compression of the trachea, or they may extend substernally and appear as masses in the superior portion of the anterior mediastinum.

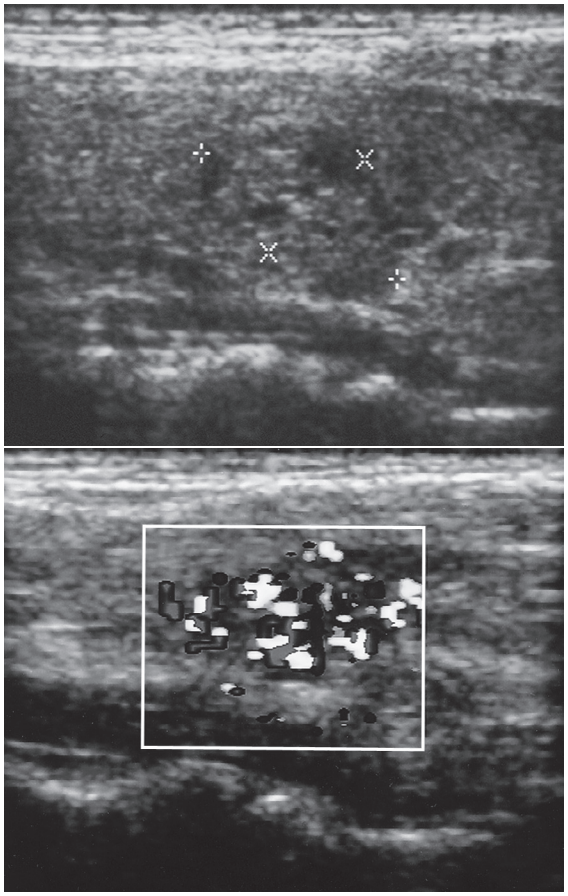

FIGURE 10-33 Multinodular goiter. (A) Ultrasound image demonstrates solid nodular lesions (8 × 15 mm) in both lobes of the thyroid (left lobe shown here). **(B)** The Doppler image demonstrates increased vascularity.

Imaging appearance. Calcification may develop within the mass of a thyroid adenoma (Figure 10-34). These tumors can appear as hot or cold nodules on radionuclide imaging, depending on their functional capacity. Ultrasound usually demonstrates an adenoma as a solid mass with a consistent echogenicity. There is often a thick and smooth peripheral hypoechoic halo caused by the fibrous capsule and blood vessels. Cystic lesions as small as 2 mm and solid lesions of 3 mm can be visualized.

Thyroid Carcinomas

The three major types of thyroid carcinomas are papillary, follicular, and medullary. **Papillary carcinoma**, the most common type, has peaks of incidence in adolescence and young adulthood and again in later life, during the third to fifth decades. The tumor is usually slow growing and cystic, and it typically spreads to regional lymph nodes, where it may remain silent for many years. Distant metastases to the lungs are rare and often cause only mild, nonspecific thickening of bronchovesicular markings, although the metastases may also appear as miliary and nodular densities that predominantly involve the lower lobes.

Follicular carcinoma has a histologic appearance that closely mimics that of normal thyroid tissue. Typically

FIGURE 10-34 Thyroid adenoma. Lateral projection of the neck shows a huge calcified thyroid mass.

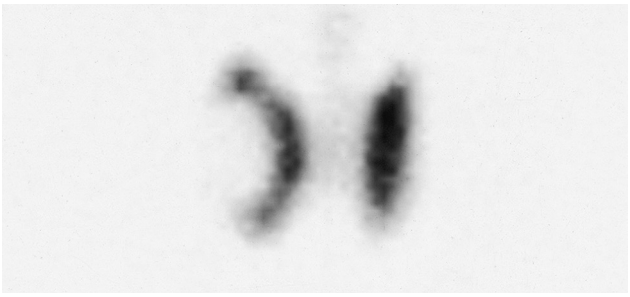

FIGURE 10-35 Thyroid carcinoma. Radioactive iodine scan shows a solitary cold nodule that corresponds to the patient's palpable mass.

(in approximately 75% of cases), this tumor occurs in women older than 40 years of age. The tumor usually undergoes early hematogenous spread, especially to the lung and bone. Skeletal metastases, which may be the initial manifestation, tend to produce entirely lytic, expansile destruction that extends into the soft tissues and is associated with little or no periosteal reaction.

Medullary carcinoma is the least common type of thyroid malignancy. At least 10% of the cases are familial, most often appearing as a component of a syndrome in which there are multiple endocrine tumors. Dense, amorphous calcifications can often be seen within the tumor. Medullary carcinomas readily metastasize via the lymphatic channels.

There is a substantially increased risk of thyroid cancer in persons with a history of therapeutic neck irradiation in childhood. In the past, such irradiation was used for benign disease, such as enlargement of the tonsils, adenoids, and thymus; middle ear disease; and a variety of skin disorders, including acne.

Imaging appearance. On radioactive iodine scans, thyroid carcinoma usually appears as a solitary cold nodule that corresponds to a palpable mass (Figure 10-35). The finding of a nodule that is functioning (hot) essentially excludes a diagnosis of thyroid carcinoma.

On ultrasound, 90% of papillary carcinomas appear as solid hypoechoic masses that may contain microcalcifications, which appear as tiny hyperechoic foci (Figure 10-36). Follicular carcinomas, which have similar tissue consistency, cannot be distinguished from adenomas unless they demonstrate irregular tumor margins and a thick irregular halo (Figure 10-37). Color Doppler imaging commonly shows a tortuous or disordered blood vessel arrangement. Medullary carcinomas appear similar to papillary carcinomas, with bright echogenic foci caused by calcifications.

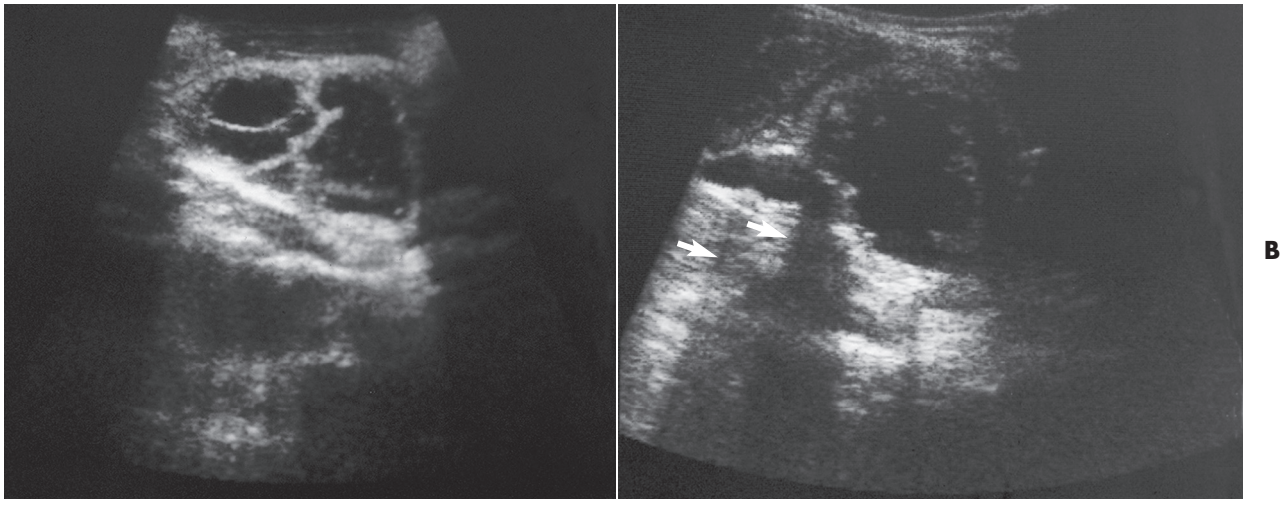

FIGURE 10-36 Ultrasound images of a complex thyroid mass. (A) The mass has solid components and intercystic septations of various thicknesses. (B) Echogenic foci with shadowing are evident (*arrows*). Together with the radioactive iodine scan, which showed a cold nodule, these findings suggest a malignant lesion.

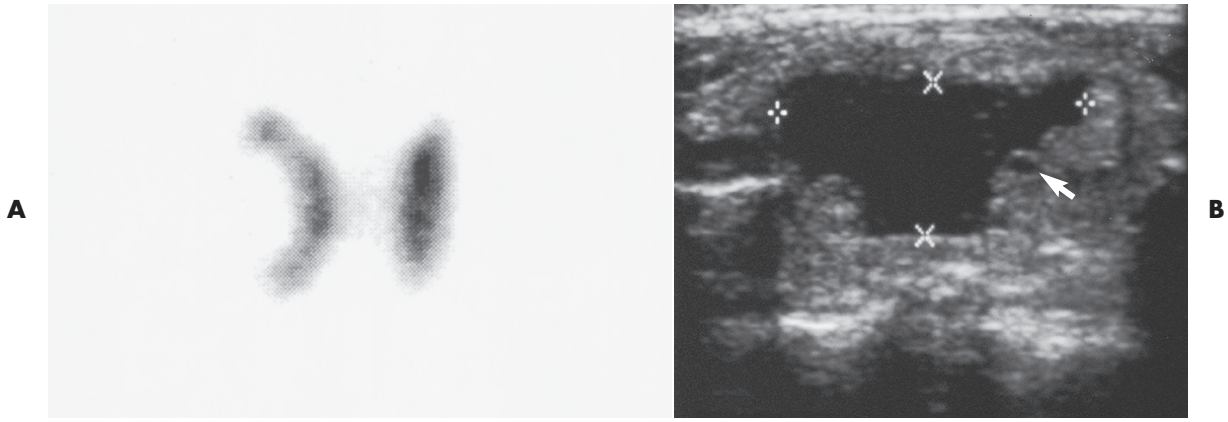

FIGURE 10-37 Degenerative follicular adenoma. (A) Radioactive iodine scan shows a prominent cold nodule. (B) Ultrasound illustrates a lesion that is not smooth (note papillary projections, *arrow*) and that lacks back wall enhancement. These features most often indicate a degenerative follicular adenoma.

MRI and CT demonstrates a substernal thyroid that ultrasound cannot detect because of bone interference. MRI may aid in defining the extent of the neoplasm.

Treatment of Thyroid Tumors

Thyroid adenoma treatment may be as simple as observation or as complex as a surgical lobectomy. Drug therapy options include TSH suppression and radioactive iodine. Appropriate treatment depends on the size and location of the thyroid adenoma.

Thyroidectomy is the first choice of treatment for thyroid carcinomas, especially for papillary carcinomas. Approximately 80% of patients survive longer than 10 years. If the patient cannot undergo surgery, alternative choices are suppressive drugs and chemotherapy with radioactive iodine, which may result in hypothyroidism. For patients with follicular carcinoma and widespread metastases, radioactive iodine treatment is the best treatment.

Summary of Findings for Diseases of the Thyroid Gland

Disorder	Location	Imaging Appearance	Treatment
Hyperthyroidism	Excessive hormone production	NM—diffuse enlarged thyroid with increased uptake	Antithyroid drugs Radioactive iodine Partial or total resection of thyroid
Hypothyroidism	Insufficient synthesis of thyroid hormone	Imaging not used for diagnosis Radiograph—retarded bone age; increased skull thickness with widened sutures and delayed suture closure Chest image (in adult)—enlarged heart with pericardial effusion	Replacement therapy If caused by tumor—surgery, radiation therapy, and chemotherapy
Goiter	Enlarged thyroid gland	NM—enlargement of thyroid gland Esophagram—thyroid gland impresses or displaces trachea and esophagus	Thyroxine to manage goiter size Resection of enlarged portion of thyroid
Benign thyroid adenomas	Encapsulated tumor	Radiography—calcification NM—hot or cold nodule US—solid homogeneous mass with peripheral hypoechoic halo	Observation Lobectomy Drug therapy
Thyroid carcinomas	Papillary, follicular, or medullary	NM—solitary cold nodule US—papillary carcinoma appears as a solid hypoechoic mass with hyperechoic foci; follicular carcinoma has irregular tumor margins and a thick irregular halo Color Doppler—tortuous or disordered blood vessel arrangement; medullary carcinomas appear similar to papillary carcinomas with bright echogenic foci MRI/CT—demonstrates substernal thyroid and may aid in defining the extent of the neoplasm	Thyroidectomy Suppressive drugs Chemotherapy with radioactive iodine Radiation therapy

NM, Nuclear medicine study; *US,* ultrasound.

FIGURE 10-38 Hyperparathyroidism. Subperiosteal bone resorption can be seen that predominantly involves the radial margins of the middle phalanges of the second, third, and fourth digits (*arrows*). Note also resorption of the terminal tufts.

FIGURE 10-39 Hyperparathyroidism. Characteristic erosion of the distal clavicle (*arrow*) is shown. Metaphyseal subperiosteal resorption beneath the proximal humeral head has led to a pathologic fracture with slippage of the humeral head.

PARATHYROID GLANDS

Physiology of the Parathyroid Glands

The parathyroids are four tiny glands, two on each side, that lie behind the upper and lower poles of the thyroid gland (see Figure 10-24). They secrete **parathormone** (parathyroid hormone [PTH]), which is responsible for regulating the blood levels of calcium and phosphate. Parathormone raises a low serum calcium level by three mechanisms. First, it increases the amount of calcium absorbed from the intestinal tract by interaction with ingested vitamin D. Second, the hormone prevents a loss of calcium through the kidneys and releases calcium from bones by stimulating osteoclastic activity. Third, serum phosphate levels are reduced.

Diseases of the Parathyroid Glands

Hyperparathyroidism

Excessive secretion of parathormone leads to a generalized disorder of calcium, phosphate, and bone metabolism that results in elevated serum values of calcium and phosphate. **Primary hyperparathyroidism** may be caused by a discrete adenoma (80%) or carcinoma (2%) or by generalized hyperplasia (18%) of all glands. Other causes include nonparathyroid tumors that secrete a parathormone-like substance and the familial syndrome of multiple endocrine neoplasia. **Secondary hyperparathyroidism** occurs more frequently than the primary form and is most often attributable to chronic renal failure. **Tertiary hyperparathyroidism** refers to the development of autonomous functioning parathyroid glands in patients who demonstrate progressive bone disease in the presence of biochemical and clinically controlled renal disease.

Imaging appearance. The radiographic findings in primary and secondary hyperparathyroidism are similar, except that in the secondary form, brown tumors (focal areas of bone destruction) are rare and osteosclerosis is more common. As a result of the predominant skeletal changes, conventional radiography is the primary image modality used for diagnosis. The earliest change is subperiosteal bone resorption, which particularly involves the radial margins of the middle phalanges (Figure 10-38), the distal clavicles (Figure 10-39), and the medial aspect of the upper third of the tibias. Loss of normal cortical definition is followed by an irregularly lacy resorption, with the endosteal margin initially remaining intact. Erosions of the terminal tufts of the fingers and loss of the lamina dura of the teeth often occur, although these findings are nonspecific and are seen in other conditions.

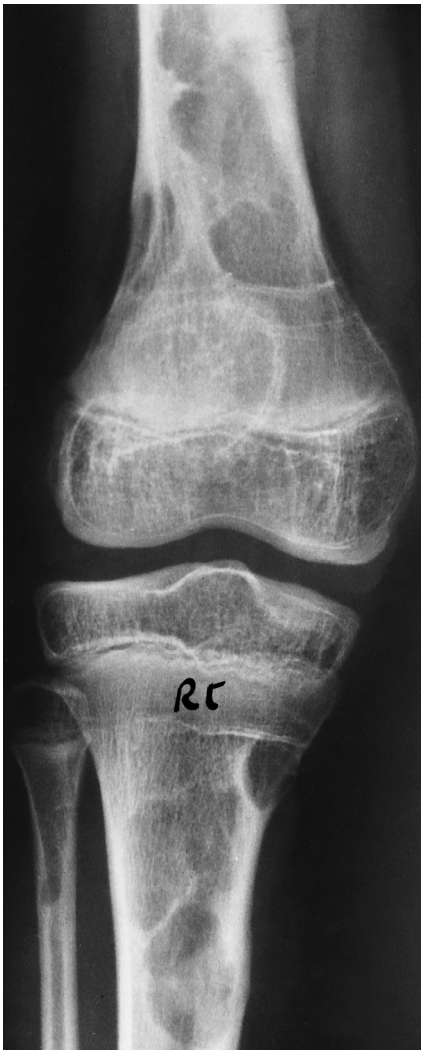

FIGURE 10-40 Hyperparathyroidism. Brown tumors have produced multiple lytic lesions about the knee.

Generalized loss of bone density may produce a ground-glass appearance. So-called brown tumors may become large and expansile and even simulate a malignant process (Figure 10-40). Pathologic fractures may lead to bizarre deformities. Irregular demineralization of the calvaria produces the characteristic salt-and-pepper skull (Figure 10-41).

A generalized increase in bone density (osteosclerosis) may develop in patients with hyperparathyroidism, especially when it is a result of renal failure. Thick bands of increased density adjacent to the superior and inferior margins of vertebral bodies produce the characteristic "rugger-jersey" spine (Figure 10-42).

Soft tissue calcification is common, especially in secondary hyperparathyroidism. Calcific deposits may develop in vessels, articular cartilages, menisci, joint capsules, and periarticular tissues (Figure 10-43). Elevation of serum calcium and decreased excretion of calcium in the urine may result in nephrocalcinosis and urinary tract stones. Increased incidences of pancreatic calculi and pancreatitis, peptic ulcer, and gallstones have also been reported in patients with hyperparathyroidism.

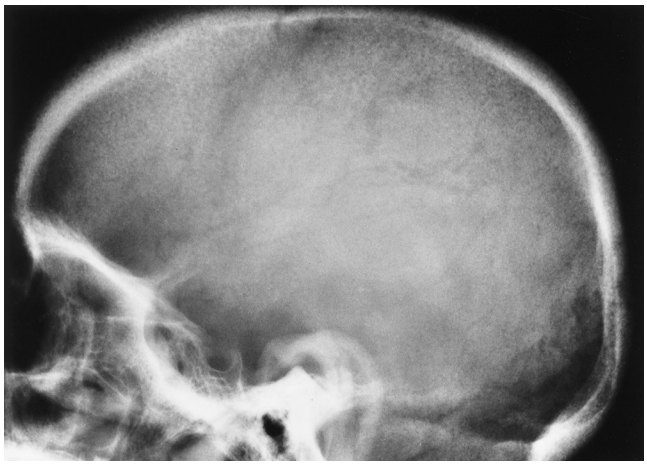

FIGURE 10-41 Hyperparathyroidism. Characteristic salt-and-pepper skull.

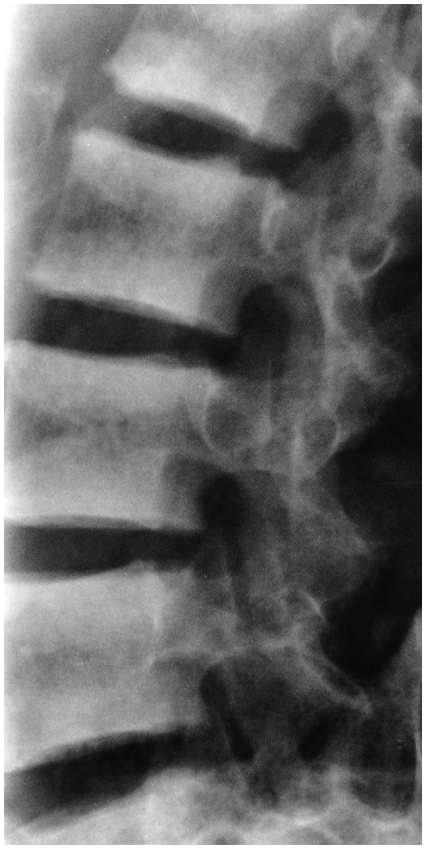

FIGURE 10-42 Hyperparathyroidism. Lateral projection of the lumbar spine demonstrates osteosclerosis of the superior and inferior margins of the vertebral bodies ("rugger-jersey" spine).

The preoperative localization of a functioning parathyroid adenoma has long been a difficult imaging problem. Ultrasound can detect 80% to 85% of parathyroid abnormalities. Parathyroid carcinomas usually have a more heterogeneous internal structure than adenomas. Preoperative parathyroid localization is not required unless the patient has had previous neck surgery. Plain radiographs and barium studies are of virtually no value unless the tumor is very large.

The major role of sophisticated imaging modalities in the localization of functioning parathyroid adenomas is in patients

who remain hypercalcemic, or in whom hypercalcemia recurs (Figure 10-44), after neck surgery for hyperparathyroidism. In these patients, normal anatomic relationships are disturbed, landmarks may be absent, and scarring and adhesions distort the field and complicate the surgical technique. Also, the elusive parathyroid tumor is more likely to be situated in an ectopic position (Figure 10-45). Indeed, the success rate for parathyroid reexploration without help from imaging is less than 65%.

FIGURE 10-43 Hyperparathyroidism. A dense mass of tumoral calcification can be seen in the joint capsules and periarticular soft tissues on the lateral aspect of the foot in a patient with chronic renal disease.

Thus, CT and MRI are required to detect ectopic parathyroid tissue location (such as in the thymus). Radionuclide subtraction imaging using technetium-99m (Figure 10-46A) and thallium can detect parathyroid adenomas with a fairly high sensitivity and specificity. An adenoma takes up only the thallium (Figure 10-46B), and a residual focus of activity appears when the technetium is subtracted from the initial image (Figure 10-46C). The normal thyroid can be distinguished from the tumor because it concentrates both radionuclides.

Using ultrasound or CT guidance for preoperative fine-needle aspiration biopsy can increase the specificity of localizing and confirming the exact site of a parathyroid adenoma, especially in patients who have undergone previous neck

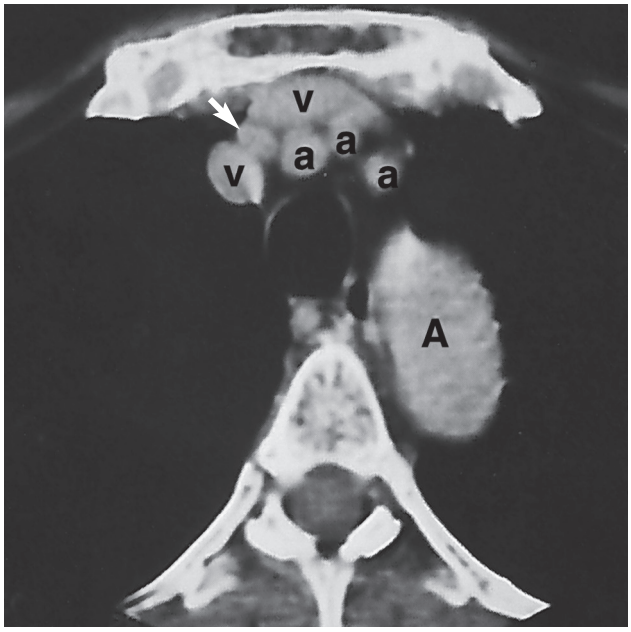

FIGURE 10-45 Ectopic parathyroid adenoma. CT scan shows a small soft tissue mass *(arrow)* in the anterior mediastinum. *A,* Aorta; *a,* three major branches of the aorta (from the patient's right to left: brachiocephalic, left carotid, and left subclavian arteries); *v,* right and left brachiocephalic veins.

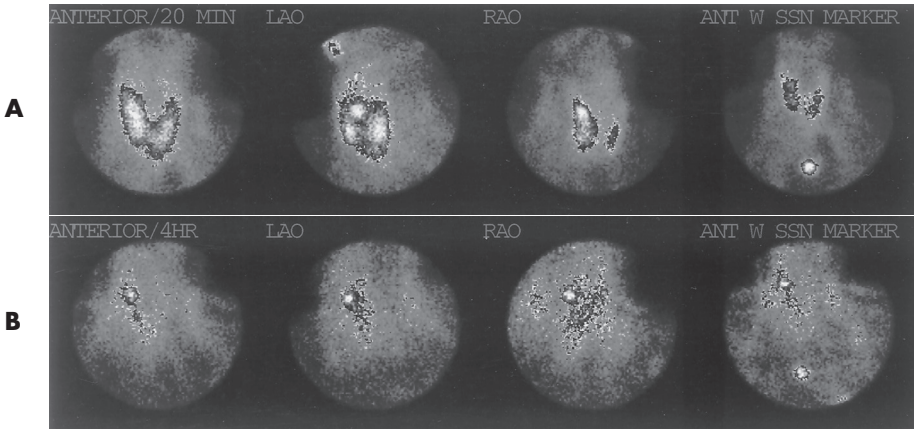

FIGURE 10-44 Parathyroid adenoma. (A) Technetium-99m sestamibi was injected, and the patient was scanned 20 minutes later; normal distribution was noted. (B) After 4 hours, washout of the activity in the thyroid tissue and a focal area of increased activity verify that the cause of hypercalcemia is a parathyroid adenoma.

dissection. When a successful aspiration biopsy of the neck shows the presence of parathyroid cells, there is no doubt that abnormal parathyroid tissue is situated at this site, and this finding eliminates the need for extensive surgical dissection.

Ultrasound, radionuclide scanning, CT, and MRI are complementary modalities for investigating the patient with hypercalcemia after parathyroid surgery. If these techniques fail to demonstrate a lesion, arteriography and venography with venous sampling may be performed for localization.

Treatment. A standard bilateral neck dissection by an experienced parathyroid surgeon can be expected to have a 95% success rate in controlling hyperparathyroidism. For hypercalcemia, specific drugs such as steroids and calcium-losing diuretics may be used.

Hypoparathyroidism

Clinically, hypoparathyroidism causes sustained muscular contraction (tetany), muscle cramps in hands and feet, and numbness and tingling of the extremities. Spasm of laryngeal muscles can cause fatal obstruction of the respiratory tract.

Imaging appearance. Hypoparathyroidism usually results from injury or accidental removal of the parathyroid glands during thyroidectomy, and this type of hypoparathyroidism is not associated with any significant radiographic abnormalities.

In **primary hypoparathyroidism**, which is less common, the most common radiographic finding on plain skull radiographs or CT of the skull is cerebral calcification, especially involving the basal ganglia (Figure 10-47),

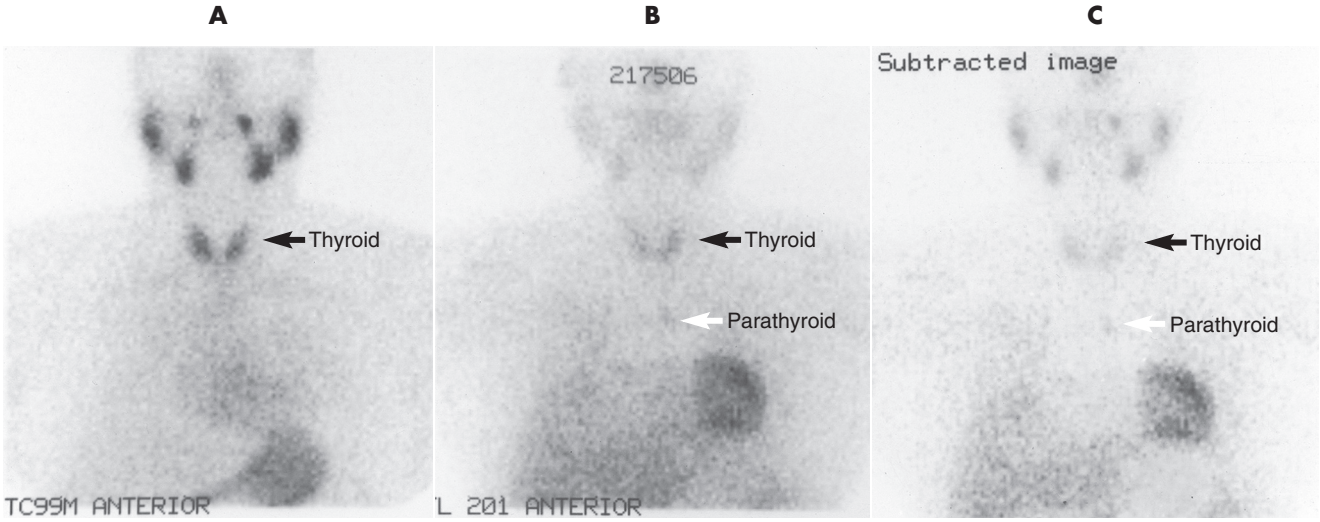

FIGURE 10-46 Radionuclide subtraction imaging. (A) Technetium uptake. (B) Thallium uptake. (C) The residual focus of thallium activity after the technetium activity is subtracted. In this case, a substernal parathyroid is demonstrated.

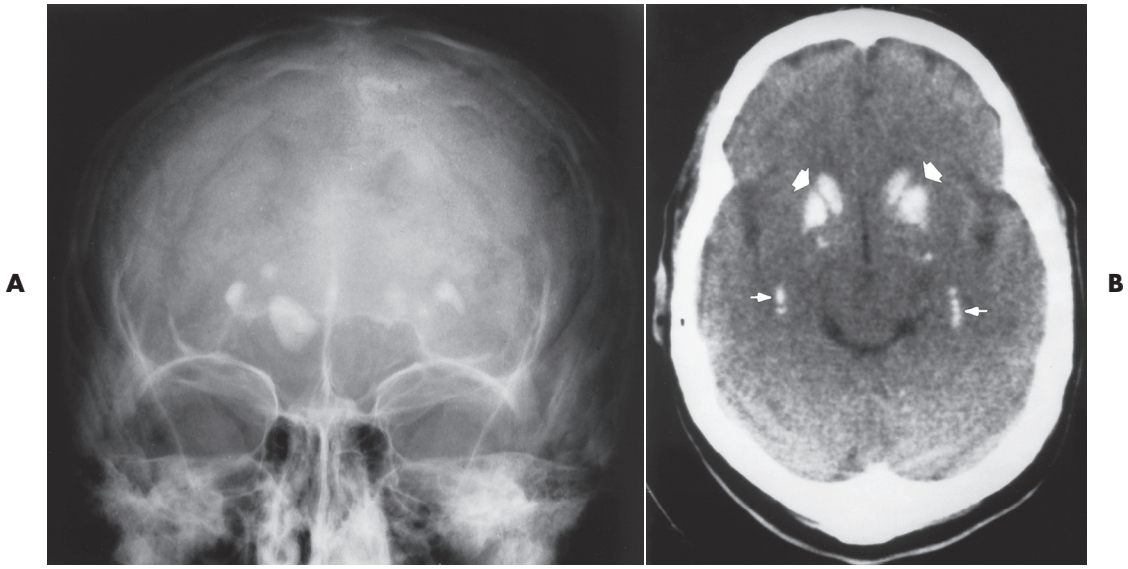

FIGURE 10-47 Hypoparathyroidism. (A) Frontal projection of the skull demonstrates calcification in the basal ganglia bilaterally. (B) CT scan shows characteristic bilateral calcification in the basal ganglia (*broad arrows*). Note also the small calcific deposits in the tail of the caudate nuclei (*thin arrows*).

the dentate (tooth-shaped) nuclei of the cerebellum, and the choroid plexus. A pattern of increased density may develop in the long bones, usually localized to the metaphyseal area.

Treatment. Synthetic parathormone decreases symptoms to a tolerable level.

Pseudohypoparathyroidism and Pseudopseudohypoparathyroidism

Pseudohypoparathyroidism is a hereditary disorder in which there is failure of normal end-organ response to normal levels of circulating parathyroid hormone. Most patients are obese and have short stature, with round faces, opacities in the cornea or lens of the eye, short fingers, and mental retardation.

Pseudopseudohypoparathyroidism refers to the presence of similar skeletal anomalies in other members of the patient's family in the absence of biochemical disturbances.

Imaging appearance. The most common radiographic abnormalities in pseudohypoparathyroidism are shortening of the tubular bones of the hands and feet (especially the fourth and fifth metacarpals) (see Figure 12-10) and calcific or bony deposits in the skin or subcutaneous tissues. An appearance similar to that of rickets may develop. As in idiopathic hypoparathyroidism, calcification is often found in the brain, especially the basal ganglia (best demonstrated on CT or MRI).

Treatment. Therapy of pseudohypoparathyroidism consists of some form of calcium supplement, either calcium carbonate or calcitriol combined with vitamin D.

Summary of Findings for Diseases of the Parathyroid Glands

Disorder	Location	Imaging Appearance	Treatment
Hyperparathyroidism	Excessive secretion of parathormone	Skeletal radiograph—subperiosteal bone resorption, erosion of distal clavicles, sclerotic stripes in vertebral bodies, salt-and-pepper skull US—carcinomas produce a more heterogeneous echo than adenomas CT/MRI—detect ectopic parathyroid tissue NM subtraction imaging—thallium appears as residual focal activity on technetium subtraction scan	Surgical resection by standard bilateral neck resection For hypercalcemia, steroids and calcium-losing diuretics
Hypoparathyroidism	Decreased secretion of parathormone	Radiograph/CT—cerebral calcification and increased density of metaphysis	Replacement therapy—synthetic parathormone
Pseudohypoparathyroidism	Failure of response by target organ	Radiograph—shortening of metacarpals and metatarsals	Some form of calcium supplement
Pseudopseudohypoparathyroidism	Similar skeletal anomalies in family members	Radiograph—shortening of metacarpals and metatarsals	Some form of calcium supplement

NM, Nuclear medicine; *US,* ultrasound.

DIABETES MELLITUS

Diabetes mellitus is a common endocrine disorder in which either beta cells in the islets of Langerhans of the pancreas fail to secrete insulin or target cells throughout the body fail to respond to this hormone. A lack of insulin prevents glucose from entering the cells, thus depriving them of the major nutrient needed for energy production. The blood glucose level rises (**hyperglycemia**).

The severity and age at onset of diabetes vary. Juvenile-onset diabetes, which develops in childhood, and insulin-dependent diabetes require the patient to undergo daily insulin injections. Non–insulin-dependent diabetes, which tends to develop later in life, is less severe and can often be controlled by diet alone. The precise cause of diabetes is unknown, although heredity is generally considered to be an important factor.

Polyuria (excessive urination) and polydipsia (drinking large quantities of liquid) are common manifestations of diabetes. The large amount of sugar filtered through the kidneys exceeds the amount that the renal tubules can absorb. This situation leads to the excretion of glucose in the urine (glycosuria), which is a major sign of diabetes.

Glucose is the major fuel of the body. However, because glucose cannot enter the cells without the action of insulin, diabetic patients are forced to metabolize a large amount of fat. This process produces a large number of acids and ketones, which can be detected in the urine. Production of fatty acids lowers the body's pH (acidosis). Severe acidosis and dehydration in a diabetic patient who fails to take enough insulin or eats a high-sugar diet can lead to diabetic coma, which may be fatal if not treated rapidly with fluids and a large dose of insulin.

A major complication of diabetes is the deposition of lipids within the walls of blood vessels (atherosclerosis). It causes arterial narrowing and even occlusion, resulting in myocardial infarction (coronary artery), stroke (carotid artery), or gangrene (peripheral artery). Excess glucose in tissues provides an excellent bacterial culture medium and leads to the frequent development of infections, which tend to heal

FIGURE 10-48 Diabetes mellitus. Typical calcification in moderate-size vessels of the hand and wrist. Evidence of a prior surgical resection of the phalanges of the fourth digit can be seen.

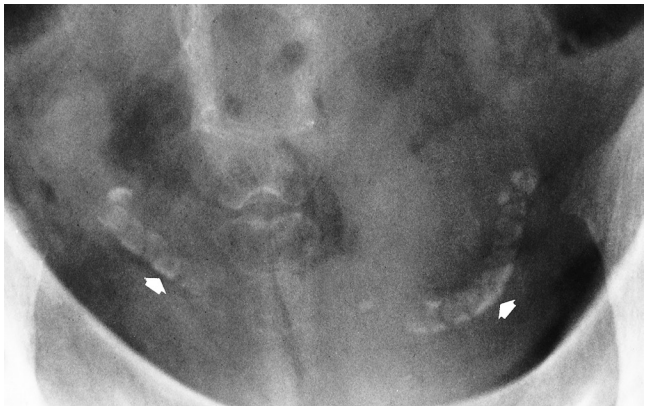

FIGURE 10-49 Diabetes mellitus. Bilateral calcification of the vas deferens (*arrows*).

FIGURE 10-50 Neuropathic joint in diabetes mellitus. Severe destructive changes with calcific debris can be observed about the intertarsal joints. Note the characteristic vascular calcification posterior to the ankle joint.

poorly because of the generally poor circulation in diabetic patients. The kidneys are always affected by long-standing diabetes, and kidney failure is frequently the cause of death. Another complication is narrowing and rupture of minute retinal blood vessels, which may lead to blindness. Poor circulation to the nervous system may produce intractable pain, tingling sensations, loss of feeling, and paralysis.

A patient with diabetes must also be wary of the development of insulin shock (hypoglycemic shock), which results from too much insulin, not enough food, or excessive exercise. The patient feels lightheaded and faint, trembles, and begins to perspire. In the radiology department, this condition may occur in diabetic patients who have not eaten or drunk before gastrointestinal examination or other special procedures. It is essential that this condition be rapidly recognized and that sugar be given, usually in the form of orange juice or candy. If the patient is unable to swallow, intravenous glucose may be administered.

Imaging Appearance

Diabetes mellitus produces a variety of radiographic findings that involve multiple organ systems. Atherosclerotic disease and subsequent ischemia involving the coronary, extracerebral, and peripheral circulations occur earlier and are more extensive in patients with diabetes, especially those who smoke. Calcifications in peripheral vessels, especially those of the hands and feet, are virtually pathognomonic of the disease (Figure 10-48). Men with diabetes may demonstrate characteristic calcification of the vas deferens, which appears as bilaterally symmetrical parallel tubular densities that run medially and caudally to enter the medial aspect of the seminal vesicles at the base of the prostate gland (Figure 10-49).

Diabetic persons have an increased susceptibility to infection, which especially affects the feet and may lead to severe osteomyelitis, producing bone destruction without periosteal reaction. Diabetic neuropathy with gait abnormalities and the loss of deep pain sensation may lead to repeated trauma on an unstable joint. Degeneration of cartilage, recurrent fracture and fragmentation of subchondral bone, soft tissue debris, and considerable proliferation of adjacent bone can lead to total disorganization of the joint (Charcot's, or neuropathic, joint) (Figure 10-50). Vascular disease with

FIGURE 10-51 Diabetic gangrene. There is diffuse destruction of the phalanges and the metatarsal head of the fifth digit. Note the large amount of gas in the soft tissues of the foot.

diminished blood supply can lead to gas gangrene, in which bubbles or streaks of gas develop in the subcutaneous or deeper tissues (Figure 10-51).

Diabetic neuropathy often causes radiographically evident abnormalities in the gastrointestinal tract. Findings include decreased primary peristalsis and tertiary contractions in the esophagus, delayed gastric emptying, and dilation of the small bowel. Emphysematous cholecystitis with gas in the lumen and wall of the gallbladder (see Figure 5-91) is a severe complication that occurs almost exclusively in diabetic patients.

Renal disease is a common complication and a leading cause of death in persons with diabetes. Acute and chronic pyelonephritis, renal papillary necrosis, and cystitis often occur. Diabetic neuropathy can cause dilation and atony (lack of normal tone) of the bladder with incomplete emptying.

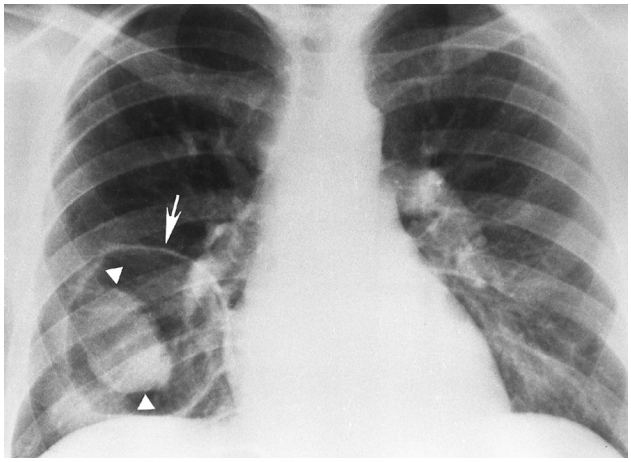

FIGURE 10-52 Mucormycosis in a patient with diabetes. A large, thin-walled cavity (*arrow*) contains a smooth, elliptic, homogeneous mass (*arrowheads*) representing the fungus ball.

Mucormycosis infection is a devastating fungal disease that occurs virtually only in persons with uncontrolled diabetes. It usually originates in the nose and paranasal sinuses, from which it can extend to destroy the walls of the sinus and invade the substance of the brain. Pulmonary mucormycosis is a progressive severe pneumonia that is widespread and confluent and often cavitates (Figure 10-52).

Treatment

The purpose of therapy in diabetes mellitus is to keep the blood glucose levels constant with a minimal variation. Oral therapy for glycemic control or short- or long-acting insulin is used when proper diet and exercise cannot maintain normal levels. In cases in which blood glucose levels are difficult to regulate, a continuous infusion pump may be used to help maintain a constant blood glucose level. Advances in therapy for this disease include islet cell transplantation and insulin gene therapy.

Summary of Findings for Diabetes Mellitus

Disorder	Location	Imaging Appearance	Treatment
Diabetes mellitus	Failure of pancreas to secrete insulin or failure of target organ to respond	Skeletal radiograph—peripheral vessel calcification, severe osteomyelitis, neuropathic joints, gas gangrene, emphysematous cholecystitis	Oral medication, insulin, proper diet Advanced therapies—islet cell transplantation, insulin gene insertion

REVIEW QUESTIONS

1. What organ in the body is responsible for the release of insulin?
   a. spleen
   b. liver
   c. pancreas
   d. small intestine
2. What organ in the body is responsible for the release of glucagon?
   a. spleen
   b. liver
   c. pancreas
   d. small intestine
3. The _____ glands secrete several types of steroid hormones and lie above each kidney.
   a. adrenal
   b. pituitary
   c. pineal
   d. thymus
4. What hormone has the ability to constrict some blood vessels while dilating others to shunt blood to active muscles where oxygen and nutrients are needed?
   a. androgen
   b. epinephrine
   c. glucocorticoids
   d. aldosterone
5. What hormones are known as the fight-or-flight hormones?
   a. androgen, epinephrine
   b. adrenaline, norepinephrine
   c. glucocorticoid, adrenaline
   d. androgen, glucocorticoid
6. Enlargement of the adrenal glands is best demonstrated by what diagnostic modality?
   a. ultrasound
   b. MRI
   c. CT
   d. plain image radiography
7. What pathologic condition is characterized by obesity of the trunk of the body, a fat pad behind the shoulders, and a moon-shaped face?
   a. Conn's syndrome
   b. Cushing's syndrome
   c. adrenogenital syndrome
   d. Addison's syndrome
8. One complication of Cushing's syndrome that radiographers must be cautious of is _____.
   a. buffalo hump
   b. spontaneous fractures
   c. hypercalciuria
   d. sella erosion
9. Excessive administration of _____ is the most common cause of adrenal insufficiency.
   a. adrenalin
   b. aldosterone
   c. steroids
   d. ACTH
10. The second most common malignancy in children is _____.
    a. pheochromocytoma
    b. neuroblastoma
    c. Wilms' tumor
    d. adenoma
11. The _____ controls the hormone secretion of the pituitary gland.
    a. cerebellum
    b. pons
    c. medulla oblongata
    d. hypothalamus
12. Enlargement of the hands, feet, and face is characteristic of what pathologic condition?
    a. adenoma
    b. acromegaly
    c. gigantism
    d. none of the above
13. A pea-sized gland suspended from the base of the brain, sometimes referred to as the master gland, is called the _____.
    a. thymus
    b. pineal
    c. pituitary
    d. pinna
14. What is the name for the butterfly-shaped gland located at the level of the larynx?
    a. thymus
    b. thyroid
    c. pituitary
    d. pineal
15. Thyroid tissue is best demonstrated by what imaging modality?
    a. CT
    b. radionuclide imaging
    c. ultrasound
    d. plain image radiography
16. Insufficient synthesis of thyroid hormone can lead to what pathologic condition?
    a. hyperthyroidism
    b. hypothyroidism
    c. exophthalmos
    d. Graves' disease
17. What is the name for an enlargement of the thyroid gland that does not result from an inflammatory or neoplastic process?
    a. exophthalmos
    b. goiter
    c. myxedema
    d. skin thickening
18. There is a significantly higher risk of thyroid cancer in people who received _____.
    a. neck irradiation in childhood
    b. steroid therapy in childhood
    c. chest radiographs in childhood
    d. skull radiographs in childhood

19. If beta cells in the islets of Langerhans fail to secrete insulin, what pathologic condition results?
- **a.** goiter
- **b.** exophthalmos
- **c.** diabetes
- **d.** hypothyroidism

20. A diabetic patient who receives insulin before reporting to the radiology department for an upper gastrointestinal study should be monitored by the radiographer for any signs of developing _____.
- **a.** ketoacidosis
- **b.** hypoglycemic shock
- **c.** acidosis
- **d.** hyperglycemic shock

21. The most common complication and leading cause of death in diabetic patients is _____.
- **a.** hypoglycemia
- **b.** hyperglycemia
- **c.** pancreatic disease
- **d.** renal disease

11

Reproductive System

OUTLINE

Infectious Diseases of Both Genders
- Syphilis
- Gonorrhea

Male Reproductive System
Physiology of the Male Reproductive System
Benign Prostatic Hyperplasia
Carcinoma of the Prostate Gland
Staging
Undescended Testis (Cryptorchidism)
Testicular Torsion and Epididymitis
Testicular Tumors
Female Reproductive System
Physiology of the Female Reproductive System
Pelvic Inflammatory Disease
Cysts and Tumors
- Ovarian Cysts and Tumors
- Dermoid Cyst (Teratoma)
- Uterine Fibroids
- Endometrial Carcinoma
- Endometriosis
- Carcinoma of the Cervix

Breast Lesions
- Breast Cancer
- Benign Breast Disease

Imaging in Pregnancy
- Ectopic Pregnancy
- Trophoblastic Disease

Female Infertility

KEY TERMS

chorion
congenital syphilis
corpus luteum
cystadenoma
ectopic pregnancy
epididymis
estrogen
hydrosalpinx
menarche
menopause
menstrual phase
oligohydramnios
ovulation
polyhydramnios
primary cystadenocarcinoma
primary stage of syphilis
progesterone
proliferative, or postmenstrual, phase
prostate gland
pyosalpinx
secondary stage of syphilis
secretory, or postovulatory, phase
seminal vesicle
spermatogenesis
tertiary stage of syphilis
testosterone
vas deferens
vasectomy

OBJECTIVES

After reading this chapter, the reader will be able to:

- Define and describe all boldface terms in this chapter
- Describe the physiology of the reproductive system
- Identify anatomic structures on both diagrams and radiographs of the reproductive system
- Differentiate various pathologic conditions affecting the reproductive system and their radiographic manifestations
- Initiate alterations that must be made in routine exposure techniques to obtain optimal-quality radiographs

INFECTIOUS DISEASES OF BOTH GENDERS

Syphilis

Syphilis is a chronic, sexually transmitted systemic infection caused by the spirochete *Treponema pallidum*. The baby of an infected mother may be born with **congenital syphilis**. In the **primary stage** of infection, a chancre, or ulceration, develops on the genitals (usually the vulva of the female and the penis of the male). If untreated, the **secondary stage** of the disease appears as a nonitching rash that affects any part of the body. At this stage, the patient is still infectious. If still untreated, the disease may become dormant for many years before the development of the most serious or **tertiary stage** of the disease, in which radiographic abnormalities become apparent. The young black male population is most often affected.

Imaging appearance. Cardiovascular syphilis involves primarily the ascending aorta, which may become aneurysmally dilated and often demonstrates linear calcification of the wall (Figure 11-1). Syphilitic aortitis often involves the aortic valvular ring and produces aortic regurgitation with enlargement of the left ventricle.

RADIOGRAPHER NOTES

Because of its nonionizing character, ultrasound has become the major modality for imaging both male and female reproductive systems. Computed tomography (CT), magnetic resonance imaging (MRI), and positron emission tomography (PET) are used for staging malignant tumors when ultrasound is inconclusive, and radionuclide studies are used to differentiate testicular torsion from epididymitis.

Conventional plain image radiography is virtually never indicated for disorders of the pregnant patient. The once common pelvimetry and gravid uterus examinations have been almost completely replaced by nonionizing ultrasound imaging. The two radiographic studies of the female reproductive system that are in current use are hysterosalpingography and mammography. Hysterosalpingography, which is performed with fluoroscopic guidance, evaluates the patency (openness) of the fallopian tubes. Plain radiographs are obtained only to provide a permanent record. Mammography requires dedicated equipment and a specially trained radiographer. Properly performed mammograms can detect breast cancer in the early stage, before it is symptomatic, thus decreasing the incidence of metastases and greatly improving patient survival rates. However, mammograms performed by poorly trained radiographers or with inadequate equipment may fail to demonstrate early lesions, condemning women with an otherwise curable disease to unnecessary suffering and even death.

It is essential that the radiographer attempt to put the patient at ease when performing an examination of the reproductive system. Although these procedures are not actually painful, they may at times be uncomfortable and are frequently embarrassing for the patient. A good professional attitude goes a long way in reassuring the patient and making these examinations as comfortable as possible.

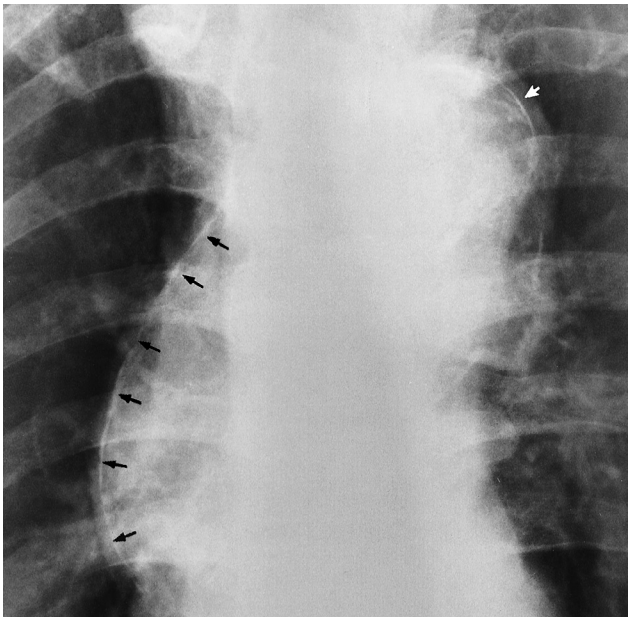

FIGURE 11-1 Syphilitic aortitis. Aneurysmal dilation of the ascending aorta with extensive linear calcification of the wall (*black arrows*). Some calcification is also seen in the distal aortic arch (*white arrow*).

Syphilitic involvement of the skeletal system most commonly produces radiographic findings of chronic osteomyelitis, which usually affects the long bones and the skull. The destruction of bone incites a prominent periosteal reaction, with dense sclerosis as the most outstanding feature (Figure 11-2). Syphilis is a major cause of neuropathic joint disease (Charcot's joint), in which bone resorption and total disorganization of the joint are associated with calcific and bony debris (Figure 11-3).

Syphilitic lesions developing in the cerebral cortex can cause mental disorders, deafness, and blindness. The cerebral lesions containing syphilis bacteria (intracerebral gummata)

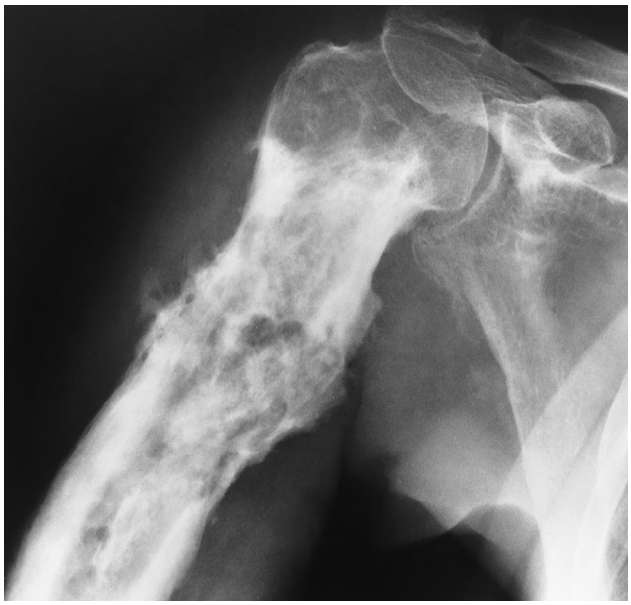

FIGURE 11-2 Syphilitic osteomyelitis. Diffuse lytic destruction of the proximal humerus with reactive sclerosis and periosteal new bone formation.

FIGURE 11-3 Neuropathic joint disease in syphilis. Joint fragmentation, sclerosis, and calcific debris about the hip.

are hypodense on nonenhanced CT. On T1-weighted MRI, the lesions appear hypointense or isointense, and they become hyperintense on T2-weighted images. The intracerebral gummata densely enhance with the administration of gadolinium. Single-photon emission computed tomography (SPECT) demonstrates the significant decrease of blood flow in the frontal and temporal cortices bilaterally. Scans obtained following therapy demonstrate a marked improvement in flow. Diffuse thickening of the gastric wall can cause narrowing of the lumen that is indistinguishable from that seen in carcinoma.

Multiple bone abnormalities can occur in infants with congenital syphilis who are born to infected mothers (Figure 11-4). Mental retardation, deafness, and blindness are common complications.

Treatment. In the primary and secondary stages of syphilis, antibiotic therapy cures the disease. The ulcerations in primary syphilis and the skin lesions and rash in secondary syphilis heal in a few days with penicillin, doxycycline, or tetracycline. The tertiary stage is incurable.

Gonorrhea

Gonorrhea is a bacterial infection, one of the most common and most widespread of the venereal diseases, which occurs more commonly in men (1.5:1). Persons of Asian and Pacific Island descent are least likely affected, whereas the African American population is experiencing the greatest increase. Symptoms usually occur a few days after infection. An acute urethritis with copious discharge of pus develops in men. Women may be asymptomatic or may have minimal symptoms of urethral or cervical inflammation. If untreated, the inflammation may become chronic, spread upward, and produce fibrosis, leading to urethral stricture in men (Figure 11-5)

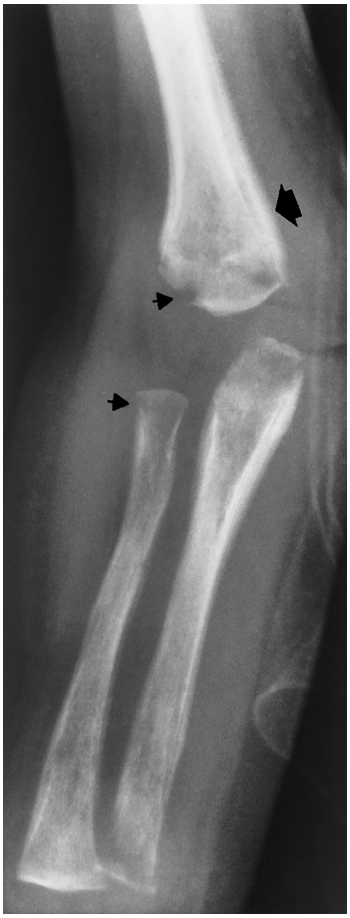

FIGURE 11-4 Congenital syphilis. Transverse bands of decreased density across the metaphyses (*small arrows*) associated with patchy areas of bone destruction in the diaphyses. Solid periosteal new bone formation (*large arrow*) is best seen about the distal humerus.

Summary of Findings for Infectious Diseases of the Reproductive System

Disorder	Location	Imaging Appearance	Treatment
Syphilis	Male and female reproductive organs	Cardiovascular—aortic dilation with possible calcification Skeletal radiograph—chronic osteomyelitis of long bones and skull; periosteal reaction with dense sclerosis CT—intracerebral gummata are hypodense on nonenhanced scans MRI—on T1-weighted images, the lesions appear hypointense or isointense; they are hyperintense on T2-weighted images; intracerebral gummata densely enhance with contrast agent SPECT—decreased cortical flow in frontal and temporal cortices bilaterally; post-therapeutic scans demonstrate a marked improvement in flow	Primary and secondary stages—antibiotics Tertiary stage—incurable
Gonorrhea	Male and female reproductive organs	Skeletal—septic arthritis with articular erosion and joint space narrowing PID—US or CT demonstrates thick, dilated fallopian tubes or abscess formation	Penicillin; if disease is penicillin-resistant, ceftriaxone

GI, Gastrointestinal; *PID,* pelvic inflammatory disease; *US,* ultrasound.

and pelvic inflammatory disease (PID) or sterility in women. A serious complication is fibrous scarring of the fallopian tubes that may result in sterility or an ectopic pregnancy.

Imaging appearance. Gonorrheal infection can cause septic arthritis, leading to articular erosion and joint space narrowing.

For patients in whom PID is suspected, ultrasound (ultrasonography) or CT is the modality of choice for demonstrating thick, dilated fallopian tubes or abscess formation. Ultrasound is superior for showing ectopic pregnancy.

Treatment. Gonorrhea usually responds rapidly to antibiotic therapy (penicillin). Penicillin-resistant gonorrhea has been reported and requires a single intramuscular dose of ceftriaxone.

MALE REPRODUCTIVE SYSTEM

PHYSIOLOGY OF THE MALE REPRODUCTIVE SYSTEM

The major function of the male reproductive system is the formation of sperm (**spermatogenesis**), which begins at approximately 13 years of age and continues throughout life. Under the influence of follicle-stimulating hormone (FSH) secreted by the anterior lobe of the pituitary gland, the seminiferous tubules of the testes are stimulated to produce the male germ cells called *spermatozoa*. In addition to producing sperm cells, the testes secrete the male hormone **testosterone**. This substance stimulates the development and activity of the accessory sex organs (prostate and seminal vesicles) and is responsible for adult male sexual behavior. Testosterone causes the typical male changes that occur at puberty, including the development of facial and body hair and alterations in the larynx that result in a deepened voice. Testosterone also helps regulate metabolism by promoting growth of skeletal muscles and is thus responsible for the greater muscular development and strength in males.

The final maturation of sperm occurs in the **epididymis**, a tightly coiled tube enclosed in a fibrous casing (Figure 11-6). The sperm spend approximately 1 to 3 weeks in this segment of the duct system, where they become motile and capable of fertilizing an ovum. The tail of the epididymis leads into the **vas deferens**, a muscular tube that passes through the inguinal canal as part of the spermatic cord and joins the duct from the **seminal vesicle** to form the ejaculatory duct. Depending on the degree of sexual activity and frequency of ejaculation, sperm may remain in the vas deferens up to 1 month with no loss of fertility. Severing of the vas deferens (**vasectomy**) is an operation performed to make a man sterile. Vasectomy interrupts the route from the epididymis to the remainder of the genital tract.

The seminal vesicles lie on the posterior aspect of the base of the bladder and secrete a thick liquid that is rich in fructose, a simple sugar that serves as an energy source for sperm motility after ejaculation. The seminal vesicles also secrete prostaglandin, which increases uterine contractions in the woman and helps propel the sperm toward the fallopian tubes.

The **prostate gland** lies just below the bladder and surrounds the urethra. It secretes a thin alkaline substance that constitutes the major portion of the seminal fluid volume. The alkalinity of this material is essential to sperm motility, which would otherwise be inhibited by the highly acidic vaginal secretions.

Intense sexual stimulation causes peristaltic contractions in the walls of the epididymis and vas deferens, propelling sperm into the urethra. At the same time, the seminal vesicles and prostate gland release their secretions, which mix with the mucous secretion of the bulbourethral glands to form semen. The ejaculation of semen occurs when intense

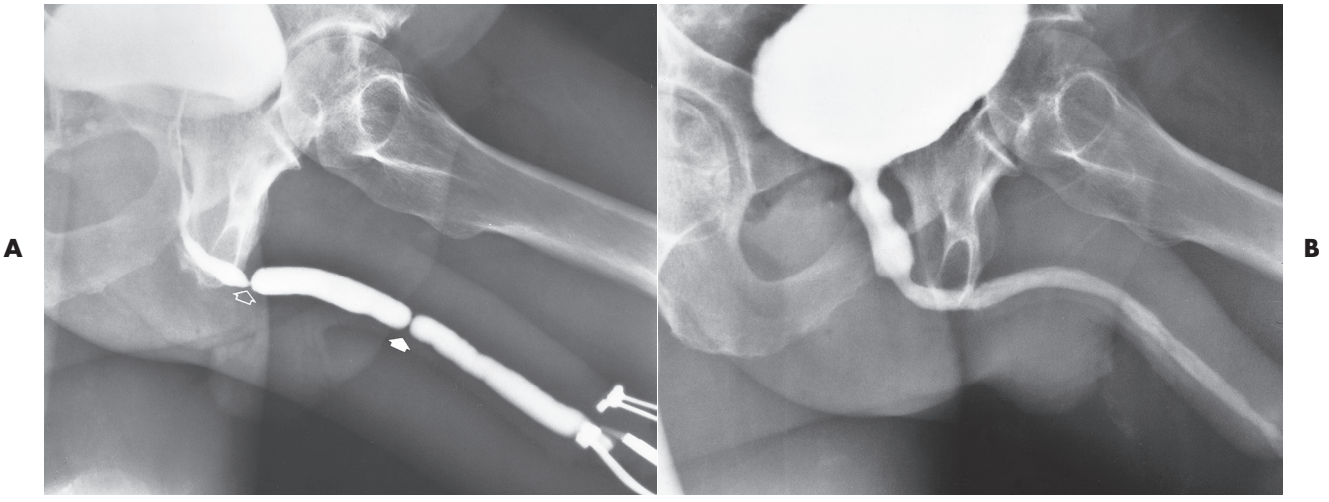

FIGURE 11-5 Gonococcal urethral stricture. **(A)** Initial retrograde urethrogram shows diffuse stricture of the bulbar urethra and high-grade stenoses in proximal (*solid arrow*) and distal (*open arrow*) portions of the urethra. **(B)** After balloon dilation, a voiding urethrogram shows considerable improvement in the appearance of the urethra.

muscular contractions of erectile tissue cause the semen to be expressed through the urethral opening.

Male fertility is related not only to the number of sperm ejaculated but also to their size, shape, and motility. Although only one sperm fertilizes an ovum, millions of sperm seem to be necessary for fertilization to occur. Indeed, it is estimated that sterility may result when the sperm count falls below approximately 50 million per milliliter of semen.

BENIGN PROSTATIC HYPERPLASIA

Enlargement of the prostate gland is common in men older than 60 years of age and may be detected on a digital rectal examination. The enlargement is probably related to a disturbance of hormone secretions from the sex glands that occurs as the period of reproductive activity declines. The major effect of prostatic enlargement is an inability to empty the bladder completely, leading to partial urinary tract obstruction, bilateral ureteral dilation, and hydronephrosis.

Imaging appearance. Transrectal ultrasound imaging, performed by means of a probe inserted into the rectum, demonstrates gland enlargement and heterogeneous signal intensity of the central portion (Figure 11-7). A circumferential surgical pseudocapsule, discrete nodules, and a thickened bladder wall may also be visualized. Moreover, an abdominal–pelvic scan can demonstrate residual urine volume and aids in the evaluation of the kidneys for the presence of hydronephrosis.

On excretory urography, the enlarged prostate typically produces elevation and a smooth impression on the floor of the contrast material–filled bladder (Figure 11-8). Elevation of the insertion of the ureters on the trigone of the bladder produces a characteristic J-shaped, or fishhook, appearance of the distal ureters. Residual urine in the bladder provides a

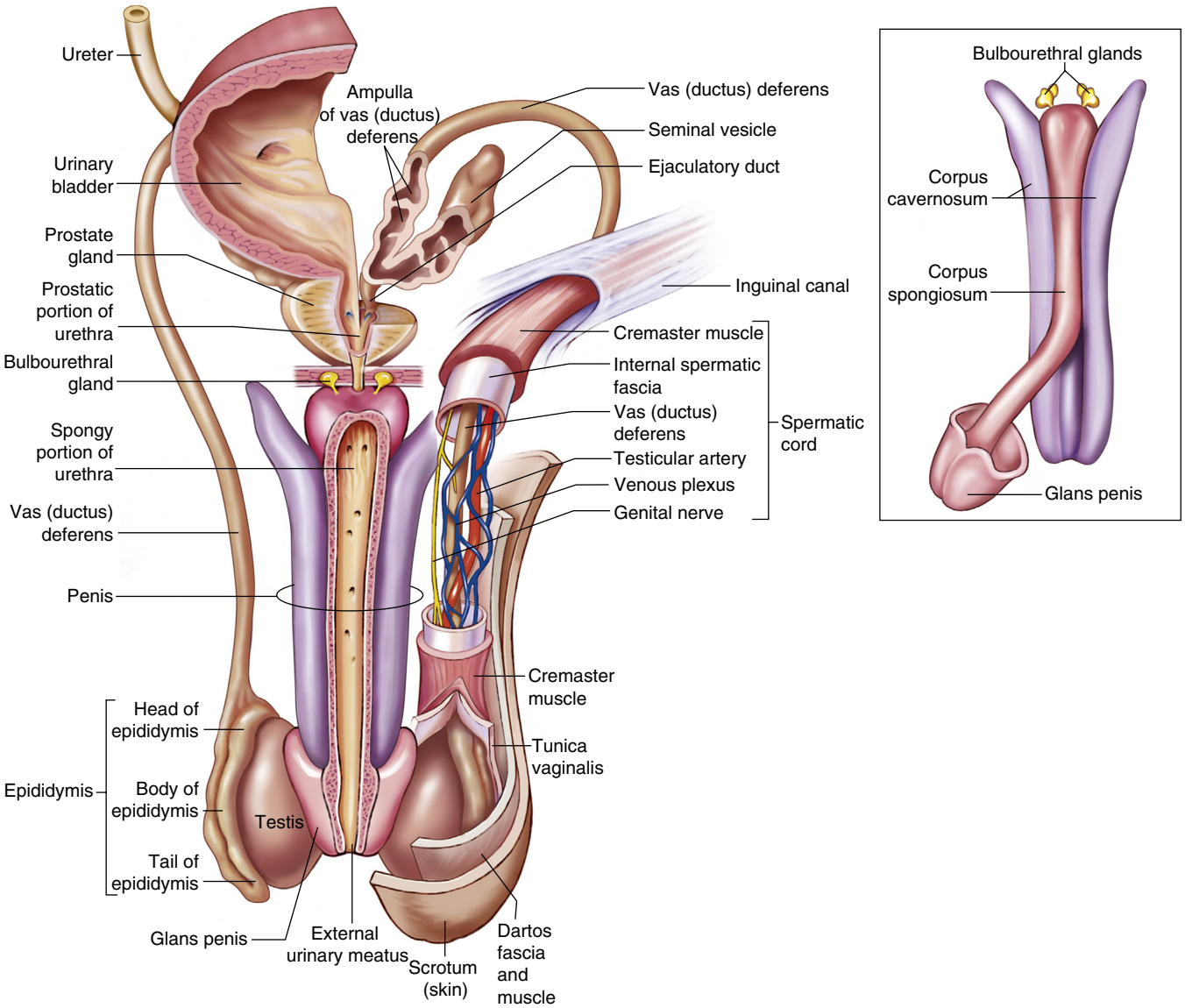

FIGURE 11-6 The male reproductive system. Illustration shows the testes, epididymis, ductus deferens, and glands of the male reproductive system.

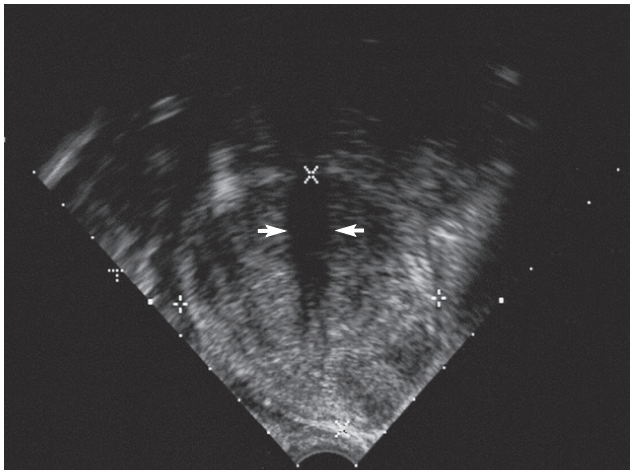

FIGURE 11-7 Benign prostatic hyperplasia. Transrectal ultrasound in the sagittal plane demonstrates enlargement of the central periurethral soft tissue consistent with benign prostatic hyperplasia (measurement *markers*). The Eiffel Tower sign is caused by an enlarged urethra (*arrows*).

FIGURE 11-8 Benign prostatic hyperplasia. Large, smooth filling defect at the base of the bladder. Note the fishhook appearance of the distal ureters and calcification in the vas deferens.

growth medium for bacterial infection, which produces cystitis; the infection may ascend from the bladder to the kidney, resulting in pyelonephritis.

On MR images, benign prostatic hyperplasia causes a diffuse or nodular area of homogeneous low signal intensity on T1-weighted images and an inhomogeneous, mixed (intermediate to high) signal intensity on T2-weighted images (Figure 11-9). A pseudocapsule, representing compression of adjacent tissue visualized as a low–signal intensity rim, often accentuates focal enlargement. Diffuse enlargement shows similar intensity changes, although the pseudocapsule is not present. Unfortunately, the intensity of benign prostatic hyperplasia may often be similar to that of the normal prostate or a region of prostatitis.

Treatment. Surgical resection of the prostate (transurethral resection [TUR]) can relieve the obstructive symptoms.

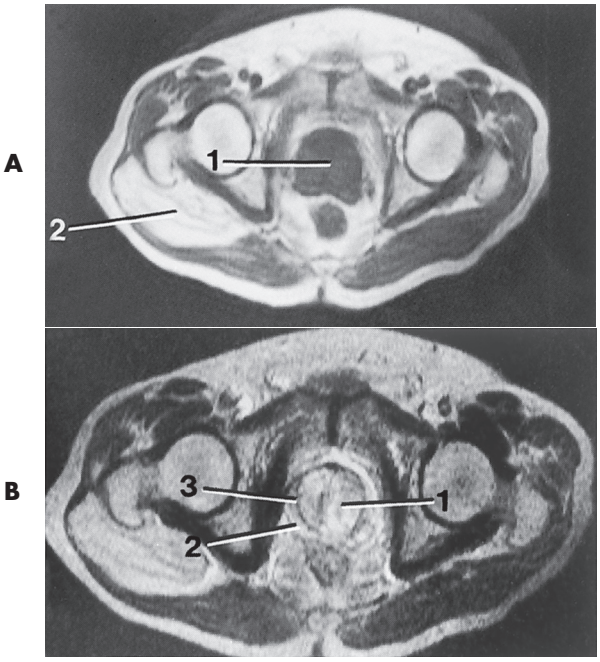

FIGURE 11-9 Benign prostatic hyperplasia. (A) T1-weighted MR image shows prostatic enlargement of homogeneous low signal intensity (1). Note the high signal intensity of the large lipoma (2) in the right gluteal region. **(B)** On a T2-weighted image, the intermediate signal intensity of the enlarged transitional zone (1) shows increased inhomogeneity and is separated from the high–signal intensity peripheral zone (2) by a low–signal intensity rim of pseudocapsule (3).

CARCINOMA OF THE PROSTATE GLAND

Carcinoma of the prostate gland is the second most common malignancy in men, with a slightly higher incidence in black men. The disease rarely occurs before 50 years of age, and the incidence increases by approximately 40% with advancing age. The tumor can be slow growing and asymptomatic for long periods or can behave aggressively with extensive metastases. Prostate carcinoma occurs most often in the peripheral zone (70%). Carcinoma of the prostate is best detected by palpation, on which it is detected as a hard, nodular, and irregular mass, on a routine rectal examination. The presence of an elevated serum PSA (prostate-specific antigen) value indicates an abnormality, although this blood test is not specific for malignancy.

Imaging appearance. Radiographically, carcinoma of the prostate often elevates and impresses the floor of the contrast-filled bladder. Unlike the smooth contour seen in benign prostatic hyperplasia, the impression on the bladder floor is usually more irregular in carcinoma (Figure 11-10). Bladder neck obstruction, infiltration of the trigone, or invasive obstruction of the ureters above the bladder may produce obstruction of the upper urinary tract.

Transrectal (TR) ultrasound is the preferred technique for detecting carcinoma of the prostate (Figure 11-11). The normal prostate has a generally homogeneous appearance with a moderate echo pattern. Early studies indicated that prostatic

FIGURE 11-10 Carcinoma of the prostate. A large, irregular mass elevates and impresses the floor of the contrast agent–filled bladder.

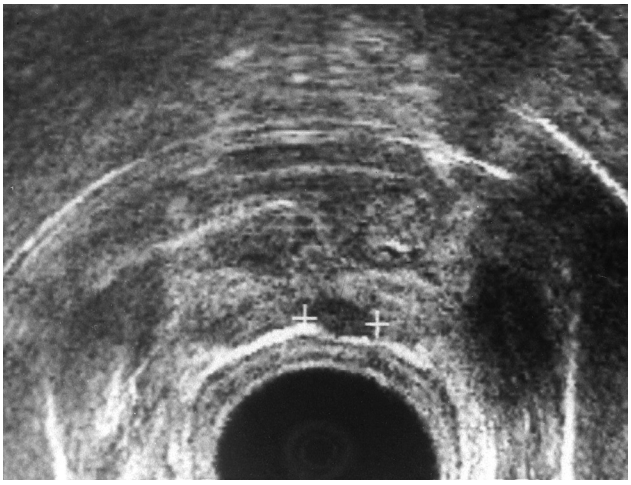

FIGURE 11-11 Cancer of the prostate. Transrectal ultrasound image demonstrates a hypoechoic mass (between *cursors*) with the capsule still intact.

carcinoma appeared as hyperechoic areas. However, with the development of newer and higher-frequency transducers, many carcinomas appear as areas of low echogenicity within the prostate. Up to 40% of carcinomas are isoechoic with normal prostate tissue and thus cannot be visualized on ultrasound. The latest studies have concluded that the wide range of sonographic patterns in carcinoma indicates that ultrasound cannot reliably differentiate prostatic malignancy from benign disease.

STAGING

Imaging appearance. MRI can superbly delineate the prostate, seminal vesicles, and surrounding organs to provide accurate staging of pelvic neoplasms. When the spin-echo technique is used, the central and peripheral zones of

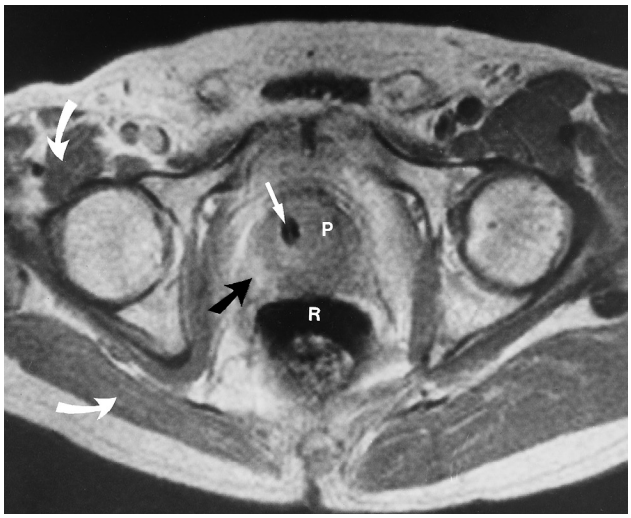

FIGURE 11-12 Carcinoma of the prostate. Axial MR image through the pelvis demonstrates an abnormal area of increased signal intensity (*black arrow*) within the prostate gland (P). A Foley catheter is in place (*straight white arrow*), and the rectum (R) contains air and feces. Note the decreased size of the pelvic musculature on the right (*curved white arrows*) in this patient, who has an above-knee amputation.

the prostate are well demonstrated and distinctly separate from the surrounding levator ani muscles. In the sagittal plane, the relation of the prostate to the bladder, rectum, and seminal vesicles is clearly shown. Prostatic carcinoma is best demonstrated on long TR images, on which it appears as disruption of the normally uniform high signal intensity of the peripheral zone of the prostate (Figure 11-12). T2-weighted images demonstrate low intensity that is surrounded by the hyperintense signal of the normal tissue. The new technique of MR lymphography aids in visualizing nonenlarged pelvic lymph nodes. However, there is much controversy regarding whether MRI is reliable for detection and diagnosis of prostate cancer, and therefore a precise diagnosis requires a biopsy and histologic examination. Research findings state that the demonstration of a normal-appearing prostate gland on MRI does not exclude the presence of a neoplasm. In addition, inhomogeneity of the gland is a common nonspecific finding that can also be seen in patients with adenoma or prostatitis.

Carcinoma of the prostate may spread by direct extension or by way of the lymphatics or the bloodstream. Spread of carcinoma of the prostate to the rectum can produce a large, smooth, concave pressure defect; a fungating ulcerated mass simulating primary rectal carcinoma; or a long, asymmetrical annular stricture. Both ultrasound and CT, especially the arterial phase of multislice CT, aid in defining extension of tumor into the bladder and seminal vesicles and in detecting metastases in enlarged lymph nodes (Figure 11-13).

The most common hematogenous metastases are to bone. They involve primarily the pelvis, thoracolumbar spine, femurs, and ribs. These lesions are most commonly osteoblastic and appear as multiple rounded foci of sclerotic density (Figure 11-14) or occasionally as diffuse sclerosis involving

an entire bone ("ivory vertebra"). Patients with bony metastases usually have strikingly elevated serum acid phosphatase values. Because significant bone destruction or bone reaction must occur before a lesion can be detected on plain radiographs, the radionuclide bone scan is the best screening technique for detection of asymptomatic skeletal metastases in patients with carcinoma of the prostate. However, because the radionuclide scan is very sensitive but not specific and may show increased uptake in multiple disorders of the bone, conventional radiography of the affected site should be performed when the scan is abnormal.

Treatment. For a tumor confined to the prostate gland, a successful cure can be achieved by a radical prostatectomy or radiation therapy. Prostate tumors with local invasion require both a radical prostatectomy and radiation therapy. Radiation therapy may consist of implantation of iodine-125 or palladium-103 seeds. Stage D prostate cancers, the most progressive, require hormonal therapy (antiandrogen drugs) to slow the spread of disease and palliative measures to reduce pain. In some cases, orchiectomy (removal of the testes) is performed.

UNDESCENDED TESTIS (CRYPTORCHIDISM)

Near the end of gestation, the testis normally migrates from its intra-abdominal position through the inguinal canal into the scrotal sac. This condition is more common in premature males and can cause infertility. If one of the testicles cannot be palpated within the scrotum, it is important to determine whether this finding represents absence of the testis or an ectopic position of the testis. The rate of malignancy is up to 40 times higher in the undescended (intra-abdominal) testis than in the descended testicle.

Imaging appearance. In the absence of a palpable testicle, ultrasound is usually used as a screening technique. This modality carries no radiation risk and has a high diagnostic

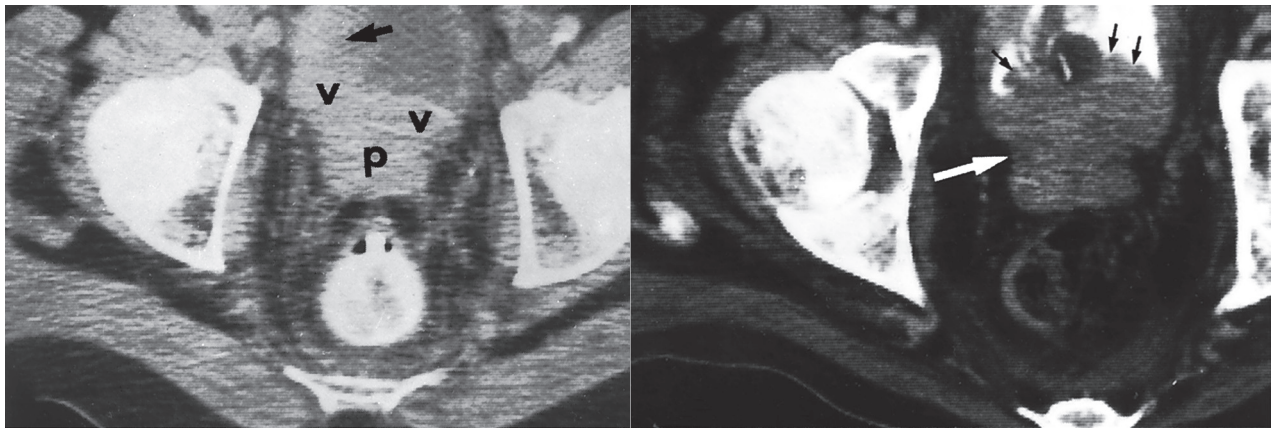

FIGURE 11-13 Metastatic carcinoma of the prostate gland. **(A)** CT scan shows prostatic carcinoma (p) invading the wall of the bladder (*arrow*) and the seminal vesicles (v). **(B)** CT scan on another patient shows prostatic carcinoma involving the bladder (*black arrows*) and seminal vesicles. The normally sharp angle between the seminal vesicles and the prostate is lost (*white arrow*).

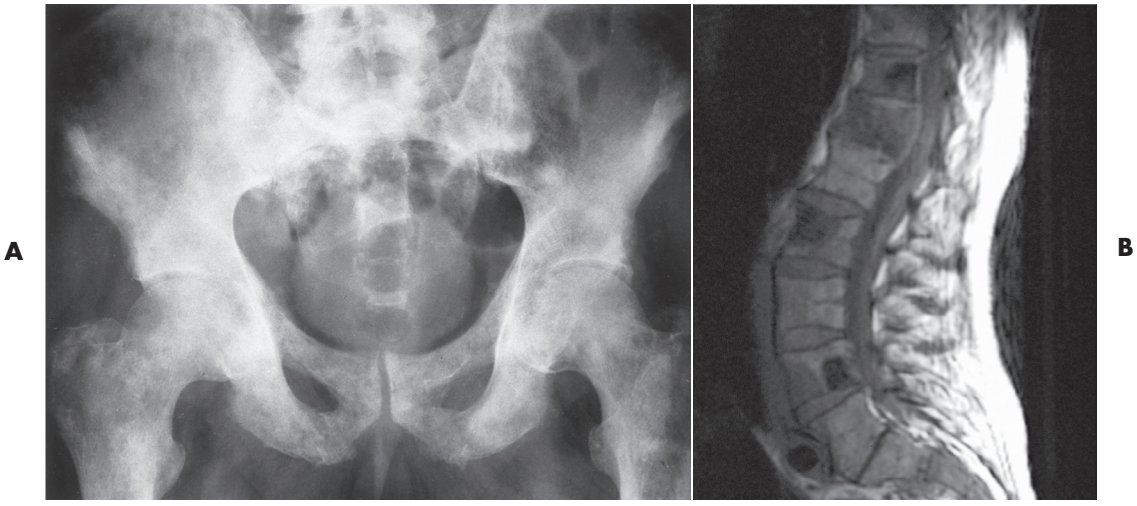

FIGURE 11-14 Metastatic carcinoma of the prostate. **(A)** Diffuse osteoblastic metastases involving the bones about the pelvis. **(B)** T1-weighted spin-echo MR image illustrates osteoblastic lesions throughout the spine.

accuracy in demonstrating undescended testicles that are located in the inguinal canal (Figure 11-15). However, sonography is not successful in detecting ectopic testicles in the pelvis or abdomen. If ultrasound fails to demonstrate an undescended testis, MRI or CT is indicated (Figures 11-16 and 11-17). MRI typically demonstrates a low signal mass on T1-weighted images that has high signal intensity on T2-weighted images. The uniform oval soft tissue mass of an undescended testis demonstrates contrast enhancement on CT.

Treatment. Because of the extremely high rate of malignancy, the diagnosis of undescended testis usually leads to orchiopexy (surgical fixation of an undescended testis into the scrotum through the inguinal canal) in patients younger than 10 years. This may be an alternative to salvage fertility. Spontaneous descent may occur in the first 6 months, and hormonal therapy may stimulate descent. Orchiectomy (surgical removal) is recommended in patients with undescended testis who are seen after puberty.

TESTICULAR TORSION AND EPIDIDYMITIS

Testicular torsion refers to the twisting of the gonad on its pedicle, which leads to compromise of the circulation and the sudden onset of severe scrotal pain. Although primarily a clinical diagnosis, the scrotal pain and swelling of testicular torsion may be difficult to distinguish from those caused by inflammation of the epididymis (epididymitis). In such cases, color Doppler ultrasound or radionuclide studies are of value.

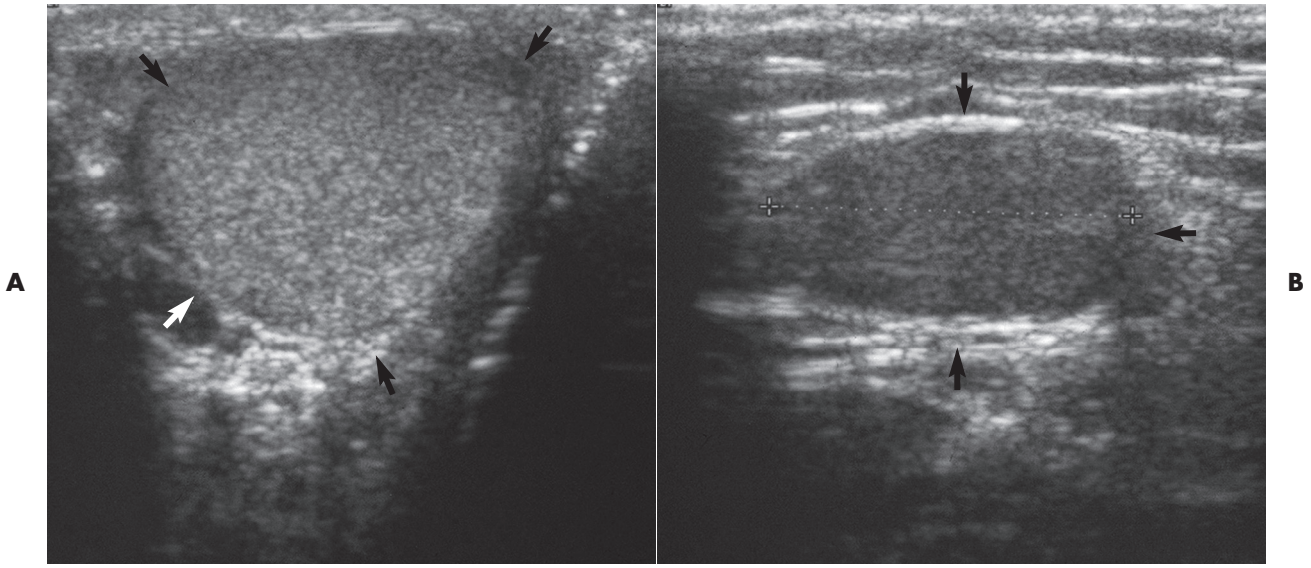

FIGURE 11-15 Undescended testes. **(A)** Ultrasound image in the transverse plane illustrates a normal right testis (*arrows*). **(B)** Another image in the longitudinal plane demonstrates the undescended left testis (*arrows*), which is smaller and less echogenic, located in the inguinal canal.

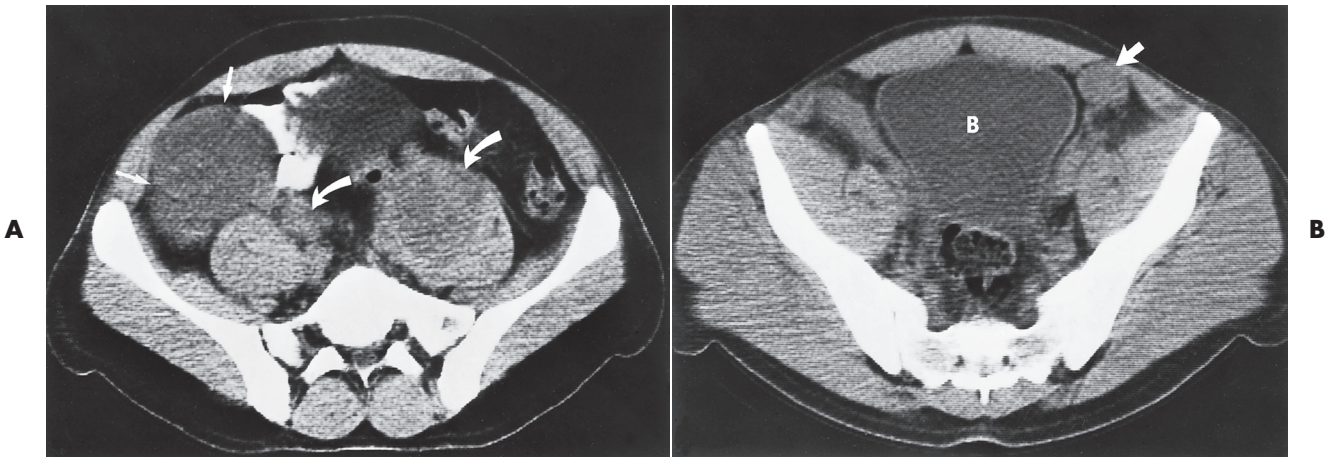

FIGURE 11-16 Malignant neoplasms developing in one of the bilateral undescended testes. **(A)** Undescended right testis is enlarged by carcinoma (*straight arrows*). The tumor has metastasized to the lymph nodes (*curved arrows*), which are enlarged. **(B)** Nontumorous intra-abdominal left testis (*arrow*) appears as a smaller, rounded structure adjacent to the bladder (B).

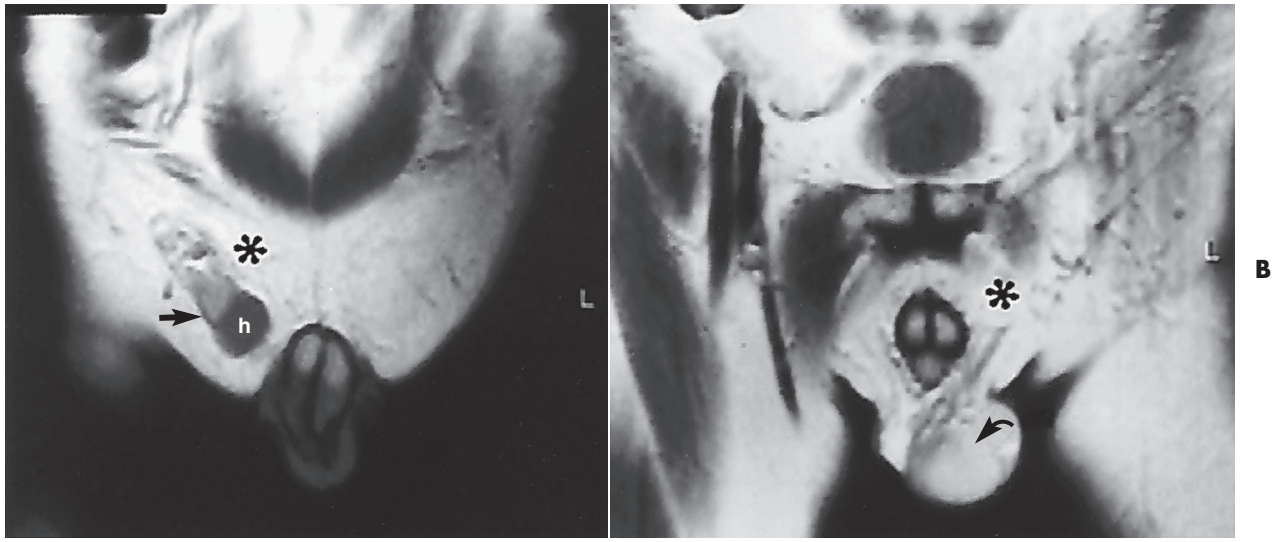

FIGURE 11-17 Atrophic undescended testis. **(A)** Coronal MR image shows a small, intermediate–signal intensity testis (*arrow*) associated with low–signal intensity hydrocele (h). The signal intensity of the testis is low compared with that of fat (*asterisk*). **(B)** Another image slightly posterior to that in panel A shows the normally descended contralateral testis (*curved arrow*), which demonstrates high signal intensity similar to that of fat (*asterisk*).

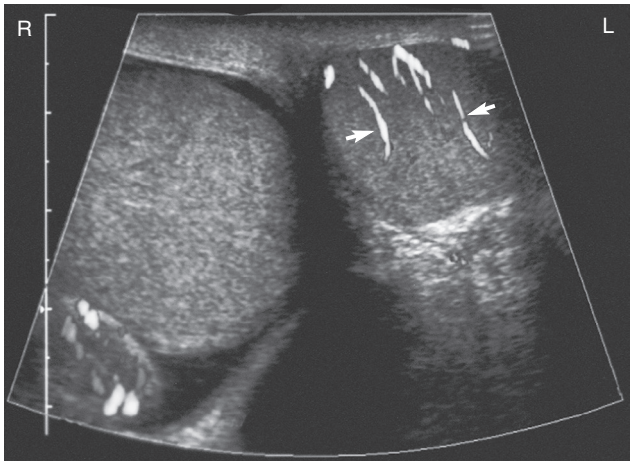

FIGURE 11-18 Testicular torsion. Doppler ultrasound image of a 3-year-old boy demonstrates abnormal to absent blood flow in the right testicle and normal blood flow (*arrows*) in the left testicle. Surgical correction was performed, saving the testis.

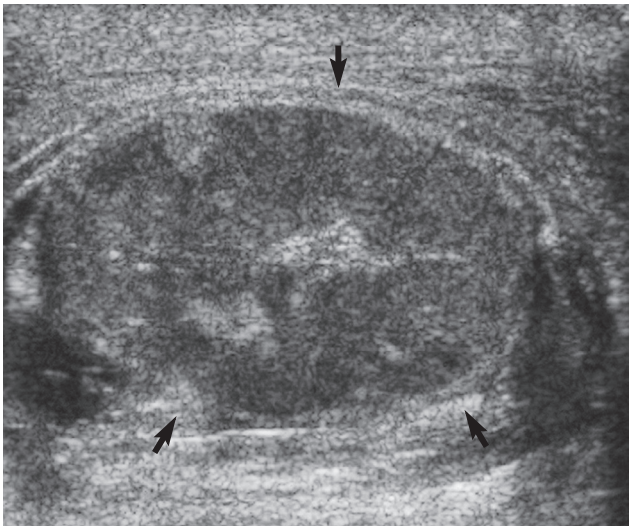

FIGURE 11-19 Testicular torsion. Scrotal ultrasound on a 16-year-old boy demonstrates the left testicle (*arrows*) without arterial blood flow, a complex heterogeneous echogenicity (indicating necrotic tissue), and a thickened scrotal wall. At surgery, the testicle remained discolored and was removed.

Imaging appearance. The preferred imaging modality for testicular torsion or epididymitis depends on the patient's age—generally, color Doppler ultrasound in adults and radionuclide studies in children. As new technology improves color and power, Doppler ultrasound is the modality of choice in most cases. Doppler ultrasound demonstrates the presence of intratesticular arterial pulsations. In testicular torsion, the arterial perfusion is diminished or absent (Figures 11-18 and 11-19), whereas in epididymitis there is increased blood flow (Figure 11-20). Similarly, the radionuclide angiogram shows isotope activity on the twisted side that is either slightly decreased or at the normal, barely perceptible level. On the uninvolved side, the perfusion should be normal. When compared with the decreased activity on the involved side, the perfusion appears to be increased. Static nuclear scans demonstrate a rounded, cold area replacing the testicle in patients with torsion (Figure 11-21) but a hot area in those with epididymitis (Figure 11-22). A nuclear testicular scan is superior to Doppler ultrasound for distinguishing between testicular torsion and epididymitis.

Treatment. Immediate surgery must be performed within 5 or 6 hours of the onset of pain to preserve the testis. For epididymitis, bed rest, scrotal support, and antibiotics are prescribed for all bacterial infections.

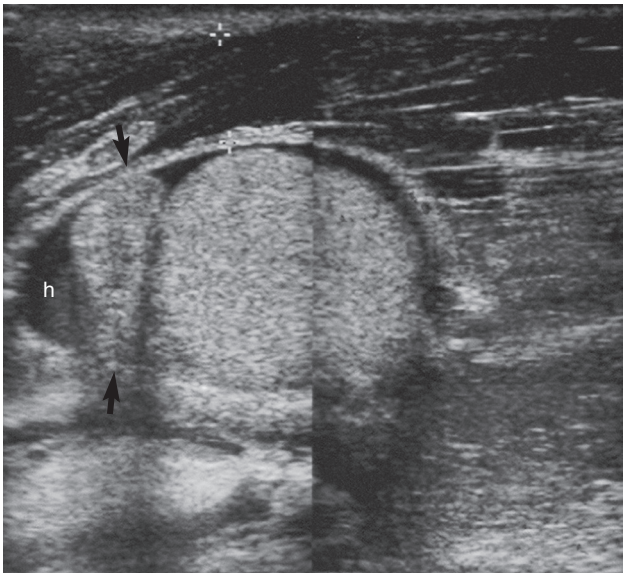

FIGURE 11-20 Epididymitis. A longitudinal ultrasound image from an 80-year-old man demonstrates an enlarged hypoechoic epididymis (*arrows*) with a moderate-sized hydrocele (h).

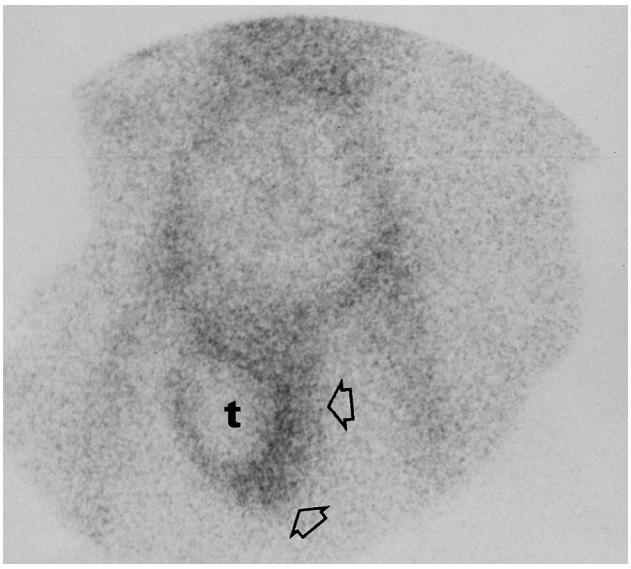

FIGURE 11-21 Testicular torsion. Severe diminished arterial perfusion causes the testicle to appear as a rounded, cold area (t) on a radionuclide scan. The surrounding rim of increased activity represents the blood supply to the scrotal sac (*arrows*).

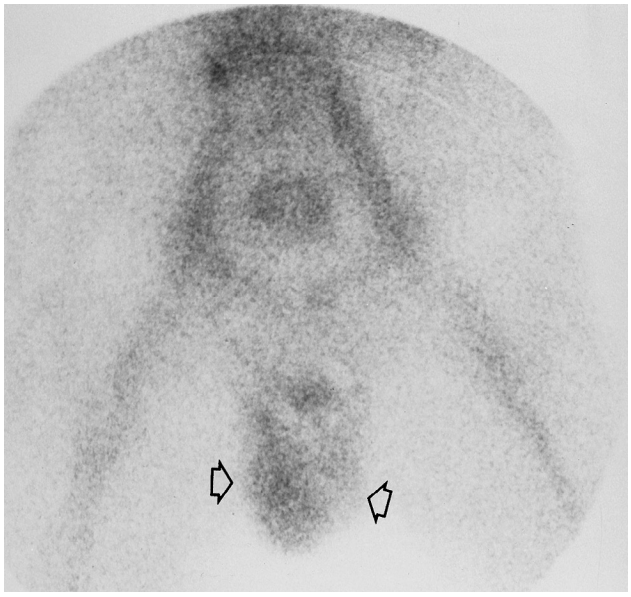

FIGURE 11-22 Epididymitis. Radionuclide scan shows high isotope uptake in the region of the testicle (*arrows*) caused by increased blood flow.

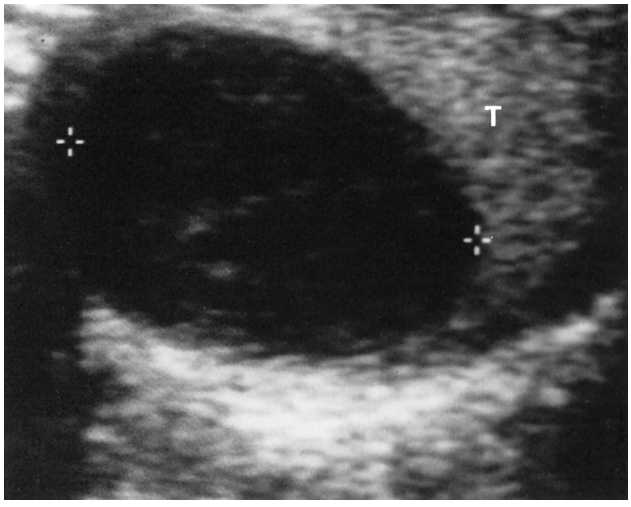

FIGURE 11-23 Seminoma. A well-circumscribed, predominantly hypoechoic, intratesticular mass (between *cursors*) with echogenicity markedly less than that of the normal adjacent testis (T) is characteristic of a seminoma.

TESTICULAR TUMORS

Testicular tumors are the most common neoplasms in men between 20 and 35 years of age. Almost all testicular tumors are malignant, and they tend to metastasize to the lymphatics that follow the course of the testicular arteries and veins and drain into para-aortic lymph nodes at the level of the kidneys.

There are two major types of testicular tumors. Seminomas constitute approximately 45% of germ cell tumors; the remaining 55% are nonseminomas that consist of teratomas and other germ cell tumors. Seminomas arise from the seminiferous tubules, whereas teratomas arise from a primitive germ cell and consist of a variety of tissues.

Imaging appearance. Testicular tumors are best diagnosed on ultrasound examination (with 98% to 100% accuracy). The normal testis has a homogeneous, medium-level echogenicity. A localized testicular tumor appears as a circumscribed mass with either increased or decreased echogenicity in an otherwise uniform-echo testicular structure. Seminomas appear as uniform hypoechoic masses without calcification or cystic areas (Figure 11-23). A teratoma appears inhomogeneous with cystic and solid areas of calcification and cartilage (Figure 11-24). Testicular tumors can also be detected

on MRI (Figure 11-25), which is required when ultrasound findings are equivocal or when there is discrepancy between the ultrasound findings and the physical examination.

Lymphatic metastases from testicular tumors typically occur at the level of the renal hilum (where the gonadal veins drain) and are best detected by CT (Figure 11-26). This modality also can detect spread of tumor to the lung or liver.

Treatment. All testicular cancers are removed (orchiectomy). Seminomas are radiosensitive, and early diagnosis and irradiation have resulted in many cures. Teratomas are surgically removed; if malignant, surgery is followed by radiation therapy and chemotherapy (consisting of several cytotoxic drugs in combination). Follow-up examinations are required to rule out metastasis.

Summary of Findings for Diseases of the Male Reproductive System

Disorder	Location	Imaging Appearance	Treatment
Benign prostatic hyperplasia	Enlargement of prostate gland	US—transrectal inner gland enlargement (relatively hypoechoic compared with the peripheral zone) IVU—elevation and smooth impression of floor in a contrast agent–filled bladder; distal ureters have a characteristic J-shaped appearance MRI—diffuse or nodular area of homogeneous low signal intensity on T1-weighted images and an inhomogeneous, mixed (intermediate to high) signal intensity on T2-weighted images	Surgical resection to relieve symptoms
Carcinoma of the prostate gland	Prostate gland	IVU—irregular elevation of the floor of a contrast agent–filled bladder with possible obstruction US—transrectal wide range of sonographic patterns, depending on glandular area involved MRI—on long TR images, loss of uniform high signal intensity of the peripheral zone	Radical prostatectomy Local invasion—surgery and radiation therapy (seeds) Stage D—hormonal therapy, palliative measures
Undescended testis	Inguinal or ectopic testicle	US—demonstrates inguinal testicle MRI—demonstrates ectopic undescended testis; low signal mass on T1-weighted images that has high signal on T2-weighted images CT—uniformly enhanced, oval soft tissue mass	Spontaneous descent Hormonal therapy Orchiopexy—surgical attachment in the scrotum Orchiectomy
Testicular torsion	Testes	Color Doppler US—arterial perfusion is diminished or absent Radionuclide angiogram—slightly decreased normal intake, cold areas on static scan	Immediate surgery to preserve testis
Epididymitis	Inflammation of the epididymis	Color Doppler US—increased blood flow Radionuclide angiogram—appears as a hot area on a static scan	Bed rest, scrotal support, and antibiotics
Testicular tumors	Seminoma (seminiferous tubules) Teratoma (primitive germ cell)	US—seminoma appears uniformly hypoechoic without calcifications; teratoma is an inhomogeneous mass with cystic and solid areas MRI—T2-weighted image demonstrates inhomogeneous signal intensity CT—demonstrates lymphatic involvement as low-attenuation nodules	Orchiectomy Seminoma—radiosensitive Cancerous teratoma—surgery, radiation therapy, and chemotherapy

IVU, Intravenous urography; *US,* ultrasound.

FEMALE REPRODUCTIVE SYSTEM

PHYSIOLOGY OF THE FEMALE REPRODUCTIVE SYSTEM

The ovaries, the female equivalent of the testes, are responsible for the production of ova and the secretion of female hormones. A woman's reproductive life begins with the onset of menstruation, **menarche**, which generally occurs between 11 and 15 years of age. Once each month, on approximately the first day of menstruation, several primitive graafian follicles and their enclosed ova begin to grow and develop, and the follicular cells start to secrete **estrogen**. In most cycles, only one follicle matures and migrates to the surface of the ovary, where it ruptures and expels the mature ovum into the pelvic cavity (**ovulation**).

After the release of the ovum, the remaining cells of the ruptured follicle enlarge and a golden-colored pigment (lutein) is deposited in their cytoplasm. This **corpus luteum** continues to grow for 7 or 8 days and secretes **progesterone**

in increasing amounts. If fertilization of the ovum has not occurred, the size and secretions of the corpus luteum gradually diminish until the nonfunctional structure is reduced to a white scar (corpus albicans) that moves into the central portion of the ovary and eventually disappears. If fertilization does occur, however, the corpus luteum remains intact throughout pregnancy.

The cyclic changes in the ovaries are controlled by a variety of substances secreted by the anterior pituitary gland. Growth of the primitive graafian follicles and ova and the secretion of estrogen are controlled by FSH, whereas rupture of the follicle, expulsion of its ripe ovum, and the secretion of progesterone are under the control of luteinizing hormone (LH).

The fallopian tubes serve as ducts for the ovaries, even though they are not directly attached to them (Figure 11-27). The union of an ovum and a spermatozoon (fertilization) normally occurs in the fallopian tubes. In the next few days, the resulting embryo reaches the uterus, where it begins to implant itself in the endometrium. Occasionally, implantation occurs in the fallopian tube or pelvic cavity instead of the uterus, resulting in an **ectopic pregnancy**. Within 10 days, there is the earliest development of the placenta, which is derived in part from both the developing embryo and the maternal tissues and serves to nourish the fetus and anchor it to the uterus. Although they are closely related, maternal blood and fetal blood do not mix, and the exchange of nutrients occurs across the important fetal membrane termed the **chorion**. *Menstrual cycle* refers to the changes in the endometrium of the uterus that occur in women throughout the childbearing years. Each cycle

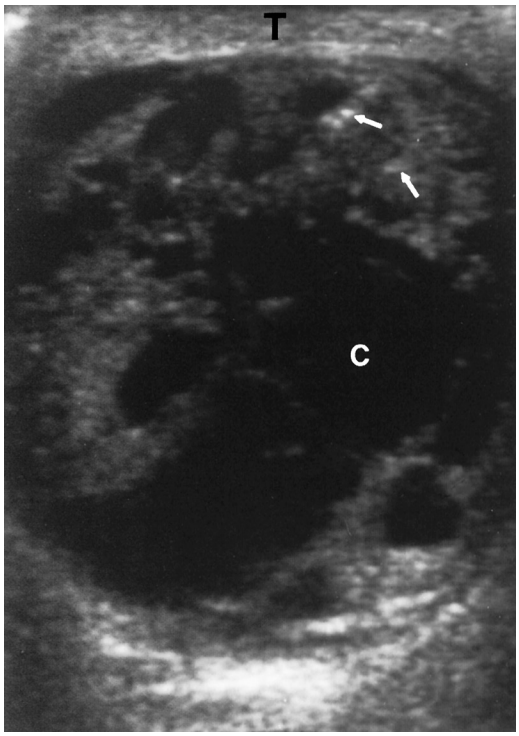

FIGURE 11-24 Malignant teratoma. A transverse testicular scan demonstrates a large malignant teratoma replacing most of the testis. Cystic (C) and solid elements with small echogenic foci (*arrows*) from small calcifications are present. *T,* Residual normal testis.

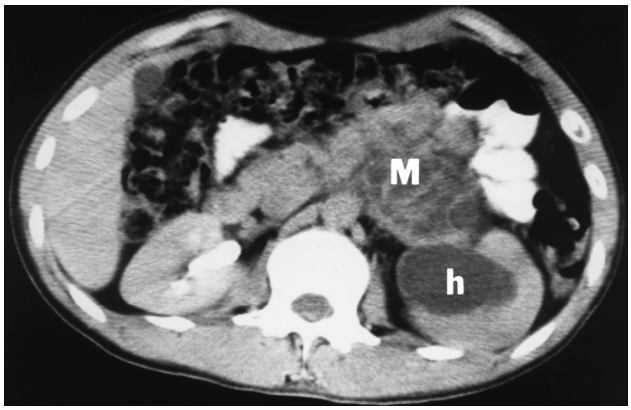

FIGURE 11-26 Metastatic testicular seminoma. CT scan through the level of the kidneys shows diffuse nodal metastases (M) containing characteristic low-attenuation areas. Extrinsic pressure on the lower left ureter has caused severe hydronephrosis with dilation of the renal pelvis (h).

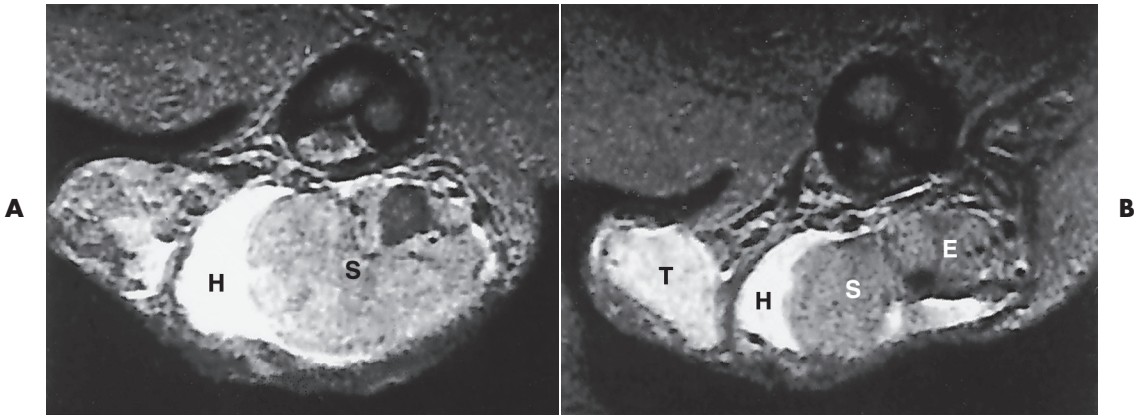

FIGURE 11-25 Testicular seminoma. (A) T2-weighted MR image shows that the signal intensity of the seminoma (S) in the left testis is inhomogeneous, and its contrast is markedly different from that of the adjacent hydrocele (H). (B) Inhomogeneous intermediate signal intensity of intratesticular tumor (S) extends into the epididymis (E). Note that the normal contralateral testis (T) demonstrates a much higher signal intensity.

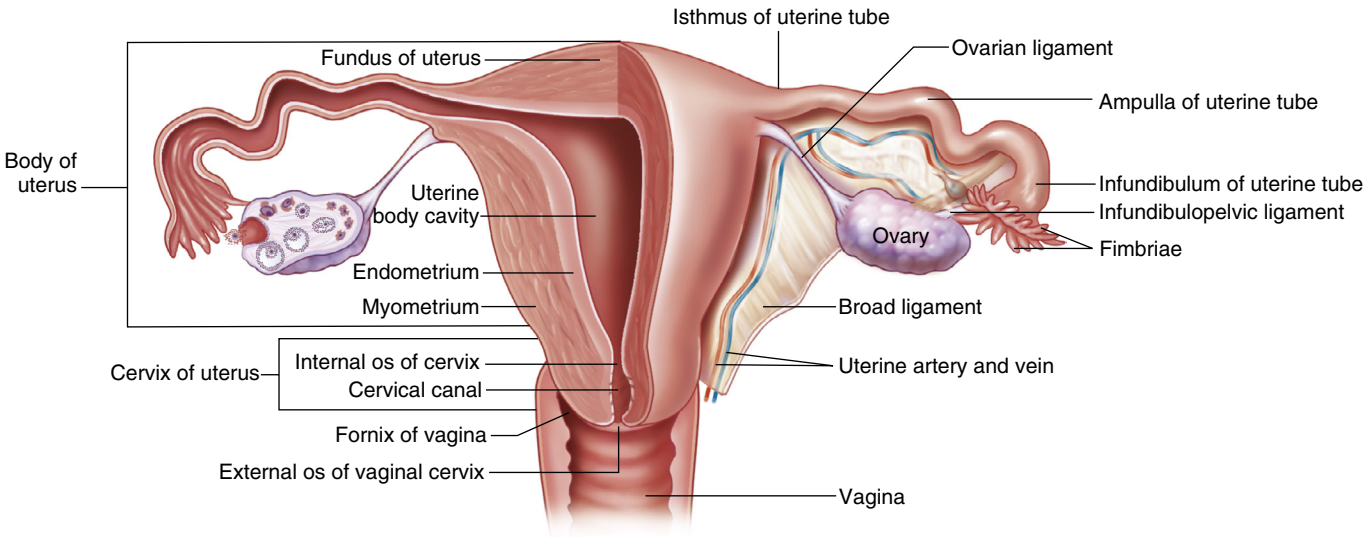

FIGURE 11-27 The female reproductive system.

lasts approximately 28 days and is divided into three phases: proliferative, secretory, and menstrual. Although the first day of menstruation is normally regarded as the first day of the cycle, for ease of description the menstrual phase is described last.

The **proliferative, or postmenstrual, phase** occurs between the end of the menses and ovulation. Production of estrogen by ovarian follicular cells under the influence of FSH causes proliferation of the endometrium of the uterus. In a typical 28-day cycle, the proliferative phase usually includes cycle days 6 to 13 or 14. However, there is far more variability in the length of this phase than in the others.

The **secretory, or postovulatory, phase** occurs between ovulation and the onset of the menses. The high level of estrogen in the blood after ovulation inhibits the secretion of FSH, and the anterior lobe of the pituitary gland begins to secrete LH. The LH stimulates the corpus luteum to produce the hormone progesterone, which stimulates a further increase in the thickness of the endometrium and prepares the uterus for implantation of the ovum should fertilization occur. The length of the secretory phase is fairly constant, usually 14 days.

If fertilization of the ovum does not occur, the high level of progesterone in the blood inhibits the secretion of LH so that the corpus luteum begins to degenerate and ceases to produce progesterone. As the superficial layers of the hypertrophied endometrium begin to break down, denuded bleeding areas are exposed. The flow of blood, mucus, and sloughed endometrium from the uterus is called the *menstrual flow*. This **menstrual phase** of the cycle lasts approximately 4 to 6 days, until the low level of progesterone causes the pituitary gland to again secrete FSH and a new menstrual cycle begins. Of course, if the ovum is fertilized, the corpus luteum does not degenerate, and the endometrium remains intact throughout pregnancy.

The reproductive years terminate with the cessation of menstrual periods (**menopause**), which usually begins when a woman is in her late 40s or early 50s.

PELVIC INFLAMMATORY DISEASE

Inflammation of the pelvic reproductive organs is usually the result of venereal disease (especially gonorrhea) in women of childbearing age, with the peak incidence between ages 20 and 24 years. It can also develop from an unsterile abortion or delivery or multiple sexual partners, or it may be a complication of intrauterine devices. If PID is not promptly and adequately treated, spread of infection to the fallopian tubes may cause fibrous adhesions that obstruct the inner portion near the uterus. If the outer ends of the tubes remain open, the spill of purulent material can lead to peritonitis and the formation of a pelvic abscess. More commonly, the outer ends close, and the fallopian tubes fill with pus (**pyosalpinx**). After antibiotic therapy, the infection subsides, and the tubes may remain filled with a watery fluid (**hydrosalpinx**). Obstruction of the fallopian tubes can result in infertility or ectopic pregnancy. Spread of infection to involve the ovaries can produce tubo-ovarian abscesses, which are usually bilateral.

Imaging appearance. Ultrasound is the imaging procedure of choice for detecting PID and pelvic abscesses. The transabdominal approach best demonstrates the extent of the disease process, whereas the endovaginal approach is most sensitive for detecting dilated tubes, inflammatory changes, and abscesses. The fluid-filled urinary bladder provides an excellent acoustic window by displacing confusing loops of small bowel. Endometritis may occur after childbirth or in association with PID. Ultrasound demonstrates a thickened endometrium, possibly with irregularity that may contain fluid (Figure 11-28). Pyosalpinx and tubo-ovarian abscesses typically are seen as tubular adnexal masses that are sonolucent and compatible with fluid collections (Figure 11-29). However, abscesses may also have thick and irregular (or "shaggy") walls or may contain echoes or fluid levels representing the layering of purulent debris (Figure 11-30). In severe cases, CT may aid in assessing the full extent of the disease. MRI is unnecessary unless the patient has an iodine allergy.

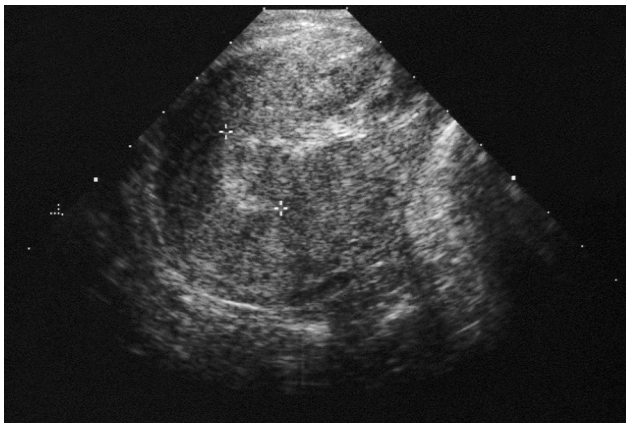

FIGURE 11-28 Endometritis. Ultrasound image illustrates an enlarged endometrial cavity with a heterogeneous echogenicity (between *cursors*) associated with a therapeutic abortion.

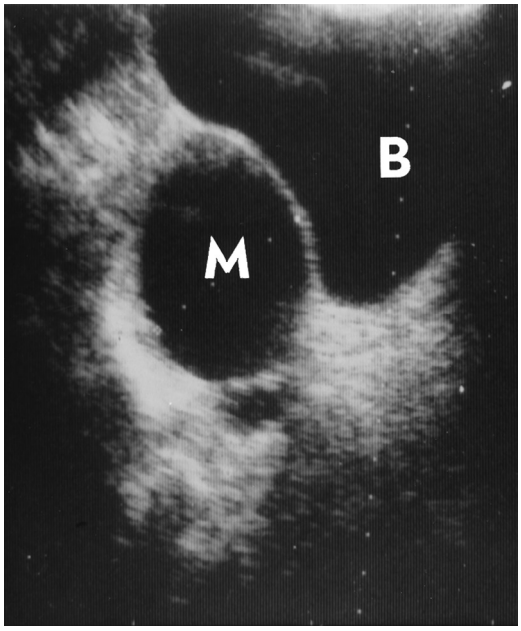

FIGURE 11-29 Tubo-ovarian abscess. Ultrasound image demonstrates a large sonolucent mass (*M*) posterior to the bladder (*B*).

The status of the fallopian tubes can be assessed radiographically by hysterosalpingography, in which the uterine cavity and fallopian tubes are opacified after the injection of contrast material into the uterus. In the woman with normal patent fallopian tubes, contrast material extravasating into the pelvic peritoneal cavity outlines the peritoneal surfaces and, often, loops of bowel within the pelvis (Figure 11-31). If the fallopian tubes are occluded by fibrosis from PID or developmental anomalies, there is no evidence of the contrast material reaching the peritoneal cavity (Figure 11-32).

Plain abdominal or pelvic radiographs are of little value in detecting PID and pelvic abscesses. Abnormal gas collections can be masked by fecal material in the rectum and in loops of small bowel.

Treatment. Antibiotic therapy and abstaining from sexual intercourse until the inflammation subsides are the usual treatments for PID. In more complex cases, ultrasound-guided aspiration and drainage may be required. Thick purulent materials require catheter drainage; most nonpurulent abscesses need only aspiration. The healing phase may leave the fallopian tubes scarred and obstructed, resulting in an inability to conceive. In vitro fertilization is an alternative method to become pregnant in these cases.

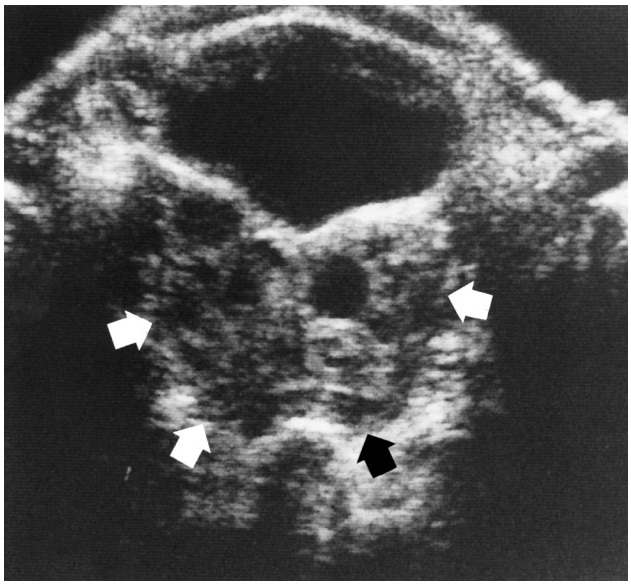

FIGURE 11-30 Chronic pelvic inflammatory disease. Transverse sonogram demonstrates large, complex cystic and echogenic masses (*arrows*) posterior to the echo-free bladder.

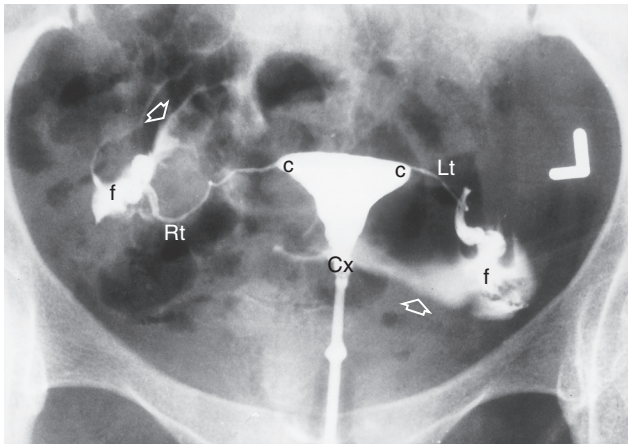

FIGURE 11-31 Normal hysterosalpingogram. *Arrows* point to a bilateral spill of contrast material into the peritoneal cavity. *c,* Cornua of the uterus; *Cx,* internal cervical os; *f,* fimbriated portion of fallopian tube; *Rt* and *Lt,* right and left fallopian tubes, respectively.

CYSTS AND TUMORS

Ovarian Cysts and Tumors

Physiologic ovarian cysts are most common in female infants and in women of childbearing age. They include follicular cysts (unruptured, enlarged follicles) and corpus luteum cysts, which occur after continued hemorrhage or lack of

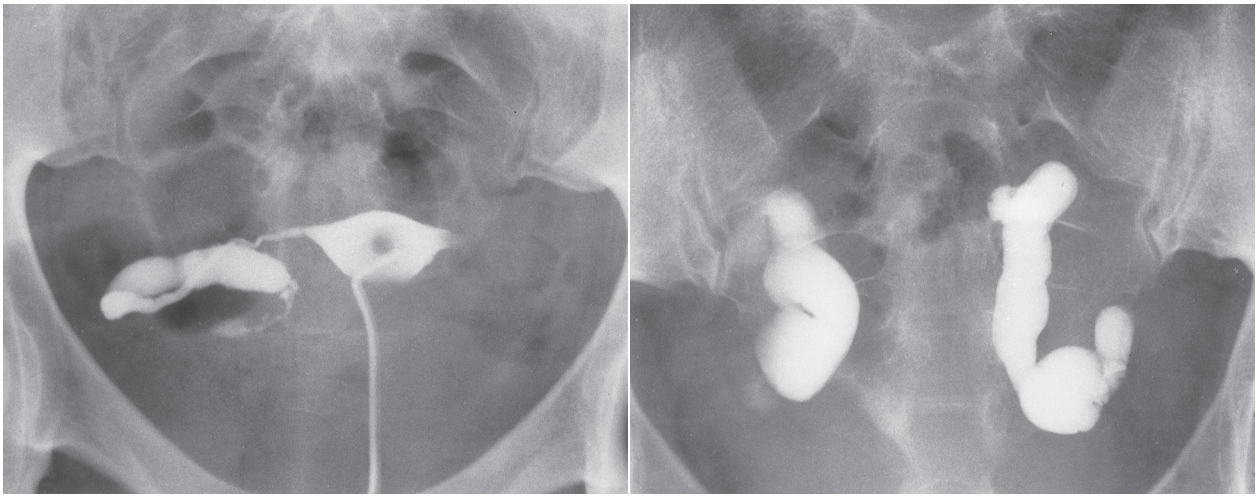

FIGURE 11-32 Hydrosalpinx. Unilateral (A) and bilateral (B) gross dilation of fallopian tubes without evidence of free spill of contrast material into the peritoneal cavity.

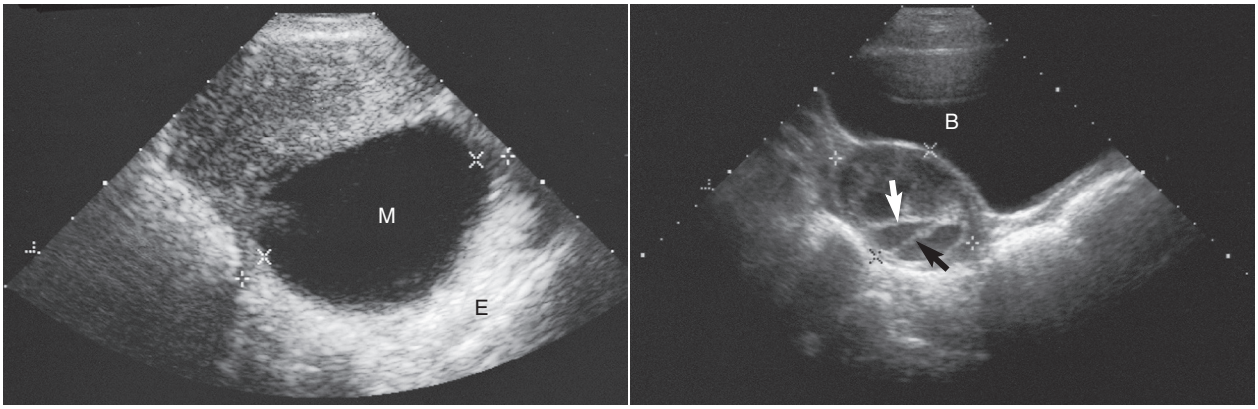

FIGURE 11-33 Ovarian cysts. (A) Ultrasound image demonstrates a large (5 × 6 cm) sonolucent mass (*M*) with back wall enhancement (E) involving the right ovary. (B) In another patient, the longitudinal image of the right ovary demonstrates a septated (*arrows*) mass (between *cursors*) with homogeneous sonolucent components measuring 5 × 6.7 cm located posterior to the bladder (B).

resolution of the corpus luteum. Polycystic ovarian syndrome (PCOS) is characterized by multiple ovarian cysts, which may interfere with the physiology of the ovary. This is considered the most common genital disorder found in young women.

The most common malignancies involving the ovaries are metastatic tumors, which arise principally from carcinomas of the breast, colon, and stomach. They are frequently bilateral and often asymptomatic.

Imaging appearance. On ultrasound, ovarian cysts appear as rounded, anechoic adnexal masses (Figure 11-33). On MRI, which is used only when ultrasound findings are indeterminate, the cysts appear hyperintense on T2-weighted pelvic images (Figure 11-34). On ultrasound, PCOS appears as 10 or more cysts located peripherally in the echodense stroma. **Primary cystadenocarcinoma** of the ovary often contains psammomatous bodies, depositions of calcium carbonate located in the fibrous stroma of the tumor that can be detected on plain abdominal radiographs. These psammomatous calcifications appear as scattered, fine, amorphous shadows that are barely denser than the normal soft tissues and can therefore be easily missed unless they are extensive (Figure 11-35). On ultrasound examination, cystadenocarcinoma typically appears as a large cystic mass with internal septa. It may be difficult to distinguish cystadenocarcinoma (Figure 11-36) from **cystadenoma** (Figure 11-37), its benign counterpart. The more solid and irregular the areas within the mass on ultrasound images, the more likely that it represents a malignant tumor. In addition, the association of ascites with an ovarian mass is strongly suggestive of underlying malignancy. MRI is a more definitive study to determine whether the tumor has benign or malignant characteristics.

Ovarian carcinomas usually spread by implanting widely on the omental and peritoneal surfaces. This pattern can produce the characteristic CT appearance of an "omental cake," an irregular sheet of soft tissue densities beneath the anterior abdominal wall (Figure 11-38). CT is also of value in detecting tumor adherence to bowel, ureteral involvement, and retroperitoneal adenopathy, making CT the modality of choice for staging and surgical planning. PET may be used in determining recurrence of ovarian carcinoma (Figure 11-39).

Treatment. Simple ovarian cysts are common, and many resolve without treatment. Cysts that are larger than 10 mm

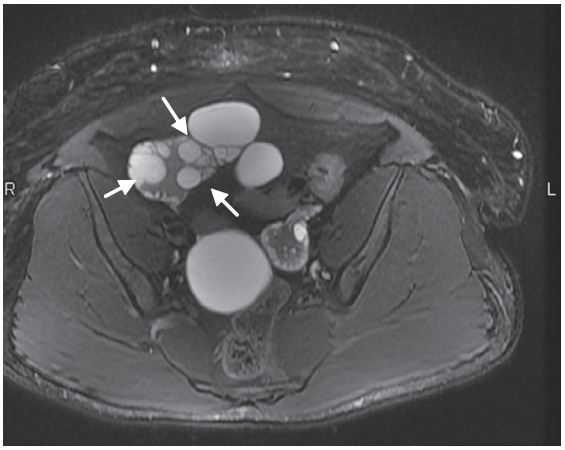

FIGURE 11-34 Ovarian cysts. On a T2-weighted axial MR image with fat saturation, multiple ovarian cysts (*arrows*) appear as high signal intensities because of the fluid within them.

FIGURE 11-35 Psammomatous calcifications. Diffuse, ill-defined collections of granular amorphous calcification are visible within this cystadenocarcinoma of the ovary.

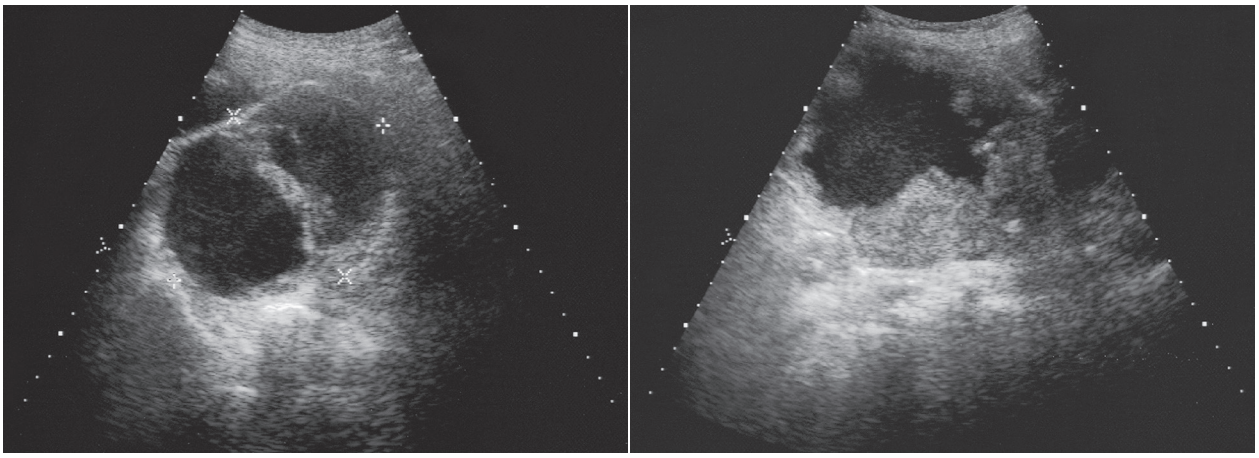

FIGURE 11-36 Endovaginal sonogram of a cystadenocarcinoma. (A) The transverse image demonstrates a thickened wall and septations within the ovary, the left measuring 9 × 7 × 10 cm. **(B)** The longitudinal image illustrates an enlarged uterus with a large, complex mass. The CT scan had shown posterior wall thickening in the cyst and irregular densities within the liver—highly suggestive of cystadenocarcinoma.

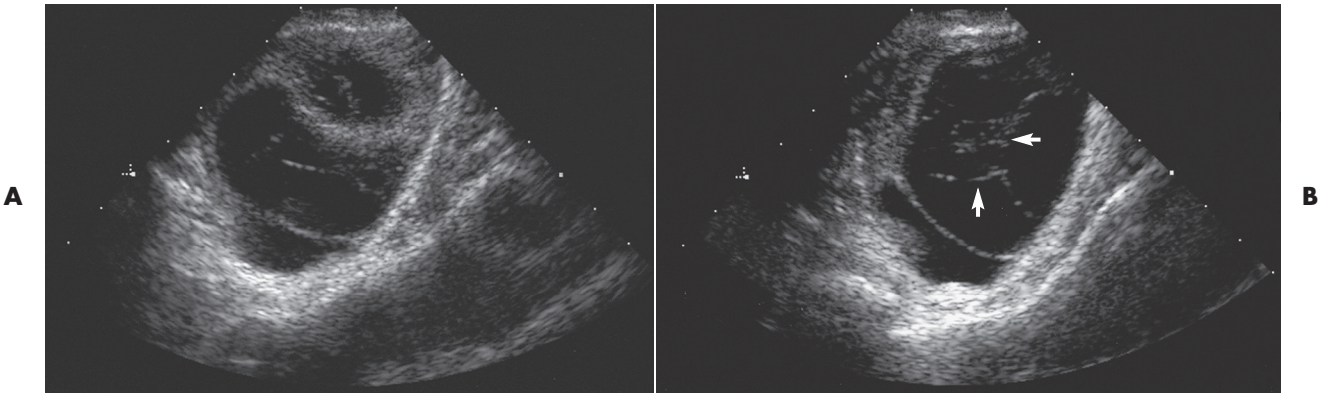

FIGURE 11-37 Cystadenoma. Longitudinal **(A)** and transverse **(B)** sonograms demonstrate a complex, predominantly cystic mass (sonolucent) containing several thin and well-defined septations (*arrows*), which suggest a benign lesion—a mucinous cystadenoma.

or are complex may require drainage or surgery. With surgical treatment, ovarian carcinoma currently has a 25% to 30% survival rate.

Dermoid Cyst (Teratoma)

A dermoid cyst, the most common type of germ cell tumor, contains skin, hair, teeth, and fatty elements, all of which typically derive from ectodermal tissue. These cysts are of no clinical significance unless they grow so large that they produce symptoms by compressing adjacent structures. Approximately half of all ovarian dermoid cysts contain some calcification. This is usually in the form of a partially or completely formed tooth (Figure 11-40); less frequently, the wall of the cyst is partially calcified.

Imaging appearance. The characteristic calcification combined with the relative radiolucency of the lipid material within the lesion is pathognomonic of an ovarian dermoid cyst.

The most common ultrasound appearance of a dermoid cyst is a complex, primarily solid mass containing high-level echoes arising from hair or calcification within the mass (Figures 11-41 and 11-42). The highly echogenic nature of these masses may make it difficult to delineate them completely and to distinguish them from surrounding gas-containing loops of bowel.

Treatment. Surgical removal is recommended because a dermoid cyst may undergo transformation and become malignant.

Uterine Fibroids

Fibroids (leiomyomas) of the uterus are benign smooth-muscle tumors that are very common; they are often multiple and vary greatly in size. Growth of fibroid tumors is stimulated by estrogen. They develop only during the reproductive years and tend to shrink after menopause. Abnormal bleeding between periods or excessively heavy menstrual flow is the most common symptom. Large tumors may project from the uterus, causing pressure on surrounding organs, which results in pelvic pain. They can also interfere with delivery or, if on a stalk (pedunculated), protrude into the vagina.

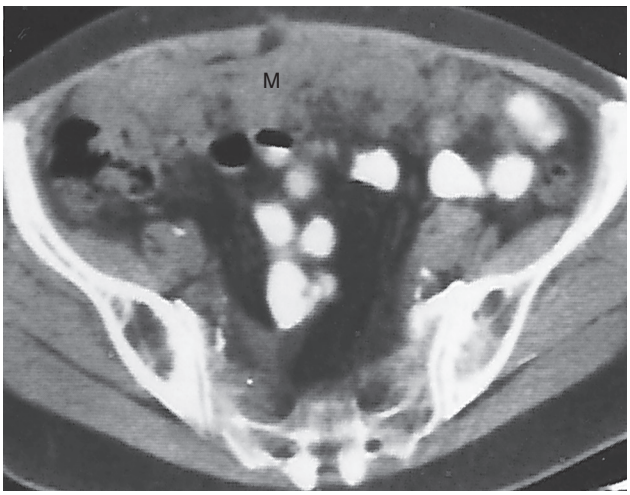

FIGURE 11-38 "Omental cake." Metastases (M) resulting from cystadenocarcinoma of the ovary cause an irregular sheet of soft tissue densities beneath the anterior abdominal wall that posteriorly displaces the adjacent, contrast-filled bowel loops.

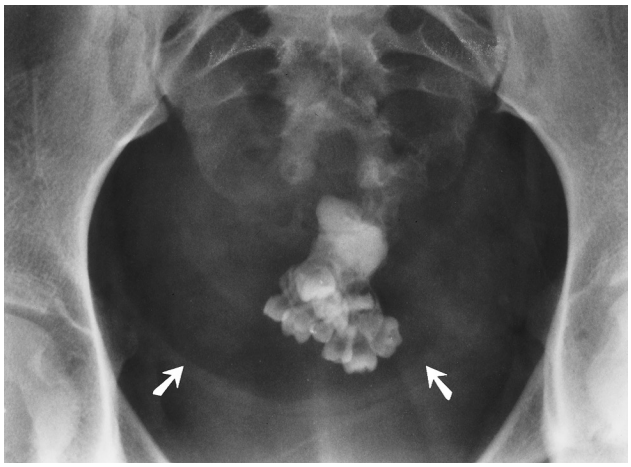

FIGURE 11-40 Dermoid cyst containing multiple well-formed teeth. Note the relative lucency of the mass (*arrows*), which is composed largely of fatty tissue.

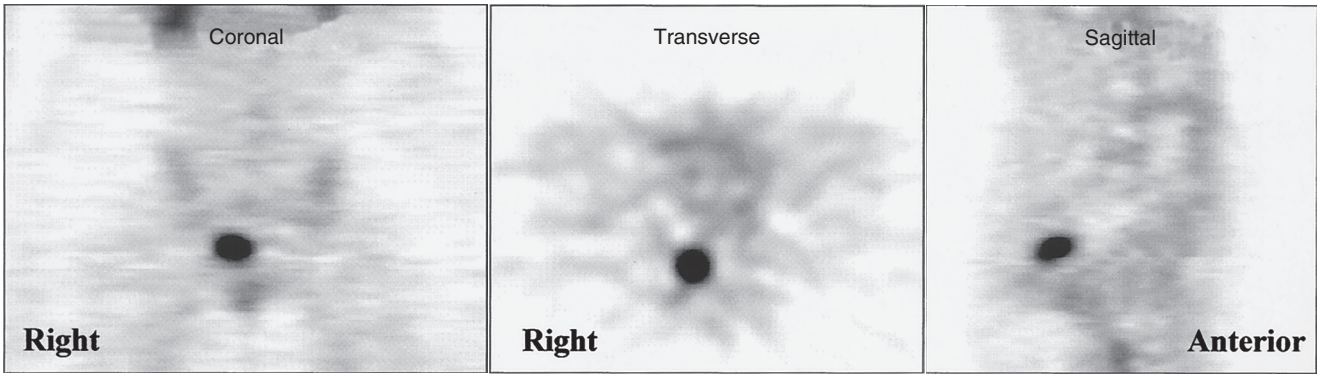

FIGURE 11-39 Recurrence of ovarian carcinoma. PET scan revealed a solitary focus of intense fluorodeoxyglucose (FDG) uptake in the right paramidline retrocystic location, suggestive of an active neoplasm and consistent with regional recurrence of the patient's ovarian carcinoma. The finding resulted in a change in treatment: The tumor focus, identified by PET–FDG to be in the right posterior pelvis, was successfully resected.

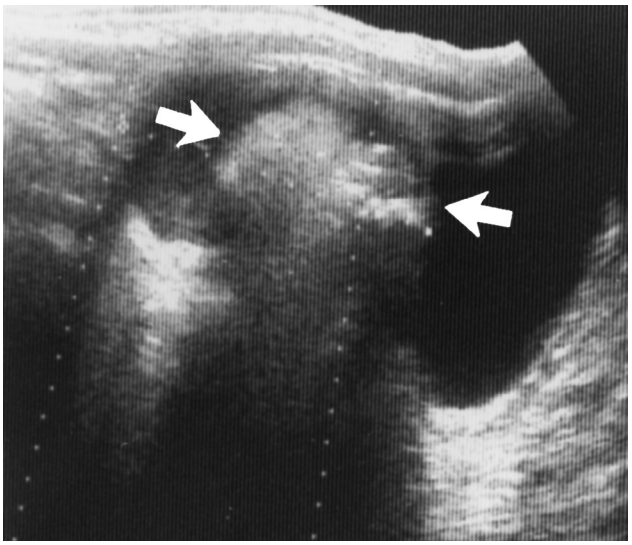

FIGURE 11-41 Dermoid cyst. Sagittal sonogram demonstrates only the near wall of the dermoid because of acoustic shadowing from a hairball (*arrows*), producing the so-called tip of the iceberg sign.

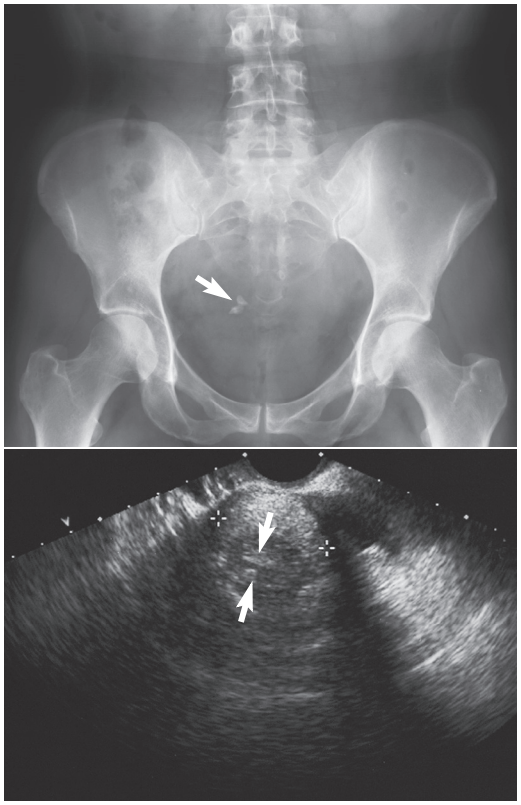

FIGURE 11-42 Dermoid cyst. (A) Kidney–ureter–bladder study demonstrates two toothlike densities (*arrow*) beside the coccyx. (B) A transverse sonogram shows a heterogeneous mass (between *cursors*) with a high-amplitude echogenic focus (*arrows*) as a result of the toothlike densities.

FIGURE 11-43 Calcified uterine fibroid. The calcified mass extends well beyond the confines of the pelvis.

FIGURE 11-44 Uterine fibroid. Excretory urogram demonstrates persistent dense opacification of a huge uterine leiomyoma (*arrows*).

Imaging appearance. Uterine fibroids are by far the most common calcified lesions of the female genital tract. They have a characteristic mottled, mulberry, or popcorn type of calcification and appear on plain abdominal radiographs as smooth or lobulated nodules with a stippled or whorled appearance. A very large calcified fibroid occasionally occupies the entire pelvis or even extends out of the pelvis to lie in the lower abdomen (Figure 11-43).

During excretory urography, persistent uterine opacification is often seen in patients with an underlying uterine fibroid tumor (Figure 11-44). The tumor typically presses on the fundus of the bladder, causing a lobulated extrinsic impression

that differs from the smooth impression usually seen with ovarian cysts. Extension of a fibroid into the adjacent tissues (parametrium) may cause medial displacement of the pelvic ureter or ureteral compression leading to hydronephrosis.

The classic ultrasound appearance of a uterine fibroid is a hypoechoic, solid, contour-deforming mass in an enlarged, inhomogeneous uterus (Figure 11-45). Fatty degeneration and calcification cause focal increased echogenicity; the calcification may result in acoustic shadowing. A subserosal fibroid projecting from the uterus, but attached to it by a large stalk, may occasionally simulate an adnexal mass or an ovarian tumor.

Endovaginal (transvaginal) ultrasound is the best modality to demonstrate small and submucosal uterine fibroids (Figure 11-46). MRI is more sensitive than CT or ultrasound but is indicated only when ultrasound is inconclusive in differentiating between uterine and adnexal masses or between leiomyoma and adenomyosis, or to search for submucosal fibroids in the patient with unexplained bleeding (Figure 11-47).

Treatment. In many cases, no treatment is required for uterine fibroids. Medications can induce a temporary chemical menopause that causes a temporary shrinkage of a fibroid. If bleeding and fibroid size cannot be controlled with medications, surgery is performed. In younger women and for superficial fibroids, a myomectomy (removal of the leiomyoma) is performed to preserve the uterus. Large or multiple tumors usually require hysterectomy, especially in a woman for whom childbearing is undesirable or complete. Many newer therapeutic techniques are available—multilaser technique, myolysis (electrical coagulation of the myoma), and uterine artery embolization—and various medications have proved to be effective.

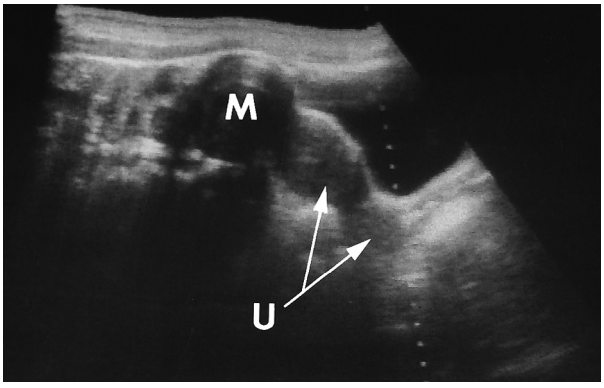

FIGURE 11-45 Uterine fibroid. Longitudinal sonogram demonstrates a pedunculated leiomyoma as a hypoechoic mass (*M*) projecting from the fundus of the uterus (*U*). Decreased sound transmission through the mass indicates its solid nature.

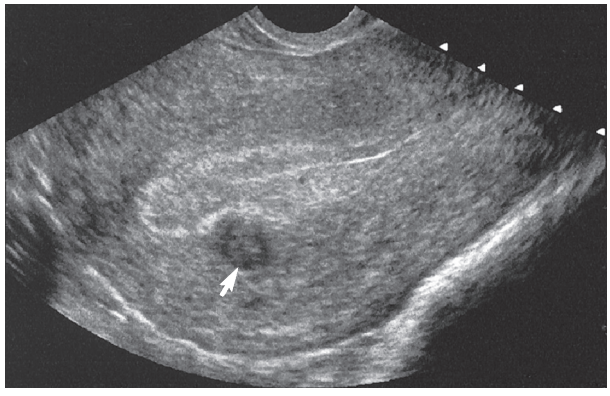

FIGURE 11-46 Submucosal uterine fibroid. Endovaginal ultrasound image of the uterus in the sagittal plane demonstrates a fibroid filling the superior endometrial cavity (*arrow*).

Endometrial Carcinoma

Adenocarcinoma of the endometrium is the predominant neoplasm of the uterine body and is the most common invasive gynecologic neoplasm. It usually occurs in postmenopausal women, especially those who have never had children. Approximately 75% of patients in whom this tumor is found are 50 years or older and are being seen clinically for postmenopausal bleeding.

Imaging appearance. Excretory urography may demonstrate an enlarged uterus impressing or invading the posterior wall and fundus of the bladder. The typical ultrasound appearance of endometrial carcinoma is an enlarged uterus with irregular areas of low-level echoes and bizarre clusters of high-intensity echoes (Figure 11-48). Unless evidence of local invasion can be demonstrated, the ultrasound findings are indistinguishable from those of fibroid tumors, which often occur in patients with endometrial carcinoma. The endovaginal approach is generally preferred to measure endometrial thickness and to determine whether dilation and curettage (D&C—dilation of the cervix to allow scraping of the uterine wall) is required for histologic examination.

CT demonstrates focal or diffuse enlargement of the body of the uterus (Figure 11-49). This modality is especially

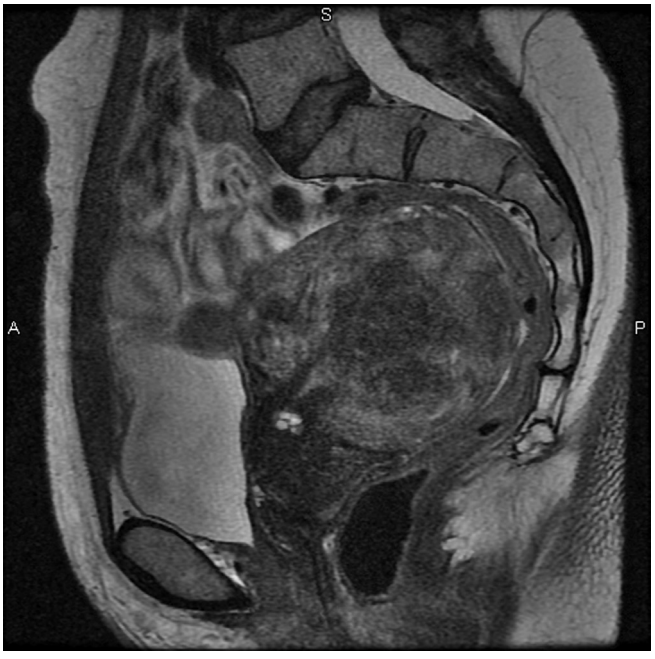

FIGURE 11-47 Uterine fibroid. T2-weighted MR sagittal image demonstrates a sharply marginated fibroid in the uterine fundus that contains both high and low signal intensity.

useful for detecting clinically unsuspected omental and nodal metastases in patients with advanced disease, for evaluating patients with suspected neoplastic recurrence, and for checking the response to chemotherapy or radiation treatment.

MRI allows differentiation of the endometrium (the inner lining) from the myometrium (the muscle layer) of the uterus and has been shown to be useful for demonstrating focal or diffuse endometrial tumors (Figure 11-50). The excellent contrast resolution of this technique may allow determination of the depth of myometrial invasion. For staging purposes, MRI is superior to CT for demonstrating extension of the tumor into the cervix, broad ligaments, and ovaries. Lymphatic involvement of the pelvis and retroperitoneal lymph nodes can also be visualized; the use of a contrast agent improves the contrast resolution.

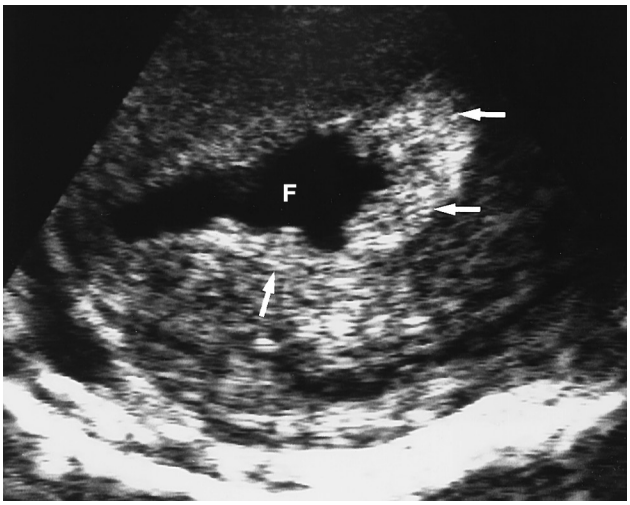

FIGURE 11-48 Endometrial carcinoma. Endovaginal sonogram localizing irregular endometrial thickening (*arrows*) with echogenic polypoid projections into the fluid-filled endometrial canal (F).

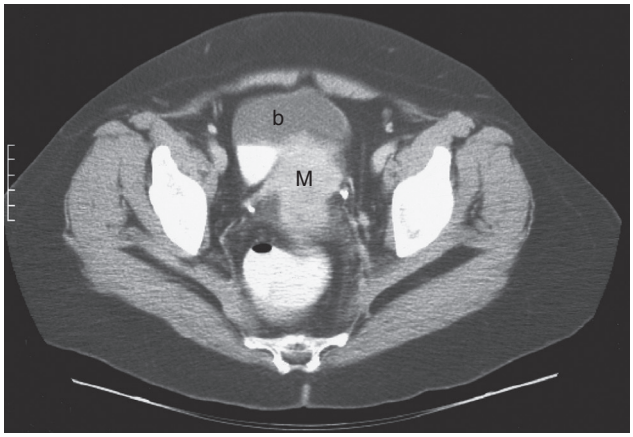

FIGURE 11-49 Bladder invasion by endometrial carcinoma. CT scan shows a mass (*M*) obliterating the fat planes between the bladder (*b*) and the uterus. Urine within the bladder outlines thickening of the posterior bladder wall. Nodular extension into the ischiorectal fossa indicates local extension of the tumor.

Treatment. The first option for treatment of endometrial carcinoma is a hysterectomy with resection of the enlarged lymph nodes. Radiation therapy may follow surgery, especially in cases of advanced disease or an incomplete resection. For inoperable cancers, the preferred choice is chemotherapy.

Endometriosis

Endometriosis is the presence of normal-appearing endometrium in sites other than their normal location inside the uterus. Although tissues next to the uterus (ovaries, uterine ligaments, rectovaginal septum, and pelvic peritoneum) are most frequently involved in endometriosis, the gastrointestinal and urinary tracts can also be affected. Current theories of the cause of endometriosis include (1) reflux of endometrial fragments backward through the fallopian tubes during menstruation, with implantation into the pelvis; (2) transformation of multipotential cells in the abdomen and pelvis; (3) implantation of endometrial fragments during surgery or delivery; and (4) spread of endometrial tissue by way of the bloodstream or lymphatic system.

Imaging appearance. Although the endometrial tissue lies outside the uterus, it still responds to hormonal changes and undergoes proliferative and secretory phases along with sloughing and subsequent bleeding. Thus, an endometrial implant within a closed space can continue to grow with each menstrual cycle (Figure 11-51). Clinical symptoms include abnormal bleeding, painful menstruation (dysmenorrhea), and pain during sexual intercourse (dyspareunia). Because endometriosis is usually clinically apparent only when ovarian function is active, most women who are symptomatic for

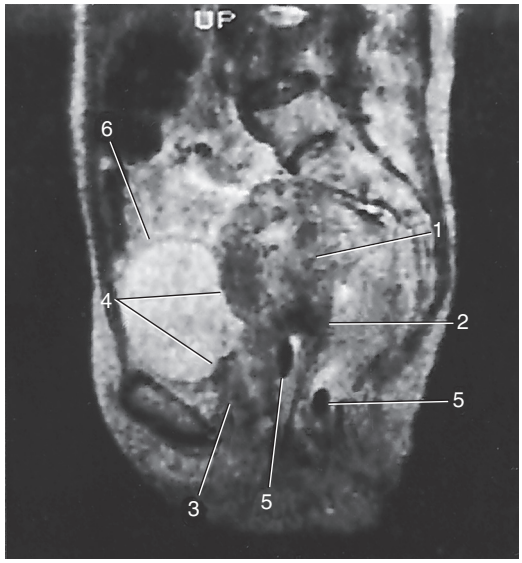

FIGURE 11-50 Endometrial carcinoma. Sagittal T2-weighted MR image shows extensive tumor of mixed signal intensity (*1*) that has invaded the endocervix and permits identification only of the ectocervix (*2*). Tumor has extended inferiorly along the serosal surface of the uterus into the vesicovaginal septum (*3*) and bladder wall (*4*). Low-intensity foci in the vagina represent radiotherapy implants (*5*). Note the normal urinary bladder wall superiorly (*6*).

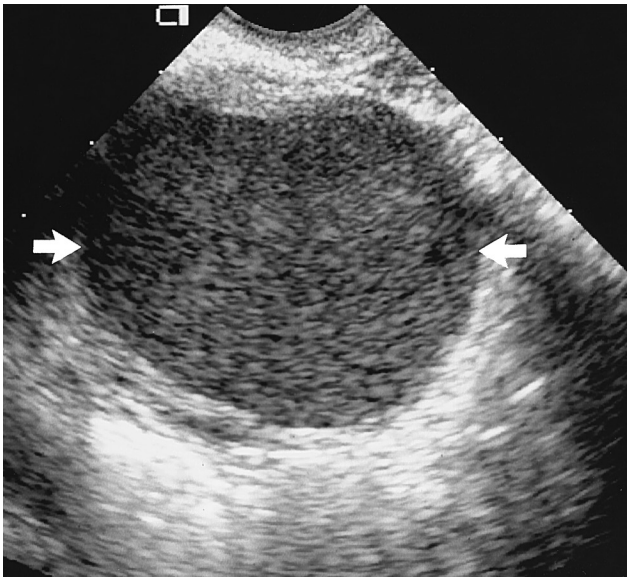

FIGURE 11-51 Endometrioma. Endovaginal sonogram demonstrating diffuse, homogeneous, low-level echoes throughout the cystic mass (*arrows*).

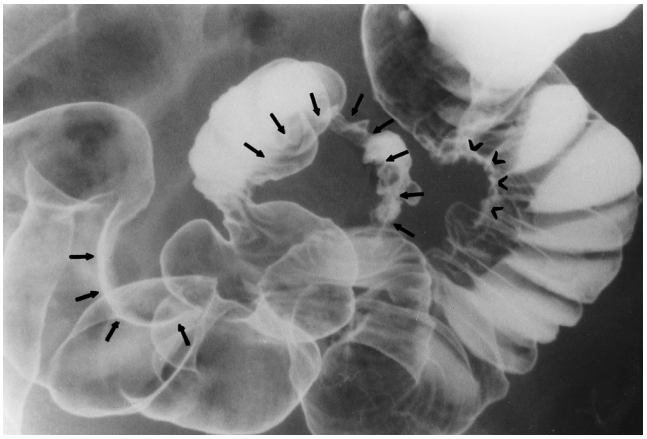

FIGURE 11-52 Endometriosis. Three separate endometrial implants (*arrows* and *arrowheads*) are seen in the sigmoid colon. The most distal lesion has a smooth interface with the bowel wall, indicating no intramural invasion. The two more proximal lesions have irregular borders, indicating intramural or submucosal invasion.

endometriosis are between 20 and 45 years of age. Ultrasound may demonstrate cystic masses filled with old blood. However, differentiation of endometriosis from other adnexal masses requires MRI.

Endometriosis involving the urinary tract most commonly produces ureteral obstruction below the level of the pelvic brim. The condition mimics a ureteral tumor and may appear as an intraluminal mass or stricture or as a smooth, rounded, or multilobular filling defect in the bladder. In the gastrointestinal tract, endometriosis primarily affects those segments that are situated in the pelvis (especially the rectosigmoid colon). It typically causes abdominal cramps and diarrhea during the menstrual period and may appear as single or multiple masses in the colon (Figure 11-52). Repeated shedding of endometrial tissue and blood into the peritoneal cavity can lead to the development of dense adhesive bands causing small bowel obstruction.

A rare complication of endometriosis with intrathoracic implants of endometrial tissue is recurrent catamenial pneumothorax, which is usually right-sided and occurs during menstrual flow.

Treatment. The main functions of treatment for endometriosis include pain management, reduction of disease progression, and prevention or reversal of infertility. To manage pain and reduce disease progression, drugs can be used to interrupt the menstrual cycle by stopping proliferation and secretion of extrauterine cells. A conservative surgical treatment, laser surgery, is used to remove visible endometrial implants that obstruct the fallopian tubes. When the pain of the disease is unbearable, the radical surgical treatment is a complete hysterectomy.

Carcinoma of the Cervix

Carcinoma of the cervix is the third most common form of cancer in women. Development of the tumor appears to be related to chronic irritation, infection, and poor hygiene. A higher incidence occurs in women who have begun sexual activity at an early age and have had multiple sexual partners. The development of the Papanicolaou smear examination has permitted detection of cervical carcinoma at a very early stage (carcinoma in situ—confined to the site of origin), when it has not yet invaded the underlying tissues and is surgically curable. Widespread cervical cancer becomes inoperable, and radiation therapy is the usual treatment.

Imaging appearance. At the time of the initial staging, one third of patients with carcinoma of the cervix have unilateral or bilateral hydronephrosis, which can be demonstrated by excretory urography or ultrasound. Indeed, the most common cause of death in patients with carcinoma of the cervix is impairment of renal function caused by ureteral obstruction. Extension of the tumor to the bladder may cause an irregular filling defect; direct infiltration of the perirectal tissues may produce irregular narrowing of the rectosigmoid colon and widening of the retrorectal space. Distant metastases to the skeleton or lungs are uncommon, even in patients with advanced disease.

Ultrasound usually demonstrates a cervical carcinoma as a solid mass behind the bladder (Figure 11-53). CT is more accurate in detecting pelvic side wall invasion and therefore is usually the initial staging procedure in patients in whom there is a clinical suspicion of advanced disease (Figures 11-54 and 11-55). This modality is also the procedure of choice for monitoring tumor response to treatment and for assessing suspected recurrence.

MRI is superior to CT and is the preferred study to distinguish the cervix from the uterus and vagina. Thus, MRI is of value in detecting and staging cervical carcinoma (Figures 11-56 and 11-57). CT cannot always differentiate tumor from adjacent normal tissue.

After radiation therapy for carcinoma of the cervix (and other types of pelvic carcinoma), it may be difficult to distinguish chronic rectal narrowing and widening of the retrorectal

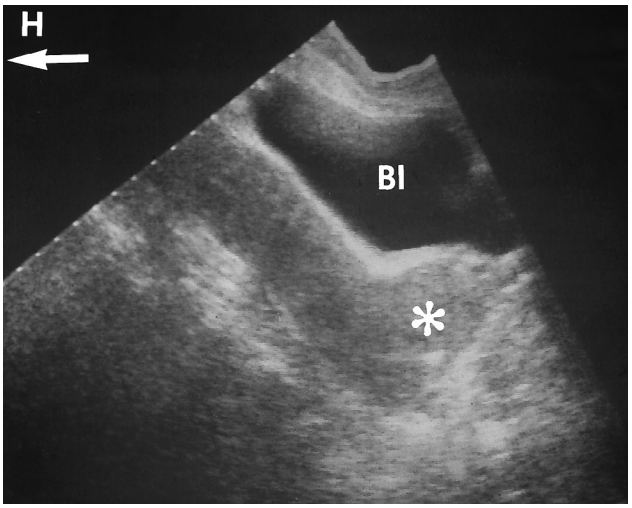

FIGURE 11-53 Carcinoma of cervix. Sonogram demonstrates a solid, echogenic mass (*asterisk*) lying behind the bladder (*Bl*) that is indistinguishable from a benign cervical myoma.

FIGURE 11-54 Carcinoma of cervix. CT scan demonstrates the inhomogeneity of an enlarged cervix (*Cx*) without evidence of bladder invasion.

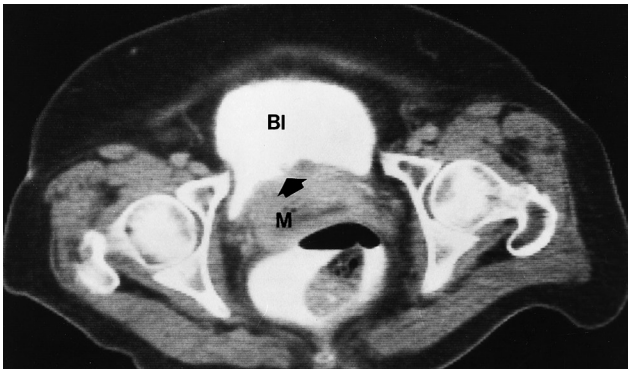

FIGURE 11-55 Bladder invasion by carcinoma of the cervix. CT scan shows irregularity (*arrow*) of the posterior margin of a contrast-filled urinary bladder (Bl) and the adjacent inhomogeneous cervical mass (M).

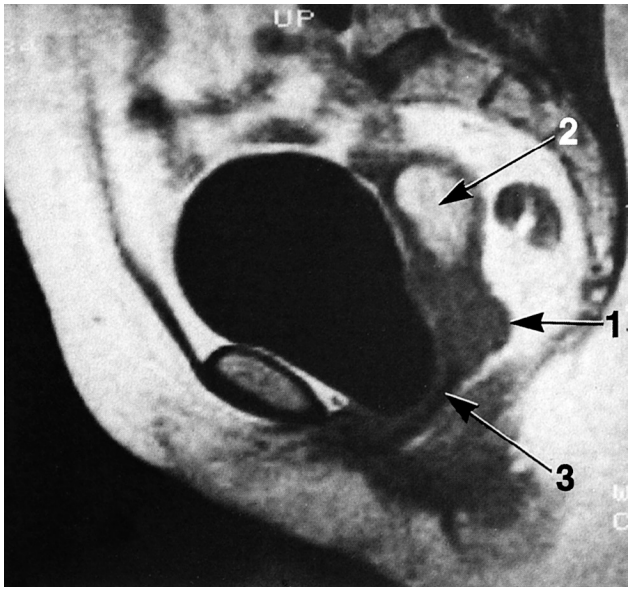

FIGURE 11-56 Cervical carcinoma. On this sagittal T1-weighted MR image, posterior cervical lobulation (1) is the only primary sign of an infiltrating cervical neoplasm. Note the considerable widening of the central uterine high-intensity zone (2) caused by an accumulation of menstrual products in the endometrial canal resulting from tumor occlusion of the endocervical canal. Urine (3) within the vagina produces low signal intensity on this imaging sequence.

FIGURE 11-57 Carcinoma of the cervix. Sagittal T2-weighted MR image shows a bulky cervical neoplasm (1) with mottled high signal intensity. The lesion has invaded the upper third of the vaginal stroma (2) anteriorly and posteriorly, but it has spared the uterus (3). The urethra (4) and urinary bladder (5) are anteriorly displaced by the tumor.

space caused by radiation effects from that caused by recurrence of tumor. Radiation therapy can also lead to the development of fibrous inflammatory adhesions between loops of bowel and the bladder, resulting in the development of fistulas between bowel loops (enteric–enteric fistula) and between a bowel loop and the urinary bladder (enteric–vesicular fistula).

Treatment. A hysterectomy with resection of the involved nodes and surrounding tissues and followed by radiation is recommended for stage I and stage II cervical cancers. Advanced lesions require surgery with a combination of radiation and chemotherapy. A pelvic exenteration (removal of all the pelvic organs to debulk the tumor) is used as a last resort.

Summary of Findings for Diseases of the Female Reproductive System

Disorder	Location	Imaging Appearance	Treatment
Pelvic inflammatory disease	Infection of uterus and fallopian tubes	US—uterus with a thickened endometrium; fallopian tubes appear as adnexal masses that are sonolucent; multiloculated, irregular mass with scattered internal echoes CT—shows full extent of severe disease Hysterosalpingography—nonvisualized fallopian tubes	Antibiotics Drainage or aspiration of abscesses
Ovarian cysts	Follicular or in corpus luteum	US—round, anechoic adnexal masses MRI—cysts produce high signal intensity on T2-weighted images	Self-resolution Aspiration and drainage Surgery
Polycystic ovarian syndrome	Multiple cysts	US—10 or more cysts peripherally	Insert drugs to induce ovulation
Ovarian tumors	Fibrous stroma	KUB—scattered tumor calcifications US—solid irregular mass with associated ascites	Surgery
Ovarian metastasis	Omental and peritoneal surface	CT—irregular sheet of soft tissue densities beneath the anterior abdominal wall—omental cake PET—determines recurrence	Surgery
Dermoid cyst (teratoma)	Germ cell tumor of ovary	Radiograph—calcifications US—complex, primarily solid mass containing high-level echoes	Surgery
Uterine fibroids (leiomyomas)	Uterine smooth muscle	KUB—mottled mulberry, popcorn calcification IVU—lobulated extrinsic impressions of fundus of bladder US—hypoechoic, solid, contour-deforming mass in an enlarged inhomogeneous uterus (endovaginal demonstrates small and submucosal fibroids) MRI—to differentiate anatomy and distinguish fibroid from adenomyosis; mixed signal intensity on images	Medications Myomectomy Myolysis Hysterectomy
Endometrial carcinoma	Uterine body	IVU—cancer invading posterior wall and fundus of bladder US—enlarged uterus with irregular hypoechoic areas and bizarre clusters of high–signal intensity echoes CT—diffuse enlargement of the uterine body; omental and nodal metastases MRI—to determine depth of myometrial invasion	Hysterectomy Radiation therapy for incomplete resection Chemotherapy for inoperable tumors
Endometriosis	Endometrium outside normal location	US—sonolucent masses MRI—differentiates endometriosis from other adnexal masses	Medications to interrupt menstrual cycle Conservative surgery—laser technique Radical surgery—hysterectomy
Carcinoma of the cervix	Cervix	US—solid mass posterior to bladder CT—demonstrates pelvic side-wall invasion MRI—differentiates uterus from vagina; used for staging	Stage I and II—hysterectomy followed by radiation Advanced stages—surgery with radiation and chemotherapy

IVU, Intravenous urography; *KUB,* kidney–ureter–bladder radiograph; *US,* ultrasound.

BREAST LESIONS

Breast Cancer

Breast cancer is the most common malignancy among women between ages 44 and 50 years. Most tumors are classified as infiltrating duct carcinomas, which occur most frequently in the upper lateral quadrant (Figure 11-58). Current surgical and radiation therapy techniques provide highly effective treatment, but only if the cancers are detected when localized to the breast itself. Today, many breast tumors are diagnosed before they are palpable because routine screening is available (especially in the United States). In these instances, the prognosis is considerably better because the mass has not extended into surrounding tissue or beyond the breast. Breast cancers diagnosed in stage I have a patient survival rate of approximately 98%. Unfortunately, most breast tumors are discovered accidentally rather than in the course of regular survey examinations. By this time, the majority have spread either to regional lymph nodes or systemically, accounting for the current high mortality (approximately 50%) that makes breast cancer the leading cause of cancer death in women.

Periodic careful physical examination of the breast, done either by a trained health professional (clinical breast examination [CBE]) or by the patient (breast self-examination [BSE]), will discover cancers that are small and more likely to be localized. Even smaller, nonpalpable, and potentially more curable lesions can be detected by mammography, a radiographic examination that is by far the most effective diagnostic procedure for breast cancer. Indeed, routine mammography combined with physical examination is the only approach currently available that promises to significantly reduce breast cancer mortality. Following a general clinical history, the accepted assessment of a suspected breast mass is a three-pronged approach, comprising physical examination, imaging (usually mammography), and needle biopsy.

With screening mammography, 7% to 10% of the patients are recalled for more extensive imaging. Of these, 15% to 20% require a biopsy, and in 5% to 7% cancer is detected. On screening examinations, 40% of the cancers detected are in situ (at the origin), and approximately 75% have no nodal involvement.

Imaging appearance. Full-field digital systems have replaced the traditional film-screen system in mammographic imaging. The digital system uses a lower dose and produces an image with increased contrast resolution that enables radiologists to better visualize anatomic structures, thus improving the sensitivity and specificity. In many cases, the digital image is interpreted by the radiologist and reviewed by computer-aided diagnosis (CAD) to improve sensitivity and specificity. Almost every breast cancer is seen mammographically as a tumor mass, clustered calcifications, or both. Either feature, when clearly demonstrated, is so indicative of malignancy that prompt biopsy is required whether the lesion is palpable or not. Secondary changes of breast carcinoma include skin thickening and nipple retraction. Magnification imaging and compression techniques greatly improve the diagnostic value of the image.

The typical malignant tumor mass is poorly defined with areas of distortion, has irregular margins, and demonstrates numerous fine linear strands or spicules radiating out from the mass (Figure 11-59). This appearance is characteristic but not diagnostic of malignancy and is in stark contrast to the typical mammographic picture of a benign mass, which has well-defined, smooth margins and a round, oval, or gently lobulated contour (Figure 11-60).

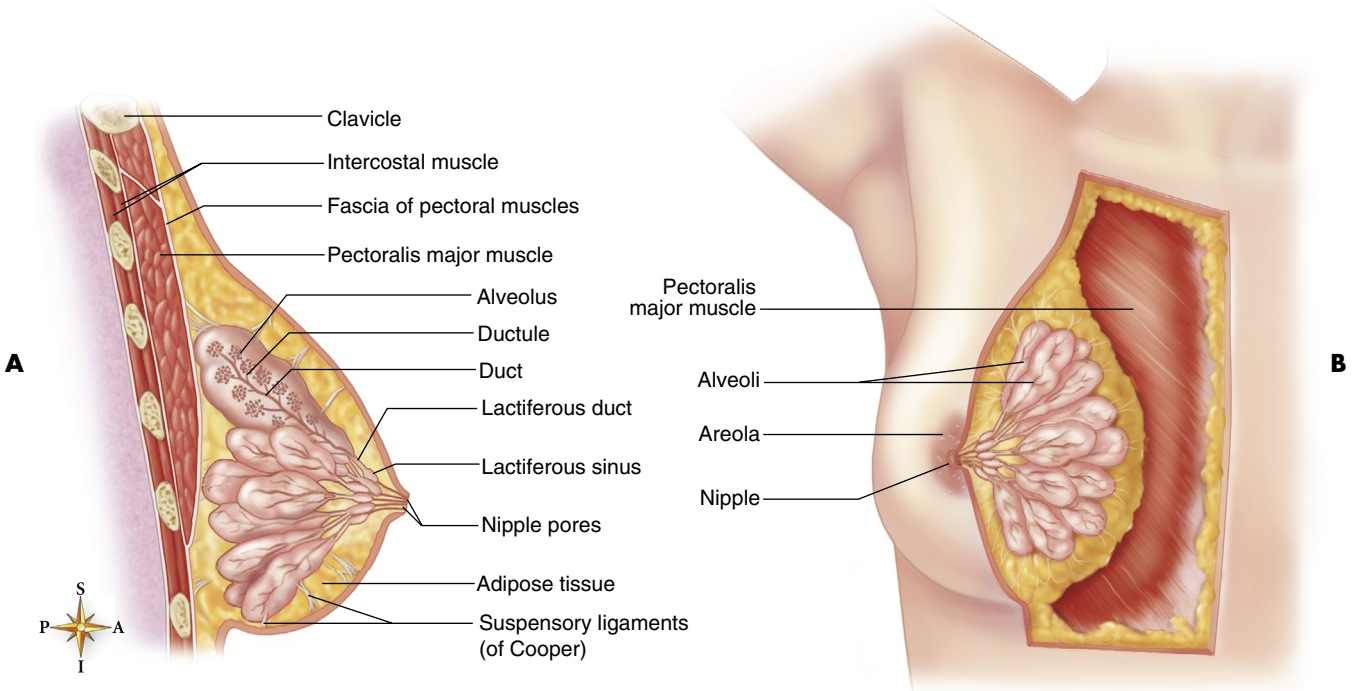

FIGURE 11-58 The female breast.

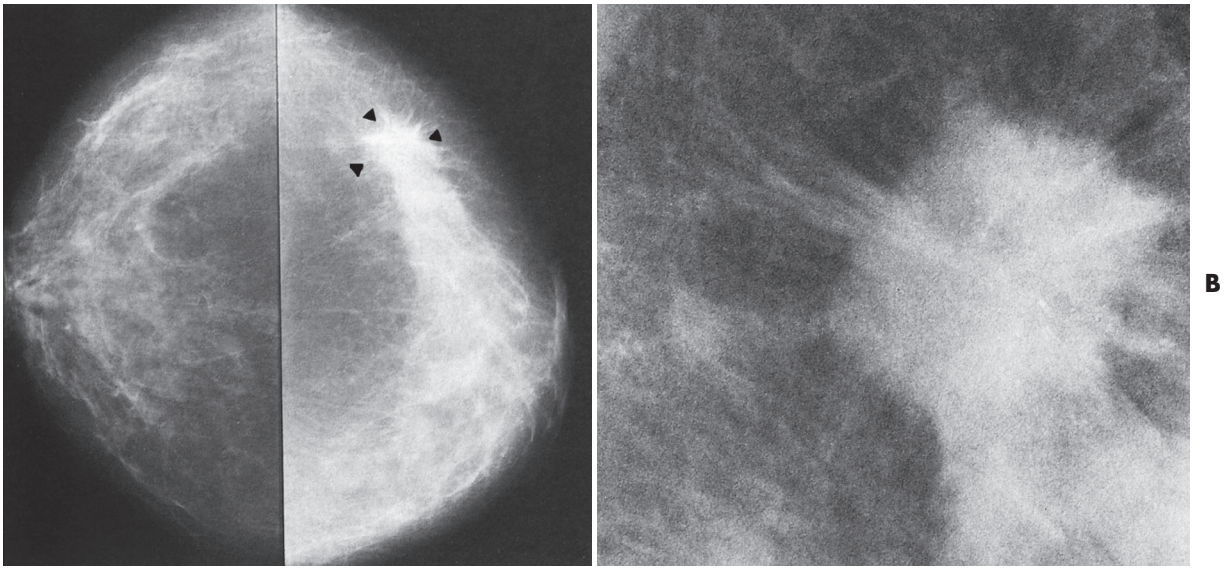

FIGURE 11-59 Breast cancer. Full (A) and magnified coned (B) views of the breast demonstrate an ill-defined, irregular mass with radiating spicules (*arrowheads*).

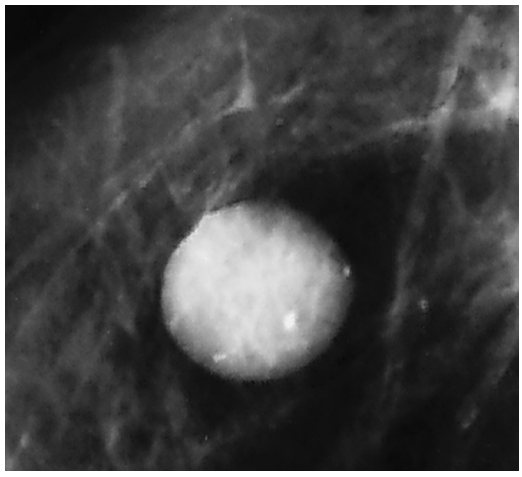

FIGURE 11-60 Benign breast mass. Screen-film mammogram demonstrates smooth, round fibroadenoma with clearly defined margins.

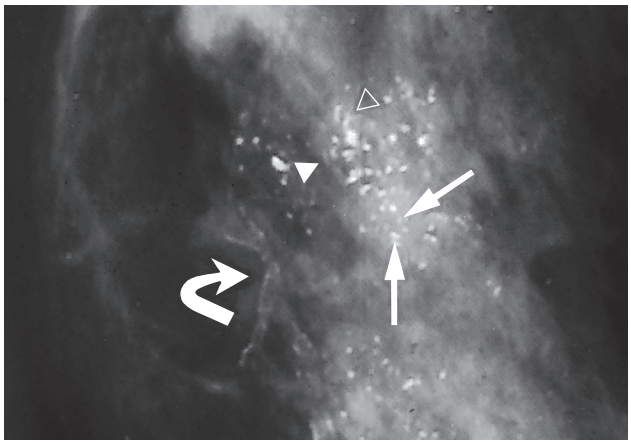

FIGURE 11-61 Malignant calcifications in breast cancer. Numerous tiny calcific particles with linear (*straight arrows*), curvilinear (*solid arrowhead*), and branching (*open arrowhead*) forms characteristic of malignancy. Note the benign calcification in the arterial wall, which is easily recognized from its large size and tubular distribution (*curved arrow*).

Clustered calcifications in breast cancer are typically numerous, very small, and localized to one segment of the breast. They demonstrate a wide variety of shapes, including fine linear, curvilinear, and branching forms (Figure 11-61). Although only approximately half of breast cancers are seen mammographically as clusters of calcifications, typical calcifications are seen in many of the nonpalpable intraductal cancers that often do not form mass lesions and may otherwise escape detection.

Ultrasound provides a secondary diagnostic tool that can differentiate a benign cyst from a solid mass, and thus it substantially reduces the number of biopsies performed for benign cysts (Figures 11-62 and 11-63) and normal fibroglandular tissue. Ultrasound is best in determining the size of a mass, and Doppler ultrasound permits visualization of blood flow patterns. However, ultrasound is of limited value in detecting nonpalpable cancers, particularly those that have calcifications alone, and thus it cannot substitute for mammography as a screening examination. In cases of ruptured silicone implants, an inflammatory process causes the development of silicone granulomas. These produce a "snowstorm" appearance (Figure 11-64), causing posterior shadowing that obscures the posterior border.

MRI with multiple sequences and contrast enhancement now has the ability to help differentiate between benign adenomas and carcinomas (Figure 11-65). The use of image subtraction (noncontrast image subtracted from the enhanced image) assists in highlighting the contrast-enhanced regions. Benign masses tend to have smooth borders, whereas malignancies appear as high–signal intensity

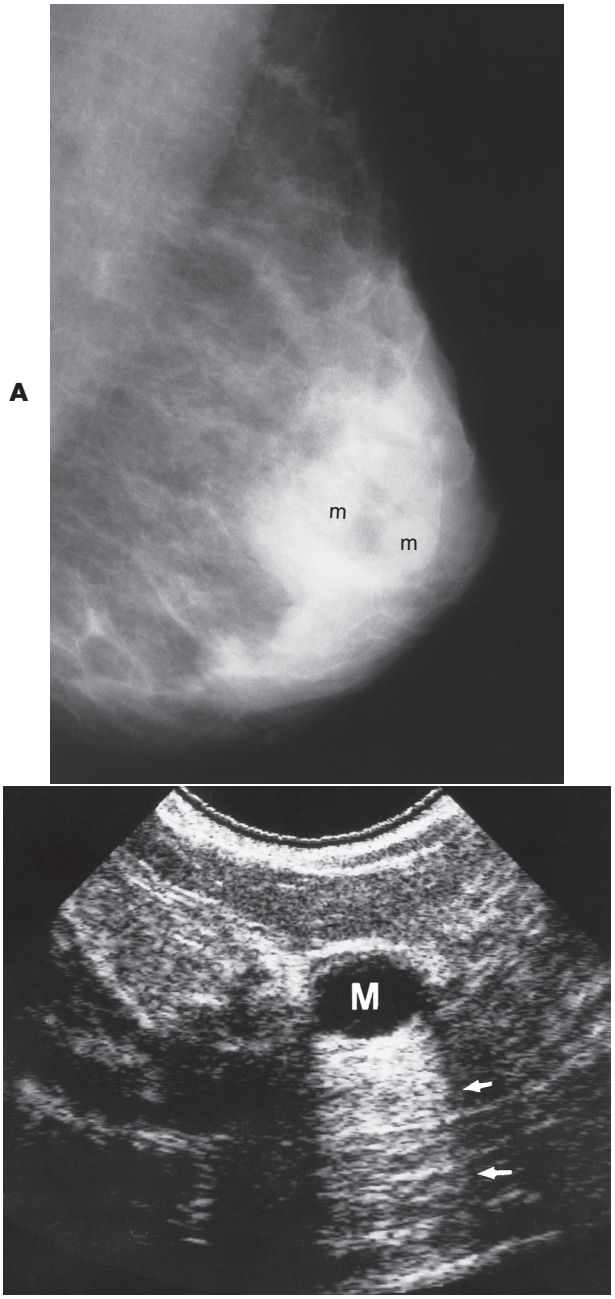

FIGURE 11-62 Sonography for breast disease. **(A)** Mammogram shows several rounded masses (m) that could be solid or cystic in a breast that is very dense anteriorly. **(B)** Sonogram clearly shows that the largest mass (M) is cystic because it contains no internal echoes and shows considerable posterior enhancement (*arrows*).

lesions with spiculation. Using longer sequences, carcinomas produce high signal intensity, whereas adenomas assume a lower signal intensity (and are not apparent). Fat suppression using water excitation best demonstrates the functional parenchyma, and this technique helps differentiate among various lesions. MRI is used in questionable cases for surgical preplanning to determine whether lumpectomy or mastectomy is the best operative approach. For patients with breast implants, MRI may best demonstrate the surrounding breast tissue (Figure 11-66). This modality also demonstrates implant twisting or rupture, which may not be visible on other imaging techniques.

Although not used routinely, CT can assist in determining extension of the disease (Figure 11-67). SPECT fusion imaging aids in determining lymphatic involvement for breast malignancies (Figure 11-68). The most sensitive imaging modality is PET. Although PET is the least used modality because of its expense and limited availability, as a molecular imaging technique it can demonstrate the metabolic activity and vascularization of the tumor at its earliest stages. Currently, PET is used to detect recurrences in scarred breasts because postoperative scarring makes mammography less effective for visualizing new lesions.

Although relatively infrequent (1 in 100), breast cancer also can develop in men. Breast cancer in men usually has a poor prognosis because it is often diagnosed in a later stage. Breast enlargement in men results from a proliferation of the glandular component and is known as *gynecomastia*.

Treatment. Imaging also plays a role in surgical planning by providing guidance (with ultrasound or mammography) for needle localization (Figure 11-69). A conservative surgical approach is lumpectomy, which is used for isolated lesions. Mastectomy, a more aggressive surgical approach, involves the removal of all breast tissue and a dissection of the lymph nodes. If the lymph nodes contain cancerous cells, the axillary nodes are removed (radical mastectomy). Chemotherapy and radiation therapy are used in more advanced cases, depending on the type of cancer cells and whether the axillary nodes are involved. Hormonal chemotherapy with synthetic antiestrogens may be used if the tumor contains estrogen receptors.

Benign Breast Disease

Fibrocystic disease of the breast is a common benign condition that occurs in approximately 20% of premenopausal women. It is usually bilateral, with cysts of various sizes distributed throughout the breasts that also contain an increased amount of fibrous tissue. The size of a cyst usually changes with the menstrual cycle, as does the amount or type of fluid in it.

Imaging appearance. A fibroadenoma is the most common benign breast tumor. It generally appears as a smooth, well-circumscribed mass with no invasion of surrounding tissue (see Figure 11-60). Ultrasound permits differentiation of a solid fibroadenoma from a fluid-filled breast cyst. Sonographically, a simple cyst has an anechoic center with a thin echogenic capsule (see Figure 11-62). High-risk patients require monitoring of the cystic lesions for possible conversion to a cancerous process. Equivocal lesions may require imaging with other modalities.

Treatment. The most conservative treatment of a benign cyst addresses pain management, usually through dietary modifications and reduction of caffeine intake. If dietary changes do not decrease pain to a tolerable level, drainage of the cyst may be performed. Hormonal therapy with synthetic antiestrogens that block estrogen and progesterone is used in cases of cyclical pain. However, these drugs may produce intolerable side effects. Surgery is not the most effective treatment unless there is only a single cyst (and most patients have multiple cysts).

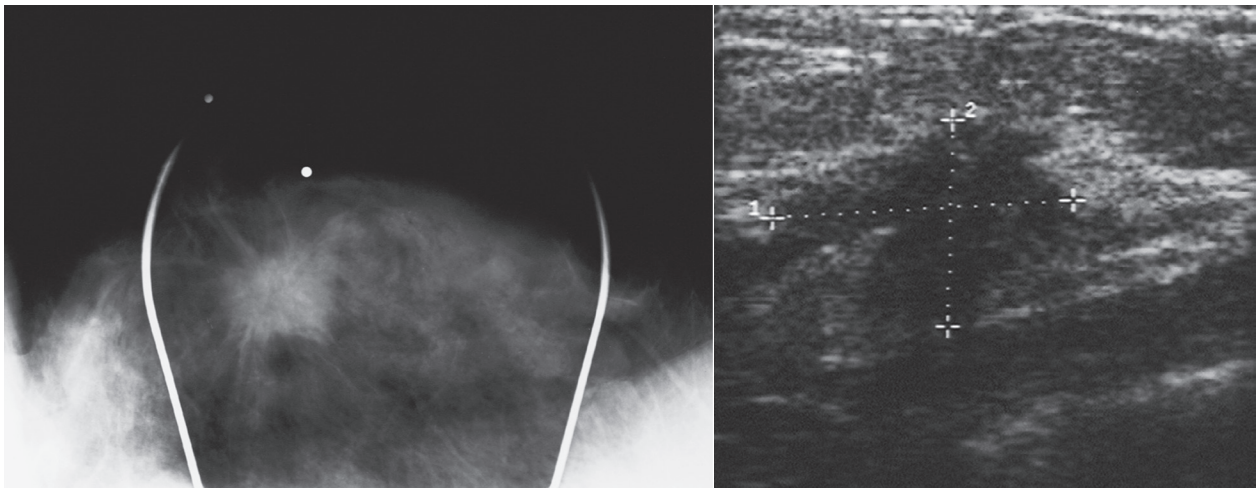

FIGURE 11-63 Spiculated lesion. (A) Mammography using magnification–spot compression demonstrates microcalcifications and a spiculated lesion. (B) Breast sonography shows finger-like projections emanating from the lesion measuring 1.8 × 1.25 cm.

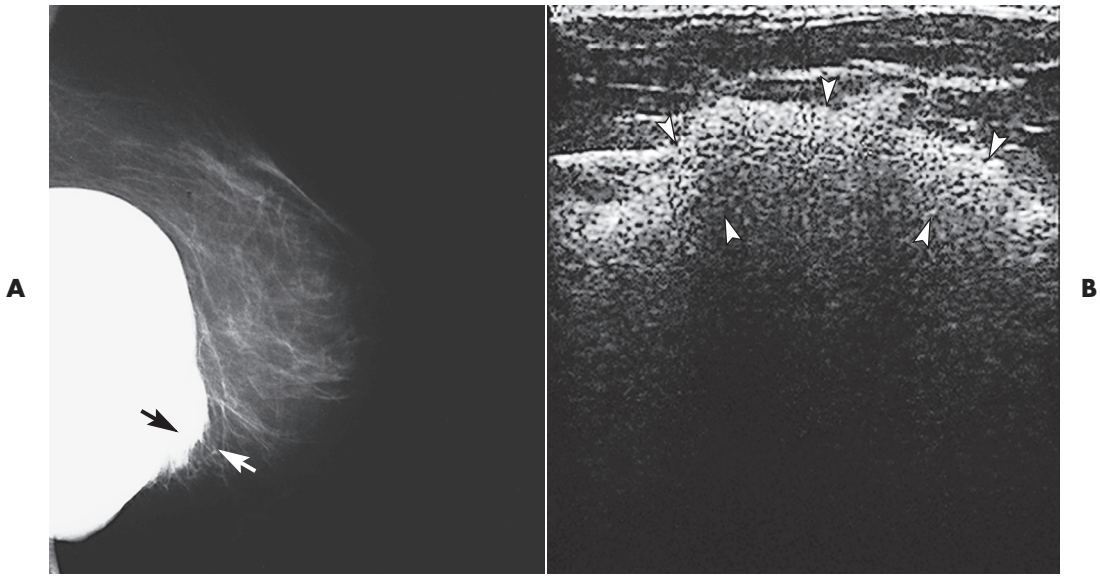

FIGURE 11-64 Ruptured silicone breast implants. (A) Mammogram shows retroglandular implant with extracapsular silicone (*arrows*). (B) Ultrasound image of the same patient shows the typical "snowstorm" appearance of free extracapsular silicone (*arrowheads*).

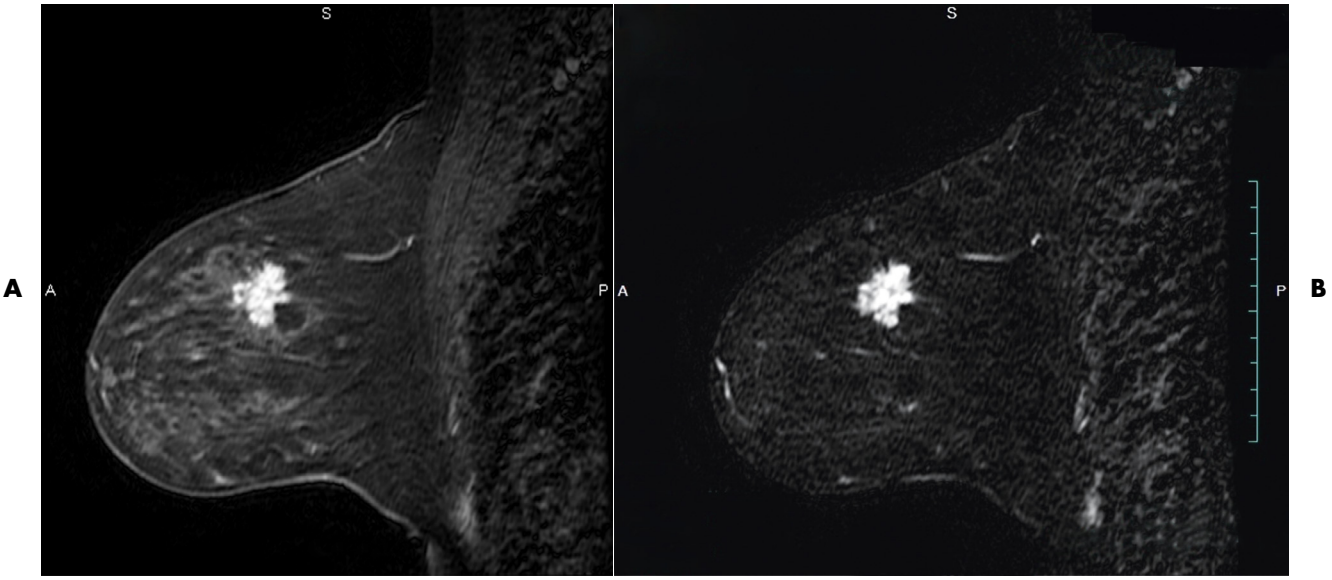

FIGURE 11-65 Breast carcinoma. (A) Unilateral sagittal T1-weighted fat-saturated postcontrast MR image demonstrates a single mass. (B) Postcontrast MR subtraction image illustrates a spiculated mass.

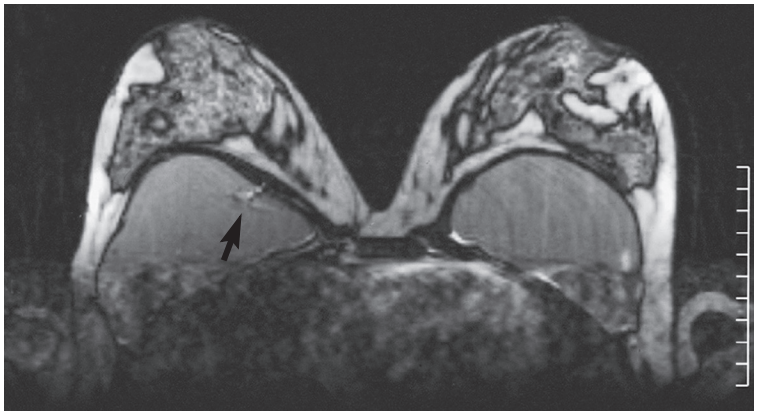

FIGURE 11-66 Breast implants. MRI distinguishes between breast tissue and implant. A fold in one implant is also visualized (*arrow*).

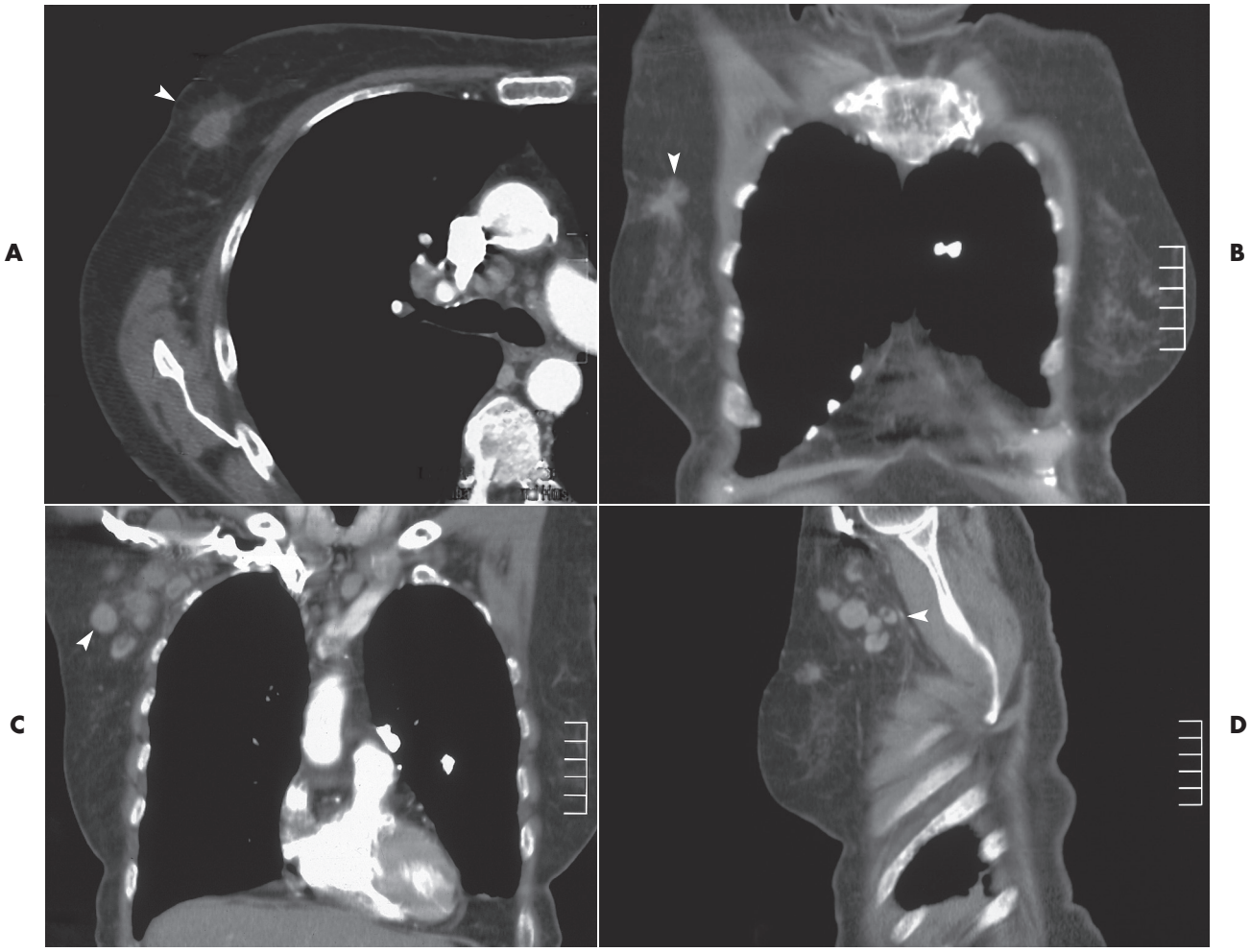

FIGURE 11-67 Breast cancer. CT scans demonstrate an enhancing breast lesion (*arrow*) in the axial **(A)** and coronal projections **(B)**. The lymph nodes (*arrows*) are enlarged, as seen on the coronal **(C)** and sagittal projections **(D)**. On lung window scans, pulmonary metastatic nodules were demonstrated.

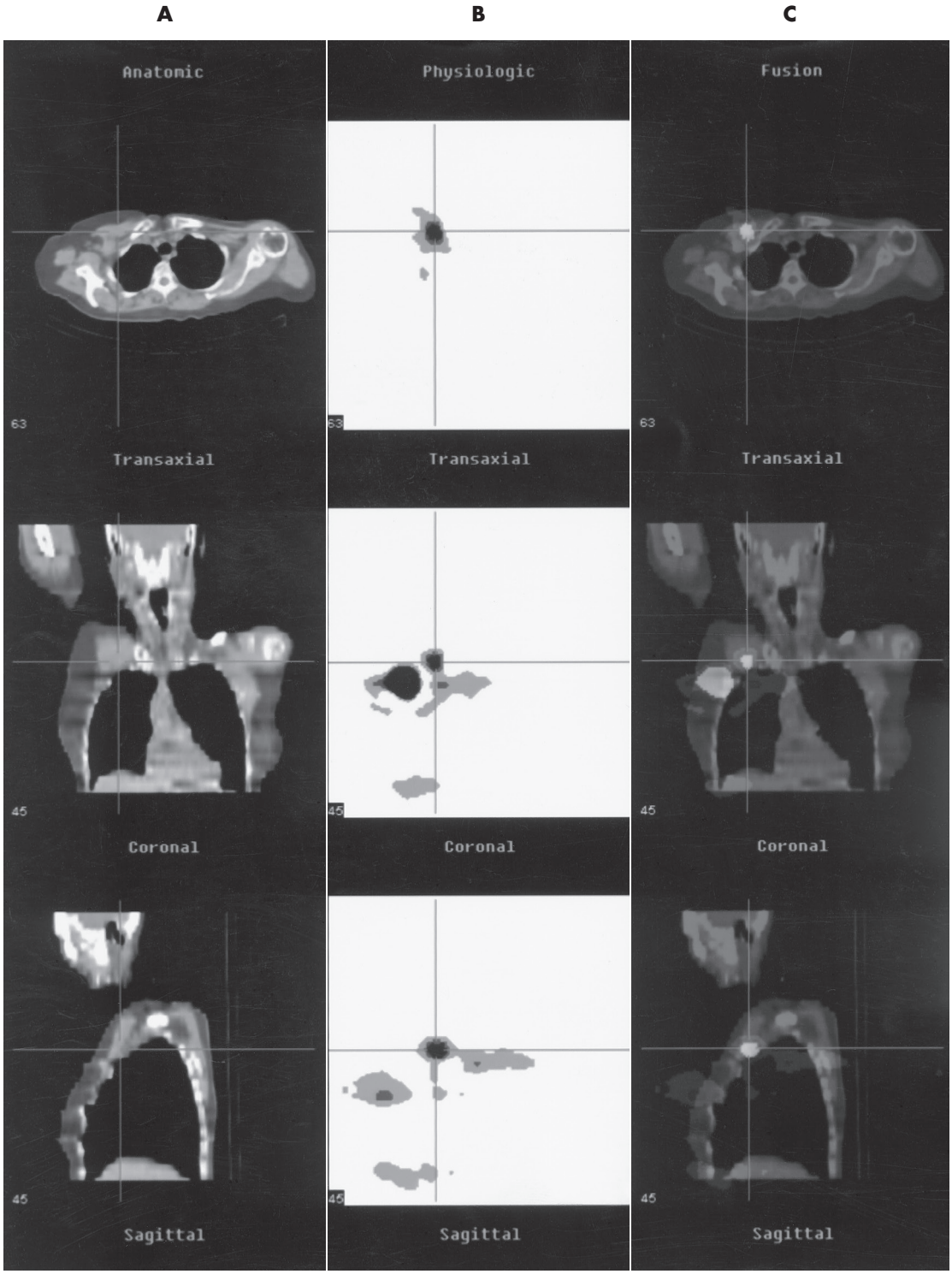

FIGURE 11-68 Right sentinel lymph node studied with SPECT and CT fusion imaging. **(A)** A triplanar anatomic CT image. **(B)** A triplanar SPECT physiologic image. **(C)** A triplanar fusion image. One sentinel node is located and marked for intraoperative removal.

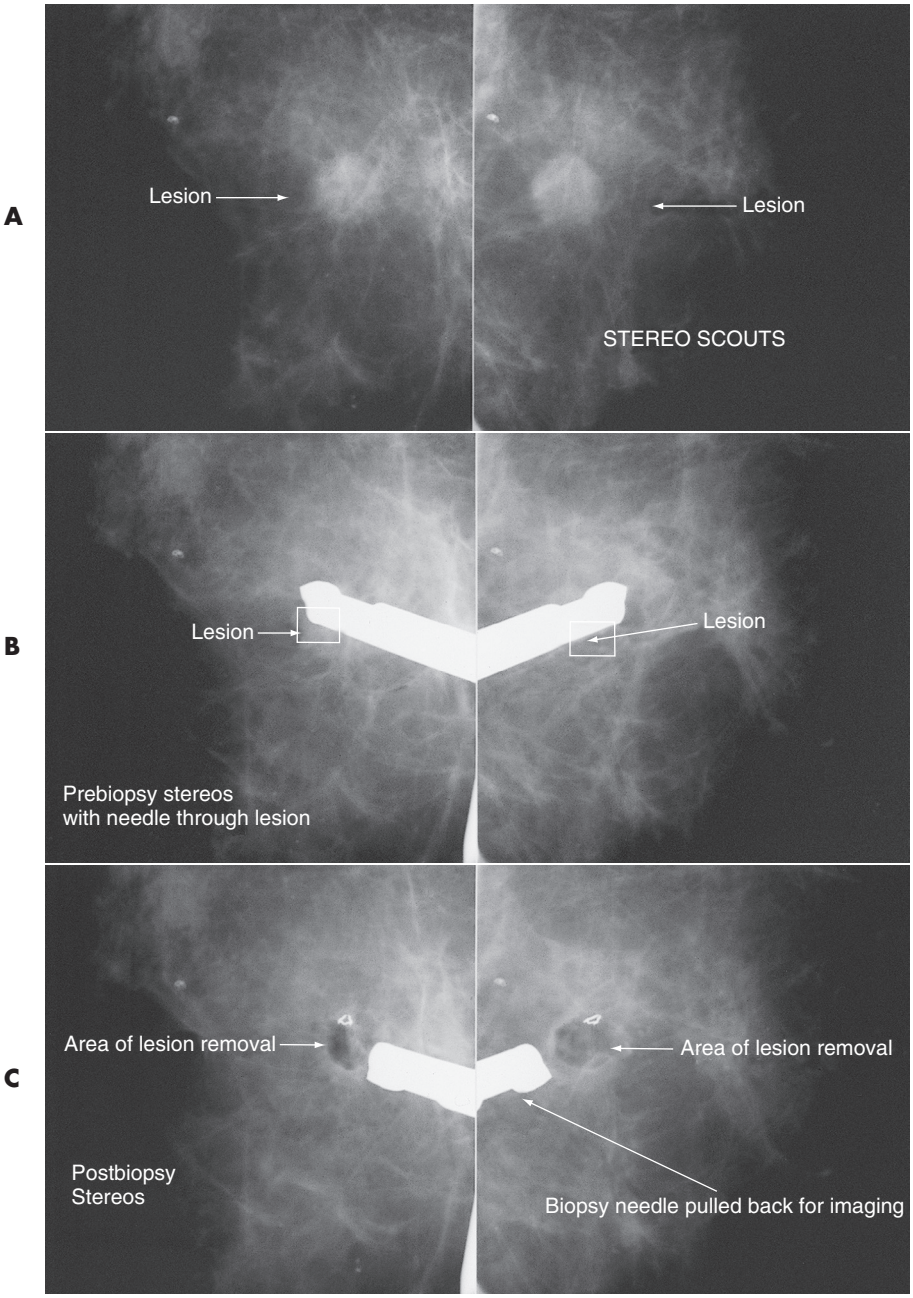

FIGURE 11-69 Stereotaxic needle biopsy. (A) Stereotaxic scout images (stereos) of breast lesion. (B) Stereotaxic images showing needle localization. (C) Postbiopsy images of lesion with the needle pulled back to demonstrate lesion removal.

Summary of Findings for Breast Lesions

Disorder	Location	Imaging Appearance	Treatment
Breast carcinoma	Breast tissue	Mammography—poorly defined with areas of distortion, irregular margins with numerous fine linear strands or spicules radiating from the mass US—differentiates benign cysts from a solid mass and its size; blood flow patterns assessed with Doppler imaging; ruptured silicone implants produce "snowstorm" appearance MRI (subtraction imaging)—benign masses tend to have smooth borders, whereas malignancies demonstrate high signal intensity with spiculation; fat suppression best demonstrates the functional parenchyma and helps differentiate lesions; best demonstrates the surrounding breast tissue in patients with implants PET—demonstrates metabolic activity and vascularization of the tumor at the earliest stages; utilized to detect recurrences in scarred breast tissue	Lumpectomy Mastectomy Radical mastectomy Chemotherapy or hormonal therapy
Benign breast disease	Fibrocystic breast or single cysts	Mammography—smooth, well-circumscribed mass without invasion of surrounding tissue US—simple cyst appears as an anechoic center with a thin echogenic capsule	Pain management through diet Hormonal therapy Surgery for single cysts

US, Ultrasound.

IMAGING IN PREGNANCY

Because of its noninvasive and nonionizing character, ultrasound is the modality of choice in the evaluation of possible complications of pregnancy. A major role of ultrasound is to assess the gestational age, a measurement that is often highly inaccurate when based on the date of the last menstrual period. Knowledge of the true gestational age may be critically important for obstetric decisions because the length of pregnancy is a major factor in interpreting the graphs that indicate the status of the fetus.

Measurements of fetal age by ultrasound include the longest biparietal diameter (BPD), the crown-to-rump length, and the length of the fetal femur. The BPD is measured from the outer margin of the skull on one side to the inner margin on the other side at the level of the thalami (Figure 11-70). A single measurement of the BPD has its greatest accuracy between 12 and 26 weeks; after this time, the size of the head and thus the BPD may be affected by a growth disturbance. *Crown-to-rump length* refers to the distance between the tip of the head and the bottom of the fetal trunk (Figure 11-71). This measurement is highly accurate for assessing gestational age in early pregnancy (less than 11 weeks). Fetal femoral length (Figure 11-72) aids in determining fetal age in the second and third trimesters by identifying epiphyseal cartilage at the knee, which indicates a gestational age beyond 33 to 35 weeks.

An early diagnosis of multiple pregnancies can be made by ultrasound (Figure 11-73). This is essential so that therapeutic measures can be taken to reduce the high complication rate associated with twin (or more) fetuses.

Ultrasound can be used to detect an abnormal volume of amniotic fluid, which is often associated with underlying fetal anomalies. **Polyhydramnios** refers to an excessive accumulation of amniotic fluid that may be caused by maternal disorders such as diabetes mellitus and Rh isoimmunization (Figure 11-74). Polyhydramnios is also caused by fetal abnormalities, especially those related to the central nervous system, the gastrointestinal tract, the circulatory system, and dwarfism. **Oligohydramnios** refers to a very small volume

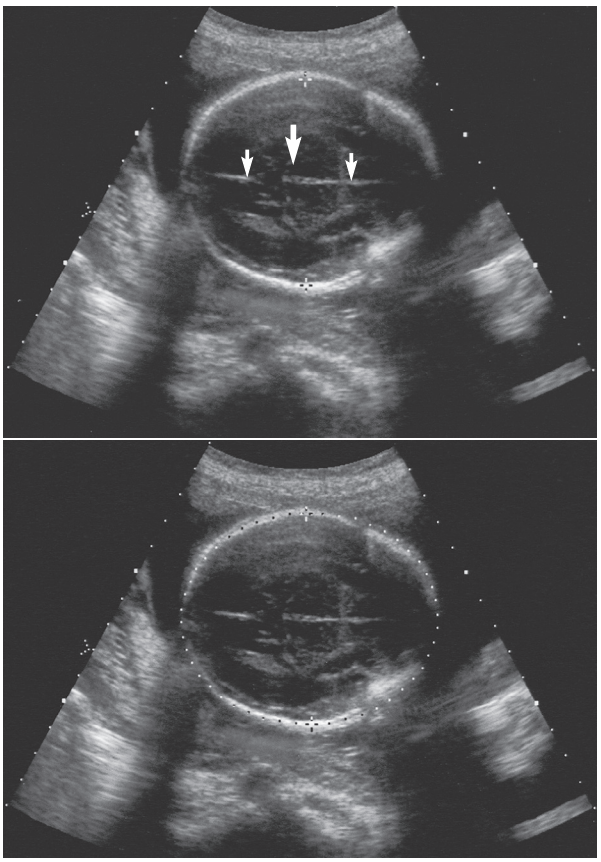

FIGURE 11-70 Biparietal diameter (BPD) in a 27-week fetus. (A) *Cursors* delineate BPD, which is measured from the outer margin of skull on one side to the inner margin on other side. *Arrows* point to the midline falx. (B) *Dotted line* indicates the head circumference.

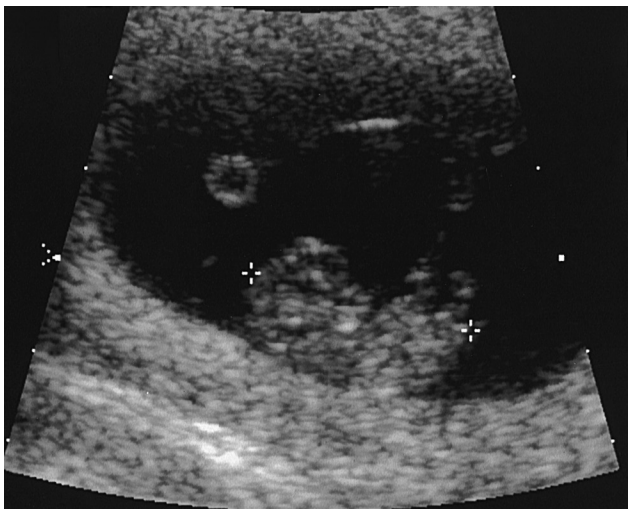

FIGURE 11-71 Crown-to-rump length measurement. *Cursors* delineate the length of the fetus from the top of the head to the bottom of the torso.

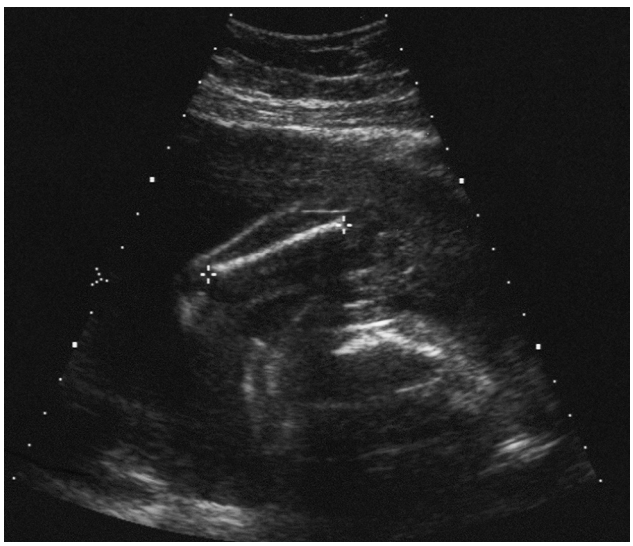

FIGURE 11-72 Fetal femur. *Cursors* demonstrate a femur length of 3.96 cm, and cartilage is not demonstrated, indicating a fetal age earlier than 33 weeks.

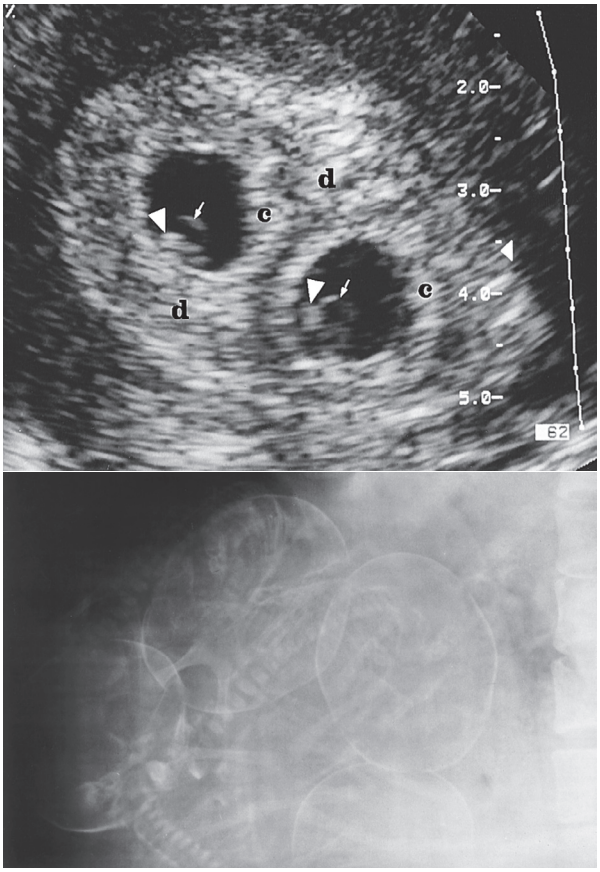

FIGURE 11-73 Multiple pregnancies. **(A)** Endovaginal sonogram shows two gestational sacs surrounded by the echogenic chorionic ring (c) composed of the decidua capsularis and the chorion laeve within the decidua vera (d). A yolk sac (*small arrow*) and live embryo (*arrowhead*) are present within each gestational sac. The crown-to-rump lengths measure 5.4 mm and 4.7 mm, corresponding to a gestational age of 6.5 weeks. **(B)** Lateral abdominal radiograph of a woman with quadruplets clearly shows four separate fetal skulls and spines.

FIGURE 11-74 Polyhydramnios. Excessive accumulation of amniotic fluid (hypoechoic area) surrounds the fetus in a mother of advanced age for pregnancy.

of amniotic fluid. This condition results primarily from fetal urinary tract disorders, such as renal aplasia, renal dysplasia, and urethral obstruction. Oligohydramnios is also associated with intrauterine growth retardation.

Clinically significant errors of morphologic development occur in up to 5% of all children. The *in utero* detection of these anomalies by ultrasound may permit *in utero* medical or surgical therapy, may provide an indication for termination of the pregnancy, or may influence the mode of delivery. Although a detailed description of the rapidly expanding field of prenatal sonography is beyond the scope of this book, some of the abnormalities that can be detected, and often treated, *in utero* are osseous (bony) and neural anomalies of the fetal cranium (Figures 11-75 and 11-76) and spine, gastrointestinal atresias and developmental cysts, cystic and obstructive

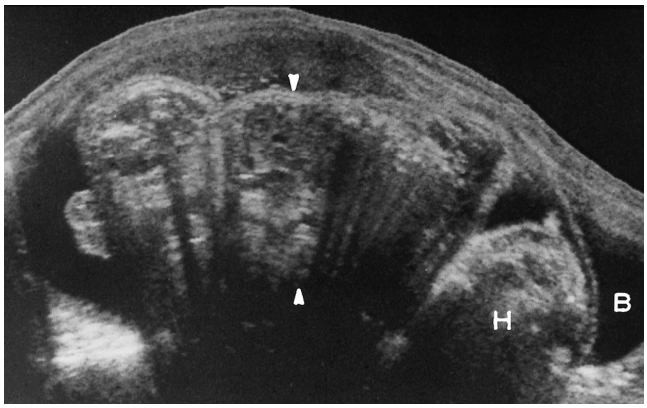

FIGURE 11-75 Anencephaly. Long-axis image of a third-trimester fetus shows that the head (H) is irregularly shaped, echogenic, and much smaller than the body (*arrowheads*). *B,* Maternal bladder.

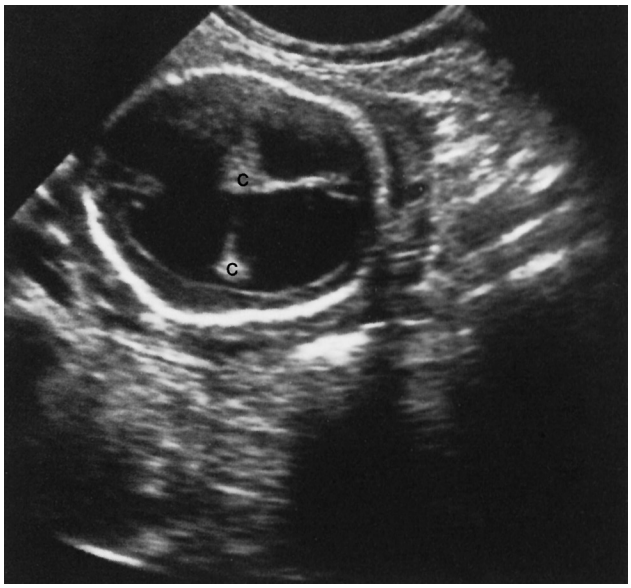

FIGURE 11-76 Ventriculomegaly. Cranial axial ultrasound image at 27 menstrual weeks shows obvious ventricular enlargement with convex surface of the lateral ventricle wall that parallels the bony calvaria. Note the dangling choroids (*c*).

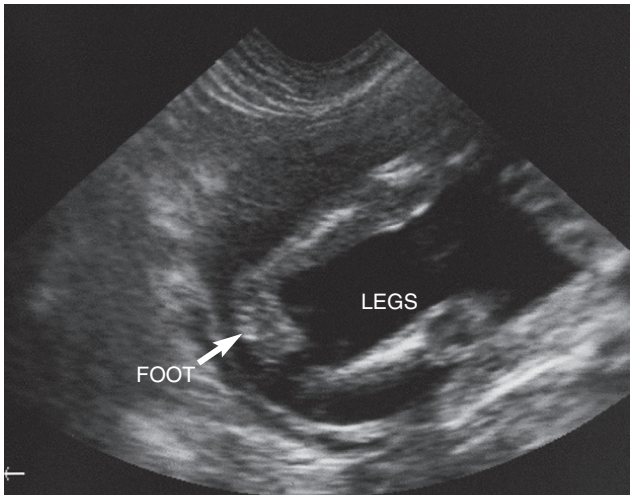

FIGURE 11-77 Clubfoot. Prenatal ultrasound image shows one foot at a right angle to the leg.

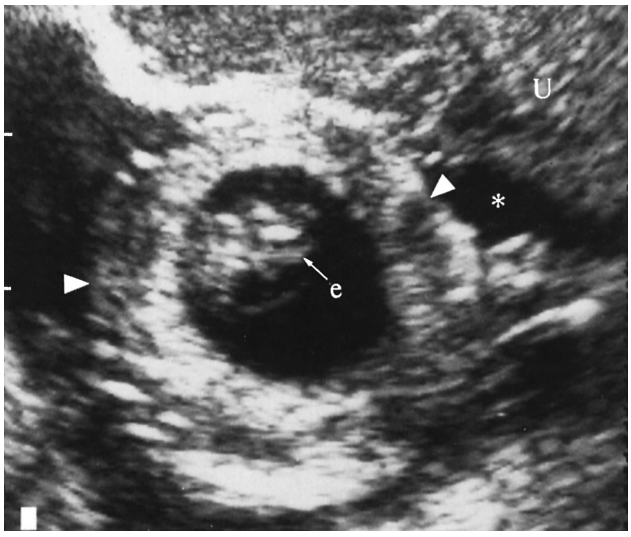

FIGURE 11-78 Ectopic pregnancy with a live embryo in the adnexa. Endovaginal sonography shows the tubal ring (*arrowheads*) and gestational sac, containing the yolk sac and live embryo (e). *Asterisk* indicates free fluid. *U,* Uterus.

lesions of the genitourinary tract, and congenital cardiac diseases and skeletal anomalies (Figure 11-77).

Because ultrasound examinations can demonstrate the fetus and placenta with no apparent risk to the mother or unborn child, ultrasonography is unquestionably the imaging study of choice for evaluating the gravid (pregnant) woman. In extremely rare instances, there may be justification for performing radiographic pelvimetry to demonstrate the architecture of the maternal pelvis and to compare the size of the fetal head with the size of the maternal bony pelvic outlet to determine whether the pelvic diameters are adequate for normal delivery or a cesarean section will be required. In almost all cases, however, the combination of careful clinical evaluation and ultrasonography is sufficient to make these decisions without the need to resort to radiographic pelvimetry with its high radiation dose. There is absolutely no indication ever to perform fetography, the radiographic demonstration of the fetus *in utero*. Ultrasound can provide far better diagnostic information and is not associated with the danger of radiation-induced fetal malformations.

Ectopic Pregnancy

Although ectopic pregnancy is a life-threatening condition, responsible for up to one fourth of maternal deaths, the diagnosis is missed by the initial examining physician in up to three fourths of cases. More than 95% of ectopic pregnancies occur within the fallopian tubes, and more than half the patients with this complication of pregnancy have a history or pathologic evidence of PID. Ectopic pregnancies are often associated with urine or plasma levels of human chorionic gonadotropin (HCG) that are substantially lower for the expected date of gestation than those in patients with normal intrauterine pregnancies.

Imaging appearance. Ultrasound is the major imaging modality for diagnosing ectopic pregnancy. The classic appearance consists of an enlarged uterus that does not contain a gestational sac and is associated with an irregular adnexal mass, an "ectopic fetal head," or fluid in the cul-de-sac (Figure 11-78). The unequivocal demonstration of an intrauterine pregnancy virtually excludes an ectopic pregnancy because the incidence of coexisting ectopic and intrauterine pregnancies is only 1 in 30,000.

Treatment. Emergency surgical intervention before a fatal hemorrhage occurs is required.

Trophoblastic Disease

Trophoblastic disease refers to a spectrum of pregnancy-related disorders ranging from benign hydatidiform mole to the more malignant and frequently metastatic choriocarcinoma. A hydatidiform mole results from abnormal fertilization when there is an absence of the female chromosome. Approximately half of choriocarcinomas follow pregnancies complicated by hydatidiform mole. The remainder occur after spontaneous abortion, ectopic pregnancy, or normal deliveries.

Imaging appearance. A hydatidiform mole typically appears on an ultrasound image as a large, soft tissue mass of placental (trophoblastic) tissue filling the uterine cavity and containing echoes of low to moderate amplitude ("bunch of grapes") (Figure 11-79) without any signs of fetal movement. Endovaginal sonography confirms that there is no evidence of a developing fetus. On ultrasound images, choriocarcinoma resembles benign hydatidiform mole and usually appears as a large complex mass of central hemorrhage, with necrosis found in the expected position of the uterus. Choriocarcinoma tends to metastasize to the lungs, where it typically produces multiple large masses that rapidly regress once appropriate chemotherapy is instituted.

Treatment. Hydatidiform moles are treated by removal of all placental tissue by suction curettage of the uterus. If suction curettage does not lower the patient's human chorionic gonadotropin level, the disease progresses, and the patient requires chemotherapy. For choriocarcinoma, folic acid antagonists have a cure rate of approximately 80% if treatment begins before brain metastasis occurs.

Summary of Findings for Pregnancy

Disorder	Location	Imaging Appearance	Treatment
Uterine pregnancy	Fetus within the uterus	US—demonstrates the fetus and placenta	Normal birth
Ectopic pregnancy	Fertilization outside the uterus	US—enlarged uterus without gestational sac and an appearance of an irregular adnexal mass	Surgical intervention
Trophoblastic disease Hydatidiform mole	Abnormal fertilization	US—large soft tissue mass with "bunch of grapes" appearance	Suction curettage
Choriocarcinoma	Malignant transformation of hydatidiform mole	US—large complex mass with necrosis	Chemotherapy of folic acid antagonist
Female infertility	Lack of fertilization or implantation	Radiograph—hysterosalpingography to demonstrate the ovaries, fallopian tubes, and uterus US—screening for congenital anomalies and to monitor treatment	Ovulation-induction agents

US, Ultrasound.

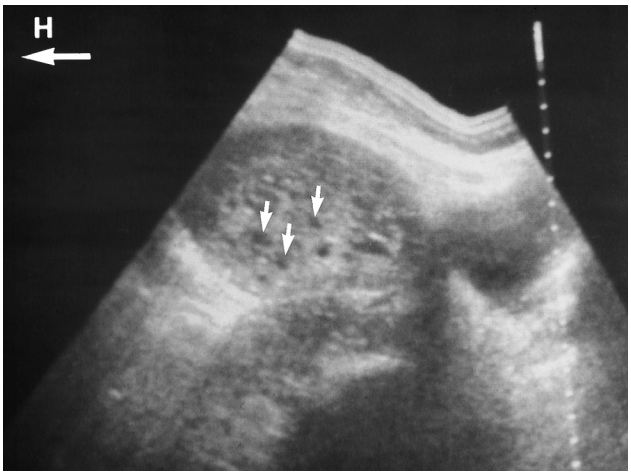

FIGURE 11-79 Hydatidiform mole. Longitudinal sonogram in a patient in her second trimester of pregnancy demonstrates a large, moderately echogenic mass filling the central uterine cavity. Note the numerous small cystic spaces (*arrows*), which represent greatly hydropic chorionic villi.

FEMALE INFERTILITY

The causes of infertility in young women include anomalies in the reproductive organs, such as an abnormal uterus that cannot hold a fetus (Figure 11-80), obstructed fallopian tubes, ovaries that are unable to produce mature ova, and disruption of the path the ova normally follow to the uterus.

Imaging appearance. The major radiographic procedure for evaluating infertile women is hysterosalpingography, in which the uterine cavity and fallopian tubes are opacified after the injection of contrast material into the uterus. In a woman with normal patent fallopian tubes, contrast material extravasating into the pelvic peritoneal cavity outlines the peritoneal surfaces (see Figure 11-31). Developmental anomalies or fibrosis from PID may cause occlusion of one or both of the fallopian tubes; in such cases, there is no evidence of the contrast material reaching the peritoneal cavity (see Figure 11-32). In addition to assessing tubal patency, hysterosalpingography can also demonstrate uterine abnormalities that contribute to infertility, such as intrauterine fibroids, severe uterine flexion or retroversion, and other congenital and acquired malformations.

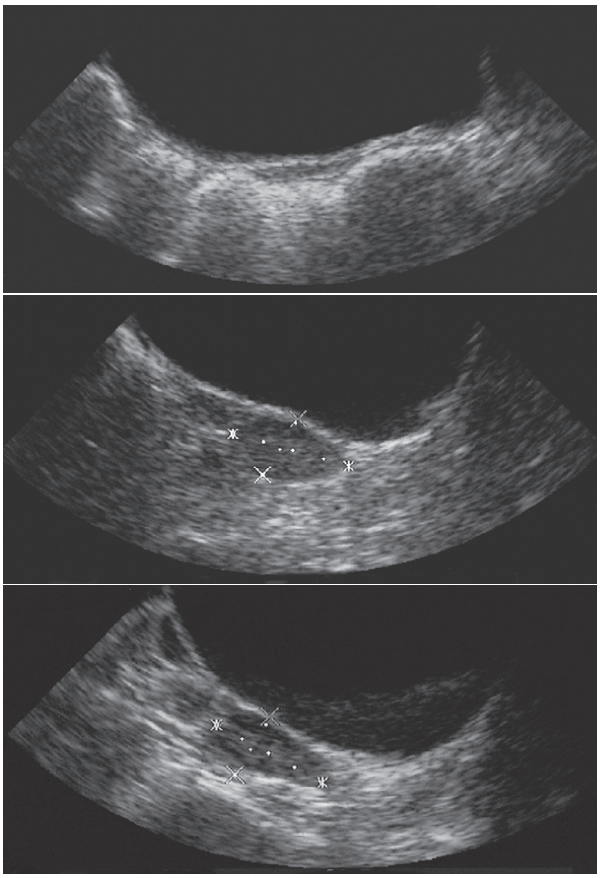

FIGURE 11-80 Uterine agenesis. Ultrasound images of a 16-year-old girl who has never had a menstrual cycle. Midline sagittal view **(A)** demonstrates the bladder (dark area) with no uterus found posteriorly. Normal left **(B)** and right **(C)** ovaries are shown in the parasagittal plane.

Treatment. For women who receive ovulation-induction agents as treatment for infertility, ultrasound can be used to monitor the maturation of ovarian follicles. Low-level internal

echoes in mature ovarian follicles appear to be a prognostic indicator of fertility. They may represent a periovulatory state, which is an appropriate time for artificial insemination or in vitro fertilization. Ultrasound can also demonstrate the characteristic bilateral multicystic ovarian enlargement in the ovarian hyperstimulation syndrome, which may develop in women receiving menotropins (Pergonal) therapy for infertility.

REVIEW QUESTIONS

1. Why has ultrasound become the major imaging modality for both the male and the female reproductive systems?
2. In addition to ultrasound, what are the main radiographic studies currently used for the female reproductive system?
3. The formation of sperm is known as _____.
4. What male hormone helps to regulate metabolism by promoting growth of skeletal muscles and is considered responsible for the greater degree of muscle development in men?
5. Severing of the vas deferens to create sterility is termed _____.
6. The second most common cause of malignancy in men is _____.
7. What imaging modality for demonstrating the prostate gland uses a probe inserted into the rectum?
8. *True or false:* Ultrasound studies of the prostate gland cannot always determine the malignant or benign status of prostatic disease.
9. Prostatic carcinoma can often spread through the bloodstream to the bone and can sometimes cause sclerosis of an entire vertebra. This pathologic condition is termed _____.
10. What screening technique is usually employed to identify the location of an undescended testicle?
11. What is the term used to describe the twisting of the male gonad on its pedicle?
12. The most common neoplasms in men between 20 and 35 years of age are tumors that tend to metastasize through the _____ system.
13. The rupture and expulsion of the mature ovum into the pelvic cavity is termed _____.
14. A pregnancy that occurs in a fallopian tube or in the pelvic cavity is termed _____.
15. What is the name of the radiographic procedure used to demonstrate the patency or status of the fallopian tubes?
16. Untreated _____ can lead to cerebral cortical lesions, causing mental disorders, and involvement of the skeletal system and affects infants born to infected mothers.
17. The most common type of germ cell tumor, often containing teeth, hair, and fatty material, is called a(n) _____.
18. Leiomyomas, which are more commonly referred to as _____, are benign smooth-muscle tumors of the uterus.
19. The most common malignancy among women occurs in the _____.
20. The second most common form of cancer in women is _____.

12

Miscellaneous Diseases

OUTLINE

Nutritional Diseases
- Vitamin Deficiencies
- Hypervitaminosis
- Protein–Calorie Malnutrition (Kwashiorkor)
- Obesity

Systemic Lupus Erythematosus

Melanoma

Muscular Dystrophy

Hereditary Diseases
- Chromosomal Aberrations
- Genetic Amino Acid Disorders

KEY TERMS

arachnodactyly
ascorbic acid
aseptic necrosis
fat-soluble vitamins
gonadal dysgenesis
microcephaly
niacin
nutritional deficiency
osteomalacia
pectus excavatum
Pelken spur
syndrome
testicular dysgenesis
thiamine
vitamins
water-soluble vitamins
Wimberger's sign of scurvy

OBJECTIVES

After reading this chapter, the reader will be able to:

- Describe nutritional disorders and their possible relationship to disorders of other organs
- Define terminology relating to nutritional disorders
- Define and describe all boldface terms in this chapter
- Distinguish the pathologic conditions caused by various vitamin deficiencies
- Describe the pathologic conditions associated with muscular dystrophy, melanoma, and systemic lupus erythematosus
- Differentiate hereditary abnormalities, including chromosomal aberrations and genetic amino acid disorders

NUTRITIONAL DISEASES

Disorders of nutrition range from malnutrition and vitamin deficiency to obesity and hypervitaminosis. In addition to inadequate intake, **nutritional deficiency** may be related to disorders of the liver, pancreas, and gastrointestinal tract that result in an inability of the body to digest and properly use proteins, carbohydrates, and lipids. In diabetes mellitus, the absence of insulin prevents entry of glucose into the cells and thus deprives the body of its major source of energy. Abnormalities of the pancreas, liver, and gastrointestinal tract that cause nutritional diseases are discussed elsewhere; this section deals with diseases caused by vitamin deficiency, malnutrition, and obesity.

Vitamin Deficiencies

Vitamins are an essential part of the enzymatic systems that are vital to the body's cellular metabolism. Vitamins are formed (synthesized) only by plants, not by animals. Therefore, humans' supply of vitamins comes directly from eating fruits and vegetables or from animals (including fish) that have eaten plants and have stored the vitamins. Vitamins are generally divided into two categories: fat soluble and water soluble. The **fat-soluble vitamins** (A, D, E, and K) can be stored within body tissues. **Water-soluble vitamins** (B and C) cannot be stored and must be a regular part of the diet to prevent a deficiency. The major B vitamins are thiamine, riboflavin, niacin, pantothenic acid, cobalamin (vitamin B_{12}), and folic acid.

RADIOGRAPHER NOTES

Radiography of patients with various nutritional diseases can be challenging because of the many effects these diseases have on all body systems. Some produce deformities; others can cause mental disorders. Obese patients can present unique problems in positioning and in selection of radiographic settings. The radiographer must be especially empathetic when dealing with these patients, who often are embarrassed because of their size and thus difficult to deal with. The manifestations of systemic lupus erythematosus cause considerable discomfort for patients. Patients with melanoma that has already metastasized or those who are facing extensive surgical intervention are usually very depressed and sometimes require special handling. Patients with muscular dystrophy can be easily agitated and are usually frustrated by their inability to control themselves. Hereditary diseases that cause abnormalities require special understanding on the part of the technologist to attain optimal patient cooperation that will result in good diagnostic radiographs. In general, patients suffering from the various diseases in the miscellaneous category in this chapter can be very demanding and require considerable patience on the part of the radiographer.

Vitamin deficiency diseases are rare in the United States but are prevalent in underdeveloped countries.

Beriberi (Thiamine Deficiency)

Beriberi results from a deficiency in thiamine (vitamin B_1), a coenzyme essential for carbohydrate metabolism that promotes growth and maintains muscle tone and heart function. Beriberi occurs primarily in rice-eating countries, such as China, where the main staple is polished rice from which the vitamin-containing skin and germ have been removed. Infantile beriberi is common in breast-fed infants 2 to 4 months of age whose mothers have **thiamine** deficiency. Noninflammatory degeneration of the myelin sheath caused by thiamine deficiency produces a peripheral neuropathy characterized by weakness of the limbs and a "pins and needles" sensation in the extremities.

Imaging appearance. Initially, peripheral vasodilation in beriberi increases cardiac output, which then produces a generalized enlargement of the cardiac silhouette and increased pulmonary vascular markings. With progression of disease, the myocardium becomes edematous and flabby and cannot function properly, leading to congestive heart failure and generalized edema (Figure 12-1).

Pellagra (Niacin Deficiency)

Pellagra, caused by a deficiency of **niacin** (vitamin B_3), is characterized by reddening and scaling of the skin on exposed parts of the body, vomiting and severe diarrhea, and nervous and mental disorders (ranging from chronic depression to violent, irrational behavior). The body requires niacin to complete the cellular process called *respiration,* in which nutrients and oxygen reach the cells through a series of chemical reactions. As a result of dietary supplements, epidemics of pellagra no longer exist; however, sporadic incidences occur among chronic alcoholics and people suffering from malabsorption.

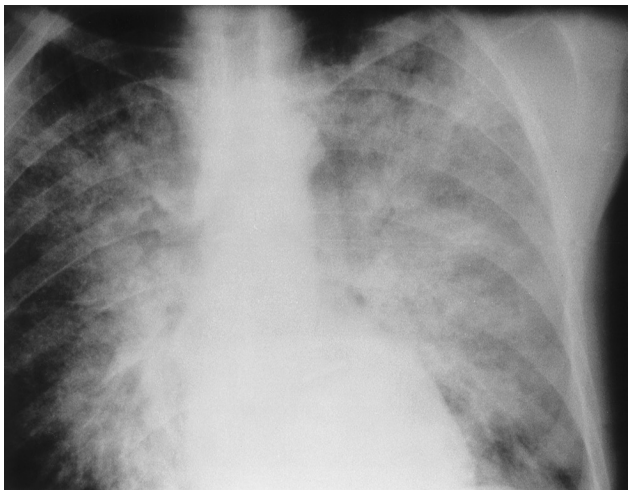

FIGURE 12-1 Beriberi. Diffuse pulmonary edema caused by severe high-output heart failure.

Scurvy (Vitamin C Deficiency)

In patients with scurvy, the deficiency of **ascorbic acid** (vitamin C) leads to an inability of the supporting tissues to produce and maintain vascular endothelium and the cementing substances that hold epithelial cells together (collagen, osteoid, and dentin). Scurvy was classically a disease of sailors and explorers deprived of fresh fruit and vegetables containing vitamin C.

Weakening of capillary walls in scurvy often results in bleeding into the skin, joints, and internal organs. The gums are especially affected and bleed easily. The open lesions provide an entry for bacteria, leading to necrosis of gum tissue and tooth loosening and loss. Impaired synthesis of collagen leads to poor and delayed wound healing.

Imaging appearance. In children, disordered chondroblastic and osteoblastic activity cause radiographic bone changes that are most prevalent where growth is normally most rapid (especially about the knee and wrist). The bones are generally osteoporotic with blurring or disappearance of trabecular markings and severe cortical thinning. Widening and increased density of the zone of provisional calcification produce the characteristic "white line" of scurvy (Figure 12-2). A relatively lucent osteoporotic zone forms on the diaphyseal side of the white line. This osteoporotic zone is easily fractured, permitting the dense bone to become impacted on the shaft and to jut laterally beyond it, thus giving rise to characteristic marginal spur formation (**Pelken spur**). The epiphyseal ossification centers are demineralized and surrounded by dense, sharply demarcated rings of calcification (**Wimberger's sign of scurvy**). If epiphyseal dislocations have not occurred, the appearance of the skeletal structures usually returns to normal after appropriate therapy.

Subperiosteal hemorrhage often occurs along the shafts of the long bones. Calcification of the elevated periosteum and underlying hematoma is a radiographic sign of healing.

Rickets (Vitamin D Deficiency)

Rickets is a bone disease of young children in which a lack of vitamin D leads to decreased absorption of calcium from

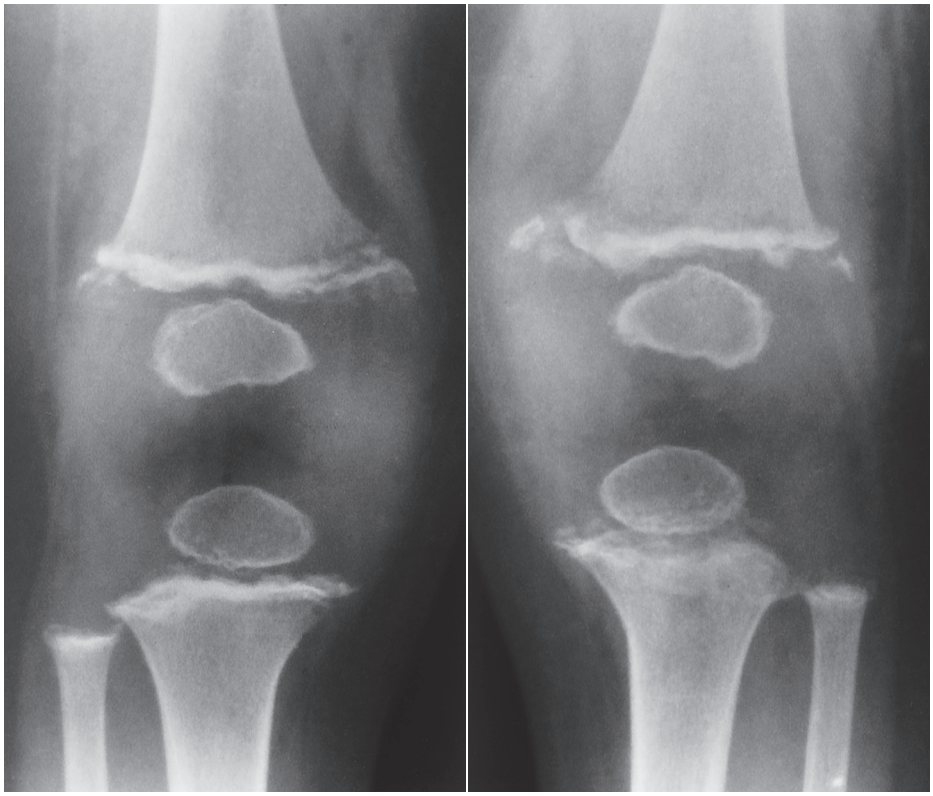

FIGURE 12-2 Scurvy. Frontal projections of both knees demonstrate widening and increased density of the zone of provisional calcification, producing the characteristic "white line" of scurvy. Note also the submetaphyseal zone of lucency and characteristic marginal spur formation (Pelken spur). Epiphyseal ossification centers are surrounded by a dense, sharply demarcated ring of calcification (Wimberger's sign).

the gastrointestinal tract, resulting in weak, deformed bones. In adults, lack of vitamin D causes generalized softening of bones (**osteomalacia**). The radiographic findings of rickets and osteomalacia are found in Chapter 4.

Vitamin A Deficiency

Vitamin A, or retinol, is essential for vision because it is a vital component of the pigment that absorbs light in the rods of the retina. A lack of vitamin A results in night blindness, an inability to see in dim light. Vitamin A also is important for maintaining the integrity of the mucous membranes lining the respiratory, gastrointestinal, and urogenital tracts. A lack of vitamin A makes these membranes dry and susceptible to cracking, permitting infectious organisms to enter the underlying tissues.

Vitamin A is derived from β-carotene, a yellow plant pigment that is converted into vitamin A by the liver. Good sources of vitamin A include dairy products, egg yolks, fish, and vegetables such as carrots, spinach, and sweet potatoes.

Vitamin K Deficiency

Vitamin K, a fat-soluble vitamin, is necessary for the formation of prothrombin, an essential ingredient in the blood-clotting mechanism. It is primarily found in green leafy vegetables. A deficiency of vitamin K results in excessive bleeding.

Treatment of Vitamin Deficiencies

Any of the following three approaches can be used to treat vitamin deficiencies: (1) The patient's diet is modified to include foods that contain the recommended daily requirements, (2) the patient is given synthetic oral supplements, and (3) vitamins are injected. Some deficiencies may be associated with absorption abnormalities resulting from a lack of the specific vitamins needed to absorb and process vitamins.

Dietary modifications for vitamin B deficiencies include increasing the intake of protein (meat), green leafy vegetables, and milk. For vitamin C deficiencies, an increase in consumption of fresh fruits and green leafy vegetables may help. Vitamin D deficiencies require the addition of cod liver oil, egg yolks, butter, and oily fish to the diet. Fortified milk and exposure to sunlight also provide vitamin D. To increase vitamin A, a diet including more liver, meat, eggs, milk, and dark green and yellow vegetables is of value. Eating more spinach, lettuce, broccoli, Brussels sprouts, and cabbage increases dietary vitamin K.

Hypervitaminosis

Long-term excessive intake of vitamin A produces a syndrome characterized by bone and joint pain, hair loss, itching, anorexia, dryness and fissuring of the lips, hepatosplenomegaly, and yellow tinting of the skin. This condition usually affects young children, who become irritable and fail to gain weight.

Imaging appearance. Excess vitamin D causes too much calcium to be absorbed from the gastrointestinal tract. The

resulting hypercalcemia leads to the deposition of calcium in the kidney, heart, lungs, and wall of the stomach (Figure 12-3).

Treatment. Because there is an excess of vitamins, treatment requires a decrease in vitamin intake and monitoring of the patient to ensure that the levels are stable.

Protein–Calorie Malnutrition (Kwashiorkor)

Severe protein–calorie malnutrition (kwashiorkor) affects millions of young children (younger than 5 years) in developing countries (approximately 182 million in 2000) and produces abnormalities involving the gastrointestinal tract and nervous system. In those affected, an imbalance between the body's supply of nutrients and its demand for energy causes a wasting away or emaciation. Fatty replacement of liver tissue and the resulting decreased levels of albumin lead to diffuse edema and ascites and the characteristic clinical appearance of a considerably protuberant abdomen. Damage to the pancreas and intestinal mucosa prevents proper digestion and absorption of nutrients.

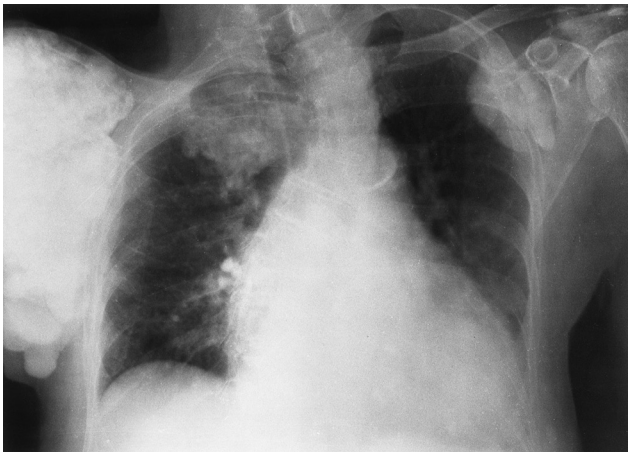

FIGURE 12-3 Hypervitaminosis D. Huge masses of calcification near the shoulder joints bilaterally.

Imaging appearance. Retarded bone growth with thinned cortices usually occurs in protein–calorie malnutrition. Atrophy of the thymus gland and lymphoid tissues diminishes the child's resistance to infection from organisms that enter the body through skin lesions and the damaged mucous membranes of the gastrointestinal tract. Mental development is also impaired, and brain atrophy can be demonstrated radiographically.

Treatment. The initial approach to protein–calorie malnutrition is to correct the child's fluid and electrolyte balance. Milk and supplementary vitamins are added to the diet. The mortality rate, which is 15% to 40%, results from the dangerous fluid imbalance.

Obesity

Obesity refers to an excess of adipose (fatty) tissue that develops when the caloric intake (from food) consistently exceeds the amount of calories required by the body to perform its daily activities. The condition may be related simply to personal habits of excessive eating combined with a lack of activity, or it may be a result of such conditions as hypothyroidism, Cushing's disease, insulinoma, and hypothalamic disorders.

Imaging appearance. Excess adipose tissue can cause displacement of normal abdominal structures, producing such radiographic patterns as widening of the retrogastric (Figure 12-4) and retrorectal spaces. An extreme increase in the intra-abdominal volume causes diffuse elevation of the diaphragm with a relatively transverse position of the heart (simulating cardiomegaly), prominence of pulmonary markings, and atelectatic changes at the lung bases. In the most severe form of obesity (pickwickian syndrome), the excursion of the diaphragm is limited, and the lungs can barely expand with breathing. This results in profound hypoventilation, hypoxia, retention of carbon dioxide, secondary polycythemia, and pulmonary hypertension with right heart failure. An excessive deposition of fatty tissue can also appear radiographically as widening of the mediastinum and prominence of the pericardial fat pads.

FIGURE 12-4 Obesity. Enlargement of the retrogastric space caused by a massive deposition of fatty tissue.

Summary of Findings for Nutritional Diseases

Disorder	Cause	Imaging Appearance	Treatment
Beriberi	Deficiency in vitamin B_1 Decrease in carbohydrate metabolism	Enlarged cardiac silhouette with increased pulmonary markings	
Pellagra	Deficiency in vitamin B_3	Not specific	
Scurvy	Deficiency in vitamin C	Osteoporosis with blurring of trabecular markings and severe cortical thinning Widening and increased density of the zone of provisional calcification, producing a white line	Increased intake by diet modification Increased intake with synthetic supplements Injections of the specific vitamin
Rickets	Deficiency of vitamin D Leads to decrease in absorption of calcium	See "Osteomalacia" in Chapter 4	Increased absorption of vitamin through association with other dietary products
Vitamin A deficiency	Deficiency of vitamin A Visual deficiencies and decreased integrity of mucous membranes	Not specific	
Vitamin K deficiency	Deficiency of vitamin K Decreased prothrombin production	Not specific	
Hypervitaminosis	Usually excessive vitamin A or D	Vitamin A—not specific Vitamin D—hypercalcemia leads to deposition of calcium in the kidney, heart, lungs, and wall of the stomach	Decreased vitamin intake
Protein–calorie malnutrition	Severe protein–calorie deficiency	Retarded bone growth Thinned cortices Brain atrophy	Balance of fluids and electrolytes Provision of milk and supplemental vitamins
Obesity	Excessive adipose tissue—due to caloric intake consistently exceeding calories required	Displacement of anatomic structures Elevated diaphragm Widened mediastinum	Weight management by dieting Nutritional counseling and behavioral therapy Dietary drugs Surgical resection to limit gastric capacity

Treatment. The simplest treatments for obesity include weight management by dieting, use of nutritional counseling and behavioral therapy, and dietary drugs. Patients with morbid obesity may undergo surgical procedures in an attempt to lose large amounts of weight. Gastric restrictive operations attempt to limit gastric capacity and limit gastric outflow, thus making the patient feel full after a small meal. This effect causes the patient to limit his or her oral intake and results in weight control. The major procedure is a gastroplasty, in which a small upper gastric remnant is connected to a larger lower gastric pouch by a narrow channel. Another procedure, gastric banding, is the placement of an adjustable band (accessed by an external port) that can be inflated to control gastric emptying. Complications of gastric restrictive procedures, which can occur in the early and late postoperative periods, include leakage, perforation, widening of the channel, and obstruction.

SYSTEMIC LUPUS ERYTHEMATOSUS

Systemic lupus erythematosus is a connective tissue disorder that affects primarily young or middle-aged women and most likely represents an immune complex disease. The cell activation is thought to be connected to genetic, environmental, and hormonal factors. The presentation and course of the disease are highly variable, from limited skin involvement to tragic systemic disease. Characteristic findings include a butterfly-shaped rash over the nose and cheeks and extreme sensitivity of the skin to sunlight.

Imaging appearance. Pain in multiple muscles and joints is the most frequent clinical complaint in patients with systemic lupus erythematosus. A characteristic finding is subluxations and malalignment of joints in the absence of erosions (Figure 12-5). Cardiopulmonary abnormalities also frequently develop. Pleural effusions, usually bilateral and small but occasionally

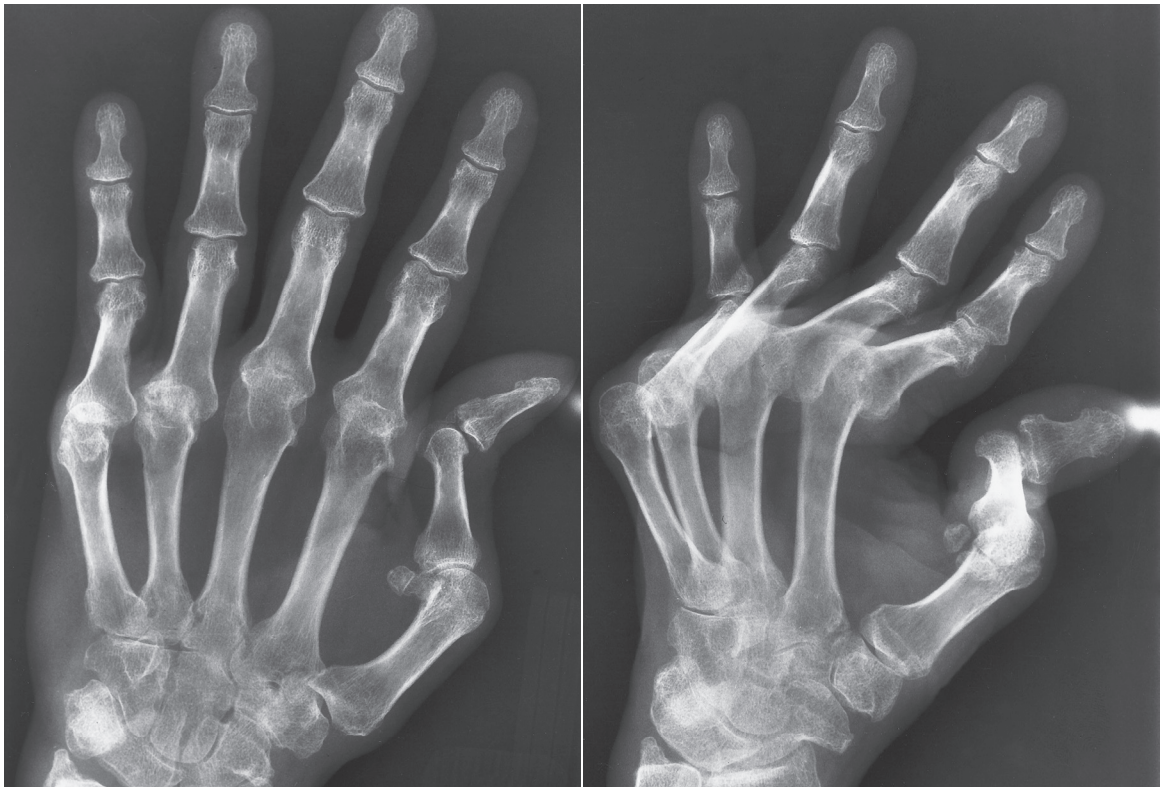

FIGURE 12-5 Systemic lupus erythematosus. Frontal and oblique projections of the hand show subluxation of the phalanges at the metacarpal articulations and hyperextension deformities of the proximal interphalangeal joints. Note the absence of erosive changes.

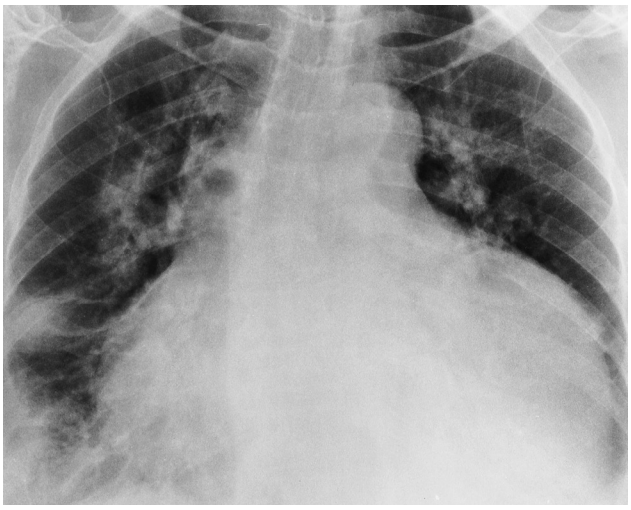

FIGURE 12-6 Systemic lupus erythematosus. Bilateral pleural effusions, more pronounced on the right, with some streaks of basilar atelectasis. Massive cardiomegaly is attributable to a combination of pericarditis and pericardial effusion.

massive, occur in approximately half of patients with the disease (Figure 12-6). Enlargement of the cardiac silhouette is generally the result of pericarditis and pericardial effusion.

Although kidney involvement (often leading to renal failure) is one of the most serious manifestations of systemic lupus erythematosus, no specific urographic findings are seen. Enlargement of the liver, spleen, and lymph nodes occurs in approximately one-fourth of patients. In the gastrointestinal system, a necrotizing inflammation of blood vessels can result in massive bleeding, multiple infarctions, and bowel perforation.

Many of the radiographic manifestations of systemic lupus erythematosus tend to disappear during spontaneous remissions or after steroid therapy.

Treatment. Anti-inflammatory drugs are used to treat pain in the muscles and joints in patients with systemic lupus erythematosus. Systemic corticosteroids help prevent pathologic conditions involving the renal and central nervous system. If skin lesions occur, antimalarial drugs are prescribed.

MELANOMA

Melanoma is an extremely malignant skin cancer that metastasizes widely throughout the body. The tumor develops from a benign mole (nevus), which changes size and color and becomes itchy and sore. The incidence of melanoma is rising, having increased in the United States approximately 2000% since 1930. Globally, cancer statistics from 2002 show that incidences in Australia and New Zealand are approximately six times higher in males and two times higher in females. Although melanoma represents only 4% of all skin cancers, the mortality rate is greater than 70%.

Imaging appearance. Metastases from malignant melanoma frequently involve the gastrointestinal tract, usually sparing the large bowel. They are typically well circumscribed, round, or oval nodules that may develop central

FIGURE 12-7 Metastatic melanoma. Large central ulcerations in two sharply defined filling defects in the small bowel (*arrows*).

necrosis and ulceration; in a barium study, such a nodule appears as a dense, barium-filled central crater surrounded by a sharply marginated nodular mass (bull's-eye, or target, lesion) (Figure 12-7). Gastrointestinal metastases can be the first clinical manifestation of metastatic melanoma; at times, it can be impossible to identify the primary tumor site.

Metastatic melanoma can also produce multiple nodules in the lung and destructive bone lesions with neither new bone formation nor reactive sclerosis.

Treatment. Carefully watching for changes in moles or in the skin and having a biopsy to assess the lesion is the best prevention of melanoma and is highly recommended. Also, continuous protection from the sun may reduce the development of these lesions. Surgical excision of the tumor and surrounding tissue may be all that is required. A lymph node biopsy determines whether chemotherapy is required for metastases. The prognosis depends on the size of the lesion and the results of the lymph node biopsy.

MUSCULAR DYSTROPHY

Muscular dystrophy refers to a group of chronic inherited conditions in which fat replaces muscle, leading to generalized weakness and eventually death due to respiratory muscle failure or pneumonia. Males are more commonly affected because of the X-linked inheritance pattern. Of the many types, the most common is Duchenne's muscular dystrophy (DMD), which has been identified on the *DMD* gene as the Xp21 band. A milder form is Becker's muscular dystrophy.

Imaging appearance. On radiographs of the extremities, the extensive accumulation of fat within the remaining muscle bundles produces a fine striated, or striped, appearance (Figure 12-8). Because most of the muscle tissue is replaced by fat, the fascial sheath bounding the muscles may stand out as a thin shadow or as increased density when it is visualized on edge. Decreased muscular tone can lead to osteoporosis, bone atrophy with cortical thinning, scoliosis, and joint contractures.

Summary of Findings for Miscellaneous Disorders

Disorder	Cause	Imaging Appearance	Treatment
Systemic lupus erythematosus	Immune complex disease (a connective tissue disorder)	Skeletal—subluxations and malalignment of joints Chest—pleural effusions, small and bilateral; cardiac enlargement	Anti-inflammatory drugs for muscle and joint pain Systemic corticosteroids help prevent renal and central nervous system pathology Antimalarial drugs for skin lesions
Melanoma	Widely metastasizing malignant skin cancer	Metastatic involvement of the gastrointestinal tract; round or oval nodules with necrosis and ulceration	Prevention—monitoring for changes in skin and reduction of sun exposure Surgical excision of lesion and surrounding tissue; biopsy needed to determine whether chemotherapy is necessary
Muscular dystrophy	Replacement of muscle by fat	Extremities—fine striated (striped) appearance of remaining muscle bundles	Nonstrenuous exercise to maintain mobility and function Drug therapy to protect muscle mass and function

An abnormal swallowing mechanism in muscular dystrophy can result in the failure to clear barium adequately from the pharynx; this problem may lead to tracheal aspiration and nasal regurgitation of contrast material (or other ingested substances).

Treatment. No curative therapy for muscular dystrophy is known. Gene therapy and cell therapy are currently under investigation as possible treatments. Currently, drug therapy is used to protect muscle mass and function. A regimen of nonstrenuous exercise is recommended to maintain mobility and function for as long as possible.

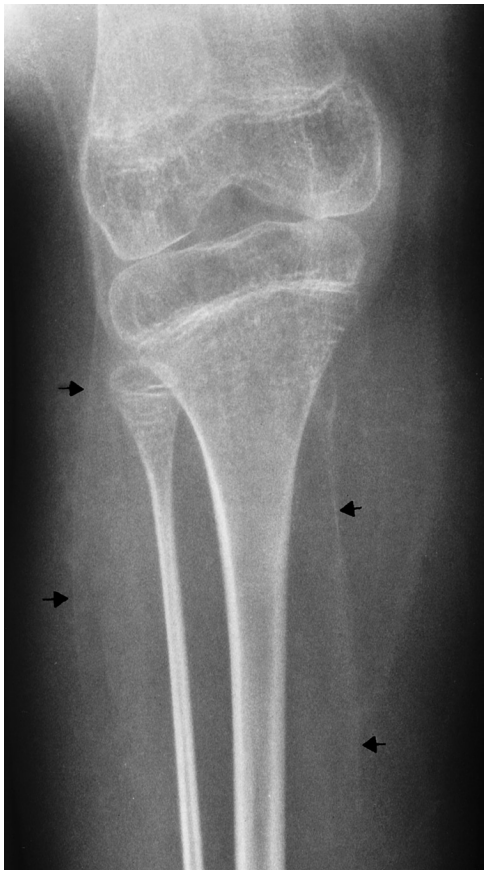

FIGURE 12-8 Muscular dystrophy. Thin, demineralized bones of the lower leg. Increased lucency, representing fatty infiltration in muscle bundles, makes fascial sheaths appear as thin shadows of increased density (*arrows*) surrounded by fat.

HEREDITARY DISEASES

Chromosomal Aberrations

The chromosomes may mutate in many different ways and cause a multitude of disease processes. The following describes chromosomal aberrations in two trisomy disorders (Down syndrome and Klinefelter's syndrome), a monosomy disorder (Turner's syndrome), and an autosomal dominant disorder (Marfan's syndrome). A **syndrome** indicates the presence of a combination of symptoms that commonly occur together and are related to a single cause.

Down Syndrome

Down syndrome, the most common of the trisomy disorders (trisomy 21), is caused by an extra-autosomal chromosome that results in an individual having three strands of chromosome 21 instead of the normal two. Down syndrome is usually diagnosed at birth because of the characteristic clinical appearance: mental deficiency, short stature, poor muscle tone, short neck, and a straight skin crease extending across the palm of the hand. The typical facial appearance includes widely set eyes, a short and flat nose, and a coarse tongue that often protrudes through a partially open mouth.

Congenital heart disease, especially septal defects, occurs in approximately 40% of patients with Down syndrome. There is also a greater-than-normal incidence of duodenal obstruction (duodenal atresia or annular pancreas) and Hirschsprung's disease and a substantially increased likelihood of development of leukemia.

Laboratory tests (chorionic villus sampling [CVS], amniocentesis, and percutaneous umbilical blood sampling [PUBS]) and the age of the mother are used to determine the risk of Down syndrome for prospective parents. Ultrasound (ultrasonography) can provide additional information. Even with these sophisticated tests, false-positive results may occur, and an accurate diagnosis can be made only after birth.

Imaging appearance. The major skeletal abnormality in infancy in a child with Down syndrome is in the pelvis, where there is a decrease in the acetabular and iliac angles with hypoplasia and noticeable lateral flaring of the iliac wings (Figure 12-9). Other common skeletal abnormalities are shortening of the middle phalanx of the fifth finger, squaring of the

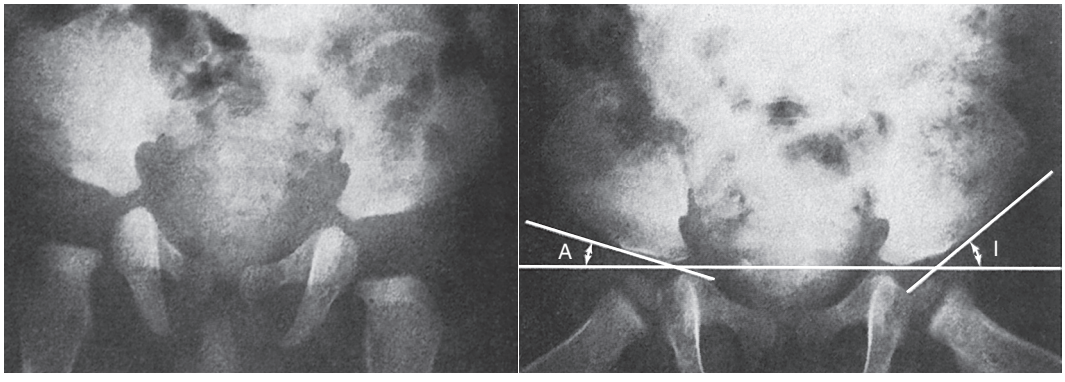

FIGURE 12-9 Down syndrome. Two examples of a typical pelvis in Down syndrome show flared iliac wings and diminished acetabular (A) and iliac (I) angles.

vertebral bodies (superoinferior length becoming equal to or greater than the anteroposterior measurement), hypoplasia of the nasal sinuses, and delayed closure of the cranial sutures.

Treatment. The many different anomalies of Down syndrome require various treatments, which generally provide a better quality of life for the affected person. Experimental dietary supplements (dimethyl sulfoxide [DMSO]–amino acid formula) are believed by some authorities to slow the retardation process, but the U.S. Food and Drug Administration has not approved these drugs.

Klinefelter's Syndrome

Klinefelter's syndrome (**testicular dysgenesis**) is a disorder characterized by small testes that fail to mature and to produce sperm and testosterone. The fundamental defect is the presence in a male of two or more X chromosomes, indicating that this disorder is another sex chromosome trisomy. The pituitary gland sends a signal for the body to produce testosterone, but the testes do not respond. At puberty, the breasts enlarge, and a female distribution of hair develops. The affected individual is tall, mentally deficient (often with language impairment), and sterile.

Imaging appearance. Radiographically, skeletal changes are both less common and less pronounced in Klinefelter's syndrome than in Turner's syndrome, its female counterpart. The metacarpal sign is present in fewer than 25% of the patients. Hypogonadism may lead to delayed epiphyseal fusion and retarded bone maturation.

Treatment. Hormonal therapy provides treatment of the symptoms of Klinefelter's syndrome. When the patient enters puberty, testosterone therapy assists the body in developing normal male attributes (male distribution of hair growth and muscular body type).

Turner's Syndrome

Turner's syndrome (**gonadal dysgenesis**), a sex chromosome monosomy disorder, is characterized by primary amenorrhea (no ovulation or menstruation), sexual infantilism, short stature, and bilateral tiny gonads. Although the patient appears to be female, she has only one X chromosome as a result of faulty cellular division.

Various urinary tract anomalies, especially horseshoe kidney and other types of malrotation, are often seen in patients with gonadal dysgenesis. Coarctation of the aorta is the most common cardiovascular anomaly. Because coarctation of the aorta most often affects men, its appearance in a woman should indicate the possibility of underlying gonadal dysgenesis.

Imaging appearance. A characteristic, but nonspecific, skeletal abnormality in Turner's syndrome is shortening of the fourth metacarpal and sometimes also the fifth metacarpal (Figure 12-10). This produces the *metacarpal sign,* in which a line drawn tangentially to the distal ends of the heads of the fourth and fifth metacarpals passes through the head of the third metacarpal (indicating the disproportionate shortening of the fourth and fifth metacarpals), rather than extending distally to the head of the third metacarpal as in an unaffected person. Skeletal surveys performed serially at specified intervals during adolescence demonstrate changes in bone growth.

Treatment. Patients with Turner's syndrome can receive treatment for their short stature and for gonadal dysfunction. Human growth hormones have been available since 1994. Hormone replacement therapy of progesterone and/or estrogen may be prescribed to treat gonadal dysfunction (lack of ovulation) and to promote female physical attributes (hair distribution and breast growth).

Marfan's Syndrome

Marfan's syndrome is an inherited generalized disorder of connective tissue with ocular, skeletal, and cardiovascular manifestations. Most patients with this autosomal dominant disorder are tall and slender, appearing emaciated because of the decrease in subcutaneous fat. A typical feature of Marfan's syndrome is bilateral dislocation of the lens of the eye caused by weakness of its supporting tissues. A laxity of ligaments about the joints leads to loose-jointedness (or double-jointedness), recurrent dislocations, and flat feet.

Almost all patients with Marfan's syndrome have abnormalities of the cardiovascular system. Necrosis of the medial portion of the aortic wall causes a progressive dilation of the ascending aorta that produces a bulging of the upper right portion of the cardiac silhouette (Figure 12-11) and an unusual prominence of the pulmonary outflow tract as it is displaced by the dilated aorta. Dissecting aneurysm, a serious complication, may kill the patient in early life.

FIGURE 12-10 Turner's syndrome. Frontal projection of a hand shows the short fourth metacarpal.

Summary of Findings for Hereditary Diseases

Disorder	Cause	Imaging Appearance	Treatment
Down syndrome	Extra autosomal chromosome—trisomy 21	Pelvis—decreased acetabular and iliac angles with hypoplasia and lateral flaring of iliac wings	Various treatments to provide a better quality of life
Klinefelter's syndrome (testicular dysgenesis)	Sex chromosome trisomy disorder—male with two or more X chromosomes	Possible delayed epiphyseal fusion and retarded bone maturation	Hormonal therapy
Turner's syndrome (gonadal dysgenesis)	Sex chromosome trisomy disorder—female with one X chromosome	Shortening of the fourth and fifth metacarpals	Growth hormones for stature Hormonal therapy for gonadal dysfunction
Marfan's syndrome	Autosomal dominant disorder of connective tissue	Elongation and thinning of tubular bones (hands and feet), arachnodactyly	No cure

Imaging appearance. The major radiographic abnormality is elongation and thinning of the tubular bones (Figure 12-12), most pronounced in the hands and feet and seen clinically as **arachnodactyly** (spider-like digits). Patients may exhibit **pectus excavatum** (concave sternum) on a lateral chest radiograph (Figure 12-13).

Treatment. Currently, no cure exists for Marfan's syndrome. The laxity of the joints makes affected patients susceptible to scoliosis; monitoring the spine and treating any curvature early help prevent spinal deformities. These patients are vulnerable to endocarditis resulting from dental procedures and commonly receive prophylactic antibiotics.

Genetic Amino Acid Disorders

The genetic amino acid disorders result from the absence of an enzyme required to produce a biochemical reaction that the body requires for normal growth and physiologic function. This genetic defect causes a decrease or an interruption in amino acid metabolism.

Homocystinuria

Homocystinuria, an inborn error of the metabolism of the amino acid methionine, causes a defect in the structure of collagen or elastin. The absence of the enzyme cystathionine B-synthase causes an elevation in methionine by not allowing the metabolic cycle to complete its process. Homocystinuria occurs only if both parents carry the gene (i.e., it is an autosomal recessive trait). Patients with homocystinuria have a tendency to demonstrate arterial and venous thrombosis, and premature occlusive vascular

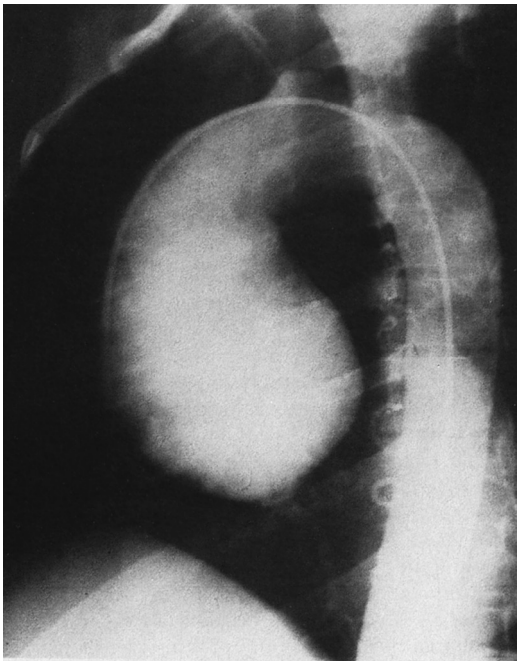

FIGURE 12-11 Marfan's syndrome. Arteriogram shows the enormous dilation of the aneurysmal ascending aorta.

FIGURE 12-12 Arachnodactyly in Marfan's syndrome. Metacarpals and phalanges are unusually long and slender.

disease is the major cause of death. Other common signs are similar to those of Marfan's syndrome (long limbs, arachnodactyly, and scoliosis). Additional symptoms are myopia (nearsightedness), dislocation of the lens of the eye, and mental retardation.

Imaging appearance. The most common and striking radiographic feature of homocystinuria is osteoporosis of the spine, which is often associated with biconcave deformities of the vertebral bodies (Figure 12-14).

Treatment. Because no cure has been found, treatment available consists of a low-methionine diet and increased doses of vitamin B_6 and folic acid or cysteine supplements. Not all patients have found this treatment effective.

Phenylketonuria

Phenylketonuria (PKU) is an inborn error of metabolism in which an enzyme deficiency results in the impaired conversion of phenylalanine to tyrosine. Fortunately, routine screening enables diagnosis of this disease at birth. If the condition is not diagnosed and treated early, the excessive phenylalanine in the blood usually causes the patient to suffer profound retardation (**microcephaly**), hyperactivity, and seizures, all related to brain atrophy. Because of an inadequate amount of tyrosine, there is impaired production of the pigment melanin, and the patient is very light in color.

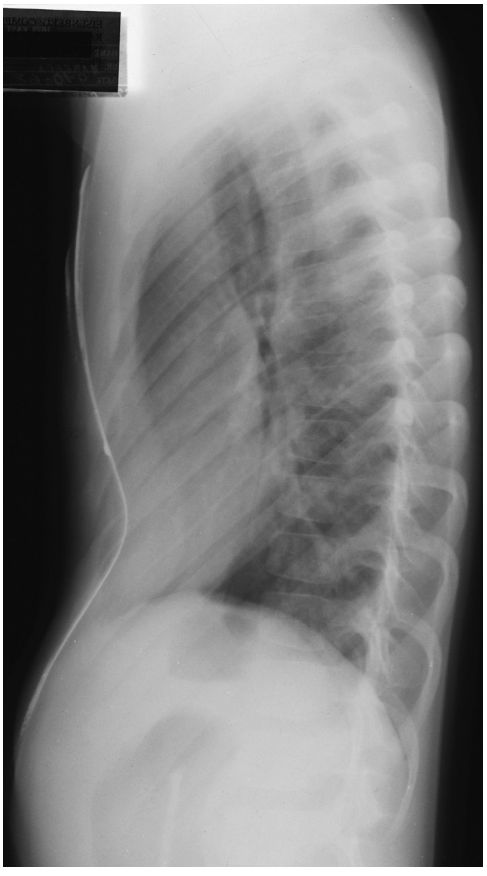

FIGURE 12-13 Pectus excavatum. Lateral chest radiograph demonstrates a concave sternum.

Imaging appearance. The brain atrophy of PKU appears as dilation of the ventricles and sulci on computed tomography (CT) or magnetic resonance imaging (MRI).

Treatment. Treatment of PKU involves a diet low in phenylalanine and protein. Dietary measures can prevent the disease process from progressing if the treatment begins before age 1 year. Treatment instituted later in life will not improve any destructive damage that has already occurred.

Alkaptonuria and Ochronosis

Alkaptonuria is a rare inborn error of metabolism in which an enzyme deficiency leads to an abnormal accumulation of homogentisic acid in the blood and urine. The urine is either very dark on voiding or becomes black after standing or being alkalinized. The disorder often goes unrecognized until middle age, when deposition of the black pigment of oxidized homogentisic acid in cartilage and other connective tissue produces a distinctive form of degenerative arthritis (ochronosis).

Imaging appearance. The pathognomonic radiographic finding in alkaptonuria is dense, laminated calcification in multiple intervertebral disks (Figure 12-15); the calcification begins in the lumbar spine and may extend to involve the dorsal and cervical regions.

Treatment. Medical therapy can inhibit the rate of pigment deposit. A low-protein diet and added vitamin C may retard the accumulation of homogentisic acid in older children and adults.

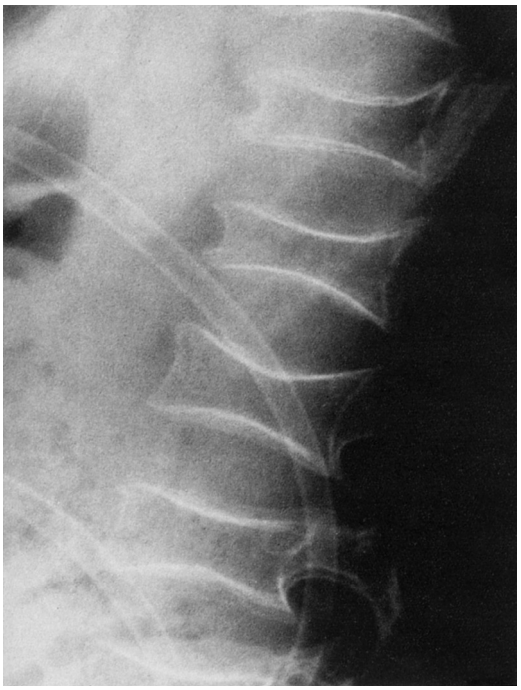

FIGURE 12-14 Homocystinuria. Striking osteoporosis of the spine is associated with biconcave deformities of the vertebral bodies.

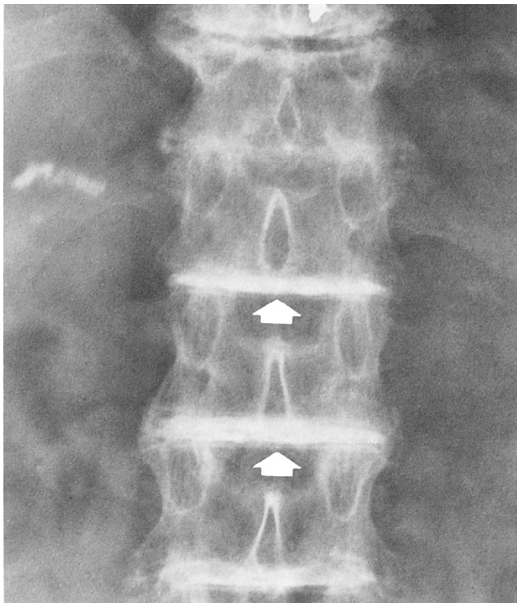

FIGURE 12-15 Ochronosis. Frontal projection of the lumbar spine shows the dense laminated calcification of multiple intervertebral disks (*arrows*).

Cystinuria

Cystinuria is an inborn error of amino acid transport characterized by impaired tubular absorption and excessive urinary excretion of several amino acids. Large amounts of cystine in the urine predispose to the formation of renal, ureteral, and bladder stones. It is common to see multiple and bilateral stones, even large staghorn calculi.

Imaging appearance. Pure cystine stones are not radiopaque and can be demonstrated only on excretory urography, where they appear as filling defects in the urinary tract. Stones containing the calcium salts of cystine appear radiopaque and can be detected on plain abdominal radiographs. Abdominal CT may define the filling defect better than intravenous urography.

Treatment. Currently, there is no cure for cystinuria. However, therapy is available to provide relief from symptoms and to prevent new stones from developing. One approach is to increase water intake to six to eight glasses a day to dilute the increased excretion of cystine in the urine. Thiol drugs may be of value in dissolving the cystine for excretion.

Glycogen Storage Diseases

The glycogen storage diseases are a group of genetic disorders that involve the pathways for the storage of carbohydrates as glycogen (in the liver) and for its use in maintaining blood glucose and providing energy. Normal or abnormal glycogen in an excess amount infiltrates and enlarges multiple organs, especially the heart and liver (Figure 12-16).

Gaucher's Disease

Gaucher's disease is an inborn error of metabolism characterized by the accumulation of abnormal quantities of complex lipids in the reticuloendothelial cells of the spleen, liver, and bone marrow. The adult (chronic) form of Gaucher's disease is most common; some cases arise in children or infants.

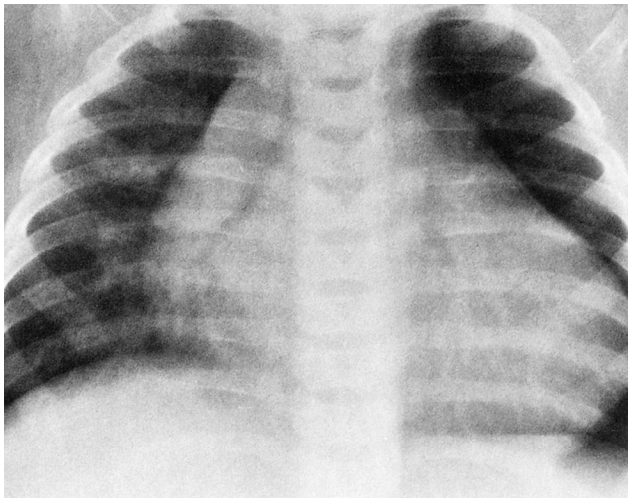

FIGURE 12-16 Glycogen storage disease. Generalized globular cardiac enlargement with left ventricular prominence.

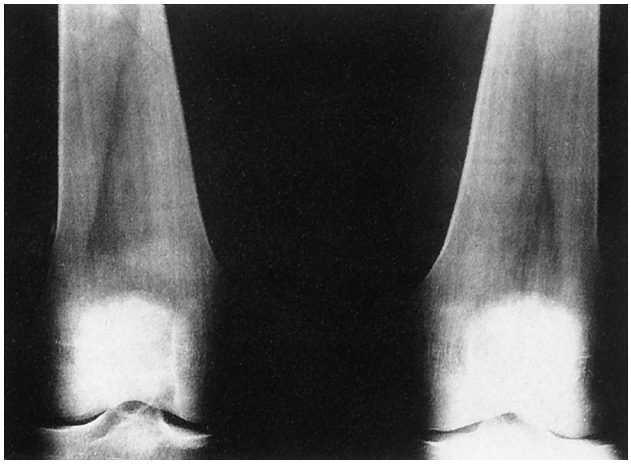

FIGURE 12-17 Gaucher's disease. The distal ends of the femurs show typical marrow infiltration of the distal femur causing abnormal modeling, flaring, and the characteristic (but nonspecific) Erlenmeyer flask deformity.

Aseptic necrosis (especially involving the femoral heads) is a common complication. The spleen is usually greatly enlarged, and hepatomegaly is common.

Imaging appearance. The most striking changes in Gaucher's disease occur in the skeletal system. Infiltration of the bone marrow with abnormal lipid-containing cells causes a loss of bone density with expansion and cortical thickening of the long bones, especially the femur. Marrow infiltration of the distal femur causes abnormal modeling, flaring, and the characteristic (but nonspecific) Erlenmeyer flask deformity (Figure 12-17).

Treatment. In the past, the traditional treatment for Gaucher's disease was splenectomy. Today, new experimental treatments are used in an attempt to inhibit the accumulation of complex lipids. Enzyme replacement is still under investigation, although initial trials have demonstrated reversal of extraskeletal symptoms.

Summary of Findings for Genetic Amino Acid Disorders

Disorder	Cause	Imaging Appearance	Treatment
Homocystinuria	Absence of cystathionine B synthase	Osteoporosis of the spine—biconcave deformities of vertebral bodies	Low methionine diet; increased vitamin B_6 and folic acid or cysteine supplements
Phenylketonuria	Enzyme deficiency leading to excessive phenylalanine	CT or MRI—brain atrophy with dilation of ventricles and sulci	Low phenylalanine and protein diet to control progression
Alkaptonuria/ochronosis	Enzyme deficiency leading to excessive homogentisic acid	Dense laminated calcification of multiple intervertebral disks	Therapy to inhibit rate of deposit
Cystinuria	Error of amino acid transport	CT—defines cystine stones in the urinary tract	No cure—increased water intake to help prevent stone formation Thiol drugs to aid in dissolving the cystine
Gaucher's disease	Abnormal accumulation of complex lipids	Extremity—loss of bone density, with expansion and cortical thickening of long bones	Treatment to inhibit the accumulation of complex lipids Enzyme replacement to reverse extraskeletal symptoms

REVIEW QUESTIONS

1. A vitamin C deficiency that years ago was common among sailors because of their lack of fresh fruit and vegetables is termed _____.
2. _____ is a vitamin deficiency disease that occurs primarily in countries in which polished rice is the main staple.
3. A deficiency of niacin, characterized by reddening and scaling of exposed skin, vomiting, diarrhea, and nervous and mental disorders, is termed _____.
4. Vitamin _____ is necessary in the blood-clotting mechanism.
5. A lack of vitamin _____ can result in night blindness.
6. When caloric intake consistently exceeds the amount needed for the body to function, _____ occurs.
7. A disease of young to middle-aged women that is most likely an immune complex disease, that can affect several systems of the body, and that is characterized by a butterfly-shaped rash across the nose and cheeks is _____.
8. A very malignant form of skin cancer, capable of metastasizing throughout the body, is _____.
9. An inherited muscular disease characterized by severe weakness and eventual death from respiratory muscle failure or pneumonia is _____.
10. The radiographer should be very alert to the possibility of _____ in patients with muscular dystrophy who lack normal swallowing ability.
11. Name three trisomy disorders: _____, _____, and _____.
12. _____ syndrome occurs when a female has only one X chromosome.
13. Arachnodactyly, or spider-like digits, occurs in which two hereditary disorders?

ANSWERS TO REVIEW QUESTIONS

CHAPTER 1

1. edema
2. phagocytosis
3. keloid
4. suppurative
5. ischemia
6. infarct
7. hematoma
8. atrophy
9. neoplasia
10. adenoma
11. epidemiology
12. mortality
13. morbidity
14. personal protective equipment (PPE)
15. transmission-based precautions
16. etiology
17. diagnosis
18. syndrome
19. asymptomatic
20. prognosis

CHAPTER 2

1. location
2. b
3. shape
4. a
5. d
6. b
7. a
8. a
9. c
10. d
11. a
12. a
13. c
14. c
15. c

CHAPTER 3

1. pneumothorax, pneumomediastinum
2. Swan–Ganz
3. superior vena cava
4. generator, electrodes
5. infarction
6. In AP and PA radiographs, the tip may *appear* to be in the proper position, but a lateral view is needed to ensure that the tip is in the anterior portion of the right ventricle—the correct position.
7. hyaline membrane disease
8. cystic fibrosis
9. croup
10. epiglottitis
11. alveolar pneumonia
12. lung abscess
13. bronchography
14. emphysema
15. silicosis, asbestosis, anthracosis
16. sarcoidosis
17. pulmonary arteriovenous fistula
18. tension pneumothorax
19. empyema
20. pneumonia
21. histoplasmosis, coccidioidomycosis
22. coughing, droplets
23. pneumothorax
24. emphysema
25. pneumoconiosis
26. mesothelioma
27. septic embolism
28. atelectasis
29. larger and more vertical mainstem bronchi
30. subcutaneous emphysema
31. c
32. mediastinal emphysema (pneumomediastinum)
33. c

CHAPTER 4

1. b
2. a
3. d
4. d
5. b
6. transitional vertebra
7. increase
8. b
9. a
10. b
11. c
12. c
13. a
14. d
15. b
16. d
17. c
18. d
19. b
20. c
21. b
22. d
23. b
24. c

25. a
26. c
27. d
28. d
29. a
30. b
31. b

CHAPTER 5

1. b
2. c
3. a
4. b
5. c
6. a
7. b
8. d
9. c
10. c
11. c
12. b
13. b
14. d
15. d
16. a
17. b
18. a
19. d
20. c
21. c
22. b
23. b
24. d
25. b
26. c
27. a
28. d
29. b
30. a

CHAPTER 6

1. d
2. d
3. b
4. a
5. c
6. d
7. c
8. a
9. c
10. a
11. b
12. a, c, e
13. urinary calculi, strictures of normal narrowing (UVJ and UPJ), ureterocele
14. hydroureter
15. polycystic kidney disease

CHAPTER 7

1. d
2. a
3. b
4. d
5. d
6. c
7. b
8. d
9. a
10. a
11. c
12. c
13. a
14. b
15. a
16. c
17. b
18. c
19. b
20. b
21. b
22. b
23. d
24. d

CHAPTER 8

1. c
2. c
3. b
4. d
5. d
6. b
7. a
8. c
9. b
10. c
11. CT
12. CT, MRI
13. transient ischemic attack
14. MRI
15. epilepsy
16. Alzheimer's disease
17. Parkinson's disease
18. horizontal, erect
19. hydrocephalus
20. cross-table lateral, horizontal

CHAPTER 9

1. c
2. a

3. c
4. b
5. b
6. c
7. c
8. c
9. a
10. c
11. b
12. b

CHAPTER 10

1. c
2. c
3. a
4. b
5. b
6. c
7. b
8. b
9. c
10. b
11. d
12. b
13. c
14. b
15. b
16. b
17. b
18. a
19. c
20. b
21. d

CHAPTER 11

1. nonionizing imaging source, high-frequency sound waves
2. hysterosalpingography, mammography
3. spermatogenesis
4. testosterone
5. vasectomy
6. cancer of the prostate
7. ultrasound
8. true
9. ivory vertebra
10. ultrasound
11. testicular torsion
12. testicular, lymphatic
13. ovulation
14. ectopic
15. hysterosalpingography
16. syphilis
17. dermoid/teratoma
18. fibroids
19. breast
20. carcinoma of the cervix

CHAPTER 12

1. scurvy
2. beriberi
3. pellagra
4. K
5. A
6. obesity
7. systemic lupus erythematosus
8. melanoma
9. muscular dystrophy
10. aspiration
11. Down syndrome, Turner's syndrome, Klinefelter's syndrome
12. Turner's
13. Marfan's syndrome, homocystinuria

ILLUSTRATION CREDITS

CHAPTER 1

Figure 1-6 from Bryk D et al: Kaposi's sarcoma of the intestinal tract: roentgen manifestations, *Gastrointest Radiol* 3:425, 1978.

CHAPTER 3

Figures 3-1 and 3-2 from Thibodeau GA, Patton KT: *Anatomy and physiology*, ed 7, St. Louis, 2010, Mosby.

Figures 3-4 and 3-8 from Dunbar RD: Radiologic appearance of compromised thoracic catheters, tubes, and wires, *Radiol Clin North Am* 22:699-722, 1984.

Figures 3-5, 3-7, 3-9 from Eisenberg RL: *Diagnostic imaging in internal medicine,* New York, 1985, McGraw-Hill.

Figure 3-10 from Swischuk LE: *Radiology of the newborn and young infant,* Baltimore, 1980, Williams & Wilkins.

Figure 3-14 from Podgore JK, Bass JW: *J Pediatr* 88:154-155, 1976.

Figures 3-18, 3-35, and 3-82 from Eisenberg R: *Atlas of signs in radiology,* Philadelphia, 1984, Lippincott.

Figures 3-41 and 3-68 from Fraser RG, Paré JAP: *Diagnosis of diseases of the chest,* Philadelphia, 1979, Saunders.

Figure 3-42 from Eisenberg R: *Atlas of signs in radiology,* Philadelphia, 1984, Lippincott.

Figure 3-62 from Lee JKT, Sagel SS, Stanley RJ, editors: *Computed body tomography,* New York, 1989, Raven Press.

Figure 3-80 from Cappitanio MA et al: *Radiology* 103: 460-461, 1972.

Figure 3-91 from Vix VA: *Semin Roentgenol* 12:277-286, 1977.

Figure 3-92 from Eisenberg RL: *Diagnostic imaging in surgery,* New York, 1987, McGraw-Hill.

CHAPTER 4

Figure 4-1 from Thibodeau GA, Patton KT: *Anatomy and physiology*, ed 7, St. Louis, 2010, Mosby.

Figure 4-14 from Brown JC, Forrester DM: Arthritis. In Eisenberg RL, Amberg JR, editors: *Critical diagnostic pathways in radiology,* Philadelphia, 1981, Lippincott.

Figure 4-27 from Forrester DM, Brown JC, Nesson JW: *The radiology of joint disease,* Philadelphia, 1978, Saunders.

Figures 4-29 and 4-35 from Rumack C, Wilson S, Charboneau JW, editors: *Diagnostic ultrasound,* ed 2, St Louis, 1998, Mosby.

Figure 4-31 from Greenspan A: *Orthopedic radiology,* Philadelphia, 1988, Lippincott.

Figure 4-56 from Eisenberg RL: *Diagnostic imaging in internal medicine,* New York, 1985, McGraw-Hill.

Figure 4-57 from Eisenberg RL: *Gastrointestinal radiology: a pattern approach,* Philadelphia, 1990, Lippincott.

Figure 4-71 from deSantos LA, Bernardino ME, Murray JA: Computed tomography in the evaluation of osteosarcoma: experience with 25 cases, *AJR Am J Roentgenol* 132:535-540, 1979.

Figures 4-72 and 4-86A from Stark DD, Bradley WG Jr: *Magnetic resonance imaging,* ed 2, St. Louis, 1991, Mosby.

Figures 4-87 and 4-123 from Eisenberg R: *Diagnostic imaging in surgery,* New York, 1987, McGraw-Hill.

Figure 4-99 from Sty JR, Starshak RJ: The role of bone scintigraphy in the evaluation of the suspected abused child, *Radiology* 146:369-375, 1983.

Figure 4-102 from Silverman FN: *Caffey's pediatric x-ray imaging,* St. Louis, 1985, Mosby.

Figure 4-110 from Bassett LW, Gold RH, Epstein HC: Anterior hip dislocation: atypical superolateral displacement of the femoral head, *AJR Am J Roentgenol* 141:385-386, 1983.

Figure 4-115 from Osborn AG: Head trauma. In Eisenberg RL, Amberg JR, editors: *Critical diagnostic pathways in radiology,* Philadelphia, 1981, Lippincott.

CHAPTER 5

Figures 5-1 and 5-2 from Thibodeau GA, Patton KT: *Anatomy and physiology*, ed 6, St. Louis, 2007.

Figure 5-3 and 5-4 from Thibodeau GA, Patton KT: *Anatomy and physiology*, ed 7, St. Louis, 2010, Mosby.

Figures 5-18, 5-19, 5-20, 5-24, 5-25, and 5-92 from Eisenberg RL: *Gastrointestinal radiology: a pattern approach,* Philadelphia, 1990, Lippincott.

Figure 5-31 from Rumack C, Wilson S, Charboneau JW, editors: *Diagnostic ultrasound,* ed 4, St. Louis, 2010, Mosby.

Figure 5-35 from Margulis AR, Burhenne JH, editors: *Alimentary tract radiology,* ed 4, St. Louis, 1989, Mosby.

Figure 5-45 from Rumack C, Wilson S, Charboneau JW, editors: *Diagnostic ultrasound,* ed 3, St. Louis, 2004, Mosby.

Figure 5-52 from Jeffrey RB: *CT and sonography of the acute abdomen,* New York, 1989, Raven Press.

Figure 5-61 from Rice RP et al: *Radiographics* 4:393-409, 1984.

Figure 5-73 from Caroline DF, Evers K: Colitis: radiographic features and differentiation of idiopathic inflammatory bowel disease, *Radiol Clin North Am* 25:47-66, 1987.

Figure 5-74 from Lichtenstein JE: Radiologic-pathologic correlation of inflammatory bowel disease, *Radiol Clin North Am* 25:3-23, 1987.

Figure 5-79 from Butch RJ: In Taveras JM, Ferruci JT, editors: *Radiology: diagnosis, imaging, intervention,* Philadelphia, 1987, Lippincott.

Figure 5-101 from Jeffrey RB, Federle MP, Laing FC: Computed tomography of mesenteric involvement in fulminant pancreatitis, *Radiology* 147:185-192, 1983.

Figure 5-108 from Federle MP, Goldberg HL: In Moss AA, Gamsu G, Genant HK, editors: *Computed tomography of the body,* Philadelphia, 1992, Saunders.

Figure 5-115 from Koehler RE: Spleen. In Lee JKT, Sagel SS, Stanley RJ, editors: *Computed body tomography,* New York, 1983, Raven Press.

CHAPTER 6

Figure 6-1 from Thibodeau GA, Patton KT: *Anatomy and physiology,* ed 7, St. Louis, 2010, Mosby.

Figure 6-2 from Brundage DJ: *Renal disorders*, St. Louis, 1992, Mosby.

Figure 6-3 from Thibodeau GA, Patton KT: *Anatomy and physiology*, ed 7, St. Louis, 2010, Mosby.

Figure 6-14 from Friedland GW et al: *Clin Radiol* 27:367-373, 1976.

Figures 6-18 and 6-19 from Tonkin AK, Witten DM: Genitourinary tuberculosis, *Semin Roentgenol* 14:305-318, 1979.

Figure 6-25 from Eisenberg R: *Gastrointestinal radiology: a pattern approach,* Philadelphia, 1990, Lippincott.

Figure 6-39 from Bosniak MA, Ambos MA: Polycystic kidney disease, *Semin Roentgenol* 10:133-143, 1975.

Figure 6-44 from Bosniak MA, Faegenburg D: *Radiology* 84:692-698, 1965.

Figure 6-47 from McClennan BL, Lee JKT: Kidney. In Lee JKT, Sagel SS, Stanley RJ, editors: *Computed body tomography,* New York, 1983, Raven Press.

Figure 6-49 and 6-55 from Friedland GW et al, editors: *Uroradiology: an integrated approach,* New York, 1983, Churchill Livingstone.

Figure 6-52 from Merten DE, Kirks DR: In Eisenberg RL, editor: *Diagnostic imaging: an algorithmic approach,* Philadelphia, 1988, Lippincott.

Figure 6-57 from Cohn LH et al: The treatment of bilateral renal vein thrombosis and nephrotic syndrome, *Surgery* 64:387-396, 1968.

CHAPTER 7

Figures 7-1 and 7-2 from Thibodeau GA, Patton KT: *Anatomy and physiology*, ed 6, St. Louis, 2007, Mosby.

Figure 7-3 from Thibodeau GA, Patton KT: *Anatomy and physiology*, ed 7, St. Louis, 2010, Mosby.

Figures 7-5, 7-6, and 7-7 from Cooley RN, Schreiber MH: *Radiology of the heart and great vessels,* Baltimore, 1978, Williams & Wilkins.

Figure 7-8 from Rumack et al: *Diagnostic ultrasound,* ed 3, vol 2, St. Louis, 2005, Mosby.

Figure 7-10 from Swischuk LE: *Plain film interpretation in congenital heart disease,* Baltimore, 1979, Williams & Wilkins.

Figure 7-13 from Schoepf UJ, Becker BM, et al. CT of coronary artery disease, *Radiology* 2004; 232: 18-37.

Figure 7-14 from Stark DD, Bradley WG, editors: *Magnetic resonance imaging,* St. Louis, 1988, Mosby.

Figure 7-17 from Fischell TA, Block PC: *Cardiovasc Reviews Reports* 6:89-99, 1985.

Figure 7-22 from Fraser RG, Pare JAP: *Diagnosis of diseases of the chest,* Philadelphia, 1979, Saunders.

Figure 7-26 from Burko H et al: In Eisenberg RL, Amberg JR, editors: *Critical diagnostic pathways in radiology: an algorithmic approach,* Philadelphia, 1981, Lippincott.

Figure 7-29 from Waltman AC: In Athanasoulis CA et al, editors: *Interventional radiology,* Philadelphia, 1982, Saunders.

Figure 7-32 from Eisenberg R: *Gastrointestinal radiology: a pattern approach,* Philadelphia, 1990, Lippincott.

Figure 7-34 from Thoeni RF, Margulis AR: In Eisenberg RL, editor: *Diagnostic imaging: an algorithmic approach,* Philadelphia, 1988, Lippincott.

Figure 7-36 from Fisher RG, Hadlock FP, Ben-Menachem Y: *Radiol Clin North Am* 19:91-112, 1981.

Figure 7-37 from Woodring JH, Pulmano CM, Stevens RK: The right paratracheal stripe in blunt chest trauma, *Radiology* 143:605-608, 1982.

Figure 7-40 from Ovenfors CO, Godwin JD: In Eisenberg RL, editor: *Diagnostic imaging: an algorithmic approach,* Philadelphia, 1988, Lippincott.

Figure 7-45 from Waltman AC: In Athanasoulis CA et al, editors: *Interventional radiology,* Philadelphia, 1982, Saunders.

Figure 7-47 from Katzen BT, van Breda A: Low dose streptokinase in the treatment of arterial occlusions, *AJR Am J Roentgenol* 136:1171-1178, 1981.

Figure 7-50 from Vickers SCW et al: *Radiology* 72:569-575, 1959.

Figure 7-60 from Miller SW, Gillian LD: In Eisenberg RL, editor: *Diagnostic Imaging: An algorithmic approach*, Philadelphia, 1988, Lippincott.

Figure 7-61 from Holden RW, Mail JT, Becker GJ: In Eisenberg RL, editor: *Diagnostic imaging: an algorithmic approach,* Philadelphia, 1988, Lippincott.

CHAPTER 8

Figure 8-1 from Thibodeau GA, Patton KT: *Anatomy and physiology*, ed 7, St. Louis, 2010, Elsevier.

Figure 8-2 courtesy of Vidic B, Suarez F: *Photographic atlas for the human body*, St. Louis, 1984, Mosby in Thibodeau GA, Patton KT: *Anatomy and physiology*, ed 7, St. Louis, 2010, Elsevier.

Figure 8-3 from Thibodeau GA, Patton KT: *Anatomy and physiology*, ed 7, St. Louis, 2010, Elsevier.

Figure 8-4 from Ross MR, Davis DO, Mark AS: *MRI Decisions* 4:24-33, 1990.

Figure 8-5 from Edelman RR, Hesselink JR, editors: *Clinical magnetic resonance imaging,* Philadelphia, 1990, Saunders.

Figures 8-7, 8-8, and 8-75 from Stark DD, Bradley WG: *Magnetic resonance imaging,* ed 2, St. Louis, 1991, Mosby.

Figures 8-20 and 8-24 from Williams AL, Haughton VM: *Cranial computed tomography,* St. Louis, 1985, Mosby.

Figures 8-26 and 8-77 from Eisenberg RL: *Clinical imaging: an atlas of differential diagnosis,* Gaithersburg, Md, 1992, Aspen.

Figure 8-28B from Levine HL, Kleefield J, Rao KCVG: In Lee SH, Rao KCVG, editors: *Cranial computed tomography,* New York, 1983, McGraw-Hill.

Figure 8-29 from Bilaniuk LT: Adult infratentorial tumors, *Semin Roentgenol* 25:155-173, 1990.
Figures 8-34A and 8-39 from Pressman BD: In Eisenberg RL, editor: *Diagnostic imaging: an algorithmic approach,* Philadelphia, 1988, Lippincott.
Figure 8-41 from Eisenberg RL: *Diagnostic imaging in surgery,* New York, 1987, McGraw-Hill.
Figures 8-46 and 8-48 from Dolan K, Jacoby C, Smoker W: *Radiographics* 4:576-663, 1984.
Figure 8-47 from Rogers LF: *Radiology of skeletal trauma,* New York, 1982, Churchill Livingstone.
Figure 8-58 from Drayer BP: Neuroradiology. In Rosenberg RN, Heinz ER, editors: *The clinical neurosciences,* New York, 1984, Churchill Livingstone.
Figure 8-65 from Bronen RA: Epilepsy: the role of MR imaging, *AJR Am J Roentgenol* 159:1165-1174, 1992.
Figure 8-73 from Johnson CE, Zimmerman RD: *MRI Decisions* 3:2-16, 1989.

CHAPTER 9

Figures 9-1 and 9-2 and Unnumbered Figure 9-1 from Thibodeau GA, Patton KT: *Anatomy and physiology*, ed 7, St. Louis, 2010, Elsevier.
Figure 9-5 from Leight TF: *Radiol Clin North Am* 1:377-393, 1963.
Figure 9-8 from Moseley JE: *Semin Roentgenol* 9:169-184, 1984.
Figure 9-25 from Stoker DJ, Murray RO: Skeletal changes in hemophilia and other bleeding disorders, *Semin Roentgenol* 9:185-193, 1974.

CHAPTER 10

Figure 10-1 from Thibodeau GA, Patton KT: *Anatomy and physiology*, ed 7, St. Louis, 2010, Elsevier.
Figure 10-3 from Lee JKT, Sagel SS, Stanley RJ, editors: *Computed body tomography,* New York, 1983, Raven Press.
Figures 10-5 and 10-6 from Karstaedt N et al: Computed tomography of the adrenal gland, *Radiology* 129:723-730, 1978.
Figure 10-9 and 10-14 from Stark DD, Bradley WG: *Magnetic resonance imaging,* ed 2, St. Louis, 1991, Mosby.
Figure 10-13 from Welch TJ et al: Pheochromocytoma: value of computed tomography, *Radiology* 148:501-503, 1983.
Figure 10-15 from Eisenberg RL: *Diagnostic imaging in surgery,* New York, 1987, McGraw-Hill.
Figure 10-17 from Friedland GW et al: *Uroradiology: an integrated approach,* New York, 1983, Churchill Livingstone.
Figure 10-19 from Thibodeau GA, Patton KT: *Anatomy and physiology*, ed 6, St. Louis, 2007, Mosby.
Figure 10-24 from Jacob S in Thibodeau GA, Patton KT: *Anatomy and physiology*, ed 6, St. Louis, 2007, Mosby.
Figure 10-26 from Palmer EL, Scott JA, Strauss HW: *Practical nuclear medicine,* Philadelphia, 1992, Saunders.
Figure 10-45 from Stark DD et al: Parathyroid scanning by computed tomography, *Radiology* 148:297-303, 1983.

CHAPTER 11

Figure 11-5 from Russinovich NA et al: Balloon dilatation of urethral strictures, *Urol Radiol* 2:33-37, 1980.
Figure 11-6 from Thibodeau GA, Patton KT: *Anatomy and physiology*, ed 7, St. Louis, 2010, Mosby.
Figure 11-9 from McCarthy S, Fritzsche PJ: In Stark DD, Bradley WG, editors: *Magnetic resonance imaging,* St. Louis, 1988, Mosby.
Figure 11-13 from Thoeni RF: In Moss AA, Gamsu G, Genant HK, editors: *Computed tomography of the body,* Philadelphia, 1983, Saunders.
Figure 11-16 from Jeffrey RB: In Moss AA, Gamsu G, Genant HK, editors: *Computed tomography of the body,* Philadelphia, 1983, Saunders.
Figure 11-17 from Fritzsche PJ, et al: Undescended testis: value of MR imaging, *Radiology* 164:169-173, 1987.
Figures 11-23, 11-24, 11-48, 11-51, 11-70, 11-71, 11-73A, 11-76, and 11-78 from Rumack CM, Wilson SR, Charboneau JW: *Diagnostic ultrasound,* St. Louis, 1998, Mosby.
Figure 11-25 from Baker LL et al: MR imaging of the scrotum: pathologic conditions, *Radiology* 163:93-98, 1987.
Figures 11-27 and 11-58 from Thibodeau GA, Patton KT: *Anatomy and physiology*, ed 6, St. Louis, 2007, Mosby.
Figures 11-30, 11-45, 11-53, 11-55, and 11-79 from Callen PW, editor: *Ultrasonography in obstetrics and gynecology,* Philadelphia, 1983, Saunders.
Figure 11-31 from Yune HY et al: Hysterosalpingography in infertility, *Am J Roentgenol Radium Ther Nucl Med* 122:642-651, 1974.
Figure 11-35 from Eisenberg RL: *Diagnostic imaging in surgery,* New York, 1987, McGraw-Hill.
Figure 11-38 from Lee JKT, Sagel SS, Stanley RJ, editors: *Computed body tomography,* New York, 1983, Raven Press.
Figure 11-41 from Eisenberg R: *Atlas of signs in radiology,* Philadelphia, 1984, Lippincott.
Figures 11-50, 11-56, and 11-57 from Lupetin AR: In Stark DD, Bradley WG, editors: *Magnetic resonance imaging,* St. Louis, 1988, Mosby.
Figure 11-52 from Gedgaudas RK, et al: The value of the preoperative barium-enema examination in the assessment of pelvic masses, *Radiology* 146:609-616, 1983.
Figure 11-54 from Gross BH et al: Computed tomography of gynecologic diseases, *AJR Am J Roentgenol* 141:765-773, 1983.
Figure 11-64 from Hagen-Ansert S: *Textbook of diagnostic ultrasound,* St. Louis, 2001, Mosby.
Figure 11-75 from Pasto ME, Kurtz AM: *Semin Ultrasound CT MR* 5:170-193, 1984.

CHAPTER 12

Figure 12-2 from Eisenberg R: *Atlas of signs in radiology,* Philadelphia, 1984, Lippincott.
Figure 12-5 from Brown JC, Forrester DM: In Eisenberg RL, Amberg JR, editors: *Critical diagnostic pathways in radiology: an algorithmic approach,* Philadelphia, 1981, Lippincott.

Figure 12-9 from James AE Jr et al: Radiological features of the most common autosomal disorders: trisomy 21-22 (mongolism or Down's syndrome), trisomy 18, trisomy 13-15, and the cri du chat syndrome, *Clin Radiol* 22:417-433, 1971.

Figure 12-11 from Ovenfors CO, Godwin JD: In Eisenberg RL, Amberg JR, editors: *Critical diagnostic pathways in radiology: an algorithmic approach,* Philadelphia, 1981, Lippincott.

Figure 12-14 from Thomas PS, Carson NA: Homocystinuria. The evolution of skeletal changes in relation to treatment, *Ann Radiol* 21:95-104, 1978.

Figure 12-17 from Levin B: Gaucher's disease: Clinical and roentgenologic manifestations, *AJR Am J Roentgenol* 85:685-696, 1961.

APPENDIX A

Prefixes/Suffixes/Roots

Prefix/Suffix/Root	Meaning	Example
a-, ab-	away from	abduction
a-, an-	without, not	asymmetric, anencephalic
ad-	toward	adduction
-algia	pain	arthralgia
ana-	up, back again	anaplastic
ante-	before, in front of	antecubital
anti-, ant-	against, antibody	antitoxin
auto-	self	autoimmune
bi-	two	bilateral, bidirectional
-blast	budding	osteoblast
cardi-	heart	cardiology, cardiac; pericardium
caudal	tail	caudal
cephal-	head	cephalic; hydrocephaly
chondro-	cartilage	chondroma, chondrosarcoma
-clast	destroyer, breaker	osteoclast
contra-	opposite	contralateral
crani-	skull	cranium, cranial
cyano-	dark blue	cyanotic
cyto-	cell	cytoplasm; erythrocyte, leukocyte
-dactyl-	finger, toe	polydactyly, arachnodactyly
deci-	tenth	decimal
derm-	skin	dermatology; epidermis
dys-	bad, difficult	dysplasia, dysuria
ecto-	outside of	ectoderm, ectopic
endo-, ento-	within	endoderm, endometrium
erythr-	red	erythrocyte
gastr-	stomach	gastric
-genic	causing	carcinogenic, pathogenic
gyn-, gyneco-	woman	gynecology
hem-, haem-	blood	hemorrhage, hemolytic
hemi-	half	hemisphere, hemidiaphragm
hetero-	different	heterogeneous
homo-	same	homogeneous
hyper-	over, excessive	hyperthyroidism, hypertension, hyperintense
hypo-	under, too little	hypothyroidism, hypotension, hypointense
iatro-	healer, healing	iatrogenic; psychiatry
infra-	below	infratemporal
intra-	within	intramural, intradermal
ipsi-	same	ipsilateral
iso-	equal	isointense
-itis	inflammation	appendicitis, diverticulitis
juxta-	near, next to	juxta-articular
kilo-	thousand	kilogram
leuko-, leuco-	white	leukocyte, leukemia
lipo-	fat	lipoma, liposarcoma
-lysis, -lytic	dissolve	lytic, osteolytic

Prefix/Suffix/Root	Meaning	Example
macro-	large	macroadenoma
magn-	great, large	magnify, magnum (foramen)
mal-	bad, ill	malunion, malalignment
mega-, megalo-	large	megadose
melan-	black	melanoma, melanin
micro-	small	microscope, microadenoma, microcirculation
milli-	thousandth	milligram, milliliter
mono-	one	monostotic, monoclonal
multi-	many	multilocular, multifaceted
myelo-	marrow	myelogram; osteomyelitis
myo-	muscle	myoma, myositis
necro-	dead	necrosis
neo-	new	neovascularity, neoplasm
non-	not	nonunion, nonviable
ocul-	eye	ocular, oculomotor (nerve)
oligo-	few	oligemia
-ology	study of	radiology, pathology
onco-	tumor	oncology
ophthalm-	eye	ophthalmology
-osis	condition of	diverticulosis
osteo-	bone	osteomyelitis, osteosarcoma
pan-	all	pansinusitis, pancytopenia
par-, para-	beside	para-aortic, paravertebral
patho-	disease	pathology; adenopathy
peri-	around	periarticular, periventricular, pericardium
plasm-, plast-	shape, form	neoplasm; anaplastic
pleur-	rib, side	pleural, pleurisy
pneumo-	air, breath	pneumothorax, pneumonia
poly-	many	polycystic, polyostotic
post-	after, later, behind	post-traumatic, postsurgical, postoperative
pre-	before, in front of	premenstrual, prepontine
pseudo-	false	pseudotumor, pseudopolyp
psych-	mind, spirit	psychiatry, psychology
re-	again, anew	reoperate, recalcify
retro-	backward, behind	retroperitoneum
-rrhea	flow, gush	diarrhea
schizo-	split	schizophrenia
sclero-	hard	sclerotic, atherosclerosis
semi-	half	semicircular
sub-	under, below	suborbital, subphrenic, subhepatic
super-, supra-	above; more than	suprarenal, supraorbital
syn-, sym-	with, together	synthesis, symmetric
tachy-	fast	tachycardia
techn-	art, skill	technology, technique
terti-	third	tertiary
tetra-	four	tetralogy (of Fallot)
thermo-	heat	thermometer
tomo-, -tome	cut	tomography; microtome
trans-	across	transverse (colon), transvenous (pacer)
tri-	three	trimalleolar, trisomy
ultra-	beyond	ultrasound
uni-	one	unilateral

Laboratory Values and Their Significance

Laboratory Values	Significance of Laboratory Values
↑ Acid phosphatase	Prostate cancer, metastatic to bone
↑ Alkaline phosphatase	Liver disease, Paget's disease, bone tumor
↑ Amylase	Pancreatitis
↑ Bilirubin	Liver disease
↑ Blood urea nitrogen (BUN)	Liver disease
↑ Calcium	Hyperparathyroidism, bone destruction
↑ Cholesterol	Tendency toward atherosclerosis
↑ Creatinine	Kidney disease
↑ Creatinine phosphokinase (CPK)	Myocardial infarction, pulmonary infarction
↑ Glucose	Diabetes mellitus, Cushing's syndrome, glucagon-secreting pancreatic tumor
↑ Lactic dehydrogenase (LDH)	Myocardial infarction, pulmonary infarction, liver disease
↑ Serum glutamic-oxaloacetic transaminase (SGOT)	Liver disease
↑ Serum glutamic-pyruvic transaminase (SGPT)	Myocardial infarction, liver disease
↑ Total protein	Dehydration, immunoglobinopathy
↑ Uric acid	Gout, antidiuretic therapy
↓ Calcium	Hypoparathyroidism, malabsorption, osteomalacia/rickets
↓ Glucose	Insulin-secreting pancreatic tumor, liver disease, hypopituitarism
↓ Total protein	Chronic liver disease, malnutrition, nephrotic syndrome

GLOSSARY

A

aberration Deviation from normal

abscess Encapsulated collection of pus

achalasia Failure of the lower esophageal sphincter to relax because of absence or destruction of cells in the myenteric nerve plexus, which results in difficulty swallowing

acid–base balance Stable concentration in body fluids

acinus Cluster of alveoli

acquired immunodeficiency syndrome (AIDS) Impairment of cellular immunity

acromegaly Gradual marked enlargement and thickening of the bones of the face and jaw

active immunity A person forms antibodies to counteract an antigen in the form of a vaccine or a toxoid

adenocarcinoma Malignancies of glandular tissue

adenoma Benign epithelial neoplasm that grows in a glandlike structure

adenopathy Enlargement of the lymphatic glands

adnexal Pertaining to the uterine appendages (ovaries, fallopian tubes, and ligaments)

adult respiratory distress syndrome (ARDS) Severe pulmonary congestion due to diffuse injury to the alveolar–capillary membrane

afferent To carry toward the center

agenesis Absence of an organ

alcoholic gastritis Inflammation of the stomach lining caused by alcohol

alveolar, or air-space, pneumonia Inflammatory exudates that replace air and cause the affected lung to become solid

amorphous Without shape or definite form

anaphylactic Reactions are characterized by hypotension and vascular collapse (shock) with urticaria (hives), bronchiolar spasm, and laryngeal edema

anaplastic Without form

androgens Any steroid hormone that increases male characteristics

anechoic Not producing internal echoes (on ultrasound)

anemia Decreased hemoglobin in the blood below normal levels

aneurysmal bone cyst Consists of numerous blood-filled arteriovenous communications

angioma Tumor composed of blood vessels

angulation Indicates an angular deformity between the axes of the major fracture fragments

ankylosing spondylitis Chronic inflammation affecting the spine

ankylosis Immobility and consolidation of a joint caused by disease, injury, or surgical procedure

annihilation Interaction produces two high-energy photons (gamma rays) in opposite directions (separated by 180 degrees)

antibodies Body's counteraction to control antigens

anticoagulant Substance that suppresses or delays coagulation of the blood

antigens Body's ability to recognize foreign substances

aortic valve Valve between the left ventricle and aorta

aplasia Lack of normal development resulting in a small size or developmental failure resulting in the absence of an organ or tissue

appositional growth Flat bones growth in size by the addition of osseous tissue to their outer surfaces

arachnodactyly Congenital condition of long, thin, spider-like fingers and toes

arachnoid membrane Middle meningeal covering

arachnoid villa Projections of fibrous tissue from the arachnoid membrane

arteriovenous malformation Abnormal communication between an artery and a vein

ascites Accumulation of fluid in the abdominal cavity

ascorbic acid Vitamin C

aseptic necrosis Cystic and sclerotic degeneration due to injury, not infection

asthma Widespread narrowing of the airways as a result of exposure to stimuli

astrocytoma Primary tumor of the brain composed of astrocytes

asymptomatic A patient showing no evidence of diseases

atresia Congenital absence or closure of a normal body orifice or tubular organ

atrial septal defect Congenital anomaly resulting in an opening between the atria

atrophy Diminished size due to wasting away

autonomic nervous system Regulates involuntary body functions

autosomes All chromosomes except gender

avulsion fracture Small fragments torn from bony prominences

B

bacteremia Bacteria spread through the circulatory system

bacterial (phlegmonous) gastritis Inflammation of the stomach lining caused by a bacterial infection

bacterial meningitis Infection of the membranes covering the brain and spinal cord caused by bacteria

basal ganglia Islands of gray matter largely composed of cell bodies

basophil Granulocyte white blood cell

Bence Jones protein Abnormal protein typically found in the blood of patients with multiple myeloma

benign Tumors that closely resemble their cells of origin in structure and function and remain localized

blowout fracture Break in the floor of the orbit

bone islands Solitary, sharply demarcated areas of dense compact bone

bougienage Passage of an instrument through a tubular structure to increase its caliber (as in the treatment of a stricture of the esophagus)

bowing fracture Plastic deformation caused by a stress

Bowman's capsule Cup-shaped end of renal tubule

boxer's fracture Fracture of the neck of the fifth metatarsal with a dorsal angulation

bronchial adenomas Neoplastic growth of glandular structures in the bronchi

bronchiectasis Chronic dilatation of the bronchi or bronchioles

bronchioalveolar carcinoma Adenocarcinoma of epithelial cells projecting into the alveolar spaces

bronchiolar (alveolar cell) carcinoma Malignant neoplastic growth of the bronchioli spreading into the alveolar spaces

bronchogenic carcinoma Primary malignancy arising from the mucosa of the bronchial tree

bullae Large air-containing space

butterfly fragment Elongated triangular fragment of cortical bone generally detached from two other larger fragments of bone

C

cachexia Ill health and malnutrition marked by weakness and emaciation that is usually associated with severe disease processes

callus New bone tissue that reunites the parts of a fracture

cancellous bone Spongy bone of the medullary cavity and bony trabeculae

cancer Collectively malignant tumors

carcinoma Malignant neoplasm of epithelial cell origins

caseation Form of necrosis in which the tissue is changed into a dry, amorphous mass resembling cheese

catamenial Pertaining to menstruation

cavitation Formation of cavities, as in pulmonary tuberculosis or neoplasm

centesis Puncture and aspiration

central nervous system (CNS) Consisting of the brain and spinal cord

cerebellum Posterior portion of the brain located behind the brainstem

cerebrovascular disease Any process that is caused by an abnormality of the blood vessels or blood supply to the brain

cerebrum Left and right larger superior portion of the brain

cervical rib An extra rib that articulates with a cervical vertebra

chest physiotherapy Chest percussions (tapping) to keep lung secretions moving

chondroblastic Forming cartilaginous tissue

chondrosarcoma Malignant tumor of cartilaginous origin

chordae tendineae Thin cords that connect each cusp of the two atrioventricular valves to papillary muscles in the heart ventricles

chorion Important fetal membrane for exchange of nutrients
choroids plexus Tangled mass of tine blood vessels within the ventricles that produce cerebrospinal fluid
chromophobe adenomas Pituitary tumor of nonstaining cells (acid or basic dyes)
chronic bronchitis Excessive tracheobronchial mucus production leading to the obstruction of small airways
chyme Gastric contents that have become mixed with hydrochloric acid and the proteolytic enzyme pepsin, resulting in a milky white product
clay shoveler's fracture An avulsion fracture of a spinous process in the lower cervical or upper thoracic spine
closed fracture Fracture that does not disrupt the skin
coagulation factors Responsible for the process of blood clotting
coalesce To merge into a single mass
coeur en sabot Appearance resembling the curved-toe portion of a wooden shoe
colic Intermittent abdominal pain whose fluctuation corresponds to smooth muscle peristalsis
collaterals Blood vessels that develop or enlarge to provide an alternative route around an obstruction
collecting tubule Funnels urine into the papillary ducts in the renal pelvis
Colles' fracture Transverse fracture of the distal radial metaphysic proximal to the wrist with a dorsal displacement of the distal fragment
collimator Containing multiple parallel channels to allow the rays to pass
colonic ileus Selective or disproportionate gaseous distention of the large bowel without an obstruction
comminuted fracture Composed of more than two fragments
communicating hydrocephalus Increased cerebrospinal fluid involving the entire ventricular system and subarchnoid space
community-acquired Infected by exposure in the public domain
compact bone Outer layer consists of which to the naked eye appears dense and structureless
complete fracture Discontinuity between two or more fragments
complete fusion Occurs in the kidneys and produces a single irregular mass that has no resemblance to a renal structure
compound fracture Overlying skin is disrupted with tissue destruction
compression fracture Compaction of bone trabeculae and results in decreased bone length or width
computed tomography Produces cross-sectional tomographic images by first scanning a slice of tissue from multiple angles with a narrow x-ray beam
congenital Existing at birth
congenital syphilis The baby of an infected mother may be born with this form of syphilis
congenital tracheoesophageal (TE) fistulas Result from the failure of a satisfactory esophageal lumen to develop completely separate from the trachea
conjunctivitis Inflammation of the delicate membrane that lines the eyelids and covers the exposed surface of the sclera (white part) of the eye
constipation Extra water is absorbed from the fecal mass to produce a hardened stool
contracture Shortening or shrinkage of a muscle or tendon resulting in persistent flexion or distortion at a joint
corpus callosum Mass of white matter connecting the two cerebral hemispheres
corpus luteum Anatomic structure on the ovary surface
corrosive gastritis Inflammation of the stomach caused by corrosive agents
cortex Outer portion of a bone or internal organ (kidney, adrenal gland, and brain)
crossed ectopic Ectopic kidney located on the same side as the normal kidney
CT number Attenuation of a specific tissue relative to that of water
curvilinear Having a curved configuration
cyst Saclike structure usually filled with fluid
cystadenoma Benign tumor forming a large cystic mass
cytology Microscopic examination to determine cell structure

D

deglutition Swallowing
demarcate To set or mark the limits of
de novo From the beginning; anew
depressed fracture Portions of the fracture fragments driven inward, such as the skull or tibial plateau
diagnosis The precise disease process affecting the patient
diaphysis Shaft of a long bone
diarrhea Results from increased motility of the small bowel, which floods the colon with an excessive amount of water that cannot be completely absorbed
diarrheogenic islet cell tumors Produce the WDHA syndrome
diastatic fracture Linear fracture intersecting a suture and courses along it to cause sutural separation
diastole Heart relaxation phase when blood enters the heart
diencephalon Lies between the cerebrum and the midbrain and consists of the third ventricle, thalamus, and hypothalamus
diffusion imaging Relies on the movement of molecules and random thermal motion
dilation and curettage Dilation of the cervix to allow the scraping of the uterine wall
diploic space Loose osseous tissue between the two tables of the skull
direct fusion Equipment designed to image two modalities simultaneously and integrate the images
dislocation Displacement of a bone no longer in contact with its normal articulation
displacement Separation of bone fragments
dissection Separation of layers
dominant Genes that always produce an effect
duplication (duplex kidney) A common anomaly that may vary from a simple bifid pelvis to a completely double pelvis ureter and ureterovesical orifice
dura mater Tough outermost meningeal covering
dysarthria Difficulty speaking
dysphagia Difficulty swallowing
dysplasia Disordered growth or faulty development of various tissues or body parts
dyspnea Shortness of breath

E

echogenic Producing a relatively strong reflection in ultrasound
ectopic Abnormally positioned
ectopic kidney Abnormally positioned kidneys that may be found in various locations, from the true pelvis (pelvic kidney) to above the diaphragm (intrathoracic kidney)
ectopic pacemaker Initiates abnormal heartbeats
ectopic pregnancy Implantation occurring in the fallopian tube or pelvic cavity
edema Accumulation of abnormal amounts of fluid in the intercellular tissue spaces or body cavities
effaced Wiped out or obliterated
efferent To carry away from the center or part
effusion Accumulation of fluid
Eisenmenger's syndrome Ventricular septal defect associated with pulmonary hypertension and cyanosis resulting from right-to-left shunting
electrolyte Element or compound that dissociates in fluid into ions
electrolyte balance Equilibrium of electrolytes in the body
embolus Any foreign matter, such as a blood clot or an air bubble, carried in the bloodstream
emphysema Pathologic accumulation of air in tissues or organs (especially as applied to a disease of the lungs)
empyema Accumulation of pus in a cavity
emulsifier Substance that acts like soap by dispersing the fat into very small droplets that permit it to mix with water
endemic Present in a particular country, nation, or region
endogenous Originating from within the body
endosteum Inner membrane lining the medullary cavity of a bone
en face Face to face, looking at
engorgement Congestion of a blood vessel or tissue with blood or other fluid
eosinophils Granulocytic bilobed leukocyte
ependymoma Tumor arising from the wall of the fourth ventricle, especially in children, and the lateral ventricles in adults
epidemiology A study of determinants that is compiled for a specific disease in a given population upon determining the type of neoplastic involvement
epididymis Tightly coiled tube enclosed in a fibrous casing in which final maturation of the sperm occurs

epiphrenic diverticula Outpouching found in the distal 10 cm of the esophagus
epiphyseal cartilage Cartilaginous plate separating the epiphysis from the diaphysis
epiphyses End of a long bone that at first is separated from the main part by cartilage but later fuses with it by ossification
erythrocytes Red blood cells
erythropoietin Protein serving as the humoral regulator of red blood cell formation
estrogen Hormonal steroid compound that promotes secondary sex characteristics in female development
etiology The study of disease causes (*not* a synonym for *cause*)
eventration Diaphragmatic—elevation of the diaphragm; abdominal—protrusion of the bowel or removal of abdominal viscera
exacerbation Increase in the severity of a disease or any of its symptoms
exenteration Removal of all organs to debulk a tumor
exogenous Arising from outside the body
exophthalmos Abnormal protrusion of the eyeball
external fixation Accomplished by the use of casts and splints
external reduction Fracture is manipulated without surgical incision
extramedullary hematopoiesis Formation of red blood cells outside the bone marrow
extrinsic asthma Environmental allergens
exudate Material (fluid, cells, or cellular debris) that has escaped from blood vessels and has been deposited in tissues or on tissue surfaces, usually as a result of inflammation

F

fat-soluble vitamins Include vitamins A, D, E, and K and can be stored within body tissues
fat-suppressed images Requires "saturation or full magnetization" on the T1 sequence to ensure a large contrast difference between fat and water
fecalith Intestinal stone formed around a center of fecal material
fibrin Essential portion of a blood clot
fibrinolysis Breaking up of a blood clot
fibromuscular dysplasia Arterial disorder characterized by intramural folds of fibrous endothelial tissue
fissures Deep grooves divide each cerebral hemisphere into lobes
fistula Abnormal connection, usually between two internal organs or from an internal organ to the surface of the body
focal Localized
follicular carcinoma Neoplasm with a follicular arrangement of cells
functional MR (fMR) Allows the localization of specific regions of the brain that correspond to various functions
fundoplication Taking tucks in the fundus of the stomach and distal esophagus
fusiform Spindle-shaped
fusiform aneurysm Bulging of the entire circumference of the vessel wall

G

Galeazzi fracture Combination fracture of the shaft of the radius with a posterior dislocation of the ulna
gamma camera A sodium iodide crystal detects the ionizing radiation emitted from the patient
giant cell tumor (osteoclastoma) Frequently occurring at the end of a long bone as a mass surrounded by a thin shell of new periosteal bone
gigantism Excessive size and stature
glioblastomas Neoplasm consisting of embryonic epithelial cells developing around the neural tube, transforming to supportive connective tissue of the nerve cells or ventricle lining
gliomas Largest group of primary brain tumors, composed of malignant glial cells
glomerulus Tuft or cluster
glucocorticoid Regulate carbohydrate metabolism and is regulated by the adrenocorticotropic hormone
glycogen Excess glucose absorbed is stored as
gonadal dysgenesis Variety of conditions related to abnormal development of the gonads
grading Assessment of malignant tumor to determine the degree of aggressiveness or malignancy
Gram's method Technique for staining microorganisms (i.e., Gram stain)
grand mal seizure Epileptic seizure characterized by generalized involuntary muscular contractions and cessation of respiration that precedes tonic and clonic spasms of the muscles
granulation tissue Combination of young developing capillaries and actively proliferating fibroblasts producing connective tissue fibers
granuloma Tumor-like mass of tissue caused by a chronic inflammatory process
greenstick fracture Incomplete fracture of one cortex
gyri Winding convolutions of the cerebral hemispheres

H

hangman's fracture Fracture of the arch of C2 anterior to the inferior facet; associated with anterior subluxation of C2 and C3
Heberden's nodes Small, hard nodules at the distal interphalangeal joints of the fingers produced by calcific spurs of the articular cartilage and associated with osteoarthritis
helical Spiral continuous motion
hematogenous spread Travels by means of the bloodstream
hematoma Hemorrhage trapped in body tissues
hemiparesis Weakness of one side of the body
hemiplegia Paralysis on one side of the body
hemodynamic Pertaining to the movements involved in the circulation of the blood
hemoglobin Complex protein–iron compound in the blood that carries oxygen
hemoptysis Coughing up blood or blood-stained sputum
hemorrhage Rupture of a blood vessel
hepatitis Inflammatory disease of the liver
hereditary Transmitted to offspring through genes
heterogeneous Composed of materials that have different structures or qualities
histology Microscopic examination to determine tissue structure
homogeneous Composed of material of similar or identical structure or quality
horseshoe kidney Fusion of the lower poles of the kidneys
hydrocephalus Enlargement of the head resulting from an abnormal increase in fluid within the ventricular system
hydronephrosis Distention of the pelvis and calyces of the kidney
hydrosalpinx Fallopian tube cystically enlarged filled with clear fluid
hydroureter Dilatation of the ureter
hyperactive Increased activity
hyperechoic A term used to make comparisons of echo intensities between adjacent structures
hyperglycemia Greater amount of glucose than normal in the blood
hyperlucency Overly black appearance on a radiograph
hypernephroma Most common renal cell carcinoma
hyperplasia Abnormal increase in the number of cells composing a tissue or organ
hypertension High blood pressure
hypoactive Decreased activity
hypocalciuria Abnormally low calcium in the urine
hypoplastic kidney Underdeveloped kidney
hypotension Low blood pressure
hypothalamus Activates, controls, and integrates peripheral autonomic nervous system, endocrine system, and somatic functions
hypoxia Deficiency (lack) of oxygen

I

iatrogenic Resulting from the activity of diagnosis or treatment by medical personnel
idiopathic Having an unknown cause for underlying disease
immune Reaction of the body provides a powerful defense against invading organisms
incomplete fracture Opposite cortex is intact
incontinence Loss of urinary bladder control
indolent Causing little or no pain; slow to heal
infarct Localized area of ischemic necrosis within a tissue or organ produced by occlusion of either its arterial supply or its venous drainage
infarction Death of tissue because of interruption of the normal blood supply
infectious gastritis Inflammation of the stomach lining caused by a microorganism
infiltrating Spreading into surrounding tissue
inflammation Initial response of body tissue to local injury
infundibulum Funnel-shaped organ or passage
inguinal Pertaining to the groin

insidious Developing in a slow or unapparent manner; more dangerous than seems evident (e.g., an insidious disease)
in situ Confined to the site of origin
insufficiency Less than the normal amount
insulinoma Hormone-secreting neoplasm most frequently in the tail of the pancreas, usually benign
integrated imaging Requires software to fuse to imaging modalities
internal fixation Surgically placed metal plates and screws, wires, rods, or nails to maintain reduction
interstitial pneumonia Inflammatory process predominantly involving the walls and lining of the alveoli, its septa, and interstitial supporting structures
intima Innermost layer of an organ or blood vessel
intraluminal Within the empty space (lumen) of a hollow viscus
intramembranous ossification Bone formation from connective tissue
intramural Within the wall of an organ
intrathoracic kidney Kidney located in the thoracic cavity
intrinsic Belonging to the real nature of a thing
intrinsic asthma Reaction to exercise, heat or cold exposure, and emotional upset
intrinsic rhythm Specialized pacemaker cells in the sinoatrial node that initiate impulses at regular intervals
ipsilateral Relating to the same side (antonym: contralateral)
irritable bowel syndrome Refers to several conditions that have an alteration in intestinal motility
ischemia Lack of blood supply in an organ or tissue
islands of Langerhans Another name for islets of Langerhans
isoechoic A term used to describe two structures that have the same echogenicity even though the tissue may not be the same

J

Jefferson fracture Comminuted fracture of the ring of the atlas involving both anterior and posterior arches
Jones fracture Transverse fracture at the base of the fifth metatarsal
juxta-articular Adjacent to a joint

K

kyphosis Anterior convexity in the curvature of the thoracic spine, sacrum, and coccyx, as viewed from the side

L

left-to-right shunt Diversion of blood from the left side of the heart to the right through a septal defect
leukocytes White blood cells
leukocytosis Abnormal amount of white blood cells in the blood
linear skull fracture Jagged or irregular sharp lucent line
lipoma Tumor composed of fat
localized ileus Isolated distended loop of small or large bowel
loop of Henle U-shaped portion of the renal tubule
lordosis Anterior concavity in the curvature of the lumbar and cervical spine, as viewed from the side
lymphangitic Spread by means of the lymphatic system
lymphatic leukemia Malignancy of the lymph nodes in which the lymphocytes are the only white blood cells to increase
lymphatic spread The major metastatic route of carcinomas, especially those of the lung and breast
lymphoma Neoplastic disorder of lymphoid tissue
lytic Destructive

M

magnetic resonance imaging (MRI) A strong magnet producing radiofrequencies at specified intervals and receives a return signal to produce an image
malabsorption disorder Multitude of conditions in which there is defective absorption in the small bowel
malaise Vague feeling of physical discomfort or uneasiness, as early in an illness
malignant Neoplasm that invades and destroys adjacent structures and spreads to distant sites
Mallory–Weiss syndrome Subsequent inflammation of the distal esophagus due to a laceration associated with bleeding and mediastinal penetration caused by severe retching and vomiting
mandibular fractures The angle of the mandible is the most common site of fracture, although fractures can involve any portion of the body and the condylar and coronoid processes
marrow Hollow, tube-like structure within the diaphysis
mast cell Connective tissue containing large basophilic granules containing heparin, serotonin, bradykinin, and histamine, which are released in response to injury or infection
mastication Chewing
matrix Basic material from which a substance (e.g., tissue) develops
medulla Inner substance of a bone (bone marrow) or an internal organ (kidney, adrenal gland)
medullary carcinoma Soft malignant neoplasm of the epithelium that contains little or no fibrous tissue
medullary cavity Hollow, tube-like structure within the diaphysis
medulloblastoma Poorly differentiated malignancy consisting of tightly packed spongioblastic and neuroblastic cells
megahertz (MHz) One million waves per second
menarche Commencement of the cyclic menstrual function
meninges Three membranes covering the brain and spinal cord
meningitis Inflammation of the coverings of the brain and spinal cord
meningocele Protrusion of the meninges through the skin
menopause Cessation of the menstrual cycle
menstrual phase Menstruation occurs, the final phase of the three
mesentery Peritoneal folds that attach the small and large bowel to the back wall of the peritoneal cavity
mesothelioma Tumor that develops from the surface of the pleura, pericardium, or peritoneum
metaphysis Wider part at the end of the shaft of a long bone, adjacent to the epiphyseal plate; located between the epiphysis and the diaphysis
metastasis Spread of disease to another organ or tissue in the body
metastasize To spread by metastasis
microcephaly Abnormal small head in relation to the body with associated underdevelopment of the brain
micturate Act of urinating
midbrain Major portion of the brainstem between the forebrain and hindbrain
mineralocorticoids Regulate salt and water balance by controlling sodium retention and potassium excretion by the kidneys
mitral valve Bicuspid valve situated between the left atrium and ventricle
monoclonal immunoglobulin Antibodies that are formed against a specific cell type
monocytes Large mononuclear leukocytes
Monteggia fracture Isolated fracture of the shaft of the ulna associated with anterior dislocation of the radius at the elbow
morbidity The rate that an illness or abnormality occurs
Morgagni hernia Protrusion of abdominal contents into the anterior and lateral aspects of the thoracic cavity
morphologic Pertaining to the form and structure of an organ
mortality The statistically expected death rate calculated by reviewing the population involved
multilocular Having many cells or compartments
multiple myeloma Bone marrow malignancy
mural thrombosis Thrombus originating in the vessel or cavity wall
mutations Alterations in the DNA structure that may become permanent hereditary changes
mycoplasma Colloquial usage for any of a genus of tiny microorganisms, smaller than bacteria but larger than viruses, that appear to be the causative agents of many diseases
mycosis Fungal infection
myelin sheath Insulated by a fatty covering
myelocytic leukemia Unregulated production of leukocytes
myelomeningocele Herniation of the spinal cord and meninges through the skin
myocardial infarction (MI) Infarction of the heart muscle (heart attack)
myxedema Puffy thickening of the skin with slowing down of physical and mental activity caused by failure of the thyroid gland

N

nasal bone fractures The most common facial fractures
navicular The most common fractures involving the carpal bones
necrosis Death of tissue
necrotic Dead or decayed
neoplasia Any new and abnormal growth, especially when the growth is uncontrolled and progressive
neoplasm Any new and abnormal growth, especially when the growth is uncontrolled and progressive
nephrocalcinosis Calcium deposits within the substance of the kidney
neurogenic Originating in the nervous system
neuron Basic nerve cell
neutrophils Polymorphonuclear granular leukocyte
niacin Vitamin B_3
nidus Focal point, especially of a stone or an inflammatory process
noncommunicating (obstructive) hydrocephalus Obstruction of cerebrospinal fluid flow in the ventricular system causing enlarged ventricles
normal-pressure hydrocephalus Defective resorption of cerebrospinal fluid or an overproduction of cerebrospinal fluid causing ventricular enlargement
nosocomial Incidences of infections being developed at the acute care facility
nuclear medicine Using radiopharmaceuticals to produce ionizing radiation that is detected by a gamma camera to produce an image
nutritional deficiency In addition to inadequate intake, may be related to disorders of the liver, pancreas, and gastrointestinal tract that result in an inability of the body to digest and properly use proteins, carbohydrates, and lipids

O

oblique fracture Runs a course of approximately 45 degrees to the long axis of the bone
octreotide Radioactive peptide tracer; a long-acting analog of the hormone somatostatin
oligemia Decreased blood volume
oligodendrocytoma Slow-growing glioma, usually arising in the cerebrum
oligohydramnios Very small volume of amniotic fluid
oncology The study of neoplasms
open fracture Overlying skin is disrupted
open reduction Surgical procedure utilizing direct or indirect manipulation of the fracture
ossification Bone formation
osteoblastic Forming bony tissue
osteoblasts Produce new bone around the outer circumference from the periosteum
osteoclastic Bone resorption
osteoclasts Enlarge the diameter of the medullary cavity by removing bone from the diaphysis walls
osteogenic sarcoma Malignant tumor composed of osteoblasts that produce osteoids and spicules of calcified bone
osteolytic Destroying bone
osteomalacia Insufficient mineralization of the adult skeleton
osteomas Tumor composed of bone tissue
ovulation Release of the ovum from the ovary

P

palpitations Rapid or fluttering beating of the heart, of which one is aware
pancreatitis An inflammatory process in which protein- and lipid-digesting enzymes become activated within the pancreas and begin to digest the organ itself
papillary carcinoma Slow-growing cystic thyroid carcinoma
paradoxical Seeming to contradict the known facts
parathormone (PTH) Secreted by the parathyroids and regulates the blood levels of calcium and phosphate
parenchyma Essential tissue of an organ
patent ductus arteriosus Abnormal connection between the pulmonary artery and aorta due to lack of the fetal ductus arteriosus
pathognomonic Especially distinctive or characteristic of a disease or pathologic condition
pathologic fracture Occurs when the bone weakens due to another process such as a tumor, infection, or metabolic disease
pectus excavatum Funnel chest: depressed sternum
pedunculated Having a stalk (pedicle)
Pelken's spur Marginal spur formation
pelvic kidney Kidney located in the pelvis
pericardium Membrane surrounding the heart
periosteum Fibrous membrane covering the outer surface
peripheral Outside or away from the central portion of a structure
peripheral nervous system Motor and sensory nerves
peristalsis Wormlike movement by which the alimentary canal or other tubular organ propels its contents
permeable Membrane allowing fluids to pass through
permeative Diffusely spreading through or penetrating a substance, tissue, or organ, as by a disease process such as cancer
pernicious anemia Progressive megaloblastic anemia that results from lack of intrinsic factor that is required for absorption of the vitamin B_{12}
petit mal The mildest type of epilepsy, which occurs primarily in children
petit mal seizure Characterized by sudden, momentary loss of consciousness
pia mater Innermost meningeal covering
pinna Cartilaginous portion of the external ear
pituitary adenomas Tumor composed of glandular tissue of the pituitary gland
platelets Smallest blood cell and contains hemoglobin
pneumococcus Genus of gram-positive bacteria
pneumoperitoneum Presence of free gas in the peritoneal cavity
polyhydramnios Excessive accumulation of amniotic fluid
polypoid Resembling a polyp
pons Part of the brainstem containing centers for some reflexes
positron emission tomography (PET) Using a radiopharmaceutical that emits a positron that the moving gamma camera detects to produce an image
postmenstrual phase Follows the menstruation phase in the menstrual cycle
postpartum After childbirth
Pott's disease Tuberculosis of the spine
primary cystadenocarcinoma Cancer of the ovary often contains psammomatous bodies, depositions of calcium carbonate located in the fibrous stroma of the tumor that can be detected on plain abdominal radiographs
primary hyperparathyroidism Hyperactivity of the parathyroid glands resulting in excessive secretion of parathyroid hormone (PTH) and is usually caused by a discrete adenoma (80%) or carcinoma (2%) or by generalized hyperplasia (18%) of all glands
primary hypoparathyroidism The most common radiographic finding on plain skull radiographs or CT of the skull is cerebral calcification, especially involving the basal ganglia, the dentate (tooth-shaped) nuclei of the cerebellum, and the choroid plexus caused by insufficient secretion of the glands
primary stage Initial phase of a disease process
progesterone Hormone secreted by the corpus luteum to help regulate menstrual cycle and fertilization
prognosis The expected patient outcome
proliferate To multiply rapidly, increase profusely
prostate gland Produces fluid that makes up the semen
proximal convoluted tubule Second part of the nephron, first part of the renal tubule
psoriatic arthritis Rheumatoid-like destructive process involving the peripheral joints in patients with psoriasis
pulmonary mycosis Fungal infection of the lung
pulmonary valve Three semilunar cusps between the right ventricle and the pulmonary trunk
punctate Marked with dots or tiny spots
purpura Spontaneous hemorrhages in the skin or mucous membrane
pyloric stenosis Also known as infantile hypertrophic pyloric stenosis (IHPS), occurs when the two muscular layers of the pylorus become hyperplastic and hypertrophic
pyogenic Bacteria that lead to the production of a thick, yellow fluid called pus
pyosalpinx Fallopian tube filled with pus

R

radiofrequency pulse (RF) Refers to that portion of the electromagnetic spectrum in which electromagnetic waves can be generated by alternating current—commonly in the 1- to 100-megahertz range—and their effect upon a body is potential heating of tissues in MRI

radiopharmaceutical A drug that is tagged to emit ionizing radiation
recessive Genes that manifest themselves only when the person is homozygous for the trait
reflex arc Simple neurologic unit to carry impulses to the CNS and impulses to the PNS
releasing hormones Control the secretion of hormones by the anterior and posterior portions of the pituitary gland
resection Partial surgical removal of an organ or bone
resorption Bone destruction by osteoclasts
retrovirus Any of a family of ribonucleic acid (RNA) viruses containing the enzyme reverse transcriptase
right-to-left shunting Ventricle septal defect and overriding aorta causes unoxygenated blood into the left ventricle
rudimentary Imperfectly developed

S

saccular Resembling a pouch-like sac
saccular aneurysm Bulging of only one side of the arterial wall
sarcoma Highly malignant tumors arising from connective tissues
sclerosis Conversion of a portion of bone into an ivory-like, densely opaque mass; an abnormal hardening of body tissues or parts, especially of the walls of arteries
seat belt fracture Transverse fracture of a lumbar vertebra that is often associated with significant visceral injuries
secondary hyperparathyroidism Occurs more frequently than the primary form and is most often attributable to chronic renal failure
secondary stage Progression of the disease process into the phase that follows the initial stage
secretory, or postovulatory, phase Occurs between ovulation and the onset of the menses
segmental fracture Consists of a segment of the shaft isolated by proximal and distal lines of fracture
seminal vesicles Paired saclike gland that secretes a thick liquid that is rich in fructose for sperm motility
sequestrum Piece of dead bone that has become separated from the surrounding healthy bone
serosa Outer layer of a viscus (especially in the alimentary tract)
serpiginous Having a wavy border
shock Acute peripheral circulatory failure
sickle cell anemia Anemia characterized by crescentic red blood cells that contain abnormal hemoglobin molecules and are susceptible to rupture
signs Measurable manifestations of a disorder; objective manifestations
silhouette (cardiac) Outer border of the heart, seen against the radiolucent lungs
simple bone cyst (unicameral) True fluid-filled cyst with a wall of fibrous tissue
single-photon emission computed tomography Gamma camera moves around the patient and detects the gamma rays produced by the radiopharmaceutical
small cell (oat cell) carcinomas Specific type of malignant bronchogenic epithelial neoplasm
somatic nervous system Supplies the striated skeletal muscles
spermatogenesis Formation of sperm
spherocytosis Anemia due to erythrocytes that have a circular rather than a biconcave shape, making them fragile and susceptible to rupture
spina bifida occulta Mild form in which there is a splitting of the bony neural canal but no clinical symptoms
spin-echo (SE) Most common pulse sequence used in MR using 90° radiofrequency pulses to excite the magnetization and one or more 180° pulses to refocus the spins to generate signal echoes
spiral fracture Encircles the shaft of a long bone
spirochete Spiral type of bacterium of the genus *Spirochaeta*
spirometry Measure of lung capacity using a spirometer
spondylolisthesis Spondylolysis with displacement of vertebral alignment
spondylolysis Cleft in the pars interarticularis situated between the superior and inferior articular process of the vertebra without displacement
squamous carcinoma Most common type of lung cancer
stable Resistant to change
staghorn calculus Renal calculi filling the entire renal pelvis of the kidney
staging Determination of the amount of spread of a neoplasm, necessary to select appropriate therapy and to predict the future course of a disease
stasis Stagnation of some fluid in the body (as of blood in veins); reduced peristalsis of the intestines resulting in the retention of feces
stenosis Narrowing
stress, or fatigue, fracture Fracture caused by repetitive stresses applied to the bone
stroke Cerebrovascular accident; denotes a sudden and dramatic focal neurologic deficit
stroma Supporting tissue of the matrix of an organ
subarachnoid space Space beneath the arachnoid and above the pia mater that contains cerebrospinal fluid
subchondral Just beneath the articular margin
subluxation Incomplete or partial dislocation
sulci Shallow depressions on the surface of an organ
supernumerary kidney An extra kidney
surfactant Agent that lowers the surface tension
symptoms Subjective manifestations; the patient feels
synapse Point of contact between two neurons for impulses to flow
syndrome Indicates the presence of a combination of symptoms that commonly occur together and are related to a single cause
systemic circulation High-pressure system that carries blood to the organs and extremities
systole Phase in which the heart contracts

T

T1-weighted image Equilibrium—high energy protons return to the low energy state
T2-weighted image Image relies on local dephasing of spins
telangiectasia Vascular lesion formed by dilatation of a group of small blood vessels
teratoma Neoplasm composed of various kinds of embryonic tissue
tertiary Third in rank or order
tertiary hyperparathyroidism Refers to the development of autonomous functioning parathyroid glands in patients who demonstrate progressive bone disease in the presence of biochemical and clinically controlled renal disease
tertiary stage Most serious stage of the disease in which radiographic abnormalities become apparent
testicular dysgenesis Characterized by small testes that fail to mature or produce sperm and testosterone
testosterone Stimulates the development and activity of the male accessory sex organs
thalamus Portion of the brain that receives and processes sensory information and relays it to the cerebral cortex
thalassemia Hemolytic anemia due to a defect in hemoglobin formation
thiamine Vitamin B_1
thrombus Blood clot in the vascular system
thymoma Tumor originating from the thymus gland
thyroxine Hormone influencing metabolic rate
tortuous Full of twists, turns, or curves
torus (buckle) fracture One cortex is intact with buckling or compaction of the opposite cortex
toxoid Chemically altered toxin
trabeculae Supporting or anchoring strands of connective tissue within body structures
traction Process of placing tension between two structures
transitional vertebra Vertebra with characteristics of another spinal region
transverse fracture Runs at a right angle to the long axis of a bone
tricuspid valve Valve between the right atrium and right ventricle that has three cusps
trigone Triangular area of the posterior bladder, between the openings for the ureters and urethra
tripod fracture Fractures of the zygomatic arch and the orbital floor or rim combined with separation of the zygomaticofrontal suture
triradiate Radiating in three directions
trisomy Presence of an additional (third) chromosome
trophoblastic Relating to the layer by which the fertilized ovum is attached to the uterine wall and from which the developing embryo receives its nourishment
tuberculous arthritis Chronic indolent infection with a slow progressive course by tuberculosis

U

ulceration Destruction of tissue creating an opening within a structure

ulcerogenic islet cell tumors (gastrinomas) Tumor found in pancreas and duodenum that is associated with peptic ulcers

ultrasound Images produced by high-frequency sound waves emitted from the transducer that are echoed back to produce an image

undifferentiated Without form

undisplaced fracture The bone is without angulation or separation

unilateral renal agenesis Absence of a kidney

unstable As a result of a fracture, alignment is uncertain

urate Salt of uric acid

uremia Presence of excessive amounts of urea and nitrogen in the blood

ureterocele A cystic dilatation of the distal ureter near its insertion into the bladder

V

vaccine Low dose of dead or deactivated bacteria or virus

valvulae conniventes Circular folds of the small bowel

vasculitis Inflammation of a vessel

vas deferens Muscular tube that passes through the inguinal canal as part of the spermatic cord connecting the epididymis and seminal vesicle to form the ejaculatory duct

vasectomy Severing of the vas deferens

vegetations Abnormal growth of tissue around a heart valve

ventricular septal defect Opening between the left and right ventricles allowing blood to flow back into the right ventricle instead of entering the systemic circulation

vermis Structure resembling a worm

villi Finger-like projections of the small bowel to increase the inner surface area

viral meningitis Inflammation of the meninges caused by virus

virus One of a group of minute infectious agents characterized by a lack of independent metabolism and by the ability to reproduce only within living host cells

viscous Thick, sticky

viscus Any large internal organ, especially in the abdomen

vitamins Organic compounds essential for normal physiologic and metabolic function

volume-rendered imaging Technique taking all the raw CT data density information and using them to simulate three-dimensional images

W

water-soluble vitamins Vitamins B and C, which cannot be stored and therefore must be included in the daily diet

Wimberger's sign of scurvy Epiphyseal ossification centers are demineralized and surrounded by dense, sharply demarcated rings of calcification

Z

Zenker's diverticula Outpouching that arises from the posterior wall of the upper esophagus

zygomatic arch fractures Demonstrated on underexposed films taken in the basal (submentovertex) projection ("jug handle" view)

INDEX

Note: Page numbers followed by "b", "f" and "t" indicate boxes, figures and tables respectively.

A

Abdomen
  contrast-enhanced MRA, 271f
  sonogram, 18f
  three-phase CT scanning protocol for, 23f
  ultrasound images, 17f
Abdominal aorta, arterial phase demonstrating, 23f
Abdominal aortic aneurysm, ultrasound/CT axial scan, 267f
Abdominal aortic stent, CTA, 268f
ABO-incompatible blood, administration of, 11
Abscess, 4t
Achalasia, 166
  esophagus, distal part (rat-tail narrowing), 167f
  functional obstruction, 166
  imaging appearance, 166
  tortuous aorta, frontal chest radiograph, 166f
  treatment, 166
Achilles tendon, insertion, 112
  bony erosion, 97f
Achlorhydria, 174
Achondroplasia, 92
  imaging appearance, 92
  pelvis, view, 94f
  posterior scalloping, 94f
  treatment, 92
Acid-base balance, 217
Acidic corrosive agents, ingestion, 160–161
Acoustic barriers, 19
Acoustic neuroma, 299–300
  CT scan, 304f
  imaging appearance, 299–300
  MR T1-weighted axial/coronal images, 303f
  treatment, 300
Acquired immunodeficiency syndrome (AIDS), 12–13
  gastrointestinal manifestations, 12
  manifestations, MRI demonstration, 12–13
  neurologic manifestations, 13f
  radiographic appearance, 12
  treatment, 13
Acquired type, of tracheoesophageal fistula, 157–158
  dentures, aspiration, 158f
  imaging appearance, 158
  treatment of, 158
Acquired vascular disease, 256–274
  findings, summary, 274t
Acromegaly, 364
  extraskeletal manifestations, 365
  heel pad, thickening, 365f
  lateral skull projection, 366f
  vertebral bodies, enlargement, 366f
Active immunity, 11
Acute appendicitis
  avoidance of barium enema examination in, 185
  clinical presentation, 185
  clinical symptoms, 184
  spot radiograph, 185f
Acute arterial occlusion, streptokinase therapy for, 273, 273f
Acute cholecystitis, 198–199
  imaging appearance, 198–199
  radionuclide hepatobiliary study, technetium-99m disofenin, 199f
Acute coccidioidomycosis, symptoms (absence), 52
Acute diverticulitis, ultrasound appearance, 187
Acute embolic occlusion, left renal artery, 273f
Acute epidural hematoma, CT scan, 311f
Acute idiopathic thrombocytopenic purpura, 350–351
Acute inflammation, 3
Acute left middle cerebral artery infarct, 318f
Acute leukemia, 342
  bone destruction, cortical erosion, 344f
  neoplastic cells, proliferation, 344f
Acute myocardial infarction, MRI, 258f
Acute osteomyelitis, 339
  proximal humerus, diffuse lytic destruction, 340f
Acute pancreatitis, 206
  CT scan, 206f
  imaging appearance, 206
  plain abdominal radiographs, 206
  symptoms, 206
  transverse sonogram, 206f
  treatment, 208
  ultrasound/CT imaging modalities, 206
Acute patellar tendinitis, 103f
Acute renal failure, 243–245
  excretory urogram, 245f
  excretory urography, 244
  imaging appearance, 243–245
  treatment, 245
  ultrasonography, selection, 244–245
Acute renal vein thrombosis, right kidney (radiograph), 244f
Acute staphylococcal arthritis, 100f
Acute subdural hematoma, 311f
Acute ureteral colic, localized ileus, 181f
Acute urinary tract obstruction, 233
Addison's disease, 357
Adenocarcinoma, 8, 63
Adenomas, pituitary, 300
Adrenal adenoma, 356f
Adrenal carcinoma, 358
  anteromedial aspect, tissue tumor, 358f
  axial MR image, 360f
  imaging appearance, 358
  treatment, 358
  ultrasound image/CT scan, 358f
Adrenal cortex
  benign/malignant tumors, 356
  diseases of, 355–359
    findings, summary, 359t
Adrenal glands, 355–363
  generalized enlargement, 355–356
  metastases, 358–359, 360f
    imaging appearance, 358–359
    treatment, 359
  physiology of, 355
  structure of, 355f
Adrenal medulla, 355
  diseases, 360–363
    findings, summary, 364t
  epinephrine, secretion, 355
Adrenal virilism, 357
Adrenocortical insufficiency, CT scan, 358f
Adrenocorticotropic hormone (ACTH), levels, decreased, 300
Adrenogenital syndrome, 357
  adrenocortical tumor, 357f
  imaging appearance, 357
  treatment, 357
Adult foot, osteogenesis imperfecta, 91f
Adult respiratory distress syndrome (ARDS), 73
  alveolar consolidation, ill-defined areas, 74f
  hypoxemia, 73
  imaging appearance, 73
  treatment, 73
Adult-type scoliosis, 147
Adynamic ileus, 180–181
  gas/fluid retention, 181f
  imaging appearance, 180–181
  intestinal motor activity, 180
  treatment, 181
  variants, 180–181
Aging
  degenerative changes of, axial MR image, 327f
  osteoporosis of, 109f

Air embolism, 272
Alcoholic gastritis, 170
Aldosteronism, 356–357
Aldosteronoma, 357f
Alkaline corrosive agents, ingestion, 160–161
Alkaptonuria, 429
Alveolar cell carcinoma (bronchiolar carcinoma), 65
Alveolar pneumonia, 45–46
  imaging appearance, 46
  right lobes, homogeneous consolidation, 46f
Alzheimer's disease, 327–328
  FDG-PET metabolic brain images, 328f
  imaging appearance, 328
  noncontrast CT scan, 328f
  presenile dementia, 327
  treatment, 328
Amyotrophic lateral sclerosis (Lou Gehrig's disease), 330
Anaphylactic reactions, 11
Anaplastic tumor, 8
Androgens (sex hormones), 355
Anechoic tissue, echo free, 17, 18f
Anemia, 337–342
  hemolytic, 338–341
  iron deficiency, 337
  megaloblastic, 341
  myelophthisic, 341
Anencephaly, long-axis image, 415f
Aneurysm, 266–267
  abdominal aortic, ultrasound/CT axial scan, 267f
  aortic, MR image, 267f
  fusiform, 266, 266f
  saccular, 266
  treatment, 267
  walls, calcification, 266f
Aneurysmal bone cysts, 122
  tibia, cystic lesion, 122f
Angina pectoris, oxygen insufficiency, 256
Angiography, comparison of contrast-enhanced CT coronary angiography and, 258f
Angiomas, 8
Angulation (fractures), 132
Ankle, bimalleolar fracture, 141f
Ankylosing spondylitis, 96–98
  imaging appearance, 96–98
  midcervical spine, oblique fracture, 97f
  sacroiliac joints, bilateral symmetric obliteration, 96f
Annihilation, 29–30
Annular carcinoma (apple-core/napkin-ring carcinoma), 192
Annulus fibrosis, tearing, 148f
Anterior mediastinal mass
  chest projections, 80f
  CT scan, 82f
  right hilar adenopathy, 80f
Anterior mediastinal/retrosternal nodes, involvement of, 344
Anterior mediastinum, lesions, 80
Anthracosis (coal worker's pneumoconiosis), 61
  diffuse reticular pattern, 62f
  imaging appearance, 61
  treatment, 61
Anthrax, 47–48
  imaging appearance, 47–48
  treatment, 48
Antibodies, reaction, 11
Antidiuretic hormone (ADH), secretion, 216–217
Antigens, 11
  immunologic responses, mechanisms, 11
Aorta
  coarctation, 254–255
    imaging appearance, 255
    plain chest radiograph, 255f
    sagittal MR image, 255f
    treatment, 255
  dissection, 268–270
    CT image, 269f
    diagnosis, aortography (usage), 270
    imaging appearance, 269–270
    MR image, 269f
    plain chest radiograph, 269f
    radiolucent intimal flap, aortogram demonstration, 270f
    treatment, 270
  traumatic rupture, 267–268
    chest radiograph, 268f
    imaging appearance, 267–268
    mediastinum widening/nasogastric tube deviation, 268f
    treatment, 268
Aortic aneurysm, MR image, 267f
Aortic arch (evaluation), echocardiography (usage), 255
Aortic insufficiency, 278
  frontal chest radiograph, 279f
Aortic knob, bulging, 255
Aortic orifice, overriding, 254
Aortic stenosis, 277–278
  aortic valve, leaflets (calcification), 278f
  cardiac apex, frontal projection, 278f
  treatment, 278
Aortic valve, 248–249
Apical lordotic projection, 49f
Aplastic anemia, 341
Appendicitis, 183–185
  imaging appearance, 184–185
  treatment, 185
  ultrasound images, 185f
Appendicolith, laminated calcification, 184f
Appendix, cecum inferomedial aspect, 153
Apple-core carcinoma (annular carcinoma/napkin-ring carcinoma), 192
Appositional growth, 87
Aqueductal stenosis, T1-weighted sagittal MR image, 331f
Arachnodactyly, 428f
Arachnoid membrane, 290
  inflammation, 290–291
Arachnoid villi, 290
ARDS. *see* Adult respiratory distress syndrome (ARDS).
Arteriovenous malformation
  axial MR image, 323f
  CT scan, 324f
Artery, acute embolic occlusion, 272–273
Arthritis
  therapy, impact, 100–101
  treatment, 100–101
Asbestosis, 60–61
  CT scan, 61f
  imaging appearance, 60–61
  PA image, 61f
Ascending aorta, aneurysmal dilatation of, 384f
Ascites (fluid accumulation), 202
  plain radiograph, 203f
Ascorbic acid (vitamin C), deficiency, 420
Aseptic necrosis, 430
Aspiration pneumonia, 47
  bilateral, nonsegmental air-space consolidation, 47f
  imaging appearance, 47
  treatment, 47
Asthma, 56–57
  imaging appearance, 56–57
  pulmonary infections, recurrence, 56f
  treatment, 57
Astrocytomas, 295–296
  cystic astrocytoma, CT scan, 299f
Asymptomatic patient, 2
Asymptomatic skeletal metastases, detection, 129
Atelectasis, 72–73
  iatrogenic cause, 72
  imaging appearance, 72–73
  treatment, 73
Atherosclerosis, 270–271
  chest, lateral projection, 270f
  Doppler ultrasound, usage, 270–271
  imaging appearance, 270–271
  superficial femoral arteries, bilateral atherosclerotic occlusion, 271f
  treatment, 271
Atlantoaxial joint, subluxation, 96f
Atrial defects (identification), Doppler echocardiography (usage), 253
Atrial septal defect, 252
  chest, frontal projection, 252f
  Eisenmenger's syndrome in, 253f
  septal closure, absence, 254f
Atrioventricular (AV) node, impulse passage, 250–251
Atrophic undescended testis, coronal MR image, 392f
Atrophy, 6
Autoimmune hepatitis, ultrasound images, 201f

Autonomic nervous system, function, 287
Autosomal dominant disorders, 10
Autosomal recessive disorders, 10
Autosomes, 9–10
Avulsion fractures, 131–132

B

Bacillus anthracis, 47
Bacteremia, 4t
Bacterial gastritis (phlegmonous gastritis), 170
Bacterial meningitis, 290–291
Bacterial organisms, toxin production, 4
Bacterial osteomyelitis, 103–106
  imaging appearance, 104–106
  treatment, 106
Bacterial pneumonia, lung abscess, 48f
Bacterial vertebral osteomyelitis, 106f
Bamboo spine, 96f
Barrett's esophagus, 159–160
  imaging appearance, 159–160
  ulcerations, development, 160f
  upper thoracic esophagus, stricture, 161f
Basal cisterns, subarachnoid enhancement, 291f
Basal ganglia, 289
Basophil, 337
Battered-child syndrome, 137
  imaging appearance, 137
  left arm, frontal radiograph, 138f
  right arm, frontal radiograph, 138f
  treatment, 137
Benign bone tumors, 119–123
  neoplasia, findings (summary), 123t
  treatment, 123
Benign breast disease, 409
Benign breast mass, screen-film mammogram, 408f
Benign gastric ulcer
  contrast material, penetration, 172f
  en face projection, 172f
  hallmark of, 172
  healing, 173
  mucosal folds, radiation, 172
Benign prostatic hyperplasia, 387–388
  bladder (base), smooth filling defect, 388f
  imaging appearance, 387–388
  prostatic enlargement, T1-weighted MR image, 388f
  transrectal ultrasound, sagittal plane, 388f
  treatment, 388
Benign solitary pulmonary nodule (tuberculoma), 62f
  CT scan, 63f
Benign thyroid adenomas, 371
Benign tumors, 7
Beriberi (thiamine deficiency), 420
  diffuse pulmonary edema, 420f
  imaging appearance, 420
Berry aneurysm
  rupture, 324f
  subarachnoid hemorrhage, 324f
Bicuspid valve (mitral valve), 248–249
Bifid renal pelvis, 221f
Bilateral cervical ribs, 89f
Bilateral orbital ecchymoses (raccoon eyes), 309
Bilateral renal vein thrombosis, 242–243
Bilateral subdural hematoma, coronal MR image, 312f
Bilateral symmetric hilar lymph node enlargement, 57–58
Bilateral undescended testes, malignant neoplasms, 391f
Bile, emulsifier, 153
Bilirubin, 338
Bimalleolar fracture, ankle, 141f
Biparietal diameter (BPD), 414
  cursor width, 414f
Black lung, 61
Bladder
  calculi, plain radiograph, 232f
  carcinoma, 240–242
    CT scan, 244f
    imaging appearance, 241–242
    treatment, 242
    tumor irregularity, 243f
  distention, CT (usage), 242
  incontinence, 89
Bleeding disorders (platelet diseases), 349–352
  findings, summary, 352t
Blood
  coagulation (clotting), 349
  electrolyte/acid-base balance, 217
  oxygenation, 38
  physiology of, 336
Blood oxygen level dependent (BOLD), 27
Blood vessels, terms for, summary of, 6t
Blowout, 129
  fracture
    cause, 314–315
    tomogram, 314f
  metastases, 130f
Body
  fluids, electrolyte/acid-base balance, 217
  waste products, removal, 38
Bone metastases, 127–131
  fluorodeoxyglucose-PET scan, 129f
  imaging appearance, 129–131
  MR image, 131f
  treatment, 131
Bones
  abscess, osteomyelitis, 104
  age, radiographic determination, 87
  benign tumors, 129
  congenital diseases, 89–92
  cysts
    aneurysmal bone cysts, 122
    simple bone cysts, 122
  destruction (resorption), 87
Bones *(Continued)*
  formation (ossification), 87
  fracture healing, 134f
  functions of, 88b
  hereditary diseases, 89–92
  infarct, 119f
  ischemic necrosis, 116–119
    imaging appearance, 117–119
    T1-weighted MR image, 118f
    treatment, 119
  islands, 122
    femoral head, 123f
  multiple abnormalities, 385
  neuroblastoma metastatic to, 362f
  quality changes (expectation), skeletal radiography (exposure factor), 2b
  radiographs, contrast requirement, 86b–87b
  sclerosis, 90f
  softening, osteomalacia, 110
Bony cortices, demineralization, 91f
Border, in imaging, 16
Bougienage, 163
Bowel obstructions, CT scans, 180f
Bowing fractures, 132
Bowman's capsule, fluid filtration, 216–217
Boxer's fractures, 138
  fifth metacarpal, distal fragment (volar angulation), 140f
Brain
  abscess, 292–293
    imaging appearance, 292–293
    T1-weighted MR image, 292f
    treatment, 293
  divisions, 289f
  neurosurgical localization, 18–19
  traumatic processes, 309–315
    findings, summary, 316t
Brainstem glioma, sagittal MR image, 297f
Breast, 407f
  benign mass, screen-film mammogram, 408f
  carcinoma, unilateral sagittal T1-weighted fat-saturated postcontrast MR image, 410f
  disease, sonography, 409f
  implants, MRI, 411f
  lesions, 407–409
    findings, summary, 413t
    removal, stereotaxic needle biopsy, 413f
Breast cancer, 407–409
  clustered calcifications, 408
  CT scans, 411f
  full/magnified coned views, 408f
  imaging appearance, 407–409
  malignant calcifications, 408f
  treatment, 409
Breast self-examination (BSE), 407
Brittle bones (osteogenesis imperfecta), 91

Bronchial adenoma, 63
imaging appearance, 63
neoplasms, low-grade malignancy, 63
Bronchial mucosa, swelling, 54
Bronchial tree, esophagorespiratory fistula, 158f
Bronchiectasis, 57
imaging appearance, 57
treatment, 57
Bronchioalveolar carcinoma, growth, 65
Bronchiolar carcinoma (alveolar cell carcinoma), appearances, 65
Bronchogenic carcinoma (malignant solitary pulmonary nodule), 63–65
airway obstruction, 63–64
cavitary right upper lobe mass, air-fluid level, 65f
cavitation, 64–65
imaging appearance, 63–65
margins, definition (problems), 62f
spread, 66f
tomography, 65f
Bronchopneumonia, 46
imaging appearance, 46
right base, consolidation, 46f
Buckle fractures (torus fractures), 132
Bullae, appearance, 55
Bursitis, 101–102
elbow, posterior aspect (transverse scan), 101f
first-line treatment, 101–102
imaging appearance, 101–102
treatment, 101–102
Butterfly fragment, 132

C

C7 vertebral body, fracture, 143f
Caffey's disease (infantile cortical hyperostosis), 7f
Calcific tendinitis, 102f
Calcified pancreatic pseudocyst, 208f
Calcified tuberculoma, 51f
Calcified uterine fibroid, calcified mass, 401f
Calor (heat), acute inflammation clinical sign, 4
Cancellous bone (spongy bone), 87
Cancerous lesion, treatment, 163
Cancers, 7
cause, 8
clinical symptoms of, 8
curable stage, 8–9
hematogenous spread of, 9
pain and, 8
Candida, 160
Candida esophagitis, 161f
Carbon dioxide, level, 39
Carcinogens (causative factors), 8
Carcinomas, 8
Cardiac pacemaker, fracture, 42f
Cardiac resting images, 32f
Cardiothoracic ratio (C/T ratio), 261
Cardiovascular system, 248–285
function, 248
objectives, 248
physiology, 248–252
radiographer notes, 249b
Carotid arteriosclerotic occlusive disease, ultrasound scan, 319f
Carotid artery
bifurcation, carotid arteriogram, 320f
MRA, 320f
Carotid artery injury, 313
Carpal navicular bone, fractures (nonunion), 135f
Cartilage, hypertrophy, 365
Cavitary right upper lobe mass, 65f
Cecal volvulus, 193–194
barium enema examination, 195f
imaging appearance, 194
Cecum, dilatation, 193f
Cell growth, alterations, 6–7
terms, summary, 6t
Centers for Disease Control and Prevention (CDC), Standard Precautions, 11
Central nervous system
components, 287
degenerative diseases, 327–330
findings, summary, 330t
diseases, findings, summary, 334t
infections, 290–295
findings, summary, 294t
tumors of, 295–309
findings, summary, 308t–309t
imaging appearance, 295
treatment, 295
vascular disease, 317–322
findings, summary, 323t
Central venous catheters, 40–41
breakage, 41
location, 41f
embolization, 41
insertion, problems, 40
Central venous pressure (CVP)
catheters, internal device (findings), 42t
measurement, 40
Cerebellar atrophy, 329
sagittal MR image, 329f
Cerebellum, 289, 289f
Cerebral arteriography, usage, 295
Cerebral contusion, 312–313
CT scan, 312f
imaging appearance, 312–313
treatment, 313
Cerebral cortex, responsibility, 288–289
Cerebrospinal fluid (CSF), 290
formation, 290
Cerebrovascular disease, 317
Cerebrum, 288, 289f
Cervical rib, 89
Cervical spine, injury, 89
Cervical spine separation, 143f
Cervix, carcinoma, 404–406
bladder invasion, CT scan, 405f
CT scan, 405f
imaging appearance, 404–406
sagittal T1-weighted MR image, 405f
sagittal T2-weighted MR image, 405f
sonogram, 405f
treatment, 406
Chest, frontal projection, atrial septal defect, 252f
Chest radiography
kVp optimum, 2b
patient positioning, 37b
performing, 37b
Chewing (mastication), 153
Chiari II malformation, 89
Childhood, rickets (system disease), 110
Children, pneumoperitoneum, 211
Cholecystitis, treatment for, 199
Cholelithiasis (gallstones), 197–198
Chondromas, 8
Chondrosarcoma, 124–125
calcification, 125f
cartilaginous origin, 124
imaging appearance, 124–125
Chordoma, 306–307
clival, sagittal MR image, 307f
CT scan, 306f
imaging appearance, 306–307
plain skull radiograph, 306f
treatment, 307
Chorion, 395–396
Choroid plexus papilloma, T1-weighted MR image, 332f
Choroid plexuses, plasma filtration, 290
Chromophobe adenomas, 300
Chromosomal aberrations, 426–428
Chronic atrophic gastritis (nonerosive gastritis), 170
Chronic bronchiectasis
bronchogram, 57f
interstitial markings, coarsening, 57f
Chronic bronchitis, 54
imaging appearance, 54
right lower lung, coned view, 55f
treatment, 54
Chronic Crohn's colitis, 190f
Chronic duodenal ulcer disease, cloverleaf deformity, 172f
Chronic glomerulonephritis, nephrotomogram, 224f
Chronic idiopathic thrombocytopenic purpura, 352f
Chronic left subdural hematoma, CT scan, 312f
Chronic leukemia, 342
indium-111 whole-body scan, 345f
splenomegaly, 345f
Chronic obstructive pulmonary disease (COPD), 54–57
Chronic osteomyelitis, 105f

Chronic pancreatitis, 206–208
diffuse pancreatic calcifications, 207f
imaging appearance, 207–208
treatment, 208
ultrasound examination, 207
ultrasound image, 207f
Chronic pelvic inflammatory disease, transverse sonogram, 397f
Chronic pyelonephritis, 225f
Chronic renal failure, 245–246
imaging appearance, 245–246
treatment, 246
ultrasound image, 246f
Chronic right middle cerebral artery infarct, low-attenuation region, 318f
Chronic sinusitis, mucosal thickening, 332f
Chronic ulcerative colitis (lead-pipe colon), 189f
Chyme, 153
Circulatory system, relative attenuation, 3b
Clay shoveler's fractures, 144
frontal/lateral projections, 145f
Clinical breast examination (CBE), 407
Clival chordoma, sagittal MR image, 307f
Closed fractures, 131
Clubfoot, 89
prenatal ultrasound, 416f
Coagulation factors, 349
Coarctation, aorta, 254–255
Coccidioidomycosis, 52–53
Coccidioides immitis, 52
imaging appearance, 52–53
posteroanterior/lateral views, 53f
pulmonary consolidations, 52
treatment, 53
Codman's triangle, periosteal elevation, 125f
Coeur en sabot appearance, 254
Cold thyroid nodules, 368
Collateral circulation (progressive development), aortic blood flow obstruction and, 254–255
Collecting tubules, urine passage, 217
Colles' fracture, 137
wrist, frontal/lateral projections, 139f
Collimator, 28
Colon, 183–197
carcinoma, 188–189
cause, 192
development, 189f
Crohn's disease, 189
diverticular disease, complication, 186
findings, summary, 196t–197t
obstruction, 182f
volvulus, 193–195
Colon cancer, 191–193
CT virtual colonoscopy, 192
^{18}F-fluorodeoxyglucose (FDG-PET), 193
imaging appearance, 191–193
transrectal ultrasound, 192
treatment, 193
Colonic diverticula, 185–186
Colonic ileus, 181
large bowel, distention, 181f
Colonic obstruction, 193
Color-flow Doppler studies, 18
Comminuted fractures, 132
Communicating hydrocephalus, 331
Community acquired disease, 2
Compact bone, 87
Compensatory hypertrophy, 219
acquired condition, 219
hypoplastic kidney, 219f
Complete fracture, 131
Completed stroke, 317
Complex thyroid mass, ultrasound images, 372f
Compound fractures (open fractures), 131
Compression fractures, 132
Compton scattering, 28
Computed axial tomography, imaging modality, 15–16
Computed tomography (CT), 20
angiography, 23f
esophagography, 157
myelogram, 22f
number (Hounsfield number), 20
scout image, 20f
single-scan protocol, change, 21
spiral scanning (helical scanning), 21
summary of, 22t
three-dimensional surface-rendered images, 24f
Computed tomography angiography, 23f
Computerized technology, imaging prevalence, 16
Coned x-ray beam, usage, 21
Congenital bone diseases, findings (summary), 93t–94t
Congenital diseases, 43–44, 218–222
findings, summary, 222t
number/size, anomalies of, 218–219
rotation/position/fusion, anomalies of, 219–220
treatment of, 221
Congenital heart disease, 252–255
findings, summary, 256t
Congenital hip dysplasia (dislocation), 92
imaging appearance, 92
treatment, 92
ultrasound imaging (ultrasonography), 92
Congenital syphilis, 383
metaphyses, transverse bands (density decreased), 385f
Congenital tracheoesophageal fistulas, 156
imaging appearance, 156–157
treatment of, 157
type I, 156
type II, 156
type III, 157, 157f
type IV (H fistula), 157, 157f
Congestive heart failure, 260–261
imaging appearance, 260–261
result, 256–257
treatment, 262–263
Connective tissue, 219–220
Consciousness, levels (decrease), 309
Constipation, 153
Contrast-enhanced CT coronary angiography, angiography (comparison), 258f
Contrast extravasation, 229f
Convulsive disorders
findings, summary, 326t
imaging appearance, 326–327
treatment, 327
Coronary angiography, 259f–260f
Coronary artery disease, 256–259
imaging appearance, 257–259
intravascular ultrasound (IVUS), 258
percutaneous transluminal coronary angioplasty (PTCA), balloon catheter (usage), 259
radionuclide thallium perfusion scanning, usage, 257
single-photon emission computed tomography (SPECT), 257, 257f
treatment, 258–259
Coronary sinus, pacemaker tip, 42f
Corpus callosum, 289
Corpus luteum, growth, 394–395
Corrosive agents, ingestion of, 160–161
imaging appearance, 161
treatment of, 161
Corrosive gastritis, 170
Cortex, 288
Craniopharyngioma, 303–304
CT scan, 305f
imaging appearance, 303–304
plain skull radiograph, 305f
sagittal MR image, 305f
treatment, 304
Craniotomy, history, 309
Cretinism, skull (lateral projection), 370f
Crohn's colitis, 189–191
benign, stricture, 190f
colon cancer, development, 190
CT demonstration, 189–190
diffuse aphthous ulcers, 190f
findings, summary, 190t
imaging appearance, 189–190
progression, 189
transverse colon, intramural fistula, 190f
treatment, 190–191
Crohn's disease (regional enteritis), 176–177
clinical spectrum, 176
cobblestone appearance, 176f
fistula formation, 176–177
imaging appearance, 176–177
skip lesions, 177f

Crohn's disease *(Continued)*
terminal ileum/sigmoid colon, fistulization, 178f
treatment, 177
ultrasound, 177f
Crossed ectopia, 219
Croup, 44
imaging appearance, 44
trachea, tapered narrowing, 45f
treatment, 44
Crown-to-rump length, 414
measurement, cursor delineation, 414f
Cryptorchidism (undescended testis), 390–391
CT. *see* Computed tomography (CT).
Cushing's syndrome, 355–356
adrenal adenoma, 356f
functioning cortical adenoma, 356f
imaging appearance, 355–356
treatment, 356
CVP. *see* Central venous pressure (CVP).
Cystadenocarcinoma, endovaginal sonogram, 399f
Cystadenomas, 8
longitudinal/transverse sonograms, 399f
Cystic astrocytoma, CT scan, 299f
Cystic fibrosis (mucoviscidosis), 43
cysts, superimposition, 43f
imaging appearance, 43
meconium ileus, bowel distention, 43f
recombinant human deoxyribonuclease (DNase) inhalation, 43
treatment, 43
Cystine stones, plain image/excretory urogram, 230f
Cystinuria, 430
Cystitis, 227, 228f
imaging appearance, 227
treatment, 227
Cysts, 234–242, 397–406
findings, summary, 242t
Cytomegalovirus, 8
Cytotoxic reaction, 11

D

Dandy-Walker cyst, 330–331, 331f
Deep venous thrombosis, 281
contrast venogram, 282f
detection, modalities, 281
Doppler image, 282f
imaging appearance, 281
treatment, 281
Degenerative diseases, 327–330
Alzheimer's disease, 327–328
normal aging, 327
Degenerative disk disease, 146f
Degenerative follicular adenoma, radioactive iodine scan, 373f
Degenerative joint disease (osteoarthritis), 98
Deglutition (swallowing), complexity, 153
Delayed reaction, 11
Demarcation, in imaging, 16, 16t
Density, in imaging, 16, 16t
Deoxygenated venous blood, return to heart, 250
Depressed fractures, 132
stellate shape, 310
Depressed nasal fracture, 314f
Dermoid cyst (teratoma), 400
imaging appearance, 400
multiple well-formed teeth, 400f
sagittal sonogram, 401f
transverse sonogram, 401f
treatment, 400
Diabetes, complication, 378–379
Diabetes insipidus, 367
Diabetes mellitus, 378–381
calcification, 379f
findings, summary, 380t
imaging appearance, 379–381
neuropathic joint, 379f
treatment, 380–381
vas deferens, bilateral calcification, 379f
Diabetic gangrene, 380f
Diabetic neuropathy, 380
Diagnosis, of disease, 2
Diagnostic imaging modalities, 15–35
Diagnostic mammogram, 16–17
Diaphragm
disorders of, 82–83
findings (summary), 83t
eventration, 83
imaging appearance, 83
treatment, 83
leaves, diffuse elevation, 83f
Diaphragm elevation
causes of, 83
imaging appearance, 83
Diaphragmatic paralysis, 82
imaging appearance, 82
treatment, 82
Diaphysis, 87
Diarrhea, 153
Diarrheogenic islet cell tumors, 209
Diastatic fracture, 309–310
Diastole (relaxation phase), 250–251
Diencephalon, 289–290, 289f
Diffuse aphthous ulcers, 190f
Diffuse lung disease, 54–61
findings, summary, 59t
Diffuse lymphomatous infiltration, 346
Diffuse osteoblastic metastases, 390f
Diffuse osteoporosis, 356
Diffuse pulmonary disease, development, 58
Diffuse pulmonary edema, demonstration, 263f
Diffusion imaging, 25–26
Digestion, occurrence, 153
Digestive organs, location, 154f
Digestive system, physiology of, 153–156
Digital mammography, advantages, 16–17
Diploic space, widening, 338
Diploic vessel, dilatation, 299
Direct fusion equipment, 31–33
Diseases, 2–9
miscellaneous, 419–431
terms, summary, 2t
Disk herniation, L5-S1 level (CT scan), 147f
Dislocations, 141–144
congenital hip dysplasia, 92
fractures, 137–140
spine, 141–144
Disorders, miscellaneous, summary of findings for, 425t
Displacement (fractures), 132
Disuse osteoporosis, 108f
Diverticula, occurrence, 185–186
Diverticulitis, 186–187
contrast material, thin projection, 186f
CT scan, 187f
fibrotic healing, spasm, 187
imaging appearance, 186–187
sigmoid, 187f
treatment, 187
Diverticulosis, 185–186
imaging appearance, 186
sawtoothed configuration, 186f
treatment, 187
DNA structure, mutations, 10
Dolor (pain), acute inflammation clinical sign, 4
Dominant genes, 10
Down syndrome, 426–427
imaging appearance, 426–427
pelvis, examples, 426f
treatment, 427
Dual-energy x-ray absorptiometry (DEXA)
bone densitometry, usage, 108
bone mineral density (BMD) scan, 109f
Duchenne's muscular dystrophy (DMD), 425
Duodenal ulcer, 171
imaging appearance, 171
ulcer niche, appearance, 171f
Duplication (duplex kidney), 220–221
Dura mater, 290
extensions, 290
Dwarfism, 92
Dysarthria, 317
Dysphagia (swallowing difficulty), cause, 161–162
Dysplasia, 7

E

Ecchymosis, 5–6
Echo free, 17
Echo time (TE), 24
Ectopic kidney, 219
Ectopic pacemaker, 251–252
Ectopic parathyroid adenoma, CT scan, 376f
Ectopic pheochromocytoma, soft tissue mass, 362f

Ectopic pregnancy, 416
adnexa, live embryo (endovaginal sonography), 416f
imaging appearance, 416
treatment, 416
Ectopic ureteroceles
appearance, 221
intravenous urogram/cystogram, 223f
Edema, 4–5
terms, summary, 5t
Eisenmenger's syndrome (pulmonary hypertension), 253
Elbow
fat pad sign, 140f
fractures, detection, 138–139
posterior aspect, transverse scan, 101f
subchondral cysts, 351f
tuberculous arthritis, 100f
Electrode fractures, 42
Electrolyte balance, maintenance, 217
Embolism, 271–274
Embolus, 272
Emphysema, 55–56
bullae, 55
chest projections, 55f
dirty chest appearance, 56
imaging appearance, 55–56
treatment, 56
vascular change, 55
Emphysematous blebs, 56f
Emphysematous cholecystitis, 199
imaging appearance, 199
lumen/gallbladder, gas, 200f
Emphysematous cystitis, 229f
Emphysematous pyelonephritis, 225, 225f
imaging appearance, 225
treatment, 225
Empyema, 79–80
imaging appearance, 79–80
large soft tissue mass, 79f
treatment, 79–80
Emulsifier, 153
Encephalitis, 291
Enchondral bone formation, decrease, 92
Enchondromas, 8f, 119–120, 120f
imaging appearance, 119–120
Endocrine system, 354–382
physiology of, 354
radiographer notes, 354b
Endometrial carcinoma, 402–403
bladder invasion, 403f
endovaginal sonogram, 403f
imaging appearance, 402–403
sagittal T2-weighted MR image, 403f
treatment, 403
Endometrioma, endovaginal sonogram, 404f
Endometriosis, 403–404
endometrial implants, 404f
imaging appearance, 403–404
treatment, 404
urinary tract, involvement, 404
Endometritis, ultrasound image, 397f
Endosteum, 87
Endotracheal tube, 40
internal devices, findings (summary), 42t
position, 40f, 73f
Enteric-enteric fistula, development, 404–406
Enzyme deficiency, 9
Eosinophils, 337
Ependymomas, 296
Epidemiology, 9
Epididymis, sperm maturation, 386
Epididymitis, 391–392
imaging appearance, 392
longitudinal ultrasound image, 393f
radionuclide scan, 393f
treatment, 392
Epidural empyema, 293
imaging appearance, 293
right frontal region, epidural fluid collection, 293f
treatment, 294
Epidural hematoma, 311
Epiglottitis, 44–45
Haemophilus influenzae, 44–45
imaging appearance, 45, 45f
treatment, 45
Epilepsy, 326–327
FDG-PET brain images, 327f
findings, summary, 326t
imaging appearance, 326–327
treatment, 327
Epinephrine (adrenaline), secretion, 355
Epiphrenic diverticula, 163, 164f
Epiphyseal cartilage, 87
Epiphyses, 87
Erosive gastritis, causative agent, 170
Erythrocytes (red blood cells), 336, 337f
Erythropoietin, kidney production, 218
Esophageal cancer, 161–163
imaging appearance, 162–163
treatment of, 163
Esophageal diverticula, 163
Esophageal varices, 163–165
complication, 165
filling defects, 165f
imaging appearance, 164–165
treatment of, 165
Esophagitis, 158–160
treatment, 160
Esophagorespiratory fistula, 158f
Esophagram, lesion infiltration, 163f
Esophagus, 156–169
carcinoma, 162f
CT staging, 163f
early, 162f
distal part, rat-tail narrowing, 167f
distal section, functional obstruction (achalasia), 166
esophagorespiratory fistula, 158f
findings, summary, 168t–169t
Esophagus *(Continued)*
fistulization, 157
fistulous communication, 157
lower cervical portion, fish bone, 167f
meat impaction, 167f
midthoracic portion, traction diverticulum, 164f
nonopaque foreign bodies, 167
perforation, 168–169
contrast material, extravasation, 169f
Estrogen, secretion, 394
Etiology, 2
Ewing's sarcoma, 125–126
diffuse permeative destruction, 126f
imaging appearance, 126
External bony callus, formation of, 134f
External carotid artery angiogram, lateral projection, 314f
External sphincter, voluntary contraction, 217–218
Extramedullary hematopoiesis, 339, 339f
Extravascular fluid, accumulation, 5
Extrinsic asthma, 56

F

Facial fractures, 313–315
imaging appearance, 314–315
treatment, 315
Facial skeleton, mandible (exposure), 315
Fallopian tubes, 395–396
unilateral/bilateral gross dilatation, 398f
Fat
CT number, 20
suppression, 26–27
Fat-soluble vitamins, 419
Fatigue fractures (stress fractures), 136–137
Feeding arteries, arteriography, 299
Feet
interphalangeal joints, bony ankylosis, 97–98
mutilating arthritis, 98f
Female breast, 407f
Female infertility, 417–418
Female reproductive system, 394–396, 396f
diseases, findings (summary), 406t
physiology of, 394–396
Femoral head
aseptic necrosis, 340f
bone island, 123f
ischemic necrosis, 118f
Femur
distal ends of, marrow infiltration in, 430f
fracture, 136f
mid shaft projections, osteoid osteoma, 121f
Fetal age measurement, BPD, 414
Fetal femur, length measurement, cursors in, 414f
Fetus
BPD in, 414f
cranial architecture in, 18f

Fibromuscular dysplasia, 264
string-of-beads pattern, 264f
Fibrous dysplasia, 116, 118t
humerus, expansile lesion, 117f
imaging appearance, 116
medullary cavities, ground-glass appearance, 117f
treatment, 116
Fifth metacarpal, neck fracture, 140f
Fifth metatarsal base, Jones fracture, 141f
Fingers
osteoarthritis, 99f
proximal interphalangeal joint of, effusion and periarticular swelling of, 112f
First metatarsophalangeal joint
rat bite erosions, 113f
soft tissue swelling, 105f
Fissures, 288
Fluid-filled structures, echoes, 17
^{18}F-fluorodeoxyglucose (18F-FDG), decreased uptake of, 31f
Fluorodeoxyglucose-PET scan, bone metastases, 129f
Focal neurologic signs, 309
Folic acid, deficiency, 341
Follicle-stimulating hormone (FSH), 364
Follicular carcinoma, 371–372
Forearm, fractures, 139–140
Foreign bodies, 166–168
Fractures, 131–137
angulation, 132
C7 vertebral body, 143f
casts, 133
classification, 132f
delayed union, 135
dislocation, 137–140
displacement, 132
elbow, detection, 138–139
external fixation, 133
lower leg, 133f
external reduction (closed reduction), 133
findings, summary, 142t
healing, 134–135
tibia, 135f
hematoma, formation, 134f
imaging appearance, 132–134
internal fixation, 133
scaphoid, 133f
malunion, 135, 135f
nonunion, 135
carpal navicular bone, 135f
complication, 138
odontoid process, 143–144
open reduction, 133
internal fixation, usage, 133f
reduction, 133
site, upper body (bone scan), 138f
spine, 141–144
stress images, 134–135
treatment, 133–134
types of, 131–134
union, dense callus formation, 134f
Frontal sinus, osteoma, 121f
Full-field digital mammography (FFDM), 16–17
Full spine images, acquisition, 147
Function, loss of, as acute inflammation clinical sign, 4
Functional MRI (fMRI), 27
Functioning parathyroid adenoma, preoperative localization, 375
Fused image, creation, 16
Fusiform aneurysm, 266, 266f
Fusiform soft tissue mass, production, 106
Fusion imaging, 31–35
PET/CT of the body, 34f
summary of, 33t

G

Gadolinium (intravenous contrast agent)
enhancement, 27f
usage, 25
Gait disturbances, 89
Galeazzi fracture, 139–140
Gallbladder, 156, 156f, 197–200
calculi, 198f
findings, summary, 200t
hypoechoic, 18f
ultrasound images, 17f
Gallstones (cholelithiasis), 197–198
diagnosis, oral cholecystography (OCG) technique, 197–198
fissuring, Mercedes-Benz sign, 198f
imaging appearance, 197–198
oral cholecystogram, 198f
radiopaque contrast material, malabsorption, 198
ultrasound image, 199f
Gamma camera, 28
Ganglion cells, damage in, 5
Gangrene, 5
Gastric atrophy, 341
Gastric banding, in obesity, 423
Gastric carcinoma
CT staging, 176f
imaging appearance, 174–176
linitis plastica pattern, 174f
polypoid mass, 174
ulceration, presence, 174f
Gastric ulcer, 171–173
evaluation, endoscopy (role), 173
healing, 173f
imaging appearance, 172–173
radiating folds, 173f
Gastrinomas, 209
Gastritis, 170
imaging appearance, 170
rugal folds, thickening, 170f
superficial gastric erosions, presence, 174f
treatment, 170
Gastroesophageal reflux disease (GERD), 158–159
Gastrointestinal system, 152–215
radiographer notes, 153b
Gastroplasty, in obesity, 423
Gaucher's disease, 430–431
femurs, distal ends (marrow infiltration), 430f
imaging appearance, 430
treatment, 430–431
Genders, infectious diseases, 383–386
Generalized osteoporosis, causes, 109
Genetic amino acid disorders, 428–431
summary of findings for, 431t
GERD. *see* Gastroesophageal reflux disease (GERD).
Germinomas, 305
Ghon lesion, 49
Giant cell tumors (osteoclastoma), 120
distal femoral metaphysis, lesion, 120f
imaging appearance, 120
Giant emphysematous bulla, 56f
Gibbous deformity, 106
Gigantism, 364
Glioblastoma multiforme, T1-weighted axial/coronal MR images, 296f
Glioblastomas, 295–296
Glioma, 295–299
brainstem glioma, sagittal MR image, 297f
imaging appearance, 296–299
infiltrating glioma, T2-weighted MR image, 298f
treatment, 299
Glomerulonephritis, 224
chronic glomerulonephritis, nephrotomogram, 224f
excretory urographic findings, 224
imaging appearance, 224
treatment, 224
Glomerulus, urine formation, 216–217
Glucocorticoids, 355
Glucose, 378
Glycogen, 155–156
Glycogen storage diseases, 430
generalized globular cardiac enlargement, with left ventricular prominence, 430f
Glycosuria, 378
Goiter, 370–371
imaging appearance, 370–371
thyroid gland, enlargement, 371f
treatment, 371
ultrasound, 371
Gonadal dysgenesis (Turner's syndrome), 427
Gonadotropins, levels, decreased, 300
Gonococcal urethral stricture, retrograde urethrogram, 386f
Gonorrhea, 385–386
Gout, 111–112
calcium, deposition, 113f
imaging appearance, 112
joint effusion, severity, 112f
periarticular swelling, 112f
tophi deposits, effusion, 112f
treatment, 112

Grading, 9
Grand mal epilepsy, 326
Granulation tissue, 4, 4t
Graves' disease, 368–369
Greenstick fractures, 132
Growth hormone, 364
  levels, decreased, 300
Gynecomastia, 409
Gyri, 288

H

Haemophilus influenzae, in meningitis, 290–291
Haemophilus influenzae type B (HiB), vaccine, inception, 44–45
Hampton's hump, 69
Hands
  calcification in moderate-size vessels of, in diabetes mellitus, 379f
  dislocation/joint destruction, posteroanterior image, 101f
  frontal and oblique projections of, 424f
  interphalangeal joints, bony ankylosis, 97–98
  in Turner's syndrome, frontal projection, 427f
Hangman's fracture, 144
  neural arch fracture/C2-C3 subluxation, 145f
Hashimoto's thyroiditis, 368
Haversian systems, 87
Head trauma, radiographic imaging purpose in, 309
Heart
  chambers, 248–249
  conduction system, 249f
  deoxygenated venous blood, return, 250
  diastole (relaxation phase), 250–251
  enlarged, 252f
  PET scan, 30f
  right atrium of, ultrasound images, 17f
  SPECT images, 30f
  systole (contraction phase), 250–251
  vascular anatomy, 249f
Heart valves
  damage, rheumatic fever, 275
  insufficiency, 275
  malfunction, 275
  narrowing (stenosis), 275
  structure, 250f
  vegetations, 275
Heberden's nodes, thickening, 98
Heel pad, thickening of, 365f
Helical scanning (CT technology), 21
Helicobacter pylori infection, 170
Hematogenous metastases, 66f
Hematogenous spread, 9
Hematoma, 5–6
Hematopoietic system, 336–353
  radiographer notes, 336b
Hemiparesis, 317
Hemiplegia, 317
Hemoglobin, 336–337
  breakdown, 338
Hemolytic anemia, 338–341
  extraskeletal abnormality, 339
  imaging appearance, 338–339
  treatment, 339–341
Hemophilia, 350
  elbow, subchondral cysts, 351f
  imaging appearance, 350
  intercondylar notch, widening, 352f
  treatment, 350
Hemorrhage, 5–6
Hemorrhoids, 195–197
  imaging appearance, 196–197
  rectal filling defects, 196f
  treatment, 196–197
Hemotympanum, fluid discharge, 309
Heparin, for thrombosis, 273
Hepatic arteries, 204f
Hepatic carcinoma metastases, In-111 octreotide scan, 29f
Hepatic metastases, 205
  CT scan, 205f
  imaging appearance, 205
  treatment, 205
Hepatitis, 201
Hepatitis A virus (HAV), 201
Hepatitis B virus (HBV), 201, 201f
Hepatitis C virus (HBC), 201
Hepatitis E virus, 201
Hepatocellular carcinoma, 203–204
  CT scan, 204f
  imaging appearance, 203–204
  treatment, 204
Hereditary bone diseases, findings (summary), 93t–94t
Hereditary diseases, 9–10, 43–44, 218–222, 426–431
  findings, summary, 222t, 428t
  number/size, anomalies, 218–219
  rotation/position/fusion, anomalies, 219–220
  terms, summary, 11t
  treatment of, 221
Hereditary disorders, findings (summary), 44t
Herniation, intervertebral disks, 144–146
  imaging appearance, 145–146
  treatment, 146
Herpesvirus, 160
Heterozygous trait, 10
Hiatal hernia, 165–166
  air-fluid level, lateral chest radiograph, 166f
  imaging appearance, 165–166
  lower quadrant pain, CT scan, 165f
  sac, ulcer, 159f
  treatment, 166
High blood pressure (hypertension), 263
  definition, 263
  prolongation, 264
High-output cardiac failure, development, 369
Hilar lymph node calcification, popcorn radiographic appearance, 52
Hilum, unilateral enlargement, 64
Hip
  calcific debris, 384f
  dislocations, 142f
  dysplasia, 95f
  osteoarthritis, 99f
Hippocampal sclerosis (mesial temporal sclerosis), 326
Histoplasmoma, 52
  central calcification, 52f
Histoplasmosis, 52
  diffuse calcifications, 52f
Homocystinuria, 428–429
  imaging appearance, 429
  spine, osteoporosis, 429f
  treatment, 429
Homozygous trait, 10
Horizontal partial-thickness tear, 103f
Hormones, 354
  chemicals, power, 355
  hyperactive production, 354
  hypoactive production, 354
Horseshoe kidney, 219–220
  nephrogram/calyceal filling, 221f
Hot thyroid nodules, 368
Human immunodeficiency virus (HIV), 12
Humerus
  expansile lesion of, 117f
  osteolytic metastasis to, 130f
Huntington's disease, 328–329
  CT scan, 329f
  imaging appearance, 328–329
  treatment, 328–329
Hyaline membrane disease (idiopathic respiratory distress syndrome), 44
  imaging appearance, 44, 44f
  lungs, progressive underaeration, 44
  treatment, 44
Hydatidiform mole, longitudinal sonogram, 417f
Hydrocephalus, 330–332
  aqueduct, obstruction, 331f
  communicating, 331
  foramen of Monro, obstruction, 330f
  fourth ventricle outlet, obstruction, 331f
  imaging appearance, 331–332
  noncommunicating (obstructive), 330–331
  normal-pressure, 331
  treatment, 332
Hydronephrosis
  distinguishing Wilms' tumor from, ultrasound in, 240
  excretory urogram, 235f
  longitudinal ultrasound images, 235f
  pelvicalyceal system, dilatation, 234f
  physiologic form, 234

Hydrosalpinx, 396
fallopian tubes, unilateral/bilateral gross dilatation, 398f
Hydroureter, 231
Hyperechoic, echo intensity, 17, 18f
Hyperglycemia, 378
Hypernephroma (renal cell carcinoma), 237–238
Hyperparathyroidism, 374–377
brown tumors, production, 375f
distal clavicle, erosion, 374f
imaging appearance, 374–377
lumbar spine, lateral projection, 375f
primary hyperparathyroidism, 374
salt-and-pepper skull, 375f
secondary hyperparathyroidism, 374
subperiosteal bone resorption, 374f
tertiary hyperparathyroidism, 374
treatment, 377
tumoral calcification, 376f
Hyperpituitarism, 364–366
imaging appearance, 364–366
treatment, 366
Hyperplasia, 7
Hypertension (high blood pressure), 263–265
imaging appearance, 263–265
renovascular, 264f
secondary hypertension, 263
treatment, 264–265
Hypertensive heart disease, 265–266
ascending aorta, generalized tortuosity/elongation, 266f
chest, lateral projection, 265f
imaging appearance, 265–266
treatment, 266
Hyperthyroidism, 368–369
imaging appearance, 369
radioactive iodine scans, 370f
treatment, 369
Hypertrophic pyloric stenosis, longitudinal sonogram, 171f
Hypertrophic spurring, 146f
Hypertrophy, 7
Hypervitaminosis, 421–422
imaging appearance, 421–422
shoulder joints, calcification, 422f
treatment, 422
Hypoadrenalism, 357
Hypoechoic, echo intensity, 17, 18f
Hypoglycemic shock (insulin shock), 379
Hypoparathyroidism, 377–378
imaging appearance, 377–378
primary hypoparathyroidism, 377–378
skull, frontal projection, 377f
treatment, 378
Hypopituitarism, 366
Hypoplastic kidney, 219
Hypothalamus, 289–290
Hypothyroidism, 369–370
Hypoxemia, ARDS, 73
Hysterectomy, involvement, 406
Hysterosalpingogram, 397f

I

Iatrogenic disease, 2
Iatrogenic pneumoperitoneum, 212
Idiopathic atrophy, 357
Idiopathic disease, 2
Idiopathic respiratory distress syndrome (IRDS), 44
Ileocecal valve, intussusception, 182
Imaging
integrated, 31–33
perfusion, 26–27
Imaging descriptors, summary of, 16t
Imaging features, 16
Immune, term (usage), 11
Immune response, suppression, 2b
Immunity disorders, 11
terms, summary, 12t
Incomplete fracture, 131
Incontinence, 217–218
Infancy, rickets (system disease), 110
Infantile cortical hyperostosis (Caffey's disease), 7f
Infantile hypertrophic pyloric stenosis (IHPS), occurrence, 170
Infantile polycystic kidney disease, excretory urogram, 238f
Infants, mediastinal emphysema, 75f
Infarct, 5
Infarction, 5
Infectious arthritis, 98–100
imaging appearance, 99–100
Infectious disease exposure, 11
Infectious disorders, 95–106, 107t
Infectious gastritis, diagnosis, 170
Infectious hepatitis. *see* Hepatitis A virus (HAV).
Infectious mononucleosis, 349
chest, frontal/lateral projections, 350f
imaging appearance, 349
treatment, 349
Infective endocarditis, 278–280
echocardiogram, 279f
imaging appearance, 278–280
treatment, 280
Infiltrating cancer, progression, 162
Infiltrating glioma, T2-weighted MR image, 298f
Inflammation, 3–4, 4t
Inflammatory disorders, 95–106, 107t, 224–227
findings, summary, 228t
Inflammatory process, summary of terms for, 4t
Inflammatory response, events in, 4b
Injuries, healing, 4
Insulin shock (hypoglycemic shock), 379
Insulinoma, 209
Integration, in imaging, 16, 16t
Internal bony callus, formation of, 134f
Internal carotid artery, ulceration, 320f
Interphalangeal joints, bony ankylosis, 97–98
Interstitial pneumonia, 46–47
diffuse peribronchial infiltrate, 47f
imaging appearance, 46
treatment, 47
Intervertebral disks
central bulging, CT scan, 147f
herniation, 144–146
imaging appearance, 145–146
MR image, 148f
treatment, 146
space, narrowing, 146f
Intraarticular components, treatment, 103
Intrabronchial foreign bodies, 74
imaging appearance, 74
nail, presence, 74f
treatment, 74
Intracerebral brainstem hematoma, 322f
Intracerebral hematoma, 313
imaging appearance, 313
lateral ventricles, acute bleeding, 313f
noncontrast CT scan, 321f
treatment, 313
Intracranial hemorrhage, 317
Intramembranous ossification, 87
Intramural fistula, 190f
Intraparenchymal hemorrhage, 320–321
Intrathoracic kidney, 219
image, 220f
Intravenous contrast agent (gadolinium), usage, 25
Intrinsic asthma, 56
Intrinsic rhythm, of pacemaker cells in SA node, 250–251
Intussusception, 181–182
colon, obstruction, 182f
doughnut-shaped lesion, ultrasound image, 183f
imaging appearance, 182
reduction, rectal insufflation, 182
treatment, 182
Iodinated contrast material, intravenous injection, 20
Ionizing radiation, 15–16
IRDS. *see* Idiopathic respiratory distress syndrome (IRDS).
Iron deficiency anemia, 337
Irritable bowel syndrome, 191
Ischemia, 5
Ischemic colitis, 191
imaging appearance, 191
soft tissue polypoid densities, 191f
treatment, 191
Ischemic heart disease, frontal projection of chest, 258f
Ischemic necrosis, bone, 116–119, 118t
Isoechoic, echogenicity, 17
Ivory vertebra, 389–390
lymphoma, 347f
Ivory vertebral body, 130
diffuse sclerosis, 130f

J

Jaundice (development), cirrhosis, 202
Jefferson fractures, 143
  frontal projection, CT scan, 144f
Joint fragmentation, 384f
Joint hemorrhages, repetition, 350
Joint space destruction, 100f
Jones fracture, 140
  fifth metatarsal, base, 141f
Juvenile-onset diabetes, 378
Juxta-articular osteoporosis, 99–100
Juxtaglomerular apparatus, 218

K

Kaposi's sarcoma, 12
  alimentary tract dissemination, 12
  small bowel study, 12f
Kidney stones, 228
  formation, 229–231
  imaging appearance, 228–231
  preventive measures, 231
  treatment, 231
Kidneys
  complete fusion of, 219–220
  excretory phase of, 23f
  function, deterioration, 243
  hypoplastic, with compensatory hypertrophy, 219f
  importance, 218
  internal structure, 218f
  intrathoracic, image, 219, 220f
  left, malrotation, 220f
  renal cysts, unifocal masses, 234
  right-sided pelvic, 220f
  solitary, excretory urogram/aortogram, 219f
  urinary system component, 216
  venous occlusion, 243
Klinefelter's syndrome, 427
Knees
  menisci, tears, 103
  multiple lytic lesions, brown tumors, 375f
  osteoarthritis, 99f
  Paget's disease, 115f
  sagittal MR image, 103f
Kwashiorkor (protein-calorie malnutrition), 422
Kyphotic angulation, 106

L

L4 vertebral body, diffuse sclerosis of, 130f
L5-S1 level, disk herniation, CT scan, 147f
Large bowel, distention, 181f
Large bowel obstruction, 193
  annular carcinoma, 195f
  cecum, dilatation, 193f
  gas pattern, upper/lower abdominal radiographs, 194f
  imaging appearance, 193
  treatment, 195
Large intestine, divisions of, 155f
Laryngeal edema, 11
Le Fort fractures, severity, 315
Le Fort II fracture, 317f
Lead lines, 116f
Lead-pipe colon (chronic ulcerative colitis), 189f
Lead poisoning, 114–115, 118t
  imaging appearance, 115
  treatment, 115
Left arm, battered-child syndrome (frontal radiograph), 138f
Left atrial calcification, mitral stenosis, 276f
Left kidney
  malrotation, 220f
  parenchyma, multiple deposits, 231f
  sagittal ultrasound image, 237f
Left main coronary artery, posteroanterior cranial projection, 259f
Left posterior rib fracture, CT scan, 78f
Left renal artery, acute embolic occlusion, 273f
Left renal pelvis, nephrostomy tube placement in, 230f
Left renal vein invasion, renal cell carcinoma, 240f
Left-sided heart failure
  cardiac enlargement, radiographic appearance, 260–261
  diffuse perihilar alveolar densities, demonstration, 261f
Left sylvian fissure, subarachnoid enhancement, 291f
Left-to-right shunts, 252–254
Left ureter, contrast extravasation, 229f
Leukemia, 342–344
Leukocytes (white blood cells), 336, 337f
  migration, 3–4
Linear skull fracture, 309–310
Lingular collapse, 74f
Lipomas, 8
Liver, 201–205
  cells, metabolism role, 155–156
  cirrhosis, 202–203
    fatty infiltration, CT scan, 202f
    imaging appearance, 202–203
    treatment, 202–203
  findings, summary, 205t
  marginated infrahepatic mass in, T1-weighted coronal MR image, 243f
  responsibility, 153–155
  three-phase CT scanning, 204f
  transverse image, 25f
Localized ileus, 180–181
Location, in imaging, 16, 16t
Loculated pleural fluid (phantom tumors), frontal chest radiograph, 263f
Long bone, 88f
  aneurysmal bone cyst, presence, 122
  Paget's disease, destructive phase, 113
Longitudinal spinal ligaments (poker spine), ossification, 96
Loop of Henle, 217
Lou Gehrig's disease (Amyotrophic lateral sclerosis), 330
Low-grade brain tumor, PET cerebral study (three-dimensional reconstruction), 297f
Lower abdomen, CT scan, 20f
Lower abdominal aorta, calcification in the walls of aneurysms of, 266f
Lower cervical portion, fish bone, 167f
Lower leg
  demineralized bones of, 426f
  external fixation, 133f
Lower lumbar spine
  lateral view, 149f
  plain lateral radiograph, 148–149
Lower respiratory system, inflammatory disorders, 45–54
  findings, summary, 48t
Lower tibial shaft, expansile lesion, 351f
Lumbar disk
  CT scan, 146f
  herniation
    MR image, 147f
    myelogram, 146f
Lumbar spine
  frontal projection of, 430f
  lateral projection of, 375f
  vertebral fusion, 97f
Lumen
  finger-like projections, 241
  gas in, 200f
Luminal obstruction, carcinoma, 162
Lung abscess, 48–49
  bacterial pneumonia, 48f
  imaging appearance, 48–49
  multiloculated capsule, CT scan, 48f
  treatment, 48–49
Lungs
  air passage, blockage, 43
  apices, 49f
  diffuse alveolar pattern, 262f
  diffuse bilateral symmetric infiltration, 262f
  diffuse calcifications in, 52f
  disorders, 72–76
    findings (summary), 76t
  high-resolution CT scan, 21f
  illustration, 39f
  interstitial spaces of, transudation of fluid into, 261–262
  metastases to, 371
  vital gas exchange, 39
Luteinizing hormone (LH), 364
Lye, ingestion (corrosive stricture), 162f
Lymphadenopathy, CT scan, 193f
Lymphangitic metastases, bronchovascular markings (coarsening), 68f
Lymphatic leukemia, 342
Lymphatic spread, 9
Lymphocytes, representation, 337
Lymphography, 346–348

Lymphoma, 344–348
chest image, 345f
CT scan, 348f
diffuse reticular/reticulonodular changes, 345f
imaging appearance, 344–348
ivory vertebra, 347f
manifestation, 346f
nodal uptake, gallium scanning, 348
right kidney, lymphomatous mass replacement, 347f
skeletal involvement, 347f
staging, 346–348
stomach, 346f
supraclavicular adenopathy, history, 348f
treatment, 348

M

Magnetic resonance angiography (MRA), 25
image, 27f
intravenous contrast agent (gadolinium), 25
Magnetic resonance imaging (MRI), 12–13, 24–28
advantages, 24–25
brain image, 26f
diffusion imaging, 25–26
disadvantage, 25
fat suppression, 26–27
functional MRI (fMRI), 27
importance, 24
patient claustrophobia, 25
perfusion imaging, 26–27
physics, 24
pulse sequence, scanning parameters, 24
radio frequency (RF) pulse, 24
receiver coil, 24
relaxation, 24
sagittal lumbar spine image, 26f
summary of, 27t
T1-weighted images, 24
T2-weighted images, 24
upper abdomen image, 25f
Magnetic resonance spectroscopy (MRS), 25
Malabsorption, sprue, 184f
Malabsorption disorder, 182
Male fertility, 387
Male reproductive system, 386–387, 387f
diseases, findings, summary, 394t
physiology, 386–387
Malignant bone tumors, 124–127
neoplasia, findings (summary), 127t–128t
treatment, 127
Malignant gastric ulcer, transition (abruptness), 173f
Malignant neoplasms, 7
Malignant solitary pulmonary nodule (bronchogenic carcinoma), 62f
CT scan, 63f
Malignant teratoma, transverse testicular scan, 395f
Malignant tumor, grading, 9
Mallory-Weiss syndrome, 168
Mammography, 16–17, 17t
magnification-spot compression, 410f
Mandibular fractures, 315
panoramic examination, 317f
Marfan's syndrome, 427–428
arachnodactyly, 428f
arteriogram, 428f
imaging appearance, 427
treatment, 428
Marrow
hyperplasia, 342
neoplastic cells, proliferation, 343
Master gland. *see* Pituitary gland.
Mastication, digestion, 153
Mastoid process, ecchymosis, 309
Maximum intensity projections (MIPs), CT postprocessing, 21
Mechanical small bowel obstruction, 178
Meconium ileus, bowel distention, 43f
Mediastinal emphysema (pneumomediastinum), 75
imaging appearance, 75
infants, 75f
lateral displacement, 75f
treatment, 75–76
Mediastinal masses, 80–82
configuration, 80
findings, summary, 81t
plain chest radiographs, 80
treatment, 80–82
Medulla, 289, 289f
Medullary carcinoma, 372
Medullary cavity (marrow), 87
Medulloblastomas, 296
Megaloblastic anemia, 341
chronic atrophic gastritis, 341f
imaging appearance, 341
treatment, 341
Melanoma, 424–425
Membranous bone formation, autosomal dominant condition, 92
Menarche, 394
Meningeal vessel, dilatation, 299
Meninges, 290, 290f
Meningioma, 299
CT scan, 301f
imaging appearance, 299
MRI, 300f
parietal meningioma, plain skull image, 301f
spinal meningioma, anteroposterior/lateral myelogram, 302f
treatment, 299
Meningitis, 290–291
bacterial meningitis, 290–291
imaging appearance, 291
subarachnoid enhancement, 291f
treatment, 291
viral meningitis, 290–291
Meningocele, 89
Meningomyelocele, 90f
Meniscal tear, 103f
Menopause, 396
Menorrhagia, 337
Menstrual cycle, 395–396
Menstruation
menstrual phase, 396
proliferative phase (postmenstrual phase), 396
secretory phase (postovulatory phase), 396
Mental deterioration, 309
Mercedes-Benz sign, fissuring, 198f
Metabolic bone disease, 108–115, 115t
Metabolism, maintenance, 217
Metacarpal sign, 427
Metaphysis, 87
Metastases, brain
axial T2-weighted/FLAIR MR image, 307f
CT scan, 307f–308f
Metastatic carcinoma, 307–309
Metastatic melanoma, small bowel (filling defects), 425f
Metastatic testicular seminoma, CT scan, 395f
Metastatic thyroid carcinoma, 66f
Microcephaly, 429
Micturate, 217–218
Midbrain, 289, 289f
Middle mediastinal mass, chest projections, 81f
Miliary tuberculosis, 50
nodules, presence, 50f
Mineralocorticoids, salt/water balance, 355
Minimum intensity projections (MinIPs), CT postprocessing, 21
Mitral insufficiency, 276–277
chest, frontal/lateral projections, 277f
Mitral stenosis, 275–276
chest, frontal/lateral projections, 276f
echocardiogram, 277f
imaging appearance, 276
left atrial calcification, 276f
treatment, 277
Mitral valve (bicuspid valve), 248–249
prosthetic replacement, 275f
Monocytes, 337
Monteggia fractures, 139–140
anterioposterior/lateral projection, 141f
Morbidity, 9
Mortality, 9
MRA. *see* Magnetic resonance angiography (MRA).
MRI. *see* Magnetic resonance imaging (MRI).
MRS. *see* Magnetic resonance spectroscopy (MRS).
Mucormycosis
homogeneous mass, fungus ball, 380f
infection, 380
roof of right orbit, destruction of, 333f

Mucoviscidosis (cystic fibrosis), 43
Mucus, production (excess), 54
Multiloculated capsule, CT scan, 48f
Multinodular goiter
  radioactive iodine scan, 371f
  ultrasound image, 371f
Multiplanar body imaging, PET scan with, 30f
Multiple myeloma, 126–127
  bone formation, absence, 127
  diffuse infiltration, 127f
  imaging appearance, 126–127, 126f
  malignancy, dissemination, 126
  osteolytic lesions, 126f
  PET oncologic survey findings, 128f
Multiple pregnancies, endovaginal sonogram, 415f
Multiple sclerosis, 324–325
  axial T2-weighted MR image, 325f
  findings, summary, 326t
  imaging appearance, 324–325
  treatment, 325
Munchausen syndrome by proxy, 137
Muscular dystrophy, 425
  imaging appearance, 425–426
  lower leg, demineralized bones of, 426f
  treatment, 426
Mutations, 10
Mycobacterium tuberculosis, 49
Myelin sheath, 287
Myelocytic leukemia, 342
Myelomeningocele, 89
Myelophthisic anemia, 341–342
Myocardial infarction, 256–257
Myocardial stress/rest perfusion single-photon emission computed tomography scan, 257f
Myocardium (perforation), intravenous electrode, 42
Myomas, 8

N

Napkin-ring carcinoma (annular carcinoma/apple-core carcinoma), 192
Nasal bone fractures, 314
Navicular fractures (scaphoid fractures), 137–138
  avascular necrosis, 140f
  detection, absence, 139f
  nonunion, complication, 138
Neck
  anteroposterior perspective, 320f
  of fifth metacarpal, fracture at, with volar angulation of distal fragment, 140f
  lateral projection of, 372f
Necrotic debris, removal, 4
Necrotic process, 226
Necrotic renal cell carcinoma, CT scan, 240f
Negative feedback mechanism, 355
Neoplasia, 7–9
  categories, 7
Neoplasms, 61–68
Neoplastic cells, proliferation, 343, 344f
Neoplastic transformation, induced by DNA and RNA viruses, 8
Nephroblastoma (Wilms' tumor), 240
  imaging appearance, 240
  treatment, 240
Nephrocalcinosis, 229
  multiple deposits, 231f
Nephrogenic diabetes insipidus, 367
Nephrostomy tube placement, 230f
Nervous system, 286–335
  physiology, 287
  radiographer notes, 287b
  radiographic contrast material, administration, 287b
  radiographs, exposure factors, 287b
Neural arch fracture, C2-C3 subluxation, 145f
Neuroblastoma, 360–363
  bone scan, 363f
  demonstration, nephrotomogram, 363f
  excretory urography, 360
  imaging appearance, 361–363
  metastatic to bone, 362f
  paravertebral stripes, bilateral widening, 363f
  treatment, 363
Neurologic patients, PET usage in, 31
Neuron, structure, 288f
Neutrophils (polymorphonuclear leukocytes), 337
Newborn, hemolytic anemia (erythroblastosis fetalis), 338
Niacin deficiency (pellagra), 420
Non-Hodgkin's lymphoma, CT scan, 349f
Non-small cell carcinoma, multiplanar PET lung scan, 67f
Noncommunicating (obstructive) hydrocephalus, 330–331
Noncontrast helical CT scanning, usage, 231
Noncontrast renal MRA, appearance, 264f
Nonerosive gastritis (chronic atrophic gastritis), 170
Noninvasive imaging modality, 17
Nonopaque urate crystals, deposition, 112
Nonpituitary tumors, ACTH production, 356
Norepinephrine, secretion, 355
Normal aging, 327
  axial MR image, 327f
  CT scan, 327f
  imaging appearance, 327
Normal-pressure hydrocephalus, 331
Nosocomial disease, 2
Nuclear magnetic resonance. *see* Magnetic resonance imaging (MRI).
Nuclear medicine, 28
  bone scan, 28f
  gamma camera, 28
  radiopharmaceutical ingestion, 28
  summary of, 29t
Nutritional deficiency, 419
Nutritional diseases, 419–423
  findings, summary, 423t
  radiographer notes, 420b

O

Oat cell carcinomas (small cell carcinomas), 63
Obesity, 422–423
  imaging appearance, 422–423
  retrogastric space, enlargement, 422f
  treatment, 423
Oblique fractures, 131–132
Obstructing ureteral calculus, 231f
Obstructive (noncommunicating) hydrocephalus, 330–331
Occluded internal carotid artery, intravenous DSA, 320f
Ochronosis, 429
  lumbar spine, frontal projection, 430f
Odontoid process, fractures, 143–144
  open-mouth frontal projection, 144f
Olecranon bursa, transverse scan, 101f
Olecranon fossa, posterior fat pad (appearance), 138–139
Oligodendrocytomas, 296
Oligohydramnios, 414–415
Omental cake
  CT appearance, 398
  metastases, 400f
Oncology, 7
Open fractures (compound fractures), 131
Oral cholecystogram, 198f
Orbital floor fracture, coronal CT scan, 315f
Ossification (bone formation), 87
Osteitis deformans (Paget's disease), 112–114
Osteoarthritis (degenerative joint disease), 98
  imaging appearance, 98
  joint space narrowing, 98
Osteoblastic metastases, 130f
Osteoblasts, 87
Osteochondromas, 119–122
  imaging appearance, 119
  long axis, tumor (presence), 119f
Osteoclasts, 87
Osteogenesis imperfecta (brittle bones), 91
  anteroposterior/lateral projections, 93f
  imaging appearance, 91, 92f
  treatment, 91
Osteogenic sarcoma, 124–127
  CT scan, 124f
  destructive lesion, 125f
  imaging appearance, 124
  MRI, 124f
Osteoid osteomas, 120–122
  femur, mid shaft projections, 121f
  imaging appearance, 121–122
Osteolytic metastases, 129

Osteomalacia, 109–110, 420–421
imaging appearance, 110
spongy bone, trabeculation (increase), 111f
treatment, 111
Osteomas, 120
frontal sinus, 121f
imaging appearance, 120
Osteomyelitis, 104, 104f
changes, 104
radionuclide bone scan, 104f
skull, 294–295
Osteopetrosis, 90–91
bones, sclerosis, 90f
imaging appearance, 90–91
treatment, 91
Osteoporosis, 108–109
aging, 109f
dual-energy x-ray absorptiometry (DEXA) bone densitometry, usage, 108
imaging appearance, 109
spine, DEXA BMD scan, 109f
treatment, 109
Osteoporotic bone, mineral salts (loss), 108
Ottonello method, 86b–87b
Ovarian carcinoma, recurrence (PET scan), 400f
Ovarian cysts, 397–400
imaging appearance, 398–400
omental cake, CT appearance, 398
T2-weighted axial MR image, 399f
treatment, 398–400
ultrasound image, 398f
Ovarian tumors, 397–400
Ovaries
cyclic changes, 395
cystadenocarcinoma, psammomatous calcifications, 399f
primary cystadenocarcinoma, 398
Overriding aorta, spin-echo MRI demonstration, 254
Ovulation, 394
Oxytocin, production, 364

P

Pacing failure, electrode failures, 42
Paget's disease (osteitis deformans), 112–114
clinical complications, 113–114
imaging appearance, 113–114
knee, cortical thickening (appearance), 115f
skull, nuclear medicine bone scan, 114f
treatment, 114
Pancreas, 156, 206–210
cancer, 209
cure, 210
detection, 209
imaging appearance, 209–210
treatment, 210
Pancreas *(Continued)*
carcinoma, noncontrast CT scan, 209f
control, 156
findings, summary, 210t
head, carcinoma, 209–210
transhepatic cholangiogram, 210f
surgical resection (total pancreatectomy), 210
tissue, cytologic examination, 209
Whipple procedure, 210
Pancreatic adenocarcinoma, 209f
Pancreatic calcifications, 207
Pancreatic pseudocyst, 208–209
calcified, 208f
CT scan, 208f
imaging appearance, 208–209
loculation, 208
pseudocysts, visibility, 208
treatment, 208–209
ultrasound examination, 208
ultrasound image, longitudinal sonogram, 208f
Pansinusitis
coronal CT scan, 333f
mucormycosis, 333f
Papanicolaou smear examination, 404
Papillary carcinoma, 371
Papillary destruction, early stage of, 226f
Papillary necrosis, 226–227
generalized saccular/club-shaped configuration, 227f
imaging appearance, 226
treatment, 226–227
Papilloma, 8
Parathormone (parathyroid hormone), 374
Parathyroid adenoma, technetium-99m sestamibi (injection), 376f
Parathyroid glands, 374–378
diseases, 374–378
findings, summary, 378t
physiology, 374
thyroid and, 368f
Paravertebral tissues, ossification, 96
Parietal meningioma, plain skull image, 301f
Parkinson's disease, 329
Passive immunity, 11
Patent ductus arteriosus, 252–253
cardiomegaly, frontal chest radiograph, 253f
Pathologic conditions, radiography, 2
Pathologic fractures, 132, 135–136, 136f
CT/MRI, usage, 136
imaging appearance, 136
treatment, 136
Pathology, introduction to, 1–14
Pectus excavatum, lateral chest radiograph, 429f
Pelken spur, 420
Pellagra (niacin deficiency), 420
Pelvic inflammatory disease, 385–386, 396–397
chronic, transverse sonogram, 397f
imaging appearance, 396–397
suspicion, 386
treatment, 397
Pelvic kidney, 219
collecting system, 220f
Pelvicalyceal system
dilatation, 234f
distortion/displacement, 241f
Pelvis
bladder calculi, plain radiograph, 232f
contrast-enhanced MRA, 271f
osteoblastic metastases, 130f
Paget's disease, sclerosis/cortical thickening, 114f
Peptic ulcer disease, 171–174
complications, 171
treatment, 174
Percutaneous transluminal coronary angioplasty (PTCA), 260f
Perfusion, in imaging, 16, 16t
Periarticular demineralization, 108f
Pericardial effusion, 280–281
cardiac silhouette, globular enlargement, 280f
demonstration
angiocardiography/intravenous carbon dioxide injection/pericardial tap, usage, 280
CT scan, usage, 280f
echocardiogram, 281f
findings, summary, 280t
imaging appearance, 280–281
MRI, transverse/sagittal images, 281f
treatment, 281
Pericardium, 252
Periosteum, 87
Peripheral bronchial adenoma, nonspecific solitary pulmonary nodule, 65f
Peripheral lung nodule, CT-guided FNAB, 65f
Peripheral nervous system (PNS), 287
Peripherally inserted central catheter (PICC)
line placement, 41f
long-term venous access device, 41
Peristalsis (smooth muscle contractions), 153
Peristaltic contractions, sexual stimulation, 386–387
Peritoneal cavity, fluid accumulation (ascites), 202
Permeable membrane, 4t
Pernicious anemia, 341
Personal protective equipment (PPE), usage, 11
Petit mal epilepsy, 326
Phagocytosis, 3–4
Phantom tumors (loculated pleural fluid), frontal chest radiograph, 263f

Phenylketonuria, 429
Pheochromocytoma, 360
  axial MR image, 362f
  ectopic, 362f
  imaging appearance, 360
  longitudinal/transverse, ultrasound images, 361f
  pear-shaped mass, 361f
  treatment, 360
Phlegmonous emphysematous gastritis, distal stomach (ulceration), 170f
Phlegmonous gastritis (bacterial gastritis), 170
Photoelectric effect, 28
Physiologic map, nuclear medicine production, 28
Pia mater, 290
  acute inflammation (meningitis), 290–291
Pica, ingestion, 116f
Pineal germinoma, sagittal T1-weighted MR image, 305f
Pineal teratoma, nonenhanced CT scan, 306f
Pineal tumor, 305–306
Pituitary adenoma, 300
  coronal CT scan, 304f
  imaging appearance, 301–303
  sagittal/coronal T1-weighted contrast-enhanced MR image, 304f
  sella turcica (ballooning), 366f
  treatment, 303
Pituitary gland, 364–367
  anterior lobe, hormones (secretion), 364
  diseases, 364–367
    findings, summary, 367t
  hormones, 365f
  physiology, 364
  posterior lobe, hormones (production), 364
Pituitary tumor
  detection/defining, MRI, 301–302
  diagnosis of, 365–366
Platelets (thrombocytes), 336, 337f
  diseases (bleeding disorders), 349–352
    findings, summary, 352t
Platelike atelectasis, 73f
Pleura
  double-walled membrane, 39
  illustration, 39f
  involvement, 345–346
Pleural disorders, 76–82
  findings, summary, 79t
Pleural effusion, 77–79, 78f
  chest, frontal projection, 79f
  chest radiograph appearance, 78
  imaging appearance, 77–79
  left posterior rib fracture, CT scan, 78f
  pleural thickening/fibrosis, 77–78
  right lateral decubitus chest radiograph, 78f
  sharp angle blunting, 78f
  treatment, 79
Pleural space, CVP catheter placement, 41f
Pneumoconiosis, 59–61
  findings, summary, 61t
Pneumocystis jirovecii pneumonia, 8
  diffuse bilateral airspace, 13f
Pneumomediastinum (mediastinal emphysema), 75
Pneumonia, 45–47
  air bronchogram sign, 46f
  single lobe infiltrate, density increase (CT scan), 47f
Pneumoperitoneum, 210–212
  cause, 211–212
  double-wall sign, 212f
  falciform ligament sign, 212f
  findings, summary, 212t
  gas accumulation, chest radiograph, 211f
  imaging appearance, 211–212
  semierect projection, intraperitoneal gas, 211f
  treatment, 212
Pneumothorax, 76–77
  frontal chest image, 77f
  imaging appearance, 76–77
  treatment, 77
Poker spine (longitudinal spinal ligaments), ossification, 96
Polycystic kidney disease, 236–237
  CT scan, 238f
  imaging appearance, 236–237
  infantile polycystic kidney disease, excretory urogram, 238f
  left kidney sagittal ultrasound image, 237f
  multiple cysts (detection), CT scans (usage), 237
  nephrogram phase, 237f
  treatment, 237
  ultrasound demonstration, 236–237
Polycystic ovarian syndrome (PCOS), 397–398
Polycythemia, 342
Polycythemia vera (primary polycythemia), 342
Polydactyly, right foot (image), 10f
Polydipsia, 367
  liquid, drinking (excess), 378
Polyhydramnios, 414–415
  amniotic fluid, accumulation (excess), 415f
Polymorphonuclear leukocytes (neutrophils), 337
Polyp, 8
Polypoid mass, localization, 162
Polyuria, 367
  urination, excess, 378
Pons, 289, 289f
Porcelain gallbladder, 199–200
  imaging appearance, 200
  mural calcification, 200f
  treatment, 200
Portal veins, branches of, in MRI, 25f
Positron emission tomography, 29–31
  annihilation, 29–30
  brain image, 33f
  chemotherapy, effectiveness of, 31f
  heart image, 32f
  imaging, signal detection, 30–31
  multiplanar body imaging, 30f
  myocardial viability, demonstrating, 32f
  radionuclides, 30
  summary of imaging for, 31t
  usefulness, 31
Post-traumatic carotid-cavernous fistula, 314f
Posterior mediastinal mass
  chest projections, 81f
  CT scan, 82f
Posterior urethral valves, 222
  treatment, 222
  voiding cystourethrogram, 224f
Pott's disease, 106
Pott's fracture, malleoli involvement, 140
Pregnancy, 414–416
  ectopic, 395–396
  findings, summary, 417t
Primary hyperparathyroidism, 374
Primary hypoparathyroidism, 377–378
Primary liver cell carcinoma, occurrence, 203
Primary polycythemia (polycythemia vera), 342
  hypoventilation, severity, 342f
  imaging appearance, 342
  treatment, 342
Primary tuberculosis, 49–50
  imaging appearance, 49–50
  right hilar lymph nodes, enlargement, 50f
  right upper lobe, consolidation, 49f
  unilateral right tuberculous pleural effusion, 50f
Probiotics, 182
Progesterone, secretion, 394–395
Prognosis, 2
Progressive fibrosis, histoplasmosis and, 52
Prolactin, 364
Prostate gland, 386
  cancer, transrectal ultrasound image, 389f
  carcinoma, 388–389
    axial MR image, 389f
    imaging appearance, 388
    mass, elevation, 389f
    staging, 389–390
  enlargement, excretory urography, 387–388
  metastatic carcinoma
    CT scan, 390f
    T1-weighted spin-echo MR image, 390f
Prosthetic aortic/mitral valves, 275f
Protein-calorie malnutrition (kwashiorkor), 422

Protrusio acetabuli, 111f
Proximal convoluted tubule, water/nutrients reabsorption, 216–217
Proximal femur, osteoblastic metastases, 130f
Proximal humerus, diffuse lytic destruction, 340f, 384f
Proximal ulna, displaced fracture, 141f
Psammomatous calcifications, ovary cystadenocarcinoma, 399f
Pseudocysts
  plain radiographs, 208
  spontaneous resolution, 208–209
Pseudohypoparathyroidism, 378
Pseudokidney, 182
Pseudopseudohypoparathyroidism, 378
Psoriatic arthritis, 96–98
  asymmetric bone destruction/subluxation/ankylosis, 98f
  imaging appearance, 97–98
  mutilating arthritis, 98f
Pulmonary arteries, embolic occlusion (physiologic consequences), 68
Pulmonary arteriogram, 71f
Pulmonary arteriovenous fistula, 72
  imaging appearance, 72
  right lung, radiographic image, 73f
  treatment, 72
Pulmonary capillary wedge (PCW) pressure, measurement, 41
Pulmonary edema, 261–263
  butterfly pattern, 262f
  diffuse pulmonary edema, demonstration, 263f
  imaging appearance, 261–262
  interstitial, 262f
  treatment, 262–263
Pulmonary embolism, 68–71
  chest projections, 69f
  CT scan, 5f
  imaging appearance, 68–71
  left main pulmonary artery, filling defect (CT scan), 71f
  plain chest radiograph, 69f
  pulmonary arteriogram, 71f
  radionuclide perfusion lung scan, 70f
  right pulmonary artery, filling defect, 71f
  treatment, 69–71
  ventilation-perfusion ratio (V/Q) scan, screening effectiveness, 69
Pulmonary hypertension (Eisenmenger's syndrome), 253
Pulmonary infections, recurrence, 56f
Pulmonary metastases, 65–68
  imaging appearance, 66–68
  PET images, 64f
  solitary nodule, growth, 67f
  treatment, 68
Pulmonary mycosis, 52–53
  findings, summary, 53t
  fungal infection, 52
Pulmonary neoplasms, findings (summary), 68t
Pulmonary neoplastic diseases, treatment of, 65
Pulmonary parenchyma, involvement, 345–346
Pulmonary stenosis, 254
Pulmonary stenosis (right ventricular outflow), spin-echo MRI demonstration, 254
Pulmonary trunk, enlargement, 252f
Pulmonary valve, location, 248–249
Pulmonary vascular diseases, findings (summary), 72t
Pulse sequence, 24
Purpura (thrombocytopenia), 350–352
Pus, pyogenic bacteria, 4
Pyelonephritis, 224–225
  chronic pyelonephritis, 225f
  CT, usage, 225
  imaging appearance, 225
  treatment, 225
Pyloric stenosis, 170
Pyogenic bacteria, 4t
  presence, 4
Pyogenic brain abscess, CT scan, 292f
Pyogenic organisms (pus-forming organisms), joint entry, 98–99
Pyosalpinx, 396

R

Raccoon eyes (bilateral orbital ecchymoses), 309
Radio frequency (RF) pulse, 24
Radioactive iodine scan
  hyperfunctioning (hot) nodules, 369f
  nonfunctioning (cold) nodules, 369f
  normal, 368f
Radioactive iodine scanning, 367–368
Radionuclide bone scan
  MRI, comparison with, 117
  screening, 129f
  sensitivity, 117
  triple-phase technique, usage, 137
Radionuclide cholescintigram, results, 199
Radionuclide subtraction imaging, 377f
Radiopharmaceuticals, 28
  usage, increase, 131
Rat bite erosions, examples, 113f
Reactivation tuberculosis (secondary tuberculosis), 50–51
Reactive sclerosis, 146f
Recessive genes, 10
Recombinant human deoxyribonuclease (DNase), inhalation, 43
Rectal carcinoma, 192f
  CT scan, 192f
Red blood cells (erythrocytes), 336, 337f
  bulging, 339
  diseases, 337–342
    findings, summary, 343t
Reduced penetrance, 10
Reflex arc, 287
Reflux (gastroesophageal reflux disease), 158–159
Reflux esophagitis
  development, 159
  long esophageal stricture, 160f
  ulcer, penetration, 159f
Regional enteritis (Crohn's disease), 176–177
Reiter's syndrome, 96–98
  bony erosion, 97f
  imaging appearance, 96–97
  metatarsophalangeal joint, erosive changes, 97f
Relaxation, 24
Releasing hormones, secretion, 289–290
Renal abnormalities, 339
Renal carcinoma, 237–240
  imaging appearance, 238–240
  treatment, 240
Renal cell carcinoma (hypernephroma), 237–238
  distortion/displacement, 238f
  left renal vein invasion, CT scan, 240f
  nephrotomogram, 239f
  sagittal T1-weighted MR image, 241f
  ultrasound image, 239f
Renal congenital anomalies, 221
Renal cyst, 234–236
  anechoic lesion, 235f
  appearance, nonenhancing left renal mass, 236f
  imaging appearance, 234–236
  nephrotomogram, 235f
  puncture, contrast material (instillation), 236f
  treatment, 236
  ultrasound, 235–236
  unifocal masses, 234
Renal disease, complication, 380
Renal disorders, findings (summary), 246t
Renal dysfunction, occurrence, 112
Renal failure
  acute, 243–245
  chronic, 245–246
Renal parenchyma (isthmus), 219–220
Renal pelvis
  anomalies, 220–221
  staghorn calculi, 230f
  ureters, relationship, 222f
Renal vein thrombosis, 242–243
  acute renal vein thrombosis, right kidney (radiograph), 244f
  imaging appearance, 242–243
  occurrence, 242
  renal venogram, 245f
  treatment, 243
Renovascular hypertension, 264f
  fibromuscular dysplasia, 264
    string-of-beads pattern, 264f
  PTA for, 265f
Renovascular lesion, presence of, 264
Repetition time (TR), 24

Reproductive system, 383–418
infectious diseases, findings (summary), 385t
radiographer notes, 384b
Resorption (bone destruction), 87
Respiration
cellular process, 420
control, 39
Respiratory syncytial virus (RSV), 53
bilateral pulmonary infiltrates, 54f
imaging appearance, 53
treatment, 53
Respiratory system, 36–84
endotracheal tube, 40
internal devices, 40–42
physiology of, 38
radiographer notes, 37b
relative attenuation, 3b
role of, 38
structure plan of, 38f
Respiratory tract, fistulization, 157
Rh-positive newborn, hemolytic anemia of, 11
Rheumatic heart disease, 275
Rheumatoid arthritis, 95–96
atlantoaxial joint, subluxation, 96f
hand, posteroanterior image, 101f
imaging appearance, 95–96
ligamentous involvement, 96
mutilation, 95f
periarticular osteoporosis, 95f
radiographic evidence, 95
Rheumatoid nodules, soft tissue masses, 96
Rheumatoid variants, 96–98
Rickets (vitamin D deficiency), 110–111, 420–421
imaging appearance, 110–111
treatment, 111
wrist, metaphyseal ends (cupping/fraying), 111f
Right arm, battered-child syndrome (frontal radiograph), 138f
Right atrioventricular valve (tricuspid valve), 248–249
Right external iliac artery stenosis, PTA, 272f
Right foot, metatarsals/digits (polydactyly), 10f
Right hemidiaphragm
eventration, 83f
paralysis, 82f
Right hip, dysplasia, 95f
Right internal jugular vein, CVP catheter in, 40f
Right kidney, lymphomatous mass replacement, 347f
Right lower lung, coned view, 55f
Right middle cerebral artery infarct, diffusion-weighted MR image, 319f
Right middle lobe, collapse, 74f
Right sentinel lymph node, SPECT/CT fusion imaging, 412f
Right-sided heart failure, 261
chest, front/lateral projections, 261f
Right-sided pelvic kidney, bone scan, 220f
Right-to-left shunting, 254
Right ventricular hypertrophy, spin-echo MRI demonstration, 254
Ring-enhancing lesions, computed tomography, 13f
Rotator cuff tears, 102–103
MR image, 102f
shoulder arthrography, 102f
Rubor (redness), acute inflammation clinical sign, 4
Rugal folds, thickening, 170f
Ruptured berry aneurysm, 324f
Ruptured silicone breast implants, mammogram, 410f

S

Saccular aneurysm, 266
Sacroiliac joints, bilateral symmetric obliteration, 96f
Sagittal lumbar spine, MRI of, 26f
Salmonella infection, 339
Salt-and-pepper skull, 375f
Salt maintenance, electrolyte/acid-base balance, 217
Sarcoidosis, 57–59, 58f
chest projections, 58f
diffuse coarse interstitial pattern, 58f
end-stage disease, 59f
high-resolution CT (HRCT), 57–58
imaging appearance, 57–59
treatment, 59
Sarcomas, 8
Scaphoid fractures (navicular fractures), 137–138
internal fixation, 133f
Scintigraphic image, 28
Sclerosis, 384f
Scoliosis, 147
anteroposterior spine image, curvature measurements, 148f
imaging appearance, 147
treatment, 147
Scotty dog sign, diagram, 149f
Screening radionuclide bone scan, 129f
Scurvy (vitamin C deficiency), 420
frontal projections, 421f
imaging appearance, 420
white line, 421f
Wimberger's sign, 420
Seat belt fracture, 144
CT scan, 146f
Secondary hyperparathyroidism, 374
Secondary polycythemia, 342
Secondary tuberculosis (reactivation tuberculosis), 50–51
bilateral fibrocalcific changes, 51f
imaging appearance, 51
Seeding, 9
Segmental fractures, 132
Seizure disorder, hippocampal sclerosis, 326f
Sella turcica
ballooning, 366f
enlargement, plain skull radiographs, 302
imaging, tomography/CT, 356
Seminal vesicle, 386
Seminoma, hypoechoic intratesticular mass, 393f
Septic embolism, 71–72
imaging appearance, 71–72
treatment, 72
Septic pulmonary emboli, cavitary lesions, 72f
Serum hepatitis. *see* Hepatitis B virus (HBV).
Severe acute respiratory syndrome (SARS), 53–54
imaging appearance, 54
treatment, 54
Sex hormones (androgens), 355
Sex-linked disorders, 10
Shaded surface rendering, CT postprocessing, 21
Shaken-baby syndrome, 137
Shaking palsy (Parkinson's disease), 329
Shape, in imaging, 16, 16t
Shoulder
arthrography, 102f
dislocation, 140
anterior/posterior dislocation, 142f
Sickle cell anemia, 338
acute osteomyelitis, 340f
biconcave indentations, 340f
complication, acute osteomyelitis, 339
femoral head, aseptic necrosis, 340f
intervertebral disks, expansile pressure, 339
red blood cells, bulging, 339
Sigmoid colon, annular carcinoma, 192f
Sigmoid diverticulitis, 187f
Sigmoid volvulus, 194–195
imaging appearance, 195
luminal tapering, 196f
Signs, characteristics, 2
Silicone breast implants, ruptured (mammogram), 410f
Silicosis, 59–60
chest tomogram, 60f
imaging appearance, 60
miliary nodules, calcification, 60f
progressive massive fibrosis, 60f
Simple bone cysts, 122
imaging appearance, 122
proximal humerus, oval configuration, 122f
Single-photon emission computed tomography, 28–29
brain images, 29f
disadvantage, 28–29
heart image, 30f
Sinoatrial (SA) node, impulse passage, 250–251

Sinusitis, 332–334
acute, mucosal thickening, 332f
chronic, mucosal thickening, 332f
imaging appearance, 332–334
treatment, 334
Sixth-generation scanners, slice performance, 21
Size, in imaging, 16, 16t
Skeletal lymphoma, right shoulder radiograph/T1-weighted axial MR image, 347f
Skeletal metastases, detection, 129
Skeletal system, 85–151
bone radiographs, contrast requirement, 86b–87b
middle kVp ranges, usage, 86b–87b
pathologic conditions, 86b–87b
physiology of, 87
radiographer notes, 86b–87b
syphilitic involvement, 384
tomography, requirement, 86b–87b
x-ray attenuation, 3b
Skull, 294–295
depression, 309
hair-on-end appearance, 338f
ossification, 91
osteomyelitis, 294–295
blastomycosis, 295f
imaging appearance, 294–295
treatment, 294–295
Paget's disease, 114f
traumatic processes, 309–315
findings, summary, 316t
Skull fracture, 309–311
CT bone-window image, 310f
imaging appearance, 309–311
lateral projection, 310f
treatment, 311
Small bowel, 176–182
diffuse dilatation, 184f
findings, summary, 183t
folds, thickening (irregularity), 184f
Small bowel obstruction, 177–180
CT diagnosis, 180f
CT scans, 180f
dilated loops, 179f
gas-filled bowel, dilated loops, 179f
imaging appearance, 177–180
impacted bezoar, barium upper gastrointestinal series, 179f
site, 178
supine/upright projections, 178f
treatment, 180
Small cell carcinomas (oat cell carcinomas), 63
Smooth muscle contractions (peristalsis), 153
Soft tissue
calcification, 375
relative attenuation, 3b
Soft tissue polypoid densities, 191f
Solitary kidney, excretory urogram/aortogram, 219f
Solitary metastases, 66–68
examination, 67f
Solitary pulmonary nodule, 61–63
CT scan, 62–63
imaging appearance, 61–63
Somatic nervous system, function, 287
Specialized imaging techniques, 15–35
radiographer notes, 16b
Sperm, formation (spermatogenesis), 386
Spherocytosis, 338
Spiculated lesion, 410f
Spina bifida, 89–90
imaging appearance, 89–90
occulta, 89f
treatment, 89–90
Spinal cord, location, 290
Spinal disorders, findings, summary, 149t
Spinal meningioma
anteroposterior/lateral myelogram, 302f
demonstration, 299
Spine
DEXA BMD scan, 109f
dislocations, 141–144
stable/unstable injury, 141–142
fractures, 141–144
stable/unstable injury, 141–142
frontal projection, 143
Spiral fractures, 131–132
Spiral scanning (CT technology), 21
Spleen, 212–214
enlargement, 212–213
imaging appearance, 212–213
lymphoma, 213f
rupture, 213–214
imaging appearance, 213–214
Splenectomy, for spherocytosis, 339
Splenic disorders
findings, summary, 214t
treatment, 213–214
Splenomegaly, CT scan, 213f
Spondylolisthesis, 148–149
imaging appearance, 148–149
lower lumbar spine, lateral view, 149f
treatment, 149
Spondylolysis, 148–149
diagnosis, 149
imaging appearance, 148–149
lumbar spine, oblique projection, 149f
Scotty dog sign, diagram, 149f
treatment, 149
Spontaneous pneumothorax, 76f
Squamous carcinoma, 65
Squamous cell carcinoma, 8
Staghorn calculi, spiral CT scan, 230f
Staging, 9
Standard Precautions (CDC), 11
Staphylococcal osteomyelitis, 105f
Steatorrhea, 182
Stenosis, luminal tapering, 196f
Stereotaxic needle biopsy, 413f
Stomach, 155f, 170–176
cancer, 174–176
imaging appearance, 174–176
Stomach *(Continued)*
treatment, 175–176
fat planes, obliteration, 175
findings, summary, 175t
lymphoma, 346f
Stress fractures (fatigue fractures), 136–137
imaging appearance, 136–137
radionuclide bone scan, triple-phase technique, usage, 137
third metatarsal, 136f
tibial, 137f
treatment, 137
Stroke syndrome, 317–319
imaging appearance, 317–319
treatment, 319
Structure, in imaging, 16, 16t
Subarachnoid hemorrhage, 313, 321–322
Subarachnoid (SA) space
enhancement, axial projection, 22f
fluid circulation, 290
nonionic contrast agent, injection, 22f
Subclavian region, central catheter (usage), 40
Subcutaneous emphysema, 75
frontal chest radiograph, 76f
imaging appearance, 75
treatment, 75–76
Subdural empyema, 293
imaging appearance, 293
T2-weighted MR image, 293f
treatment, 294
Subdural hematoma, 311–312
imaging appearance, 311–312
Submucosal bleeding, 350
Subperiosteal hemorrhage, occurrence, 420
Subsecond scanning, 21
Sudden infant death syndrome, 137
Sulci, 288
Superficial gastric erosions, 173–174
gastritis, presence, 174f
Supernumerary kidney, 219
Supraspinatus tendon, low signal intensity, 102f
Surfactant, components, 44
Suspected non-accidental trauma (SNAT), 137
Swallowing
deglutition, complexity, 153
difficulty (dysphagia), 161–162
Swan-Ganz catheters, 41
complication, 41
internal devices, findings (summary), 42t
position, 41
Symptoms, characteristics, 2
Synapse, 287
Syndrome, 2
indication, 426
Synovial membrane, inflammation of, 95
Syphilis, 383–385
congenital syphilis, 383
imaging appearance, 383–385
neuropathic joint disease, 384f
primary stage, 383

Syphilis *(Continued)*
secondary stage, 383
tertiary stage, 383
treatment, 385
Syphilitic aortitis, 384f
Syphilitic lesions, 384–385
Syphilitic osteomyelitis, 384f
Systemic arterial system, 251f
Systemic circulation, 250
Systemic lupus erythematosus, 423–424
bilateral pleural effusions, 424f
hand, frontal/oblique projections, 424f
imaging appearance, 423–424
treatment, 424
Systemic manifestations, acute inflammation and, 4
Systole (contraction phase), 250–251

T

T1-weighted images, 24
T2-weighted images, 24
TB. *see* Tuberculosis (TB).
Technetium-99m-labeled bone scintigraphy, 28f
Tension pneumothorax, 77f
Teratomas, 305
dermoid cysts, 400
Terminal ileum/sigmoid colon, fistulization, 178f
Tertiary hyperparathyroidism, 374
Testicular dysgenesis, 427
Testicular seminoma, T2-weighted MR image, 395f
Testicular torsion, 391–392
arterial perfusion, diminished, 393f
Doppler ultrasound image, 392f
imaging appearance, 392
scrotal ultrasound, 392f
treatment, 392
Testicular tumors, 393–394
imaging appearance, 393–394
treatment of, 394
types of, 393
Testosterone, 386
Tetralogy of Fallot, 254
imaging appearance, 254
plain chest radiograph, 254f
treatment, 254
Thalamus, 289–290
Thalassemia, 338
extramedullary hematopoiesis, 339f
lateral projection (skull), hair-on-end appearance, 338f
medullary spaces, widening, 338f
Thiamine deficiency (beriberi), 420
Third metatarsal, stress fracture, 136f
Thoracentesis, procedure, 79
Thoracic vertebroplasty, demonstration, 110f
Three-phase CT scanning protocol, 23f
Thrombectomy catheter (AngioJet catheter), usage, 273
Thrombocytes (platelets), 336, 337f
Thrombosis, 271–274
Thrombus (intravascular clot development), 271
Thumbprinting, in ischemic colitis, 191
Thyroid adenoma, neck (lateral projection), 372f
Thyroid carcinomas, 371–373
imaging appearance, 372–373
radioactive iodine scan, 372f
Thyroid gland, 367–373
diseases, 367–373
findings, summary, 373t
and parathyroid, 368f
physiology, 367
Thyroid goiter, ultrasound image, 370f
Thyroid tumors, treatment, 373
Thyroidectomy, 373
Thyrotropic hormone, levels, decreased, 300
Thyroxine, 367
Tibia
aneurysmal bone cyst, 122f
healed fracture in, 135f
Tissue death (necrosis), 5
Tortuous aorta, frontal chest radiograph, 166f
Torus fractures (buckle fractures), 132
Total pancreatectomy (surgical resection), 210
Toxic megacolon, ulcerative colitis, 188f
Toxic multinodular goiter, 370–371
Toxoid, 11
Trabeculae, 87
Tracheobronchial tree, fistulous communications, 157
Tracheoesophageal fistula, 156–158
acquired type, 157–158
congenital type, 156–157
types of, findings for, 158t
Traction diverticula, 163
esophagus, midthoracic portion, 164f
Transducer, recording, 17
Transient ischemic attacks, 319–320
Transitional vertebrae, 89f
Transmission-based precautions, 11
Transurethral resection (TUR), 388
Transvenous cardiac pacemakers, 42
internal devices, findings (summary), 42t
Transverse colon, intramural fistula, 190f
Transverse fractures, 131–132
Traumatic splenic rupture, CT scan, 213f
Treponema pallidum, 383
Tricuspid valve (right atrioventricular valve), 248–249
Trigone, 217–218
Triiodothyronine (T_3), 367
Tripod fracture, 315
orbital rim, interruption, 315f
Trisomy disorders (trisomy 21), 426
Trophoblastic disease, 416
Tuberculoma, 51–52
benign solitary pulmonary nodule, 62f
imaging appearance, 51
treatment, 51–52
Tuberculosis (TB), 49–52, 225–226
bladder, involvement, 226
findings, summary, 51t
imaging appearance, 226
large cavities, air-fluid levels, 50f
Mycobacterium tuberculosis, 49
papillary destruction, early stage, 226f
treatment, 226
ureter, involvement, 226
ureteral tuberculosis, 227f
Tuberculous arthritis
imaging appearance, 99–100
joint space destruction, 100f
Tuberculous autonephrectomy, plain image, 226f
Tuberculous osteomyelitis, 106
imaging appearance, 106
midthoracic vertebrae, vertebral collapse/anterior wedging, 108f
treatment, 106
Tubo-ovarian abscess, ultrasound image, 397f
Tumors, 7, 234–242, 397–406. *see also* specific tumor
extensiveness, staging, 9
findings, summary, 242t
swelling, acute inflammation clinical sign, 4
Turner's syndrome, 427
hand, frontal projection, 427f
imaging appearance, 427
treatment, 427

U

Ulcer
hiatal hernia sac, 159f
treatment of, 174
Ulcerative colitis, 187–189
disease, progression, 188f
double-contrast studies, 188
findings, summary, 190t
imaging appearance, 187–189
rectosigmoid, involvement, 188f
toxic megacolon, 188f
treatment, 190–191
Ulcerogenic islet cell tumors (gastrinomas), 209
Ultrasound, 17–20
abdominal, 18
imaging
knowledge requirement, 19
modality, 17
role, expansion, 19
limitation, acoustic barriers, 19
needle localization, 19f
safety, advantage, 18
summary of, 20t
Ultrasound-guided localization, 19f
Unconsciousness, 309
Undescended testis (cryptorchidism), 390–391
atrophic undescended testis, coronal MR image, 392f

Undescended testis *(Continued)*
bilateral undescended testes, malignant neoplasms, 391f
imaging appearance, 390–391
treatment, 391
ultrasound image, transverse plane, 391f
Undifferentiated tumor, 8
Undisplaced fractures, 132
Unilateral pulmonary edema, diffuse alveolar pattern, 262f
Unilateral renal agenesis, 218–219
Unilateral renal vein thrombosis, 242–243
Unilateral right tuberculous pleural effusion, 50f
Unilateral ureterocele, filled with contrast material, 223f
Upper abdomen
MRI of, 25f
plain image of, 362f
Upper bladder, CT scan of, 244f
Upper body, fracture sites (bone scan), 138f
Upper pelvis, CT scan of, 185f
Upper respiratory system, inflammatory disorders, 44–45
findings (summary), 45t
Upper thoracic esophagus, stricture, 161f
Urate crystals, deposition (continuation), 112
Uremia, 245
Ureter
anomalies, 220–221
distal portion, kidney stone (nonopaque filling defect), 232f
left ureter, contrast extravasation, 229f
renal pelvis, relationship, 222f
Ureteral calculus
obstructing, 231f
stone, 232f
Ureteral tuberculosis, 227f
Ureterocele, 221–222
bilateral, contrast material, 223f
ectopic, excretory urogram/cystogram, 223f
imaging appearance, 222
treatment, 222
unilateral, contrast material, 223f
Urinary bladder
inflammation, 227
structure/location, 218f
Urinary calculi, 228–231
imaging appearance, 228–231
treatment, 231
Urinary obstructions, findings (summary), 234t
Urinary system, 216–247
organs, location, 217f
physiology of, 216–218
radiographer notes, 217b
scout image, 217b
Urinary tract, congenital/hereditary anomalies, 221
Urinary tract obstruction, 231–234
excretory urogram, 233f
imaging appearance, 231–234
treatment, 234
Uterine agenesis, ultrasound images, 417f
Uterine fibroids, 400–402
excretory urogram, 401f
imaging appearance, 401–402
longitudinal sonogram, 402f
submucosal, endovaginal ultrasound, 402f
T2-weighted MR sagittal image, 402f
treatment, 402

V

Vaccine, bacteria/viruses (presence), 11
Valvular disease, 275–280
findings, summary, 279t
Variable expressivity, 10
Varicose veins, 281–284
blood, stasis, 283
imaging appearance, 283–284
lower extremity venogram, 282f
soft tissues, calcifications, 283f
treatment, 283–284
Vas deferens, 386
Vascular anatomy, 249f
Vascular diseases, 68–72
Vascular studies, 18
Vascular system, in MRA, 25
Vasectomy, 386
Vasopressin (ADH), production, 364
Vegetations, 275
Venous disease, 281–284
findings, summary, 283t
Ventricles, midline shift, 6f
Ventricular defects (identification), Doppler echocardiography (usage), 253
Ventricular septal defect, 252
heart enlargement, 252f
septal closure, absence, 254f
spin-echo MRI demonstration, 254
Ventricular system, generalized enlargement of, 328f
Ventriculomegaly, cranial axial ultrasound, 415f
Vermis, 289
Vertebral anomalies, 89
imaging appearance, 89
treatment, 89
Vertebral bodies
enlargement of, 366f
fracture, 145f
softening, 111
Vertebral fusion, 97f
Vertebral marrow, caseous necrosis, 106
Vesicoureteral reflux/infection, 220–221
Villi, digestion, 153
Viral meningitis, 290–291
Virtual reality (VR), CT postprocessing, 21
Virtual reality (VR) reconstructions, 21
Viruses, findings (summary), 54t
Visceral peritoneum, penetration, 9
Visual impulses, transmission, 288–289
Vitamin A deficiency, 421
Vitamin B deficiencies, dietary modifications, 421
Vitamin B_{12} deficiency, 341
Vitamin C (ascorbic acid) deficiency (scurvy), 420
Vitamin D deficiency (rickets), 420–421
Vitamin deficiencies, 419–421
treatment, 421
Vitamin K deficiency, 421
Vitamins, 419
Voiding cystourethrogram, 224f
Volume-rendered imaging, 21
Volvulus, 193
treatment, 195

W

Wagging jaw, 86b–87b
Warfarin (Coumadin), for thrombosis, 273
Water-soluble vitamins, 419
Whipple procedure, 210
White blood cells (leukocytes), 336, 337f
diseases, 342–349
findings, summary, 349t
Wilms' tumor (nephroblastoma), 240
CT scan, 242f
hydronephrosis (contrast), ultrasound (usage), 240
right kidney
pelvicalyceal system, distortion/displacement, 241f
ultrasound, 241f
T1-weighted coronal MR image, 243f
Wimberger's sign of scurvy, 420
Window level, 20
Window width, 20
Work-related lung disease, 59–60
Wrist
calcification in, in diabetes mellitus, 379f
Colles' fracture, frontal/lateral projections, 139f
musculoskeletal architecture, ultrasound image, 19f

X

X-linked inheritance pattern (muscular dystrophy), 425
X-rays, relative attenuation, 3b
circulatory system, 3b
decreased, 3b
increased, 3b
respiratory system, 3b
skeletal system, 3b
soft tissue, 3b

Z

Zenker's diverticula, 163
saccular outpouching, 164f
Zygomatic arch fractures, 315
submentovertex projection, 315f
Zygomatic arch vulnerability, 315